

Proceedings  
of International Conference  
in Prague, 19-20 February 2009

# **APPLICATIONS OF STRUCTURAL FIRE ENGINEERING**



[eurofiredesign.fsv.cvut.cz](http://eurofiredesign.fsv.cvut.cz)

---

Czech Technical University in Prague

**Proceedings of International Conference  
Applications of Structural Fire Engineering**  
hold during the Czech Presidency of the Council of the EU  
in Prague, 19-20 February 2009  
[eurofiredesign.fsv.cvut.cz](http://eurofiredesign.fsv.cvut.cz)

The preparation of the Proceedings was supported by the research centre of the Ministry of education, youth and sports CIDEAS No. 1M0579 and the Research plan Sustainable construction No. 6840770005. The illustrative figures on the cover prepared by Nuno R.R. Almeida represent the opportunity of colleagues from Czech Technical University in Prague, University in Coimbra and Slovak Technical University in Bratislava to work on the seventh large fire test in Cardington.

Ed. Wald F., Kallerová P., Chlouba J.  
ISBN 978-80-01-04266-3

Print Pražská technika, Czech Technical University in Prague  
January 2009, 200 copies

## Contents

|   |    |
|---|----|
| Preface .....   | 11 |
| Burgess I., <i>United Kingdom</i>   |    |
| Twenty two years of structural fire engineering in Czech Republic .....   | 13 |
| R. Kaiser, F. Wald, <i>Czech Republic</i>   |    |
| <b>Session 1: Case studies</b>  |    |
| Visible steel for a fire safe structure, case study office building “Junghof” .....                                 | 18 |
| Lange J., Ewald K., <i>Germany</i>  |    |
| Structural fire analysis for a perimeter braced-frame structure .....   | 22 |
| Jowsey A., Lim. L., Lane B., <i>United Kingdom</i>  |    |
| Simulation and study of natural fire in a wide-framed multipurpose hall with steel roof<br>truss .....              | 28 |
| Pada D., <i>Finland</i>   |    |
| An innovative approach to design fires for structural analysis of non-conventional<br>buildings, a case study ..... | 34 |
| Stern-Gottfried J., Rein G., Lane B., Torrero J.L., <i>United Kingdom</i>   |    |
| Evaluation of the fire resistance of a sport hall using structural fire engineering .....                           | 41 |
| Vila Real P., Lopes N., <i>Portugal</i>   |    |
| Design of cold-formed stainless steel tubular columns at elevated temperatures .....                                | 47 |
| To E.Ch.Y., Young B., <i>Hong Kong</i>  |    |
| Application of structural fire engineering to the steelwork design of Cannon Place, London. 53                      |    |
| Ding S.J., Harries D., Hermouet E., <i>United Kingdom</i>   |    |
| <b>Session 2: Fire modelling</b>  |    |
| Fire scenario and structural behaviour of underground parking lots exposed to fire .....                            | 60 |
| Bamonte P., Felicetti R., <i>Italy</i>  |    |
| Definition and selection of design fire scenarios .....   | 66 |
| Gkoumas K., Crosti Ch., Giuliani L., Bontempi F., <i>Italy</i>  |    |
| Generalised thermal and structural fire analysis with GENISTELA and GENISTRUC .....                                 | 72 |
| Liang H., Welch S., Faure L., Gillie M., <i>United Kingdom</i>  |    |
| Experimentation of the subway smoke control system .....  | 78 |
| Ni Z, Kan Q., <i>P. R. of China</i>   |    |

|   |     |
|---|-----|
| Experimental study on baggage fires of subway passenger .....   | 84  |
| Kan Q., Ni Z., <i>P. R. of China</i>  |     |
| Numerical simulation on vertical fire spread, effects of wall pier and overhanging eave<br>in preventing vertical fire spread ..... | 90  |
| Huang X., Ni Z., Lu S., <i>P. R. of China</i>   |     |
| Decrease in fire load on structures by timely fire detection .....  | 96  |
| Dudáček A., <i>Czech Republic</i>   |     |
| Adiabatic surface temperature, a sufficient input data for a thermal model .....  | 102 |
| Sandström J., Wickström U., Veljkovic M., <i>Sweden</i>   |     |
| <br><b>Session 3: Material modelling</b>  |     |
| Material properties loss of fibred-SCC due to fire action .....   | 110 |
| Alonso C., Rodriguez C., <i>Spain</i>   |     |
| Variations of steel strength characteristics in fire temperatures .....   | 116 |
| Domański T., <i>Poland</i>  |     |
| Fire damage of stone structures .....   | 122 |
| Hajpál M., <i>Hungary</i>   |     |
| Thermal characteristics measurements of an inorganic intumescent coating system .....   | 128 |
| Choi J.Y., Jang H.M., Chun Ch., <i>Korea</i>  |     |
| Stress-strain relationship of reinforcing steel, subjected to tension and high temperature ...                                      | 134 |
| Abramowicz M., Kowalski R., <i>Poland</i>   |     |
| Decomposition of intumescent coatings: comparison between numerical method and<br>experimental results .....                        | 140 |
| Mesquita L.M.R., Piloto P.A.G., Vaz M.A.P., Pinto T.M.G., <i>Portugal</i>   |     |
| Thermal behaviour of alkali activated slag composites: effect of aggregates .....   | 146 |
| Rovnaník P., Bayer P., Rovnaníková P., <i>Czech Republic</i>  |     |
| Thermal conductivity of gypsum at high temperatures, a combined experimental and<br>numerical approach .....                        | 152 |
| Rahmanian I., Wang Y., <i>United Kingdom</i>  |     |
| Thermal conductivity of gypsum plasterboards, at ambient temperature and exposed<br>to fire .....                                   | 158 |
| de Korte A.C.J., Brouwers H.J.H., <i>The Netherlands</i>  |     |
| Effective characteristics of fire protection materials .....  | 164 |
| Wald F., Strejček M., Cinař R., <i>Czech Republic</i>   |     |

#### Session 4: Concrete structures

|   |     |
|---|-----|
| Basic approach for the diagnosis of concrete after fire exposure .....  | 172 |
| Annerel E., Taerwe L., <i>Belgium</i>   |     |
| Heating-induced prestress variation in unbonded post-tensioned construction, potential consequences for post-fire performance ..... | 178 |
| Bisby L., <i>United Kingdom</i> , MacLean K., MacDougall C., <i>Canada</i>  |     |
| Fire resistance of axially loaded slender concrete filled steel tubular columns.....  | 184 |
| Espinós A., Hospitaler A., Ibáñez C., Romero M.L., <i>Spain</i>   |     |
| Numerical and experimental determination of residual concrete strength after action of fire .....                                   | 190 |
| Cvetkovska M., Cvetanovski P., Mihajlov V., <i>Macedonia</i>  |     |
| Fire resistance curves for RC columns .....   | 196 |
| Cvetkovska M., Cvetanovski P., Mihajlov V., <i>Macedonia</i>  |     |
| Spalling of concrete, implications for structural performance in fire .....   | 202 |
| Deeny S., Stratford T., Dhakal R., Moss P., <i>United Kingdom</i><br>Buchanan A., <i>New Zealand</i>                                |     |
| Combined while-drilling techniques for the assessment of the fire damaged concrete cover .....                                      | 208 |
| Felicetti R., <i>Italy</i>  |     |
| Experimental analysis of concrete strength at high temperatures and after cooling .....   | 216 |
| Klingsch E., Frangi A., Fontana M., <i>Switzerland</i>  |     |
| Numerical analysis of concrete columns in fire, advanced versus simplified calculation methods .....                                | 222 |
| Gonçalves M.C., Abrantes V., Rodrigues J.P.C., <i>Portugal</i><br>Franssen J.M., <i>Belgium</i>                                     |     |
| Analysis of the behavior in fire of concrete loadbearing walls .....  | 228 |
| Gonçalves M.C., Rodrigues J.P.C., Abrantes V., <i>Portugal</i>  |     |
| Self-compacting concrete at high temperature: a critical survey and recent test results .....                                       | 234 |
| Bamonte P., Gambarova P.G., <i>Italy</i>  |     |
| The effect of elevated temperatures on aerated concrete blocks .....  | 240 |
| Hardie B., Nadjai A., Ali F., <i>United Kingdom</i>   |     |

|  |     |
|--|-----|
| Experimental and numerical study of high performance concrete columns subjected to fire loading .....                                      | 246 |
| Huisman S., Korzen M., <i>Germany</i>  |     |
| Behaviour of R.C. beams under elevated temperature .....   | 252 |
| Lakshmiathy M., Jayasree G., Santhanaselvi S., <i>India</i>  |     |
| Simplified layered approach for analysis of RC slabs subjected to fire .....   | 258 |
| Bacinskas D., Geda E., Kaklauskas G., Gribniak V., <i>Lithuania</i>  |     |
| Performance based fire design of concrete-filled steel columns .....   | 264 |
| Kodur V., Fike R., <i>USA</i>  |     |
| Fire resistance of fibre reinforced concrete columns .....   | 271 |
| Rodrigues J.P.C., Laím L., <i>Portugal</i> , Mihailovschi G., <i>Argentina</i>   |     |
| Fire resistance tests on concrete columns with restrained thermal elongation .....   | 277 |
| Martins A.M.B., Rodrigues J.P.C., <i>Portugal</i>  |     |
| Compressive strength of fibre reinforced concretes .....   | 283 |
| Santos S.O., Rodrigues J.P.C., <i>Portugal</i> , Toledo R., <i>Brazil</i>  |     |
| Numerical evaluation of load induced thermal strain in restraint structures, calculation of a tunnel cross section subjected to fire ..... | 289 |
| Schneider U., Schneider M., <i>Austria</i> , Franssen J.M., <i>Belgium</i>   |     |
| Structural safety assessment of tunnels subjected to fire loading .....  | 295 |
| Ring T., Zeiml M., Lackner R., <i>Austria</i>  |     |
| A numerical model for prediction of spalling of concrete exposed to elevated temperatures .....  | 301 |
| Zhang H., Davie C.T., Pearce Ch.J., Bićanić N., <i>United Kingdom</i>  |     |
| A theoretical model for RC columns subjected to natural fire .....   | 307 |
| Yao Y., <i>USA</i> , Tan K.H., <i>Singapore</i>  |     |
| Different types of pre-stressed hollow core panels, and their fire resistance according to Eurocodes .....                                 | 313 |
| Čajka R., Matečková P., <i>Czech Republic</i>  |     |
| Effect of temperature on the behaviour of confined fibre reinforced high strength concrete   | 318 |
| Sharma U.K., Babu C.R., Bhargava P., Gupta V.K., <i>India</i>  |     |
| Recovery behavior of hybrid fibre reinforced high strength concrete after fire exposure ....   | 325 |
| Horiguchi T., <i>Japan</i> , Suhaendi S.L., <i>Singapore</i>   |     |

## Session 5: Steel structures

|   |     |
|---|-----|
| Investigation into methods for predicting connection temperatures .....   | 332 |
| Anderson K., Gillie M., <i>United Kingdom</i>   |     |
| Structural fire engineering assessments of the FRACOF and Mokrsko fire tests,<br>an engineering prediction .....  | 338 |
| Abu A.K., Block F.M., Butterworth N.A., Burgess I.W., <i>United Kingdom</i>   |     |
| A new design method for industrial portal frames in fire .....  | 344 |
| Song Y., Huang Z., Burgess I., Plank R., <i>United Kingdom</i>  |     |
| An experimental study of structural behaviour of joints in restrained steel frames in fires ..  | 350 |
| Dai X.H., Wang Y.C., Bailey C.G., <i>United Kingdom</i>   |     |
| Effects of flame radiation on temperature elevation of steel members in large space<br>building fire .....  | 356 |
| Du Y., Li G.Q., <i>P. R. of China</i>   |     |
| Application of structural fire design to steel buildings, New Zealand experience<br>1986 to 2008 .....  | 362 |
| Feeney M., Clifton G.Ch., <i>New Zealand</i>  |     |
| Influence of fire on steel bridge, over Vistula river in Puławy .....   | 368 |
| Głuch G., <i>Poland</i>   |     |
| Design method for restrained steel columns in fire .....  | 374 |
| Li G.Q., Wang P., <i>P. R. of China</i> , Wang Y.C., <i>United Kingdom</i>  |     |
| Integrated fire engineering of steel skeleton, using well established fire sources .....  | 380 |
| Heinisuo M., Hietaniemi J., Kaitila O., Laasonen M., Outinen J., <i>Finland</i>   |     |
| Buckling behaviour of steel columns in fire conditions and comparison with Eurocode 3 ..  | 386 |
| Hozjan T., Kurnjek L., Planinc I., Saje M., Srpčič S., <i>Slovenia</i>  |     |
| Behaviour of high strength grade 10.9 bolts under fire conditions .....   | 392 |
| González F., Lange J., <i>Germany</i>   |     |
| Stainless steel beam-columns interaction curves in case of fire with and without lateral<br>torsional buckling .....  | 398 |
| Lopes N., Real P.V., Simões da Silva L., <i>Portugal</i> , Franssen J.M., <i>Belgium</i>  |     |
| Fire protection of steel structures using sprinkler systems .....   | 406 |
| Outinen J., Kansa J., <i>Finland</i>  |     |
| FSE Analysis of a 19th century cast-iron bridge structure, a performance based analysis<br>of a solution that combines water suppression and ventilation to avoid passive<br>protection ..... | 411 |
| Ugartetxe R., Morente F., Aurtenetxe J., Pérez Ch., De la Quintana J., <i>Spain</i>   |     |

|   |     |
|---|-----|
| Experimental research on the fire behaviour of steel columns embedded on walls .....  | 417 |
| Correia A.J.P.M., <i>Portugal</i> , Rodrigues J.P.C., <i>Brazil</i> , Silva V.P., <i>Portugal</i>   |     |
| Numerical simulation of steel columns in fire .....   | 423 |
| Carvalho L.T., Rodrigues J.P.C., Gonçalves M.C., Correia A.M., <i>Portugal</i>  |     |
| Unprotected steel in multi-storey car parks, 15 min fire resistance of unprotected steel<br>and composite members in a multi-storey car park system .....             | 429 |
| Schaumann P., Kirsch T., <i>Germany</i>   |     |
| Steel beam-column under thermal gradient, combined axial-bending capacity of steel<br>double-T cross-sections subjected to non-uniform temperature distribution ..... | 435 |
| Tsalikis C., Koltsakis E., Baniotopoulos C.C., <i>Greece</i>  |     |
| Behaviour of screwed shear sheeting connection in fire .....  | 441 |
| Lu W., Mäkeläinen P., Outinen J., <i>Finland</i>  |     |
| Unprotected bi-axially loaded steel columns under fire conditions .....   | 447 |
| Yao Y., <i>USA</i> , Tan K.H., <i>Singapore</i>   |     |
| Computer program for fire check of concrete members .....   | 453 |
| Štefan R., Procházka J., <i>Czech Republic</i>  |     |
| Connections of trapezoidal sheets at elevated temperature .....   | 459 |
| Kallerová P., Sokol Z., Wald F., <i>Czech Republic</i>  |     |
| Structural analysis of steel structures under fire loading .....  | 465 |
| Crosti Ch., Giuliani L., Gkoumas K., Bontempi F., <i>Italy</i>  |     |
| Connection temperatures during the fire test in Mokrsko .....   | 471 |
| Chlouba J., Wald F., <i>Czech Republic</i>  |     |
| <b>Session 6: Composite structures</b>  |     |
| Assessment of steel-concrete-steel shear wall .....   | 478 |
| Dunne D., Subedi N., <i>United Kingdom</i>  |     |
| Long span composite beams subjected to fire, effects of fire on lateral stability .....   | 484 |
| Flint G., Lane B., <i>United Kingdom</i>  |     |
| Performance of shear studs in fire .....  | 490 |
| Choi S., Han S., Nadjai A., Ali F., <i>United Kingdom</i> , Kim S., Choi J., <i>Korea</i>   |     |
| Fire composite floor cellular steel beams for buildings .....   | 496 |
| Goodfellow N., Nadjai A., Tee K.F., Ali F., Choi S., <i>United Kingdom</i>  |     |

|  |     |
|--|-----|
| Experimental study on full scale composite floor slabs under fire condition .....                                    | 502 |
| Zhang N.S., Li G.Q., Lou G.B., Jiang S.Ch., Hao K.Ch., <i>P. R. of China</i>   |     |
| Thermal restraint effects on the fire resistance of steel and composite steel and concrete columns .....             | 512 |
| Korzen M., <i>Germany</i> , Rodrigues J.P.C., Correia A.M., <i>Portugal</i>  |     |
| Fire resistance of bar-reinforced concrete-filled steel tube columns .....   | 518 |
| Park S.H., Song K.Ch., Chung K.S., Min B.Y., Choi S.M., <i>Korea</i>   |     |
| Calculation of temperature distribution in composite columns .....   | 524 |
| Yuan W., Tan K.H., <i>Singapore</i>  |     |
| Parametric numerical analysis of steel and concrete composite floors exposed to ISO fire .                           | 530 |
| Roosefid M., Zhao B., <i>France</i>  |     |
| Cellular composite beams at elevated temperatures, experimental investigation .....                                  | 537 |
| Bihina G., Zhao B., <i>France</i> , Vassart O., <i>Luxembourg</i>  |     |
| Concrete and composite slabs in fire, discussion of the load bearing characteristics .....                           | 543 |
| Mensingher M., Stadler M., <i>Germany</i>  |     |
| <br><b>Session 7: Timber structures</b>  |     |
| Tests and modelling of wood in shear at elevated temperatures .....  | 550 |
| Audebert M., Bouchaïr A., Dhima D., <i>France</i>  |     |
| Timber connections under fire loading, a component model for numerical modelling .....                               | 557 |
| Cachim P., <i>Portugal</i> , Franssen J.M., <i>Belgium</i>   |     |
| Evaluation of natural and parametric temperature-time curves for the fire design of cross-laminated wood slabs ..... | 563 |
| Friquin K.L., <i>Norway</i>  |     |
| Experimental study on fire protection of timber assemblies .....   | 569 |
| Ni Z., Qiu P., <i>P. R. of China</i> , Mehaffey J., <i>Canada</i> , Winter S., <i>Germany</i>                        |     |
| Fire resistance of trusses with punched metal plate fasteners .....  | 575 |
| Kuklík P., Starý J., Tajbr A., Vodolan M., <i>Czech Republic</i>   |     |
| <br><b>Session 8: Other questions</b>  |     |
| Seismic and fire design of composite frames, a multi-disciplinary approach for an integrated design .....            | 580 |
| Alderighi E., Salvatore W., <i>Italy</i>   |     |

|   |     |
|---|-----|
| Fire analysis of structures in seismic areas .....  | 586 |
| Zaharia R., Pintea D., Dubina D., <i>Romania</i>  |     |
| Incorporation of load induced thermal strain in finite element models .....   | 592 |
| Law A., Gillie M., Pankaj P., <i>United Kingdom</i>   |     |
| Fire resistance assessment for differentiated safety requirements .....   | 598 |
| Maślak M., <i>Poland</i>  |     |
| Performance of structural systems in fire .....   | 604 |
| Mostafaei H., Sultan M.A., Bénichou N., <i>Canada</i>   |     |
| Integrity of fire resistant construction, developing a methodology to control fire induced<br>progressive structural collapse ..... | 610 |
| Wang Y.C., <i>United Kingdom</i>  |     |
| Super element in structural analysis .....  | 616 |
| Yuan W., Tan K.H., <i>Singapore</i>   |     |
| Authors index .....   | 622 |

## Preface

Current European practice in structural fire engineering is tending more and more to acceptance of the benefits to be gained from performance-based approaches to fire-resistant design. These proceedings, from the *Applications of Structural Fire Engineering* conference, presents the state of the art in the development and application of both simple and advanced performance-based design methods for concrete, steel and timber structures. Internationally acknowledged research experts and specialists in design against fire are represented in these articles, offering an opportunity to share contemporary ideas and knowledge within both the background science and practical case studies. The spectrum of relevant research themes covered encompasses fire modelling, heat transfer to structural elements, numerical modelling of thermo-structural behaviour at elevated temperatures, structural fire testing at elemental and structural scales, the development of simplified design methods and studies based on the structural Eurocodes. Practical design case studies demonstrating the ways in which performance-based structural fire safety design methods have been applied to real projects, and the economic and safety implications of using these methods in place of the traditional prescriptive rules, are included.

Ian Burgess

### **Scientific Committee**

Farid ALFAWAKHIRI, USA  
Zdeněk BITTNAR, Czech Republic  
Ian BURGESS, United Kingdom  
    Chairman  
Frank DEHN, Germany  
Aleš DUDÁČEK, Czech Republic  
Jean-Marc FRANSSSEN, Belgium  
Pietro G. GAMBAROVA, Italy  
Sengkwan CHOI, Korea  
Gabriel A. KHOURI, United Kingdom  
Venkatesh KODUR, USA  
Jürgen KÖNIG, Germany  
Rudolf KAISER, Czech Republic  
Petr KUKLÍK, Czech Republic  
J.M.LEJTENA, The Netherlands  
Qiang Guo LI, China  
Ming Chun LUO, China (Hong Kong)  
Mahen MAHENDRAN, Australia  
Fernando Belmez MORENTE, Spain  
Ali NADJAI, United Kingdom  
Tuuli OKSANEN, Finland  
Jaroslav PROCHÁZKA, Czech Republic  
Peter SCHAUMANN, Germany  
Luc TAERWE, Belgium  
Kang Hai TAN, Singapore  
Olivier VASSART, Luxembourg  
Milan VELJKOVIC, Sweden  
Paulo VILA REAL, Portugal  
František WALD, Czech Republic  
Yong WANG, United Kingdom  
Raul A ZAHARI, Romania  
Bin ZHAO, France

### **Organizing Committee**

Aleš DUDÁČEK, Czech Republic  
Jiří CHLOUBA, Czech Republic  
Rudolf KAISER, Czech Republic  
Petra KALLEROVÁ, Czech Republic  
František KREGL, Czech Republic  
Petr KUKLÍK, Czech Republic  
Jaroslav PROCHÁZKA, Czech Republic  
Zdeněk SOKOL, Czech Republic  
Magdaléna ŠTUIBEROVÁ, Slovak Republic  
Jitka VAŠKOVÁ, Czech Republic  
František WALD, Czech Republic  
    Chairman

## TWENTY TWO YEARS OF STRUCTURAL FIRE ENGINEERING IN CZECH REPUBLIC

Rudolf Kaiser <sup>a</sup>, František Wald <sup>b</sup>

<sup>a</sup> Ministry of Interior, Fire and Rescue Service of the Czech Republic, General Directorate

<sup>b</sup> Czech Technical University, Faculty of Civil Engineering, Prague, Czech Republic

### FIRE DESIGN IN CZECHOSLOVAKIA

The background of the today fire engineering in Czechoslovakia starts in 1965, when the fire engineering solutions were incorporated into the overall architectural and engineering design. The standard related to fire testing, which was introduced in 1967, takes into account the compartmentisation, the fire risks, the escape solutions and the building separation. The whole set of standards, which is marked ČSN 73 08xx and related to fire testing of the construction products, the data of the material properties and the valorisation of structures, was prepared by a new standard committee established in the area of fire safety in 1971. The standard ČSN 73 0810 Fire protection of buildings - Requirements determination in civil engineering was in the set of documents localised at the position between the experimental and design national specifications. The document [10] represents the latest issue of this key provision, which creates the foundation of the structure of the national standards.

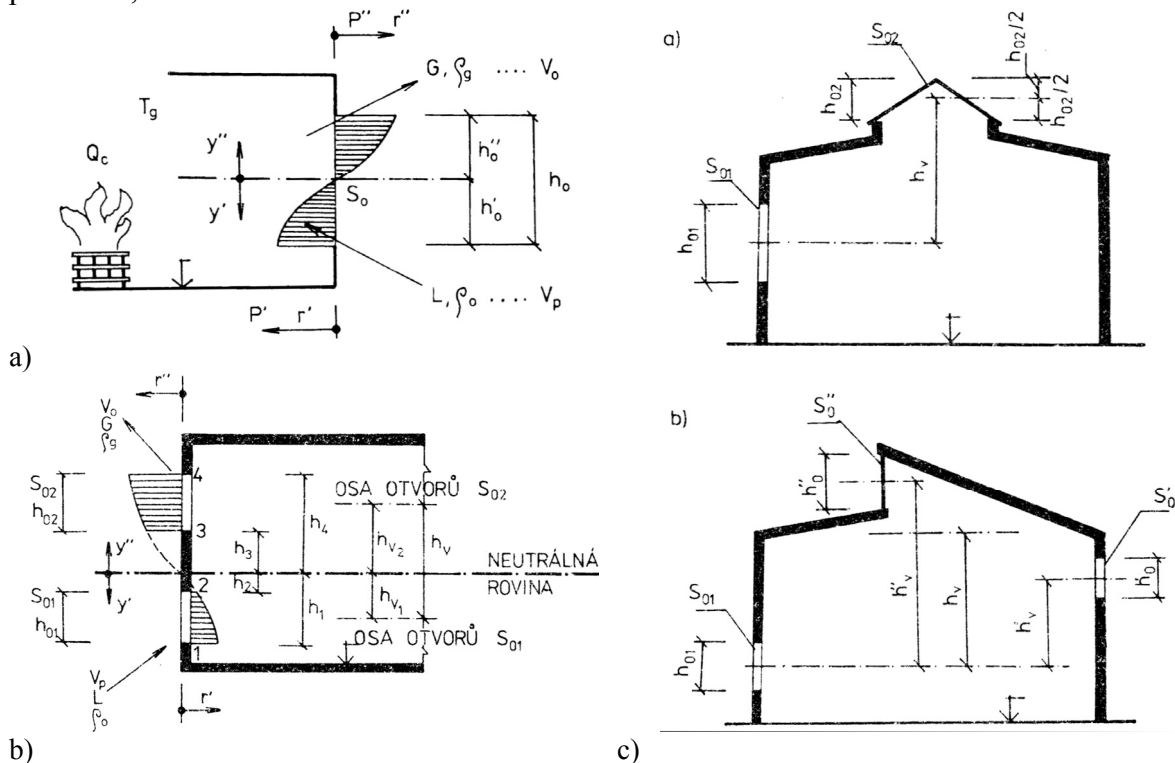


Fig. 1 Example of application of the zone model for prediction of temperature in the industrial building, a) model, b) openings in different heights, c) application to industrial hall, see [4]

The today prescriptive rules are based on the publication prepared by Karpaš and Zoufal, see [1], which brings not only the properties and rules of application of the fire protection, but also the material properties of the structural steel and the basic rules of the design of steel

structures. In the same year was published the first contribution for the fire design by dr. Reichel, see [2], which creates the background of the today compartmentisations, the estimation of the fire load, and most importantly it incorporate the fire risk into the Ultimate Limit State design. The second volume of this book takes care among others of the fire separation walls, the bearing structures and the fire safety distances, see [3].

The important steps for fire safety of structures was the foundation of the research centre in Veselí nad Lužnicí, where the colleagues from PAVUS a.s., see [www.pavus.cz](http://www.pavus.cz), successfully continue to ensure the good level of the products at European market to develop European material fire standards as well as national fire safety regulations and standards. The integral part of the reached level of the fire safety is shearing of knowledge with the young colleagues at the Faculty of Safety Engineering of Ostrava University, see [www.fbi.vsb.cz](http://www.fbi.vsb.cz), for forty years already and in the part of the safety and risk engineering related to the structures at Czech Technical University in Prague as well, see [www.fsv.cvut.cz/baris](http://www.fsv.cvut.cz/baris).

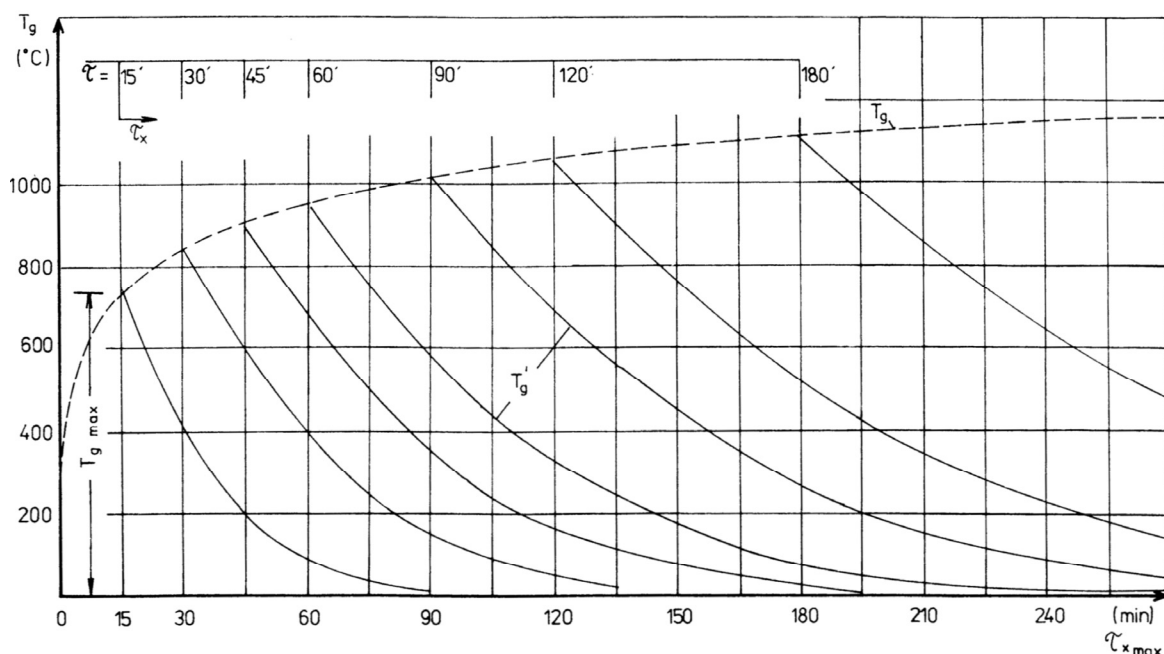


Fig. 2 Structure of the parametrical fire curve based on the time of the maximal temperature, see [4]

The background to the structural fire engineering in Czechoslovakia itself was introduced by the work of dr. Reichel, see [4], in 1987. The publication is contributing to the evaluation of the fire risk, the fire load, the structural behaviour and the economical aspects of the fire hazards. It brings the explanation of the background principles and its application in the current Czechoslovak standards. In the part devoted to the fire load is introduced for the utilisation of the Ultimate Limit State principles. A special chapter is focussed to the heat release and its importance for estimation of prediction of fires. The zone models and parametrical fire curve are used for the fire modelling. The simple zone model allowed predicting of the importance of the openings and its position in the fire compartment in the horizontal and vertical directions. The example of the application of the zone model to the influence of the openings at different height is documented on Fig. 1. The parametrical fire curve, presented in the book, modified the nominal standard fire curve based on the fire load and the ventilation. The simple solution gives a conservative estimation based on an assumed maximal reached temperature, see Fig. 2. Only one cooling speed is assumed. The publication brings useful worked examples for the calculation of the fire load, the equivalent



the specialists with appropriate qualification take care of the fire engineering for constructions. These methods of evaluation do not need to be specified in detail for these specialists. The procedure of evaluation contains basically from the location of fire, type of fire, the potential fire hazard, the systems and features impacting on fire, the people response, the event tree, the consideration of probability, the consideration of consequence, the risk ranking, and the final selection and documentation. These fire scenarios for quantitative analysis will become the design fire. The data related to the risk probability are under preparation at Ministry of Interior.

## SUMMARY

The fire engineering in Czech Republic, which is based on a good connection between the prescriptive rules and the performance based solutions, starts in 1965. The reached knowledge in connection with growing application of the active fire measurements and the information technologies in the fire engineering brings the opportunity to keep the good level of the fire safety for the challenging complex structural solutions, e.g. the mixed building technologies, introduction of the new materials, the high raised buildings, as well as the solutions for the sustainable constructions.

## ACKNOWLEDGMENT

For the preparation of this contribution Dr. Reichel kindly offered his lecture, which presented at the Faculty of Safety Engineering Ostrava University in September 2008. The material was prepared with the support of the Research plan No. 6840770005.

## REFERENCES

- [1] Karpaš J., Zoufal R., Fire protection of steel structures, in Czech Ochrana ocelových konstrukcí před požárem, ČSP Zabraňujeme škodám, vol. 6, Prague 1978, p. 43.
- [2] Reichel V., Fire design of buildings, in Czech Navrhování požární bezpečnosti staveb, Zabraňujeme škodám, Česká státní pojišťovna, part I, vol. 11, Prague 1978, p. 72.
- [3] Reichel V., Fire design of buildings, in Czech Navrhování požární bezpečnosti staveb, Zabraňujeme škodám, Česká státní pojišťovna, part II, vol. 12, Prague 1978, p. 67.
- [4] Reichel V.: Fire design of industrial structures, in Czech Navrhování požární bezpečnosti výrobních objektů, Zabraňujeme škodám, Česká státní pojišťovna, vol. 17, Prague 1987, p. 125.
- [5] Karpaš J., Zoufal R., Fire safety of steel and concrete structures, in Czech Požární odolnost ocelových a železobetonových konstrukcí, publikace ČSP Zabraňujeme škodám, svazek 28, Prague 1989, p. 43.
- [6] ČSN 73 0810, Fire protection of buildings - General requirements, in Czech Požární bezpečnost staveb - Požadavky na požární odolnost stavebních konstrukcí, ČNI, Prague 2005, p. 40.
- [7] ČSN 73 0802, Fire protection of buildings - Non-industrial buildings, in Czech Požární bezpečnost staveb - Nevýrobní objekty, ČNI, Prague 2000, p. 116.
- [8] ČSN 73 0804, Fire protection of buildings - Industrial buildings, in Czech Požární bezpečnost staveb - Výrobní objekty, ČNI, Prague 2002, p. 146.
- [9] Regulation MI No. 23/2008, Technical conditions of the fire protection of the buildings, in Czech O technických podmínkách požární ochrany staveb, Czech Ministry of Interior, Prague 2008.
- [10] Law ČR No. 133/1985, Fire protection and related provisions, in Czech O požární ochraně a související předpisy, Czech Republic, Prague 1985.
- [11] ISO/TR 13387-2, Fire engineering - Part 2: Design fire scenarios and design fire, Genève 1999.

Proceedings of International Conference  
Applications of Structural Fire Engineering  
Prague, 19-20 February 2009

**Session 1**

**Case Studies**

## VISIBLE STEEL FOR A FIRE SAFE STRUCTURE Case Study Office Building “Junghof”

Prof. Dr.-Ing. Jörg Lange <sup>a</sup>, Dipl.-Ing. Karsten Ewald <sup>b</sup>

<sup>a</sup> Technische Universität Darmstadt, Department of Civil Engineering and Geodesy, Darmstadt, Germany

<sup>b</sup> Lange + Ewald Ingenieure, Rödermark, Germany

### INTRODUCTION

In the centre of Frankfurt the office building “Junghof” had to be refurbished to make it attractive for modern use. When it was built in the 1950s five storeys were located around a central court. The new concept (*Fig. 1*) developed by the architects “Schneider und Schumacher” of Frankfurt added two storeys, raising the building above the critical height into the class of high-rise buildings. This led to additional requirements with regard to the fire-safety, mainly escape routes and fire resistance of structural elements.



*Fig.1.* View of the “Junghof” in Frankfurt

The building is located close to a district with many sky scrapers that rise up to 200 m. Because it is visible from most of these the architects invested much effort into the 5th façade. The roof was given a free form, clad with aluminium panels.

### 1 GEOMETRY

All four wings of the existing building have different depths. This led to varying geometric patterns in each corner. Spline-functions were used by the architects to define the form of the roof. These functions could not be used for further processing of the structural analyses and shop drawings, so an equivalent mathematical model was developed. To prepare buildable structural details it became necessary to develop plane glass surfaces and a roof structure with constant depth. This was done by defining a mathematical net for the outer surface. Relating to the net nodes, all additional design depths of the structure and dry ceiling were defined.

The system lines of the structural model for the calculation of the design forces were also taken from this net. This structural model then served as the basis for the final design drawings.

## 2 STRUCTURE

The concrete cores for the staircases in the four corners of the building had to be strengthened for the additional loads of the added storeys. Between these cores no additional loads were allowed to be transferred to the existing structure. Due to the difficulties related to improving the strength of the structure the added two storeys had to be light. Therefore, and because of the long span over the old structure, a steel construction was chosen.



Fig. 2. Primary structure of the 7<sup>th</sup> floor office space

A structure was designed that resembles an arch bridge (Fig. 4a). In fact only the sides located towards the court act like an arch (spanning 36 m) in structural terms. The outside structures are trusses with cantilevers showing top chords having the form of an arch. They have a total length of 57 and 60 m respectively. The cantilevers have a length of up to 12 m. These arches are made of circular steel sections (diameter: 355.6 mm, wall thickness: 12 to 20 mm). The tension element tying the arches horizontal bearing forces is an I-beam. All arches, tension elements, and bottom chords are fire protected with fire board.

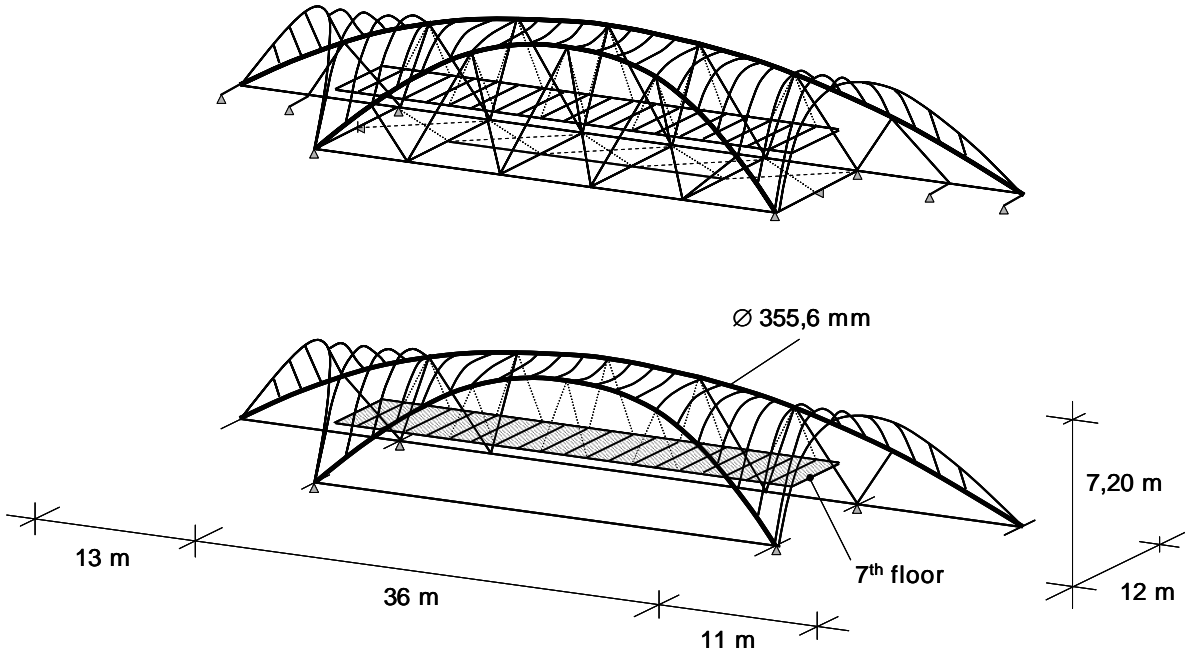


Fig. 3. Roof beams

The need for a light structure combined with the architects goal to produce a transparent, open office space led to the use of composite slabs (depth = 160 mm, spanning nearly 2 m without temporary support) on composite beams spanning from outside wall to outside wall (maximum span = 7.5 m) without any interior columns (*Fig. 2*). This led to a common design of the 7<sup>th</sup> floor slab but to very odd shapes of the roof-beams on account of the shell-like roof (*Fig. 3*). Due to the use of a suspended ceiling it was possible to protect these beams with a cementitious coating that gave them 90 minutes fire resistance.

The design for heating and cooling required the use of material with high heat capacity in the roof since no air-conditioning was installed. Therefore slopes of up to 70° had to be formed in concrete. Up to 30° composite slabs with in-situ concrete were cast. A re-entrant composite profile (with a depth of 51 mm), needing no fire protection was used for the slab. It was flexible enough to follow the curve of the roof (*Fig. 3*). In bigger slopes pre-cast concrete elements were used (see also *Fig. 3* lower left area). They were bolted in three points to the steel structure. The joints were filled with fireproofing-material. Due to a careful planning process 90% of the roof-area was made of identical elements.

The 7<sup>th</sup> floor frames into a stringer that is suspended from the arch using circular sections (diameters of 40 and 56 mm) with fire-protection made of calcium-silicate shells.



*Fig. 4. Structural System*  
top: a) Serviceability state  
bottom: b) System for fire design

### 3 FIRE DESIGN

A special feature of this building is the design of the ties that are part of the arch. They are designed without any fire protection. As shown in *Fig. 4a* a structural system was developed that in case of fire neglected most of the ties and the wind-loaded truss connecting the bottom chords (*Fig. 4b*). This system was analyzed under all dead and live loads. The wind loads were reduced, because it was reasonable to neglect the area of the windows. If the fire is strong enough to reduce the strength of the ties the windows will be broken.

Due to redistribution of the loads for some members the fire-design was the governing load case.

This design procedure, guided by references [1] to [9] not only saved cost but also reduced the visible width of the ties. In some load cases they have to carry compressive loads. Therefore it was not possible to reduce their diameter below 273 mm.

## REFERENCES

- [1] Fontana, M.; Favre, J. P.; Fetz, C., A survey of 40,000 building fires in Switzerland. *Fire Safety Journal* 32, Elsevier Science Ltd., 1999
- [2] Eurocode 3: Design of steel structures, part 1.2: General rules, Structural fire design. April 2001
- [3] Grundlagen zur Festlegung von Sicherheitsanforderungen für bauliche Anlagen. *Beuth Verlag, Berlin*, 1981
- [4] Richtlinie 019 „Brandsicherheit von Stahl- und Verbundbauteilen in Büro- und Verwaltungsgebäuden“ *Deutscher Ausschuss für Stahlbau, Düsseldorf*, November 2001
- [5] Schaumann, P.; Heise, A., Erläuterungen zur DAST-Richtlinie 019: Brandsicherheit von Stahl- und Verbundbauteilen in Büro und Verwaltungsgebäuden. *Stahlbau* 71, Ernst & Sohn, Berlin, 2002
- [6] Schleich, J.-B., Globales Brandsicherheitskonzept. *Stahlbau* 67, Ernst & Sohn, Berlin, 1998
- [7] Zehfuss, J., Risikogerechte brandschutztechnische Bemessung mehrgeschossiger Wohn- und Bürogebäude am Beispiel der Stahlbauweise. *Bauingenieur* 7/8, 2002
- [8] Lange, J.; Ewald, K., Das Düsseldorfer Stadttor – ein 19-geschossiges Hochhaus in Stahlverbundbauweise. *Stahlbau* 67, Ernst & Sohn, Berlin, 1998
- [9] Schaumann, P., Brandschutznachweise für ungeschützte Stahlkonstruktionen, *BbauBl., Heft* 7, 1999

# STRUCTURAL FIRE ANALYSIS FOR A PERIMETER BRACED-FRAME STRUCTURE

Allan Jowsey<sup>a</sup>, Linus Lim<sup>a</sup>, Barbara Lane<sup>a</sup>

Arup, 13 Fitzroy Street, London, W1T 4BQ, United Kingdom

## 1 INTRODUCTION

This paper presents a detailed analysis of the structural performance of a braced perimeter tube in fire, based on a proposed landmark 63 storey office building in the City of London, UK. The aim of the analysis was to study the robustness of this iconic structure and to address any weaknesses in the proposed structural form. The analysis quantified the heating and cooling phase over the entire 3,000m<sup>2</sup> floor-plate and its effects on connections and structural elements, including the non-uniform perimeter bracing layout.

The outcome of the study presented in this paper allowed for an understanding of the strengths and weaknesses of structural design in terms of fire both for tall buildings in general and specific to this structure. The analyses have identified key performance issues which would not have been identified if the building were protected to typical Building Codes. This project has highlighted the need for more research into large diameter circular hollow sections filled with un-reinforced concrete and research into performance of connections.

## 2 THE BUILDING

The Pinnacle is 288m tall and comprises 3 basement levels and 63 upper floors (*Fig 1*). The building will be mainly occupied by offices. The structural system that is discussed in this paper is a braced perimeter tube, which is a system that is suited for very high rise buildings.

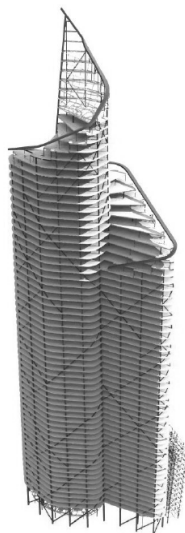


*Fig 1*: Structural representation of the building

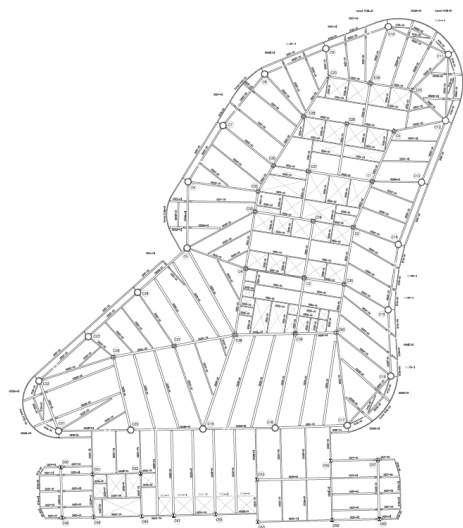


*Fig 2*: Typical beam layout for lower floor (Floor 5)

This building has several unique features. It has a highly irregular floor plan which has a beam layout that changes from floor to floor (*Fig 2*). The perimeter columns of the building are inclined due to the tapered elevation of the building. The layout of the perimeter diagonal

braces is non-uniform as it has been optimised to resist the worst case wind condition. The braces connect to the perimeter columns at megaframe levels which are located at every third floor and act together with the beams to resist the wind and other horizontal forces.

### **3 STRUCUTRAL FIRE ANALYSIS**

A series of non-linear structural fire analyses were performed by Arup Fire to assess the robustness of the building in a fire and to develop an engineered fire protection strategy for the structural steel members of the building. The engineered fire protection strategy incorporated unprotected secondary beams and reduced fire rating (90 minutes) to all structural frame elements, rather than relying on the prescriptive guidance defined by Building Regulations[1] which requires 2 hour fire protection to all structural elements. Three representative floors of the building (levels 5, 6 and 44) were selected to represent the structural fire response of the typical office floors and to address various aspects of the structure. The analyses of only one of the three floors (level 5) are presented here. There were several challenges in undertaking the structural fire analysis for this project:

- The architects expressed their desire to have large, clear spans with a minimum number of internal columns to provide flexibility for the building tenants.
- To minimise the inter-storey height, cellular beams with composite steel-concrete trapezoidal floor decks were to be used. The cellular beams allowed the building services to be passed through the beam webs while the trapezoidal floor system reduced overall building weight.
- Unreinforced concrete filled steel tube columns were also proposed to be used around the perimeter of the building.
- Other aspects that had to be considered in the analyses were the increased temperatures of the shear studs due to the proposed trapezoidal decking system (without fire protection to fill the voids) and any effects of partial composite action on structural fire performance.
- Web-post buckling of the protected cellular beams had to be mitigated.

#### **3.1 Acceptance criteria for analyses**

The main acceptance criteria for the analyses considered maintaining stability and compartmentation throughout the duration of the design fire, specifically:

- Columns to maintain their load carrying capacity and no runaway deflections of the floor system to occur for the duration of the fire scenarios
- Strains in the concrete floor slab, specifically at connections, are within acceptable limits.

#### **3.2 Design Fire**

The parametric fire curve described in Eurocode 1: Part 1-2 (BS EN 1991-1-2:2002) [2] was used to determine a credible natural, office design fire (*Fig 3*). This design fire was applied throughout the entire floor plate, assuming simultaneous uniform heating throughout a single floor. Multi-floor fires were not considered. In determining the worst case design fire, various amounts of ventilation were considered, ranging from 25% to 100% to consider different amounts of glass breakage in the fire. The fire with 25% ventilation was chosen and agreed with the Approving Authorities (City of London) as it was considered to have the greatest impact on the protected structural elements and to be the most conservative design fire.

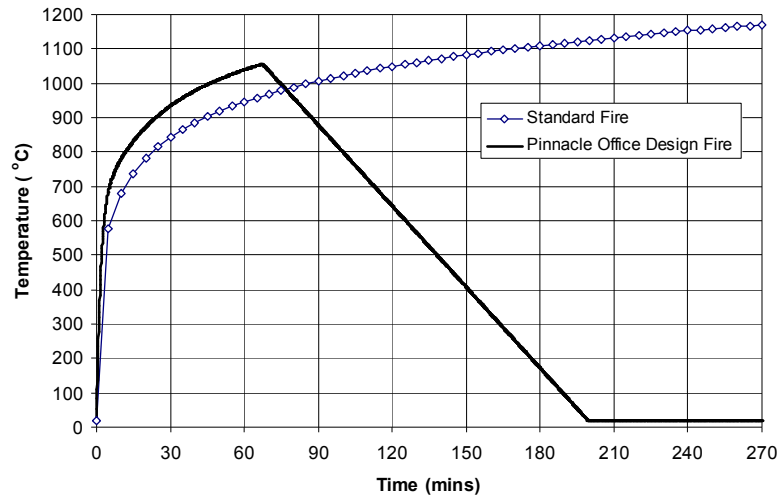


Fig 3: Comparison of design fire with the Standard Fire

#### 4 MODELLING OF THE GLOBAL STABILITY SYSTEM

The program used for the analysis of The Pinnacle is the ABAQUS [3] Finite Element Analysis (FEA) software, incorporating the non-linear temperature dependant material properties based on the Eurocodes [4],[5],[6].

Fig 4 shows the 3D structural model to simulate a fire on level 4, which heats the Level 5 floor and the megaframe levels between Levels 2 to 8. The unheated floors (Levels 3, 4, 6, 7 and 8) were assumed to behave as and modelled as rigid diaphragms because the in-plane stiffness of the unheated floors was considered to be significantly greater than the bending resistance of the columns. This was modelled using kinematic rigid links which tie all the columns to a central reference point, which represents the centre of gravity of the building.

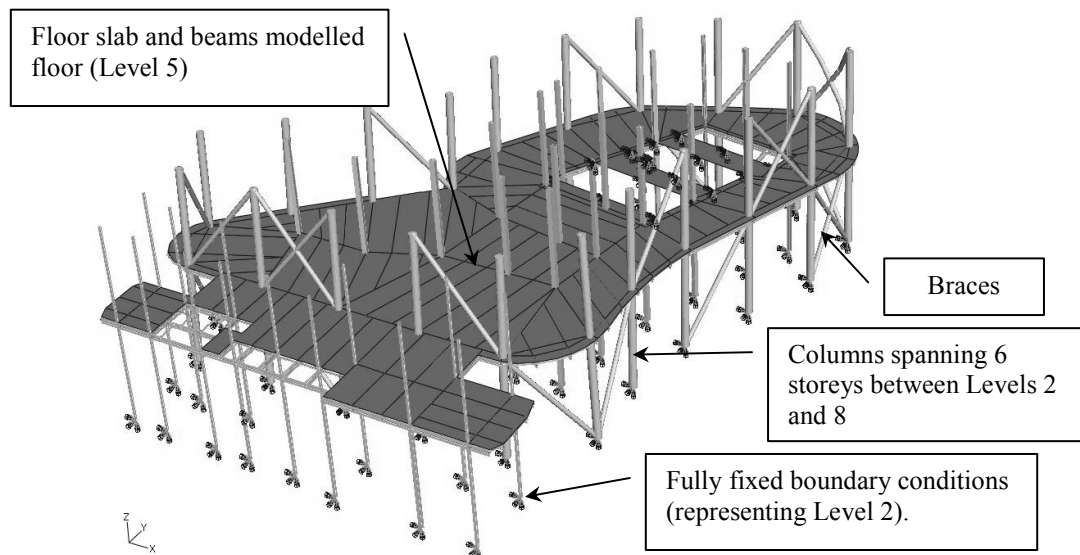


Fig 4: Level 5 global finite element model showing boundary conditions and mega-frame structure between floors 2 to 8. (The unheated floor diaphragms representing the unheated floors are not shown)

Many structural fire analyses in commercial applications involve buildings with regular beams and column layouts which can be analysed using simplified representative portions of

part of a floor to represent its overall response. Also, the lateral stability system usually consists of a reinforced concrete core which is assumed to be relatively unaffected by fire and as such the building is assumed to be laterally restrained. However, for The Pinnacle, the entire 2800m<sup>2</sup> floor plate had to be modelled because of the irregular floor shape, the irregular bracing and because the entire perimeter frame has to resist the lateral loads due to wind at the fire limit state. The assumption that the lateral stability system was not affected by fire could not be applied for this building.

In the model, all columns and bracing in the model were extended to the next megaframe level above and below the analysed floor to accurately simulate the column and bracing boundary conditions.

To minimise the loss of lettable area caused by intrusion of the braces into office spaces, the braces have to change direction where they touch the intermediate levels between megaframe levels. This is structurally less efficient and can cause significant forces to be passed into the intermediate floors. This had to be modelled and monitored in the structural fire analysis to ensure that the forces do not cause failure of the beams and floor slab.

The applied live, dead and wind loads were factored in accordance with BS 5950 Part 8 (2003) [7]. Lateral wind forces which apply the most significant loading onto the structure were included by applying the resultant forces on the columns and the braces.

Four node shell elements were used to model the slab. Two node linear beam elements (B31) were used for all beams, columns and braces. The reinforcing steel in the slab was modelled based on a smeared model, assuming a thin sheet of steel of equivalent area to the specified reinforcing bars.

The modelling of composite columns on a large global finite element model was challenging although there has been research into modelling the performance of concrete filled tubes [8]. Two different beam finite element sections were linked together to model the single concrete filled composite steel section. One of the beam sections had a circular hollow profile with steel properties to represent the steel tube while the other had a solid circular section with concrete properties. The concrete used for infill was C80 high strength concrete. The concrete was conservatively modelled as having uniform temperatures, with temperatures 20% higher than the steel tubes.

#### **4.1 Modelling of web penetrations and partial composite action in beams**

The primary and secondary beams are 625mm deep cellular beams and have circular web penetrations to allow mechanical and electrical services to be passed through. In the global structural models, the beams were modelled with the full web thickness of the beams and without web openings. The beam finite elements cannot model the web penetrations and any effects on the beam behaviour in fire due to these penetrations.

A separate analysis of a detailed subassembly of part of the structure using only shell finite elements was undertaken to assess and capture any fire related phenomena on the web penetrations, such as web-post buckling of the beams, and partial shear composite action between the slab and beam.

#### **4.2 Beam connections**

Typically, beam connections are modelled as either fully pinned or fully fixed, for simplicity. For The Pinnacle, the beam connection capacities were available from the structural engineers and they were specified with temperature dependent capacity limits (shear, axial and/or

moment), based on the Eurocode strength reduction curves [5]. This allows the transfer and redistribution of forces due to local connection weaknesses. The connectors can continue to deform once they reach their maximum capacity, but the limiting force (in tension, bending or shear) is not surpassed.

## 5 MODELLING RESULTS

To make the models run and cope numerically with the large number of variables and the highly complex nature of the structure in fire required creative application and integration of software and hardware. The analyses for Level 5 showed that global stability was maintained throughout the entire fire duration and there were no runaway deflections in the slab or beams (Fig 5). There was also no failure of the columns due to buckling. The largest mid-span deflections (beam 28) and the adjacent parallel protected secondary beam are shown in Fig 6. The floor system supported by unprotected beams performed well due to tensile membrane action. The unprotected beams did not suffer runaway failure because of catenary action while the protected beams were able to resist the loads by bending action. The detailed submodel of part of level 5 (Fig 7) showed that although the unprotected secondary beams suffered large lateral distortions, the protected primary beams with the 90 minute fire protection did not buckle and were relatively undeformed.

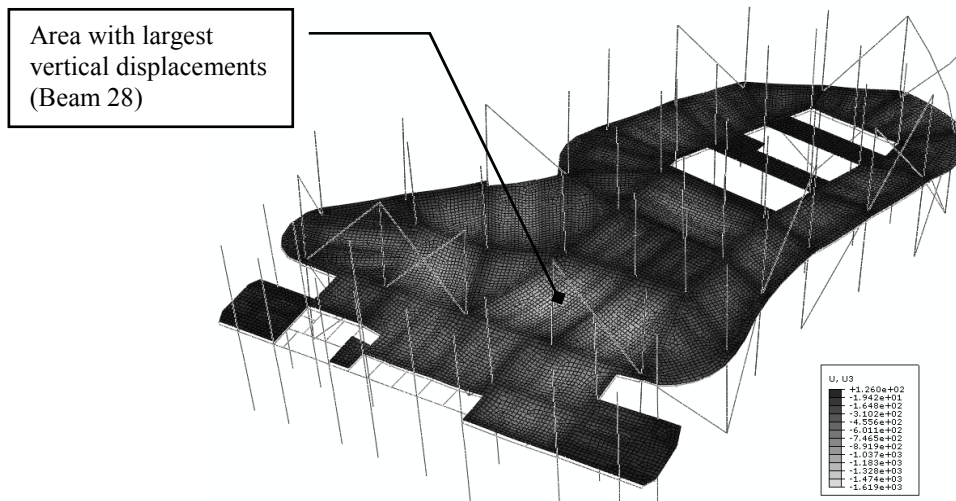


Fig 5: Vertical displacements at end of the analysis for Level 5.

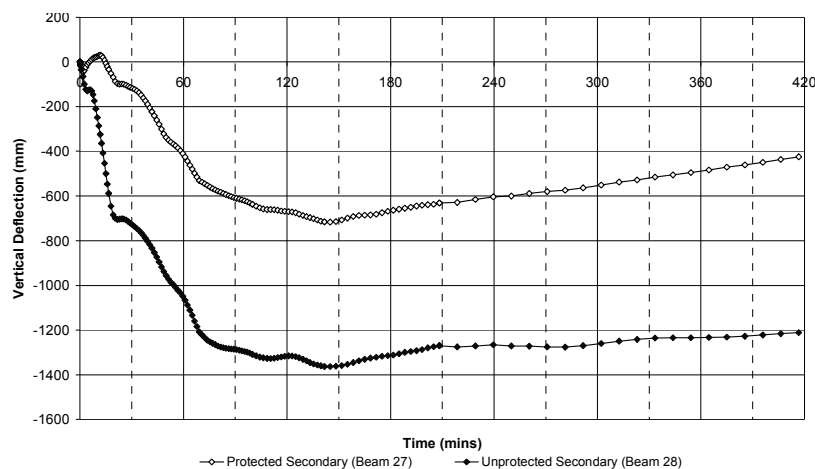
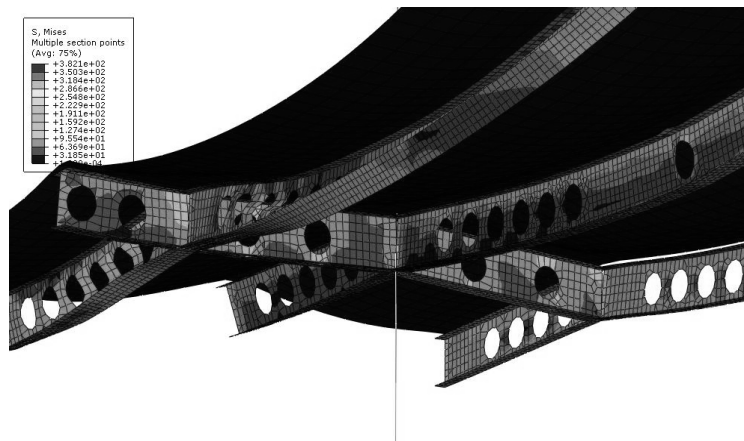


Fig 6: Mid-span deflections with time for selected worst-case beams.



*Fig 7: Submodel showing detailed deformation of beams on level 5.*

The bracing elements had a significant influence on the deformation and forces within the structure. The analyses showed that the expansion of the protected braces due to heating can impose significant axial forces on the columns. The heating of the braces in a non-uniform bracing arrangement can influence the deformation of the floor plate due to thermal expansion.

## 6 CONCLUSIONS

This paper describes the 3D structural fire analysis for a complex high rise structural system to check its robustness when exposed to a realistic fire. The analyses showed that the structure retained its stability throughout the entire duration of the design fire. The analysis showed that a engineered fire protection strategy incorporating a reduced fire rating and also removal of fire protection to the secondary beams could be safely applied. This project has also highlighted the need for more research into un-reinforced concrete filled hollow steel sections.

## 7 REFERENCES

- [1] Approved Document B Vol. 2, The Building Regulations 2000 Fire Safety. 2006 Edn.
- [2] British Standards Institution, "Eurocode 1 - actions on structures general actions - actions on structures exposed to fire", BS EN 1991-1.2:2002, 2002
- [3] Hibbett, Karlsson & Sorenson Inc., "ABAQUS v6.7.1 Manuals", ABAQUS Manual Set, 2007.
- [4] British Standards Institution, Eurocode 2 – "Design of concrete structures general rules - structural fire design", BS EN 1992-1.2:2004, 2004
- [5] British Standards Institution, "Eurocode 3 - design of steel structures general rules - structural fire design", BS EN 1993-1.2:2005 , 2005
- [6] British Standards Institution, "Eurocode 4 - design of composite steel and concrete structures general rules - structural fire design", BS EN 1994-1.2:2005 , 2005
- [7] British Standards Institution, "Structural use of steelwork in building code of practice for fire resistant design", BS 5950-8:2003 , 2003
- [8] Edwards M. The Performance in Fire of Fully Protected Utilised Concrete Filled SHS Columns with External Fire Protection Proceedings of the 9th International Symposium on Tubular Structures, Balkema, Rotterdam, Netherlands, 2000.
- [9] British Steel plc (now Corus). The Behaviour of Multi-Storey Steel Framed Buildings in Fire – A European Joint Research Programme. 1999.

## **SIMULATION AND STUDY OF NATURAL FIRE IN A WIDE-FRAMED MULTIPURPOSE HALL WITH STEEL ROOF TRUSS**

Dan Pada

Helsinki University of Technology, Faculty of Engineering and Architecture, Espoo, Finland

### **INTRODUCTION**

As a part of an extensive long-term plan for the development of the Helsinki Fair Centre a new 14500 m<sup>2</sup> multipurpose hall will be built in Helsinki, Finland. The design of the hall was carried out in co-operation between Finnish and German architects and it is intended to be able to host both exhibitions and indoor sporting events with up to 6000 spectators. In Figure 1, the new multipurpose hall can be seen to the left.

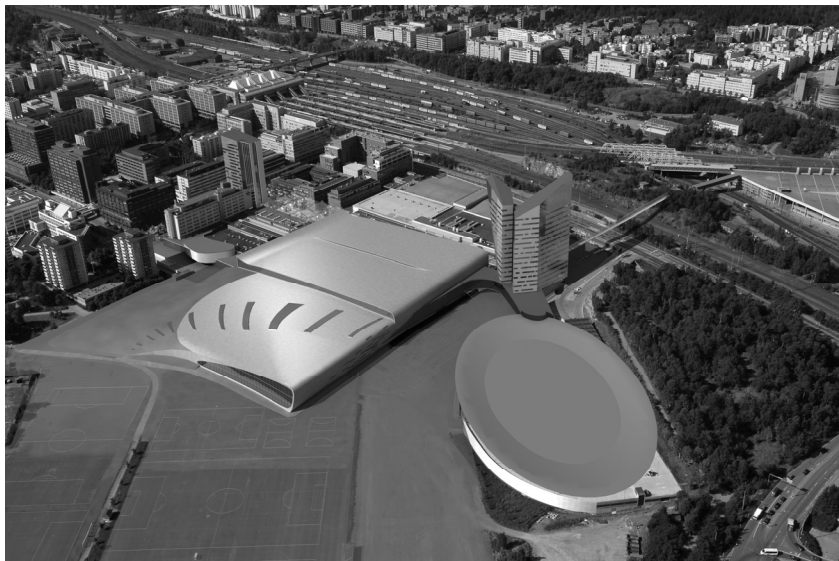


*Fig. 1.* Air photo of the architects' suggestion for the Helsinki Fair Centre

The Finnish Building Code allows the fire safety design of a building to be performed according to either the prescriptive regulations or the natural fire safety concept, NFSC. In this study the NFSC was used to do a performance-based structural fire safety design of the steel roof trusses in the above described multipurpose hall. This made it possible to estimate whether the roof trusses can be safe in the case of fire without passive fire protection, such as intumescent painting, or not.

### **1 STRUCTURE DESCRIPTION**

#### **1.1 General**

The main frame of the hall is made up of reinforced concrete columns and three dimensional steel roof trusses. See Figure 2 for a view of the frame. The frame spacing is 9,0 m, except in the middle of the hall where it is 13,05 m. The span of the roof trusses is 78 m with a splice in the middle of the span and the total number of trusses is 17. The free height inside the hall varies from 10 m to 16 m. The total length of the building is just over 170 m and the total width is about 88 m.

The height of the steel roof trusses varies between 4,5 m and 7 m, the bottom width of the truss is about 1,3 m and the top width is 3,0 m. The trusses are made up of structural steel hollow sections of varying dimensions with a steel quality of S355.

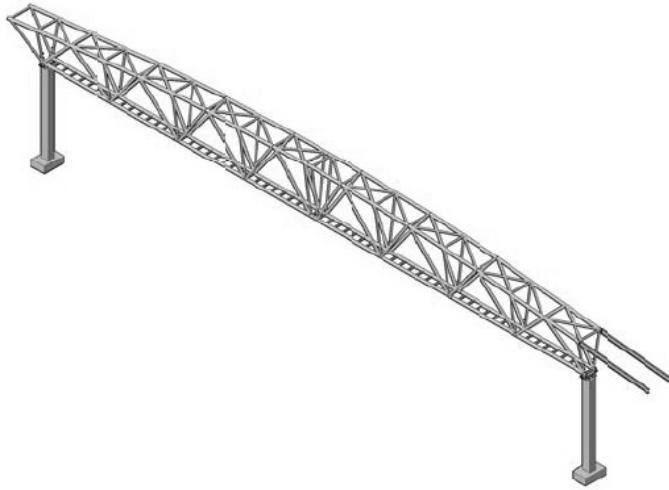


Fig. 2. Main frame

The roof structure will consist of wooden elements with mineral wool insulation supported by the roof trusses. A large part of the exterior walls will be made of glass, which is assumed to break when the temperature reaches 200 °C. The rest of the exterior walls will be made of steel sheets with mineral wool insulation and concrete sandwich structures.

The new hall will form one single fire compartment together with an existing hall at the Helsinki Fair Centre. Hence the total area of the fire compartment will be in the order of 33000 m<sup>2</sup>.

## 1.2 Fire resistance requirement

In this study focus was only on the first part of the essential requirement for the limitation of fire risks according to the Construction Products Directive 89/106/EEC, i.e. “The load bearing resistance of the construction can be assumed for a specified period of time” [1]. The required time period in this case study was 60 minutes.

## 2 DESIGN FIRES

Two prescribed design fires were used in this study. They were chosen from the project’s performance-based fire safety design report [2], where a rough risk analysis has been made and several different fires have been considered, and a report by Hietaniemi [3]. The choice of the design fires from these reports was based on the possible severity of their effect on the steel roof trusses.

### 2.1 Spectator stand fire

The spectator stand fire represents the case when the multipurpose hall is used for e.g. indoor sport events or concerts. As spectator stands can be placed also above floor level the design fire is closer to the roof than a fire on floor level, hence posing a larger threat to the load-carrying structure.

According to Hietaniemi [3] the maximum rate of heat release, RHR, of the seat material for a spectator stand fire can be assumed to be 2000 kW/m<sup>2</sup>, giving a maximum RHR of the spectator stand of 1500 kW/m<sup>2</sup>, while the total fire load being 510 MJ/m<sup>2</sup>. The studied spectator stand section measured 8,0 x 13,6 m<sup>2</sup> with a height of 3 m. It was placed 5,2 m above floor level in the lower part of the hall, leaving only about 2 m of free height to the bottom chord of the roof truss. The whole section was assumed to be on fire, giving a maximum RHR of 163,2 MW. In Figure 3 the RHR curve for the spectator stand design fire is presented.

## 2.2 Exhibition stand fire

The exhibition stand fire represents one of the main purposes of use where the fire load can be very high. Also this design fire was based on Hietaniemi's report [3], a 10 x 10 m<sup>2</sup> exhibition stand, made of burnable materials, for small motor vehicles, e.g. motorcycles or ATV's, placed on floor level in the lower part of the hall just below a roof truss. The maximum RHR of the design fire was 53 MW, the total fire load was 1720 MJ/m<sup>2</sup> and the height of the stand was assumed to be 2 m. The RHR curve for the exhibition stand fire can be seen in Figure 4.

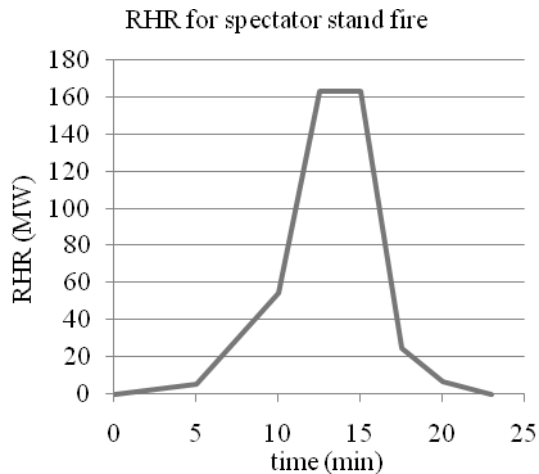


Fig. 3. RHR curve for spectator stand fire

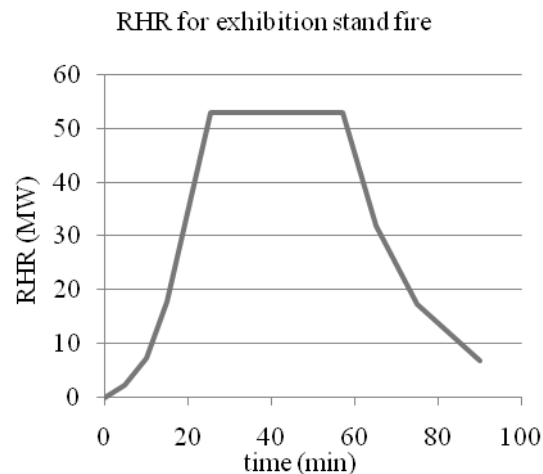


Fig. 4. RHR curve for exhibition stand fire

## 2.3 Sprinkler system fail

As the sprinkler system usually is considered to be one of the most effective and reliable active fire protection systems in a building, a total sprinkler system fail was not considered in this study. However, a partial sprinkler system fail, where two nozzles above the design fire were inoperative, was considered in both the design fires.

## 3 FDS MODEL CREATION

### 3.1 General

The design fires were simulated with Fire Dynamics Simulator, FDS, version 5.2 and the input files were made with Pyrosim. The whole multipurpose hall was modeled in Pyrosim with a cell size ranging from 0,2 x 0,2 x 0,2 m<sup>3</sup> to 0,8 x 0,8 x 0,8 m<sup>3</sup>, hence the total number of cells was kept at about 2 millions.

### 3.2 Sprinkler system

The model was equipped with an automatic sprinkler system that activated when the temperature of the nozzle reached 74 °C. The sprinklers' effect on the gas temperature and the combustion occurring in the gas phase was taken into account in the simulation. The sprinklers' suppressing effect on the design fire was however not taken into account in the two original simulations, as there was no way of determining how large the effect could be without carrying out real fire tests. In a second additional simulation of the spectator stand fire, the effect was however taken into account according to a method described in Hietaniemi's report [3]. According to this method the RHR is only allowed to double from the value it has when the sprinkler system is activated. As the model was so large, the time

when 20 nozzles had been activated in the original simulation, i.e. at approximately 7 minutes into the simulation, was used as the sprinkler activation point. At that point the RHR was about 28 MW and was hence allowed to grow to 56 MW.

### 3.3 Smoke exhaust system

The model was also equipped with a smoke exhaust system. The hall was divided into different smoke sections so that one section was about 2400 m<sup>2</sup>, assuming that that the system could be active only in two sections at the same time. The time at which the smoke exhaust system was activated in the spectator stand fire was assumed to be 400 s and in the exhibition stand fire 600 s. These times were approximated based on simulation tests of the sprinkler activation times, assuming that the smoke exhaust system would be activated roughly at the same time as the sprinklers.

### 3.4 Data measured

The most important data measured during the fire simulation, from the structural fire safety design's point of view, was the adiabatic surface temperature every 5 m of the bottom chord of the steel roof trusses situated above and near to the fire. The adiabatic surface temperature is the temperature that the bottom chord "sees" and is the quantity that is representative of the heat flux to the solid surface [4]. This temperature was used to calculate the temperature of the steel cross section.

The gas temperature of the building was also measured at several different heights and points to get a picture of the total temperature development in the building as a function of time.

## 4 SIMULATION OF FIRE

### 4.1 Spectator stand fire 1

The original spectator stand fire simulation was ended at 1400 s, as the fire only lasted 1380 s. The RHR reached a maximum value of 167 MW during the simulation, i.e. very close to the intended value of 163,2 MW. The first sprinkler nozzle activated a bit sooner than expected, already at 308 s, being one of the sprinklers above the fire. In total 251 out of the 310 functional sprinkler nozzles in the model were activated during the simulation.

The temperature inside the hall remained quite low in general, except of course over and near to the fire. Close to the roof the temperature reached about 65 °C, while it at 5 m above floor level remained just above 20 °C.

The measured adiabatic surface temperature of the bottom chord just above the fire is plotted in Figure 5 and this was also the measurement used to calculate the temperature of the steel.

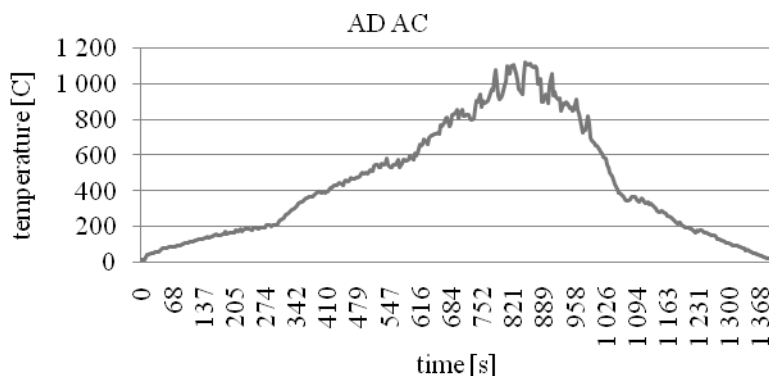


Fig. 5. Adiabatic surface temperature of the bottom chord above the spectator stand fire 1

## 4.2 Spectator stand fire 2

In the additional simulation of the spectator stand fire, where the sprinklers' suppressing effect on the design fire was taken into account, the RHR reached a maximum value of 56 MW.

As the sprinklers were removed from the model in order to speed up the simulation, the only measured data taken into consideration was the adiabatic surface temperature of the bottom chord just above the fire. This temperature is plotted in Figure 6.

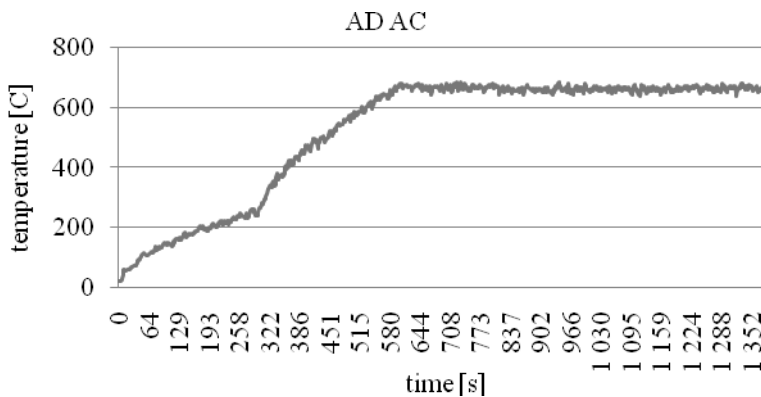


Fig. 6. Adiabatic surface temperature of the bottom chord above the spectator stand fire 2

## 4.3 Exhibition stand fire

The exhibition stand fire was ended at 3670 s, as there was no need to study the fire situation beyond one hour. The maximum RHR measured during the simulation was just over 53 MW, i.e. almost exactly the intended value. The first sprinkler nozzle activated a bit later than expected, at 668 s. In total only 148 out of the 310 functional sprinkler nozzles were activated.

The temperature close to the roof reached circa 60 °C while it at 5 m above the floor level only increased a few degrees above the original temperature of 20 °C, again except close to and over the fire.

The adiabatic surface temperature of the bottom chord above the fire is plotted in Figure 7.

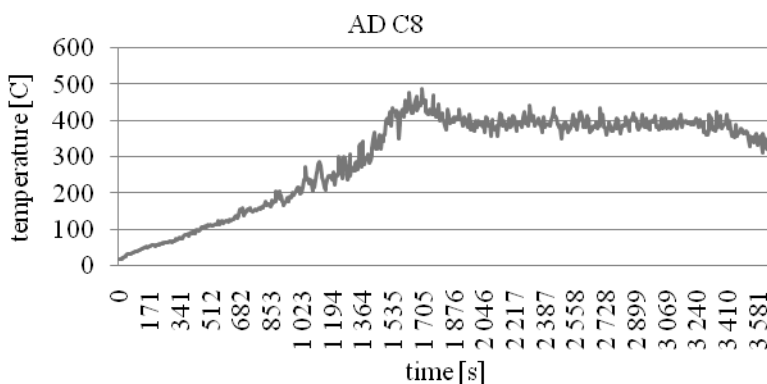


Fig. 7. Adiabatic surface temperature of the bottom chord above the exhibition stand fire

## 5 FIRE SAFETY DESIGN OF STEEL ROOF TRUSS

The temperature development of the unprotected steel members was calculated according to Eurocode 1 and 3 just above the fire. The temperature was assumed to be vertically equivalent.

### 5.1 Steel temperature

In the original spectator stand fire the maximum temperature of the bottom chord with a wall thickness of 10 mm was established to be 727 °C whereas it was 897 °C for the diagonals with a wall thickness of 5 mm.

In the additional simulation of the spectator stand fire the temperature of the bottom chord reached 614 °C whereas the diagonals reached a temperature of 661 °C.

In the case of the exhibition stand fire the maximum temperature of the bottom chord was 387 °C and of the diagonals 396 °C, i.e. almost the same temperature was reached in all steel sections, independent of wall thickness.

### 5.2 Structural analysis

A FEM-model of the roof truss was made in Robot Millennium 21. In the model the truss was subjected to snow load, self-weight of the roof structure, self-weight of equipment, such as lighting and ventilation ducts, hanged to the bottom chord of the truss and of course the self-weight of the truss itself. The temperature of the truss was assumed to be uniform in order to simplify the calculations and to avoid having to take the effect of heat conduction inside the roof truss into consideration. The effective yield strength and the modulus of elasticity of the steel were changed to correspond to the values at the different elevated temperatures.

With the help of the FEM-model the critical temperature of the roof truss could be established to be 590 °C. At this temperature the highest degree of utilization was 0,94 and took place in the diagonals in compression closest to the ends of the truss. The deflection was established to be 400 mm in the middle of the truss, without taking the pre-camber of 100 mm into consideration. Hence the actual deflection would be in the order of 300 mm, which equals the length of the truss, 78 m, divided by 260.

## 6 CONCLUSIONS

By comparing the temperature of the steel reached in the different design fires to the critical temperature of the truss, it could be established that the truss well could withstand the exhibition stand fire without any fire protection. However, in the case of the spectator stand fire the temperature proved to be too high for the unprotected truss to endure the fire, even though the temperature did not rise that much above the critical temperature when taking the sprinklers' suppressing effect on the fire into account.

## REFERENCES

- [1] European Committee for Standardization. SFS-EN 1991-1-2 Eurocode 1: Actions on structures. Part 1-2: General Actions. Actions on structures exposed to fire. Finland: Finnish Standards Association, 2003
- [2] Hämäläinen, S. Toiminnallisen palosuunnittelun määrittely ja käytettävät lähtöarvot, Suomen messut / Näyttelyhallin laajennus. Helsinki, Finland, 12.06.2008
- [3] Hietaniemi, J. Palon voimakkuuden kuvaaminen toiminnallisessa paloteknisessä suunnittelussa. Finland: VTT, 2007
- [4] McGrattan K. et al. NIST Special Publication 1019-5, Fire Dynamics Simulator (Version 5) User's Guide. Washington, USA: U.S. Government Printing Office, 2007

## **AN INNOVATIVE APPROACH TO DESIGN FIRES FOR STRUCTURAL ANALYSIS OF NON-CONVENTIONAL BUILDINGS**

### **A Case Study**

Jamie Stern-Gottfried<sup>a,b</sup>, Guillermo Rein<sup>a</sup>, Barbara Lane<sup>b</sup>, Jose L. Torrero<sup>a</sup>

<sup>a</sup> BRE Centre for Fire Safety Engineering, The University of Edinburgh, Edinburgh, UK

<sup>b</sup> Arup Fire, London, UK

## **INTRODUCTION**

Structural fire safety analysis is a fast developing discipline within the overall fire safety community. There is substantial research being done in the mechanical response of buildings to thermal loadings. The results of this research are being applied commercially in the design of real buildings in numerous countries globally.

While a great deal of effort is being placed in the analysis of structures, there is a dearth of research on determining appropriate thermal inputs for such a structural analysis. Much of the structural fire safety work being carried out is based on one of two traditional methods of determining the fire environment; the standard temperature-time curve (which has its origins in the late 19th century [1]) or parametric temperature-time curves such as that specified in Eurocode 1 [2].

While both of these methods have great merits and represented breakthroughs in the discipline at their times of adoption, they have inherent limitations with regards to their range of applicability [3]. For example, Eurocode 1 states that the design equations are only valid for compartments with floor areas up to 500 m<sup>2</sup> and heights up to 4 m, the enclosure must have no openings through the ceiling, and the compartment linings are also restricted to a thermal inertia between 1000 and 2200 J/m<sup>2</sup>s<sup>1/2</sup>K, which means that highly conductive linings such as glass facades and highly insulated materials can not be taken into account. As a result, common features in modern construction like large enclosures, high ceilings, atria, large open spaces, multiple floors connected by voids, and glass façades are excluded from the range of applicability of the current methodologies. These limitations, which are largely associated with the physical size and geometric features of the experimental compartments on which the methods are based, ought to be carefully considered when the methods are applied to an engineering design. This is particularly relevant given the large floor plates and complicated architecture of modern buildings.

Another limitation of the existing methods is that they assume only uniform temperature conditions throughout the whole floor of the compartment. A fire that would cause these types of conditions burns uniformly within the enclosure and generates high temperatures for a relatively short duration. This is opposed to a travelling fire that burns locally but spreads through the enclosure with time, generating lower temperatures for longer times. Buchanan [4] notes that post-flashover fires in open plan offices are unlikely to burn throughout the whole space at once. Real, large fires that have lead to structural failure, such as those in the World Trade Center towers 1, 2 [5] and 7 [6] in September 2001, the Windsor Tower in Madrid, Spain in February 2005 [7] and the Faculty of Architecture building at TU Delft in the Netherlands in May 2008 [8] were all observed to travel across floor plates, and vertically between floors, rather than burn uniformly for their duration. Travelling fires have also been

observed experimentally in compartments with non-uniform ventilation [9, 10]. Clifton [11] has developed a methodology to examine a spreading fire within a floor plate, but there is a lack of experimental data to validate this approach [4].

Therefore a methodology is being developed that allows for a wide range of possible fires, including both uniform burning and travelling fires, by considering the fire dynamics within a given building [3]. This new methodology also facilitates the collaboration between fire safety engineers and structural fire engineers, which is an identified need within the structural fire community [12], to jointly determine the most challenging fire scenarios for a structure.

This paper presents a case study of the application of this new methodology to a large, non-conventional structure.

## 1 NEW METHODOLOGY

The key aspect of the new methodology being developed is to characterise the thermal environment for structural analysis accounting for the fire dynamics specific to the building, including a wide range of possible fires. In order to achieve this a tool to capture the spatial and temporal changes of the fire-induced thermal field is selected. This tool is then applied to a particular floor of the building accounting for a family of fires that range between one that burns in a small area and travels across the floor plate for a long duration and one that is well distributed across the whole floor plate but burns for a short duration.

### 1.1 Temperature Field

The methodology divides the effect of a fire on structural elements into the near field and the far field [3]. The near field is when a structural element is exposed directly to the flames of the fire and the far field is when it is exposed to the hot gases, i.e. the smoke layer, away from the flames, as shown in *Fig. 1*. This division of the thermal field allows the methodology to overcome a well-known inaccuracy of fire modelling; calculation of the flame temperature.

A ceiling jet correlation, as developed by Alpert [13] and given below in *Eq. (1)*, was selected for this case study to determine the temperature field as a function of distance from the fire. The use of such a correlation is deemed appropriate if the floor area is large and the smoke layer is thin relative to the floor to ceiling height.

$$T_{\max} - T_{\infty} = \frac{5.38(\dot{Q}/r)^{2/3}}{H} \quad (1)$$

where  $T_{\max}$  is the maximum ceiling jet temperature (K)  
 $T_{\infty}$  is the ambient temperature (K)  
 $\dot{Q}$  is the total heat release rate (kW)  
 $r$  is the distance from the centre of the fire (m)  
 $H$  is the floor to ceiling height (m)

Note that while Alpert gives a piecewise equation for maximum ceiling jet temperatures to describe the near field ( $r/H \leq 0.18$ ) and far field ( $r/H > 0.18$ ) temperatures, only the far field equation is utilised in the present case study as the near field temperature is assumed to be the flame temperature, as described in Section 1.3.

The ceiling jet correlation characterises the spatial variation of the temperature field in only a one dimensional manner, as it has been assumed that the fire area always extends between the

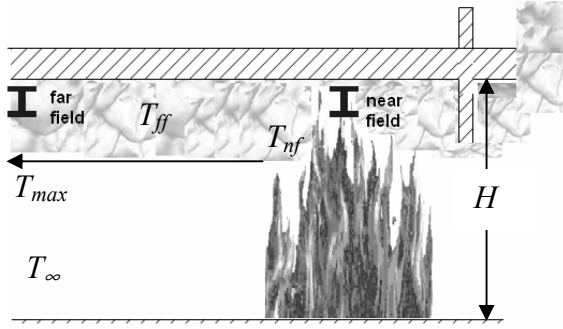


Fig. 1. Illustration of near and far fields

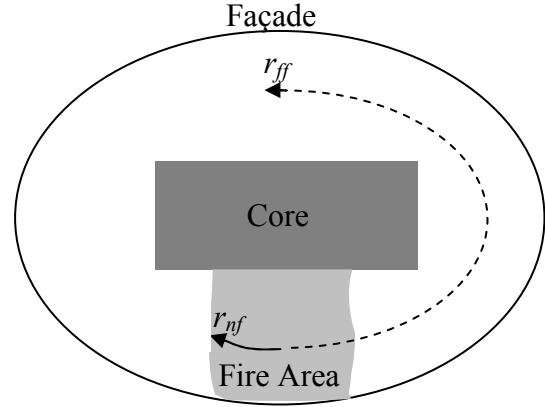


Fig. 2. Plan view of a possible fire path

core and façade of the building (see Fig. 2). The correlation was chosen to provide a straightforward description of the temperature field that is qualitatively sufficient to progress the development of the methodology. It is noted that alternative methods of characterising the temperature field, including computational fluid dynamics, can be utilised instead [3].

## 1.2 Family of Fires

A family, or set, of fires that covers the range of possible fires, both travelling and uniformly burning, needs to be selected as an input for the temperature field. To do this it was assumed that each fire in the family would burn over a surface,  $A_b$ , which is a percentage of the total floor area,  $A_t$ , of the building, ranging from 1% to 100%. The burning area of the fire that is equal to 100% of the floor area is a well distributed fire. All other burning areas represent travelling fires of different sizes.

It is assumed that there is a uniform fuel load across the fire path and the fire will burn at a constant heat release per unit area typical of the building load under study. Thus the burning time can be calculated by Eq. (2).

$$t_b = \frac{q_f}{\dot{Q}''} \quad (2)$$

where  $t_b$  is the burning time (s)  
 $q_f$  is the fuel load density (MJ/m<sup>2</sup>)  
 $\dot{Q}''$  is the heat release rate per unit area (MW/m<sup>2</sup>)

Note that the burning time is independent of the burning area [3]. Thus the 100% burning area and the 1% burning area will both consume all of the fuel in the same time  $t_b$ . However, a travelling fire moves from one burning area to the next so that the total burning duration,  $t_{total}$ , across the floor plate is extended. This time is given in Eq. (3).

$$t_{total} = \frac{t_b}{A_b/A_t} \quad (3)$$

This means that there is a longer total burning duration for smaller burning areas.

## 1.3 Near Field vs. Far Field

In the case of the 100% burning area, all of the structure will experience near field (flame) conditions for the total burning duration (which is equal to the burning time,  $t_b$ ). However, for

the travelling fire cases, any one structural element will feel far field (non-flame) conditions for the majority of the total burning duration and near field (flame) conditions for the burning time as the fire burns locally to the element. The time one element experiences far field conditions prior to the arrival of the flame is defined as  $t_{pre}$  and the time the element experiences far field conditions after the departure of the flame is defined as  $t_{post}$ . Fig. 1 illustrates the difference between the near field and far field.

The near field temperature,  $T_{nf}$ , is taken here as the flame temperature, which for the accuracy levels required in structural fire analysis, is more or less constant and approximately 1200°C to 1300°C for a typical office fire [14]. The far field conditions vary as a function of distance away from the fire. However, it is desirable to express the results in simple terms but without loss of generality in order to be of valuable engineering use. Thus, the far field is reduced to a single characteristic temperature,  $T_{ff}$ , which keeps the amount of information passed to the structural analysis manageable. To do this, the far field temperature is taken as the fourth-power average of  $T_{max}$  (to favour high temperatures in a bias towards radiation heat transfer and worst case conditions) over the distance between the end of the near field,  $r_{nf}$ , and the end of the far field,  $r_{ff}$ . This average is calculated by Eq. (4).

$$T_{ff} = \frac{\left[ \int_{r_{nf}}^{r_{ff}} (T_{max})^4 dr \right]^{1/4}}{(r_{ff} - r_{nf})^{1/4}} \quad (4)$$

Once the far field temperature is determined for a given fire size, the temperature time history of a point can be described, as shown in Fig. 3. Determining both  $t_{pre}$  and  $t_{post}$  is dependant on the path of the fire and the exact position being examined. However, it is not possible to establish a fire's path of travel *a priori* to a real incident; therefore assumptions must be made for worst case conditions. For the present case study, it is assumed that the fire will travel in a ring around the building core in one direction only, as illustrated in Fig. 2. Clearly other paths of fire travel are possible and the sensitivity of this parameter on the structural response will need to be explored as the methodology is further developed.

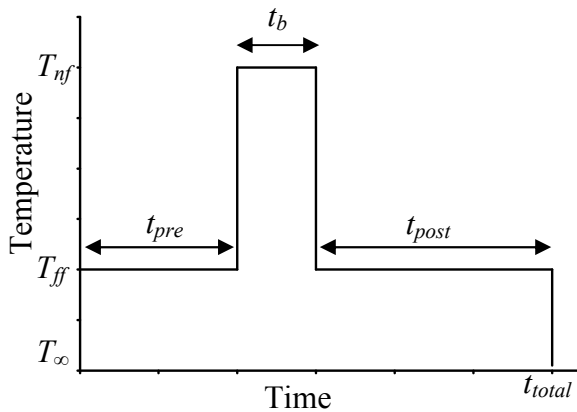


Fig. 3. Temperature-time curve at a general location of the ceiling for a travelling fire



Fig. 4. Mumbai C70 by James Law Cybertecture

## 2 THE CASE STUDY

### 2.1 The Building

The above methodology was applied to a real building, currently being designed. The building, Mumbai C70 by James Law Cybertecture shown in *Fig. 4*, is a large, modern, architecturally complex building in which a traditional temperature-time curve (standard or parametric) does not fully describe the range of possible fire dynamics.

The building has 13 storeys and is approximately 60 m tall. The building has an external diagrid megaframe consisting of hollow structural steel members, designed to carry wind loads and a proportion of the gravity load. The building is also provided with an internal reinforced concrete core system designed to carry gravity load. A hat truss is proposed at the top of the building. *Fig. 2* shows a generic plan view of a single floor. The exact shape and area of each floor varies. Most floors have an area over 2000 m<sup>2</sup> and much of the external façade is glazed, thus this building lies outside the range of applicability of the traditional design methods.

The 9<sup>th</sup> floor was selected by the structural fire engineers on the project as the most onerous floor from a structural perspective, as this floor has the longest beam spans as well as slender diagrid members compared to those found lower in the building. This is where a severe fire is most challenging for the structure and therefore the first location to be studied. It is anticipated that as the methodology becomes more mature, the assessment of the most onerous floor, or floors, will also be made from a fire perspective and the assessment done on both the most onerous fire floor (worst case fire) and most onerous structural floor (worst case structural floor).

### 2.2 Input Parameters

The specific dimensions of the 9<sup>th</sup> floor of the Mumbai C70 building have been applied to the methodology presented. The total floor area,  $A_f$ , is 2846 m<sup>2</sup> and the floor to ceiling height,  $H$ , is 3 m.

The fuel load density,  $q_f$ , is taken as 570 MJ/m<sup>2</sup>, as per the 80<sup>th</sup> percentile design value [15] for office buildings. The heat release rate per unit area,  $\dot{Q}''$ , is taken as 500 kW/m<sup>2</sup> which is deemed to be a typical value for densely furnished spaces, as design guidance [16] gives this value for retail spaces. Based on these two values, the characteristic burning time,  $t_b$ , is calculated by *Eq. (2)* to be 19 minutes.

## 3 RESULTS

Applying this methodology to a family of fires results in a range of far field temperatures and total burning durations, as shown in *Table 1*. These results illustrate the concept that hotter far field temperatures will occur for larger fires, but for shorter durations.

The far field temperatures are plotted in *Fig. 5* along with the temperature-time curves of traditional design methods. The growth and decay phases of the gas temperatures for the curves from this methodology are assumed to be very fast [3]. This is because the larger an enclosure is, the lower the importance of the thermal inertial of its linings are, thus the faster the growth and decay phases will be, i.e. the transport of the hot gases in the smoke layer is faster than the heat transfer to the surfaces. Note that the cooling is not neglected in the structural analysis, only the decay phase is eliminated from the fire environment.

| Percentage of Floor Area | Burning Area $A_b$ (m <sup>2</sup> ) | Total Heat Release Rate $\dot{Q}$ (MW) | Total Burning Duration $t_b$ (min) | Far Field Temperature $T_{ff}$ (°C) |
|--------------------------|--------------------------------------|--|------------------------------------|-------------------------------------|
| 1%                       | 28                                   | 14                                     | 1900                               | 156                                 |
| 2.5%                     | 71                                   | 36                                     | 760                                | 258                                 |
| 5%                       | 142                                  | 71                                     | 380                                | 376                                 |
| 10%                      | 285                                  | 142                                    | 190                                | 543                                 |
| 25%                      | 711                                  | 356                                    | 76                                 | 803                                 |
| 50%                      | 1423                                 | 711                                    | 38                                 | 1118                                |
| 100%                     | 2846                                 | 1423                                   | 19                                 | 1200 (near field only)              |

Table 1. Results for the family of travelling fires

The standard temperature-time curve extends to a region of temperatures and burning times that for the present building cannot be explained in terms of the possible fire dynamics. Two Eurocode 1 Parametric temperature-time curves are given to represent different amounts of assumed glass breakage; 25% glass breakage to produce a longer, relatively cool fire and 100% glass breakage to produce a shorter, relatively hot fire. Note that Fig. 5 provides the far field values that need to be combined with the near field to produce curves of the type shown in Fig. 3. Every point on the floor plate will at some point experience the near field temperature for the burning time (19 minutes) and the far field temperature for the rest of the total burning duration, as illustrated in Fig. 1.

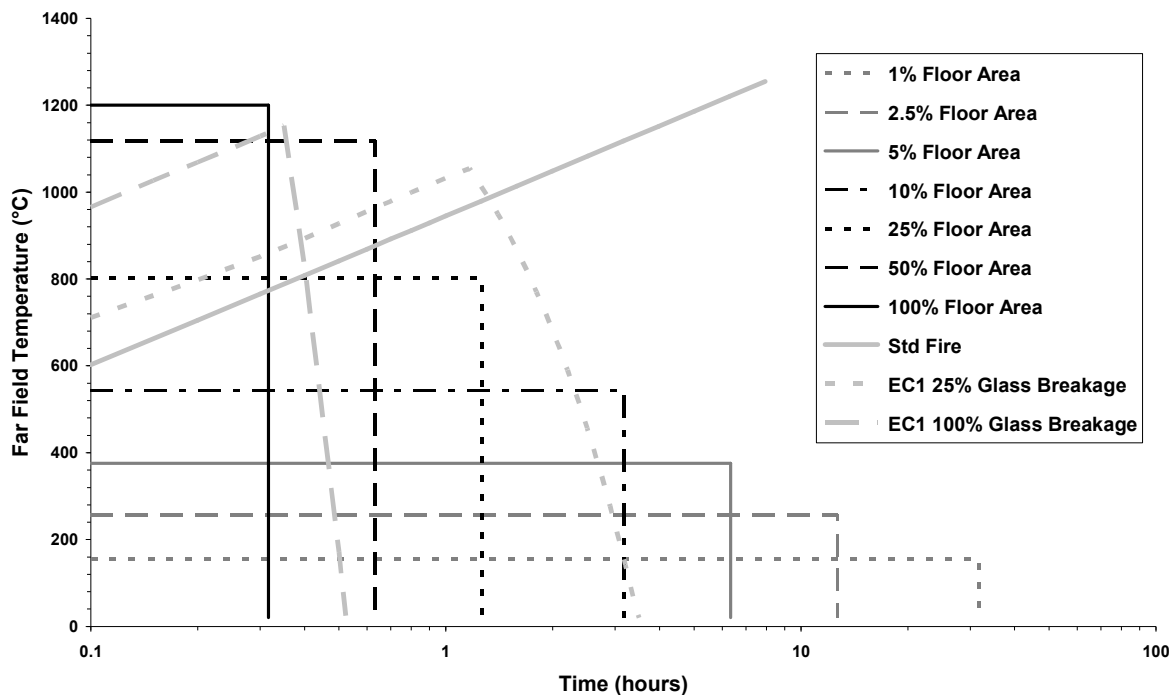


Fig. 5. Far Field Temperatures for the Family of Fires and Nominal Design Methods

The next step of this methodology is to apply these curves to a structural fire model. The fire engineer and structural engineer should work together to identify which curves are the most challenging to the structure. It is anticipated that the smaller area fires (1% through 5% of the floor area) would be less challenging, while the larger area fires (10% and above) would be more challenging, especially the cases with longer total burning durations.

## 4 CONCLUSIONS

This work develops a novel methodology to determine design fires for structural fire analysis of modern buildings that are outside the range of applicability of traditional methods. It has been applied to determine a family of fires for a floor in the Mumbai C70 building. The family of fires was generated by considering different burning areas that travelled on the floor plate. The methodology calculated both the near and far field temperatures to characterise the thermal environment for structural analysis. Future work will develop the tool used to determine the temperature fields, examine the effect of the path of fire travel, as well as determine the impact of this family of fires on the structure.

## 5 ACKNOWLEDGMENTS

The authors acknowledge the contributions of Allan Jowsey, Linus Lim and Pascal Steenbakkens of Arup Fire and Charlotte Röben, Frank Gusto and Colin Kupris of the University of Edinburgh.

## REFERENCES

- [1] Babrauskas, V. and Williamson R.B., "The historical basis of fire resistance testing – Part II." *Fire Technology*, 14(4), pp. 304-316, 1978.
- [2] Eurocode 1: Actions on structures – Part 1-2: General actions – Actions on structures exposed to fire, European standard EN 1991-1-2, 2002. CEN, Brussels.
- [3] Rein, G. et al, "Multi-story Fire Analysis for High-Rise Buildings," Proceedings of the 11th International Interflam Conference, London, Sept. 2007.
- [4] Buchanan, A., *Structural Design for Fire Safety*, John Wiley & Sons, 2001
- [5] Gann, R.G. et al, *Reconstruction of the Fires in the World Trade Center Towers*, NIST NCSTAR 1-5, September 2005.
- [6] McAllister, T.P. et al, *Structural Fire Response and Probably Collapse Sequence of the World Trade Center Building 7*, NIST NCSTAR 1-9, November 2008.
- [7] Fletcher, I. et al, "Model-Based Analysis of a Concrete Building Subjected to Fire," Advanced Research Workshop on Fire Computer Modelling, Santander, Spain, October 2007.
- [8] Zannoni, M. et al, *Brand bij Bouwkunde*, COT Instituut voor Veiligheids – en Crisismanagement, December 2008.
- [9] Thomas, I.R. and Bennets, I.D., "Fires in Enclosures with Single Ventilation Openings – Comparison of Long and Wide Enclosures," The 6<sup>th</sup> International Symposium on Fire Safety Science, Poitiers, France, 1999.
- [10] Kirby, B.R. et al, *Natural Fires in Large Scale Compartments*, British Steel, 1994
- [11] Clifton, G.C., *Fire Models for Large Firecells*, HERA Report R4-83, 1996.
- [12] Buchanan, A., "The Challenges of Predicting Structural Performance in Fires." The 9<sup>th</sup> International Symposium on Fire Safety Science, Karlsruhe, Germany 2008 (in press).
- [13] Alpert, R.L., "Calculation of Response Time of Ceiling-Mounted Fire Detectors," *Fire Technology*, Vol. 8, pp. 181–195, 1972.
- [14] Drysdale, D., *An Introduction to Fire Dynamics*, 2nd Edition, John Wiley & Sons, 1999.
- [15] PD 6688-1-2:2007, *Background Paper to the UK National Annex to BS EN 1991-1-2*.
- [16] TM19, *Relationships for Smoke Control*, CIBSE, 1995

## EVALUATION OF THE FIRE RESISTANCE OF A SPORT HALL USING STRUCTURAL FIRE ENGINEERING

Paulo Vila Real <sup>a</sup>, Nuno Lopes <sup>a</sup>

<sup>a</sup> University of Aveiro, LABEST-Department of Civil Engineering, Aveiro, Portugal

### INTRODUCTION

It is the purpose of this paper to present a study on the needs of passive fire protection in the steel roof structure of the Oporto Football Club (FCP) sport hall, to fulfil a fire resistance of 60.

Due to the large dimension of the sport hall a prescriptive approach using the standard fire curve ISO 834 revealed to be too severe, quite unrealistic and uneconomical. Indeed the fire load of this type of construction is generally rather small being not possible to reach the high temperatures of the ISO curve. On the other hand a large amount of air is available, which is a second factor for reducing the temperatures in a real fire [1]. The results obtained with the ISO fire curve were compared with the ones obtained using the natural fire, in accordance with the advanced calculation methods included in the recently approved part 1-2 of EC1 [2]. The program Ozone V2.2 [3,4] was used to simulate the natural fire, and the thermo-mechanic behaviour of the structure was modelled by the finite elements program SAFIR [5].



Fig. 1. FCP sport hall plant



Fig. 2. FCP sport hall

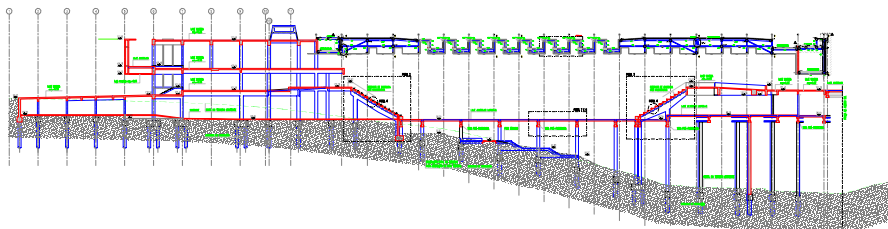


Fig. 3. Inside draw of the FCP sport hall

### 1 FIRE SCENARIOS

From the point of view of the characterization and prediction of the fire development, it was studied an equivalent compartment to the pitch zone and the main entrance, with the same air

volume, being considered localized fire and fire in whole pitch zone, in a total of seven fire scenarios.

Although Eurocode 1 allows for the consideration of the beneficial effect provided by active safety measures against fires, in this study these measures were not considered, according the Portuguese National Annex.

In the natural fires studied was considered a value for the maximum Rate of Heat Release (RHR) of  $250\text{kW/m}^2$ , a fire load density of  $200\text{MJ/m}^2$  and a medium fire grow rate ( $t_\alpha = 300\text{ s}$ ) or a fast fire grow rate ( $t_\alpha = 150\text{ s}$ ) depending on the situation [1].

### 1.1 Fires in the entire pitch

The pitch has an area of  $26.2 \times 48 = 1257.6\text{m}^2$  (being equal to the fire area). The height of the compartment is  $13.5\text{m}$ . The area of openings is  $97.4\text{m}^2$  located at a height of  $6.6\text{m}$ . The maximum fire area was  $2262.5\text{m}^2$ .

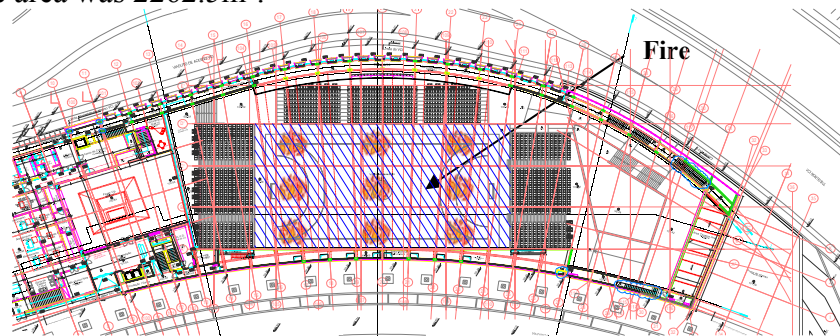


Fig. 4. Fire in the entire pitch

The first three scenarios are related to the existence of fire in the entire pitch.

*Scenario 0* - standard fire ISO834.

*Scenario 1* - natural fire with a linear openings variation from 10% at  $20^\circ\text{C}$  until 50% at temperature of  $400^\circ\text{C}$  and after until 100% openings at  $500^\circ\text{C}$  and a medium fire grow rate.

*Scenario 2* - natural fire with constant opening area during the fire. Several constant percentage of openings were tested (from 10% until 100%), resulting on the use of the most severe case (60% openings) and a medium fire grow rate.

The graphics in figures 5 and 6 show the temperature evolution in the compartment for the two last fire scenarios, obtained with the program Ozone [3, 4].

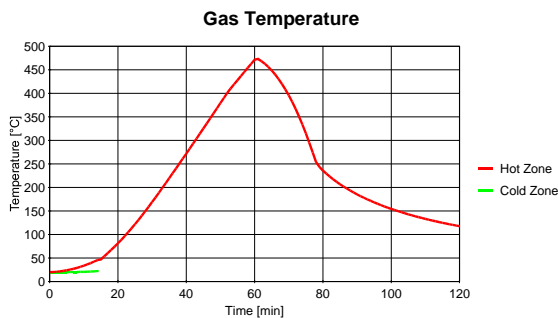


Fig. 5. Temperature in scenario 1

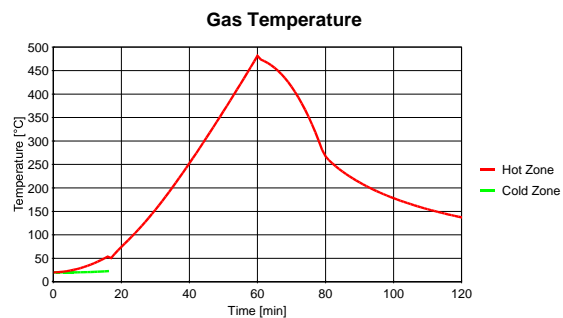


Fig. 6. Temperature in scenario 2

### 1.2 Localized fire in the pitch

*Scenario 3* - The fire area was  $9\text{m}^2$ , corresponding to a diameter of  $3.4\text{m}$  [4], at the pitch level (Figure 7). The opening variation was equal to the one on scenario 1, however due to the large

amount of oxygen it was found that the fire is controlled by the fire load not depending on the openings. Again, the maximum fire area was  $2262.5\text{m}^2$  and a medium fire grow rate.

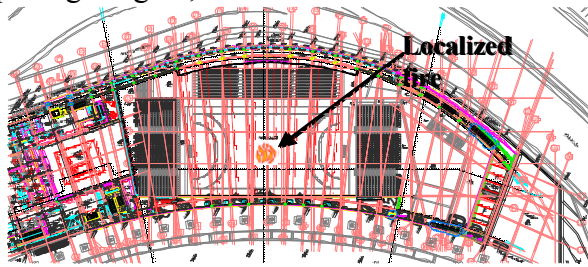


Fig. 7. Localized fire in the pitch

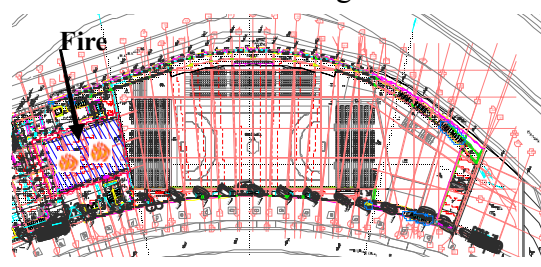


Fig. 8. Fire in the vip foyer

Figure 9 show the average temperature evolution in the compartment for this fire scenario.

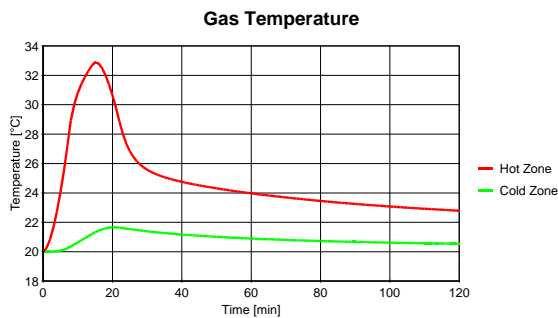


Fig. 9. Temperature in scenario 3

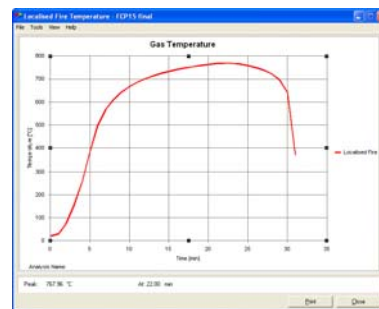


Fig. 10. Temperature in scenario 4

In this case the fire remained localized, and the flame did not impact the ceiling. With the Heskestad model [2, 6] it was possible to determine the maximum temperature at the covering with the value of  $60^{\circ}\text{C}$ , slightly higher than the one obtained in OZone V2.2 for the average temperature in the compartment (see Figure 9).

### 1.3 Localized fire in the Media balcony

*Scenario 4* - The fire area was  $36\text{m}^2$ , corresponding to a diameter of  $6.8\text{m}$  [4], at media balcony (10.2m from the pitch level). The opening variation was the same used on scenario 1, however due to the large amount of oxygen it was found that the fire is controlled by the fire load not depending on the openings. The maximum fire area was  $2262.5\text{m}^2$  and a fast fire grow rate.

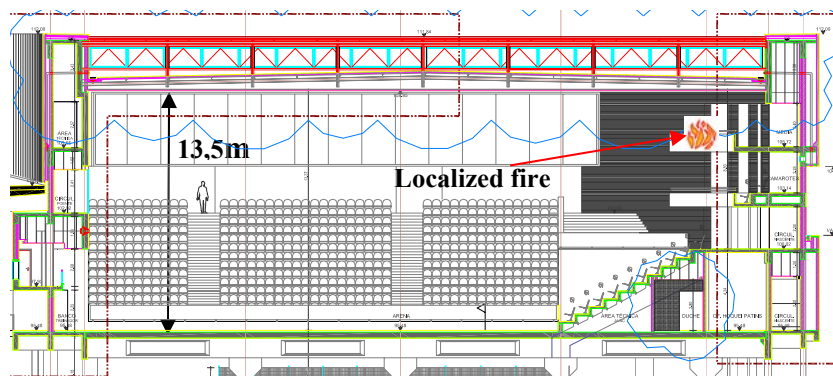


Fig. 11. Localized fire in the media balcony

In this case the fire remained localized, and the flame was impacting the ceiling. With the Hasemi model [2] and a RHR of  $500\text{kW}/\text{m}^2$  it was possible to determine the maximum

temperature at the lower cord level (767.96 °C), which was significantly higher than the average temperature obtained with OZone V2.2. Figure 10 show the temperature evolution in the compartment for this localized fire.

#### 1.4 Fires in the vip foyer

The vip foyer has an area of  $22 \times 15 = 330 \text{m}^2$  (being equal to the fire area and to maximum fire area). The height of the compartment is 3.0m. The openings area is  $45 \text{m}^2$ , corresponded to the façade turned into the pitch (see Figure 8).

Two scenarios were considered:

*Scenario 5* - natural fire with a linear openings variation from 10% at 20°C until 50% at temperature of 400°C and after until 100% openings at 500°C.

*Scenario 6* - natural fire with constant opening area during the fire. Several constant percentage of openings were tested (from 10% until 100%), resulting on the use of the most severe case (100% openings)

The graphics in figures 12 and 13 show the temperature evolution in the compartment for this two fire scenarios where a medium fire grow rate was considered.

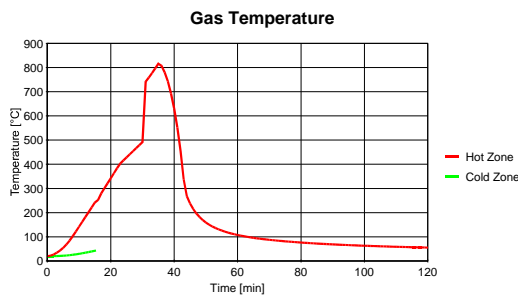


Fig. 12. Temperature in scenario 5

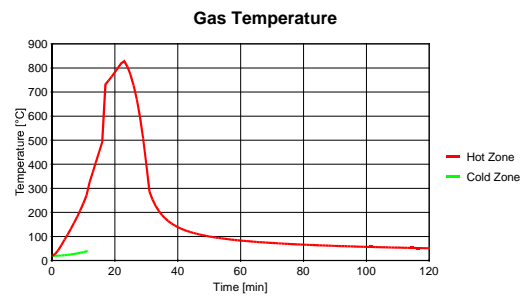


Fig. 13. Temperature in scenario 6

## 2 MECHANICAL ANALYSIS

In the safety evaluation of the steel structure were used: simplified methods prescribed in part 1.2 of EC3 [7] and implemented in the software Elefir-EN [8] (developed at Universities of Aveiro and Liege); and advanced calculation model using the software SAFIR [3] (developed at University of Liège).

The structural system analysed was a truss in steel S275, with a span with 36m length. It was chosen to evaluate only the truss subjected to the most severe conditions. The profiles used in the truss were: HEA 120, HEA 140, HEA 160, HEA 240, HEA 260, HEA 280 and HEB 240.

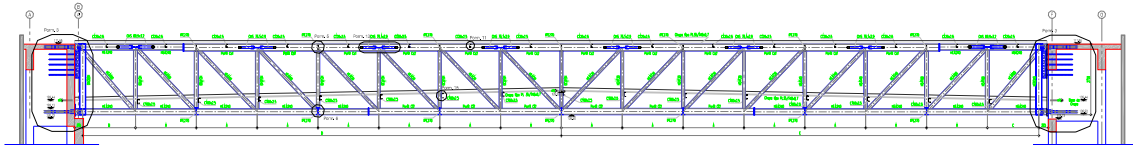


Fig. 14. Truss subjected to the most severe conditions

### 2.1 Mechanical actions

EN 1990 [9] defines fire as an accidental situation and according to the Portuguese National Annex the following load combination was used:

$$\sum G_k + \psi_{1,1} \cdot Q_{k,1} + \sum \psi_{2,i} \cdot Q_{k,i} + \sum A_d \quad (1)$$

According to the Annex A1 of EN1990 the combination factors  $\psi_1$  and  $\psi_2$  take the value of 0.0 for variable imposed loads on roofs and the accidental combination of actions results in

$$1.0G_k + \psi_{1,1}Q_{k,1} = 1.0G_k + 0.0Q_{k,1} = G_k \quad (2)$$

## 2.2 Simplified methods

For this accidental combination, the most severe efforts for the several profiles are presented in table 1. In this table it is found also the critical temperatures obtained with Elefir-EN and the maximum temperatures in the steel profiles obtained with Ozone V2.2.

Table 1. Most severe efforts at 20°C, critical temperatures corresponded to the fire scenarios

| Profiles | Efforts [kN] |         | Critical Temp. (Elefir-EN) [° C] | T <sub>max</sub> scenario 2 (OZone) [° C] | T <sub>max</sub> scenario 6 (OZone) [° C] | Critical time ISO834 [min] | Temp. after 60min of ISO834 [°C] |
|----------|--------------|---------|----------------------------------|---|---|----------------------------|----------------------------------|
|          | Compr.       | Tension |                                  |   |   |                            |                                  |
| HEA280   | -110.3       |         | 943                              | 435                                       | 735                                       | 62                         | 938                              |
| HEA260   |              | 144.1   | 899                              | 438                                       | 736                                       | 47                         | 938                              |
| HEA240   | -212.5       |         | 774                              | 440                                       | 738                                       | 29                         | 939                              |
| HEB240   |              | 3.74    | 1195                             | 404                                       | 781                                       | 320                        | 954                              |
| HEA160   | -82          | 113     | 808                              | 451                                       | 753                                       | 27                         | 940                              |
| HEA140   | -60          | 89      | 814                              | 455                                       | 765                                       | 26                         | 941                              |
| HEA120   | -40          | 56      | 859                              | 457                                       | 769                                       | 26                         | 941                              |

Table 1 shows that the maximum temperatures never reach the critical temperatures with natural fire. In here it is shown the results for the fire scenarios 2 and 6. Regarding the fire scenario 4 the maximum temperature of the compartment at the level of the lower cord of the truss is 767.96 °C (Fig. 10), meaning that again the critical temperatures are never reached (as an example it should be mentioned that for the profile with the biggest section factor, HEB 240, the maximum temperature obtained in this scenario is 707 °C). It can be concluded that there is no need to use passive protection against fire, which would not be true if the standard fire curve ISO834 was used.

## 2.3 Advanced calculation methods

The most loaded truss was analysed (Figure 14) with the load combination (2) and the fire scenario 2 or the ISO834 fire curve in all the 4 sides of the profiles. With these fire scenarios it was first performed thermal analysis to each profile, using the program SAFIR (figure 15).

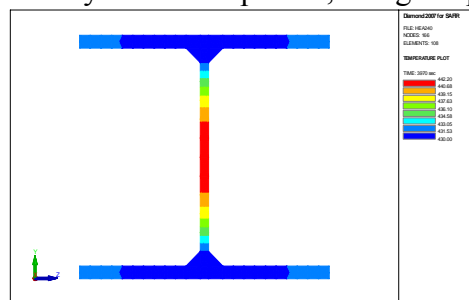


Fig. 15. Maximum temperatures in the HEB240

Following the thermal analysis, it was made a 2D structural analysis, using a material and geometrical non-linear analysis, with beam finite elements.

The analyses performed were:

1. Truss without the possibility of expanding longitudinally subjected to ISO834;
2. Truss with the possibility of expanding longitudinally subjected to ISO834;
3. Truss without the possibility of expanding longitudinally subjected to scenario 2;
4. Truss with the possibility of expanding longitudinally subjected to scenario 2;

Figures 16 and 17 show the deformed shapes immediately before collapse for analysed cases 3 and 4.

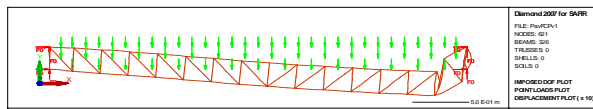


Fig. 16. Deformed shape for case 3

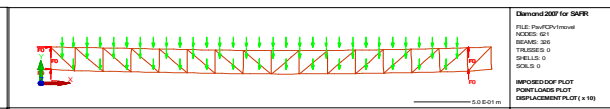


Fig. 17. Deformed shape for case 4

Table 2 shows the time needed for the collapse, the maximum horizontal reaction in the supports and the maximum horizontal displacements in the supports.

Table 2. Final results

| Case study    | Collapse time [min] | Reaction [kN] | Displacement [cm] |
|---------------|---------------------|---------------|-------------------|
| 1) ISO 834    | 24.8                | 2100          | -                 |
| 2) ISO 834    | 26.6                | -             | 43                |
| 2)* ISO 834   | 60                  | 2100          | -                 |
| 3) scenario 2 | 66.1                | 2100          | -                 |
| 4) scenario 2 | No collapse         | -             | 21                |

2)\* truss protected to hold 60 min of ISO834 fire curve

### 3 CONCLUSIONS

It was shown that the temperatures at the level of the roof are relatively low and no passive protection against fire in the steel structure was needed, as a prescriptive evaluation using the standard ISO834 fire curve would impose. Adopting the natural fire, was proven that the steel profiles of the truss have a fire resistance higher than the 60 minutes, being even able to not collapse during the entire fire development, if the truss can freely expand in the supports. This can be obtained from the structure configuration or possible yielding of the supports for the horizontal reactions of 2100kN. However this possibility does not require to be used, due to the fact that the structure holds without collapse 66 minutes, enough time for the evacuation of the occupants and for fire brigades intervention.

### REFERENCES

- [1] European Commission, *Development of Design Rules for Steel Structures Subjected to Natural Fires in Large Compartments*, EUR 18868 EN, 1999.
- [2] CEN, EN 1991-1-2, Eurocode 1 – Basis of design and actions on structures – Part 1-2: General rules – Structural fire design, 2005.
- [3] Ozone V2.2 – University of Liege, PROFILARBED - Research
- [4] Cadorin, J.-F., *Compartment Fire Models for Structural Engineering*, Thèse de doctorat, University of Liège, 2003.
- [5] SAFIR. *A Thermal/Structural Program Modelling Structures under Fire*, Franssen J.-M., Engineering Journal, A.I.S.C., Vol 42, No. 3, 143-158, 2005.
- [6] Heskestad, G., Luminous heights of turbulent diffusion flames, *Fire Safety Journal*, Elsevier, 1983.
- [7] CEN, EN 1993-1-2, Eurocode 3 – Design of steel structures – Part 1-2: Actions on structures exposed to fire, 2005.
- [8] Elefir-EN – Fire design of steel structural members according to Eurocode 3, University of Aveiro and University of Liege.
- [9] CEN, EN 1990, Eurocode – Basis of structural design, 2005.

# **DESIGN OF COLD-FORMED STAINLESS STEEL TUBULAR COLUMNS AT ELEVATED TEMPERATURES**

Ernest Chiu-Yin To, Ben Young

The University of Hong Kong, Department of Civil Engineering, Pokfulam Road, Hong Kong

## **INTRODUCTION**

In the past 15 years, there has been a growing interest in the use of stainless steel in structural applications owing to the high strength, attractive appearance, corrosion resistance and fire resistance of the stainless steel material [1]. Recently, significant progress has been made on the experimental investigation of the structural behaviour of stainless steel columns which enables improvement of the existing design specifications [2]. Comprehensive design guidance for the design stainless steel structural members at ambient temperature is given in the European Code [3], American Specification [4] and Australian/New Zealand Standard [5]. The fire resistance of stainless steel, however, receives relatively little attention with only a few design guidance available, such as the European Code and design guidance proposed by Gardner and Baddoo [6] and Ng and Gardner [7]. These design guidance were developed to determine the failure temperature of a stainless steel structural member subject to a constant load. The performance of cold-formed steel structural members at elevated temperatures has been investigated by Ranby [8], Feng et al. [9], Dharma and Tan [10], Tan et al. [11], Lim and Young [12] and Chen and Young [13], but the works have been focused on carbon steel rather than stainless steel structural members. In order to improve our understanding on fire resistance of stainless steel members, the structural performance of stainless steel members at elevated temperatures has to be investigated.

While physical tests are time consuming and expensive to conduct, numerical analyses can be carried out efficiently and with sufficient accuracy in terms of both time and cost. To and Young [14] investigated the performance of concentrically loaded cold-formed stainless steel tubular columns at elevated temperatures using FEA and performed a parametric study to study the effects of cross-section geometries and temperature on the strength and behaviour of the columns. Based on the numerical results obtained, two design rules for cold-formed stainless steel tubular columns at elevated temperatures have been proposed and presented in this paper. Furthermore, reliability analysis was also performed to assess the validity of the proposed design rules.

## **1 FINITE ELEMENT ANALYSIS**

To and Young [14] developed a finite element model (FEM) to assess the structural performance of cold-formed stainless steel tubular columns at elevated temperatures using the finite element package ABAQUS. The model was developed to simulate fixed-ended columns. The two ends of the column were fixed against all degrees of freedom except that the column was allowed to displace along the loading direction at the loaded end, and all other nodes in the column were free to translate and rotate in any directions. The four-noded doubly curved shell element S4R with six degrees of freedom per node was used in the model. A mesh size of approximately 20 mm × 10 mm (length by width) was chosen for the flat portions of the columns and finer mesh was used at the corners. Initial imperfections and material non-linearity described by the stress-strain model proposed by Chen and Young [15] were incorporated in the model. The FEM involves two types of analyses: (1) the Eigenvalue analysis to determine the buckling modes of the column and (2) the load-displacement non-linear analysis to determine the ultimate loads, failure modes and axial shortenings of the columns. The model has been verified against column test results obtained by Young and Lui [16]. Both the failure loads and failure modes of the columns have been accurately predicted by the FEM. The mean value of the tested-to-FEA load ratio is 1.00 and the

corresponding coefficient of variation (COV) is 0.065 in the verification. The good agreement of the results has demonstrated the validity of the FEM.

A parametric study has been carried out by To and Young [14] using the verified FEM to study the effects of cross section geometries, plate thickness, effective column length and temperature on the strengths and failure modes of the columns. Three series of rectangular hollow sections (Depth×Width): R1 (120mm×60mm), R2 (80mm×50mm) and R3 (140mm×80mm) and one series of square hollow section S1 (50mm×50mm) were investigated in the parametric study. The series have different thicknesses ranging from 1mm to 6mm and different column lengths ranging from 300mm to 3600mm. The temperatures ranged from 22°C to 900°C were investigated. A total of 327 columns were analysed in the study. The developed finite element model and the parametric study are detailed in To and Young [14].

## 2 DESIGN RULES

Based on the numerical results obtained from the parametric study conducted by To and Young [14], two different methods to determine the failure loads of cold-formed stainless steel tubular columns at elevated temperatures were proposed. First, the column strength equations in Eurocode 3 Part 1.4 [3] were employed with the substitution of reduced material properties at elevated temperatures into the equations. Second, the column design rules were developed based on the ultimate strength of stainless steel material and gross sectional area of the columns rather than the yield strength (0.2% proof stress) and effective area.

### 2.1 Column strength design rules in Eurocode 3 Part 1.4

The column strengths obtained by To and Young [14] were compared with the design strengths calculated from Eurocode 3 Part 1.4 [3] but with the replacement of ambient temperature mechanical properties by the elevated temperatures mechanical properties. It is shown that the column strengths agree fairly well with the strengths obtained from FEA. As shown in *Fig. 1*, the mean value of the FEA-to-design load ratio  $R_{FEA} / R_{EC3}$  is 1.27 and the COV is 0.12, where  $R$  is ratio of the failure stress  $f_f$  of the column (failure load divided by gross sectional area) obtained from either the EC3 equations or FEA to the ultimate strength of stainless steel  $f_{U,T}$  at temperature  $T$ °C.

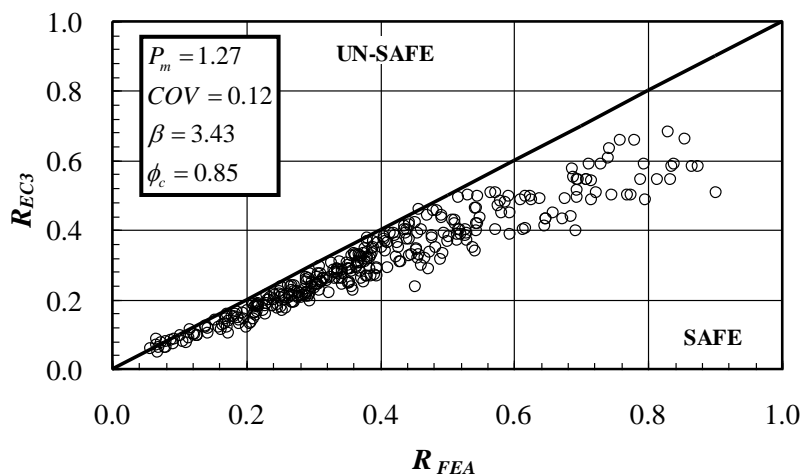


*Fig. 1.* A plot of  $R_{EC3}$  against  $R_{FEA}$

In order to ensure a reliable design rule, reliability analysis was performed, in which the reliability is measured by the reliability index  $\beta$ . The NAS Specification [17] for cold-formed steel structures recommended a minimum reliability index of 2.5 for structural members, while the ASCE Specification [4] for cold-formed stainless steel structures recommended a minimum reliability

index of 3.0. In this study, a minimum reliability index of 2.5 was adopted. The resistance factor  $\phi_c$  of 0.85 was used in the analysis for concentrically loaded compression members, which is given by the NAS Specification [17] and ASCE Specification [4]. A load combination of 1.2DL + 1.6LL as specified in the American Society of Civil Engineers Standard [18] was used in the analysis, where DL is the dead load and LL is the live load. The dead load-to-live load ratio is 0.2. The statistical parameters  $M_m = 1.10$ ,  $F_m = 1.00$ ,  $V_M = 0.10$ , and  $V_F = 0.05$ , which are the mean values and COVs for material properties and fabrication factors were obtained from Table F1 of the NAS Specification [17]. The statistical parameters  $P_m$  and  $V_P$  (COV) are the mean value and coefficient of variation of FEA-to-predicted load ratio respectively, as shown in Fig. 1. A correction factor  $C_P$  was used to account for the influence of a small number of tests, and a factor  $C_P$  is given in Eq. (F1.1-3) of the NAS Specification [17]. The equation to obtain  $\beta$  is shown in Eq. (1) below:

$$\beta = \frac{\ln\left(\frac{M_m F_m P_m}{0.657 \phi_c}\right)}{\sqrt{(V_M^2 + V_F^2 + C_P V_P^2 + 0.21^2)}} \geq 2.5 \quad (1)$$

The reliability index was calculated to be 3.43, which is greater than the minimum required value of 2.5. Therefore, the column strengths calculated from the buckling resistance equations in the Eurocode 3 Part 1.4 [3] using the reduced material properties at elevated temperatures is reliable. It can be seen from the plot of  $R_{EC3}$  against  $R_{FEA}$  in Fig. 1 that the design equations of Eurocode 3 are generally conservative as most of the data points lie below the 45° straight line. Hence, it is suggested that this design rules could be used for determining the buckling resistance of cold-formed stainless steel tubular columns at elevated temperatures using reduced material properties.

## 2.2 Column strength design rules based on ultimate strength of material and gross sectional area

In the existing design specifications, the calculation of column strength of cold-formed stainless steel structural members is always based on the yield strength (0.2% proof stress) of the material. However, this philosophy may not be appropriate as it can be seen in the cold-formed stainless steel square hollow section column tests conducted by Young and Lui [16] and Liu and Young [19] that the failure stress for some of the short columns, in which the failure mode is yielding, was close to the ultimate strength of the stainless steel material instead of its yield strength. The existing design specifications might therefore underestimate the strengths of the short columns. In addition, the determination of strength of thin-walled sections is normally based on the concept of effective area  $A_e$ . Its calculation, however, could be somewhat tedious. In view of these, this study attempts to propose design rules for stainless steel columns based on ultimate strength of the stainless steel material and the gross sectional area, in which the concept is similar to the direct strength method [20, 21]. To start with, the failure load of the column  $P$  is related to the gross area of the section  $A_g$  with the failure stress  $f_f$  as shown in Eq. (2):

$$P = A_g f_f \quad (2)$$

Analytically, the failure stress could be written as a function of the ultimate strength of stainless steel material  $f_{U,T}$ , the elastic flexural buckling stress  $f_{F,T}$ , and the elastic local buckling stress  $f_{L,T}$  of the column at temperature  $T^\circ\text{C}$  given by:

$$f_f = F(f_{U,T}, f_{F,T}, f_{L,T}) \quad (3)$$

Normalizing both sides by the ultimate strength  $f_{U,T}$  of the stainless steel material at temperature  $T^\circ\text{C}$ , Eq. (3) becomes:

$$R_U = \frac{f_f}{f_{U,T}} = F\left(\frac{f_{F,T}}{f_{U,T}}, \frac{f_{L,T}}{f_{U,T}}\right) \quad (4)$$

In Eq. (4), the temperature effect on the strength of the column would not be obvious as the normalization of ultimate strength is temperature dependent as well as the elastic flexural buckling stress and elastic local buckling stress are also temperature dependent. The temperature effect could be considered by including the elastic modulus at a temperature normalized with the elastic modulus at room temperature  $E_{22}$ . Hence, Eq. (4) can be modified as:

$$R_U = F \left( \frac{f_{F,T}}{f_{U,T}}, \frac{f_{L,T}}{f_{U,T}}, \frac{E_T}{E_{22}} \right) \quad (5)$$

Now, postulate that the load ratio  $R_U$  can be expressed as a function of a dimensionless slenderness ratio  $\lambda$  given by:

$$R_U = F \left[ \lambda = \left( \frac{f_{F,T}}{f_{U,T}} \right)^a \left( \frac{f_{L,T}}{f_{U,T}} \right)^b \left( \frac{E_T}{E_{22}} \right)^c \right] \quad (6)$$

where  $a$ ,  $b$  and  $c$  are constants. Appropriate values of  $a$ ,  $b$  and  $c$  have to be determined such that the  $R_U$ - $\lambda$  relation can be represented by a simple mathematical function. By trial and error, it was proposed that  $a = -0.25$ ,  $b = -0.25$  and  $c = -0.45$  and hence Eq. (6) can be re-written as:

$$R_U = F \left[ \lambda = \left( \frac{f_{U,T}^2}{f_{F,T} f_{L,T}} \right)^{0.25} \left( \frac{E_{22}}{E_T} \right)^{0.45} \right] \quad (7)$$

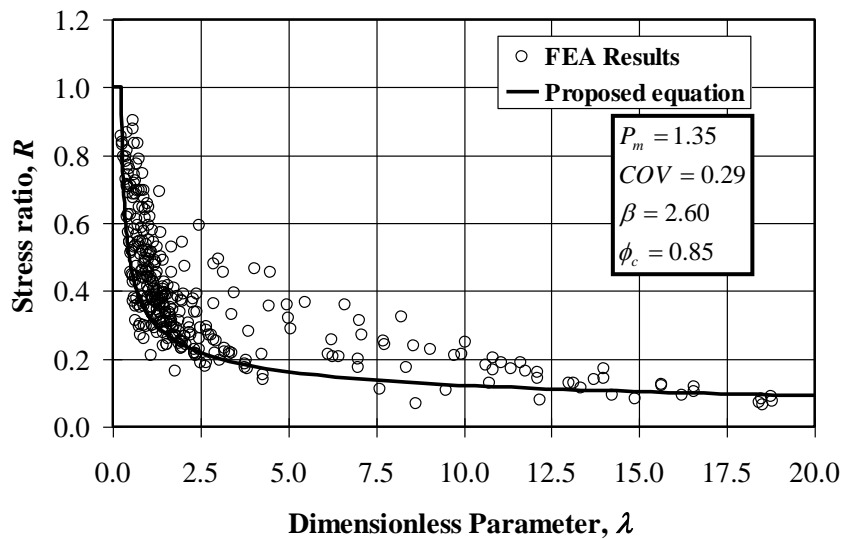


Fig. 2. Comparison of FEA results with the proposed equation

Fig. 2 shows the plot of  $R_U$  against  $\lambda$ , in which a decreasing trend of  $R_U$  with increasing value of  $\lambda$  was observed. The next step is to devise the function  $F$  to describe the  $R_U$ - $\lambda$  relationship. Subjected to the constraint that the reliability index must be greater than or equal to 2.5, and that the mean value of the FEA-to-predicted load ratio is to be as close to 1.0 as possible, an iterative curve fitting process was carried out. Finally, the following equations are proposed:

$$R_U = 1.0 \quad \text{for } \lambda \leq 0.24 \quad (8)$$

$$R_U = 0.34 \left( \frac{\lambda}{0.75} - 0.25 \right)^{-0.4} \quad \text{for } \lambda > 0.24 \quad (9)$$

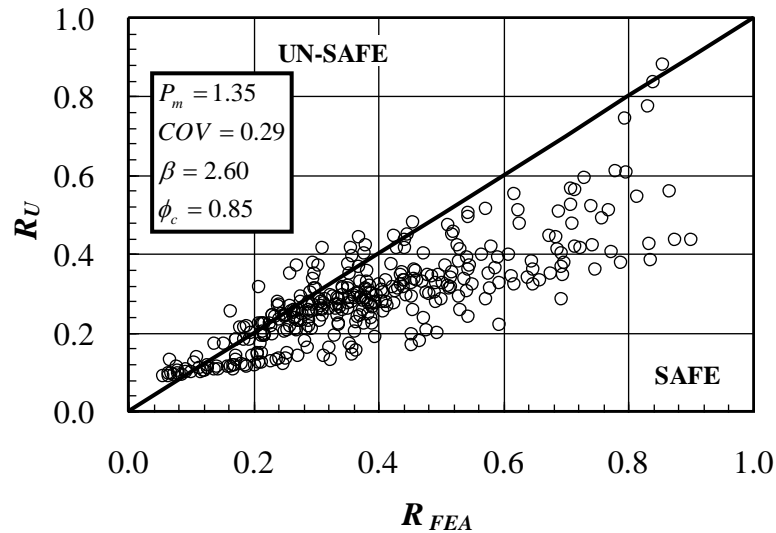


Fig. 3. A plot of  $R_U$  against  $R_{FEA}$

Fig. 2 compares the FEA results with the prediction by the proposed equations. Reliability analysis was carried out and the results give  $\beta = 2.60$ ,  $P_m = 1.35$  and  $COV = 0.29$ . A plot of  $R_U$  against  $R_{FEA}$  is also shown in Fig. 3. Hence, it can be concluded that the proposed equations are reliable and slightly conservative. Finally, the failure load of a column can be computed from:

$$P = R_U f_{U,T} A_g \quad (10)$$

The derivation of the proposed design equations and the comparison of the predicted column strengths with test results are detailed in To and Young [14].

### 3 CONCLUSIONS

Design rules of cold-formed stainless steel tubular columns at elevated temperatures have been proposed. Two design rules based on different design philosophies have been studied. The first design rules is simply the substitution of the mechanical properties of stainless steel material at elevated temperatures into the buckling resistance equations of columns at room temperature specified in the European code for stainless steel structures. The second design rules was developed based on the ultimate strength of the material and the gross sectional area of the column, in which the failure stress of the column is said to be a function of the elastic local buckling stress, elastic flexural buckling stress and the elastic modulus at the temperature of concern. The calculated column strengths were compared with the finite element analysis results of 327 columns, and the reliability analysis showed that both design rules are generally reliable and conservative. Therefore, it can be concluded that the two design rules can be safely employed for estimating the column strengths of concentrically loaded cold-formed stainless steel tubular columns at elevated temperatures.

### REFERENCES

- [1] Gardner L., The use of stainless steel in structures, *Progress in Structural Engineering and Materials*, 7(2): 45 – 55, 2005.
- [2] Gardner L., Stainless steel structures in fire, *Proceedings of the Institution of Civil Engineers: Structures and Buildings*, 160(3): 129 – 138, 2007.
- [3] EC3, Eurocode 3: Design of steel structures – Part 1.4: General rules – Supplementary rules for stainless steels, *Brussels: European Committee for Standardization, EN 1993-1-4, CEN, Brussels*, 2006.

- [4] American Society of Civil Engineers (ASCE), Specification for the design of cold-formed stainless steel structural members, *American Society of Civil Engineers, SEI/ASCE-8-02, Reston, Virginia*, 2002.
- [5] AS/NZS Cold-formed stainless steel structures, *Australian/New Zealand Standard, AS/NZS 4673:2001. Sydney (Australia): Standards Australia*, 2001.
- [6] Gardner L., Baddoo N.R., Fire testing and design of stainless steel structures, *Journal of Constructional Steel Research*, 62: 532 – 543, 2006.
- [7] Ng K.T., Gardner L., Buckling of stainless steel columns and beams in fire, *Engineering Structures*, 29(5): 717 – 730, 2007.
- [8] Ranby A., Structural fire design of thin walled steel sections, *Journal of Constructional Steel Research*, 46(1-3): 303 – 304, 1998.
- [9] Feng M., Wang Y.C., Davies J.M., Structural behaviour of cold-formed thin-walled short steel channel columns at elevated temperatures. Part 1: Experiments, *Thin-Walled Structures*, 41(6): 543 – 570, 2003
- [10] Dharma R.B., Tan K.H., Rotational capacity of steel I-beams under fire conditions Part I: Experimental study, *Engineering Structures*, 29(9): 2391 – 2402, 2007.
- [11] Tan K.H., Toh, W.S., Huang Z.F., Phng G.H., Structural responses of restrained steel columns at elevated temperatures Part 1: Experiments. *Engineering Structures*, 29(8): 1641 – 1652, 2007.
- [12] Lim J.B.P., Young B., Effects of elevated temperatures on bolted moment-connections between cold-formed steel members, *Engineering Structures*, 29(10): 2419 – 2427, 2007.
- [13] Chen J., Young B., Cold-formed steel lipped channel columns at elevated temperatures, *Engineering Structures* 29(10): 2445 – 2456, 2007.
- [14] To E.C.Y., Young B., Performance of cold-formed stainless steel tubular columns at elevated temperatures, *Engineering Structures*, 30(7): 2012 – 2021, 2008.
- [15] Chen J., Young B., Stress-stain curves for stainless steel at elevated temperatures, *Engineering Structures*, 28(2): 229 – 239, 2006.
- [16] Young B., Lui W.M., Tests of cold-formed high strength stainless steel compression members, *Thin-Walled Structures*, 44(2): 224 – 234, 2006.
- [17] North American Specification (NAS), North American Specification for the design of cold-formed steel structural members, *North American Cold-formed Steel Specification, American Iron and Steel Institute, Washington, D.C.*, 2001.
- [18] American Society of Civil Engineers (ASCE), Minimum design loads for buildings and other structures, *ASCE Standard 7-05. New York*, 2005.
- [19] Liu Y., Young B., Buckling of stainless steel square hollow section compression members, *Journal of constructional steel research*, 59(2): 165 – 177, 2003.
- [20] Schafer B.W., Pekoz T., Direct strength prediction of cold-formed steel members using numerical elastic buckling solutions. *Proceedings of the 14th Int. specialty conference on cold-formed steel structures, University of Missouri-Rolla, Rolla, Mo*, 69 – 76, 1998.
- [21] Schafer B.W., Local, distortional, and Euler buckling of thin-walled columns, *Journal of Structural Engineering, ASCE*, 128(3): 289 – 299, 2002.

# APPLICATION OF STRUCTURAL FIRE ENGINEERING TO THE STEELWORK DESIGN OF CANNON PLACE, LONDON

Summer Jun Ding<sup>a</sup>, David Harries<sup>a</sup>, Etienne Hermouet<sup>b</sup>

<sup>a</sup> Bodycote Warringtonfire Consulting, Manchester, UK

<sup>b</sup> Bodycote Warringtonfire Consulting, London, UK

## INTRODUCTION

Cannon Place is a new office building that is currently being built above Cannon Street Station in Central London, with train lines running below the building. The building is over 30m in height and is served by four firefighting cores located around the perimeter of the building. There are two atria that run the height of the building and are linked at the lowest level of the atria.

The project involves the design of the new office building as well as extensive modifications to the station below. The architectural and structural design of the office building is being carried out by Foggo Associates. Bodycote warringtonfire are designing the fire safety strategy for the project.

The structural design uses a highly innovative approach, incorporating an extensive external framed structure that is cantilevered to the front and rear of the building. As the structure is external, the visible appearance of the structural elements is crucial to the architectural concept for the building.

Bodycote warringtonfire have carried out detailed fire engineering analysis on the entire structure of the building based on the approaches in PD 7974 and the Eurocodes. The analysis included an assessment of the impact of fire on the internal structure as well as flame projection and impact on the external structure, resulting in recommendations on the amount of fire protection required to ensure that the structure will not fail in the event of a fire.

## 1 OVERVIEW OF ANALYSIS

To comply with Approved Document B<sup>[1]</sup> (ADB), for office buildings more than 30m above ground level the building need to be sprinklered throughout and the elements of structural frame need to be constructed to achieve a 120 minute standard of fire resistance when tested to BS 476<sup>[2]</sup>. The aim of this investigation is to show that the requirements of the UK Building Regulations 2000<sup>[3]</sup> can be met with a reduced level of fire protection using structural fire engineering analyses.

Requirement B3 of the Building Regulations states that “The building shall be designed and constructed so that, in the event of a fire, its stability will be maintained for a reasonable period.”

The intention is to go beyond that requirement and to demonstrate that, in the event of a foreseeable fire, the building will suffer no structural collapse throughout the entire duration of the fire. The reduction in the amount of fire protection in certain areas of the building will therefore not reduce the level of safety or reduce the performance of the building in a fire. The reduction in fire protection is simply to reduce or eliminate fire protection for parts of the structure where it performs no useful purpose. Any structure that only supports a roof would not need any fire protection (as recommended in ADB) and so has not been analysed.

Different elements of structure will be subject to different fire scenarios depending on their location and characteristics and as such, the assumptions taken for the analysis would differ from one element to another. It should also be noted that the deck structure and any element of structure penetrating the deck or going through the concourse would be protected to a 120 minute standard to maintain an adequate level of separation between the station and office building.

## 2 ANALYSIS METHODS

The intention is to carry out an analysis of the 'reasonable worst case' fire in each individual area to determine its impact on the structure. The sprinkler intervention has also been ignored, in respect of its actions upon the fire, however the provision of sprinklers allows the selection of a less

conservative fire load and thus the provision is taken into account in an indirect manner. The fire is assumed to burn until it runs out of fuel. Fire brigade intervention is ignored, which is a highly onerous assumption as the fire service would be likely to either extinguish or, at least significantly reduce the severity of any fire.

The procedure of the analysis is:

- a) Analyse the potential fires in each area of the building that are to be reviewed;
- b) From a), determine the temperature and duration of flames that may impact on any structure in the vicinity;
- c) Analyse the impact of the flames on the structure (i.e. the temperature that the steel may be heated to);
- d) Determine whether the maximum calculated steel temperatures would lead to structural failure, and if so, what level of fire protection would be required when tested to BS 476.

## 2.1 Potential Fire Sizes

One of the factors that needs to be assessed in the analysis is the potential size and duration of any fire that might occur. In order to predict this it is necessary to understand how fires develop.

One of the most important factors for this is to determine the risk of a flashover occurring. Flashover is a phenomenon that occurs when the smoke layer above a localised fire in one part of a compartment reaches about 600°C. At this point the level of radiation from the smoke layer is sufficient to cause spontaneous ignition of all the combustible surfaces within that room. This causes a very rapid transition from a localised fire in one part of the room to a fully developed fire that involves the entire space.

If a fire occurs within an enclosed space, there is a risk of flashover occurring. However, if there is no possibility of a hot smoke layer developing, then flashover cannot occur. This is the situation in cases where the ceiling is well above the fire or where there is a large amount of permanent ventilation. In these scenarios the potential fire size would be considerably smaller as the only method of fire spread would be via radiation from the flames, which is a much slower process.

It is therefore necessary to determine the likelihood of a flashover fire occurring in each area and then to determine the potential fire size.

## 2.2 Impact of Fires on Structural Steel

Steel gradually reduces in strength as it is heated, so the structure of a building would stay in place until the steel is heated to the point at which the remaining strength is insufficient to sustain the load imposed on it. At this point the steel would begin to sag. Tests carried out by BRE at Cardington showed that when this happens, the load that is supported by that member tends to become redistributed to other elements within the structure, so that full failure is unlikely to occur.

This analysis is intended to ensure that any structural element will not be heated to the point at which it may start to fail and will always have sufficient strength to support the imposed load, so that even the initial sagging will not occur.

Steel has approximately half its strength remaining when it reaches 550°C. General structural design codes tend to end up with designs that have a factor of safety of at least 2. This is in addition to the fact that the structural design is generally based on the highest loading that will ever occur during the lifetime of the building. During normal conditions, the structure is loaded to a relatively low level. It can therefore be concluded that as long as the steel is kept below approximately 550°C, it will not fail. This corresponds with the guidance of BS 5950: Part 8<sup>[4]</sup>.

Even steel that is unprotected has a certain degree of fire resistance that depends on its section size. The larger the steel section, the longer it will take to heat up in a fire. Providing fire protection to a steel element slows the rate at which it heats up, effectively increasing its fire resistance.

## 3 FIRE SCENARIOS

The building will be used as an office building. Due to the height of the building, every floor would be constructed as a 120 minute compartment floor. There are two fully glazed atria of equal size

that run the full height of the office levels and are joined at the base by a large reception area. A temperature control smoke extraction system is provided to the atria as such the glazing enclosing the atria will only be smoke retarding but not fire rated. The building would also be protected by an automatic sprinkler system. Therefore, it is reasonable to assume that a fire would be limited to the area of operation of the few sprinkler heads directly in the vicinity of the fire and would not involve a complete compartment (a whole floor in this case). However, in order to add a margin of safety to the results, it is proposed to assume sprinkler failure and the fire involving the compartment of origin, as detailed below. This will allow additional confidence in the results.

Potential tenancies may subdivide the internal layout in a variety of ways. This sub-division can affect the temperature and duration of the fire and in order to take this into account a number of fire scenarios were assumed and then modelled:

- a) Fire involving the whole main floor plate;
- b) Fire affecting a single tenancy (approx 1/3 of the floor plate);
- c) Fire affecting an area approx 1/3 of a tenancy;
- d) Fire affecting an office layout, area approx 100m<sup>2</sup>;
- e) Fire affecting an office layout as designed by Foggo architects, being equivalent to 2/3 of a tenancy.

The scenarios of the fires were assumed to be post-flashover fires within that space. The amount of ventilation that is available to the fire was included in the analysis. This would be dependent on how much of the enclosure of the room was open at the start of the fire (e.g. an open door or window) and on the failure of any additional sections of the enclosure during the fire. Glazing will often stay in place during the early stages of a fire, but once flashover occurs the temperatures within the room tend to be sufficient to cause most, if not all, of the glass to fail.

The external wall to the building on all levels is glazed. Sensitivity studies were therefore carried out on the amount of ventilation that might be available. The maximum limit would be to assume all the glass failed. The minimum assumed was that only 75% of this failed. Further sensitivity studies involved examining different fire loads and wall linings.

The fire load was taken to be the 80% fractile for office accommodation (570MJ/m<sup>2</sup>) as given in PD 7974: Part 1, and then examined with the following safety factors specified in PD 7974: Part 3:

$$\gamma_1 = 2.2; \quad \gamma_2 = 1.2; \quad \gamma_3 = 0.6$$

These safety factors relate to the height, use and occupancy of the building and are used to calculate the final fire loads that are used in the analysis.

The structures that could be affected by these types of fire are:

- a) The external façade bracing;
- b) The internal frame columns and beams above deck level;
- c) The floor slabs above deck level.

The deck structure and the structure below deck level will not be affected by these office fires.

## 4 INTERNAL STRUCTURE

### 4.1 Details of Analysis

The initial stage of the analysis of a fire within the internal floor areas was to model the potential severity of a fire within this space and compare this with an equivalent period within the standard BS 476: Part 20 fire resistance furnace test. This approach is called the Time Equivalent method. Two different methods were used to achieve this: a) Direct Method; b) Graphical Method. The use of two independent methods gives additional confidence in the results of the analysis.

The Direct Method consists of an equation, which was derived from experimental data that directly compares the compartment data (i.e. compartment size, ventilation area, amount of fire load etc.) to an equivalent duration within the standard fire resistance furnace test. This is a relatively simple approach that does not give specific data on the temperatures reached within the compartment, but gives an easily understood result. Equation 31 from PD 7974: Part 3 was used.

The Graphical Method is a more detailed calculation that consists of a number of stages:

- a) Predict the time/temperature curve that would occur in the event of a fire within the compartment (based on input data such as compartment geometry, ventilation area and fire load). The Parametric Fire Curve from Eurocode 1-1-2<sup>[5]</sup> was used for this stage.
- b) Analyse the effect of the fire on a typical protected steel section. Modify the thickness of the fire protection until the peak temperature of the steel reaches 550°C (other limiting temperatures could also be used). Equation 66 from PD 7974: Part 3 was used for this stage.
- c) Analyse the same steel element with the same thickness of fire protection when exposed to BS 476 and calculate the time at which the steel reaches the same maximum temperature as was reached in the predicted fire. This would give the equivalent severity of the predicted fire in terms of duration within the BS 476 test.

## 4.2 Results

The analysis was carried out using an in-house computer program. In total 24 different scenarios have been investigated. The detailed results of the analysis are presented in Table 1.

Table 1. Description of Fire Scenarios and Results

|    | Scenario  | Direct Method | Graphical Method |
|----|---|---------------|------------------|
| 1  | Whole floor plate, level 2, BASE                      | 52 mins       | 54 mins          |
| 2  | One tenancy, level 2, BASE                            | 51 mins       | 49 mins          |
| 3  | 1/3 of a tenancy, level 2, BASE                       | 51 mins       | 47 mins          |
| 4  | Office floor plate, level 2, BASE                     | 51 mins       | 36 mins          |
| 5  | Whole floor plate, level 2, 75% glazing failure       | 63 mins       | 67 mins          |
| 6  | One tenancy, level 2, 75% glazing failure             | 54 mins       | 57 mins          |
| 7  | 1/3 of a tenancy, level 2, 75% glazing failure        | 53 mins       | 55 mins          |
| 8  | Office floor plate, level 2, 75% glazing failure      | 51 mins       | 36 mins          |
| 9  | Whole floor plate, level 2, Eurocode 1 fire load 80%  | 46 mins       | 49 mins          |
| 10 | One tenancy, level 2, Eurocode 1 fire load 80%        | 46 mins       | 38 mins          |
| 11 | 1/3 of a tenancy, level 2, Eurocode 1 fire load 80%   | 46 mins       | 37 mins          |
| 12 | Office floor plate, level 2, Eurocode 1 fire load 80% | 46 mins       | 35 mins          |
| 13 | Whole floor plate, level 2, Reduced lining factor     | 52 mins       | 54 mins          |
| 14 | One tenancy, level 2, Reduced lining factor           | 51 mins       | 49 mins          |
| 15 | 1/3 of a tenancy, level 2, Reduced lining factor      | 51 mins       | 47 mins          |
| 16 | Office floor plate, level 2, Reduced lining factor    | 51 mins       | 37 mins          |
| 17 | Foggo tenancy, Level 2, BASE                          | 51 mins       | 49 mins          |
| 18 | Foggo tenancy, Level 2, 75% glazing failure           | 54 mins       | 57 mins          |
| 19 | Foggo tenancy, Level 2, Eurocode 1 fire load 80%      | 46 mins       | 38 mins          |
| 20 | Foggo tenancy, Level 2, Reduced lining factor         | 51 mins       | 49 mins          |
| 21 | 1/3 of tenancy, Lev 2, Centre, BASE                   | 67 mins       | 71 mins          |
| 22 | 1/3 of tenancy, Lev 2, Centre, 75% glazing failure    | 86 mins       | 88 mins          |
| 23 | 1/3 of tenancy, Lev 2, Centre, Eurocode 1             | 60 mins       | 65 mins          |
| 24 | 1/3 of tenancy, Lev 2, Centre, Reduced lining fact    | 67 mins       | 71 mins          |

In some of the scenarios (for the Graphical Method and the Direct Method) the amount of ventilation that was available was above the upper limit of applicability of the equations. The amount of ventilation used by the computer program was therefore artificially reduced in order to keep it within its range of applicability. This effectively meant that the scenarios that were analysed were based on only a proportion of the glazed enclosure failing. At the high levels of ventilation that were available it would be a fuel load controlled fire (as opposed to a ventilation controlled fire) and further increasing the ventilation would result in less heat being retained within the enclosure and so a reduction in the fire severity. The artificial reduction in the ventilation that has been carried out would therefore increase the severity (i.e. the analysis will over-predict the fire severity).

The results of the analysis predict that the severity of the fire would require an equivalent (BS 476 test) fire protection to the structure in the order of 35 to 88 minutes. Therefore for the internal structure above deck level an equivalent fire rating of 90 minutes should be sufficient.

## 4.3 Secondary Beams

The structural engineers have allowed for a degree of redundancy in the layout and design of the secondary beams supporting the floors. It is such that localised failure of one beam and the

associated redistribution of load to adjacent beams would not cause structural collapse. Given the other assumptions in the structural fire strategy (specifically the 550°C temperature limit), this requires that the utilisation ratio of the adjacent beams does not exceed approximately 50%.

It is therefore proposed to increase the reinforcement of the slab and fire-rate only 50% of the secondary beams, providing fire protection to every other beam. In the event of a fire located below an unprotected structural beam, the beam may be exposed to temperature sufficient to cause it to fail, however, the next beam on each side would be fire rated and this, coupled with the enhanced slab, would ensure that the integrity of the floor remains.

## 5 EXTERNAL STRUCTURE

### 5.1 Scenarios

A separate analysis was carried out for the external structure. This structure would be outside the fire compartment itself and so would only be affected by any flames and radiation that project out of the windows. The severity of this would normally be significantly lower than for the internal structure.

Using the same scenarios as in the above analysis the effects of external flaming and radiation upon the external structure was analysed. Of the differing scenarios from above, those that produced the highest external flame temperatures were used to analyse the effect on the external members.

### 5.2 Flame Projection

The external flaming was calculated using guidance laid out in PD 7974: Part 3. The study into the effects of flame projection produced the following results, refer to Table 2. The results show that there is so much ventilation that combustion is able to take place completely within the floor plate and that flames would not project out of the windows. Any external structure would not experience any flame impingement, however it would receive radiation from the fire within the compartment. The compartment fires in numerous scenarios reached temperatures of over 1300°C and as such the radiation received by the external members would be likely to heat the structure to such a degree that fire protection would be required.

Table 2. Analysis of Flame Projection

| Scenario                           | Flame projection | Scenario                           | Flame projection |
|------------------------------------|------------------|------------------------------------|------------------|
| <b>Full glazing failure</b>        |                  | <b>75% glazing failure</b>         |                  |
| Full floor area, north elevation   | N                | Full floor area, north elevation   | N                |
| Full floor, west elevation, corner | N                | Full floor, west elevation, corner | N                |
| Full floor, west elevation, centre | N                | Full floor, west elevation, centre | N                |
| 1/3 of floor area (one tenancy)    | N                | 1/3 of floor area (one tenancy)    | N                |
| 1/3 of a tenancy                   | N                | 1/3 of a tenancy                   | N                |
| 100m <sup>2</sup> office space     | N                | 100m <sup>2</sup> office space     | N                |

### 5.3 Details of Analysis

An analysis was carried out to determine whether the external elements need any fire protection and if so the amount of fire protection that they would require. The structural elements investigated include the X-frames on the east and west façades and the Circular Hollow Sections supporting the north and south external bracings. This analysis consists of a number of stages:

- a) The time/temperature curve of the compartment fire was taken as the one of the worst-case scenario (scenario 22) calculated for the internal structure protection analysis using Graphical Method. This time/temperature curve was then reduced by a factor corresponding to the losses during the radiation process through the air. As a result, the worst fire scenario would have a maximum air temperature of 1063°C on the heated surface of the external structure. The fire then burned for a total of 22 minutes before running out of fuel.
- b) Computer program SAFIR was used to calculate the effect of fire on the external structural members. The effects of radiation only were analysed upon the elements of structure as it

was shown that there would be no flame engulfment. If the steel temperature was lower than 550°C during the worst fire scenario, no fire protection will be required. In the case where the steel had a temperature higher than 550°C, fire protection would be required.

- c) For the structural element which requires fire protection, the required thickness of insulation was calculated using SAFIR to insure that the element would survive the worst fire scenario.
- d) The same structural element with the same thickness of insulation was then analysed using BS 476 furnace fire and the time at which the steel reaches 550°C was calculated. This would give the equivalent severity of the predicted fire in terms of duration within the BS 476 test.

## 5.4 Results

The study indicates that there will be no flame impingement upon the external structure and would mean that the only heating the steel would undergo would either be from radiation from the compartment fire or a localised fire next to the external structure. Therefore the external structure is exposed to the radiative heat flux on one side only. The analysis result in recommendations on the amount of fire protection required on various external structural elements, as summarised in Table 3. Since the external structure is only exposed to heat on one side, only the surface facing the building needs to be protected if the structural element requires any fire protection.

Table 3. Summary of Fire Protection Required on Various External Structural Elements

| External Structural Elements   | Fire protection required when tested to BS 476 |
|--|--|
| X Frame – 500x500x50 fabricated box section                            | Not required                                   |
| X Frame – 400x400x16 SHS   | 41 minutes                                     |
| X Frame Joints – 100mm plate   | Not required                                   |
| X Frame Compression bars – 711x40 CHS                                  | 45 minutes                                     |
| X Frame Compression bars – 752x35.5 CHS                                | 43 minutes                                     |
| X Frame Tension bars – 550x300 solid bar                               | Not required                                   |
| External Perimeter Bars – 500x200x16 RHS                               | 45 minutes                                     |
| External Elements – 457 CHS with thickness varying between 8mm to 25mm | 42 minutes                                     |

## 6 CONCLUSIONS

An analysis has been carried out looking at fires within the various office areas in the building to determine whether a reduction in fire protection from the standards laid out in Approved Document B would be achievable. The intention of the analysis is to determine the likely level of fire protection that would be required to comply with the functional requirements of The Building Regulations. The amount of fire protection was designed to ensure that there would be no significant structural failure even in the event of the most onerous fire that could reasonably occur.

## REFERENCES

- [1] Approved Document B – Fire Safety, 2000 Edition, *TSO*.
- [2] BS 476: Fire Tests on Building Materials and Structures, *British Standard*.
- [3] The Building Regulations 2000, DCLG, *TSO*.
- [4] BS 5950: Structural use of steelwork in building. Part 8: Code of practice for fire resistant design, *British Standard*, 1990.
- [5] Eurocode 1: Actions on Structures. Part 1.2: General Actions - Actions on Structures Exposed to Fire, *European Committee for Standardisation (CEN)*, 2002.

Proceedings of International Conference  
Applications of Structural Fire Engineering  
Prague, 19-20 February 2009

**Session 2**

**Fire Modelling**

## **FIRE SCENARIO AND STRUCTURAL BEHAVIOUR OF UNDERGROUND PARKING LOTS EXPOSED TO FIRE**

Patrick Bamonte, Roberto Felicetti

Department of Structural Engineering, Politecnico di Milano, Milan, Italy

### **INTRODUCTION**

The increasing diffusion of underground parking lots, mainly in congested urban areas, makes the fire safety of these structures a real challenge during the entire design process. As a matter of fact, (a) the reduced extension of the in-plan areas puts strict limits on the evacuation paths, that require an accurate design, and (b) the rather low ceiling and lack of openings can significantly influence both the fire scenario and the ensuing thermal field, making it imperative to study each single case, without relying on the usual standard fire curves. As a consequence, the resulting temperatures can be higher than in typical buildings and the structural members can be more severely damaged than in usual cases.

All these factors, and especially the exposure to unusual fire scenarios, makes prescriptive design hardly applicable and performance-based design a must, from the identification of the most appropriate temperature-time curve, to the evaluation of the bearing capacity of each structural member. This phase is crucial, since parking lots are often built with rather thin structural members, such as prestressed open-section or double-tee beams and slabs. In the former case, for example, the pre-tensioned reinforcement is very close to the heated surface, and thus prone to thermally-induced mechanical decay, to the detriment of the overall bearing capacity. In the latter case, the thermal damage in concrete outer layers may significantly reduce the structural ductility, in so favouring brittle phenomena like – for instance – punching-shear failures.

The objective of this paper is to investigate the main factors governing the fire behaviour of a typical underground parking lot consisting of a flat slab supported by a number of relatively slender columns. On the basis of the available literature [1] and of reasonable assumptions, the fire scenario is worked out firstly, by properly modelling the heat transfer between the ambient and the structural members. This preliminary step is instrumental in determining the temperature-time curve required by the thermal analysis of the structural members. On the basis of the calculated thermal field, it is possible to evaluate the decay of the mechanical properties (strength and stiffness) as a function of the temperature [2]. The strength decay results in a general reduction of the bearing capacity, that can be studied by means of well-established simplified methods. The stiffness decay, together with the thermal deformations, often brings in significant redistributions of the internal forces [3,4]. The main factors – and especially the role played by materials' nonlinearity – are studied and some general considerations are drawn on the overall safety of the structure under examination.

### **1 GEOMETRY AND MATERIALS**

The structure considered in the following is a rectangular flat slab resting on square columns and on four perimeter walls (Fig. 1). The two rows of columns divide the slab in a main span (= 8.00 m), and two minor lateral spans (= 4.50 m): thus, there is a central lane for the car movement, and two side aisles for car parking. For the sake of simplicity, the spans comprised between adjacent columns and the columns themselves have been numbered (spans = C1-C15; columns = P1-P8).

The thickness of the slab is assumed to be 35 cm, thus yielding a structural slenderness of  $\approx 23$ , which is a reasonable value for these kind of structures. The structure is made of normal-strength concrete ( $f_{ck} = 25 \text{ MPa}$ ,  $E_c = 31000 \text{ MPa}$ ,  $\nu = 0.16$ ), and reinforced with ordinary steel ( $E_s = 200000 \text{ MPa}$ ,  $f_y = 500 \text{ MPa}$ ).

The external loads consist only of the soil, which is assumed to be about 1 m deep. Therefore, the distributed load per unit area is assumed to be  $30 \text{ kN/m}^2$  (self-weight  $\approx 9.00 \text{ kN/m}^2$ ; permanent loads  $\approx 21 \text{ kN/m}^2$ , corresponding to  $\approx 1.20 \text{ m}$  of ground above the slab).

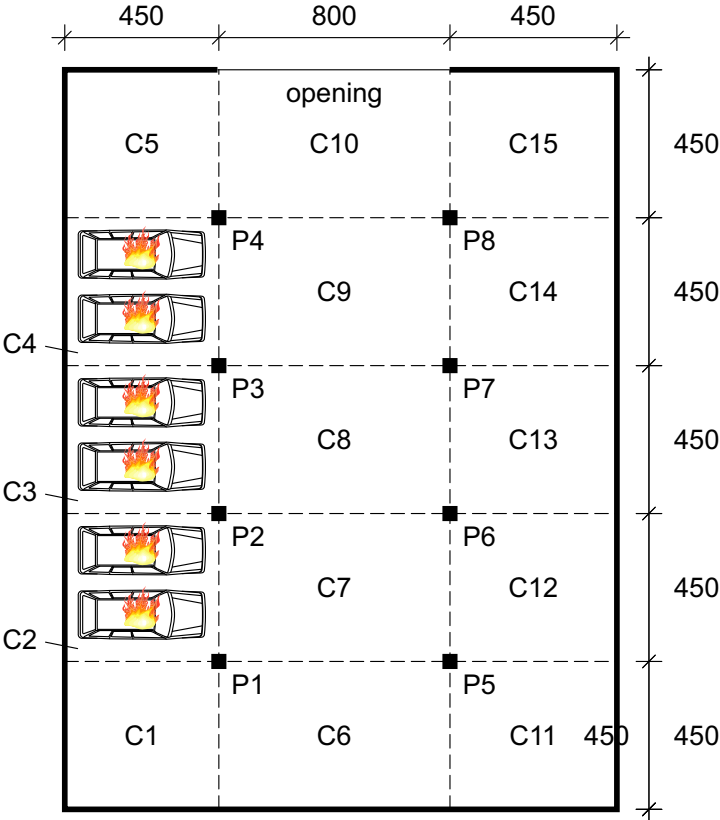


Fig. 1. Plan view of the structure considered

## 2 FIRE SCENARIO

The fire event considered is due to the ignition of six cars in the left aisle of the parking lot. It is assumed that the fire starts at the car near column P1, and then propagates to the nearby cars. Each car takes fire approximately 15 minutes after the previous one; the resulting fire duration is close to 120 minutes.

The number of cars involved in the fire implies that almost the whole left aisle will be subjected to fire. However, the resulting fire remains localized, and the condition for flash-over to occur is not reached. The evolution of the temperature inside the compartment could be evaluated properly only by means of a CFD calculation; this would be rather time-consuming, and CFD calculations are not suited to be performed easily by a structural engineer, especially in the design phase. As an alternative, the EN 1991-1-2 allows the use of simplified models, such as one- and two-zone models, which are based on simplified balance equations between the different heat contributions involved in the fire event inside a given compartment.

Two-zone models have been implemented in several free-downloadable softwares: in our case, reference was made to OZone (developed at the University of Liège, Belgium) and CFAST (developed at NIST, USA).

Both softwares require the input of the fire scenario in terms of HRR (Heat Release Rate) curve. In the present case, the evaluation of the power developed by the burning of one single car was performed in accordance to the experiments carried out by Li and Spearpoint [1] on different means of transportation. The HRR curve measured during the ignition of a normal-size car (Austin Maestro) was used in the following (Fig. 2a).

In the case of CFAST, the single curve can be used as input for the calculation: the different cars igniting are then represented as single fires, characterized by the same HRR curve, but different starting and location points (in space and time). In the case of OZone, the total HRR needs to be input: therefore, the total HRR was evaluated as the sum of the six HRR-curves properly delayed in time, and input into the software. The result is shown in Fig. 2b: the continuous line represents the input, the dashed line represents the input computed by the software (which represents a sort of average of the real input curve).

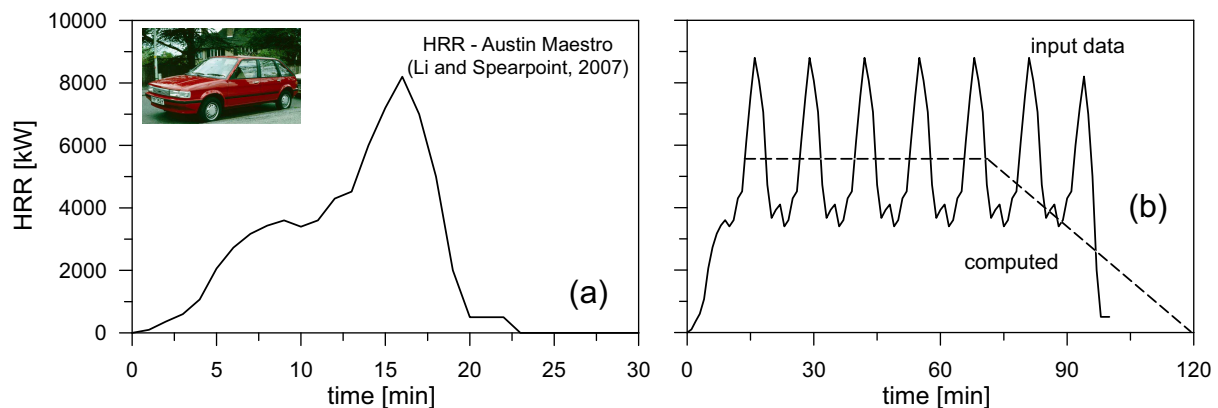


*Fig. 2.* (a) HRR measured from a car fire experiment [1]; (b) total HRR, calculated as the sum of the curves of 6 cars igniting (each car is assumed to start burning approximately 15 minutes after the previous one)

The resulting temperatures of the “hot layer” as a function of time (as evaluated by means of the two softwares) are depicted in Fig. 3a. It is worth noting that the temperature-time curve computed by OZone is smoother (probably because of the smoother input curve); moreover, the temperature-time curves evaluated by means of the two softwares, are in very good agreement.

The most crude approximation of these calculations is the assumption that the whole compartment of the parking lot behaves as a unique ambient (although subdivided into a hot and a cold layer), and thus the evaluation of a unique temperature-time curve. A possible refinement is to divide the lot into 15 compartments (C1-C15, see Fig. 1); this subdivision is only virtual, since no partitions are placed between adjacent compartments. This circumstance was incorporated in CFAST, by introducing 15 different compartments with great openings as partitions. In this case, the thermal input is implemented by placing the burning cars (each described by the single HRR curve in Fig. 2a) in compartments C2, C3 and C4. By working out the temperatures in the “virtual” compartments C1-C15, the evolution of temperature in space (and not only in time) can be assessed.

The resulting temperatures in the hottest compartments (C1-C5) are shown in Fig. 3b: the trends are rather serrate, probably because of the sharp shape of the input HRR curve

(Fig. 2a). Comparing the results with the curves obtained under the assumption of one single compartment (Fig. 3a), it is worth noting that the maximum temperatures are significantly higher. There are also sizable differences between the different compartments: for example, T1 is approximately half of T4, at least beyond 30 minutes from the beginning of the fire.

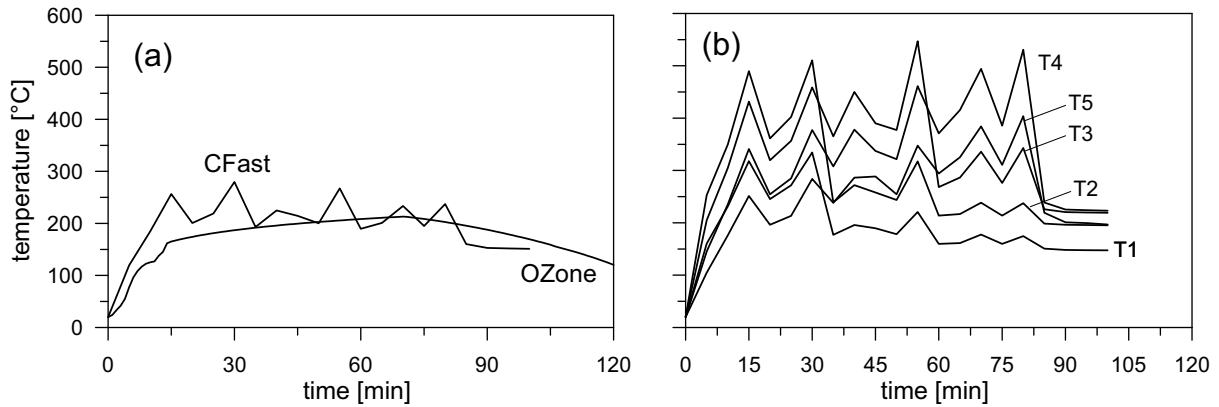


Fig. 3. (a) Temperature-time curves, calculated by the two codes used under the assumption of a single compartment; (b) temperature-time curves for the compartments on the left aisle (as evaluated with CFAST).

### 3 FINITE ELEMENT MODEL

The structural behaviour was studied by means of a finite elements model. The slab was modelled by means of plate elements, allowing for a sequentially-coupled thermo-mechanical behaviour (i.e. the temperature affects the stress and displacement variables, but not vice versa). Different analyses were carried out, under different assumptions concerning the thermal input, the boundary restraints and, above all, the geometrical and materials' non-linearity. The different assumptions were implemented individually, in order to better highlight their specific effect on the overall behaviour.

A first set of analyses was carried out under the assumption that the behaviour of the material be elastic and temperature-independent. Therefore, since cracking of the concrete is not explicitly introduced, the reinforcement needs not be considered.

In the first analysis (A1) the boundary walls and columns are modelled as simple supports (i.e. the confining effect of the soil, as well as the bending stiffness of the walls and columns, are neglected). The thermal input consists of the temperature-time curves shown in Fig. 3b for the left compartments, together with the other curves (not plotted in Fig. 3b) for the remaining 10 compartments. The thermal flux entering the heated surface of the slab is determined by convection (convection coefficient = 35 W/[m<sup>2</sup>K], see EN 1991-1-2), and radiation (emissivity of the heated surface = 0.8, see EN 1991-1-2).

The resulting axial loads on the columns as a function of time are shown in Fig. 4a: the most significant increase in the axial load ( $N^{\text{fire}}/N^{20} = 2.5\div 4.0$ ) occurs in the columns belonging to the left aisle of the parking lot (P1-P4, see Fig. 1), as should have been expected, since they are closer to the localized fires. The axial load on the remaining columns exhibits either a minor increase (P5 and P8,  $N^{\text{fire}}/N^{20} = 1.5$ ), or remains practically constant (P6 and P7). It is worth noting that the sequence of the peaks of the axial loads in columns P1-P4 as a function of time is closely related to the sequence of the 6 cars igniting (from C2 to C4), with P1 being the first column to reach the peak of the axial load, and P4 the last: therefore, the 6 burning cars generate a sort of "heat wave" propagating from C2 towards C4. A possible consequence

is the fact that the column characterized by the highest peak in the axial load is P4, with a peak of the compression force during the fire almost 4 times the value at ambient temperature. The sensitivity of the structure to the various factors (thermal input, confining effect of the soil, boundary restraints) coming into play has been ascertained by means of a set of three more numerical analyses. More in detail:

- A2: the temperature-time curve is the same for all spans (i.e. the variability of the temperature with space is neglected), and equal to the smooth curve of Fig. 3a (determined by means of OZone);
- A3: the boundaries are modelled as perfect in-plane restraints for the slab, and the second-order effects (= geometrical non-linearity) are taken into account;
- A4: the boundaries of the slab are considered to be built in.

The comparison between the various analyses was carried out with reference to column P4, that exhibits in all cases the largest increase of the axial load.

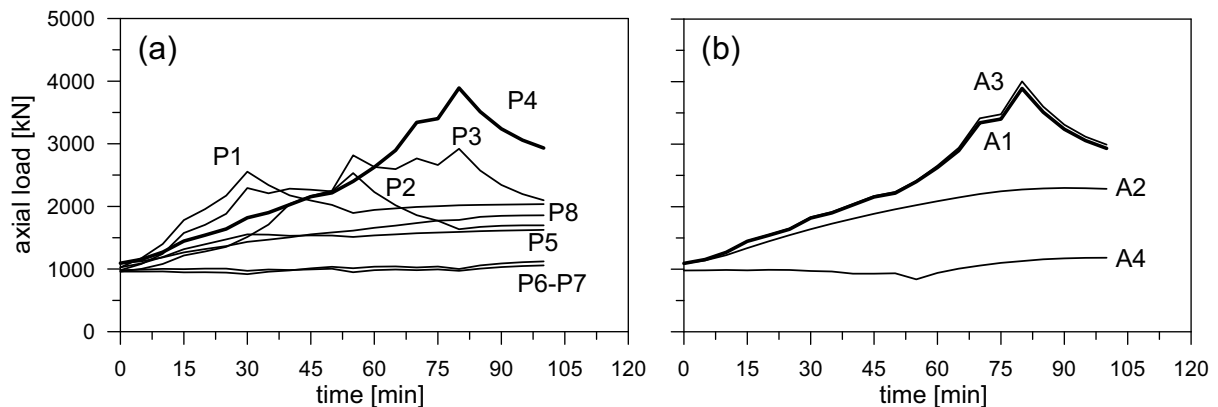


Fig. 4. (a) Axial loads in columns P1-P8 as a function of time; (b) axial load in column P4 for different assumptions concerning thermal input, boundary restraints and 2<sup>nd</sup> order effects.

The comparison between curves A1 and A2 shows that the effect of a non-uniform heating is detrimental, probably because different values of the thermal curvature in adjacent spans tend to increase the shear force at the interface; this increase results in a higher axial load on the columns. Consequently, a uniform heating leads to a lower increase of the axial load during the fire.

As for the 2<sup>nd</sup>-order effects due to the confining effect of the boundaries (A3), they seem to play a minor role, most probably because the displacements reached during the fire are limited by the presence of the columns: as a matter of fact, membrane effects are significant for slab structures characterized by larger slenderness (and thus large displacements in fire). Finally, if the slab has built-in edges (A4), the axial load is hardly affected by the fire.

Two further analyses were then performed, to account for the decay of the elastic modulus with temperature (evaluated in accordance to the provisions given in EN 1992-1-2); the thermal inputs were the same as in the case of A1 and A2. The comparison was carried out in terms of axial load on column P4, and the results are shown in Fig. 5.

If the dependence on temperature of the elastic modulus of concrete is taken into account, both in the case of non-uniform (dashed curve) and uniform heating (dash-dotted curve), the resulting axial load on column P4 is significantly lower than in the corresponding reference cases (A1 and A2 respectively); however, the value is still 50% higher than at room temperature.

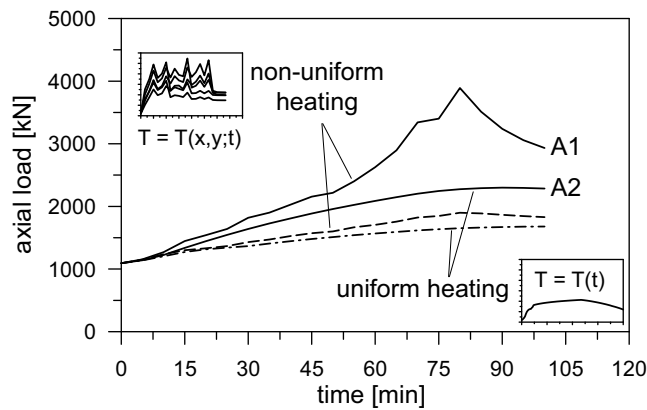


Fig. 5. Axial load on column P4 as a function of time, assuming a constant elastic modulus (A1 = non-uniform heating and A2 = uniform heating), or taking into account its reduction with temperature (dashed and dash-dotted curve respectively).

#### 4 CONCLUDING REMARKS

The thickness of thin flat slabs supported by columns is usually designed by limiting the displacements under the service loads, and by ensuring a satisfying level of safety against punching shear at ultimate. In the case of the roof of a parking lot subjected to the fire of a limited number of cars, a generalized increase of the axial load on the columns is to be expected. This increase becomes even more significant, if the localized nature of car fires is taken into account, and properly introduced by considering the dependence of ambient temperature not only from time, but also from space. The differences ensuing from the distribution of temperature in space (non-uniform heating vs. uniform heating) tend to vanish, if the reduction of the elastic modulus with temperature is taken into account; the same would probably be observed, if concrete cracking and rebar yielding were considered. However, the axial load can still exhibit an increase of up to 50% with respect to its value at 20°C, making these structures very sensitive to punching shear failures triggered by fire.

#### 5 ACKNOWLEDGMENTS

The authors are grateful to Prof. Pietro Gambarova for his valuable suggestions. The contribution of Antonio Buccinnà in the numerical simulations concerning the fire scenario is also gratefully acknowledged.

#### REFERENCES

- [1] Y. Li and M. Spearpoint (2007): “Analysis of Vehicle Fire Statistics in New Zealand Parking Buildings”, *Fire Technology*, 43, pp. 93–106.
- [2] G.A. Houry (2000): “Effect of Fire on Concrete and Concrete Structures”, *Progress in Structural Engineering Materials*, 2000, 2, pp. 429-447.
- [3] F. Biondini and A. Nero (2006): “Nonlinear Analysis of Concrete Structures under Fire”, 2<sup>nd</sup> *fib* Congress, Paper 12-5, Naples, June 5-8, 2006.
- [4] P. Riva and J.-M. Franssen (2008): “Structural Behavior of Continuous Beams and Frames”, Chapter 4 in *fib* Bulletin 46 “Fire design of concrete structures – structural behavior and assessment”, 210 pp.

## **DEFINITION AND SELECTION OF DESIGN FIRE SCENARIOS**

Konstantinos Gkoumas, Chiara Crosti, Luisa Giuliani, Franco Bontempi  
University of Rome “La Sapienza”, School of Engineering, Rome, Italy

### **INTRODUCTION**

The problem of structural fire safety in the recent years has gained a predominant role in the engineering design. This is because nowadays, always bigger and more complex structures are designed and build, making use of particularly fire sensitive materials such as steel, and also, because there is an increasing belief that structures not only have to resist to the design loads, but to maintain a minimal performance in accidental situations as well. The necessity to pursue these goals, has led to the growth of the branch of Fire Safety Engineering, especially after the 9-11 events, which led to the WTC tower collapses in the United States.

Although at present there is no internationally agreed definition of Fire Safety Engineering (FSE), it can be defined as the application of engineering principles, rules and expert judgement based on a scientific understanding of the fire phenomena, of the effects of fire and of the reaction and behaviour of people, in order to:

- save life, protect property and preserve the environment and heritage;
- quantify the hazards and risk of fire and its effects;
- evaluate analytically the optimum protective and preventative measures necessary to limit, within prescribed levels, the consequences of fire.

In a FSE complying strategy, a number of objectives is identified (safety of life, conservation of property, continuity of business operations, preservation of heritage, etc.). These (qualitative) objectives, must be characterised by setting specific performance criteria. Regarding in particular safety of life, the principal aim is to ensure the necessary time for the safe evacuation. In [1] NIST recommends a number of measures, starting from “hard” measures related to building performance factors, such as the checking of the structural integrity and the endurance under fire, and extending to issues related to the human performance, such as the evacuation measurements, training of the personnel etc.

Regarding in particular the performance of the structure under fire, performances can be assessed with the implementation of analytical and computational tools, tools which require a very good understanding of the fire phenomenon. In a second paper presented at the same conference [2], some fundamental considerations regarding the structural safety of steel structures, are presented, as a practical exemplification of many of these concepts.

From what said above, the performance evaluation of the structure becomes important. In this perspective, within the approach assumed in a FSE complying context, two single concepts have found application (the second one, also as a complement to the other):

- The Performance Based Fire Safety Design (PBFSD) of the structure;
- The Fire Risk Assessment (FRA) of the structure.

With aid from the above concepts it is possible to define and select design fire scenarios, leading to the identification of design fires implemented within finite element analysis, in order to inquire on the requested performances.

# 1 PERFORMANCE BASED FIRE SAFETY DESIGN

Performance Based Design (PBD) in general, is the design that meets a specified performance level rather than prescribe specific design criteria (see for example [3]). Performance Based Fire Safety Design (PBFSD) is a new concept within Fire Safety engineering, and it is based on the premises of PBD.

PBFSD allows the use of any design that demonstrates compliance with the fire safety goals of the code. Fire safety goals commonly addressed include life safety, property protection, continuity of operations, and environmental protection. These fire safety goals are explicitly stated in the code, as are the methods that can be used to demonstrate compliance.

A PBFSD starts with an analysis of fire scenarios to determine which design alternatives will meet those fire safety goals. These goals are either referred to the structural performance or to the performance of the system in general. In the first case, the focus is on the structural performance in the presence of fire and includes requirements of fire resistance for the structural elements (e.g. beams, slabs, columns) or for the structural system as a whole (avoidance of excessive vibrations, avoidance of progressive collapse, etc.). In the second case, the focus is on the general design for safety in the case of fire, dealing mostly with the evacuation provisions, at conditions extended well before an eventual structural failure or collapse. In both cases the final goal is the same: the minimization of the consequences to the public. This is in generally attained by assuring a minimum performance (both structural and operational) for the evacuation time.

The PBFSD becomes important especially in the case of complex structural systems or unique buildings, for which a prescriptive approach is difficult to apply for several reason, among else, aesthetics.

## 1.1 Performance Based Structural Design for Fire Safety

The performance approach for the structural design of structures begun to diffuse in the last sixty years, mostly for facilities with elevated risk of fire. This kind of Performance Based approach, has been applied in other circumstances, particularly for seismic design.

The focus is on the structural performance in the presence of fire and includes requirements of fire resistance for the structural elements (e.g. beams, slabs, columns) or for the structural system as a whole (avoidance of excessive vibrations, of progressive collapse, etc.). A very important step to guarantee a determinate level of safety is to verify that the resistance of the structure under fire is higher than the fire severity (fire resistance > fire severity). There are three techniques of checking for the fire resistance (in the time, temperature or resistance domain), as explained among else in the Italian Building Code [4], as shown in *Table 1*.

*Table 1.* Fire resistant checks (from [4])

| Domain      | Units     | Fire resistance                                 | Fire severity                           |
|-------------|-----------|---|---|
| Time        | Hours     | Time over that the structure is weakened        | Duration of fire                        |
| Temperature | °C        | Temperature over that the structure is weakened | Maximum temperature reached during fire |
| Resistance  | KN or KNm | Load bearing capacity at high temperature       | Applied load during fire                |

Generally, when assessing the performance of a structure subject to fire, a conventional collapse is defined, related to the typology of structural element and to the function that it must accomplish. For additional details, the reader is referred to [2] presented at the same conference.

## 1.2 Performance Based Design for Fire Safety - human performance/system response

The principal issue again is the evacuation of a building. The evacuation time is strongly related to some characteristics related to the building geometry and inner organization (e.g. the number of emergency doors per floor, the door dimensions, the maximum travel distance to the exit). While in a prescriptive code, specific data are given, on the basis of the building usage, a performance based code, investigates on how to achieve the same goal as of the numerical prescriptive requirements.

As an example [5] indicates a number of PBD indications, that could substitute specific numerical prescriptive requirements of a prescriptive code:

- provide a maximum travel distance over which safe conditions for egress;
- provide a sufficient number of exits from an area of generally high density occupant load to allow for safe egress;
- provide a sufficient number of exits from a floor area where the large number of people need more than two exits from the area in the event of an evacuation (instead of providing a specific number of exits).

## 2 DESIGN FIRE SCENARIOS AND DESIGN FIRES

For the appropriate fire performance assessment of the structure, fire scenarios have to be identified, with the consequent selection of design fire scenarios, and finally, of the design fires.

In the process of selecting a design fire, several phases have to be identified. These are documented in many International codes and standards (see for example [6,7]). In *Fig. 1*, a schematic flowchart is presented, closely based on indication provided in [7], in which the various phases leading to the selection of design fires are described.

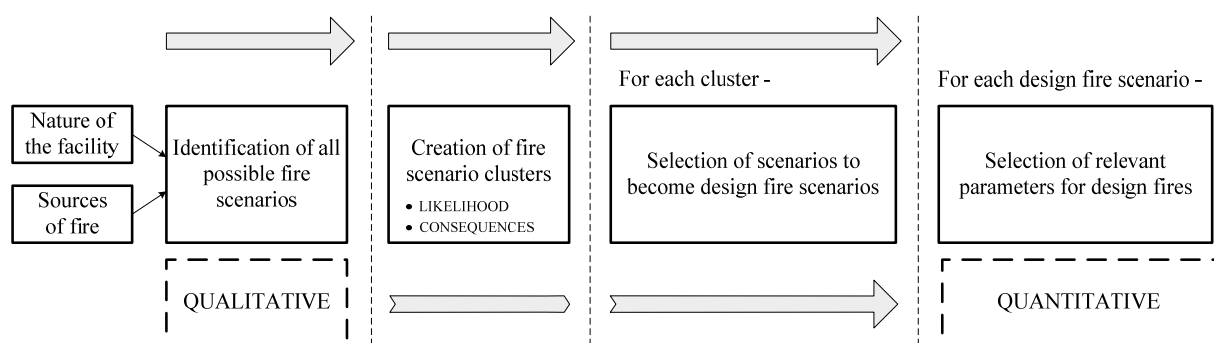


*Fig. 1.* Selection of design fires

With reference to the above flowchart, in a first place, all apparently possible fire scenarios are identified on the basis of the nature of the facility and the possible sources of fire. This leads to the identification of a vast number of -qualitatively described- possible fire scenarios. These scenarios have to be “filtered” and categorised in cluster of scenarios. For each cluster, a risk is associated characterised in terms of the likelihood of occurrence of the cluster and the resultant consequence. The estimated risk can be either qualitative or quantitative (depending on the risk analysis performed and the necessity on a case by case basis). From each cluster of scenarios, those candidate to become design fires are selected. The selection can be based on different processes, ranging from pure judgement to risk analysis techniques such as risk ranking or the construction of event trees. Some additional considerations regarding the fire risk assessment of a structure are given in paragraph 3, while a practical exemplification of

the construction of event trees is presented in paragraph 4. Finally, for each fire scenario selected, a design fire scenario is obtained on the basis of a ranking process.

From the obtained design fire scenarios, one or more design fires are obtained, characterised by quantified data, specific for a given fire safety design objective. Briefly stated, a design fire is characterized by quantities such as its heat release rate at any moment in time, its growth rate, the combustion product rate (such as smoke particulate, toxic or corrosive species, etc.) and the production rate [6]. In the process of selecting the design fire, burning rate data on actual materials should be used. A broadly accepted way to classify design fires is in function the heat release rate: in [7] design fires are classified as slow, medium, fast and ultra fast fires. Other ways to classify a design fire are proposed in literature, e.g. by default curves as a function of the type of the building (see for example [8]).

### **3 FIRE RISK ASSESSMENT OF THE STRUCTURE**

The Fire Risk Assessment (FRA) of the structure, is an incorporated part of the PBFSD, and is codified in many Standards [5,9-11]. One of the aims of the Standards is to provide the methodology on how to evaluate the scenarios to be considered for further analysis, by means of standard methods of Risk Analysis (e.g. qualitative, quantitative, probabilistic etc.).

In particular, within a Risk Management Process, system hazards, their contributing factors and possible sources, must be identified, analyzed and ranked. In particular, any object that emits sufficient heat to ignite combustibles, based on proximity and ignitability, constitutes an initiating hazard, having potential to initiate an unwanted fire. In the first place, the use of a Preliminary Hazards Analysis (PHA) method is suitable. This method includes the ranking of hazards by severity and probability, the inquiry of operational constraints and a list of recommended actions to eliminate or control the hazards. The advantage of a PHA approach is that an inventory of possible hazards can be easily generated. On the downside, some hazards can be missed, thus it is not easy to have an insight into overall risk associated with the system. More systematic and detailed methods to System Hazards Identification include Hazard and operability study (HAZOP) and Failure modes and effects analysis (FMEA). The first is a method of group examination to identify hazards and their consequences, while the latter identifies the modes in which each element can fail and determines the effect on the system. The reader is referred to specialized texts for additional details.

### **4 DEFINITION OF DESIGN FIRE SCENARIOS FOR A STRUCTURAL SYSTEM**

The previous exposed theoretical arguments, find a practical exemplification in the Fire Risk Assessment of a complex structural system, exposed in detail in [12]. The object under inquiry is an industrial facility in steel frame, used for the storage and maintenance of helicopters.

Due to the particular usage, this facility presents an elevated fire risk. The structure is 64.64 meters long, 32.85 meters wide and has a maximum height of 12.9 meters. The triggering event consider is the fire ignition on a helicopter.

The choice of important fire scenarios for the case studied is focused on three areas that, after an initial evaluation, seem to produce the most adverse fire scenarios (in the sense of “likelihood *times* consequence”).

The identified most severe areas for the starting of the fire give birth to a number of scenarios, localized in zone of about 50 m<sup>2</sup>, that accounts for about the 2,5% of all the building surface.

The fire risk prone areas identified are three (*Fig. 2*):

1. The central zone of the building (Area A).
2. The central zone of the span (Area B).
3. The outer zone (Area C).

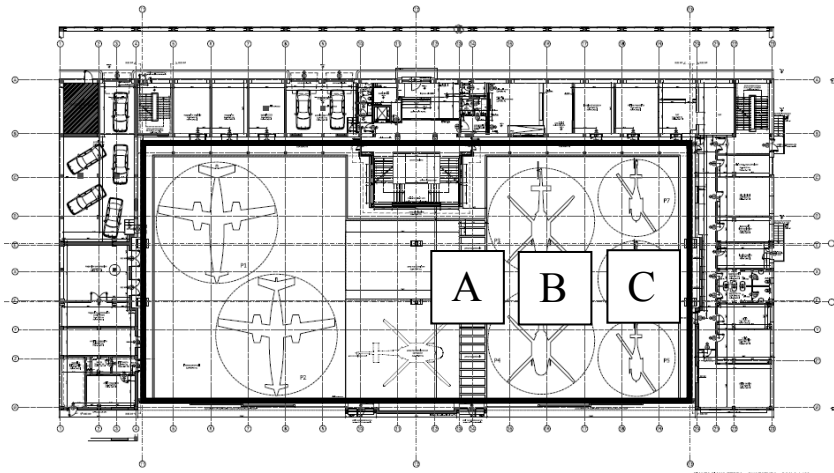


Fig. 2. Plan of the industrial facility

The event tree representing the evolution of a generic triggering event is further divided to take account for more than one initial situations. The one presented here, is relevant to a condition where the doors of the facility are closed, however, there are employees inside. In the event tree of Fig. 3, the consequences of an initiative event are followed in a series of possible paths.

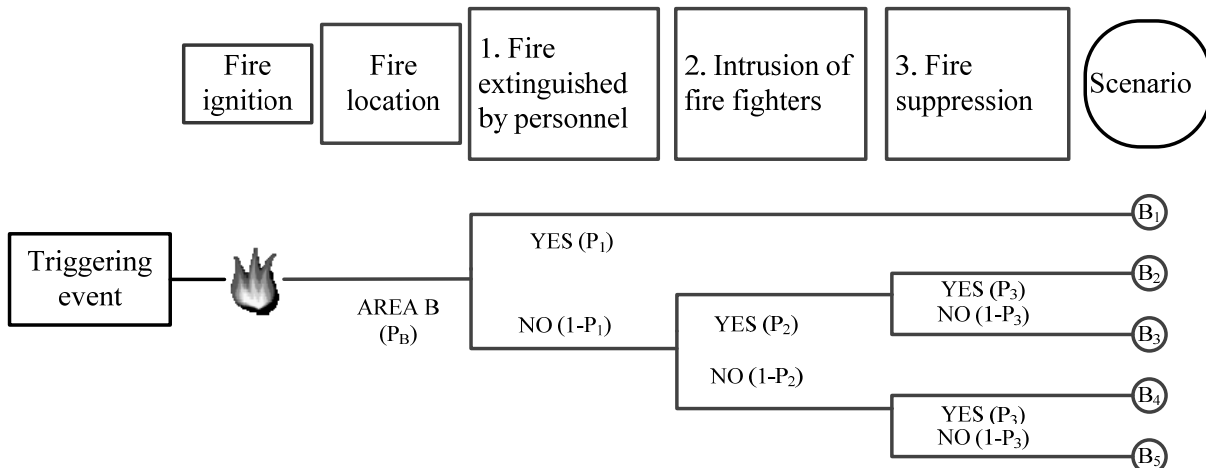


Fig. 3. Event tree after a fire ignition in the industrial facility

The analysis can be quantified by assigning numerical values to the probabilities (e.g. making use of appropriate historical values) as shown for example in Table 2 in the case of a triggering event in area B.

Table 2. Probabilities for the occurrence of different scenarios

| Scenario       | Probability   |
|----------------|---|
| B <sub>1</sub> | $P_B * P_1$   |
| B <sub>2</sub> | $P_B * (1 - P_1) * P_2$                               |
| B <sub>3</sub> | $P_B * (1 - P_1) * (1 - P_2) * P_3 * P_4$             |
| B <sub>4</sub> | $P_B * (1 - P_1) * (1 - P_2) * P_3 * (1 - P_4)$       |
| B <sub>5</sub> | $P_B * (1 - P_1) * (1 - P_2) * (1 - P_3) * P_4$       |
| B <sub>6</sub> | $P_B * (1 - P_1) * (1 - P_2) * (1 - P_3) * (1 - P_4)$ |

The indicated probabilities are intended as in function of time, that is,  $P = P(t)$ . In this sense,  $P_4$  is not the same after condition 3 (intrusion of the fire fighters), since the expansion of the fire is different for the two cases. For the same reason, probabilities of the various branches are different for the 3 different areas (e.g. the probability  $P_2$  of the fire being extinguished by the sprinklers, is different for each one of the Areas, since the sprinkler arrangement is different in each area). The same stands for probabilities assigned for the different fire locations (not shown here for the sake of brevity), due to the different geometric characteristics and the different internal configuration of each area.

## 5 FURTHER CONSIDERATIONS

The aspects covered in this paper show that only with a faithful representation of the system, a truthful definition of fire scenarios and, as will be shown, detailed advanced analysis, it is possible to have a clear view on the consequences of a fire. Design fire scenarios identified and selected in this paper, led to the implementation of design fires in FEM (as shown in the 2<sup>nd</sup> application in [2] presented at the same conference), aiming at the assessment of specific structural performances, in particular the collapse resistance of the structure. Although the process of defining design fire scenarios is complex and characterised by uncertainties, the authors believe that with scrupulous applications of engineering principles that have found ground in the recent years, and the necessary engineering judgement, it is possibly to realistically depict the phenomena in the civil engineering field.

## REFERENCES

- [1] NIST NCSTAR 1, WTC Investigation, Chapter 9, Recommendations. Available online on 01/2008 at <http://wtc.nist.gov/NCSTAR1>
- [2] Crosti, C., Giuliani, L., Gkoumas, K., Bontempi, F., Structural analysis of steel structures under fire loading, Book Proceedings: Applications of Structural Fire Engineering, Prague 19-20 February 2009.
- [3] Foliente, G., Developments in Performance-Based Building Codes and Standards, Forest Products Journal., Vol.50, No 7/8, 2000.
- [4] D.M. 14/09/2005- Norme Tecniche per le Costruzioni (in Italian), Ministry of Infrastructures and transportation, Italy 2005.
- [5] ISO/TS 16732, Fire Safety Engineering - Guidance on fire risk assessment, 2005.
- [6] SFPE- Society of Fire Protection Engineers, Handbook of Fire Protection Engineering, National Fire Protection Association, 3rd Edition, 2002.
- [7] ISO/PDTS 16733, Fire Safety Engineering - Selection of design fire scenarios and design fires, Committee draft 2005.
- [8] Sundström, B., A methodology to create a design fire, NIST Workshop on Fire Growth and Spread on Objects, March 4-6, 2002.
- [9] SFPE- Society of Fire Protection Engineers, Engineering Guide to Application of Risk Assessment in Fire Protection Design, *Review Draft*, October 2005.
- [10] ASTM- American Society for Testing Materials, E1776 Standard Guide for Development of Fire-Risk-Assessment Standards, 2007.
- [11] NFPA- National Fire Protection Association 551, Guide for the Evaluation of Fire Risk Assessments, Edition 2007.
- [12] Gkoumas, K., Crosti, C. and Bontempi, F., Risk Analysis and Modelling Techniques for Structural Fire Safety, in Proceedings of the CST2008 & ECT2008 Conferences, Athens, 2-5 September 2008.

## **GENERALISED THERMAL AND STRUCTURAL FIRE ANALYSIS WITH GENISTELA AND GENISTRUC**

Hong Liang, Stephen Welch, L'oc Faure, Martin Gillie

University of Edinburgh, BRE Centre for Fire Safety Engineering, Edinburgh, UK

### **INTRODUCTION**

Increasing interest in assessing the performance of structures in fire is driving the development of an array of modelling methodologies to be used in fire safety engineering design. Whilst traditionally most code-based design has been invoked simple calculations, referencing measured fire performance in standard tests, the progressive shift towards performance-based design has opened the door to use of advanced methods exploiting numerical models. These approaches will not replace standard testing, but they can already be used in a complementary fashion, to extend the application of test data, or in cases where standard test results are not applicable.

Some simplified modelling methods have also been established, such as the protected member equation in Eurocode 3 (EC3) [1], but as with all semi-empirical methods the results will tend to be conservative and there are of necessity a number of simplifying assumptions. CFD-based methodologies can in principle provide a much more detailed description of the thermal environment in fire and the effects of localised heating, which could be used in conjunction with thermal analysis models to examine structural fire performance. In previous work [2], a dedicated fine-mesh thermal modelling tool, known as STELA (Solid ThErmaL Analysis), has been implemented within the RANS CFD code SOFIE [3]. However, the practical application of these techniques suggests that detailed thermal analysis of structural members in the context of simulations of full-scale building fires remains problematic. This is partly due to the difference of scale between the mesh which can be afforded for the fire and that required for the thermal analysis of the structure, a particular problem with structured meshes, and also the generally high computational demands for coupled analyses. Moreover, existing approaches are limited to consideration of a specific structural arrangement of interest, since it is necessary to define all model parameters in advance. Simulations must be repeated from the beginning if details such as the structural geometry or the thermal properties are changed, a very inefficient procedure.

To overcome the above limitations, a more general and flexible methodology has been developed, still within the context of a CFD fire simulation. This novel methodology is called GeniSTELA (Generalised Solid ThErmaL Analysis) and is currently implemented in SOFIE. It has been verified and validated as reported elsewhere [4-6]. Moreover, the computational requirements are also assessed considering a number of aspects, such as the number of simultaneous parametric cases, the required frequency of the GeniSTELA steel temperature field computation and, hence, the overall balance between fluid and solid-phase analysis.

This paper includes a demonstration of the intended operation of GeniSTELA in application to a hypothetical scenario, with simultaneous computation of 72 parametric variants. GeniSTELA provides a large amount of output, including the predicted steel temperature field throughout the compartment for all combinations of structural members and protections considered. By this means, an efficient approach to determining the worst case steel temperatures is provided, with no requirement to repeat simulations of the fire itself. On the

other hand, a special methodology is required to directly use of those outputs for mechanical analysis of structures. An extended methodology called GeniSTRUC (Generalised STRUCture analysis) is developed, exploiting the closed form solutions for simple structural forms (a connected beam/column assembly). It is currently used to predict the plastic collapse and buckling behaviour. For validation, the method has been compared with the FEM method (ABAQUS). A comparison to the experimental measurements obtained in the CTICM external column fire tests is also undergoing.

### 1 GENISTELA

As mentioned elsewhere [4-6], the GeniSTELA methodology is based on computation of a set of "steel temperature field" parameters within the whole of the calculation domain, accommodating, by means of simultaneous calculations, both uncertainties in the input parameters and possible variants to the specification. Hence the need for repeat simulations is bypassed. Furthermore, by predicting the member temperatures at each point in space the limitations of existing methods with regards to the position of the structural component are overcome. Considering the potentially great computational costs associated with the large numbers of thermal analysis calculations required (equal to the number of gas-phase cells times the number of variants studied in the simultaneous calculations), approximate methods are employed to reduce the full 3D thermal response problem down to treatments which are essentially 1D but which include appropriate representations of the heat transfer processes in the other dimensions to reconstruct a quasi-3D solution. The computations are performed in each gas-phase CFD cell in the computational domain. The heat transfer within the structure and CFD calculation are solved separately and then coupled together by exchanging data, such as temperatures and velocities at their mutual boundaries at the end of the time step. For generalisation and accuracy, heat transfer submodels are also implemented within GeniSTELA to treat the important factors which might have great impact on the transient thermal response, such as the convection coefficient and material thermal properties. The details of the model development are described previously [4-6]. Figures below provide schematics which reference the various concepts of quasi-3D model (Fig. 1 for 1D model and 2 for 2/3D corrections).

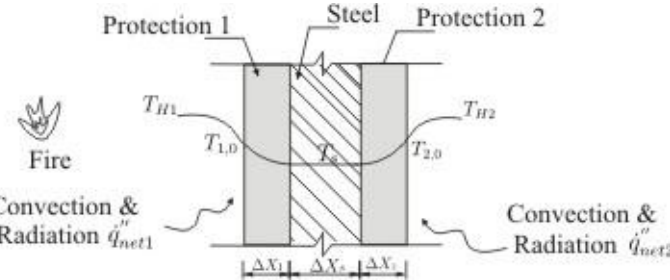


Fig. 1. Schematic of heat transfer for 1D model

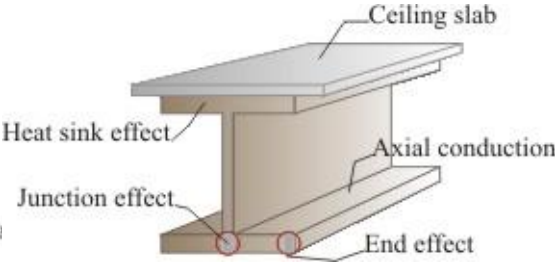


Fig. 2. Correction effects for 2/3D

## 2 APPLICATION TO HYPOTHETICAL SCENARIO

### 2.1 Background

GeniSTELA has been applied to a ‘hypothetical benchmark scenario’ defined in the RFCS FIRESTRUC project [7]. This involves a series of steel tubes and I-profile columns and beams inside an open-ended compartment 30 m by 20 m in floor area and 10 m high. The fire was specified as a heptane pool in a 5-m square tray, following a t-squared fast-growing curve

and reaching 30 MW in 800s, remaining steady thereafter. A more detailed description of the test scenarios is available in the report [7]. In this work, as a demonstration of GeniSTELA for practical use, the methodology was applied in the reported case with fire at location A, representing the non-symmetrical fire position.

72 simultaneous parametric variants were examined, spanning different steel sections and protection properties, etc, with a single parameter modified from the defaults in each case. For the default case, a IPE B 500 section long beam was adopted with Fendolite MII fire protection material with 1-hour fire rating thickness. Eurocode properties were assumed for the steel and the surface emissivity was set as 0.8. The other parameters varied where the steel section (dimensions and weight), protection materials specification including material type (sprayed fibre, board and intumescent) and thickness, together with the thermal-related properties of the material, including moisture content, thermal conductivity, specific heat, density and surface emissivity. On case without protection was also analysed, using a simpler variant of the standard GeniSTELA analysis, to provide a limit for the expected worst case condition and allowing the comparison with the ‘hypothetical benchmark test’ results obtained from other models in earlier work [7].

Various locations on the surfaces of beams and columns studied in the earlier work were examined for comparison of steel temperature field predictions, as shown in Fig. 3 below:

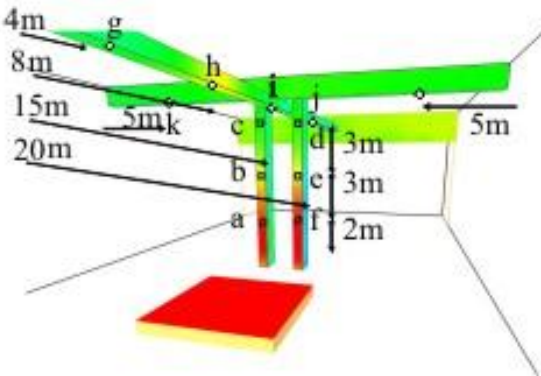


Fig. 3. Locations studied

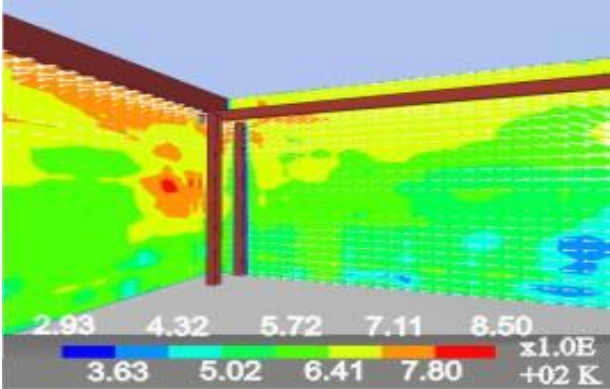
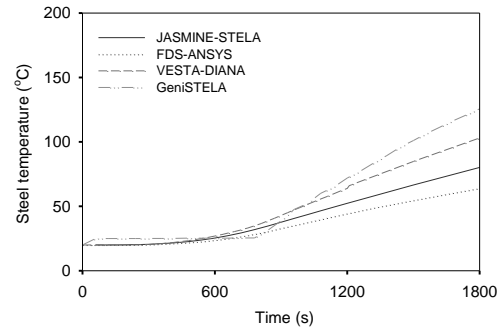
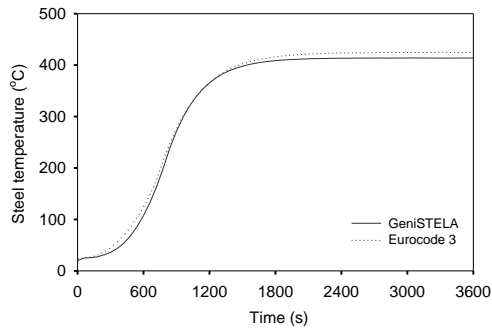


Fig. 4. Example graphical output from GENISTELA at 3600 s

**2.2 Results and analysis**

The simulation provided steel temperature field results for all parametric cases within an affordable computational time (roughly double that required for the fire itself, when the steel temperature was computed at the end of each timestep). Fig. 4 is an illustration of the results, which shows the calculated steel temperature field and flowfield vector distributions at 3600s, for the default case. As expected, increased temperatures are predicted at locations close to the fire source and in the hot layer, confirming that these are the most critical areas for structural member performance for this particular fire scenario.

The results presented below (Figs. 5-8) focus on the steel temperatures at some of the locations specified in Fig. 3. The results have also been compared with EC3 [1] method and those obtained from other modelling methodologies exploited in the FIRESTRUC project [7], whilst model sensitivities have been examined and demonstrated.



*Fig. 5.* Comparison of steel temperatures for *Fig. 6.* Comparison of steel temperatures for unprotected member between GeniSTELA and unprotected member between GeniSTELA and EC3 at location g other models at location e

Fig. 5 shows that the prediction for unprotected steel is in good agreement with the EC3 method the unprotected steel. These temperatures exhibit the same trend as those obtained using other code pairs, see Fig. 6.

Regarding structural fire design, the protected cases are more of interest. A series of predicted steel temperatures at various locations for the default case have been studied, including locations a, c, g, h and j (see Fig. 3). These cover most typical steel structure locations of interest during a fire, i.e. either structure in a cold layer or hot layer, above the fire source or away from the fire source, close to the ventilation opening or far away from the opening. The results also suggest that higher temperatures would be expected at the locations close to the fire source in the hot layer.

Sensitivity study has been carried out. Fig. 7 and 8 demonstrates some of the key factors that affect the prediction results, based on location g. The sensitivity study results indicate the final steel temperature is strongly affected by the structural element geometry and the fire protection materials as well as the thermal conductivity. The moisture content could be an important factor within a certain temperature range before the moisture has vanished. Emissivities in the range 0.1 to 1.0 were examined and differences of up to 20% found in the later stages of the heating. Effects are much smaller initially, when convective heat transfer is dominant, consistent with the findings by Staggs and Phylaktou [8]. The results guide the definitions of default parameters for reasonable worst cases and suggest the possible exploitation opportunities in structural fire design.

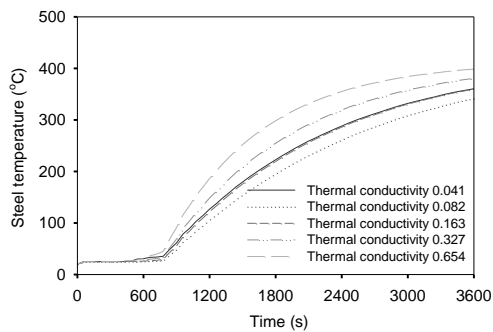


*Fig. 7.* Effect of protection thermal conductivity on calculated steel temperatures

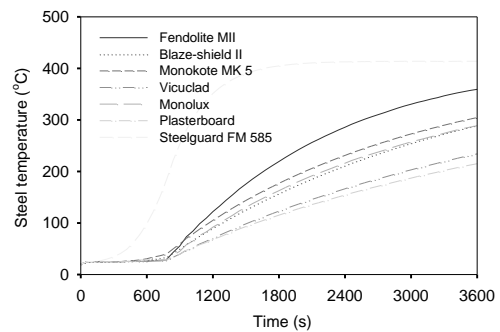


*Fig. 8.* Effect of protection type on calculated steel temperatures at 1 hour fire rating thickness

### 3 GENISTRUC

#### 3.1 Methodology

The ultimate goal of this work is to assess the mechanical performance of structures in fires, but so far no failure criteria beyond traditional critical temperature methods have been considered. In light of the advantages of GeniSTELA, the potential for using simplified structural analysis methods, exploiting closed-form solutions, to establish a more robust means of predicting the ultimate structural performance within this generalised framework is explored and a generalised methodology called GeniSTRUC is proposed.

GeniSTRUC is developed as a ‘simple’ method by considering a simplified structural assembly as a whole, cf. the method of Quiel and Garlock [9]. A simplified model is adopted for representing interactions between the two components, adding a spring where appropriate to represent the flexural stiffness and strength of the column. The members are thereafter subjected to thermal expansion and thermal bowing actions due to the temperature elevation. Each part of the component is then analysed separately, with the stiffness of the spring varying according to time and temperature in order to represent the interaction. Under the temperature elevation, the beam expands and as a result of the partial restraint brought by the column, an axial force is developed in the beam. The beam is considered to be composed of different segments which are in fact corresponding to the meshing of GeniSTELA. As the temperature elevation is different in each segment, the Young’s modulus and the ultimate strength are different. Then the ultimate plastic moment ( $M_u$ ) can be computed for each segment and is a function of the geometry of the cross section, the axial force and the ultimate strength of the beam. The optimum number of segments is chosen by the user depending on the affordable computing time and the required accuracy. The method could also be applied to the column, where the lateral force is brought by the expansion of the beam instead.

#### 3.2 Analysis

The model has been implemented in a spreadsheet and compared with FEA (Finite Element Analysis) modelling using ABAQUS. Its performance has also been examined in a validation scenario based on the CTICM external column fire tests though the work is still undergoing.

Table 1 shows the comparison between GeniSTRUC and ABAQUS regarding to the failure time. The prediction difference is within reasonable range and generally conservative for GeniSTELA.

*Table 1.* Failure time prediction comparison

| Load (KN) | Time of failure (s) |        |
|-----------|---------------------|--------|
|           | GeniSTRUC           | ABAQUS |
| 175       | 570                 | 600    |
| 180       | 510                 | 600    |
| 185       | 420                 | 480    |

### 4 CONCLUSION

Along with the case study, the simulation results demonstrate the simultaneous computation capability of GeniSTELA. The detailed method-to-method comparison results demonstrate

the practical use of GeniSTELA in terms of the prediction sensitivities and the associated computational costs, hence the possible use in the field of the structural fire design.

In addition, the framework of GeniSTRUC has been formed to assess the structural integrity by doing plastic and buckling analysis, using temperature field results from GeniSTELA, while taking into account its direct surroundings. GeniSTRUC has been proved to be a very efficient tool for structural analysis as the extension of GeniSTELA, based on the initial tests.

Overall, GeniSTELA and GeniSTRUC are demonstrated as comprehensive but practical tools for structural fire design, providing far more flexibility in assessing the thermal and mechanical responses of steel structures to fire than has been available hitherto, with potential to improve the efficiency and safety of the relevant constructions.

## REFERENCES

- [1] BSI. Eurocode 3: Design of steel structures – Part 1-2: General rules – Structure fire design. British Standards Institution. 2005.
- [2] Kumar S, Welch S, Miles SD, Cajot L-G, Haller M, Ojanguren M et al. Natural Fire Safety Concept - The development and validation of a CFD-based engineering methodology for evaluating thermal action on steel and composite structures, report No. ISBN 92-894-9594-4. European Commission, 2005. 150 pp.
- [3] Rubini PA. SOFIE-simulation of fires in enclosures. Cranfield University. 1997.
- [4] Liang H. GeniSTELA - A generalised engineering tool for thermal analysis of structural members in fire. PhD thesis, University of Edinburgh, 2008. 215 pp.
- [5] Liang H, Welch S. A novel engineering tool for thermal analysis of structural members in natural fires. *Proc 4th Int Workshop on Structures in fire*. Aveiro, Portugal, 2006.
- [6] Liang H, Welch S, Stratford T, Kinsella EV. Development and validation of a generalised engineering methodology for thermal analysis of structural members in fire. *Proc 5th Int Seminar Fire and Explosion Hazards*. Edinburgh, UK, 2007.
- [7] Welch S, Miles SD, Kumar S, Lemaire T, Chan A. FIRESTRUC - Integrating advanced three-dimensional modelling methodologies for predicting thermo-mechanical behaviour of steel and composite structures subjected to natural fires. *IAFSS 9*, Karlsruhe, Germany, 2008.
- [8] Staggs JEJ, Phylaktou HN. The effects of emissivity on the performance of steel in furnace tests. *Fire Safety J. vol. 43, pp. 1-10*, 2008.
- [9] Quiel SE, Garlock MEM. A performance-based design approach for steel perimeter columns subject to fire. *Proc 4th Int Workshop on Structures in fire*. Aveiro, Portugal, 2006.

## Experimentation of the Subway Smoke Control System

Ni Zhaopeng , Kan Qiang

Tianjin Fire Research Institute, the Ministry of Public Security, Tianjin, P.R.China

### INTRODUCTION

As a fast, comfortable urban transport tool with big capacity, subway has a history of more than a hundred years. It has been widely adopted in most of the major developed countries or regions and has been playing an important role in easing urban traffic pressure. However, because of the special structure of the subway, in the event of fire, large amount of smoke is generated, heat is not easy to spread, firefighting and rescue work is difficult to be carried out; serious casualties could be caused. In a subway fire, smoke is the major factor threatening life safety. It not only impedes people's sight for escape, causes suffocation, but also makes the fire-fighting and rescue work difficult<sup>[1]</sup>. As one of the major fire facilities in subway, Smoke control system plays an irreplaceable role in the guarantee of the safety of people and facilitating the fire-fighting and rescue work. Therefore, field test were done by Tianjin Fire Research Institute of the Ministry of Public Security to analyze the performance of the smoke control system in a new subway before it was put into operation. The field test and numerical simulation analysis could not only provide an objective and accurate evaluation, but also help us to find problems and to put forward suggestions for improvement. The research will also provide basic data for amendments to the related existing technical specifications of China.

### 1 FIELD TEST PROCEDURE

#### 1.1 Brief introduction to the subway station

The subway station is two-story island-type. The concourse is on the first floor of the underground. It has 4 entrance/exits to the ground, namely 1,2,3 and 4. The second floor of the underground is the platform. Two stairs and two escalators connect the platform and the concourse, namely stair 1 and 2 and escalator 1 and 2. The layout of the concourse and the platform is shown in Figure 1 and Figure 2 respectively.

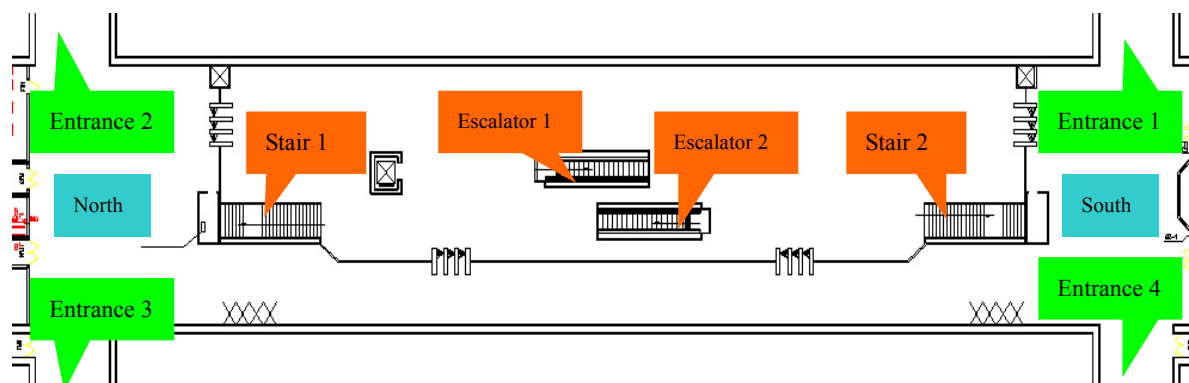


Fig.1. Layout of the concourse

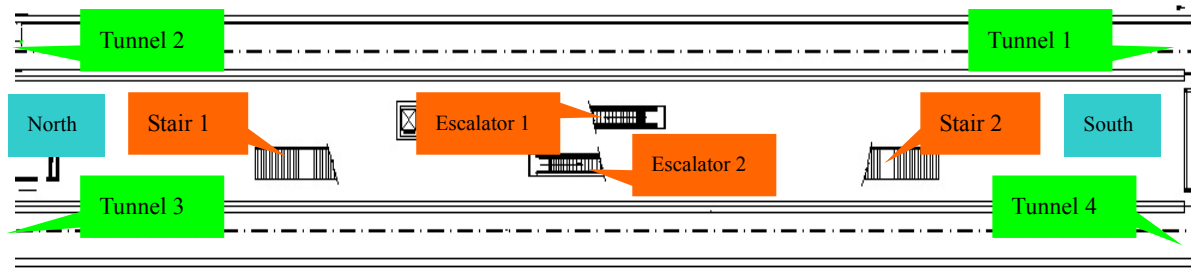


Fig.2. Layout of the platform

According to the design, the platform and the concourse were respectively divided into 2 separate smoke-proof divisions -A, B and C, D, with an area of 537m<sup>2</sup>, 560m<sup>2</sup>, 854m<sup>2</sup> and 856m<sup>2</sup> respectively. The concourse has exclusive exhaust ducts, arranged in two rows with a total of 52 outlets; the ventilator at the top of the platform, with 66 outlets in two rows, serves as a smoke exhauster for the public area. The exhaust ducts at the top of the two tracks, a total of 108 outlets with 54 outlets for each exhaust duct, also used to exhaust smoke. The main smoke-proof parameters of the station are shown in Table 1:

Table 1 Main parameters of smoke proof/exhaust design of the subway station

| Location       | Area of smoke-proof division ( m <sup>2</sup> ) |                        | Arrangement of exhausters, exhaust ducts and outlet |   |
|----------------|---|------------------------|---|---|
|                | smoke-proof division A                          | smoke-proof division B | Over platform                                       | Over tracks                             |
| Platform floor | 537m <sup>2</sup>                               | 560m <sup>2</sup>      | 2 rows of exhaust ducts<br>33×2 outlets             | 2 rows of exhaust ducts<br>54×2 outlets |
|                | 854m <sup>2</sup>                               | 856m <sup>2</sup>      | 2 rows of exhaust ducts<br>26×2 outlets             |   |

## 2.2 Test method

On-site tests can check the installation and operation of the smoke prevention/exhaust system of the subway, as well as the difference between the design and actual effects. In order to simulate the real circumstances of the fire, the test were carried out in 2 ways: one is to use smoke cake to produce smoke with industry alcohol auxiliary heating method to increase buoyancy of the smoke. The other is to use wood crib to simulate the actual fire with a certain scale.

Baggage fire commonly occurred in the concourse and platform of subway station. The average fire scale of the common luggage fire was determined as 200kW~400kW according to some related research report<sup>[2]</sup>. In order to obtain a better repeatability, wood crib fire was applied to simulate the actual fire of this scale.

Wood crib was prepared in accordance with national standard *Characteristics and tests for transportable fire extinguishers*(GB 8109-1987)<sup>[3]</sup>. Through the results of several different sizes of wood crib fire tests with large-scale calorimeter, the size of the wood crib used in the actual test was defined as: 500mm × 1300mm × 6-layers, the scale of the fire were 0.5MW ~ 0.7MW.

As the smoke produced by wood crib was relatively different from that produced in the actual fire, it wasn't able to get a good result in testing the performance of the station's smoke proof/exhaust system. Therefore, wood crib fire plus smoke cake methods was used in hot smoke test.

## 2.3 Contents of the full-scale test

According to the purpose of the test as well as the structure of the station, 3 scenarios (smoke-free,

cold smoke and hot smoke) were adopted at 2 areas- concourse and platform.

1 ) Performance test of ventilation status of the concourse and platform at normal condition: To test the performance of exhaust system and internal environmental status of subway station under normal condition;

2) Smoke-proof division test: in case of fire in platform/concourse, hot and cold smoke tests were carried out at typical locations such as the stair exit, escalator mouth, platform and concourse center so as to test the actual effects of the smoke-proof divisions and smoke-proof Facilities;

3) Cross-section wind speed measurement on the concourse and platform: in case of fire in platform/ concourse, hot and cold smoke tests were carried out at typical locations such as the stair exit, escalator mouth, platform and concourse center so as to observe the flow of gas and to measure continuously the cross-section wind speed of the stairs and the escalators;

### 3 Full-scale test of the station

#### 3.1 Concourse fire

##### 3.1.1 ventilation / smoke exhaust system operation mode of the station

In case of concourse fire, the station concourse’s ventilation / smoke exhaust system adopts the smoke exhaust mode, to stop air supply and exhaust the smoke of the concourse through the smoke tower to the ground. At the same time, the ventilation/smoke exhaust system adopts the wind blowing mode, so that smoke will not spread to the platform. the fresh air enter the concourse through the entrances/exits of the platform in order to facilitate the evacuation of passengers from the concourse to the ground. The smoke control method of the concourse is as shown in Table 2:

Table 2 smoke control mode in concourse fire

| Location of fire source | Exhausters in concourse |               | Exhausters in platform |                 | Exhausters above tracks |               |
|-------------------------|-------------------------|---------------|------------------------|-----------------|-------------------------|---------------|
|                         | Scenario                | Outlet number | Scenario               | Outlet number   | Scenario                | Outlet number |
| concourse               | Smoke exhaust           | 52            | Wind supplement        | 34 at south end | —                       | —             |

##### 3.1.2 Test results

In case of concourse fire, the main content of the test is the wind speed of the smoke outlet in the concourse. During the test, the wind speed of 5 different locations for each smoke outlet among 52 outlets was measured. After filtering and data processing, the average wind speed of the smoke outlets in concourse was 3.7m/s.

The dimension of smoke outlets in the concourse was 500mm × 500mm with deflection grilles. Its designed wind capacity was 5262m<sup>3</sup>/h. the average wind speed measured in the test was 3.7m/s, which was equivalent to the wind capacity of 3330m<sup>3</sup>/h (55.5 m<sup>3</sup>/min)-about 63% of the value of the design value. According to the actual construction area of the concourse (1710m<sup>2</sup>), the actual amount of smoke exhaust is calculated as (55.5m<sup>3</sup>/min × 52) / 1710 m<sup>2</sup> = 1.69 m<sup>3</sup>/m<sup>2</sup> min.

Test results showed that the smoke ventilation/smoke exhaust system designed for the concourse couldn’t meet the design requirements. The duct’s pressure loss and the fan performance were tested. Only to find that when the concourse’s ventilation/smoke exhaust system was switched to the fire mode, serious leakage occurred at valves and ducts, and the exhaust amount couldn’t meet the design requirements.

After the adjustment and improvement of the system, another test was carried out. The average wind speed of the concourse's smoke outlet increased to 4.04m/s; the air flow of a single smoke outlet is 3636m<sup>3</sup>/h (60.6 m<sup>3</sup>/min), which was about 70% of the value of the design. As a result, the smoke exhaust capacity of the concourse measured in the test was  $(60.6\text{m}^3/\text{min} \times 52) / 1710 \text{ m}^2 = 1.84 \text{ m}^3/\text{m}^2 \text{ min}$ , which still couldn't meet the design requirements.

### 3.1.3 Hot smoke test in case of concourse fire

In case of concourse fire, the hot smoke test was carried out. Figure 3 showed the smoke movement in the concourse during the hot smoke test.

According to the observation, the visibility in the concourse was less than 2m when the fire developed to its medium-term, which meant that the ventilation/smoke exhaust system behaved badly in fire. By improving the ventilation/smoke exhaust system, the smoke exhaust capacity was improved obviously, and the visibility reached to 5m. However, smoke at entrance/exit 1 gathered and settled due to the incompleteness of the entrance/exit, which led to poor air circulation.



Figure.3. smoke movement in concourse during hot smoke test (fire source at the center of the concourse)

## 3.2 Platform fire

### 3.2.1 ventilation / smoke exhaust system operation mode of the station

In case of platform fire, the ventilation / smoke exhaust system of the platform and the hot smoke exhauster at top of the tracks adopted smoke exhaust mode. The smoke in the platform was exhausted through the smoke tower to the ground. Fresh air entered the platform through the entrances/exits, concourse, and mouths between the concourse and platform. The smoke control method of the platform is shown in Table 3:

Table 3 Smoke control in platform fire

| Location of fire source | Exhausters at concourse |               | Exhausters at platform |               | Exhausters above tracks |               |
|-------------------------|-------------------------|---------------|------------------------|---------------|-------------------------|---------------|
|                         | Scenario                | Outlet number | Scenario               | Outlet number | Scenario                | Outlet number |
| platform                | —                       | —             | Smoke exhaust          | 66            | Smoke exhaust           | 108           |

### 3.2.2 Test results

In case of platform fires, the wind speed of the smoke exhaust outlets at the top of the platform and tracks was measured. The average wind speed of the smoke exhaust outlets above platform was 3.8m/s, the average wind speed of the smoke exhaust outlets above tracks was 1.65m/s.

500mm × 500mm double layer smoke exhaust outlets, with an designed air capacity of 5454.5m<sup>3</sup>/h, were used at the top of the platform. The average wind speed measured in the test was 3.8m/s, which was equivalent to the wind capacity of 3556.8m<sup>3</sup>/h (59.3 m<sup>3</sup>/min)-about 65% of the value of the design. According to the actual construction area of the platform (1097m<sup>2</sup>), the actual amount of smoke exhaust of the smoke exhauster at the top of the platform was calculated as (59.3m<sup>3</sup>/min × 66)/1097 m<sup>2</sup>=3.56 m<sup>3</sup>/m<sup>2</sup>·min.

500mm × 1000mm smoke exhaust outlets were used at the top of the tracks. The average wind speed measured in the test was 1.65m/s, which was equivalent to the wind capacity of 2970m<sup>3</sup>/h (49.5 m<sup>3</sup>/min) . The actual amount of smoke exhaust of the smoke exhauster at the top of the tracks was calculated as (49.5m<sup>3</sup>/min × 108)/1097m<sup>2</sup>=4.87 m<sup>3</sup>/m<sup>2</sup>·min.

In case of platform fire, downward wind speed was tested at different locations of the two stairs and two escalators. According to test results, the actual downward wind speed of stairs was between 0.82 m/s ~ 1.15 m/s.

**3.2.3 Cold and hot smoke test in case of platform fire**

In case of platform fire, cold smoke test was carried out at the centre of the platform, platform stairs, and the tunnel near the platform respectively. Figure 4 shows the smoke movement observed at the escalator when cold smoke released at the centre of the platform. Figure 5 shows the smoke movement observed at the stairs when cold smoke released at the stairs.



*Fig.4.* status at the mouth of the escalator under platform cold smoke test ( cold smoke source was in the center of platform )



*Fig.5.* status at the mouth of the escalator under platform cold smoke test ( cold smoke source was in the mouth of escalator )

According to the observation, regardless of locations of the smoke source, under the effect of the downward airflow at the stair and escalator mouths and the around retaining walls, smoke was not found spreading to the concourse from the stair and escalator mouths.

In case of platform fire, hot smoke test was carried out with the smoke source at the centre of the platform. Under the joint action of the downward airflow (0.82m/s ~ 1.15m/s) and the retaining wall at the mouths of the stairs and the escalators, no smoke spread from the platform to the concourse when hot smoke released at the maximum heat release rate of 0.5 ~ 0.7MW.

Through the cold and hot smoke tests, we can see that although the measured downward air flow speed at the stair mouths can not meet 1.5m/s, which is stipulated in the national standard "Code for Design of Metro" (GB50157-2003)<sup>[4]</sup>, the existing design achieves the desired results. The evacuation of passengers has been secured and the objectives of stopping the spread of smoke to the concourse through the mouths of the stairs and the escalators have been achieved.

Figure 6 and Figure 7 shows the smoke flow of the platform under the hot smoke test condition. We can see from them that the effect of the smoke-proof divisions divided by the retaining walls is not satisfactory. The entire platform has become one division. The reason for this phenomenon is that the retaining walls were not built above the tracks at the side of the platform, but only built along the centre of the platform.



*Fig.6.* hot smoke test: south end of platform  
( the hot smoke source was at the center of  
the platform )



*Fig.7.* hot smoke test: north end of platform  
( the hot smoke source was at the center of  
the platform )

#### 4 CONCLUSION

Through the systematic full-scale fire test, the newly built subway is able to meet basic requirement for safe evacuation of people in case of a fire. But there are still some problems that need to be further improved. For example, the closeness of the switching valve and ducts of the ventilation / exhaust system should be further dealt with, and the capacity of the smoke exhaust system should be improved; entrance 1 of the station should be constructed timely and be improved to ensure smooth flow of the air and avoid settlement and gathering of smoke; the smoke exhaust effect of the concourse and the smoke-proof division of the platform need to be improved, is necessary to build smoke retaining wall above the tracks near platform. In addition, it has been found from the test that in the existing “code for Design of Metro”, the value given for the smoke exhaust volume of platform is low while the downward wind speed at stair mouth is high. We suggest that those requirements should be adjusted.

#### REFERENCES

- [1] Tianjin Fire Research Institute, Case Study on Typical Subway/Tunnel Fire, *Research Report of Research project of the Ministry of Public Security*, 2003.
- [2] Tianjin Fire Research Institute, Experimental Study on Baggage Fires of Subway Passenger, *Research Report of 10<sup>th</sup> five-year plan of China*, 2006.
- [3] Ministry of Public Security of the P.R.China, GB 8109-1987: Characteristics and tests for transportable fire extinguishers, 1987.
- [4] Ministry of Construction of the P.R.China, GB 50157-2003: Code for Design of Metro, 2003.

## Experimental Study on Baggage Fires of Subway Passenger

Kan Qiang , Ni Zhaopeng

Tianjin Fire Research Institute, the Ministry of Public Security, Tianjin, P.R.China

### INTRODUCTION

Subway fire safety has been paid much attention to because of its special structure. There are many causes that result in subway fire, among which baggage fire in the platform and concourse is one of them. In order to find out the rule of baggage fire, typical baggage fire tests were carried out. Fire heat release rate curves of baggage fire were obtained so as to provide the basis for fire protection design of subway station.

### 1 BAGGAGE FIRE TEST

#### 1.1 Field survey

To ascertain the categories and the weights of subway passengers' baggage, field survey on Beijing Subway was carried out. The idiographic survey locations were subway stations of Beijing railway station and Xizhimen subway station. Questionnaires, baggage weighting and video recording were used to do the survey. Some survey results are as follows:

Table 1 average weights of passengers' baggage

| Subway station                             | Beijing railway station | Xizhimen subway station |
|--|-------------------------|-------------------------|
| average weight of passengers' baggages /kg | 3.9                     | 1.67                    |

Table 2 Categories and average weights of baggage in the subway station of Beijing railway station

| Categories of baggage | keister | satchel | plastic bag | briefcase | suitcase |
|-----------------------|---------|---------|-------------|-----------|----------|
| average weight /kg    | 1.22    | 3.01    | 2.5         | 2.49      | 6.37     |

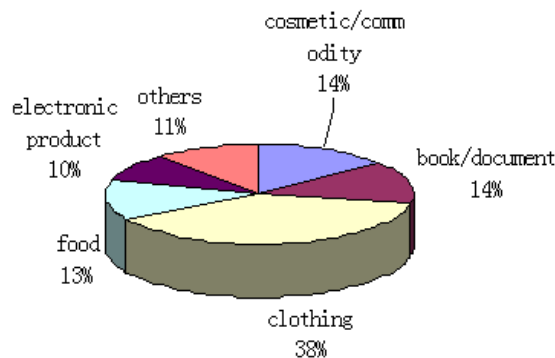


Fig.1. Categories of baggage

#### 1.2 Determination of categories and weight of baggage

Fire tests on shopping mall for clothing and shoes have been carried out in Tianjin Fire Research Institute<sup>[1]</sup>. One test was 5kg mixed quality clothing burning on the shelf. According to the test, the heat release rate reached the maximum 98.67kW when the clothing was ignited 251s later. The result proved that both 3.9kg -- average weight of the survey result of subway station of Beijing railway station and 1.67kg --average weight of the survey result of Xizhimen station could only cause small scale fire, which should be put out easily. The worst case would be fires caused by large baggage. Therefore, two kinds of baggage were considered. As shown in Table 3, 6.37kg was the average weight of suitcase; 11.00kg was the largest baggage in the survey.

Table 3 Categories and weights of baggage of the tests

| weight of a baggage ( kg ) | clothing ( kg ) | food ( kg ) | Electronic product ( kg ) | book/document ( kg ) | Cosmetic/commodity ( kg ) | other ( kg ) |
|----------------------------|-----------------|-------------|---------------------------|----------------------|---------------------------|--------------|
| 6.37                       | 2.42            | 0.83        | 0.64                      | 0.89                 | 0.89                      | 0.70         |
| 11.00                      | 4.18            | 1.43        | 1.10                      | 1.54                 | 1.54                      | 1.21         |

Different types of goods in baggage were identified as follows: ‘clothing’ were clothes made with different materials, mainly cotton clothing; ‘food’ was instant noodles and biscuits; ‘electronic product’ were demolition materials of obsolete computers; ‘book and document’ were books, newspapers, etc.; ‘cosmetics and commodity’ were sanitary towels. As ‘other’ items can not be precisely defined, so the synthetic bag was regard as other goods. If the weight of synthetic bag was less than the required weight, then clothing were added.

|   |  |   |
|---|--|---|
|  |  |  |
| clothing ( dress/bedsheet/cap )   | cosmetic/commodity(sanitary napkin)  | food(instant noodles)   |
|  |  |  |
| book/document(book/newspaper)   | electronic products (demolition materials of obsolete computers)                     | one baggage   |

Fig.2. Goods in Test

### 1.3 Test method

The ignition sources of the tests were cotton balls dipped with petrol. In the process of fire tests, the whole process of fire development was recorded. In some tests, fire sources were taken photos by infrared camera. Fire heat release rates were measured by large-scale calorimeter, temperatures around the fire source were measured by K-sheathed nickel chromium - nickel silicon thermocouples.



Fig.3. Large-scale calorimeter



Fig.4. Data acquisition instrument

A total of 6 group of tests were carried out. Scenarios were shown in Table 4. Forms of baggage's location of the tests were shown in Figure 5~Figure 7.

Table 4 Test scenarios

| NO.                       | 1A  | 2A   | 3A  | 1B                               | 2B  | 3B  |
|---------------------------|---|--|---|----------------------------------|---|---|
| Test equipment            | Large-scale calorimeter   |  |   |                                  |   |   |
| Pieces of baggage         | one piece of baggage ( 6.37kg )   | Two pieces of baggage (6.37kg for every baggage) | three pieces of baggage(6.37kg for every baggage) | one piece of baggage ( 11.00kg ) | two pieces of baggage(11kg for every baggage) | three pieces of baggage(11kg for every baggage) |
| goods in baggage          | categories and weights of goods in every baggage were determined according to Table 3 |  |   |                                  |   |   |
| placement                 | stack on shelves  |  |   |                                  |   |   |
| ignition sources          | cotton balls dipped with petrol   |  |   |                                  |   |   |
| place of ignition sources | clothing in the baggage   | clothing in any of the baggage                   | clothing in the middle baggage                    | clothing in the baggage          | clothing in any of the baggage                | clothing in the middle baggage                  |



Fig.5. Test 1A/1B

Fig.6. Test 2A/2B

Fig.7. Test 3A/3B

## 2 TEST RESULT ANALYSIS

### 2.1 Test result of series A

A total of 3 groups of tests were carried out in series A tests. The main measurement data were shown in Table 5.

Table 5 Test result of series A

| Test NO. | Maximum heat release rate(kW ) | Time of the heat release rate reached the maximum(s) | Maximum temperature ( ) | Time of the temperature reached the maximum(s) |
|----------|--------------------------------|--|-------------------------|--|
| 1A       | -                              | -  | 60                      | 228  |
| 2A       | 196                            | 392  | 81                      | 454  |
| 3A       | 324                            | 408  | 152                     | 342  |

Note: Because the weight of baggage in Test 1A was light, the heat release rate was less than the measuring range of large-scale calorimeter, exact measurement result was not gained.

Figure 8 showed the heat release rate curves of Test 2A and Test 3A. It showed that the maximum heat release rate of Test 3A was 1.65 times of that of Test 2A. The fire growth rate of Test 3A was more or less the same as the slow speed  $t^2$  fire, while the fire growth rate of Test 2A was more or less the same as the medium speed  $t^2$  fire at the first 140s, but it decreased after 140s. When the heat release rate of two groups of tests reached their peak values respectively, peak value of Test 2A lasted for a longer time than that of Test 3A. The time of the heat release rate of Test 2A reached its maximum heat release rate was almost the same as that of Test 3A. Test 3A lasted slightly longer than Test 2A.

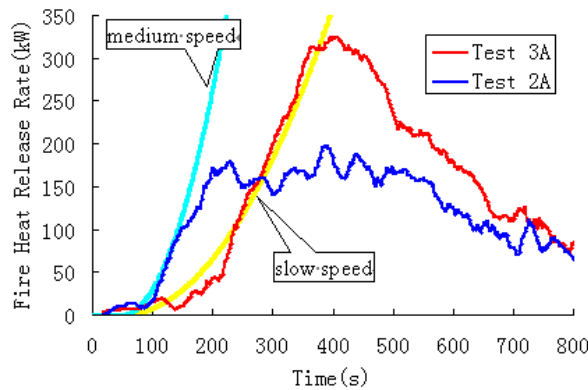


Fig.8. Comparison of heat release rate curve of test series A

## 2.2 Test result of series B

A total of 3 groups of tests were carried out in series B tests. The main measurement data were shown in Table 6.

Table 6 Test result of series B

| Test NO. | Maximum heat release rate(kW ) | Time of the heat release rate reached the maximum(s) | Maximum temperature ( ) | Time of the temperature reached the maximum(s) |
|----------|--------------------------------|--|-------------------------|--|
| 1B       | 250                            | 326  | 157                     | 247  |
| 2B       | 262                            | 381  | 119                     | 501  |
| 3B       | 356                            | 570  | 207                     | 690  |

From Table 6, although the number of baggage of Test 2B was more than that of Test 1B, but the maximum temperature of 2B tests was less than that of Test 1B, which may be caused by the location of the baggage. In Test 1B, a piece of baggage was just under a thermocouple, so the temperature measured by that thermocouple was higher; In Test 2B, two pieces of baggage were put

in the bottom of both sides of a thermocouple, and the location of those two pieces of baggage had a certain angle with other thermocouples, so the temperature measured by that thermocouple was lower.

Figure 9 showed the heat release rate curves of 3 groups of tests of series B. The maximum heat release rate of Test 2B and Test 3B were 1.05 times and 1.42 times of that of Test 1B respectively. The fire growth rate of Test 1B and 2B were between slow and medium speed  $t^2$  fire. The fire growth rate of Test 3B was less than slow speed  $t^2$  fire. However, with the full combustion of the fuel, the fire growth rate of Test 3B was faster than that of Test 1B and Test 2B.

In Test 1B, 2B and 3B, the time of the heat release rate reached their maximum values lagged one after another. When the heat release rate of Test 1B reached the maximum value, it decreased rapidly. While Test 2B and Test 3B fire lasted longer because the number and weight of the baggage was more than that of the Test 1B. The duration of Test 3B was the longest.

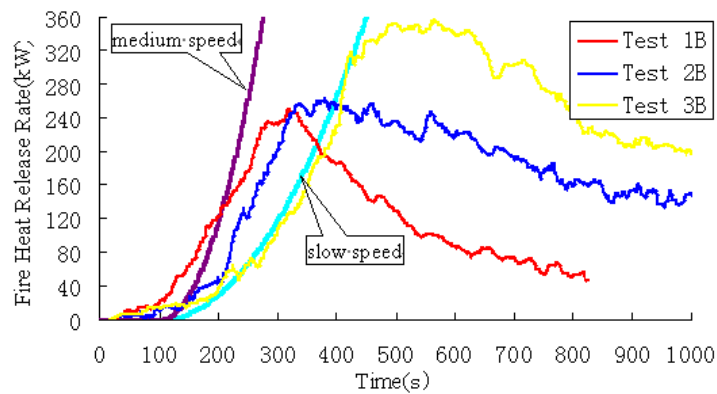


Fig.9. Comparison of heat release rate curve of test series B

### 2.3 Comparison of test results of Series A and Series B

The test conditions of Test 2A and Test 2B, Test 3A and Test 3B, including the number of baggage, the categories of goods and the location of baggage were the same respectively, only the weight of individual baggage was different. Figure 10 and 11 showed the heat release rate curves of Test 2A and Test 2B, Test 3A and Test 3B respectively. Figure 10 showed that the heat release rate curves of Test 2A and Test 3A were very similar, not only in the growth stage but also in the decay stage. Figure 11 showed that the overall trend of heat release rate curves of Test 3A and Test 3B was similar. Compared Test series A with Test series B, the maximum heat release rate of Test series B was bigger. The maximum heat release rate of Test 2B was 1.34 times of that of Test 2A. While the maximum heat release rate of Test 3B was 1.10 times of that of Test 3A. The time of heat release rate of Test series B to reach its peak value was a little later than that of Test series A.

Compared Figure 10 with Figure 11, the similarity degree of the heat release rate curves of Test 3A and Test 3B was less than that of Test 2A and Test 2B. Furthermore, the difference between the maximum heat release rate of Test 3A and that of Test 3B was not obvious. This may be caused by the fact that the number and weight of baggage in 3A and 3B was more than that in 2A and 2B and the combustion was inadequate.

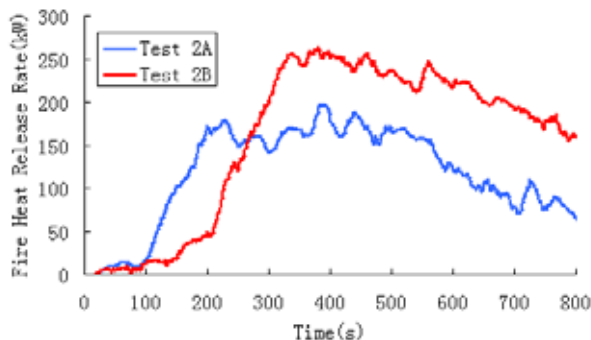


Fig.10. Comparison of heat release rate curves of Test 2A and Test 2B

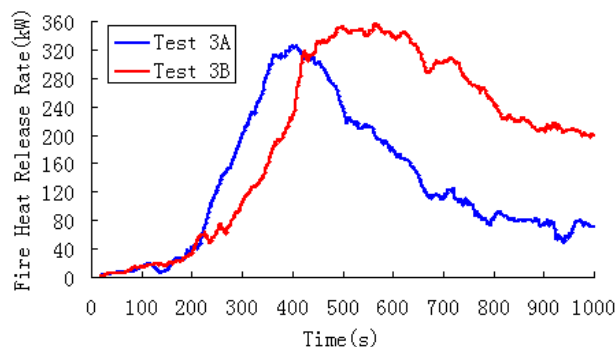


Fig.11. Comparison of heat release rate curves of Test 3A and Test 3B

### 3 CONCLUSION

The tests proved that ordinary baggage fire scale is 200kW~400kW. Ordinary baggage fire growth rate is between slow and medium speed  $t^2$  fire. In practice, baggage fire growth rate is identified as medium speed fire due to uncertainties.

When using fire simulation software to evaluate building fire safety, heat release rate is an important input parameter. In order to make sure that the evaluate result is reliable and conservative, the chosen heat release rate should consider the worst case. In reality, baggage in the subway station scatters around without piling up. The worst condition is that one baggage ignites 4 pieces of baggage around it at the same time. The test results show that the maximum heat release rate of the single 11Kg baggage was 250kW. The time of one piece of baggage ignites the adjacent baggage was 57s~127s. Based on the fire heat release rate curve of the 11Kg baggage, the assumption is that one piece of baggage ignites 4 pieces of baggage around it at the same time 57S later. Then the heat release rate curve can be obtained, as shown in Figure 12. Based on Figure 12, the maximum heat release rate is 1.2MW. Considering the safety factor, the maximum baggage fire heat release rate used in subway fire safety evaluation can be defined as 1.5MW. Of course, in other building fire safety evaluation, fire design should consider the fire heat release rate curve gained by test, together with the spatial distribution of baggage in buildings.

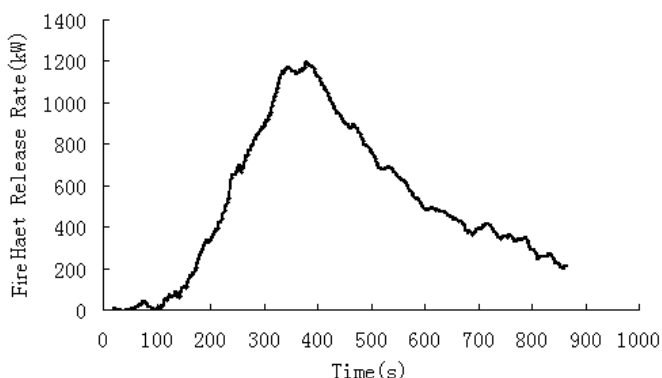


Fig.12. Heat release rate curve of subway baggage fire

### REFERENCES

[1] Tianjin Fire Research Institute, Study on Large-scale Underground Shopping Mall Fire , *Research Report of 9<sup>th</sup> five-year plan of China*, 1999.

## NUMERICAL SIMULATION ON VERTICAL FIRE SPREAD Effects of Wall Pier and Overhanging Eave in Preventing Vertical Fire Spread

Huang Xin, Ni Zhaopeng, Lu Shichang

Tianjin Fire Research Institute, the Ministry of Public Security, Tianjin, P.R.China

### INTRODUCTION

Building with French windows has the advantages of brightness, wide view and beautiful appearance. Nowadays this kind of structure has been applied in many commercial and residential buildings. However, exterior windows in adjacent stories in this kind of buildings are too close and the fire can spread easily to upper stories.

In order to prevent the fire from spreading vertically through the exterior openings, the minimum height of wall pier is required in the related codes of many countries. NFPA 5000 and *International Building Code* require that openings in exterior walls in adjacent stories shall be separated vertically at least 3 feet (914mm) by spandrel girders, exterior walls or other similar assemblies that have a fire-resistance rating of at least 1 hour<sup>[1,2]</sup>. Hong Kong's Code also prescribes that there should be a wall pier with height not less than 900mm between the top of one window and the bottom of the next window above. Chinese code requires that an annexed solid non-combustible wall with height not less than 800mm shall be constructed at the outer edge of each floor slab where there is no wall between two windows in vertical directions and a wall pier with height not less than 800mm shall be built up on the upper portion over the opening on the exterior wall of residential buildings<sup>[3,4]</sup>. However, some kinds of buildings such as buildings with French windows can not satisfy these requirements.

If the wall pier is too short, fire resistant overhanging eave can be built up to replace wall pier for protecting against fire spread on the exterior of the buildings. NFPA 5000 and *International Building Code* require that the overhanging eave should extend horizontally at least 30 inches (762mm) beyond the exterior wall<sup>[1,2]</sup>. Chinese code requires that the width of overhanging eave should not below 500mm for residential building<sup>[4]</sup>.

Different countries have different requirements for wall pier and fire resistant overhanging eave. In order to study the effects of wall pier and fire resistant overhanging eave in preventing vertical fire spread, computational fluid dynamics (CFD) simulation was performed and typical office fire scenarios, hotel fire scenarios and shop fire scenarios were designed.

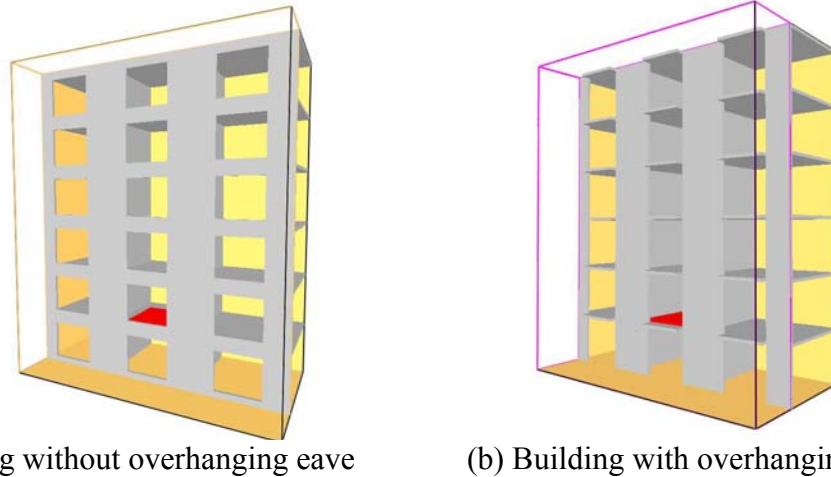
## 1 FDS MODEL SET-UP

### 1.1 Physical model

CFD simulations were carried out with fire dynamics simulator (FDS), a software package released by the National Institute of Standards and Technology (NIST), USA. It is now a popular CFD tool in fire related researches that describe the flow of smoke and hot gases from a fire. The recent version of FDS 4.0.7 released in March, 2006 was used.

Office fire, hotel fire and shop fire were chosen as simulated objectives. The basic outline of the simulated building is shown in *Fig.1*. The simulated building had six stories. Each storey was 3.4m high and had three rooms. Each room was 6m×6m and had one 3m wide window. The height of the window was changed with the wall pier. The heights of the simulated wall piers ( $H$ ) were 0.2m, 0.4m, 0.6m, 0.8m, 1.0m and 1.2m, respectively. Both the floor and the side wall were 0.2m thick. There was only a floor between windows in adjacent stories in the simulated building with fire resistant overhanging eave. The widths of the fire resistant overhanging eaves ( $W$ ) were 0.2m, 0.4m, 0.6m, 0.8m, 1.0m and 1.2m, respectively. The fire source was 4m×4m being set in the middle room of the second

storey. The simulation domain was 18m×9m×21.6m. All grids were 0.2m×0.2m×0.2m.



(a) Building without overhanging eave (b) Building with overhanging eave

Fig.1. 3D view of the simulated building (all windows were open)

The simulation adopted the following parameters: ambient temperature (23 °C), no wind, concrete side wall and floor, glass window and wood crib fuel. Time for the simulation of all cases ( $t$ ) was 1200s.

## 1.2 Design fire

The office fire, hotel fire and shop fire were all set as  $t$ -squared fires (the heat release rate is assumed to be proportional to the square of the elapsed time). The fire growth coefficients of office fire, hotel fire and shop fire were all set as  $0.05\text{kW/s}^2$  by referring to the experiments results of the office fire tests and sofa fire tests performed by NIST<sup>[5,6]</sup> and the clothes fire tests performed by Tianjin Fire Research Institute<sup>[7]</sup>.

NFPA 92B recommends that the heat release rate per unit area of office fire, hotel fire and shop fire be  $290\text{kW/m}^2$ ,  $249\text{kW/m}^2$  and  $568\text{kW/m}^2$  respectively<sup>[8]</sup>. SNZ PAS 4509 recommends that the heat release rate per unit area of office fire and shop fire be  $250\text{kW/m}^2$  and  $500\text{kW/m}^2$  respectively<sup>[9]</sup>. In our FDS model, the heat release rate per unit area of office fire and hotel fire were both set as  $250\text{kW/m}^2$  and the heat release rate per unit area of shop fire was set as  $500\text{kW/m}^2$ . Therefore, the maximum fire sizes of office fire and hotel fire were 9MW and the maximum fire size of shop fire was 18MW.

## 2 SIMULATION RESULTS

### 2.1 Effects of wall pier

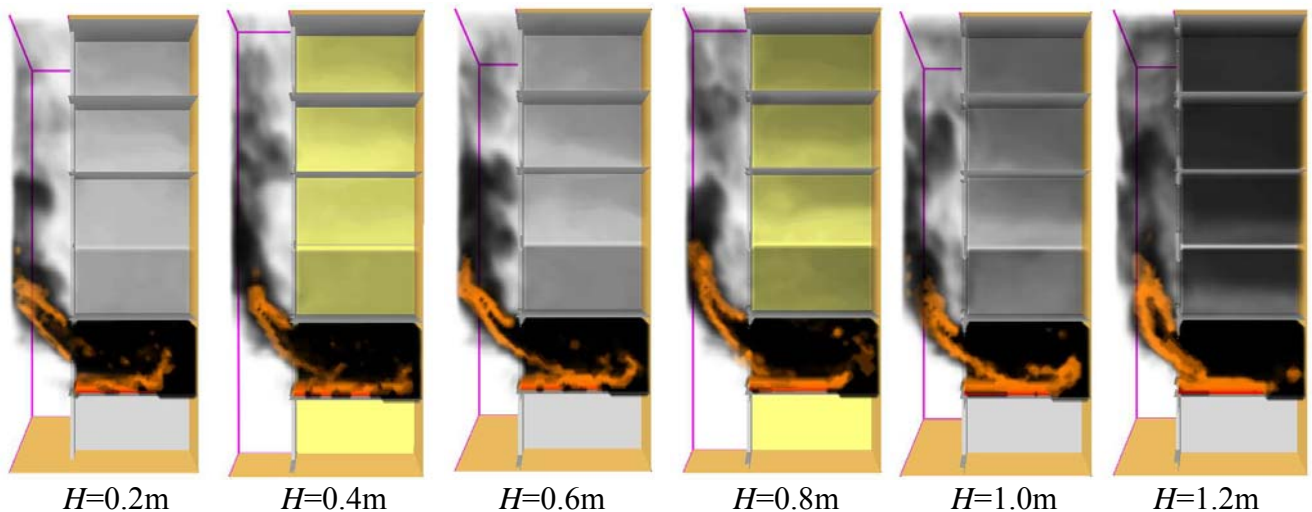


Fig.2. Smoke and fire spread profile (all windows were open, 9MW fire,  $t=1200\text{s}$ )

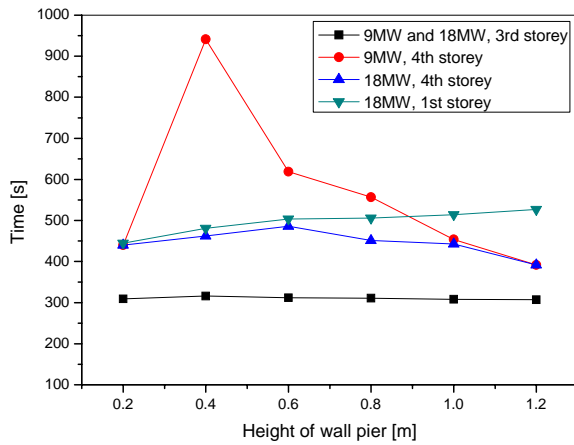


Fig.3. Time to reach 10kW/m<sup>2</sup> at the openings

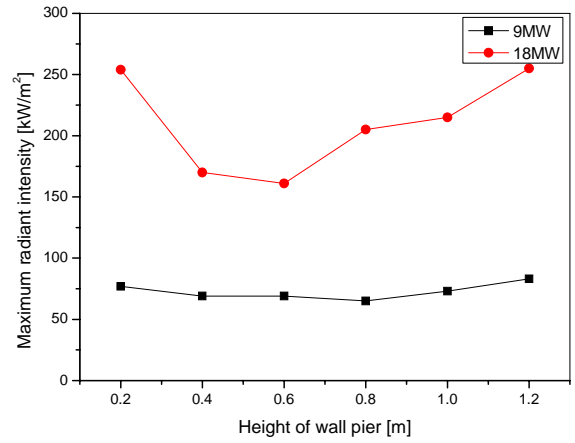


Fig.4. Maximum radiant intensity at the middle opening of the 3rd storey

Fig.2. — Fig.4. show the simulation results of the wall piers at different heights with all windows open. After the fire was ignited, the smoke flew out of the fire room with a radial velocity and there was a certain distance between the outside smoke and the exterior wall. The flame also stretched out of the window when the fire was big enough and an angle was formed by the flame and the exterior wall. Since all the windows were open, smoke flew into the rooms at upper stories.

Fig.3. shows the times to reach 10kW/m<sup>2</sup> radiant intensity at the openings at different heights of wall pier. 10kW/m<sup>2</sup> is the minimum radiant intensity to ignite combustibles like thin curtain<sup>[10]</sup>. The radiant intensity at the openings of the 3rd and the 4th storey could reach 10kW/m<sup>2</sup> in both 9MW and 18MW fire and that of the 1st storey could also reach 10kW/m<sup>2</sup> in 18MW fire. The openings of the non-fire stories were further away from the fire room with increasing the height of wall pier. Therefore, the radiant intensity would decrease with the height of wall pier increased within a certain range. As shown in Fig.3, the time at which radiant intensity of the 1st storey reach 10kW/m<sup>2</sup> was prolonged by an increase in the height of wall pier. However, increasing the height of wall pier would induce the outside smoke and the flame closer to the exterior wall at the same time and the radiant intensity at the openings of the upper stories would reach 10kW/m<sup>2</sup> faster. Fig.2 also shows that the soot density inside the middle rooms of the upper stories would increase with the increases in the height of wall pier because the outside smoke was closer to the exterior wall. As shown in Fig.4, the maximum radiant intensity at the middle opening of the 3rd storey first decreased and then increased with the increase in the height of wall pier. The simulation results showed that the optimum heights of wall pier were 0.4m and 0.6m for 9MW and 18MW fire respectively if windows were open. Generally speaking, wall pier could not prevent vertical fire spread effectively with windows open.

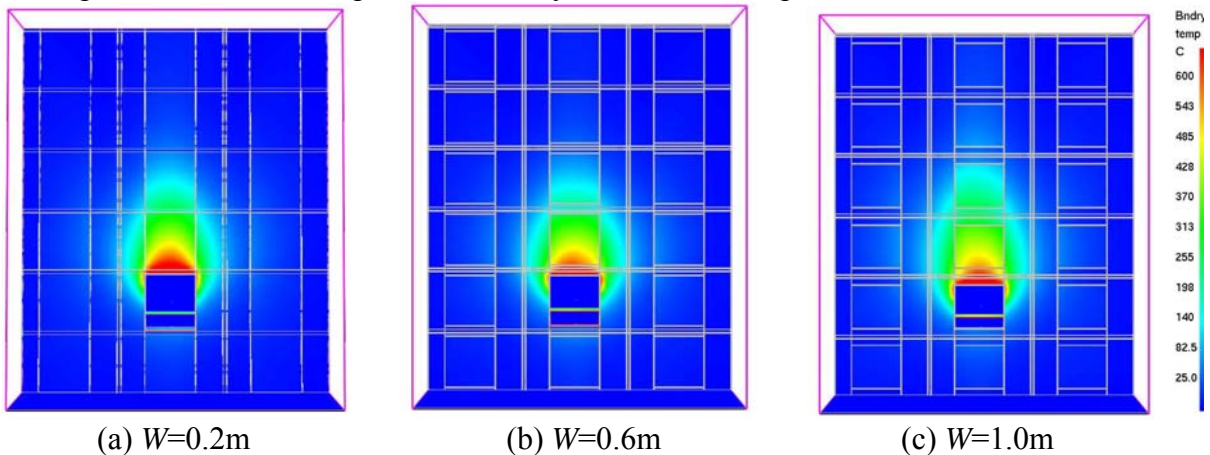


Fig.5. Temperature profile at the windows (all windows were close, 18MW fire,  $t=1200s$ )

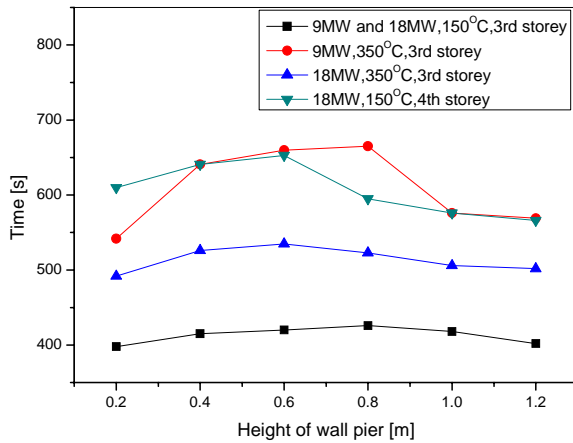


Fig.6 Time to reach 150°C or 350°C at the windows

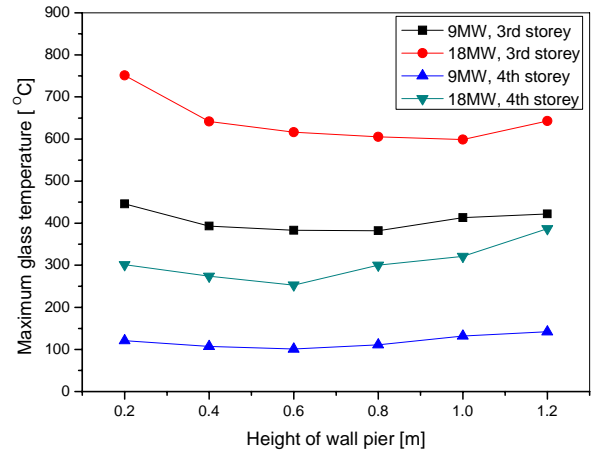


Fig.7. Maximum glass temperature at the middle windows of the 3rd and 4th storey

Fig.5.—Fig.7. show that the simulation results of the wall piers at different heights with all windows close. Fig.5 shows that the temperature on the portion closer to the fire of the windows was higher. With increasing the height of wall pier, the maximum temperatures at the exterior side of the windows first decreased and then increased. The maximum temperature at the middle window of the 3rd storey was lowest when the heights of wall pier were 0.8m and 1.0m for 9MW and 18MW fire respectively. However, for both 9MW and 18MW fire, when the heights of wall pier were 0.6m, the maximum temperature at the middle window of the 4th storey was lowest. And in larger fires, the influence of the wall pier on the maximum temperature was more prominent.

Fig.6. shows the time to reach 150°C and 350°C on the exterior side of the middle windows at different heights of wall pier. 150°C and 350°C are breaking temperatures for plain glass and tempered glass respectively<sup>[11]</sup>. The simulation results showed that the radiant intensity has reached 10kW/m<sup>2</sup> when the glass temperature reached the breaking temperature. That is, if the window broke, the fire would be able to spread into the room. In 9MW fire, only the temperature at the middle window of the 3rd storey could reach 150°C. In 18MW fire, only the temperature at the middle window of the 3rd storey could reach 350°C and that of the 4th storey could reach 150°C. The time at which the temperatures on the exterior side of the windows reached to 150°C and 350°C were first increased and then decreased by the increase in the height of wall pier. The simulation results showed that the optimum heights of wall pier were 0.8m and 0.6m for 9MW and 18MW fire respectively if windows were close. Increasing the height of wall pier also could not prevent vertical fire spread effectively with windows close.

## 2.2 Effects of fire resistant overhanging eave

Fig.8.—Fig.10. show that the simulation results of the overhanging eaves at different widths with all windows open. The results showed that fire resistant overhanging eave could prevent vertical fire spread effectively. With the overhanging eave, the fire could not spread to the 4th storey for 9MW fire and to the 1st storey for 18MW fire by radiation. Fig.9 shows that the time at which radiant intensity of the 3rd and 4th storey reached 10kW/m<sup>2</sup> increased with an increase in the width of overhanging eave. When the width of overhanging eave increased to 0.8m, the fire could not spread to the 4th storey for 18MW fire. Fig.10 shows that the maximum radiant intensity at the middle opening of the 3rd storey decreased with an increase in the width of overhanging eave, while the decreasing rate was slower if the width was larger. And the effects of the overhanging eave were better for larger fire size. However, too wide overhanging eave would reduce the radial velocity of the smoke when it flew out of the fire room since the overhanging eave would obstruct the upward movement of the smoke. Therefore, increasing the width of overhanging eave would make the smoke flow into the middle rooms of the

upper stories easily and the soot densities and room temperatures in these rooms were higher as shown in Fig.8.

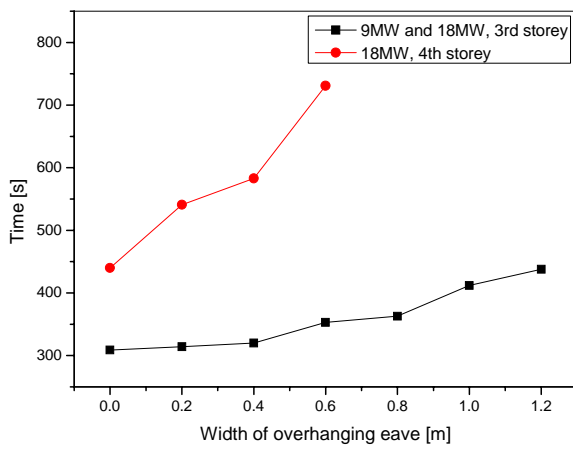
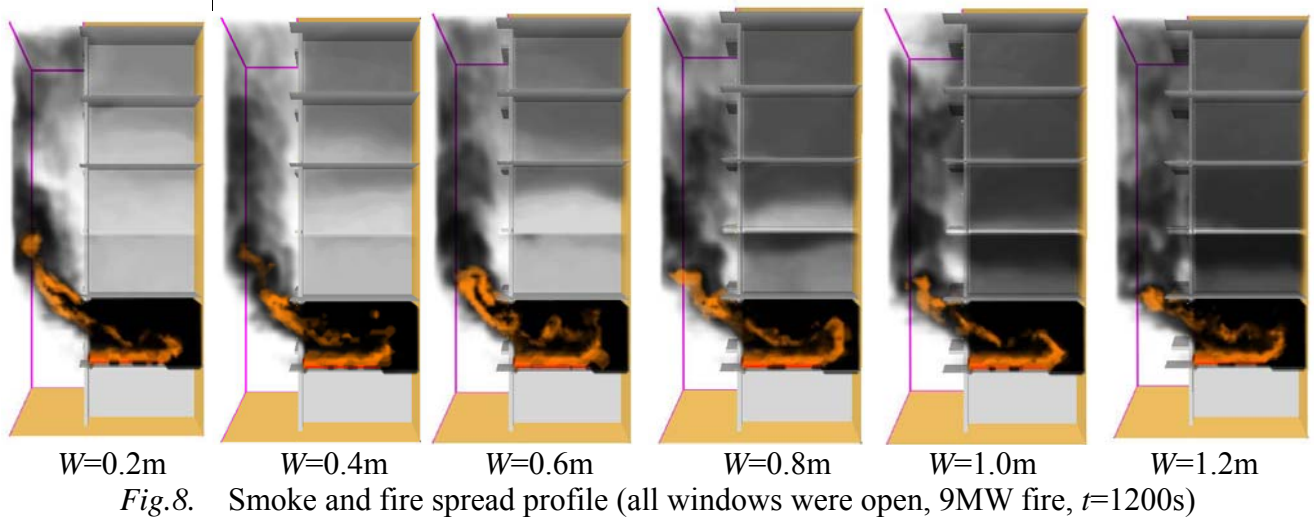


Fig.9. Time to reach  $10kW/m^2$  at the openings

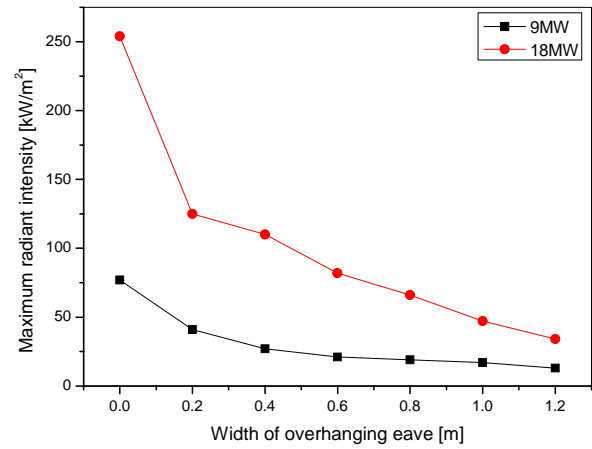


Fig.10. Maximum radiant intensity at the middle opening of the 3rd storey

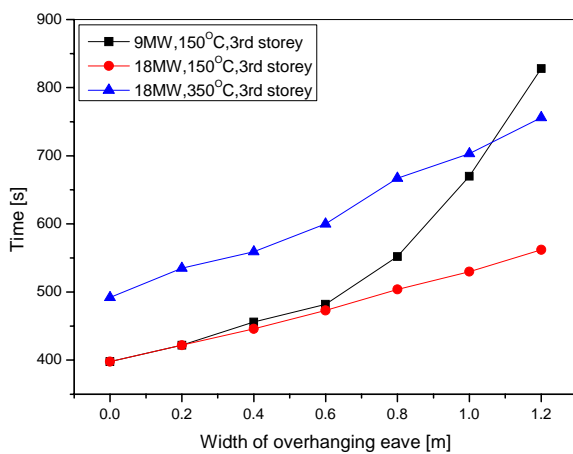


Fig.11 Time to reach  $150^{\circ}C$  or  $350^{\circ}C$  at the windows

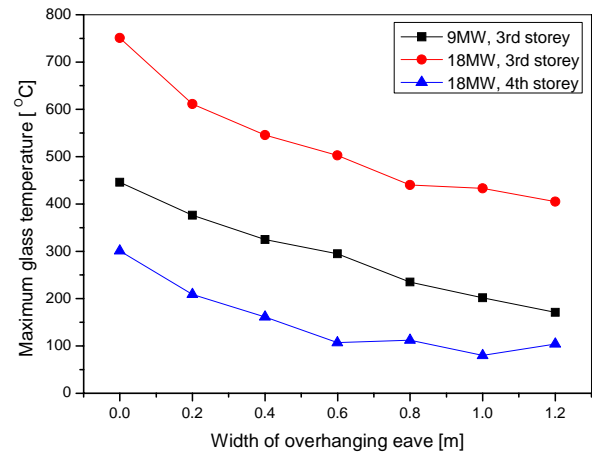


Fig.12. Maximum glass temperature at the middle windows of the 3rd and 4th storey

*Fig.11.* and *Fig.12.* show that the simulation results of the overhanging eaves at different widths with all windows close. With the overhanging eave, only the temperature at the middle windows of the 3rd storey could reach 150°C for 9MW fire and reach 350°C for 18MW fire. When the width of overhanging eave increased to 0.4m, the temperature at the middle windows of the 3rd storey was below 350°C. When the width of overhanging eave increased to 0.6m, the temperature at the middle windows of the 4th storey was below 150°C. *Fig.11.* shows that the time at which the temperatures on the exterior side of the windows reached to 150°C and 350°C increased with the increase of the width of overhanging eave. The maximum temperature at the middle window of the 3rd storey was decreased by an increase in width of the overhanging eave. However, the maximum temperature at the middle window of the 4th storey increased slightly when the width of overhanging eave increased from 1.0m to 1.2m. The reason was that too wide overhanging eave blocked the smoke movement and made the smoke get together under the overhanging eave. Then the temperature at the upper portion of the window increased.

### 3 CONCLUSIONS

CFD simulations were carried out to study the effects of wall pier and fire resistant overhanging eaves in preventing vertical fire spread. The fires at 9MW and 18MW were set to represent the typical office fire, hotel fire and shop fire. The simulation results show that increasing the height of wall pier has little effects on preventing vertical fire spread. There is an optimum height of wall pier for different fire scenarios. Excessive increasing the height of wall pier will induce the outside smoke and flame closer to the exterior wall and make the fire spread vertically easily. The fire resistant overhanging eave has a much better effect on preventing fire from spreading vertically than wall pier. Increasing the width of fire resistant overhanging eave will reduce vertical fire spread. However, too wide overhanging eave will obstruct the upward movement of the smoke and make more smoke flow into the room in the upper stories through the openings.

### REFERENCES

- [1] National Fire Protection Association. NFPA 5000: Building Construction and Safety Code, 2006.
- [2] International Code Council, 2006 International Building Code, *ICC Inc*, 2005.
- [3] Ministry of Construction of the P.R.China, GB 50016-2006: Code of Design on Building Fire Protection and Prevention, 2006.
- [4] Ministry of Construction of the P.R.China, GB 50368-2005: Residential Building Code, 2005.
- [5] Thomas J.O., George W.M., Fire Tests of Single Office Workstations, *National Institute of Standards and Technology Report NIST-NCSTAR-1-5C*, 2005.
- [6] National Institute of Standards and Technology, Sofa Fire, <http://www.fire.nist.gov/fire/fires/sofa/>
- [7] Tianjin Fire Research Institute, Fire Risk Analysis and Assessment, *Research Report of 10<sup>th</sup> five-year plan of China*, 2004.
- [8] National Fire Protection Association. NFPA 92B: Guide for Smoke Management Systems in Malls, Atria, and Large Areas, 2000.
- [9] Standards New Zealand, SNZ PAS 4509: New Zealand Fire Service Fire Fighting Water Supplies Code of Practice, 2003.
- [10] Bukowski, R.W., Clarke, F.B., Fire Risk Assessment Method: Description of Methodology, *National Fire Protection Research Foundation*, 1990.
- [11] Hadjisophocleous, G.V., Benichou, N., and Tamim, A.S., Literature Review of Performance-Based Fire Codes and Design Environment, *Journal of Fire Protection Engineering*, 9(1): 12-40.

## **DECREASE IN FIRE LOAD ON STRUCTURES BY TIMELY FIRE DETECTION**

Aleš Dudáček <sup>a</sup>

<sup>a</sup> VŠB – Technical University of Ostrava, Faculty of Safety Engineering, Ostrava, Czech Republic

### **INTRODUCTION**

One way of increasing fire safety in buildings is the use of fire safety devices (henceforth referred to as FSD). The basic division of them is presented in Decree No. 246/2001 Coll. of Ministry of the Interior. The fire safety devices that are of key importance to an increase in fire safety are listed in Section 4 of the above-mentioned Decree and are designated as reserved kinds of fire safety devices. Depending upon function and purpose, some reserved fire safety devices influence directly the course of a fire (e.g. fixed fire fighting systems) and can be used, in the framework of dealing with fire safety in buildings, for fire risk reduction. However, in a case of the devices that do not have any direct influence on the course of a fire, the installation of these devices cannot lead to fire risk reduction. But the use of such devices can be a condition for including another fire risk reducing coefficient into calculations (e.g. the use of fire detection and alarm system (FDAS) is a condition for including the reducing coefficient for fire brigade intervention into calculations). Timely fire detection and alarm are also of great importance to the evacuation of persons, and shortening the time to evacuation thanks to the timely raising of the alarm by the FDA system makes it possible, e.g. to extend unprotected escape routes. The fast intervention of fire brigades, the use of fixed fire fighting systems and smoke and heat exhaustion systems have direct effects on the course of a fire in space, and thus also on thermal load on structures. The obvious condition is the reliable function of fire safety devices and their correct design and installation. In the text below the analysis of function of fire detection and alarm system (FDAS), fixed fire fighting system (FFS) and smoke and heat exhaustion system (SHES) in the course of fires in the Czech Republic in the years 2006 and 2007 will be provided and the influence of SHES on the course of a fire will be shown by means of software for fire modelling.

### **1 ANALYSIS OF THE FUNCTION OF SELECTED FIRE SAFETY DEVICES IN THE COURSE OF FIRES IN THE CZECH REPUBLIC**

The Ministry of the Interior – General Directorate of Fire and Rescue Service of the Czech Republic keeps the national statistics on fires and other incidents (Statistical Observation of Events – SOE) [2], in which fire brigades intervened. This statistical observation of events provides valuable data for the analysis of fires, the causes of fires and the courses of fires, and can also be used for the analysis of function of selected fire safety devices during the fires.

The main objective of use of FDASs is shortening the time to fire discovery, notification and acceptance of other needed measures. On the basis of data from SOE in the period from 1997 to 2003, a comparison between the time to fire discovery and the time to fire notification to the emergency call centre in the case of correct function of FDAS and without the influence of FDAS on these times was carried out [1]. The influence of automatic fire detection on the shortening of the time to fire discovery in buildings, which is taken into account when considering fire alarm application, i.e. buildings of classes 1, 2, and 3 from the point of view of ID, can help us to get a better picture. On the basis of data on times to fire discovery and receiving the emergency call, distribution functions of times to discovery (Fig. 1) and to

receiving the emergency call (Fig. 2) in cases without FDAS influence and in cases, when FDAS fulfilled its function in fire detection were created for these classes of buildings. The FDAS influence on the increase in the number of fires discovered, or reported shortly after their origin is clear from Figs. 1 and 2.



*Fig. 1.* Distribution functions of times to discovery

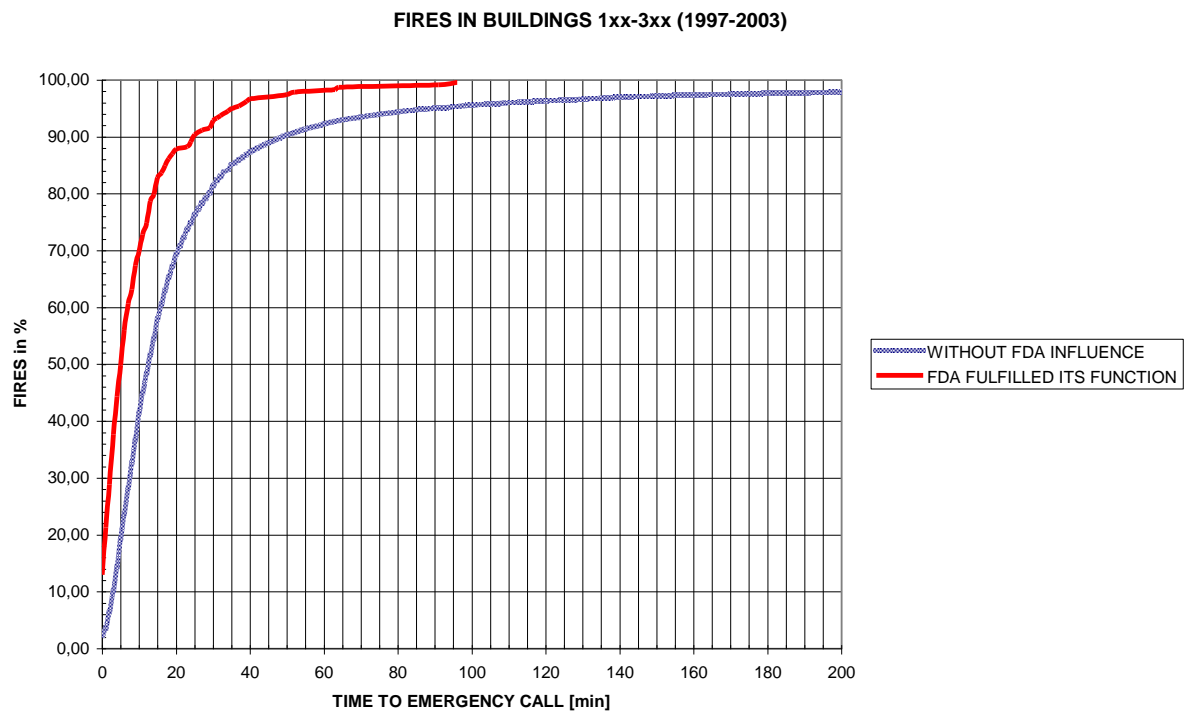


*Fig. 2.* Distribution functions of times to receiving the emergency call

## 1.1 Overview of Fires in the Years 2006 and 2007

On the basis of statistical data on SOE, the analysis of function of fire detection and alarm system (FDAS), fixed fire fighting system (FFS), combustible gas and vapour detection system (CGVDS) and smoke and heat exhaustion system (SHES) during the fires in the Czech Republic in the years 2006 and 2007 was made. For the analysis, only fires in buildings relevant for the use of mentioned fire safety devices were considered; according to the SOE code-list, it was the case of buildings of 1xx, 2xx, 3xx, 4xx, 530, 531, 550, 552, 554, 555, 556, 557 and 992 classes. A basic overview of fires in the given buildings in the years 2006 and 2007 is presented in Table 1.

Table 1. Overview of selected fires in the years 2006 - 2007

|  | YEAR   |        |
|--|--------|--------|
|  | 2006   | 2007   |
| Total number of fires in the Czech Republic                                | 20 540 | 22 394 |
| Number of fires in buildings of selected classes                           | 5 491  | 5 532  |
| Number of members of Integrated Emergency System killed in selected fires  | 0      | 0      |
| Number of members of Integrated Emergency System injured in selected fires | 116    | 110    |
| Number of persons killed in selected fires                                 | 86     | 60     |
| Number of persons injured in selected fires                                | 471    | 542    |
| Number of persons rescued from selected fires                              | 352    | 409    |
| Number of persons evacuated in the course of selected fires                | 3 082  | 3 055  |

Thus, approximately one quarter of all the fires (26.7% in 2006 and 24.7% in 2007) in the years 2006 and 2007 occurred in buildings relevant to the use of selected fire safety devices; nevertheless, the proportions of killed and injured persons in the total number were markedly higher.

## 1.2 Function of Selected FSDs in the course of Fires

As for fires in buildings of the above-mentioned selected classes, the function of FDAS, FFS, CGVDS and SHES was observed. For clarification, the function of each system was merely divided into two categories – the device fulfilled the task or the device did not fulfil the task in the fire, although it had been installed in the building. Into the category, when FSD did not fulfil the task in the fire, cases of installations of the device outside the space of fire origin, cases of device failure, device switching off and cases when the functional device did not respond to the fire (also the release of combustible gases and vapours) were included. An overall overview of function of selected FSDs in the fires is provided in Fig. 3. From the figure, it is evident that only in FDASs, the proportion of cases when the system fulfilled the task is markedly higher than the proportion of cases when the system did not fulfil the task in the fire. In the other FSDs, differences are not obvious so much; in FFSs and SHESs, cases when the device did not fulfil the task in the fire prevailed in both the years. Here it is necessary to state that the most frequent cause for the not fulfilment of the task in the fire was the installation of the device outside the space of fire origin. Non-functionality in the fire was found out in five EDASs, four FFSs and three SHESs. In one case, technically functional FDAS and also in one case, technically functional FFS did not respond to fire origin. On the basis of Fig. 3, it is also possible to state that in the year 2007, in the case of all selected FSDs the FDS number in fire-affected buildings was reduced. This should be evaluated, with regard to the positive influence of FSDs on the reduction of fires and fire consequences, negatively.

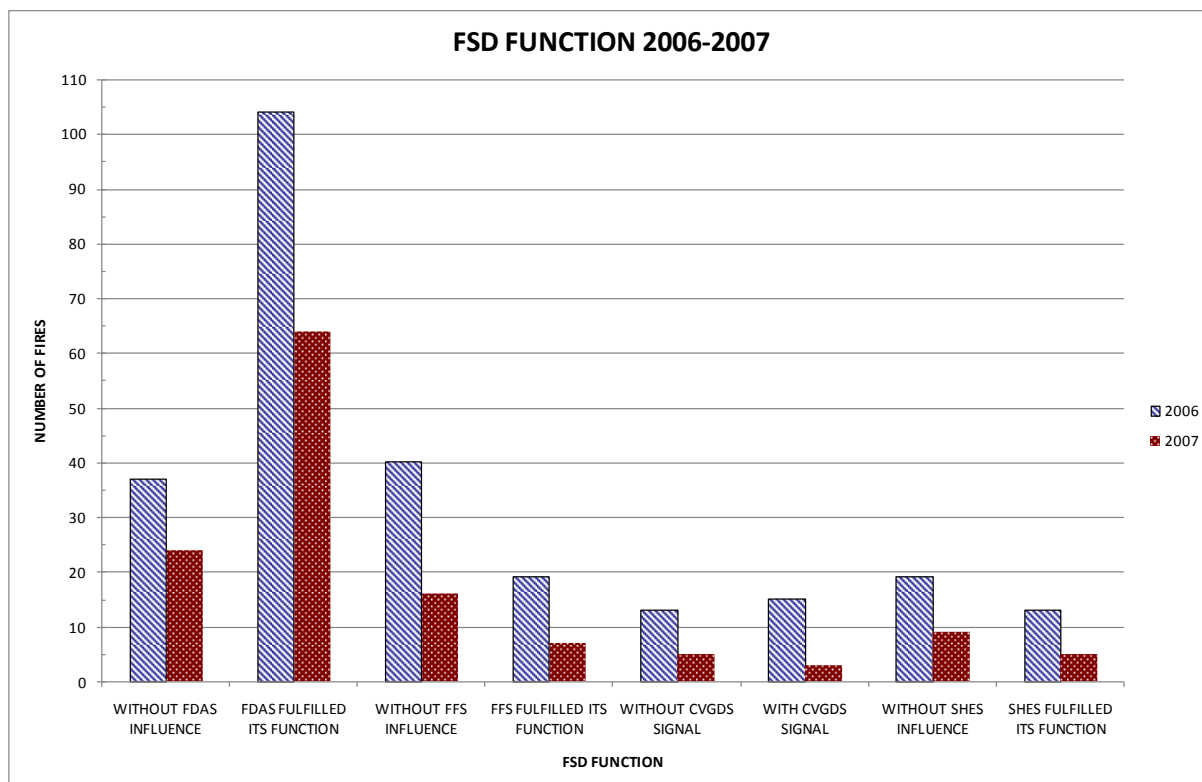


Fig. 3. Overview of the function of selected FSDs in the fires

## 2 INFLUENCE OF SOME FSD'S ON THE COURSE OF A FIRE

As already stated in Introduction, some fire safety devices influence directly the course of the fire, and it is possible to use them for influencing the fire risk when designing fire safety in buildings. For the purposes of evaluation of their influence, the mathematical modelling of the course of the fire by means of an ARGOS zone model was used. Software ARGOS is a product of Danish Institute of Fire and Security Technology (DIFT) from Copenhagen; at present, version 5.3 is used. The CFD models (e.g. FDS program developed at the National Institute of Standards and Technology (NIST) – Building and Fire Research Laboratory in Gaithersburg, U.S.A.) provide, in a number of cases, more accurate results; on the other hand, they are more computationally intensive. An advantage of FDS program is also the fact that results can be graphically plotted by means of Smokeview software.

For calculations, a dummy single-storeyed hall for wood processing of the floor size 12 m x 18 m and the height of 5 m. was used. The structure of the building is reinforced concrete. For the considered fire load  $p_n$  of  $60 \text{ kg.m}^{-2}$ , the fire safety level II is required for the building according to the new draft standard ČSN 73 0802. In the hall, automatic fire alarms with temperature and smoke detectors were used; the temperature ones having the value (temperature) of response of  $70 \text{ }^\circ\text{C}$  and the response time index  $\text{RTI} = 300 \text{ (m.s)}^{1/2}$ , the smoke ones with the sensitivity of  $0.30 \text{ dB.m}^{-1}$ . If SHES was considered in the calculations, it was a case of natural exhaustion of smoke and heat triggered by a thermal fuse with the reaction temperature of  $70 \text{ }^\circ\text{C}$  and the response time index  $\text{RTI} = 100 \text{ (m.s)}^{1/2}$ . The aerodynamic area of SHES, which was determined on the basis of SHES hole area with using the discharge coefficient  $c_v = 0.60$ , is presented in Table 3. The time delay in opening (proper opening time) was set at 10 sec. The hall was connected with the surrounding environment by means of two doors, two gates and altogether three holes. The size, opening and closing of them in the

course of individual tests are given in Table 3. For the calculations, four variants of initial fires were used; they were variants of stacked Euro pallets. The basic description of them is presented in Table 2. For each variant of initial fire, six calculations under various conditions were executed. Altogether, 24 fire scenarios were dealt with.

*Table 2. Initial fires used*

|                                     | Initial fire |        |        |        |
|-------------------------------------|--------------|--------|--------|--------|
|                                     | A            | B      | C      | D      |
| Height of pallets [m]               | 1.0          | 1.5    | 1.7    | 2.0    |
| Width of pallets [m]                | 0.8          | 1.6    | 1.6    | 1.6    |
| Length of pallets [m]               | 6.0          | 6.0    | 6.0    | 6.0    |
| Volume of pallets [m <sup>3</sup> ] | 4.80         | 14.40  | 16.32  | 19.20  |
| Heat release rate [MW]              | 16.80        | 50.40  | 57.12  | 67.20  |
| Total energy released [MJ]          | 16 130       | 48 400 | 54 800 | 64 500 |

*Table 3. Conditions used in calculation – fire scenarios*

|   | Number | Fire scenario |       |       |       |       |       |
|---|--------|---------------|-------|-------|-------|-------|-------|
|   |        | 1             | 2     | 3     | 4     | 5     | 6     |
| Door 140 x 210 cm                       | 2      | Close         | Close | Close | Close | Close | Close |
| Gate 300 x 300 cm                       | 2      | Close         | Close | Close | Close | Close | Close |
| Hole 50 x 50 cm, 200 cm above the floor | 1      | Open          | Open  | Open  | Open  | Open  | Open  |
| Hole 300 x 300 cm                       | 1      | Close         | Open  | Open  | Open  | Open  | Open  |
| Hole 300 x 300 cm                       | 1      | Close         | Close | Close | Close | Close | Open  |
| SHES aerodynamic area [m <sup>2</sup> ] | 1      | N/A           | N/A   | 2.16  | 4.32  | 6.50  | 6.50  |

*Table 4. Time of occurrence of Flash-over phenomenon according to fire scenarios*

| Occurrence of Flash-over phenomenon [mm:ss] | Fire scenario |       |       |       |       |    |
|---|---------------|-------|-------|-------|-------|----|
|   | 1             | 2     | 3     | 4     | 5     | 6  |
| Type of initial fire                        |               |       |       |       |       |    |
| A   | No            | No    | No    | No    | No    | No |
| B   | 09:45         | No    | No    | No    | No    | No |
| C   | 08:45         | 09:55 | 10:35 | No    | No    | No |
| D   | 07:36         | 08:35 | 09:05 | 09:25 | 09:55 | No |

From Table 4 it is evident that smaller aerodynamic areas of SHES were not sufficient to prevent the Flash-over phenomenon. If in the case of scenario B2, natural ventilation through a 3 m x 3 m hole in the wall was sufficient to prevent the Flash-over, then in the case of scenario D5, SHES with the aerodynamic area, which corresponded to 3% of floor area, did not prevent the Flash-over. The reason was the insufficient supply of air into the ventilated compartment (open area of 9 m<sup>2</sup>). If this area was doubled (scenario D6), the Flash-over did not occur any more.

Basic data on the course of the fire according to some selected scenarios are presented in Table 5.

Table 5. Course of the fire according to some selected scenarios

|   | Fire scenario |       |       |       |       |       |       |
|---|---------------|-------|-------|-------|-------|-------|-------|
|   | A1            | B1    | B2    | C3    | C4    | D5    | D6    |
| Flash-over [min:sec]                    | N/A           | 09:45 | N/A   | 10:35 | N/A   | 09:55 | N/A   |
| Temperature detector response [min:sec] | 03:25         | 03:01 | 03:01 | 02:57 | 02:57 | 02:54 | 02:54 |
| Smoke detector response [min:sec]       | 01:10         | 01:10 | 01:10 | 01:10 | 01:10 | 01:10 | 01:10 |
| SHES opening [min:sec]                  | N/A           | N/A   | N/A   | 02:32 | 02:32 | 02:32 | 02:32 |
| Maximum temperature of upper layer [°C] | 222           | 1 123 | 461   | 1 160 | 462   | 1 178 | 458   |

In Table 5 the great difference in the achieved temperature of upper layer between the case when the Flash-over occurs and the case when it does not occur can be seen. It is possible to demonstrate this difference on an example of scenarios D5 and D6; curves of upper layer temperatures are there in Figs. 4. and Fig. 5.

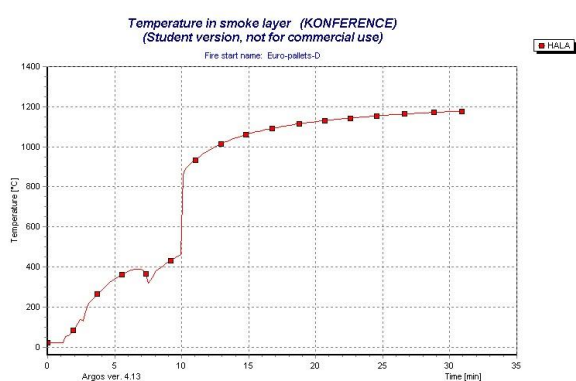


Fig. 4. Upper layer temperature, D5

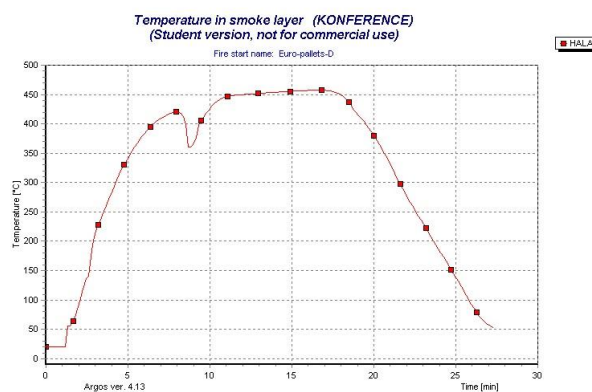


Fig. 5. Upper layer temperature, D6

To complete the view of theoretical temperatures of the fire, comparison with the standard temperature curve according to ČSN EN 1363-1 (also according to ISO 834:1975) or, as the case may be, with the hydrocarbon temperature curve according to ČSN EN 1363-2 is possible.

### 3 SUMMARY AND ACKNOWLEDGMENT

The made analysis of fire statistics shows clearly the importance of use of automatic fire detection to shorten the time to fire notification, and thus to fire brigade intervention. By ARGOS software, the impact of SHES application on Flash-over phenomenon prevention was calculated. The prevention of Flash-over leads unambiguously to markedly lower temperatures in the fire, and thus to the limitation of damage to structures as well as internal equipment. The calculation confirms the expected faster response of smoke fire detector in comparison with the temperature detector.

### REFERENCES

- [1] Dudáček, Aleš – Stryková, Zuzana. Problematika používání automatických hlásičů požáru v budovách pro bydlení a ubytování. In *Zborník Wood & Fire Safety 2004*. Zvolen: TU Zvolen, 2004. pp. 35 – 44.
- [2] Statistické sledování událostí. Praha: GŘ HZS ČR, 2008.

## ADIABATIC SURFACE TEMPERATURE A Sufficient Input Data for a Thermal Model

Joakim Sandström<sup>a</sup>, Ulf Wickström<sup>b</sup>, Milan Veljkovic<sup>c</sup>

<sup>a</sup> Luleå University of Technology/Brandskyddslaget AB, Karlstad, Sweden

<sup>b</sup> Luleå University of Technology/SP Technical Research Institute of Sweden, Borås, Sweden

<sup>c</sup> Luleå University of Technology, Luleå, Sweden

### INTRODUCTION

Two computational models are employed in this paper to predict structural performance in fire:

- A fire model created using a numerical code based on Computation Fluid Dynamic (CFD). The model predicts the development of a fire and the heat flux in a fire compartment with a simple geometry consisting of solid objects for the purpose of estimating their temperature.
- A thermal/structural model using numerical software based on the Finite Element Method. The model predicts structural behaviour based on an "effective gas temperature", which is denoted *adiabatic surface temperature*. This temperature may be obtained either from fire modelling or from measurements. An important question is which parameter values from the fire model are required to transfer information at the gas-solid interface.

A thorough and common understanding of heat transfer to structural elements of a building is very important for realistic prediction of the temperature and resistance of structural components. Researchers and test standard developers have different ways of expressing and measuring the various forms of convective and radiative heat flux.

The net heat flux to a surface computed by a fire model is often seen as a valuable information to be used in thermal/structural model to perform detailed heat transfer calculation within the structural elements. However the net heat flux calculated in the fire model depends on the corresponding surface temperature and is therefore limited to be used in thermal calculations only with the same structural geometry as used in the fire model.

This paper is intended to promote use of *adiabatic surface temperature (AST)* [1] as a practical means of expressing the thermal exposure of structural surfaces independent of the structural properties in the fire model. The concept is useful when calculating temperatures and structural resistance in a fire.

The concept of AST may be used when the exposure conditions are obtained either from a fire model, calculated by the Fire Dynamic Simulator, FDS [2] or directly from measurements using Plate Thermometer temperatures [3].

# 1 THEORETICAL BACKGROUND OF HEAT TRANSFER

Heat is transferred from hot fire gases to structures by radiation and convection. The contributions of these two models of heat transfer are in principal independent and must be treated separately.

Thus the total heat flux  $\dot{q}''_{tot}$  to a surface is:

$$\dot{q}''_{tot} = \dot{q}''_{rad} + \dot{q}''_{con} \quad (1)$$

where  $\dot{q}''_{rad}$  is the net radiation heat flux and  $\dot{q}''_{con}$  the heat transfer to the surface by convection. The net contribution by radiation  $\dot{q}''_{rad}$  depends on the incident radiation  $\dot{q}''_{inc}$ , on the surface emissivity/absorptivity, Stefan-Boltzmanns constant,  $\sigma$ , and on the fourth power of the absolute temperature  $T_s$  of the targeted surface. The heat exchange at a surface is illustrated by *Fig. 1*.

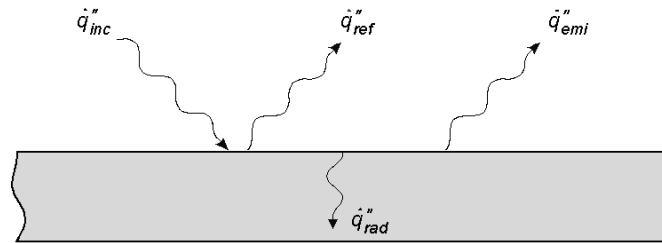


*Fig. 1* The heat transfer by radiation to a surface depends on incident radiation and the surface absolute temperature and the surface emissivity.

A part of the incident radiation is absorbed and the rest  $\dot{q}''_{ref}$  is reflected. Then the surface emits heat by radiation  $\dot{q}''_{emi}$  depending of the emissivity and the surface absolute temperature to the fourth power. Thus

$$\dot{q}''_{rad} = \alpha_s \dot{q}''_{inc} - \varepsilon_s \sigma T_s^4 \quad (2)$$

where  $\alpha_s$  and  $\varepsilon_s$  are the target surface absorptivity and emissivity, respectively. The surface emissivity and absorptivity are assumed equal according to the Kirchhoff's identity, and the incident radiation is expressed in terms of a radiation temperature,  $T_r$ . Then (2) becomes:

$$\dot{q}''_{rad} = \varepsilon_s \sigma (T_r^4 - T_s^4) \quad (3)$$

The heat transferred by convection from adjacent gases to a surface varies a lot depending on adjacent gas velocities and geometries. It may be written as

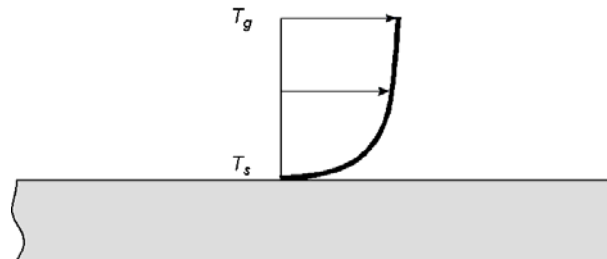


*Fig. 2* Gas velocity profile. The heat transfer by convection depends on the temperature difference between the adjacent gases and the target surface, and on the gas velocity.

$$\dot{q}_{\text{con}}'' = h(T_g - T_s) \quad (4)$$

The convective heat transfer coefficient  $h$  depends mainly on flow conditions near the surface and not so much on the surface or the material properties.

The total heat transfer to a surface may now be obtained by adding the contributions by radiation and convection:

$$\dot{q}_{\text{tot}}'' = \varepsilon_s \sigma (T_r^4 - T_s^4) + h(T_g - T_s) \quad (5)$$

### 1.1 Adiabatic Surface Temperature (AST)

The two boundary temperatures in (5),  $T_r$  and  $T_g$  may be combined to one effective temperature  $T_{\text{AST}}$ , the adiabatic surface temperature. This temperature is defined as the temperature of an ideally perfectly insulated surface when exposed to radiation and convection heat transfer [1]. Thus  $T_{\text{AST}}$  is defined by the surface heat balance equation

$$\varepsilon_s \sigma (T_r^4 - T_{\text{AST}}^4) + h(T_g - T_{\text{AST}}) = 0 \quad (6)$$

The value of  $T_{\text{AST}}$  is always between  $T_r$  and  $T_g$ .

By combining (5) and (6) the total heat transfer may be written as

$$\dot{q}_{\text{tot}}'' = \varepsilon_s \sigma (T_{\text{AST}}^4 - T_s^4) + h(T_{\text{AST}} - T_s) \quad (7)$$

## 2. PRACTICAL APPLICATION OF AST

Three components are assumed or calculated in thermal response of fire exposed structures. The first component and the most common to assume is the time-temperature curve, or fire temperature based on the assumed surrounding conditions, used to heat the structural element. The second and third is the heat flux and surface temperature which are calculated based on the properties of the structural element.

FDS can calculate the fire progression for a desired scenario and with a 1-D heat flow model calculate the second and third components of the thermal response calculation. These values are only valid for the structural properties used in the FDS calculation but can be seen as fairly accurate [4].

By knowing the surface temperature,  $T_s$  and the heat flux from radiation,  $\dot{q}_{\text{rad}}''$  and convection,  $\dot{q}_{\text{con}}''$  FDS can use equation 6 to iteratively calculate the assumed fire temperature in each time step [5] representing the surrounding temperature and therefore valid for any structural element. This fire temperature calculated in FDS is denoted  $T_{\text{AST}}$ .

By specifying  $T_{\text{AST}}$  as an output in FDS it is possible to obtain a time-temperature curve in each direction of fire exposure of a structural element that is calculated for the specific

scenario used in the fire model. This time-temperature curve can be used in thermal FEM-calculations the same way as fire curves such as the ISO834 or ASTM 119-E with the difference that there are different values for each side whereas the temperature exposure of ISO834 and ASTM 119-E are uniform.

**2.1 Numerical example**

To show that, by knowing  $T_s$  and  $\dot{q}''_{tot}$ , it is possible to derive a fire curve with  $T_{AST}$  that is valid for other structural elements than the one used in the first calculation. Two different fire simulations were performed in a room of the dimension 1.6 m by 1.6 m and 1.6 m high with a steel beam (tubular cross section) in the ceiling. An opening of 1.2 m by 0.8 m was modelled at the wall opposite of a heat source, see Fig. 3.

The heat source in the fire model was 0.2 m by 0.2 m with a constant heat release of 500 kW. Grid cells of 2.5 cm. The simulations were performed with different beam sizes: RHS 300 (300 mm by 200 mm with a thickness of 9.5 mm) and RHS 200 (200 mm by 100 mm with a thickness of 10.5 mm).  $T_{AST}$  was calculated in both cases, on each side of the beam and in the concrete at three reference cross-sections of the beam, positions indicated in Fig 4.

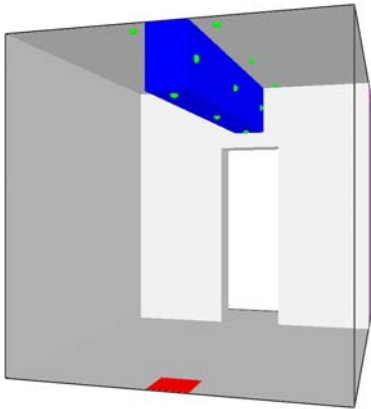


Fig. 3 The room used to model different scenarios. The red rectangle symbolizes the heat source.

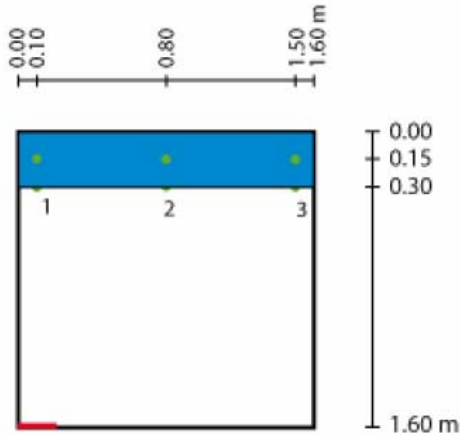


Fig. 4 Position of reference cross-sections at the steel beam.

The temperature distributions in the steel beams were calculated using Tasef [6].  $T_{AST}$  from the corresponding reference points obtained from the fire model (FDS analyses) in each reference cross-section were the only boundary conditions used in the thermo-model, see Fig. 5. Different boundary conditions were assumed on each side of the beam (see fig 6.). The set up of the Tasef model is shown in fig 7.

Following assumptions were made to simplify the steel temperature calculations in Tasef:

- The model is symmetric around y-axis.
- Nodes in the steel section close to each other are coupled (restricted to get the same temperature) to save computational time.
- Heat transfer by radiation and convection inside the beam is considered.

All surfaces have an emission coefficient of 0.8 and the convection heat transfer coefficient  $h = 25 \text{ W}/(\text{m}^2\text{K})$ .

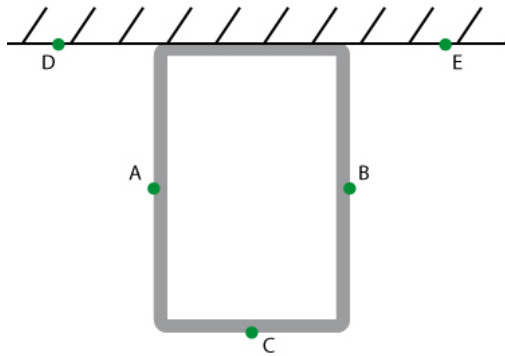


Fig. 5 Reference points in the fire model at the cross section of the beam in which the time- $T_{AST}$  relations were calculated.

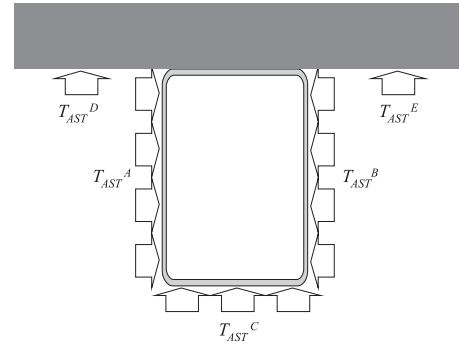


Fig. 6 The surfaces in the thermal model were exposed to the time-temperature cure with  $T_{AST}$  obtained from the corresponding surface in the fire model.

By assuming that:

- $T_{AST}$  can be used in thermal calculations with good results [4]
- $T_{AST}$  is valid for other structural elements than the one used in the fire model.

a comparison was made between thermal calculations on the larger beam (RHS 300) with  $T_{AST}$  from each of the fire simulations.

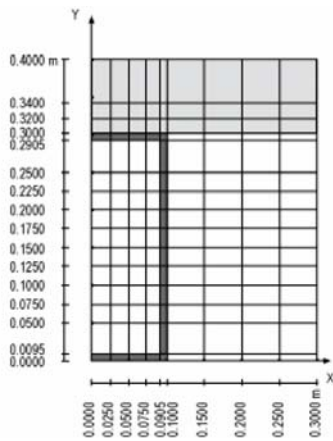


Fig. 7. 2D thermo-model used in the Tasef calculations.

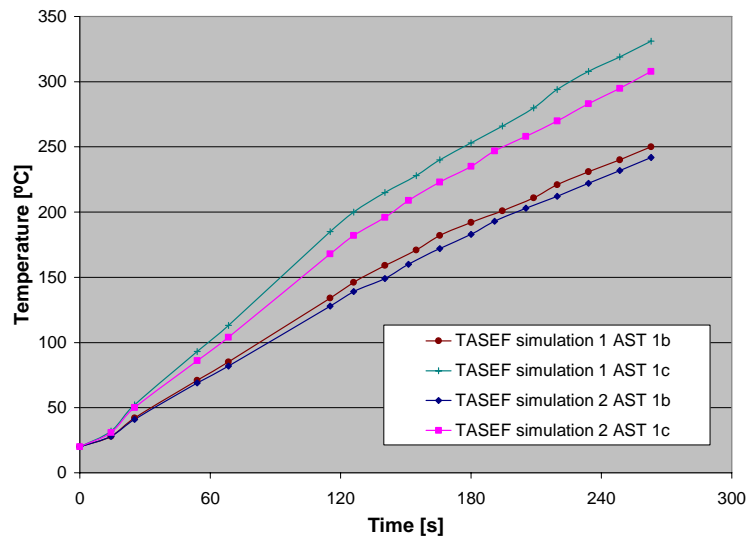


Fig. 8 Comparison of the temperature calculations performed in Tasef with the use of  $T_{AST}$  from two different FDS-calculations.  $T_{AST}$  taken as output from cross-section 1 and used as input in reference points b and c.

The results of the calculations are shown in Fig. 8 to show the influence of  $T_{AST}$  obtained in the two fire models. Temperature evaluation at the section 1 of the steel beam, in the middle of the bottom flange and in the web, points c and b, respectively are shown

One can conclude from Fig. 8 that it is possible to use  $T_{AST}$  obtained from the fire model with different beam sections as input for the thermo model. The shape of the curves are rather similar, but of course, differences exist for the various reference points due to the fact that geometry is a factor in the near field as in the case.

### 3 SUMMARY AND RECOMMENDATION FOR FURTHER WORK

The general idea of using the concept of adiabatic surface temperature  $T_{AST}$  in modelling heat transfer to fire exposed structures is illustrated in the paper. This is an initial part of the research planned to be performed at LTU.

The uncertainties introduced by employing  $T_{AST}$  are most often negligible as it has been shown in ref. [4]. There is a need to better understand, and allow compensation for, these uncertainties. After that it will be possible to perform thermal calculations in structural elements exposed to fire with the improved accuracy and flexibility needed in a new generation of the design process.

### REFERENCES

- [1] Wickström, U., (2007). Methods for Predicting Temperature in Fire Exposed Structures, *SP Draft*, SP - Swedish National Testing and Research Institute, Borås, 2007
- [2] McGrattan, K.B., Hostikka S., J.E. Floyd, H.R. Baum and R.G. Rehm, Fire Dynamics Simulator (Version 5), Technical Reference Guide, *NIST SP 1018-5*, National Institute of Standards and Technology, Gaithersburg, Maryland, December 2008
- [3] Wickström, U., Heat Transfer and Temperature Calculations Based on Plate Thermometer Measurements, *SP Draft*, SP - Swedish National Testing and Research Institute, Borås, 2008
- [4] Wickström, U., Duthinh, D. and McGrattan, K.B., Adiabatic Surface Temperature for Calculating Heat Transfer to Fire Exposed Structures, *Interflam 2007*
- [5] McGrattan, K., Hostikka S., Floyd, J., Klein, B., Fire Dynamics Simulator (Version 5), User's Manual, *NIST SP 1019-5*, National Institute of Standards and Technology, Gaithersburg, Maryland, December 2008
- [6] Sterner, E. and Wickström, U., TASEF - Temperature Analysis of Structures Exposed to Fire, *SP Report 1990:05*, Swedish National Testing and Research Institute, Borås, 1990
- [7] EN 1991-1-2, Eurocode 1: Actions on structures – Part 1-2: General actions – Actions on structures exposed to fire



Proceedings of International Conference  
Applications of Structural Fire Engineering  
Prague, 19-20 February 2009

**Session 3**

**Material Modelling**

## **MATERIAL PROPERTIES LOSS OF FIBRED-SCC DUE TO FIRE ACTION**

Alonso, C. and Rodriguez, C.

Eduardo Torroja Institute of Construction Sciences (IETcc) – CSIC ,Madrid, Spain

### **INTRODUCTION**

Traditionally concrete is identified as a material showing good resistance against fire, but it is also known that different changes take place in chemical composition, pore structure and water content when concrete is exposed to high temperatures, that together with thermal expansions finally produce losses in mechanical strength properties [1, 2]. Furthermore other type of damage exists that affects the integrity of the structure under fire, associated with a type of explosion. The risk of spalling of concrete at high temperature implies reduction of the effective section and concrete cover, and facilitates the exposure of new faces of concrete to the high temperatures developed during the fire [3].

High dense concretes, as high and ultra high strength concretes, are more prone to spalling when exposed to high temperatures than normal concretes, the reason is associated with the fineness of the pore structure that does not facilitate the water vapour easily to be evacuated, what induces increase of the vapour pressures inside the pores and then the risk of spalling [4]. In addition SCC is also considered to show less fire resistance [5-8], although no agreement between authors is found. A challenge appears trying to understand the mechanism of spalling to allow more efficient design of new concretes.

Experiences with high strength concrete reinforced with polypropylene fibers have showed that a certain favourable effect is noticed to reduce the spalling risk of the concrete cover, although some fails have indicated that the risk still remains and the reason is not yet well understood, it would depend on the dosage and type of fibers used [9-15].

Present work focuses on mechanical and microstructure properties evolution under fire of self compacting concrete (SCC) and the modification due to fibers addition, polypropylene and steel, used separately or mixed, in order to analysed the response at high temperatures and the influence of the type of fibre.

## **1 EXPERIMENTAL PROGRAM**

### **1.1 Materials**

Self-Compacting Concrete was manufactured with 426 kg/m<sup>3</sup> of Ordinary Portland Cement (OPC) (CEM I 52.5 R), 963 kg/m<sup>3</sup> of crushed limestone aggregates with a grading of 0-5 mm for the sand and 5/12 mm for the gravel, 647 kg/m<sup>3</sup> of limestone filler and 6.40 kg/m<sup>3</sup> of polycarboxylate-based superplasticizer, the water/cement ratio (w/c) was 0.45.

Additions of fibers were also used in several proportions: 1) 3 kg/m<sup>3</sup> of polypropylene (PPF) of 54 mm of length and 0.05 mm of diameter, 2) 40kg/m<sup>3</sup> of steel fiber (SF) with 30mm of length and 0.48mm of diameter, and 3) mix of PPF + SF, 1.5 kg/m<sup>3</sup> and 20kg/m<sup>3</sup> respectively.

Beams of 40x10x10cm were fabricated, but tests were carried out using cylindrical cores of 7.5x10 cm taken from the beams.

## 1.2 Test method

The SCC concrete cores were exposed to several temperatures in an electrical furnace and heated at a heating rate of 2°C/min until the temperature selected and maintained for two hours. Then, the cooling of the samples was allowed inside the furnace, following a cooling rate <1°C/min.

After cooling, in residual state, changes in microstructure and mechanical properties of the heated concrete samples were measured.

The temperatures considered were: 20°C (as initial), 200, 300, 500, 700 and 1200 °C: After heating, each specimen was introduced in a plastic bag and then in a box free of humidity and CO<sub>2</sub> to avoid any negligible effect due to contact with the atmosphere before testing. The characterisation tests were:

- *Residual mechanical properties*: Compressive strength and indirect tensile strength.
- *Pore structure*: Total porosity and pore size distribution using mercury porosimetry.
- *TG/DTA*: Transformations taking place in hydrated phases of cement paste and aggregates of SCC and in the PPF fiber.
- *Microscopy*: to determine the microstructure in pore density, microcracks and dehydrated phases distribution using back-scattered-SEM and stereoscopic microscopy.

## 2 RESULTS AD DISCUSSION

### 2.1 Chemical composition changes in SCC after exposure to high temperatures

The transformations occurring in chemical composition of hydrated phases in SCC at high temperatures have been identified using thermo-gravimetric tests (TG/DTA) in samples previously exposed to several temperatures (20, 105, 300, 500, 700 and 1200°C) are included in *Fig.1-left* and in *Table 1*. The results follow similar performance than a conventional cement paste up to temperatures of 500°C, as indicated in [2]. The main differences appear in temperatures > 600°C, showing higher weight losses associated to the decomposition of either the filler and the aggregate, both calcareous (carbonates based) that chemically decompose at those high temperatures. For temperatures < 100°C the weight losses detected in the initial SCC are due to the evaporation of the free water, which is not detected in the samples exposed to higher temperatures. The weight losses recorded between 100-350°C are associated to the dehydration of the cement paste, mainly CSH, which after 300°C has practically disappeared. The weight losses taking place in the region of 350-500°C are due to the decomposition of the portlandite. The sample exposed at 1200°C shows that all the components of the concrete have been altered and no more transformations take place.

The polypropylene fiber shows a melting point at 133°C and combustion (evaporation) at 444°C, as determined from TG/DTA given in *Fig.1-right*. This ability of the PPF to melt at relatively low temperatures, would affect the transport process of vapour released from the dehydration of the concrete.

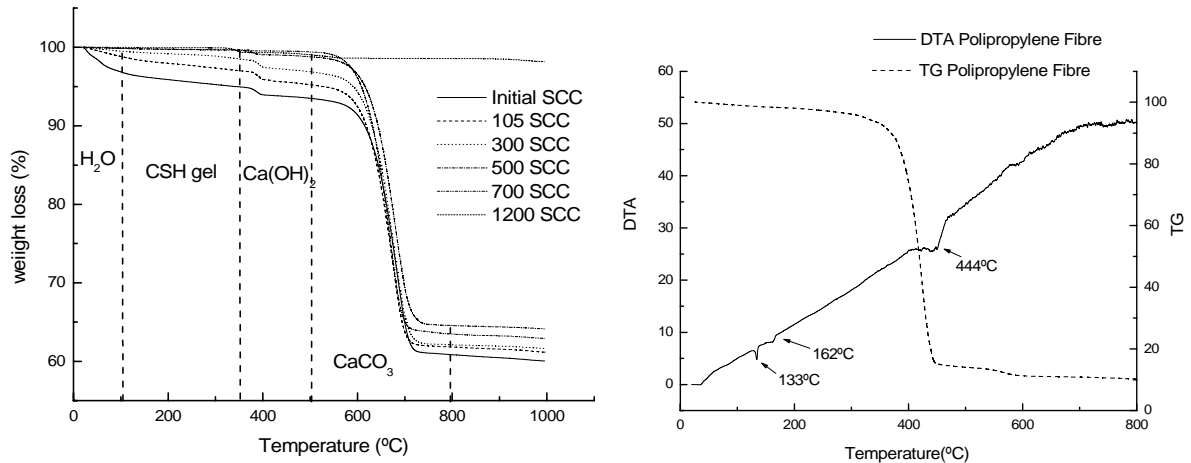


Fig. 1. TG of SCC after high temperature (left). DTA/TG of PPF (right).

Table 1. % of weight loss in different ranges of temperature

| Temperatrue | 100-350°C | 350-500°C | 500-800°C |
|-------------|-----------|-----------|-----------|
| Initial SCC | 1.98      | 1.74      | 32.02     |
| 105 SCC     | 1.81      | 1.79      | 33.41     |
| 200 SCC     | 1.20      | 1.85      | 34.95     |
| 300 SCC     | 0.97      | 1.71      | 34.66     |
| 500 SCC     | -         | -         | 35.24     |
| 700 SCC     | -         | -         | 35.90     |
| 1200 SCC    | -         | -         | 0.52      |

## 2.2 Pore structure changes in SCC with fibers after exposure to high temperature

The pore structure of the SCC concretes undergoes a progressive increase due to heat action, associated with the dehydration of the cement paste components and thermal stresses in the paste, aggregates, filler and PPF, creating open pores, microcracks and empty spaces, as shown in Fig. 2. No differences are detected with respect SF, but some curious behaviour is observed in the case of SCC+PPF.

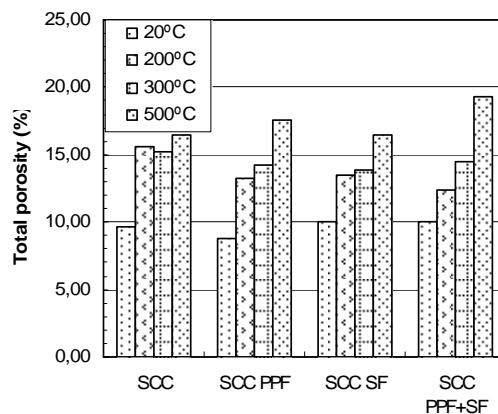
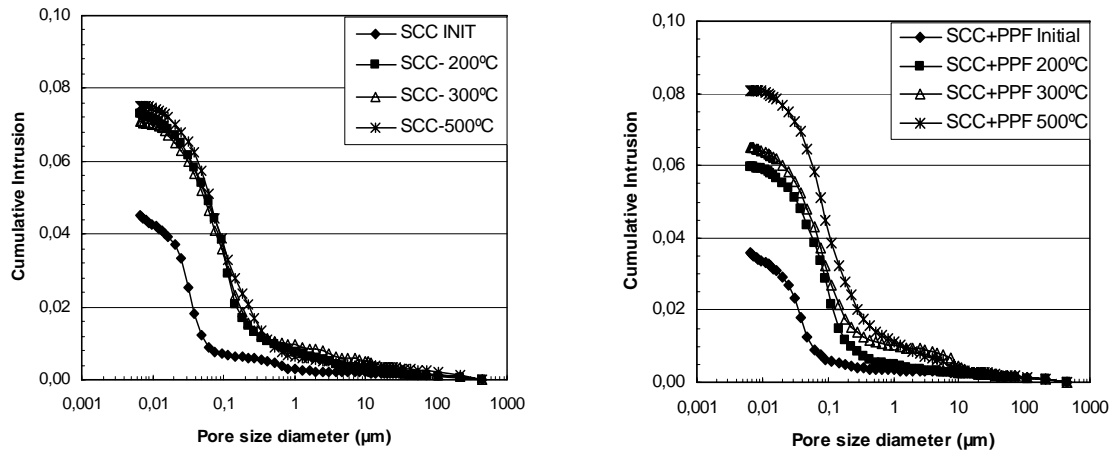


Fig. 2. Total porosity at different temperatures

Small pores, <0.01 $\mu$ m, decrease more intensively in SCC+PPF than for the plain SCC, which no necessarily represents an increase in creation of pores of higher capillary size, the reason is associated to the fact that the melted PPF, occurring 133°C, might disuse into the small pores

of the surrounding concrete that do not produce the expected increase of porosity, as shown in *Fig. 3, left and right*. The efficiency of the PPF to create more open capillary pores is not noticed until the melted PPF evaporates, which does not occur until 444°C, present behaviour confirms the previously found by [10, 14].



*Fig. 3.* Pore structure size distribution of plain SCC and SCC+PPF after high  $T^a$

### 2.3 Influence of fibers in mechanical properties of SCC under fire

The loss in compressive and indirect tensile strength after exposure to 20, 300, 500 and 700°C are given in *Fig. 4 left and right*. The presence of fibres seems not to affect the compressive strength evolution, no important differences in compressive strength losses between SCC with and without fibers is determined. However tensile strength decreases more quickly in SCC+PPF than in the others, this fact is attributed first to the PPF loss their beneficial effect in the tensile strength properties after melting; later at higher temperatures after evaporation of the melted fiber creates empty spaces that behave as defects in the concrete. On the contrary the SCC+SF maintain the tensile strength in a higher level up to higher temperatures. At 700°C the steel fiber is chemically altered (oxidised). The most beneficial in tensile strength at  $T^a > 300^\circ\text{C}$  is the cocktail of fibers: the SF are beneficial due to their better fire resistance which maintain the interaction with concrete, the PPF contribute to open porosity spaces. At 700°C the behaviour is very similar in all SCC, with and without fibers as both the PPF and the SF have been altered at that temperature.

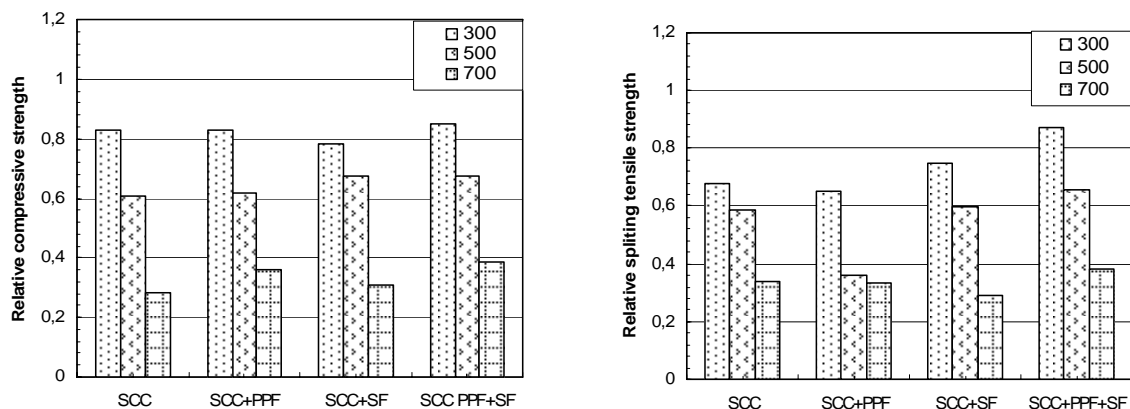


*Fig. 4.* Relative compressive strength (left) and Relative indirect tensile strength at different temperatures after cooling

## 2.4 Microstructure changes. Microscopy

When analysing the microstructure of a SCC exposed to high temperature, the progressive loss of density in the material is detected due to the dehydration of the cement paste phases. The main difference observed is in the limestone filler, which loss easily the interaction with the cement paste, as observed in *Fig. 5-left*. Other significant change is related to the presence of the fiber, in particular the PPF, at temperatures bellow 300°C when the fiber is melted and penetrates into the pores of the surrounding concrete, as observed in *Fig 5-right*.

This response of PPF at high temperatures is important because it is believed that the use of PPF in concrete avoids the risk of explosion under fire due to their ability to melt at the temperature where the risk of explosion is higher up to 300°C [6, 11, 12] due to the increase of empty spaces leaved by the heat decomposition of the fibers, which relax the high pore pressures generated during heating from dehydration of cement paste. However, recent studies have demonstrated that the risk of spalling due to vapour released still remains even in presence of PPF; the reason can be attributed to the close of pores at temperatures lower than 200-300°C that not always can be compensated by an increase in pore size due to dehydration of cement paste, so the beneficial effect of PPF in concrete at high temperatures with respect to spalling would also depend on the pore size distribution of concrete, adequate content of polypropylene fibers and w/c ratio of concrete, or the use of PPF fibers with lower range of temperature between melting and evaporation.

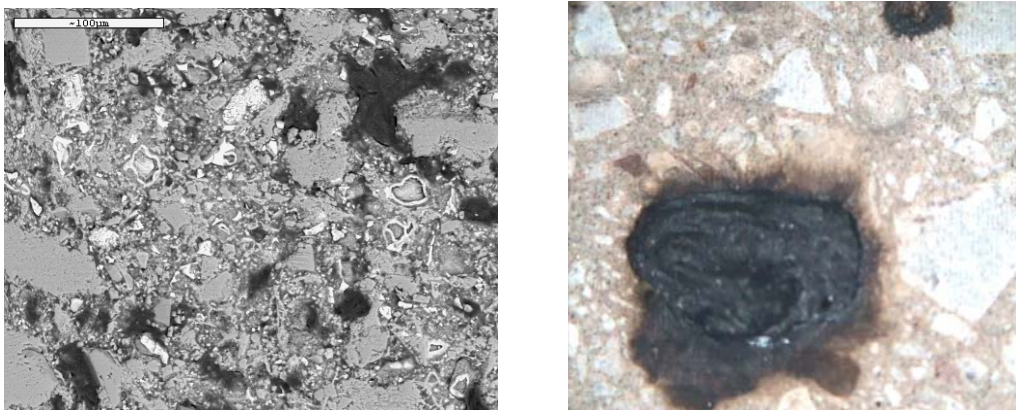


*Fig. 5.* Left, Backscattered electron microscopy of SCC at 700°C, x 350. Right, Melting and diffusion of PPF after 300°C.

## 3 CONCLUSIONS

- SCC follows similar transformations in microstructure and mechanical properties than plain concrete except that of the filler.
- The changes in pore structure of SCC+PPF suggest close of capillary porosity after the fusion of the fiber, that does no significantly increase until combustion has occurred.
- Mechanical properties of SCC + PPF show higher losses of strain strength.
- SCC +SF contribute to confine dehydrated paste and to control crack developing, until oxidized at T<sup>a</sup> above 500°C.
- SCC with mix of PPF+S F can contribute better to improve the resistance of concrete to fire.

#### 4 ACKNOWLEDGMENT

The authors acknowledge the funding received from the Spanish Ministry of Education and Science PSE-380000-2006-4 / PSE-380000-200681, HABITAT 2030.

#### REFERENCES

- [1] Z.P. Bazant and M.F. Kaplan. Concrete at high temperatures: Material properties and mathematical models. Logman Grp. Ltd., England (1996)
- [2] Alonso, C., Fernandez-Municio, L.. Int. WS on Fire Design of concrete structures- From materials modelling to structural performance, Univ. of Coimbra, Portugal, (2007) 69-78.
- [3] Fib Bul. n° 38, Fire design of concrete structures, materials structures and modelling. (2007)
- [4] Schneider, U., RILEM Int. WS on Durability of high performance concrete. Edt. H. Sommer, Vienna Feb (1994) 237-242.
- [5] Ye G., Liu X., De Schutter, Taerwe L., Vanndeveld P.. *Cement and Concrete Research*, 37, (2007) 978-987.
- [6] Jansson, R. and Boström, L. Int. WS on fire design of concrete structures from materials modelling to structural performance. *Univ. of Coimbra, Portugal. (2007) 177-188.*
- [7] Persson, B. Self-Compacting concrete at fire temperatures TVBM-3110, Lund Institute of Technology. Lund Univ, Division of Building Materials (2003).
- [8] Persson, B, *Cement and Concrete Research*, 31, (2001)193-198.
- [9] Alonso, C., Andrade, C., Gallo, E. and Menendez, E. 2005. ACI International, SP-229(2005) 289-302.
- [10] Kalifa, P. Chéne, G. and Cálle, C. *Cement and Concrete Research*, 31, 10, (2001) 1487-1499.
- [11] Khoury, G.A., Majorana, C., Int. WS on fire design of concrete structures from materials modelling to structural performance. Univ. of Coimbra, Portugal. (2007) 211-224.
- [12] Suhaendi, S. and Horiguchi, T. Int. WS on design of concrete structures from materials modelling to structural performance. Univ. of Coimbra, Portugal. (2007) 189-197.
- [13] György, L. Balázs, Éva, L. 8<sup>th</sup> International Symposium on Utilization of High-Strength and High-Performance Concrete. Nagoya, Japan, 2008.
- [14] Alonso, C., Andrade, C., Gallo, E. and Menendez, E., ACI International, SP-229(2005) (2005) 289-302.
- [15] Alonso, M.C., Sanchez, M., Rodriguez, C. and Barragan, B., 11<sup>th</sup> Int inorganic bonded fiber composite conference, Madrid, Nov, 2008.

## VARIANCES OF STEEL STRENGTH CHARACTERISTICS IN FIRE TEMPERATURES

Tomasz Domański

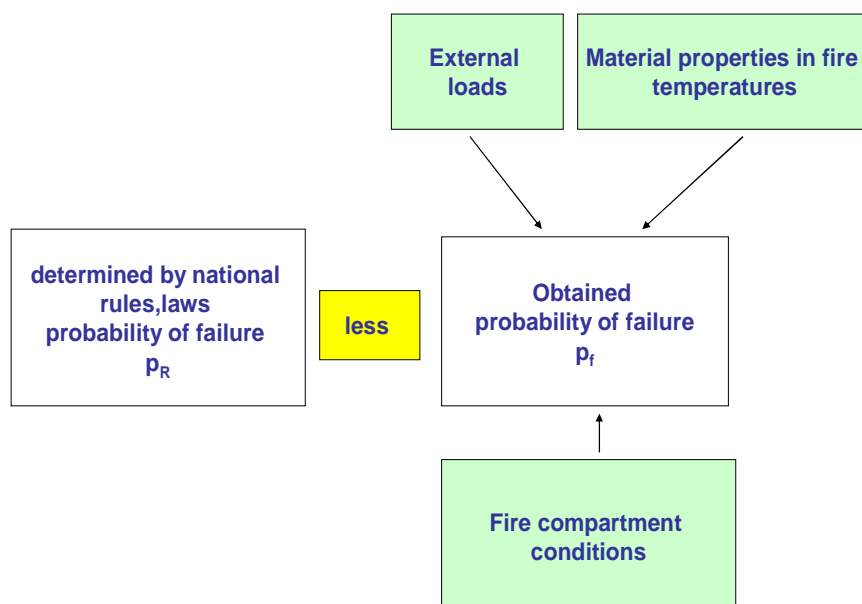
Cracow University of Technology, Faculty of Civil Engineering, Krakow, Poland

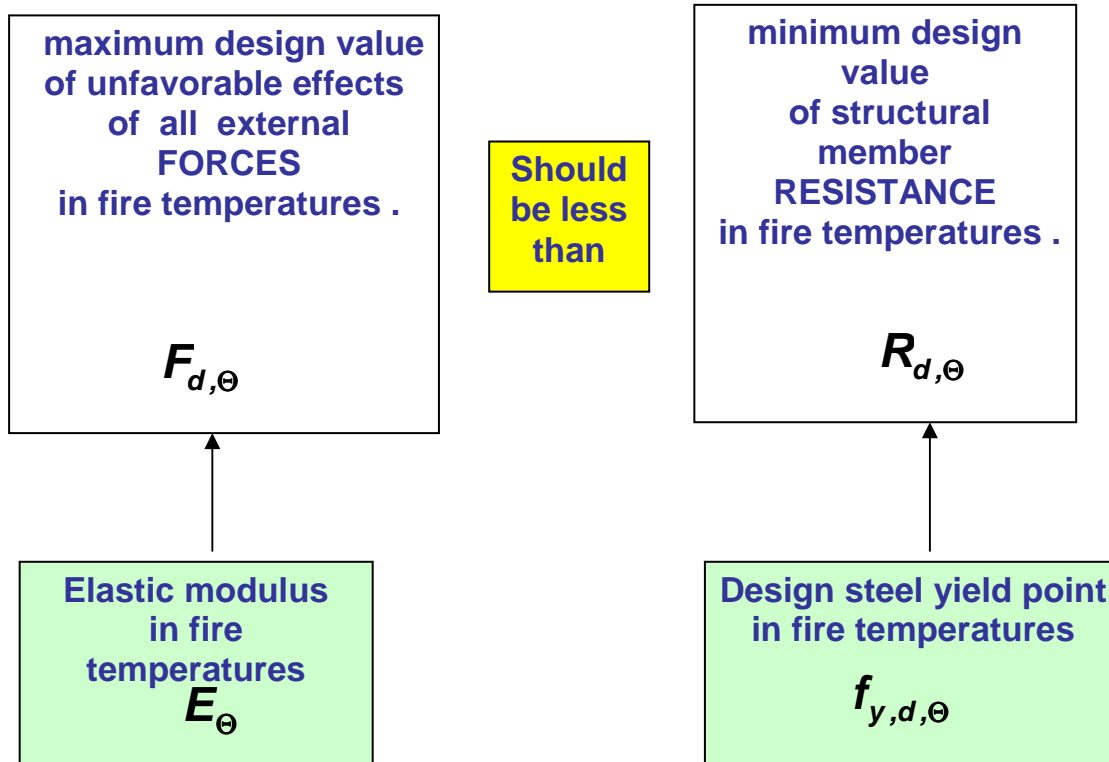
### INTRODUCTION

Laboratory tests provide the only practicable basis for specifying safety margin for ultimate strength of structural members in fire. The reliable safety measure in design of steel member in fire is probability of failure  $p_f = P(Ex, Ex^2; t)$ . The probability function  $P(Ex, Ex^2; t)$  depends on two parameters: expected value  $Ex$  of strength in temperature  $t$  (mean or median value) and variation parameter  $Ex^2$  (variance or coefficient of variation). The relationship between expected value of strength (mean, median value) and temperature is well known but relations between variation parameters (variance, coefficient of variations) are still taken into consideration. In this paper, the results of laboratory tests of strength characteristics in fire temperatures for two kinds of steel (F 230JR, F350JR) and for two kinds of shapes are presented. The basic question which ought to be stated is which variation parameters (variance or coefficient of variation) are constant in fire temperatures to create probability function of strength characteristics and consequently probability function of failure in fire temperatures. Then, it is necessary to test two equivalent hypotheses:  $H_0$ : variance is constant versus  $H_1$ : coefficient of variation is constant in fire temperatures. The analysis of variance in two-way hierarchical classification case was applied to estimate variance from fixed effects of different kinds of steel and shapes. The Bartlett's statistic  $B$  to verify hypothesis  $H_0$  and  $H_1$  which is asymptotically convergent to chi-squared distribution was applied.

The results of these investigations make possible to create probability function of fire resistance which is essential to estimate fire safety of steel structure

### 1 DESIGN CONDITIONS





It is assumed that structural member could support external and accidental fire forces according to EN 1991-1-1, repeated in particular standard EN 1993-1-2 [5],[6],[7] as follows:

$$F_{d,\Theta} \leq R_{d,\Theta} \quad (1)$$

Where :  $F_{d,\Theta}$  is the maximum design value of unfavorable effects of all the external force combinations in fire temperature  $\Theta$ .  
 $R_{d,\Theta}$  is the minimum design value of structural member resistance in fire temperature  $\Theta$ .

### 1.1 Design value of steel yield point in fire temperatures

The yield point  $f_{y,k}$  decreases when fire temperatures  $\Theta$  are grown, then

$$f_{y,k,\Theta} = k_{y,\Theta} f_{y,k,20}, \quad f_{y,k,20} = \check{f}_y \exp(-1.64v_{fy,20} - 0.5v_{fy,20}^2) \quad (2)$$

Where;  $\check{f}_y, v_{fy,20}$  are the median and log-normal coefficient of variation of the steel yield point in temperature  $\Theta = 20^\circ C$ .

It has been assumed that applied value of characteristic strength  $f_{y,k,20}$  is described in normal – room temperature  $\Theta = 20^\circ C$ . The reduction coefficient  $k_{y,\Theta}$  for different fire temperatures  $\Theta$  is presented in standard EN 1993-1-2. This relation is described as:

$$R_{k,\Theta} = k_{y,\Theta} R_{k,20}$$

Constant value of  $\gamma_{M,fi}$  in fire duration (particularly  $\gamma_{M,fi} = 1$ ) provides to the following formula for design value of the steel yield point in fire temperature  $\Theta$ .

$$f_{y,d,\Theta} = \frac{f_{y,k,\Theta}}{\gamma_{M,fi}} = \frac{k_{y,\Theta} f_{y,k,20}}{\gamma_{M,fi}} = k_{y,\Theta} f_{y,d,20} \quad f_{y,d,20} = \bar{f}_y \exp(-3.04v_{fy,20} - 0.5v_{fy,20}^2), \quad (3)$$

and also for design resistance

$$R_{d,t,\Theta} = R_{d,t}(\Theta_a) = k_{y,\Theta} R_{d,20} \quad (4)$$

The  $R_{\Theta}$  is the random variable described by log-normal probability distribution function  $\mathcal{N}(\bar{R}_{\Theta}, v_R)$  -  $\bar{R}_{\Theta}$  is median value and  $v_R$  is the log-normal coefficient of variation. Reduction coefficient  $k_{y,\Theta}$  is defined for different fire temperatures  $\Theta$ . Temperature  $\Theta$  will be treated as no-random in this analysis. There is the relation :

$$\bar{R}_{\Theta} = k_{y,\Theta} \bar{R}_{20} \quad (5)$$

It has been assumed that log - normal coefficient of variation  $v_R$  does not depend on temperature  $\Theta$ , then:

$$v_{R,\Theta} = v_{R,20} = const \quad \text{and} \quad v_{fy,\Theta} = v_{fy,20} = const \quad (6)$$

The problem of acceptance equality (8) will be taken into consideration in the next part of this paper.

## 2 VARIATION PARAMETERS – STATISTICAL TESTS IN FIRE TEMPERATURES

### 2.1 Populations, groups, samples

Let  $\underline{Y}_{ijk}$  be the set of measured values of the basic variables (e.g., steel yield point, modulus of elasticity) for a particular test specimen. A set of n identical specimens constitutes a sample from the population of all possible specimens built to the same specified values of  $\underline{Y}$ . The statistical properties, such as the variances or coefficients of variation of  $\underline{Y}$ , may be approximated by the variance, coefficient of variation of  $\underline{Y}_{ijk}$  from the samples and a calibration for the population will be based on these properties. The samples  $\underline{Y}_{ijk}$  were defined for two kinds of steel grades  $i=1,2$ (S235JR,S355JR) , for two kinds of steel members  $j=1,2$  (bars, hot rolled sections) and for  $k=1...4$  temperatures (20,300,400,500 °C).

The tests were performed for “small-sample size”  $n=6$  estimating yield point  $f_{e, ij,k,v}$  and  $E_{i,j,k,v} - v=1...6$ . The  $N=96$  laboratory data were obtained.

### 2.2 Outline of used statistical methods – assumptions

- There were different grades and shapes of steel members to get large variance inside samples  $\underline{Y}_{ijk}$  taken into the consideration
- The variances from permanent effects (different factors-grades, shapes) for group  $\underline{Y}_k = \bigcup_{ij} \underline{Y}_{ijk}$  for temperatures  $k=1...4$ . were obtained. It is supposed that variations

parameters of  $\underline{Y}_k$  can be constant, can increase or decrease but can not be non-monotonic in fire temperatures  $\Theta$ .

- There were two parameters of variations taken into consideration:
  - standard deviation  $\sigma_k = (\text{Var}(Y_k))^{1/2}$
  - coefficient of variations  $V_k \equiv \vartheta_k = (\text{Var}(\ln \underline{Y}_k))^{1/2}$ ,  $\vartheta_k$  -log-normal coefficient of variation.
- Analysis of variance was applied to estimate  $\sigma_k$  and  $V_k$  to separate gross laboratory errors. Two levels of factor A (steels S235Jr,S355JR  $r=2$ ) and two levels of factor B(bars,

hot rolled sections s=2) within each levels of factor A were considered. Analysis of variance was applied for laboratory results for each k=1..4 temperatures  $\Theta$  separately.

## 2.3 Analysis of variance

### 2.3.1 Outline of methodology

It was accepted that :formula for “v” test results  $Y_{ijv}$  (steel yield point, modulus of elasticity) in temperature  $\Theta$  (k) separately, for “j” level of factor B within “i” level of factor A [1]:

$$Y_{ijv} = \mu + a_i + b_{ij} + e_{ijv}. \quad (7)$$

Where:  $i=1\dots r, j=1\dots s, v=1\dots 6,$

$\mu$  - mean value in sample  $Y_{ijk}$

$a_i, b_{ij}, e_{ijv}$  – non correlated random variables with expected value equal null and partial variances :  $\text{var}(a_i) = \sigma_a^2, \text{var}(b_{ij}) = \sigma_b^2, \text{var}(e_{ijv}) = \sigma_e^2$  for all  $i, j, v.$

Variances  $\sigma_a^2, \sigma_b^2, \sigma_e^2$  are partial of complete variance in temperatures  $\Theta$  (k);

$$\sigma^2 = \text{var}(Y_{ijv}) = \sigma_a^2 + \sigma_b^2 + \sigma_e^2. \quad (8)$$

The result of permanent effect actions are variances  $\sigma_a^2, \sigma_b^2$  (steel grades and shapes). The problem is to estimate variances from permanent actions  $\sigma_k^2$  free from laboratory errors:

$$\sigma_{\text{per}}^2 = \sigma_a^2 + \sigma_b^2. \quad (9)$$

The estimation of variances  $\sigma_a^2, \sigma_b^2, \sigma_e^2$  should be calculated upon classic analysis of variance methods [1] and variance from permanent actions factor – A and B ;

$$\hat{\sigma}_{\text{per}}^2 = \hat{\sigma}_a^2 + \hat{\sigma}_b^2. \quad (10)$$

### 2.3.2 Influence of factors A and B on variance $\hat{\sigma}_{\text{per}}^2$ .

It is necessary to test the null hypothesis  $H_0: \sigma_{\text{per}}^2 \neq 0$  against the alternative hypothesis  $H_1$ : the variances are equal ;  $\sigma_{\text{per}}^2 = 0$  [2]. Hypothesis about existing treatment A –  $H_0$  is accepted when  $MQ_A/MQ_R \leq F_{\alpha}(f_A, f_R)$  and is rejected when  $MQ_A/MQ_R > F_{\alpha}(f_A, f_R)$ , where  $F_{\alpha}(f_A, f_R)$  is the critical value of the F-Snedecor distribution with  $f_A, f_R$  degrees of freedom. Null hypothesis will be tested at the  $\alpha$  level of significance. Alternatively, we test the null hypothesis  $H_0$  about existing treatment B. We accept hypothesis  $H_0$  when  $MQ_B/MQ_R \leq F_{\alpha}(f_B, f_R)$  and reject it when  $MQ_B/MQ_R > F_{\alpha}(f_B, f_R)$ . The variances of two variables (steel yield point, modulus of elasticity in fire temperatures) and for two statistics :  $\sigma = (\text{var}(Y))^{1/2}$  and  $V = \sigma_{\ln} = (\text{var}(\ln Y))^{1/2}$  were analysed. The influences – interactions of factors A and B on variation parameters of yield point ( $Y=f_d$ ) are shown in Table 1 [3],[4].

Table 1. Influence of factors A,B on standard deviation  $\sigma$  of the steel yield point ( $Y=f_d$ )

| $\Theta$ [°C] | $MQ_A/MQ_R$ | $F_{0.05}(1,20)$ | Interaction A | $MQ_B/MQ_R$ | $F_{0.05}(2,20)$ | Interaction B | $\hat{\sigma}_{\text{st}}(f_y)$ [Mpa] |
|---------------|-------------|------------------|---------------|-------------|------------------|---------------|---------------------------------------|
| 20            | 294.42      | 4.35             | exist         | 24.24       | 3.49             | exist         | 76.74                                 |
| 300           | 49.10       | 4.35             | exist         | 4.45        | 3.49             | exist         | 60.92                                 |
| 400           | 66.68       | 4.35             | exist         | 2.42        | 3.49             | exist         | 62.89                                 |
| 500           | 83.21       | 4.35             | exist         | 6.30        | 3.49             | exist         | 42.75                                 |

Analysis of above tables gives basis to state existing influence of factor A,B for yield point of steel parameters of variations , that is  $\sigma_k(f_y) \neq 0$  and  $V_k(f_y) \neq 0$  for any fire temperatures  $\Theta$ . These thesis cannot be supported for variation parameters of modulus of elasticity  $E$  in fire temperatures. Then upon *Table 2* we can state that :  $\sigma_k(E) = 0$  and  $V_k(E) = 0$

*Table 2.* Influence of factors A,B on variation parameters of modulus of elasticity  $E$  ( $Y=E, Y=\ln E$ )

| $\Theta$ [°C]             | 20        | 300       | 400       | 500       |
|---------------------------|-----------|-----------|-----------|-----------|
| $MQ_A/MQ_R$ for $Y=E$     | 1.75      | 0.25      | 0.35      | 4.15      |
| $MQ_A/MQ_R$ for $Y=\ln E$ | 1.76      | 0.74      | 0.496     | 1.21      |
| $F_{0.05}(1,20)$          | 4.35      | 4.35      | 4.35      | 4.35      |
| Interaction A,B           | no- exist | no- exist | no- exist | no- exist |

#### 2.4 Standard deviation $\sigma$ and coefficient of variation $V$ of the steel yield point in fire temperatures

Now, it is necessary to test hypothesis  $H_0$  - equality of variances :  $\sigma_k^2 = \text{var}(Y_k)$  in fire temperatures. The null hypothesis  $H_0$  is :  $\sigma_1^2 = \sigma_2^2 = \dots = \sigma_k^2$  against alternative hypothesis  $H_1$ :  $\sigma_1^2 \neq \sigma_2^2 \neq \dots \neq \sigma_k^2$  for all fire temperatures  $\Theta(k)$  and adequately for  $V_k^2 = \sigma_{\ln, k}^2$  the null hypothesis  $H_0$ :  $\sigma_{\ln, 1}^2 = \sigma_{\ln, 2}^2 = \dots = \sigma_{\ln, k}^2$  against alternative hypothesis  $H_1$ :  $\sigma_{\ln, 1}^2 \neq \sigma_{\ln, 2}^2 \neq \dots \neq \sigma_{\ln, k}^2$ . Above hypothesis will be verified by using Bartlett's test which is supported upon following statistic[2]:

$$b = \frac{\left( \prod_{i=1}^k \sigma_i^2 \right)^{n/(N-k)}}{\sigma_p^2}, \quad (11)$$

where:  $n$ - sample quantity ,  $n=24$ ,  $i=1 \dots k=4$ ,  $N = k n = 96$ ,

$$\sigma_p^2 = n \sum_{i=1}^k \sigma_i^2 / (N-k) \quad (12)$$

We accept hypothesis  $H_0$  at the  $\alpha$  level of significance when :  $b < b_k(\alpha; n)$

$b_k(\alpha; n)$  – critical value for Bartlett's test ,  $k$  – number of populations in fire temperatures ,  $\alpha$  – level of significance ,  $n$  – sample quantity.

The Bartlett's statistic  $b_{fe}$  to verify hypothesis about equality of yield point standard deviation in fire temperatures  $\sigma_1^2 = \sigma_2^2 = \dots = \sigma_k^2$  was estimated as follows;

$$b_{fe} = 1.171 > b_4(0.01, 24) = 0.882 \quad (13)$$

then hypothesis  $H_0 (\sigma_1^2 = \sigma_2^2 = \dots = \sigma_k^2)$  is rejected,  $\sigma_k^2$  - variance of the steel yield point in fire temperature.

Consistently, the Bartlett's statistic  $b_{lnfe}$  to verify hypothesis about equality of yield point coefficient of variations in fire temperatures  $V_1^2 = V_2^2 = \dots = V_k^2$  was estimated ;

$$b_{lnfe} 0.247 < b_4(0.01, 24) = 0.882. \quad (14)$$

In this case we accept hypothesis  $H_0$ :  $V_1^2 = V_2^2 = \dots = V_k^2 = const$  and  $v_{fy,\Theta} = v_{fy,20} = const$ .

$V_k^2$  – coefficient of variation of the steel yield point in fire temperatures.

### 3 SUMMARY

- It can be assumed at the  $\alpha$  level of significance that the variations parameters of the steel modulus of elasticity  $E$  in fire temperatures is equal null.
- The variations parameters of the steel yield point (coefficient of variations, variance) in fire temperatures are significant and are not equal null.
- For reasons given above the coefficient of variation of the steel yield point is constant in fire temperatures
- More research is needed on the coefficients of variations, as found in practice, of some of the basic variables, and on the assumption that the distribution of the steel yield point in fire temperatures is log-normal.

### REFERENCES

- [1] Dunn O.J., Clark V.A., Applied Statistic: Analysis of Variance and Regression, *John Wiley Sons* N.J.,1987
- [2] Walpole R.E., Myers R.H., Myers S.L., Probability & Statistics for Engineers & Scientists, *Prentice Hall*.N.J.2002
- [3] Domański T., Variation Parameters of Structural Steel, Characteristics in Fire Temperatures. *Eurosteel 2008, 5<sup>th</sup> Conference on Steel and Composite Structures,2008 Graz, Austria. Publishing by ECCS,1200 Bruseels, Belgium.*
- [4] Maślak M., Domański T., Safety factors in design of steel members for accidental fire situation. In: *Proc. of the DFE2008 Int. Conf. "Design ,Fabrication and Economy of Welded Structures .Miskolc. Horwood Publishing Ltd.London,2008.*
- [5] EN 1990: Eurocode –Basis of Structural Design.
- [6] EN 1991-1-2:Eurocode 1:Actions on Structures – part 1-2:General Actions-Actions on Structures Exposed to Fire.
- [7] EN 1993-1-2:Eurocode 3:Design of Steel Structures – Part 1-2:General rules – Structural Fire Design.

## FIRE DAMAGE OF STONE STRUCTURES

Mónika Hajpál

ÉMI – Non-profit Company for Quality Control and Innovation in Building, Budapest, Hungary

### INTRODUCTION

Nowadays mostly the historic buildings are built of stone, they have also stone structural elements, the modern buildings contains only stone parts (embellishment, floor-plate). Natural stones were frequently used as building material in our historical monuments due to their advantageous properties. The finely carvable and well workable ones were applied as raw material of trim-stones, frontal ornamentations or sculptures. The hard, compact types were exceedingly applicable for load-bearing, structural elements (cope, vault, column, pillar, stairs, access balcony, lintel, bracket, etc.). The most popular types were able to be used both ways. Stone buildings were damaged by fire from ancient times until quite recently. In the stone material the fire causes irreversible changes, which influence the strength and static behaviour of the whole monument.

Some fires at the end of 20<sup>th</sup> century brought attention to the severe damage that fires can cause to historic buildings and their building stones.

There are some example mentioned without requiring completeness for historic fire incidents, which are well known since they were published in the world press:

- York Minster (1984)
- Hampton Court Palace (1986)
- Chiado, Lisbon, Portugal (1988)
- Uppark House, England (1989)
- Katarina Church, Stockholm Sweden (1990)
- Windsor Castle, England (1992)
- Odd Fellow Palace, Copenhagen (1992)
- St. Michaels Church in Newquay (1993)
- Redoutensal, Hofburg Palace, Vienna, Austria (1992)
- Theatre “La Fenice”, Venezia (1996)
- Cathedral of Torino “Sacra Sindone”, Torino (1997)
- St. Michael Church, Budapest (1998)

Till the 1990s mostly only fire resistance of wood, steel and concrete have been investigated. Due to prefabricated buildings the studies have been limited to the role of stone as an aggregate for concrete. Previous researches on the effects of fire on monumental stones have mainly focussed on morphological changes taking place on stone surfaces such as cracking, scaling [1, 2] or analyses of colour changes [3]. A few mechanical properties of fire-damaged sandstones or heated specimens were also measured [4, 5, 6]. Previously few researcher [7, 8, 9] have shown that sandstones are sensitive to heat by oven tests under laboratory conditions. They provide valuable information on the thermal behaviour of sandstones, the mineralogical and textural changes have been also published in detail.

In this paper first the traces of deterioration by fire are shown, then the results of petrological and petrophysical laboratory tests made on different stone type samples are demonstrated. The futur research will focus on the statical analysis of fire damaged stone structures. A computer model will be used for analyzing the statical behaviour and load carrying capacity of structural part simultaneously subjected to normal loading and high temperature.

### 1 DECAYS, TRACE OF FORMER FIRES

The measure of damage caused by fire depends on many factors. The changes at the natural stones could be influenced by the burning circumstances, e.g. is the heating one-sided or more-sided, homogenous or heterogeneous, the size of the burned stone, velocity of heating, the maximum burning temperature, stone type and its characteristics.

The one-sided and quick heating is much more disadvantageous. Thin elements like plates become warm sooner and thus are suffering less than the blocks. Fires can be small and localized, which generally do not generate much heat and their damaging effect is limited to surface effects and soiling of the surface by smoke. On the other hand the large and widespread fire generates more heat and as a result it has a significant effect on the physical-chemical properties of stone structure. The maximum temperature is 800°C in case of small fires, by large-scale catastrophic fires some hundred degrees more, but by burning significant amount of inflammable materials could cause much higher burning temperature.

The decay is a form of physical and chemical changes in stone. The changing of the rock constituent minerals and the inner structure induce the character and degree of the decay on effect of heat.

The **colour changes** in natural stones almost corresponds to the dehydration of iron compounds. Heat causes the development of a pink or reddish-brown colouration in brown or buff-colour (Fig.1.). It does not occur among white or grayish stones, which are relatively free from iron oxide. The colour changes start at a temperature of 200-300°C in most rocks and it may not be apparent until a somewhat higher temperature. By testing of big stoneblocks is a sharp boundary between the heated, red-coloured stone surface and the unaltered stone behind. These zone has a width about 2-3 cm or less. Some stones contain a small amount of organic substance which cannot be seen and which is seldom found in analysis. At about 500°C this organic matter begins to turn into coal and effects a grey colour covering the red one. At an increased temperature the carbon is burnt away and the original colour is visible again.

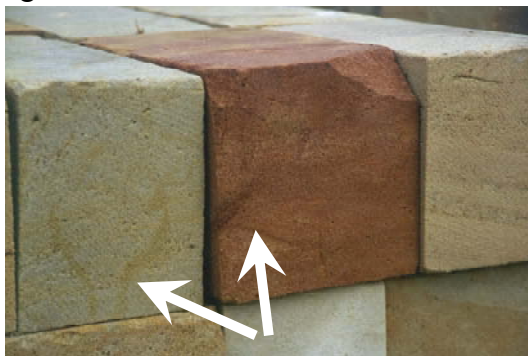


Fig. 1. Colour changing

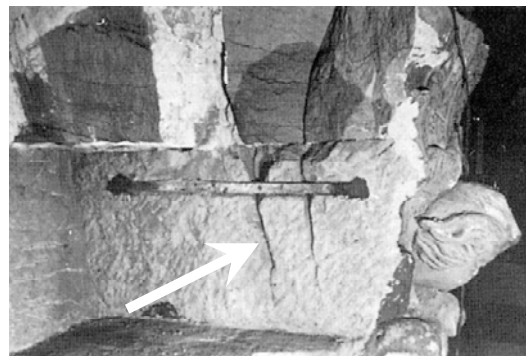


Fig. 2. Cracking

Other significant kinds of decay of stones by burning are cracking (Fig.2.), shattering, scaling, spalling, which completely destroy the richer carved forms of architecture and damages the smoother forms. They are often so badly spoiled that they have to be replaced by new ones.

Heat effect related **spalling** of sandstone is to be seen on Fig.3. At this window of the Monastery in Lobenfeld, in Germany the stone was quickly heated from one side, but it was still cold in its inner parts. The process of scaling is continued during the fire, therefore the strength of the stone is surpassed and a bursting of the hot outer part is forced and the rock peels like an onion. In the simplest cases the bursting of occurs in shells parallel to the surface: a sphere will burst in spherical calottes, a column in cylindrical shells.

**Rounding off the edges** can occur if there is an edge the heat can work from two sides. This form of decay is regularly seen on steps, edges of pillars and window-heads. Fig.4. shows a rounding of edges by fire a sandstone column at the Heidelberg Castle (Germany).

**Breaking** is typical where single parts are jutting out of a plane (Fig.5.). It heat up more quickly and burst off easier, since the stresses find the way out more quickly (e.g. scaling of bosses just to the depth of groove, the bursting of the ribs of channelled columns, etc.).

If the jutting part is sharply divided from its neighbourhood often arise additional notch effects. All kinds of carving in stones will influence the form of bursting. At a very long

heated construction (e.g. a door post or the longstep of a staircase) a distribution of the stress is not effected across the whole length, the length will be subdivided by means of small transverse cracks into divisions which will scale separately and the result will be a range of pillow-formed surfaces [2, 8].

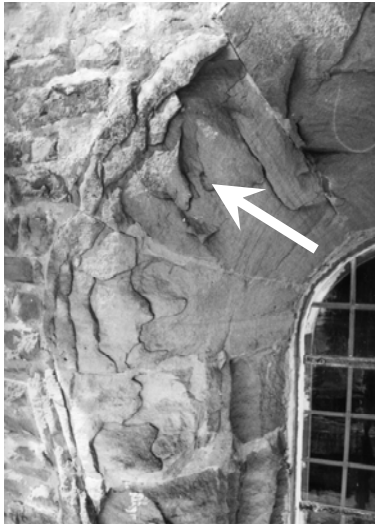


*Fig. 3. Spalling*



*Fig. 4. Rounding edges*

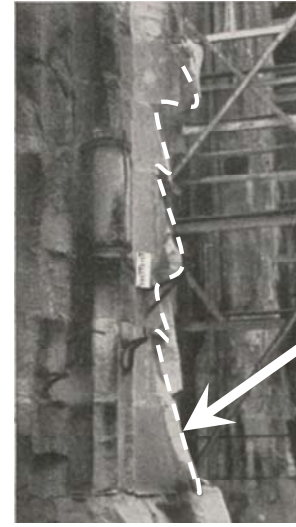


*Fig. 5. Breaking*

The texture will heavily influence the form of decay by inhomogeneous stones. Layers of mica, lamination, other cleavage planes or fine capillary cracks are always spots of failure and they will burst off at any rate. In stone structures tensions are by means of heating, differential dilation, and also from payloads and deadloads. In highly loaded pillars the exterior parts can be already overloaded and the additional heat stresses may cause disintegration. It is very important that we don't have to know only the behaviour of building stones, but we have to face the whole construction.

## 2 MATERIAL PROPERTIES

Hungarian stone types frequently used in historical monuments were taken into the experiments. Three types of sandstone, three types of limestone and a rhyolite tuff were chosen for the investigation. Besides I applied in my research seven types of German sandstones, and in cooperation with other researcher Portuguese and Spanish stones are also examined. The selected stone types showed a wide range of their feature (colour, grain size, cement type, age, rock constituent minerals, porosity, strength). This compositional variation enables us to achieve a better understanding of how such properties influence the behaviour of natural stones under heat.

Three types of Hungarian sandstones were used for the thermal tests: Balatonrendesi, Ezüsthgyi and Rezi. Seven German sandstone types were also investigated. The analysed quartz sandstones have different characteristics (grain size, porosity). The mineralogy of cements and the colour also varies [6, 8]. The three types of limestones (Tardos compact limestone, Süttő travertine, Sósút oolitic limestone), which were used for the thermal tests represent the most widely used monumental stones in Hungary [10]. The creamy colour rhyolite tuff from Egertihámér is used as ashlar in one of the most visited historic site of North-Hungary, in the Eger Castle and in environs.

## 3 INVESTIGATION METHODS

Because of the complexity of the processes taken place in case of fire and the lack of knowledge of the behaviour of stone material a simplified heating method was used for the simulation of the effect of fire. From the stone blocks cylindrical specimens (40 mm in

diameter and 40 mm to 80 mm in height) were prepared. The specimens were heated in an oven at 6 different temperatures (150, 300, 450, 600, 750, 900°C) for 6 hours. Warming up took 1 hour, and after controlled heating the specimens cooled down slowly in the oven. The samples were tested before and after the heating processes carried out at each temperature. The mineralogical composition of the samples heated to the different temperatures was determined by X-ray powder diffraction (XRD: Siemens D500) and by differential thermal analyses (DTA: MOM Derivatograph, 20-1000°C). Textural and mineralogical alterations were visualized under polarizing microscope in thin sections and by scanning electron microscopy (Cambridge Stereoscan). The petrophysical analyses included the measuring of specific and bulk density, porosity, water adsorption, duroskop hardness, ultrasonic sound velocity. Indirect tensile strength test and uniaxial compressive tests were also made. The colour changes were tested with CIELAB method.

## 4 RESULTS

### 4.1 Mineralogical analyses

As result of the mineralogical analyses the changes of the texture and inner structure and hereby the increasing in porosity, the disappearance of minerals or formation of new mineral phases and the colour change are observable. On effect of heating the quartz and K-feldspar do not show significant alteration up to 900°C. As major effects the transformation of  $\alpha$ -quartz to  $\beta$ -quartz (580-595°C) and the formation of micro-cracks at quartz and feldspar grain boundaries above the 600°C heating temperature were detectable. Micro-cracks develop also within the crystals but only at higher temperatures (above 750°C). Clay minerals and phyllosilicates show several transformations on heat effect. In the ferruginous sandstone (Balatonrendes) the changing of the iron-hydroxide and the kaolinite was shown. The micas iron contents oxidize and the clayey cement comes away from the pore wall in Ezüsthegy sandstone and hereby the mineral become dark. The structure of kaolinite mineral partly collapse after 750°C the, but thanks to the extremely large crystal size it is recognizable yet. Illite-smectite structures are more stable than kaolinite, it can be still detected at 900°C, although at 553°C it loses its hydroxyl radicals. The jarosite mineral in the Rezi sandstone changed its colour to yellowish brown by heating and it modified to hematite above 450°C. Kaolinite and chlorite first coloured by increasing the temperature then ruined additionally in the inner structure and in quartz grains cracks occurred. Due to calcination processes at limestones in the carbonate minerals the major changes took place at 450°C and above. At 750°C the structure of calcite collapsed and at 900°C calcite and dolomite was not possible to detect; however after leaving the samples at room temperature for two hours at about 45% relative humidity a new mineral phase, portlandite was detected. This is a reaction product of air humidity (water) and CaO and associated with a volume increase of 20% in average and leads to the disintegration of cylindrical specimens. In Tardos limestone a thin film of iron oxides cover the calcite crystals in some places and this degrades with the heating. In the Süttő travertine the calcite crystals are very rough, which show that the deposition was very quick. Thermal cleavage, inter-granular crackings and incipient surface dissolution of grains occurred at the effect of heat. In Sósút coarse limestone the heating makes small inter- and intragranular cracks arisen, which occur decided porosity increasing at elevated temperature. In Egertihámér rhyolite tuff bentonite flakes cover the surface of lithic clasts as a thin film. Above 750°C this is not yet recognizable.

## 4.2 Petrophysical investigations

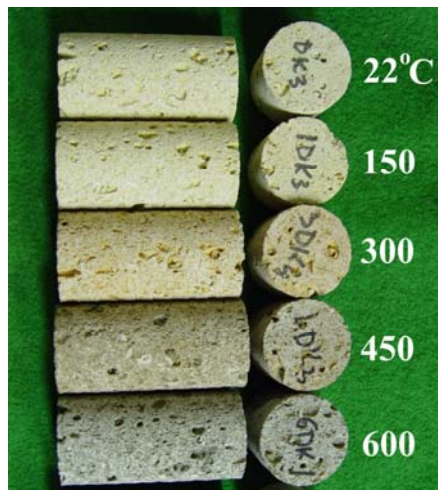


Fig. 6. Colour changing by Sós-kút coarse limestone samples

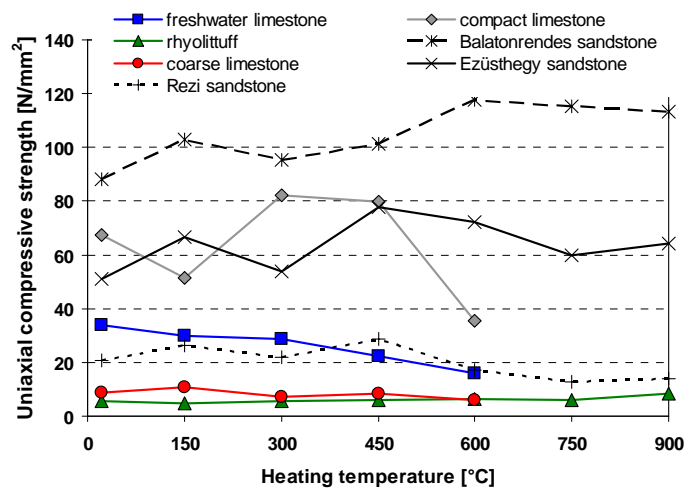


Fig. 7. Uniaxial compressive strength values as function of heating temperature at different stone types

The limestone samples were sensitive at the heating. On the compact limestones specimens small hairline cracks arised already after at heating on 450°C and over the 600°C heating temperature the samples exploded. These specimens faded at the elevated temperature (750°C). The travertine samples grown dark till 450°C and smelt foul due to organic matter content, but after this there also paled. These specimens survived the heating, but some hours after the test the CaO had reaction with the air moisture and due to nascent portlandite and the volume increment the samples crumbled. The coarse limestone samples also stand out the effect of heat at 750°C and 900°C, but they have falled into dust soon (Fig. 6). Some reports [3, 7] mention this process by high temperature tests of calcite containing stones. The heating did not result similar problems at the sandstones and the rhyolite tuff samples.

The colour changing was detectable by eyes (Fig. 6), but for the correct determination instrumental testing was (CIELAB method) also used. The colour modification of stone types was different. The dark grey colour of travertine samples at elevated temperature and the nascent hum indicates to organic matter content. Fig. 7 shows the results of the compressive strength test as function the heating temperature. It can be observed, that the heating does not causes a decrease in the strength in all cases. The Balatonrendes and Ezüsthegy sandstone and also the Egertihámér rhyolite tuff has higher strength after the heating at 900°C as in the beginning state before heating. The limestone types lost their strength not promptly but only at elevated temperature.

## 5 SUMMARY

At the effect of heat changes take place in the inner structure and mineral composition of the natural stones, which influences the petrophysical parameters (porosity, strength, water adsorption, colour). This changing is not always adverse, but we have to take it to account for instance at the restoration of a fire damaged stone building. The mineralogical composition and texture of natural stones significantly influence their resistance to fire and the thermal changes. The heat resistance of different quartz sandstone depends on the type of the cementing mineral, the amount of cement (grain/cement ratio), the grain size (fine, medium, coarse) and the grain to grain or matrix to grain contacts. The initial porosity, compactness influences the behaviour of limestone and rhyolite tuff at heat effect. The compact stones show more dramatic change in porosity at elevated temperatures than the less cemented ones and they are more rigid. At a porous and cement rich stone is more adaptable, these can adopt

the addition strength caused by thermal expansion. The mineral composition is also determinant factor. The silica cemented, ferruginous or clayey stones are less sensitive than the carbonatic ones, which disintegrate at higher temperature. It is to be regretted that it is not possible to use the sequence of colours as a scale of temperature. The amount of colouring substances is different with every square stone, and one can see the most varied degrees of colours on a heated wall. The degree of temperature and the duration of heating can replace each other to a large extent.

In the future the results of petrological and petrophysical laboratory tests can help as input at the calculation by fire damaged stone structure. This kind of computer model will be used for statical analyzing the statical behaviour and load carrying capacity of structural part simultaneously subjected to normal loading and high temperature.

## 6 ACKNOWLEDGMENT

The author gratefully acknowledges the support of her earlier workplace the Budapest University of Technology and Economics (BUTE), Department of Building Energetics and Building Services, Laboratory of Building Physics and her supervisor, Dr. Ákos Török (BUTE, Department of Construction Materials and Engineering Geology) for his valuable help during the research work in the last years.

## REFERENCES

- [1] Kieslinger A., *Zerstörungen an Steinbauten*, Franz Deuticke. Leipzig und Wien, 1932
- [2] BRE, *Repair of Damaged Buildings—the repair of stonework damaged by fire. Garston Building Research Establishment Note 21:1–5*, 1945
- [3] Chakrabarti B., Yates T., Lewry A., Effect of fire damage on natural stonework in buildings. *Construction and Building Materials (10)*, pp. 539–544, 1996
- [4] Chakrabarti B., An assessment of effects of fire damage to stone in buildings & procedures for restoration and conservation of stone in some historic stone buildings. *Building Research Establishment Note 93(15)*, pp 2–14, 1993
- [5] Allison RJ, Goudie AS, The effects of fire on rock weathering: an experimental study. In: Robinson DA, Williams RBG (eds) *Rock Weathering and Landform Evolution*. Wiley, Chichester, pp 41–56, 1994
- [6] Hajpál M, Török Á., Mineralogical and colour changes of quartz sandstones by heat. *Environmental Geology*, 46 (3-4), pp. 311-322, 2004
- [7] Török Á., Hajpál M., Effect of Temperature Changes on the Mineralogy and Physical properties of Sandstones. A Laboratory Study. *International Journal for Restoration of Buildings and Monuments*, 11 (4), Freiburg, pp. 211-217, 2005
- [8] Hajpál M., Changes in sandstones of historical monuments exposed to fire or high temperature. *Fire Technology* 38(4), pp. 373–382, 2002
- [9] Hajpál M., The behaviour of natural building stones by heat. *Fracture and Failure of Natural Building Stones. Applications in the Restoration of Ancient Monuments*, pp. 439-445, 2006
- [10] Gomez-Heras M., Alvarez de Buego M., Fort, R, Hajpál, M., Török Á., Varas M.J., Evolution of porosity in Hungarian building stones after simulated burning. In: Fort, R, Alvarez de Buego M., Gomez-Heras M. & Vazquez-Calvo C. (Eds): *Heritage Weathering and Conservation, Taylor & Francis/Balkema, London. Vol. I*, 513-519, 2006

## **THERMAL CHARACTERISTICS MEASUREMENTS OF AN INORGANIC INTUMESCENT COATING SYSTEM**

J. Yoon Choi, Hyun Min Jang, Chaemin Chun <sup>a</sup>

<sup>a</sup> Korea Institute of Construction Materials, Weathering Technology Center, Seoul, Korea

### **1 INTRODUCTION**

Intumescent coatings are widely used to improve thermal resistance of steel building structures under fire conditions. By knowing the thermal characteristics of an applied intumescent coating system as a function of temperature, the insulating properties of intumescent coating protected steel structure could be better understood.

However, intumescent coatings, as their nature, exhibit time and temperature dependant changes of physical and chemical properties when they are exposed at thermal sources. These time and temperature dependant properties include thermal diffusivity, density and specific heat capacity etc. These would be some of the important values to be used for the prediction of structural safety under fire conditions.

Substantial amount of commercially available intumescent coating systems are comprised of polymer resin with ingredients such as intumescent agents, fillers and property enhancers. In depth polymer resin contained intumescent system has been investigated [1-3]. Although advantageous aspects, which would include harder expanded insulating layer and low gas evolution during expansion, can be achieved by excluding polymer resin, a few intumescent systems exclude polymer resin as the continuous medium [4] [5].

A commercially available inorganic intumescent coating system, of which applicability as a passive fire protection product under ISO 834 fire test condition is reported, was chosen and physical and chemical changes were measured and reported in this paper.

### **2 EXPERIMENTAL**

A commercially available inorganic intumescent coating product named FC-MAX [6], which is a water dispersion of inorganic particles, was used for this work. Reported main ingredients include sodium silicate as the expanding agent, titanium dioxide and aluminium oxide as fillers and Kaolinite as the substitute of polymer resin.

Intumescent coating samples were prepared using an automatic film applicator, PA2101 Byk Gardner, to achieve uniform sample thickness of wet coated film, and then the film was dried under room condition until no further weight decrease was measured. The dried samples were used here after experiments unless otherwise specified. For heat treatment, samples were located within an electric oven that was set up at wanted temperature for 30 minutes.

Images of samples were acquired using a HITACHI S-3000H SEM. To characterize time and temperature dependent behaviours of the interested sample, NETZCH STA 409PC, QMS 403C STA-MS was used between room temperature and 1400 °C at elevating temperature

speed of 10 °C/min. Under the same test conditions NETZCH STA 409PC was used to analyze the weight changes. To characterize evolving gases during the heating period MS was used simultaneously. Specific heat capacity measurements were performed using NETZCH DSC 404 to increase accuracy at higher temperature ranges. Also these samples were used to measure thermal diffusivities using a laser flash apparatus, NETZCH LFA 457

### 3 RESULTS AND DISCUSSION

Intumescent coating solution was diluted with water then particles within the solution were collected with a filter paper. Surface image of the collected particles is presented at Figure 1. The image indicates the particle size of the ingredients of the dried coating is within the order of  $\mu\text{m}$ . Hexagonal flake shape particles shown at the figure represent Kaolinite. This image would indicate that lab scale thermal experiments including DSC, TG, MS and LFA that only use mg scale samples would be sufficient enough to represent the whole system. Figure 2 shows the intumescent system after expansion at 600 °C.

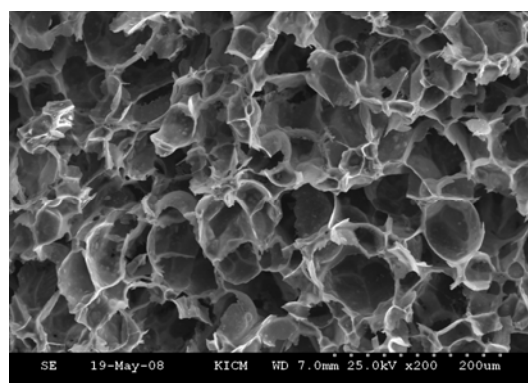
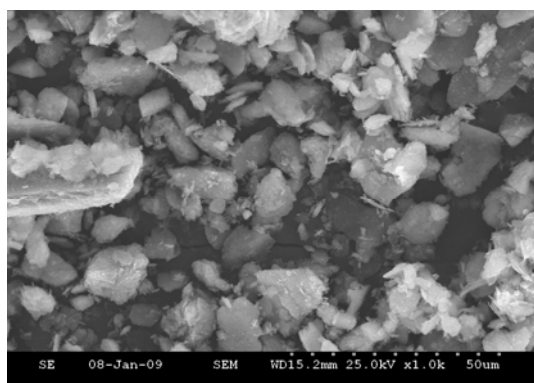


*Fig. 1.* SEM image of ingredient particles *Fig. 2.* Expanded intumescent coating at 600 °C

To analyze thermal reactivity of the system, DSC and TG were applied and the result is shown at Figure 3. This indicates that endothermic reaction appears between ca 118.8 °C and 168.2 °C. During this period approximately 9.2% w/w mass decrease was measured. At this temperature range inflation of the sample i.e., intumescent characteristics could be observed as well. As was reported sodium silicate and Kaolinite lose absorbed water around 100 °C and the process ends at 200 °C [7], [8]. For the case of Kaolinite, dehydration process of physically adsorbed water goes on between 400~700 °C.

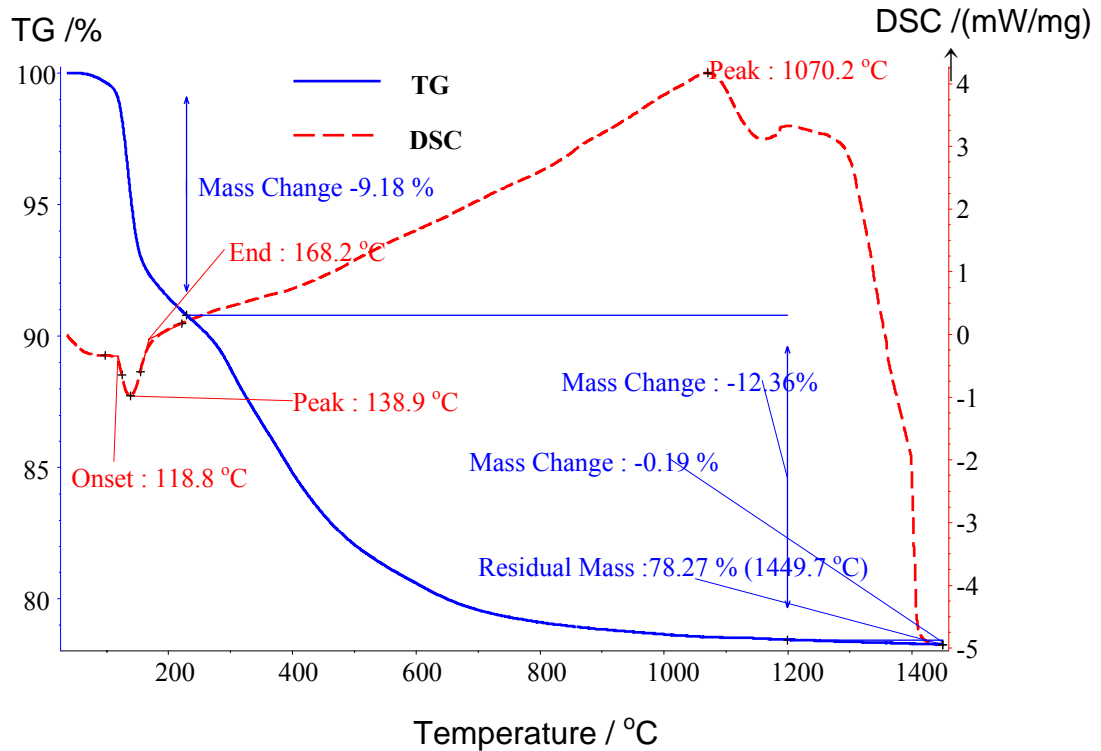


Fig. 3. DSC and TG results of the intumescent coating system

Therefore it could be suggested that the rapid decrease of mass within the system is due to loss of water from sodium silicate and Kaolinite until 200 °C and then gradual decrease thereafter is from dehydration of Kaolinite. This could be supported by the analysis of MS TG-MS measurements shown at Figure 4. This indicates that most of the evolving gas is only water and hydroxide ion. After the intumescent process the system is structured by several 10~100 um size pores constructed with wall thickness of single order um or less. This could be seen from the SEM image at fully expanded state of a cross sectional one after sample was experienced at 600 °C (see Figure 2)

Because of the weight decreases until ca 1200°C, thermally treated samples at every 100°C were prepared to measure more reliable thermal properties at dynamic state. Density, heat capacity and thermal diffusivity were measured at each temperature state and presented at Figures 5~8. As could be observed by TG data after 200 °C gradual weight decreases due to dehydration process appears. This causes linear trend of weight and density decreases through out the measured temperature range. Comparing with the dried coating at the initial state, density decreases over 88% at 200 °C and 92% at 700°C could be observed. The dehydration process also causes gradual decrease of heat capacity. Thermal diffusivity measurements are presented at Figure 7.

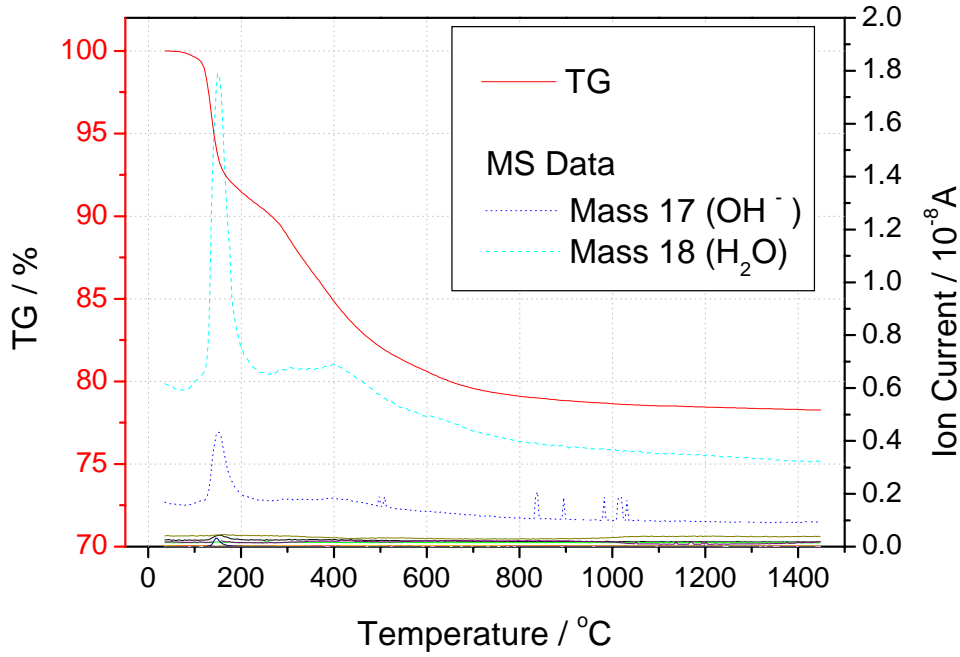


Fig. 4. TG and MS spectra results

These measurements and a mathematical equation (1) allow calculating thermal conductivity changes and the values are shown at Figure 8. As could be seen at the figure thermal conductivity slightly decreases from 200 °C to 400 °C then increases until 600 °C, which is near the starting value at 200°C. Comparing with the increasing thermal conductivity values of general materials without phase or chemical structural changes, the investigated system holds the low value from 200°C to 700°C and this allows the system applicable for passive fire protection

$$\lambda = \alpha \rho C_p \quad (1)$$

where  $\lambda$  is the thermal conductivity,  $\alpha$  the thermal diffusivity,  $\rho$  the density and  $C_p$  the heat capacity

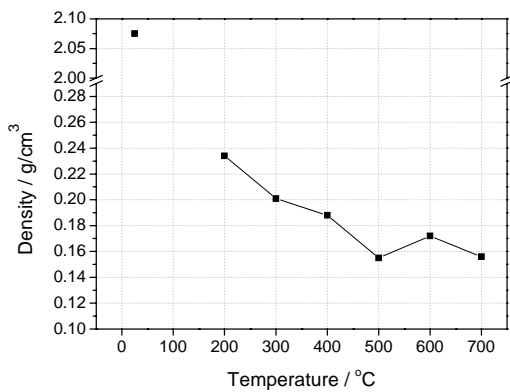


Fig. 5. Density changes as a function of temperature

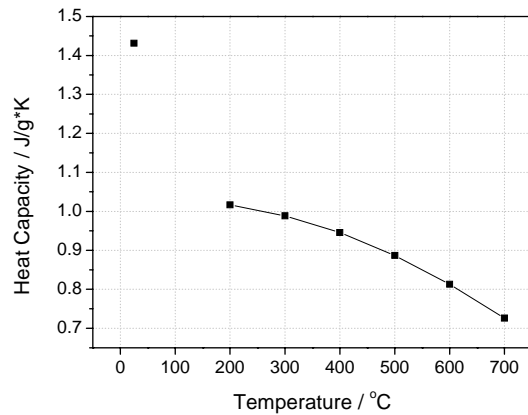


Fig. 6. Heat capacity changes as a function of temperature

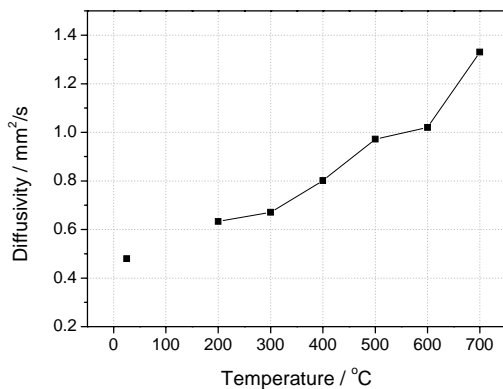


Fig. 7. Thermal diffusivity changes as a function of temperature

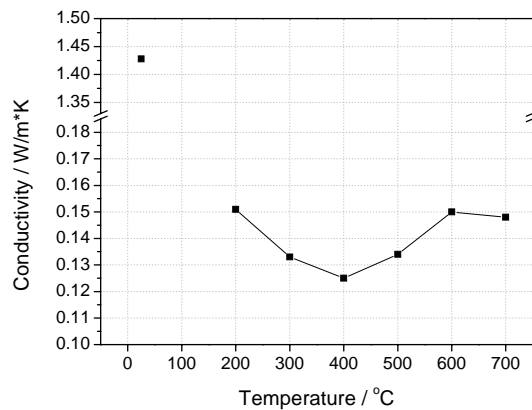


Fig. 8 Thermal conductivity changes as a function of temperature

#### 4 SUMMARY AND ACKNOWLEDGMENT

The present study describes methods to characterise thermal properties of intumescent coating system of which thermophysical values changes as a function of temperature. For the presented intumescent coating system, lab scale experiments of measuring thermophysical properties including thermal diffusivity and specific heat constant could be enough to represent overall system.

Due to the nature of the intumescent coating system, at different temperature density, specific heat constant and thermal diffusivity changes so samples were prepared to represent at different temperature and the above thermal properties were measured. When the system was experienced at higher temperature, density and heat capacity constants decreased but thermal diffusivity increased. Hence thermal conductivity of the system could be kept similar state until 700 °C.

The authors would like to thank Eunho Lee at Ajou University for valuable helps during LFA experiments and Hitem co. ltd for kindly supplying FC-Max samples. The work presented in this paper was undertaken as part of the research projects issued by Ministry of Knowledge Economy and Ministry of Land, Transport and Maritime Affairs. The authors gratefully acknowledge the financial assistance of the ministries.

## 5 REFERENCES

- [1] Duquesnea, S., Delobela R., Brasa, M. and Caminob, G., *Polymer Degradation and Stability* 77 (2002) 333-344
- [2] Duquesnea, S., Bras, M. L., Bourbigot, S., Delobel, R., Camino, G. C., Eling, B., Linsay, C., and Roels, T, *Polymer Degradation and Stability* 74 (2001) 493-499
- [3] Zverev, V. G., Gol'din, V. D., Nesmelov, V. V., and Tsimbalyuk, A. F. *Combustion, Explosion and Shocks Waves*, Vol. 34 (1998) 198-205
- [4] Koo J. H., *Fire Technology* 34 (1998) 59-71
- [5] Langille, D., Nguyen, D. and Veinot, D. E., *Fire Technology* 35 (1999) 99-110
- [6] [www.hitem.co.kr](http://www.hitem.co.kr)
- [7] Vauhan, F., *Clay Microporous and Meroporous Materials* 2 (1955) 265-274
- [8] Selvam, T., Bandarapu, B., Mabande, G.T.P., Toufar, H., and Schwieger, W *Microporous and Meroporous Materials* 64 (2003) 41-50

## **STRESS-STRAIN RELATIONSHIP OF REINFORCING STEEL Subjected to Tension and High Temperature**

Marian Abramowicz <sup>a</sup>, Robert Kowalski <sup>b</sup>

<sup>a</sup> Main School of Fire Service, Warsaw, Poland

<sup>b</sup> Warsaw University of Technology, Poland

### **INTRODUCTION**

Due to popularisation of legal regulations [1] and Eurocodes [2, 3, 4] one can expect that in the nearest future during analyses of especially important buildings or buildings where people's safety is especially threatened more and more often fire is going to be considered the accidental design situation. It means that calculations of load bearing capacity of RC elements subjected to fire conditions will be required more and more often. In these calculations an appropriate estimation of stress-strain relationship of reinforcing steel plays a crucial role.

When separated structural elements are analysed the estimation of real values of reinforcement elongations is necessary for cross-section load bearing capacity calculation. When a part of a structure is considered or when a global structural analysis is performed the appropriate estimation of reinforcement elongations is also necessary for cross-sections stiffness decrease calculation. The appropriate estimation of element stiffness decrease is necessary for prediction of internal forces redistribution which often appears due to fire. Additionally in some cases as a result of stiffness decrease and significant deflections of elements heated up to high temperature a secondary static scheme of the structure might appear.

The basic stress-strain relationship of reinforcing steel subjected to high temperature is given in Eurocode [4] but before taking Eurocode model into calculations concerning fire design situation some comments and considerations should be given.

### **1. WAYS OF TESTING STEEL HEATED UP TO HIGH TEMPERATURE**

In room temperature analyses the mechanical properties of reinforcement are usually considered in two coordinate system stress-strain ( $\sigma$ - $\varepsilon$ ). In analyses concerning fire design situation the third coordinate (temperature ( $\theta$ )) appears. However, testing specimens in presence of three variable parameters ( $\sigma$ - $\varepsilon$ - $\theta$ ) could be difficult and would not lead to satisfying practical results. As a result in practice two the most important ways of testing reinforcing bars subjected to high temperature are usually used [5, 6]:

- at constant temperature (steady temperature state),
- at variable (increasing) temperature.

When the first type of testing is performed the specimens are at first heated up to high temperature. This temperature takes various values but it is kept constant in each particular test. At constant high temperature values the stress-strain relationships are examined. The way of testing is usually more or less the same as the one used at room temperature. As a result the tests performed at constant high temperatures are relatively easy to realise in practice and their results can be compared with the results obtained in room temperature tests. The Eurocode [4] model is based on the test results performed at constant temperature [5].

When the second type of testing is performed the specimens are at first loaded. The level of stress is various but it is kept constant in each particular test. During the test the specimens are heated up and the elongation (in practice displacement) is measured. In this way the temperature-strain relationships for various stress values are obtained.

Before comparing these two ways of testing it is worth to have a brief look at the problem of steel elongation at high temperature. The total elongation of reinforcing bar heated up to high temperature ( $\varepsilon_{tot}$ ) can be expressed as the sum of three components as follows [5, 7]:

$$\varepsilon_{tot} = \varepsilon_0 + \varepsilon_\sigma + \varepsilon_{cr}. \quad (1)$$

In formula (1):

$\varepsilon_0$  – is the free thermal steel strain (appearing without any load action),

$\varepsilon_\sigma$  – is the elongation appearing due to load action; sometimes the  $\varepsilon_\sigma$  elongation can be divided in two parts: the elastic and the ductile part but in the Authors' opinion the division of  $\varepsilon_\sigma$  is not important from the practical fire design analyses point of view,

$\varepsilon_{cr}$  – is the creep elongations; it appears due to long term simultaneous action of load and high temperature.

In the tests performed at constant temperature the specimens are at first heated up and after that the measurement of the elongation begins. As a consequence the free thermal steel strain ( $\varepsilon_0$ ) is usually neglected in the test results. In addition due to the relatively short time of the stress-strain relationship testing the significant part of the creep elongation ( $\varepsilon_{cr}$ ) is also neglected. Reassuming it can be noticed that during the tests performed at constant high temperature only the elongation appearing due to the load action ( $\varepsilon_\sigma$ ) is measured. The test performed at constant high temperature does not simulate the real conditions to which the structural elements are subjected during the real fire.

The real fire conditions can be simulated during the tests performed at variable (increasing) temperature. The reinforcing bars of real structural elements are stressed before the fire starts. During the fire the bars are heated up while stressed. In this conditions the total bar elongation consists of the sum of the free thermal strain ( $\varepsilon_0$ ), the elongation appearing due to the load action ( $\varepsilon_\sigma$ ) and the part of the creep elongation ( $\varepsilon_{cr}$ ). The significance of this part depends on the rate of heating. When the rate of heating simulates bar temperature increase during the fire the test results can be appropriate for analyses of structural elements stiffness decrease.

## 2. EUROCODE [4] MODEL ANALYSIS

The basic assumption of Eurocode [4] model gives a general stress-strain relationship shown in Fig. 1. This relationship consists of three line segments and the part of ellipse inscribed between them. Mathematical formulas of the ellipse and the coefficients necessary for the calculation of values of steel mechanical properties appearing on the vertical axis are given in [4]. Table 1 shows the examples of the coefficients for hot rolled reinforcing bars.

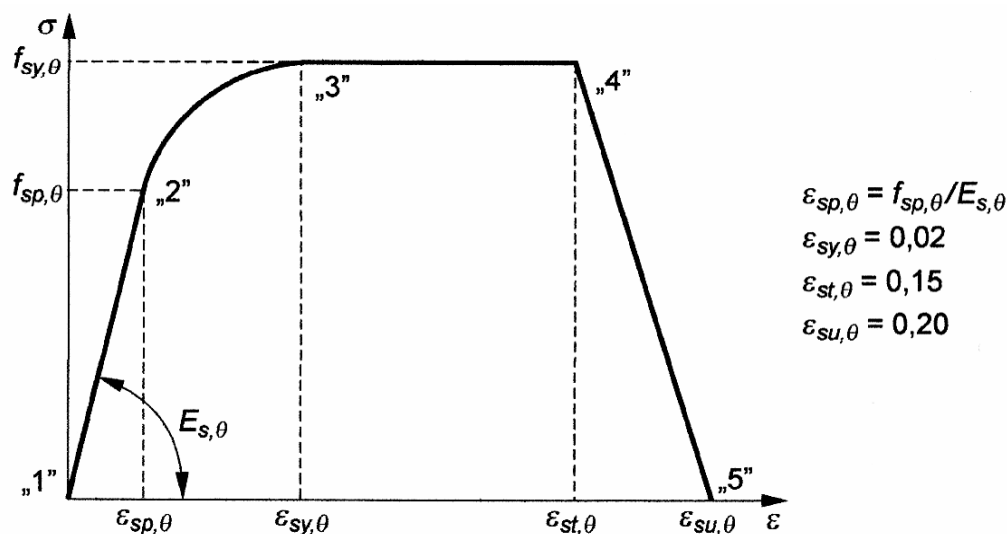


Fig. 1. The general stress-strain relationship for reinforcing steel heated up to high temperature [4]

Table 1. Coefficients for calculation of hot rolled steel mechanical properties at high temperature [4]

| Temperature ( $\theta$ ), °C | Yield strength           | Proportional limit       | Modulus of elasticity |
|------------------------------|--------------------------|--------------------------|-----------------------|
|                              | $f_{sy,\theta} / f_{yk}$ | $f_{sp,\theta} / f_{yk}$ | $E_{s,\theta} / E_s$  |
| 20                           | 1.00                     | 1.00                     | 1.00                  |
| 100                          | 1.00                     | 1.00                     | 1.00                  |
| 200                          | 1.00                     | 0.81                     | 0.90                  |
| 300                          | 1.00                     | 0.61                     | 0.80                  |
| 400                          | 1.00                     | 0.42                     | 0.70                  |
| 500                          | 0.78                     | 0.36                     | 0.60                  |
| 600                          | 0.47                     | 0.18                     | 0.31                  |
| 700                          | 0.23                     | 0.07                     | 0.13                  |
| 800                          | 0.11                     | 0.05                     | 0.09                  |
| 900                          | 0.06                     | 0.04                     | 0.07                  |
| 1000                         | 0.04                     | 0.02                     | 0.04                  |
| 1100                         | 0.02                     | 0.01                     | 0.02                  |
| 1200                         | 0.00                     | 0.00                     | 0.00                  |

For practical use of Eurocode [4] model it is necessary to put the values calculated according to the Tab. 1 into the relationship shown in the Fig. 1. However, doing this one can realise that the abscissa of point „2” in the Fig. 1 is given as  $\varepsilon_{sp,\theta} = f_{sp,\theta} / E_{s,\theta}$ , the value of proportional limit  $f_{sp,\theta}$  depends on  $f_{yk}$ , and  $E_{s,\theta}$  depends on  $E_s = 200$  GPa. As a result the value of  $f_{yk}$  has to be assumed for calculation of the elongation  $\varepsilon_{sp,\theta}$ . It means that it is impossible to prepare the general relationship with relative values of reinforcing steel mechanical properties on vertical axis. Figure 2 shows the examples of stress-strain relationships prepared by the Authors for hot rolled reinforcing steel of the yield strength of  $f_{yk} = 500$  MPa.

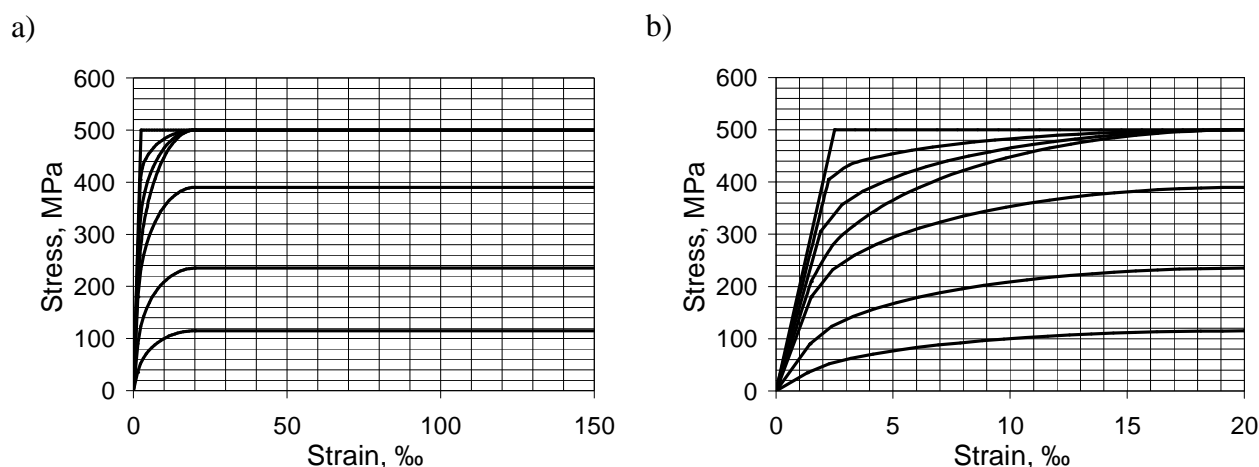


Fig. 2. Stress-strain relationships of hot rolled reinforcing steel ( $f_{yk} = 500$  MPa) at high temperatures. Looking from the left side of the figure the successive lines refer to the temperature 100, 200, 300, 400, 500, 600 and 700 °C respectively: a) in the strain range of 0-150‰, b) the part of Fig. a in the strain range of 0-20‰.

Comparing figures 1 and 2a one can notice that the relationship shown in the Fig. 1 does not respect the scale of the horizontal axis. Almost all area of Fig. 2a is covered by the horizontal lines situated between strain values of 20 and 150‰. These lines can influence the calculation results only when advanced analysis is performed. When simplified calculation method is used the appearance of reinforcement elongation in point „3” in the Fig. 1 means that the cross-section ultimate limit state is reached. As a result in practical simplified analysis the cross-section ultimate limit state will always be reached when the steel elongation is equal to 20‰ irrespectively of the temperature.

In the Authors’ opinion the point „3” should rather take a variable placement on the horizontal axis of Fig. 1. The elongation  $\varepsilon_{sy,\theta}$  could be lower than 20‰ for the relatively low temperature and

higher than 20‰ for the relatively high temperature. It should also be reminded that in the original version [5] of the Eurocode [4] model the line segment situated between points „3” and „4” in the Fig. 1 was not horizontal but took higher and higher values with the strain increase.

The Eurocode [4] model is based on the test results performed in steady temperature state conditions [5]. It means that the steel elongation obtained according to the Fig. 1 is only this part of the total reinforcing bar elongation which appears due to stress ( $\varepsilon_\sigma$ ). The Authors suggest that for RC elements calculation in fire the free thermal steel elongation ( $\varepsilon_\theta$ ) should be added to elongation calculated according to the Fig. 1. The Fig. 3 shows the stress-strain relationships for reinforcing steel ( $f_{yk} = 500$  MPa) prepared by the Authors. The elongation shown in the Fig. 3 is the sum of the values taken from the Fig. 2b and free thermal steel elongation estimated according to Eurocode [4] recommendation. Comparing figures 2b and 3 one can conclude that the elongation of RC elements bars can be larger than the one calculated according to the Eurocode [4] model.

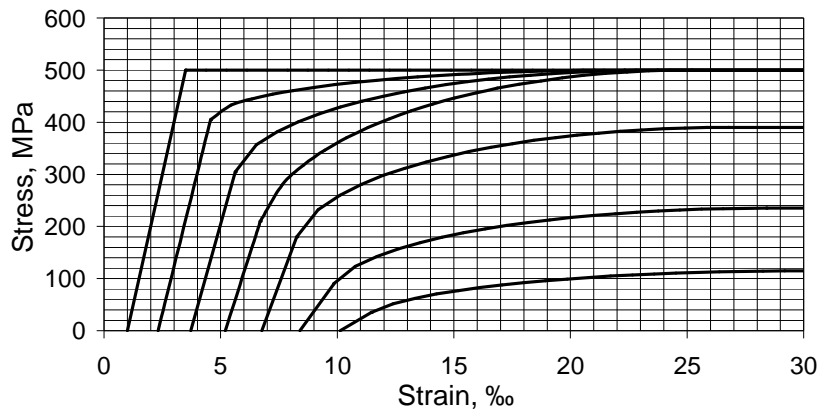


*Fig. 3. Stress-strain relationships of hot rolled reinforcing steel ( $f_{yk} = 500$  MPa) at high temperatures. Looking from the left side of the Figure the successive lines refer to the temperature 100, 200, 300, 400, 500, 600 and 700 °C respectively. The strain is the sum of values taken from Fig. 2b and free thermal steel elongation estimated according to [4] recommendation.*

### 3. REINFORCEMENT ELONGATION IN HEATED UP RC BEAMS

The sum of the average strain values of the external cross-section fibres can be estimated on the base of the beam deflection. For that purpose, one should consider generally known formulas. The beam deflection is expressed with the following formula:

$$a = \alpha \cdot \frac{Ml^2}{EJ} \quad (2)$$

The beam axis curvature can be expressed with two formulas:

$$\frac{1}{r} = \frac{M}{EJ} \quad (3)$$

and

$$\frac{1}{r} = \frac{\varepsilon_s + \varepsilon_c}{d} \quad (4)$$

In the formula (4)  $\varepsilon_s$  is the average value of reinforcing bar elongation,  $\varepsilon_c$  is the average value of the contraction of the external fibre of concrete compressed zone and  $d$  is the cross-section depth.

With the above formulas (2, 3 and 4) the sum of the average values of concrete and reinforcement strains can be expressed as follows:

$$\varepsilon_s + \varepsilon_c = \frac{d \cdot a}{\alpha \cdot l^2} \quad (5)$$

When the ratio of  $\epsilon_s$  to the sum of  $\epsilon_s + \epsilon_c$  is assumed the average values of  $\epsilon_s$  can be estimated according to the formula (5) on the base of the beam deflection.

The Authors tested RC beams under simultaneous action of high temperature and constant load. The cross-section of tested beams was  $b \times h = 12 \times 14$  cm and their length was 120 cm. Two types of concrete: C30/37 and C60/75, with siliceous aggregate and three different reinforcement ratios were used. The main reinforcement of each beam consisted of two bars. Cold rolled 6 mm diameter bars of  $f_y = 674$  MPa steel and hot rolled 10 and 14 mm diameter bars of  $f_y = 580$  MPa steel were used. The concrete cover of the bars in each beam was 15 mm.

The beams were put into the furnace chamber, heated up to the temperature of 670 °C and immediately loaded to the load level of 54 % of their load bearing capacity obtained experimentally at room temperature. The temperature inside the chamber increased to the value of 800 °C in about 15 minutes and then it was kept constant. The beams were tested under simultaneous action of high temperature and constant load up to the failure. During the test the deflection of beams and the temperature inside some places of their cross-sections were measured. More details about specimens and testing procedure can be found in [8, 9].

Table 2 shows the average beam deflections and the values of the average reinforcement bar elongation estimated on the base of beam deflection according to formula (5) and assumption shown in the column 2 of the Table 2 at various temperatures. Because the deflections of beams made of C30/37 and C60/75 concrete were more or less equal in the Table 2 only the average values of both concrete type beams are shown.

Table 2. Average values of beam deflection and estimated average reinforcement elongations at various temperatures

| Reinforcement type | $\frac{\epsilon_s}{\epsilon_s + \epsilon_c}$ | Average beam deflection, mm                          |       |       |       |        |
|--------------------|--|--|-------|-------|-------|--------|
|                    |  | Average reinforcement elongation ( $\epsilon_s$ ), ‰ |       |       |       |        |
|                    |  | 100°C  | 200°C | 300°C | 400°C | 500°C  |
| 1                  | 2  | 3  | 4     | 5     | 6     | 7      |
| 2 $\phi$ 6         | 0.95   | 3.6  | 6.1   | 8.6   | 12.5  | 23.1*  |
|                    |  | 3.49   | 5.91  | 8.34  | 12.07 | 22.34* |
| 2 $\phi$ 10        | 0.89   | 5.8  | 7.8   | 11.2  | 15.9  | 33.6   |
|                    |  | 5.22   | 7.08  | 10.12 | 14.44 | 30.46  |
| 2 $\phi$ 14        | 0.77   | 8.0  | 11.1  | 14.8  | 20.4  | 41.4   |
|                    |  | 6.28   | 8.68  | 11.63 | 15.99 | 32.25  |

\*The deflection and the elongation obtained at the temperature of 475°C.

Figure 4 shows the comparison of the average reinforcement elongations obtained in tested beams (Tab. 2) and the elongations calculated by the Authors according to the Eurocode model [4].

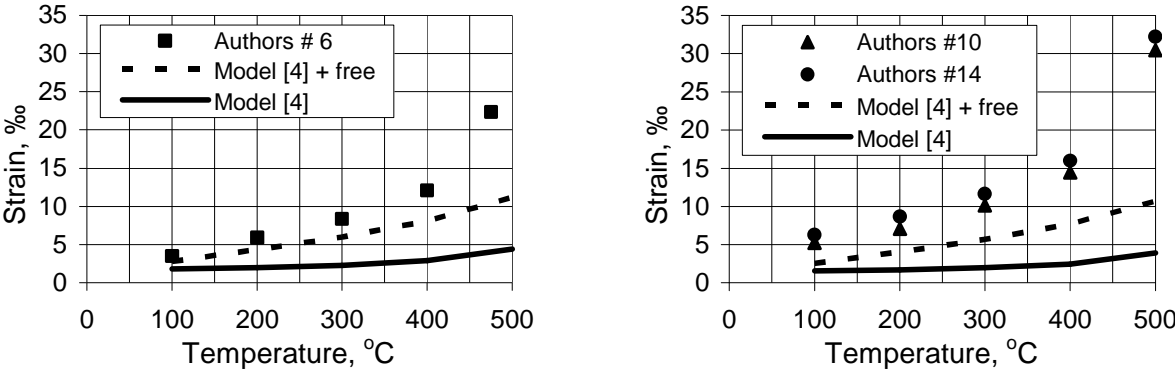


Fig. 4. Comparison of reinforcement elongation obtained in tested beams and Eurocode [4] prediction: marks – the Authors’ test results, solid line – elongation calculated according to the Eurocode [4] stress-strain relationship model, detached line – the sum of Eurocode [4] model and free thermal steel strain

In the Fig. 4 the marks referring to reinforcement elongations obtained in tested beams are situated much higher than both lines calculated according to the Eurocode [4] model. It might suggest that the elongation of real bent RC elements is higher than values estimated according to Eurocode [4] due to the steel creep elongation ( $\varepsilon_{cr}$ ) or that Eurocode [4] model underestimates reinforcement elongation.

#### 4. CONCLUSIONS

The stress-strain relationship recommended in the Eurocode [4] is based on the test results performed in steady temperature state conditions. This type of testing does not simulate the conditions to which the real RC structural elements are subjected during the real fire.

The reinforcing bars of real RC structural elements are stressed before the fire starts and during the fire the bars are heated up while stressed. The real fire conditions can be simulated by the tests performed under constant load and increasing temperature. In these tests the sum of the free thermal steel strain and the elongation appearing due to load action is measured.

When the stiffness decrease of bent RC structural elements in fire is going to be considered the reinforcement elongation should be calculated according to the Eurocode [4] as the sum of the elongation estimated on the base of stress-strain relationship and free thermal steel elongation.

#### REFERENCES

- [1] Interpretative Document (to Council Directive 89/106/EEC), Essential Requirement No 2 "Safety in Case of Fire".
- [2] EN 1990: 2002: Eurocode: Basis of structural design.
- [3] EN 1991-1-2:2002: Eurocode 1: Actions on structures – Part 1-2: General actions – Actions on structures exposed to fire.
- [4] EN 1992-1-2: 2004: Eurocode 2: Design of concrete structures – Part 1.2: General rules - Structural fire design.
- [5] Anderberg Y.: Modelling Steel Behaviour. Fire Safety Journal 13, 1988, p. 17-26.
- [6] Kirby B.R., Preston R.R.: High Temperature Properties of Hot-rolled, Structural Steels for Use in Fire Engineering Design Studies. Fire Safety Journal 13, 1988, p. 27-37.
- [7] Skowroński W.: Fire Safety of Metal Structures. PWN, Warsaw 2004.
- [8] Kowalski R.: Load bearing capacity calculation of bent RC elements in fire (in Polish). Publishing House of the Warsaw University of Technology. Scientific Works. Building Engineering 149/2008.
- [9] Kowalski R.: Deformation and Load Bearing Capacity of RC Flexural Cross-Section Subjected to Fire. 7<sup>th</sup> International Congress Concrete: Construction's Sustainable Options. Dundee, Scotland, 2008. Conf. Proc. Concrete for Fire Engineering p. 35-46.

## DECOMPOSITION OF INTUMESCENT COATINGS: COMPARISON BETWEEN NUMERICAL METHOD AND EXPERIMENTAL RESULTS

Luís M.R. Mesquita<sup>a</sup>, Paulo A.G. Piloto<sup>a</sup>, Mário A.P. Vaz<sup>b</sup> and Tiago M.G. Pinto<sup>a</sup>

<sup>a</sup> Polytechnic Institute of Bragança, Applied Mechanics Department, Portugal.

<sup>b</sup> University of Porto, Faculty of Engineering, Portugal.

### INTRODUCTION

Passive fire protection materials insulate steel structures from the effects of the elevated temperatures that may be generated during fire. They can be divided into two types, non-reactive, of which the most common types are boards and sprays, and reactive, being intumescent coatings an example. They are available as solvent or water based systems applied up to approximately 3[mm]. One problem associated with the use of such systems is the adhesion of the charred structure to the steel element during fire and upon it. It is very important that the char remains in the steel surface to insure the fire protection.

The intumescent chemistry has changed little over the past years and almost all coatings are largely based on the presence of similar key components. The chemical compounds of intumescent systems are classified in four categories: a carbonisation agent, a carbon rich polyhydric compound that influences the amount of char formed and the rate of char formation; an acid source, a foaming agent, which during their degradation release non-flammable gases such CO<sub>2</sub> and NH<sub>3</sub>, [1].

Activated by fire or heat, a sequential chemical reaction between several chemical products takes place. At higher temperatures, between 200-300 [°C], the acid reacts with the carboniferous agent. The formed gases will expand, beginning the intumescence in the form of a carbonaceous char.

Different models handle the intumescent behaviour with char forming polymers as a heat and mass transfer problem. Other existing models provide a suitable description regarding the intumescence and char formation using kinetic studies of thermal degradation, accounting the complex sequence of chemical reactions, thermal and transport phenomenon, [[2]-[5]].

Due to the thermal decomposition complexity of intumescent coating systems, the models presented so far are based on several assumptions, being the most relevant the consideration of one-dimensional heat transfer through material, temperature and space independent thermal properties and the assumption of a constant incident heat flux where the heat losses by radiation and convection are ignored, [3]. Some authors also assume that the thermochemical processes of intumescence occur without energy release or energy absorption, [6]. Results show that the insulation efficiency of the char depends on the cell structure and the low thermal conductivity of intumescent chars result from the pockets of trapped gas within the porous char which act as a blowing agent to the solid material.

The authors, in a previous work, considering the results obtained from coated steel plates tested in a cone calorimeter studied the intumescence as one homogenous layer. The steel temperature variation was considered and with the intumescence thickness time variation an inverse one-dimensional heat conduction problem (IHCP) was applied to determine the intumescence effective thermal conductivity and thermal resistance [7].

This work presents an experimental study to assess the performance of water-based intumescent paints used as a passive fire protection material. These tests were performed in a cone calorimeter, in steel plates coated with two different paints, three dry film thicknesses and considering two different radiant heat fluxes. During tests, among other quantities, the steel temperature, the intumescence mass loss and thickness variation were measured. A numerical model is also presented to study the intumescence behaviour. The paint thermal decomposition numerical model is based on the conservation equation of energy, mass and momentum.

### 1. EXPERIMENTAL TESTS PERFORMED IN THE CONE CALORIMETER

To assess the performance of two commercial water-based intumescent paints a set of experimental

tests was performed in a cone calorimeter, see Fig. 1 and Fig. 2. The steel plates are 100 [mm] squared and 4, 6 [mm] thick, coated in one side with different dry film thicknesses and tested in a cone calorimeter as prescribed by the standard ISO5660, [8]. Temperatures are measured by means of four thermocouples, type k, welded at the plate in the heating side and at the opposite side, at two different positions. The samples were weighted before and after of being coated allowing for the initial coating mass. The dry thickness was also measured in 16 different points, being the mean values and the standard deviation presented in the Fig. 1.

| Specimens identification |            | Initial mass [g] | Final mass [g] | Coating mass [g] | Thick (mean) [μm] | σ (SD) [μm] |
|--------------------------|------------|------------------|----------------|------------------|-------------------|-------------|
| B                        | 35 4 0.5 1 | 366.73           | 375.36         | 8.63             | 571               | 41.6        |
| B                        | 35 4 0.5 2 | 365.38           | 374.88         | 9.5              | 626               | 38.6        |
| B                        | 35 4 0.5 3 | 364.95           | 373.95         | 9                | 603               | 49.5        |
| B                        | 35 4 1.5 1 | 366.63           | 390.10         | 24.47            | 1510              | 70.2        |
| B                        | 35 4 1.5 2 | 365.82           | 391.42         | 25.6             | 1570              | 64.1        |
| B                        | 35 4 1.5 3 | 364.80           | 390.67         | 25.87            | 1580              | 66.5        |
| B                        | 35 4 2.5 1 | 365.49           | 409.85         | 44.36            | 2640              | 90.9        |
| B                        | 35 4 2.5 2 | 366.29           | 409.12         | 42.83            | 2560              | 89.0        |
| B                        | 35 4 2.5 3 | 366.40           | 407.77         | 41.37            | 2510              | 85.7        |
| B                        | 75 4 0.5 1 | 362.92           | 371.94         | 9.02             | 581               | 35.9        |
| B                        | 75 4 0.5 2 | 366.00           | 375.97         | 9.97             | 662               | 53.9        |
| B                        | 75 4 0.5 3 | 367.53           | 377.53         | 10               | 631               | 31.2        |
| B                        | 75 4 1.5 1 | 366.27           | 390.71         | 24.44            | 1530              | 79.5        |
| B                        | 75 4 1.5 2 | 364.69           | 389.63         | 24.94            | 1550              | 67.8        |
| B                        | 75 4 1.5 3 | 359.09           | 384.05         | 24.96            | 1560              | 74.9        |
| B                        | 75 4 2.5 1 | 359.79           | 399.66         | 39.87            | 2520              | 211         |
| B                        | 75 4 2.5 2 | 364.28           | 405.30         | 41.02            | 2520              | 91.4        |
| B                        | 75 4 2.5 3 | 364.80           | 404.97         | 40.17            | 2490              | 126         |
| B                        | 35 6 0.5 1 | 528.60           | 537.10         | 8.5              | 533               | 56.7        |
| B                        | 35 6 0.5 2 | 528.91           | 571.74         | 42.83            | 2570              | 105         |
| B                        | 75 6 0.5 1 | 525.47           | 534.86         | 9.39             | 607               | 65.9        |
| B                        | 75 6 2.5 1 | 529.04           | 570.00         | 40.96            | 2610              | 75.8        |
| A                        | 35 4 0.5 1 | 363.77           | 373.56         | 9.79             | 575               | 47.3        |
| A                        | 35 4 0.5 2 | 363.82           | 373.35         | 9.53             | 574               | 56.4        |
| A                        | 35 4 0.5 3 | 364.54           | 373.19         | 8.65             | 528               | 60.4        |
| A                        | 35 4 1.5 1 | 361.10           | 387.74         | 26.64            | 1670              | 107         |
| A                        | 35 4 1.5 2 | 362.17           | 388.06         | 25.89            | 1610              | 72.2        |
| A                        | 35 4 1.5 3 | 361.38           | 385.42         | 24.04            | 1450              | 84.9        |
| A                        | 35 4 2.5 1 | 362.81           | 403.37         | 40.56            | 2530              | 149         |
| A                        | 35 4 2.5 2 | 365.81           | 407.89         | 42.08            | 2590              | 122         |
| A                        | 35 4 2.5 3 | 363.49           | 415.12         | 51.63            | 2590              | 121         |
| A                        | 75 4 0.5 1 | 363.46           | 372.34         | 8.88             | 549               | 60.3        |
| A                        | 75 4 0.5 2 | 363.58           | 373.20         | 9.62             | 581               | 61.1        |
| A                        | 75 4 0.5 3 | 368.44           | 377.85         | 9.41             | 582               | 48.6        |
| A                        | 75 4 1.5 1 | 369.59           | 394.82         | 25.23            | 1510              | 83.7        |
| A                        | 75 4 1.5 2 | 371.11           | 396.24         | 25.13            | 1530              | 87.7        |
| A                        | 75 4 1.5 3 | 364.87           | 391.13         | 26.26            | 1620              | 98.7        |
| A                        | 75 4 2.5 1 | 366.97           | 407.71         | 40.74            | 2590              | 122         |
| A                        | 75 4 2.5 2 | 365.11           | 404.90         | 39.79            | 2590              | 134         |
| A                        | 75 4 2.5 3 | 370.60           | 410.77         | 40.17            | 2530              | 167         |
| A                        | 35 6 0.5 1 | 527.37           | 535.05         | 7.68             | 476               | 33.1        |
| A                        | 35 6 2.5 1 | 526.65           | 565.71         | 39.06            | 2420              | 150         |
| A                        | 75 6 0.5 1 | 522.90           | 530.58         | 7.68             | 494               | 33.9        |
| A                        | 75 6 2.5 1 | 525.71           | 564.89         | 39.18            | 2490              | 112         |

Fig. 1. Set of experimental tests. Reference: Paint/Heat Flux/Steel Thick./Dry Thick/Test N°.



Fig. 2. Coated steel plates, with fixed thermocouples. Tested samples at 35 [kW/m<sup>2</sup>] and at 75 [kW/m<sup>2</sup>]. Reference and position of the thermocouples.

Between the steel plate and the sample older two silicate plates were used to put the specimen in place and also a thermocouple was placed to measure its temperature variation. The distance between the sample surface and the heater remained unchanged, at approximately 60 [mm], which means that with the increasing intumescence the top of the sample came closer to cone surface. Due to the large amount of results, only a set of samples will be referenced in this paper.

## 1.1 Experimental Results

The temperature evolution in a steel plate without protection was also tested to attain the efficiency of this fire protection. The measured temperatures are presented in the Fig. 3 for a radiant heat flux of 35 [KW/m<sup>2</sup>] and then resetting the cone to 75 [KW/m<sup>2</sup>].

Fig. 4 represents the mass loss of each sample and shows a variation almost linear with time mainly for a heat flux of 35 [kWm<sup>-2</sup>].

Using discrete frames obtained from digital camera during tests and by image processing techniques using Matlab, the intumescence development was measure over time. Fig. 5 presents the intumescent development (free boundary L(t)) for specimens with paint A and B, different thicknesses and radiant heat fluxes.

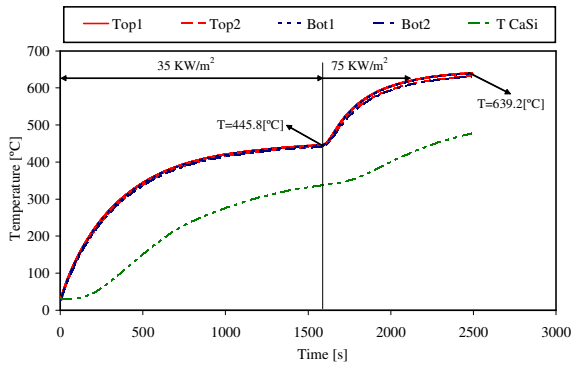


Fig. 3. Measured temperature in the steel plate without protection.

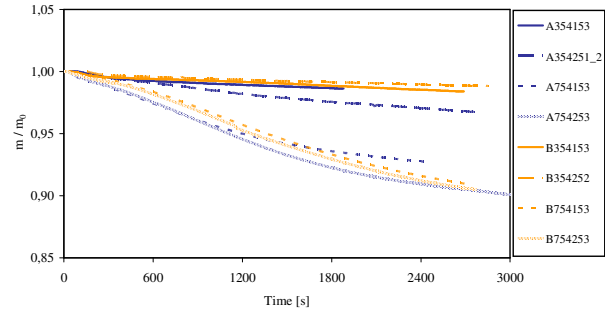


Fig. 4. Measured mass loss with time.

Higher intumescence may be noticed in sample right region coincident to the thermocouples wire position responsible for coating accumulation. The presented values are mean values determined from four central measures.

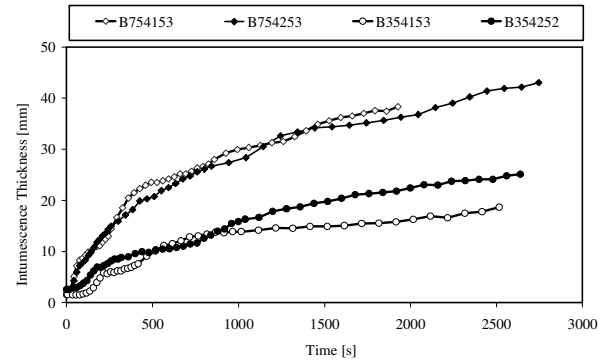
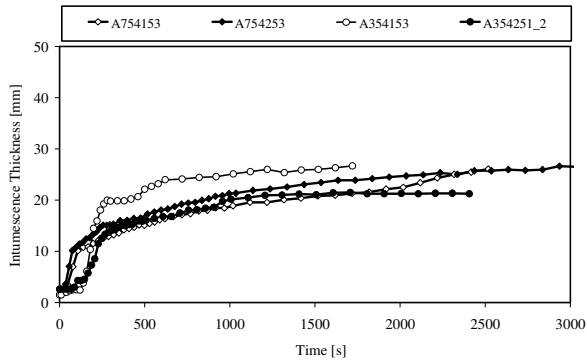


Fig. 5. Intumescence thickness mean values of four central measurements.

The figures shown that for the lower heat flux the intumescence becomes stable, but for the higher it continues to increase. Coating A presents a higher expansion at the initial stage compared to the coating B. For longer exposure periods of exposure coating B continues to expand.

The steel temperature profiles and temperatures at the middle of the silicate plates are reported in Fig. 6 and Fig. 7. Measured values from the thermocouples welded on the bottom of the plate are very close to the temperatures at the top. For the same heat flux, the time to reach a same temperature increases with the increase of the dry thickness.

The behaviour is very similar for both coatings, but for all cases the time to reach, for example a temperature of 200 [°c] is always higher when the paint B is used. For these conditions it gives an improved fire protection.

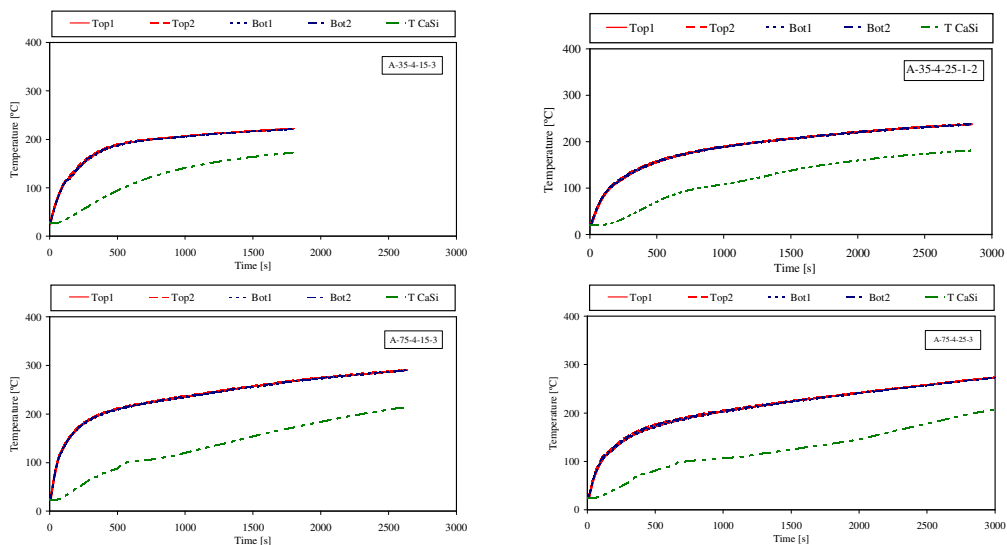


Fig. 6. Temperature variation of steel and silicate plates for coating A.

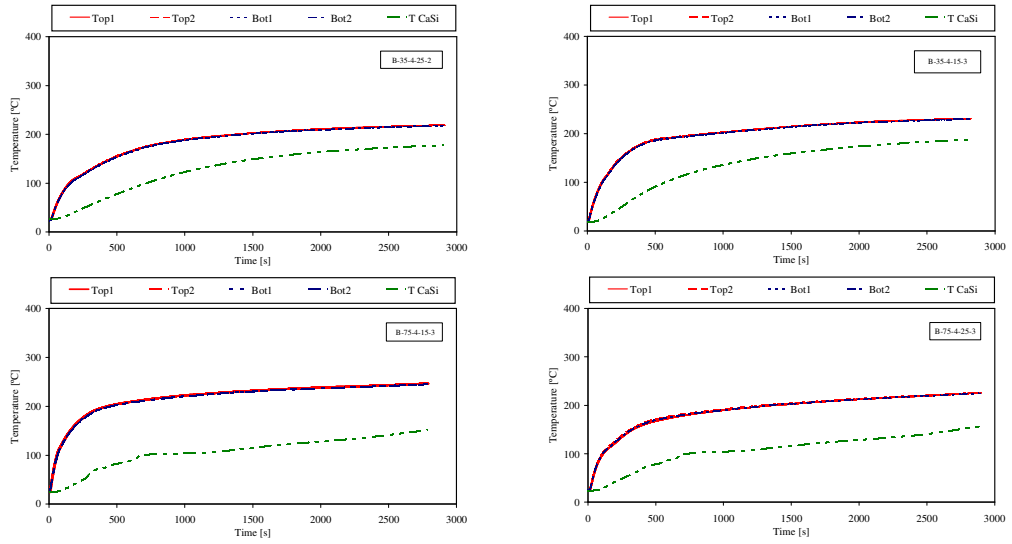


Fig. 7. Temperature variation of steel and silicate plates for coating B.

## 2 MATHEMATICAL MODEL OF THE INTUMESCENCE BEHAVIOUR

The problem to determine the temperature field in an intumescent material involves the solution of a phase transformation problem with two or more moving boundaries that characterize its state, initial, softened and carbonaceous char. Different methodologies can be found in the literature to model the thermal decomposition of a polymer or polymer based materials. The methodology followed in this work was to consider that the decomposition occurs not only at the outside surface but also inside, for temperatures above the pyrolysis temperature,  $T_p$ . In this case the moving boundary regression rate must be determined considering the motion of all domain. This strategy implies that a mass diffusion term needs to appear in the energy equation due its motion. This term was disregarded due to the small thickness of the virgin layer for this types of applications, about 1-3 [mm].

Considering a first order reaction, the mass loss is given by

$$\dot{m}(T(x,t)) = \frac{\partial \rho_v}{\partial t} = -\rho_v A_0 e^{-\frac{E_0}{RT(x,t)}} \quad \text{for } T \geq T_p \quad (1)$$

where  $\dot{m}$  is the local mass loss [ $\text{kg} \cdot \text{m}^{-3} \cdot \text{s}^{-1}$ ],  $T(x,t)$  is the temperature at point  $x$  at instant  $t$ ,  $A_0$  is the pre exponential factor [ $\text{s}^{-1}$ ],  $E_0$  the activation energy [ $\text{J} \cdot \text{mol}^{-1}$ ], and  $R$  the universal gas constant [ $\text{J} \cdot \text{mol}^{-1} \cdot \text{K}^{-1}$ ]. The position of the moving boundary is obtained by summing all the mass loss and dividing by the specific mass.

The energy equation for the steel and virgin layers is based on the one-dimensional conduction heat equation.

The conservation equation for the solid virgin material phase is given by

$$\frac{\partial \rho_v V_v}{\partial t} = -\dot{w}_v^{m,d} V_v \quad (2)$$

Where  $\dot{w}_v^{m,d}$  represents the destruction rate of virgin material per unit volume, originated by the thermal decomposition. The virgin material decomposition produces a fraction of gas, equal to the porosity,  $\phi$ , and a solid char fraction equal to  $(1 - \phi)$ .

The formation rate of char and gas mass is:

$$\dot{w}_{gas}^p = -\left(1 - \frac{\rho_c}{\rho_g}\right) \chi \rho_v A \frac{ds(t)}{dt} \quad \dot{w}_{char}^p = -\left[1 - \left(1 - \frac{\rho_c}{\rho_g}\right) \chi\right] \rho_v A \frac{ds(t)}{dt} \quad (3)$$

$\chi$  represents the fraction of the bulk density difference between the virgin and char materials that is converted to gas. In this study the value used was  $\chi = 0.66$ , [9].

The conservation of gas mass equation is given by eq. (4).

$$\frac{\partial(\rho_g \varphi)}{\partial t} + \frac{\rho_g \varphi}{V} \frac{\partial V}{\partial t} + \frac{\partial \dot{m}_g''}{\partial x} = 0 \quad (4)$$

In the previous equation  $\partial V/\partial t$  represents the intumescence rate. The gas mass flux,  $\dot{m}_g''$ , is calculated accordingly to Darcy's law and it is assumed that the gases present in the intumescent material behave as a perfect gas. The thermodynamic properties are related by the ideal gas law and, assuming that the gas is a mixture of 50wt%CO<sub>2</sub> and 50wt%H<sub>2</sub>O, the generated gas molar mass used in the model  $M_g$  is 31[g/mol].

The conservation of gas mass equation with the Darcy's and the ideal gas laws combined can be used to give a differential equation for the pressure inside the intumescence. In the numeric calculations, the intumescence rate is assumed to be known, provided by the experimental results, so the pressure calculation is disregarded being assumed that the internal pressure is constant and equal to the atmospheric pressure. An energy equation for the conservation of energy within the intumescence zone can be obtained by combining the energy equation for the gases with that of the solid char material. The equation for the conservation of energy per unit bulk volume can be written as:

$$(\rho Cp)_{eff} \frac{\partial T}{\partial t} + \frac{\partial}{\partial x} (\dot{m}_g'' T_g C p_g) = \frac{\partial}{\partial x} \left( k_{eff} \frac{\partial T}{\partial x} \right) - C p T \frac{\partial \rho}{\partial t} - (\rho Cp)_{eff} \frac{T}{V} \frac{\partial V}{\partial t} \quad (5)$$

where  $(\rho Cp)_{eff} = \varphi \rho_g C p_g + (1 - \varphi) \rho_c C p_c$  and  $k_{eff} = \varphi k_g + (1 - \varphi) k_c$ .

The effective thermal conductivity for the intumescence bulk material, including gas and char, is equal to the thermal conductivity of the gas per unit bulk volume, plus that of the solid material. The same thing applies to the effective heat capacity.

In the steel plate back surface it is assumed an adiabatic boundary condition and at the boundary steel/virgin layers it is assumed a perfect thermal contact. At the moving front, the boundary conditions are:

$$\begin{aligned} k_v \frac{\partial T}{\partial x} &= \varepsilon \dot{q}_r'' - \varepsilon \sigma (T^4 - T_a^4) - h_c (T - T_a) & \text{for } T(s(t), t) < T_p \\ k_v \frac{\partial T}{\partial x} - k_c \frac{\partial T}{\partial x} &= Q_H & \text{for } T(s(t), t) = T_p \end{aligned} \quad (6)$$

In which  $Q_H$  is the heat flux due to the endothermic decomposition of the virgin material, given by  $Q_H = -h_p \rho_v \dot{s}(t)$ , where  $h_p$  represents the decomposition enthalpy. A wide range of values are reported in the literature for the heat of pyrolysis and go from a few units to units of millions. The value used in the calculations was 50 [J/kg].

The intumescent coating specific mass was measured by the pycnometer method given a value of 1360 and 1250 [kg/m<sup>3</sup>] for the virgin coating and a value of 692.4 and 450 [kg/m<sup>3</sup>] for the char material, for paints A and B, respectively. Steel properties are assumed constant, with a specific heat value of 600 [J/kgK] and a specific mass equal to 7850 [kg/m<sup>3</sup>]. The intumescent coating specific heat was considered constant and equal to 1000 [J/kgK].

The mathematical model is based on the following major simplifying assumptions: there is no heat between gas and char, the thermophysical properties and the pressure at both layers are constant.

The solution method was implemented in a Matlab routine using the Method Of Lines (MOL), [10], and the integrator *ode15s* to solve the set of ordinary differential equations.

The temperature field is determined by the steel and virgin energy equations. When the front reaches the pyrolysis temperature, equal to 250 [°C], starts to decompose and to move. Then the moving front rate is determined and the intumescence forms. The position the free boundary is set equal to the experimental results and the intumescence temperature field is determined. In each time step the virgin and char layers are remeshed.

The input parameters are listed as follows:  $k_v = 0.5 W m^{-1} K^{-1}$ ;  $k_c = 0.1 W m^{-1} K^{-1}$ ;  $C p_v = 2600 J k g^{-1} K^{-1}$ ;  $C p_c = 3000 J k g^{-1} K^{-1}$ ;  $h_c = 20 W m^2 K^{-1}$ ;  $\varepsilon = 0.92$ ;  $T_p = 525 K$ ;  $A_0 = 4.67 e^{12} s^{-1}$ .

Two case studies are presented in Fig. 8 and Fig. 9. In the first one the steel temperature variation and the moving front position are determined based on a value of the activation energy equal to  $E_0 = 125 \text{ KJmol}^{-1}$ . The numerical results follow reasonably well the experimental values. The major differences occur at intermediate times probably because a transition state of molten polymer was not considered.

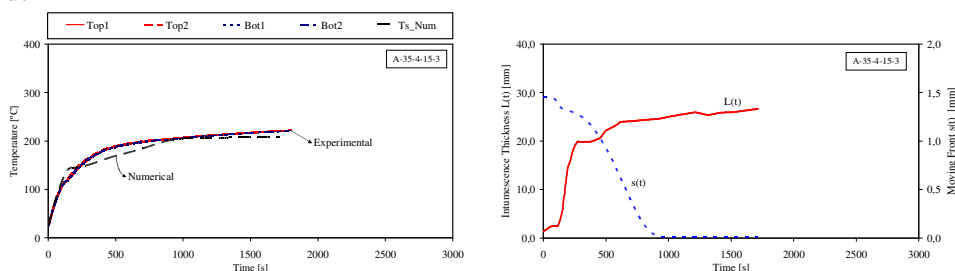


Fig. 8. Comparison of measured and computed steel temperatures and position of the moving front,  $E_0 = 125 \text{ KJmol}^{-1}$ .

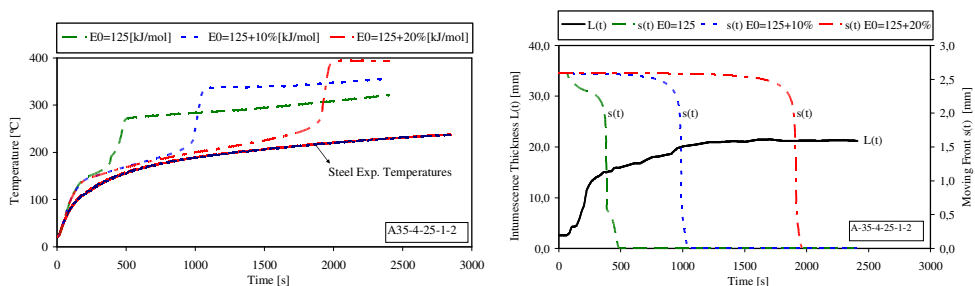


Fig. 9. Influence of the activation energy in the steel temperature and in the moving front.

Both the determined steel temperatures and the moving front are strongly dependent on the activation energy that defines the amount of mass loss of virgin paint, as presented in Fig. 9. It must be said that the value used in the simulations was obtained from the literature, but the correct value of both paints are needed. The reaction kinetics parameters can be obtained from thermogravimetric analysis.

## ACKNOWLEDGMENTS

The authors acknowledge the financial support from the Portuguese Science and technology Foundation, project PTDC/EME-PME/64913/2006, “Assessment of Intumescent Paint Behaviour for Passive Protection of Structural Elements Submitted to Fire Conditions”, and fellowship SFRH/BD/28909/2006. The authors acknowledge also the contribution from the paints producers: CIN, Nullifire.

## REFERENCES

- [1]. Duquesne, S.; Bourbigot, S. Delobel, R., “Mechanism of fire protection in intumescent coatings”, European Coatings Conference: Fire Retardant Coatings II, Berlin, 2007.
- [2]. Staggs J. E. J., “A discussion of modelling idealised ablative materials with particular reference to fire testing”, Fire Safety Journal, Vol. 28, 47-66, 1997.
- [3]. Moghtaderi B., Novozhilov V., Fletcher, D., Kent J. H., “An integral model for the transient pyrolysis of solid materials” Fire and Materials, Vol. 21, 7-16, 1997.
- [4]. Lyon R. E., “Pyrolysis kinetics of char forming polymers”, Polymer Degradation and Stability, N° 61, pp. 201-210, 1998.
- [5]. Jia F., Galea E. R., Patel M. K., “Numerical Simulation of the Mass Loss Process in Pyrolyzing Char Materials”, Fire And Materials, N° 23, 71-78, 1999.
- [6]. Kuznetsov, G. V., Rudzinskii, V. P., “Heat transfer in intumescent heat- and fire-insulating coatings”, Journal of Applied Mechanics and Technical Physics, Vol. 40, No. 3, 1999.
- [7]. Mesquita, L.M.R.; Piloto, P.A.G.; Vaz, M.A.P.; Pinto, T.; “Numerical Estimation For Intumescent Thermal Protection Using One-Dimensional IHCP”, WCCM8-ECCOMAS2008, ISBN: 978-84-96736-55-9, Venice, Italy, June 30 – July 5, 2008.
- [8]. ISO 5660-1:2002, Reaction-to-fire tests - Heat release, smoke production and mass loss rate. Part 1: Heat release rate (cone calorimeter method), International Organization for Standardization, 2002.
- [9]. C. Lautenberger, A Generalized Pyrolysis Model for Combustible Solids, Ph.D. thesis, University of California at Berkeley, Berkeley, CA, 2007.
- [10]. Wouwer A.V, Saucz P., and W. E. Schiesser, “Simulation of Distributed Parameter Systems Using a Matlab-Based Method of Lines Toolbox: Chemical Engineering Applications”, Ind. Eng. Chem. Res. 2004, 43, 3469-3477.

# THERMAL BEHAVIOUR OF ALKALI ACTIVATED SLAG COMPOSITES

## Effect of Aggregates

Pavel Rovnaník<sup>a</sup>, Patrik Bayer<sup>a</sup>, Pavla Rovnaníková<sup>a</sup>

<sup>a</sup> Brno University of Technology, Faculty of Civil Engineering, Brno, Czech Republic

### INTRODUCTION

Portland cement is widely used as a part of many building materials among which the most common is concrete. This material is highly inflammable and does not support combustion of other material. However, its undesirable fast degradation, when exposed to very high temperature, connected with compressive strength decrease, cracking and spalling limits the utilization of concrete in constructions endangered by fire [1-3]. Concretes based on alkali activated slag (AAS) exhibit a very good resistance against high temperatures and fire [4-6]. Due to its different porosity no spalling occurs even during thermal shock treatment. This property can be improved by application of artificial thermally stabilized aggregates with low extensibility. We have examined the influence of burnt clay (chamotte) and andalusite on the behavior of alkali activated slag composite during heat loading up to 1200 °C and the mechanical properties after high temperature exposure. This study is partially focused on the interstitial transition zone between the aggregate and AAS binder.

## 1 EXPERIMENT

### 1.1 Materials

For the investigation of material properties, specimens of finely granulated blast furnace (BF) slag from Kotouč, s r.o. Štramberk activated with dried sodium silicate Portil A (Henkel AG) were prepared. Chamotte, andalusite and quartz sand were used as an aggregate. The specific surface of the slag was 380 m<sup>2</sup>/kg and its basicity modulus was 1.07. The chemical composition of slag is given in table 1.

Table 1. Chemical composition of blast furnace slag

| Component  | SiO <sub>2</sub> | Al <sub>2</sub> O <sub>3</sub> | Fe <sub>2</sub> O <sub>3</sub> | CaO  | MgO  | MnO | S <sub>total</sub> |
|------------|------------------|--------------------------------|--------------------------------|------|------|-----|--------------------|
| Content, % | 37.8             | 6.9                            | 0.2                            | 34.9 | 12.8 | 0.5 | 0.5                |

Dried sodium silicate Portil A with  $M_s = 1.9$  was used as an activator. The grain size of chamotte and andalusite aggregate was in the range 0-5 mm. The maximum grain size of standard quartz sand was 2.5 mm.

### Testing Methods

The mixture of slag, activator, aggregate and water was placed into moulds of 40×40×160 mm dimension. The hardened specimens were stored in water for 28 days. Afterwards the composite was pulled out and left at an ambient temperature for 3 days. Then, the specimens were exposed to elevated temperatures 200, 400, 600, 800, 1000, and 1200 °C with 1 h dwell, and afterwards they were let cool down spontaneously. Reference samples were stored at 20 °C. The microstructure of composites was investigated by means of mercury intrusion porosimetry (Micromeritics Poresizer 9300) and electron scanning microscopy (JEOL U 3). Composition of the mixtures is listed in table 2.

Table 2. Composition of alkali activated slag and Portland cement mortars

| Component                  | Slag | Aggregate | Portil A | Water |
|----------------------------|------|-----------|----------|-------|
| Content, kg/m <sup>3</sup> | 586  | 1758      | 117      | 235   |

## 2 RESULTS AND DISCUSSION

The properties and microstructure of AAS composites with inspected aggregates were compared with composite containing only standard quartz sand as aggregate. As reference samples we considered the specimens which were treated only at an ambient temperature. Bulk density of described specimens is presented in table 3. The compressive strengths of AAS with chamotte reached the value for AAS matrix itself [7], therefore the aggregate seems not to be a limiting factor for the mechanical properties of such composite. On the contrary, the quartz sand causes a strength decrease by approx. 20 MPa and andalusite even by 40 MPa (Fig. 1). This might be explained by weaker contacts between AAS matrix and aggregate that is, in the case of andalusite, indicated by cracks on the surface of specimens (Fig. 2). After exposure to elevated temperature, the compressive strengths gradually decrease. The trend, however, appears to be the same for all three composites, therefore it can be attributed to dehydration and decomposition of AAS matrix. Strength decrease of AAS composite with quartz above 600 °C is partly caused by phase transformation of quartz at 573 °C ( $\alpha$ -quartz $\leftrightarrow\beta$ -quartz), accompanied by the change of volume. Exposure of AAS material to temperatures above 800 °C enables the crystallization and formation of several crystalline phases, among which akermanite is predominant [5]. These phases are responsible for increase of strengths that reach 53% of original strength for AAS with chamotte, 23% for AAS with andalusite, and 36% of that obtained for AAS with quartz, respectively.

Table 3. Bulk density of alkali activated slag composites

| Aggregate type                  | Chamotte | Andalusite | Quartz |
|---------------------------------|----------|------------|--------|
| Bulk density, kg/m <sup>3</sup> | 2230     | 2520       | 2150   |

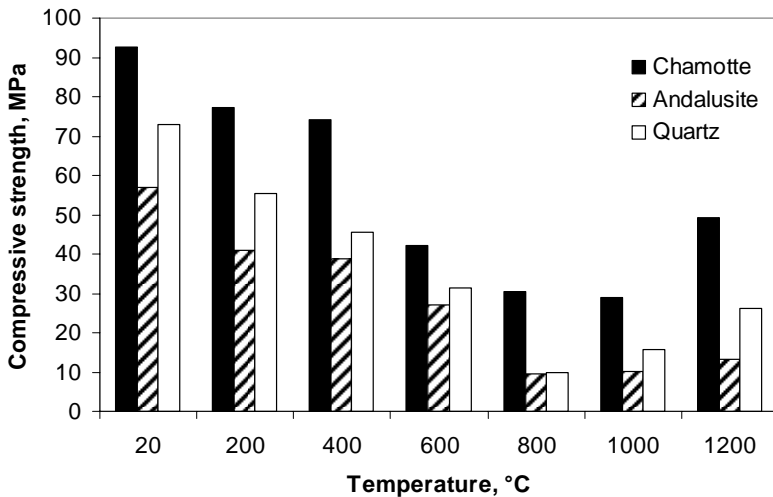


Fig. 1. Compressive strengths of AAS composites for different temperatures of exposure

Fig. 2. Cracks on the surface of andalusite composite

Flexural strengths of all AAS composites follow the same trend that has been observed for compressive strengths (Fig. 3). However, at elevated temperature the composite with chamotte performs much better values by approx. 3 MPa in comparison with AAS filled with quartz sand. Flexural strengths of heated AAS filled with andalusite are by 4 MPa lower than those obtained for

AAS with chamotte. The significant increase of flexural strength for chamotte composite after exposure to 1200 °C, that even exceeds the reference value, can be ascribed to the reaction of AAS matrix with surface of aggregates that results in the formation of tight ceramic bond.

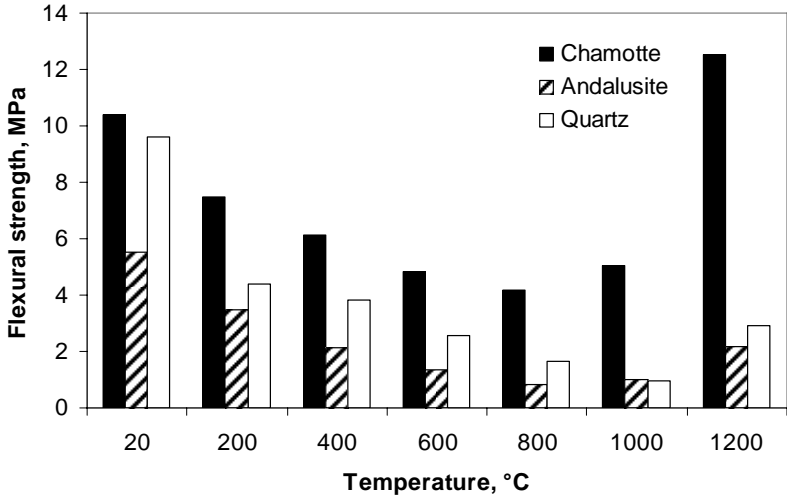


Fig. 3. Flexural strengths of AAS composites for different temperatures of exposure

The mechanical properties of inspected AAS composites after exposure to elevated temperature can be explained by changes in microstructure. Distribution of pores smaller than 100 μm for unexposed composites is almost independent of the aggregate type used, although some minor cracks were observed on specimens with andalusite. Dehydration and decomposition of AAS matrix starts upon heating that results in its shrinkage and finally in an increase of porosity. The first difference is obtained after heating to 600 °C. The porosity of quartz composite increases due to rapid reversible change between α-quartz and β-quartz modifications at 573 °C (Fig. 4).

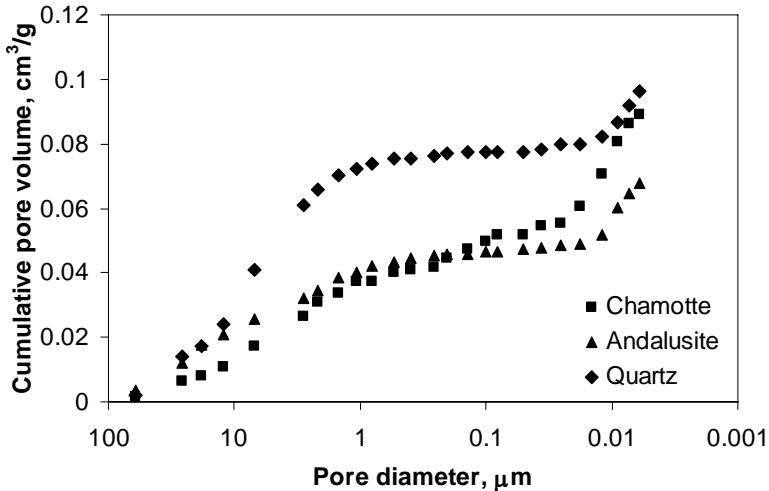


Fig. 4. Comparison of pore distribution of AAS composites after exposure to 600 °C

Upon further heating very small gel pores completely disappear and above 1000 °C only pores larger than 1 μm remain. However, the total porosity differs according to the aggregate type used (Fig. 5). The biggest apparent porosity was observed for AAS composite with quartz sand and the least porous seems to be andalusite composite, but mercury intrusion porosimetry does not provide results for voids larger than 100 μm. Photograph of the specimen with andalusite aggregate after exposure to 1200 °C shows large crack that do not appear in the porosimetric curve (Fig. 6). Such

considerable cracking of the specimens was observed for composites neither with chamotte nor with quartz sand. Therefore, total porosity of the latter two composites is formed mainly by pores of size between 1 and 100  $\mu\text{m}$ .

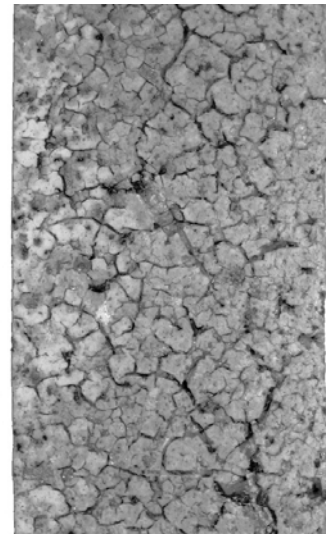
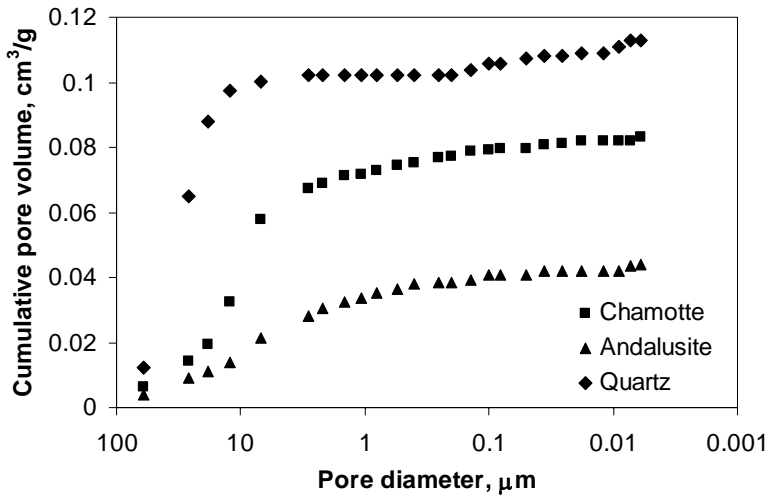


Fig. 5. Comparison of pore distribution of AAS composites after exposure to 1200 °C

Fig. 6. Surface of andalusite composite specimen after exposure to 1200 °C

Alkali activated slag material exhibits amorphous gel structure at 20 °C. The contact zone between AAS paste and aggregate grains were studied by means of scanning electron microscopy. Presented micrographs show the contact zone of binder and aggregate grains of andalusite (Fig. 7) and chamotte, respectively (Fig. 8). Since surface of andalusite is quite flat, it is only sparsely connected to the binder and so it does not prevent the AAS matrix from significant drying shrinkage. This effect is predominantly responsible for crack formation and finally also for noticeable strengths' deterioration when compared to other composites. On the contrary, the surface of chamotte aggregate is so rugged that bonds with matrix are stronger and the composite is more compact.

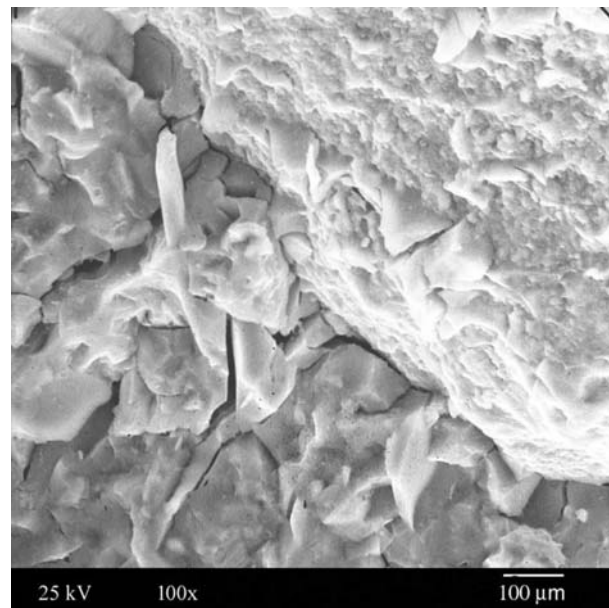
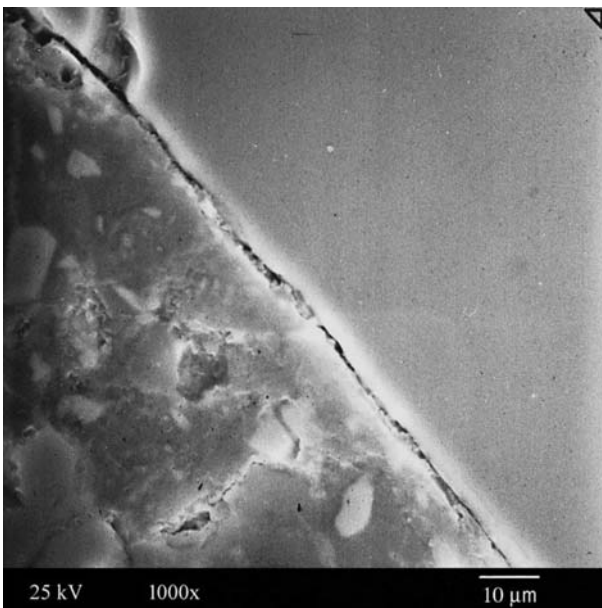
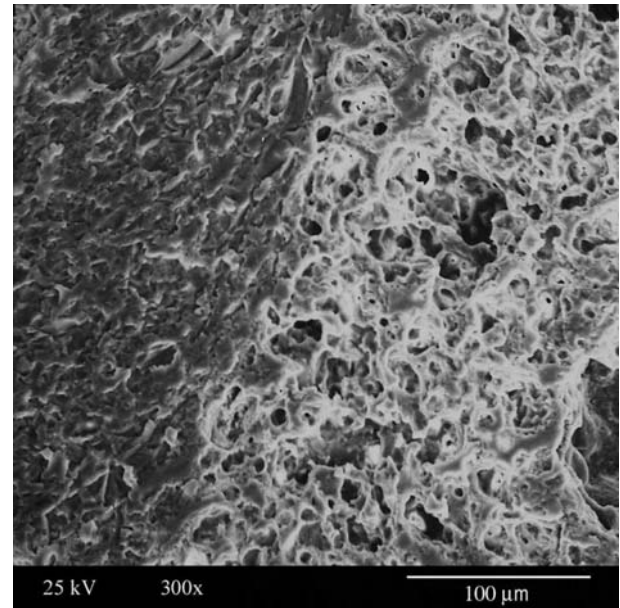
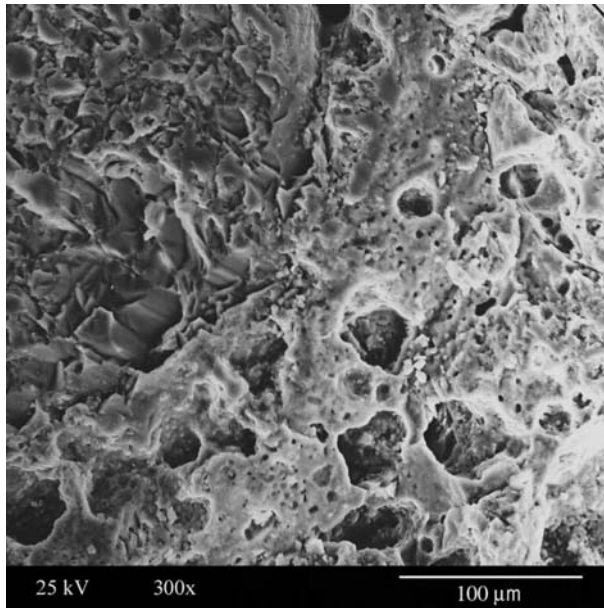


Fig. 7. SEM micrograph of AAS composite with andalusite

Fig. 8. SEM micrograph of AAS composite with chamotte

As the temperature increases, decomposition and further shrinkage of the AAS matrix can be observed, which implies enlargement of pores evoking spongy structure of the AAS paste. This weakening of AAS structure is the main reason for strengths' deterioration that has been discussed above. At temperature that reaches 1200 °C the formation of very strong connection between alkali activated slag and the surface layer of chamotte aggregate can be observed (Fig. 10). This ceramic bond is so strong that fracture of aggregate grains occurs during mechanical testing. Such sintering of aggregate with a binder in the contact zone does not occur either for quartz or andalusite type of aggregate (Fig. 9). This effect is also the main reason for enormous increase in especially flexural strength and better performance of composite material with chamotte aggregate after exposure to extremely high temperatures



*Fig. 9.* SEM micrograph of AAS composite with andalusite after exposure to 1200 °C *Fig. 10.* SEM micrograph of AAS composite with chamotte after exposure to 1200 °C

### 3 SUMMARY AND ACKNOWLEDGMENT

The properties of alkali activated slag material and its behavior upon heating up to 1200 °C considerably depend on the type of aggregate that is used as filler. Alkali activated slag paste itself performs much better compared to concrete made of ordinary Portland cement when subjected to very high temperatures or fire but mechanical properties of this material are strongly affected by aggregates. It turned out that the main factor for good mechanical performance of AAS composites is the quality of interface between aggregate grains and binder. Stronger connection with aggregate mitigates the action of mechanical stress on binder that is caused by its shrinkage and it impedes the formation of larger cracks that contribute to strength's deterioration.

Utilization of chamotte as an aggregate in alkali activated slag composites seems to be the most effective among other studied aggregates. Chamotte is a material that is produced from natural clay in rotary kiln at 1350 °C, and therefore it is more thermally stable than quartz or andalusite. Quartz exhibits phase modification at 573 °C and andalusite forms very weak connection with AAS binder which results in the formation of large cracks. From the viewpoint of mechanical properties, chamotte aggregate does not limit mechanical strengths of AAS paste at temperatures up to 1000 °C and it even considerably improves the flexural strength of the composite at 1200 °C. Although some deterioration occurs upon heating, the compressive strength decreases to the limit of 29 MPa at 1000 °C. However, it is still 31% of the original strengths. The flexural strength falls to limit of 4.2

MPa at 800 °C, which is 40% of the original strength. All these very good properties predetermine chamotte aggregate especially in alkali activated slag composites for application in structures that might be exposed to elevated temperatures.

This paper was elaborated with the financial support of the project granted by Ministry of Education, Youth and Sport (MSM 0021630511).

## REFERENCES

- [1] Husem, M. The effects of high temperature on compressive and flexural strengths of ordinary and high-performance concrete, *Fire Safety Journal* 2006, vol. 41, 155-163.
- [2] Li, M., Qian, C., Sun W. Mechanical properties of high-strength concrete after fire, *Cement and Concrete Research* 2004, vol. 34, 1001-1005.
- [3] Kalifa, P., Menneteau, F.-D., Quenard D. Spalling and pore pressure in HPC at high temperatures, *Cement and Concrete Research* 2000, vol. 30, 1915-1927.
- [4] Zuda, L., Rovnaník, P., Bayer, P., Černý, R. Effect of High Temperatures on the Properties of Alkali Activated Aluminosilicate with Electrical Porcelain Filler. *International Journal of Thermophysics* 2008, vol. 29, 693-705.
- [5] Rovnaníková, P., Bayer, P., Rovnaník, P., Novák, J. Properties of Alkali-Activated Aluminosilicate Materials with Fire-Resistant Aggregate after High Temperature Loading. *Cement Combinations for Durable Concrete, Proceedings of the International Conference*. Dundee, UK: Dhir, R.K., Chana, P., Caliskan, S., Lavingia, R. (Eds.), Thomas Telford Ltd., London, UK, 2005, pp. 277–286.
- [6] Rovnaník, P., Bayer, P., Rovnaníková, P. Utilisation of alkali activated aluminosilicates as fire protecting materials. In *Concrete for Fire Engineering, Proc. 7th Int. Congress – Concrete: Construction's Sustainable Option*. Dundee, UK: Dhir, R.K., Harrison, T.A., Newlands, M.D. (Eds.), IHS BRE Press, Brecknell, UK, 2008, pp. 273-282.
- [7] Bayer, P. PhD thesis, Brno University of Technology, Brno 2005 (in Czech)

# THERMAL CONDUCTIVITY OF GYPSUM AT HIGH TEMPERATURES

## A Combined Experimental and Numerical Approach

Ima Rahmanian<sup>a</sup>, Yong Wang<sup>a</sup>

<sup>a</sup> University of Manchester, School of Mechanical, Aerospace and Civil Engineering, Manchester, UK

### INTRODUCTION

Gypsum board based systems are now widely used in buildings, as walls or ceilings, to provide passive fire protection. The basis of the fire resistance of such systems lies in low thermal conductivity and the evaporation of the water content of the gypsum board, which absorbs a considerable amount of heat, thereby delaying temperature rise through the system. To accurately model the performance of such systems in fire condition, their thermal properties should be known. Thermal properties of gypsum are temperature-dependent and among them, thermal conductivity has a critical influence, but there is a wide difference in reported values in literature. Given the effects of porosity, non-homogeneity and moisture in gypsum, direct experimental measurement of thermal conductivity of gypsum at high temperatures is not an easy task. As an alternative, this paper proposes a hybrid numerical and experimental method to extract thermal conductivity of gypsum. A one-dimensional finite difference heat conduction programme has been developed to predict the temperature development through the thickness of the gypsum board, based on an initial estimate of the thermal conductivity-temperature relationship as a function of porosity and radiation within the voids. This relationship is then calibrated by comparing numerical results with the experimental ones from small-scale fire tests, so that the temperature history of the specimen calculated by the programme closely matches those recorded during the test. This method has been found to yield more consistent results than those reported in literature.

### 1 OUTLINE OF THE NUMERICAL ANALYSIS METHOD

The transient heat transfer through a gypsum board is modelled using one-dimensional Finite Difference formulation. A computer program has been developed and implemented in the familiar environment of Microsoft Excel using VBA. The modelling procedure has been thoroughly validated<sup>[1]</sup> by comparisons with a number of analytical solutions and simulation results using ABAQUS/Standard. The following describes the basis of the modelling method.

#### 1.1 One-Dimensional Finite Difference Formulation

The Fourier's law of conduction in one dimension with no heat generation is expressed as:

$$\frac{\partial}{\partial x} \left( k(T) \frac{\partial T(x,t)}{\partial x} \right) = \rho c \frac{\partial T(x,t)}{\partial t} \quad (1)$$

where  $T(x,t)$  is temperature (°C);

$k(T)$  is thermal conductivity (W/m.°C);

$\rho$  is material density (kg/m<sup>3</sup>);

$c$  is specific heat of material (J/kg.°C);

$t$  is time (sec);

$x$  is the coordinate ( $0 \leq x \leq L$ ,  $L$  being the thickness of the panel).

Choosing the explicit technique, the temperature of a volume cell (refer to *Figs 1* and *2*) at a time step is computed directly based on the temperatures of the adjacent cells in the last time step which leads to a very simple scheme of computation<sup>[2]</sup>:

(i) For a typical node  $m$  within the material (Fig. 1):

$$T'_m = F_0 \left[ \frac{2(k_{m-1,m}T_{m-1} + k_{m+1,m}T_{m+1})}{k_{m-1,m} + k_{m+1,m}} + T_m \left( \frac{1}{F_0} - 2 \right) \right] \quad (2)$$

where  $F_0$  is defined as: 
$$F_0 = \frac{(k_{m-1,m} + k_{m+1,m})\Delta t}{2\rho c(\Delta x)^2} \quad (3)$$

$T'_m$  is the temperature of  $m$  in the subsequent time step and  $k_{i,j}$  is the thermal conductivity at the average temperature of cells  $i$  and  $j$ : 
$$k_{i,j} = k \left( \frac{T_i + T_j}{2} \right) \quad (4)$$

Numerical stability under the explicit scheme requires: 
$$\Delta t \leq \frac{\rho c(\Delta x)^2}{(k_{m-1,m} + k_{m+1,m})} \quad (5)$$

(ii) For a boundary node, when subjected to convective and radiative boundary conditions (Fig. 2):

$$T'_1 = 2F_0 \left[ T_2 + \frac{h\Delta x}{k_1} T_\infty + \left( \frac{1}{2F_0} - 1 - \frac{h\Delta x}{k_1} \right) T_1 \right] + \phi E \sigma [(T_\infty + 273)^4 - (T_1 + 273)^4] \frac{2\Delta t}{\rho c \Delta x} \quad (6)$$

where  $F_0$  is  $F_0 = \frac{k_1 \Delta t}{\rho c(\Delta x)^2}$

$h(T)$  is convection heat transfer coefficient ( $\text{W}/\text{m}^2 \cdot ^\circ\text{C}$ );

$T_\infty$  is the ambient temperature ( $^\circ\text{C}$ );

$\phi$  is a geometric “view factor”

$E$  is the effective emissivity

$\sigma$  is Stefan-Boltzmann constant ( $5.67 \times 10^{-8} \text{ W}/\text{m}^2 \cdot \text{K}^4$ ).

Numerical stability limits the time step to:

$$\Delta t \leq \frac{0.5\rho c(\Delta x)^2}{k_1} \left[ 1 + \frac{h\Delta x}{k_1} + \frac{\phi E \sigma \Delta x}{k_1} \cdot \frac{(T_1 + 273)^4}{T_1} \right]^{-1} \quad (7)$$

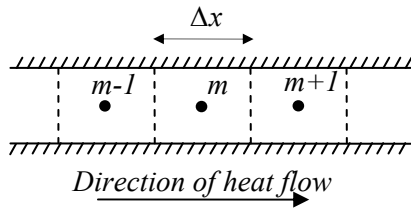


Fig. 1. Finite Difference discretization for node  $m$  within the material

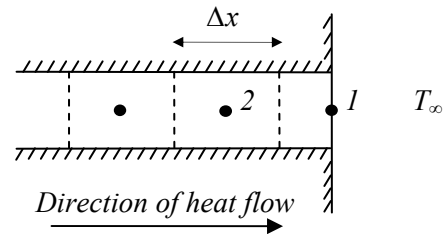


Fig. 2. Finite Difference discretization for a boundary node

## 1.2 Initial and Boundary Conditions

Gypsum board is assumed to have a uniform initial temperature equal to the ambient temperature. On the unexposed boundary, the convective heat transfer coefficient ( $h$ ) is assumed to be constant and the value is taken as  $10 \text{ W}/\text{m}^2 \cdot ^\circ\text{C}$ . The surface of gypsum plasterboards is laminated by paper with emissivity of 0.8-0.9 as reported in reference [3]. Thus, the surface emissivity of the board is taken as 0.8 and the view factor equals unity. For extraction of thermal conductivity based on fire test results, the recorded temperatures on the exposed surface are used as input data.

## 1.3 Specific Heat and Density

The temperature-dependent specific heat of gypsum experiences two peaks corresponding to the two dehydration reactions of gypsum as shown in Fig. 3. These peaks represent the energy consumed to dissociate and evaporate water and include the effect of water movement and

recondensation of water in cooler regions of gypsum [4]. The base value of the specific heat is 950 J/kg.°C as reported by Mehaffey *et al* [5] and the additional specific heat at each dehydration reaction can be expressed by [4]:

$$\Delta c = \frac{2.26 \times 10^6}{\Delta T} (e_d f_1 + e_{free}) f_2 \quad (\text{J/kg.}^\circ\text{C}) \quad (8)$$

where  $\Delta c$  is the average additional specific heat

$e_d$  is the dehydration water content (percentage by total weight)

$e_{free}$  is the free water content (percentage by total weight)

$\Delta T$  is the temperature interval

$f_1, f_2$  are correction factors to account for heat of reactions and effects of water movement

According to Ang and Wang [4],  $f_1=1.28$  and  $1.42$  for the first and second dehydration reactions, respectively. For standard fire conditions  $f_2=1.4$ .

Due to evaporation of water, the density of gypsum reduces with temperature increase. *Fig. 4* shows the density used in the modelling as a percentage of the original density of gypsum at ambient temperature.

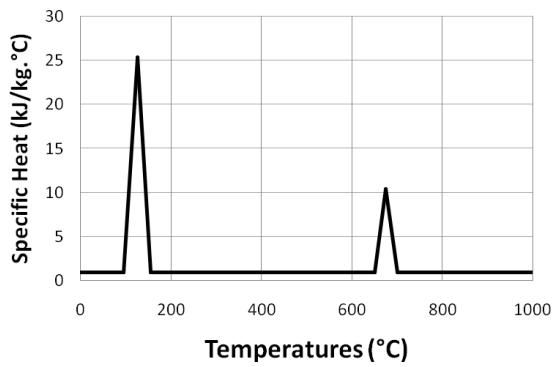


*Fig. 3.* Specific heat of gypsum as used in the analysis

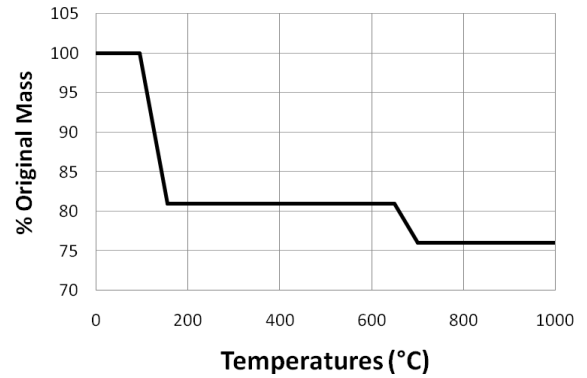


*Fig. 4.* Density of gypsum as used in the analysis (% of the original density)

#### 1.4 Thermal Conductivity

Since gypsum is a porous material, heat transfer through gypsum is a combination of all three modes: conduction through the solid and convection and radiation through the pores. Therefore the effective thermal conductivity of gypsum should include these effects. This effective thermal conductivity can be affected by many factors such as temperature, density, moisture content and porosity of the material. Such sensitivity contributes to the diverse data reported in literature as demonstrated in *Fig.5*. Assuming gypsum is made of solid substrate and uniformly distributed spherical pores, the effective thermal conductivity of gypsum may be calculated using the following

equation [6]:

$$k^* = k_s \frac{k_g \varepsilon^{\frac{2}{3}} + (1 - \varepsilon^{\frac{2}{3}}) k_s}{k_g (\varepsilon^3 - \varepsilon) + (1 - \varepsilon^3 + \varepsilon) k_s} \quad (9)$$

where  $k^*$  is the effective thermal conductivity of gypsum

$k_g$  is effective thermal conductivity of gas to account for heat transfer in the pores

$k_s$  is the thermal conductivity of the solid

$\varepsilon$  is the porosity of the material (the ratio of the volume of void to the overall volume)

In this study, the thermal conductivity of solid gypsum ( $k_s$ ) is 0.12 W/m.°C. The porosity of gypsum is 0.25. Since the size of the pores is very small (never larger than 5mm), natural convection in the pores can be neglected. Therefore the effective thermal conductivity of the gas is [6]:

$$k_g = 4.815 \times 10^{-4} T^{0.717} + \frac{2}{3} \times 4d_e \sigma T^3 \quad (10)$$

where  $T$  is absolute temperature and  $d_e$  is the effective diameter of the pores. In this study  $d_e = 1\text{mm}$ . Hence, the effective thermal conductivity-temperature relationship consists of three parts as demonstrated in *Fig. 6*: 1) Constant thermal conductivity up to  $95^\circ\text{C}$  before water evaporation, equal to that at ambient temperature reported by the manufacturer; 2) Linear reduction of conductivity to  $0.1\text{ W/m}\cdot^\circ\text{C}$  at  $155^\circ\text{C}$ ; 3) Non-linear increase in thermal conductivity based on equations 9 and 10.

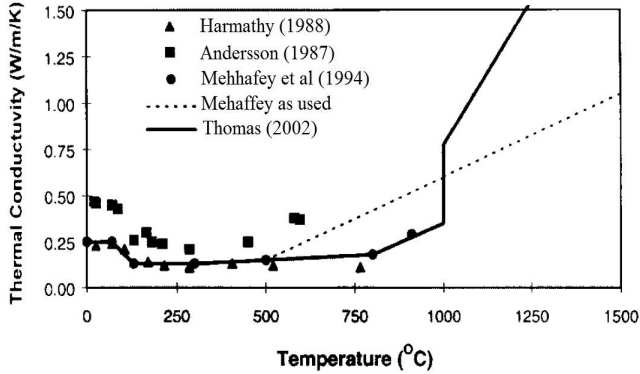


*Fig. 5.* Thermal conductivity of gypsum as reported by various researchers [7]

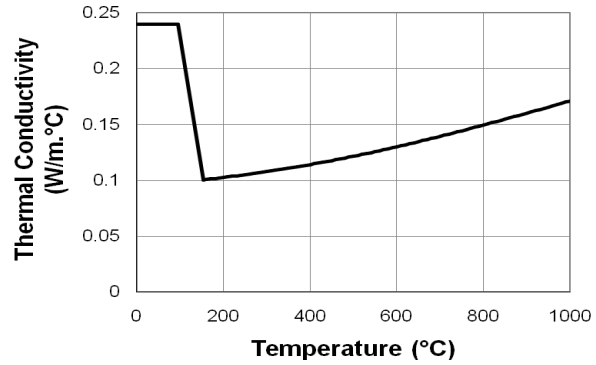


*Fig. 6.* Effective thermal conductivity of gypsum as used in this study

## 2 SMALL-SCALE HIGH TEMPERATURE TESTS

A limited number of small-scale experiments have been performed. The specimens tested were gypsum board panels of two different types;  $12.5\text{mm}$  *Gyproc Fireline* plasterboard and  $9.5\text{mm}$  *Gyproc Wallboard* plasterboard, both *British Gypsum* products. A total number of 8 specimens were tested as specified in *Table 1*. All specimens were with approximate dimensions of  $400 \times 400\text{ mm}$ . Each specimen was placed horizontally on top of an electric kiln, as the source of heat, so that one side of the panel was subjected to kiln temperature and the other side faced up to the room temperature ( $19\text{-}25^\circ\text{C}$ ). An opening of  $280 \times 265\text{ mm}$  on the top lid of the kiln allowed the lower side of the panel to be exposed to the elevated kiln temperatures. A  $30\text{mm}$  layer of glass wool (with an opening of the same size as that in the kiln lid) was laid underneath the specimen to insulate the contact surface between the top lid and the plasterboard. *Fig. 7* shows typical set-up of the experiments. *Fig. 8* shows the heating curve achieved in the kiln which is compared to a standard cellulosic fire (BS476) [8]. Temperatures were measured on the unexposed side, the midpoint (for double layered panels) and the exposed side of the gypsum panel using Type K thermocouples.

*Table 1.* Specifications of gypsum board specimens

| Test No | Plaster board Type | Layers | Total Thickness (mm) | Density (kg/m <sup>3</sup> ) | Free Water (% by weight) | Initial Thermal Conductivity (W/m.°C) |
|---------|--------------------|--------|----------------------|------------------------------|--------------------------|---------------------------------------|
| 1       | Gyproc Fireline    | Single | 12.5                 | 784                          | 3.5                      | 0.24                                  |
| 2       | Gyproc Fireline    | Single | 12.5                 | 784                          | 3.5                      | 0.24                                  |
| 3       | Gyproc Fireline    | Double | 25                   | 784                          | 3.5                      | 0.24                                  |
| 4       | Gyproc Fireline    | Double | 25                   | 784                          | 3.5                      | 0.24                                  |
| 5       | Gyproc Wallboard   | Single | 9.5                  | 663                          | 3.5                      | 0.19                                  |
| 6       | Gyproc Wallboard   | Single | 9.5                  | 663                          | 3.5                      | 0.19                                  |
| 7       | Gyproc Wallboard   | Double | 19                   | 663                          | 3.5                      | 0.19                                  |
| 8       | Gyproc Wallboard   | Double | 19                   | 663                          | 3.5                      | 0.19                                  |

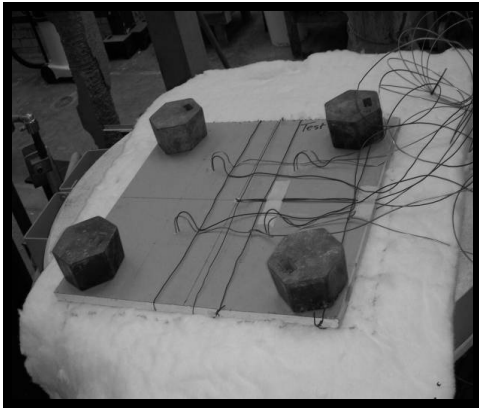


Fig. 7. Typical set-up for the small-scale fire tests

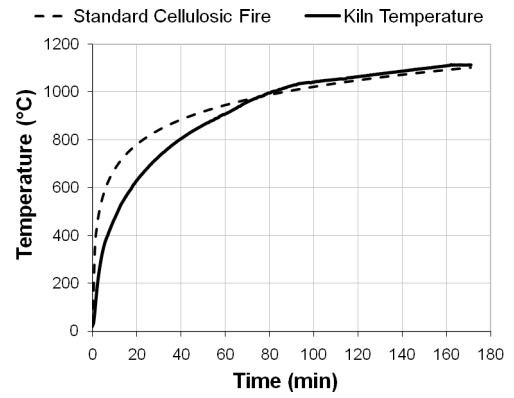


Fig. 8. Time-temperature curve for the kiln against standard cellulosic fire curve

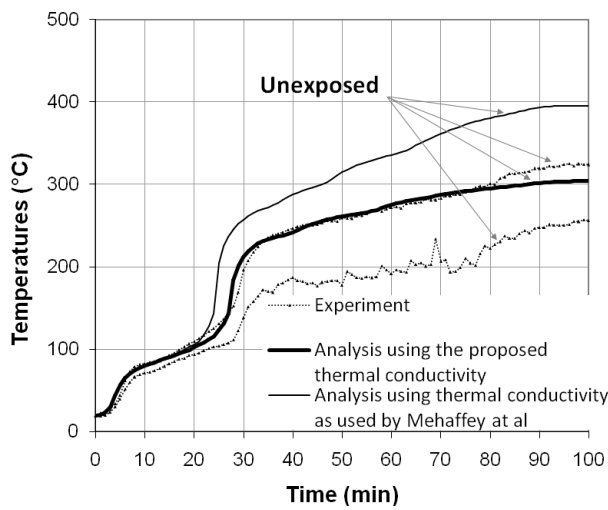


Fig. 9. Temperature history for 12.5mm Fireline gypsum panel

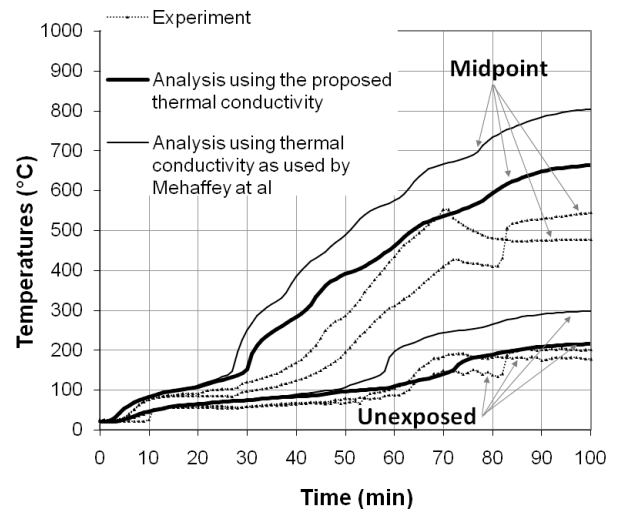


Fig. 10. Temperature history for 25mm Fireline gypsum panel

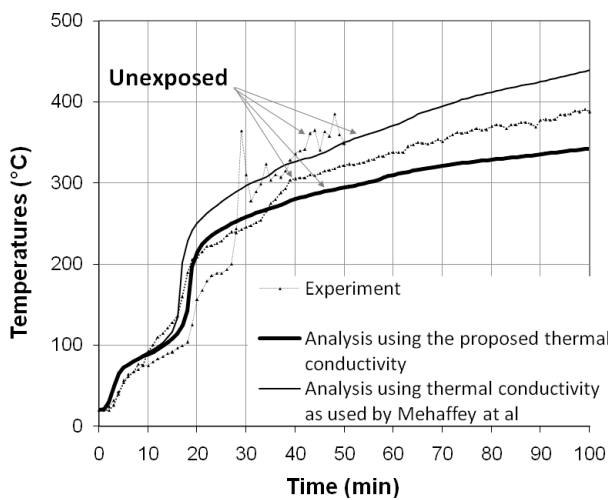


Fig. 11. Temperature history for 9.5mm Wallboard gypsum panel

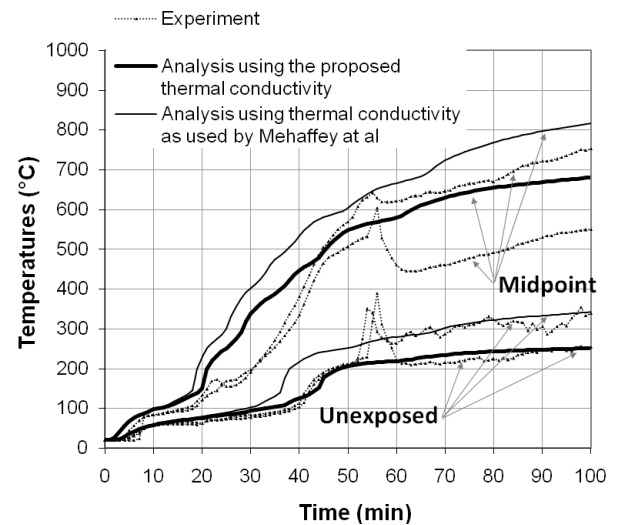


Fig. 12. Temperature history for 19mm Wallboard gypsum panel

### 3 RESULTS

In Figs. 9 to 12, the temperature histories measured from the tests (data points) and calculated by the program using pore size of 1mm (solid thick line) are compared. Also plotted in these figures are the numerical results utilizing thermal conductivity of gypsum as used by Mehaffey *et al* [5] (thin solid line). The results demonstrate a considerable improvement in prediction of temperature development through gypsum when using the new thermal conductivity model described in this paper.

### 4 CONCLUSIONS

This paper has presented a hybrid method to determine the effective thermal conductivity of gypsum at high temperatures, based on using small-scale experimental results and a thermal conductivity model which includes the effects of radiation in voids. Despite the simplicity of the method, the results are in good agreement with test measurements and show great improvement when compared to those produced using thermal conductivity values reported in literature. This method will aid manufacturers to develop their products without having to conduct numerous large-scale fire tests. Further planned research includes investigating the effects of discrete large cracks in gypsum on heat transfer in gypsum board systems and gypsum falling-off at high temperatures.

### 5 ACKNOWLEDGMENT

The authors would like to thank British Gypsum for their financial support and Drs. Kane Ironside and Jan Rideout for their interest and technical support. The technical assistance by the laboratory staff at the University of Manchester is greatly appreciated.

### REFERENCES

- [1] Rahmanian I., Fire Resistance of Gypsum Board Based Systems, First year PhD progression report, *School of Mechanical, Aerospace and Civil Engineering*, University of Manchester, UK, 2008
- [2] Wang, H.B., Heat Transfer Analysis of Components of Construction Exposed to Fire, *Department of civil Engineering and Construction*, University of Salford, U.K., 1995
- [3] Ozisik, M.N., Heat Transfer: A Basic Approach, New York; London: *McGraw-Hill*, 1985
- [4] Ang, C.N. and Wang, Y.C., The Effect of Water Movement on Specific Heat of Gypsum Plasterboard in Heat Transfer Analysis Under Natural Fire Exposure, *Construction and Building Materials*, **18**: p. 505-515, 2004
- [5] Mehaffey, J.R., Cuerrier, p., and Carisse, G.A., A Model for Predicting Heat Transfer Through Gypsum-Board/Wood-Stud Walls Exposed to Fire, *Fire and Materials*, **18**: p. 297-305, 1994
- [6] Yuan J., Fire Protection Performance of Intumescent Coating under Realistic Fire Conditions, PhD Thesis, *School of Mechanical, Aerospace and Civil Engineering*, University of Manchester, UK, 2009
- [7] Thomas, G., Thermal Properties of Gypsum Plasterboard at High Temperatures, *Fire and Materials*, **26**: p. 37-45, 2002
- [8] BS476, Fire tests on building materials and structures, Part 20: Method for determination of the fire resistance of elements of construction (general principles), *British Standards Institution*, 1987

## **THERMAL CONDUCTIVITY OF GYPSUM PLASTERBOARDS**

At ambient temperature and exposed to fire

A.C.J. de Korte, H.J.H Brouwers

University of Twente, Faculty of Engineering Technology, Department of Construction Management and Engineering, Enschede, The Netherlands

### **INTRODUCTION**

One of the more complicated thermal properties to calculate for gypsum plasterboard is the thermal conductivity. The thermal conductivity is important because it plays an important role in the fire behaviour of gypsum plasterboards. Plasterboard often protects steel structures of buildings, because it conducts heat slowly and absorbs the heat of the fire by its volumetric enthalpy. This paper will focus on the first role.

The thermal conductivity becomes more complicated for porous media, which consist of different phases. Kaviany (1995) points out that the heat conduction through fully saturated matrix depends on the structure of the matrix and the thermal conductivity of each phase. The same principle applies for any heterogeneous material. One of the most difficult aspects of the analysis of heat conduction through a porous medium is the structural modelling. The thermal conductivity of the solid phase is generally larger than that of the fluid, the manner in which the solid is interconnected influences the conduction. Plasterboard consists of a solid phase and water/air mix in the voids. The thermal conductivity of the voids depends strongly on the amount of moisture (absorbed water) in the voids, since the thermal conductivity of water is 23 times the thermal conductivity of air.

This article will try to solve this problem partly by assuming that gypsum plasterboards can be assumed to be a three-phase system consisting of two different two-phase systems. This concept is applied to various types of gypsum/limestone plasterboards. The models are validated by comparing the results of the models with experiments. Based on these results and models conclusions are drawn in regard to the amount of absorbed water.

Finally the concept of thermal conductivity is applied on gypsum plasterboards under fire.

### **1 TWO-PHASE SYSTEMS**

This section will focus on the description of thermal conductivity for two phase systems (fluid-solid). For these systems, several equations have been suggested during the last two centuries. Côté and Konrad (2008) point out that heat conduction through a two-phase porous media depends on the thermal conductivity as well as the structure of the solid matrix. In terms of thermal behaviour, the structure of the solid matrix determines the contact resistance and the continuity of the solid phase (Kaviany, 1995). Hamilton and Crosser (1962) showed theoretically that the thermal conductivity of particle packings decrease with increasing sphericity of particles. This effect was also noticed by Johansen (1975) and Côté and Konrad (2005) in air-saturated geomaterials where the thermal conductivity of natural particle packing (rounded/sub-rounded particles) were systematically lower than those of crushed particle packings (angular/sub-angular particles). A possible reason for this effect could be found in the smaller contact areas among the spherical particles compared to the more angular particles. Since the amount of contact area is related to the possible amount of solid-solid conductivity, which is always more than solid-fluid conductivity.

Within this article two equations are used, which take into account the structure of the solid. The first equation was introduced by Hadley (1986). This equation uses a so called mixture factor, which depends on the sphericity of the particles and the ratio of the thermal conductivity of the different phases. Another possibility is to describe the thermal conductivity with method of Zehner and Schlünder (1972). Zehner and Schlünder take into account the shape of the particles and therefore their surface connectivity. For the description of the form of the particle the factor C is used. These values are for particles which can be freely move in/through the matrix. In the case of a gypsum core there are a high number of so-called solid-phase bridges. This higher connectivity leads to a higher conductivity compared to a system with the same void fraction but with lower connectivity. For such systems with high number of solid-phase bridges, a C-value of 5 is proposed (Zehner and Schlünder, 1970).

## 2 THEORY VERSUS EXPERIMENTAL DATA

This section describes the experimental data on thermal conductivity of gypsum plasterboards found in literature, which are used to compare with the results of the theoretical equations. This experimental data is often found together with a description of the apparent density and chemical composition. Both these parameters are important in order to predict the thermal conductivity of plasterboards. The density is important because it is closely related to the void fraction of plasterboards. As can be seen in the previous section, the void fraction is one of the main parameters for the calculation of the thermal conductivity. The chemical composition of gypsum plasterboards influences the thermal conductivity of the solid phase within the board.

Table 1 shows values which are presented in literature. The experimental data is compared with the equations of the previous section. For this comparison the thermal conductivity of the solid needs to be known. Since the solid phase of gypsum plasterboards consist of several phases, the thermal conductivity of the solid phases has to be calculated. There are different calculation methods available for thermal conductivity of the composite solid.

Table 1. Experimental values of gypsum plasterboards as describes in literature

| Source                | Apparent density<br>$\rho_e$<br>[kg/m <sup>3</sup> ] | Composition              |                       |                       | $k_{meas}$<br>[W/(m K)] |
|-----------------------|--|--------------------------|-----------------------|-----------------------|-------------------------|
|                       |  | % $m_{CSH_2}$<br>[kg/kg] | % $m_{CC}$<br>[kg/kg] | % $m_{MC}$<br>[kg/kg] |                         |
| Wullschlager (2008)   | 810  | 81                       | 9.5                   |                       | 0.28                    |
| Ang and Wang (2004)   | 836.4  |                          |                       |                       |                         |
| Grazi Wakali (2007)   | 810  | 81                       | 9.5                   |                       | 0.28                    |
| Mehaffey (1994) 1     | 732  |                          |                       |                       | 0.25                    |
| Mehaffey (1994) 2     | 648  |                          |                       |                       | 0.24                    |
| Clancy (2001)         |  |                          |                       |                       | 0.18                    |
| Sultan (1996)         | 698  |                          |                       |                       | 0.25                    |
| Thomas (2002)         |  |                          |                       |                       | 0.25                    |
| Ghazi Wakali (2008) 1 | 735  | 80.9                     | 12.3                  |                       | 0.28                    |
| Ghazi Wakali (2008) 2 | 840  | 62.2                     | 32.3                  |                       | 0.30                    |
| Ghazi Wakali (2008) 3 | 740  | 76.5                     | 4.2                   | 4.7                   | 0.23                    |
| Ghazi Wakali (2008) 4 | 870  | 98                       |                       |                       | 0.32                    |

The geometric mean (eq. (1)) is a type of average, which indicates the central tendency or typical value of a set of numbers, and is often used for exponential data. As it is the most realistic model, it is used for the calculation of the solid thermal conductivity. Côté and

Konrad (2005) recommend this geometric method for the calculation of the thermal conductivity of dry soil. The method uses the volume-based composition. This equation reads;

$$k_s = \prod k_i^{\delta_i}, \quad (1)$$

with  $k_i$  is the thermal conductivity of  $i^{\text{th}}$  phase and  $\delta_i$  the volume fraction of  $i^{\text{th}}$  solid phase. Table 4 shows the results of the thermal conductivity of the solid phase based on eq. (1), the chemical composition from Table 1 and properties from Table 2.

Table 2. Thermal conductivities and specific density

| Substance                            | Thermal conductivity [W/(m K)] | Specific density [kg/m <sup>3</sup> ] |
|--------------------------------------|--------------------------------|---------------------------------------|
| CaSO <sub>4</sub> ·2H <sub>2</sub> O | 1.255                          | 2310                                  |
| CaCO <sub>3</sub>                    | 3.58                           | 2720                                  |
| MgCO <sub>3</sub>                    | 5.83                           | 2990                                  |
| H <sub>2</sub> O                     | 0.60                           | 1000                                  |
| Air (dry)                            | 0.026                          | 1.3                                   |

Table 3. The solid thermal conductivity for the solid phase only based on the geometric method and the solid composition

|                       | Solid thermal conductivity [W/(m K)] |
|-----------------------|--------------------------------------|
| Wullschlager (2008)   | 1.38                                 |
| Mehaffey (1994) 1     | 1.26                                 |
| Mehaffey (1994) 2     | 1.26                                 |
| Sultan (1996)         | 1.26                                 |
| Grazi Wakali (2008) 1 | 1.42                                 |
| Grazi Wakali (2008) 2 | 1.72                                 |
| Grazi Wakali (2008) 3 | 1.40                                 |
| Grazi Wakali (2008) 4 | 1.26                                 |

Next, the two-phase conductivities are computed based on the expressions from Section 1 and the calculated solid thermal conductivities from Table 3. The results of these computations are presented in Table 4.

Table 4. Results of different theoretical equations for the dry thermal conductivity

|                             | $k_{\text{meas}}$ | Zehner and Schlünder (1972) |
|-----------------------------|-------------------|-----------------------------|
| Wullschlager (2008)         | 0.28              | 0.171                       |
| Wullschlager (2008)         | 0.28              | 0.165                       |
| Wullschlager (2008)         | 0.28              | 0.167                       |
| Mehaffey (1994) 1           | 0.25              | 0.145                       |
| Mehaffey (1994) 2           | 0.24              | 0.126                       |
| Sultan (1996)               | 0.25              | 0.137                       |
| Grazi Wakali et al (2008) 1 | 0.28              | 0.152                       |
| Grazi Wakali et al (2008) 1 | 0.28              | 0.146                       |
| Grazi Wakali et al (2008) 1 | 0.28              | 0.149                       |
| Grazi Wakali et al (2008) 2 | 0.30              | 0.189                       |
| Grazi Wakali et al (2008) 2 | 0.30              | 0.175                       |
| Grazi Wakali et al (2008) 2 | 0.30              | 0.181                       |
| Grazi Wakali et al (2008) 3 | 0.23              | 0.154                       |
| Grazi Wakali et al (2008) 3 | 0.23              | 0.147                       |
| Grazi Wakali et al (2008) 3 | 0.23              | 0.149                       |
| Grazi Wakali et al (2008) 4 | 0.32              | 0.181                       |

The best results were obtained with Zehner and Schlünder with  $C = 5$ <sup>1</sup>. The obtained value from the equation of Zehner and Schlünder (1972) are too low compared to the results obtained from experiments. This could be the result of the current assumption that the voids

<sup>1</sup> A comparison of more equations and the experimental data can be found in De Korte and Brouwers (2009).

are filled with dry air, while in reality the fluid in the voids is usually moistured. Building materials, like gypsum plasterboards, are porous media in which moisture transfer occurs in both the vapor/gas and liquid phase. Bouguerra (1999) points out that the thermal conductivity is strongly influenced by the moisture content migrating through porous material. Since the thermal conductivity of water vapour is similar to the thermal conductivity of air there will no clear difference. But the thermal conductivity of liquid water is 23 times the thermal conductivity which will lead to clear difference. The next section will focus on the effect of moisture on the thermal conductivity of the gypsum plasterboards.

### 3 THREE-PHASE SYSTEM

This section will focus on the calculation of the thermal conductivity of a solid porous medium with a mixture of a liquid (water) and a gas (dry air) in the voids. Somerton et al. (1973) have derived the following equation for porous medium filled by a mixture of two fluids

$$k_e = k_g + \sqrt{s_1} (k_l - k_g) \quad . \quad (2)$$

Here  $k_g$  is the effective thermal conductivity of the porous medium filled with dry air,  $k_l$  is the effective thermal conductivity of the porous medium filled with water and  $s_1$  is the water saturation in the voids. Both  $k_g$  and  $k_l$  can be calculated with the equations for two-phase effective conductivity given in Section 2, with  $k_{air}$  and  $k_{water}$  as the  $k_f$  respectively.

Here, this method proposed by Somerton et al. (1973) is used to derive the amount of water needed to comply with the thermal conductivity as measured in the literature. During this derivation the effect of the moisture on density needs to be taken into account. A higher moisture content means a lower dry mass, so lower dry density. The dry density, in turn, is related to the void fraction of the material. So the density, void fraction and moisture content are all interrelated.

Table 5 shows the results of both the Zehner & Schlünder equation The sorbed water values are all in line with values from literature. Ang and Wang (2004) also give a moisture content of 3% m/m. This value is furthermore mentioned by Thomas (2002), Belmiloudi and Le Meur (2005). Therefore one can conclude that all three equations are close to the values from literature.

Table 5. Water content derived to match the experimental value

|                       | Zehner & Schlünder<br>C=5 |
|-----------------------|---------------------------|
| Wullschlager (2007)   | 2.08 %                    |
| Mehaffey (1994) 1     | 2.32 %                    |
| Mehaffey (1994) 2     | 3.42 %                    |
| Sultan (1996)         | 2.95 %                    |
| Ghazi Wakali (2008) 1 | 3.37 %                    |
| Ghazi Wakali (2008) 2 | 1.72 %                    |
| Ghazi Wakali (2008) 3 | 1.78 %                    |
| Ghazi Wakali (2008) 4 | 3.24 %                    |

### 4 APPLICATION TO THERMAL CONDUCTIVITY DURING FIRE

In the previous sections the thermal conductivity at ambient temperatures were analysed. In this section, the developed method is used for the determination of the thermal conductivity during fire, i.e. for elevated temperatures.

The thermal conductivities can be computed as the composition of the system is known for all temperatures. The decomposition process is described in more detail in de Korte and Brouwers (2009). Figure 1 shows the comparison of the results of the three-phase system with the experimental results of Mehaffey (1994). The used gypsum plasterboard of Mehaffey (1994) has a density of  $732 \text{ kg/m}^3$  and consists of 100% gypsum. The thermal conductivity is simulated with the Zehner and Schlünder equation with a shape-factor (C) of 5 and an initial moisture content of 2.8% on the gypsum mass is used. This is based on the result from Section 3. The equation of Zehner and Schlünder is used because it depends on a few parameters. Furthermore the thermal conductivities of the solid and fluid phases are assumed to be equal to the data in Table 2, so the thermal conductivities are assumed to be constant, i.e. not a function of temperature. Also the thermal expansion of the solids is ignored. Upon heating, the solids expand, which reduces the void fraction.

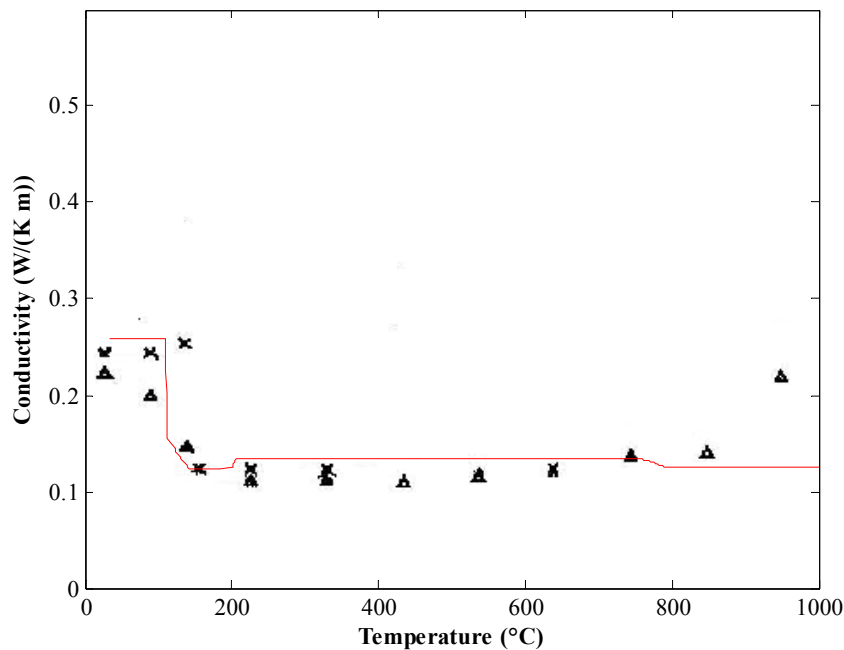


Fig. 1. Simulated thermal conductivity according to the proposed model (thin line) and experimental thermal conductivity (Mehaffey, 1994).

Notwithstanding these and other simplifications, it can be seen from Figure 1 that the simulated value have a good fit with the experimental value obtained from literature. The raise in thermal conductivity beyond  $850^\circ\text{C}$  in the experiments is probably caused by shrinkage cracks in the material. Due to cracks the air flows through the cracks more easy, increasing the apparent thermal conductivity. Obviously, this system change is not dealt with by the present model.

## 5 SUMMARY/CONCLUSION

The thermal conductivity of gypsum plasterboard up to a temperature of  $105^\circ\text{C}$  can be described best by a three-phase system as first introduced by Somerton et al (1973). This method requires information about the thermal conductivities which are provided by two-phase systems and the saturation of the voids. The two two-phase systems govern the cases with no saturation and full saturation of the voids.

For the two-phase system the Zehner and Schlünder equation met shape-factor of 5 yields good results. Furthermore, a moisture content of 2.8 % on plasterboard mass appears to be needed to explain the thermal conductivity of the board.

Using this moisture content of 2.8%, and the equations of Zehner and Schlünder with  $C=5$  and Somerton, measured values for the thermal conductivity of several plasterboards from literature up to 105°C can be predicted excellently. This amount of moisture content is in line with the values reported in literature, and here it appears to depend only on the gypsum content of the solid phase. For more elevated temperatures, the two-phase equations (air/solid) also proves to be useful, when one takes account of the appropriate changes in the type of solid (dehydration, decarbonation) and volume (void fraction).

## ACKNOWLEDGEMENTS

The author wishes to express their sincere thanks to the European Commission (I-SSB Project, Proposal No. 026661-2) and the following sponsors of the research group: Bouwdienst Rijkswaterstaat, Rokramix, Betoncentrale Twenthe, Betonmortelcentrale Flevoland, Graniet-Import Benelux, Kijlstra Beton, Struyk Verwo Groep, Hülskens, Insulinde, Dusseldorp Groep, Eerland Recycling, Enci, Provincie Overijssel, Rijkswaterstaat Directie Zeeland, A&G Maasvlakte, BTE, Alvon Bouwsystemen and V.d Bosch Beton (chronological order of joining).

## REFERENCES

- Ang, C. N., and Wang, Y. C. (2004). The effect of water movement on specific heat of gypsum plasterboard in heat transfer analysis under natural fire exposure. *Construction and Building Materials*, 18(7), 505-515.
- Belmiloudi, A., and Le Meur, G. (2005). Mathematical and numerical analysis of dehydration of gypsum plasterboards exposed to fire. *Applied Mathematics and Computation*, 163(3), 1023.
- Bouguerra, A. (1999). Temperature and moisture dependence on the thermal conductivity of wood-cement-based composite: experimental and theoretical analysis. *Journal of Physics D: Applied Physics*, 32, 2797-2803.
- Côté, J., and Konrad, J. M. (2008). Assessment of structure effects on the thermal conductivity of two-phase porous geomaterials. *International Journal of Heat and Mass Transfer*, Accepted.
- de Korte, A.C.J. and Brouwers, H.J.H. (2009). Thermal conductivity of gypsum plasterboards. Submitted to *Fire and Materials*.
- Grazi Wakali, K. and Hugi, E (2008) Four types of gypsum plaster boards and their thermo-physical properties under fire condition. Submitted to *Journal of Fire Sciences*.
- Hadley, G. R. (1986). Thermal conductivity of packed metal powders. *International Journal of Heat and Mass Transfer*, 29(6), 909-920.
- Hamilton, R. L., and Crosser, O. K. (1962). Thermal Conductivity of Heterogeneous Two-Component Systems. *Industrial & Engineering Chemistry Fundamentals*, 1(3), 187-191.
- Johansen, O. (1975). *Varmeledningsevne av jordarter*, Ph.D. Thesis, Norge tekniske hogskole, Trondheim, Norway.
- Kaviany, M. (1995). *Principles of Heat Transfer in Porous Media* (Second ed.). Springer, Berlin.
- Mehaffey, J. R., Cuerrier, P., & Carisse, G. (1994). A model for predicting heat transfer through gypsum-board/wood-stud walls exposed to fire. *Fire and Materials*, 18(5), 297-305.
- Somerton, W. H., Chu, S. L., & Keese, J. A. (1973). Thermal behavior of unconsolidated oil sands. *Soc. Pet. Eng. AIME, Pap*, 4506(48).
- Sultan, M. A. (1996). A model for predicting heat transfer through noninsulated unloaded steel-stud gypsum board wall assemblies exposed to fire. *Fire Technology*, 32(3), 239-259.
- Thomas, G. (2002). Thermal properties of gypsum plasterboard at high temperatures. *Fire and Materials*, 26(1), 37-45.
- Wullschleger, L., and Wakili, K. G. (2008). Numerical parameter study of the thermal behaviour of a gypsum plaster board at fire temperatures. *Fire and Materials*, 32(2), 103-119.
- Zehner, P. and Schlünder, E. U. (1970). Thermal conductivity of granular materials at moderate temperatures. *Chemie Ingenieur Technik*, 42(14), 933-941.
- Zehner, P., & Schlünder, E. U. (1972). Einfluß der Wärmestrahlung und des Druckes auf den Wärmetransport in nicht durchströmten Schüttungen *Chem. Ing.-Tech*, 44(23), 1303-1308.

## EFFECTIVE CHARACTERISTICS OF FIRE PROTECTION

Michal Strejček <sup>a</sup>, Richard Cinař <sup>a</sup>, Vilém Stanke <sup>b</sup>, František Wald <sup>a</sup>

<sup>a</sup> Czech Technical University, Faculty of Civil Engineering, Prague, Czech Republic

<sup>b</sup> Promat a.s., Prague, Czech Republic

### INTRODUCTION

Reliability of a steel structure exposed to fire conditions depends basically on the affect of mechanical and thermal actions. To predict the behaviour of the structure during the fire the gas temperature in the compartment, the temperature transfer into the structure element, the mechanical loading during the fire and the mechanical resistance of the structure is calculated. The collapse of the structural element occurs at the moment of reaching the critical temperature in the structure. High thermal conductivity of structural steel is the main disadvantage which causes the fast growth of the temperature in structural element. Application of the fire protection materials directly on the steel element can significantly affect the temperature growth. Thereby the structural collapse can be put behind.



*Fig. 1* The fire test of Promapaint SC, see [7]

A number of fire protection materials are available to provide required fire resistance of the structure. Commonly used fire protection materials for structural steelwork include, except for traditional concrete protective layer, board type products, sprayed fire-resistive materials, thin-film intumescent materials and intumescent mat wrap materials, see [1]. All these materials are required to assure thermal insulation and carry its integrity at elevated temperatures during the fire. Selection of the specific type of fire protection material is managed by many factors, which classifies fire protection ability, durability, maintenance and aesthetic factor. Intumescent materials are ideal choice for uncovered members of steel structures. They are directly applied on the steel structure in thin layer from 450 to 2500  $\mu\text{m}$ ,

depending on required fire resistance of the structure. At elevated temperatures the thin layer goes through a chemical process, which causes the foaming. Initial layer is able to change its thickness more than 30 times during the heating. Foamed layer can provide the fire resistance commonly up to 2 hours. Board type products and sprayed fire-resistive materials are usually applied in cases of completely hidden structure. Board products, which are currently most used in commercial buildings, can provide the fire resistance up to 3 hours. Modern mixtures, improved by the reinforce fibres, ensure its integrity at high temperatures. Dry process during the construction and shape variability are their main advantages. Sprayed fire-resistive materials can be divided into two categories depending on the mixture which widely affect, except for the layer thickness, the fire resistance rating. Sprayed mineral fibre and sprayed cementitious mixtures can be recognized. Taking into account their mechanical and weather resistance are appropriate for offshore and industrial structures.

Temperature calculation of the structure during the fire can be described by a number of different ways. Prediction by the manufacturer's table values, verified experimentally, is the most used method in established practice. Analytical design models, which provide more specific solution, are used in this article for temperature calculations of thermally protected steel elements. In spite of using the finite element approach is the most fitting method, remains this solution, due to its complicated calculation, in field of research.

## 1 ANALYTICAL MODEL

The temperature growth in the structural steel element can be delayed against the gas temperature in the fire compartment by using the fire protection material covering the structure. The temperature evaluation for a structural element protected by a thermal insulation layer includes considering the thermal equilibrium of heat emitted by hot gases, heat absorbed by the protection material and heat absorbed by the structural element. The heat is transferred through the insulation layer by conduction and the temperature increase  $\Delta\theta_{a,t}$  during a time interval  $\Delta t$  can be obtained from Eq. (1) expecting uniform temperature distribution in cross-section [2].

$$\Delta\theta_{a,t} = \frac{\lambda_p A_p / V}{d_p c_a \rho_a} \frac{\theta_{g,t} - \theta_{a,t}}{1 + \phi/3} \Delta t - (e^{\phi/10} - 1) \Delta\theta_{g,t}, \text{ but } \Delta\theta_{a,t} > 0 \quad (1)$$

with: 
$$\phi = \frac{c_p \rho_p}{c_a \rho_a} d_p \frac{A_p}{V}$$

where:  $\lambda_p$  is thermal conductivity of the fire protection material [ $\text{J kg}^{-1}\text{K}^{-1}$ ];  $A_p / V$  is the section factor of insulated steel member [ $\text{m}^{-1}$ ];  $\theta_{g,t}$  is the ambient gas temperature at time  $t$  [ $^{\circ}\text{C}$ ];  $\theta_{a,t}$  is the steel temperature at time  $t$  [ $^{\circ}\text{C}$ ];  $d_p$  is the thickness of the fire protection material [m];  $c_p$  and  $c_a$  are specific heat of the fire protection material and of steel [ $\text{J kg}^{-1}\text{K}^{-1}$ ];  $\rho_p$  and  $\rho_a$  are unit mass of the fire protection material and of steel [ $\text{kg/m}^3$ ];  $\Delta\theta_{g,t}$  is the gas temperature increase during the time interval  $\Delta t$  [K], where value of  $\Delta t$  should be considered less than 30 seconds. Recommended equation is useless for section factor  $A_p / V$  less than  $10 \text{ m}^{-1}$ . With  $A_p / V$  ratio higher than  $350 \text{ m}^{-1}$  it has not practical sense, because the element temperature equals to the gas temperature,  $\theta_{a,t} \approx \theta_{g,t}$ .

The temperature growth depends basically on thermal properties of the fire insulation layer, its thickness and on the  $A_p / V$  ratio, where  $A_p$  is inner surface of the insulation layer. The fire protection material is exposed to significant chemical process during the heating, which considerably changes its material characteristics. Conservative values of different materials at respective temperatures, determined from experimental results, are shown in Tab. 1, see [3].

For perfect prediction of the temperature growth in the steel member is necessary to take into account the material characteristics changes. The temperature inconsistency limits practical usage of analytical prediction model mentioned above. Values of material characteristics at respective temperatures can be replaced by an effective value.

## 2 EFFECTIVE CHARACTERISTICS

Two fire tests in FIRES s.r.o. laboratory in Batizovce (Slovakia) were prepared to study the temperature increase in the steel element protected by boards PROMATEC<sup>®</sup>-H and sprayed material TERFIX-P, see [4] and [5]. The temperature growth was observed during the heating in steel elements of different section factor and different thickness of thermal insulation. The gas temperature in the test furnace followed nominal standard fire curve.

*Tab. 1* Properties of the enclosure surface materials at elevated temperatures

| Material                   | Temperature<br>$\theta^\circ$<br>C | Unit mass<br>$\rho_p$<br>kg/m <sup>3</sup> | Thermal conductivity<br>$\lambda_i$<br>W m <sup>-1</sup> K <sup>-1</sup> | Specific heat<br>$c$<br>J kg <sup>-1</sup> K <sup>-1</sup> | Coefficient<br>$b = \sqrt{\rho c \lambda}$<br>J m <sup>-2</sup> s <sup>-1/2</sup> K <sup>-1</sup> |
|----------------------------|------------------------------------|--|--|--|---|
| Normal concrete            | 20                                 | 2300                                       | 2,00   | 900  | 2030  |
|                            | 200                                | 2300                                       | 1,63   | 1022   | 1960  |
|                            | 500                                | 2300                                       | 1,21   | 1164   | 1800  |
|                            | 1000                               | 2300                                       | 0,83   | 1289   | 1570  |
| Steel                      | 20                                 | 7800                                       | 54   | 425  | 13380   |
|                            | 200                                | 7800                                       | 47   | 530  | 13940   |
|                            | 500                                | 7800                                       | 37   | 667  | 13870   |
|                            | 1000                               | 7800                                       | 27   | 650  | 11700   |
| Gypsum insulating material | 20                                 | 128  | 0,35   | 800  | 190   |
|                            | 200                                | 128  | 0,06   | 900  | 80  |
|                            | 500                                | 128  | 0,12   | 1050   | 130   |
|                            | 1000                               | 128  | 0,27   | 1100   | 190   |
| Sealing cement             | 20                                 | 200  | 0,0483   | 751  | 90  |
|                            | 250                                | 200  | 0,0681   | 954  | 110   |
|                            | 450                                | 200  | 0,1128   | 1052   | 150   |
|                            | 1050                               | 200  | 0,2016   | 1059   | 210   |
| CaSi board                 | 20                                 | 450  | 0,0685   | 748  | 150   |
|                            | 250                                | 450  | 0,0786   | 956  | 180   |
|                            | 500                                | 450  | 0,0951   | 1060   | 210   |
|                            | 800                                | 450  | 0,157  | 1440   | 320   |

Results of the test for boards PROMATEC<sup>®</sup>-H of minimal thickness 8 mm are compared to analytical prediction Tab. 2. Analytical prediction was realized based on effective material characteristics of the boards. The thermal conductivity development at elevated temperatures can be described by its effective value  $\lambda_{p,eff}$ . From experimental results were identified ideal values of the thermal conductivity at respective temperatures. Using the method of least squares the effective thermal conductivity formula for every board thickness can be derived, see *Fig 1*. For PROMATEC<sup>®</sup>-H boards with nominal thickness 7,6 mm the effective thermal conductivity is  $\lambda = 3 \times 10^{-7} \theta_{a,t}^2 - 0,0001 \theta_{a,t} + 0,14$ ; where  $\theta_{a,t}$  is the steel temperature.

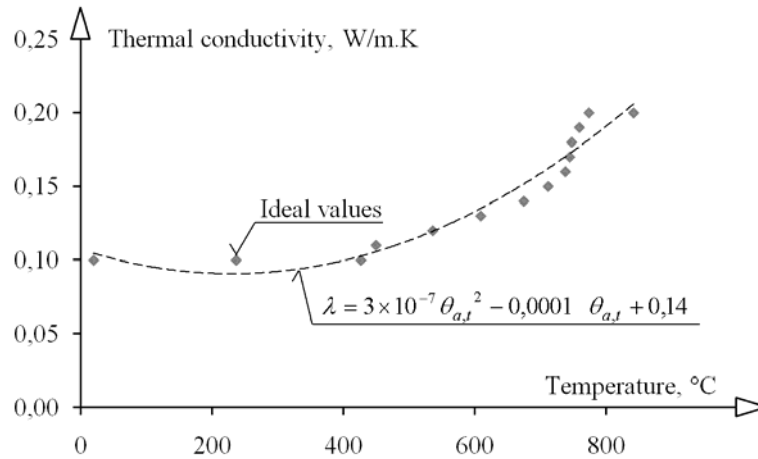


Fig. 2 Effective value of thermal conductivity  $\lambda_{p,eff}$  for PROMATEC<sup>®</sup>-H, thickness 7,6 mm

Temperature prediction during the fire is slightly conservative, see Fig. 2. Black circular points represent manufacturer's table values, see [6]. Conservative prediction in 30<sup>th</sup> min of the fire can be noticed.

Tab. 2 Test temperature compared to analytical prediction for PROMATEC<sup>®</sup>-H

| Time [min] | ISO curve [°C] | EXPERIMENT           |                          | ANALYTICAL MODEL |                |                          |                          |
|------------|----------------|----------------------|--------------------------|------------------|----------------|--------------------------|--------------------------|
|            |                | Gas temperature [°C] | Element temperature [°C] | $C_a$ [J/Kg°C]   | $C_p$ [J/Kg°C] | $\lambda_{p,eff}$ [W/mK] | Element temperature [°C] |
| 0          | 20             | 35                   | 23                       | 440              | 800            | 0,000                    | 20                       |
| 5          | 576            | 357                  | 72                       | 450              | 838            | 0,137                    | 39                       |
| 10         | 678            | 679                  | 122                      | 482              | 875            | 0,133                    | 97                       |
| 15         | 739            | 729                  | 189                      | 516              | 913            | 0,132                    | 172                      |
| 20         | 781            | 779                  | 257                      | 541              | 950            | 0,133                    | 239                      |
| 25         | 815            | 809                  | 322                      | 563              | 988            | 0,137                    | 302                      |
| 30         | 842            | 838                  | 385                      | 586              | 1025           | 0,142                    | 361                      |
| 35         | 865            | 864                  | 445                      | 612              | 1063           | 0,150                    | 417                      |
| 40         | 885            | 889                  | 498                      | 642              | 1100           | 0,158                    | 470                      |
| 45         | 902            | 901                  | 551                      | 678              | 1138           | 0,168                    | 519                      |
| 50         | 918            | 913                  | 600                      | 718              | 1175           | 0,178                    | 564                      |
| 55         | 932            | 927                  | 642                      | 761              | 1213           | 0,188                    | 606                      |
| 60         | 945            | 942                  | 680                      | 799              | 1250           | 0,199                    | 644                      |
| 65         | 957            | 960                  | 713                      | 877              | 1288           | 0,210                    | 680                      |
| 70         | 968            | 978                  | 738                      | 1096             | 1325           | 0,220                    | 711                      |
| 75         | 979            | 978                  | 762                      | 2318             | 1363           | 732                      | 732                      |

An analytical prediction of temperature development in steel element protected by sprayed coating TERFIX-P was realized using the effective value of thermal conductivity which was derived from experimental results. Comparison of experimental measured temperature and predicted temperature is shown in Fig. 4. An inaccurate prediction can be noticed until 15<sup>th</sup> minute. Manufacturer's table values are inaccurate in 30<sup>th</sup> min.

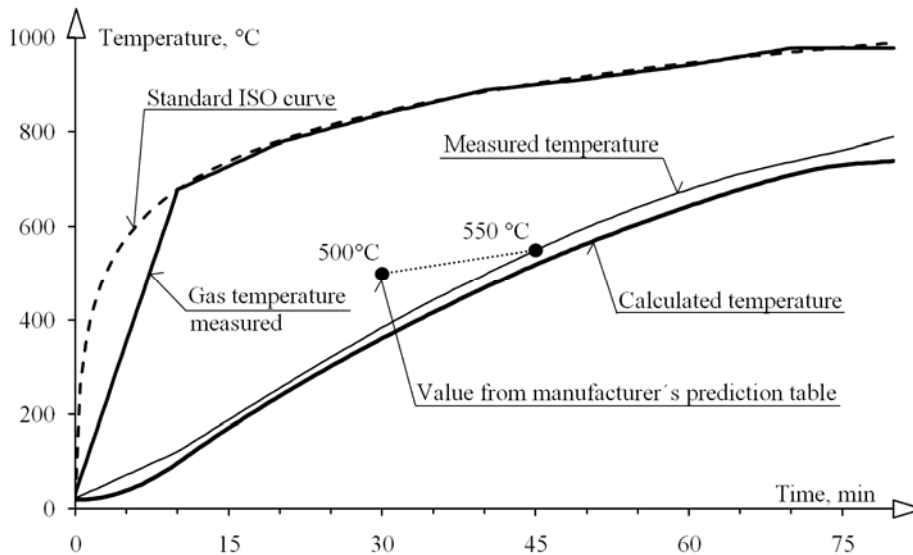


Fig. 3 Comparison of the measured temperature and calculated temperature for PROMATEC<sup>®</sup>-H boards of thickness  $d_p = 7,6$  mm

Intumescent painting, except its density, thermal conductivity and specific heat, also changes its thickness. To determination of effective thickness was tested PROMAPAIN<sup>®</sup>-SC intumescent painting on opened and box cross-section columns in experimental furnace in laboratory Veselí nad Lužnicí, Czech Republic, see [7]. Three thicknesses were observed during the loading by a Standard fire curve: thin  $d_{dry,thin} = 470$   $\mu\text{m}$ , medium  $d_{dry,medium} = 1200$   $\mu\text{m}$  and thick  $d_{dry,thick} = 2500$   $\mu\text{m}$ . Analytical prediction of temperature development in opened cross-section HEA 300 column covered with thin layer of intumescent painting is demonstrated in Fig. 5. For minimal initial thickness  $d_{dry,min} = 470$   $\mu\text{m}$  was derived an effective thickness  $d_{p,eff} = 8$  mm. Other material characteristics were considered constant with values of density  $\rho_p = 350$   $\text{kg/m}^3$ , thermal conductivity  $\gamma_p = 0,20$   $\text{W m}^{-1}\text{K}^{-1}$  and specific heat  $c_p = 1100$   $\text{J kg}^{-1}\text{K}^{-1}$ . An inaccurate prediction until 15<sup>th</sup> minute of the fire is caused by time-delayed of the foaming. Effective thickness for medium and thick initial layer can be considered by 18 and 20 mm.

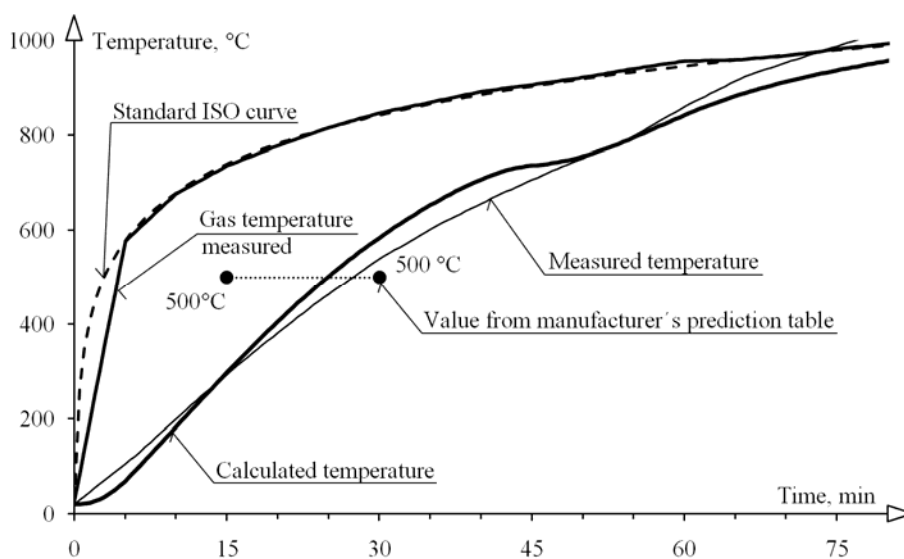


Fig. 4 Comparison of the measured temperature and calculated temperature for sprayed coating TERFIX-P of thickness  $d_p = 7$  mm

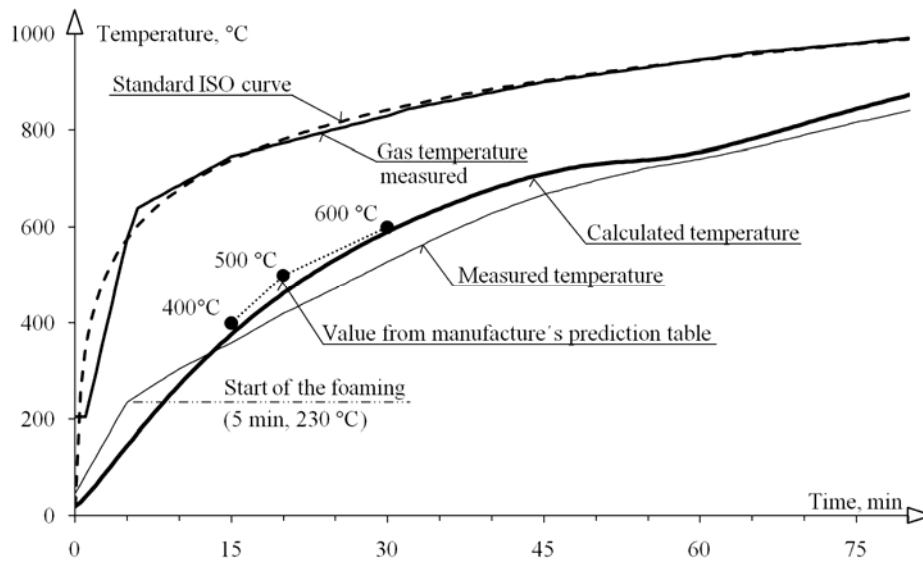


Fig. 5. Comparison of the measured temperature and calculated temperature for Promapaint SC intumescent painting using effective thickness  $d_{p,eff} = 8$  mm

### 3 SUMMARY AND ACKNOWLEDGMENT

The calculations of the heat transfer to structures protected against fire are based on experimentally verified times of the completeness of fire protection elements. Thermal properties can be determined conservatively using nominal values shown in the respective tables or more accurately by evaluating the tests. The contribution documents a good accuracy of the analytical prediction for commonly used fire protection materials.

The authors would like to thank PROMAT a.s. and TORA s.r.o. for publishing of the experimental results.

### REFERENCES

- [1] Parker A.J., Beitel J.J., Iwankiw N.R., Fire Protection Materials for Architecturally Exposed Structural Steel (AESS), *STRUCTURE magazine*, 2005.
- [2] EN 1993-1-2:2005, Design of steel structures – Part 1-2: General rules – Structural fire design, *European Committee for Standardization*, Brussels, 2005.
- [3] Vassart, L.G., Cajot, L.G., Brasseur, M., Thermal & Mechanical Actions – Part 1, DIFISEK<sup>+</sup>, www.difisek.eu, 2007.
- [4] Gorlický M., Protocol of the test, in Slovak Protokol o zkoušce FIRES FR 018/04CP, obklad ocelových konstrukcí, Typ PROMATEC<sup>®</sup>-H, No. 415 a 445, Batizovce, Slovakia, 2004.
- [5] Gorlický M., Protocol of the test, in Slovak Protokol o zkoušce FIRES FR 057/04CP, nástřik ocelových konstrukcí, Typ TERFIX P, Batizovce, Slovakia, 2004.
- [6] Design tables of products PROMAT s.r.o., Praha, 2005, www.promatpraha.cz
- [7] Louma, M., Protocol of the fire test resistance, in Czech Protokol o zkoušce požární odolnosti, Pavus a.s., protocol č. Pr-06-2.019, Veselí nad Lužnicí, 2006.
- [8] Wald, F., Střejček, M., The effective properties of the fire protection materials, in Czech Účinné vlastnosti požárně ochranných materiálů, *Konstrukce*, roč. 6, č. 5, pp. 29 - 31. ISSN 1213 8762, 2007.



Proceedings of International Conference  
Applications of Structural Fire Engineering  
Prague, 19-20 February 2009

**Session 4**

**Concrete Structures**

## BASIC APPROACH FOR THE DIAGNOSIS OF CONCRETE AFTER FIRE EXPOSURE

Emmanuel Annerel <sup>a</sup>, Luc Taerwe <sup>b</sup>

<sup>a,b</sup> Ghent University, Laboratory Magnel for Concrete Research, Ghent, Belgium

### INTRODUCTION

Generally, concrete structures have a very good fire resistance. Although damage to the concrete gradually appears with increasing temperature, it is possible to repair the structure after an adequate assessment. To do this in a systematic way, knowledge is necessary concerning residual material properties and methods to assess this strength. The residual strength varies between additional strength loss due to internal expansion reactions and strength recovery due to possibly rehydration processes ([1], [2] and [3]). Since the residual strength is temperature dependent, methods may be used to assess the strength indirectly by measuring the alteration in the material as function of the temperature. [1] and [2] illustrate how cracks appear and the colour of the concrete changes from red (300-600°C) to whitish grey (600-900°C) and buff (900-1000°C). Once these temperatures are obtained, simple calculations based on EN1992-1-2 [4] may be used to determine the residual capacity of concrete elements, as elaborated in [5].

### 1 RESIDUAL STRENGTH

*Table 1* summarizes the mix design of a self-compacting concrete (SCC), a traditional vibrated concrete with siliceous aggregates (TC) and calcareous aggregates (Tck), as well as a high strength concrete (HPC). One hundred fifty millimetre cubes are cured for 4 weeks in an air-conditioned room at a RH >90% and a temperature of 20±1°C, after which they are stored at 60% RH and 20±1°C for drying until testing age (> 17 weeks). Two cubes are heated for each of the examined temperature levels (till 800°C), occurring at a heating rate of 3.5°C/min. The target temperature is kept constant for 750 minutes. The cubes are allowed to cool slowly in the oven, after which they are immediately tested for compression. *Fig. 1* shows how the results are situated around the curves mentioned in EN 1992-1-2 [4]. Tests are executed to determine the influence of the heating rate, duration at target temperature (350°C, 550°C) and cooling method on the residual strength immediately after cooling [1]. The heating rate is changed to 10°C/min for TC and 20°C/min for SCC. The duration at the target temperature is altered to 3600 minutes and the cooling regime is modified into a rapid cooling by quenching under water. Results show that only the cooling method is an important parameter to consider, resulting in an extra drop of the residual strength of 30-35%.

*Table 1.* Concrete mix design

|   | SCC<br>siliceous | TC<br>siliceous | Tck<br>calcareous | HPC<br>siliceous |
|---|------------------|-----------------|-------------------|------------------|
| sand [kg/m <sup>3</sup> ]                     | 782              | 640             | 663               | 650              |
| gravel 2-8 mm [kg/m <sup>3</sup> ]            | 300              | 525             | -                 | 530              |
| gravel 8-16 mm [kg/m <sup>3</sup> ]           | 340              | 700             | -                 | 720              |
| limestone 2/6                                 | -                | -               | 450               | -                |
| limestone 6/20                                | -                | -               | 759               | -                |
| portland cement I 52.5 [kg/m <sup>3</sup> ]   | 400              | 350             | 350               | 400              |
| water [kg/m <sup>3</sup> ]                    | 192              | 165             | 165               | 132              |
| limestone powder [kg/m <sup>3</sup> ]         | 300              | -               | -                 | -                |
| superplasticizer 1 [l/m <sup>3</sup> ]        | 2.90             | -               | -                 | -                |
| Superplasticizer 2 [l/m <sup>3</sup> ]        | -                | -               | -                 | 16.5             |
| W/C [-]                                       | 0.48             | 0.47            | 0.47              | 0.33             |
| compressive strength 28d [N/mm <sup>2</sup> ] | 65.9             | 56.5            | 60.3              | 77.3             |

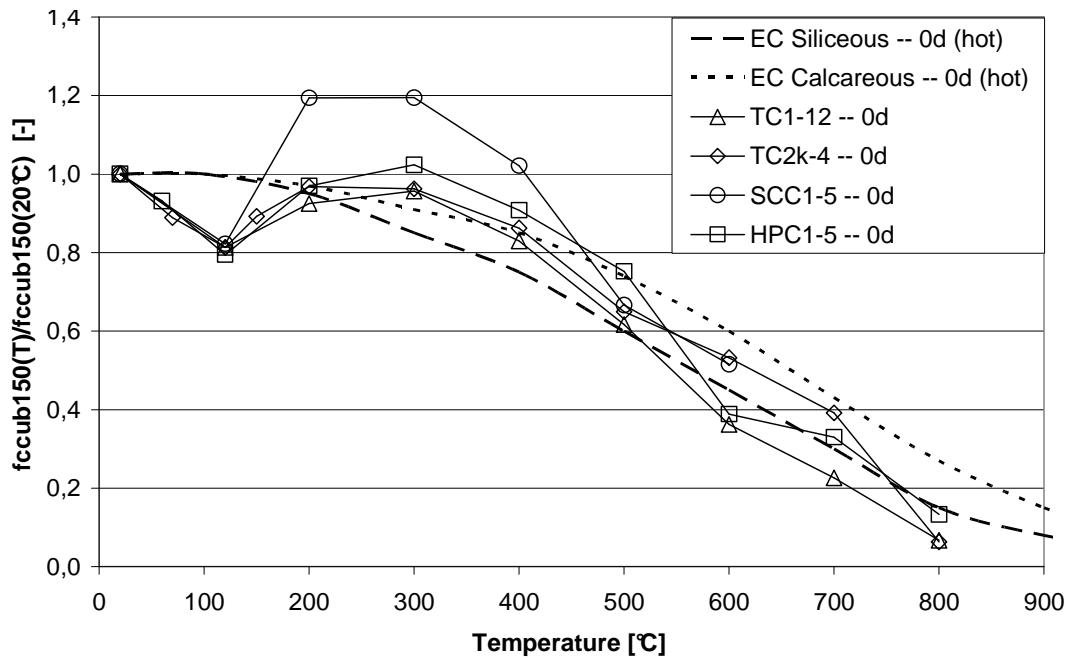


Fig. 1. Residual compressive strength

Besides the test conditions, storage after heating influences the residual strength. One hundred and fifty millimetre cubes TC2k are heated to different target temperatures according to the standard conditions as mentioned before. Furthermore, TC1 cylinders ( $\varnothing 113\text{mm} \times 320\text{ mm}$ ) are heated at a rate of  $1^\circ\text{C}/\text{min}$ , kept for 750 minutes at target temperature and slowly cooled in the oven. Fig. 2 shows an additional strength decrease above  $200^\circ\text{C}$  compared to the strength loss due to heating (Fig. 1) of about 20% when testing the cubes and cylinders after a period (28 days; 12 weeks) of storage at RH 60% and  $20 \pm 1^\circ\text{C}$ . These experiments have been repeated for  $350^\circ\text{C}$  and  $550^\circ\text{C}$ , after which they were stored under water and ambient air [1]. Again an additional strength decrease of 20-30% was observed around 7 days of storage, from where the strength slowly recovers. Strength recovery of up to 10% was found when storing for 56 days under water.

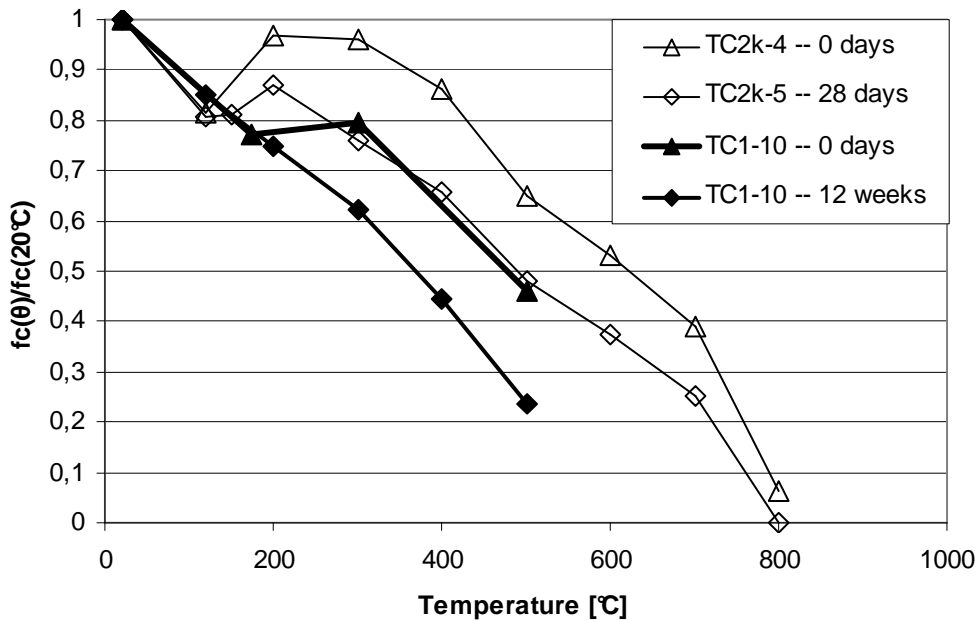
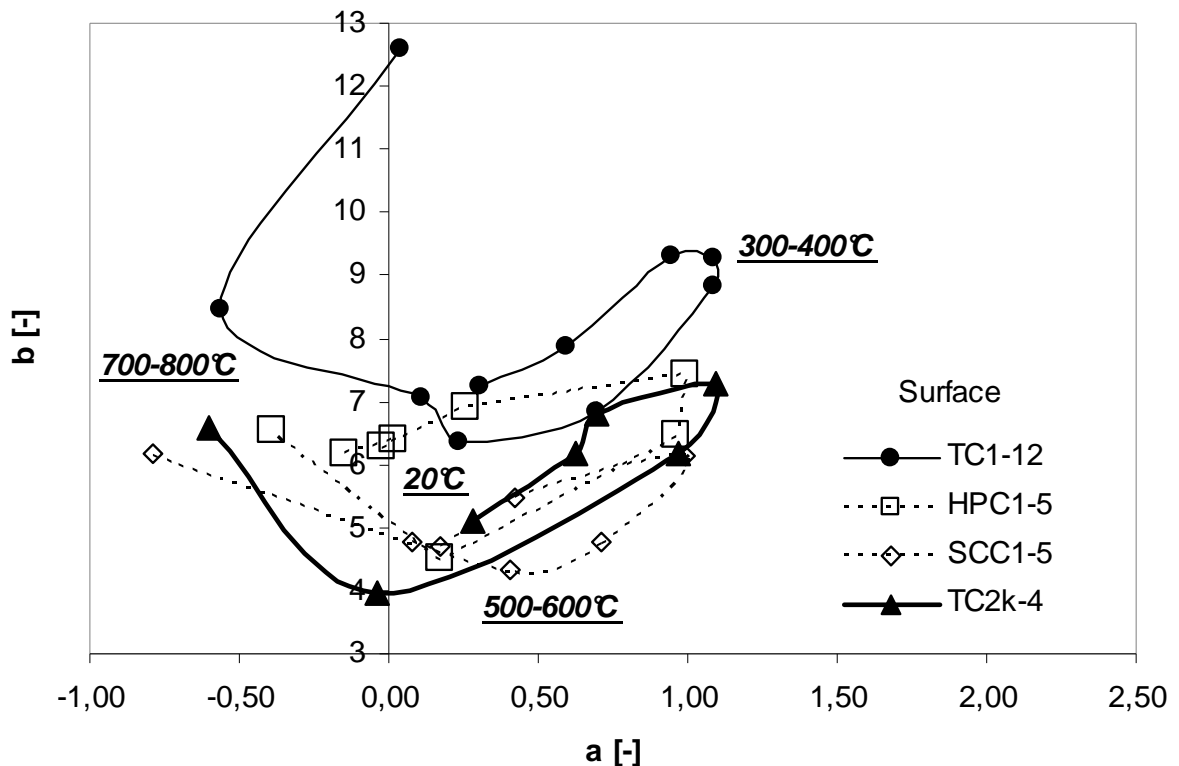


Fig. 2. Further strength decrease of TC2k cubes and TC1 cylinders due to storage in ambient air after heating

## 2 ASSESSMENT OF THE TEMPERATURE PROFILE

### 2.1 Colorimetry

The colour is measured with an X-rite SP60 spectrophotometer (aperture 8 mm) according to the CIE Lab-colour space. In this colour system 'L' is the lightness with values between 0 (black) and 100 (white), while 'a' is spread between magenta (positive values) and green (negative values) and 'b' is positioned between yellow (positive values) and blue (negative values). *Fig. 3* shows how the colour measured on cast surfaces describes an elliptical path in the a\*b\*-colour space. However, differences are noticeable between the 4 concrete types. The measurements are executed immediately after cooling down to ambient temperatures and before the compression test (*Fig. 1*). When storing these cubes under RH 60% and at temperatures of  $20\pm 1^\circ\text{C}$  for several weeks, a shift towards the inner part of the ellipse is found [1]. This shift can probably be attributed to the moisture absorption, because a linear relationship between the colour change (L, a, b) and the weight increase exist with a  $R^2$  of 0.7-0.8. Further studies are executed on TC and SCC discs cut from drilled cores, after polishing and masking of the colourful aggregates [1]. These colour alterations provide information to identify the temperature reached inside the concrete after fire exposure.



*Fig. 3.* Colour development at concrete surface

*Fig. 4* shows the colour paths described by some heated siliceous aggregates. They are named after their initial colour which is visible when wetting the aggregates. Generally, these aggregates alter in colour towards a reddish tint above  $300^\circ\text{C}$  due to the oxidation process of the iron. However, knowledge about the exact colour path could provide more detailed information on the temperature distribution inside a concrete element. The link to the aggregates composition is important, since once changed to red, it is difficult to distinct the different aggregates.

From a batch of siliceous gravel, aggregates which are most present are selected. These aggregates are grinded to powder, after which their composition is determined with EDX under a SEM in low vacuum mode at 200x magnification (*Table 2*). Group 1 is determined by silicon Si with a mutual ratio of around 97 %. Group 2 consists of the same ions (Al, Si, K and Fe) in comparable proportion. The aggregates of group 3 shows higher mutual percentage of calcium Ca, but lower for

silicon Si. Group 4 is characterised by the presence of magnesium Mg. The powders are heated for 3 hours in an electric oven for different target temperatures at a rate of about 30°C/min. The target temperature is raised successively by 50°C: 120°C, 200°C, 250°C, 300°C, ..., 1100°C and 1150°C. Between two heating regimes, the colour of the powders is measured with an X-rite SP60 spectrophotometer. The colour of group 1 and 2 alter gradually towards a more orange tint with a maximum at 700°C. From there, the colour changes back to a more grey tint and even white above 1000°C. The path of group 3 is more complicated: a jump is recognisable at 250°C with further increase till 450°C, from where the colour turns halfway back till approximately 700°C. At 1100°C, the aggregate 'blue' is coloured white, while the aggregate 'brown' has turned into orange. Group 4 keeps travelling to an orange tint till around 950°C, from where it turns back in a loop. This green aggregate also shows a jump at 250°C, which is supposed to be caused by the oxidation of the iron oxides. This assumption seems to be right since the aggregates with the largest amount of iron (green, brown) do show a larger colour jump. However, even for the aggregates with no detection of iron (white, blue), a smaller jump is visible. Fig. 4 illustrates also the colour shift of calcareous aggregates. Although the colour changes from black over blue to white (>700°C: decarbonation), the displacements are small compared to siliceous aggregates.

Table 2. EDX results

|      | Group 1 |              | Group 2      |            | Group 3 |       | Group 4 |
|------|---------|--------------|--------------|------------|---------|-------|---------|
| At % | white   | white-yellow | yellow-brown | brown-iron | brown   | blue  | green   |
| MgK  | -       | -            | -            | -          | -       | -     | 2.55    |
| AlK  | 1.29    | -            | 3.73         | 7.12       | 2.24    | -     | 4.92    |
| SiK  | 97.30   | 96.76        | 90.43        | 86.93      | 72.40   | 56.28 | 85.03   |
| KK   | -       | -            | 3.74         | 4.01       | -       | -     | -       |
| CaK  | 1.42    | -            | -            | -          | 22.17   | 43.73 | -       |
| FeK  | -       | 3.24         | 2.12         | 1.95       | 3.21    | -     | 7.51    |

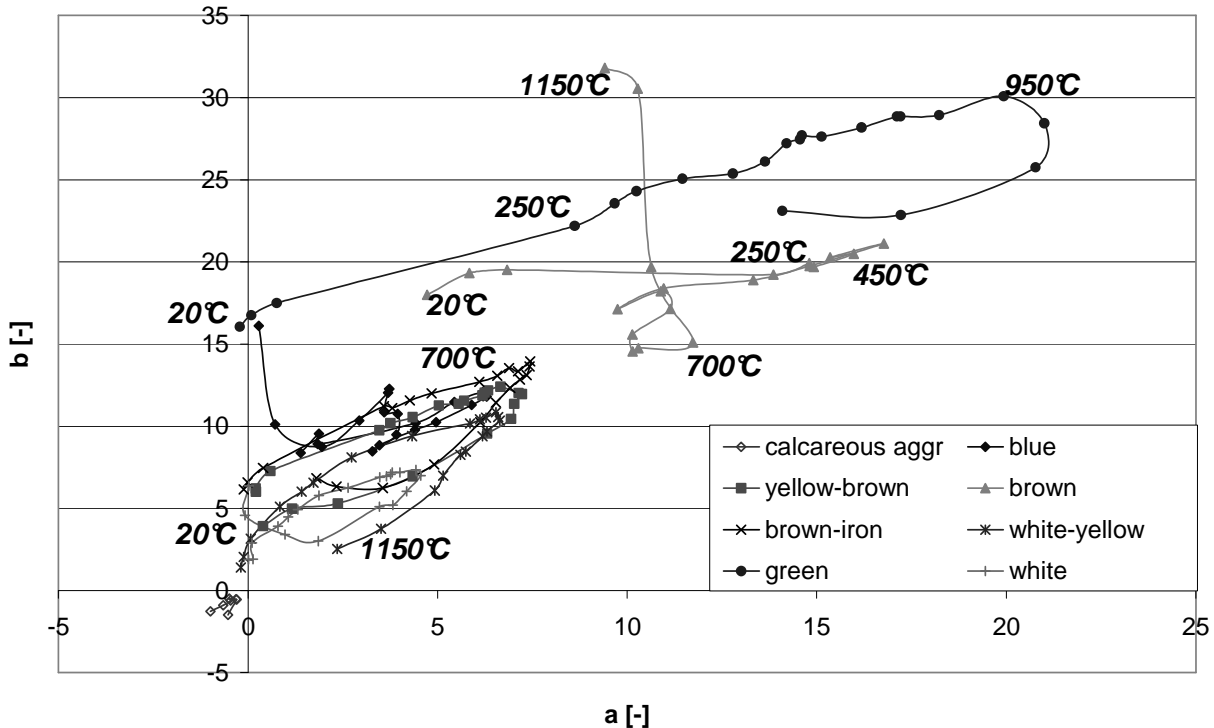


Fig. 4. Colour path of aggregates

## 2.2 Water immersion

Heating of concrete introduces stresses, resulting in cracks. Meanwhile, chemical alterations, such as dehydration and decarbonation, lead to the disappearance of the hydration products, which increases the pore space (Fig. 5) [6]. Hence, these two effects cause an increase of the porosity when heating concrete. Remark that immersion of concrete under water will fill the pores and cracks with water. Then, the weight increase can be used to assess the internal damage due to heating.

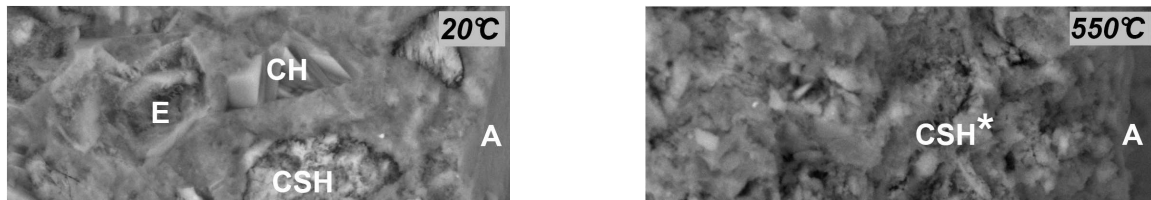


Fig. 5. ESEM images of ordinary Portland concrete at 20°C and heated up to 550°C. (E = ettringite, CH = portlandite, A = aggregate, CSH\* = fire altered CSH)

The total water absorption can be defined as the difference in weight after storage under water and a reference weight, for instance the weight at uniform target temperature ( $M_{0d,hot}$ ). After already 7 days, the weight increase flattens. Under in situ circumstances,  $M_{0d,hot}$  can be determined from the drilled core by drying it till constant mass. Drying is necessary to eliminate the moisture absorbed due to climatic exposure. Notice that the heated sample itself functions as reference, which is more convenient than searching for an adequate reference concrete that has not been exposed to fire. New made hydration products which may fill some small cracks and thus may hinder the water absorption are neglected in this method. In laboratory conditions, this reference weight is measured during the test when the concrete is at target temperature or after cooling down to 60°C (Fig. 6). Fig. 7 illustrates the water immersion of half cubes (TC1-8, TC2k-1) and small discs (TC1-10) with Ø80mm and 15mm height. These results are transformed in percentages by dividing with the reference weight  $M_{0d,hot}$ . For the discs, different cooling methods are used: 1) slowly cooling in the oven ('L, oven'); 2) cooling outside the oven at ambient air ('L, 20°C'); 3) cooling by quenching into water ('Water'). The results on half cubes and small discs are comparable, as is visible on the graph for the water absorption of specimens slowly cooled in the oven.

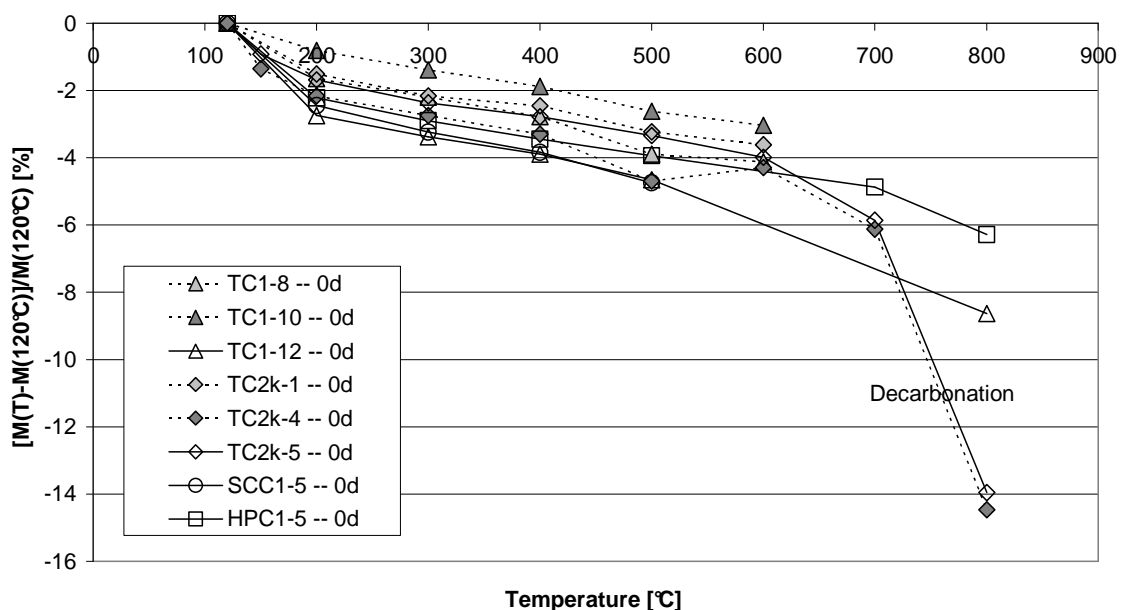


Fig. 6. Weight loss due to heating

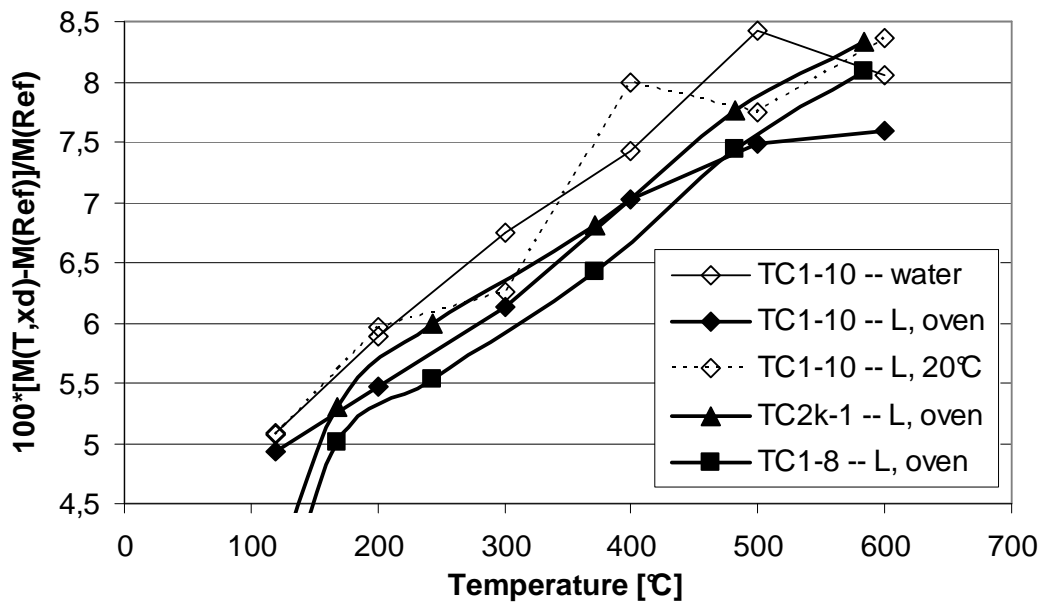


Fig. 7. Water immersion

### 3 SUMMARY

- The residual strength is mainly influenced by the temperature during heating, the way of cooling and the time of storage after fire.
- Colour analysis and water immersion provide an adequate basis to assess the temperature history of concrete.

### 4 ACKNOWLEDGMENT

The authors would like to thank the Fund for Scientific Research in Flanders (FWO) for the financial support through the research grant “Damage assessment and estimation of the residual strength of concrete members after exposure to fire”. The authors are thankful for the help of TNO Delft and TU Delft (Netherlands) for their contribution to the microscopic research.

### REFERENCES

- [1] Annerel E., Taerwe L., Approaches for the Assessment of the Residual Strength of Concrete Exposed to Fire. *Proceedings of the International Workshop, Fire Design of Concrete Structures, From Materials Modelling to Structural Performance*, Coimbra, 8<sup>th</sup> and 9<sup>th</sup> November, 2007, pp. 489-500
- [2] Fib TG 4.3.2, *fib bulletin 46: Fire design of concrete structures – structural behaviour and assessment, state-of-the art report*, july 2008, 209 p.
- [3] Fib TG 4.3.1, *fib bulletin 38: Fire design of concrete structures – materials, structures and modelling, state-of-the art report*, april 2007, 97 p.
- [4] EN 1992-1-2: 2004 - *Eurocode 2: Design of Concrete Structures – Part 1-2: General Rules – Structural Fire Design*, CEN, Brussels, 2004, 97 p.
- [5] Taerwe L., Poppe A.-M., Annerel E., Vandeveldel P., Structural Assessment of a Pretensioned Concrete Girder after Fire Exposure. *Proceedings of the 2<sup>nd</sup> fib Congress*, Napels, 5-8 june, 2006
- [6] Liu X., *Microstructural investigation of self-compacting concrete and high-performance concrete during hydration and after exposure to high temperatures*, PhD thesis, Ghent University, 2005-2006, 174 p.

# HEATING-INDUCED PRESTRESS VARIATION IN UNBONDED POST-TENSIONED CONSTRUCTION

## Potential Consequences for Post-Fire Performance

Luke Bisby<sup>a</sup>, Kevin MacLean<sup>b</sup>, Colin MacDougall<sup>c</sup>

<sup>a</sup> University of Edinburgh, BRE Centre for Fire Safety Engineering, Edinburgh, Scotland, UK

<sup>b</sup> Read Jones Christoffersen Ltd., Toronto, Canada

<sup>c</sup> Queen's University, Department of Civil Engineering, Kingston, Canada

## 1 INTRODUCTION

Unbonded post-tensioned (UBPT) concrete is a popular form of construction that allows for rapid erection of economical and sustainable buildings. UBPT buildings are more efficient than non-prestressed concrete construction and make optimal use of the structural materials from which they are constructed [1]. However, this efficiency also causes concerns associated with the performance of UBPT structures at elevated temperatures. In particular, prestressing steel is much more sensitive to temperature than mild steel reinforcement, and it suffers proportionally greater losses in strength and stiffness as temperatures increase. Experimental results from few, limited large-scale furnace tests on isolated UBPT slabs have recently led to concern, and considerable debate, regarding their performance in fire [2]. However, while available tests are instructive, in many important respects their results may not be representative of the performance of real UBPT structures in fire.

Current design requirements for UBPT floors are based on a fundamentally limited understanding of full structural response in fire. Available fire tests on UBPT members have either been furnace tests on isolated beams or slabs [2,3,4], with their numerous, well-documented shortcomings, or are so old as to be of limited relevance to today's advanced concretes and construction methods [4]. There are a number of factors that may be important for UBPT systems in fire that have not yet been identified or adequately considered. In particular, because UBPT structures are typically continuous across multiple bays, sometimes with two-way action within a floor plate and with higher span-to-depth ratios than reinforced concrete slabs, furnace tests on isolated, simply-supported, one-way members with short unbonded lengths cannot be considered as representative (or necessarily conservative). Tendon continuity, compression and tension membrane actions, restraint, spalling, thermal deformations, and non-uniform heating and cooling can all be expected to play important roles in real UBPT structures, both during and after a fire.

Experiments and modelling aimed at predicting the effects of localized heating on UBPT tendons and the potential consequences for the post-fire response of UBPT members are presented in this paper. The issues discussed are related to creep of the stressed tendons at high temperature and are specific to UBPT construction – arising as a consequence of continuity of unbonded tendons, with varying cover, over multiple bays of a structure (some of which may not be heated during a fire).

## 2 BACKGROUND AND OBJECTIVES

For a given metal, transient creep strains increase with time, temperature, and stress. Since both stress and temperature may be high in the tendons of a fire-affected, post-tensioned structure, large creep strains may develop in shorter times than are normally considered in structural engineering. In the absence of other effects, these creep strains will, along with changes in the elastic properties of the prestressing and thermal expansion, reduce the effective prestress in the structure. This will affect the capacity of the structure both during heating and, since creep strains are irrecoverable on cooling, after a fire. They may also contribute to tendon rupture in extreme cases of localized heating (due to localized cover spalling during fire for example). Creep strains in steel tendons under transient temperature and stress conditions therefore need to be accurately quantified before realistic fire testing or modelling of UBPT members can be performed with confidence.

Data on the creep behaviour of modern post-tensioning tendons under high-stress, high-temperature conditions is scarce, and no high temperature creep data are apparently available for tendon stresses in excess of 690 MPa [5], despite the fact that in-service stress levels in UBPT members may be in the range of 1000-1200 MPa [1]. The objectives of the research presented herein were to: (1) develop a better understanding of, and ability to model, the creep behaviour of prestressing tendons at elevated temperature subjected time-varying stress and non-uniform heating; (2) study the effects of varying the concrete cover and heated length ratio (i.e., the ratio of the heated length of tendon to the overall length of tendon) on the observed/predicted reductions in prestressing force for a typical UBPT flat-plate slab both during and after a fire; and (3) highlight potential concerns for the performance of real UBPT structures during and after a fire.

### 3 EXPERIMENTS ON LOCALLY-HEATED PRESTRESSING TENDONS

Experiments were performed on locally-heated, prestressed, unbonded, restrained tendons to measure the changes in stress under localized heating and cooling regimes. These tests have been described in detail by MacLean et al. [6]. Fig. 1 shows the testing apparatus used. A single tendon 6300 mm long was passed through a 610 mm long tube furnace and stressed in a fixed-abutment prestressing bed to a target initial stress of 1000 MPa (after losses). The restrained tendon was then locally heated using one of a number of preselected ramp-soak-cool regimes. The ramp rate for all tests was 10°C/min, chosen to represent typical heating rates for tendons in UBPT concrete slabs. Soak temperatures of 200, 300, 400, 500, and 700°C were held for between 5 and 90 minutes before slow cooling to room temperature. Load cells at both ends of the tendon were used to measure prestress variation, and temperatures were continuously recorded along the tendons' length.

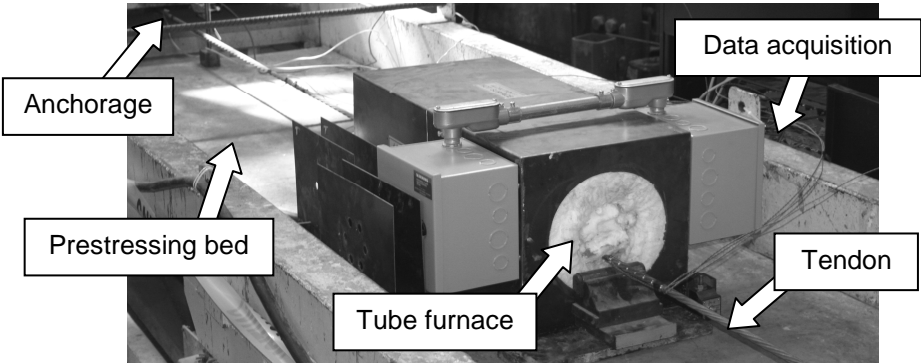


Fig. 1. Experimental apparatus used in relaxation tests on locally-heated unbonded steel prestressing tendons

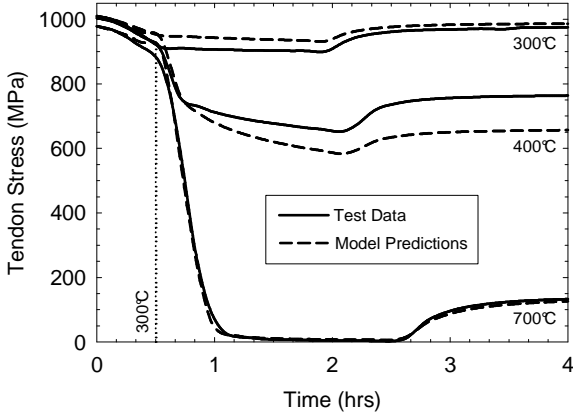


Fig. 2. Comparison of observed and predicted variation in tendon stress levels with localized heating (ramp-soak-cool) to various soak temperatures [8]

As an example of the data obtained during these tests, Fig. 2 shows the measured variation in tendon stress with exposure to one of three ramp-soak-cool regimes (to 300, 400, or 700°C). The

initial reductions in tendon stress are essentially linear, and are due to thermal expansion of the tendon in the heated region. However, at temperatures above 300°C, the stress reductions accelerate (due to creep/relaxation), causing considerable reductions in effective prestress. The irrecoverability of effective prestress for exposure temperature above 300°C is also clearly evident in this figure.

**4 MODELING HIGH-TEMPERATURE CREEP/RELAXATION OF STEEL TENDONS**

The transient variation in tendon stress noted in the tests presented above can be predicted using an appropriate computational model which accounts for the spatial and temporal variation in temperature along the length of a heated tendon inside a concrete slab. Such a model has been developed by the authors and is presented in detail by Gales et al. [7]. The analysis procedure divides the tendon into a series of longitudinal thermal regions of assumed constant temperature during a given time step. At the beginning of the analysis, the stress in the tendon is known from the service prestress condition. Given the known time-temperature history of each thermal region along the length of the tendon (taken as measured temperatures from tests [6] or from a simple heat transfer analysis of the structure under consideration [8]) the continuous thermal exposure is discretized into finite time steps of small duration. The changes in strain of each thermal region due to thermal expansion, degradations in elastic properties, and creep can be computed using steady-state high-temperature creep models and parameters available in the literature [7]. The change in length of each thermal region during a given time step can therefore be determined, and the changes in length of all regions subsequently summed over the length of the tendon to determine the stress change required for no net change in length (using temperature-dependent elastic properties). By repeating this procedure at multiple time steps, the full stress-time history can be predicted.

In addition to showing experimental stress-time histories for the tests by MacLean et al. [6], Fig. 2 includes predictions made using the authors’ computational model [7]. The agreement between the test data and model predictions is satisfactory, with the model being conservative in the critical temperature range between 300 and 700°C. It must be stressed that the model is based on an extrapolation of creep parameters derived from steady-state testing up to only 690 MPa [5]. Additional tests are needed to verify the use of these parameters at initial stress levels of 1000 MPa or more, as can be expected under service loading in UBPT structures [1].

**5 POTENTIAL CONSEQUENCES: TYPICAL UBPT FLAT SLAB**

Given the wide variety of possible forms of UBPT construction, it is difficult to make generalizations regarding their performance in fire. However, for the purposes of illustrating the potential importance of irrecoverable creep-induced tendon stress reductions for locally-heated multiple span tendons in UBPT slabs, a series of analyses were performed using the previously described computational model in conjunction with a typical UBPT flat-slab structure; this is shown in Figs. 3 and 4 (from Example 3-37 of the CPCI design manual [9], which can be consulted for complete details of the design and reinforcement details).

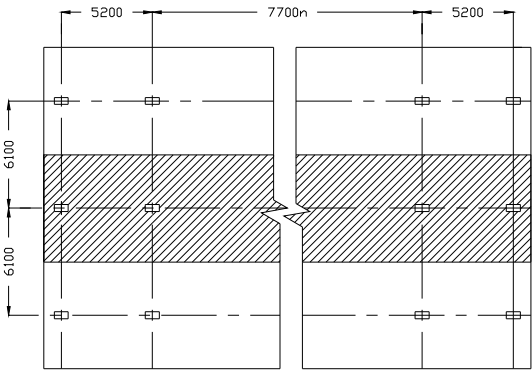


Fig. 3. Example slab with ‘n’ interior spans (plan view)

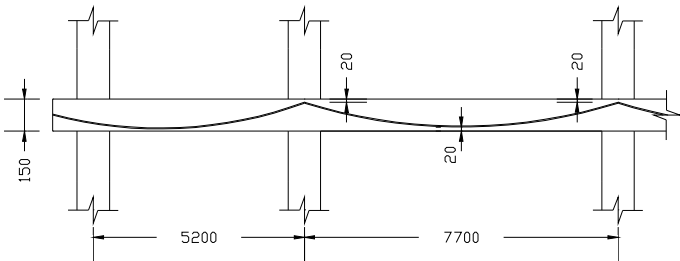


Fig. 4. Example slab end span and interior span (partial elevation view)

The spatial and temporal variation in tendon temperatures along its entire length were determined using a simple one-dimensional heat transfer analysis programmed previously by Bisby [8], and the transient variation in tendon stress was determined using the previously described computational model. During parametric analyses the total tendon length was varied by changing the number of internal bays in the structure while maintaining the same interior and exterior bay dimensions and tendon profiles. The heated length ratio was varied by changing the number of internal bays exposed fire (from below) according to the ASTM E119 [10] standard fire curve. Note that the parabolic tendon profile causes a continuously varying tendon temperature, with higher temperatures in regions with smaller concrete cover.

Fig. 5 shows the predicted variation in tendon stress for three arbitrarily selected heated length ratios: 3 spans with only the interior span heated, 5 spans with one interior span heated, and 5 spans with all three interior spans heated. Also shown in Fig. 5 are the predicted tendon stress profiles that would be generated if only thermal expansion were considered (i.e., by ignoring creep strains and degradation of elastic properties); the importance of properly accounting for transient effects when modelling these structures is clear. It is also clear that larger heated length ratios show a slightly larger reduction in prestress during heating – due to greater overall thermal expansion of the tendon – although the irrecoverable component is less for these cases (since thermal strains are recoverable). This implies that larger heat length ratios may be more critical *during* a fire, but smaller heated length ratios may be more important in for residual prestress *after* a fire.

Fig. 6 shows the effect of the heated length ratio on the reduction in prestress during fire at 45 minutes, 60 minutes, and 75 minutes. This figure confirms that the influence of the heated length ratio in causing tendon stress reductions is minor during heating, and also highlights the speed with which tendon stress reductions might realistically occur in a fire – again stressing the importance of properly accounting for prestress reductions when modelling (or testing) UBPT structures in fire. More recent work [11] has shown that smaller heated length ratios may lead to tendon rupture.

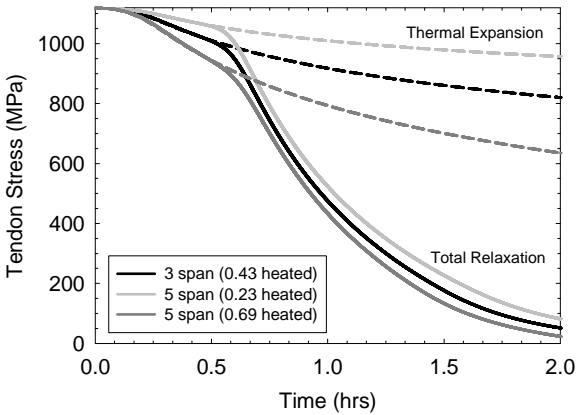


Fig. 5. Predicted variation in tendon stress with for the example structure (effect of heated length ratio)

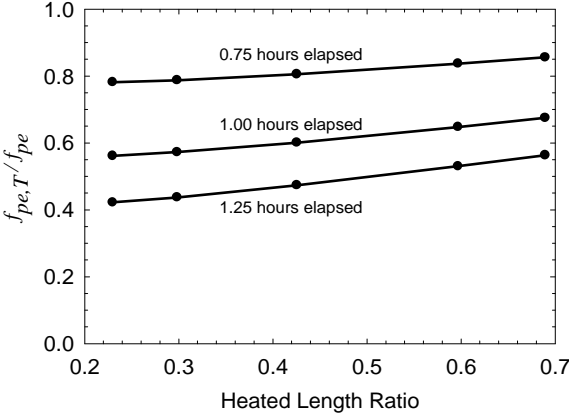


Fig. 6. Predicted effect of heated length ratio on tendon stress levels for the example structure (during exposure to an ASTM E119 [10] fire)

Adequate fire resistance of UBPT structures is currently ensured during the design process by providing sufficient concrete cover to maintain the temperature of the prestressed reinforcement below reasonable limits [1]. Typical specified covers may range between 20 (0.5 or 1 hrs rating) to 80 mm (4 hrs rating), depending on the jurisdiction and on local requirements. To highlight the importance of actually achieving design concrete covers for assuring adequate fire performance, and also to conceptually illustrate the potential consequences of loss of cover due to localized spalling, Fig. 7 shows the effects of varying the concrete cover at midspan between 10 and 30 mm for the example structure (shifting the tendon profile up or down during the heat transfer analysis) with one internal bay exposed to an ASTM E119 [10] fire.

As expected, Fig. 7 shows that concrete cover to the prestressed reinforcement has a profound impact on the transient variation in tendon stress, both during and after a fire. For example, after

one hour of fire exposure, the total reductions in tendon stress (from an initial tendon stress value of 1116 MPa, or 60% of ultimate) are 180, 617, and 1028 MPa for 30, 20, and 10 mm concrete cover respectively. Perhaps just as importantly, the irrecoverable portion of the prestress loss for these three cases is 76, 478, and 849 MPa respectively, showing the importance of the above considerations for engineers involved in structural evaluations of fire-damaged UBPT structures, even when damage appears localized.

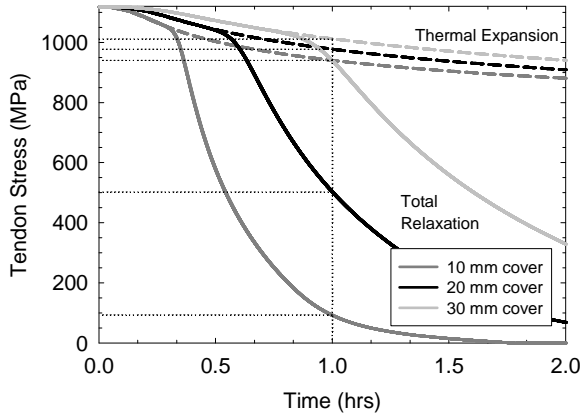


Fig. 7. Predicted variation in tendon stress with for the example structure (effect of concrete cover to the prestressed reinforcement)

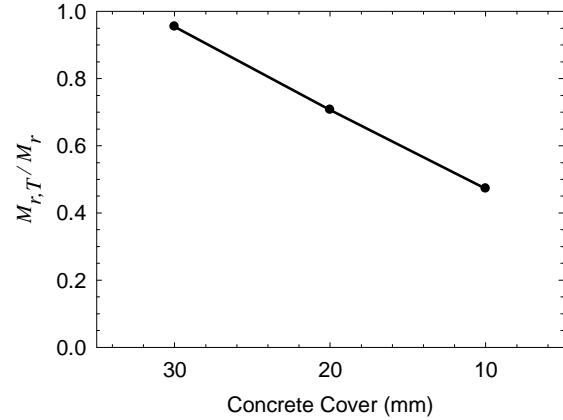


Fig. 8. Predicted variation of post-fire residual midspan positive bending moment capacity with different concrete covers for the example structure (after one hour of fire exposure)

Given that localized heating of UBPT tendons results in irrecoverable reductions in tendon stress both during and after a fire, an obvious question is: what might be the consequences of this for failure of the structure during a fire (when subjected to fire design loads only) or after a fire (when the full design loads must be considered)? Structural performance during a fire depends on many factors that have not been considered in the current analysis. In particular, membrane actions and thermal deformations of the slab must be considered in any rational analysis of the capacity of a real UBPT structure during fire – this is beyond the scope of the current paper and is not treated here.

However, for the purposes of illustration, Fig. 8 illustrates the potential consequences of localized heating for the post-fire (residual) cross-sectional flexural capacity of the example UBPT slab (at midspan) according to Canadian UBPT slab design guidelines [12]. Very briefly, for a partially-prestressed beam or slab strip, the moment capacity at ultimate limit state can be expressed as sum of the respective moment contributions from the tensile non-prestressed ( $A_s$ ), prestressed ( $A_{ps}$ ), and compressive non-prestressed ( $A'_s$ ) reinforcement, about the compressive stress resultant, giving:

$$M_r = \phi_s A_s f_s \left( d_s - \frac{\beta_1 c}{2} \right) + \phi_{ps} A_{ps} f_{pr} \left( d_p - \frac{\beta_1 c}{2} \right) - \phi'_s A'_s f'_s \left( d'_s - \frac{\beta_1 c}{2} \right) \quad (1)$$

where  $\phi_s$ ,  $\phi_{ps}$ , and  $\phi'_s$  are code-specified material resistance factors,  $\beta_1$  is a code-specified concrete stress block parameter,  $d$  represents the distances of the respective reinforcements from the extreme compression fibre,  $f$  represents the stresses in the respective reinforcements at the ultimate condition, and  $c$  represents the depth to the neutral axis, determined from force equilibrium at a section as:

$$c = \frac{\phi_s A_s f_s + \phi_{ps} A_{ps} f_{pr} - \phi'_s A'_s f'_s}{0.85 \phi_c f'_c b \beta_1} \quad (2)$$

All of the terms in Eq. 2 are known or can be determined directly, with the exception of tendon stress at ultimate,  $f_{pr}$ . For UBPT structures this value is partially dependent on the strain in the concrete at the level of the tendon caused by member deflections, and therefore consists of two

components: (1) the stress created by prestressing operations *after all losses* (the effective prestress force),  $f_{pe}$ , and (2) the increase in stress created by member deflection,  $\Delta f_{pr}$ , so:

$$f_{pr} = f_{pe} + \Delta f_{pr} \quad (3)$$

Rational determination of  $\Delta f_{pr}$  is complicated even at ambient temperature because it depends on many factors, including: patterned loading, the span-to-depth ratio, and the amount of bonded non-prestressed reinforcement present. The Canadian code [12] uses an empirical expression defining tendon stress at ultimate in a UBPT concrete member. Tendon stress is defined as:

$$f_{pr} = f_{pe} + \frac{8000}{l_e} (d_p - c_y) \leq f_{py} \quad (\text{MPa}) \quad (4)$$

where  $l_e$  is the total tendon length between anchorages divided by the minimum number of plastic hinges required to create a failure mechanism in the span being designed, and  $c_y$  is the neutral axis depth determined assuming the yield stress of  $f_{py}$  in the tendons. The above equations were used to derive the data shown in *Fig. 8*, which shows the importance of reductions in tendon prestress levels after a fire-affected structure has cooled to room temperature and is expected to resist its full factored design load. While this simple illustration should obviously not be considered a rigorous treatment of the problem, it nonetheless confirms the importance of careful consideration of the effects of localized heating of prestressing tendons, particularly given that changes in prestress will manifest themselves not only in the fire damaged region, but also in areas of the structure which may have remained remote from the fire.

## 6 ACKNOWLEDGMENT

The Authors would like to acknowledge the support of the Natural Sciences and Engineering Research Council of Canada, Queen's University, and Dr. Ivan Campbell.

## REFERENCES

- [1] Khan, S. & Williams, M., *Post-Tensioned Concrete Floors*, Laxton's, 1995.
- [2] Kelly, F. & Purkiss, J., Reinforced concrete structures in fire: a review of current rules, *The Structural Engineer*, 86(19): 33-39, 2008.
- [3] Ellobody, E. & Bailey, C., Testing and modelling of bonded and unbonded post-tensioned concrete slabs in fire. *Proc. 5<sup>th</sup> Int. Conf. on Structures in Fire*, Singapore, pp. 392-405, 2008.
- [4] Lee, D. & Bailey, C. The behaviour of post-tensioned floor slabs in fire conditions, *Proc. Int. Congress on Fire Safety in Tall Buildings*, Santander, Spain, pp.183-201, 2006.
- [5] Harmathy, T. & Stanzak, W., *Elevated-temperature tensile and creep properties of some structural and prestressing steels*, National Research Council, Ottawa, Canada, 1970.
- [6] Maclean, K., Bisby, L. & MacDougall, C., Post-fire assessment of unbonded post-tensioned slabs, *ACI-SP 255*, American Concrete Institute, USA, 2008.
- [7] Gales, J., Bisby, L., MacDougall, C. & MacLean, K., Transient high-temperature stress relaxation of prestressing tendons in unbonded construction, *Fire Safety J.*, in press, 2009.
- [8] Bisby, L., *Fire Behaviour of Fibre-Reinforced Polymer (FRP) Reinforced or Confined Concrete*, Ph.D. Thesis, Civil Engineering, Queen's University, Kingston, Canada, 2003.
- [9] CPCI, *Design Manual*, Canadian Prestressed Concrete Institute, Ottawa, Canada, 1996.
- [10] ASTM, *Test Method E119-01: Standard Methods of Fire Test of Building Construction and Materials*, American Society for Testing and Materials, West Conshohocken, PA, USA, 2001.
- [11] Gales, J., Bisby, L. & MacDougall, C., Irrecoverable prestress loss in unbonded post-tensioned concrete slabs in fire, *Fire & Materials*, San Francisco, USA, 2009.
- [12] CSA, *Design of Concrete Structures*, Canadian Standards Association, Ottawa, Canada, 1994.

## **FIRE RESISTANCE OF AXIALLY LOADED SLENDER CONCRETE FILLED STEEL TUBULAR COLUMNS**

### **Development of a three-dimensional numerical model and comparison with Eurocode 4**

Ana Espinós, Antonio Hospitaler, Carmen Ibáñez, Manuel L. Romero

Instituto de Ciencia y Tecnología del Hormigón (ICITECH)

Universidad Politécnica de Valencia, Camino de Vera s/n, 46022 Valencia (Spain)

aespinos@mes.upv.es, ahospitaler@cst.upv.es, caribus@etsii.upv.es, mromero@mes.upv.es

## **INTRODUCTION**

Filling hollow steel columns with concrete is an interesting way for improving their fire resistance [7]. The temperature at the surface of a hollow structural section without external protection increases quickly during the development of a fire. On the other hand, if the steel tube is filled with concrete, while the steel section loses gradually its resistance and rigidity, the load is transferred to the concrete core, that heats up more slowly, thus increasing the fire resistance of the column.

Besides its structural function, the steel tube acts as a radiation shield to the concrete core, what, combined with a steam layer in the steel-concrete boundary, leads to a lower temperature rise in the concrete core when compared to exposed reinforced concrete structures [7].

During a fire, the temperature distribution in the cross-section of a CFT column is not uniform: steel and concrete have very different thermal conductivities, what generates a behaviour characterized by noticeable heating transients and high temperature differentials across the cross-section. Due to these differentials, CFT columns can reach high fire resistance times without external fire protection [7]. However, it is necessary to resort to numerical models in order to predict accurately these temperature profiles along the fire exposure time [8], [9].

In this work, the finite element analysis package ABAQUS [1] was employed to model the behaviour of slender axially loaded CFT columns exposed to fire. With this software, a sequentially coupled nonlinear thermal-stress analysis was conducted. The results of the simulations were compared with a series of fire resistance tests available in the literature [11], as well as with the predictions of the Eurocode 4 [6] simplified calculation model.

## **1 DEVELOPMENT OF THE NUMERICAL MODEL**

### **- Finite element mesh**

A three-dimensional numerical model was developed in ABAQUS [1], with variable parameters such as the length of the column ( $L$ ), the external diameter ( $D$ ), the thickness of the steel tube ( $t$ ) and the thermal and mechanical material properties. It consisted of two parts: the concrete core and the steel tube. Due to symmetry on the geometry and boundary conditions, only a quarter of the column was modelled.

The three-dimensional eight-node solid element C3D8RT was used to mesh the model. It is an eight-node thermally coupled brick, with trilinear displacement and temperature, reduced integration and hourglass control. The mesh density was controlled to have a maximum element size of 2 cm, what proved to be sufficient to predict with enough accuracy the thermal and mechanical behaviour of the CFT columns under fire.

## - Material properties

The numerical model took into account the temperature dependent thermal and mechanical properties of the materials. For concrete, Lie's model [12] was employed, provided that it proved to be the one that best predicted the behaviour of the concrete infill in CFT columns, as said by Hong & Varma [9]. The mechanical model implemented in ABAQUS employed the hyperbolic Drucker-Prager yield surface. The thermal properties for concrete at elevated temperatures were extracted from EN 1992-1-2 [4]. For steel, the temperature dependent thermal and mechanical properties recommended in EN 1993-1-2 [5] were adopted. The isotropic multiaxial plasticity model with the Von Mises yield surface was employed.

The values of the thermal expansion coefficient for concrete and steel recommended by Hong and Varma [9] were employed:  $\alpha_s = 12 \times 10^{-6} \text{ }^\circ\text{C}^{-1}$ ,  $\alpha_c = 6 \times 10^{-6} \text{ }^\circ\text{C}^{-1}$ . The moisture content of the concrete infill was not modelled in this research, what lies on the safe side.

## - Thermal analysis

For conducting the thermal analysis, the standard ISO-834 [10] fire curve was applied to the exposed surface of the CFT column model as a thermal load. The thermal contact in the steel-concrete boundary was modelled by employing the "gap conductance" and "gap radiation" options. For the governing parameters of the heat transfer problem, the values recommended in EN 1991-1-2 [3] were adopted.

## 2 VALIDATION OF THE NUMERICAL MODEL

The three-dimensional numerical model was validated by comparing the simulations with experimental fire resistance tests [11] and with the EC4 simplified calculation model [6].

### 2.1 Comparison with experimental results

The numerical model was employed to predict the standard fire behaviour of a series of CFT column specimens listed in *Table 1*. These specimens were tested at the NRCC, and their results published by Lie & Caron [11]. All the specimens tested were circular, filled with siliceous aggregate concrete and subjected to concentric compression load. Their total length was 3810 mm, although only the central 3048 mm were directly exposed to fire. Because of the loading conditions, all the tests were assumed as fix-ended.

*Table 1.* List of CFT columns analyzed, from the NRCC research report [11]

| Column specimen | D (mm) | t (mm) | $f_y$ (N/mm <sup>2</sup> ) | $f_{ck}$ (N/mm <sup>2</sup> ) | N (kN) | $\mu = N / N_{pl,Rd}$ | FRR (min) |
|-----------------|--------|--------|----------------------------|-------------------------------|--------|-----------------------|-----------|
| 1               | 141    | 6.5    | 401.93                     | 28.62                         | 131    | 8.90%                 | 57        |
| 2               | 168    | 4.8    | 346.98                     | 28.62                         | 218    | 15.37%                | 56        |
| 3               | 219    | 4.8    | 322.06                     | 24.34                         | 492    | 26.19%                | 80        |
| 4               | 219    | 4.8    | 322.06                     | 24.34                         | 384    | 20.44%                | 102       |
| 5               | 219    | 8.2    | 367.43                     | 24.34                         | 525    | 18.88%                | 82        |
| 6               | 273    | 5.6    | 412.79                     | 26.34                         | 574    | 17.08%                | 112       |
| 7               | 273    | 5.6    | 412.79                     | 26.34                         | 525    | 15.63%                | 133       |
| 8               | 273    | 5.6    | 412.79                     | 26.34                         | 1000   | 29.76%                | 70        |

For each simulation, the axial displacement at the top of the column versus the fire exposure time was registered, comparing this curve with the one obtained in the fire resistance test [11]. *Fig. 1* shows an example of the comparison between both curves for one of the specimens studied.

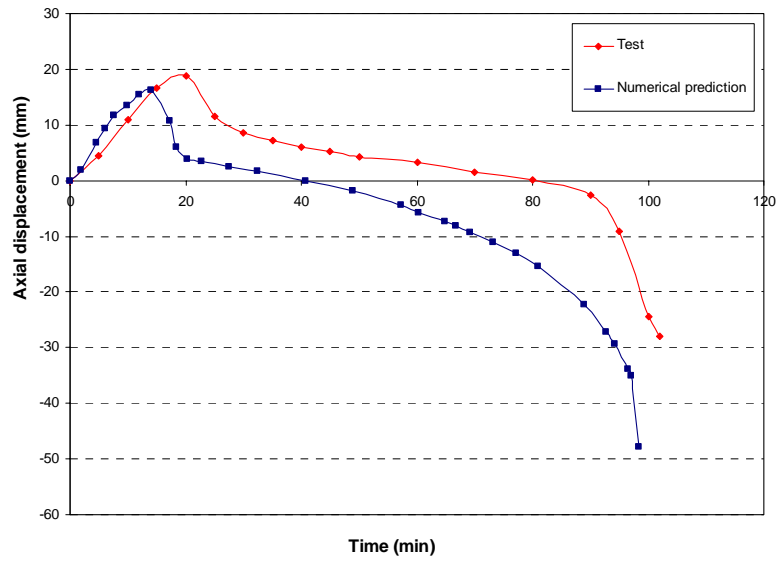


Fig. 1. Comparison between calculated and measured axial displacement, for test no. 4

From this curves, the fire resistance rating (FRR) was obtained for each one of the specimens under study. The failure criteria from EN 1363-1 [2] were adopted. This standard establishes that the failure time is given by the most restrictive from the following two limits: maximum axial displacement and maximum axial displacement velocity. By applying these criteria, the values in Table 2 were obtained. As it can be seen in Fig. 2, most of the values obtained lie in the region of the 15% error, apart from two values, corresponding to column specimens no. 1 and 2, which have the smallest diameters.

The maximum axial displacement ( $\delta_{max}$ ) was also obtained for each of the column specimens studied. Table 2 shows the calculated and measured values, which are plotted in Fig. 3, were it can be seen again that most of the cases lie in the region of the 15% error, apart from specimens no. 3 and 8, corresponding to those with a higher loading level, over the 20% of the maximum load bearing capacity of the column at room temperature.

Table 2. Predicted and measured FRR and maximum axial displacement ( $\delta_{max}$ )

| Column specimen | FRR (min)                 |            | $\xi_{FRR} = \frac{FRR_{test}}{FRR_{NS}}$ | $\delta_{max}$ (mm)       |            | $\xi_{\delta_{max}} = \frac{\delta_{max, test}}{\delta_{max, NS}}$ |
|-----------------|---------------------------|------------|---|---------------------------|------------|--|
|                 | Test                      | Simulation |   | Test                      | Simulation |  |
| 1               | 57                        | 72         | 0.79                                      | 24.09                     | 24.35      | 0.99   |
| 2               | 56                        | 75         | 0.75                                      | 20.48                     | 19.25      | 1.06   |
| 3               | 80                        | 74         | 1.08                                      | 18.13                     | 12.36      | 1.47   |
| 4               | 102                       | 97         | 1.05                                      | 18.77                     | 16.23      | 1.16   |
| 5               | 82                        | 68         | 1.21                                      | 20.36                     | 19.30      | 1.05   |
| 6               | 112                       | 126        | 0.89                                      | 16.40                     | 17.71      | 0.93   |
| 7               | 133                       | 137        | 0.97                                      | 19.67                     | 18.61      | 1.06   |
| 8               | 70                        | 70         | 1.00                                      | 5.51                      | 10.35      | 0.53   |
|                 | <b>Average</b>            |            | <b>0.97</b>                               | <b>Average</b>            |            | <b>1.03</b>  |
|                 | <b>Standard deviation</b> |            | <b>0.15</b>                               | <b>Standard deviation</b> |            | <b>0.26</b>  |

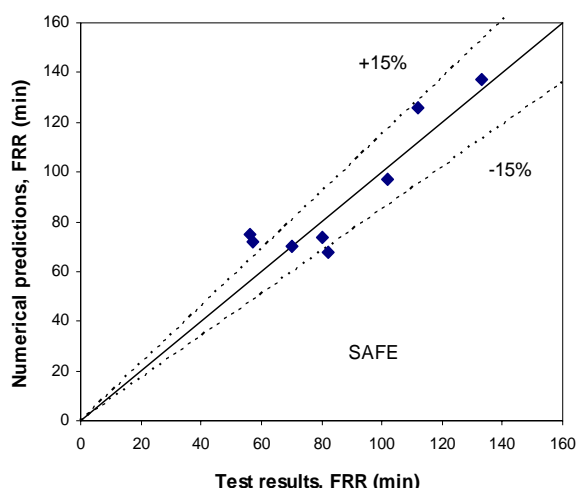


Fig. 2. Comparison of the fire resistance ratings, calculated VS test results

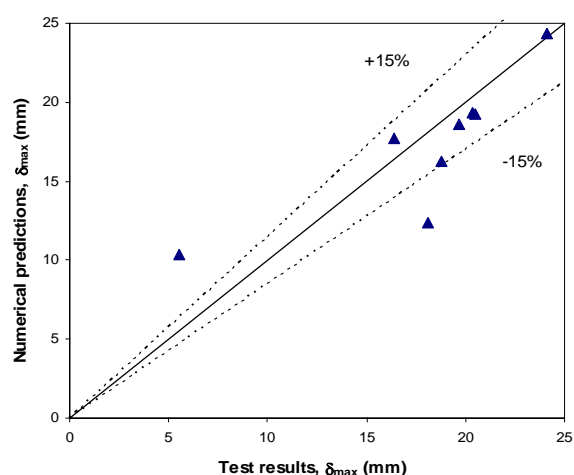


Fig. 3. Comparison of the maximum axial displacement, calculated VS test results

### 3.2 Comparison with Eurocode 4 simplified calculation model

In this section, the numerical model is compared with the predictions of the EC4 simplified calculation model [6], obtaining the results shown in *Table 3*. It can be seen in *Fig. 4* that the proposed numerical model gives a better prediction of the fire resistance rating, showing a very accurate trend. On the other hand, the EC4 simplified model turns out to be excessively conservative, as shown in the figure. We must note that the EC4 simplified model doesn't take into account the thermal expansion of the materials, nor the air gap at the steel-concrete boundary, what lies on the safe side and gives a very conservative prediction. If we apply these simplifications to our numerical model, smaller values of the fire resistance ratings are obtained, very similar to those predicted by EC4, as shown in *Table 3*. As it can be seen in *Fig. 5*, our predicted values reproduce quite well the results of EC4, except for those tests with fire resistance ratings around 120 minutes, where our numerical model provides more accurate results, what produces a more close to reality trend.

Table 3. Comparison of the numerical model and EC4 predictions with the tests

| Column specimen           | FRR (min) |            |                           |     | $\xi_{FRR} = \frac{FRR_{test}}{FRR_{calc}}$ |                           |             |
|---------------------------|-----------|------------|---------------------------|-----|---|---------------------------|-------------|
|                           | Test      | Simulation | Simulation (no expansion) | EC4 | Simulation                                  | Simulation (no expansion) | EC4         |
| 1                         | 57        | 72         | 49                        | 49  | 0.79  | 1.16                      | 1.16        |
| 2                         | 56        | 75         | 46                        | 46  | 0.75  | 1.22                      | 1.22        |
| 3                         | 80        | 74         | 52                        | 49  | 1.08  | 1.54                      | 1.63        |
| 4                         | 102       | 97         | 63                        | 61  | 1.05  | 1.62                      | 1.67        |
| 5                         | 82        | 68         | 52                        | 51  | 1.21  | 1.58                      | 1.61        |
| 6                         | 112       | 126        | 118                       | 91  | 0.89  | 0.95                      | 1.23        |
| 7                         | 133       | 137        | 126                       | 96  | 0.97  | 1.06                      | 1.39        |
| 8                         | 70        | 70         | 58                        | 56  | 1.00  | 1.21                      | 1.25        |
| <b>Average</b>            |           |            |                           |     | <b>0.97</b>                                 | <b>1.29</b>               | <b>1.39</b> |
| <b>Standard deviation</b> |           |            |                           |     | <b>0.15</b>                                 | <b>0.25</b>               | <b>0.21</b> |

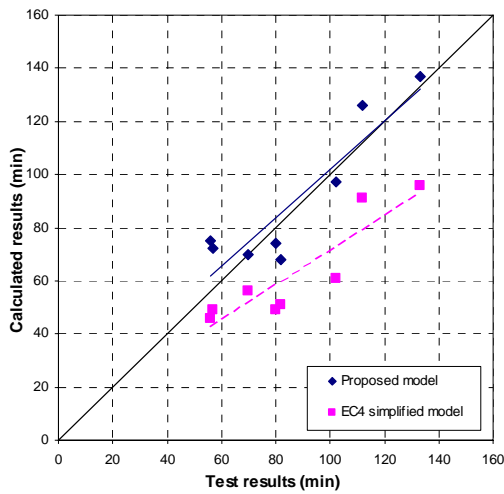


Fig. 4. Comparison of FRR, proposed numerical model VS EC4 model

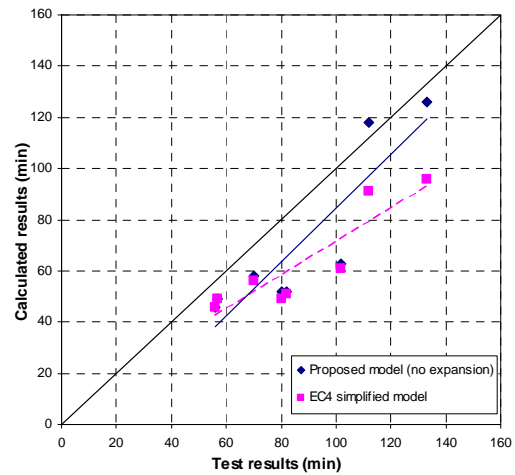


Fig. 5. Comparison of FRR, proposed model (without expansion) VS EC4 model

#### 4. SUMMARY AND CONCLUSIONS

A three-dimensional numerical model for axially loaded slender CFT columns under fire was presented. By means of this model, the behaviour under standard fire conditions of eight column specimens previously tested by the NRCC research group [11] was predicted. The proposed numerical model showed better behaviour for columns with low slenderness and loading levels under 20%. Despite these two aspects, the model shows an accurate response when contrasted with the fire tests.

This study also proved that the predictions of EC4 simplified calculation model [6] can be reproduced with the proposed numerical model by eliminating the thermal expansion of the materials, which lies on the safe side. Nevertheless, if the real behaviour of CFT columns under fire wants to be predicted, this aspect must be taken into account, extending the failure time. The expansion of the steel tube produces an opposed axial strain in the early stages of heating, as well as an opening of the gap in the steel-concrete interface, which delays the heating of the concrete core and thus increases the fire resistance rating.

The proposed numerical model proved to give better predictions than the EC4 simplified model, which turned out to be excessively conservative.

## REFERENCES

- [1] ABAQUS. ABAQUS/Standard Version 6.6 User's Manual: Volumes I-III. Pawtucket, Rhode Island: Hibbit, Karlsson & Sorenson, Inc.; 2005.
- [2] EN (European Committee for Standardisation). EN 1363-1: Fire resistance tests. Part 1: General requirements. Brussels: CEN; 1999.
- [3] CEN (European Committee for Standardisation). EN 1991-1-2, Eurocode 1: Actions on structures, Part 1.2: General actions - Actions on structures exposed to fire. Brussels: CEN; 2002.
- [4] CEN (European Committee for Standardisation). EN 1992-1-2, Eurocode 2: Design of concrete structures, Part 1.2: General rules – Structural fire design. Brussels: CEN; 2004.
- [5] CEN (European Committee for Standardisation). EN 1993-1-2, Eurocode 3: Design of steel structures, Part 1.2: General rules – Structural fire design. Brussels: CEN; 2005.
- [6] CEN (European Committee for Standardisation). EN 1994-1-2, Eurocode 4: Design of composite steel and concrete structures, Part 1.2: General rules - Structural fire design. Brussels: CEN; 2005.
- [7] CIDECT. Twilt L, Hass R, Klingsch W, Edwards M, Dutta D. Design guide for structural hollow section columns exposed to fire. CIDECT (Comité International pour le Développement et l'Etude de la Construction Tubulaire). Cologne, Germany: Verlag TÜV Rheinland; 1996.
- [8] Ding J, Wang YC. Realistic modelling of thermal and structural behaviour of unprotected concrete filled tubular columns in fire. *Journal of Constructional Steel Research* 2008; 64:1086-1102.
- [9] Hong S, Varma AH. Analytical modeling of the standard fire behavior of loaded CFT columns. *Journal of Constructional Steel Research* 2009; 65:54-69.
- [10] ISO (International Standards Organization). ISO 834: Fire resistance tests, elements of building construction. Switzerland: International Standards Organisation; 1980.
- [11] Lie TT, Caron SE. Fire resistance of circular hollow steel columns filled with siliceous aggregate concrete: Test results. Internal report No. 570. Ottawa, Canada: Institute for Research in Construction, National Research Council of Canada; 1988.
- [12] Lie TT. Fire resistance of circular steel columns filled with bar-reinforced concrete. *Journal of Structural Engineering-ASCE* 1994; 120(5):1489-1509.

## NUMERICAL AND EXPERIMENTAL DETERMINATION OF residual concrete strength after action of fire

Meri Cvetkovska<sup>a</sup>, Petar Cvetanovski<sup>b</sup>, Viktor Mihajlov<sup>c</sup>

<sup>a</sup> Ss. "Cyril and Methodius" University, Faculty of Civil Engineering, Skopje, Macedonia

<sup>b</sup> Ss. "Cyril and Methodius" University, Faculty of Civil Engineering, Skopje, Macedonia

<sup>c</sup> Ss. "Cyril and Methodius" University, Faculty of Civil Engineering, Skopje, Macedonia

### INTRODUCTION

A reinforced concrete structure exposed to fire should undergo a significant damage. Based on experience and on data collected through detailed visual survey of fired structural elements, the following characteristic damages can be recorded: change of the concrete colour (red, grey-yellow, yellow, fig.1); fissures and cracks inside the concrete mass; cracks along main reinforcement in columns, beams and slabs; crushing of concrete and falling off the concrete parts along the edges of linear elements up to the reinforcement. The possibility for adequate repair of the damaged elements and the measures that have to be done in that case, directly depend on the level of the damages caused during the fire action, as well as in the cooling period. One of the most important factors that directly influence the repairing possibility is the residual compressive strength of concrete. The mechanical properties of the reinforcement decrease as well, but in the cooling phase they increase again.

Temperature over 400<sup>0</sup>C causes irreversible reduction of the compressive strength and other mechanical properties of concrete. The compressive strength of concrete does not recover in the cooling phase because of initial degradation and chemical decomposition of the cement past. The residual compressive strength of concrete should be determinate by laboratory tests of specimens taken from the RC elements exposed to fire, but very often this procedure is impractical because additional destruction of the damaged elements is not advisable. Because of the position of the reinforcement in the surface layers of the cross section, taking the specimens from columns and beams is more complicated and is not advisable. In such cases the problem can be solved by using a numerical procedure, based on the nonlinear transient heat flow analysis and the nonlinear stress-strain analysis. When the residual compressive concrete strength is numerically determined, it's value is assumed to be the same as the value that corresponds to the maximum concrete temperature.

The program FIRE solves this problem. This program carries out the nonlinear transient heat flow analysis (modulus FIRE-T) and nonlinear stress-strain response associated with fire (modulus FIRE-S). The solution technique used in FIRE is a finite element method coupled with time step integration.

### 1 NUMERICAL PROCEDURE FOR RESIDUAL CONCRETE STRENGTH DETERMINATION

The residual concrete strength directly depends on the maximum achieved temperature in the cross section of the fire exposed concrete elements. The temperature distribution in the cross section of the elements can be calculated once the Theory of Heat Transfer is used. The governing differential equation of heat transfer in conduction is:

$$\frac{\partial}{\partial x}(\lambda_x \frac{\partial T}{\partial x}) + \frac{\partial}{\partial y}(\lambda_y \frac{\partial T}{\partial y}) + \frac{\partial}{\partial z}(\lambda_z \frac{\partial T}{\partial z}) = \rho c \frac{\partial T}{\partial t} \quad (1)$$

where:  $\lambda$  is a thermal conductivity (temperature dependent);  
 $\rho$  is a density of the material (temperature dependant);  
 $c$  is a specific heat (temperature dependent).

The fire boundary conditions can be modelled in terms of both convective and radiative heat transfer mechanisms. The heat flow caused by convection is:

$$q_c = h_c(T_z - T_f) \quad (2)$$

where  $h_c$  is coefficient of convection (for surface directly exposed to fire  $h_c=25\text{W/m}^2\text{K}$ , and for the unexposed surface  $h_c=9\text{W/m}^2\text{K}$ . These values are recommended in EC 2, part 1.2);  
 $T_z$  is the temperature on the boundary of the element;  
 $T_f$  is the temperature of the fluid around the element.

The heat flow caused by radiation is:

$$q_r = V\varepsilon\sigma_c(T_{z,a}^4 - T_{f,a}^4) = h_r(T_z - T_f) \quad (3)$$

$$h_r = V\varepsilon\sigma_c(T_{z,a}^2 + T_{f,a}^2)(T_{z,a} + T_{f,a}) \quad (4)$$

where:  $h_r$  is coefficient of radiation (temperature dependant);  
 $V$  is a radiation view factor (recommended  $V = 1.0$ );  
 $\varepsilon$  is a resultant coefficient of emission  $\varepsilon = \varepsilon_f\varepsilon_z$ ;  $\varepsilon_f = 0.8$  is coefficient of emission for the fire compartment;  $\varepsilon_z = 0.7$  is coefficient of emission for the surface of the element;  
 $\sigma_c$  is Stefan-Boltzmann constant;  
 $T_{z,a}$  is the absolute temperature of the surface;  $T_{f,a}$  is the absolute temperature of the fluid.

Using a typical Galerkin finite element approach Eq. (1) assumes the form:

$$\int_V N^T \left[ \lambda_x \frac{\partial^2 T}{\partial x^2} + \lambda_y \frac{\partial^2 T}{\partial y^2} + \lambda_z \frac{\partial^2 T}{\partial z^2} - \rho c \frac{\partial T}{\partial t} \right] dV = 0 \quad (5)$$

where the approximation field function is expressed in terms of the interpolation function as:

$$T = N \times T_e \quad (6)$$

Integration of Eq. (5) by parts yields:

$$\begin{aligned} \int_V \left( \left[ \frac{\partial N}{\partial x} \right]^T \lambda_x \frac{\partial T}{\partial x} + \left[ \frac{\partial N}{\partial y} \right]^T \lambda_y \frac{\partial T}{\partial y} + \left[ \frac{\partial N}{\partial z} \right]^T \lambda_z \frac{\partial T}{\partial z} \right) dV - \int_S N^T \left( \lambda_x l_x \frac{\partial T}{\partial x} + \lambda_y l_y \frac{\partial T}{\partial y} + \lambda_z l_z \frac{\partial T}{\partial z} \right) ds \\ + \int_V \rho c N^T T dV = 0 \end{aligned} \quad (7)$$

$$\text{where: } q = q_c + q_r = (h_c + h_r)(T_z - T_f) \quad (8)$$

Finally, the governing equation takes the form:

$$C\dot{T} + (K_1 + K_2)T + RT = P \quad (9)$$

where:  $C$  is a heat capacity matrix (temperature dependent):  $C = \int_V \rho c N^T N dV$

$K_1$  is the conductivity matrix (temperature dependent):  $K_1 = \int_V B^T D B dV$

$K_2$  is the convective matrix:  $K_2 = \int_S h_c N^T N dS$

$R$  is the radiative matrix (temperature dependent):  $R = \int_S h_r N^T N dS$

$P$  is the external heat flow vector (caused by convection and radiation on the surface of the element and is temperature dependent): 
$$P = \int_S h_c T_f N^T dS + \int_S h_r T_f N^T dS$$

$\dot{T}$  is the vector of temperature derivatives

$T$  is the vector of unknown temperatures in the nodal points of the element.

If the heat capacity of the material is taken under consideration and if thermal load is time dependent, the problem becomes transient and for solving the Eq. (9) an iterative procedure has to be used. In a small time interval we assumed that the time derivative of the temperature is constant:

$$\dot{T}_t = \dot{T}_{t+\Delta t} = \frac{T_{t+\Delta t} - T_t}{\Delta t} \quad (10)$$

By summarizing Eq. (9) for time  $t$  and  $t + \Delta t$  and assuming that the capacity matrix in small time interval is constant:  $C_t = C_{t+\Delta t}$ , the heat flow equation for a small time step becomes:

$$\left[ K_{t+\Delta t} + \frac{2}{\Delta t} C_t \right] T_{t+\Delta t} = \left[ -K_t + \frac{2}{\Delta t} C_t \right] T_t + P_{t+\Delta t} + P_t \quad (11)$$

Eq. (11) together with the initial and boundary conditions completely solves the problem. Taking the radiation into account makes the problem nonlinear. This problem is solved by involving new iterative procedure in every time step. Problem becomes nonlinear too, when temperature dependent physical properties of the materials are assumed. In that case the conductivity and capacity matrix are defined at the beginning of each time step based on the temperature from the previous time step. The modulus FIRE-T solves the governing differential equation of heat transfer in conduction and in that purpose the following assumptions are made: a fire can be modelled by a single valued gas temperature history: ASTM E119, ISO 834 or SDHI (short duration, high intensity) fire model; no contact resistance to heat transmission at the interface between the reinforcing steel and concrete occurs; the fire boundary conditions can be modelled in terms of both convective and radiating heat transfer mechanisms; the temperature dependant material properties are known (recommended in Eurocode 2, part 1.2); while cracks appear, or same parts of the element crush, the heat penetrates in the cross section easier, but in this study it is neglected. It has been assumed that the heat flow is separable from the structural analysis.

The modulus FIRE-S defines the nonlinear stress-strain response of structure in case of fire. This modulus enables use of temperature dependant  $\sigma - \varepsilon$  curves for steel and concrete based on experimental data, or use of theoretical curves. A stress-strain law for concrete under uniaxial loading consists of two parts: a compressive part and a tensile part. Parameters that completely define this curve are temperature dependant and for various temperature intervals they are given in EC 2, part 1.2. The compressive concrete strength “ $f_c$ ” decreases with temperature, strain at compressive strength “ $\varepsilon_{cl}$ ” increases with temperature and the ultimate crushing strain “ $\varepsilon_{cu}$ ” increases with temperature.

## 2. TEST EXAMPLE FOR NUMERICAL PROCEDURE

A twenty storey building structure was in fire and two apartments at the seventh and eighth floor were completely burned. Primary, the fire was caused by gas explosion, but the synthetic materials in the apartment were additional fire load, so very high temperatures were reached and the fire time was more than four hours. Thermal and structural response of four-bay, five-story reinforced concrete frame (only one part of the whole frame with defined support conditions) exposed to fire scenario at the two floors only, has been investigated analytically. Elements geometry; support conditions; concrete cover thickness; type of aggregate; compression strength of concrete; steel ratio and defined fire scenario were taken into account while the nonlinear and transient temperature field and the concrete strength reduction in the cross section of the elements exposed to fire were determined.

The most damaged column was incorporated into the wall, so it was exposed to fire only from the inside of the compartment, but the temperature on the other side (in the hall) was raising proportionally to the temperature in the fire compartment (the fire flames were coming out through the open door) and the heating was from the both sides, but not with the same intensity. The dimensions of the cross section of this column are 60×60cm, the compressive strength of the concrete before action of fire was  $f_c=40\text{MPa}$  (according to national codes this value corresponds to concrete type MB30).

The concrete strength was reduced as a result of high temperatures in the surface layers of the cross section (Fig.1). Calculation results indicate that on the side of the fire, in 4-5cm thick layer, which is 17% of the cross section of the column, the strength reduction is significant and the residual strength of concrete is 15Mpa (MB11) in average (Fig.2). These results correspond well with experimental results obtained by laboratory testing of specimens taken from the nearest RC wall (B8, Table 1). In the cross section core the strength of concrete is not reduced.

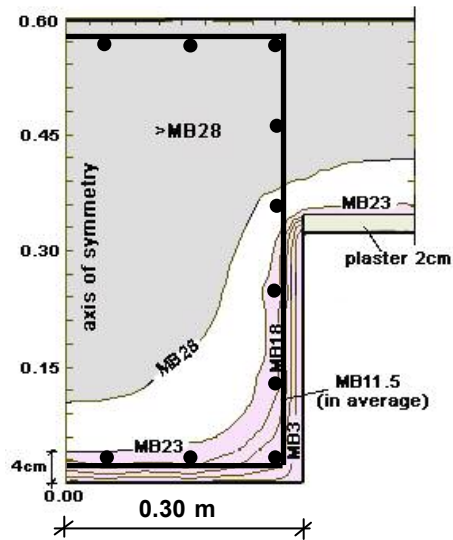
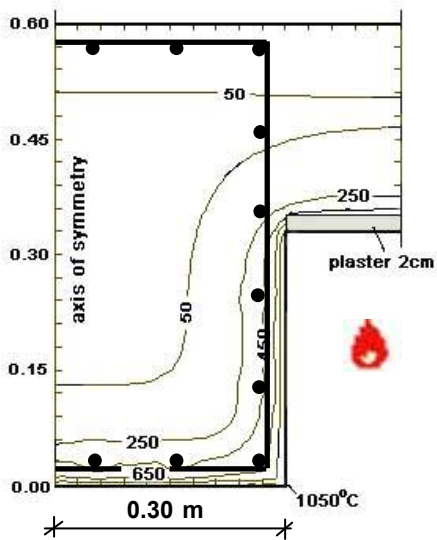


Fig. 1. Temperature distribution in the cross section of the column exposed to fire from two sides

Fig. 2. Residual concrete strength in the cross section of column

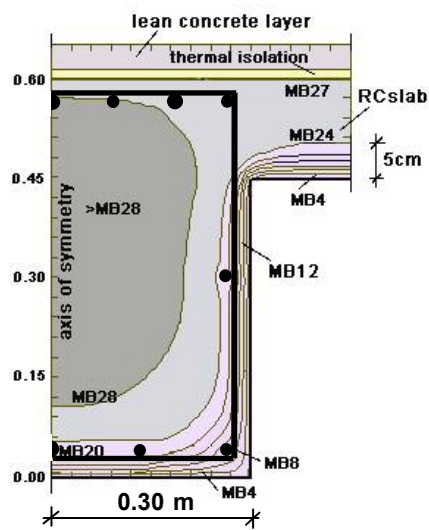
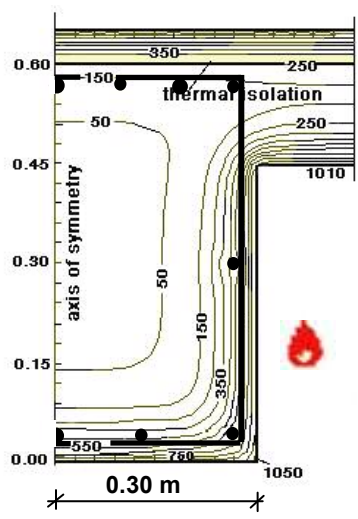


Fig. 3. Temperature distribution in the cross section of the beam exposed to fire from both sides

Fig. 4. Residual concrete strength in the cross section of beam

Results obtained by the thermal and static analysis of the frame structure show that fire had the most negative influence upon the beam elements over the 7<sup>th</sup> floor, where the fire started. These results correspond well with experimental results obtained by laboratory testing of specimens taken from the elements from that floor and with visually recorded changes in concrete colour (V7, G7, D7, E7, *Table 1*). The fire intensity on the 8<sup>th</sup> floor was less than that of the 7<sup>th</sup> floor and the degree of damage was less too (for B8 the reduction of concrete strength is less than for the other specimens). Beams over the 7<sup>th</sup> floor were fire exposed from both sides, but from the upper side, as a part of the RC slabs, they were covered with 1cm thermal isolation and 4cm lean concrete, that directly influenced upon the cross section temperature field (*Fig.3*) and the concrete strength reduction (*Fig.4*).

## 2. EXPERIMENTAL DETERMINATION OF THE RESIDUAL CONCRETE STRENGTH

The experimental testing of the residual concrete strength after the fire action was done by the Institute for Materials Testing and Development of New Technologies “Skopje”-Skopje. According to the previous Schmidt hammer testing results, the locations of the eight concrete specimens, taken only from RC walls and RC slabs, were defined. Hammer testing of concrete elements from apartments that were not fired confirmed that the compressive strength of the concrete before the action of fire was  $f_c=40\text{MPa}$  (MB30).

The concrete specimens taken from the RC walls (B8, V7, G7, D7, E7) were exposed to fire from one side. The corresponding surface layers (3-5cm thick) had changed the colour (red, grey-yellow, yellow) and were more deteriorated than the inner layers (*Fig.5*). Before testing all the specimens were divided in two slices. The deteriorated (burned) slices had small height (3-6cm) and rough surface therefore they were specially prepared by adding plaster layers (*Fig.6*). In that case the measured values for the compressive concrete strength were reduced with coefficients depending on the shape and height (h) of the deteriorated concrete specimens [4].



*Fig. 5.* Change of concrete colour and deterioration of surface layers of specimens



*Fig. 6.* Deteriorated concrete specimens, prepared for testing

Table 1. Concrete strength testing results

| Position            | Dimensions of specimens (cm) |             |     | Concrete compressive strength (MPa) |                        | Concrete strength (MB) |
|---------------------|------------------------------|-------------|-----|-------------------------------------|------------------------|------------------------|
|                     | total H                      | h (testing) | D   | cylinder                            | reduc.to cube 20/20/20 |                        |
| RC wall (B8)        | 15                           | 9.9         | 9.9 | <b>26.0</b>                         | 26.5                   | <b>20.0</b>            |
| (after fire expose) |                              | 3.5         |     | <b>15.8*</b>                        | 16.1                   | <b>12.0</b>            |
| RC slab (MS)        | 18                           | 10.3        | 9.9 | <b>33.8</b>                         | 34.5                   | <b>26.0</b>            |
| (after fire expose) |                              | 6.5         |     | <b>12.5*</b>                        | 12.8                   | <b>9.5</b>             |
| RC slab (SII)       | 18                           | 9.6         | 9.9 | <b>38.4</b>                         | 39.1                   | <b>29.4</b>            |
| (after fire expose) |                              | 4           |     | <b>13.0*</b>                        | 13.3                   | <b>10.0</b>            |
| RC wall (V7)        | 25                           | 9.9         | 9.9 | <b>35.4</b>                         | 36.1                   | <b>27.0</b>            |
| (after fire expose) |                              | 5           |     | <b>14.5*</b>                        | 14.8                   | <b>11.0</b>            |
| RC wall (G7)        | 19.4                         | 10          | 9.9 | <b>25.4</b>                         | 25.9                   | <b>20.0</b>            |
| (after fire expose) |                              | 3.5         |     | <b>14.5*</b>                        | 14.5                   | <b>11.0</b>            |
| RC wall (D7)        | 18                           | 10          | 9.9 | <b>30.7</b>                         | 31.3                   | <b>24.0</b>            |
| (after fire expose) |                              | 3.5         |     | <b>14.5*</b>                        | 14.8                   | <b>11.0</b>            |
| RC wall (E7)        | 16                           | 10          | 9.9 | <b>31.9</b>                         | 32.6                   | <b>25.0</b>            |
| (after fire expose) |                              | 3           |     | <b>14.1</b>                         | 14.4                   | <b>10.5</b>            |

\* Values are reduced with coefficients depending on the shape and height (h) of the deteriorated concrete specimens.

Results obtained by the thermal analysis and experimental testing of specimens show that during the fire action, as well as in the cooling period, the compressive strength of concrete is continually reduced. Numerically achieved results correspond well with experimental results obtained by laboratory tests of specimens taken from fired elements (RC walls and slabs). All these confirms that the numerical procedure, based on the nonlinear transient heat flow analysis, can be used for defining the residual concrete strength with grate accuracy.

## REFERENCES

- [1] Cvetkovska M., Nonlinear stress strain behavior of RC elements and RC frames exposed to fire, *Phd. thesis, University St.Cyril and Methodius, Skopje, 2002*
- [2] Cvetkovska M., Lazarov Lj., Examination and assessment of degree of damage of fired elements of building structure K2-Karpos IV, *Civil engineering faculty-Skopje, May 2005*
- [3] Cvetkovska M., Lazarov Lj., The repair project of the RC structure of the building K2-Karpos IV-Skopje, damaged by fire, *Civil engineering faculty-Skopje, June 2005*
- [4] Manov Z., Determination of the residual concrete strength after action of fire on building structure K2-Karpos IV-Skopje, *Institute for materials testing and development of new technologies "Skopje"-Skopje, May 2005*

## FIRE RESISTANCE CURVES FOR RC COLUMNS

Meri Cvetkovska<sup>a</sup>, Petar Cvetanovski<sup>b</sup>, Viktor Mihajlov<sup>c</sup>

<sup>a</sup> Ss. "Cyril and Methodius" University, Faculty of Civil Engineering, Skopje, Macedonia

<sup>b</sup> Ss. "Cyril and Methodius" University, Faculty of Civil Engineering, Skopje, Macedonia

<sup>c</sup> Ss. "Cyril and Methodius" University, Faculty of Civil Engineering, Skopje, Macedonia

### INTRODUCTION

The response of complex structure subjected to a real fire loading is estimated by methods of computational modelling of thermo dynamic and thermo mechanical processes. However, the development of various numerical methods for the analysis of the nonlinear response of structures under fire does not reduce the necessity and the importance of the experimental tests. They are necessary to determine the mechanical properties of materials at elevated temperatures, as well as to check the adequacy of the developed computational methods.

The columns as structural elements have an important role in preventing loss of global stability of structures under fire. If these elements do not suffer failure, damages shall be of a local character, which shall enable evacuation and efficient extinguishing of the fire. This paper describes the analytically achieved results for the fire resistance of centrally and eccentrically loaded RC columns incorporated in a wall for separating the fire compartment. The influence of: element geometry, concrete cover thickness, steel ratio and intensity of the axial force and bending moment are analyzed and the results are presented by curves which enable determination of the fire resistance of these columns without use of numeric procedure. For that purpose the program FIRE is used. This program carries out the nonlinear transient heat flow analysis (modulus FIRE-T) and nonlinear stress-strain response associated with fire (modulus FIRE-S). The solution technique used in FIRE is a finite element method coupled with time step integration.

### 1. FIRE RESISTANCE OF CENTRICALLY LOADED RC COLUMNS

*Fig.1a* shows a column, fixed at A and free to move vertically at B, allowing a free expansion in longitudinal direction; and *Fig.1b* shows the cross section of the column. The steel ratio is  $\mu = 1\%$ . The yield strength of the reinforcing bars is  $f_y(20^\circ C) = 400 \text{ Mpa}$  and the strength of the siliceous concrete is  $f_c(20^\circ C) = 30 \text{ Mpa}$ . The column is exposed to a standard fire only from one side of the wall. At the other side the column is part of a concrete wall, which is not fire exposed.

The column is discretised by three elements and each element is further discretised by five subelements. Because of the symmetry of the cross section and the symmetry of the fire load, only one half of the column is analyzed. For the thermal analysis the cross section of the column and the associated part of the wall is discretised by isoparametric 4 nodes rectangular elements (subslices). In the stress-strain analysis the wall elements are excluded, reducing the number of elements. For the surface layers a finer discrete mesh is adopted because of the high temperature gradient ( $\Delta x = 1.0\text{cm}$ ), while for the inner layers the size of the subslices is  $2.0 \leq \Delta x \leq 3.0\text{cm}$ . The time step is  $\Delta t = 0.025\text{h}$  and it is adopted to the size of the subslices. Temperature dependent thermal and mechanical properties of concrete and steel are taken as recommended by Eurocode 2, part 1.2.

For the regions with high seismic risk it is recommended stresses in concrete not to exceed:  $\sigma_c \leq 0.35f_{cd} \leq 0.35 \cdot 0.85f_c \leq 0.3f_c$ . In this research the load ratio is defined as:  $\alpha = \sigma_c / f_c(20^\circ C)$ , but its value is varied in more wide range:  $0 \leq \alpha \leq 0.5$ . Dimensions of the cross section, concrete cover thickness, steel ratio and intensity of the axial force are varied and the results are presented by curves from which the fire resistance of the column can be determined without any additional calculations.

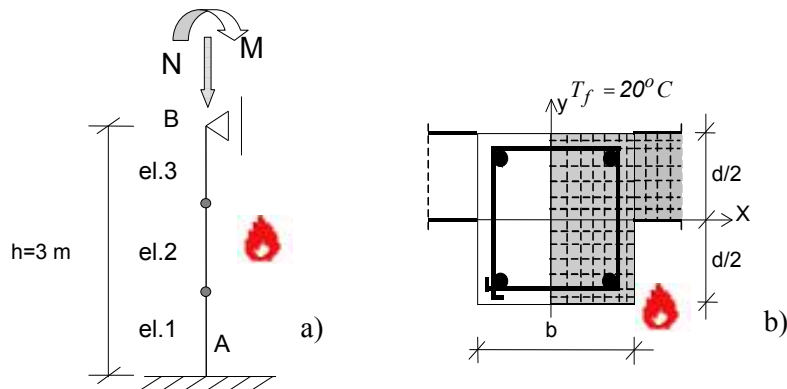


Fig. 1. a) Geometry and support conditions. b) discretization of the cross-section when column is part of a wall for separation the fire compartment

The results of the thermal analysis, in case when the dimensions of the cross section are  $30 \times 30\text{ cm}$ , are presented on Fig. 2. Isobars in the cross section at support B, for the case when the load ratio is  $\alpha = 0.3$ , are shown on Fig.3.

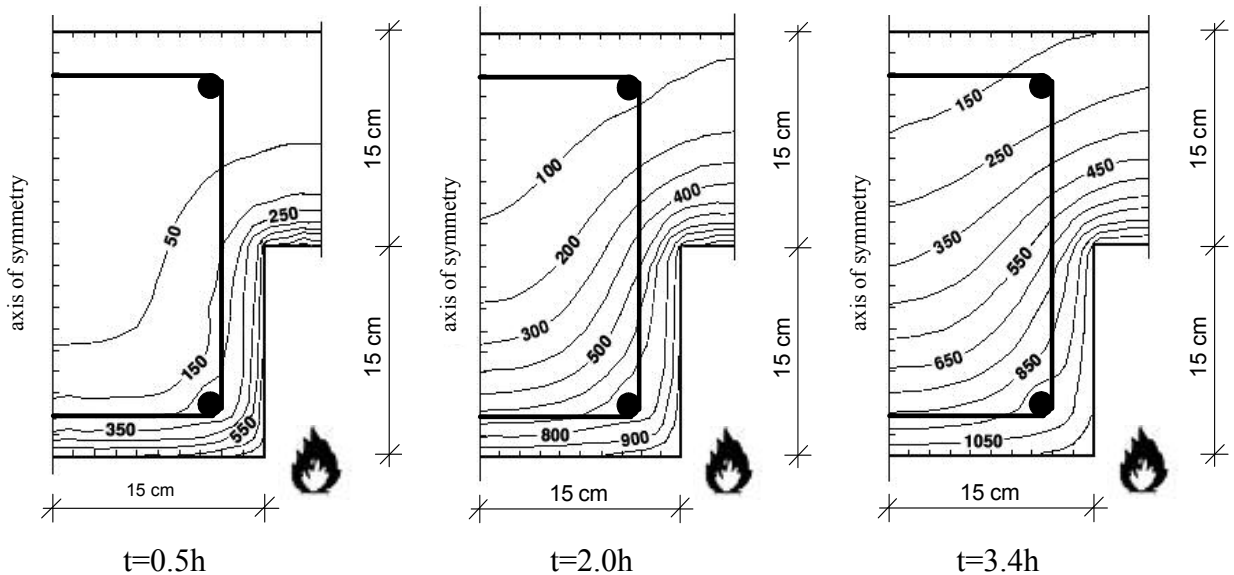


Fig.2: Isotherms in the cross section of a column  $30 \times 30\text{ cm}$ , that is a part of a wall for separation the fire compartment

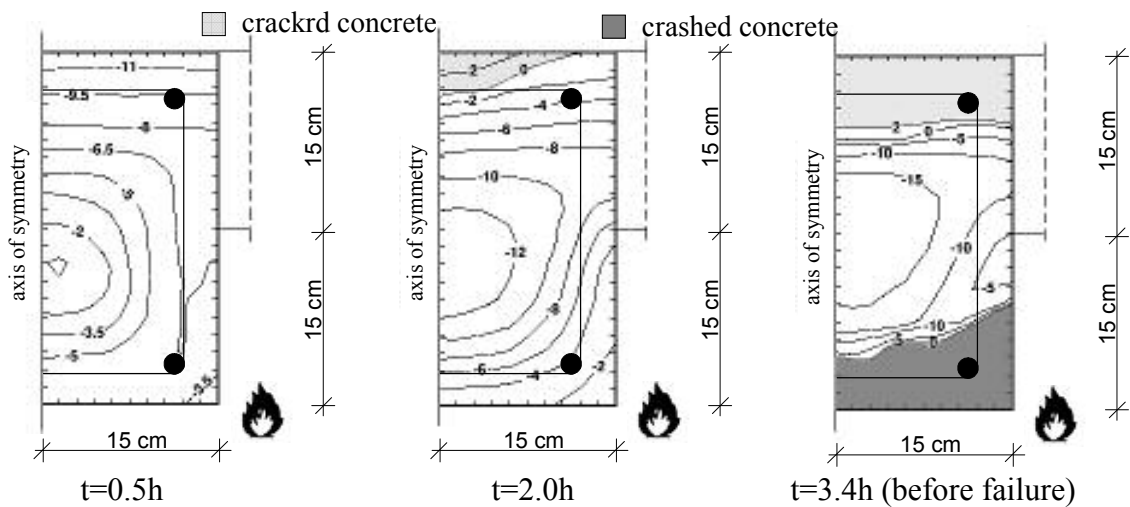


Fig.3: Isobars in the cross section at support B (load ratio  $\alpha = 0.3$ , concrete cover thickness  $a=2.0\text{ cm}$ )

The differential heating causes the end B of the column to separate from the support thus causing negative reaction. This action results in an initialization of negative moment at support A (Fig.4), but after some time the moment changes the sign. The outside reinforcement at support A (el.2A at Fig.5) remains cold for a long period of time, its yield strength is not reduced and the axial force produces compressive stresses, so the negative moment can be accommodated. The reinforcing bar that is on the side of the fire (el.1A) is in compression by the axial force, bending moment and the action of the fire. The yield strength is reduced because of the high temperatures, so stresses are close to the yield strength very soon, but after some time the moment changes the sign and the stresses decrease. Element 1B, at support B, is in compression all the time by the axial force and the fire action and yields first. Failure occurs at support B (Fig.3,  $t=3.4h$ ).

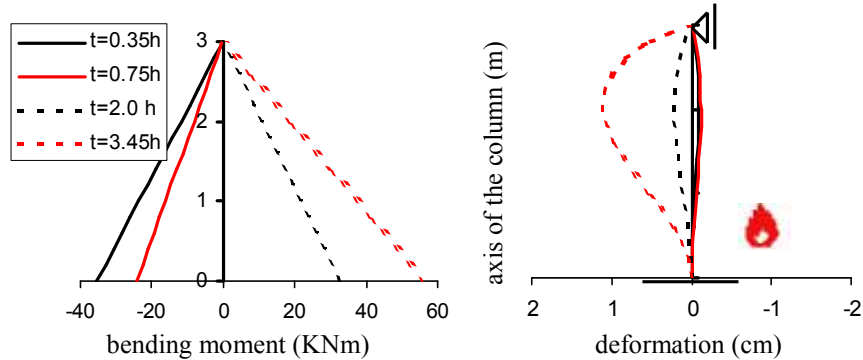


Fig.4: Bending moment and deformation redistribution during a fire exposure, (load ratio  $\alpha = 0.3$ )

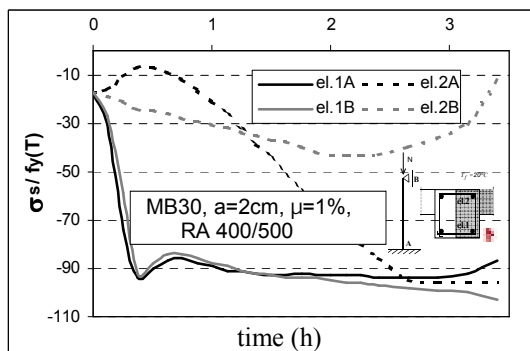


Fig.5: Time redistribution of stresses in the reinforcement at support A and B,  $\alpha = 0.3$

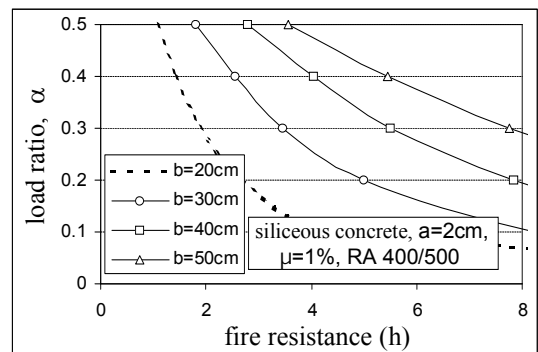


Fig.6: Fire resistance curves for centrally loaded columns

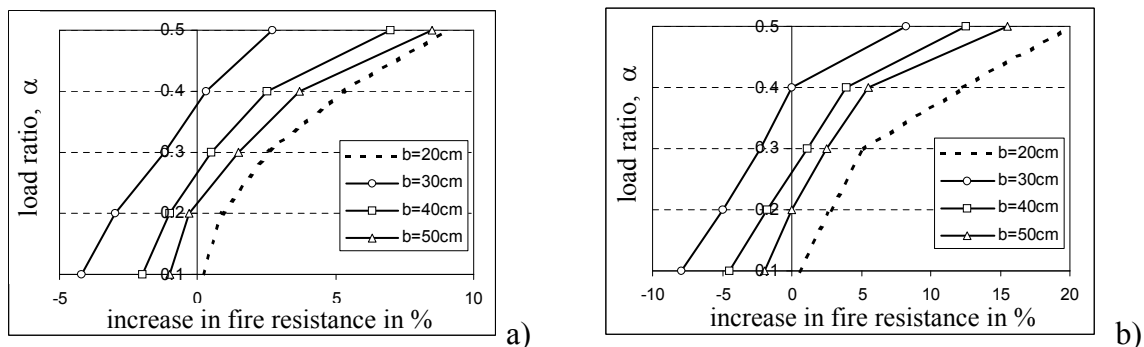


Fig.7: Increase in fire resistance of centrally loaded columns when the concrete cover thickness is increased: a)  $a=3cm$ , b)  $a=4cm$ , (reference column has  $a=2cm$ )

If dimensions of the cross section, intensity of the axial force (load ratio  $\alpha$ ) and concrete cover thickness are known, fire resistance of centrally loaded column that is part of a wall for separation

the fire compartment, can be directly defined from the diagram presented on Fig.6. If the concrete cover thickness is  $a = 2\text{cm}$ , the results are presented on Fig.6. For all other cases ( $a = 3\text{cm}$  or  $a = 4\text{cm}$ ) a correction has to be made according to the values on Fig.7.

## 2. FIRE RESISTANCE OF ECCENTRICALLY LOADED RC COLUMNS

Fire resistance of RC columns subjected to eccentric loads is determined in this example. Columns are part of a wall for separation the fire compartment, so they are exposed to ISO 834 standard fire only from the inside of the compartment. This is the most usual case in practice. Geometry and support conditions of the columns analyzed in this example are presented on Fig.1. Dimensions of the cross section; concrete cover thickness; steel ratio; intensity of the axial force and bending moment are significant factors affecting fire resistance of these columns.

The differential heating causes redistribution of bending moments (Fig.8). The outside reinforcement remains cold for a long period of time (el.2A, Fig.9), its yield strength is not reduced and the axial force produces compressive stresses, so that the change of the moment sign can be accommodated. The reinforcing bars that are on the side of the fire are all the time in compression by the dominant axial force and the action of the fire (el.1A and el.1B, Fig.9). The yield strength is reduced because of the high temperatures, so they start to yield very soon. Failure occurs at support B where the bending moment and the fire cause the same effect.

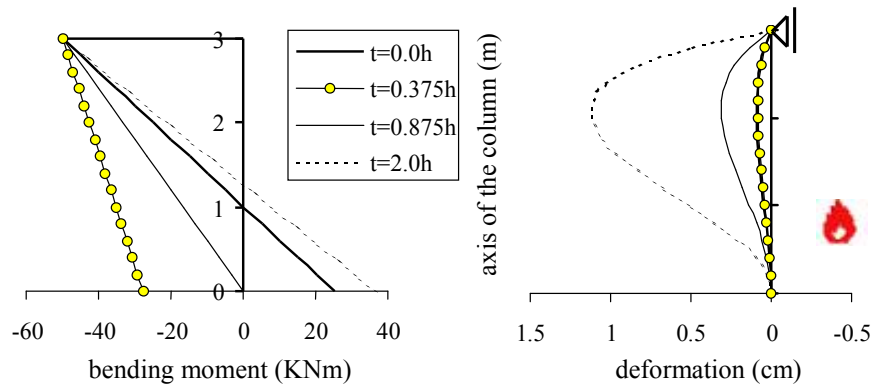


Fig.8. Deformation and bending moment redistribution during fire for column  $30 \times 30\text{cm}$  ( $\eta = 0.2$ ,  $\beta = 0.4$ ,  $a = 2\text{cm}$ ,  $\mu = 1\%$ )

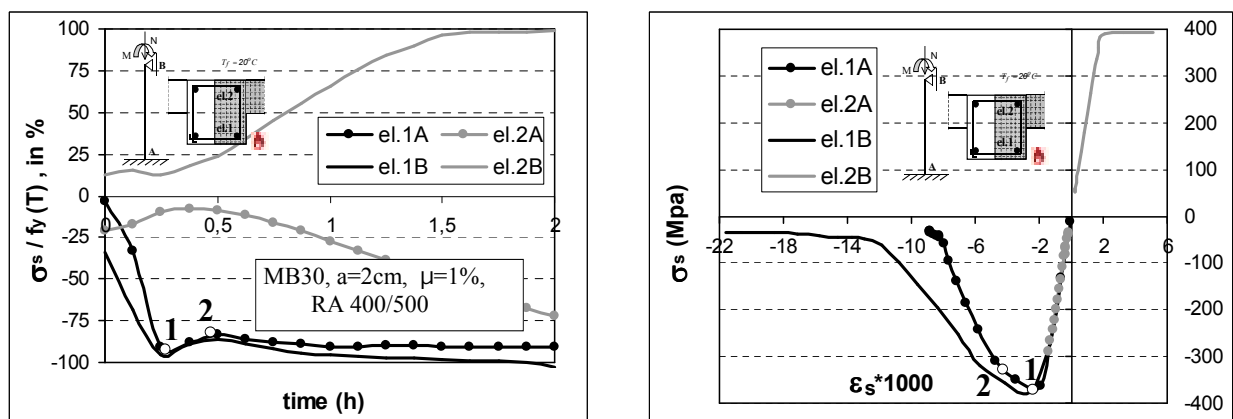


Fig.9. Time redistribution of stresses in a column  $30 \times 30\text{cm}$  ( $\eta = 0.2$ ,  $\beta = 0.4$ ,  $a = 2\text{cm}$ ,  $\mu = 1\%$ )

Stresses on Fig.9a are presented as a per cent of the yielding strength for the corresponding temperature of the reinforcement, but on Fig.9b they are presented with the real values, so typical stress-strain diagrams for steel at high temperature are obtained.

If the column is designed according to current design standards, the fire resistance can be directly defined from the diagrams presented on Fig.10a, when concrete cover thickness is  $a = 2\text{cm}$ . For

that purpose the M-N diagram of the column at ambient temperatures has to be defined and the load coefficients for the axial force and bending moment to be calculated:

$$\eta = \frac{N}{N_{u,max}} \quad , \quad \beta = \frac{M}{M_u} \quad (1)$$

- where:
- $\eta$  - load coefficient for axial force
  - $N$  - axial force before action of fire
  - $N_{u,max}$  - ultimate axial force when the bending moment is zero  
(defined from the M-N diagram)
  - $\beta$  - load coefficient for the bending moment
  - $M$  - bending moment before action of fire
  - $M_u$  - ultimate bending moment corresponding to the ultimate axial force  $N_u$   
(defined from the M-N diagram according to Equation 2)

$$N_u = N_g \gamma_{ug} + N_p \gamma_{up} = N \gamma_u \Rightarrow M_u = f(N_u) \quad (2)$$

For all other cases ( $\mu = 0.6\%$  or  $\mu = 1.5\%$ ;  $a = 3\text{cm}$  or  $a = 4\text{cm}$ ) a correction has to be made according to the values on *Fig.10b* and *Fig.11*. Such diagrams are obtained for columns  $40 \times 40\text{cm}$  and  $50 \times 50\text{cm}$ , but they are not presented.

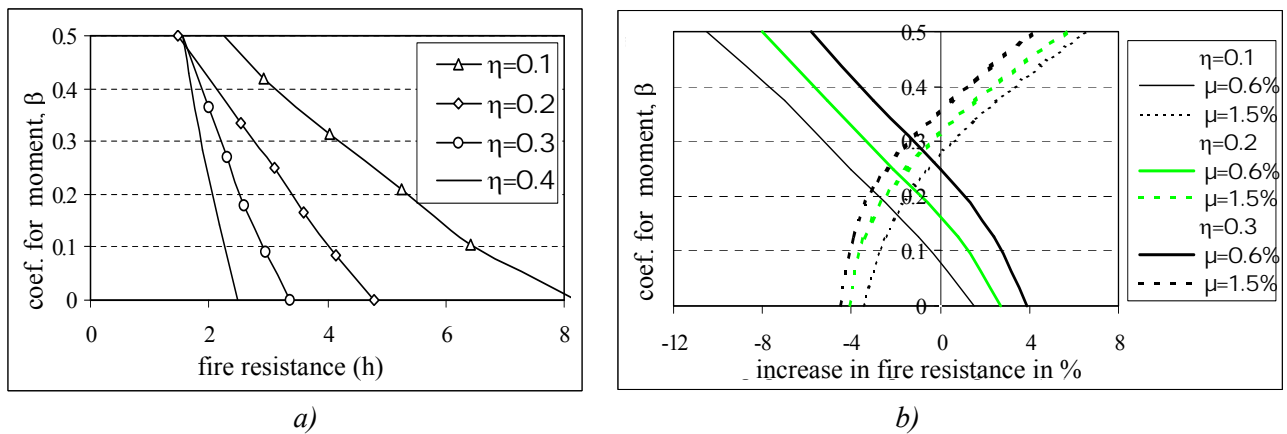


*Fig.10.* Effect of a) load intensity b) steel ratio (referent column  $\mu=1\%$ ) upon the fire resistance of eccentrically loaded column  $30 \times 30\text{cm}$  (concrete cover  $a = 2\text{cm}$ )

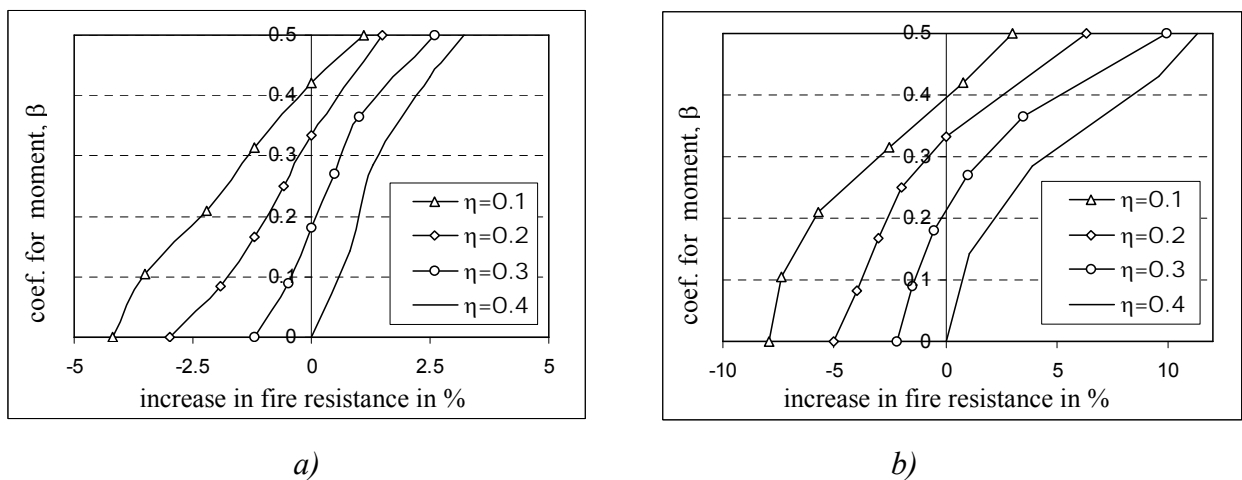


*Fig.11.* Increase in fire resistance of eccentrically loaded columns  $30 \times 30\text{cm}$ , when concrete cover thickness is increased: a)  $a = 3\text{cm}$ , b)  $a = 4\text{cm}$ , (reference column has  $a = 2\text{cm}$ )

### 3. SUMMARY AND ACKNOWLEDGMENT

As a result of parametric studies, the following conclusions are made: dimensions of the cross section, intensity of the axial force (load ratio  $\alpha$ ) and the type of the aggregate (siliceous or carbonate) are significant factors affecting fire resistance of centrally loaded columns exposed to standard fire from all sides. When dimensions of the cross section are small temperature penetrates deeper in a short time period and the fire resistance is lower. When the load ratio is increased, the fire resistance is decreased, and opposite. If load ratio  $\alpha = 0.3$  is decreased to  $\alpha = 0.2$ , the fire resistance is increased for 30%. If carbonate aggregate concrete is used instead of siliceous aggregate concrete, the fire resistance is increased for 30% in average. Experimental results indicate even higher effect, which leads to a conclusion that recommendations for the temperature dependant physical characteristics of carbonate aggregate concrete, given in Eurocode 2 part 1.2, are conservative but are on the side of safety.

With the increase of the strength of concrete, the fire resistance increases in proportion to the assigned load capacity. The steel ratio has a negligible effect on the fire resistance of the centrally loaded columns, exposed to fire from all sides. As a result of that the concrete cover thickness has a negligible effect. Because of the symmetry of the axial load and fire exposure, support conditions and height of the column have no influence on the fire resistance (the used analysis procedure does not account for the effects of large displacements on equilibrium equations). The effect of axial restraint on the fire resistance is negligible. Experimental results indicated that fully restrained column didn't significantly decrease its fire resistance, and only columns with high slenderness ratio failed in buckling.

Eccentrically loaded columns that are part of a wall for separation the fire compartment have the lowest fire resistance. Dimensions of the cross section; concrete cover thickness; steel ratio; support conditions; fire scenario and intensity of the axial force and bending moment are significant factors affecting fire resistance of these columns. The effect of increasing the steel ratio is positive. It was not a case when the column was centrally loaded ( $\beta = 0$ ). When the bending moment is increased and the axial force is decreased the positive effect is more expressive. For optimally loaded columns ( $\eta \leq 0.3$ ) the concrete cover thickness has a positive effect in increasing the fire resistance, but not more than 5% for columns with small dimensions, and up to 10% for larger columns.

### REFERENCES

- [1] Anderberg, Y. Magnusson, S.E. Pettersson, O. Thelandersson, S. & Wickstrom, U., An analytical approach to fire engineering design of concrete structures. *International Symposium on Concrete and Structures. ACI Publications* 1986.
- [2] Bazant, Z.P. & Kaplan, M.F., Concrete at high temperature: Material properties and mathematical models. *London: Longman Group Limited*, 1996.
- [3] Cvetkovska, M., Nonlinear stress strain behaviour of RC elements and RC frames exposed to fire. *Phd. thesis. Skopje: University St. Cyril and Methodius*, 2002.
- [4] Ellingwood, B. & Lin, T.D., Flexure and shear behavior of concrete beams during fires. *Journal of the Structural Engineering. Vol.117 No.2*, 1991.
- [5] Iding, R. Bresler, B. & Nizamuddin, Z., FIRES-RC II A computer program for the fire response of structures-reinforced concrete frames. *Report No. UCG FRG 77-8. Berkeley: University of California*, 1977
- [6] Lin, T.D. Zwiers, R.I. Burg, R.G. Lie, T.T. & McGrath R.J., Fire resistance of reinforced concrete columns. *PCA Research and Development Bulletin RD101B. Skokie, Illinois: Portland Cement Association*, 1992.

## **SPALLING OF CONCRETE**

### **Implications for Structural Performance in Fire**

Susan Deeny<sup>a</sup>, Tim Stratford<sup>a</sup>, Rajesh Dhakal<sup>b</sup>, Peter Moss<sup>b</sup>, Andy Buchanan<sup>b</sup>

<sup>a</sup> The University of Edinburgh, BRE Centre for Fire Safety Engineering, Edinburgh, UK

<sup>b</sup> University of Canterbury, Department of Civil and Natural Resource Engineering, Christchurch, New Zealand

## **INTRODUCTION**

Spalling involves the breaking off of layers or pieces of concrete from the surface during thermal exposure. Spalling can broadly be classified into 3 different types: aggregate spalling, corner spalling (or sloughing off) and explosive spalling. Aggregate spalling and corner spalling are generally not considered to be critical for the performance of concrete structures in fire and are, therefore, not considered further here. Explosive spalling involves the ejection of pieces of concrete from the heated surface at high velocities. It typically occurs in the early stages of the fire when heating rates are high [1, 2]. Explosive spalling (hereafter referred to as spalling for brevity) poses the greater threat to structural stability; it is, therefore, the form of spalling focused upon in this paper.

Current research is predominantly concerned with establishing and modelling the precipitating mechanisms. Prediction of the stress state leading to spalling requires complex hygro-thermal-mechanical modelling; the reliability and accuracy of such models however is not yet sufficient to formulate design guidelines; hence, there is little guidance provided under BS 8110 part 2 [3] and the new Eurocode 2 [4] with regards to protection of concrete structures in the event of spalling. In this paper, a preliminary investigation on the effect of spalling on structural stability is performed through the finite element analyses of a reinforced concrete beam subjected to the Eurocode 1 [5] standard temperature – time curve. It is not the intention of this investigation to model explicitly the hygro-thermal-mechanical processes, rather to develop a framework for consequence modelling of spalling in a finite element analysis.

## **1 MECHANISMS OF SPALLING**

Spalling of concrete can generally be categorised as pore pressure induced spalling, thermal stress induced spalling or a combination of the two. In general terms, pore pressure spalling occurs when migration of evaporated free water from the heated surface leads to increased pore pressure at some distance from the heated surface. Continued heating will result in the pore pressure reaching the tensile strength of the concrete, causing explosive local failure. No pore pressures have yet been measured which would exceed the tensile strength of concrete [6, 7]. Thermal stress induced spalling is thought to occur due to the steep thermal gradients which develop in concrete as it is heated. These gradients induce compressive stresses at the surface due to restrained thermal expansion and tensile stresses in the cooler interior. Surface compression may be augmented by applied loading or pre-stress. It is most likely that spalling results as a combination of the tensile stresses induced by thermal expansions and increased pore pressure. Much debate still surrounds the identification of the key mechanism (pore pressure or thermal stress). However, it is noted that the key mechanism may change depending upon the section size, material composition and moisture content [8].

## 2 SPALLING MODEL

### 2.1 Spalling Criteria

From the previous discussion of the governing mechanisms of spalling, it is evident that the stress state within the concrete will dictate whether spalling will occur. The stress state due to moisture migration and thermal stress will be influenced by several parameters; these parameters can be categorised as follows [1, 2]:

- Material Parameters: Initial moisture content, permeability, porosity, presence of cracks, aggregate type and size, amount of reinforcement.
- Geometric Parameters: Section shape and size.
- Environmental Parameters: Heating rate and profile, temperature level and thermal restraint.

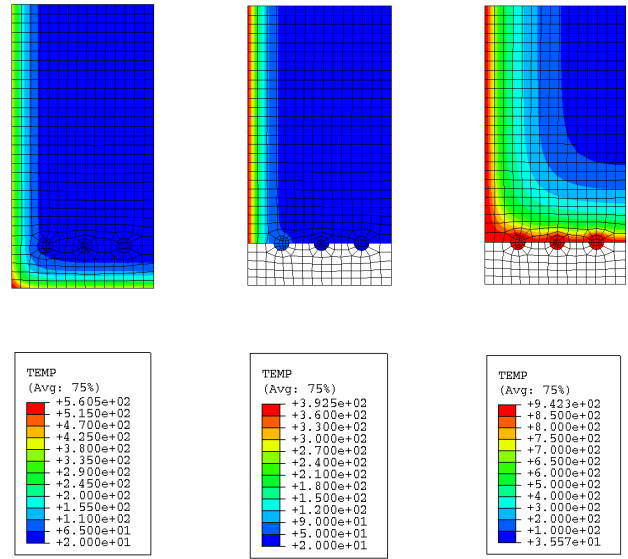
It is not the intention of this investigation to model explicitly the hygro-thermal-mechanical processes which determine this stress state leading to spalling. A comprehensive review of the substantial body of research which has sought to characterise the conditions under which spalling occurs has been undertaken to identify critical conditions or parameters for spalling which are applicable within a structural analysis. The fundamental assumption in this analysis is that spalling *will* occur, thus it is assumed that the material and geometric conditions which trigger spalling are satisfied.

Assuming that spalling will occur, it is then necessary to define *when* spalling will occur during fire exposure. The environmental parameters of heating rate and temperature level are useful indicators in a thermal analysis of when spalling may occur. From the literature it is found that heating rates in the range of 20–32°C/min are significant for spalling [2]. Such high heating rates normally occur in the early stages of the fire which is consistent with the experimental observations. Several researchers have identified critical temperature ranges for the exposed surface at the onset of spalling. Aktaruzzaman and Sullivan [9] have cited exposed surface temperatures in the range of 375–425°C for normal weight concretes.

### 2.2 Spalling Implementation

A 2-D heat transfer analysis of the member cross section is performed using ABAQUS finite element software [10]. The onset of spalling is triggered when the bottom surface temperature reaches the range of 375-425°C. Spalling is modelled by removing all the elements making up the bottom concrete cover. The analysis is continued and the temperature distribution for the reduced cross section is calculated. Figure 1 presents typical temperature contour plots just prior to and just after spalling and one hour from the beginning of the analysis for the abrupt spalling analysis.

Removing all of the concrete cover instantaneously when the bottom surface reaches a certain temperature greatly simplifies the progressive nature of spalling. Slower and more progressive spalling can also be modelled by employing the same temperature criteria but only removing single layers of elements at time. The thickness of the layers removed will be a function of the element thickness used in the finite element analysis.



(a) Pre Spalling (b) Immediately post spalling (c) Final temp distribution

Fig. 1. Beam cross section temperature profile (°C) for abrupt spalling.

#### 4 CASE STUDIES

The performance of a simply supported RC beam exposed to the EC1 [5] standard temperature-time curve (Figure 2) and subject to spalling is investigated.

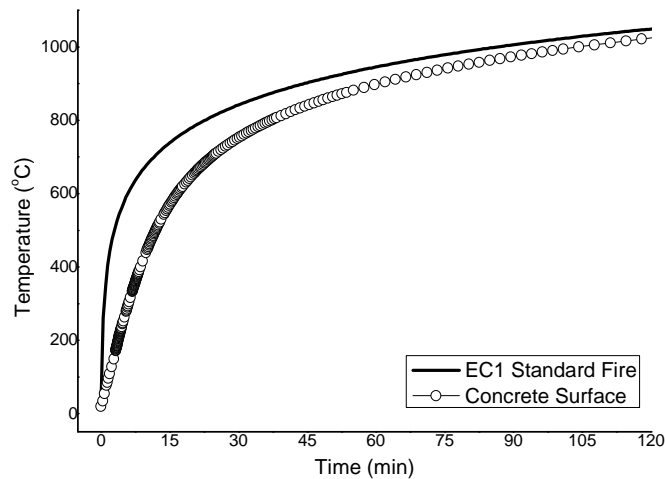


Fig. 2. Eurocode 1 standard temperature curve and concrete surface temperature.

The beam cross section is 600 mm deep by 300 mm. The concrete strength  $f_{cu}$  is assumed to be 30 MPa. The beam is reinforced with six 16 mm steel bars of yield strength,  $f_y = 500$  MPa. The cover depth is assumed to be 45 mm. Temperature dependant material properties for both the concrete and reinforcing steel are taken from Eurocode 2

Advantage is taken of symmetry and half of the beam cross section is analysed for the case of no spalling, progressive spalling (8 mm layers) and abrupt spalling. The rapid evolution of concrete surface temperature in Figure 2 would indicate that varying the criterion temperature

between 375°C- 425°C would have little effect on the final temperature distribution therefore the surface temperature criterion for the onset of spalling is taken as a single value of 400°C.

For each case the resulting evolution of temperature in the reinforcement is plotted in Figure 3 (a). The corresponding reduction in reinforcing steel yield strength is plotted according to the reduction factors provided in Eurocode 2 is plotted in Figure 3 (b).

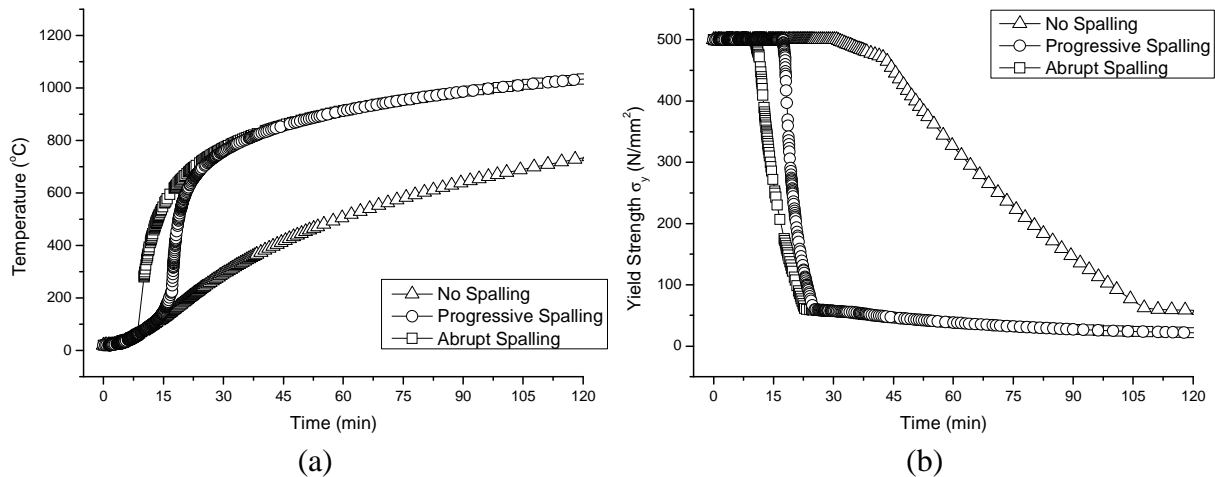


Fig. 3. (a) Temperature development and (b) reduction in yield stress in reinforcing steel on exposure to the standard fire.

For the case of no spalling the steel temperatures rise gradually, being insulated by the concrete cover. Removal of the concrete cover due to spalling instantly results in a sharp increase in steel temperatures and a corresponding reduction in steel strength.

#### 4.1 Single span simply supported RC beam

For a simply supported beam a single point of failure will result in a stability failure. Thus, failure times can be calculated by comparing the load ratio,  $r_{load}$ , with the residual steel strengths. The load ratio,  $r_{load}$ , is defined as per Equation 1 below:

$$r_{load} = M^*_{fire} / R_{cold} \quad (1)$$

Where  $M^*_{fire}$  Applied bending moment in fire conditions

$R_{cold}$  Ambient ultimate capacity

Table 1. Failure times for simply supported beam under standard heating.

| $r_{load}$ | No spalling (min) | Progressive spalling (min) | Abrupt Spalling (min) |
|------------|-------------------|----------------------------|-----------------------|
| 0.4        | 78                | 21                         | 17                    |
| 0.45       | 73                | 20                         | 16                    |
| 0.5        | 71                | 20                         | 16                    |

The failure times for each scenario and a variety of load ratios representative of those expected in a real building [11] are presented in Table 1. It is apparent that spalling significantly reduces the failure time of the simply supported concrete beam when exposed to the standard fire. Note that the failure time predicted with spalling (even in progressive spalling) is well short of the time when the cooling phase typically starts in ‘natural’ or

parametric fires (EC1 2002). Hence it can be argued that consideration of the cooling phase will not alter the prediction of failure time.

#### 4.2 Two span simply supported RC beam

Continuous beams generally exhibit improved fire performance due to their ability to maintain stability through alternate load paths (moment redistribution). The fire affected moment capacity is calculated using the simplified method from EC2 [4] which assumes that concrete above 500°C is structurally insignificant and below 500°C the concrete is unaffected, the results can be seen in Table 2.

Table 2. Failure times for a two span RC beam under standard heating.

| Spalling |        | Single steel layer<br>(min) | Double steel layer<br>(min) |
|----------|--------|-----------------------------|-----------------------------|
| Span 1   | Span 2 |                             |                             |
| No       | No     | 177                         | 224                         |
| Yes      | Yes    | 24                          | 258                         |
| No       | Yes    | 99                          | 188                         |

Figure 4 shows the bending moment distribution for the case of unsymmetrical spalling. Yielding at the mid span and near the support creates a failure mechanism in the spalling affected span.

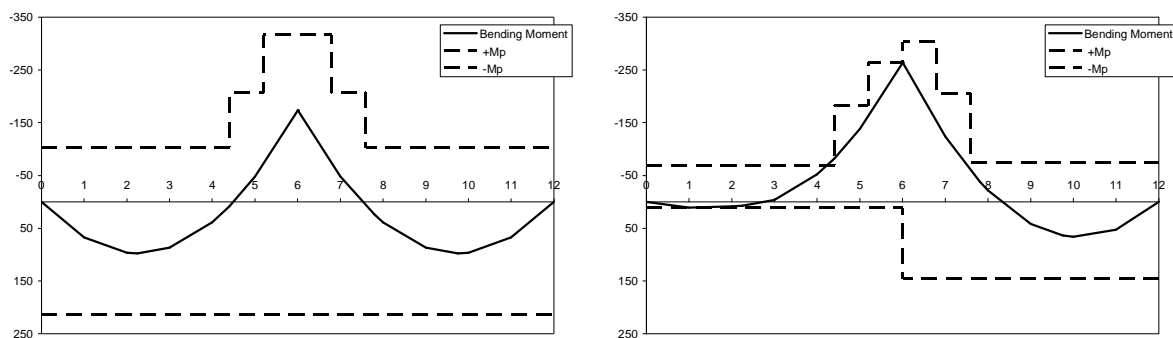


Fig. 4. (a) Ambient BMD (b) BMD at failure

The beam analysed has a 2 hour fire rating according to the requirements of EC2. For the normal design of a single layer of tensile steel failure times in the event of spalling are significant less than prescribed in design. The analysis was repeated using an equivalent quantity of steel but distributed in two layers thus increasing the insulation to 50% of the steel. This simple change significantly increases the performance of the beam.

In both analyses the standard temperature-time curve has been used to define the thermal exposure for the beam. This assumes a uniform thermal exposure along the length and across the width of the beam which, in conjunction with a thermal criterion for spalling predicts spalling affects the entire beam length. In reality this is not the case, because spalling may be localised to regions of high thermal exposure. The effects of localised spalling become more complicated in the case of a continuous multi-span beam or a slab.

## 6 CONCLUSIONS

Explosive spalling is a very complex phenomenon which poses a great threat to structural performance of some reinforced concrete structures in fire. There is a large body of research

concerning the prediction of whether spalling will occur, but rather less research concerning the implications that spalling has for structural performance. Current design guidance for the consideration of spalling is limited thus spalling is largely ignored in the design process of concrete structures despite its potential consequences.

The results of the analysis of a simply supported beam indicate that spalling threatens stability of the structure by exposure of the reinforcement to high and rapidly rising temperatures. It is shown that under exposure to the standard fire, failure times are significantly reduced for both models of spalling (abrupt and progressive spalling).

Multi-span beams perform better due to their ability to utilise alternate load paths. However, in the presented example, extensive spalling still leads to premature failure. More sophisticated calculation methods considering the effects of end restraint are required to better establish performance in fire and spalling. In the future, the study will be extended to consider spalling implications in a finite element mechanical analysis using non-uniform heating definitions for multi-span beams and slabs.

## **7 SUMMARY AND ACKNOWLEDGMENT**

The authors gratefully acknowledge sponsorship and support of the first author by Buro Happold FEDRA Ltd and EPSRC. Thanks are also due to the Royal Society of Edinburgh Lessells Travel Scholarship without which this collaboration would not have been possible.

## **REFERENCES**

1. Hertz, K.D., Limits of Spalling of Fire-exposed Concrete. *Fire Safety Journal*, 2003. 38(2): p. 103-116.
2. Khoury, G.A., Effect of fire on concrete and concrete structures. *Progress in Structural Engineering and Materials*, 2000. 2(4): p. 429-447.
3. BSI, Design of Concrete Structures: General rules - Structural Fire Design. 2004, BSI: London. p. NA to BS EN 1992-1-2:2004.
4. EC2, Design of Concrete Structures; General Rules - Structural Fire Design. 1996, European Committee for Standardisation: London. p. BS EN1992-1-2:1996.
5. EC1, Actions on Structures: General Actions - Actions on Structures Exposed to Fire. 2002, European Committee for Standardisation: Brussels. p. BS EN1991-1-2.
6. Khoury, G.A., Anderberg, Y, Concrete Spalling Review. 2000, *Fire Safety Design*.
7. Jansson, R., Bostrom, L. The influence of pore pressure in the pore system on fire spalling of concrete. in *Structures in Fire - SiF'08*. 2008. Singapore.
8. Davie, C.T., Zhang, H., Pearce C.J., Bicanic, N. Computational modelling of concrete exposed to fire: The effects of coupled hydro-thermal-mechanical behaviour of the development of spalling in concrete structures. in *Structures in Fire - SiF'08*. 2008. Singapore.
9. Akhtaruzzaman, A.A., Sullivan, P.J, Explosive spalling of concrete exposed to high temperature, in *Concrete structures and Technology Research Report*. 1970, Imperial College: London.
10. Simulia, ABAQUS 6.6-2. 2006, Simulia: U.S.A.
11. Buchanan, A.H., *Structural Design for Fire Safety*. 2001: John Wiley & Sons. 444.

## **COMBINED WHILE-DRILLING TECHNIQUES for the assessment of the fire damaged concrete cover**

Roberto Felicetti

Politecnico di Milano, Milano, Italy, roberto.felicetti@polimi.it

### **INTRODUCTION**

Concrete is known to exhibit a good behaviour when submitted to fire, thanks to its incombustible nature and low thermal diffusivity. These qualities guarantee a slow propagation of the thermal transients within the structural elements, but they also trigger very steep temperature gradients within the concrete cover. As a consequence, pronounced variations of the mechanical properties take place in the outer layer of the heated members, making difficult to ascertain the actual depth of the visible damage suffered by the structure.

A number of other properties are affected by the physicochemical transformations experienced by the material, casting the base for the indirect assessment of the effects of fire via the Non-Destructive Testing techniques [1]. Most of these methods are generally meant to smooth the effect of the inherent heterogeneities of the material at the scale of the coarse aggregate, which is also the significant range of the problem at issue. Hence, they can hardly outline more than the average response of the investigated cover layer.

Despite of the possible detriment to the integrity of the structure, a very analytical approach to the assessment of fire damaged concrete is based on the extraction of cores, to be examined as they are (visual observation, colour measurement, ultrasonic scan) or to be cut into slices for subsequent laboratory analyses [1-4]. A number of investigation techniques are available to this latter purpose, involving the mechanical response of each slice (splitting test, punching-load compression, dynamic Young's modulus), their physical and morphological properties (colour, micro-crack density, porosity, air permeability, petrographic and SEM examinations) and their physicochemical features (X-ray diffraction, thermal and chemical analyses). The results pertaining to each slice can then be sorted into a profile depicting the evolution within the concrete cover of the property under study.

This wide assortment of inspection techniques paves the way for the implementation of combined methods, in which an improved accuracy is achieved by properly merging different sets of results. In this perspective, the operation of coring a concrete member can be itself considered as a way of scanning the material soundness at increasing depth, which comes at no cost after having decided to take samples of the deteriorated concrete.

To date, the potential of monitoring the core cutting process, that is a well established practice in geophysical prospection, has not been studied systematically for the assessment of construction materials. On the contrary, several examples of this kind of approach applied to the simple drilling of holes are available in the literature. By means of suitably modified drills, different operational parameters can be surveyed, like the thrust or the torque to be exerted to keep a constant feed rate [5] and the mechanical work spent for a unit penetration of the bit [6]. The attractive pros of this technique are the little time required to run a test, the immediate availability of the results and the limited damage to the member under consideration. Compared to the core extraction, the main limitation is the lack of a material sample to analyse, though the remaining hole and the ensuing ground-concrete powder could be in principle the object of additional investigations.

In this paper a comparison among some drilling and coring resistance indicators is performed first, in order to ascertain the sensitivity of these methods to a steep gradient of the mechanical properties. Further studies aimed to go beyond some limitations of the drilling technique will be also briefly illustrated. Then the potentials of the visual observation of the drilled hole and the of analysis of the ensuing powder are checked, as a way to implement the combination of different assessment techniques even in the absence of an undisturbed concrete sample.

# 1 CORING AND DRILLING RESISTANCE

In order to monitor the process of cutting a concrete core, a common core drill has been fitted with a set of sensors for measuring the rotational speed, the longitudinal stroke, the exerted thrust and the electric power consumption (Fig. 1a). The most significant parameters that can be worked out for revealing the quality of the material are the specific work ( $J/mm^3$  - work per unit notched volume) and the time spent for a unit advance of the tool ( $s/mm$ ).

In a first series of tests, the effect of the working variables (bit diameter, exerted thrust, rotation rate) has been studied by coring some ordinary concrete cubes (side = 150 mm, average cubic strength  $R_{cm} = 50 N/mm^2$  - Fig. 2). At the reference rotational speed (600 rpm), the results show a relatively stable specific work consumption for increasing tool size and thrust (Fig. 2), whereas a concurrent reduction of the drilling time and rise of the electrical power input are observed. The same trends have been recognized by increasing the rotational speed (1250 rpm, not reported here). The slower rotation and the intermediate thrust ( $1.36 N/mm^2$ ) have been adopted in the following series of tests, together with the smallest core bit ( $\varnothing_{int} = 44$  mm), which has the advantage of a minor damage to the investigated member.

The sensitivity of the two cited coring resistance indicators to the mechanical weakening of a deteriorated material has been ascertained on two sets of cubes, made of an ordinary and a lightweight concrete (average cubic strength  $R_{cm} = 50 N/mm^2$  - max aggregate size = 16 mm). The samples have been tested as they were or after being uniformly damaged by way of a slow thermal cycle ( $T_{max} = 200\div 800^\circ C$ , heating/cooling rates =  $0.5/0.2^\circ C/min$ , 1 hour spell at  $T_{max}$ ). Identical samples were used also in other studies in order to compare the effectiveness of a series of ND techniques [1, 7]. Among them, a like method based on the measurement of the drilling resistance via a modified hammer-drill has been also thoroughly deepened (Fig. 1b [6]). A summary of all the results is presented in Fig. 3.

In principle the coring and the hammer-drilling techniques are based on the same micro-fracturing mechanism induced by a hard indenter scratching the concrete surface. However, the diamond-tipped bit of the core drill is fitted with a number of small hard grains, which have the effect of finely milling the material. On the contrary, the bit of a hammer-drill ends with a single large indenter submitted to strong pressure pulses, leading to a deeper propagation of cracks and a coarser fragmentation, especially in stiff and brittle materials like rock and high grade concrete. Hammer-drilling is then far less energy demanding than coring, but a rise of both the drilling work and time can be observed in slightly damaged concretes, when the increased deformability and almost constant fracture energy give way to less efficient penetration mechanisms (plastic crushing and milling rather than chipping [6]).

For this reason, even being the most promising parameter to be monitored in hammer-drilling, the dissipated work proved to be not enough sensitive to low levels of damage. On the other hand, the

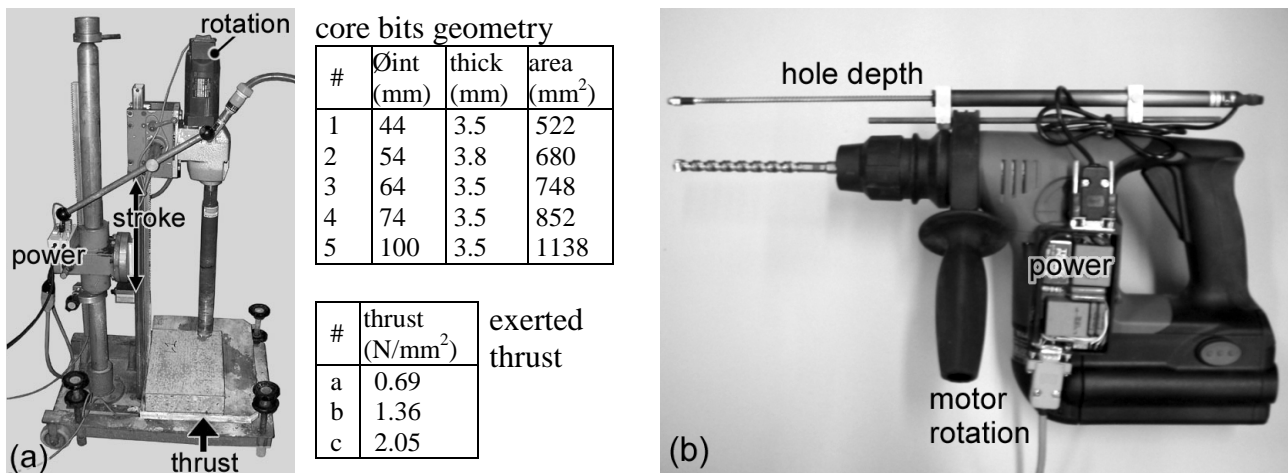


Fig. 1. (a) The core drill fitted with the sensors for monitoring the functioning parameters and investigated variables; (b) modified hammer-drill for measuring the drilling resistance [6].

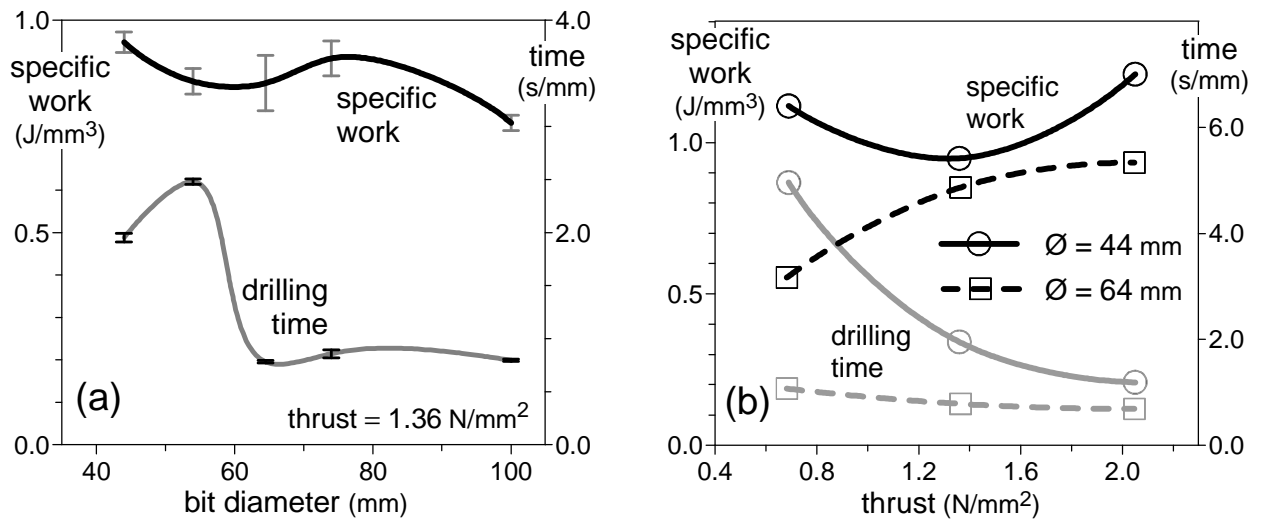


Fig.2 . Results of the preliminary core drilling tests under varying bit diameter and exerted thrust (rotational speed 600 rpm).

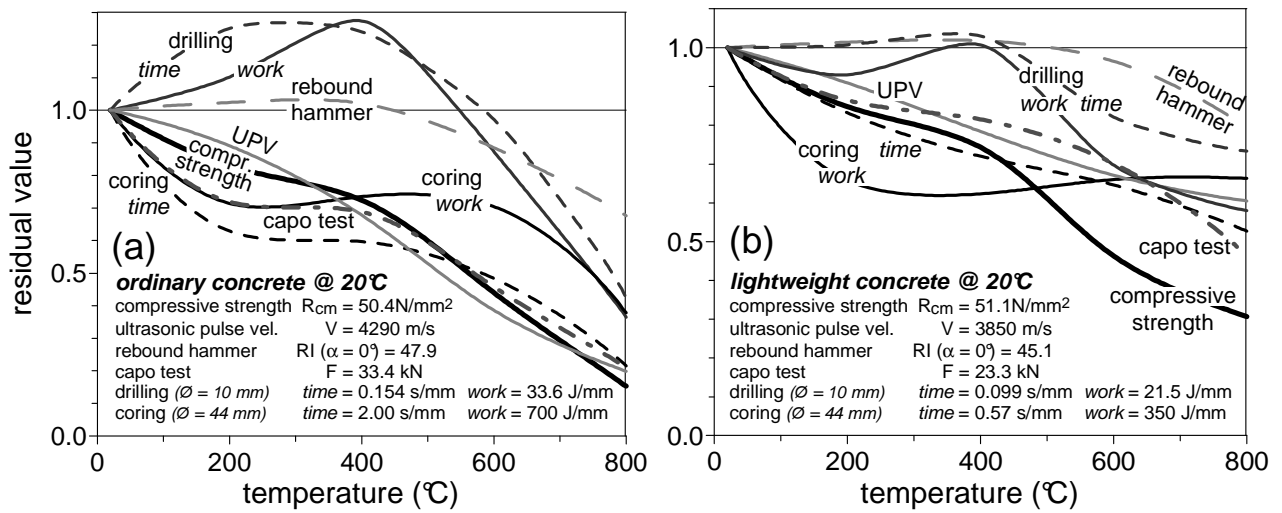


Fig.3 . Sensitivity to a uniform thermal damage of some common ND techniques and of the two drilling methods herein investigated.

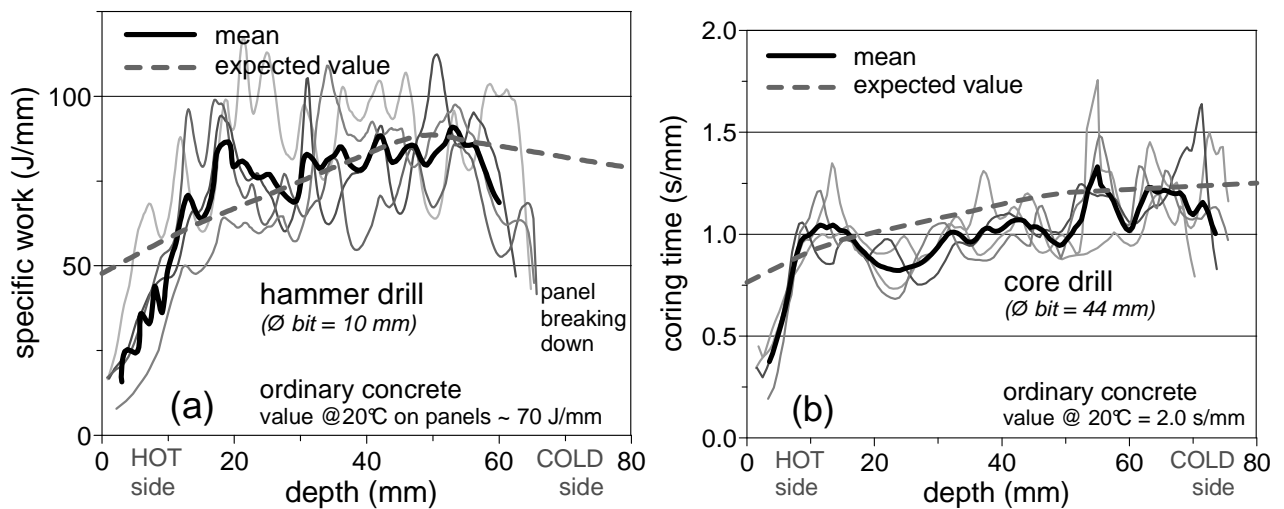


Fig. 4. Profiles of the most significant drilling and coring resistance indicators in the case of a concrete panel exposed to a steep thermal gradient.

elapsed time is the most responsive parameter in core drilling, provided that a careful control of the exerted thrust is performed. The fairly good sensitivity to thermal damage of this latter value can be compared to some well established ND techniques (ultrasonic pulse velocity and capo test) and to the compressive strength itself.

The interesting feature of both the discussed drilling techniques is their ability to continuously scan the material response at increasing depth, even in presence of strong gradients due to the concrete exposure to fire. As an example, Fig. 4 reports the profiles recorded while drilling a ordinary-concrete panel (thickness = 80 mm) that was preliminarily exposed to a steep thermal gradient (675 to 230°C left to right [7]). Based on the maximum temperatures reached in the panel and on the calibration curves of Fig. 3a, the expected drilling resistance profiles have been also worked out for reference. The general good agreement with the measured profiles confirms the reliability of this approach. Other features to be noted are the lower initial resistance due to the settlement of the cutting-tools, the remarkable sensitivity of the core drilling time to low damage levels (a 30% decay compared to unheated concrete is recognized already on the cold side) and the higher influence of the hard aggregate pebbles on the hammer drilling results, which requires to average some tests in order to recognize a clear trend. In the common case of shallow degradation of relatively thick members, a steady resistance value is reached in the end of the drilling process, when the pristine material is inspected. This allows to plot the profiles in relative terms, releasing from the need of specific calibration curves for a first assessment of the damaged depth.

Further studies are in progress, aimed to go beyond the limitation of the hammer-drilling technique in the case of slightly damaged concrete. One direction is focused on the propagation along the bit of the strong pulses induced by the hammering mechanism of the drill. This mechanism (Fig. 5a) is generally based on a crankshaft which activates a cylinder containing a striker (the so called “flying piston”). A quick succession of vacuum and pressure is exerted on the striker on its rebounds against the rammer-bit line, leading to resonance and then considerably boosting the impact energy. The compressive stress-wave generated by the impact propagates towards the tip of the drill bit, where it is partly reflected in the form of a backward tensile stress-wave. This propagation can be effectively captured by means of a couple small dual-grid strain gages glued on the bit shank (Fig. 5b) arranged in a full-bridge scheme and connected to a wide band signal conditioner.

Some preliminary tests have been performed on a concrete block by allowing the striker to drop from 2.2 m height (impact energy = 1 J) on the vertical drill bit and rammer. The results (Fig. 5c) are quite repeatable and in good agreement with those reported in the literature for the case of rock indentation with slender rods [8]. The reflected wave has practically the same amplitude as the incident wave, but the duration and the enveloped area are quite different in the two cases. This is particularly true for stiff and hard materials, being higher the share of impact energy transmitted to the workpiece. The next step will be to monitor the strain-waves propagation during the normal operation of the hammer drill, so to scan the material hardness at increasing depth. The sensitivity of the reflected waves to the material thermal degradation is another open issue to be deepened.

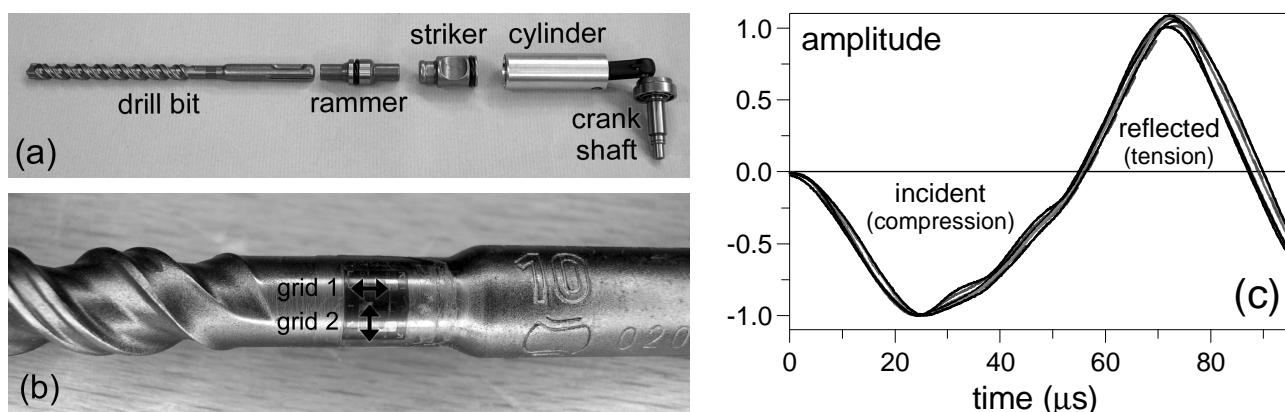


Fig. 5. (a) Components of the pneumatic hammering mechanism of the drill; (b) one strain gauge glued on the bit shank and (c) incident and reflected strain waves induced by one hit of the striker .

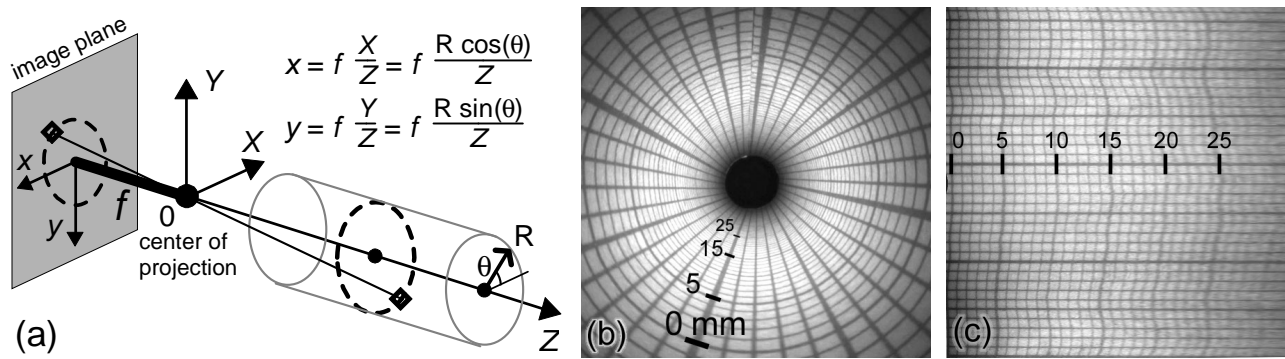


Fig. 6. (a) Endoscopic image projection on the CCD sensor of the digital camera; (b) original and (c) unwrapped views of a rolled graph paper.

## 2 VISUAL INSPECTION OF THE DRILLED HOLES

One advantage of taking a core from a member, compared to hammer-drilling, is the opportunity to observe the extracted samples for ascertaining the material morphology and condition. Nonetheless, the point of view can be reversed by examining the small-diameter drilled holes through an optical endoscope. The limitation of this instrument is to provide a magnified view of a just a small portion of the cavity, making difficult to gather a complete representation of the inner surface and to preserve the geometrical proportion of the observed details. A number of techniques have been proposed, mainly for medical and surgical applications, aimed at the calibration, projection and merging of the endoscope images.

In this study a rather simple approach has been implemented so to allow a first check on the viability and significance of this kind of observation. A rigid endoscope with frontal view and a wide field of vision (100 deg) has been fitted with a digital USB camera, in order to automatically store a series of digital images at regular steps (generally every 10 mm). The images are processed in order to switch from the central perspective to a front view of the unwrapped cylindrical surface of the hole. The transformation is based on the pinhole-model of the image projection on the CCD sensor of the camera (Fig. 6a [9]). By assuming a fixed radius of the hole ( $R = 5$  mm in this case) and a perfect alignment of the endoscope axis, a simple relationship can be established between the coordinates of the cylindrical surface and the pixels on the image plane. After deciding the resolution of the unwrapped image, an array of target coordinates ( $R \cdot \theta_i, Z_j$ ) is converted into image coordinates and the RGB values are determined from the sampled pixels via a cubic-spline interpolation scheme. A proper adjustment of the focal length  $f$  allows to match the longitudinal and the circumferential representation scales, as can be checked on the image of a rolled graph paper (Fig. 6b,c). Finally, the unwrapped frames are merged by means of a software for image editing.

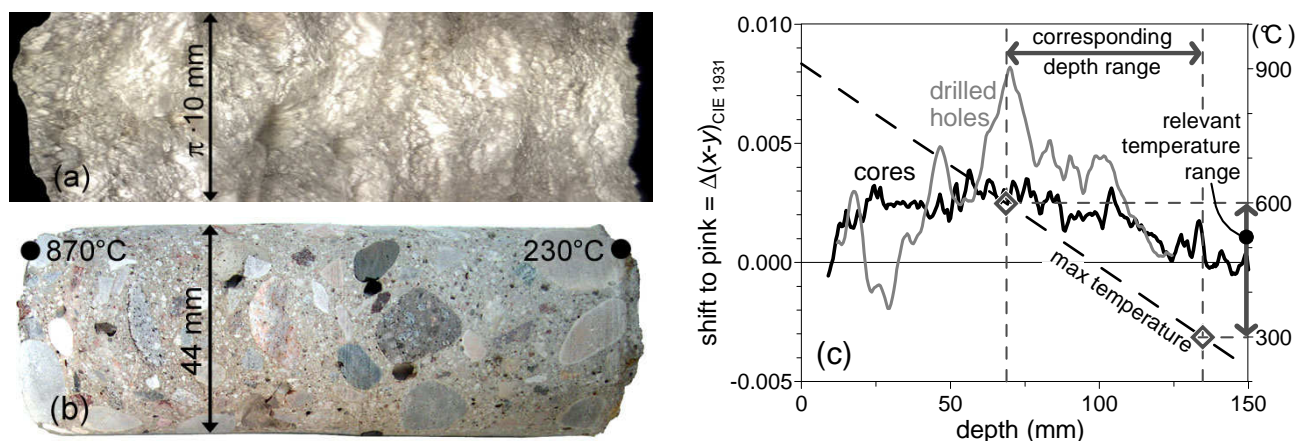


Fig. 7. View of (a) the unwrapped inner surface of a drilled hole and (b) a core taken from the same concrete panel submitted to a thermal gradient; (c) colour alteration profiles within the panel determined via the digital image analysis.

The comparison between the internal image of one hole drilled in a heated concrete panel (Fig. 7a) and the side view of a core taken from the same sample (Fig. 7b) allows to point out the limitations and the potential of this technique. As expected, the limited size of the drilled hole doesn't allow to recognize the material texture nor the shape and nature of the coarse aggregate. Moreover, the significant roughness of the hole produced by hammer-drilling makes the visual recognition of small pores and flaws quite a difficult task.

Nevertheless, some averaged values can still be measured, like the slight discoloration occurring along the hole axis. In a former study, the analysis of the digital images of concrete samples has been regarded as a method for detecting the colour variations induced by the exposure of concrete to high temperature [10]. This technique can be implemented on both kinds of image, though a change of the illuminant generally produces a shift of the chromaticity diagrams (a halogen source and the natural daylight have been used in the two images at issue). However, being significant the colour variation compared to pristine concrete, this bias can be deleted by zeroing the plots in the range pertaining to the undamaged material. It can be observed that the two images provide comparable trends of the pink discoloration which generally affects heated concrete in the range 300-600°C (Fig. 7c). A greater noise characterizes the plot obtained from the drilled hole, which is also more sensitive to the return to whitish-grey taking place at higher temperatures. Far less sophisticated observation techniques are required in case of stronger colour variations, as those produced by the common pH indicators for revealing the carbonation depth.

### 3 ANALYSIS OF DRILLING-POWDER SAMPLES

Several physicochemical analyses on concrete require a preliminary grinding of the material into a fine powder (X-ray diffraction, chloride-ions content, Differential Thermal Analysis, Thermo-Gravimetric Analysis, etc). Moreover, some tests that are normally performed on the intact samples, may be in principle carried out also on the material in pulverized form (carbonation depth, colour measurement, etc).

This evidence casts the base for merging the results of the hammer-drill perforation test and the following examination of the ensuing powder. Compared to the ordinary laboratory practice, the main limitation is the impracticality of controlling whether to include or not the coarse aggregate in the sample, leading to some uncertainties for small diameter holes. In case of steep variations of the investigated properties with the drilling depth, an important requirement is to preserve the order of extraction, so to obtain a sorted sample of powder. Dividing the drilling operation in regular steps is a viable solution to this problem.

In order to check the viability of this kind of test, different types of analysis have been performed on sorted samples of powder obtained by drilling concrete with a 10 mm diameter bit. The first example concerns again the discoloration of heated concrete. By collecting the powder in a transparent test tube, the slight concrete colour variations induced by the exposure to high temperature can be measured via the digital image analysis technique (Fig. 8), as already discussed

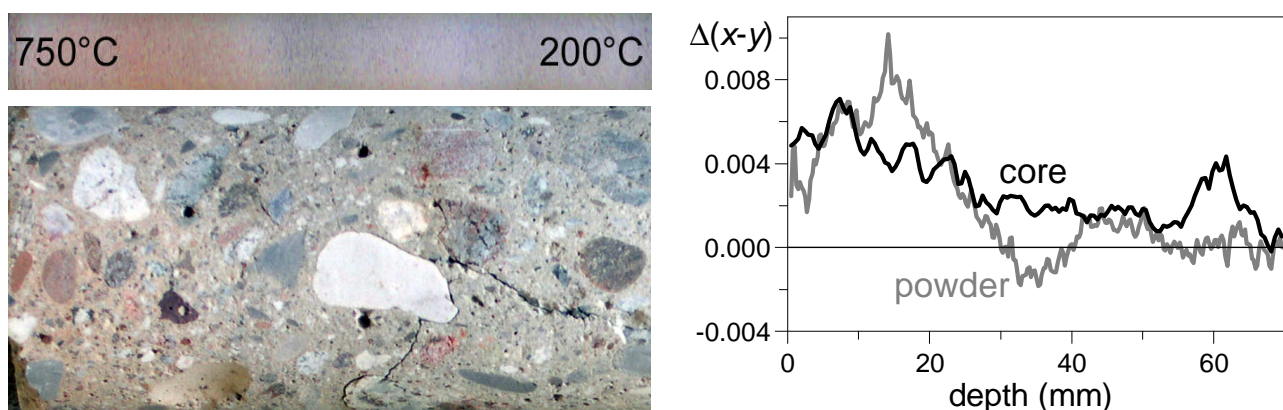


Fig. 8. Discoloration of a powder sample and a core taken from the same heated panel and corresponding colour variation profiles obtained via the digital image analysis.

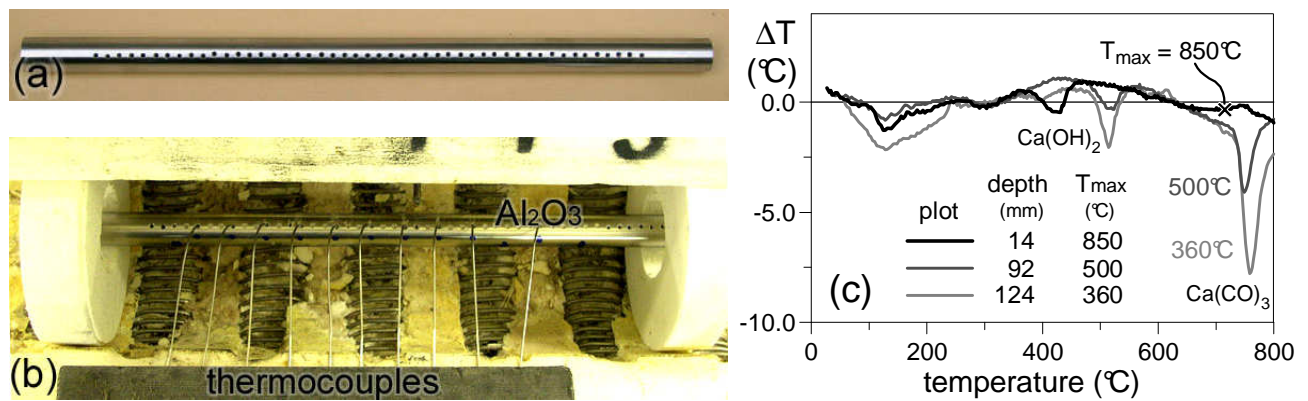


Fig. 9. (a) Nickel-chromium perforated pipe to be filled with a sorted sample of drilling-powder and (b) test setup in the split-tube furnace; (c) temperature differentials pertaining to different depths in a heated panel (see Fig. 7).

in the previous section. After having determined the appropriate scale factor between the hole depth and the length of the powder sample, the discoloration profile can be plotted. Compared to the conventional analysis of cores, an increased noise is observed, probably because of the random influence of the coarse aggregate (see the analogy between Fig. 8 and Fig. 7b). Nonetheless, the relevant features of the material alteration can still be detected.

The second example regards the differential thermal analysis (DTA), that involves the heating a small sample of powdered concrete together with a similar amount of inert material (e.g. aluminium oxide Al<sub>2</sub>O<sub>3</sub>). Both samples are monitored to trace their temperature difference, which ensues from the transformations occurring in the tested material. This method has been proposed as a way for analyzing fire damaged concrete, because during this second heating minor or different transformations should occur until the maximum temperature experienced during the fire is exceeded [11]. In the case a temperature profile through the cover has to be worked out, the DT analysis has to be repeated on a series of samples taken at increasing depth, which is quite a demanding procedure.

In order to overcome this limitation, a sorted sample of drilling-powder has been collected in a metal pipe, together with a small amount of aluminium oxide. The pipe (Fig. 9a) is made of a thermally stable alloy (nickel-chromium) and it is perforated at regular steps along one generatrix so to allow to vent the developing gases and to reach the inner powder with a series of thin shielded thermocouples (1 mm diameter - Fig. 9b). By heating the pipe in a split-tube furnace (5°C/min) several DT analyses can be performed in one take. Though less rigorous than adopting the standard test procedure and a dedicated device, this method is far less time demanding and still allows to detect the onset of the relevant transformations. The first results (Fig. 9c) pertaining to the same panel already mentioned in Fig. 7 seem in good agreement with the trends reported in the literature [11]. The anticipated dissociation of the calcium-hydroxide resulting from the calcium-oxide rehydration compared to unheated portlandite (350-500°C) and the disappearance of the peak ascribable to the calcium-carbonate dissociation (700-800°C) are the main features to trace on the thermo-differential plots.

#### 4 CONCLUSIONS

In this paper the idea to monitor the resistance encountered while drilling a concrete member and then to analyse the ensuing material has been regarded as a combined method for detecting the deterioration of the concrete cover due to fire exposure. In this perspective, the well established practice of analysing the drilled cores can take advantage of this preliminary scan of the material response, which comes at no cost once the acquisition of samples has been planned. On the other hand, the faster and less invasive monitoring of the hammer-drilling resistance, that in principle is not intended to provide any material sample, can be fostered by the analysis of both the ground-concrete powder and the remaining hole. The results obtained in these different directions can be summarized as follows.

The penetration rate of the core bit, at constant exerted thrust, is the most responsive parameter to be monitored while drilling a concrete member. The sensitivity is comparable to other effective ND techniques, with the additional benefit of a point-by-point analysis at increasing depth. As concerns the hammer-drilling technique, the energy spent to penetrate the material is the most significant parameter to be surveyed, with the limitation of a poor sensitivity to low levels of material damage. Further studies are in progress in order to offset this limitation

A valuable support to the visual inspection of the drilled holes is the proper processing of the endoscopic images, aimed to provide a front view of the unwrapped cylindrical surface of the cavity. However, the limited size and the considerable roughness characterizing the holes produced by hammer-drilling make the recognition of the material texture and the detection of any small flaws quite a difficult task. On the contrary, the analysis of more sketchy features like the pink discolouration of heated concrete may still compete with the traditional inspection of cores.

Collecting the powder produced while drilling a member is a convenient alternative to cores in case the laboratory analyses require a preliminary grounding of concrete into a fine powder. The tests concerning the colour alterations and the physicochemical response of the material seem to confirm the viability of this method. The only drawback is the impracticality of controlling the effect of the coarse aggregate, whose local influence may prevail in relatively small drilled holes.

These results are intended as a first check on the viability and significance of the testing techniques herein proposed. A systematic study on the reliability of the most promising methods will be necessary in order to factually merge different test results in the assessment of the fire damaged concrete cover.

## REFERENCES

- [1] Felicetti R., Gambarova P.G., Expertise and assessment of structures after fire, in *Fire design of concrete structures - Structural behaviour and assessment*, Fib Bulletin n.46, 2008, p.64-114.
- [2] Laboratoire Central des Ponts et Chaussées, Présentation des techniques de diagnostic de l'état d'un béton soumis à un incendie, Report ME 62, 2005, 114 p. (in French).
- [3] Short N.R., Purkiss J.A., Guise S.E., Assessment of Fire-Damaged Concrete, *Proc. of the Concrete Communication Conference*, BCA, 29-30 June, 2000, Crowthorn, UK, pp.245-254.
- [4] Dilek U., Leming M.L., Comparison of pulse velocity and impact-echo findings to properties of thin disks from a fire damaged slab, *Journal of Performance of Constructed Facilities*, ASCE, Vol. 21, Nr.1, February 2007, pp.13-21.
- [5] Chagneau F., Levasseur M., Contrôle des matériaux de construction par dynamostratigraphie, *Materials and Structures*, Vol. 22, 1989, pp.231-236 (in French).
- [6] Felicetti R., The drilling resistance test for the assessment of fire damaged concrete, *Journal of Cement and Concrete Composites*, Vol.28, 2006, pp.321-329.
- [7] Colombo M., Felicetti R., New NDT techniques for the assessment of fire-damaged concrete structures, *Fire Safety Journal*, Vol.42, 2007, pp.461-472.
- [8] Li, X., Lok, T.S., Summers, D.A., Rupert, G., Tyler, J., Stress and energy reflection from impact on rocks using different indentors, *Geotechnical and Geological Engineering*, Vol. 19, 2001, pp.119-136.
- [9] Trucco E., Verri, A., Introductory techniques for 3-D computer vision, *Prentice Hall*, 1998.
- [10] Felicetti R., Digital-Camera Colorimetry for the Assessment of Fire-Damaged Concrete, *Proc. Int. Workshop on "Fire Design of Concrete Structures: What now? What next?"*, fib Task group 4.3, 2-3 December, 2004, Milan, Italy, 2005, pp.211-220.
- [11] Alarcon-Ruiz L., Platret G., Massieu E., Ehrlacher A., The use of thermal analysis in assessing the effect of temperature on a cement paste, *Cem. and Concr. Res.*, Vol.35, 2005, pp. 609-613.

## **EXPERIMENTAL ANALYSIS OF CONCRETE STRENGTH AT HIGH TEMPERATURES AND AFTER COOLING**

Eike Klingsch, Andrea Frangi, Mario Fontana

Institute of Structural Engineering, Steel, Timber and Composite Structures, ETH Zurich, Switzerland

### **INTRODUCTION**

Since some years, the cement industry invests in the development of new, environmental friendly blended cement products, like e.g. supersulfated slag cement (SSC). This cement is mainly made out of blast furnace slag, a by product of iron making; hence less energy is used during the manufacturing process and less carbon dioxide is produced compared to Portland cement.

The thermal and mechanical properties of concrete change at elevated temperatures. This change of material properties influences the load carrying and deformation behavior of concrete structures in case of fire. The rate of increase of temperature across the section in a concrete element is relatively slow and inner zones are protected against heat. Therefore reinforced concrete structures with adequate structural detailing like minimum dimensions and cover thicknesses of the reinforcement usually reach a satisfactory fire resistance without any additional fire protection [EN 1992-1-2]. However after the fire has been extinguished the heat penetration into the cross section may continue for hours and is inverted during the cooling phase leading to thermal stresses and cracks [Frangi 2006]. Additionally chemical reactions like the reformation of calcium hydroxide during the cooling phase can widen up micro cracks. The combination of these two phenomena may lead to a significant reduction of the compressive strength of concrete after fire [Hertz 2005]. Investigations carried out by Felicetti and Gambarova [CEB 46] find that the minimum strength is reached after the concrete has cooled down to normal temperature.

For general application of concrete made of supersulfated slag cement, there is a lack of basic knowledge on the mechanical behaviour during and after a fire. A research project on the fire behaviour of concrete made of supersulfated slag cement is currently carried out at the Institute of Structural Engineering at ETH Zurich. The research project aims at enlarging the theoretical and experimental data on the performance of concrete made of supersulfated slag cement during and after a fire. An extensive testing program using the IBK electric furnace is performed to study the temperature dependent loss of strength of concrete and to develop temperature dependent stress-strain relationships for concrete made of supersulfated and other types of cement for a complete temperature cycle (including cooling phase). The stress-strain relationships can be used as material input parameters for finite-element analysis and the development of calculation models.

### **TEST SET UP AND TESTING PROCEDURE**

The tests were performed using an electric-powered furnace that can reach a temperature of up to 1000°C. The attainable heating rate at the concrete surface of cylindrical specimens with a diameter of 150 mm and a length of 300 mm can be up to 4.5 K/min. The furnace consists of two U-shaped shells, allowing the test specimen to be placed in the middle of the oven in a metal cage to protect the furnace in case of concrete spalling.

The concrete specimen is loaded with a hydraulic cylinder. At the contact zones a thin layer of gypsum ensures an even and central force transmission. The test set-up is shown in figure 3.

All tests were carried out within a very short time-frame and the specimens were kept in a controlled climate (20°C/50%) to reduce the influences of concrete age and moisture content. The tests specimens were heated up slowly to the maximum temperature of 300°C, 500°C and 700°C. After maintaining the temperature level for two hours, the test specimens were cooled down linearly. The compressive strength at maximum temperature (hot strength) as well as the residual strength during the cooling down phase and after being cooled down to ambient temperature of 20°C were measured. The general thermal cycle is shown in figure 1. The corresponding target temperatures for the hot and residual strength are given in table 1.

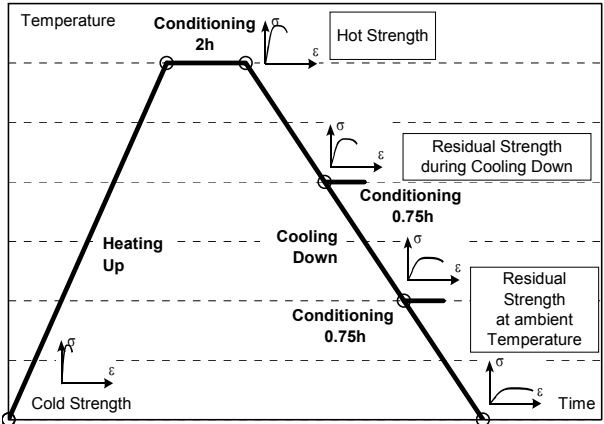


Fig.1 Full thermal cycle

Table 1. Testing Procedure

| Testing Series | Max. Temperature | Tests at target temperature (hot and residual strength) |       |       |      |
|----------------|------------------|---|-------|-------|------|
|                |                  | Hot strength  |       |       | 20°C |
| 1              | 300°C            | Hot strength  |       |       | 20°C |
| 2              | 500°C            | Hot strength  |       | 300°C | 20°C |
| 3              | 700°C            | Hot strength  | 500°C | 300°C | 20°C |

In order to minimize temperature gradients in the cross section and related thermal stresses slow heating up and cooling down rates and a conditioning time of 2h at maximum temperature were chosen. According to test results presented in [CEB 46], the heating up rate can be as high as 5 K/min while the cooling down rate should not exceed 1.0 K/min, higher values reduce the formation of calcium hydroxide, causing a higher residual strength which decreases within days after cooling down. First simple finite element analysis were carried out to predict the maximum heat gradient during heating up and cooling down. According to this first analysis, literature results and preliminary test, the heating up rate at the surface was chosen as 1.5 K/min and the surface cooling down rate as 0.9 K/min. During the entire heating cycle, the concrete was loaded with a maximum pressure of roughly 0.3 MPa which is less than 0.75% of the cold strength; hence, the cylinders can be assumed as unloaded as the concrete’s thermal expansion is not affected by any load effects. The free expansion, internal damages caused by cracks and debonding of the cement matrix lead to a lower hot and residual strength compared to loaded specimens [CEB 46]. A test series with loaded concrete specimens is planned. At the end of the thermal cycle, when reaching the target temperature, the concrete strength was determined inside the furnace. The furnace was not opened; hence the concrete surface temperature remained constant. The load was applied deformation controlled with a constant speed of 0.005 mm/s. The stress-strain curve was continuously monitored and the test was stopped manually post fracture. The concrete cold strength was determined in an analogous manner with the same deformation speed.

After the testing procedure, the specimens were visually inspected with respect to crack formation and spalling. None of the tested concrete specimens showed loose or missing concrete parts caused by spalling. Equalizing the contact zones of the specimens with a thin layer of gypsum lead to proper results, since the fracture pattern was shaped like a truncated cone.

## TEST SPECIMENS

The tests were conducted using cylindrical specimens ( $d=150\text{mm}$  /  $L=300\text{mm}$ ) made of three different concrete mixtures, a superfulfated slag cement (SSC), a Portland-limestone cement (CEM II-A-LL), and an ordinary Portland cement (CEM I). The concrete's mixing properties were identical, apart from the cement used. The cement content was always  $300\text{ kg/m}^3$  with a w/c ratio of 0.55. Common types of carbonate and siliceous aggregates up to 32 mm were used to prepare the test specimens. The fresh concrete density was  $2420\text{ kg/m}^3$ , it decreased to  $2390\text{ kg/m}^3$  during conditioning in  $20^\circ\text{C}/50\%$  atmosphere.

Before concreting, a petro graphic analysis of the aggregates was carried out. The gravel plant is located in the area of an end moraine, hence the main component are based on limestone gravel. The petro graphic analysis shows that roughly 57% of the aggregates consist of carbonate, while 38% of the gravel components are siliceous.

The specimen diameter used in hot material testing, is mostly smaller than 100 mm. These small-scale specimens are insufficient for grading curves with a maximum aggregate size of 32 mm. To ensure adequate compacting of the fresh concrete, cylindrical specimens with a diameter of 150 mm and a height of 300 mm were used.

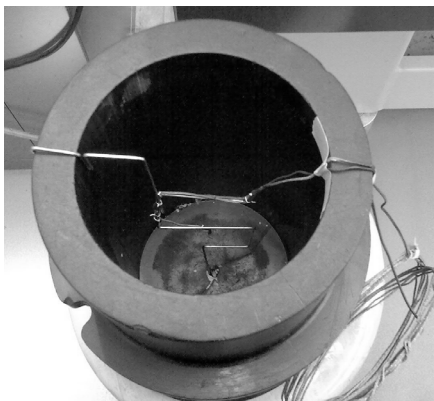


*Fig.2* Thermocouple and formwork

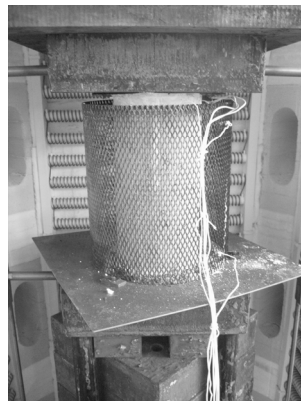


*Fig.3.* Concrete specimen in furnace



*Fig.4.* Concrete specimen after the test

The specimens were produced under laboratory conditions. The facilities were climate controlled with a relative humidity of 65% and a temperature of  $20^\circ\text{C}$ . As formwork, a non-absorbent plastic cylinder was used. Four thermocouples were placed into this formwork before concreting: two in the core, and additionally two in 30 mm depth, as shown in figure 2. The thermocouples had at least a distance of 30 mm between each other, to minimize perturbation due to electric fields. The thermocouples were fixed to a 2 mm welding wire to ensure that the couples will stay in position during concreting and compacting. This set-up followed generally accepted guidelines [ABM 1990].

The concrete was poured into the formwork in two stages and was compacted after each stage using a vibrating table. Striking times and storage conditions for hardened concrete are respected according to [EN 12390]. According to these regulations, the specimens were cured for three days after concreting; they were then placed either in water or in very humid conditions, i.e. temperature of  $20^\circ\text{C}$  and a relative humidity of at least 95% up to the age of 28d from the time of concreting.

According to [EN 1363-1], the specimens have to be conditioned in a dry atmosphere for at least 90d. The surrounding temperature should not exceed  $23^\circ\text{C}$  and the moisture level should be around 50% rel. humidity. All cylinders were stored in a  $20^\circ\text{C}/50\%$  conditioning room; the loss of weight of the concrete was monitored on a weekly basis until the specimen was tested in the furnace. At the time of testing, the specimens showed no significant loss in weight.

## TEST PROGRAM

Table 2 shows the test program carried out. While steps one to four are carried out for all cement types, steps five and six are conducted on a few specimens only. The interim values at step four are determined during cooling down cycle (see figure 1). The first temperature in table 2 (step 4 - right) indicates the maximum temperature, while the second temperature is the temperature for testing during cooling down.

Table 2. Testing Program

| Step | Measured Category                                       | Temperature Level   |
|------|---|---|
| 1    | Cold Strength   | 20°C  |
| 2    | Hot strength  | 300°C ; 500°C; 700°C  |
| 3    | Residual Strength                                       | After concrete cooled down to 20°C from the three hot strength temperature levels from step 2 |
| 4    | Interim Values  | 700°C – 500°C; 700°C – 300°C; 500°C – 300°C   |
| 5    | Slow heating rate<br>(on CEM II-A-LL cement only)       | 500°C – hot strength<br>500°C – 20°C (residual strength after cooling down)                   |
| 6    | Magnetic Resonance Imaging<br>(one CEM I specimen only) | 300°C - 20°C  |

## TEST RESULTS

The tested specimens showed no significant difference in strength at room temperature, the average coefficient of variation was less than 5%. The cylindrical cold strength after 90d was 33.1 MPa for the SSC concrete, 34.3 MPa for the CEM II-A-LL concrete and 40.3 MPa for the CEM I concrete.

During the heating cycle, the temperature at the concrete surface and at the core of the specimen was constantly monitored. It was assured that the average temperature gradient between surface and core during the heating cycle was never higher than 1 K/mm.

The measured stress-strain curves for the SSC concrete tests are shown in figure 5. The left picture includes the cold strength stress-strain curve. The interim values during cooling down are presented as well. It could be observed, that at hot stage, the curves' gradient is monotonic, while at residual stage, the gradient shows one inflexion point. This effect increases with increasing maximum temperature and lower cooling temperatures respectively. This is caused by the loss in bond between the aggregates and the cement matrix during cooling down. The stress strain curves for the CEM II-A-LL and the CEM I cement were similar; the SSC showed higher strains at ultimate load.

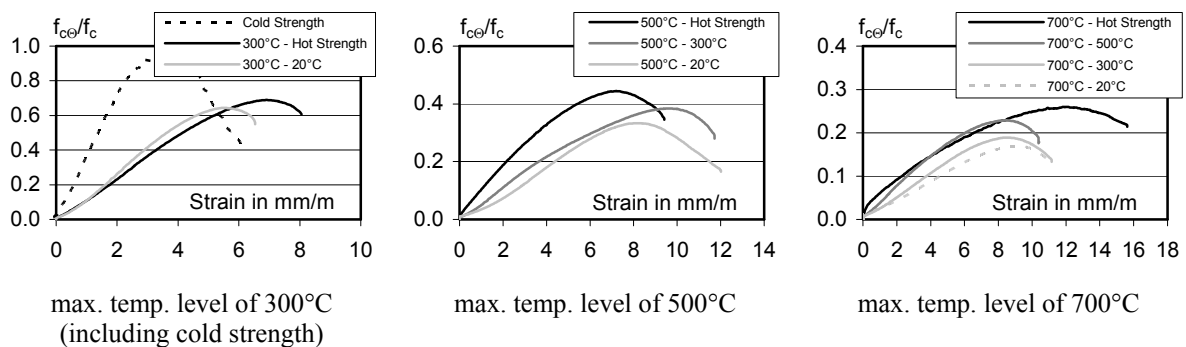


Fig.5. Stress-Strain relation for the SSC concrete for different heating up levels.

Figure 6 shows the reduction factors for hot and residual strength of the specimen with the three different types of cement used. All results are normalized to the corresponding cold strength before testing (cold strength = 1.0). Starting at the relative cold strength of 1.0 at 20°C, the relative hot strength is given by the continuous line, the dots corresponding to the test results at temperature levels of 300°C, 500°C or 700°C. After reaching the maximum temperature level, the loss in strength during and after cooling down is found by following the dotted line to the left until reaching the residual strength at ambient temperature of 20°C after a full thermal cycle.

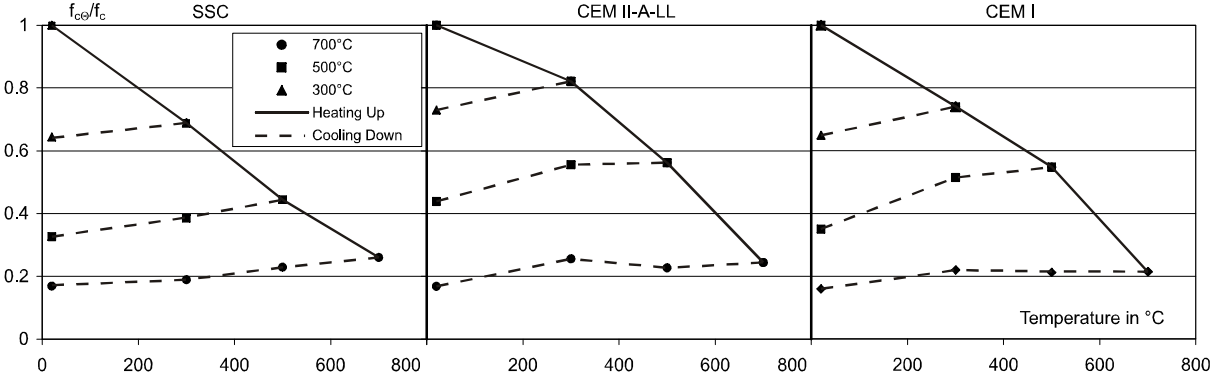


Fig.6. Temperature-Strength relation for three different cements during heating up and cooling down phase

As shown in figure 6, the specimens with SSC show slightly lower hot strength compared to the CEM II-A-LL and CEM I cement at the 300°C and 500°C temperature level. At higher temperature levels, i.e. 700°C, all cements show similar performances. While the loss in strength during cooling down for the SSC was nearly linear CEM I and II show a non-linear residual strength development, with an increased losses in strength while cooling down from 300°C to 20°C.

In general, the losses in strength from hot to residual stage at ambient temperature increase with increasing maximum temperature levels. The concrete specimens cooled down from a maximum temperature of 300°C had an average residual strength of 91% compared to the hot strength. At 500°C it was 72%, and after cooling down from 700°C, the average residual strength was 69%.

**Magnetic resonance imaging**

Using magnetic resonance imaging the entire concrete cylinder was scanned slice by slice. Higher densities of any scanned objects inside the concrete cylinder, like aggregates, are shown in brighter greyscales, hence, cracks, voids and air pores are shown as black lines or dots in the image.

After heating one CEM I specimen up to 300°C, it was cooled down and inspected by magnetic resonance imaging. The main aim was to study crack formation inside the specimen, and to investigate if any loss in bond between the cement matrix and the aggregates occurred. Scans on SSC and CEM II-A-LL samples are planned.

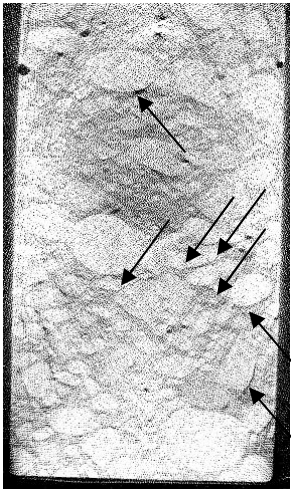


Fig.7. Magnetic resonance imaging

Figure 7 shows that the bond between the aggregates and the cement matrix became loose over the entire cross section. The arrows indicate the zones, where the bond was affected.

## CONCLUSIONS

The results of this first series of test on the hot and on the residual strength of concrete after a fire, including cooling can be summarized as follows:

- The difference in strength at hot and residual stage after cooling down to ambient temperature is significant. The losses in residual strength during cooling down increases with higher temperatures.
- During the cooling down phase, a non-linear material behaviour for CEM I and CEM II is observed.
- Even after cooling down from a moderate temperature of 300°C debonding effects between the cement matrix and the aggregates could be observed by magnetic resonance imaging.
- The supersulfated slag cement (SSC) performs not much different compared to ordinary Portland cement.

## ACKNOWLEDGEMENTS

Thanks to Holcim Group Support Ltd. for the supply of the test specimen.

## REFERENCES

- [Frangi 2006] A. Frangi, C. Tesar, M. Fontana; Tragwiderstand von Betonbauteilen nach dem Brand; Bauphysik 2006; 28: pp. 170–183
- [CEB 46] CEB-FIP state-of-art report bulletin 46; Fire design of concrete structures – structural behaviour and assessment, 2008
- [ABM 1990] ABM-Paper 2A by German Federal Institute for Materials Research and Testing, 1990
- [EN 12390] EN 12390-2:2008; Testing hardened concrete - Part 2: Making and curing specimens for strength tests
- [EN 1363-1] EN 1363-1:1999; Fire resistance tests - Part 1: General requirements
- [Hertz 2005] K. D. Hertz, Concrete strength for fire safety design; Magazine of Concrete Research 2005; 57: p. 445-453
- [EN 1992-1-2] EN 1992-1-2:2004; Eurocode 2: Design of concrete structures; Part 1-2: General rules - Structural fire design

## NUMERICAL ANALYSIS OF CONCRETE COLUMNS IN FIRE Advanced versus simplified calculation methods

Miguel C. Gonçalves<sup>a</sup>, Jean Marc-Franssen<sup>b</sup>, Vitor Abrantes<sup>a</sup> & João Paulo C. Rodrigues<sup>c</sup>

<sup>a</sup> University of Porto, Faculty of Engineering, Porto, Portugal

<sup>b</sup> University of Liège, ArGEnCo, Liège, Belgium

<sup>c</sup> University of Coimbra, Faculty of Sciences and Technology, Coimbra, Portugal

### INTRODUCTION

A column is a structural element whose main function is to support axial forces. When these forces are high, lateral deformation will occur, inducing an increment in the bending moment, known as second order effects. These second order effects have a great effect on the behavior of the column in fire and must be taken into account in fire analysis methods.

Two issues are important in the assessment of the fire resistance of concrete columns: for the resistance, the definition the interaction  $N$ - $M$  diagram of the column, and for the actions, the geometrical and material non-linearity, which are both highly temperature dependent.

The authors describe a simplified calculation method named SimFIRc [1], developed for the analysis of reinforced concrete (RC) columns in fire. The results are compared with those obtained with an advanced calculation method, the finite element program SAFIR, [2]. This program, developed by Jean Marc-Franssen, in the University of Liège, Belgium, can perform the geometric and material non-linear analysis of building elements in fire.

### 1 CALCULATION PROCESS

The evaluation of the behavior of building structures in fire is very easy using numerical modeling. Two types of model are available in the Eurocodes for that purpose: simplified and the advanced calculation models [3].

#### 1.1 SAFIR

The main objective of analyzing structures is to determine the mechanical behavior of a structure until failure. SAFIR has been developed with the specific aim of modeling structures in fire, with an effort having been made to achieve a wider and more general field of application [2].

The software takes the effects of large displacements into account, using a fiber model where the section is divided into fibers. Each fiber is considered to have a different temperature. The mechanical model was based on a 3D Bernoulli beam finite element.

The thermal and the mechanical analyses are performed separately, in that order, which means that the temperature distribution will obviously deeply influence the mechanical response. However the determination of the temperatures in the fire compartment is a prerequisite of this software, and this can be done with the ISO 834 or some other fire curve.

The program has databases of thermal and mechanical properties for steel, concrete and aluminum and several fire curves.

## The thermal analysis

Heat transfer by conduction in solid materials is described by the Fourier equation that is solved in SAFIR according to the standard finite element procedure. The main hypotheses are:

- The materials are isotropic, not submitted to movement, not compressible and have no mechanical dissipation;
- There is no thermal resistance in the interface between adjacent materials.

The local equation describing conduction in solid materials has the form of equation 1 in a Cartesian system of coordinates:

$$K \left( \frac{\partial^2 T}{\partial x^2} + \frac{\partial^2 T}{\partial y^2} + \frac{\partial^2 T}{\partial z^2} \right) + Q - C\rho \frac{\partial T}{\partial t} = 0 \quad (1)$$

Where:

|           |                              |        |   |
|-----------|------------------------------|--------|---|
| $K$       | = thermal conductivity, W/mK | $T$    | = temperature, K                              |
| $x, y, z$ | = coordinates, m             | $Q$    | = internally generated heat, W/m <sup>3</sup> |
| $C$       | = specific heat, J/kgK       | $\rho$ | = specific mass density, kg/m <sup>3</sup>    |
| $t$       | = time, s                    |        |   |

The classical shape functions,  $N$ , are used. If the temperature of Equation (1) is replaced by the approximation  $T = N_i T_i$ , multiplied by a weighting function and integrated into the volume of the element, then:

$$\int_{element} k \{ \nabla N_i \} \{ \nabla N_j \} dv T_i + \int_{element} C \rho N_i N_j dv \dot{T}_i + \int_{element} Q N_j dv = \int_{boundary} N_j q_n dS \quad (2)$$

Where  $\nabla$  means  $\langle \partial/\partial_x; \partial/\partial_y; \partial/\partial_z \rangle$  and  $q_n$  is the heat flux at the boundary of the element.

Finally, when the contributions of all the elements are summed, the matrix (Equation 3) is obtained, describing the equilibrium of heat fluxes in the structure at any given instant of time:

$$[K] \{T\} + [C] \{\dot{T}\} = \{g\} \quad (3)$$

Where:

|       |                          |               |  |
|-------|--------------------------|---------------|--|
| $[K]$ | = matrix of conductivity | $\{\dot{T}\}$ | = vector of temperatures at the nodes                      |
| $[C]$ | = matrix of capacity     | $\{g\}$       | = vector accounting for the heat exchange at the boundary. |

The fact that the thermal properties are temperature dependent is taken into account in equation 3, which expresses thermal equilibrium at a given time.

## The mechanical analysis

The basis of the mechanical analysis of structures that have large displacements is the incremental form of the principal of virtual work. If a total co-rotational configuration is used it as given by equation 4:

$$\int_V (\bar{D}_{ijkl} d\bar{E}_{kl} \delta \bar{E}_{ij} + S_{ij} \delta d\bar{E}_{ij}) dV = \int_V (d\bar{f}_i \delta \bar{u}_i + \bar{f}_i \delta d\bar{u}_i) dV \quad (4)$$

Where:

|               |  |
|---------------|--|
| $V = \bar{V}$ | = the undeformed volume of the element |
|---------------|--|

|                             |  |
|-----------------------------|--|
| $S_{ij}$                    | = tensor of the second Piolo-Kirchoff stress                               |
| $\bar{D}_{ijkl} = D_{ijkl}$ | = tensor defining the incremental constitutive law of the material         |
| $\delta\bar{E}_{ij}$        | = Green tensor of the virtual field of displacement                        |
| $\bar{f}_i$                 | = volume forces  |
| $\delta\bar{u}_i$           | = virtual field of displacements from the deformed position of the element |

In order to solve this equation in a displacement-based finite element formulation, we obtain the matrix equation that governs the iteration from one position to the next position of equilibrium:

$$\int_v B^T DBdVdp + \int_v S^T \delta dedVdp = (K_u + K_s)dp = f^{ext} - f^{int} \quad (5)$$

Where:

|           |   |
|-----------|---|
| $K_u$     | = comprises the linear elastic and the geometric stiffness matrices |
| $K_s$     | = is the stress generated stiffness matrix                          |
| $f^{ext}$ | = nodal forces energetically equivalent to the applied forces       |
| $f^{int}$ | = nodal forces obtained equivalent to the applied forces            |

## 1.2 SimFirC

The SimFIRc model was developed for structural elements of reinforced concrete subjected to second order effects with an axial load. It is inspired by the method of nominal stiffness described in EN 1992-1-1, [4].

But there are two aspects to consider in the evaluation of the fire resistance of a column, in analysis at high temperatures:

- For the resistance of the element it is necessary to calculate the diagram of the bending resistance of one section of the RC column (interaction diagram  $N-M$ ), which depends on a great many parameters, such as considerations of material non-linearity as a function of temperature. This diagram establishes the possible domain of the combinations of actions  $N_{Rd,fi}$  and  $M_{Rd,fi}$  for an RC section subjected to fire at a certain instant of time;
- For the action it is necessary to take into account both geometric non-linearity and material non-linearity (thermal effect). This is accomplished through the method of nominal stiffness.

It will be the intersection of these two curves, calculated for the same instant, that will give the resistance of the column.

The second order effect is calculated with equation 6, which is a function of the first order moment of the critical load and of the load to which the column is subjected.

$$M_{Ed} = M_{0Ed} \cdot (1 + \beta / (N_B / N_{Ed} - 1)) \quad (6)$$

where:

|           |   |
|-----------|---|
| $M_{0Ed}$ | = Design value of first order moment, kN.m  |
| $\beta$   | = $\pi^2 / c_0$ with $c_0 = 9,8$ ; first order moment (parabolic distribution), - |
| $N_{Ed}$  | = Design value of the axial load, kN  |
| $N_B$     | = Buckling load based on the reduction of stiffness, or $N_{cr}$ , kN             |

The main calculation procedure for SimFIRc is shown in Fig. 1:

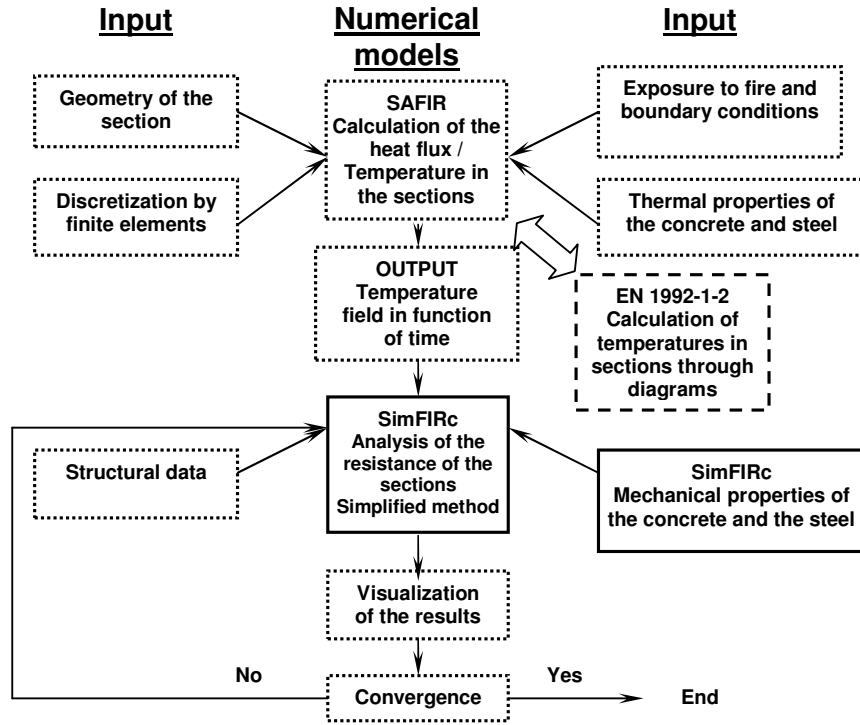


Figure 1. Procedure of calculation of the simplified method “SimFIRc”.

The interaction diagram can be created with the equations of equilibrium (7) and (8) established for a certain instant to which correspond certain temperatures in the reinforcement bars and in each of the six zones of concrete.

$$N_{Rd,fi} = \sum_{i=1}^6 b_{fi} \cdot a_i \cdot f_{cd,fi}(\theta_i, \varepsilon_{c,i}) + \sum_{j=1}^m A_{sj} \cdot f_{sy,fi}(\theta_j, \varepsilon_{s,j}) \quad (7)$$

With  $m$  being the number of reinforcement bars,

$$M_{Rd,fi} = \sum_{i=1}^3 b_{fi} [a_i \cdot f_{cd,fi}(\theta_i, \varepsilon_{c,i})] \cdot \left[ \frac{h}{2} - a_z - \frac{a_i}{2} - a_n \right] - \sum_{k=4}^6 b_{fi} [a_k \cdot f_{cd,fi}(\theta_k, \varepsilon_{c,k})] \cdot \left[ -\frac{a_k}{2} - a_l \right] + \sum_{j=1}^{m(armad)} A_{sj} \cdot f_{sy,fi}(\theta_j, \varepsilon_{s,j}) \cdot z_j \quad (8)$$

$n < i$   
 $l < k$

and  $l$  and  $k$  are the number of concrete zones respectively above and below the center of the section. The other variables are presented in Figure 2.

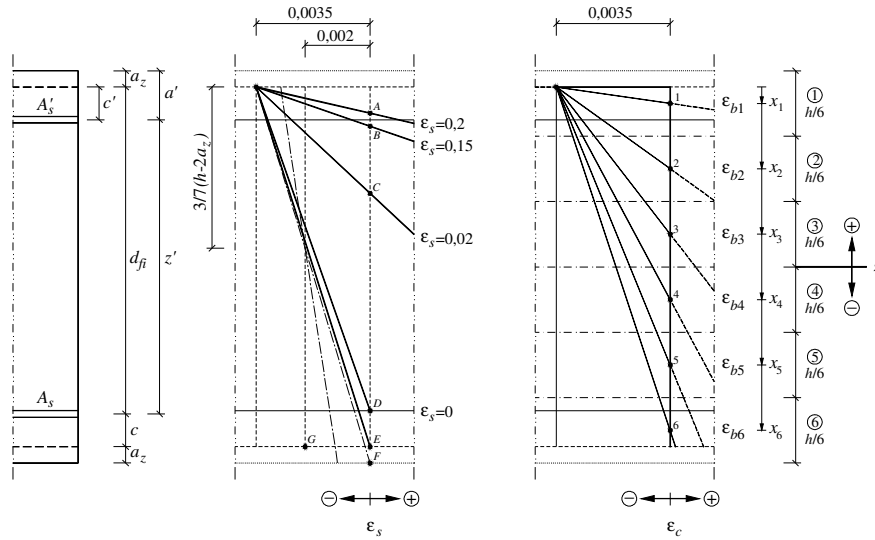


Figure 2. Limit strains in the reinforcement steel bars and in the 6 concrete zones (SimFIRc).

## 2 EXAMPLE

The RC columns analyzed were made of concrete C35/45 with siliceous aggregate and steel reinforcement bars S500 [3].

Figure 3 shows the mechanical boundary conditions and the accidental eccentricities (a trigonometrical function with maximum value of 2cm at middle height) and the application of the axial load in the top of the column (a). The discretization of the finite elements in the thermal analysis at the level of the section (b) is also given.

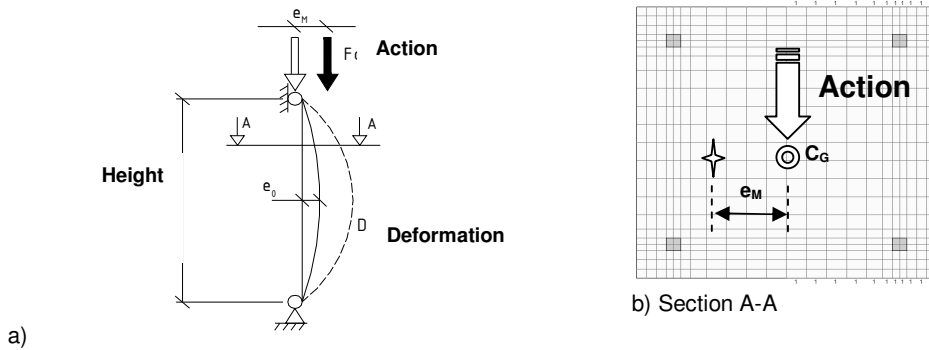


Figure 3. a) Mechanical model; b) Discretization of the section.

### 2.1 Analysis of the results

Figure 4 shows the values of the interaction graphs  $N_{R,fi}-M_{R,fi}$  and  $N_{S,fi}-M_{S,fi}$  obtained by the simplified calculation method (SimFIRc), corresponding to the loadbearing capacity for 30, 60, 90 and 120 minutes (R30, R60, R90 and R120) of an 8 m tall RC column, with a cross-section of 0.3 m x 0.3m and where the distance from the axis of the reinforcement bars to the surface is  $a=4\text{cm}$ , considering steel reinforcement bars with diameters:  $4\phi 12$ ,  $4\phi 16$  and  $4\phi 25$ . The values obtained with the advanced calculation method (SAFIR) are also given.

Figure 5 gives the loadbearing capacity for 30, 60, 90 and 120 minutes of an RC with a cross-section of 0.3m x 0.3m, reinforcement bars with diameter  $4\phi 25$ ,  $a=4\text{cm}$ , and 4, 8 and 12 m tall, using the advanced calculation method (SAFIR) and the simplified calculation method (SimFIRc).

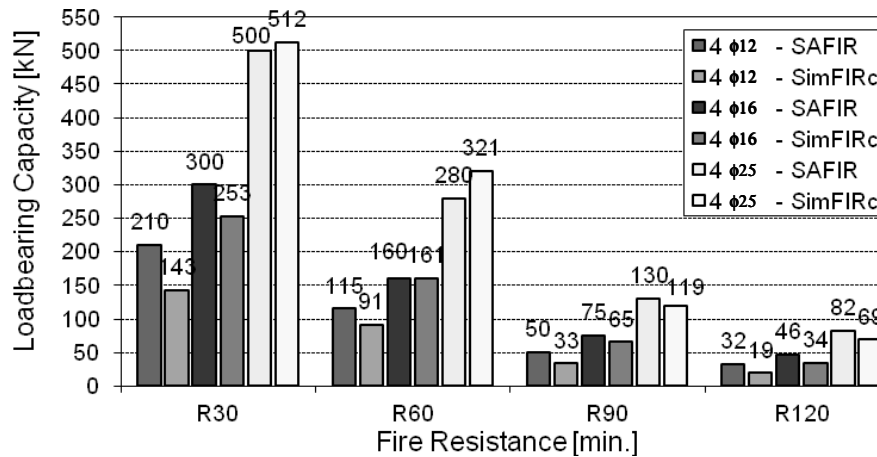


Figure 4. Loabearing capacity of an RC column 8 m tall for different fire resistances.

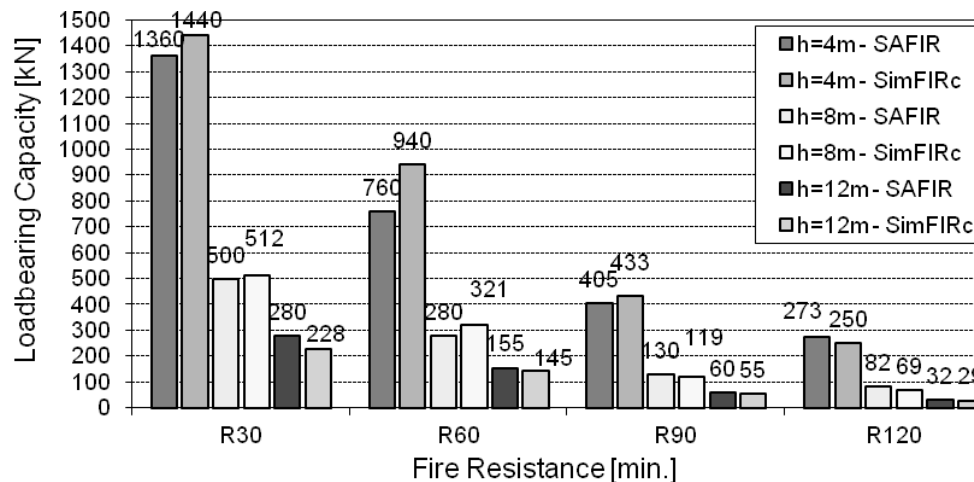


Figure 5. Loabearing capacity of RC columns with 4, 8 and 12 m tall

### 3. FINAL REMARKS

The formulation of EN 1992-1-1 [4] indicated for the calculation of the resistance of concrete sections at room temperature was suitably adapted by the author [1] to the specificity of thermal action (SimFIRc). The results are at the level of the ones obtained with the advanced calculation models (SAFIR), [2]. A relatively simple and powerful tool has been created which provides results on the side of safety.

### REFERENCES

- [1.] Miguel Chichorro Gonçalves, *Fire Behaviour of Structural Concrete Elements – Numerical Analysis and Methodology*, Ph.D. Thesis, Faculty of Engineering of the University of Porto, 2006
- [2.] Jean-Marc Franssen, *SAFIR: A thermal/structural Program for Modeling Structures Under Fire*, Engineering Journal /Third Quarter/2005
- [3.] EN 1992-1-2: *Design of concrete structures, part1-2: General rules - Structural fire design*, European Committee for Standardization, Brussels, 2004.
- [4.] EN 1992-1-1: *Design of concrete structures, part 1-1: General rules and rules for buildings*, European Committee for Standardization, Brussels, 2004.

## **ANALYSIS OF THE BEHAVIOR IN FIRE OF CONCRETE LOADBEARING WALLS**

Miguel C. Gonçalves<sup>a</sup>, João Paulo C. Rodrigues<sup>c</sup> & Vitor Abrantes<sup>a</sup>

<sup>a</sup> University of Porto, Faculty of Engineering, Porto, Portugal

<sup>c</sup> University of Coimbra, Faculty of Sciences and Technology, Coimbra, Portugal

### **INTRODUCTION**

When a fire occurs in a building, the high temperatures developed introduce important thermal and mechanical actions in the loadbearing elements. Walls are loadbearing elements that are greatly affected, due to the large surface exposed to fire. The boundary conditions, especially at the top, will also influence the performance of walls in fire.

The horizontal elements adjacent to the wall, like the slabs and beams, when heated in fire will apply horizontal forces perpendicular to the wall surface. These forces induce important bending moments and shear forces in the cross-section of the wall. At the same time, the structure surrounding the wall restrains its thermal elongation. The imposed forces and the thermal restraint both have a great influence on the reduction of the fire resistance of walls.

This paper presents the results of numerical simulations for the behavior in fire of loadbearing concrete walls restrained in their thermal elongation. The simulations were performed with the finite element program SAFIR [1], developed by Jean Marc-Franssen, in the University of Liège, Belgium, and the simplified calculation method SimFIRb developed by the authors of the paper. The parameters considered in the analysis were the thickness of the wall, the height, the load level, the mechanical reinforcement ratio, the distribution of reinforcement in the cross-section, the number of floors adjacent to the walls and the boundary conditions. Walls that were built in at the base, with the top free or restrained against the horizontal displacement were considered.

### **1 CALCULATION PROCESS**

The advanced calculation model used was the finite element program SAFIR [1], which, in addition to determining the ultimate load bearing capacity of the walls after a certain duration of fire, tracks the behavior of the element during the fire. The calculation process of SAFIR is described in other paper submitted by the same authors to this conference [2]. The simplified calculation model SimFIRb is a new model developed by the authors to evaluate the loadbearing capacity of concrete beam sections in fire [3].

#### **SimFIRb**

The field of temperatures as a function of time can be calculated with the SAFIR model, taking into account the variation of the material properties with the temperature. SimFIRb reads the field of temperatures as input data. The analysis of the bending moment resistance is based on the balance of the forces mobilized in each part of the concrete and the forces mobilized in the steel reinforcement bars (equation 2). Equation 1 makes it possible to determine the height of the concrete compression zone, and consequently the lengths (moment arms) necessary for the calculation of the bending moment resistance in equation 2. The

analysis of the variation of the bending moment resistance of the walls subjected to a certain loading and the standard fire ISO 834, with the time is described by:

$$\sum (f_{sy,\theta_i} \cdot A_{s,i}) - \sum (f_{cd,\theta_j} \cdot A_{c,j}) = 0 \quad (1)$$

$$M_u = \sum (f_{cd,\theta_j} \cdot A_{c,j} \cdot y_j) \quad (2)$$

where:

- $M_u$  - Bending moment resistance for a field of temperatures [kN.m]
- $f_{cd,\theta_j}$  - Design value of the compression strength of the concrete  $j$  at temp.  $\theta_j$  [MPa]
- $\theta_j$  - Temperature of the concrete element  $j$  [°C]
- $A_{c,j}$  - Area of the concrete element  $j$  subjected to compression [m<sup>2</sup>].
- $f_{sy,\theta_i}$  - Value of the effective yield strength of the reinforcement bar  $i$  at temperature  $\theta_i$  [MPa]
- $\theta_i$  - Temperature of the reinforcement bar  $i$  [°C]
- $A_{s,i}$  - Area of the reinforcement bar  $i$  [m<sup>2</sup>]
- $y_j$  - Moment arm of the resulting force of the concrete element in compression,  $j$  [m].

The calculation procedure was as follows:

- 1 - Determine a strain at the level of the center of gravity of the section: initial value  $\epsilon_g=0$ ;
- 2 - Determine a curvature for the section (initial value  $K=1 \times 10^{-5} \text{ cm}^{-1}$ );
- 3 - Once these two degrees of freedom are defined, just vary  $\epsilon_g$  (expression of the diagram of strain in the section) until the resulting normal force, from the corresponding stresses in the section, balances with the acting normal force (which may be other than 0);
- 4 - For the balanced position in terms of normal force, calculate the resulting bending moment;
- 5 - Increase the value of the curvature (initial value of the increment  $\Delta K=2 \times 10^{-5} \text{ cm}^{-1}$ ) and keep returning to point 3 until one of the following conditions is verified:
  - The  $M-K$  enters a plateau;
  - The strains in the concrete and the steel reach limit values;

This process is repeated for each distribution of temperatures in the cross-section, thereby finding the variation of the bending resistance capacity of a section over time (evaluated every 5 minutes).

The iterative process allows the increments, either from the curvature, or from the strain at the level of the center of gravity of the section, to be variable so as to guarantee the desired precision compatible with the discretization of the section with elements.

## 2 EXAMPLE OF CALCULATION

Concrete C30/32, made with siliceous aggregates, and steel S500 were used in the numerical simulations. Walls built in at the base and with the top free or against to the horizontal displacement (Figure 1a and b, respectively) were analyzed.

The structural evaluation finishes with the analysis of a more complex structure (Figure 1c), which is a wall similar to the previous ones but with adjacent building's floors. This wall has two supports, one at the top and other at mid height, corresponding to the floors.

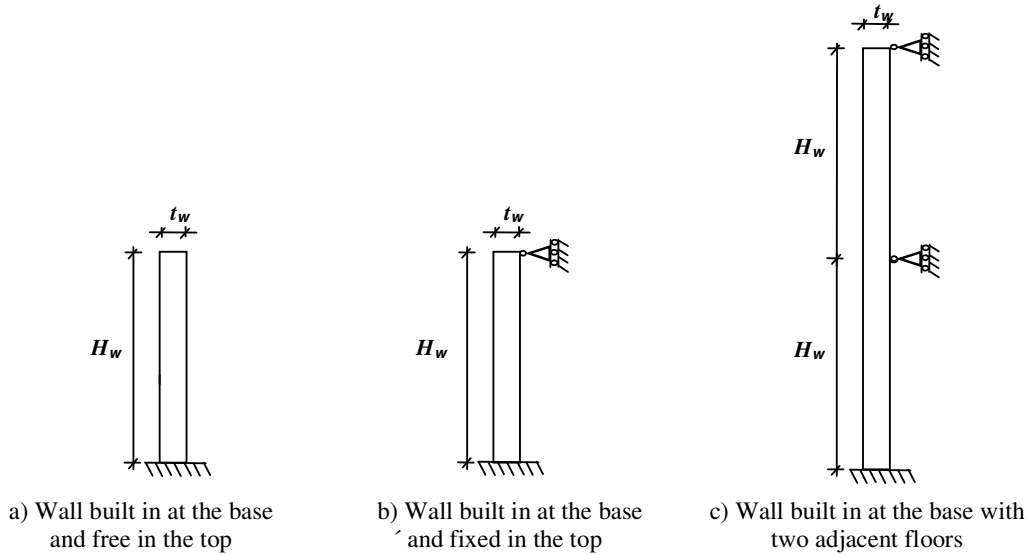


Figure 1. Structural models of the RC walls analyzed.

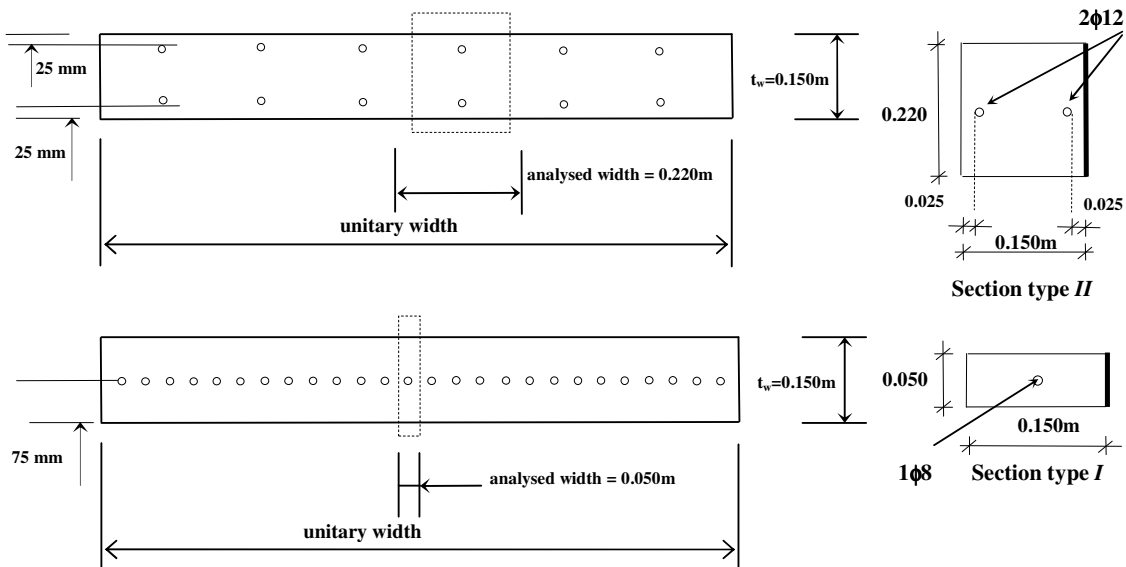


Figure 2. Cross-sections of the RC walls analyzed - sections type.

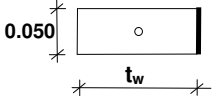
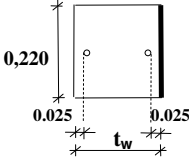
The cross-sections of the walls analyzed in the numerical simulations, thermal and mechanical analyses, are presented in Figure 2. The wall surface was completely subjected to the ISO 834 fire. The type I section is 0.150 m thick, has steel reinforcement bars  $\phi 8$ , spaced 0.050 m

apart. The type II section is 0.150 m thick, two steel reinforcement bars  $\phi 12$ , spaced 0.220 m apart with a 0.025 m concrete covering.

### 3 RESULTS

Simplified calculations were performed in order to determine the expected loadbearing capacity for the sections under analysis. The results are summarized in Table 1.

Table 1 – Bending moment resistance for 0, 30, 60, 90 and 120min, (SimFIRb).

| $t_w$         |  |       |       |       |  |       |            |             |             |  |
|---------------|---|-------|-------|-------|---|-------|------------|-------------|-------------|--|
|               | 0.125   | 0.150 | 0.200 | 0.250 | 0.150   | 0.200 | 0.150      |             |             |  |
| Reinforcement | 1 $\phi 8$  |       |       |       | 2 $\phi 12$   |       | 2 $\phi 8$ | 2 $\phi 10$ | 2 $\phi 16$ |  |
| $t$ [min.]    | $M_{r,fi}$ [N.m]  |       |       |       |   |       |            |             |             |  |
| 0             | 1164  | 1419  | 1948  | 2477  | 6463  | 8897  | 3018       | 4673        | 10323       |  |
| 30            | 1166  | 1419  | 1948  | 2477  | 5745  | 7846  | 2623       | 4144        | 9321        |  |
| 60            | 1081  | 1375  | 1949  | 2477  | 4840  | 6485  | 2150       | 3424        | 7915        |  |
| 90            | 960   | 1288  | 1900  | 2478  | 4000  | 5256  | 1679       | 2730        | 6669        |  |
| 120           | 830   | 1189  | 1820  | 2442  | 2964  | 3915  | 1197       | 1973        | 4964        |  |

Figures 3 and 4 give the results of the horizontal displacement at the top of the built-in base walls for different wall heights and thicknesses (Figure 3) and for a wall 6 m tall, varying the percentage of steel reinforcement for the type I and II sections (Figure 4).

The main conclusions drawn from Figures 3 and 4 are that, qualitative and quantitatively, the horizontal displacements of the wall are inversely proportional to its thickness and the percentage of steel reinforcement.

Figure 5 shows the horizontal displacements at the mid point of the walls built in at the base and fixed at the top, 6, 8 10 and 12 m tall and 0.125 m, 0.150 m, 0.200 m and 0.250 m thick. From this figure it can be observed that the horizontal displacements at mid height increase as the wall height increases and the wall thickness decreases.

Figure 6 presents the results of the bending moment of a wall with two heights (3 + 3 m) and with loads applied at the two floors, corresponding to a certain percentage of the resistance capacity of the wall at room temperature, and not considering buckling. The bending moment below the first support, in the base of the walls with different levels of axial load, varies with time, as shown in Figure 6. The walls subjected to high axial loads exhibit greater variation of the bending moment in all phases of the fire.

For an instant prior to failure, for  $F=0\%$  or  $F=10\%+10\%$ , the largest bending moments are mobilized in the sections mentioned below the first support and in the base of the walls. For higher axial loads, the larger bending moments occur in the section that is immediately below the first support. From Figure 6 it can be concluded that the mobilization of bending moments in these two sections is about double for axial loads of  $10\%+10\%$ .

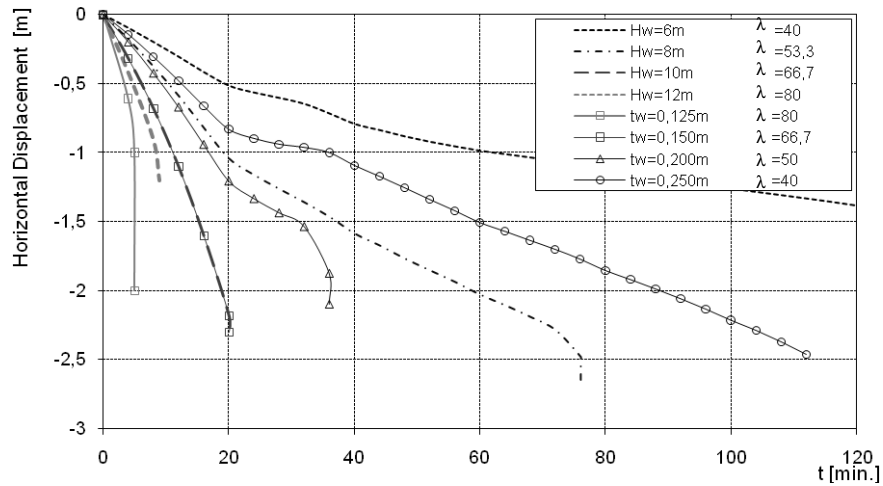


Figure 3. Horizontal displacement in the top of walls built in at the base for different wall slenderness.

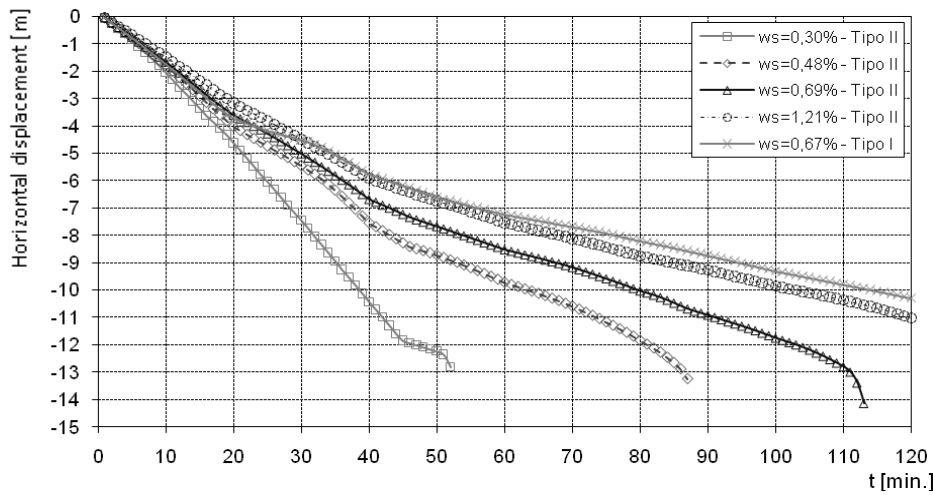


Figure 4. Horizontal displacement at the top of a wall built in at the base, 6 m tall, for different percentages of steel reinforcement.

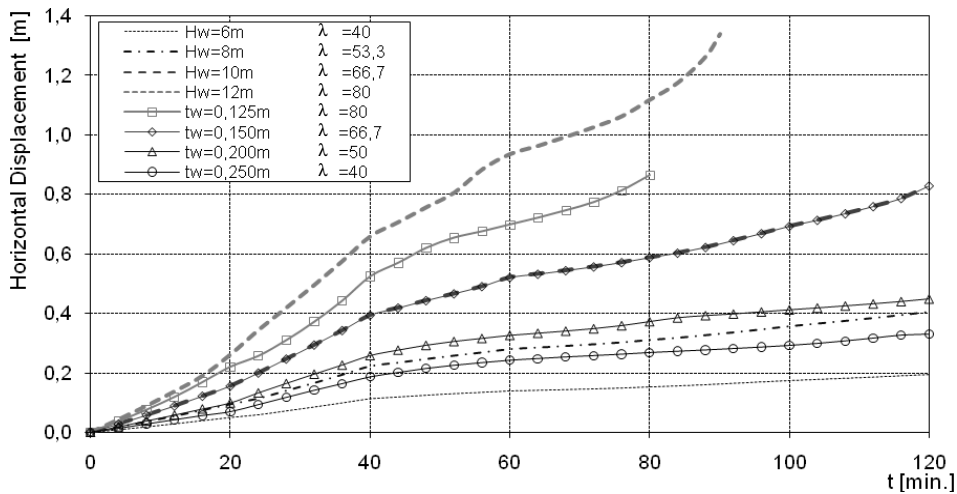


Figure 5. Horizontal displacements at mid height of walls of different heights and thicknesses.

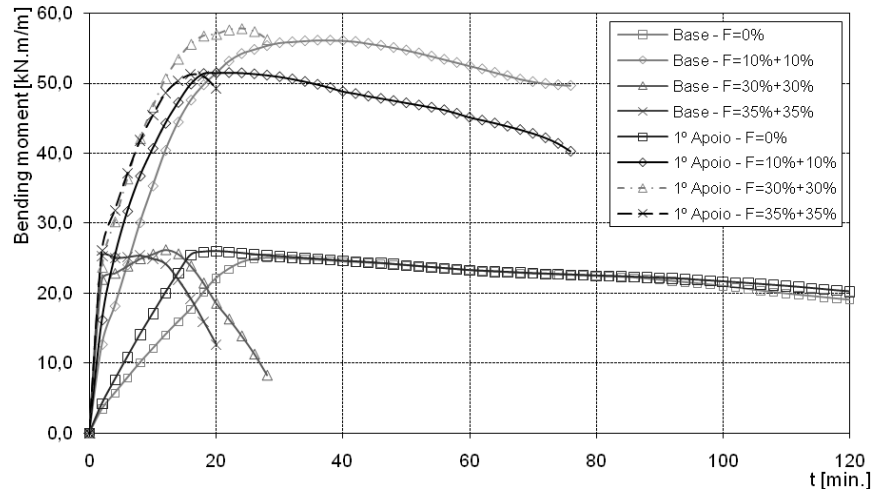


Figure 6. Bending moments at the base and at the first support of walls of 3m+3m tall and subjected to different axial loads

### 3 CONCLUSIONS

The analyses show that the walls only built in at the base reach great horizontal displacements at the top when subjected to the ISO 834 fire. The percentage of steel reinforcement generally used in normal practice in these walls is inadequate for slenderness ratios higher than 50 because it does not provide enough resistance to bending to avoid large deformations. The major deflections of thermal origin generate large bending moments at the base of the wall. Once the foundation of the walls is adapted, the large displacements cause their collapse by yielding of the steel reinforcement at the base of the wall or by buckling.

Walls built in at the base and with a support at the top present small horizontal deformations. The failure mode of those walls varies between the yielding of the steel reinforcement at the base of the wall due to bending, and buckling. This study shows that the fire resistance of these walls decreases with the increasing wall height. As the height of the walls decreases, the imposed horizontal force in the support due to the thermal curvature increases.

### REFERENCES

- [1] Jean-Marc Franssen, SAFIR: A thermal/structural Program for Modelling Structures Under Fire, Engineering Journal /Third Quarter/2005.
- [2] Miguel C. Gonçalves, Jean Marc-Franssen, Vitor Abrantes and João Paulo C. Rodrigues: Numerical Analysis of Concrete Columns in Fire - Advanced versus simplified calculation methods, Application of Structural Fire Engineering, 19-20 February 2009, Prague, Czech Republic.
- [3] Miguel Chichorro Gonçalves, Fire Behaviour of Structural Concrete Elements – Numerical Analysis and Methodology, Ph.D. Thesis, Faculty of Engineering of the University of Porto, 2006.

## **SELF-COMPACTING CONCRETE AT HIGH TEMPERATURE: A CRITICAL SURVEY AND RECENT TEST RESULTS**

Patrick Bamonte, Pietro G. Gambarova

Department of Structural Engineering, Politecnico di Milano, Milan, Italy

### **INTRODUCTION**

Self-Compacting/Consolidating Concrete (SCC) is certainly one of the most innovative materials used today by the Construction Industry, because of its astonishing workability ensured by large amounts of fine aggregates, special additives and fillers, that characterize its mix compared to traditionally-vibrated concrete – VC. SCC is increasingly used in tunnels, bridges, dwelling houses and office buildings, to reduce the labor cost and to increase the safety of the building site, even if stiffer and stronger shutters are required to withstand the higher pressure exerted by SCC during casting.

Many of the above-mentioned structures are often required to face severe environmental conditions, such as high temperature and fire. While the thermal effects on VC have been extensively investigated in the last 20 years (see for instance [1]) and several studies have been devoted to SCCs spalling in fire (see for instance [2]), scanty attention has been paid so far to the mechanical properties of SCCs at high temperature (“hot” properties) and/or after cooling (“residual” properties) [3-7]. Furthermore, comparing the experimental results coming from different sources is not as simple as one may presume, because of the different heating rates, specimen types, and procedures in data treatment and presentation.

On the basis of a recently-completed project on the hot and residual behavior of a family of Self-Compacting Concretes (“limestone” concretes, 2008;  $f_c = 50, 80$  and  $90$  MPa, first part of this paper), a survey on the main results published so far on SCC’s thermo-mechanical behavior is presented in the second part of this paper, to highlight the general trends, to make comparisons with VC and to check the consistency of the tests.

### **1 MIX DESIGN AND TEST MODALITIES**

The mix design of each concrete is shown in Table 1. The binder is a limestone cement in concrete No.1, and a portland cement in concretes No. 2 and 3.

The tests in compression (to measure the  $\sigma_c$ - $\epsilon_c$  curve,  $E_c$  and  $f_c$ ) were performed on cylinders ( $d = 100$  mm;  $d/h = 1/2$  in all specimens). Besides the room temperature ( $T = 20^\circ\text{C}$ ), three “reference” temperatures were adopted ( $T = 200, 400$  and  $600^\circ\text{C}$ ). The temperature  $600^\circ\text{C}$  was considered a suitable target since above this temperature both the compressive strength and the elastic modulus rapidly decrease and above  $700^\circ\text{C}$  calcination is activated.

The tests were displacement controlled. Both the heating and the cooling processes were performed in a furnace ( $T_{\max} = 1000^\circ\text{C}$ ; size of the chamber  $300 \times 500 \times 600$  mm) and the heating rate  $\Delta T/\Delta t$  was limited to  $\pm 1^\circ\text{C}/\text{minute}$ , to avoid dangerous self-stresses.

The tests in 4-point bending made it possible to measure  $f_{ct,fl}$  (tensile strength in bending) and  $G_f$  (fracture energy) in residual conditions [3]. Prismatic, notched specimens were adopted (size:  $a \times b \times L = 150 \times 150 \times 600$  mm; notch at midspan; notch depth / section depth = 0.3).

Table 1. Mix design of the 3 SCCs investigated in this research project.

| Concrete No. and type                                   | 1 – NSC      | 2 – HPC    | 3 – HSC    |
|---|--------------|------------|------------|
| Cement type   | II/A-LL 42.5 | I 52.5     | I 52.5     |
| Cement content (c) [kg/m <sup>3</sup> ]                 | 350          | 480        | 520        |
| Calcareous filler [kg/m <sup>3</sup> ]                  | 130          | 100        | 100        |
| Acrylic superplasticizer/cement                         | 1.2%         | 2.0%       | 2.0%       |
| Water [kg/m <sup>3</sup> ] (w/c)                        | 175 (0.50)   | 168 (0.35) | 172 (0.33) |
| Aggregate/d <sub>a</sub> [mm]/mass [kg/m <sup>3</sup> ] | n/16/1700    | n/16/1600  | n/16/1600  |
| Mass per unit volume [kg/m <sup>3</sup> ]               | 2359         | 2358       | 2402       |
| f <sub>c</sub> [MPa]                                    | 51           | 82         | 90         |

n = natural, round river gravel;  
concrete age at the onset of testing = 180, 90 and 50 days.

As shown in Fig.1a, in the tests at high temperature two specimens were heated in the furnace, after being insulated with a 20 mm-thick rock-wool blanket, to prevent the specimens from cooling too quickly after the extraction from the furnace. In order to keep the insulated specimens at the reference temperature during the tests, the temperature of the furnace was set to values 5-20% higher than the reference temperatures (240, 480 and 630°C, that were maintained for 2-2.5 hours for T = 200 and 400°C, and for 4-4.5 hours for T = 600°C). Then each specimen was placed in turn between the platens of a press (Fig.1b) and was tested. Between the platens and the end sections of each specimen two pre-heated steel cylinders were inserted (thickness 50 mm), to protect the platens from high temperature and to mitigate the thermal shock in the specimens during the early phase of each test (for more details see [3]). During the first 10-15 minutes of each test the temperature of the specimens was rather constant and close to the reference temperature; this time length (past the extraction from the furnace) was more than adequate to move the specimen from the furnace to the press and to carry out the test up to the peak of the load (the tests were displacement-controlled).

In the hot and the residual tests, slightly different set-ups were used for the 3 LVDTs, that measured the relative displacement of the platens.

In Fig. 2 the stress-strain diagrams in compression are shown both in the “hot” and “residual” conditions, as will be explained later.

The tensile strength was measured in residual conditions, both by splitting and in 4-point bending [3]. The latter tests made it possible to evaluate the residual fracture energy, that turned out to an increasing function of the temperature up to 300-400°C, and then started decreasing [3]. As for the tensile strength, the splitting strength was slightly more temperature-sensitive than the flexural strength, but on the whole the strength decay with the temperature was practically the same in both cases.

Also the thermal diffusivity was evaluated by inserting a couple of thermocouples inside the specimen, in the mid-span section [3]. However, no differences were observed with respect to vibrated concretes. The slight increase with concrete grade was confirmed as well.

## 2 STRESS-STRAIN CURVES, PEAK STRAINS AND ELASTIC MODULUS

The stress-strain curves in compression are shown in Fig.3a,b,c (T = 400°C), together with the plots of the strain at the peak stress (Figs.3d,e,f). Since the LVDTs are placed between the press platens and are not directly fastened to the specimens, the measured displacements had

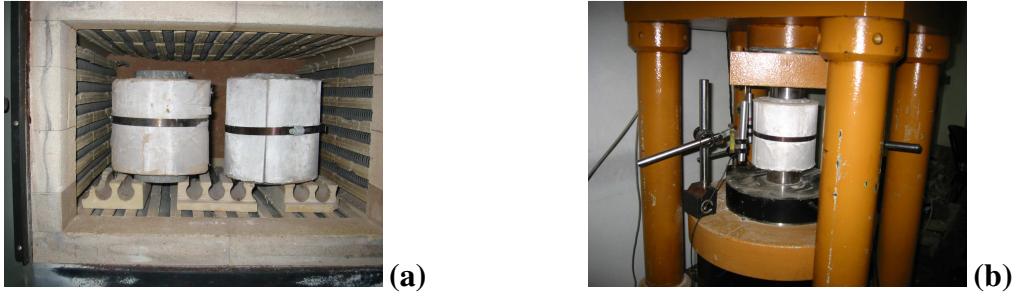


Fig.1. (a) Couple of insulated specimens inside the furnace; and (b) a pre-heated specimen between the press platens, ready to be tested.

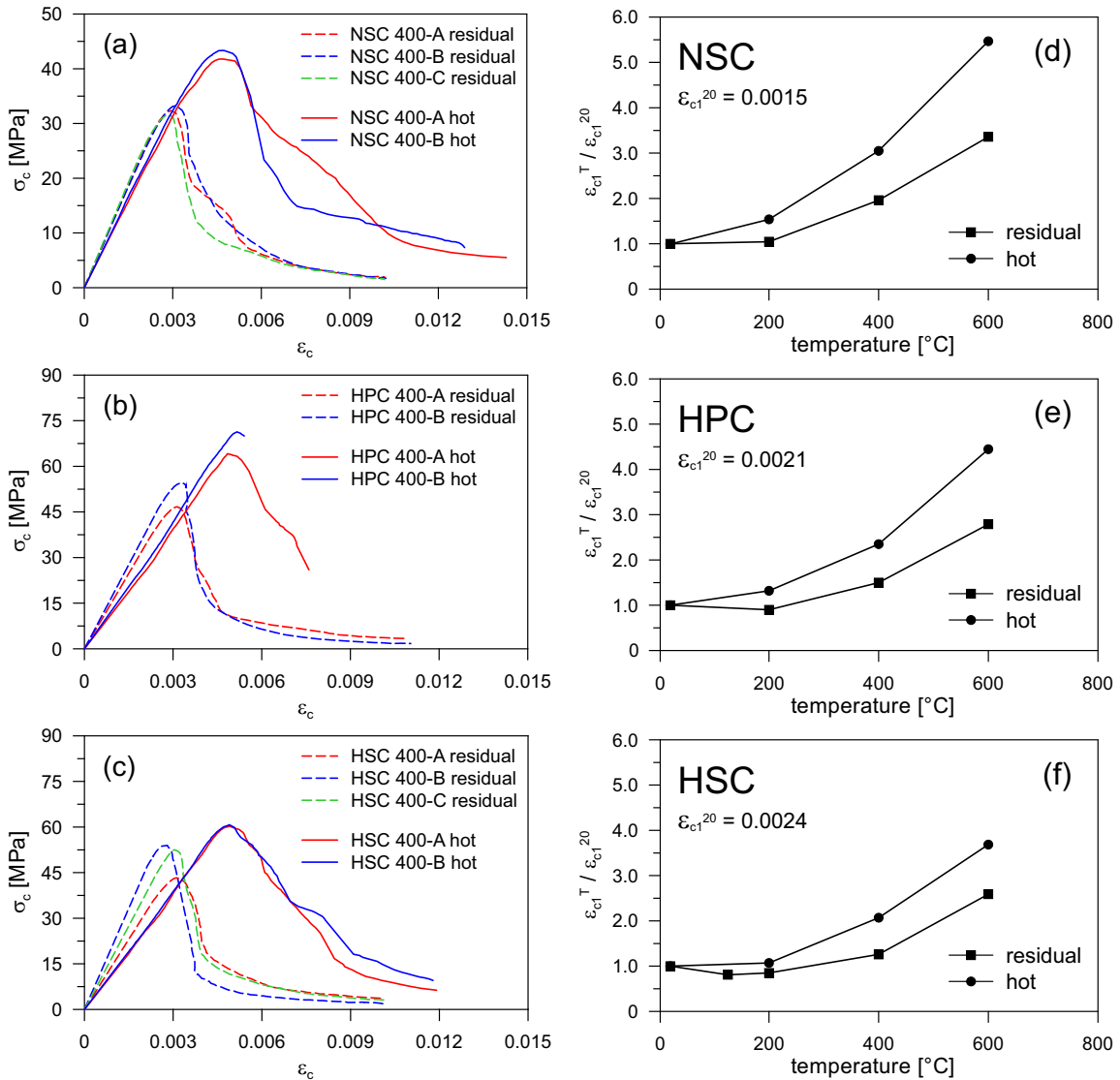


Fig. 2 . T = 400 °C: (a,b,c) Hot and residual stress-strain curves in compression; and (d,e,f) plots of the strain at the peak stress.

to be cleared of the possible disturbances occurring in the end zones. This extra deformability was taken care of by testing a dummy specimen before starting the tests. This procedure was instrumental also in evaluating the elastic modulus.

The relative compressive strength is plotted in Figs.4a,b,c as a function of the temperature. The dashed curves represent the curves indicated by EC-2 for calcareous (top) and siliceous (bottom) concretes. In Figs.4d,e,f, the secant elastic modulus is plotted versus the temperature.

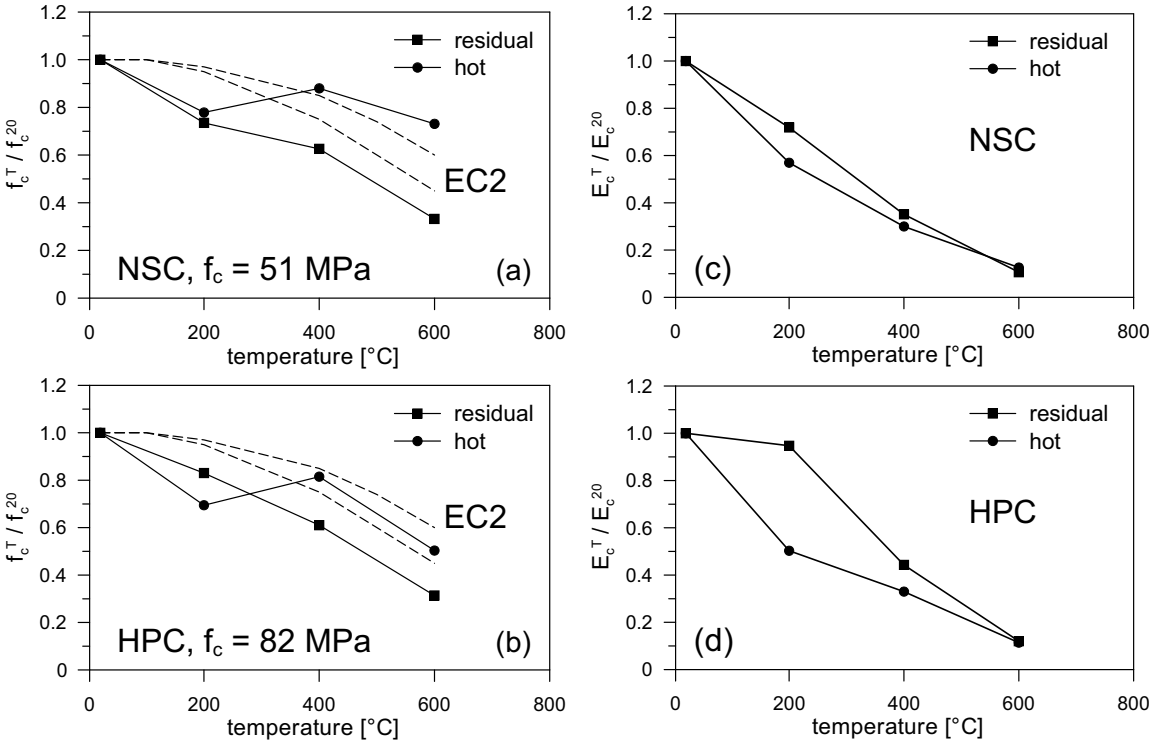


Fig. 3 . SC-NSC and SC-HPC tested in this study: (a,b) normalized compressive strength; and (c,d) normalized elastic (secant) modulus.

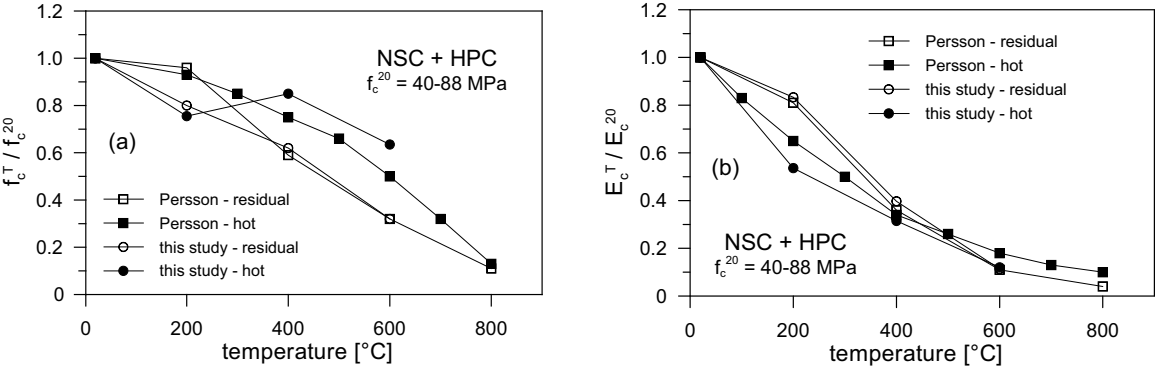


Fig. 4 . Normalized strength (a) and elastic modulus (b): this study and Persson’s results [4].

**3 COMPARISON WITH AVAILABLE RESULTS**

Among the many papers (more than 120) published in 15 international journals in the last 20 years on concrete exposed to high temperature, the authors have found not more than 4 papers dealing with SCC exposed to high temperature and containing well-documented information [4-7]. However, even in these papers scanty results are presented about the “hot” and “residual” stress strain curves in compression, the fracture energy, the tensile strength and the thermal diffusivity. As for the experimental procedures, the heating rate varies between 0.5 and 8°C/minute, the geometry of the specimens is either cylindrical or cubic, the cylindrical

specimens are either cast in a formwork or cored from cubic specimens, the mix designs are different and the materials are NSCs and/or HPCs in the various experimental campaigns. In the following, the main results presented in the four above-mentioned papers are recalled.

- Persson [4],  $\Delta T/\Delta t = +4/-1^\circ\text{C}/\text{minute}$ ,  $T = 20, 200, 400, 600, 800^\circ\text{C}$ , cylindrical specimens,  $f_c = 40\text{-}88$  MPa; hot and residual tests; total number of the mixes 16 (4 VCs and 12 SCCs with/without pp fibers). Here reference is made to 10 SCC mixes (8 with blended cement = limestone cement, and 2 with portland cement, all containing a limestone powder); the aggregates were crushed gneiss and granite. The comparison between the results of this project (SC-NSC and SC-HPC) and Persson's results concerns the mean values of the compressive strength and of the elastic modulus. The agreement is satisfactory above  $400^\circ\text{C}$  for the compressive strength (Fig.4a), with no sizable differences compared to VC (EC-2); the agreement is very good indeed for the elastic modulus (Fig.4b).
- Sideris [5],  $\Delta T/\Delta t = +5^\circ\text{C}/\text{minute}$ ,  $T = 20, 100, 300, 500, 700^\circ\text{C}$ , cubic specimens,  $R_c = 42\text{-}75$  MPa; residual tests; total number of the mixes 8 (4 VCs and 4 SCCs, without fibers), all containing blended cement and crushed granite aggregates. Here reference is made to 2 SCC mixes and 1 VC mix ( $R_c = 54, 55$  e  $62$  MPa). The comparison with the results of this project concerned the normalized compressive strength of the SC-NSC (Fig.5a). The agreement is rather good. (Sideris' results were corrected, since the ratio of the compressive strengths measured on cylinders and cubes depends on the temperature).
- Noumowé et al. [6],  $\Delta T/\Delta t = +0.5/-0.5^\circ\text{C}/\text{minute}$ ,  $T = 20, 400^\circ\text{C}$ , cylindrical specimens,  $f_c = 75\text{-}81$  MPa; residual tests; total number of the mixes 4 (2 VCs and 2 SCCs, with/without fibers, all containing silica fume and calcareous aggregates). Here reference is made to 3 mixes, the first (called "HSC",  $f_c = 75$  MPa) without fibers, the second (called "HSC-F",  $f_c = 79$  MPa) with pp fibers, and the third (called "SC-HSC-F",  $f_c = 76$  MPa) with pp fibers,  $\square\triangle\lozenge$  in Fig. 5b. The comparison with the results of this project (mean values for SC-NSC and SC-HPC) was limited to  $T = 400^\circ\text{C}$ ; the agreement is good (Fig.5b).
- Reinhardt and Stegmaier [7], ( $\Delta T/\Delta t$  variable between 2 and  $8^\circ\text{C}/\text{minute}$ ),  $T = 20, 500\text{-}600^\circ\text{C}$ , short cylindrical cores,  $R_c = 33\text{-}76$  MPa,  $f_c = 30\text{-}68$  MPa, residual tests; total number of the mixes 9 (8 SCCs and 1 VC, no fibers). Here reference is made to 5 SCC mixes ( $f_c = 50\text{-}76$  MPa, two with  $f_c \cong 53$  MPa -  $\blacksquare$ , and three with  $f_c \cong 72$  MPa -  $\blacktriangle$  in Fig. 5b), containing quartzitic aggregates, fly ash and a calcareous powder; two mixes contained also a viscosity agent.

The cylinders were cored out of large cubes (side 300 mm) subjected for 120 minutes to the standard fire (ISO 834). The length of the cylinders was reduced to 100 mm ( $h/\varnothing = 1$ ) by cutting off the extremities that were subjected to very high temperatures ( $T_{\max} = 1038^\circ\text{C}$ ). According to the numerical analysis performed in this study, the average temperature reached in the core of the cubes  $T_{\text{av}}$  was comprised between  $450$  and  $500^\circ\text{C}$  (in [7] a higher temperature was declared =  $720^\circ\text{C}$ ). The values of the strength measured in [7] were corrected to take care of the differences between "short" cylinders ( $h/\varnothing = 1$ , whose strength is close to that of cubic specimens) and "long" cylinders ( $h/\varnothing = 2\text{-}3$ ). Even if the results shown in [7] are doubtful, the agreement is very satisfactory (Fig.5b).

## CONCLUDING REMARKS

The closeness of the mechanical behavior of Self-Compacting Concrete to the behavior of Vibrated Concrete at high temperature is confirmed by this study, where SCC is shown to

exhibit a markedly linear loading branch in compression and a rather steep softening branch, at any temperature.

The closeness of SCC and VC at high temperature is confirmed by the satisfactory agreement with the results found in the literature, in terms of hot/residual strength and elastic modulus, in spite of the differences concerning concrete mixes, specimen types, heating ramps and concrete grades.

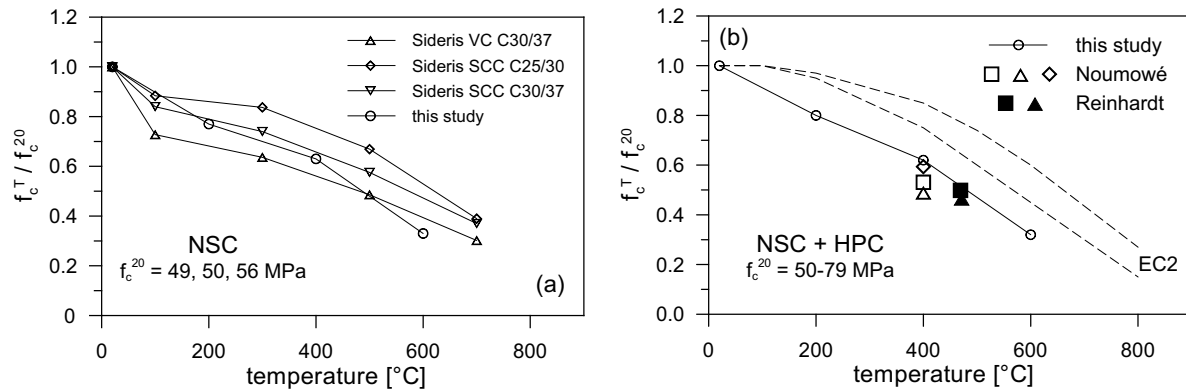


Fig. 5. This study and Sideris' results [5] (a); and this study and Noumowé's + Reinhardt and Stegmaier's results [6,7] (b), ■  $f_c^{20} = 53$  MPa; ▲  $f_c^{20} = 72$  MPa.

## ACKNOWLEDGEMENTS

This project was jointly financed by CTG-Italcementi (Bergamo, Italy) and by the Italian Ministry of Higher Education within the National Project-PRIN 2006 "Optimization of Construction Methods and Materials in Tunnel Linings".

## REFERENCES

- [1] Felicetti R. and Gambarova P.G. Effects of High Temperature on the Residual Compressive Strength of High-Strength Siliceous Concretes. *ACI-Materials Journal*, Vol.95, No.4, 1998, 395-406.
- [2] Jansson R. and Boström L. Experimental Investigation on Concrete Spalling in Fire. *Int. Workshop "Fire Design of Concrete Structures: What now? What next?" - fib Task Group 4.3*, ed. by P.G. Gambarova, R. Felicetti, A. Meda and P. Riva, publ. by Starrylink (2005, Brescia, Italy), Milan (Italy), December 2004, 109-113.
- [3] Bamonte P., Felicetti R. and Gambarova P.G.: "Mechanical Properties of Self-Compacting Concrete at High Temperature and after Cooling", *Proc. of SCC 2008 - 3<sup>rd</sup> North American Conf. on the Design and Use of SCC : Challenges and Barriers to Application*, Chicago (USA), November 2008, 6 pp. (in press).
- [4] Persson B. Fire Resistance of Self-Compacting Concrete – SCC. *Materials and Structures-Matériaux et Constructions*, Vol.37, No.11, 2004, 575-584.
- [5] Sideris K.K. Mechanical Characteristics of Self-Consolidating Concretes Exposed to elevated Temperatures. *ASCE-J. of Materials in Civil Engineering*, Vol.19, No.8, 2007, 648-654.
- [6] Noumowé A., Carré H., Daoud A. and Toutanji H. " High-Strength Self-Compacting Concrete Exposed to Fire Test", *ASCE Journal of Materials in Civil Engineering*, Vol. 18, No. 6, 2006, 754-758.
- [7] Reinhardt H.W. and Stegmaier M. Self-Consolidating Concrete in Fire. *ACI-Materials Journal*, V.103, No.2, 2006, 130-135.

## THE EFFECT OF ELEVATED TEMPERATURES ON AERATED CONCRETE BLOCKS

BRIAN HARDIE<sup>1</sup>, ALI NADJAI<sup>1</sup> & FARIS ALI<sup>1</sup>

University of Ulster, School Built Environment, FireSERT, Belfast, United Kingdom [brianhardie45@hotmail.com](mailto:brianhardie45@hotmail.com)

**KEY WORDS:** - Concrete Blocks, Elevated Temperatures, Mechanical properties

### INTRODUCTION

The tests were part of ongoing experimental research in walling systems at elevated temperatures being carried out at the University of Ulster FireSERT. In the event of a fire, masonry walls in buildings serve as a fire barrier in addition to their architectural and structural functions. Often the subdivision of a building into isolated compartments is achieved by masonry walls in conjunction with fire resisting floors above and below. The dominant factors are the thermal, physical and chemical properties of the constituent masonry units and the joint mortar, the dimensions of the walls, the end restraints and the load conditions.

The role of a single leaf masonry wall in a fire situation is generally seen to be three fold:

- a) Firstly a load bearing wall must provide structural stability to prevent collapse. This provision is termed structural adequacy
- b) The wall is required to maintain integrity, i.e. prevent the passage of flame from one side of the wall to the other, in an attempt to compartment the fire.
- c) The wall must provide adequate insulation properties to prevent excessive temperature on the unexposed face creating further spread of flame.

It is well known that due to their low thermal conductivity [1], masonry walls will experience highly non-linear temperature gradients through their thickness, when subject to fire on one side of the wall. This non-linear temperature will, due to plane-sections-remaining-plane, induce internal thermal stresses [2-3]. To develop performance –based fire design methods, these thermal stresses, together with mechanical stresses (and the influence of transient strains for concrete blocks) need to be estimated and the structural response determined. In order to reliably model walls subjected to fire the mechanical properties at discreet points (temperatures) through the thickness of the wall are required [4].

## SPECIMENS AND TESTING EQUIPMENT

Testing procedures were carried out where 15 specimens of aerated concrete block were observed there conduction, and compressive strength at elevated temperature was recorded. The heat flow from one pre loaded and one unloaded specimen was also recorded using infra red camera.

These results were benchmarked with  $5\text{N/mm}^2$  and  $7\text{N/mm}^2$  concrete blocks as well as previously tested prism testing [5]

### Specimen sampling and preparation

The specimens were assembled from lightweight aerated block of  $3.6\text{N/mm}^2$  crushing strength. The blocks are constructed utilising pulverised fuel ash, a by product from coal powered electrical generation plant they are very light weight and fuel efficient thus making them particularly attractive material in terms of fuel efficiency, recycling of waste materials, and manual handling. The blocks were selected at random from suppliers and no particular conditioning was carried out prior to the tests. Mortars were mixed utilising ordinary Portland cement, sand and water. The cement and sand was mixed in the portions measured by volume. The water was added to a consistent workable mix and was measured in proportion to the cement, giving a water to cement ratio of 1 to 2. All test samples were placed in the laboratory with a background heat maintaining at least  $5^\circ\text{C}$  for 28 days prior to the test, allowing any excess moisture build up to evaporate and the initial 28 day strength of the mortar to be achieved.

### Large scale envelope testing

In order to determine the compressive strength at elevated temperatures 15 tests were carried out utilising the 2.5MW gas furnace figure 3 which has an exposed area of 1.5m in length x 1.5m in height. Samples were constructed in the form of three blocks 210mm in length by 100mm in depth, constructed on top of each other thus forming a column. The mortar mix and curing was identical to the prism samples with a 1 in 4 cement sand mix being adopted.

The samples top block was drilled to accommodate thermo couples every 25mm into the blocks. Additional thermo couples were placed, two on the surface exposed within the furnace and one on the unexposed face. The samples were placed in a rig detailed (figure 1 and 2) and connected to the furnace. Hydraulic rams were connected to a compressor which had its pressure, prior to the testing, calibrated using a calibration device. 13 of the samples were pre loaded to one third of the designed service load. The time/temperature curve adopted for the furnace was to IS0 834. Once the resultant temperature was attained, the burners in the furnace were switched off and the pressure induced via the hydraulic rams. The failure compression was recorded together with any observations on the type of failure



*Fig.1. Testing equipment*

## Testing equipment used

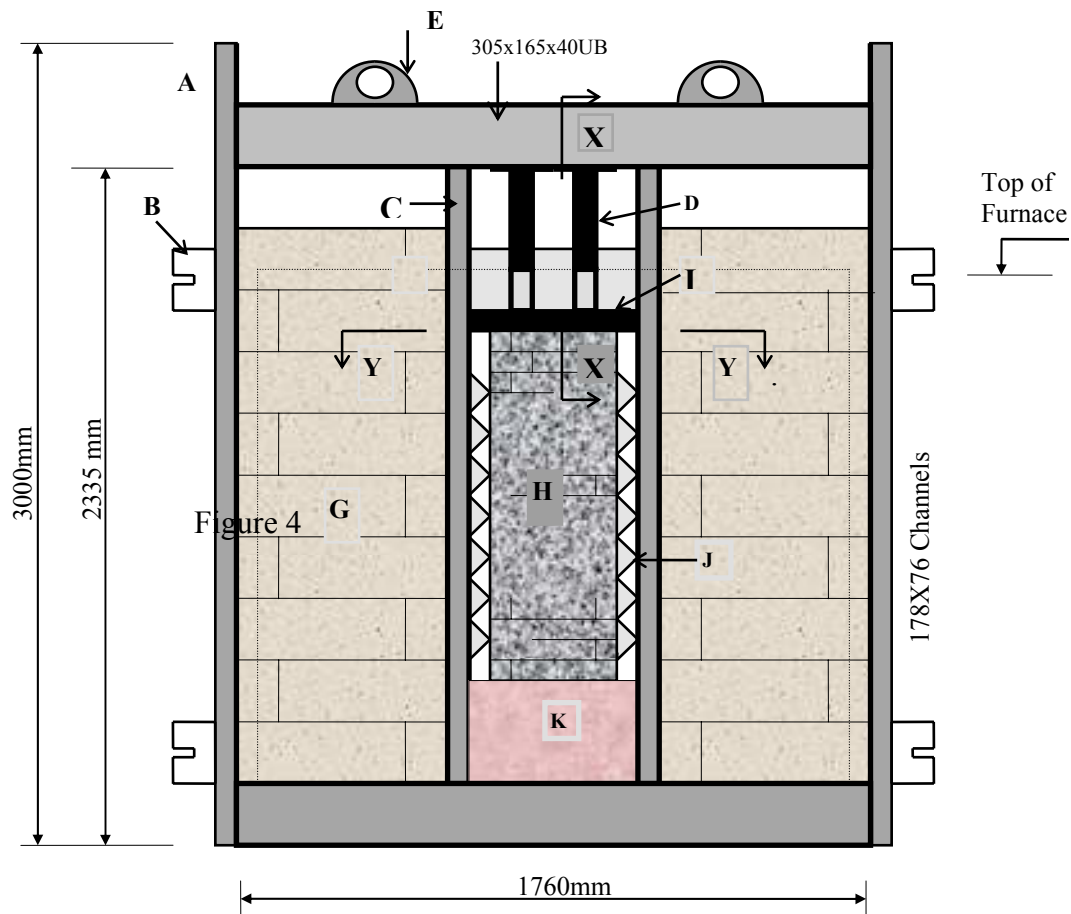


Fig.2. Testing frame details

|             |  |   |   |
|-------------|--|---|---|
| <u>Key:</u> | Jacking Frame  | G | Permanent 150mm thick pre cast concrete with 20mm fibreboard protection to furnace side       |
| A           |  | H | Test specimen 680 high 210mm wide 100mm thick 3 blocks  |
| B           | Bracket Connection to Furnace  | I | 210mm by 100mm 200mm in height by 10mm thick plate on 3mm fire resisting compressible surface |
| C           | 100x100 L Lateral restraint to panels                                      | J | 40mm thick fibreboard with 7mm fire resistant edge seals                                      |
| D           | 25T Hydraulic Jacks protected with fire resisting material including hoses | K | Pre formed steel framed supports no more than 870mm in height lined with fibreboard           |
| E           | Lifting eye  |   |   |

## COMPRESSIVE STRENGTH RESULTS

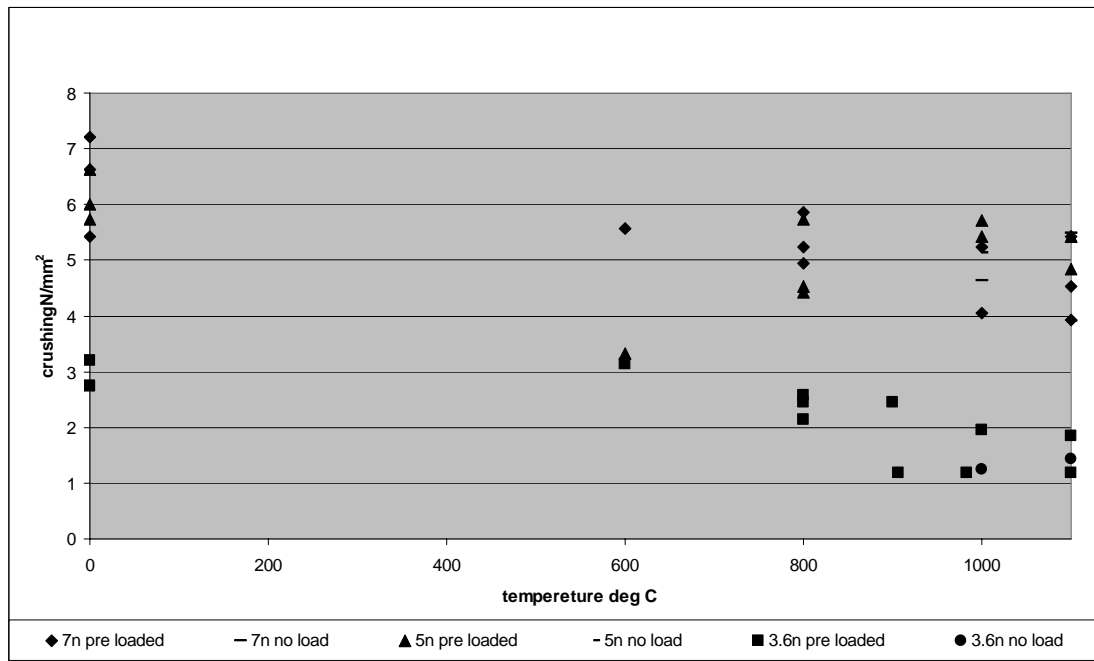


Fig.3. Compressive strength, 3.6N/mm<sup>2</sup>, 5N/mm<sup>2</sup> and 7N/mm<sup>2</sup> block work

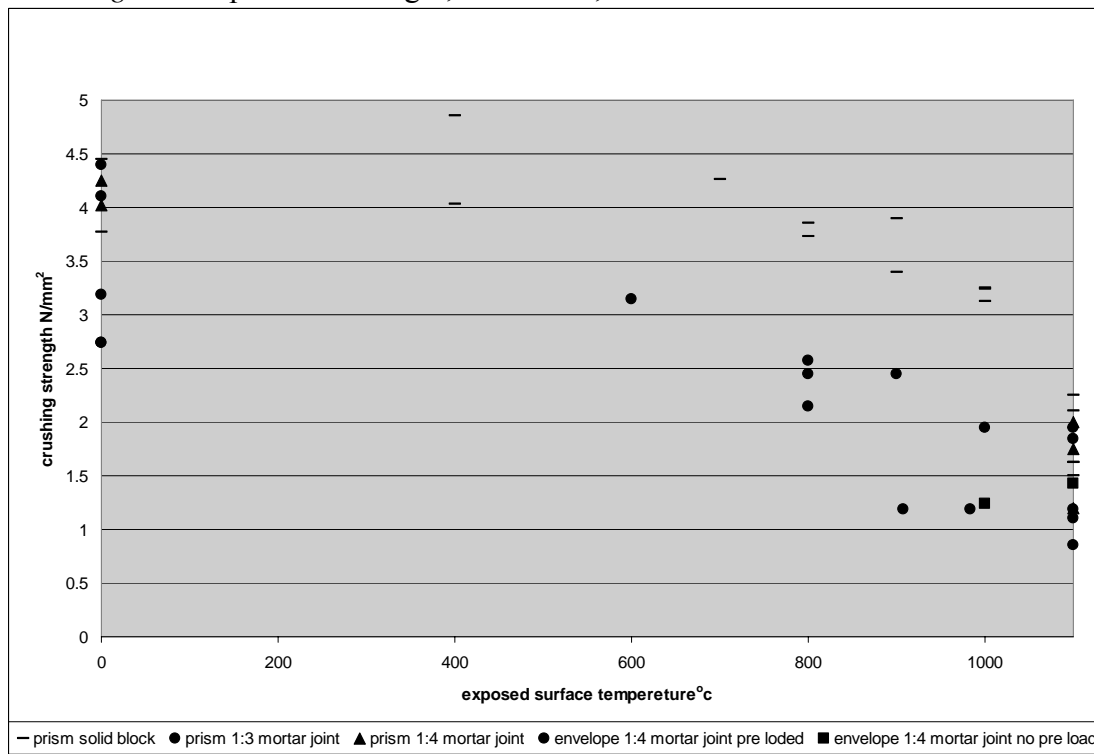


Fig.4. Compressive strength 3.6N/mm<sup>2</sup> blocks (prism samples [5])

### Discussion of results

Figure 3 details the results of the aerated block work compared to concrete aggregated block work. At temperature of 900°C, little more than half the designed compressive strength remains within the specimens. Two samples exhibited premature failure with their service load at 900°C and 980°C and were recorded accordingly. From unloaded

and loaded envelopes there was little evidence of a large variation in their results, Figure 4 gives additional benchmarking between the previous prism testing [5] which indicated that the prism samples retained a higher residual compressive strength however the loss in compressive strength, was evident at the requisite temperatures observed in the envelope tests.

### RESULTING FAILURE CRACKING

Figure 5 details the crushing results from an aerated block. The picture was taken from the unexposed side with the sample subjected to 1100°C on the exposed face. All blocks tested at and over 1000°C exhibited a sheering parallel to the surface in the bottom two blocks. The sheering varied in the samples from 20mm to 30mm from the unexposed surface. From the conduction data these areas within the block work attained a temperature of 100°C to 367°C. At the lower temperatures the block work failure was evident similar to aggregate concrete block work, where cracking was observed within the base block and extending into the mid block. The exposed face pictured in figure 6 from the same sample in figure 5, exhibited the break down of the block work from an



*Fig .5. 1100°C unexposed face*



*Fig.6. 1100°C exposed face*



*Fig.7. 1100°C concrete block unexposed face*

Exposure temperature of 800°C and above a dry shrinkage pattern on the face which extended into the block, not unlike a dried river bed, the depth of penetration varies with temperature. The face remained intact and remained as a barrier to the heat

source. Figure 7 indicates a  $5\text{N/mm}^2$  aggregate. Concrete block which exhibits its typical failure through the base and partially into the mid block which was typical to all this type of block at all temperatures. These types of block did not disintegrate on the application of the load the cracking was observed but the block remained in place to give some resistance to radiation

## CONCLUSION

- I. Critical temperature of  $900^\circ\text{C}$  was observed as a temperature that triggered a marked loss of compressive strength
- II. With temperatures in excess of  $1000^\circ\text{C}$  there is a risk of spontaneous disintegration on the application of a load at or above one third of the service load.
- III. Despite a limited number of samples there was no evidence of different results between unloaded and one third loaded specimens
- IV. There is evidence of gains in compressive strength in the cooling phase, as demonstrated in figure 4 residual compressive strength of the prisms as compared with hot crushing of envelopes.
- V. There was little evidence of distress in the mortar joints

## REFERENCES

1. Cook, GME. Thermal bowing and how it affects the design of fire separating constructions. Interflam 88 – Fourth International Fire Conference. 22-24 March, Church College Cambridge, 1988, pp 230-236
2. Khoury GA, Grainger BN, and Sullivan PJE. Transient Thermal Strain of Concrete: Literature Review, Conditions within Specimen and Behaviour of Individual Constituents. Magazine of Concrete Research, vol 37, No 132, 1985, pp 131-144
3. Anderberg Y, and Thelandersson S. Stress Deformation Characteristics of Concrete at High Temperatures. Division of Structural Mechanics and Concrete Construction, Lund Institute of Technology, Bulletin 54 1076
4. Nadjai A, O'Garra M, and Ali F. A Numerical Model for the Behaviour of Masonry Under Elevated Temperatures, Fire & Materials, Vol 27, pp 163-182, 2003.
5. Hardie B, Nadjai A, and Ali F. concrete block work at elevated temperatures, fib conference proceedings Cabrera Portugal 2007

## EXPERIMENTAL AND NUMERICAL STUDY OF HIGH PERFORMANCE CONCRETE COLUMNS SUBJECTED TO FIRE LOADING

Sven Huismann <sup>a</sup>, Manfred Korzen <sup>b</sup>

<sup>a</sup> Federal Institute for Materials Research and Testing, Division Building Materials, Berlin, Germany

<sup>b</sup> Federal Institute for Materials Research and Testing, Division Fire Engineering, Berlin, Germany

### INTRODUCTION

This paper presents an experimental and numerical study on the thermo-mechanical behaviour of high performance concrete (HPC) columns subjected to fire loading in accordance with ISO 834. The objective is to perform numerical simulations of the thermo-mechanical behaviour of the columns on the basis of the thermo-mechanical material properties which will actually be investigated.

### 1 EXPERIMENTAL STUDIES

Two HPC square type columns have been tested under ISO 834 fire exposure and mechanical loading of 3200 kN.

#### 1.1 Test Specimens

The two columns had a cross section of 30 x 30 cm<sup>2</sup> and length of 3.6 m. The longitudinal reinforcing bars of diameter 25 mm and axis distance of 50 mm were welded at end plates of thickness 30 mm. They had an axis distance of 50 mm. The transversal reinforcement has been realized with circular stirrups of 10 mm thickness with a spacing of 150 mm within a distance of 600 mm from the supports, and a spacing of 300 mm in the central part. The ties had 135° bent ends. The column temperatures were measured by 40 thermocouples of type K at 4 measuring stations along the column axis with at least 7 sensors per station. They were positioned inside the concrete and welded at the reinforcements. The concrete mix is shown in Table 1. Column I was made of the concrete HU-9 with a compressive strength of 131.9 MPa (100 mm cube) at the test day and column II of HU-10 with a strength of 124.4 MPa. The age was more than 90 days. The relative humidity was 4.3 % in both columns at the test day.

*Table 1. Mix proportions*

| Materials [kg/m <sup>3</sup> ] |          | HU-9 | HU-10 |
|--------------------------------|----------|------|-------|
| Cement CEM I 42,5 R            |          | 580  |       |
| Water                          |          | 173  |       |
| Aggregates (siliceous)         | 0 – 2 mm | 769  |       |
|                                | 2 – 4 mm | 231  |       |
|                                | 4 – 8 mm | 538  |       |
| Silica fume                    |          | 63.8 |       |
| Superplasticizer               |          | 17.4 |       |
| Polypropylene Fibres           |          | 2    |       |
| Steel fibres                   |          | no   | 100   |
| W/C ratio                      |          | 0.3  |       |

## 1.2 Experimental Set-Up

The tests were carried out in a special column-furnace (see Fig. 1) with a loading capacity of 6300 kN. Mechanical and thermal actions are applied through this device to the specimen under test. Six electro-hydraulic control channels equipped with displacement and force sensors are available to influence the mechanical boundary conditions, i.e. two bending rotations each at top and bottom, one axial displacement at the bottom and one horizontal displacement at the top. During the experiments under discussion only the axial load has been applied whereas the other degrees of freedom were fixed. The furnace is operating with six oil burners and the gas temperatures are controlled with plate thermometers according to [2].

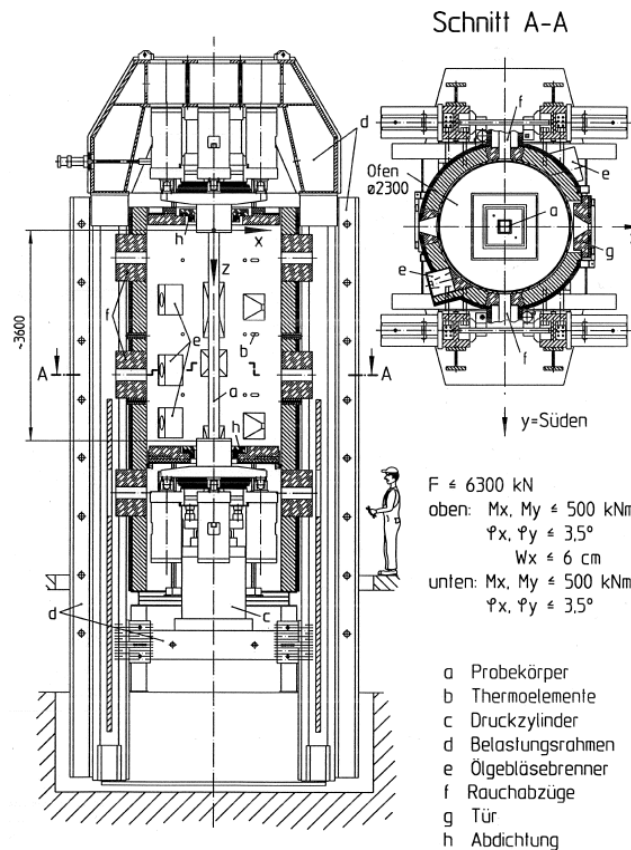


Fig. 1. column-furnace

## 1.3 Test Conditions and Procedure

The four sided fire loading was in accordance to the ISO 834 standard and in good agreement with EN-1365-1 [2]. Two types of mechanical boundary conditions have been applied to the specimens: Column I fixed at the bottom and with a 25 mm eccentric hinge at the top and column II fixed at both ends. The axial load of 3200 kN, characterized by 75 % of the design load, was kept constant during the tests. The axial displacements as well as the temperatures of the specimens and the gas temperature of the furnace have been measured.

## 2 RESULTS AND DISCUSSION

### 2.1 Failure behaviour

Failure of column I and II was observed after 94 minutes and 116 minutes of fire exposure, respectively. The failure mode of column II was compression and not buckling (see Fig.2).

Spalling has been observed only at column I at the side of the concrete charging after 14 minutes. The reason seems to be the abrasion of the fresh concrete at the surface of column I during the production. It was not observed at column II, which was not abraded.

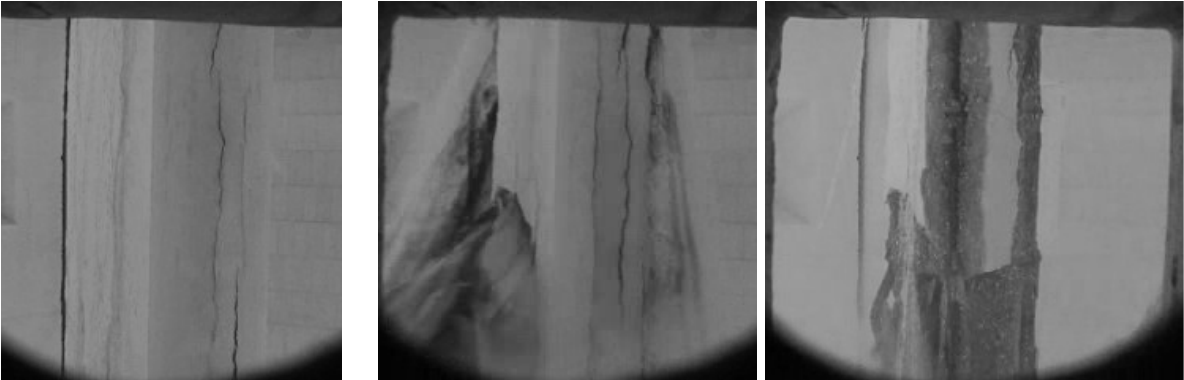


Fig. 2. Failure of column II

**2.2 Deformations**

The deformations of the two columns are shown in Fig. 3. Both columns expand in the first phase. Column I reached the initial deformation after 30 minutes. In minute 34 was a switch in the deformation of column I, which does not represent the overall failure of the column. This phenomenon is induced by the concentrated load, which results in local failure of the concrete at the top. After the test a large deformation in the top plate was observed. It is not clear in how far this effect contributes to the axial deformation. For this reason the deformation of column I is taken out of the evaluation. Column II reached the initial deformation after 75 minutes.

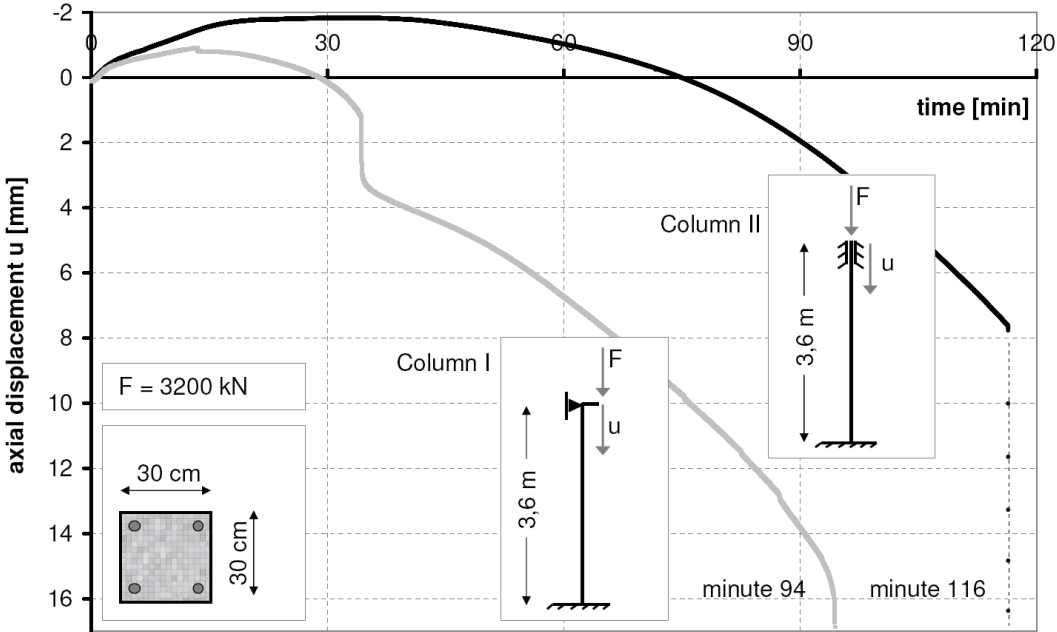


Fig. 3. Axial displacement

## 2.3 Temperatures

The temperatures were measured in four cross sections at different heights. Fig. 4 shows the temperatures vs. time in the height of 89 cm from the bottom and at middle height of column II.

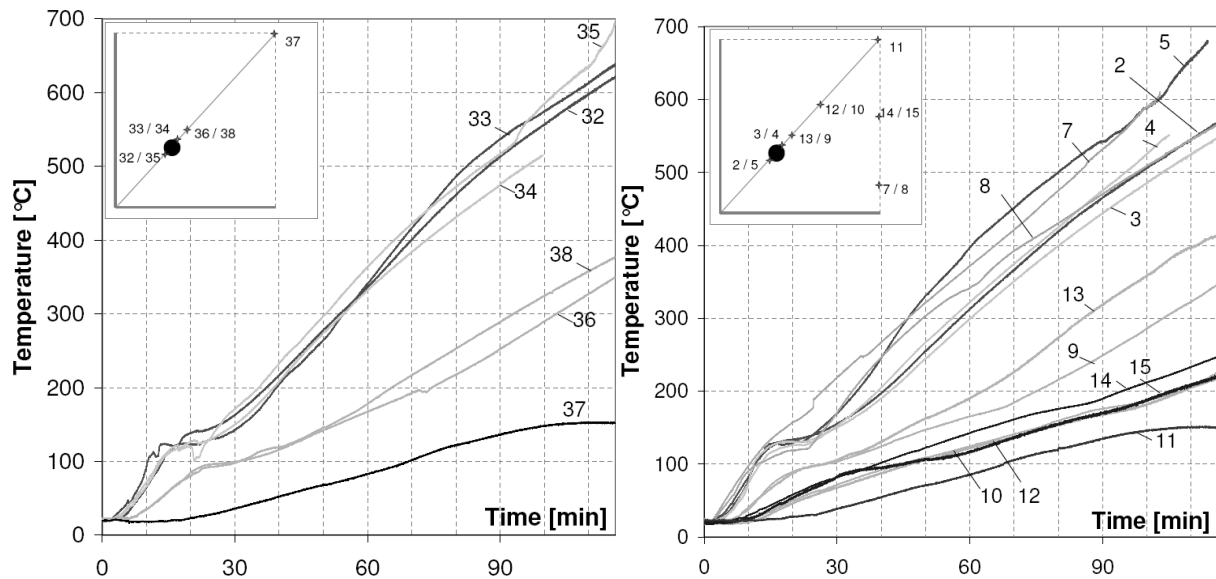


Fig. 4. Temperature in the cross section of column II (left: 89 cm from the bottom, right: middle-height)

The temperatures at the time of failure in the reinforcement bars and the centre were about 600 °C and about 160 °C, respectively.

The temperatures in column I with additional steel fibres were somewhat higher than in column II. The difference arises mostly at the temperatures of 100 °C to 200 °C when the phase transformation of the water appears.

The temperatures are in good correlation with the calculated temperatures in [2], but they are much higher than in [5]. The reason for this difference is not yet clarified and still under discussion.

## 2 NUMERICAL STUDIES

### 2.1 Numerical Model

For the numerical simulation of the thermal and mechanical behaviour of column II the finite element program DIANA from TNO was used. With a three dimensional model a quarter of the cross section which implies that no buckling occurs was simulated. The element size of the twenty node volume element was about 10 mm at each edge.

The longitudinal reinforcement bars were modelled with the embedded reinforcement option without any bond slip. The reinforcement material properties were assumed according to [4]. At the heated surfaces of the column the conditions for the heat transfer with convection and radiation according to [3] were applied. As thermal input heating due to the ISO 834 fire curve was assumed. The mechanical load was set constant to 35.5 MPa which corresponds to the load of 3200 kN.

The thermal conductivity of the concrete is higher than in [3] because of the smaller maximum aggregate size. For this reason the thermal conductivity was set to 2.5 W/mK in the range up to 100 °C and at 150 °C to the lower bound of [3]. Between 100 °C and 150 °C the values were linear interpolated. The heat capacity was also assumed according to [3].

For the temperature dependent stress-strain relations in compression similar curves as defined in [3] were used in which the elastic, plastic and transient creep strains are implied. The tensile behaviour was assumed linear below the tensile strength. After reaching the tensile strength the stress-strain diagram was assumed as constant. All temperature dependent mechanical properties were taken from [3] and related to the measured properties at 20°C. It should be mentioned that the properties in [3] are measured from normal strength concrete.

### 2.2 Numerical Results

The calculated temperature fields are in relatively good agreement with the measured temperatures. There are differences especially until 150 °C because the finite element program does not consider the change of the thermal properties due to the phase transformation of the water.

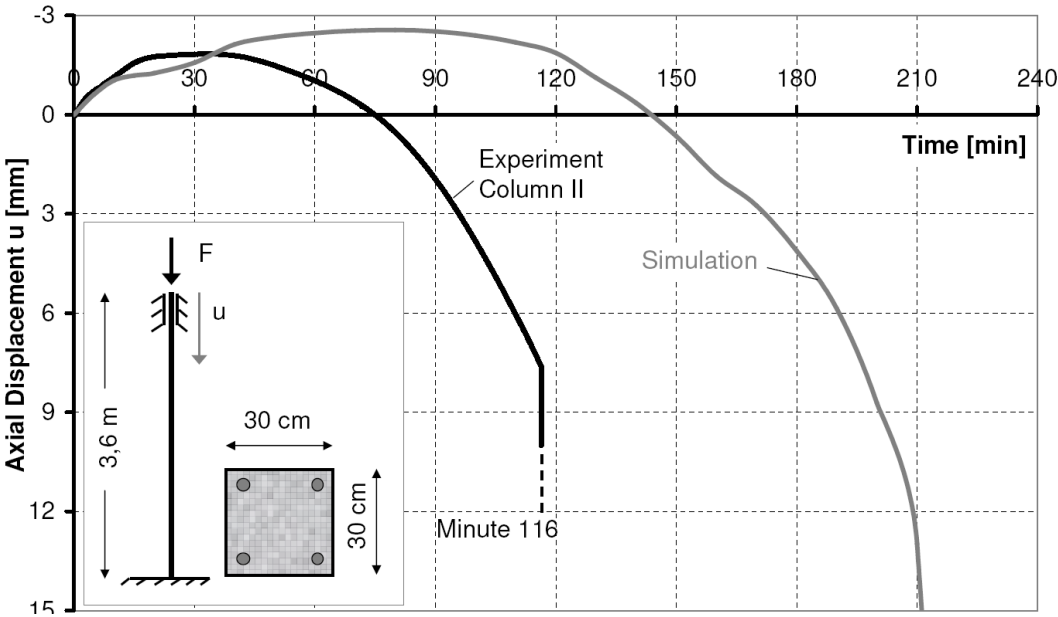


Fig. 5. Comparison of the calculated and measured axial displacement

The results of the axial displacement are presented in Fig. 5. The simulated axial displacement reaches its maximum at about 75 minutes and the initial deformation at about 140 minutes. At 210 minutes failure occurred.

It can be seen that the numerical results of the axial displacement based on material properties according to [3] are not in good agreement with the experimental results. Especially for high strength concrete the transient creep strains are higher than for normal strength concrete [1,6] due to its higher amount of cement. This seems to be the main reason for the difference in the axial displacement predictions in comparison with the experimental results. Therefore more knowledge of the thermo-mechanical properties of high strength concrete is necessary. Material values from ordinary concrete cannot be used. These properties such as strength, thermal expansion and transient creep are currently determined experimentally through a test equipment, which has been specially developed for those purposes. Based on the corresponding identified material properties further simulations will be done.

### **3 SUMMARY, CONCLUSION AND FUTURE RESEARCH**

The subject of this paper was an experimental and numerical study of high strength concrete columns. Two high strength concrete columns were tested under fire conditions. The first one was excluded from evaluation because of its undefined failure. The results of the second test were compared to numerical results. The material properties were assumed according to the Eurocode. But with these properties there was no accordance to the experimental results of the axial displacement. The reason is that the properties according to the Eurocode are related to normal strength concrete. Compared to normal strength concrete the high strength concrete strains are higher. Therefore investigations on the thermo-mechanical properties of the used high strength concrete are in process using recently developed test equipment.

### **REFERENCES**

- [1] Diederichs, U. et al., Behaviour of high strength concrete at high temperatures, Report 92, Helsinki University of Technology, Department of Structural Engineering, Espoo, 1989
- [2] EN 1363-1:1999 Fire resistance tests - Part 1: General requirements, October 1999
- [3] Eurocode 2: Design of concrete structures - Part 1-2: General rules - Structural fire design, EN 1992-1-2:2004, July 2004
- [4] Eurocode 4: Design of composite steel and concrete structures – Part 1-2: General rules – Structural fire design, EN 1994-1-2:2005, November 2006
- [5] Kodur, V.K.R., Fire Resistance of High-Performance Concrete Columns, Report IRC-IR-834, National Research Council Canada, 2002
- [6] Schneider, U. et al., Hochtemperaturverhalten von Festbeton, Sonderforschungsbereich 148 – Brandverhalten von Bauteilen, Technische Universität Braunschweig, Braunschweig, 1987

## BEHAVIOUR OF R.C. BEAMS UNDER ELEVATED TEMPERATURE

Lakshmipathy.M<sup>a</sup>, Jayasree.G<sup>b</sup> and Santhanaselvi.S<sup>c</sup>

<sup>a</sup> Dean and Professor, <sup>b</sup> Ph.D. Research Scholar, <sup>c</sup> Assistant Professor

School of Civil Engineering, SRM University, Kattankulathur-603 203, Tamil Nadu, India.

### 1 INTRODUCTION

Concrete is a complex material subjected to a range of heat more severe than that caused by weather. There are important cases in which concrete is exposed to much higher temperatures when subjected to accidental fires in buildings, nuclear reactors, RC chimneys, runways of jet aircraft and rocket launching pads. Such fires or elevated temperatures result in most cases in considerable damages to structures. Generally concrete is thought to have good fire resistance property but the fire resistance capacity of concrete is very complicated because not only is concrete a composite material with components having different thermal characteristics, it also has properties that depend on moisture and porosity. The extensive use of concrete as a structural material had led to the need to fully understand the effects of sustained elevated temperature on concrete. Elevated/high temperature represents one of the most severe exposure conditions and provisions of appropriate resistance of the structural members are the major safety requirements in design.

### 2 RESEARCH SIGNIFICANCE

From the literature survey it is found that there is a lack of experimental data for concrete heated under a constant preload to simulate the stress conditions in the real field conditions. It is also brought out that data from the stressed test will be of interest, which simulate the conditions of structural elements when exposed to fire in real conditions. The study on the behaviour of RC beams tested under preloaded condition is found limited and there is a scope for attempting studies pertaining to these areas. The dramatic fire accidents/incidents have emphasized the need for safety concerning reinforced concrete (RC) structures made of both ordinary concrete (NSC) and high-strength/ high performance concrete (HPC/HSC). Fire was the main reason in bringing down both of the WTC towers during the tragic event of September 2001 in New York, USA. This has renewed the interest in the area of research on concrete subjected to elevated temperature. A better understanding of behaviour of structural elements under elevated temperature and its implementation will allow improvements to be made in the design of structures for high temperature applications and for accidental exposures. By use of specific concretes, structural configuration and structural detailing the effects of the underlying processes driving this behaviour may be reduced. Such improvements will allow structural safety and consequences of damage due to thermal loading is minimized.

### 3 OBJECTIVE AND SCOPE OF THE WORK

The main objective and scope of this study is to experimentally investigate the residual characteristics of RC beams subjected to sustained elevated temperature under unstressed and stressed test conditions by considering various aspects given below.

- Grade of concrete : Normal Strength Concrete of grade M20
- Type of beam : Varying % of steel  
: Type I – Steel in one face. (  $p_t\% = 0.8\%$ ,  $V_{st} = 1\%$  approx.)  
: Type II – Steel in both faces. (  $p_t\% = 1.5\%$ ,  $V_{st} = 2\%$  approx)
- Temperature level : Normal(28°C), 100°C, 200°C, 300°C, 400°C and 500°C
- Exposure period : Sustained exposure period of 4 hrs

- Test conditions : Residual properties under unstressed test condition and stressed test condition
- Type of loading : Static loading

#### **4 EXPERIMENTAL INVESTIGATIONS**

The details of experimental investigations carried out in this work are covered in the following sections.

##### **4.1 Properties of materials used and concrete mix details**

Ordinary Portland cement of 53 grade [10] and of specific gravity 3.15 is used. Locally available river sand, which is free from organic impurities and specific gravity 2.60 and of Zone III grading is used. The coarse aggregate of 12.5mm maximum size and specific gravity of 2.65 and conforms to grading of IS383:1970 is used. [7]. Clean water as available in SRM University campus, which is free from all impurities is used for the entire work of concrete preparation and curing. The yield strength of 8mm and 4mm diameter steel reinforcement bars of Fe 415 and Fe 250 grade steel provided for beams are  $397.9\text{N/mm}^2$  and  $238.2\text{N/mm}^2$  respectively. The concrete of grade M20 is designed as per IS method IS10262-1982.[9] and the mix proportion by weight is 1:1.29:2.28 and w/c ratio of 0.48.

##### **4.2 Casting of R.C. Beams**

The dimension of the beam is 120mmx120mmx1500mm and the reinforcement details are shown in Figure1. The R.C beams are provided with reinforcement in the tension zone and without any hanger bars and designated as Type I beams (RCB1) to simulate singly reinforced beam in ideal conditions and it is ensured while casting the beam, the stirrups are held vertical in position and effective in resisting shear. The other set of beams are provided with reinforcement bars on both faces designated as Type II beams (RCB2) [8]. A clear cover of 10mm is provided for the beams. The curing of the specimens are initiated after 10 hours by covering with wet gunny bags and cured in clean water for 28 days.

##### **4.3 Testing of R.C. beams**

The details of the testing of the R.C. beams for its residual characteristics under unstressed and stressed test conditions are presented below.

##### **4.3.1 Preloading of R.C. beams in stressed test conditions**

It is believed 20 to 40% of the ultimate load act during service load conditions and accordingly 40% of the ultimate load of the R.C. beam is taken for the level of preloading [3]. In the stressed test, the R.C. beams are kept in a simply supported condition in an assembly specially fabricated for the purpose and placed in the Universal testing machine for preloading. The beams are preloaded by applying a concentrated load through the middle threaded rod and the nuts tightened to retain the load. A preload of 5kN and 10kN is applied to the Type I (RCB1) and Type II (RCB2) reinforced beams equivalent to 40% of the ultimate capacity of the beam in normal temperature conditions. After the preload is applied, the nuts are tightened so that the stresses of preload are retained in the beam as shown in Figure2.

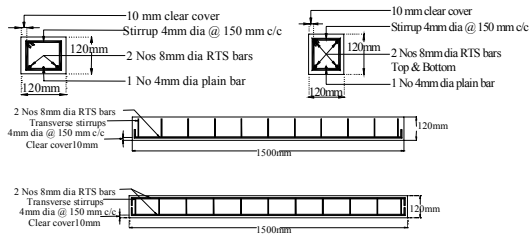


Fig. 1. Reinforcement details of beams

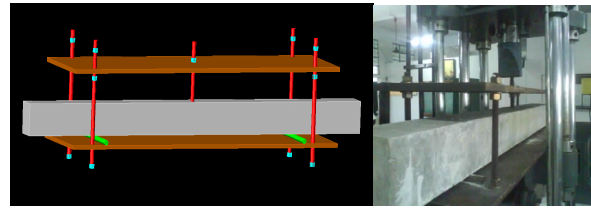


Fig. 2. Preloading of beams

### 4.3.2 Heating of the specimens

The overall dimension of the oven is 2.26m x 0.36m and 0.57m height and the maximum range of temperature that can be measured is 1000°C and a minimum of room temperature. The beam specimens are heated to the target temperature of 100°C, 200°C, 300°C, 400°C and 500°C after the temperature has reached steady state and is sustained for 4 hours of exposure. In the stressed test the beams are exposed to heating in the oven in a preloaded condition. The specimens are then cooled down to room temperature and tested for the residual properties. The heating and the loading histories in unstressed and stressed conditions are shown in Figure 3. The heating of the specimens in the oven in unstressed and stressed test conditions are shown in Figure 4.

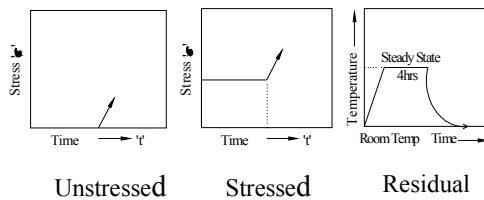


Fig. 3. Heating and loading histories



Fig. 4. Heating of beam specimens in oven

### 4.3.3 Testing arrangement and instrumentation

The two point bending test is conducted on the R.C. beams in the Universal testing machine of capacity 400kN. To measure the central deflection of the beam, dial gauge of 0.01mm accuracy is fixed to the under side of the beam at mid span. In order to evaluate the behaviour of the R.C. beams, the following behavioral parameters are measured and recorded during testing. (i) Load at initial crack is recorded. (ii) Ultimate load capacity of the beam specimen is noted. (iii) Initial stiffness of the beam is determined from the load-deflection curve of the beams. (iv) Stiffness of the beam at 50% stress level is found from the load-deflection curve of the beam. (v) Failure pattern of the beams are noted and crack pattern is recorded in the beam.

## 4.4 Results and Discussions

### 4.4.1 Residual characteristics of beams

The load at initial crack of the R.C. beams at various temperatures 100° C, 200° C, 300° C 400° C and 500° C are compared in Figure 5 for the unstressed and stressed test conditions. The ultimate load at various elevated temperatures are compared with the ultimate load at normal temperature and their ratio T°C/Normal is reported as Residual Strength Ratio (RSR) and compared in Figure 6. The damage suffered by the beams are determined as  $((1-RSR)*100)$  due to elevated temperature exposure and expressed in %. The Type II beams are suffering higher % of damage than Type I

beams as more volume of steel in the beam conducts more heat and transfer to the surrounding mass of concrete and causes more damage to the R.C. beams and also due to complex phenomena of loss of bond strength of concrete. The ultimate load at failure determined theoretically for the two types of beams Type I and Type II tested under unstressed test and stressed test conditions are compared with experimental values in Figure7 and Figure8 respectively.

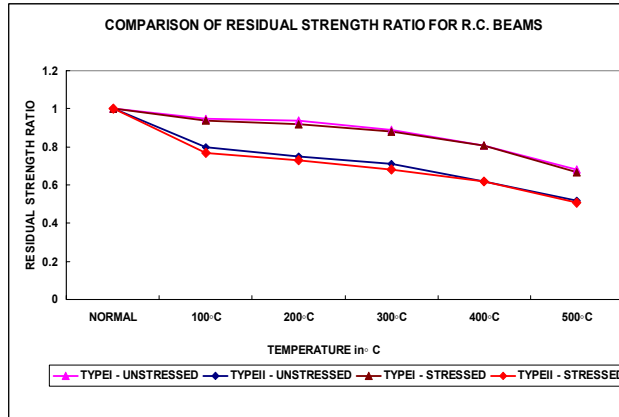
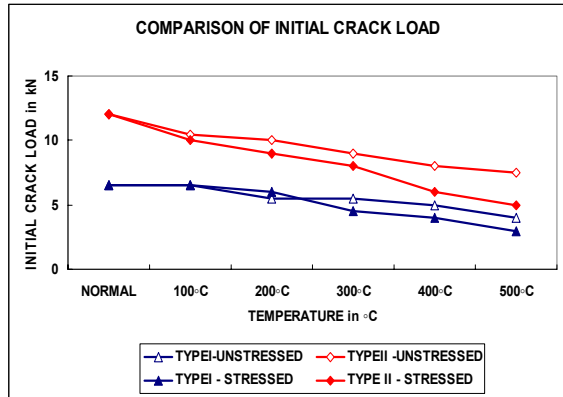


Fig. 5. Comparison of load at initial crack

Fig. 6. Comparison of residual strength ratio

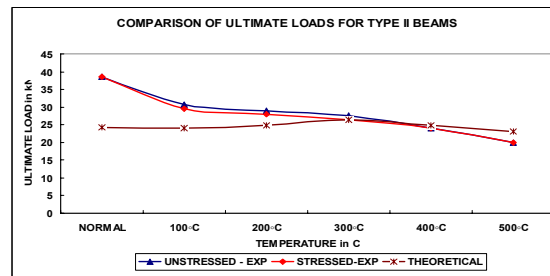
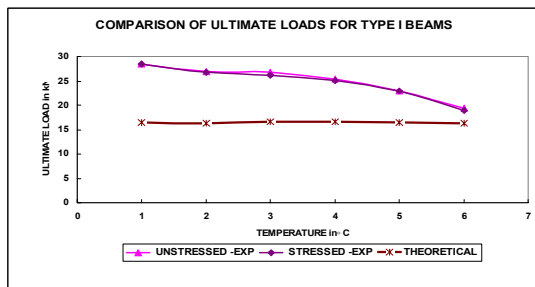


Fig. 7. Comparison of ultimate load Type I beams

Fig. 8. Comparison of ultimate load for Type II beams

#### 4.4.2 Comparison of stiffness of R.C. beams

The initial stiffness of the beam is determined as slope of the load-deflection curve before initial cracking load. Similarly the stiffness of the beam at 50% of the ultimate load is also determined as slope of the tangent drawn at that point. The stiffness as determined are recorded for the beams in unstressed test condition and stressed condition in Table1 and Table 2 respectively.

Table 1 Comparison of stiffness in unstressed test condition

| Type of beam        | Temperature (°C) | Initial stiffness kN/mm | Stiffness at 50% load kN/mm | Stiffness degradation (%) |          |
|---------------------|------------------|-------------------------|-----------------------------|---------------------------|----------|
|                     |                  |                         |                             | Initial                   | 50% Load |
| Type I Beam (RCB1)  | Normal           | 3.28                    | 1.97                        | ----                      | ----     |
|                     | 100°C            | 3.47                    | 1.80                        | +5.8%                     | -8.63%   |
|                     | 200°C            | 3.94                    | 1.85                        | +20%                      | -6.1%    |
|                     | 300°C            | 2.176                   | 1.84                        | -33.66%                   | -6.6%    |
|                     | 400°C            | 2.03                    | 1.75                        | -38.11%                   | -11.17%  |
|                     | 500°C            | 1.41                    | 1.0                         | -57%                      | -49.23%  |
| Type II Beam (RCB2) | Normal           | 3.72                    | 2.56                        | ---                       | ---      |
|                     | 100°C            | 4.025                   | 2.11                        | +8.2%                     | -17.6%   |
|                     | 200°C            | 2.99                    | 1.921                       | -19.6%                    | -25%     |
|                     | 300°C            | 2.136                   | 1.84                        | -42.6%                    | -28%     |
|                     | 400°C            | 2.0                     | 1.75                        | -46%                      | -31.64%  |
|                     | 500°C            | 1.88                    | 1.67                        | -49%                      | -35%     |

Table 2 Initial stiffness and stiffness at 50% of ultimate load in stressed test condition

| Type of beam        | Temperature (°C) | *Initial stiffness KN/mm | *Stiffness at 50% load KN/mm | Stiffness degradation (%) due to temperature exposure |          |
|---------------------|------------------|--------------------------|------------------------------|---|----------|
|                     |                  |                          |                              | Initial   | 50% Load |
| Type I Beam (RCB1)  | Normal           | 3.28                     | 1.97                         | ----  | ----     |
|                     | 100°C            | 3.68                     | 1.77                         | +12.20%   | -10.15%  |
|                     | 200°C            | 3.44                     | 1.93                         | +4.90%  | -2.03%   |
|                     | 300°C            | 3.20                     | 1.80                         | -2.44%  | -8.63%   |
|                     | 400°C            | 2.10                     | 1.20                         | -36%  | -39%     |
|                     | 500°C            | 1.50                     | 0.70                         | -54%  | -65%     |
| Type II Beam (RCB2) | Normal           | 3.72                     | 2.56                         | -----   | -----    |
|                     | 100°C            | 3.33                     | 2.52                         | -10.50%   | -1.56%   |
|                     | 200°C            | 3.19                     | 2.40                         | -14.2%  | -6.25%   |
|                     | 300°C            | 2.62                     | 2.32                         | -29.6%  | -9.4%    |
|                     | 400°C            | 1.85                     | 0.88                         | -50.26%   | -65.63%  |
|                     | 500°C            | 1.00                     | 0.60                         | -73%  | -76.6%   |

## 5 CONCLUSIONS

From the results and discussions on the experimental investigations, the following facts are presented.

- At 500°C the initial crack started at lower load and is lower by 38.5% in Type I beams and 37.5% in Type II beams when compared to normal temperature conditions.
- Also the ultimate load decreased and the damage suffered by Type I and Type II beams are to an extent of 32% and 48% respectively in unstressed test condition. In the stressed test condition it is to an extent of 33% and 49% respectively. The reduction in the strength is about 50% at 500°C.
- The ultimate loads from experimental investigations are greater than the theoretical estimation due to the considerations of lower strength of concrete ( $0.447f_{ck}$ ) and yield strength of steel ( $0.87f_y$ ) in theoretical calculations of the moment capacity of the beams.
- The ultimate load at failure of R.C. beams tested in stressed condition are lower marginally by 5% than the beams under unstressed test condition. The amount of preload is smaller in magnitude in the laboratory tested specimens.

- The degradation in initial stiffness and stiffness at 50% load is also nearly 35% to 50% in unstressed test and is about 54 %to 77% in stressed test for the elevated temperature considered in this study.
- All the beams fail in flexure as expected forming cracks in the tension zone.

It can be concluded that the R.C. beams loses its strength and stiffness at higher elevated temperature and is quantified in this study.

## ACKNOWLEDGEMENT

The authors expresses their sincere gratitude to the Management, SRM University, for the continuous encouragement and support by providing facilities for conducting the experimental part of this work.

## REFERENCES

- [1] Crozier, D. A., Sanjayan, J. G. and Liew, E. M., Residual strength of High Strength Concrete beams exposed to high temperatures, *International Conference on HPHSC, Perth, Australia*, 1998
- [2] Phan Long, T and Carino Nicholas, J., Review of mechanical properties of HSC at elevated temperature, *Journal of materials in Civil Engineering*, 1998
- [3] Phan Long, T. and Carino Nicholas, J., Effect of test conditions and mixture proportions on behaviour of High strength concrete exposed to high temperatures, *ACI Materials Journal*, V.99, No.1,2002
- [4] Kodur, V. K. R., World Trade Center building disaster: Stimulus for innovations, *The Indian Concrete Journal*, 2008
- [5] Kodur, V. K. R. and Dwaikat, M., A numerical model for predicting the fire resistance of reinforced concrete beams, *Cement and Concrete composites*, No.30.2008
- [6] Potharaju, M., Srinivasa Rao, .K, Srinivasa Rao, P.V. and Nalini, M., Theoretical assessment of flexural strength of heated reinforced concrete beams, *Proceedings of the Congress 2008 on Concrete for Fire Engineering, University of Dundee, Scotland*, 2008.
- [7] IS: 383-1970, Specification for coarse and fine aggregate from natural sources for concrete (Reaffirmed 1997), *Bureau of Indian standards, New Delhi*
- [8] IS:456-2000, Plain and Reinforced concrete–Code of Practice, *Bureau of Indian standards, New Delhi*
- [9] IS:10262-1982,Recommended guidelines for concrete mix design(Reaffirmed 1999), *Bureau of Indian standards, New Delhi*
- [10] IS:12269-1987, Specification for 53 Grade Ordinary Portland Cement,(Reaffirmed 1999), *Bureau of Indian standards, New Delhi*

## **SIMPLIFIED LAYERED APPROACH FOR ANALYSIS OF RC SLABS SUBJECTED TO FIRE**

Darius Bacinskas<sup>a</sup>, Edgaras Geda<sup>a</sup>, Gintaris Kaklauskas<sup>a</sup>, Viktor Gribniak<sup>a</sup>

<sup>a</sup> Vilnius Gediminas Technical University, Department of Bridges and Special Structures, Vilnius, Lithuania

### **INTRODUCTION**

Around 8 million fire rise on the earth every year. Average losses in EU countries due to fire reach 1% of gross national product [1]. During fire, building structures have to carry mechanical loads to assure safe evacuation of people and safe activities of fire brigades. In most practical cases, behaviour of reinforced concrete structures at fire is assessed by simplified analytical-empirical techniques. However, such simplified analysis makes only a rough assessment of behaviour of concrete structures subjected to fire and mechanical loads. At present time, using advanced finite element software packages such as DIANA, ATENA, ABAQUS etc., it has become possible to assess the influence of various physical phenomena. However, due to complexity of these phenomena, the analysis results (deflections, time of resistance) may differ up to 5–7 times [2]. The reason for that is that presently known thermal and physical models of materials due to lack of experimental investigations are not accurate. Need for huge computing resources is another disadvantage of numerical techniques. Analysis of relatively simple members by standard software packages may last tens of hours.

A new statistically verified constitutive model [3] has been developed for deformational analysis of flexural RC members subjected to short-term loading. The model (called the *Flexural model*) has been developed by means of innovative method [3, 4] aimed at deriving constitutive relationships from flexural tests of RC members. The proposed constitutive relationship in a simple averaging manner (convenient for FE formulation) includes concrete cracking and tension stiffening effects.

In this paper, an attempt has been made to extend application of the *Flexural model* to stress and strain analysis of flexural RC members subjected to high temperature. Constitutive models and key material parameters describing thermo-mechanical behaviour of concrete and reinforcement steel are discussed. A powerful calculation technique based on layered approach is briefly described. Comparison of the experimental [5] and modelling results has shown that the proposed model has satisfactorily captured the load-deflection behaviour of the pre-cast concrete slabs.

### **1 MATERIAL MODELS**

In fire analysis, the material properties have to be considered as temperature-dependent. Mechanical properties of different materials (steel, concrete, aluminium and stone) according to the appropriate *Eurocodes* are presented by Pintea et al [6]. This section briefly describes constitutive relationships for concrete and reinforcement steel used in the present study. Constitutive models are mainly based on *Eurocode 2* specifications [7].

During the last four decades many investigations have been reported on the effect of fire on concrete and concrete structures. The temperature dependent behaviour of concrete was summarized by Schneider and Horvath [8], including most of the test data published on concrete subject during the recent 30 years.

The theoretical stress-strain relationships of compressed and tensile concrete are given in *Fig. 1*. On the compression side, the curve consists of a parabolic branch followed by a

descending curve until crushing occurs. On the tension side, the curve consists of a bilinear diagram. An initial stiffness of concrete in tension is equal to that in compression. At tensile strains greater than this value of  $\varepsilon_{cr}$  the concrete is assumed to follow the descending branch of the stress-strain curve. Once tensile strains exceed  $\varepsilon_{cu}$ , the concrete in tension is ignored. It should be noted that behaviour of concrete in tension under fire condition is not fully investigated. So far few investigations have been carried out, mainly aimed to overall and stress-strain behaviour of structures.

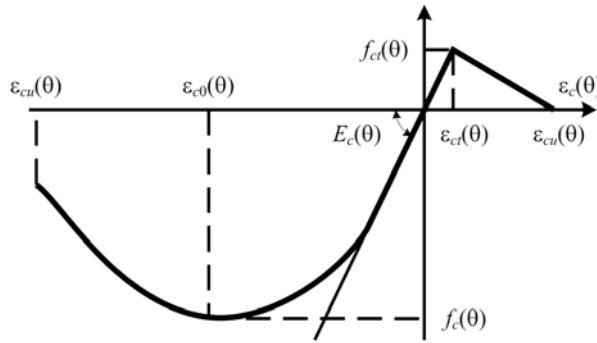


Fig. 1. Theoretical model of the stress-strain relationship of compressive and tensile concrete

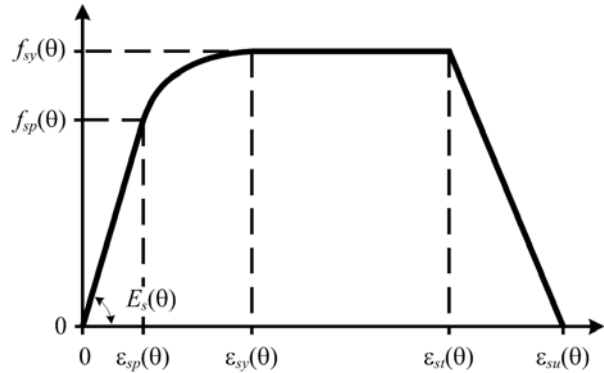


Fig. 2. Stress-strain relationship of steel

Variation of concrete parameters  $f_c(\theta)$ ,  $f_{cr}(\theta)$ ,  $E_c(\theta)$ ,  $\varepsilon_{c0}(\theta)$ ,  $\varepsilon_{cu}(\theta)$  under increasing temperatures are defined using *Eurocode 2* [7]. To the authors' knowledge, investigations regarding the limit strain  $\varepsilon_{cu}(\theta)$  of tensile concrete are practically absent. In reference [9] it is taken as  $15\varepsilon_{cr}(\theta)$ . The same source also notes that the analysis of RC beams at ambient temperature is very sensitive to the assumed tensile behaviour of concrete. In the present study, the limit strain of tensile concrete is expressed as  $\varepsilon_{cu}(\theta) = \beta\varepsilon_{cr}(\theta)$  [4]. Parameter  $\beta$  defining the length of the descending branch of stress-strain curve is equal to such tensile strain which corresponds to zero stress. Parameter  $\beta$  is expressed as  $\beta = 32.8 - 27.6p + 7.12p^2$ , where  $p$  is reinforcement ratio.

The constitutive model for heated and loaded steel is shown in *Fig. 2*. For a given steel temperature  $\theta$ , the stress-strain curves are defined by three parameters: the slope of the linear elastic range  $E_s(\theta)$  for reinforcement, the proportionality limit  $f_{sp}(\theta)$ , and the maximum stress level  $f_{sy}(\theta)$ . The strength and deformation properties of reinforcing steel at elevated temperatures are obtained from [7].

## 2 ANALYSIS OF RC SLABS SUBJECTED TO FIRE

Modelling of behaviour of structures subjected to high temperature conditions consists of 3 separate steps [10]. The first step is associated with the fire dynamics. Computational fluid dynamics models may be applied to get heat transport from fire source to the boundary of structure. In the second step, heat transfer analysis is performed to get temperature distribution within cross section of the member. Experimental fire tests, tables or graphs, numerical or empirical calculations can be employed for this case. Heat transfer analysis is a link between the first and the final step which is related to the mechanical response of the structure due to simultaneous time-dependent thermal and mechanical loads. Although, some

authors proposed a unified computer model [11], these steps usually, are not integrated, i.e. the thermal calculations are carried out first for the entire duration of the fire and then fed into the mechanical analysis program to produce the stresses and strains for the member.

In this section, a simple iterative technique for mechanical analysis (3rd step) of RC slabs under high temperature is presented. The calculation is based on fundamental techniques of mechanics of materials extended to application of layered approach. As shown in *Fig. 3, a*, a member may contain one or more levels of reinforcement, and is subjected to coupled thermo-mechanical loading. *Fig. 3, c* shows the thermal part of loading. The member's cross-section is divided into a number of horizontal layers corresponding to either concrete or reinforcement (*Fig. 3, b*).

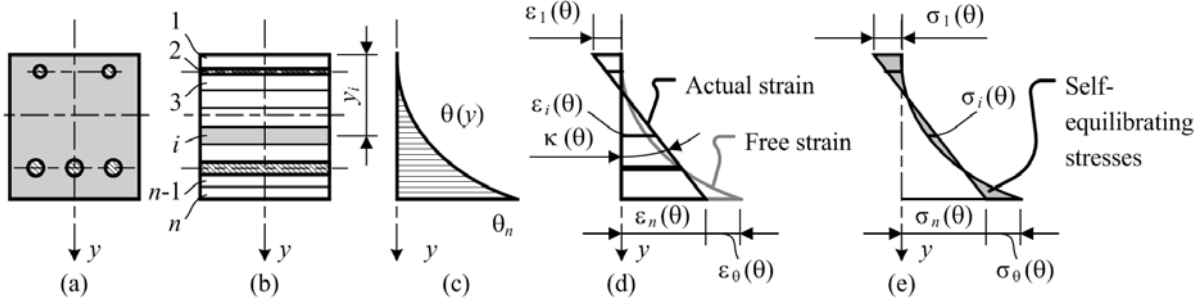


*Fig. 3.* Stress and strain caused by non-linear temperature gradient: cross-section (a); layered section (b); temperature gradient (c); distribution of strain (d) and distribution of stress across the section (e)

The material properties are assessed in iterative calculation by means of secant deformation modulus and assumed to be constant over the layer thickness. The cross section analysis is performed on the so-called transformed section. The area of bonded steel reinforcement is transformed into an equivalent area of concrete. Thickness of the reinforcement layer is taken from the condition of the equivalent area.

The proposed calculation technique is based on the following approaches and assumptions: 1) smeared crack approach; 2) linear distribution of strain within the depth of the section; 3) perfect bond between concrete and reinforcement; 4) the model is valid only for the ascending temperature regime, i. e. cooling faze can not be assessed.

The strain components can be modelled using the superposition theory whereby the total strain is considered to be the sum of various strain components [12]:

$$\varepsilon_{tot}(T, \sigma) = \varepsilon_{\sigma}(T, \sigma) + \varepsilon_{th}(T, \theta) + \varepsilon_{tc}(T, \sigma), \quad (1)$$

where  $\varepsilon_{\sigma}(T, \sigma)$  is the stress-related strain,  $\varepsilon_{th}(T, \theta)$  is the thermal strain,  $\varepsilon_{tc}(T, \sigma)$  is the transient thermal creep strain,  $\theta$  is the temperature,  $T$  is the time,  $\sigma$  is a stress.

Thermal strain of concrete during heating is a simple function of temperature  $\varepsilon_{th,i}(\theta) = \alpha_i \Delta\theta_i$ , where  $\alpha_i$  is the coefficient of thermal expansion of  $i$ -th layer;  $\Delta\theta_i$  is the increment of temperature in this layer. In *Eurocode 2* [7], empirical expressions for strain  $\varepsilon_{\theta}$  in terms of  $\Delta\theta$  are given for concrete and reinforcement.

The transient thermal creep strain of tensile concrete has not been taken into account. Meanwhile the transient creep for each compressive layer is calculated using the relationship proposed by Anderberg and Thelandersson [12]:

$$\varepsilon_{tc,i}(T, \sigma) = -\varepsilon_{th,i}(\theta) \beta \sigma_i / f_c(20^{\circ}\text{C}), \quad (2)$$

where  $\beta$  is a material parameter,  $\sigma_i$  is the stress in the layer,  $f_c(20^\circ\text{C})$  is the compressive strength of concrete under normal ambient temperature.

As plane sections tend to remain plane, a non-linear temperature gradient and transient thermal creep produces internal, self-equilibrating stresses  $\Delta\sigma_\theta$  and  $\Delta\sigma_{tc}$ , respectively. These strains of each fibre are restrained by the adjacent fibres resulting in the internal stress distribution. The total restraining axial force  $\Delta N = \Delta N_\theta + \Delta N_{tc}$  and bending moment  $\Delta M = \Delta M_\theta + \Delta M_{tc}$  required to prevent these deformations. These restraining actions are obtained by integrating the internal relaxation stresses  $\Delta\sigma_\theta$  and  $\Delta\sigma_{tc}$  and their first moments about the top edge. The restraining forces are added to the external ones ( $N = N_{ext} + \Delta N$ ,  $M = M_{ext} + \Delta M$ ). Thus, the resultant changes in stresses and strains due to high temperature loads are obtained. Expressions for the initial top fibre strain  $\varepsilon_1(\theta)$  and curvature  $\kappa(\theta)$  in terms of applied axial force  $N$  and bending moment  $M$  are as follows:

$$\varepsilon_1(\theta) = -\frac{I_{c,eff}N + S_{c,eff}M}{E_c(20^\circ\text{C})(A_{c,eff}I_{c,eff} - S_{c,eff}^2)}, \quad \kappa(\theta) = \frac{S_{c,eff}N + A_{c,eff}M}{E_c(20^\circ\text{C})(A_{c,eff}I_{c,eff} - S_{c,eff}^2)} \quad (3)$$

Here  $A_{c,eff}$  is the area of transformed section,  $S_{c,eff}$  is the first moment of transformed area,  $I_{c,eff}$  is the second moment  $I_{c,eff}$  of transformed area about the top edge,  $E_c(20^\circ\text{C})$  is the modulus of elasticity of concrete under normal ambient condition.

Total strain at any point of the section below the top surface is expressed as:

$$\varepsilon_{\sigma,i}(\theta, \sigma) = \varepsilon_1(\theta) - \varepsilon_{th,i}(T, \theta) - \varepsilon_{tc,i}(T, \sigma) + y_i\kappa(\theta) \quad (4)$$

Based on  $\varepsilon_{\sigma,i}(\theta, \sigma)$ , the stress at any fibre of cross section is obtained according to the respective material model (steel or concrete). A computer program for the mechanical problem has been developed for assessing stress and strain state of a beam as well as for calculation of curvatures and deflections. For a given external moment, the computation is performed in iterations. For deflection calculation *Mohr's* integral technique has been applied.

### 3 COMPARISON TO TEST DATA

This section presents a comparison between the computed (using the described procedure) and the measured RC slab deflections reported by Cook [5]. Totally 14 pre-cast concrete floor slabs were exposed to standard ISO 834 and Norwegian Petroleum Directorate (NPD) fires (*Fig. 4, a*). Present paper includes results of modelling of six slabs, namely S1, S2, S3, S5, S6 and S10 data of which was reported in [5]. The specimens were 4700 mm long, 150 mm (S1÷S3) and 250 mm high (S5, S6, S10) and 925 mm wide. All slabs were simply supported at 4.5 m centres. The fire exposed length was 4.0 m. The slabs were cast of concrete mixes with siliceous aggregates and designed to have characteristic cube strength of 30 MPa. The moisture content of slabs varied between 3.5 and 4.5% by weight. The reinforcing steel bars were of high yield ribbed bar having yield strength of 460 MPa. Slabs S1÷S3 were reinforced with 10 bars of 8 mm diameter, whereas slabs S5, S6, S10 were reinforced with 6 bars of 8 mm diameter. The reinforcement cover was 25 mm.

Experimental temperature distributions within cross section of slabs after 30, 60, 90 and 120 min fire exposure are presented in *Fig. 4, b and c*. These temperature profiles were used for the respective time-deflection analysis. As temperature dependent material properties were not given in the reference [5], they were assumed according to *Eurocode 2* [7]. Loading of

slabs S1, S3, S5, S10 was due to selfweight, whereas slabs S2 and S6 were additionally subjected to live distributed load of 1.5 kN/m<sup>2</sup>.

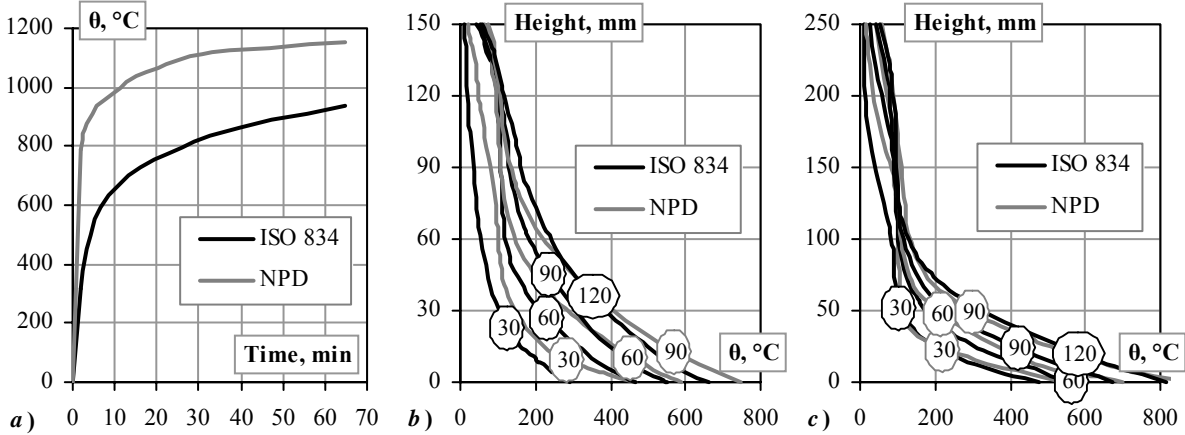


Fig. 4. Temperature-time curves used in tests (a) and temperature profiles for S1÷S3 (b) and S5, S6, S10 (c) slabs

The modelled time-deflection diagrams along with the experimental curves are presented in Fig. 5 in terms of normalized deflections,  $f / f_{max}$ . Here  $f_{max}$  is the maximal deflection at the end of fire exposure. It can be seen from Fig. 5 that the shape of the experimental load-deflection diagrams was well captured in the present analysis. Agreement of the calculated and measured deflections is within reasonable limits.

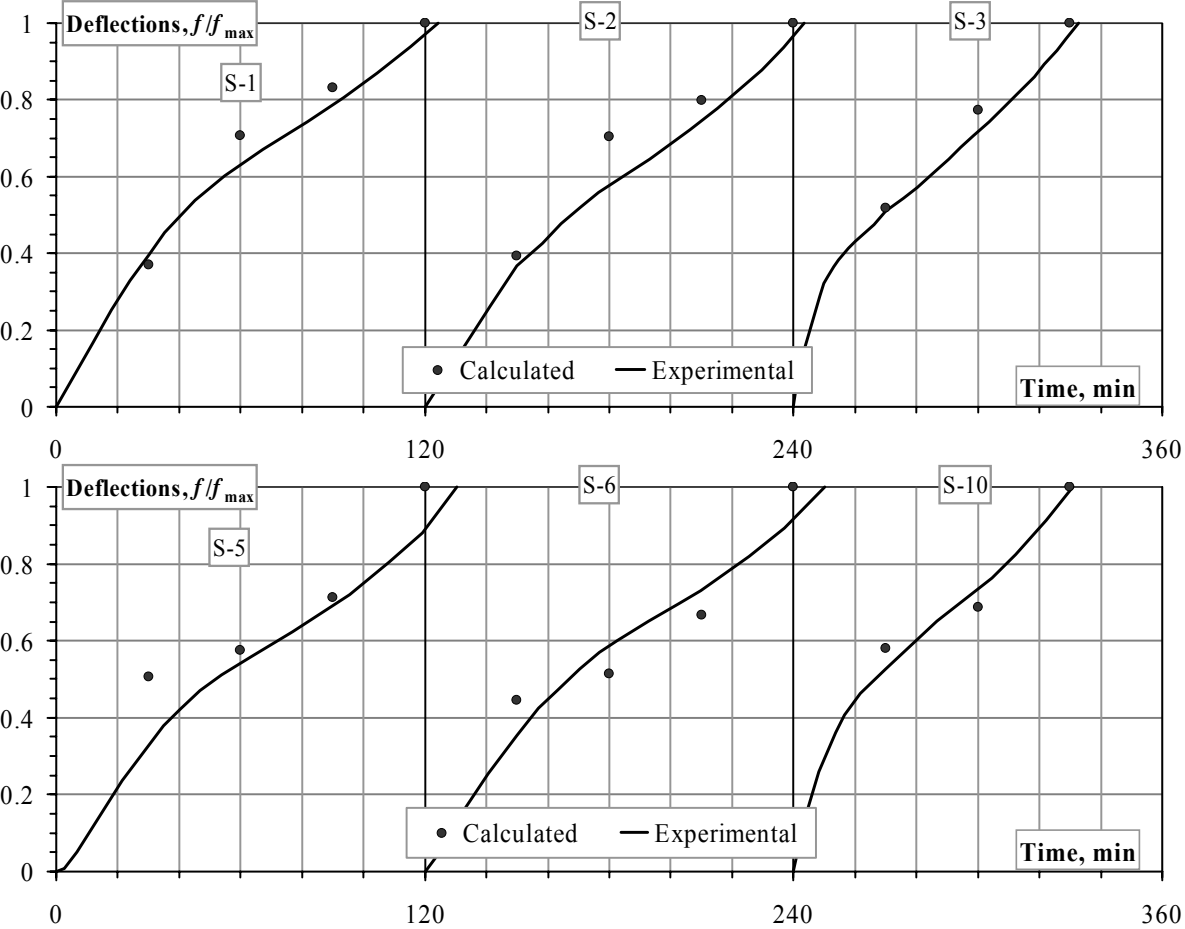


Fig. 5. Comparison of calculated deflections to test results [5]

#### 4 CONCLUDING REMARKS

In this paper, an attempt has been made to extend application of the *Flexural model* to stress and strain analysis of flexural reinforced concrete members subjected to high temperature. Constitutive models and key material parameters describing thermo-mechanical behaviour of concrete and reinforcement are discussed. A powerful calculation technique based on layered approach has been developed. Variation of material properties within the section due to different loading and temperature gradient was assessed in the analysis. Restrained thermal deformations as well as transient thermal creep were modelled by means of fictitious equivalent forces. Comparison of the experimental and modelling results has shown that the proposed model has satisfactorily captured the load-deflection behaviour of the pre-cast reinforced concrete slabs.

#### 5 ACKNOWLEDGMENT

The authors wish to express their gratitude to the *European Community* and the *Agency of International Programs of Scientific and Technology Development in Lithuania* for the financial support provided under the COST action C26. The authors also gratefully acknowledge the financial support provided by the *Lithuanian State Fund of Research and Studies*.

#### REFERENCES

- [1] World Fire Statistics, Report N 10, second edition. *International Association of Fire and Rescue Service (CTIF)*. Available online <http://www.ctif.org>.
- [2] Cervenka, J., Surovec, J., Fellingner, J., Feron, C., Wageneder, J., Kaklauskas G., Corsi, F. FE Simulations of a Suspending Ceiling. Comparison of Fire Test Analyses. *UPTUN Report 441*, 2005.
- [3] Kaklauskas, G., Ghaboussi, J. Stress–Strain Relations for Cracked Tensile Concrete from RC Beam Tests. *ASCE Journal of Structural Engineering* 127(1), 2001, pp. 64–73.
- [4] Kaklauskas, G. Flexural Layered Deformational Model of Reinforced Concrete Members. *Magazine of Concrete Research* 56(10), 2004, pp. 575–584.
- [5] Cooke, G. M. E. Behaviour of Precast Concrete Floor Slabs Exposed to Standardised Fires. *Fire Safety Journal* 36(5), 2001, pp. 459–475.
- [6] Pintea, D.; Zaharia, R.; Kaliske, M.; Kaklauskas, G.; Bacinskas, D.; Gribniak, V.; Torok, A.; Hajpal, M. Mechanical Properties of Materials. Proceedings of International COST C26 Symposium, Malta, 23-24 October 2008, *Datasheet No. 1.5*, 2008, pp. 28–33.
- [7] EN 1992-1-2. Eurocode 2: Design of Concrete Structures – Part 1.2: General Rules – Structural Fire Design. *European Committee for Standardization*, Brussels, 2004.
- [8] Schneider, U., Horvath, J. Behaviour of Ordinary Concrete at High Temperatures. *Research Report, Vol. 9*. Vienna University of Technology, 2003.
- [9] Cai, J., Burgess, I., Plank, R. A Generalised Steel/Reinforced Concrete Beam-Column Element Model for Fire Conditions. *Engineering Structures* 25(6), 2003, pp. 817–833.
- [10] Wang, Y. C.; Wald, F. Heat Transfer Analysis. Proceedings of International COST C26 Symposium, Malta, 23-24 October 2008, *Datasheet No. 1.4*, 2008, pp. 22–27.
- [11] Ren, A., Shi, J., Shi, W. Integration of Fire Simulation and Structural Analysis for Safety Evaluation of Gymnasiums – With a Case Study of Gymnasium for Olympic Games in 2008. *Automation in Construction* 16(3), 2007, pp. 277–289.
- [12] Anderberg, Y.; Thelandersson, S. Stress and Deformation Characteristic of Concrete at High Temperatures. Part 2: Experimental Investigation and Material Behaviour Model. *Bulletin* 54, Lund University of Technology, 1976.

## **PERFORMANCE BASED FIRE DESIGN OF CONCRETE-FILLED STEEL COLUMNS**

Venkatesh Kodur <sup>a</sup>, Rustin Fike <sup>b</sup>

<sup>a</sup> Michigan State University, Professor of Civil and Environmental Engineering, E. Lansing, MI, USA

<sup>b</sup> Michigan State University, Ph.D. Candidate Civil and Environmental Engineering, E. Lansing, MI, USA

### **1 INTRODUCTION**

Steel hollow structural sections (HSS) are very efficient in resisting compression, torsional and seismic loads, and are widely used as compressions members in the construction of framed structures. Fire safety is one of the primary considerations in the design of high-rise buildings, and hence, building codes specify fire resistance requirements for HSS columns to maintain overall structural stability in the event of fire. Providing such external fire protection to HSS columns involves additional cost, reduces aesthetics, increases weight of the structure, and decreases usable space. Also, durability of fire proofing (adhesion to steel) is often a questionable issue, and hence, requires periodic inspection and regular maintenance, which in turn, incurs additional cost during the lifetime of the structure [1,2].

Often these HSS sections are filled with concrete (CFHSS) to enhance the stiffness, torsional rigidity and load-bearing capacity. The two components of the composite column complement each other ideally at ambient temperatures. In addition, high fire resistance can be obtained without using external fire protection for the steel. Further, a wide range of fire resistance can be obtained by selecting different types of concrete filling, namely plain concrete (PC) steel fiber reinforced concrete (FC) and bar reinforced concrete (RC) [8]. Design guidelines for achieving fire resistance through concrete filling have been incorporated into codes and standards [3-5]. However, the current fire guidelines are limited in scope and restrictive in application since they were developed based on standard fires (ASTM E-119 and ISO 834) [6,7]. Hence, they are valid only for the standard fire exposure conditions, and for column parameters (length, load, etc.) dictated by the capacity of available testing furnaces.

To overcome some of the drawbacks in current design specifications a numerical study is carried out on a set of CFHSS columns exposed to various fire and loading scenarios. The analysis was carried out using finite element based computational model SAFIR, wherein the material and geometric non-linearity, and stability-based failure criterion are considered. Results from the analysis are used to present a framework for a performance-based fire engineering methodology. It is demonstrated that required fire resistance for HSS columns in the practical range can be achieved through concrete filling.

### **2 PERFORMANCE BASED DESIGN**

Recently there has been an increased impetus on moving toward a performance-based approach for fire safety design [7]. This is mainly due to the fact that the current prescriptive-based approach has serious limitations and does not provide alternate, cost effective and innovative solutions. One of the key components in performance based design is the use of a rational approach for evaluating fire resistance. Numerical/computational simulations can be used to evaluate the structural performance under fire conditions. The most important factors to be considered in any performance-based fire safety design are fire scenario, load level, failure criterion and geometric conditions [9]. Research efforts in the last two decades have

lead to inclusion of recommendations for the use of design fire scenarios, load level, and failure criterion in codes and standards [10]

### 3 FACTORS GOVERNING FIRE RESISTANCE

Fire resistance of CFHSS columns depends on a number of factors. While the effects of critical factors under standard fire exposure are well understood [11], the influence of critical parameters under realistic fire, loading, and failure criterion are not well understood. To investigate the influence of different parameters on fire resistance of CFHSS columns, a set of numerical studies were carried out using the computer program SAFIR. For the parametric studies, 20 CFHSS columns were selected. Fourteen of the selected columns were the ones tested at the National Research Council of Canada [12,13], while the remaining six columns were variations of the test columns selected to cover a wider range of column variables. In order to fully investigate the effect of length on fire resistance, columns with 3.81, 5, 6, 7, 8, 9 and 10 m (12.5, 16.4, 19.7, 23.0, 26.3, 29.5 and 32.8 ft) length were modeled for each cross-section. Fire exposure was assumed on all four sides with the bottom and top 5% of the column length unexposed to fire. The applied loads on the column were modified to maintain a constant load ratio for all of the lengths modeled for a specific cross-section according to the AISC analysis procedure [4]. The applied load on the composite column takes into account the contribution of different types of concrete filling with steel fiber and bar reinforced concrete-filled HSS columns having higher load capacity. Each of these cross section-length combinations were modeled under seven fire scenarios. Five of the scenarios are shown in Figure 1, the remaining two fire scenarios were also design fires. This parametric study generated a total of 980 numerical simulations covering a wide range of load, geometry, concrete types, and fire scenarios. Detailed results from the parametric studies are presented elsewhere and only the main highlights of the most important parameters are addressed below [11]. The trends (results) discussed below were observed for all of the filling types (plain, bar and steel fiber reinforced) considered unless otherwise noted.

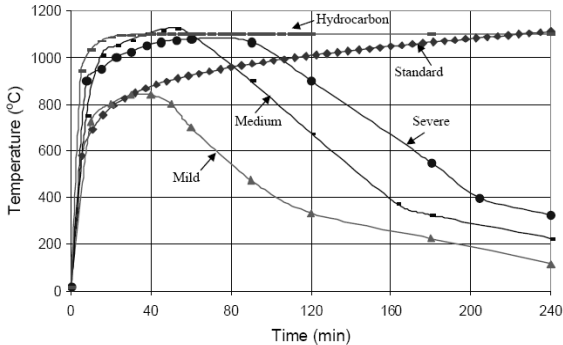


Fig. 1. Time-temperature relationships for various fire scenarios

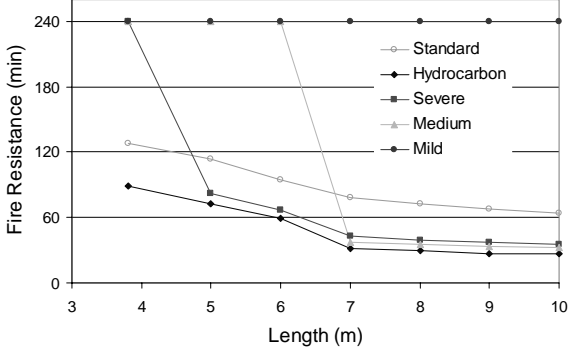


Fig. 2. Fire resistance as a function of length for a PC-HSS under different fire scenarios

#### 3.1 Effect of Fire Exposure

Results from parametric studies indicate that the fire resistance of a column increases as the fire severity decreases. It can be seen in Figure 2 that fire resistance of four hours or more can be obtained for columns up to 10m long under mild fire conditions. However, for other fire exposures, fire resistance decreases with an increase in length. A closer look at Figure 2 reveals that fire resistance of a 5 m (16.4 ft) long CFHSS column ranges from sufficient to withstand compartment burnout for medium and mild fire exposure, to 68 minutes under severe exposure. The reason for this decreased fire resistance with increased fire severity can

be attributed to the higher internal temperatures attained in the concrete under severe fire exposure. Consequently, the column loses its strength and stiffness at a faster rate leading to early failure.

### 3.2 Effect of Length

Results presented in Figure 2 can also be used to demonstrate the effect of length on the fire resistance of CFHSS columns. As would be expected, fire resistance for a given fire exposure decreases with an increased length of the column. This is due to higher slenderness that accompanies the increased length which in turn governs the failure pattern of the column. Fire resistance is drastically reduced when the failure mode switches from crushing to buckling with increased length. This is most pronounced for the “medium” and “severe” fire exposure as can be seen in Figure 2. Fire resistance under the “medium” fire drops from 240 to 45 minutes when length is increased from 5 to 7 m (16.4 to 23 ft). Under severe fire exposure, the fire resistance decreases from 240 to 75 minutes for an increase in length from 3.81 to 5 m (12.5 to 16.4 ft). However, under mild fire exposure, fire resistance remains high for all cases, and the length does not have any influence. This study clearly illustrates that length has a significant influence on the resulting fire resistance, specifically under severe fire exposures.

### 3.3 Effect of Concrete Filling

The effect of the type of concrete filling on fire resistance is illustrated in Figure 3. HSS columns with different concrete filling types were analyzed under standard fire exposure and the fire resistance evaluated. As was the case with the effect of length, the applied load was modified according to AISC analysis procedures [4] to account for the higher strength capacity resulting from FC and RC filling. As seen in Figure 3, the fire resistance decreases with an increase in length for all of the filling types. However, columns with RC or FC filling demonstrate higher fire resistance than PC-filled columns at all lengths. This can be attributed to the increased load carrying capacity of the concrete core provided by the inclusion of reinforcement, and also due to the slower loss of strength in RC and FC filled columns resulting from the presence of reinforcement in the concrete core. These results indicate that it is possible to significantly enhance the fire resistance of CFHSS columns by changing the type of concrete filling. The required fire resistance in most practical situations can be obtained for columns up to 10 m (32.8 ft) in length by simply altering the type of concrete filling.

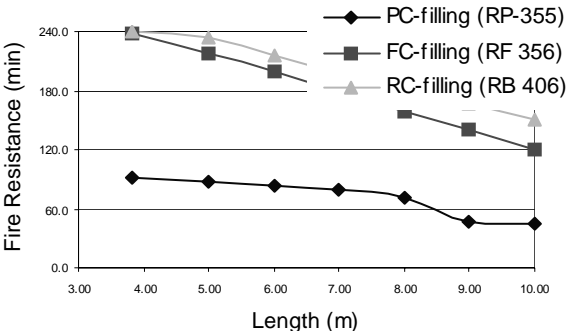


Fig. 3. Effect of length and concrete filling on fire resistance of CFHSS columns

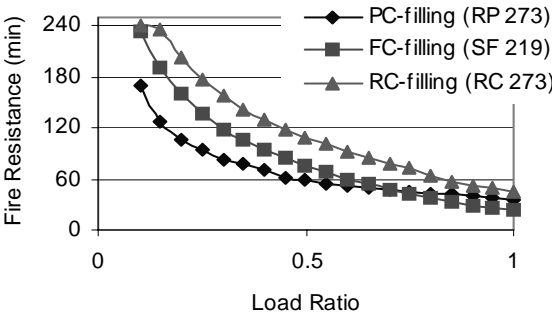


Fig. 4. Effect of load ratio on the fire resistance of CFHSS columns

### **3.4 Effect of Load Ratio**

The effect of load ratio on fire resistance was investigated by analyzing three CFHSS columns under standard fire with load ratios ranging from 10% to 100% (0.1 to 1.0). Load ratio is defined as the ratio of the load on the column under fire conditions to the ambient temperature capacity of the column. The analysis was carried out for three types of concrete filling, namely: PC, FC, and RC, and the results are shown in Figure 4. A RC-filled HSS column withstood the ASTM E-119 [6] fire for 240 minutes with a load ratio of 10% (0.1). The FC and PC-filled columns lasted for 234 and 170 minutes respectively. The fire resistance decreases rapidly with an increase in load ratio up to 0.4. After which point the rate of decrease in resistance is slower as seen in Figure 4. This can be attributed to the fact that concrete filling generally provides a load bearing contribution of about 30%-40% of the overall composite column capacity. In a fire scenario, the steel shell loses its strength very quickly, and concrete carries most of the load. Thus, for load ratios higher than 40%, the concrete filling has to be strengthened either through the use of bar-reinforcement, or through the use of steel fibers to achieve higher fire resistance.

### **3.5 Effect of Aggregate Type**

Results from the analysis indicate that the type of aggregate has a moderate influence on the fire resistance of CFHSS columns. The two common types of aggregate used in concrete are: carbonate (mainly consisting of limestone) and siliceous (mainly consisting of quartz) aggregate. Carbonate aggregate concrete typically demonstrates higher fire resistance than siliceous aggregate concrete [14,15]. This is due to an endothermic reaction occurring in carbonate aggregate at 600-800 °C, in which the dolomite within the aggregate dissociates. Consequently, the heat capacity of carbonate aggregate increases significantly and is approximately 10 times higher than siliceous aggregate in the same temperature range. As a result, there is a slower increase in temperature in the carbonate aggregate concrete, and thus, a slower loss of strength. Therefore, the fire resistance of CFHSS columns filled with carbonate aggregate concrete is about 10% higher than siliceous aggregate concrete-filled HSS columns.

### **3.6 Effect of Failure Criterion**

The two limit states generally considered for defining failure of steel columns under fire conditions are: critical steel temperature and stability (strength) of the column. ASTM E-119 [6] defines fire resistance as the time it takes to reach a maximum average section temperature of 538 °C, or a maximum point temperature of 649 °C. On the contrary, stability-based failure criterion are based on the duration of time during which a column maintains structural stability (strength) during fire exposure. In the case of CFHSS columns, use of critical temperature criterion does not reflect realistic fire resistance since CFHSS columns derive fire resistance primarily from the concrete core. As an illustration, a PC-filled HSS column that has a fire resistance of 128 minutes as per SAFIR analysis (based on strength limit state), only has a fire resistance of 38 minutes when critical temperature criterion is applied. Clearly, thermal failure criteria do not reflect the contribution of the concrete filling to the fire resistance of CFHSS columns. As such, it is necessary to employ stability-based failure criterion for the evaluation of the fire resistance of CFHSS columns.

## **4 STRATEGIES FOR REALIZING UNPROTECTED CFHSS COLUMNS**

In recent years, the performance-based approach to fire safety design has become popular since cost-effective and rational fire safety solutions can be developed using this approach [8]. One of the key aspects in any performance-based design is the fire resistant design of

structural members. Through the application of a performance-based approach, and by utilizing different concrete filling types, the full benefits of CFHSS columns can be realized. For developing such strategies, numerical models that can simulate the response of CFHSS columns under realistic fire, loading and restraint scenarios have to be used. The main steps involved in undertaking a rational approach for performance-based fire design of CFHSS columns are: 1) identifying proper design (realistic) fire scenarios and realistic loading level on the column, 2) carrying out detailed thermal and structural analysis by exposing the column to fire conditions; and 3) developing relevant practical solutions, such as the use of different types of concrete filling, to achieve the required fire resistance.

#### **4.1 Development of Fire Scenario and Loading**

The design fire scenarios for any given situation can be established either through the use of parametric fires (time-temperature curves) specified in Eurocode 1 [16] or through design tables [17] based on ventilation, fuel load and surface lining characteristics. To use the design tables, the ventilation factor,  $F_v$ , has to be established using  $F_v = \frac{A_v}{A_t} \sqrt{H_v}$ . Where  $A_v$  is the

area of the window opening ( $m^2$ ),  $A_t$  is the total internal area of the bounding surface ( $m^2$ ), and,  $H_v$ , is the height of the window opening (m) [18]. The fuel load in the compartment is determined by considering the total bounding surface (not just the floor surface area). Typical fuel loads for common compartment types are available [9,18]. Figure 1 shows typical design fire curves that can be generated using performance-based fire safety design. The presence of sprinklers can also be accounted for in the development of design fire scenarios.

The loads that are to be considered on concrete-filled HSS columns under fire conditions should be estimated based on the guidance given in ASCE-07 standard or Eurocode, [16, 19] (1.2 dead load + 0.5 live load) or through actual calculations based on different load combinations.

#### **4.2 Structural Analysis Under Fire Exposure**

Once the fire scenarios and load level are established, the next step is to avail of a computer program for the analysis of CFHSS columns exposed to fire. The computer program should be able to trace the response of the CFHSS column in the entire range of loading up to collapse under fire. Using the computer program, a coupled thermal-structural analysis shall be carried out at various time steps. In each time step, the fire behavior of a CFHSS column is estimated using a complex, coupled heat transfer/strain equilibrium analysis, based on theoretical heat transfer and mechanics principles. The analysis shall be performed in three steps: namely, calculation of fire temperatures to which the column is exposed (as detailed in 4.1), calculation of temperatures in the column, and calculation of resulting deflections and strength, including an analysis of the stress and strain distribution.

The temperatures (in the concrete, and reinforcement), strength capacities, and computed deflections of the column shall be used to evaluate failure of the column at each time step. At every time step, the failure of the column shall be checked against a pre-determined set of failure criteria. The time increments continue until a certain point at which the strength failure criterion has been reached, or the axial deformations reach their limiting state. At this point, the column becomes unstable and will be assumed to have failed. The time to reach this failure point is the fire resistance of the CFHSS column.

#### **4.3 Development of Practical Alternatives**

Results from the above analysis can be utilized to develop practical solutions for achieving the required fire resistance in CFHSS columns. The most feasible solution is through the use

of appropriate concrete filling (PC, FC, and RC). Other factors, such as reinforcement in the column or load level can be varied to achieve the required fire resistance in HSS columns. Once the parameters are selected, a detailed analysis can be carried out to assess the fire resistance of the column under a specific fire and loading scenario. The analysis is repeated until the required fire resistance is obtained for the CFHSS column. As an example, while PC-filling can provide one-two hours of fire resistance in HSS columns, by switching to FC or RC-filling, up to three hours of fire resistance can be obtained even under severe design fire scenarios. It should be insured that stem vent holes are provided at the top and the bottom of compartment elevations to alleviate the steam pressure generated inside the HSS column [20].

## 5 CONCLUSIONS

Based on the results of this study, the following conclusions can be drawn:

- Type of fire exposure has a significant influence on the fire resistance of CFHSS columns. The fire resistance of CFHSS columns under most design fire scenarios is higher than that under standard fire exposure.
- Apart from fire exposure, the other significant factors that affect the fire resistance of CFHSS columns are length, type of concrete filling, load ratio and failure criterion.
- It is possible to achieve unprotected CFHSS columns up to 10m (32.8 ft) in length, capable of withstanding complete compartment burnout through the use of different types of concrete filling.
- Through the use of a performance-based design approach, it is possible to significantly enhance the fire resistance of CFHSS columns by varying parameters such as load level, concrete filling type, and type of aggregate in the concrete.
- The limiting criterion, used for determining failure, has a significant influence on the fire resistance of CFHSS columns. The conventional failure criterion, such as limiting steel temperature can not be applied to CFHSS columns. Strength and deformation failure criteria should be considered for evaluating fire resistance of CFHSS columns.

## 6 ACKNOWLEDGMENTS

The research, presented in this paper, is primarily supported by the American Institute of Steel Construction through AISC Faculty Fellowship Award to Prof. Kodur. Any opinions, findings, and conclusions or recommendations expressed in this paper are those of the authors and do not necessarily reflect the views of the sponsors.

## 7 REFERENCES

- [1] FEMA, “World Trade Center Building Performance Study: Data Collection, Preliminary Observations, and Recommendations”, Federal Emergency Management Agency, Washington, DC. 2002
- [2] NIST, “Final Report of the National Construction Safety Team on the Collapse of World Trade Center Towers”, NCSTAR1, National Institute of Standards and Technology, Gaithersburg, MD 20899. 2005
- [3] ASCE/SFPE 29, “Standard Calculation Method for Structural Fire Protection”, American Society of Civil Engineers, Reston, VA. 1999
- [4] AISC, “Steel Construction Manual 13th Edition”, American Institute of Steel Construction, Chicago, IL. 2005
- [5] NBC, “National Building Code of Canada”, National Research Council of Canada, Canada. 2005
- [6] ASTM, “Standard Methods of Fire Test of Building Construction and Materials”, Test Method E119-00, American Society for Testing and Materials, West Conshohocken, PA. 2007
- [7] ISO 834, “Fire Resistance Tests – Elements of Building Construction”, International Organization for Standardization, Geneva, Switzerland 1975,
- [8] Kodur, V.K.R., “Performance-based Fire Resistance Design of Concrete-filled Steel Columns”, *Journal of Constructional Steel Research Institute*, Vol. 51, pp. 21-36. 1999
- [9] Parkinson, D.L. and Kodur, V.K.R., “Performance-Based Design of Structural Steel for Fire Conditions – A Calculation Methodology”, *International Journal of Steel Structures* Vol. 7, No. 3, pp. 219-226. 2007

- [10] Eurocode 4, ENV 1994 1-2: "Design of Composite Steel and Concrete Structures" European Committee for Standardization 2005.
- [11] Kodur, V.K.R. and Fike, R.F. "Performance-Based Fire Resistant Design for Concrete-Filled HSS Columns" Proceedings of the 2008 Annual Stability Conference, Nashville TN April 2-5, 2008
- [12] Kodur, V.K.R. and Lie, T.T., "Fire Performance of Concrete-filled Hollow Steel Columns", *Journal of Fire Protection Engineering*, Vol. 7, No. 3, pp. 89-98. 1995
- [13] Lie, T.T. and Chabot, M., "Experimental Studies on the Fire Resistance of Hollow Steel Columns Filled With Plain Concrete", IRC Internal Report No. 611, National Research Council of Canada. 1992
- [14] Kodur, V.K.R. and Lie, T.T., "Fire Resistance of Circular Steel Columns Filled With Fiber-reinforced Concrete", *Journal of Structural Engineering*, ASCE Vol. 122, No. 7, pp. 776-782. 1996
- [15] Kodur, V.K.R. and Lie, T.T., "Evaluation of Fire Resistance of Rectangular Steel Columns Filled With Fiber-Reinforce Concrete", *Canadian Journal of Civil Engineering*, Vol. 24, pp. 339-349. 1997
- [16] Eurocode 1, ENV 1991 1-2: "General Actions – Actions on Structures Exposed to Fire", European Committee for Standardization. 2002
- [17] Magnusson, S.E. and Thelandersson, S., "Temperature-Time Curves of Complete Process of Fire Development; Theoretical Study of Wood Fuel Fires in Enclosed Spaces", *Civil Engineering and Building Series 65*, Acta, Polytechnica, Scandinavia. 1970
- [18] Buchanan, A.H., "Structural Design for Fire Safety", John Wiley and Sons Ltd., New York, NY. 2005
- [19] ASCE 7-05, "Minimum Design Loads for Buildings and Other Structures", American Society of Civil Engineers, Reston, VA. 2005
- [20] Kodur, V.K.R. and Mackinnon, D.H. "Design of Concrete-Filled Hollow Structural Steel Columns for Fire Endurance" *American Institute of Steel Construction Engineering Journal* Vol. 37 pp. 13-24 2000

## **FIRE RESISTANCE OF FIBER REINFORCED CONCRETE COLUMNS**

João Paulo C. Rodrigues <sup>a</sup>, Luís Laím <sup>a</sup>, Georgina Mihailovschi <sup>b</sup>

<sup>a</sup> Faculty of Sciences and Technology, University of Coimbra, Coimbra, Portugal

<sup>b</sup> INTI-Construccion, Buenos Aires, Argentina

### **INTRODUCTION**

In this paper are presented results of fire resistance tests on fiber reinforced concrete columns. The concrete used has a mixture of polypropylene (pp) and steel (st) fibers. The pp fibers have the function to control the spalling while the st fibers have the function to give the concrete the capacity to resist the thermal stresses generated in fire and increase the ductility of the concrete.

The percentage of st fibers varied in the different mixtures studied according to the percentage of steel reinforcement. In other words, it was done a replacement of steel reinforcing bars by steel fibers, maintaining in each column the same quantity of steel reinforcement (st fibers + steel reinforcement). The columns were then tested in fire resistance tests.

The studies developed in the area of fire behavior in fiber reinforced elements are still very premature. Nevertheless, for concrete material, with and without fibers, there are already a lot of tests by Kalifa et al [1] and Han C.G et al (2004) [2]. The most important findings of those studies were that in case of fire the pp fibers will volatilize and micro-channels will be formed in the concrete which served as a way for the release of water vapor to the outside, and, consequently, they allowed a reduction in the spalling of concrete. Another important finding is that the use of st fibers or a mixture of both fibers (pp + st) reduces the loss of residual compression strength and elastic modulus of concrete at high temperatures.

### **1. FIRE RESISTANCE TESTS ON FIBRE CONCRETE COLUMNS**

The main objective of this work was to study the behavior of fiber concrete columns when exposed to fire, being the steel reinforcement partially replaced by st fibers. Four fire resistance tests were carried out, one in a column without fibers (reference test) and three others with a fixed quantity of pp fibers and a variable quantity of st fibers. In these three tests, the steel reinforcing bar of the columns was replaced partly by st fibers so that the total amount of steel in the column (st fibers + steel reinforcing bars) was always the same.

#### **1.1. Composition of concrete**

The concrete was constituted by cement type I 42,5 R (C), superplasticizer (SP), calcareous filler (CF), fine (FS), middle (MS) and coarse sand (CS), grain of rice (GR), fine (CS1: 5-12 mm) and middle crushed stone (CS2: 14-20 mm), polypropylene fibers (PP) and steel fibers (ST), being the respective quantities of each column described in Table 1. Relatively to the total amount of steel in each column the percentage of steel fibres varied between 36% (Column C3) and 84% (Column C1).

Table 1. Composition of concrete columns [per m<sup>3</sup>]

| Column | C [kg] | SP [% CEM] | CF [kg] | FS [kg] | MS [kg] | CS [kg] | CS [kg] | CS1 [kg] | CS2 [kg] | PF [kg] | SF [kg] | W/C  |
|--------|--------|------------|---------|---------|---------|---------|---------|----------|----------|---------|---------|------|
| 1      | 200.0  | 3.0        | 100     | 539     | -----   | -----   | 407     | 319      | 422      | 1.5     | 38.80   | 0.67 |
| 2      | 200.0  | 3.0        | 100     | 539     | -----   | -----   | 407     | 319      | 422      | 1.5     | 27.24   | 0.67 |
| 3      | 200.0  | 3.0        | 100     | 539     | -----   | -----   | 407     | 319      | 422      | 1.5     | 16.56   | 0.67 |
| 4      | 190.0  | 2.9        | 100     | 260     | 380     | 250     | -----   | 940      | -----    | -----   | -----   | 0.59 |

Table 2 presents the quantities of st fibers and steel reinforcement bars in each column.

Table 2. Quantity of steel fibers and steel reinforcement bars in columns

| Column | Dia. of steel bars | Steel reinforcement bars [kg] | Steel fibers [kg] | Total steel [kg] |
|--------|--------------------|-------------------------------|-------------------|------------------|
| C1     | 4 $\phi$ 10        | 7.40                          | 38.80             | 46.20            |
| C2     | 4 $\phi$ 16        | 18.96                         | 27.24             | 46.20            |
| C3     | 4 $\phi$ 20        | 29.64                         | 16.56             | 46.20            |
| C4     | 4 $\phi$ 25        | 46.20                         | -----             | 46.20            |

Table 3 presents the compression strength of the concrete at 28 days, where  $f_{cm}$  and  $f_{ck}$  are the mean and the characteristic value of the compressive strength of concrete, respectively.

Table 3. Compression resistance of concrete at 28 years

| Column | $f_{cm}$ [Mpa] | $f_{ck}$ [Mpa] | Class resistance |
|--------|----------------|----------------|------------------|
| C1     | 23.8           | 16.0           | C12/15           |
| C2     | 27.0           | 19.0           | C12/15           |
| C3     | 25.1           | 17.1           | C12/15           |
| C4     | 29.4           | 21.4           | C16/20           |

## 1.2. Columns

The columns tested presented all a square section 250 mm x 250 mm with 3 meters high. The longitudinal steel reinforcing bars varied according to the values presented in Table 2, while the stirrups had in all columns 8 mm of diameter (Fig. 1).

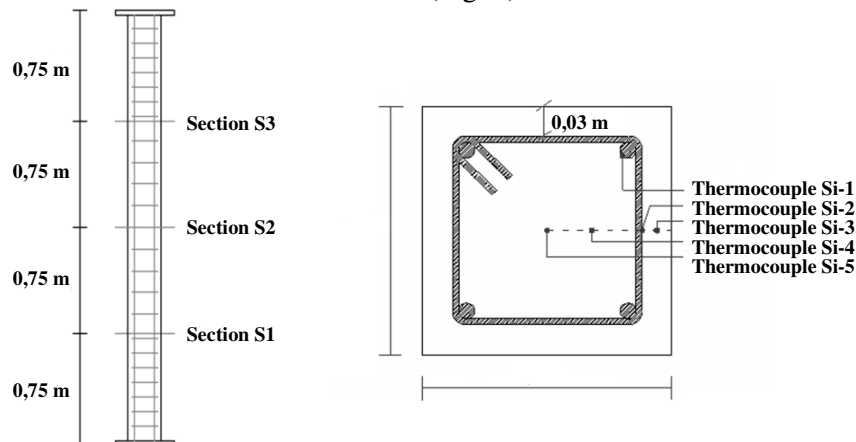
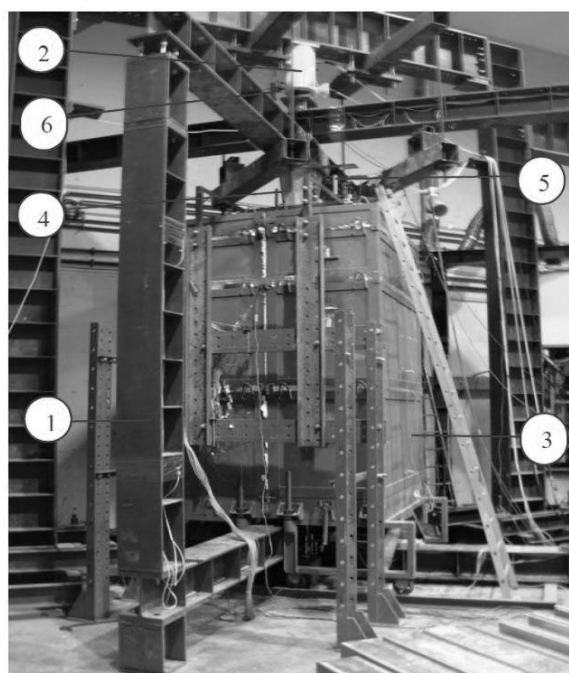


Fig. 1. Scheme of the columns and localization of the thermocouples

The temperature was measured with type K (chromo-alumel) thermocouples located at different depths in three sections of the column as represented in figure 1. Thermocouples Si-1 and Si-2 were welded in steel reinforcing bars, while thermocouples Si-3, Si-4 and Si-5 were embedded in the concrete.

### 1.3. Test procedure

In the experimental tests was used a new test set-up for fire resistance test of columns with restrained thermal elongation, that has been developed in development in the Faculty of Sciences and Technology of the University of Coimbra (Fig. 2). This system is composed by a restraining frame of variable stiffness (1), although in these tests was adopted a stiffness of 13 KN/mm (stiffness determined experimentally). This restraining frame had the function to simulate the stiffness of the surrounding structure to the column when exposed to fire.



*Fig. 2.* Test set-up for fire resistance tests on building columns

The columns were subjected to a constant compressive load, during the whole test, of 686 KN. This load was controlled by a load cell of 1 MN, located on the head of the piston of hydraulic jack (6). The applied load corresponded to 70% of the design value of buckling resistance of the column at room temperature. This load was calculated to the reference column C4, through the method of the nominal stiffness, according to EC 2 part 1-1 [3]. Thus, it was pretended to simulate the serviceability load of the column when part of a real structure. The load was applied by an hydraulic jack (2) controlled by a servo hydraulic system.

The thermal action was applied by a modular electric furnace (3) and followed nearly the ISO 834 fire curve [4].

The restraining forces generated in the column due to heating were measured by load cell of 3 MN located into a steel piston (4). This piston was placed between the testing column and the restraining frame, as shown in figure 2.

The axial displacements and rotations on top and base of the column were also measured by displacement transducers (5) orthogonally arranged in three different points, forming a deformation plan.

Besides, as noted, the temperatures in different sections and depths in the cross section of the column and the temperatures of the column were measured.

#### 1.4. Results

Figure 3 presents the furnace temperature during the four tests. The temperature followed nearly the ISO 834 fire curve and was very uniform in the four tests.

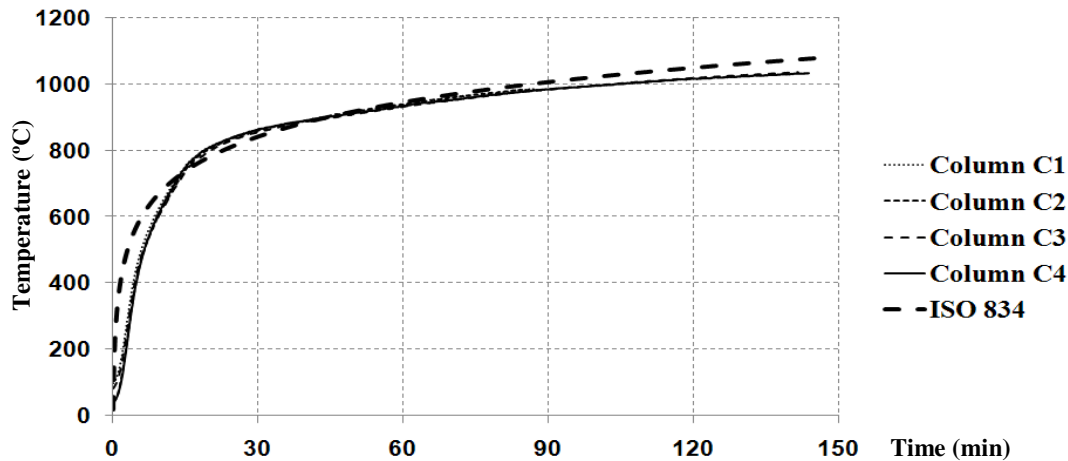


Fig. 3. Temperature in the furnace in tests

Figure 4 shows, as example, the evolution of temperature at different points in section S3 and figure 5 the temperature along the height of column C2.

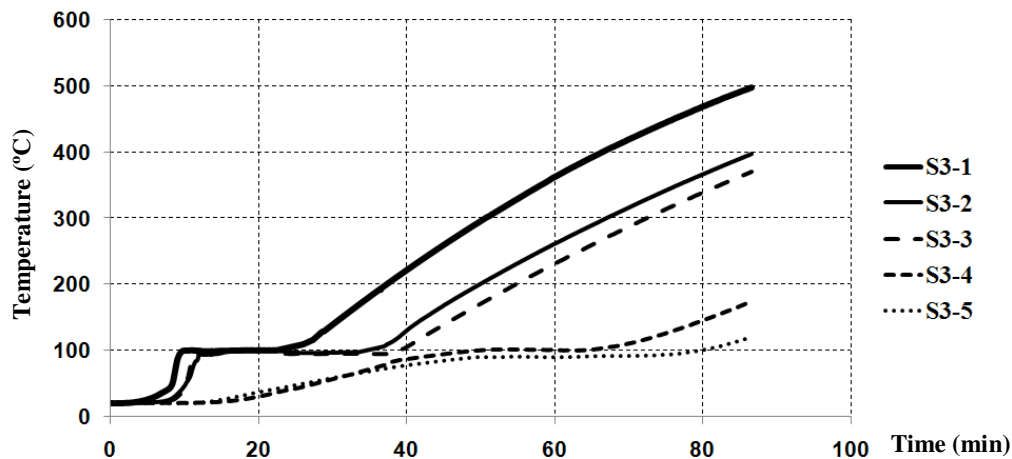


Fig. 4. Evolution of temperature in section S3 of column C2

In figure 4 it can be observed that the temperature remained practically unchanged up to nearly 40 min and then started to increase more in thermocouples near the surface. The temperature in the thermocouples did not exceed 500 °C while the temperature of the furnace reached around 1100°C. The difference of temperatures between the surface and inner thermocouples was more than 400°C, showing a very big thermal gradient along the cross-section of the concrete column. The low thermal conductivity of the concrete associated to the maintenance of the integrity of the element due to the use of pp fibers in the concrete was the responsible for this fact [5].

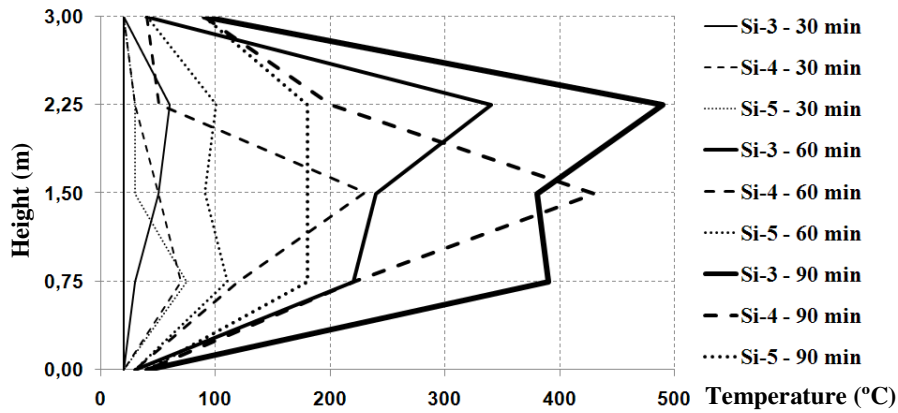


Fig. 5. Evolution of temperature in concrete along the height of the column 2

The thermal gradients in height were also strong and increased throughout time as shown in figure 5.

Figure 6 shows the restraining forces in columns throughout time. In this graph it can be observed that column C1 presented a small increasing in restraining forces. The higher the percentage of steel reinforcement bars the higher was the increasing in restraining forces and the fire resistance. Column C3 with steel reinforcing bars dia. 20 mm and an amount of 16,56 Kg/m<sup>3</sup> of steel fibers presented a development of restraining forces similar to column C4 (reference column). Column C4 had steel reinforcing bars dia. 25 mm and no st fibers.

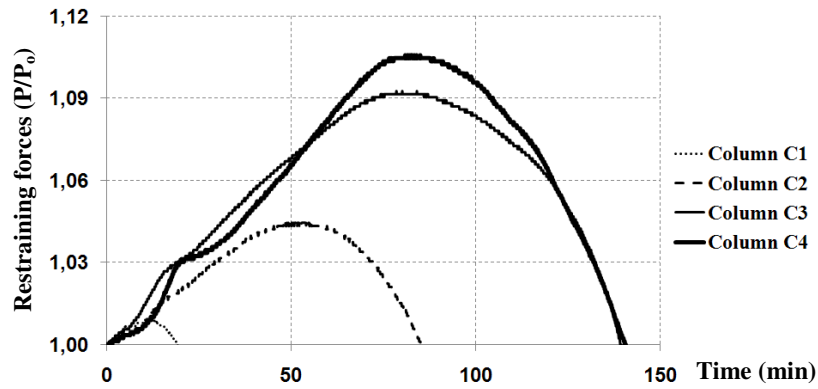


Fig. 6. Restraining forces in columns throughout time

Concerning the displacements and rotations in the ends of the columns (top and bottom) they were very small as expected for a concrete column (Figs. 7 and 8).

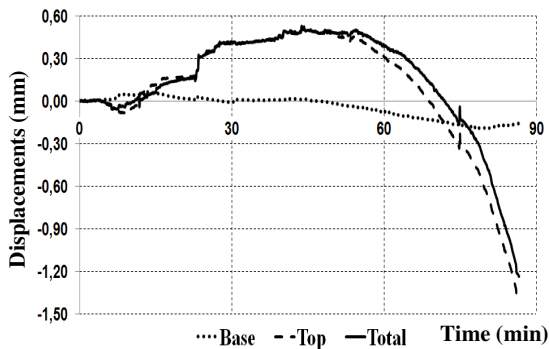


Fig. 7. Axial displacements in column C2

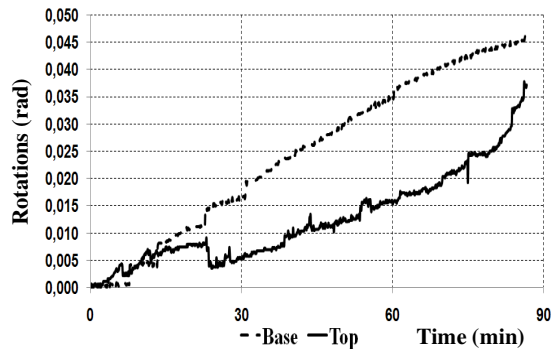


Fig. 8. Rotations in column C2

The columns made of concrete with pp fibers (fig. 9) didn't show any spalling after test in opposition to the reference column C4 (fig. 10) that showed the detachment of big pieces of concrete in the edges of the cross-section and in the more compressed areas of the column.



Fig. 9. Column C1 after test



Fig. 10. Column C4 after test

## 2. CONCLUSIONS

As main conclusions of this work, we may see that the use of pp and st fibers in concrete improves the fire behavior of the columns. The pp fibers volatilize and create paths where the water vapour generated inside the concrete can escape, while the steel fibers give the concrete the capacity to resist to the thermal stresses developed in fire.

A day after the test, the reference column showed extensive spalling, exposing the steel reinforcing bars, while the columns with pp and st fibers were not altered. Thus, the use of pp fibers and a small quantity of st fibers in concrete can provide benefits in controlling the spalling of concrete.

The replacement of steel reinforcing bars by steel fibers in big quantity didn't show a significant advantage in the fire behavior of the columns, since the columns that had greater fire resistance were those with steel reinforcing bars with bigger diameter.

## REFERENCES

- [1.] Kalifa, P., Chéné, G. e Gallé, C. (2001). "High-temperature behaviour of HPC with polypropylene fibres from spalling to microstructure". *Cement and Concrete Research*. Vol. 31, pp. 1487–1499.
- [2.] Cheon-Goo Han, Yin-Seong Hwang, Seong-Hwan Yang & N. Gowripalan (2004). "Performance of spalling resistance of high performance concrete with polypropylene fiber contents and lateral confinement". *Science Direct 35* (2005), pp 1747–1753.
- [3.] EN 1992-1-1: Design of concrete structures, part 1-1: General rules and rules for buildings, European Committee for Standardization, Brussels, 2004.
- [4.] EN 1992-1-2: Design of concrete structures, part1-2: General rules - Structural fire design", European Committee for Standardization, Brussels, 2004.
- [5.] Zeiml, M., Leithner, D., Lackner, R. e Mang, H. A. (2006). "How do polypropylene fibers improve the spalling behavior of in-situ concrete?". *Cement and Concrete Research*, Vol. 36, pp. 929–942.

## **FIRE RESISTANCE TESTS ON CONCRETE COLUMNS WITH RESTRAINED THERMAL ELONGATION**

Alberto Miguel B. Martins <sup>a</sup>, João Paulo C. Rodrigues <sup>a</sup>

<sup>a</sup> Department of Civil Engineering, Faculty of Sciences and Technology, University of Coimbra, Portugal

### **INTRODUCTION**

The high temperatures experienced in a fire, lead to thermal elongation of the structural members. However, other parts of the structure may remain at lower temperatures and this will restrain their thermal elongation. The result is to increase stresses in the elements and, if these exceed their buckling resistance the elements will collapse. It is therefore important to analyze the influence of the restraint of the structure on the behaviour of structural elements in the event of fire.

The effect of the boundary conditions on the fire behaviour of reinforced concrete columns has not yet been sufficiently studied [1], [2], [3]. In a recent experimental study [2] it was found that the values of the restraining forces generated were less than 15% of the column's design load. The test models used in this study were small scale, however, (cross-section of 125×125 mm<sup>2</sup> and 1800 mm in height), and were made of high-strength concrete. Thus it cannot be stated with certainty that the results can be extrapolated for larger elements made of other types of concrete.

The Eurocodes allow the use of simplified calculation methods to guarantee that the structures offer appropriate fire resistance, instead of using traditional fire resistance tests. But those methods fail to take account of all the parameters present in real fires in which a structural element may be involved. One parameter not considered is the restraint of the structure according to the thermal elongation of the element.

The main objective of the work described in this paper was to study the fire behaviour of reinforced concrete columns with restrained thermal elongation.

### **1 EXPERIMENTAL PROGRAMME**

Several fire resistance tests were carried out on reinforced concrete columns. The variables studied in the experimental tests were the longitudinal steel reinforcement ratio, the slenderness of the column and the stiffness of the structure surrounding the column.

#### **1.1 Experimental models**

The specimens tested were reinforced concrete columns 3000 mm long, with cross-sections of 250×250 mm<sup>2</sup> and 160×160 mm<sup>2</sup>, with S355 steel plates measuring 450×450×30 mm at their ends. These plates were used to fix the testing column to the restraining frame in the tests.

The columns were connected to the steel end plates out by welding the longitudinal steel reinforcement bars to the steel plates prior to casting.

Table 1. Characteristics of the columns

| Column Reference | Cross-section                      |                                   | Longitudinal Reinforcement |                                   | Reinforcement Ratio $A_s/A_c$ [%] |
|------------------|------------------------------------|-----------------------------------|----------------------------|-----------------------------------|-----------------------------------|
|                  | $h \times b$<br>[mm] $\times$ [mm] | Area, $A_c$<br>[mm <sup>2</sup> ] | Number and Diameter        | Area, $A_s$<br>[mm <sup>2</sup> ] |                                   |
| P16-10-k13       | 160 $\times$ 160                   | 25600                             | 4 $\phi$ 10                | 314.2                             | 1.23                              |
| P16-10-k45       | 160 $\times$ 160                   | 25600                             | 4 $\phi$ 10                | 314.2                             | 1.23                              |
| P16-16-k13       | 160 $\times$ 160                   | 25600                             | 4 $\phi$ 16                | 804.2                             | 3.14                              |
| P16-16-k45       | 160 $\times$ 160                   | 25600                             | 4 $\phi$ 16                | 804.2                             | 3.14                              |
| P25-16-k13       | 250 $\times$ 250                   | 62500                             | 4 $\phi$ 16                | 804.2                             | 1.27                              |
| P25-16-k45       | 250 $\times$ 250                   | 62500                             | 4 $\phi$ 16                | 804.2                             | 1.27                              |
| P25-25-k13       | 250 $\times$ 250                   | 62500                             | 4 $\phi$ 25                | 1963.5                            | 3.14                              |
| P25-25-k45       | 250 $\times$ 250                   | 62500                             | 4 $\phi$ 25                | 1963.5                            | 3.14                              |

Table 1 gives the characteristics of the columns tested. In this table the first column indicates the label of each column tested. Thus the label P25-16-k13 indicates that the dimensions of the cross-section are 250 mm $\times$ 250 mm, the longitudinal steel reinforcement are 16 mm diameter bars and the stiffness of the surrounding structure in the test was 13 kN/mm.

The strength classes of the materials used to make the columns were C20/25 for the concrete and A500 NR for the steel.

## 1.2 Experimental set-up

This comprised a large number of pieces arranged in a very complex system that is described in the following sections. Figure 1 gives a general view of the experimental set-up.

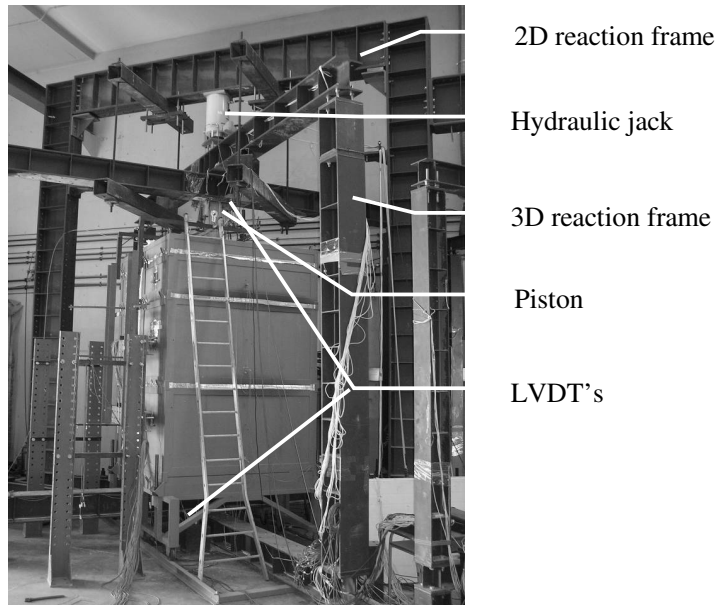


Fig. 1. Experimental set-up

## 1.3 Boundary conditions

The boundary conditions for the tests were formed by two steel frames: a 2D reaction frame and a 3D reaction frame. This latter frame is hereunder referred to as the “restraining frame”.

The 2D reaction frame consisted of two S355 steel HEB500 columns and an HEB600 beam of the same material, connected with bolts M24 class 8.8.

The 3D reaction frame consisted of four HEB300 columns and four HEB 300 beams made of S355 steel, arranged orthogonally. The purpose of this restraining frame was to simulate the effect of the stiffness of the building structure surrounding the column, in a fire. All the elements were connected with bolts M24 class 8.8.

It was possible to change the position of the columns and beams of the 3D restraining frame so that the column being tested could have different stiffness values. Stiffness of 13 kN/mm (*k13*) and 45 kN/mm (*k45*) were tested.

#### 1.4 Mechanical action

The mechanical action imposed on the models was a compression force, applied by a hydraulic jack with 3 MN maximum capacity, fixed in the beam of the 2D reaction frame. The hydraulic jack was controlled by a servo-hydraulic control unit.

This load simulated the serviceability load of the column when part of a real structure. This load was 70% of the value of the column's design load at room temperature, calculated according to EC2-1-1 [4, 5].

#### 1.5 Thermal action

The thermal action on the experimental models was applied by a modular electric furnace with internal dimensions of 1.5m×1.5m×2.5m capable of temperatures up to 1200°C and fire curves with different heating curves.

In all tests the heating curves applied were close to the standard curve ISO 834.

#### 1.6 Instrumentation and data acquisition

The applied load was recorded by a compression load cell of 1 MN. The load cell was placed on the top of the hydraulic jack.

The restraining forces that developed due to the heating of the column were measured by a load cell of 3 MN placed inside a cylindrical piston made of high stiffness steel.

The axial displacements were measured at the top with 3 LVDTs and at the bottom with 4 LVDTs placed orthogonally to form a plane of deformation. The LVDT model used was TML CDP-100.

The temperatures were measured by type K chrome-alumel thermocouples in three sections along the length of the column. Five thermocouples were used in each section, two welded to the steel reinforcement bars and the others embedded in the concrete at various depths (one

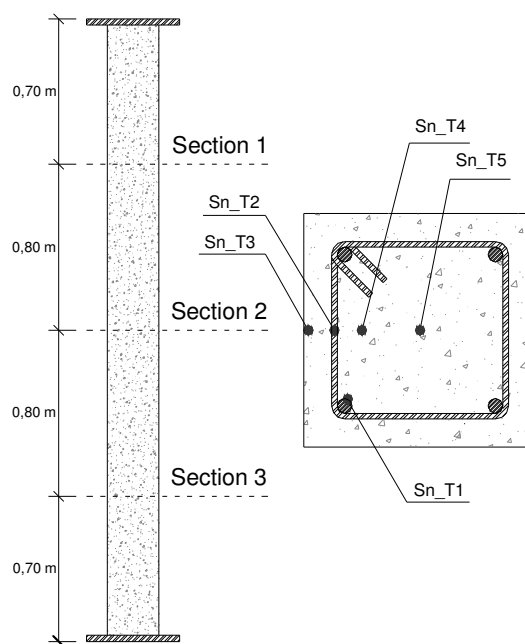


Fig. 2. Location of the thermocouples (n indicates the section number)

nearer the surface Sn\_T3, another in the center of section Sn\_T5 and the third midway between these two Sn\_T4) (Fig. 2).

All parameters were recorded with datalogger model TML TDS-530.

## 2 TEST RESULTS

### 2.1 Temperatures

As an example Fig. 3 shows the temperature distribution in the top cross-section S1\_Ti of column P25-16-k45 as a function of time. The very high thermal gradients between the inner parts of the concrete and the surface can be seen.

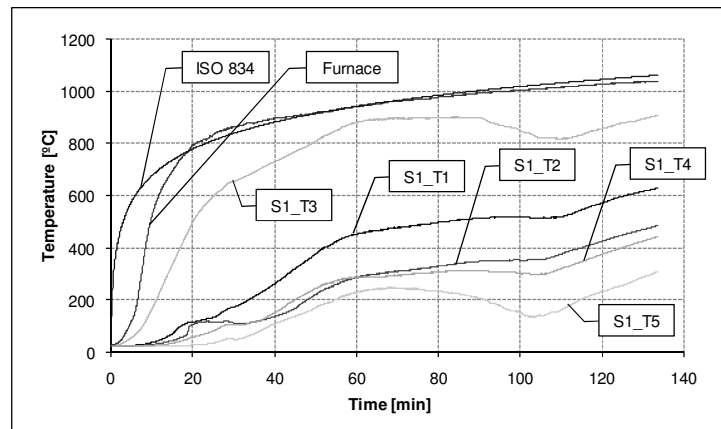


Fig. 3. Temperature in the thermocouples as a function of time (column P25-16-k45)

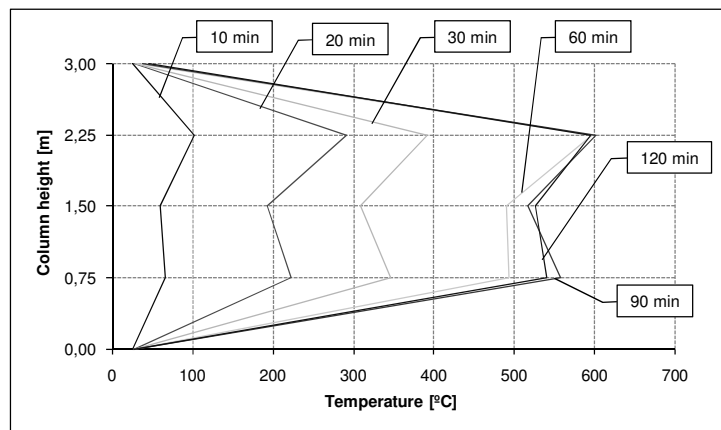


Fig. 4. Thermal gradients in height as a function of fire duration (column P25-16-k45)

Figure 4 shows the thermal gradients vertically in the column, as a function of the heating time. The large thermal gradients registered between the central part of the column and the ends were due to the fact that the ends were protected and not exposed directly to the heating. On the other hand, the graph shows that after 60 min the temperatures in the central part are almost unchanged.

## 2.2 Restraining forces and fire resistance

Figures 5 and 6 give the graphs for the variation of the restraining forces as a function of time. These graphs show the influence of the longitudinal steel reinforcement ratio and the stiffness of the surrounding structure on the restraining forces and on the fire resistance of the columns

All the results are summarized in Table 2.

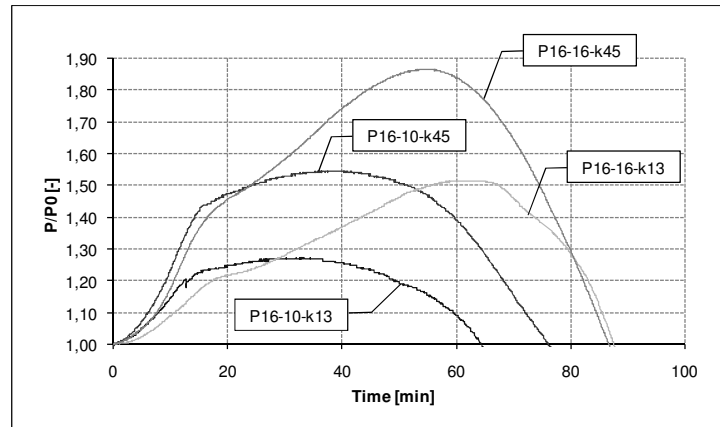


Fig. 5. Restraining forces versus time for columns  $160 \times 160 \text{ mm}^2$

The increase in the steel reinforcement ratio led to an increase in the fire resistance of 29.9% and 13.4%, for the  $160 \times 160 \text{ mm}^2$  columns, and an increase of 5.4% and a reduction of 10.4%, for the  $250 \times 250 \text{ mm}^2$  columns, respectively for stiffness  $k13$  and  $k45$  of the surrounding structure.

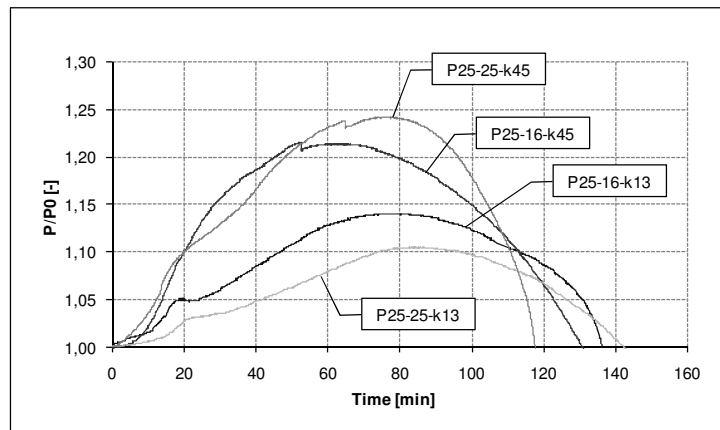


Fig. 6. Restraining forces versus time for columns  $250 \times 250 \text{ mm}^2$

The increasing of the steel reinforcement ratio led to an increase in the restraining forces of 23.8% for stiffness  $k13$  and 31.7% for stiffness  $k45$ , in the  $160 \times 160 \text{ mm}^2$  columns, while for the  $250 \times 250 \text{ mm}^2$  columns a reduction of 3.3% for stiffness  $k13$  and an increase of 2.7% for stiffness  $k45$  was observed. The increased stiffness of the surrounding structure also showed an increase in the restraining forces from 27.4% to 35.4%, for the  $160 \times 160 \text{ mm}^2$  columns, and from 7.5% to 13.5% for the  $250 \times 250 \text{ mm}^2$  columns, respectively for the smaller and higher steel reinforcement ratio.

Table 2. Experimental results for the restraining forces and fire resistance

| Column Reference | $P_0$ [kN] | $P_{rest}$ [kN] | $P_{rest}/P_0$ [-] | Fire resistance [min] |
|------------------|------------|-----------------|--------------------|-----------------------|
| P16-10-R1        | 143.82     | 39.43           | 27.4%              | 64.70                 |
| P16-10-R2        | 152.29     | 83.52           | 54.8%              | 76.58                 |
| P16-16-R1        | 181.06     | 92.72           | 51.2%              | 87.73                 |
| P16-16-R2        | 184.71     | 159.89          | 86.6%              | 86.87                 |
| P25-16-R1        | 494.71     | 68.85           | 13.9%              | 136.22                |
| P25-16-R2        | 507.40     | 108.78          | 21.4%              | 131.67                |
| P25-25-R1        | 656.34     | 69.36           | 10.6%              | 143.53                |
| P25-25-R2        | 675.32     | 162.81          | 24.1%              | 118.02                |

$P_0$  – Applied load;  $P_{rest}$  – Maximum value of the restraining forces.

### 3 CONCLUSIONS

The main conclusions of this work are:

- Increasing the longitudinal reinforcement ratio has a beneficial effect on the fire resistance of the columns, but the use of 25 mm diameter bars contradicts this tendency [6];
- Increasing the stiffness of the surrounding structure led to an increase in the generated restraining forces;
- Increasing the slenderness leads to a reduction in the fire resistance, with that reduction being more significant for columns with a smaller longitudinal reinforcement ratio;
- If the thermal restraint is increased a general tendency towards reduction of the fire resistance is observed;
- Spalling occurred in all tests but explosive spalling occurred in just one case;
- Spalling occurred mainly in the compressed zones and at the edges of the columns.

### REFERENCES

- [1] Benmarce, A., Guenfoud, M., Behaviour of axially restrained high strength concrete columns in fire, *Construction and Building Materials*, article in press, 2005;
- [2] Fletcher, I.A., Welch, S., Torero, J.L., Carvel, R.O., Usmani, A., The behaviour of concrete structures in fire, *Thermal Science*, Vol. 11, No. 2, 2007, pp. 37-52
- [3] Correia Rodrigues, J.P., Valente, J.C., Cabrita Neves, I., Experimental research on the critical temperature of compressed steel elements with restrained thermal elongation, *Fire Safety Journal*, 35, 2000, pp. 77-98
- [4] CEN, Eurocode 2: Design of Concrete Structures – Part 1-1: General rules and rules for buildings, CEN – Comité Européen de Normalisation, Brussels, April 2004;
- [5] CEN, Eurocode 2: Design of Concrete Structures – Part 1-2: General rules – Structural Fire Design, CEN – Comité Européen de Normalisation, Brussels, December 2004;
- [6] Dotreppe, J.-C., Franssen, J.-M., Bruls, A., Baus, R., Vandeveld, P., Minne, R., van Nieuwenburg, D. and Lambotte, H., Experimental research on the determination of the main parameters affecting the behaviour of reinforced concrete columns under fire conditions, *Magazine of Concrete Research*, 49, No. 179, 1997, pp. 117-127

## COMPRESSIVE STRENGTH OF FIBRE REINFORCED CONCRETES

Susana O. Santos<sup>a</sup>, João Paulo C. Rodrigues<sup>a</sup>, Romildo Toledo<sup>b</sup>

<sup>a</sup> Faculty of Science and Technology of University of Coimbra, Portugal

<sup>b</sup> Federal University of Rio de Janeiro, Department of Civil Engineering, COPPE, Rio de Janeiro, Brazil

### INTRODUCTION

During the last 20 years, concrete has been developed to have better performances for normal and extreme actions. The changes made in the composition of the mixtures (reduction of water content, use of superplasticizers, optimization of grain size distribution, use of particles with pozzolanic activity, addition of fibers, etc.) lead to striking improvements in many properties such as strength, reology of fresh concrete, ductility and compactness. The latter yields in most cases a better durability, but it may also lead to a brittle behavior of high-performance concrete (HPC) in fire conditions. Under certain thermal and mechanical stresses, HPC may spall. [1]

Spalling can be defined as the violent or non-violent breaking off of layers or pieces of concrete from the surface of a structural element when it is exposed to high and rapidly rising temperatures, as experienced in fires [2]. It results from two concomitant processes: (i) the thermo-mechanical process associated with the thermal expansion/shrinkage gradients that occur within the element being heated and (ii) the thermo-hydral process that generates high-pressure fields of gas (water vapour and enclosed air) in the porous network [3]

During last year, in Europe, fires occurred in several tunnels which caused loss of lives as well as significant damages in the concrete structure. Some of these tunnels such as the "Channel Tunnel" and "Great Belt Tunnel" were recently built, which shows that spalling phenomenon is not yet completely known in order to be prevented in the construction process.

This paper intended to contribute to the understanding of concrete behavior at high temperatures, and to the characterization of the spalling phenomenon, through the development of concretes with improved fire behavior. Thus, it is presented a Portuguese and a Brazilian study carried out to develop fiber concrete compositions with better fire behavior.

## 2 EXPERIMENTAL STUDIES

### 2.1 Portuguese Tests

In the Laboratory of Testing Materials and Structures of the University of Coimbra, studies are being carried out to develop a high-strength concrete (HSC) with improved fire behavior. So, three compositions of concrete were developed, one without fibers, one with steel and polypropylene fibers together and a third one with glass fibers. Compressive strength tests at high temperatures were carried out in cylindrical specimens made from these three different concrete compositions [4].

#### Concrete compositions

In *Table 1* are presented the three compositions developed. All compositions had cement Portland (CEM) type II 42,5R, superplasticizer (SP) SIKA 3002 HE, limestone filler (LF) and four different aggregates: fine sand (FS) with a fineness modulus of 1.87, coarse aggregate

(CA) with maximum size of 9.5mm and two calcareous crushed stone (CS1 and CS2 with maximum sizes of 12.5 mm and 25 mm, respectively).

Table 1. Concrete compositions (per  $m^3$ )

|        | CEM<br>[kg] | CS1<br>[kg] | CS2<br>[kg] | CA<br>[kg] | FS<br>[kg] | LF<br>[kg] | W/<br>C | SP<br>[%CEM] | PF<br>[kg] | SF<br>[kg] | GF<br>[kg] |
|--------|-------------|-------------|-------------|------------|------------|------------|---------|--------------|------------|------------|------------|
| HSC    | 400         | 600         | 321         | 230        | 470        | 200        | 0.3     | 2.9          | -          | -          | -          |
| HSCSPF | 400         | 600         | 321         | 230        | 470        | 200        | 0.3     | 11.6         | 1          | 70         | -          |
| HSCGF  | 400         | 600         | 321         | 230        | 470        | 200        | 0.3     | 11.6         | -          | -          | 1.5        |

The compositions differ only in the fiber type, or lack of them. For the first composition (HSC) fibers were not incorporated, in the second there were used steel fibers (SF) DRAMIX RC ZP305 with length of 30 mm, diameter of 0.55 mm, relation length/diameter of 55, tensile strength of 1100MPa, together with polypropylene fibers (PF) DURO-FIBRIL, with diameter of 31  $\mu$ m and length of 6 mm (HSCSPF); in the third composition were used glass fibers (GF) VIMACRACK, with length of 12 mm and diameter of 14  $\mu$ m (HSCGF).

In Table 2 are presented the resistance classes for each concrete composition, obtained through the European Standard EN 206-1 (2000) by the realization of compressive strength tests at room temperature, after 28 days. This table also incorporates the values correspondent to the compression load of  $0.7f_{cd}$  applied in the compressive strength tests of concrete at high temperatures.

Table 2. Compressive resistance classes

|        | $f_c$ (MPa) | $f_{cm}$ (MPa) | $f_{ck}$ (MPa) | Resistance Class | Compression load<br>( $0.7f_{cd}$ ) (kN) |
|--------|-------------|----------------|----------------|------------------|--|
| HSC    | 73.04       | 71.33          | 63.33          | <b>C50/60</b>    | 130.5                                    |
|        | 72.25       |                |                |                  |  |
|        | 68.69       |                |                |                  |  |
| HSCSPF | 75.79       | 76.21          | 68.21          | <b>C55/67</b>    | 140.6                                    |
|        | 77.18       |                |                |                  |  |
|        | 75.65       |                |                |                  |  |
| HSCGF  | 65.19       | 64.16          | 56.16          | <b>C45/55</b>    | 115.8                                    |
|        | 57.04       |                |                |                  |  |
|        | 70.23       |                |                |                  |  |

The polypropylene fibers, when exposed to high temperatures, form pathways that allow the output of steam, thereby reducing the pressure accumulated in the porous network of the concrete element, while the steel fibers increase the ductility of the concrete, thus allowing a more mechanically and thermally resistant concrete. The aim of include glass fibers in concrete composition was to assess to which point these fibers can replace the polypropylene and steel fibers, taking into account the concrete strength at high temperatures.

### Specimens

The specimens were cylinders of 75 mm diameter ( $\varnothing$ ) and 225 mm height (h), where the ratio  $h/\varnothing$  is 3.

Five thermocouples type K (Cromo-Alumel), with diameter of 0.5 mm, were placed within the specimen and its surface to measure the temperature during high temperatures tests.

The location of thermocouples was defined according to the recommendations of RILEM TC-200 HTC [5].

### Test procedure

The test system used is presented in *Fig. 1*, comprising a press machine AMSLER with a capacity of 5 MN (a), a cylindrical furnace with a inner diameter of 90 mm and 300 mm of height and capacity to reach temperatures up to 1200°C (b) and a datalogger TML TDS-601 for data acquisition (force, displacement, and furnace and specimens temperature) (c).

The tests procedures were adopted according to the recommendations of the RILEM TC-200 HTC [5]. The specimen was initially loaded with a load equal to 70% of the design value of concrete compressive strength at room temperature ( $0,7f_{cd}$ ). When the load level was reached, the specimen was heated at a heating rate of 3°C/min, until the desired level of temperature. Three levels of maximum temperature were experimented (300°C, 500°C and 600°C). The level of temperature was reached when the average temperatures on the three specimen thermocouples of the surface match the temperature of the furnace. The specimen was then kept at that temperature for an hour to stabilize. The difference of temperatures inside and outside the specimen, given by thermocouples at the same level, was also verified. This difference should not be above 20°C.

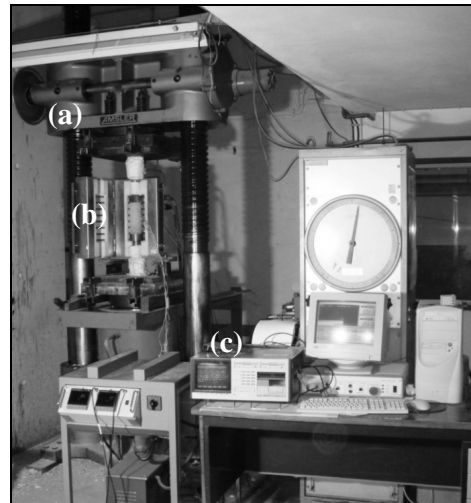


Fig. 1. Test system

### Results

In *Fig. 2* is presented a graph with the variation of concrete compressive strength versus the maximum temperature that specimens were subjected in the experimental tests.

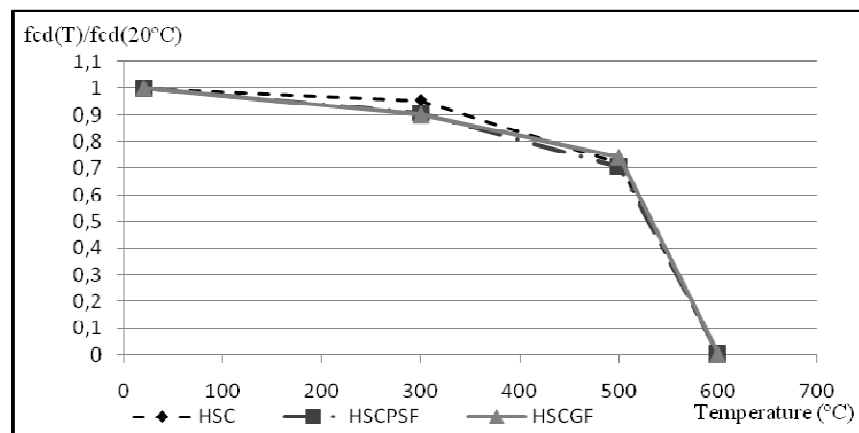


Fig. 2. Concrete compressive strength vs maximum temperature.

In tests carried out up to 300 ° C, all specimens had a slight loss of strength. However, the samples of HSC had a smaller loss of strength (5%) that those made of HSCPSF and HSCGF (10%).

In the 500°C tests, the HSC and HSCPSF specimens lost about 30% of its strength at room temperature while the samples made of HSCGF suffered a strength decrease of approximately 26%.

In the maximum temperature tests, 600°C, all the specimens collapsed before reaching the stabilization of the temperature.

It was observed a less explosive failure in HSCPSF specimens confirming the effectiveness of steel fibers in obtaining more ductile concrete and control of cracking.

Explosive spalling was not observed in any of the heating-cooling tests, only some cracks. It was verified an aggravation of cracking, for tests up to 500°C. For this level of temperature, the HSCSPF specimens suffered exfoliation at the top.

In tests for 300°C, the HSC specimens showed only some surface cracks.

## 2.2 Brazilian Tests

Tests to assess the stress-strain behavior of polypropylene fiber reinforced high performance concrete exposed to ambient temperature (27°C) and to temperatures of 400, 650 and 900°C, were carried out in the Laboratory of Structures of COPPE of the Federal University of Rio de Janeiro [6].

The residual compressive strength and elastic modulus were determined after allowing the samples to cool down to room temperature.

The role of polypropylene fiber to control the spalling of high performance concrete (HPC) was also investigated.

### Concrete composition

In specimens composition was used Portland cement (CPIII-40), sand with a fineness modulus of 2.70, crushed syenite with a maximum size of 9.50 mm and a specific weight of 2.70 g/cm<sup>3</sup>, naphtalene sulphonate based superplasticizer (SP) with a total amount of solid particles of 40% and silica fume. The polypropylene fibres (PP) were 40 mm long and had a specific weight of 0.91 kg/dm<sup>3</sup> and an elastic modulus value of 3500 MPa.

The mixtures were produced in order to reach compressive strength levels at 28 days of 65 MPa (C65) and 85 MPa (C85). They were reinforced with 0.25% and 0.5% by volume of polypropylene fibers (C65PP0.25/C85PP0.25 and C65PP0.5/C85PP0.5 series, respectively).

The mix proportions of the mixtures are summarized in *Table 3*.

*Table 3.* Mix proportions for the polypropylene fiber reinforced concrete -HPC (per m<sup>3</sup>)

| <i>Series</i> | <i>Cement [kg]</i> | <i>Silica [kg]</i> | <i>Sand [kg]</i> | <i>Agg. [kg]</i> | <i>Water [l]</i> | <i>SP [l]</i> | <i>Fibres [kg]</i> |
|---------------|--------------------|--------------------|------------------|------------------|------------------|---------------|--------------------|
| C65           | 365                | 37                 | 780              | 857              | 156              | 8.30          | -                  |
| C85           | 414                | 42                 | 694              | 895              | 151              | 8.49          | -                  |
| C65PP0.25     | 365                | 37                 | 780              | 857              | 156              | 8.30          | 2.28               |
| C65PP0.5      | 365                | 37                 | 780              | 857              | 156              | 8.30          | 4.56               |
| C85PP0.25     | 414                | 42                 | 694              | 895              | 151              | 8.49          | 2.28               |
| C85PP0.5      | 414                | 42                 | 694              | 895              | 151              | 8.49          | 4.56               |

## Specimens and test procedure

In the compression tests were used cylindrical specimens with 100 mm x 200 mm. These tests were carried out in a 2500 kN MTS testing machine, at a loading rate of 0.00078mm/s. Three samples were tested for each mixture. Average values were taken as representative for each analyzed mixture.

Prismatic specimens (150 mm x 260 mm x 100 mm) were used in the spalling and total porosity studies. They were heated in a computer-controlled electric furnace at a rate of 10°C/min. Three maximum temperatures (400°C, 650°C and 900°C) were chosen. After the peak temperature was reached, it was maintained for one hour and then cooled down at a rate of 0.4-0.5°C/min until room temperature.

Total porosity was measured by means of water absorption tests on cylindrical specimens (60 mm height, with a diameter of 25.4 mm) extracted from the prismatic samples.

## Results

Typical compressive stress-strain curves for the HPC matrices and polypropylene fiber reinforced-HPC, at room temperature and after exposure to high temperatures, are presented in Fig. 3.

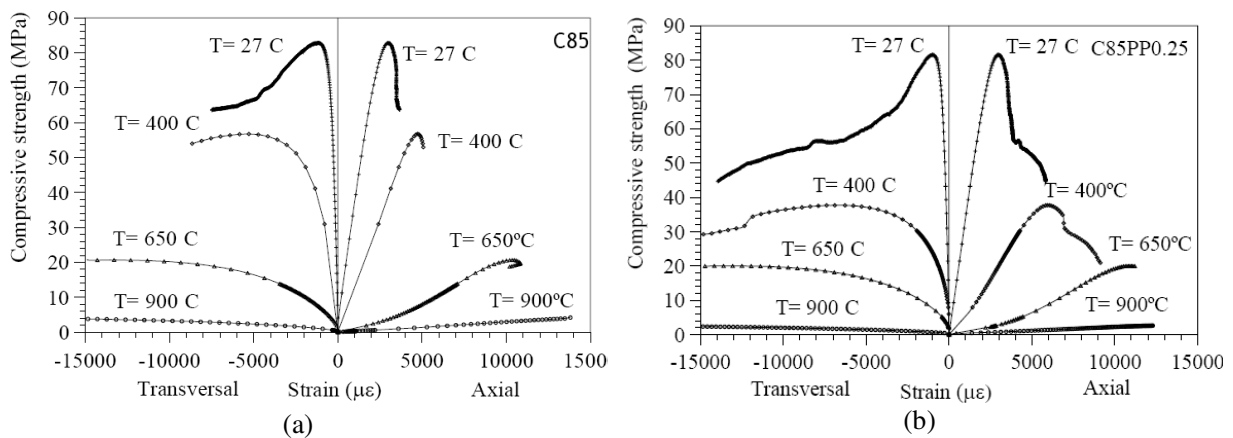


Fig. 3 Compressive stress-strain curves at room temperatures after exposure to high temperatures: (a) Concrete series C85; (b) Composite series C85PP0.25

At room temperature, the addition of small volume fractions of polypropylene fibers did not change significantly the behavior in compression of the matrices.

The results indicate that at the temperature of 400°C, the concrete specimens reinforced with polypropylene fiber show a strength and rigidity loss more pronounced than those observed to the plain HPC mixtures. At higher temperatures (650°C and 900°C) all specimens experienced a similar strength and rigidity loss, independently of the presence of fibers in the mixtures.

The worst behavior of the reinforced concrete specimens is associated with the melting of polypropylene fibers at about 170°C. During the melting process occurs a slight dilatation of about 10% [3] of the polypropylene generating extra pore-pressure in the concrete leading to a crack density higher than that observed in the plain concrete. The fiber beds led in the matrix after fiber melting can also help in the nucleation of cracks locally as they have sharp angles favoring the distribution of microcracking.

In this study, spalling was observed in prismatic samples of concrete C85 when they were being heated to the temperature of 400°C. The spalling of the HPC prismatic sample occurred at about 200-220°C. The addition of 0.25% by volume of polypropylene fibers to the C85 matrix prevented concrete spalling.

### 3 CONCLUSIONS

In the Portuguese studies, it could be concluded that the inclusion of PP fibers in the concrete compositions avoided spalling. The specimens of concrete with steel and polypropylene fibers had better performance than those with glass fibers. It has been observed a small detachment of concrete surface in the last ones.

In compression tests, it was noticed a more explosive rupture in specimens without fibers as well as those with glass fibers. It was confirmed the benefit of steel fibers in the crack control.

The incorporation of steel fibers with a lower length and a lower amount of polypropylene fibers conferred greater strength to the concrete specimens.

In this study, in compression tests, the glass fibers have an identical behavior to the polypropylene and steel fibers. The loss of strength of HSCGF specimens, at high temperatures, was only slightly lower than the HSC and HSCPSF ones. Thus, it was concluded that glass fibers not had the intended effect, the effect of winning the mechanical and thermal stresses, which are developed in the concrete at high temperatures. However, further studies in this area have to be performed, given the small number of tests performed in this experimental work.

In the Brazilian studies it was concluded that at high temperatures, the concrete specimens reinforced with PP fiber showed a strength and rigidity loss more pronounced than those observed to the plain HPC mixtures. The increase in porosity was also higher for the reinforced specimens. This behavior can be associated with melting of polypropylene fibers at about 170°C.

In this study, it could also be concluded that the addition of polypropylene fibers to the C85 matrix prevented concrete spalling.

Given these findings, we can state that polypropylene fibers prevent the spalling occurrence. These fibers melt at approximately 170°C being then partially absorbed by the microcracked cement matrix leaving a pathway for gas, reducing the intensity of the pore pressure.

### REFERENCES

- [1]Kalifa, P., Menneteau, F. and Quenard D. (1999); "Spalling and pore pressure in HPC at high temperatures", *Cement and Concrete Research*, Vol. 30, pp. 1915-1927.
- [2]Khoury, G. A. (2000); "Effect of fire on concrete and concrete structures", *Prog. Struct. Engng Mater.*, Vol 2, pp. 429-447.
- [3]Kalifa, P., Chene, G., Galle, C. (2001); "High-temperature behaviour of HPC with polypropylene fibres. From spalling to microstructure.", *Cement and Concrete Research*, Vol 31, pp 1487-1499.
- [4]Santos, S. and Rodrigues, J. P. (2008); "Spalling on concrete structures", *Proceedings of the National Conference on Structural Concrete*, Guimarães, Portugal.
- [5]Recommendations of RILEM TC 200-HTC (2005); "Mechanical concrete properties at high temperature – Modeling and applications". *Materials and Structures*, V. 38, pp. 913-919.
- [6]Velasco, R. V., Toledo, R. D., Fairbairn, E. M. R., Lima, P. R. L. and Neumann, R.; "Spalling and stress-strain behaviour of polypropylene fibre reinforced HPC after exposure to high temperatures".

## NUMERICAL EVALUATION OF LOAD INDUCED THERMAL STRAIN IN RESTRAINT STRUCTURES

### Calculation of a tunnel cross section subjected to fire

Ulrich Schneider <sup>a</sup>, Martin Schneider <sup>b</sup>, Jean-Marc Franssen <sup>c</sup>

<sup>a</sup> Univ. of Techn. Vienna, Karlsplatz 13/206, 1040 Vienna, Austria, ulrich.schneider+e206@tuwien.ac.at

<sup>b</sup> Univ. of Techn. Vienna, Karlsplatz 13/206, 1040 Vienna, Austria, e0527948@student.tuwien.ac.at

<sup>c</sup> Univ. of Liege, 1, Ch. des Chevreuils, 4000, Liège, Belgium, jm.franssen@ulg.ac.be

### INTRODUCTION

Calculations to predict the deformation rate and load bearing capacity of concrete structures at high temperatures are often based on material models according to the model of the Eurocode 2 (EC2-Model). In Europe most of the calculations of structures are based on this model. The model is very usable and provides a high level of safety for members under bending and standard fire test conditions. It has not been tested for natural fire conditions which include decreasing temperature conditions.

The load bearing capacity of concrete structures can be optimized with models representing a transient material behaviour. Models which are approximated by transient data are more realistic. The following investigation describes the potential when using a new transient concrete model. This model considers thermal induced strain with external load or internal restraint load during heating up. For this model, a realisation of all components of concrete strain is needed. The concrete behaviour is influenced by transient temperature and load history.

A material model for calculation of siliceous concrete is given in [1]. This new model is based on a Thermal-Induced-Strain-Model (TIS-Model) and is called advanced transient concrete model (ATCM). Transient conditions during the whole calculation routine are taken into account. The transient load and the real temperature development are considered. Generally an ATCM can be used for every type of concrete; only some parameter must be changed. This examination is based on ordinary concrete with siliceous aggregates. Using this model, the finite element analysis (FEA) is applied to the calculation [2].

Both concrete models, EC2-Model and ATCM based on material properties according to TIS-Model (see equation (1)), show a very different behaviour for deformation and restraint stresses during calculation. The influence of load during heating is essential [3]. A cut and cover rectangular-shape reinforced concrete tunnel is calculated with the new model in the followed paper.

### 1 GENERALS ADVANCED TRANSIENT CONCRETE MODEL

It is generally agreed that the total strain  $\varepsilon_{tot}$  comprises the following parts:

$$\varepsilon_{tot} = \varepsilon_{el} + \varepsilon_{pl} + \varepsilon_{tr} + \varepsilon_{th} \quad (1)$$

where:

$\varepsilon_{tot}$  total strain,  $\varepsilon_{el}$  elastic strain,  $\varepsilon_{pl}$  plastic strain,  $\varepsilon_{tr}$  total transient creep strain,  $\varepsilon_{th}$  thermal dilatation

It is therefore convenient to write for the pure mechanical strain:

$$\varepsilon_m = \varepsilon_{el} + \varepsilon_{pl} + \varepsilon_{tr} = \varepsilon_{tot} - \varepsilon_{th} \quad (2)$$

According to [4], in this case the term  $\varepsilon_m$  is called „load induced thermal strain“. It consists of transient creep (transitional thermal creep and drying creep), basic creep and elastic strains. The shrinkage during the first heating is accounted for by the observed thermal strain (load 0%). Eq. 3 is used to calculate the thermal induced creep strain:

$$\varepsilon_{tr}(T, \alpha) = \frac{\varphi^* \sigma(t)}{E(T)} - \varepsilon_{pl}(T, \alpha) - \Delta\varepsilon_{el}(T, \alpha) \text{ with: } \Delta\varepsilon_{el}(T, \alpha) = \varepsilon_{el}(T) - \varepsilon_{el}(T, \alpha) \quad (3)$$

$\varepsilon_{tr}(T, \alpha)$  is called “thermal induced creep strain“ but the definition is different compared to [4]. The pure transient creep will not be calculated numerically within the proposed calculation procedure described above, but the exact extended relationship is given in equation (3). The  $\varphi$ -function is calculated by the equation (4). It utilizes new parameters, those were obtained by recent scientific results [5, 6] based on ongoing research.

$$\varphi = C_1 * \tanh \gamma_w * (T - 20) + C_2 * \tanh \gamma_0 * (T - T_g) + C_3 \quad (4)$$

with:  $C_1 = 2.50$ ,  $C_2 = 0.70$ ,  $C_3 = 0.70$ ,  $\gamma_0 = 7.5 * 10^{-3} \text{ C}^{-1}$ ,  $T_g = 800^\circ\text{C}$  for quarzit concrete [7].

The moisture content of concrete is taken into account using equation (5).

$$\gamma_w = 0.3 * 10^{-3} * w^{0.5} + 2.2 * 10^{-3} \text{ with } \gamma_w \leq 2.8 * 10^{-3} \quad (5)$$

It is concluded that the irreversible character of the main material properties must be incorporated in a calculation model to ensure a realistic consideration of the behavior of concrete.

## 2. CALCULATION OF A TUNNEL CROSS SECTION

### 2.1 Model of the calculation of a tunnel cross section

In general, calculation methods have two separate arithmetic steps: a thermal and a mechanical analysis. For further information, please see the references [8].

In the following example, a single-bay frame is calculated. It is a model of a tunnel taken from a research project, shown in Figure 1 [9].

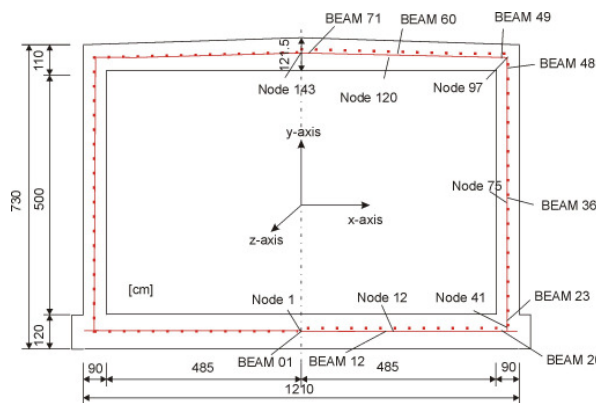


Fig. 1: Principle sketch of the tunnel; according to [9].

The simulation calculates a tunnel cross section with an exposition of a HCI curve. Derived from the Hydrocarbon curve, the maximum temperature of the HCI curve is 1300°C instead of the 1100°C, standard HC curve. Such fires may in accidents of tank trucks.

The arithmetic model is based on a section with a width of 1 meter. General calculations utilize the semi-probabilistic concept of the Eurocode 1. The bedding is considered with the help of a spring component under every beam element of the ground plate. The used material is ordinary siliceous concrete C25/30 and steel BSt500. The heating is calculated for transient heating. Before the structure is subjected to fire, the basic combination must be used to determine the amount of reinforcement, which is to be used for comparison purposes during the fire exposure. It is assumed that no spalling occurs during the fire.

## 2.2 Results of the Calculation of a tunnel cross section

The various displacements demonstrate the whole structure responds during heating. The system's stiffness is changing as a function of time [10]. Most of the deformations show a lower deformation with the ATCM. Only in node 1 the deformation in y-axis is a little bit larger with the ATCM than with the EC2-Model. These results show the effect of the higher load utilisation of the new model. Without considering the load history the influence of the load under temperature exposure is not sufficient reflected in the calculation of deformation of the structure. The figures 2 to 3 show the results of the deformation with the EC2-Model with the maximum value of PSS and with the ATCM.

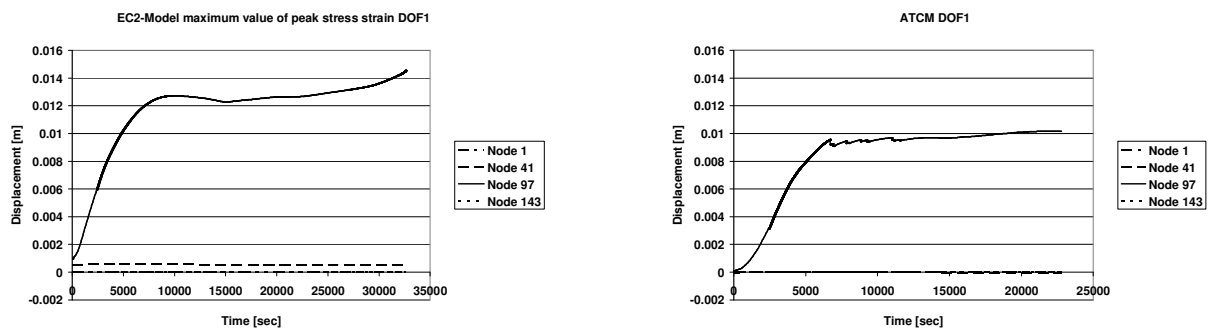


Fig. 2: Displacement in x - axis in various nodes.

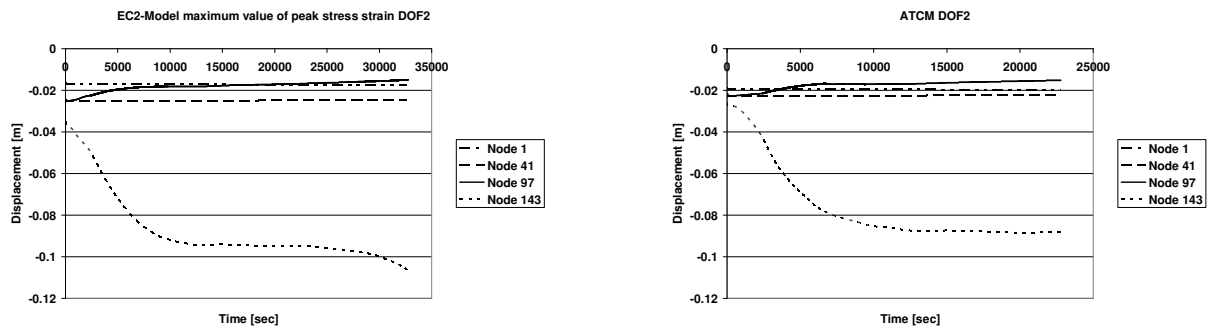


Fig. 3: Displacement in y - axis in various nodes.

The axial forces of the ground plate, the wall and the ceiling are generally higher according to simulations with the EC2-Model compared to the ATCM. Due to the lower deformation in the ATCM lower axial forces occur. An insignificant difference between the two models is seen in the calculation of the bending moment. The positive bending moments are lower with the ATCM than with the EC2-Model. The negative bending moments are higher with the ATCM than with the EC2-Model. The next figures show these mechanical properties of the structure with respect to the axial forces and the bending moments.

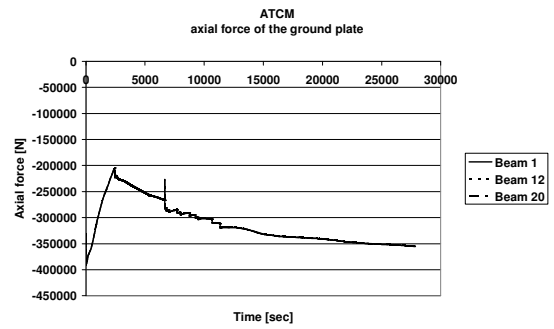
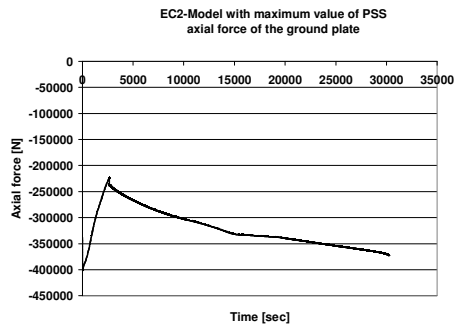


Fig. 4: Axial forces in various beams in the ground plate.

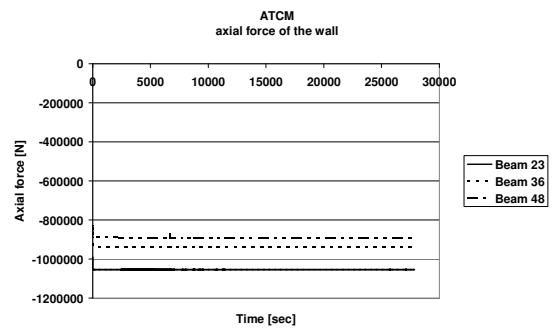
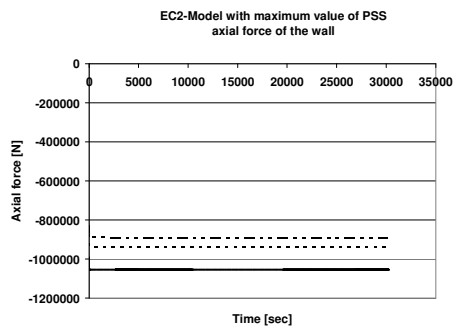


Fig. 5: Axial forces in various beams in the wall.

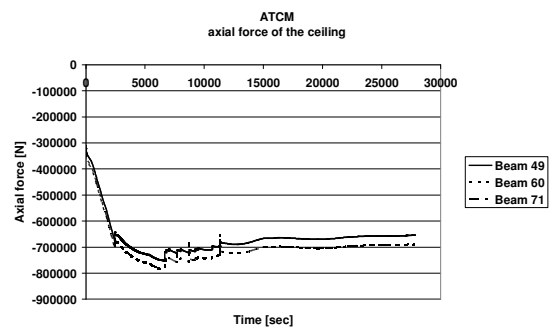
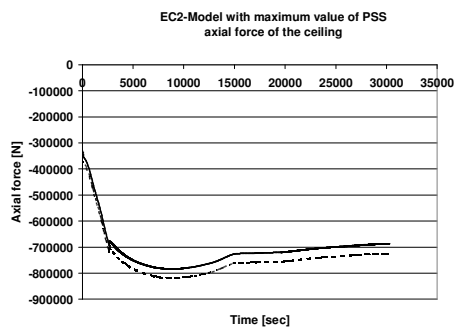


Fig. 6: Axial forces in various beams in the ceiling.

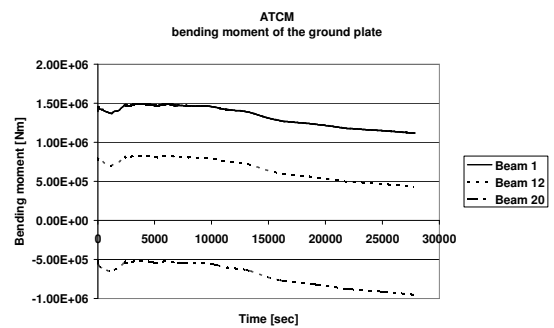
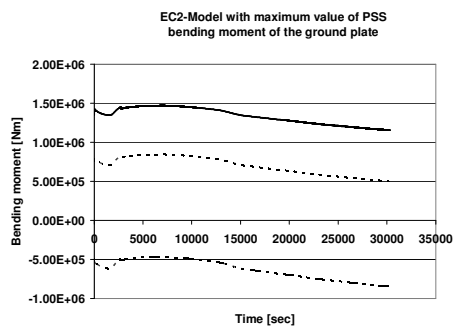


Fig. 7: Bending moments in various beams in the ground plate.

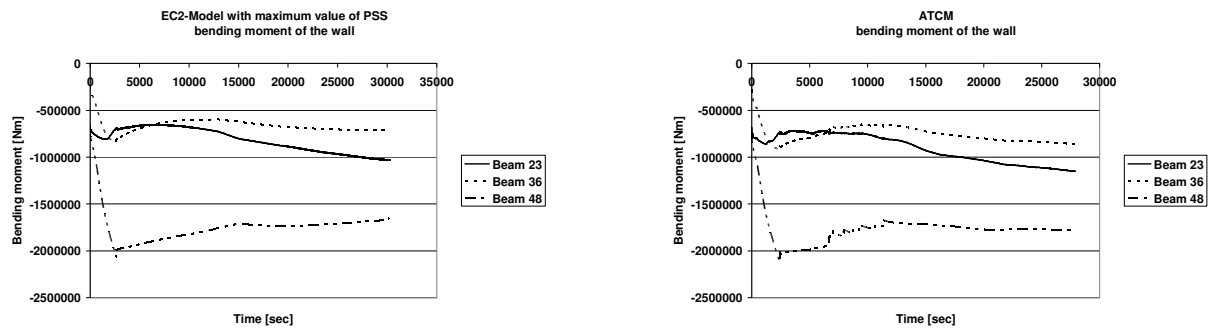


Fig. 8: Bending moments in various beams in the wall.

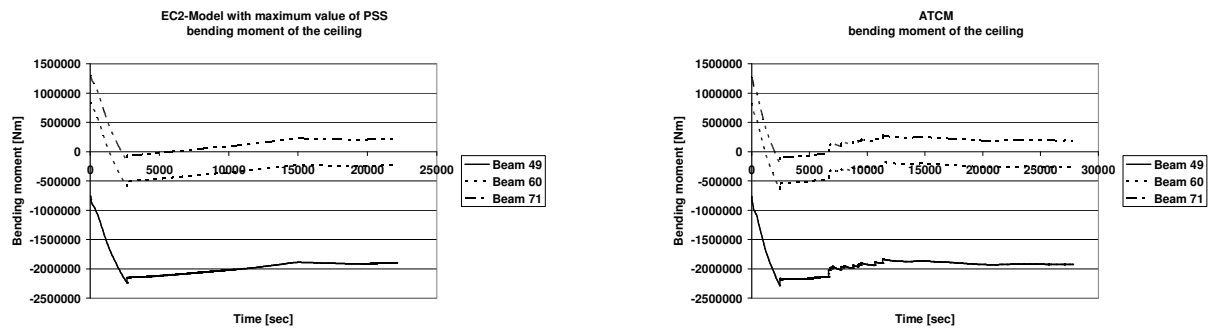


Fig. 9: Bending moments in various beams in the ceiling.

### 3 DISCUSSION OF THE RESULTS

For the calculation of the load bearing capacity and behaviour of structures subjected to fire, new material equations for the most important material properties of ordinary concrete were developed [1, 4]. This model was developed to complete the existing concrete model of EC2 with respect to the transient thermal creep and the effect of load history. It is possible with this new model to consider the load history in all phases of thermal exposure. With this complex model one can calculate total strain taking into account a wide range of variations of load history and temperatures. Different parts of deformations are approximated with discrete equations interacting in the new concrete model. This technique is usable to calculate realistic behaviour of structures, especially in the case of restraint.

By considering the load history during heating up in several cases an increasing load bearing capacity due to a higher stiffness of concrete may be obtained. With this model it is possible to consider the thermal-physical behaviour of material properties for the calculation of reinforced concrete structures. By applying this model instead of the calculation system of EC2 this will lead to a better evaluation of the safety level. This opens space for optimizing reinforced concrete structures under temperature exposure.

A calculation of a tunnel cross section of cut and cover single bay frame was performed and presented above. Lower deformations are calculated in all parts of the structures using the new advanced transient concrete model (ATCM). Due to this lower deformation a lower axial force during heating occurs.

The results of the calculation of the bending moments show a lower moment at the inside of the tunnel surface and a higher bending moment outside of the tunnel if one compares results of the ATCM with those of EC2-Model. The differences between the calculations are very small. Here we don't observe a significant difference in this structure by using the new model of concrete.

## 4 CONCLUSION

It is shown that the recommended model of EC2 doesn't calculate realistic values of deformations of concrete structures under high temperature if one compares to the results of an advanced transient concrete model (ATCM) which is based on measured data. A maximum value of peak stress strain is necessary for describing a relatively realistic behaviour of the structure. For calculation of tunnels with concrete with siliceous aggregates the EC2-Model should be taken with the maximum value of the peak stress strain. For calculation a higher load bearing member the ATCM should be applied. Note, only with the TIS-Model with the equations of the ATCM the full concrete behaviour is used in the structure. The calculation with the ATCM has a high potential for optimizing concrete structures, more than the EC2-Model. The reliability of the load bearing capacity is higher with the ATCM because the deformations are lower than with the EC2-Model. The calculated axial forces with the ATCM are close to the EC2-Model. A potential is observed for more detailed calculations of complex structures. In the concept of structures it may be applied with lower safety factors, i.e. lower excess charges may be used in the design.

## 5. REFERENCES

- [1] Schneider, U.; Schneider, M.; Franssen, J.-M.: Consideration of nonlinear creep strain of siliceous concrete on calculation of mechanical strain under transient temperatures as a function of load history. Proceedings of the *Fifth International Conference – Structures in Fire SIF 08*, pp. 463-476, Singapore 2008
- [2] Franssen J.-M.,: SAFIR. A Thermal/Structural Program Modelling Structures under Fire, *Engineering Journal, A.I.S.C.*, Vol. 42, No. 3 (2005), 143-158
- [3] Schneider, U.; Schneider, M.; Franssen, J.-M.: Numerical evaluation of load induced thermal strain in restraint structures compared with an experimental study on reinforced concrete columns, Proceedings of the *11th International Conference and Exhibition, FIRE AND MATERIALS 2009*, 26<sup>th</sup> - 28<sup>th</sup> January 2009, Fisherman's Wharf, San Francisco, USA
- [4] Khoury, G.A.; Grainger, B.N.; Sullivan, P.J.E.: Transient thermal strain of concrete: Literature review, conditions with specimens and behaviour of individual constituents, *Magazine of Concrete Research Vol. 37 No. 132*, 1985
- [5] RILEM TC HTC 200: Mechanical Concrete Properties at High Temperature – Recommendation Part 1: *Mat. & Struct.*, Vol. 44, Paris, June 2007
- [6] Schneider, U.: Ein Beitrag zur Frage des Kriechens und der Relaxation von Beton unter hohen Temperaturen, *Habilitationschrift, Institut für Baustoffe, Massivbau und Brandschutz, TU Braunschweig, Heft 42, Braunschweig*, 1979
- [7] Schneider, U.; Lebeda, C.; Franssen, J.-M.: *Baulicher Brandschutz, Bauwerk Verlag GmbH, Berlin*, 2008
- [8] Franssen, J.-M.: Contributions à la Modélisation des Incendies dans les Bâtiments et leurs Effets sur les Structures, *Université de Liège, Belgium* 1998
- [9] Franssen, J.-M.; Hanus, F.; Dotreppe, J.-C.: Numerical Evaluation of the Fire Behaviour of a Concrete Tunnel Integrating the Effects of Spalling in Proceedings *fib Workshop – Ciombra*, November 2007
- [10] Schneider, U.; Horvath, J.: *Brandschutz – Praxis in Tunnelbauten, Bauwerk Verlag GmbH, Berlin*, 2006

# STRUCTURAL SAFETY ASSESSMENT OF TUNNELS SUBJECTED TO FIRE LOADING

Thomas Ring<sup>a</sup>, Matthias Zeiml<sup>a</sup>, Roman Lackner<sup>b</sup>

<sup>a</sup>*Institute for Mechanics of Materials and Structures,  
Vienna University of Technology, Karlsplatz 13/202, 1040 Vienna, Austria*

<sup>b</sup>*Material-Technology Unit,  
University of Innsbruck, Technikerstraße 13, 6020 Innsbruck, Austria*

## 1 STATE OF THE ART

Tunnel structures have to fulfill requirements as regards their bearing capacity and serviceability before as well as during/after fire accidents. Currently, the determination of the structural safety of tunnels subjected to fire loading is based on the so-called equivalent-temperature concept, assuming linear-elastic material behavior. As illustrated in [1], the equivalent-temperature load is calculated from the real (nonlinear) temperature distribution within a clamped (layered) beam, using the stress-resultants  $N_{equ}$  and  $M_{equ}$  (see Fig. 1):

$$T_m = \frac{N_{equ}}{\alpha E_{equ} A} \quad \text{and} \quad \Delta T = \frac{M_{equ}}{\alpha E_{equ} I}. \quad (1)$$

In Eq. (1) and (2),  $A$  [m<sup>2</sup>] and  $I$  [m<sup>4</sup>] are the cross-sectional area and the moment of inertia, respectively, whereas  $\alpha$  [K<sup>-1</sup>] is the thermal expansion coefficient of concrete.  $E_{equ}$  [MPa] is the equivalent Young's modulus, given by

$$E_{equ} = \sum_{i=1}^N \frac{E_{c,i}(T_i) A_i}{A}, \quad (2)$$

where  $E_{c,i}(T_i)$  [MPa] and  $A_i$  [m<sup>2</sup>] are Young's modulus and cross-sectional area of the  $i$ -th layer (with  $N$  [-] as the number of layers). The parameters  $T_m$  [°C],  $\Delta T$  [°C/m], and  $E_{equ}$  serve as input for the linear-elastic analysis.

In this paper, selected results from a structural safety assessment of different tunnel cross-sections under fire are presented. Hereby, the influence of different material models and modes to consider fire loading (equivalent temperature loading or nonlinear temperature distribution) is investigated.

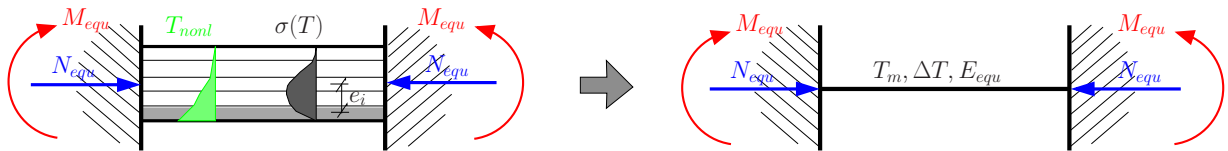


Fig. 1. Model for determination of equivalent temperature loading ( $T_m$  and  $\Delta T$ ) [1], giving the same stress resultants  $N_{equ}$  and  $M_{equ}$

## 2 NUMERICAL MODEL

The finite-element analyses are performed using thick (layered) shell elements (see Fig. 2 and [2–4]). The layer concept enables for (i) assignment of different temperatures and, hence, of temperature-dependent material parameters to the respective layers and (ii) consideration of spalling by de-activation of the respective near-surface layers. Concrete and steel are considered by separate layers, the reinforcement bars are transformed into a homogeneous steel layer of

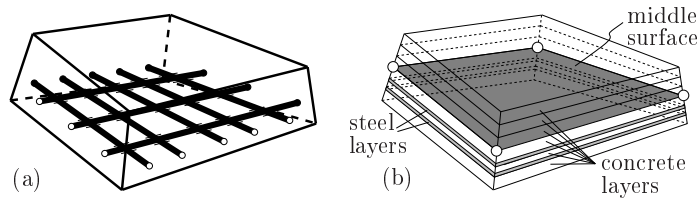


Fig. 2. Illustration of employed layer concept [2–4]: (a) real cross-section, (b) layered finite element

equivalent thickness. As mentioned in [4], a plane-stress plasticity model for concrete is used, whereas the steel reinforcement is simulated by a 1D plasticity model formulated in the direction of the reinforcement bars. The temperature-dependent material parameters are taken from national/international standards [5,6].

### 3 APPLICATION

#### 3.1 Geometric properties and loading conditions

The numerical model described in the previous section is used to analyze different double-track railway tunnel cross-sections (see Fig. 3). Hereby, the mechanical load consists of the self-weight of the tunnel, earth load with an overburden of 1.50 and 1.75 m, respectively, and the traffic load resulting from a road crossing above the tunnel. The bottom of the tunnel is covered by a gravel layer as rail bedding which is considered to protect this part of the tunnel structure from fire loading. Therefore, temperature loading (representing a fire of stacked car tires) is applied only at the side wall and the top of the tunnel. The duration of the fire load is set to 180 min with an increase of the surface temperature up to 900°C within the first 20 min and a constant surface temperature of 900°C until the end of the fire load (see [1] for details). In addition to fire load, different spalling scenarios are considered, with a final spalling depth  $d_s^\infty$  [m] to be reached after 30 min of fire loading (with  $d_s^\infty = 0$  m,  $d_s^\infty = 0.1$  m, and  $d_s^\infty = 0.2$  m,

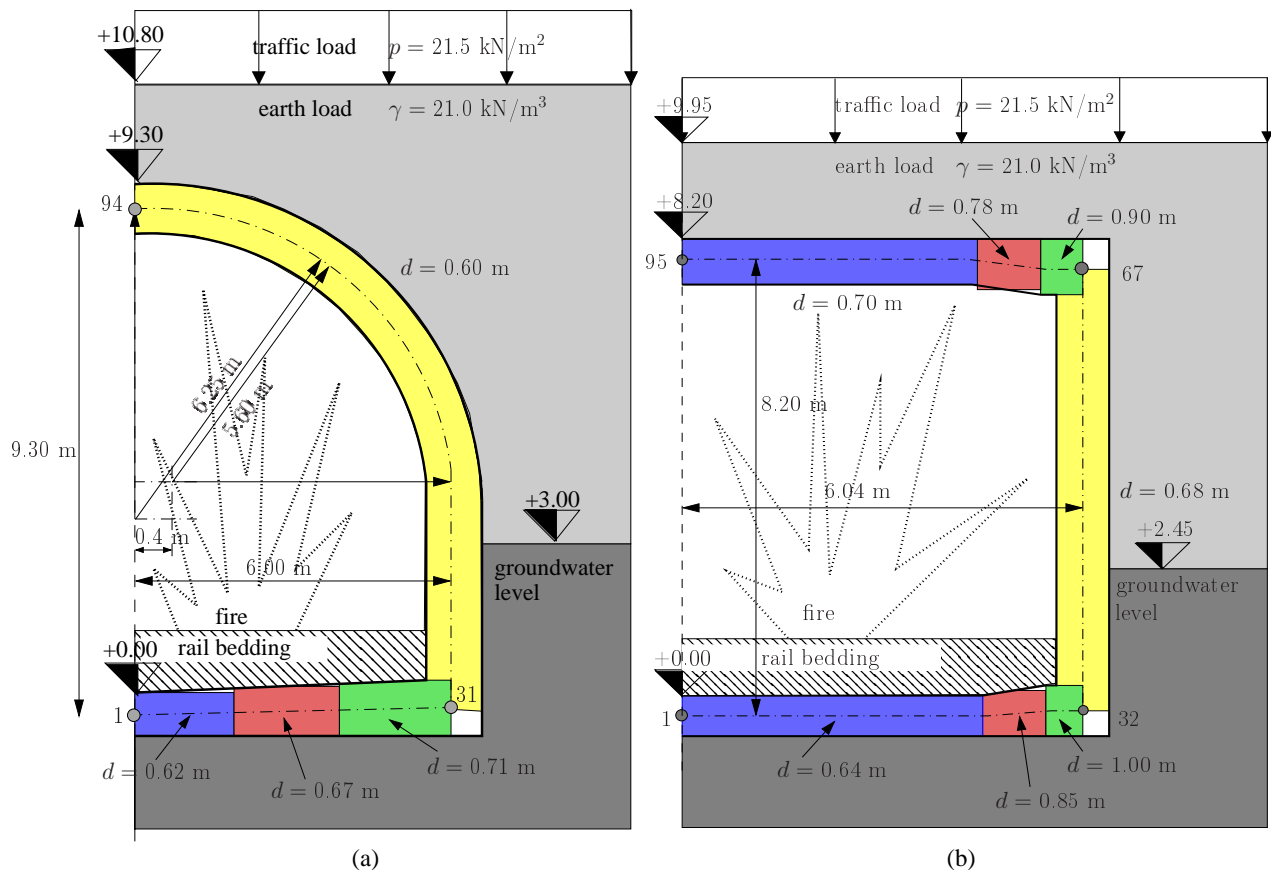


Fig. 3. Investigated concrete structures: (a) circular and (b) rectangular tunnel cross-section

see [3] for details). Furthermore, different material models and modes of temperature loading are employed, i.e.,

- Linear-elastic material behavior and equivalent temperature (LE –  $T_m, \Delta T$ ), and
- Linear-elastic/ideal-plastic material behavior and nonlinear temperature (LE/IP –  $T_{nonl}$ ).

### 3.2 Results – circular tunnel cross-section

In the following, representative numerical results are presented. In order to determine whether the reinforcement steel exhibits plastic behavior, the level of loading  $L$  [-] is determined at significant sections of the tunnel cross-section (e.g., upper corner, shoulder), with  $L$  defined as the ratio between the actual steel stress  $\sigma_s$  [MPa] and the (temperature-dependent) yield strength  $f_y(T)$  [MPa]. In case of  $L = 0$ , the steel reinforcement is unloaded, whereas  $L = 1$  indicates that the maximum possible loading is reached. Additionally to  $L$ , the bending-moment distribution over the tunnel cross-section is presented for selected time instants (before and after 180 min of fire loading). Finally, the relative top displacement  $v_{rel}$  [cm] is shown in order to evaluate the compliance of the tunnel.

In Fig. 4, the level of loading of the reinforcement at the shoulder of the tunnel cross-section is presented. Hereby, the consideration of linear-elastic/ideal-plastic material behavior and the nonlinear temperature distribution (LE/IP –  $T_{nonl}$ ) leads to significantly higher steel stresses. In case of spalling ( $d_s^\infty = 0.1$  m and  $0.2$  m), the inner reinforcement layer is lost and, lateron,

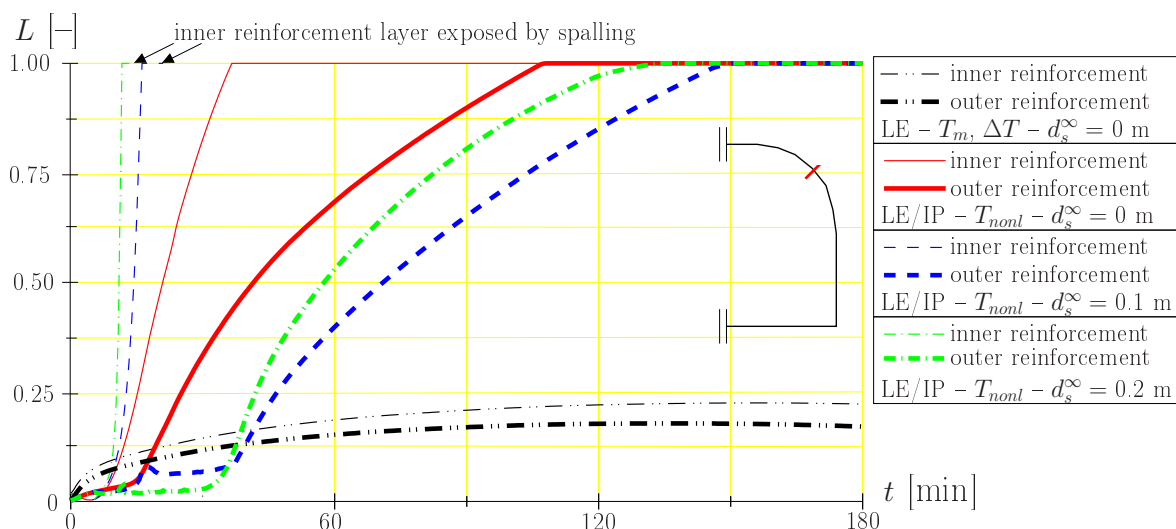


Fig. 4. Circular cross-section – level of loading of reinforcement at the tunnel shoulder for different material models and spalling scenarios

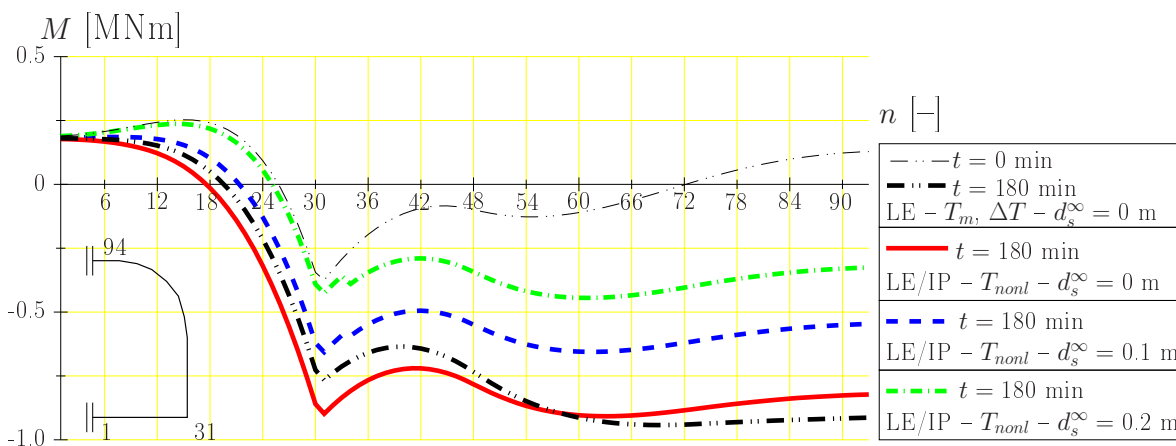


Fig. 5. Circular cross-section – distribution of bending moment for different material models and spalling scenarios before ( $t = 0$  min) and after 180 min of fire loading

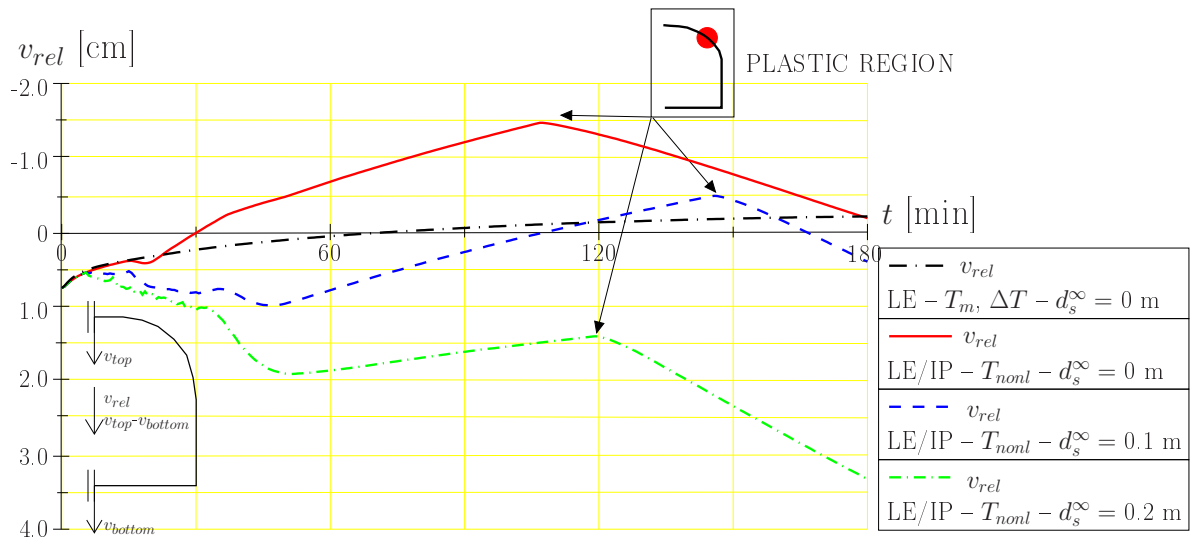


Fig. 6. Circular cross-section – vertical convergence for different material models and spalling scenarios

the outer reinforcement experiences plastic deformations.

The bending-moment distributions (see Fig. 5) indicate a significant increase of the bending moment at the fire-exposed regions. The differences between cases  $LE - T_m, \Delta T$  and  $LE/IP - T_{nonl}$  are small (see results for  $d_s^\infty = 0$  m). In case of  $LE/IP - T_{nonl}$ , however, the redistribution of forces in consequence of changing stiffness from the fire-exposed towards the unexposed parts of the cross-section (lower corner and bottom) can be observed. In general, the reduction of the cross-section in consequence of spalling resulted in a reduction of the bending moments.

The history of the vertical convergence of the tunnel cross-section is presented in Fig. 6. In case of the analysis using a linear-elastic material behavior and the equivalent temperature distribution ( $LE/IP - T_m, \Delta T$ ), a continuous decrease of convergence in consequence of heating of the cross-section is observed. In case of  $LE/IP - T_{nonl}$ , the upward deformation of the cross-section is even more pronounced. After about 105 min of fire loading, a plastic hinge is formed, leading to a continuous increase of deformations. The development of this plastic hinge was already indicated in Fig. 4, where both the inner and the outer steel layer exhibits  $L = 1$  after 105 min of fire loading. Consideration of spalling leads to an increase of the compliance and, thus, of the downward motion of the top of the tunnel.

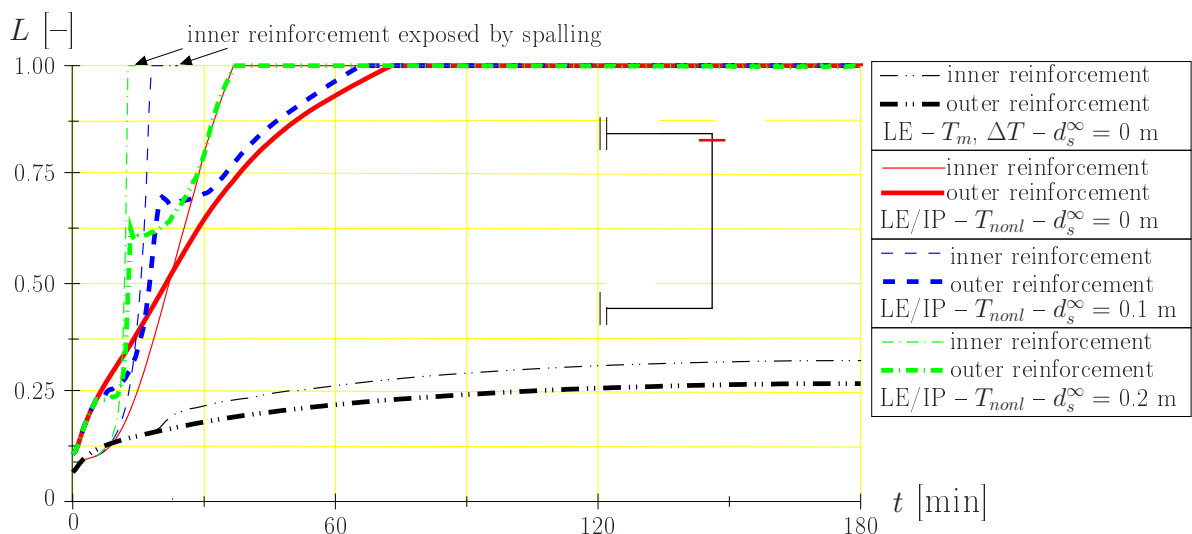


Fig. 7. Rectangular cross-section – level of loading of reinforcement at the upper corner for different material models and spalling scenarios

### 3.3 Results – rectangular tunnel cross-section

Fig. 7 depicts the level of loading of the reinforcement in the upper corner of a rectangular cross-section. Similar to the case of the circular cross-section, the analysis characterized by LE/IP –  $T_{nonl}$  leads to significantly higher stresses (compare with LE –  $T_m, \Delta T$  for  $d_s^\infty = 0$  m). The stresses, however, increase faster and plastic deformations occur earlier than in case of the circular cross-section. When spalling is considered, the inner steel layer is deactivated at a certain time instant and plastic deformations of the outer reinforcement occur even earlier as in case of no spalling.

The bending moment depicted in Fig. 8 indicates a shift of loading from the fire-exposed upper tunnel corner to the bottom corner when plastic deformation and the nonlinear temperature distribution are considered (compare with LE –  $T_m, \Delta T$  for  $d_s^\infty = 0$  m). Again, spalling leads to a reduction of the bending moment, explained by the reduced cross-sections inducing smaller thermal constraints.

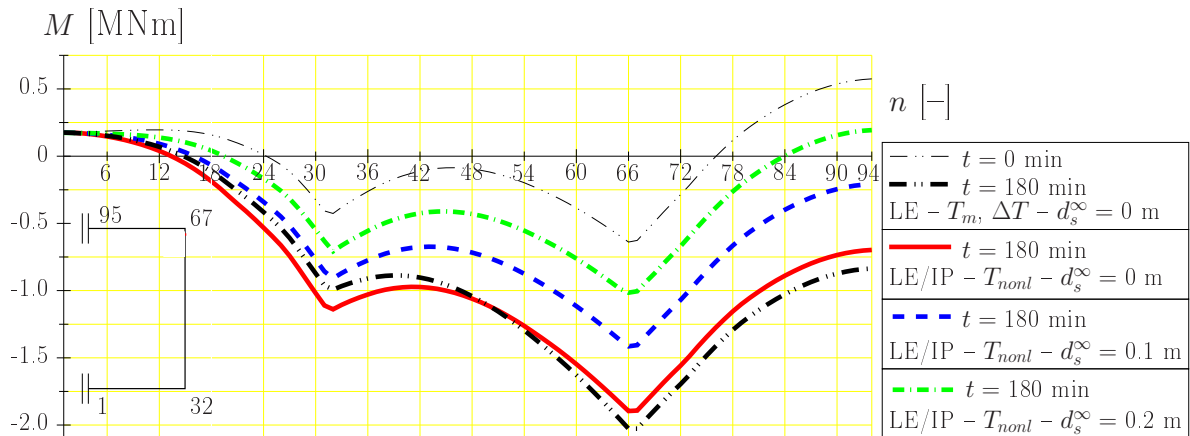


Fig. 8. Rectangular cross-section – distribution of bending moment for different material models and spalling scenarios before ( $t = 0$  min) and after 180 min of fire loading

The vertical convergence of the tunnel (see Fig. 9) illustrates the influence of the underlying material model on the compliance of the tunnel lining (compare cases LE –  $T_m, \Delta T$  and LE/IP –  $T_{nonl}$  for  $d_s^\infty = 0$  m with increased deformations in the latter case). Comparison of the results of the two considered cross-sections for LE/IP –  $T_{nonl}$  and  $d_s^\infty = 0$  m (Fig. 6 and 9) shows a higher structural safety of the circular cross-section. This difference is more pronounced in case of spalling. For  $d_s^\infty = 0.2$  m, the increase in deformations of the rectangular cross-section is

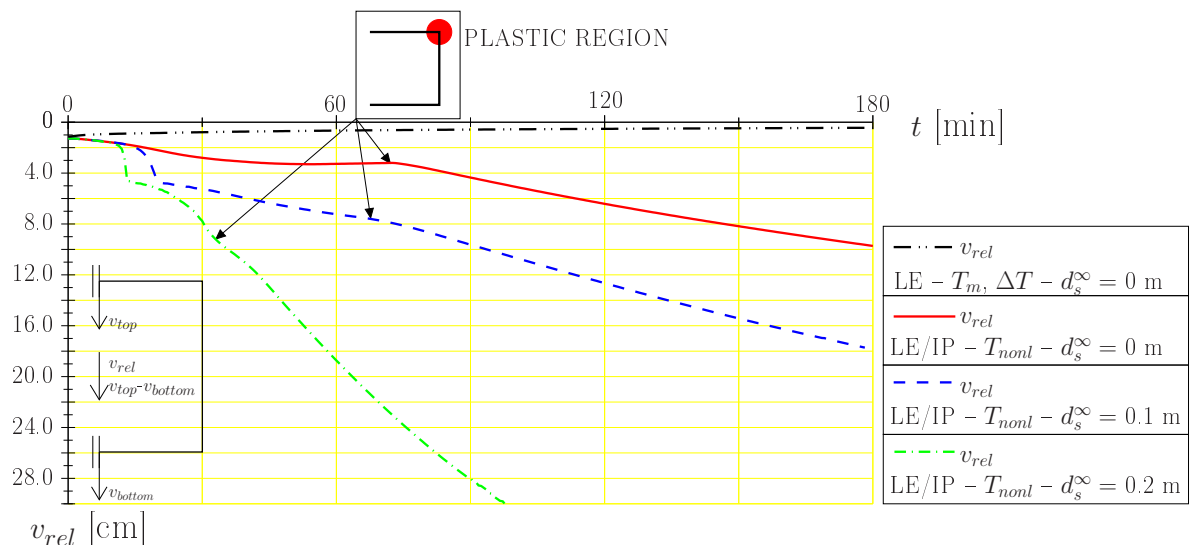


Fig. 9. Rectangular cross-section – vertical convergence for different material models and spalling scenarios

significantly higher as for  $d_s^\infty = 0$  m and 0.1 m (see Fig. 9) because of a positive bending moment in the tunnel ceiling (see Fig. 8) and deactivation of the inner reinforcement in consequence of spalling. However, collapse of the tunnel is not observed (even for  $d_s^\infty = 0.2$  m) which would result in a sudden and steep increase of deformation. Moreover, collapse would require the development of a second plastic hinge.

## 4 CONCLUSIONS

As illustrated by results for different tunnel cross-sections, the structural safety of tunnels subjected to fire loading strongly depends on the considered material model and whether spalling is taken into account. In contrast to the state-of-the-art analysis mode, characterized by linear-elastic material behavior and the so-called equivalent temperature loading, the application of linear-elastic/ideal-plastic material models and consideration of the real (nonlinear) temperature distribution leads to force redistribution within the tunnel cross-section. For the investigated cross-sections and loading conditions, however, the difference in stress resultants (e.g., bending moment) is small. The level of loading of the steel reinforcement, on the other hand, reveals large differences between the two different modes of analysis. A realistic prediction of plastic deformations within the reinforcement requires consideration of linear-elastic/ideal-plastic material behavior allowing the formation of plastic hinges and, hence, the realistic determination of tunnel deformations.

The geometric properties of the tunnel cross-section have a significant influence on the sensitivity of the structure to fire loading. The analyses showed that the rectangular cross-section is more sensitive to fire loading than the circular cross-section because of the more efficient geometry of the latter. Consideration of spalling leads to an increase of the compliance of the lining, with the rectangular cross-section again being more sensitive.

Ongoing research focuses on the improvement of the employed material model, considering the influence of combined thermal and mechanical loading on the strain behavior of heated concrete, giving numerical results in better agreement to reality.

## REFERENCES

- [1] W. Kusterle, W. Lindlbauer, G. Hampejs, A. Heel, P.-F. Donauer, M. Zeiml, W. Brunnsteiner, R. Dietze, W. Hermann, H. Viechtbauer, M. Schreiner, R. Vierthaler, H. Stadlober, H. Winter, J. Lemmerer, E. Kammeringer, Brandbeständigkeit von Faser-, Stahl- und Spannbeton [Fire resistance of fiber-reinforced, reinforced, and prestressed concrete], Tech. Rep. 544, Bundesministerium für Verkehr, Innovation und Technologie, Vienna, in German. (2004).
- [2] K. Savov, R. Lackner, H. A. Mang, Stability assessment of shallow tunnels subjected to fire load, *Fire Safety Journal* 40 (2005) 745–763.
- [3] M. Zeiml, R. Lackner, F. Pesavento, B. A. Schrefler, Thermo-hydro-chemical couplings considered in safety assessment of shallow tunnels subjected to fire load, *Fire Safety Journal* 43 (2) (2008) 83–95.
- [4] T. Ring, Finite element analysis of concrete structures subjected to fire load considering different element types and material models, Master's thesis, Vienna University of Technology, Vienna, Austria (2008).
- [5] CEB, Fire Design of Concrete Structures, Bulletin d'Information 208, CEB, Lausanne, Switzerland (1991).
- [6] ÖNORM EN1992-1-2, Eurocode 2 – Bemessung und Konstruktion von Stahlbeton- und Spannbetontragwerken – Teil 1-2: Allgemeine Regeln – Tragwerksbemessung für den Brandfall [Eurocode 2 – Design of concrete structures – Part 1-2: General rules – Structural fire design], European Committee for Standardization (CEN), in German (2007).

## A NUMERICAL MODEL FOR PREDICTION OF SPALLING OF CONCRETE EXPOSED TO ELEVATED TEMPERATURES

**Honglin Zhang<sup>a</sup>, Colin T. Davie<sup>a</sup>, Chris J. Pearce<sup>b</sup> and Nenad Bićanić<sup>b</sup>**

<sup>a</sup>School of Civil Engineering and Geosciences, Newcastle University, Newcastle upon Tyne, UK

<sup>b</sup>Department of Civil Engineering, University of Glasgow, Glasgow, UK

### 1 INTRODUCTION

When concrete structures are exposed to elevated temperatures, extremely complex phenomena, such as dehydration of cement paste, evaporation of water in pores and restrained thermal expansion of the structures will occur, which result in build-up of pore pressure and thermally induced stresses inside the structures. If high enough, pore pressure or thermally induced stresses could lead to spalling of the structures, i.e., the fracturing and loss of material from the surface of concrete elements. The increase in temperature will also cause decrease in strength and stiffness of concrete, further facilitating the occurrence of spalling.

In the last few decades, extensive experiments have been performed to gain a better understanding of the spalling mechanism [1-3]. Meanwhile, several numerical models were presented for simulation of the complex phenomena at different levels of simplification [4-9]. The past research suggests that spalling is influenced by a combination of heating rate, section shape and size, moisture content, permeability and restraint of concrete structure. However, as for the driving force of spalling, there still exists controversy. Some researchers state that pore pressure is the most importance factor, some emphasise the significance of thermally induced stresses, while others believe spalling is caused by the combination of these two factors.

In this paper, taking a one-dimensional and a two dimensional benchmark problem as examples, the significance of pore pressure and thermally induced stresses for spalling of concrete with different permeability and moisture content is investigated using a finite element method solution procedure, which can capture the coupled hygro-thermo-mechanical behaviour of concrete exposed to elevated temperatures.

### 2 MATHEMATICAL MODELLING

In the mathematical formulation, concrete is treated as a multiphase system consisting of solid, liquid and gas phases. The solid skeleton is assumed to undertake isotropic elastic-damage deformations under mechanical and thermal loadings. The liquid phase is considered to include adsorbed water and the gas phase to be a mixture of dry air and water vapour, both of which are assumed to behave as ideal gases. The material parametric relationships are given based on the work conducted by previous researchers. The complete description of the mathematical formulation was given in [10]. Here, only governing equations, mechanical constitutive equation and damage model were briefly described in the following.

The model is composed of four governing equations, defining the conservations of mass of dry air, mass of moisture, energy and momentum Eqs. (1) - (4).

$$\frac{\partial(\varepsilon_G \tilde{\rho}_A)}{\partial t} = -\nabla \cdot \mathbf{J}_A \quad (1)$$

$$\frac{\partial(\varepsilon_G \tilde{\rho}_V)}{\partial t} + \frac{\partial(\varepsilon_L \rho_L)}{\partial t} - \frac{\partial(\varepsilon_D \rho_L)}{\partial t} = -\nabla \cdot (\mathbf{J}_V + \mathbf{J}_L) \quad (2)$$

$$(\rho C) \frac{\partial T}{\partial t} - \lambda_E \frac{\partial(\varepsilon_L \rho_L)}{\partial t} + (\lambda_D + \lambda_E) \frac{\partial(\varepsilon_D \rho_L)}{\partial t} = \nabla \cdot (k \nabla T) + \lambda_E \nabla \cdot \mathbf{J}_L \quad (3)$$

$$\nabla \cdot (\boldsymbol{\sigma}' - P_{pore} \mathbf{I}) + \mathbf{b} = 0 \quad (4)$$

Mechanical strains are developed by way of an isotropic damage model, which accounts for the loss of the elastic stiffness that is caused by the micro-fracturing of concrete that develops under loading and under heating. The classical mechanical damage formulation is modified to include a second thermal damage parameter in a multiplicative form Eq. (5).

$$\boldsymbol{\sigma} = (1 - \omega)(1 - \chi) \mathbf{E}_0 : \boldsymbol{\varepsilon}^e = \mathbf{E}_{sec} : \boldsymbol{\varepsilon}^e \quad (5)$$

The mechanical damage parameter,  $\omega$ , is defined by the temperature dependent function shown in Eq. (6)

$$\omega = 1 - \frac{\kappa_0^{md}(T)}{\kappa^{md}} e^{-\gamma(T)(\kappa^{md} - \kappa_0^{md}(T))} \quad (6)$$

where,  $\kappa_0^{md}$ , which defines the onset of fracturing, is a function of the tensile strength,  $f_t(T)$ , and elastic modulus,  $E(T)$ .

$$\kappa_0^{md} = \frac{f_t(T)}{E(T)} \quad (7)$$

The thermal damage parameter is defined by the temperature dependent function shown in Eq. (8), which is derived from the degradation of the elastic modulus that results from increased temperatures,  $E(T)$ .

$$\chi = 0.2\theta - 0.01\theta^2 \quad (8)$$

### 3 NUMERICAL PROCEDURE

Employing the Galerkin weighted residual method and application of the divergence theorem the weak form of the governing equations (1) - (4) is obtained and may be expressed in matrix-vector form as (9).

$$\mathbf{C}\dot{\mathbf{x}} + \mathbf{K}\mathbf{x} = \mathbf{f}^{ext} \quad (9)$$

where, the coefficient matrices,  $\mathbf{C}$  &  $\mathbf{K}$ , and the array of nodal variables,  $\mathbf{x}$ , are given below for the chosen set of primary variables (10).

$$\mathbf{C} = \begin{bmatrix} 0 & 0 & 0 & 0 \\ 0 & \mathbf{C}_{TT} & \mathbf{C}_{TP} & \mathbf{C}_{TV} \\ 0 & \mathbf{C}_{AT} & \mathbf{C}_{AP} & \mathbf{C}_{AV} \\ 0 & \mathbf{C}_{MT} & \mathbf{C}_{MP} & \mathbf{C}_{MV} \end{bmatrix}; \quad \mathbf{K} = \begin{bmatrix} \mathbf{K}_{uu} & \mathbf{K}_{uT} & \mathbf{K}_{uP} & \mathbf{K}_{uV} \\ 0 & \mathbf{K}_{TT} & \mathbf{K}_{TP} & \mathbf{K}_{TV} \\ 0 & \mathbf{K}_{AT} & \mathbf{K}_{AP} & \mathbf{K}_{AV} \\ 0 & \mathbf{K}_{MT} & \mathbf{K}_{MP} & \mathbf{K}_{MV} \end{bmatrix}; \quad \mathbf{x} = \begin{Bmatrix} \mathbf{u} \\ \mathbf{T} \\ \mathbf{P}_G \\ \boldsymbol{\rho}_V \end{Bmatrix} \quad (10)$$

The governing equations are discretised using the standard finite element approximation and the chosen primary variables of displacements,  $u$ , temperature,  $T$ , gas pressure,  $P_G$ , and vapour content,  $\tilde{\rho}_v$ , are expressed in terms of their nodal quantities Eq. (11).

$$u = \mathbf{N}_u \mathbf{u}; \quad T = \mathbf{N}_T \mathbf{T}; \quad P_G = \mathbf{N}_P \mathbf{P}_G; \quad \tilde{\rho}_v = \mathbf{N}_\rho \boldsymbol{\rho}_v \quad (11)$$

The formulation is completed with the following boundary conditions. Transfer of heat across the boundary is described by Eq. (12).

$$\frac{\partial T}{\partial n} = \frac{h_{qr}}{k} (T_\infty - T) \quad (12)$$

Transfer of water vapour across the boundary is described by Eq. (13).

$$\frac{\partial \tilde{p}_v}{\partial n} = -\frac{K_{vT}}{K_{vV}} \frac{h_{qr}}{k} (T_\infty - T) + \frac{\beta}{K_{vV}} (\tilde{p}_{v,\infty} - \tilde{p}_v) \quad (13)$$

Finally, the gas pressure on the boundary is given by Eq. (14).

$$P_G = P_{G,\infty} \quad (14)$$

#### 4 ONE-DIMENSIONAL PROBLEM

The significance of pore pressure for the development of spalling can be investigated by application of the model to the analysis of the one-dimensional problem as shown in Fig. 1, which may be considered as a simplified representation of a concrete wall exposed to fire from one side. One (left) side is constraint-free and heated by the standard ISO834 fire, far-field temperature of which can be expressed as Eq. (15).

$$T_\infty = 20 + 345 \log_{10}(8t + 1) + 273.15 \quad (15)$$

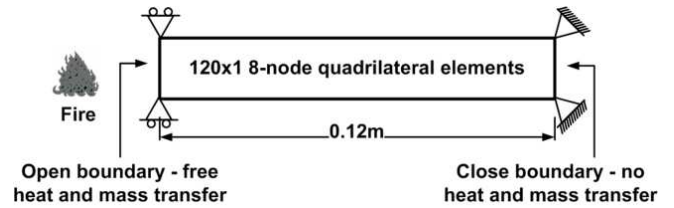


Fig. 1 Schematic diagram of the 1D problem

In the simulation, the initial internal temperature, gas pressure and porosity of the concrete are 293K, 0.1MPa and 12.2%. Initial Young's modulus, tensile strength and Poisson's ratio are 30GPa, 3MPa and 0.2, respectively. As the magnitude of gas pressure built-up in concrete during heating is significantly affected by the permeability and moisture content of the concrete, different levels of initial permeabilities in combination with different levels of initial relative humidities were used in the analysis.

Fig. 2 gives distributions of mechanical damage and gas pressure at different times for an initial permeability of  $1 \times 10^{-17} \text{m}^2$  and a relative humidity of 10%. The occurrence of mechanical damage starts from the surface after about 1200s, developing towards the inside. The maximum built-up gas pressure, as seen in the figure, is much lower than the tensile strength of concrete. Moreover, the advancement of the damage zone front falls behind the advancement of the peaks of gas pressure. Therefore, the development of damage is not due to the build-up and transport of pore pressure. Rather, it is mainly caused by the degradation of the elastic modulus due to high temperature, which results in high strains.

Fig. 3 gives distributions of mechanical damage and gas pressure for an initial permeability of  $1 \times 10^{-19} \text{m}^2$  and a relative humidity of 65%. As compared to Fig. 2, the occurrence of mechanical damage starts earlier (i.e., at about 800s), with the higher maximum built-up gas pressure reaching as high as 2.3MPa. This indicates that pore pressure accelerates the occurrence of damage.

Similarly, Fig. 4 shows distributions of mechanical damage and gas pressure for an initial permeability of  $5 \times 10^{-21} \text{m}^2$  and a relative humidity of 90%. As can be seen, the maximum pressures are higher than 3.2MPa, and the advancement of the damage zone front is almost synchronous with that of the peak of gas pressure. It should also be noticed that mechanical damage does not start from the surface as in the previous cases, but a few centimetres beneath the surface.

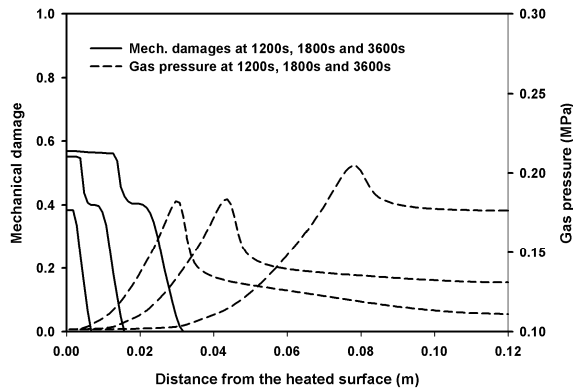


Fig. 2 Distributions of mech. damage and gas pressure. Perm. =  $1 \times 10^{-17} \text{ m}^2$ ; R.H. = 10%

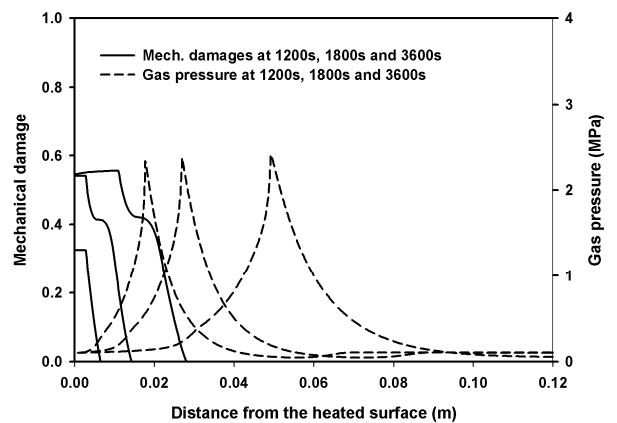


Fig. 3 Distributions of mech. damage and gas pressure. Perm. =  $1 \times 10^{-19} \text{ m}^2$ ; R.H. = 65%

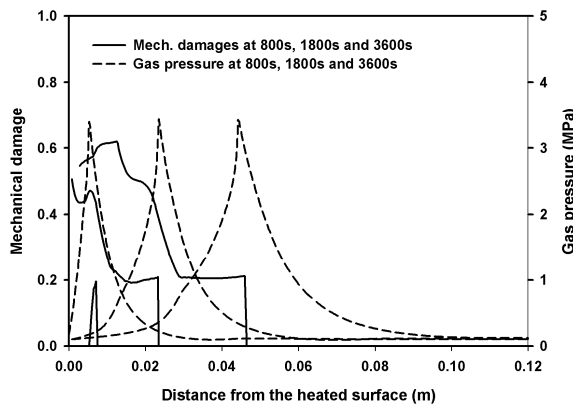


Fig. 4 Distributions of mech. damage and gas pressure. Perm. =  $5 \times 10^{-21} \text{ m}^2$ ; R.H. = 90%

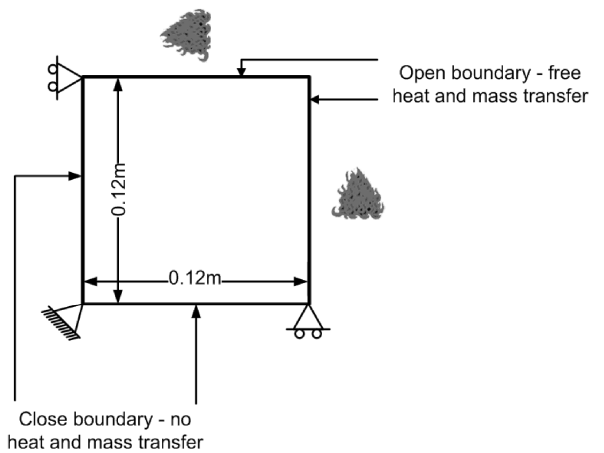


Fig. 5 Schematic diagram for the 2D problem

## 5 TWO-DIMENSIONAL PROBLEM

The significance of thermally induced stresses, in addition to the presence of pore pressures, is now investigated by application of the model to the analysis of the two-dimensional problem as shown in Fig. 5. This problem may be considered a simplified representation (in quarter symmetry) of a cross-section through a concrete column exposed to fire on all sides. Similarly to the one-dimensional problem, the top and right-hand sides of the concrete column are heated by the standard ISO834 fire while the other two sides are isolated. Unless explicitly stated otherwise, the material properties of the concrete are the same as those used in the one-dimensional problem.

Figures 6-8 give the development of mechanical damage, first principal stress and gas pressure for the concrete with permeability of  $1 \times 10^{-19} \text{ m}^2$  and relative humidity of 65%. The most severely damaged zone occurs almost at the same location as the maximum stress, but in a different location to the maximum gas pressure. Moreover, the maximum stress (i.e., about 8MPa) is much higher than gas pressure ( $\sim 1 \text{ MPa}$ ). Therefore, the damage is mainly caused by the thermally induced stress and not by the gas pressure.

For further investigation of the role played by thermally induced stresses, another case using extremely low relative humidity (10%) and high permeability ( $1 \times 10^{-17} \text{ m}^2$ ) was run. As seen in Fig. 9, very low gas pressure is built-up since the low moisture content is easily transported and dissipated.

However, the damage pattern is almost the same as the former case (see Fig. 6). This means that thermally induced stresses can themselves lead to the occurrence of damage, even for concrete where pore pressure build-up is very small, because thermally induced stresses can be built-up rapidly to a higher value than the tensile strength of the concrete.

To illustrate the importance of pore pressure for concrete of low permeability and high relative humidity, where higher pore pressure is expected to build-up, simulation using a relative humidity of 80% and a permeability of  $1 \times 10^{-21} \text{m}^2$  was performed (Fig. 10). As can be seen, although a higher maximum gas pressure is built-up, it seems not to have significant effect on the damage pattern.

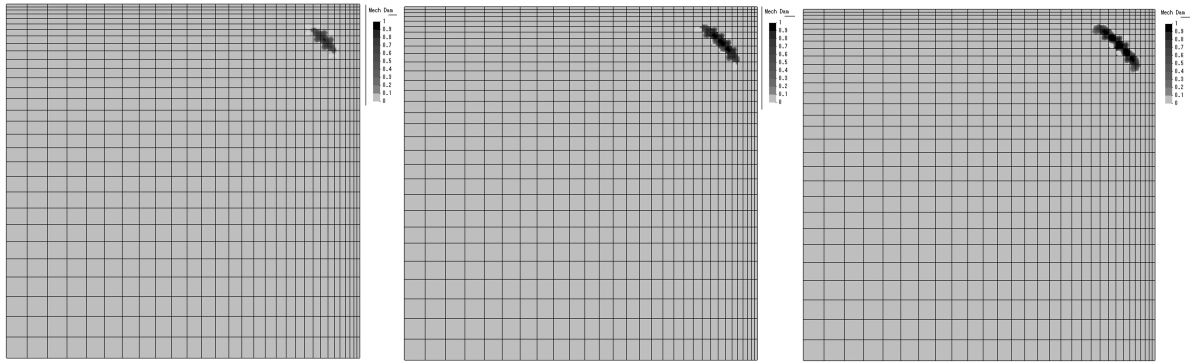


Fig. 6 Evolution of damage. Perm. =  $1 \times 10^{-19} \text{m}^2$ ; R. H. = 65%; at (a) 160s; (b) 180s and (c) 200s

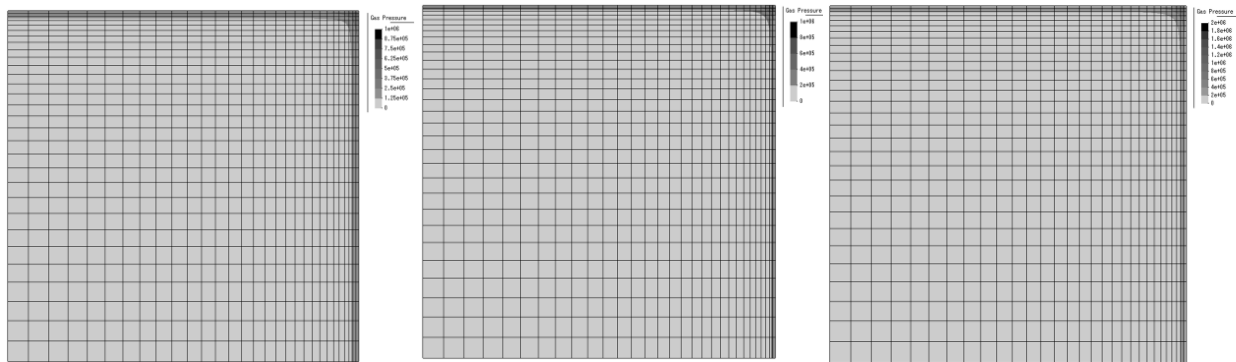


Fig. 7 Evolution of gas pressure. Perm. =  $1 \times 10^{-19} \text{m}^2$ ; R. H. = 65%; at (a) 160s; (b) 180s and (c) 200s

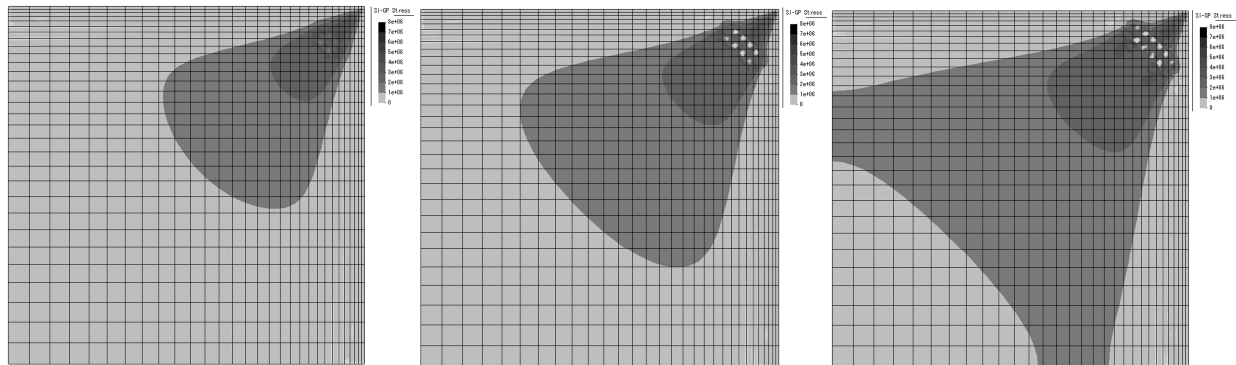


Fig. 8 Evolution of stress. Perm. =  $1 \times 10^{-19} \text{m}^2$ ; R. H. = 65% at (a) 160s; (b) 180s and (c) 200s

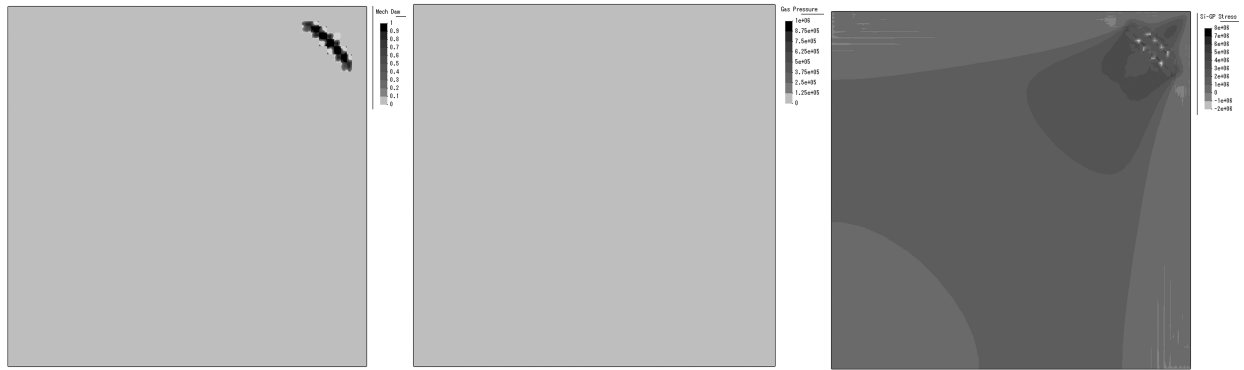


Fig. 9 Distributions of: (a) mech. dam; (b) gas pre. (c) stress. Perm. $=5 \times 10^{-17} \text{ m}^2$ ; R.H.=1%; t=200s

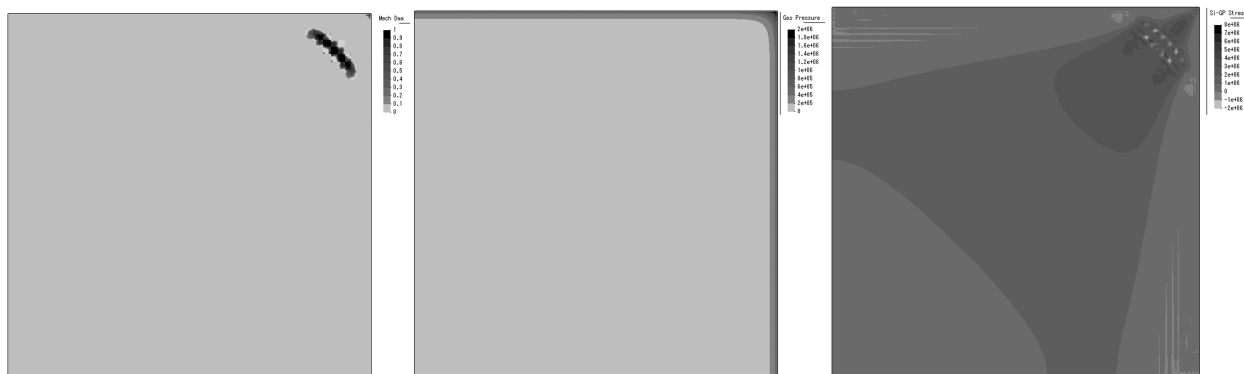


Fig. 10 Distributions of: (a) mech. dam.; (b) gas pre.; (c) stress. Perm. $=1 \times 10^{-21} \text{ m}^2$ ; R.H.=80%; t= 200s

## REFERENCES

- [1] Anderberg, Y. (1997). "Spalling phenomena of HPC and OC." International Workshop on Fire Performance of High-Strength Concrete, Gaithersburg, MD.
- [2] Kalifa, P., Menneteau, F.-D., and Quenard, D. (2000). "Spalling and pore pressure in HPC at high temperatures." *Cement and Concrete Research* 30 1915-1927.
- [3] Phan, L. T. (1996). "Fire performance of high-strength concrete: A report of the state-of-the-art." NIST, Gaithersburg, MD.
- [4] Gawin, D., Majorana, C. E., and Schreßer, B. A. (1999). "Numerical analysis of hygro-thermal behaviour and damage of concrete at high temperature." *Mech. Cohes.-Frict. Mater.*, 4, 37-74.
- [5] Stabler. (2000). "Computational modelling of thermo-mechanical damage and plasticity in concrete," PhD, The University of Queensland.
- [6] Houry, G. A., Majorana, C. E., Pesavento, F., and Schrefler, B. A. (2002). "Modelling of heated concrete." *Magazine of Concrete Research*, 54(2), 71-101.
- [7] Tenchev, R., and Purnell, P. (2005). "An application of a damage constitutive model to concrete at high temperature and prediction of spalling." *Int. J Solids Struct*, 42 (26), 6550–6565.
- [8] Gawin, D., Pesavento, F., and Schrefler, B. A. (2006). "Towards prediction of the thermal spalling risk through a multi-phase porous media model of concrete." *Comput. Methods Appl. Mech. Engrg.*, 195 5707–5729.
- [9] Davie, C. T., Pearce, C. J., and Bicanic, N. (2006). "Coupled heat and moisture transport in concrete at elevated temperatures - effects of capillary pressure and absorbed water." *Numerical Heat Transfer, Part A*, 49, 733-763.
- [10] Davie, C. T., Zhang, H. L., Pearce, C. J., and Bicanic, N. (2008). "Computational modelling of concrete exposed to fire: the effects of coupled hygro-thermal-mechanical behaviour on the development of spalling in concrete structures." The 5th International Conference for Structures in Fire, Singapore.

# A THEORETICAL MODEL FOR RC COLUMNS SUBJECTED TO NATURAL FIRE

Yao Yao<sup>a</sup>, \*Tan Kang Hai<sup>b</sup>

<sup>a</sup>ExxonMobil Upstream Research Company, Houston, Texas, USA

<sup>b</sup>Nanyang Technological University, School of Civil and Environmental Engineering, Singapore

(\*corresponding author)

## INTRODUCTION

In the European and the American codes, the design of reinforced concrete (RC) columns exposed to fire is generally based on the national and international code recommendations. They are largely derived from empirical test results under the standard ISO 834 or ASTM E119 fire curves. In view of the current global trend towards performance-based design, it is helpful and necessary to develop a simple, robust and yet rational design method for structural engineers to calculate the fire resistance of RC columns under natural fire conditions. Drawing from the limitations of standard fire curve, it is important to extend the Rankine method for RC columns under natural fire conditions. This takes account of actual fire load, ventilation conditions and thermal characteristics of compartment walls. It should be noted that failure of a particular column in a fire scenario does not in itself signify the collapse of an entire structure.

## 1 FIRE MODELLING ANALYSIS FOR RC COLUMNS

Generally, there are three phases in the fire resistance calculations, viz. fire modeling, heat transfer and structural analysis. The benchmark tests consist of fire modeling using either Ozone software or parametric fire curves. Through the heat transfer process, the predicted thermal field is then input into finite element software SAFIR to determine the mechanical responses of RC columns subject to elevated temperature. In the same sequence, for heat transfer analysis, the authors adopt a time-equivalence approach coupled with empirical formulas (Tan and Yao 2003). This is then followed by the application of Rankine method for fire resistance calculations. A well-established finite element computer code SAFIR is available for the simulation of the mechanical response of steel, concrete, and composite structures under elevated temperatures (Dotreppe et al. 1999). Since the software has been validated with extensive test data, in the absence of available test results for columns subjected to natural fire conditions, the authors used SAFIR as a numerical tool for the development of the proposed methodology. This paper presents a framework to deal with the fire resistance of RC columns in a natural compartment fire. The emphasis is on the proposed methodology and simplifications based on Rankine method. Thus, it represents a performance-based approach taken at the member level.

For design purpose, a formula recommended in Eurocode 1 (1994) can be applied. The equivalent time of exposure to ISO 834 fire test  $t_e$  (min) is given by:

$$t_e = k_b w Q_f \quad (1)$$

where  $k_b$  (min m<sup>2</sup>/MJ) is a parameter to account for different compartment linings; it depends on thermal conductivity  $k$ , density  $\rho$ , and specific heat  $c$  of compartment materials, and the value of  $k_b$  is given in Table 1;  $Q_f$  is the fire load (MJ/m<sup>2</sup>) of floor area and the ventilation

factor  $w$  is given by:  $w = \left( \frac{6.0}{H_c} \right)^{0.3} \left[ 0.62 + \frac{90(0.4 - \alpha_v)^4}{1 + b_v \alpha_h} \right] > 0.5$ ;  $H_c$  is the compartment height (m);  $\alpha_v = A_v/A_f = B_v H_v / L_1 L_2$  for  $0.05 \leq \alpha_v \leq 0.25$ ;  $\alpha_h = A_h/A_f = B_h H_h / L_1 L_2$  for  $\alpha_h \leq 0.20$ ; if there is no horizontal opening,  $\alpha_h = 0$ ;  $L_1, L_2$  are the length and width of fire compartment, respectively;  $B_v, H_v$  are the width and height of vertical opening, respectively;  $B_h, H_h$  are the width and height of horizontal opening, respectively, and  $b_v = 12.5(1 + 10\alpha_v - \alpha_v^2)$ ;  $A_f$  is the floor area (m<sup>2</sup>) of the compartment;  $A_v$  is the total area (m<sup>2</sup>) of vertical wall openings;  $A_h$  is the total area (m<sup>2</sup>) of horizontal roof openings.

It is instructive to compare the temperature-time predictions of fire gas in the compartment using time equivalence, zone modeling, and parametric fire curves, since temperature has a direct effect on fire resistance calculations. For a compartment which has geometrical and thermal conditions given in Table 1, the respective equivalent time  $t_e$  and gas temperature  $T_{ISO}$  corresponding to different fire loads and ventilation factors are given in Table 2a. Table 2b and Table 2c show the time  $t_d$  when a fire reaches its maximum temperature  $T$  predicted by parametric fire curves and Ozone, respectively. Comparing Table 2a with Table 2b and 2c, it shows that the time equivalence formula consistently gives higher estimates of equivalent ISO 834 temperature, thus leading to conservative lower column fire resistance. Besides, the applicable range of time equivalence (Table 2a) is limited compared with the parametric fire curves (Table 2b) and Ozone (Table 2c). However, for fire load equal to 200 MJ/m<sup>2</sup>, the parametric fire predictions are not comparable with time equivalence and Ozone predictions. To verify the approach for design purpose, a range of generalized design fire curves are presented with geometry and materials defined in Table 2. It should be noted that Ozone can only be used to calculate the temperature-time relation of single compartment and sprinklers are assumed to be out of order. The following fire load and compartment parameters are used in Ozone: Fire load density of 200, 400, 800, 1200 MJ/m<sup>2</sup> of floor area; Vertical ventilation factors  $A_v \sqrt{h} / A_f$  of 0.02, 0.04, 0.08 and 0.12 m<sup>0.5</sup>; Horizontal ventilation factor  $\alpha_h = 0$ ; Compartment construction – concrete.

Table 1. Geometrical and thermal conditions of analyzed compartment

|                                  |  |
|----------------------------------|--|
| Compartment Length $L_1$         | 5.0 m  |
| Compartment Width $L_2$          | 5.0 m  |
| Compartment Height $H_c$         | 3.0 m  |
| Ventilation Opening Height $H_v$ | 2.0 m  |
| Ventilation Opening Width $B_v$  | 0.778, 1.556, 3.111, 4.667 m                   |
| Enclosing Boundary               | Walls, ceiling and floor all of heavy concrete |
|                                  | Density $\rho$ 2300 kg/m <sup>3</sup>          |
|                                  | Specific Heat $c$ 1230 J/kg K                  |
|                                  | Thermal Conductivity $k$ 1.3 W/mK              |
|                                  | Thickness 0.200 m                              |

Table 2a. Equivalent time and peak temperature of the gas temperature

| Time Equivalence                    | $Q_f = 200 \text{ MJ/m}^2$ |                      | $Q_f = 400 \text{ MJ/m}^2$ |                      | $Q_f = 800 \text{ MJ/m}^2$ |                      | $Q_f = 1200 \text{ MJ/m}^2$ |                      |
|-------------------------------------|----------------------------|----------------------|----------------------------|----------------------|----------------------------|----------------------|-----------------------------|----------------------|
|                                     | $t_e(\text{min})$          | $T_{ISO}(\text{°C})$ | $t_e(\text{min})$          | $T_{ISO}(\text{°C})$ | $t_e(\text{min})$          | $T_{ISO}(\text{°C})$ | $t_e(\text{min})$           | $T_{ISO}(\text{°C})$ |
| $v_f = 0.02$                        | 25                         | 815                  | 49                         | 915                  | 98                         | 1019                 | 147                         | 1079                 |
| $v_f = 0.04$                        | 15                         | 739                  | 30                         | 842                  | 61                         | 948                  | 92                          | 1009                 |
| $v_f = 0.08$                        | 9                          | 663                  | 18                         | 766                  | 36                         | 869                  | 54                          | 930                  |
| $v_f = 0.12$ (note: not applicable) |                            |                      |                            |                      |                            |                      |                             |                      |

Table 2b. Peak temperature/time of Eurocode parametric fire curves

| Parametric Fire curve | $Q_f = 200 \text{ MJ/m}^2$ |                | $Q_f = 400 \text{ MJ/m}^2$ |                | $Q_f = 800 \text{ MJ/m}^2$ |                | $Q_f = 1200 \text{ MJ/m}^2$ |                |
|-----------------------|----------------------------|----------------|----------------------------|----------------|----------------------------|----------------|-----------------------------|----------------|
|                       | $t_d(\text{min})$          | $T(\text{°C})$ | $t_d(\text{min})$          | $T(\text{°C})$ | $t_d(\text{min})$          | $T(\text{°C})$ | $t_d(\text{min})$           | $T(\text{°C})$ |
| $v_f = 0.02$          | 27                         | 384            | 55                         | 559            | 109                        | 699            | 164                         | 754            |
| $v_f = 0.04$          | 20                         | 261            | 27                         | 700            | 55                         | 788            | 82                          | 841            |
| $v_f = 0.08$          | 20                         | 261            | 20                         | 593            | 27                         | 882            | 41                          | 944            |
| $v_f = 0.12$          | 20                         | 261            | 20                         | 593            | 20                         | 806            | 27                          | 1006           |

Table 2c. Peak temperature/time of zone modeling analysis (Ozone)

| Parametric Fire curve | $Q_f = 200 \text{ MJ/m}^2$ |                | $Q_f = 400 \text{ MJ/m}^2$ |                | $Q_f = 800 \text{ MJ/m}^2$ |                | $Q_f = 1200 \text{ MJ/m}^2$ |                |
|-----------------------|----------------------------|----------------|----------------------------|----------------|----------------------------|----------------|-----------------------------|----------------|
|                       | $t_d(\text{min})$          | $T(\text{°C})$ | $t_d(\text{min})$          | $T(\text{°C})$ | $t_d(\text{min})$          | $T(\text{°C})$ | $t_d(\text{min})$           | $T(\text{°C})$ |
| $v_f = 0.02$          | 23                         | 540            | 40                         | 600            | 100                        | 740            | 138                         | 780            |
| $v_f = 0.04$          | 17                         | 640            | 21                         | 730            | 45                         | 860            | 65                          | 930            |
| $v_f = 0.08$          | 15                         | 740            | 17                         | 800            | 27                         | 920            | 37                          | 990            |
| $v_f = 0.12$          | 12                         | 760            | 16                         | 840            | 25                         | 990            | 35                          | 1060           |

Note:  $v_f=0.02$ ,  $\alpha_v=0.062$ ;  $v_f=0.04$ ,  $\alpha_v=0.124$ ;  $v_f=0.08$ ,  $\alpha_v=0.249$ ;  $v_f=0.12$ ,  $\alpha_v=0.373$ ; (the idea of time equivalence is not applicable)

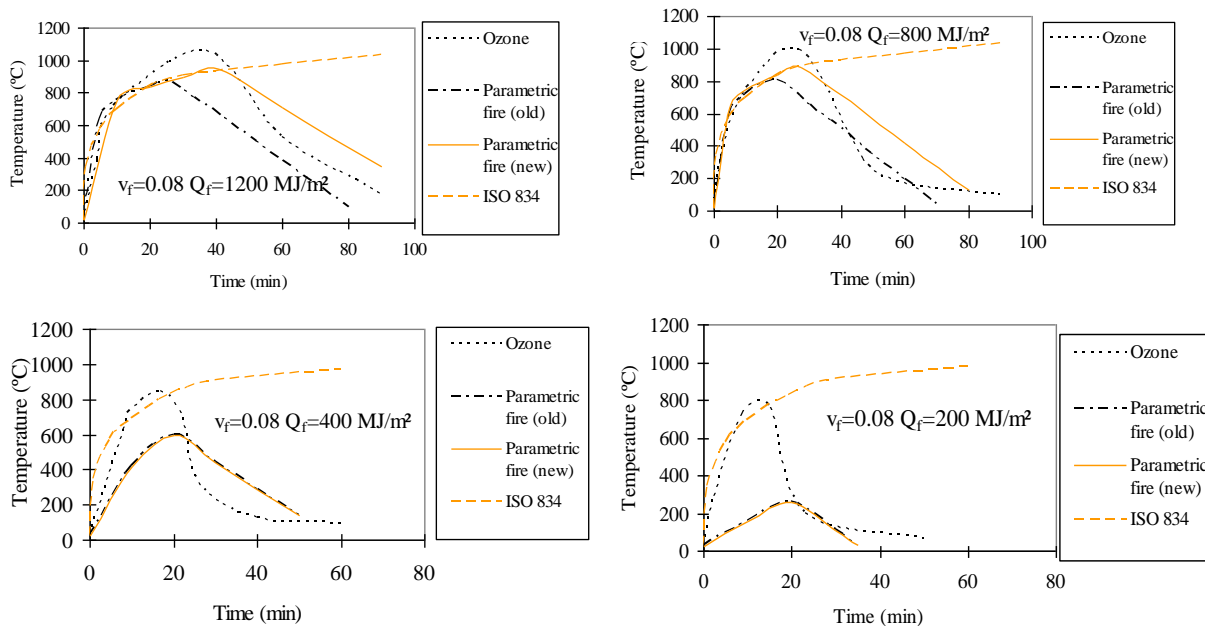


Fig. 1. Gas time-temperature relationship predictions by Ozone and Parametric fire curve

Due to the limit of paper length, only part of the comparison is presented here, as shown in Fig. 1, in which  $Q_f$  is the fire load and  $v_f$  is the ventilation factor. Basically, it is found that the predicted heating curves by different zone modeling and parametric fire equations are similar

for  $Q_f$  greater than 200 MJ/m<sup>2</sup>; the higher the fire loads, the greater the similarity in predictions by zone modeling and parametric fire curve equations. However, for fire loads equal or smaller than 200 MJ/m<sup>2</sup>, Ozone gives very conservative predictions compared with parametric fire equations. It should be noted that for  $Q_f$  less than 200 MJ/m<sup>2</sup>, most columns will not fail and therefore, the comparisons are only academic. Moreover, it can be found that predictions of modified parametric fire curves in the new edition (EC1 2003) are closer to Ozone predictions compared with the old version (EC1 1994) for higher fire loads (say above 400 MJ/m<sup>2</sup>). And for smaller fire loads (say less than 400 MJ/m<sup>2</sup>), the two versions of the parametric fire curves give similar predictions. However, for fire loads smaller than 200 MJ/m<sup>2</sup>, both editions of parametric fire curves have significant differences compared with Ozone predictions. From comparison, it can be concluded that for most cases, the new parametric fire curves and Ozone give similar predictions to temperature-time relationship of the compartment. Thus, both methods can be applied to verify the time equivalence approach.

## 2 STRUCTURAL ANALYSIS

Having presented the fire modeling calculations, this section presents the comparison of fire resistance calculations using Rankine method and finite element program SAFIR. SAFIR accommodates various elements for different idealizations, calculation procedures, and various material models for incorporating the stress-strain behavior. The stress-strain material laws are generally linear-elliptic for steel and nonlinear for concrete. SAFIR can be used for performing two different types of calculation, namely, thermal and structural analyses.

The Rankine formula has the following form:

$$\frac{1}{P_R} = \frac{1}{P_p} + \frac{1}{P_e} \quad (2)$$

where  $P_R$ ,  $P_p$  and  $P_e$  are the Rankine load, plastic collapse load, and elastic critical load, respectively.

Although it is derived for ambient-temperature analysis, the Rankine formula can be extended to columns in fire conditions by taking account of the deterioration of material properties at elevated temperatures (Tang et al. 2001). Thus, Eq. (2) can be expressed as:

$$\frac{1}{P_R(t)} = \frac{1}{P_p(t)} + \frac{1}{P_e(t)} \quad (3)$$

where  $t$  is the time of fire exposure.

The capacity of a real column in fire conditions may be less than that expected from Eq. (2), as both the plastic collapse load and elastic critical load are over-estimated by ignoring secondary effects such as load eccentricity and initial crookedness. The reduced plastic collapse load  $P_{pr}(t)$  and the reduced elastic critical load  $P_{er}(t)$  are introduced to account for secondary effects. Thus, if the secondary effects are significant, a modified form of Rankine formula can be used:

$$\frac{1}{P_{Rr}(t)} = \frac{1}{P_{pr}(t)} + \frac{1}{P_{er}(t)} \quad (4)$$

where  $P_{Rr}(t)$  is the reduced Rankine load for imperfect columns.

The following equations are useful in dealing with the modified Rankine formula:

$$P_{pr}(t) = u_{pr} P_p(t) \text{ and } P_{er}(t) = u_{er} P_e(t) \quad (5)$$

where  $u_{pr}$  and  $u_{er}$  are the plastic load reduction factor and elastic critical load reduction factor,

respectively. The values can be obtained from the method recommended by Tang et al. (2001).

There are 4 steps in the Rankine method to determine the fire resistance of RC columns (Tan and Yao 2003). The first step is to determine the equivalent ISO 834 fire exposure time. The second step is to calculate the plastic squashing and elastic buckling loads of columns, followed by the third step to determine the imperfection parameter which explicitly includes secondary effects such as load eccentricity. The last step is to calculate column failure loads. Although the proposed method is developed based on standard fire curve, for general conditions, different heating rates can be incorporated into the proposed method by applying the time equivalence formula. . To verify the proposed method, a series of case studies for RC columns is conducted in the following section.

### 3 CASE STUDY FOR RC COLUMNS UNDER NATURAL FIRE

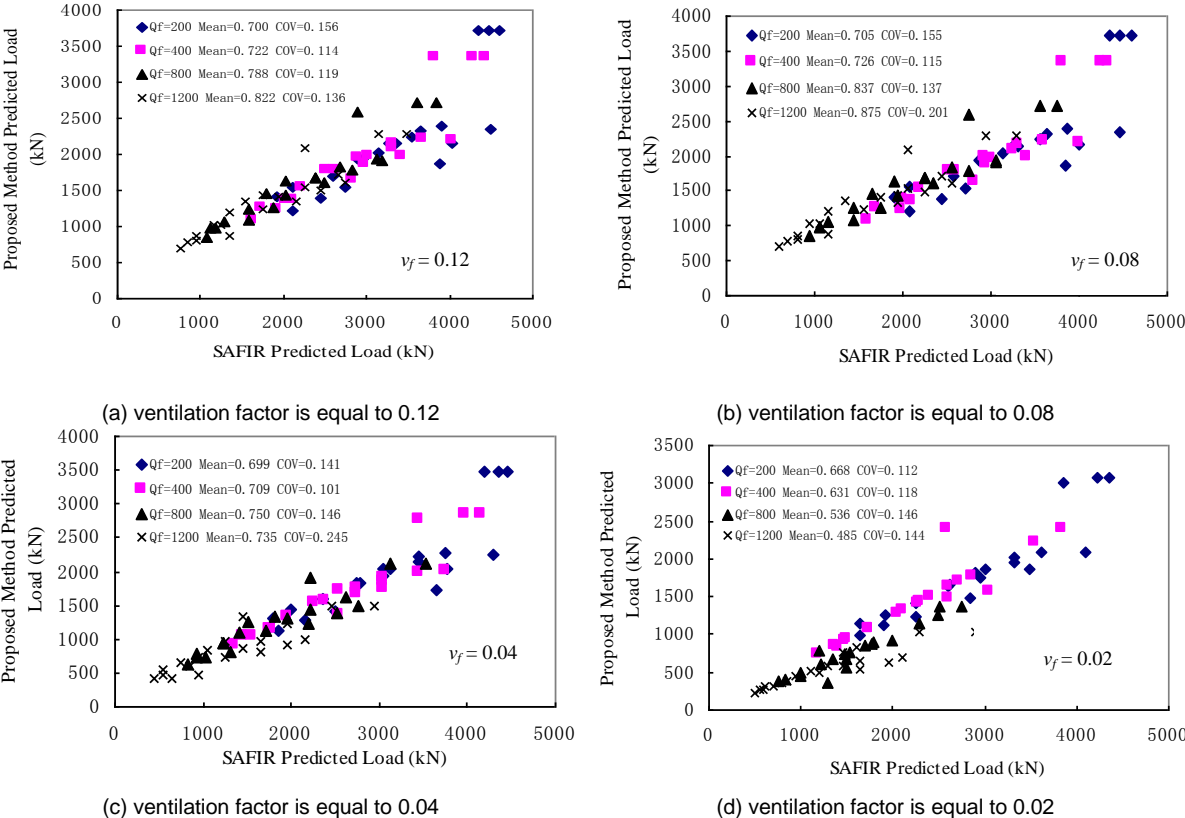


Fig. 2. Comparison of RC columns failure load under different heating conditions predicted by the proposed method (with Euro code formula) and SAFIR (with Ozone modeling); fire loads from 200 to 1200 MJ/m<sup>2</sup>

For more general heating conditions, the predictions of the proposed method are compared with SAFIR and Ozone. The fire resistance predictions of a large pool of RC columns with different slenderness ratios (from 20 to 100), load levels (from 20 to 80% of design load) (100 to 4500 kN), load eccentricities  $e/h$  (from 0 to 0.4), cross section areas (from 200×200 to 600×600mm<sup>2</sup>), concrete strengths (from 20 to 80 MPa), and concrete covers (from 20 to 60mm) were analyzed. The comparisons between the proposed approach (using Eq. (1) to

predict equivalent ISO 834 fire exposure time  $t_e$ ) with Ozone and SAFIR predictions corresponding to fire loads from 200 to 1200 MJ/m<sup>2</sup>, and ventilation factors from 0.02 to 0.12 are given in Fig. 2. From the comparison study, the predictions by the proposed method are consistent and conservative with a mean value ranging from 0.699 to 0.875, and a COV of 0.101 to 0.245 for ventilation factors ranging from 0.04 to 0.12. The conservative predictions of the proposed method may be due to the physical meaning of the concept of time equivalence as discussed before. Thus, the approach is suitable for design purpose under natural fire conditions. However, it should be noted that when the ventilation factor is 0.02, the predictions by the approach are too conservative. This is partly because the predictions by zone modeling may not be accurate within this range.

#### 4 CONCLUSION

A theoretical model based on Rankine method is proposed to predict the fire resistance of RC columns. Comparison between zone modeling, parametric fire curves, and time equivalence are first conducted. Based on time equivalence formula recommended in the EC 1 (1994), the Rankine method can be applied to different fire curves. A large pool of columns with different slenderness ratios, load levels, eccentricities, cross sectional areas, material strengths and concrete covers have been analyzed with Zone modeling, parametric fire curves and Finite Element program SAFIR. Comparisons of predictions between the Rankine method (combining with the Eurocode time equivalence formula) and SAFIR (with fire curves predicted by Ozone) are performed. The results show that the proposed method can be safely applied for design purpose for most natural fire curves and for different thermal boundary conditions in a compartment fire. Only when the ventilation factor is equal to 0.02, the proposed method is too conservative.

#### 5 ACKNOWLEDGEMENT

The authors would like to acknowledge funding support from the Ministry of Education, Singapore, for research project titled "Failure modes and ultimate strength of tubular joints under elevated temperatures" with account number ARC 2/07.

#### REFERENCES

- [1] Dotreppe, J.C., Franssen, J.M. and Vanderzeypen, Y. "Calculation Method for Design of Reinforced Concrete Columns under Fire Conditions," ACI Structural Journal, 1999, V. 96, No. 1, 9-18.
- [2] Eurocode 1 (1994). "Basis of design and Actions on Structures. Part 2-2: Actions on structures Exposed to Fire," European Committee for Standardization.
- [3] Eurocode 1 (2003). "Basis of design and Actions on Structures. Part 2-2: Actions on structures Exposed to Fire," European Committee for Standardization.
- [4] Tan, K.H. and Yao, Y. (2003). "Fire Resistance of Four-Face Heated Reinforced Concrete Columns", J. of Struct. Engrg. ASCE, 129(9), pp. 1220-1229.
- [5] Tang, C. Y., Tan, K. H. and Ting, S. K. (2001). "Basis and Application of a Simple Interaction Formula for Steel Columns under Fire Conditions," J. of Struct. Engrg., ASCE, 127(10), 1214 –1220.

## **DIFFERENT TYPES OF PRE-STRESSED HOLLOW CORE PANELS And their fire resistance according to Eurocodes**

Radim Čajka<sup>a</sup>, Pavlína Matečková<sup>a</sup>

<sup>a</sup> VSB – Technical University Ostrava, Faculty of Civil Engineering, Ostrava, Czech Republic

### **INTRODUCTION**

Calculation of the fire resistance demands apposite determination of temperature distribution in the cross-section (heat-exposure model) and analysis of mechanical responses of the structure exposed to increased temperature (structural response model).

The transient thermal array was solved numerically using FEM analysis and appropriate computer program.

Mechanical response of pre-stressed cross-section was analysed on the basis of published dependences of thermal and mechanical characteristics of concrete and pre-stressing steel on temperature.

The temperature distribution in the cross-section, mechanical behaviour of the structure and final fire resistance are compared with test results (if available).

### **1 HEAT-EXPOSURE MODEL**

#### **1.1 Air in hollow core**

Analysis of transient thermal array in hollow core cross-section demands setting up of boundary conditions and thermal characteristics of concrete and air in hollows. Boundary conditions are given in Eurocode 1 [2] by standard time-temperature curve and parameters of convection and radiation. Thermal characteristics of concrete are given in Eurocode 2 [3]. Thermal characteristics of air in hollows were determined on the basis of inverse analysis. Several reports about testing the fire resistance of pre-stressed panel are available. During the fire resistance testing both the temperatures on unexposed side and the temperatures in cross-section were measured.

The basis of inverse analysis were thermal properties of air. Complex process of convection in hollow cores is defined in a simplified way through substitutive coefficient of thermal conductivity [4].

#### **1.2. Comparison of measured and calculated temperatures**

In the Table 1 calculated and measured temperatures are presented. Temperatures on the bottom of hollow and temperatures on unexposed side are compared for pre-stressed panel Spiroll 250 mm. Measured and calculated temperatures on the bottom of hollow respond with acceptable divergence, calculated temperatures on unexposed side are significantly higher than measured temperatures. Inverse analysis was elaborated so that the measured and calculated temperatures respond together, but the temperatures on the bottom of hollow in preference because it is nearer the reinforcement. Besides, measured temperatures are represented with average values and measured temperatures have wide variance, even temperatures measured on particular panel.

Table 1. Spiroll 250 mm, calculated and measured temperatures

|      | Temp. on the bottom of hollow |             |         | Unexposed side |             |         |
|------|-------------------------------|-------------|---------|----------------|-------------|---------|
|      | calculation                   | measurement |         | calculation    | measurement |         |
| Time | EN                            | panel 1     | panel 2 | EN             | panel 1     | panel 2 |
| min  | °C                            | °C          | °C      | °C             | °C          | °C      |
| 0    | 20                            | 12          | 11      | 20             | 11          | 11      |
| 15   | 112                           | 92          | 46      | 21             | 12          | 11      |
| 30   | 202                           | 225         | 115     | 32             | 14          | 15      |
| 45   | 261                           | 347         | 162     | 55             | 23          | 34      |
| 60   | 307                           | 413         | 238     | 84             | 33          | 49      |
| 90   | 379                           | 472         |         | 148            | 53          |         |

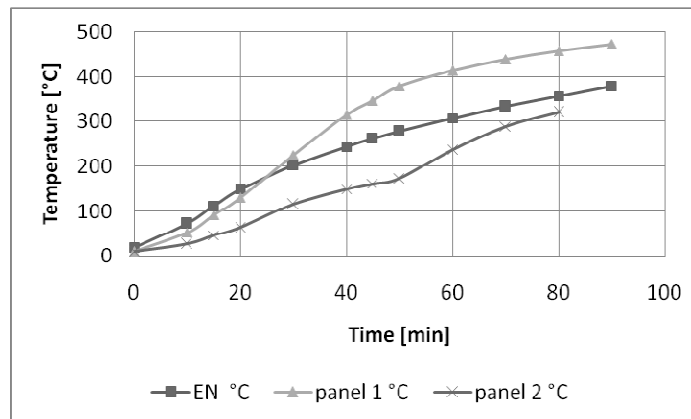


Fig. 1. Spiroll 250 mm, calculated and measured temperatures

### 1.3. Comparison of different types of panel

In the Table 2 calculated temperatures for different types of hollow core panels are presented. Temperatures in reinforcement and temperatures on unexposed side are compared for pre-stressed panel, thickness 200 mm, type Echo with oval hollow core and type Elematic with circle hollow core, see Fig.2. Temperatures both in reinforcement and on unexposed side are more favourable for panel Echo due to higher portion of concrete in cross-section. Insulation limit state is 90 minutes for panel type Echo and 60 minutes for panel type Elematic.

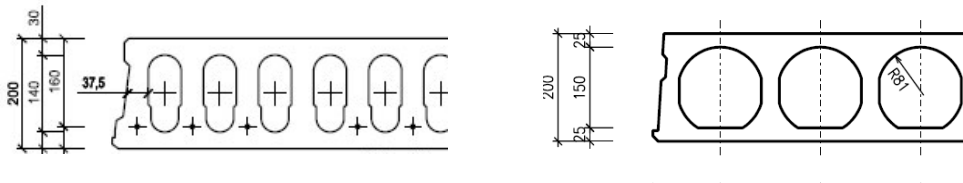


Fig. 2. Different types of pre-stressed panel, Echo 200 mm, Elematic 200 mm

Table 2. Temperatures in cross-section, Echo 200 mm, Elematic 200 mm

| Time | Echo     |           | Elematic |           |
|------|----------|-----------|----------|-----------|
|      | reinfor. | unexposed | reinfor. | unexposed |
| min  | °C       | °C        | °C       | °C        |
| 0    | 20       | 20        | 20       | 20        |
| 15   | 119      | 21        | 118      | 25        |
| 30   | 246      | 31        | 261      | 55        |
| 45   | 333      | 57        | 362      | 102       |
| 60   | 396      | 90        | 438      | 151       |
| 75   | 447      | 126       | 498      | 196       |
| 90   | 489      | 160       | 549      | 237       |

## 2 STRUCTURAL RESPONSE MODEL

### 2.1 Load bearing capacity and fire resistance

Mechanical response of pre-stressed cross-section was analysed on the basis of published dependences of concrete and pre-stressing steel mechanical characteristics on temperature. In the Table 3 fire resistance 40 minutes of pre-stressed panel Elematic is determined according to final version of Eurocode 2 [3], see Fig. 3. As the thermal properties of concrete and parameters of heat transfer are more favourable according to P ENV version of Eurocode, the fire resistance according to P ENV version was stated to value 45 minutes. Laboratory testing of fire resistance was quitted for panel 1 after 65 minutes and for panel 2 after 74 minutes, fire resistance on the basis of laboratory testing was settled 45 minutes.

In the Table 4 fire resistance determined for panel Echo and Elematic is compared and again is more favourable for panel type Echo. In the Table 4 the concrete cover is also analysed. Higher concrete cover responds to mildly decrease of load bearing capacity for permanent design situation but significant increase of fire resistance.

Table 3. Fire resistance, Elematic 200 mm

| Time | reinforcement |              | concrete |              | $M_{Rd,fi}$ | $M_{ed,fi}$ |
|------|---------------|--------------|----------|--------------|-------------|-------------|
|      | Temp °C       | Strength MPa | Temp °C  | Strength MPa |             |             |
| min  | Temp °C       | Strength MPa | Temp °C  | Strength MPa | kNm         | kNm         |
| 0    | 20            | 1593         | 20       | 41,67        | 66,24       | 40,22       |
| 15   | 118           | 1543         | 25       | 41,67        | 64,19       | 40,22       |
| 30   | 261           | 1241         | 55       | 41,67        | 51,91       | 40,22       |
| 45   | 362           | 889          | 102      | 41,64        | 37,39       | 40,22       |
| 60   | 438           | 575          | 151      | 40,62        | 24,31       | 40,22       |
| 75   | 498           | 328          | 196      | 39,68        | 13,91       | 40,22       |
| 90   | 549           | 257          | 237      | 38,04        | 10,92       | 40,22       |

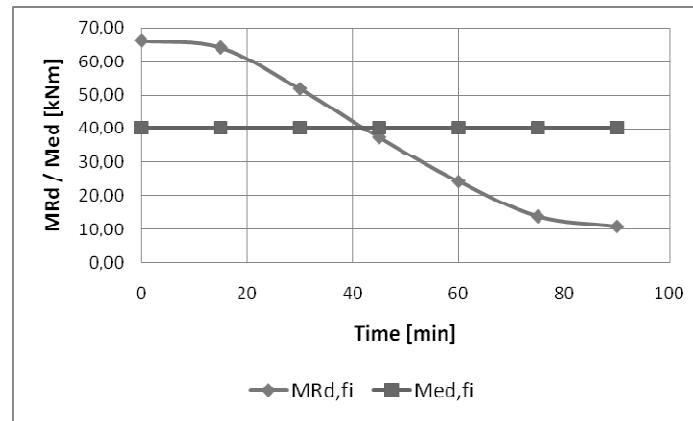


Fig. 3. Elematic 200 mm, fire resistance determination

Table 4. Fire resistance, Echo 200 mm, Elematic 200 mm

| Type of panel                | Elematic         |      | Echo             |       |
|------------------------------|------------------|------|------------------|-------|
| Reinforcement                | 5 x cable 9,3 mm |      | 6 x cable 9,3 mm |       |
| Weight [kg.m <sup>-2</sup> ] | 240              |      | 315              |       |
| Concrete cover [mm]          | 35               | 40   | 35               | 40    |
| Bearing capacity [kNm]       | 57,5             | 55,7 | 68,56            | 66,41 |
| Fire resistance [min]        | 40               | 50   | 45               | 60    |

## 2.2 Decrease of pre-stressing force

Decrease of pre-stressing force during the fire influences especially deformation of particular panel. Owing to irregular decrease of pre-stressing force and reinforcement strength the bearing capacity of pre-stressing panel could be exceeded. Decrease of pre-stressing force in fire resistance calculation was considered according to Eq. (1):

$$P(\theta) = A_s \cdot \varepsilon_s(\theta) \cdot E_s(\theta) \quad (1)$$

where  $P(\theta)$  pre-stressing force versus temperature

$A_s$  area of reinforcement

$\varepsilon_s(\theta)$  specific thermal elongation of reinforcement versus temperature

$E_s(\theta)$  modulus of elasticity of reinforcement versus temperature

Specific thermal elongation versus temperature is creasing function and modulus of elasticity versus temperature is descending function. After multiplying those functions the result  $P(\theta)$  form local minimum. Decreasing values of pre-stressing force for Elematic 200 mm are sequenced in the Table 5.

Table 5 . Decrease of pre-stressing force, Elematic 200 mm

| Time | Temp. | $\varepsilon$ | E   | $\Delta P$ | P      |
|------|-------|---------------|-----|------------|--------|
| min  | °C    |               | Gpa | kN         | kN     |
| 0    | 20    | 0,000000      | 195 | 0,00       | 284,76 |
| 15   | 118   | 0,001034      | 190 | 50,80      | 233,96 |
| 30   | 261   | 0,002675      | 177 | 122,38     | 162,38 |
| 45   | 362   | 0,003946      | 163 | 166,36     | 118,40 |
| 60   | 438   | 0,004946      | 138 | 176,36     | 108,40 |
| 75   | 498   | 0,005767      | 106 | 158,74     | 126,02 |
| 90   | 549   | 0,006490      | 93  | 155,94     | 128,82 |

### 3 SUMMARY

In the paper the fire resistance of pre-stressed hollow core panels is analysed. Calculation of transient thermal array in cross-section is based on inverse analysis and measured and calculated temperatures confrontation. Field of temperature and final fire resistance is compared for different types of pre-stressed panel, Echo 200 mm with oval hollow core and Elematic 200 mm with circle hollow core. Calculated temperatures and final fire resistance are more favourable for panel Echo due to higher portion of concrete in cross-section. Concrete cover was also analysed. Higher concrete cover responds to mildly decrease of load bearing capacity for permanent design situation but significant increase of fire resistance. Decrease of pre-stressing force is also mentioned.

### ACKNOWLEDGMENT

This outcome has been achieved with the financial support of the Ministry of Education, Youth and Sports of the Czech Republic, project No. 1M0579, within activities of the CIDEAS research centre.

### REFERENCES

- [1] Zidkova, P., Fire resistance calculation of concrete slab structures with respect to physical and geometrical non-linearity, *PhD. thesis*, 2004 (in Czech)
- [2] CSN EN 1991-1-2: Eurocode 1: Actions on structures, part 1-2: Action on structures – Action on structures exposed to fire, CNI, 2004
- [3] CSN EN 1992-1-2, Eurocode 2: Design of concrete structures, part 1-2: General rules – Structural fire design, CNI, 2006
- [4] Sazina, M., Kmonicek, V.: Heat, SNTL, Prague 1989 (in Czech)

## **EFFECT OF TEMPERATURE ON THE BEHAVIOUR OF CONFINED FIBER REINFORCED HIGH STRENGTH CONCRETE**

**U.K. Sharma, C.R. Babu , P. Bhargava and V.K. Gupta**

Department of Civil Engineering, Indian Institute of Technology Roorkee, Roorkee, India

### **INTRODUCTION**

With the development and application of high strength concrete (HSC), understanding of its behavior when subjected to elevated temperature in the event of fire is needed to insure its safe application [1]. HSC exhibits superior performance in many aspects e.g. possesses high strength, durability and workability. Given the many benefits of HSC and its increased use in structural applications, it is essential that the fundamental behavior of HSC at elevated temperatures be understood to ensure that structural fire design involving HSC will be safe. Recently, some studies have been conducted to investigate the performance of HSC at elevated temperature [2-3].

In the structural design, inelastic deformability to the structural elements is ensured by providing sufficient amount of lateral confining steel. The requirements of confinement are well established now at ambient temperature, however, it remains to be seen that how confined concrete would behave after having exposed to elevated temperature. Further, the use of fibers in concrete at ambient and elevated temperature has also picked up recently [4]. In view of the above, the present study aims to establish the behavior of confined fibre reinforced HSC after exposure to a single cycle of high temperature.

### **1. EXPERIMENTAL PROGRAM**

#### **1.1 Test specimens**

One hundred specimens of 100 mm diameter and 200 mm height cylinders were cast (Table 1). These included plain and hoop reinforced cylinders in two grades of concrete with discrete polypropylene fibers at 0.1%, 0.2% and 0.3% by volume. The transverse reinforcement was provided in the form of 4 mm tor steel hoops at various spacings. The spacing varied from as small as 34 mm to as large as 85 mm so as to achieve a very light to heavy confinement. Longitudinal reinforcement of 4 numbers of 4 mm tor steel was provided for holding the transverse reinforcement in the position. Plain concrete specimens (S0V0 and V0S0) were also cast as control specimens.

#### **1.2 Properties of materials**

Two grades of High Strength Concrete of compressive strength 60 MPa and 80 MPa were designed and used in this study. The control cubes and cylinders were cast in all the two mixes to determine the compressive strength of cubes and cylinders. The specimens were cured under water (28 days) and in air (28 days) and tested after 56 days. The details of the designed concrete mixes along with the 28 days compressive strengths are given in Table 2. Ordinary Portland Cement 43 grade (OPC 43) from a single lot was used throughout the course of the investigation. Locally available river sand was used as fine aggregate. Locally available crushed stone aggregate of maximum nominal size of 10 mm was used as coarse aggregate. Commercially available high range Superplasticizer (Glenium 51) based on modified polycarboxylic ether and conforming to ASTM C494 type F and IS: 9103-1999 with specific gravity as 1.09 was used throughout the investigation. Micro Silica was obtained

from M/S Elkem (India) Private Limited was used in the present study. A fly-ash obtained from combined fields of the electrostatic precipitator of the thermal power plant at Dadri was used. Polypropylene fibers were used throughout the investigation. Physical properties of Polypropylene fibers are 0.3 mm diameter, 20 mm length and 150-170<sup>0</sup> C melting point.

**Table 1-Details of Test Specimens**

| Mix | $f_{ck}$ ( $f_c$ )<br>(MPa) | Specimen Label | Pitch of Transverse Hoop<br>(mm) | Fibers Volume (%) |
|-----|-----------------------------|----------------|----------------------------------|-------------------|
| M60 | 73.52 (66.33)               | S0V0           | -                                | -                 |
|     |                             | S1V1           | 34                               | 0.1               |
|     |                             | S2V1           | 57                               | 0.1               |
|     |                             | S3V1           | 85                               | 0.1               |
|     |                             | S1V2           | 34                               | 0.2               |
|     |                             | S2V2           | 57                               | 0.2               |
|     |                             | S3V2           | 85                               | 0.2               |
|     |                             | S1V3           | 34                               | 0.3               |
|     |                             | S2V3           | 57                               | 0.3               |
|     |                             | S3V3           | 85                               | 0.3               |
| M80 | 93.09 (83.97)               | V0S0           | -                                | -                 |
|     |                             | V1S1           | 34                               | 0.1               |
|     |                             | V1S2           | 57                               | 0.1               |
|     |                             | V1S3           | 85                               | 0.1               |
|     |                             | V2S1           | 34                               | 0.2               |
|     |                             | V2S2           | 57                               | 0.2               |
|     |                             | V2S3           | 85                               | 0.2               |
|     |                             | V3S1           | 34                               | 0.3               |
|     |                             | V3S2           | 57                               | 0.3               |
|     |                             | V3S3           | 85                               | 0.3               |

**Table.2 Concrete Mix Proportions**

| Mix | Cement<br>(Kg/m <sup>3</sup> ) | Sand<br>(Kg/m <sup>3</sup> ) | Aggregate<br>(Kg/m <sup>3</sup> ) | Water<br>(Kg/m <sup>3</sup> ) | Silica<br>Fume<br>(Kg/m <sup>3</sup> ) | Fly Ash<br>(Kg/m <sup>3</sup> ) | Super-<br>plasticizer<br>(Kg/m <sup>3</sup> ) | 28 days<br>Cylinder<br>Compressive<br>Strength* $f_c$<br>MPa | 28 days<br>Cube<br>Compressive<br>Strength* $f_c$<br>MPa |
|-----|--------------------------------|------------------------------|-----------------------------------|-------------------------------|--|---------------------------------|---|--|--|
| M60 | 535                            | 688                          | 1085                              | 166                           | 27                                     | 0                               | 5.35  | 61.63  | 68.61  |
| M80 | 555                            | 700                          | 868                               | 155                           | 55.5                                   | 63                              | 11.07   | 78.36  | 86.72  |

### 1.3 Heating of specimens

The tests to determine residual properties of confined fiber reinforced High Strength Concrete after subjecting to thermal loads were conducted at room temperature (27° approx., 100°, 200°, 400°, 800°. A digitally controlled electric furnace was used to heat the specimens. After the specimens reached to desired temperature, the same temperature was maintained for 60 minutes in order to achieve steady state condition. After that, furnace was switched off in order to bring the heated specimen to room temperature. After the fire resistance test, spalling was examined with the naked eye, and weight reduction ratio was calculated by measuring the weight of specimens before and after the fire resistance test. The real time-temperature curve of the furnace and specimens are shown in Fig.1. The specimen is heated without preload at a prescribed rate to the target temperature, which is maintained until a thermal steady state is reached within the specimen. The specimen is then allowed to cool.

### 1.4 Residual Testing of specimens

All specimens were tested after 56 days of ageing, under axial compression. Before testing, the cylinders were capped with a rich cement paste to ensure parallel loading faces and constant height of the test specimens. The complete load-displacement and stress-strain response of confined fiber reinforced concrete was obtained by testing the specimens in a 2500 kN capacity INSTRON make Universal Testing Machine. Displacement controlled in-plane loading was applied at a relatively slow rate of 0.2 mm per minute until the specimens fails. The load is applied from top collar and all precautions are taken to avoid loading eccentricity on the specimens.

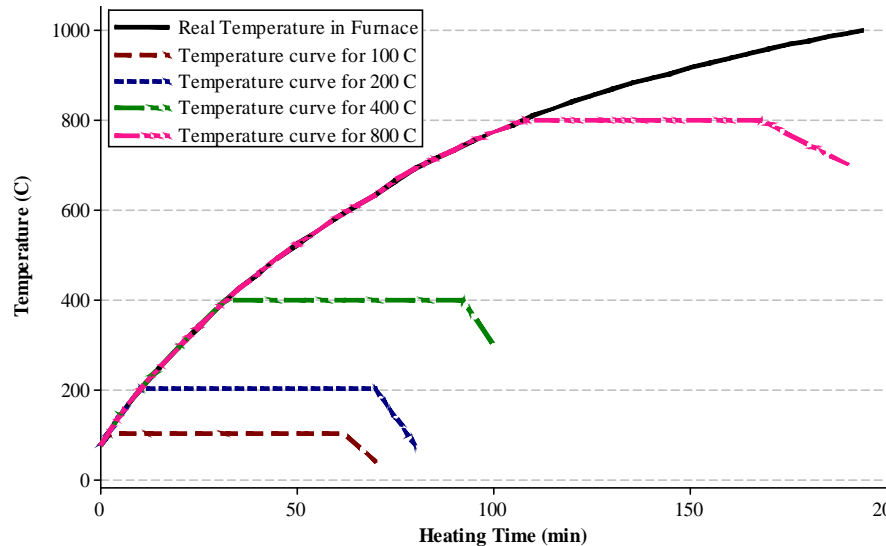


Fig.1 Temperature Curve for Electric Furnace

Before testing, the specimens were loaded and unloaded once or twice up to 5% of the expected maximum load to take care of all loose joints and reduce as much as possible the curvilinear response that would otherwise distort the initial portion of the load displacement curve. The shape of uniaxial load-displacement curve is strongly affected by the testing conditions namely stiffness of testing machine, size and shape of specimens, rate of loading etc. and concrete characteristics like water/cement ratio, aggregate type etc. To minimize the effects of testing conditions, careful attention was exercised to avoid variation in the testing setup.

## 2. TEST RESULTS

The test programme included measurement of axial load, displacements and mass loss after fire test. The test results of all the specimens are given in Table 3. The discussion presented below focuses on the residual load-displacement behavior of confined fiber reinforced high strength concrete, comparing the effects of temperature, amount of transverse reinforcement, fiber volume fraction and concrete strength. Crack patterns at the time of fire test and the failure modes after the compression test are also discussed below.

### 2.1 Observations and Failure modes

When the specimens were heated to 100° C and 200° C, no cracks were found on the surface of the specimens. The specimens heated to 400° C, minor cracks appeared in the specimens containing confinement and polypropylene (PP) fibers. Same minor cracks appeared, but the number of cracks was more on plain concrete specimens. At 800° C, major cracks were formed on the surface for the specimens containing confined PP fiber concrete and the plain concrete specimens disintegrated completely especially for M80 plain concrete specimens. The spalling was observed in plain concrete specimens only. However, when PP fiber percentage was more than 0.1% with confinement, spalling did not occur in any of the specimens. There are two reasons for this behavior: one is that as PP fiber in concrete melts at the high temperature (at about 170 °C) and vapor pressure is relieved. The other reason may be that lateral confinement pressure provided by the confining material is higher than the pressure induced by the internal vapor pressure. On surface of the specimens; black spots were formed after heating to 400° C due to melting of PP fibers, whereas colour of the surface became ash white after heating to 800° C. After the fire test the weight reduction ratios were recorded.

In the case of specimens without PP fiber and confinement, the weight reduction ratio is high as compared to the specimens with PP fiber and confinement. At 100° C and 200° C temperatures for M60 grade concrete specimens as the mixing ratio of PP fibers is increased there is more or less no change in the weight reducing ratios. But at 400° C and 800° C the weight reducing ratio is high at 0% of mixing ratio of PP fibers. When the mixing ratio of PP fibers is increased from 0% to 0.1% the weight reducing ratio is decreased. At this point it is observed that for 800° C rate of decreasing of weight reducing ratio is more than that of 400° C. As the mixing ratio of PP fibers is increased from 0.1% to 0.3% there is more or less no change in the weight reducing ratio both for 400° C and 800° C. From the Table 3, it can be observed that M80 grade concrete specimens also follow the same trend as the M60 grade concrete specimens. These results corroborate the cracking/spalling observation mentioned in previous paragraph. The effect of confinement was negligible on weight reduction ratio due to its high melting temperature. The temperature was one of the primary variables investigated extensively in the test programme. The specimens exposed to 100° C and 200° C, behavior and strengths are more or less same as the specimens tested at room temperature.

After 200° C as the temperature was increased to 800° C the displacement increased but the axial load decreased for both M60 and M80 grade concrete specimens. As the temperature increases from 200° to 400° C, strength ratio decreased to 0.78 and 0.85 for plain concrete and confined fiber reinforced concrete respectively. When the temperature increased from 400° to 800° C, strength ratio reduced drastically upto 0.2 in the plain concrete specimen, but the confined fiber reinforced concrete showed much better improvement in the behavior and strength ratio reduced to 0.4. At 0.1%, 0.2% and 0.3% volume fraction of fibers, the variation of strength ratio with the temperature is almost same.

### 3 SUMMARY

At high temperature, the weight reduction ratio increases as the grade of concrete increases for both plain and fiber reinforced concrete. Addition of polypropylene fibers to the concrete reduces the weight reduction ratio. The effect of fibers in reducing the weight reduction is more at high temperatures. Upto 200<sup>0</sup> C, the effect of temperature on the strength of concrete is negligible for both plain and confined polypropylene fiber reinforced concrete. As the temperature increases, the strength of concrete decreases.

**Table 3 Test Results**

| Specimen Label | Temperature (°C) | M60               |                 |             | M80               |                 |             |
|----------------|------------------|-------------------|-----------------|-------------|-------------------|-----------------|-------------|
|                |                  | Displacement (mm) | Axial Load (kN) | % Mass Loss | Displacement (mm) | Axial Load (kN) | % Mass Loss |
| S0V0           | 27               | 1.314             | 520.92          | 0           | 1.221             | 659.52          | 0           |
|                | 100              | 1.287             | 506.15          | 0.248       | 1.319             | 663.43          | 0.253       |
|                | 200              | 1.361             | 528.28          | 0.500       | 1.261             | 682.13          | 0.496       |
|                | 400              | 1.811             | 404.29          | 5.434       | 1.593             | 501.85          | 5.477       |
|                | 800              | 1.125             | 109.98          | 11.073      | ---               | ---             | 12.039      |
| S1V1           | 27               | 1.465             | 684.40          | 0           | 1.497             | 814.38          | 0           |
|                | 100              | 1.424             | 692.96          | 0.238       | 1.603             | 826.00          | 0.243       |
|                | 200              | 1.482             | 688.24          | 0.477       | 1.239             | 830.09          | 0.496       |
|                | 400              | 2.191             | 577.90          | 4.513       | 2.461             | 694.84          | 4.523       |
|                | 800              | 2.964             | 261.30          | 6.398       | 3.055             | 307.56          | 7.747       |
| S1V2           | 27               | 1.512             | 655.10          | 0           | 1.558             | 813.20          | 0           |
|                | 100              | 1.660             | 649.45          | 0           | 1.583             | 817.91          | 0.254       |
|                | 200              | 1.625             | 652.35          | 0.714       | 1.642             | 821.06          | 0.525       |
|                | 400              | 2.050             | 558.50          | 3.941       | 1.807             | 691.47          | 4.500       |
|                | 800              | 2.677             | 246.77          | 6.573       | 2.802             | 321.70          | 6.863       |
| S1V3           | 27               | 1.494             | 650.78          | 0           | 1.673             | 802.52          | 0           |
|                | 100              | 1.312             | 658.09          | 0           | 1.702             | 810.69          | 0.241       |
|                | 200              | 1.620             | 650.15          | 0.246       | 1.626             | 809.12          | 0.512       |
|                | 400              | 2.163             | 544.12          | 4.276       | 2.268             | 684.32          | 4.077       |
|                | 800              | 2.774             | 238.29          | 6.566       | 2.977             | 315.10          | 6.835       |
| S2V1           | 27               | 1.768             | 645.13          | 0           | 1.555             | 774.95          | 0           |
|                | 100              | 1.524             | 643.01          | 0.239       | 1.704             | 783.28          | 0           |
|                | 200              | 1.613             | 652.90          | 0.450       | 1.684             | 771.58          | 0.521       |
|                | 400              | 2.161             | 558.26          | 4.282       | 2.197             | 672.93          | 4.847       |
|                | 800              | 2.902             | 252.98          | 6.651       | 2.357             | 313.06          | 6.699       |

**Table 3 (Contd.)**

| Specimen Label | Temperature ( <sup>0</sup> C) | Displacement (mm) | Axial Load (kN) | % Mass Loss | Displacement (mm) | Axial Load (kN) | % Mass Loss |
|----------------|-------------------------------|-------------------|-----------------|-------------|-------------------|-----------------|-------------|
| S2V2           | 27                            | 1.565             | 606.64          | 0           | 1.548             | 753.67          | 0           |
|                | 100                           | 1.521             | 612.14          | 0.254       | 1.533             | 759.24          | 0.254       |
|                | 200                           | 1.447             | 614.73          | 0.515       | 1.601             | 755.63          | 0.522       |
|                | 400                           | 2.617             | 528.18          | 4.293       | 2.354             | 660.98          | 4.381       |
|                | 800                           | 2.960             | 232.63          | 6.398       | 2.717             | 288.48          | 6.718       |
| S2V3           | 27                            | 1.735             | 610.49          | 0           | 1.676             | 756.42          | 0           |
|                | 100                           | 1.398             | 601.77          | 0.238       | 1.534             | 762.70          | 0           |
|                | 200                           | 1.723             | 610.10          | 0.487       | 1.753             | 763.96          | 0.249       |
|                | 400                           | 2.314             | 518.91          | 4.208       | 2.304             | 644.18          | 4.381       |
|                | 800                           | 2.901             | 239.86          | 6.147       | 2.914             | 287.77          | 6.806       |
| S3V1           | 27                            | 1.566             | 575.46          | 0           | 1.626             | 680.39          | 0           |
|                | 100                           | 1.519             | 561.01          | 0.232       | 1.667             | 692.25          | 0.243       |
|                | 200                           | 1.482             | 566.51          | 0.500       | 1.617             | 685.10          | 0.514       |
|                | 400                           | 2.261             | 471.08          | 4.167       | 2.292             | 578.37          | 4.556       |
|                | 800                           | 3.094             | 209.39          | 6.527       | 2.671             | 244.27          | 6.983       |
| S3V2           | 27                            | 1.381             | 524.10          | 0           | 1.726             | 665.15          | 0           |
|                | 100                           | 1.538             | 537.68          | 0           | 1.613             | 659.73          | 0           |
|                | 200                           | 1.453             | 527.63          | 0.253       | 1.644             | 657.69          | 0.748       |
|                | 400                           | 2.133             | 413.20          | 4.167       | 2.064             | 553.08          | 4.106       |
|                | 800                           | 2.193             | 200.90          | 6.599       | 2.940             | 243.00          | 6.959       |
| S3V3           | 27                            | 1.308             | 526.92          | 0           | 1.466             | 657.61          | 0           |
|                | 100                           | 1.366             | 530.77          | 0           | 1.498             | 653.06          | 0.258       |
|                | 200                           | 1.232             | 518.24          | 0.723       | 1.572             | 656.83          | 0.480       |
|                | 400                           | 1.809             | 450.90          | 4.239       | 2.506             | 551.90          | 4.639       |
|                | 800                           | 2.453             | 205.62          | 6.733       | 2.750             | 257.85          | 6.700       |

At 400<sup>0</sup> C, the compressive strength decreases to 75 to 80% for plain concrete. Whereas for concrete containing polypropylene fibers and confinement, the compressive strength reduces to approximately 90%. At 800<sup>0</sup> C, compressive strength reduces to approximately 20% for M60 grade plain concrete, but for M80 grade concrete the reduction is still more. Whereas for concrete containing polypropylene fibers and confinement the average compressive strength reduces to approximately 40% for both M60 and M80 grade of concrete.

## REFERENCES

1. Kodur, V.K.R., and Sultan, M.A., Effect of temperature on thermal properties of high-strength concrete, Journal of Materials in Civil Engineering, ASCE,2003, pp. 101-107.

2. Phan, L.T., Lawson, J.R. and Davis, F.L., Effects of elevated temperature exposure on heating characteristics, spalling, and residual properties of high performance concrete, *Materials and Structures/Materiaux et Constructions*, Vol. 34, March 2001, pp 83-91.
3. Wu, B., Su, X., Li, H. and Yuan, J., Effect of High temperature on Residual Mechanical Properties of Confined and Unconfined High-Strength Concrete, *ACI Materials Journal*, Vol. 99, No.4 2002, pp. 399-407.
4. Sharma, U., Bhargava, P. and Kaushik, S.K., Behavior of Confined High Strength Concrete Columns under Axial Compression, *International Journal of Advanced Concrete Technology*, Japan Concrete Institute, Vol. 3. No. 2, pp. 267-281, June, 2005.

## RECOVERY BEHAVIOR OF HYBRID FIBER REINFORCED HIGH STRENGTH CONCRETE AFTER FIRE EXPOSURE

Takashi Horiguchi <sup>a</sup>, Sofren Leo Suhaendi <sup>b</sup>

<sup>a</sup> Hokkaido University, Faculty of Engineering, Sapporo, Japan

<sup>b</sup> STO Singapore Transportation Office, Singapore

### INTRODUCTION

High-strength concrete shows particular characteristic behaviour at elevated temperatures, such as explosive spalling, that is rarely observed in normal-strength concrete. This behaviour has been attributed to the very dense concrete matrix usually associated with high-strength concrete [1-3]. Recently the addition of polypropylene fibres into high-strength concrete was reported to be very effective against the explosive spalling [4,5]. As heating increases, the fibres in the cement matrix start to melt at about 160 °C and increase the total pore area. This melting effect mitigates the explosive spalling as it provides pore space in which moisture vapour can accumulate at lower vapour pressures. However, it is hopeless to maintain the residual strength and the fracture toughness when the fibres melt. Steel fibre reinforcement can help to maintain the residual strength and fracture toughness after heated.

In this point of view, authors have proposed the hybrid fibre reinforcement systems with the combination of polypropylene and steel fibres for improving the residual strength as well as the residual fracture characteristics after heating [6,7]. This paper investigates the residual properties as well as recovery possibility of heated hybrid fibre reinforced high-strength concrete.

### 1 EXPERIMENTAL PROCEDURE

#### 1.1 Materials

The cement was a normal Portland cement, and river gravel (Sand stone) (5 - 20 mm of particle size) was used as the coarse aggregate and river sand was used as the fine aggregates. A maleic acid based super-plasticizer (SP), air entraining agent (AE), and bubble cutter agent (BC) were used. For bubble cutter agent, this chemical admixture was used only in the concrete mix containing fibres since this particular mix had the tendency to form more additional air bubble.

Steel and polypropylene fibres with the properties as shown in Table 1 were added into concrete mix in this study. The steel fibres came in bundles where each bundle consisted of 10 to 12 single steel fibres bound by special glue that would dissolve in water. As for polypropylene fibres, they came in fine fibrillated bundles that would disperse into monofilament fibres inside the concrete mix.

Table 1. Properties of polypropylene and steel fibres

| Fiber material | Length (mm) | Shape           | Denier | Effective diameter (mm) | Aspect ratio (l/d) | Specific gravity |
|----------------|-------------|-----------------|--------|-------------------------|--------------------|------------------|
| Polypropylene  | 6           | Fibrillated     | 20     | 0.06                    | 100                | 0.9              |
|                | 30          |                 |        |                         | 500                |                  |
| Steel          | 30          | Straight-hooked | -      | 0.6                     | 50                 | 7.8              |

## 1.2 Mix Design of Concrete

There were eleven series of concrete mix as shown in Table 2 to be tested in this experimental study. These are plain concrete, four series of polypropylene fibre reinforced concrete (PFRC), two series of steel fibre reinforced concrete (SFRC), and four series of hybrid fibre reinforced concrete (HFRC). In this mix proportions, all series had the same value of these factors: water to cement ratio (W/C) of 0.3, sand to aggregate ratio (s/a) of 60 %, and unit water content of 170 kg/m<sup>3</sup>. The main factor differentiated each series of concrete mix was the fibres. The valuable included fibre material (polypropylene fibre, steel fibre, and combination of the two fibres), fibre volume fraction (Vf), fibre length (lf), and Vf composition. The Vf composition in hybrid fibre reinforced concrete was selected intentionally so that correlation between single type fibre reinforced concrete and hybrid fibre reinforced concrete could be maintained.

Table 2. Mix design of plain and fibre reinforced high-strength concrete

| Series                                     | Code     | w/c | s/a (%) | Fiber volume (%) |       | SP <sup>1</sup> (% x c) | AE <sup>2</sup> (A) | BC <sup>3</sup> (T) |
|--|----------|-----|---------|------------------|-------|-------------------------|---------------------|---------------------|
|  |          |     |         | pp               | steel |                         |                     |                     |
| Plain                                      | Plain    | 0.3 | 60      | ~                | ~     | 1.3                     | 7                   | ~                   |
| PFRC 6 - 0.25                              | P6-0.25  |     |         | 0.25             | ~     | 1.3                     | 3                   | 1                   |
| PFRC 6 - 0.5                               | P6-0.5   |     |         | 0.5              | ~     | 1.3                     | 3                   | 1                   |
| PFRC 30 - 0.25                             | P30-0.25 |     |         | 0.25             | ~     | 1.7                     | 3                   | 2                   |
| PFRC 30 - 0.5                              | P30-0.5  |     |         | 0.5              | ~     | 1.9                     | 3                   | 2                   |
| SFRC 30 - 0.25                             | S30-0.25 |     |         | ~                | 0.25  | 1.3                     | 3                   | 1                   |
| SFRC 30 - 0.5                              | S30-0.5  |     |         | ~                | 0.5   | 1.3                     | 3                   | 1                   |
| P <sub>6</sub> -0.25 S <sub>30</sub> -0.25 | H1       |     |         | 0.25             | 0.25  | 1.35                    | 3                   | 2                   |
| P <sub>6</sub> -0.25 S <sub>30</sub> -0.5  | H2       |     |         | 0.25             | 0.5   | 1.3                     | 1                   | 4                   |
| P <sub>6</sub> -0.5 S <sub>30</sub> -0.25  | H3       |     |         | 0.5              | 0.25  | 1.4                     | 1                   | 4                   |
| P <sub>6</sub> -0.5 S <sub>30</sub> -0.5   | H4       |     |         | 0.5              | 0.5   | 1.5                     | 1                   | 4                   |

<sup>1</sup> Superplasticizer= Paric FP300U

<sup>2</sup> Air entraining agent= Flowric AE200, 1A= 0.004% x cement (by weight)

<sup>3</sup> Bubble cutter agent, 1T= 0.0002% x cement (by weight)

## 1.3 Experimental test procedures

For fresh concrete, the performed tests included slump and air content tests. Some features of the hardened concrete like density, voids, and ultrasonic pulse velocity (UPV test according to ASTM C 597-83) were also conducted. The main tests in this study consisted of compressive strength (ASTM C 39-86 and ASTM C 469-87a), splitting tensile strength (ASTM C 496-90), and permeability test (modified DIN 1048).

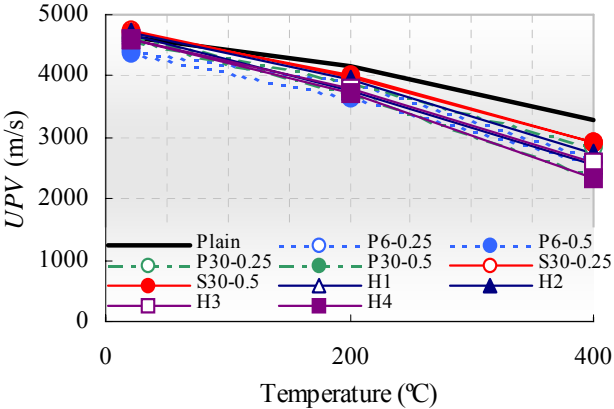
Specimens were heated using computer-controlled electric furnace. The heating rate was set at 10 °C per minute with peak temperature maintained at 200 °C and 400 °C for 2 hours.

## 2 TEST RESULTS AND DISCUSSION

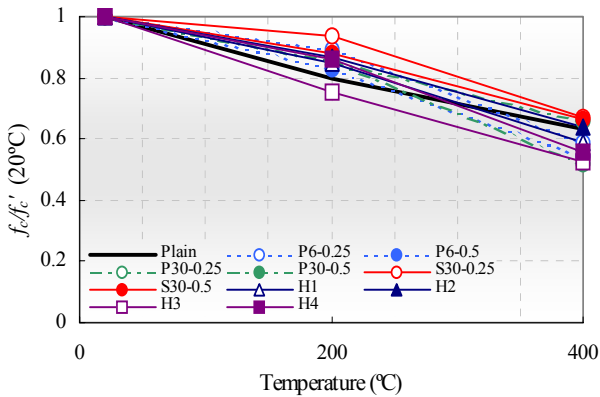
### 2.1 Residual properties of heated concrete

Fig.1(a) shows the heating effect on quality of concrete based on UPV test as it detect the presence of cracks, voids, and other imperfections inside the concrete.

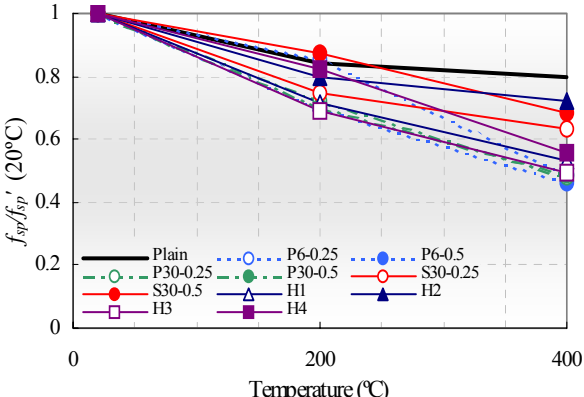
Fig. 1(b), and (c) show the heating effect on relative compressive strength and relative tensile strength of heated concrete, respectively. Similarly, heating effect on relative Young's modulus and relative permeability coefficient were shown in Fig. 1(d) and (e). Generally, concrete properties will tend to undergo further deterioration with the increase in maximum temperature. In mechanical point of view, modulus of elasticity decreases very significantly compared to compressive and splitting tensile strength. Average reduction of 30%, 20%, and 15% was observed in modulus of elasticity, splitting tensile strength, and compressive strength, respectively, for specimens heated up to 200°C. For specimens heated up to 400°C, average reduction in modulus of elasticity of 70% was observed while both compressive strength and splitting tensile strength showed an average reduction of 40%.



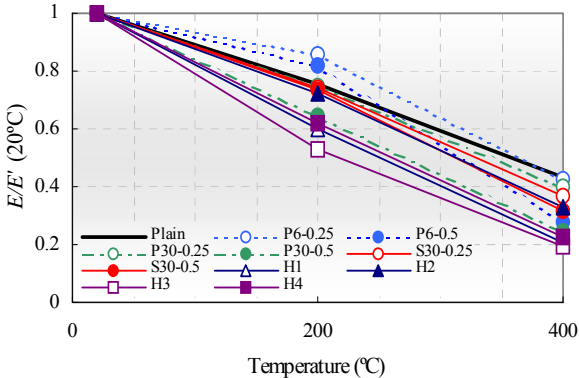
(a) Relative UPV value



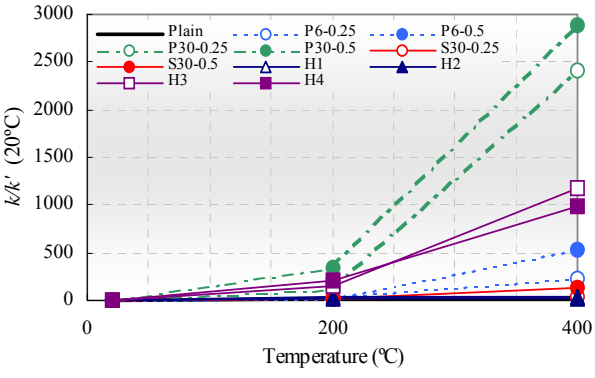
(b) Relative compressive strength



(c) Relative splitting tensile strength



(d) Relative Young's modulus



(e) Relative permeability

Fig. 1. Relative residual properties of plain and fibre reinforced concrete after heat exposure

As polypropylene fibers melted at its fusion point of 160-170°C, PFRC showed more reduction in its residual properties compared to SFRC. More inclusion of polypropylene fibers will tend to reduce most of PFRC and HFRC residual properties.

As shown in the Fig.1(c), more inclusion of steel fibers may improve the splitting tensile strength of SFRC and HFRC, especially at 400°C. Inclusion of 0.5% of steel fibers might lead to a better performance in modulus of elasticity compared to inclusion of 0.25% of steel fibers at both 200°C and 400°C, in both series also containing 0.25% and 0.5% of polypropylene fibers.

In residual permeability performance, more inclusion of polypropylene fibers will tend to reduce most of PFRC and HFRC residual permeability performance as shown in the Fig.1(e). More inclusion of steel fibers was found to be quite effective in the series also consisting 0.25% of polypropylene fibers in the HFRC, at both 200°C and 400°C. For PFRC, fiber length significantly affected the residual water permeability coefficient. The longer the fiber, the higher the residual water permeability coefficient

**2.2 Recovery properties of heated concrete**

Fig.2 to Fig.5 show the properties of heated concrete after being cured under ambient temperature (dry curing) and under water (saturated curing), respectively.

The compressive strength, tensile strength and Young’s modulus do not seem to recover clearly in the case of heated concrete specimens being cured under ambient temperature. Meanwhile, for heated concrete specimens that had been cured under saturated curing, the recovery in UPV, compressive strength, tensile strength and Young’s modulus can be observed as shown in Fig.2 to Fig.4. This might indicate that re-hydration of heated concrete had taken place for the heated specimens cured under saturated condition. The recovery rate under saturated curing showed a rapid increase in the first 2 months and slows down after that. As shown in the Fig.5, recovery in permeability performance was observed significantly in the case where heated concrete specimens were cured under saturated condition while no significant change in these properties on heated concrete specimens under ambient temperature.

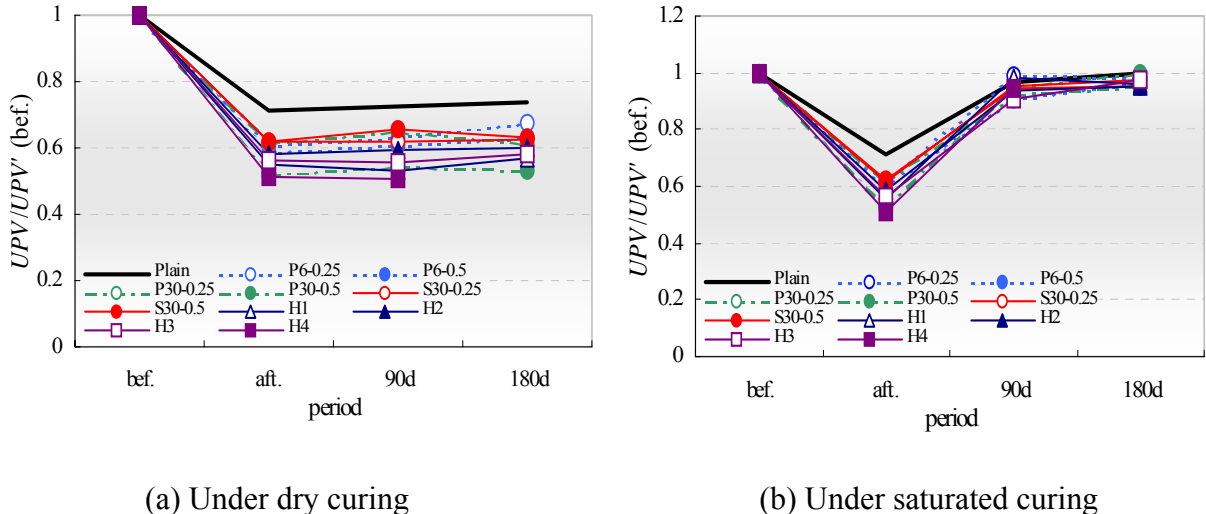
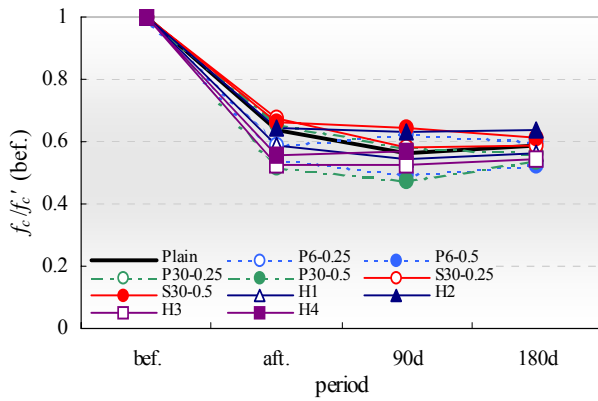
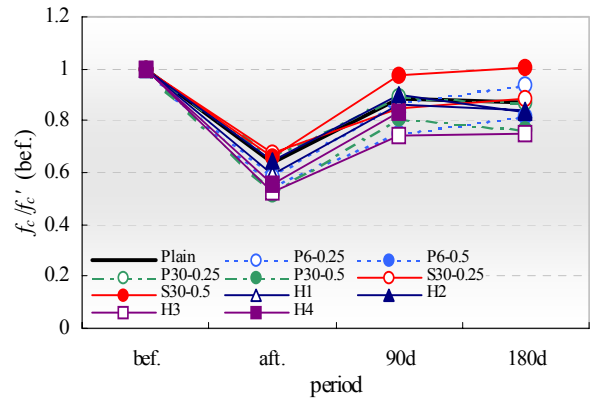


Fig. 2. Relative UPV value before and after heat exposure under dry curing

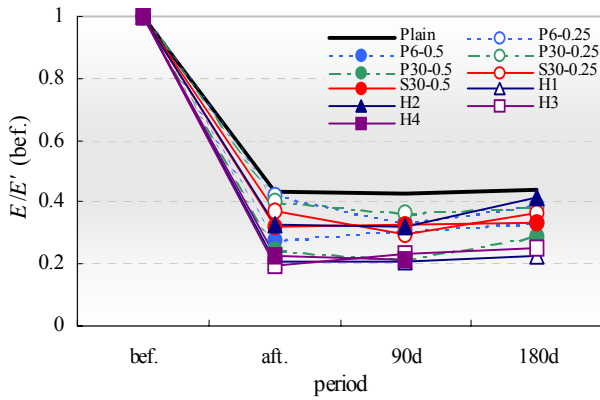


(b) Under saturated curing

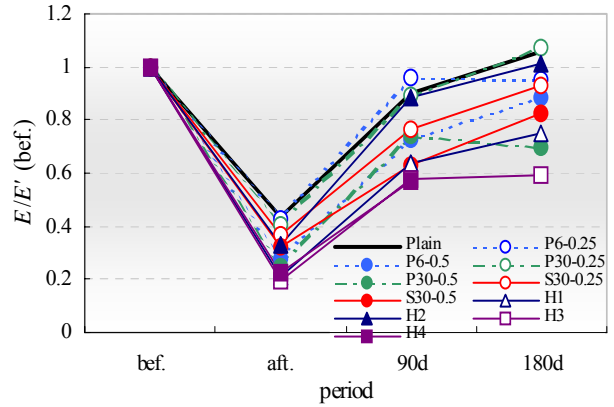


(a) Under dry curing

Fig. 3. Relative compressive strength before and after heat exposure

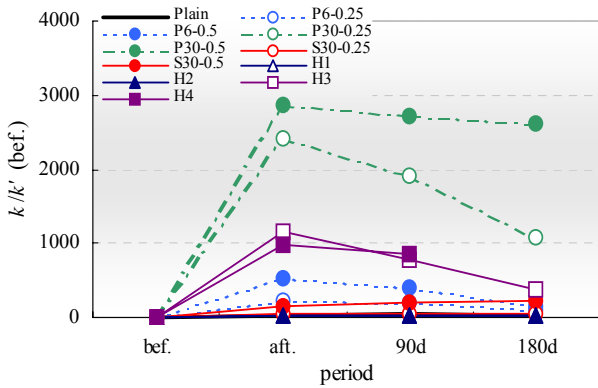


(a) Under dry curing

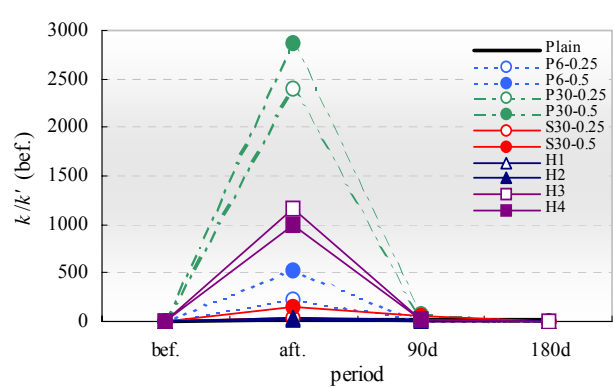


(b) Under saturated curing

Fig. 4. Relative Young's modulus before and after heat exposure



(a) Under dry curing



(b) Under saturated curing

Fig. 5. Relative permeability coefficient before and after heat exposure

### 3 SUMMARY

From the experimental test results, the following conclusions were made:

1. Average reduction of 30%, 20%, and 15% was observed in modulus of elasticity, splitting tensile strength, and compressive strength, respectively, for specimens heated up to 200°C. For specimens heated up to 400°C, average reduction in modulus of elasticity of 70% was observed while both compressive strength and splitting tensile strength showed an average reduction of 40%.
2. As polypropylene fibers melted at its fusion point of 160-170°C, polypropylene fiber reinforced concrete (PFRC) showed more reduction in its residual properties compared to steel fiber reinforced concrete (SFRC). More inclusion of polypropylene fibers will tend to reduce most of PFRC and HFRC residual properties, especially its residual permeability performance. On the other hand, more inclusion of steel fibers may improve the splitting tensile strength of SFRC and HFRC.
3. In residual permeability performance, more inclusion of steel fibers was found to be quite effective in the series also consisting 0.25% of polypropylene fibers in the HFRC, at both 200°C and 400°C. For PFRC, fiber length significantly affected the residual water permeability coefficient. The longer the fiber, the higher the residual water permeability coefficient
4. Properties recovery was observed significantly on heated concrete specimens cured under saturated condition compared to the ones cured under ambient temperature.
5. The recovery rate showed a rapid increase in the first two months on heated concrete being cured under saturated condition and slowed down after that

### REFERENCES

- [1] Ali, F.A., Connolly, R. and Sullivan, P.J.E., "Spalling of High Strength Concrete at Elevated Temperatures," *Journal of Applied Fire Science*, Vol.6, No.1, pp.3-14, 1996-97
- [2] Phan, L.T., "Fire Performance of High-Strength Concrete: A Report of the State-of-the-Art," NISTIR 5934, NIST 1996
- [3] Khoury, G.A. and Algar, S., "Mechanical behavior of HPC and UHPC concrete at high temperatures in compression and tension," *ACI International conference on State-of-the-Art in High Performance Concrete*, Chicago, 1999
- [4] Takano, T., Shimura, K., Horiguchi, T. and Saeki, N., "Fire Resistance of High-strength Mortars with Several Types of Fibers and Polymers," *3rd Joint Symposium on the Structural Materials between Korea & Japan*, pp.65-72, 2000
- [5] Horiguchi, T., Takano, T., N. Saeki, T. D. Lin, "Effect of Fiber Reinforcement on Residual properties of high strength concrete under elevated temperature," *American Concrete Institute, ACI SP-209*, 53-64, 2002
- [6] Suhaendi, S. L. and Horiguchi, T.: Effect of short fibres on residual permeability and mechanical properties of hybrid fibre reinforced high strength concrete after heat exposition, *Cement and Concrete Research*, Vol.36, Issue 9, pp.1672-1678, 2006.
- [7] Horiguchi, T., Watanabe, K. and Suhaendi, S. L. : Study on fracture toughness of hybrid fiber reinforced high strength concrete at high temperature environment, *Proceedings of 11th International Conference on Durability of Building Materials and Components*, 11dbmc, pp.117-124, 2008

Proceedings of International Conference  
Applications of Structural Fire Engineering  
Prague, 19-20 February 2009

**Session 5**

**Steel Structures**

## INVESTIGATION INTO METHODS FOR PREDICTING CONNECTION TEMPERATURES

Kate Anderson<sup>a</sup>, Martin Gillie<sup>a</sup>

<sup>a</sup> University of Edinburgh, School of Engineering and Electronics, Edinburgh, United Kingdom

### INTRODUCTION

Structural fire design is, to a large extent, based on single member tests. Due to the nature of these tests, the behaviour of the connections is neglected suggesting that they do not play a critical role in fire. In support of this theory, connections generally have a lower temperature than the surrounding structure during fires and are usually protected. This assumption of cooler connections is valid but this does not justify ignoring them in fire design. During both heating and cooling, connections will be subject to conditions, for example large moments and shear forces, which they will not typically have been designed for [1]. The response of connections to these conditions is complex and is largely based on the material strength degradation and the interactions between the various components of the connection. To predict how the behaviour of connections affects global performance in fire, temperature profiles must initially be established in order to evaluate the material strength degradation over time.

This paper examines two current methods available for predicting connection temperatures as defined in Eurocode 3 [2]. The first of these methods suggests that connection temperatures can be defined as a percentage of the adjacent beam temperature and a second is based on the lumped mass of material at the connection. A 3D finite element model is also created to predict connection temperatures using the commercial software package Abaqus[3]. Abaqus uses heat transfer theory to predict connection temperatures over time. These methods are all compared to experimental data and the validity and accuracy of each is evaluated and its limitations explored.

### 1 THEORY

#### 1.1 Eurocode Percentages Method

Eurocode 3 details two methods for predicting connection temperatures. The first assumes that connection temperatures follow the same general trend as local beam temperatures but are a percentage lower. This method simplifies connections into 2 categories based on whether the connecting beam is less than or equal to 400mm deep or greater than that. In the first case, where the top of the connection is adjacent to the concrete slab, connection temperatures are approximated at 88% of the beam lower flange mid-span temperature at the bottom of the connection, 75% at mid-height and 62% at the top. Between these points the temperature is assumed to vary linearly. Where the connecting beam is more than 400mm deep, temperatures are calculated as 88% of the beam temperature at the bottom and mid-height of the connection, tapering to 70% at the top.

Connections are cooler at the top for two main reasons. The largest contributor to heating is radiation from hot surfaces such as compartment or furnace walls. Where there is no direct line of sight between these walls and the member, in this case the connection, the radiative heating will decrease. This phenomenon is known as shadowing and causes the top of the

connection to be cooler than the rest. The provision of a heat sink in the form of a concrete slab will also reduce connection temperatures.

## 1.2 Lumped Capacitance

Connection temperatures can also be predicted using the ratio of material volume to exposed surface area. An average connection temperature or the that of a specific connection component, such as a bolt or end plate, can be calculated, assuming the gas temperature-time curve is known.

The lumped capacitance method [4] calculates the uniform temperature rise in an unprotected steel member using a series of finite time steps  $\Delta t$  as given in Eq (1).

$$\Delta T_s = \frac{h}{C_s (W/D)} (T_f - T_s) \Delta t \quad (1)$$

where  $h$  heat transfer co-efficient,  
 $T_f$  gas temperature,  
 $T_s$  steel temperature,  
 $C_s$  steel specific heat,  
 $D$  heated perimeter  
 $W$  steel volume per meter length

When applied to connections, this method must take into consideration the large volume of steel at the connection therefore the equation has been modified to use the ratio of volume of steel,  $V$ , to heated surface area,  $A$ , as shown in Eq (2).

$$\Delta T_s = \frac{h}{C_s (V/A)} (T_f - T_s) \Delta t \quad (2)$$

This method does not account for the concrete slab above the connection and as the effect of the slab on connection temperatures has not been well researched, the validity of applying this method to connections is uncertain.

## 1.3 Finite Element Modelling

An alternative means of predicting structural temperatures is to carry out a finite-element heat transfer analysis. Detailed temperature profiles can be created and this information can be used as direct input for a structural model. In principle, this method is highly accurate, however obtaining correct values for the all input parameters is very challenging. The modelling process is outlined below.

For the purpose of this paper, the gas temperature-time curve to which a connection is exposed is assumed to be known, therefore the modelling will be limited to the convective and radiative heat transfer between the gas and solid, and to the conduction between the connection components. Perfect conduction is assumed between the various connection components such as bolts and bolt holes and through the welds.

Convective heat transfer is heating by movement of the hot gases where the heat flux due to convection,  $q_c''$  and is given by:

$$q_c'' = h (T_f - T_{su}) \quad (3)$$

where  $T_{su}$  is the surface temperature.

The heat transfer coefficient varies with temperature and depends on the hot gas velocity. Its value for structural steel is given in Eurocode 3 as  $25\text{W/m}^2\cdot\text{K}$  [2]. At the connections, the convective heating will be less due to lower gas velocities in these areas, however, no practical methods exist for accurately calculating heat transfer coefficient at connections. This

paper has therefore used the Eurocode recommended value. This assumption was verified with a sensitivity study.

Radiative heat transfer is heating directly between one item and another or between the fire source and a structural element or between one structural element and other. Emissivity is used to describe the radiative power of an object and can be defined as the ratio of the radiative power of the object to the radiative power of a black body where a black body is a perfect emitter and emissivity can never be greater than 1.

Emissivity varies with temperature and in large building fires is usually the dominant mode of heating. There are a huge number of factors which affect radiative heating, for example the make up of the air in the room: if the air contains soot particles the radiation between objects will be lower than in clear air or if an element becomes charred or sooty its emissive power will reduce, i.e. less heat will be absorbed by the element. Due to the many variables affecting emissivity, predicting radiative heating is extremely difficult: for one structural member, there will be variations not only with temperature but also with factors such as location in the building, fuel type and ventilation conditions.

The heat flux due to radiative heating, or total emissive power of an object is given in *Eq (4)*.

$$q_e'' = \varepsilon \sigma T_{su}^4 \quad (4)$$

where  $\varepsilon$       emissivity and  
 $\sigma$       Stefan Boltzmann constant

The emissivity at a connection will be lower than that of the local beams and columns due to the shadow effect, as discussed in section 1.1. Eurocode 3 suggests that for ‘shadowed’ areas a reduction factor for unprotected steel temperatures can be defined as shown in *Eq (5)*.

$$k_{sh} = [A_m/V]_b/[A_m/V] \quad (5)$$

where  $[A_m/V]_b$       box section factor  
 $[A_m/V]$       section factor  
 $A_m$       surface area of the member per unit length

This method is suggested for beams but has not yet been validated for connections. Further research is required to validate this assumption.

## 2 RESULTS

Two sets of experimental data have been used to investigate the accuracy of these methods for predicting connection temperatures. These are briefly summarised here.

- Manchester University furnace tests carried out in 2008 [5-6] consisting of 4 beams spanning from one column with a concrete slab on top. The steel members were all unprotected. This whole assembly was tested in a furnace where the gas temperatures followed a 60 minute standard fire. Connection temperatures were recorded at several locations. Cooling was not considered. 4 connection types were used: flush and flexible end plate, fin plate and web cleats. The flush end plate and fin plate have been used for validation in this paper.
- Cardington full scale tests from January 2003 [7]. This was a compartment fire test on the 4<sup>th</sup> storey of an 8 storey building where one of the main objectives was to monitor the connection behaviour including temperature evolution during the heating and cooling phases. The interior beam to column connections were flexible end plates. The columns were protected to the underside of the beams whilst the connection remained unprotected.

**2.1 Eurocode Percentages Method**

The Eurocode percentages method was used to predict the temperatures of two connections, a flush end plate from the Manchester University tests and a flexible end plate from the Cardington tests. The results of these are shown in Figs 1 and 2.

Figure 1 shows the predicted temperatures at 3 locations on the connection, bottom, mid-height and top, in comparison to the recorded temperatures at the same locations. For the first 15 minutes the predicted temperatures are of reasonable accuracy but after this point predicted temperatures are much higher than experimental ones. After 50 minutes the predicted temperature of the bottom of the connection is 900°C whereas the measured temperature was 250°C lower at 650°C; there is a similar error margin for the mid-height temperature. The peak temperature of the connection is estimated to be at around 50 minutes, coinciding with the peak beam temperature. Connections, however, can continue to heat after the surrounding structure has started cooling and experimental results show that this connection does not start cooling until 15 minutes later. During the cooling stage the connection temperatures are under-predicted by between 150°C and 250°C for the 60 minute cooling period at all locations.

The results for the flush end plate, Fig. 2, shows that the temperatures at three locations on the connection are initially over conservative by up to 200°C but are equally under conservative after about 25 minutes until the conclusion of the test. The trend of connection temperatures relative to one another is also not shown: The experimental test shows connection temperatures varying by around 75°C from top to bottom whereas the Eurocode method shows a variation of close to 200°C.

This method provides a very simple means of estimating connection temperatures where the only information required is the beam mid-span temperature and depth. However, results show it to be unreliable in both heating and, to a larger extent, in cooling. The implication of this is that using this method is inappropriate except for very crude calculations.

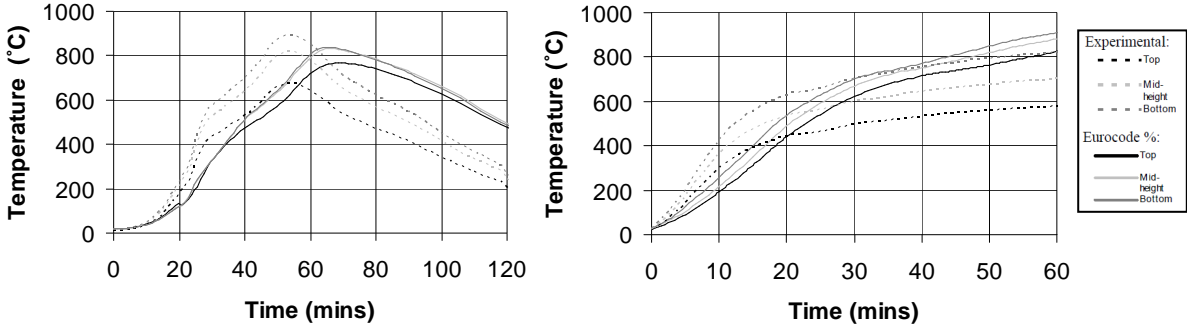


Fig. 1. EC % Method: Flexible End Plate

Fig. 2. EC % Method: Flush End Plate

**2.2 Lumped Capacitance**

The lumped capacitance method has been used to predict the average temperature of a fin-plate connection from the Manchester University tests and of the flexible end plate used in the Cardington tests. The results are shown in Fig. 3 and compared to the recorded average connection temperature.

For fin-plate, the average temperature is predicted well. However it is noteworthy that this experiment was carried out in a highly controlled environment. The same lumped capacitance method is then used to calculate the average temperature for the flexible end plate. The temperatures predicted are consistently higher than the experimental results by between 30°C

and 90°C and are therefore conservative however there is a good correlation between the predicted and experimental trend.

More input data is required for this method than for the percentages method: connection geometry and gas temperature-time curve. Despite calculations being basic, results show that good average temperatures are predicted. There are, however, many factors that could affect the results such how much of the beam or column is considered to be part of the connection and what effect the concrete slab has on the heating rate. As the effect of the slab on connection temperatures has not been well researched, this assumption may be invalid. Also, temperature gradients are present over connections and mechanical response may vary notably between a connection with one average temperature to that with a temperature profile therefore an average temperature may not be adequate for detailed calculation purposes.

### 2.3 Finite Element Modelling

A model of the flexible end plate created in Abaqus for the 200 minute fire which includes a 140 minute cooling phase. In creating the finite element model there were three main areas for consideration: radiative heating, convective heating and the inclusion of a concrete slab.

A sensitivity study was carried out to look at these three parameters and examine their effect on results. It was found that varying the heat transfer coefficient, and therefore the level of convective heating, at the connection had a negligible affect on results. When the concrete slab was included in the model the temperatures of the upper flanges of the beams were affected but other temperature predictions remained unchanged. Based on these results the concrete slab was excluded from further modelling.

The value of emissivity affected results and therefore the area near to the connection was assigned a lower emissivity that the rest of the structure. This is based on the shadow effect in this location as discussed in section 1.1.

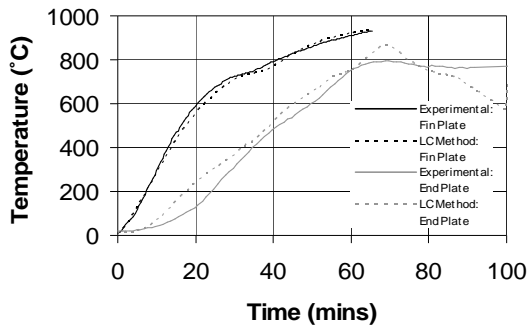


Fig. 3. Lumped Capacitance Method for Fin Plate and Flexible End Plate

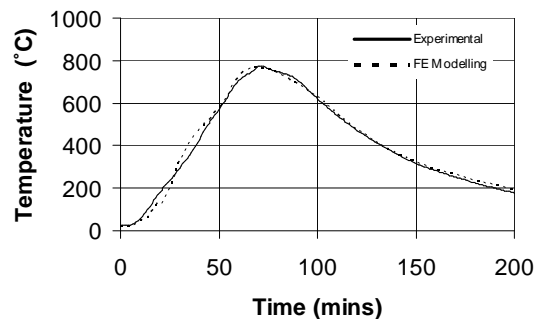


Fig. 4. Finite Element for Flexible End Plate: Top of Connection

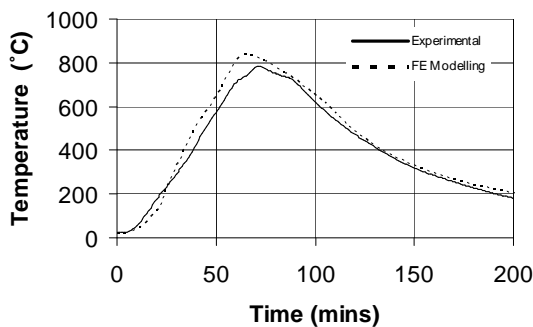


Fig. 5. Finite Element for Flexible End Plate: Bottom of Connection

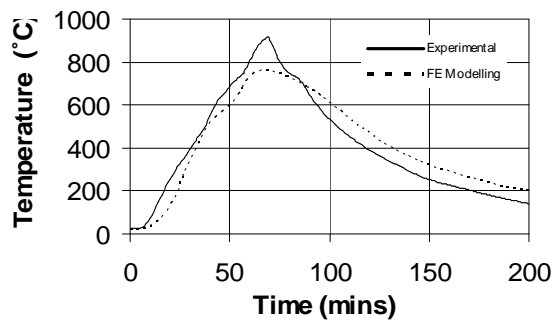


Fig. 6. Finite Element for Flexible End Plate: Top Flange of Beam

The known gas temperature over time was input to the model and heating assumed on all faces apart from the upper flanges of the beams and top of the column where there was contact with the concrete slab.

Results from the finite element modelling are shown in Figs. 4 and 5 and all show close correlation with experimental data. Figure 6 shows that the biggest difference between predicted and experimental temperatures is on the underside of the beam upper flange. This is due to the concrete being excluded from the analysis.

For detailed calculations where the exact connection geometry is known, this method provides accurate results. It can be used for all connection types where a detailed knowledge of its response in fire is required. This method, however, is time consuming both in model creation and simulation run time therefore it could not be a day to day modelling approach.

### **3. CONCLUSIONS**

This paper has investigated three methods for predicting connection temperatures. The Eurocode suggests connection temperatures can be calculated as percentages of the mid-span beam flange temperature. However, results show this method to be unreliable and should therefore be used with caution.

The lumped capacitance method, based on the heated surface area of the connection and its volume, showed good correlation with average connection temperatures. More work should be done to look at predicting temperatures of individual connection elements and to define what volume of the connection beams and columns should be included in calculations.

The Abaqus modelling also showed good correlation with experimental results. This method can therefore be recommended if a detailed temperature profile is needed for mechanical analysis. During the modelling it was found that the inclusion of the concrete slab did not affect the predicted temperatures of the connection therefore it in need not be included allowing for much quicker computational times.

A detailed yet simple method for predicting connection temperatures is still unavailable and therefore more work is required in this field.

### **4. ACKNOWLEDGEMENT**

The authors wish to thank Arup Fire and EPSRC for funding this research. They also thank Dr. Y. Wang and Dr. X. Dai of the University of Manchester for allowing access to experimental results in advance of publication.

### **REFERENCES**

- [1] Bailey, CG, Lennon, T and Moore, DB, "The behaviour of full-scale steel framed buildings subjected to compartment fires", *The Structural Engineer*, pp. 15-21, April 1999
- [2] CEN, EC 3: Design of Steel Structures part 1.2: General rules - Structural Fire Design, BS EN 1993-1-2:2005, Brussels: CEN, European Committee for Standardisation, 2006b
- [3] ABAQUS User's Manual, version 6.6, Providence, RI, USA
- [4] Incropera, FP, DeWitt, DP, Bergman, TL and Lavine, AS, 'Fundamentals of Heat and Mass Transfer' John Wiley & Sons, Hoboken, USA, Sixth Edition , 2005
- [5] Dai, XH, Wang, YC & Bailey, CG, 'Temperature distributions in unprotected steel connections in fire' *Proc. Steel & Composite Structures*, Manchester, UK , pp. 535-540, 2007
- [6] Dai, XH, Wang YC & Bailey CG, 'Effects of partial fire protection on temperatures developments in steel joints protected by intumescent coating' *Fire Safety J.*, pp. 16-32, Jan. 2009
- [7] Lennon, T. and Moore, DB, 'Results and observations from full-scale fire test at BRE Cardington, 16 January 2003' BRE, Watford, UK, 2004

## **STRUCTURAL FIRE ENGINEERING ASSESSMENTS OF THE FRACOF AND MOKRSKO FIRE TESTS An Engineering Prediction**

Anthony K. Abu<sup>a</sup>, Florian M. Block<sup>a</sup>, Neal A. Butterworth<sup>a</sup> and Ian W. Burgess<sup>b</sup>

<sup>a</sup> Buro Happold Ltd., FEDRA, Leeds, United Kingdom

<sup>b</sup> University of Sheffield, Department of Civil and Structural Engineering, Sheffield, United Kingdom

### **INTRODUCTION**

The fire engineering of steel and composite frame buildings has become more and more standard practice in the UK in recent years. Simplified design methods allow structural engineers to omit fire protection from large numbers of composite beams. However, there are always buildings which fall outside the relatively tight boundaries of the simplified methods, and more advanced analysis approaches, normally implying the use of general or specialist finite element programs, are used. Although, these programs have been extensively validated during their development against available test data, the way in which a model is created and its results interpreted is extremely important. This was seen during the “Round Robin” CFD modelling of the Dalmarnock fire test [1]. Acknowledging that modelling of the dynamics of a fire is inherently less deterministic than that of the structural response of a building in fire, a similar lesson should be learned, as the effects of possible “modelling” mistakes could lead to catastrophic consequences.

As mentioned above, the FEM programs used to predict the structural response to fire have been validated against available test data. However, the bulk of the available test data comes from a series of just seven fire tests on a single building constructed in an old airship hanger in Bedfordshire, UK. The Cardington test building was designed as a typical composite frame building of the early 1990s, using standard UK building practice and details, which limits the available validation cases for the FEM programs to one particular type of construction. None of the tests led to the collapse of the building. The fact that the building techniques have developed further, and that finite element analyses of buildings in fire are conducted all over the world, means that programs are likely to be used outside the boundaries of the validations conducted. It is therefore even more important that parametric studies are carried out and that special care is given to the “modelling” assumptions and interpretation during the design process in order to give robust answers.

The year 2008, provided the opportunity for more diverse validation cases, with two full scale fire tests on parts of composite steel frame buildings. The first was the FRACOF fire test in Metz, France, in which a single slab panel with two unprotected secondary beams was tested under exposure to a 120-minute ISO834 Standard Fire. The second was the Mokrsko fire test, south of Prague in the Czech Republic, which exposed a purpose-built single-storey building to a natural fire. Buro Happold Ltd and the University of Sheffield used these opportunities to predict the structural behaviour prior to the tests, using the specialist finite element program *Vulcan*. During the assessments a number of parameters were varied within the normal range expected on site. For the FRACOF test two models were analysed before the test, with a more detailed follow-up in its aftermath. For the Mokrsko test the majority of the analyses were initiated before the test. The analyses were treated no differently from those for normal structural fire engineering projects, and it was expected to see conservative results. The results of the FRACOF assessment will be shown first, followed by the Mokrsko predictions.

## 1 THE FRACOF FIRE TEST

The FRACOF test was designed to demonstrate the benefits of incorporating tensile membrane action into the design of steel-framed composite floor systems in the European Community, and to assist in preparation of design guidance for its implementation. The test was therefore to investigate the performance of slab panels, as documented in the SCI document P-288 [2], and the effects of different construction details on their fire resistance.

### 1.1 Test description

The test was set up as an 8.74m x 6.66m composite slab panel, representative of a corner compartment. It included four equally-spaced IPE 300 downstand secondary beams spanning in the longer direction, with IPE 400 primary beams. The floor arrangement was supported by HEB 260 steel columns, using simple connections. The slab was 155mm deep, on COFRAPLUS 60 decking, acting compositely with the steel beams. Beams and columns at the edge of the structure were wrapped in 50mm of Cerablanket protection (density = 128kg/m<sup>3</sup>; specific heat capacity = 1130J/kgK; thermal conductivity = 0.06 – 0.2W/mK). Continuity across the two adjacent “internal” edges was simulated by welding the anti-crack mesh (7mm diameter bars at 150mm centres, placed 50mm below the top of the slab) to the flanges of horizontally-aligned HEB 200 sections before the concrete slab was cast. A gravity load of 3.87kN/m<sup>2</sup> was placed on the slab to simulate live loading at the fire limit state. The base of the structural assembly was exposed to the Standard Fire for 120min. Details of the test setup and results can be found in Reference [3].

### 1.2 Test predictions

Five finite element test predictions are reported here; the first two were made before the test, with the subsequent three conducted afterwards, to correct differences in assumptions between the test design brief and the models. An overall slab thickness of 160mm had been specified in the brief, with no specific data on concrete strength. The applied load was given as 3.75kN/m<sup>2</sup>, and it was assumed that the intended slab continuity would be achieved along the two adjacent “internal” edges. Based on the design brief and an assumed concrete cube strength of 40N/mm<sup>2</sup> the first predictions were made with protected beam and column temperatures following Eurocode 3: Part 1.2 [4] calculations, making a conservative assumption of Cerablanket thermal conductivity of 0.2W/mK. One-dimensional heat transfer was assumed for the concrete slab. The structural response predictions were made using *Vulcan* [5].

The first model considered the 8.74m x 6.66m slab as an isolated slab panel, supported vertically at its corners, with protected beams providing the necessary vertical support along the slab edges. The model used no axial restraints along its edges, but rotational restraints along two adjacent edges to simulate slab continuity across those boundaries. For conservatism, the 102mm thick continuous concrete layer above the decking troughs was modelled as a flat slab. The second *Vulcan* assessment used a full model of the test setup. It included the columns at the corners of the panel and the two horizontally-aligned HEB 200 sections along the “internal” adjacent edges for continuity. The orthotropic nature of the slab was accounted for by the using the *Vulcan* effective stiffness representation, developed by Huang *et al.* [6]. In this approach the full depth of the composite slab is modelled as a flat slab with different bending stiffnesses in the two orthogonal directions to account for the contribution of the ribs. The two models are shown in *Fig. 1*.

Test observations showed that the continuity condition was only practically achieved across the shorter edge. It was also observed that the protected beams and columns were not entirely within the furnace, and so did not attain appreciable temperatures or deformations.

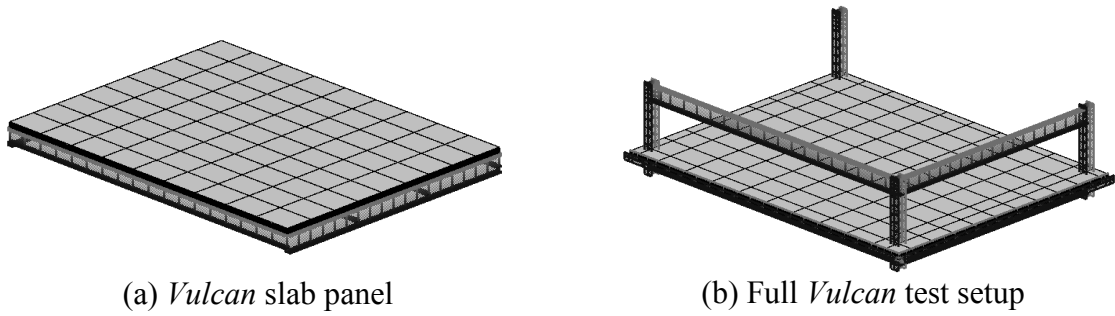


Fig.1. Vulcan models

This kept the slab panel boundaries supported vertically throughout the test. At 105mins however, fracture of a welded lap joint in the mesh caused an integrity failure of the central region of the slab. The *Vulcan* analyses are described in *Table 1*, and the central slab panel displacements predicted are plotted in *Figs. 2* and *3* together with the central vertical displacement from the test.

Table 1. Modified parameters in the *Vulcan* analyses

| Parameter                               | V1                       | V2                  | V3                  | V4                  | V5                 |
|---|--------------------------|---------------------|---------------------|---------------------|--------------------|
| Concrete strength [N/mm <sup>2</sup> ]  | 40                       | 40                  | 37                  | 37                  | 37                 |
| Overall Slab thickness [mm]             | 160                      | 160                 | 155                 | 155                 | 155                |
| Applied load [kN/m <sup>2</sup> ]       | 3.75                     | 3.75                | 3.87                | 3.87                | 3.87               |
| Thermal conductivity [W/mK]             | 0.2                      | 0.2                 | 0.06                | 0.06                | 0.06               |
| Protected beam temperature distribution | Uniform                  | Uniform             | Uniform             | Non-uniform         | Non-uniform        |
| Edge continuity condition               | 2 edges                  | 2 edges             | 1 edge              | 1 edge              | 1 edge             |
| Slab modelling approach                 | Thin continuous concrete | Effective stiffness | Effective stiffness | Effective stiffness | Average slab depth |

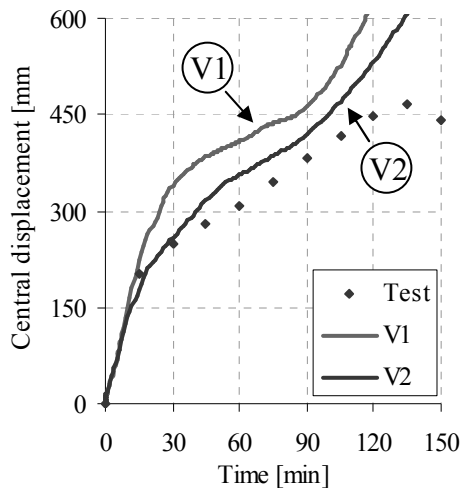


Fig. 2. Vulcan pre-test predictions

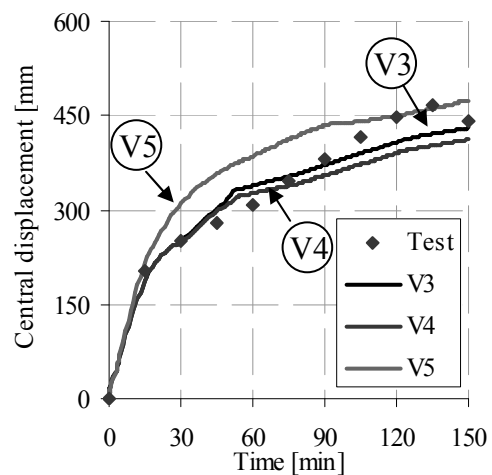


Fig. 3. Vulcan post-test predictions

It is observed that the initial predictions (*Fig. 2*) conservatively estimated the test deflection, although exact structural detail was not available. The subsequent analyses however showed better predictions (*Fig. 3*) using more realistic protected beam temperatures, non-uniform temperature distributions and the average slab depth approach. It is noticeable that the software's estimate of deflection worsened as the integrity failure point was approached.

## 2 THE MOKRSKO FIRE TEST

This fire test was conducted on the 18 September 2008 at Mokrsko, Czech Republic, by the Department of Steel and Timber Structures of the Czech Technical University of Prague.

The structure represented one floor of a steel and concrete composite office building consisting of four bays with a size of 9m x 6m each, and tested three different floor systems, namely “Angelina” composite beams developed by Arcelor-Mittal with elongated web openings, beams with corrugated webs made from thin steel plate, and precast hollow-core panels. The steel beams supported a composite slab with a total thickness of 120mm supported on CF46 metal decking. The slab was reinforced with a smooth mesh, providing a steel area of  $196\text{mm}^2/\text{m}$  in each direction, situated 20mm from the top of the slab as well as 12mm bars in each rib. The connections of the Angelina beams were by specially designed endplates which only connected the top flange and a small part of the web of each beam. The bases of the columns were constructed as pinned. The imposed load of  $3.0\text{kN}/\text{m}^2$  on the slab was generated by sand bags, and the self-weight of the floor system was  $2.6\text{kN}/\text{m}^2$ . Timber cribs generated a total fire load of about  $620\text{MJ}/\text{m}^2$ , and two  $2.5\text{m} \times 4\text{m}$  openings at the front provided ventilation to the fire. Steelwork fire protection was omitted from all Angelina beams, as well as the beams with corrugated webs. The rest of the steelwork was fire-protected using fire-board. This protection arrangement generated a  $9\text{m} \times 12\text{m}$  bay of unprotected Angelina beams, and a  $9\text{m} \times 6\text{m}$  bay of beams with corrugated webs, surrounded by protected beams. However, it left one edge column restrained in only one direction by fire-protected beams.

The fire burned a little cooler than expected, but after about 61 minutes three quarters of the structure collapsed; this is the only large-scale structural fire experiment which has generated a structural collapse. The corrugated web beams developed shear buckles near their ends, but their overall vertical deflections were relatively small; this can be explained by their greater depths and flange thicknesses compared with the Angelina beams. The Angelina beams showed severe Vierendeel bending across their first two openings, and after about 50 minutes the bottom flanges of some of the Angelina beams deformed laterally, folding the beams along their longitudinal axes. More details are given by Wald and Kallerová [7].

### 3.2 *Vulcan* modelling of the Mokrsko fire test

Before the test, the experiment was modelled using *Vulcan*, using only the fairly limited data available at the time. For simplification only the 3 bays with the composite slab were modelled, and the Angelina beams and the corrugated-web beams were represented using an effective web thickness approach which calculates a reduced web thickness based on the net cross section. This approach usually gives good overall results for beams with web openings but cannot adequately represent local effects around the openings.

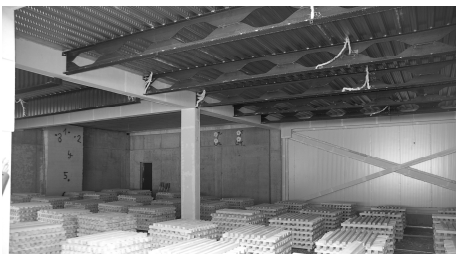


Fig. 4. Fire test set-up

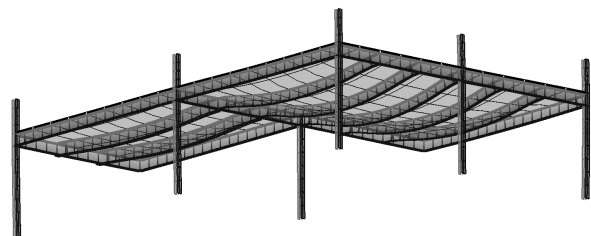


Fig. 5. Deformed *Vulcan* model

As with a normal structural fire engineering project a number of parameters were varied in order to test the robustness of the solution. Firstly, the fire was altered to produce a short-hot fire and a cooler-longer fire. The position of the reinforcement in the slab was then varied by

$\pm 15\text{mm}$  to account for normal construction tolerances. The beam connections were modelled as rigid, which tends to be acceptable for normal composite connections designed to UK design rules in braced frames. Because of space restrictions here, only the results for the different fire curves are shown below.

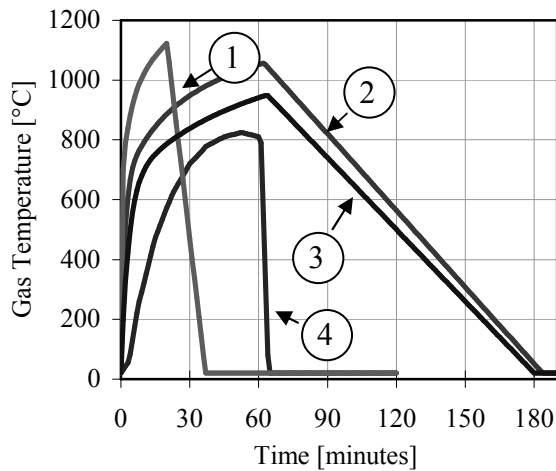


Fig. 6. Fire curves

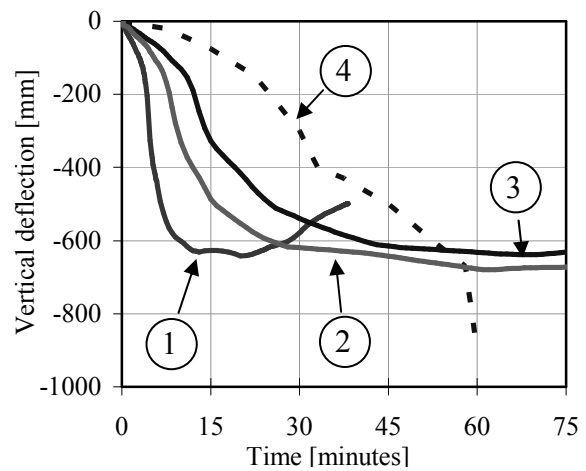


Fig. 7. Vulcan deflection prediction

It can be seen from Fig. 6 that the real fire (4) in the experiment burned significantly cooler than the predicted fire (2). Fig. 7 shows the resulting vertical deflections from the test and the three different design fires at the middle of the large bay of Angelina beams (V3).

The predictions show a much earlier increase in deflections than the experimental results. This is because the parametric fire curves represent post-flashover fires, and should therefore be moved by about 15 minutes to give a realistic representation of the fire. This greatly improves the estimation of the fire test deflections. The models continued beyond the failure point of the test at about 61 minutes, and do not show any indication of collapse, however the vertical deflections of the slab are in excess of span/15, which would normally result in an increase of reinforcement to limit the vertical deflections. Furthermore, all beams framing into columns would be protected in a robust design for fire.

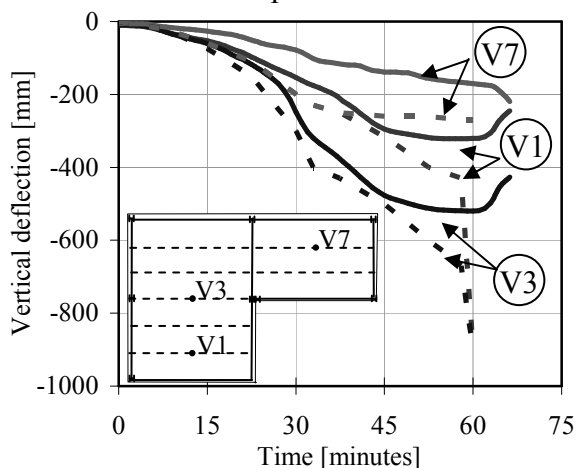


Fig. 8. Prediction using the average test temp.

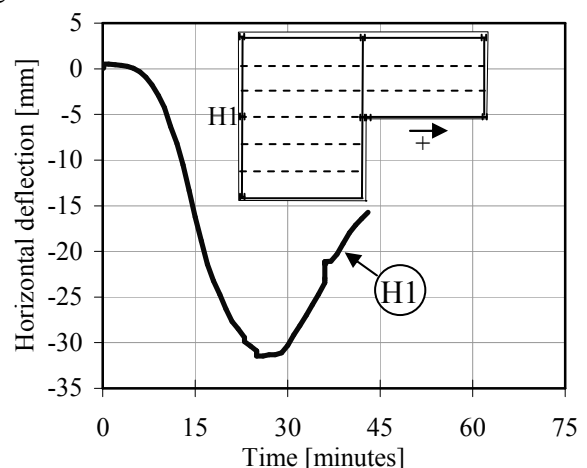


Fig. 9. Deflection of column head

After the test results were released, the actual temperature data was used as more accurate input data to the *Vulcan* model. Fig. 8 shows that when the real temperature data is used the vertical deflections are represented relatively accurately up to about 44 minutes. The small vertical differences are due to the edge beam deflections, which are lower than those seen in the test, as well as to the use of average compartment gas temperatures to heat all elements.

The difference between prediction and reality for the beams with corrugated webs (V7) can be explained by the observed shear buckling of the thin webs, which cannot be represented by the chosen way of modelling the beams.

Due to the very flexible beam connections, another set of analyses were conducted in which the connections were modelled as pinned. In these cases the *Vulcan* models predict failure at around 43 minutes using the experimental fire temperature data. From *Fig. 8* it can be seen that this is the point at which the *Vulcan* and test results diverge. *Fig. 9* shows the horizontal displacement at the top of the edge column connected to an unprotected Angelina beam. It can be seen that, after an initial outwards movement due to thermal expansion of the structure, the column moves inwards due to pull-in by the vertically-deflecting Angelina beams. This observation may prompt speculation about a possible cause of the test failure, but due to the lack of test data and further in-depth analyses at this time, this is not investigated further here.

#### 4 CONCLUSION

In this paper, it is again confirmed that it is possible to make conservative overall predictions of the response of composite structures to fire using sophisticated finite element programs and that modelling can be accurate with accurate data. However, in both test cases it was not possible to predict the exact failure mode or time prior to the tests. With the accurate data given by the tests a fairly accurate representation of the structural behaviour can be made, and this implies that conservative assumptions will produce conservative predictions.

The integrity failure in the FRACOF test was undoubtedly related to the lap-welding of the mesh, but it will be necessary in future to develop programmable criteria for this local slab fracture. The unexpected collapse in the Mokrsko test is at present unexplained, but probably relates to construction details (pinned column bases, connections with limited tying capacity, columns connected to unprotected beams, poor connection between slabs and edge beams) which lack robustness. It is essential that robust construction details are developed and specified if fire protection is to be omitted from structural elements. If finite element analyses are used to justify the behaviour of non-standard forms of construction, which are most likely to lie outside the bounds of software validation, great care should be taken when modelling these problems, using detailed parametric studies and possibly even physical fire testing.

#### REFERENCES

- [1] G Rein, JL Torero, W Jahn, J Stern-Gottfried, NL Ryder, S Desanghere, M Lázaro, F Mowrer, A Coles, D Joyeux, D Alvear, JA Capote, A Jowsey, C Abecassis-Empis, P Reszka, *Round-Robin Study of a priori Modelling Predictions of The Dalmarnock Fire Test One*, Fire Safety Journal (in press), 2009.
- [2] Newman, G. M., Robinson, J. T. and Bailey, C. G., *Fire Safe Design: A New Approach to Multi-Storey Steel-Framed Buildings*, Second Edition, SCI Publication P288, The Steel Construction Institute, UK, 2006
- [3] Zhao, B., Roosefid, M. and Vassart, O., *Full scale test of a steel and concrete composite floor exposed to ISO fire*, Proceedings of the 5<sup>th</sup> Structures in Fire Workshop SiF'08, Singapore City, Singapore, 2008, 539-550.
- [4] European Committee for Standardization, *Eurocode 3: Design of Steel Structures – Part 1.2: General Rules – Structural Fire Design*.
- [5] Vulcan Solutions Limited: <http://www.vulcan-solutions.com>
- [6] Huang, Z., Burgess, I.W. and Plank, R.J., *Effective Stiffness Modelling of Composite Concrete Slabs in Fire*, Engineering Structures 22 (9), 2000, 1133-1144
- [7] Wald, F. and Kallerová, P., *Description of Fire Test on Experimental Structure in Mokrsko*, [http://fire.fsv.cvut.cz/firetest\\_Mokrsko/pdf/Test\\_report.pdf](http://fire.fsv.cvut.cz/firetest_Mokrsko/pdf/Test_report.pdf)

## A NEW DESIGN METHOD FOR INDUSTRIAL PORTAL FRAMES IN FIRE

Yuanyuan Song <sup>a</sup>, Zhaohui Huang <sup>b</sup>, Ian Burgess <sup>c</sup>, Roger Plank <sup>d</sup>

<sup>a</sup> Safe Consulting Limited, Manchester, UK

<sup>b,c</sup> Department of Civil and Structural Engineering, University of Sheffield, UK

<sup>d</sup> School of Architectural Studies, University of Sheffield, UK

### INTRODUCTION

For single-storey steel portal frames in fire, especially when situated close to a site perimeter, it is imperative that the boundary walls stay close to vertical, so that fires which occur are not allowed to spread to adjacent properties. A current UK fire design guide [1] requires either that the whole frame be protected as a single element, or that the rafter can be left unprotected but the column bases and foundations should be designed to resist the forces and moments necessary to prevent collapse of rafter, in order to ensure the lateral stability of the boundary walls. Some arbitrary assumptions regarding the behaviour of the frame in fire, which are used to simplify this current design model, can lead to very uneconomical foundation design and base-plate detailing. Further understanding of the behaviour of portal frames in fire is required, to provide other design options so that over-design of column bases and foundations can be avoided, and a more reasonable prediction of real critical temperatures can be made.

On the basis of fire tests, a simplified method to estimate the critical temperatures of portal frames in fire was developed by Wong in 2001 [2] for single-span portal frames with simple base connections. It was shown by numerical modelling that this method could predict the temperature at which the rafters initially lose stability in fire. A recently developed quasi-static analysis [3], implemented in the program *Vulcan*, using a combination of static and dynamic solvers, has also shown that the strong base connections recommended by the current design method may not always lead to a conservative design. A second-phase failure mechanism observed in numerical modelling corresponds with the failure mode shown in one of the previous fire tests. The critical temperature at which run-away collapse occurs may be higher than that at which the roof initially loses its stability, because of re-stabilisation.

In this paper, a new method for estimating critical temperatures of single-span frames in fire, using these two failure mechanisms, is presented. Numerical tests on typical industrial frames are used to calibrate this new method against the current design method.

### 1 BEHAVIOUR OF SINGLE-STOREY PORTAL FRAMES IN FIRE

As early as 1979 the behaviour of steel portal frames in accidental fires was described in the report of a study [4] of fires in a number of portal frames in the UK. A typical variation of the overturning moment at the column base with time, after a fire is ignited in a pitched-roof portal frame is described in the CONSTRADO design guide [5]. It was believed that the stability of the column was mainly determined by the resistance provided by the column base connections. However, the fire test on a scaled pitched-roof portal frame performed in 1999 [2] showed that the steel columns, connected to their foundations by a fairly flexible connection, could stand almost upright throughout the fire while the rafters snapped-through to an inverted

shape. This indicates that strong column bases are not always essential to the stability of an industrial frame under fire conditions.

It has been postulated by O’Meagher *et al.* [6] that unaffected parts of a building can act as anchorage for the fire-affected zone, provided that the forces developed in the purlins are reasonably small and that they have sufficient capacity at high temperatures, so that cold frames will also deform in an acceptable mode. The results of a series of parametric studies [2] using the two- and three-dimensional modelling showed that the initial collapse of a portal frame with semi-rigid bases initially loses stability in a combined mechanism, which differs from the assumption used in the current design method. Further deformation could not be simulated because of the limitations of the static solver.

In a previous paper the behaviour of single-span pitched portal frames was simulated using the recently-developed quasi-static solver [3] in *Vulcan*. This showed that collapse of the frame happens in two phases [7]. It was also found that initial collapse of the rafter is always caused by a plastic hinge mechanism which is based on the frame’s initial configuration. If the frame can re-stabilize when the roof is substantially inverted, a second plastic mechanism based on the re-stabilized configuration leads to eventual failure of the whole frame.

## 2 NEW DESIGN METHOD

A single-span portal frame fails either in the first-phase mechanism when it initially loses stability, or may re-stabilise for a while before collapsing in the second-phase mechanism. The simple method developed by Wong [2] is based on the initial configuration of the frame. Hence, it is capable of explaining the reason why frames initially lose stability in fire, but is not valid for frame collapse in the second mechanism, in which the deformation of the frame is significant. The estimation of the critical temperatures for a two-phase failure mechanism should be based on different initial configurations for each of the two phases.

### 2.1 Estimation of First-Phase Failure

When the roof of the frame starts to deform downward under the loading and fire temperature, the columns are pushed outward due to the change of geometry and to thermal expansion of the rafters. For a portal frame with frictionless pinned base connections, high rotations can be generated at these bases, caused by either elastic or plastic deformation. These rotations, together with the fire hinges formed at the apex and eaves, can generate a “combined” plastic mechanism. Wong’s simple model, as shown in *Fig. 1*, uses this mechanism, whose kinematics is referred to the initial configuration of the portal frame. This method can only apply to the frame’s initial loss of stability at relatively low deflections. According to plastic theory, for the mechanism shown in *Fig. 1*, the fire hinge moments at corners 1 and 2 can be calculated. The ratio of the fire hinge moment to the normal moment capacity is given by the strength reduction factor at the critical temperature, so the critical temperature of this frame can be interpolated from stress-strain curves defined in Eurocode 3 Part 1. 2 [8].

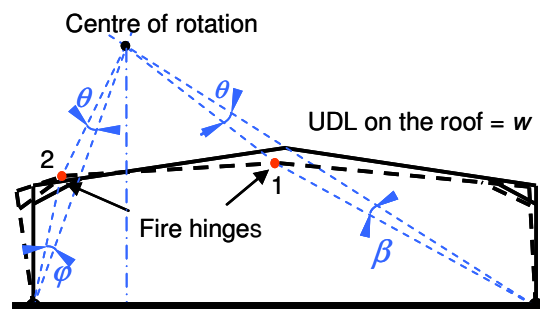


Fig. 1. The model of Wong’s simple design method.

### 2.2 Estimation of Second-Phase Failure

The initial collapse of the roof frame may initiate a “combined” mechanism leading to

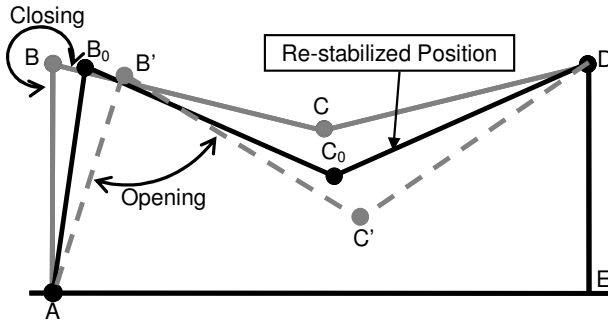


Fig. 2. Illustration of the second phase mechanism.

moments of the columns increase again. When the rotation of the column AB is faster than the rotation of the adjacent rafter, the moment on one eave (corner B) starts to reverse, leading to locking of the adjacent plastic hinge. This causes the frame to re-stabilise at this position (Shape  $AB_0C_0DE$  in Fig. 2), at which the internal angle ( $AB_0C_0$ ) between column  $AB_0$  and the connected rafter  $BC_0$  stops closing and starts opening. With further increase of the pulling force at the column top caused by catenary action of the inverted roof, the fire hinges at the eave and column base can be mobilised again (shape  $AB'C'DE$  in Fig. 2), and a new mechanism, referred to as the second-phase failure mechanism, is established which leads to complete collapse of the frame.

The new design method developed here focuses mainly on collapse caused by the second-phase mechanism in fire, and aims to predict the critical temperatures which initiate formation of the second-phase failure mechanism. The method is based on calculating the strength reduction factor of the fire hinge moment according to the work balance within the frame.

Because of the significant deformation of the roof frame before the start of the second failure

mechanism, this new model has to identify the re-stabilised position of the frame and its critical position at the start point of the second-phase mechanism. Both the thermal elongation of rafters and degradation of fire hinge moments at elevated temperatures are considered under some temperature assumption. Moreover, because a plastic hinge at one column base is essential to generate a second-phase mechanism, the strength of the column bases is also included in this new method.

When the second-phase mechanism of the frame is established, the elongation of the rafters is significant. This should not be ignored when the work balance is calculated within this system. Estimation of the critical temperature for the second-phase mechanism of the frame is also based on the reduced moment capacity of

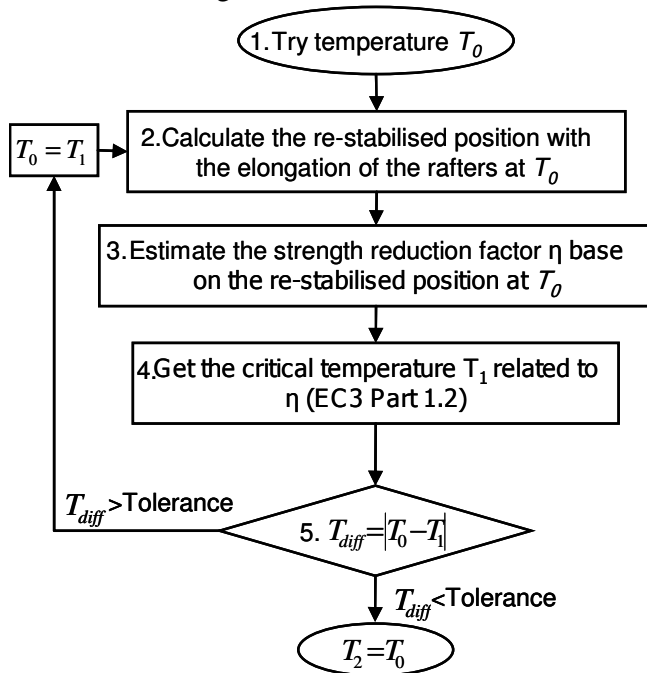


Fig. 3. The procedure for estimating the critical temperature of second phase failure.

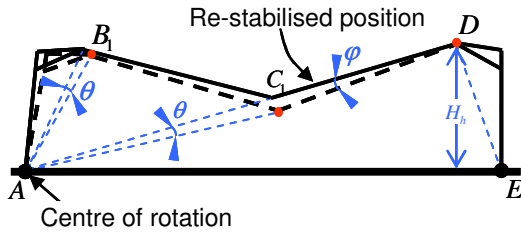


Fig. 4. The model of the second-phase failure

of the frame, including the elongation of the rafter, at temperature  $T_0$ . The fire hinge moment can also be calculated on the basis of the configuration of the frame at the re-stabilised position (as shown in Fig. 4) and the work balance based on plastic theory. The critical temperature  $T_1$  can be obtained from the strength reduction factor given by dividing the fire hinge moment by the moment capacity of the rafter section, and relating this to the corresponding temperature, as defined in Eurocode 3 Part 1.2 [8]. If the difference between  $T_0$  and  $T_1$  is larger than the tolerance required, Steps 2 to 5 as defined in Fig. 3 are repeated, using the elongated lengths of the rafters at  $T_1$ , until  $T_{diff}$  is smaller than the tolerance required. The temperature  $T_1$  estimated from the final iteration is the critical temperature of the frame at the beginning of the second-phase mechanism.

### 3 VALIDATIONS AGAINST NUMERICAL TESTS

In order to validate the new design method a series of comparison between critical failure temperatures predicted using the new design method and those obtained from previous numerical tests [9], have been conducted. Because the two-phase mechanisms are included in this method, critical temperatures for the creation of both the first- and the second-phase mechanisms are compared.

Figs. 5 and 6 compare the critical temperatures predicted by the new design method and numerical analysis results for two typical portal frames. The results presented in Fig. 5 are for the portal frame designed without haunches but with varying base strength. Results for the other portal frame, which is designed with typical-sized haunches and modelled with different base strengths, are shown in Fig. 6.

The first re-stabilised position of the frame is reached when the rafter is deformed into the inverted position and the vertical displacement of the apex is around 5m. The prediction of the new design method is 5m. This confirms that re-stabilisation during the collapse of the portal frame is caused by locking of the plastic hinge near to an eave, which disables the first-phase mechanism. Once the opening of the locked angle exceeds the elastic rotation limit, the frame loses its stability again.

the rafters. Because the strength reduction factor and the steel elongation at the critical temperature are both unknown, an iterative solution procedure, illustrated by the flow chart in Fig. 3, is required.

At the beginning of the second-phase calculation, an initial temperature  $T_0$  is assumed, so the re-stabilised position can be estimated on the basis of the geometry

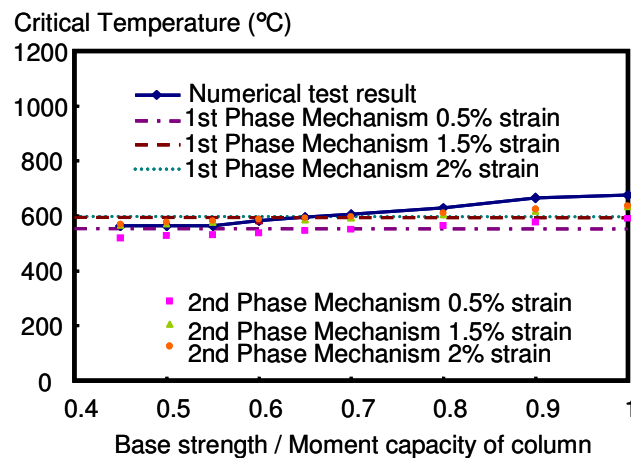
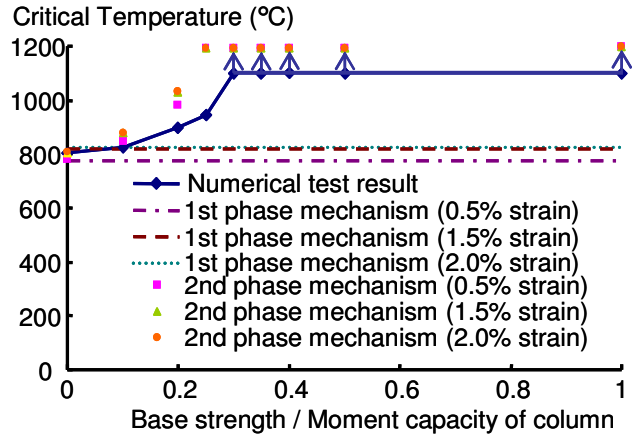


Fig. 5. Portal frames without haunches.

For the frame with haunches, the re-stabilised position predicted by the new design method is about 0.4m lower than for the numerical results. This is because, in the new design method, a re-stabilised position is assumed to occur when, in the first-phase mechanism, the rafter ceases to rotate relative to the column at hinge B (*Fig. 4*) and this hinge consequently locks itself. When the hinge finally begins to rotate again, in the opposite sense to its original rotation, the second-phase mechanism is created and failure occurs. Locking of the plastic hinges



*Fig. 6.* Portal frames with haunches

developed at one of the column bases could also be encountered when the column is pulled inward and passes its original position, so collapse is arrested until the plastic hinge at the base A is unlocked. When this hinge is mobilised, the frame is capable of continuing to collapse until the fire hinge near the end of the haunch locks itself. This explains the difference between the re-stabilised positions predicted by numerical tests and this new design method. It is worth noting that the main purpose for estimating the re-stabilised position is to determine the critical configuration of the frame on the basis of the principle of work balance. Therefore the final equilibrium position of the frame before it collapses again should be adopted in order to estimate the critical temperature.

From the previous numerical studies, the portal frame would fail in its first-phase mechanism when the ratio between the base strength and moment capacity of the column is lower than 0.55 for the unhaunched case and 0.1 for the haunched case. The reduced “yield stress” at 0.5% steel strain leads to a better prediction of the critical temperature of the frame without haunches in the new design method. As shown in *Fig. 5* the critical temperatures predicted by the new method for the second-phase mechanism according to the strength reduction factors at 1.5% and 2.0% strain show a similar trend to the numerical results.

From *Fig. 6* it is evident that, for a haunched frame with base strength equal to 10% of the moment capacity of the column section, the critical temperatures predicted by the new design method for the first-phase mechanism are very close to the numerical results. However, the numerical analyses give higher limiting temperatures for cases with base strength greater than 20% of the moment capacity of the column.

In the new design method the strength reduction factor obtained from equilibrium on the basis of the second-phase mechanism, becomes negative when the base strength is higher than 30% of the moment capacity of column. This means that the work done by the plastic hinges developed at the bases exceeds the work done by the external forces, and hence the second-phase mechanism can not happen, and the frame will stand in its re-stabilised position under further temperature increases.

#### 4 CONCLUSION

A new design method, extended from Wong’s model is presented in this paper. In this method, instead of relying on a single failure mechanism, the two most common failure mechanisms for pitched portal frames under fire conditions are considered to predict the critical temperatures of the frame. The critical temperatures predicted by the new design method on the basis of the first-phase failure mechanism show very good agreement with the numerical results at which a typical frame initially loses stability in fire. Very reasonable

predictions about the re-stabilised position and the final collapse temperatures of the frames were achieved using this new design method. It is evident from this study that the initial collapse of the frame due to the first failure mechanism is often a temporary instability, and that after this the frame can experience a second-phase mechanism with a higher critical temperature, which depends on the base strength and the loading conditions of the frame. When the frame collapses at the beginning of the first-phase mechanism, the inclination of the columns may be relatively small, so this could be a lower bound for the design of portal frames in a fire boundary condition. The re-stabilisation after the initial loss of stability of the frame can be estimated from the critical temperature predicted on the basis of the second-phase mechanism. In this new design method, when the strength reduction factor, calculated from work equilibrium for the second-phase mechanism of the frame, becomes negative it is possible that the portal frame could remain in its re-stabilised state after snap-through of the pitched roof, and may not collapse until a very high temperature is achieved.

## REFERENCES

- [1] Simms, W. I. and Newman, G. M., SCI Publication P313: Single Storey Steel Framed Buildings in Fire Boundary Conditions (2002 edn.), *The Steel Construction Institute*, 2002.
- [2] Wong, S. Y., The Structural Response of Industrial Portal Frame Structures in Fire, *PhD Thesis, University of Sheffield*, 2001
- [3] Song, Y., Huang, Z., Burgess, I. W. and Plank, R. J., The Behaviour of Single-Storey Industrial Steel Frames in Fire. *Acc. Advanced Steel Construction: an International Journal*, 2008.
- [4] CONSTRADO, The Study of the Behaviour of Portal Frames in Fire When Subject to Boundary Conditions, *The Constructional Steel Research and Development Organisation*, 1979.
- [5] CONSTRADO, Fire and Steel Construction: The Behaviour of Steel Portal Frames in Boundary Conditions, *The Constructional Steel Research and Development Organisation*, 1980.
- [6] O’Meagher, A. J., Bennetts I. D., Daywansa, P. H., Thomas, I. R. and BHP Research, Melbourne Laboratories, Design of Single Storey Industrial Buildings for Fire Resistance. *Journal of Australian Institute of Steel Construction*, Vol. 26, No.2, 1992.
- [7] Song, Y., Huang, Z., Burgess, I. W. and Plank, R. J., A New Design Method for Industrial Portal Frames in Fire, *Proc. Structures in Fire Workshop*, pp302-312, 2008.
- [8] CEN, BS EN 1993-1-8:2005: Eurocode 3: Design of Steel Structures: Part 1.2: General Rules-Structural Fire Design, *European Committee for Standardization*, 2005.
- [9] Song, Y., Analysis of Industrial Steel Portal Frames under Fire Conditions, *PhD Thesis, University of Sheffield*, 2009.

## AN EXPERIMENTAL STUDY OF STRUCTURAL BEHAVIOUR OF JOINTS IN RESTRAINED STEEL FRAMES IN FIRES

X. H. Dai, Y.C. Wang and C. G. Bailey

School of Mechanical, Aerospace and Civil Engineering, University of Manchester, UK

### INTRODUCTION

Joints are important members in steel framed structures and play a critical role in controlling progressive collapse of the structure under accidental fire attacks. Although previous research studies on steel-framed structures in fire have resulted in the development of fire engineering design methods (Wang 2002) that are now being widely adopted in practical steel structural fire resistant design, gaps still exist in understanding joint performance in fires. In order to understand joint performance in fire and develop feasible methods to quantify joint behaviour under complex loading conditions, a research project at the University of Manchester, in collaboration with the University of Sheffield, has been carried out to investigate the robustness of steel joints in fires. This collaborative research programme includes determination of temperatures in connection components with different fire protection schemes, bolt tests, elevated temperature tests on isolated joint assemblies and steel framed structures, development of component based methods etc. This paper only presents experimental results of the fire tests on structural assemblies. The results have revealed different possible failure modes of joint components and effects of column size and different joint types on structural fire behaviour of the connected beams. These tests have also demonstrated catenary action in restrained steel frames (Yin and Wang 2004, 2005a,b), which may be used to control progressive collapse of steel framed structures under exceptional fire attacks.

### 1 DESCRIPTION OF FIRE TESTS

In total ten fire tests were carried out in the fire testing laboratory at the University of Manchester. Each test used a fresh specimen specially designed in the form of “rugby-goalpost”. UB 178 x 102 x 19 was used as the beam in all ten tests. The two column sections were Grade S355 UC 254 x 254 x 73 (for Tests 1 - Test 5) and Grade S275 UC 152 x 152 x 23 (for Test 6 –Test 10). All the bolts and nuts were M20 Grade 8.8 except for the bolts in Test 5 (using extended endplate connection and large column section) which used M20 Grade G10.9 bolts and nuts to prevent premature failure of the bolts and nuts due to thread stripping. All connection components (including fin plates, end plates and web cleats) were grade S275 steel. *Table 1* summarises the beam size, the column size, the joint type and the main joint component size for all the ten tests.

All specimens were tested in the fire testing furnace which had internal dimensions of 3000mm x 1600mm x 900mm. *Fig.1* presents the elevation view of the test set up. The internal faces of the furnace were lined with ceramic fibre wool materials of thickness 200mm which could efficiently transfer heat to the test specimen. The furnace temperatures were recorded by using six conventional bead thermocouples whose average temperature was intended to follow the standard fire condition in ISO 834 (1975) in all tests.

In order to simulate the heat-sink effect of the concrete slab on beam top, the top flange of the steel beam was wrapped with a layer of 15 mm thick ceramic fibre blanket. A specially designed steel truss was bolted to the beam top flange to account for the lateral restraining effect of the concrete slab. Except for the top flange of the beam and the additional truss, all other members of the test specimen were unprotected. As shown in *Fig.1*, the columns were restrained from lateral movement at both ends and were only free to move in the longitudinal direction at the top end where a 25mm gap between the column top and the reaction frame to allow the column to develop free axial movement. To ensure that the loading jacks remained attached to the test beam, the hydraulic loading jacks were attached to the test beam using a special pin bracket system.

The target load of 40kN was applied to the steel beam in each hydraulic loading jack at ambient temperature, followed by fire exposure until the end of the test. This target load corresponds to a nominal load ratio of 0.5 in the beam, calculated as the ratio of the theoretical maximum bending moment in the simply supported beam to the plastic bending moment capacity of the beam at ambient temperature using a nominal steel yield stress of 275 N/mm<sup>2</sup>. It was recognised that the presence of a compressive load in the column would affect the performance of the system. However, due to limitations in the laboratory, the columns were unloaded in all tests.

Table 1: Summary of specimen dimensions

| Test ID | Joint type        | Connection component dimension (mm) | Column section | Beam section  |
|---------|-------------------|-------------------------------------|----------------|---------------|
| Test-1  | fin plate         | 150x130x10                          | UC 254x254x73  | UB 178x102x19 |
| Test-2  | flexible endplate | 150x130x8                           |                |               |
| Test-3  | flush endplate    | 150x200x8                           |                |               |
| Test-4  | web cleat         | 90x150x10 (depth: 130)              |                |               |
| Test-5  | extended endplate | 150x250x8                           |                |               |
| Test-6  | fin plate         | 150x130x10                          | UC152x152x23   |               |
| Test-7  | flexible endplate | 150x130x8                           |                |               |
| Test-8  | flush endplate    | 150x200x8                           |                |               |
| Test-9  | web cleat         | 90x150x10 (depth: 130)              |                |               |
| Test-10 | extended endplate | 150x250x8                           |                |               |

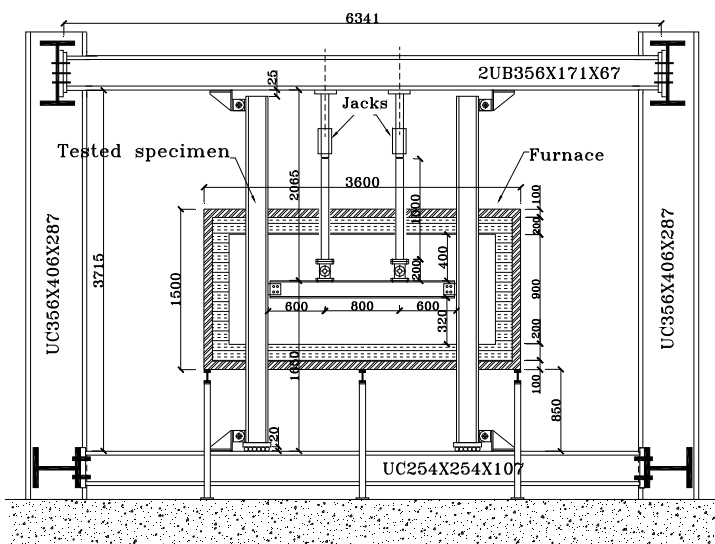


Fig.1: Elevation view of the test set up

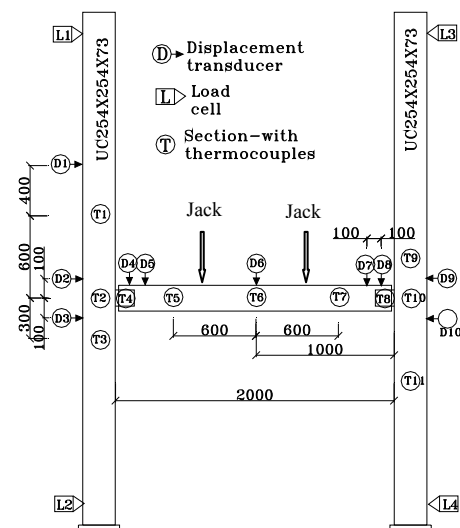


Fig.2: Arrangement of measurement devices on a specimen

To capture the temperature distribution in the tested specimen, numerous thermocouples were installed in the beam, columns and joint components. Fig.2 shows the thermocouple stations. Since this paper will only concentrate on the structural behaviour, detailed temperature information will not be presented here. Fig.2 also shows the displacement transducers (D1-D10) placed on the beam, the columns and around the joint zone to measure the beam deflections and column deformations. In order to obtain the axial load in the test beam, the horizontal reaction force at each column end was measured by a pin load cell (L1-L4) as shown in Fig.2.

## 2 TEST OBSERVATIONS AND FAILURE MODES OF JOINTS

The “failure” definition adopted here is to reflect the main objective of this study: to provide an insight into joint behaviour in terms of its contribution to preventing progressive collapse of the steel structure in fire. Therefore, as long as the structure is not physically detached from each other (fracture), it is assumed that the structure is still functioning or has not failed. Based on this

definition, *Table 2* summarised the main observations and failure modes (if observed) in each test. *Fig.3* shows possible connection failure modes. The following conclusions may be drawn based on the test observations: (1) With axial restraint to the steel beam, there will be axial force in the steel beam in fire. However, there was no failure in the structure when axial compression was developed in the beam. Failure was a result of the development of tension in the beam. (2) Failure occurred in the connections, not in the beams. When failure occurred, it was due to inadequate shear resistance of the beam web (Test-2) or weld fracture or bolt thread stripping due to a combination of the tensile forces from catenary action and hogging bending moment in the connection. (3) Although no quantitative analysis has been undertaken, it is possible to suggest that the web cleat connection would appear to be the most robust connection. Its good bending flexibility reduced the concentration of tensile axial force which reduced the extent of any tensile failure. Flush end plate and extended end plate connection could also provide sufficient connection robustness, but high strength bolts should be used to avoid thread stripping. Fin plate and flexible end plate connections performed poorly. (4) Catenary action is often relied on to ensure robustness of steel framed structures in fire. Although it is necessary for the joint to possess sufficient axial stiffness in order to develop catenary action in the steel beam, too large an axial restraint stiffness could attract a great catenary force to fracture the connection components.

*Table 2: Summary of specimen observations and failure modes*

| Test ID | Joint type        | Main observations   | Failure mode                       |
|---------|-------------------|---|------------------------------------|
| Test-1  | fin plate         | Beam flange bearing against column flange, little column deformation  | Weld fracture                      |
| Test-2  | flexible endplate | Beam web fractured mainly in shear, complete detachment of beam from column, little column deformation                              | Beam web fracture & detachment     |
| Test-3  | flush endplate    | Thread-stripping of bolts and nuts, complete detachment of beam from column, little column deformation                              | Bolt thread stripping & detachment |
| Test-4  | web cleat         | Web cleat large deformation, thread-stripping of bolts and nuts of top bolts but connection not detached, little column deformation | Some bolt thread stripping         |
| Test-5  | extended endplate | Classical end plate ductile deformation, compressive buckling in beam lower flange, little column deformation                       | -                                  |
| Test-6  | fin plate         | Beam flange bearing against column flange, plastic hinges in column   | Weld fracture                      |
| Test-7  | flexible endplate | Large flexible end plate and column flange deformations   | Slight weld fracture               |
| Test-8  | flush endplate    | Large column flange deformations, moderate end plate deformation  | -                                  |
| Test-9  | web cleat         | Large web cleat and column flange deformations  | -                                  |
| Test-10 | extended endplate | Moderate end plate deformation, large column flange deformations, plastic hinges in column flanges                                  | -                                  |

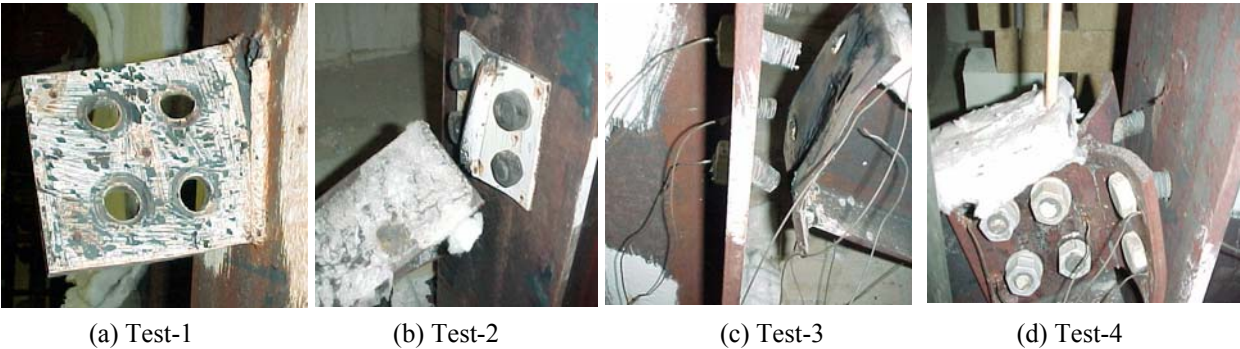


*Fig. 3: Failure modes of joint components*

### 3 EFFECTS OF COLUMN SIZE AND JOINT TYPES ON STRUCTURAL FIRE BEHAVIOUR

The qualitative behaviour of an axially restrained beam is now well established (Wang 2002) and confirmed by a theoretical study by Yin and Wang (2004, 2005a, 2005b). Generally, the temperature at which the axial force of an axially restrained steel beam returns to zero is the same as the limiting temperature of the same beam without axial restraint. However, when the beam enters catenary stage, its ability to survive high temperature will depend on the connection's ability to resist the tension force due to catenary action and hogging bending moment. There are many factors may influence the connection's ability, such as joint types, structural member size, structural material, fire characteristics etc. The paper will only focus on effects of the two factors considered in this study: column size and connection types.

#### 3.1 Effects of column sizes on structural fire behaviour

As a demonstration, *Fig.4(a)* compares beam mid-span deflections between frames using flush endplate connection with the two column section sizes. It can be seen that the beam experienced rapid increase in deflections within a very narrow temperature range. *Fig.4(b)* compares the corresponding beam axial forces. It can be seen that the temperature at which the beam experienced rapid increase in deflection is the same temperature at which the beam's axial force returns to zero, or changing from compression to tension. As expected, the beam temperature at which the beam started to experience large deflections (beam running away) in the frame using the larger columns was higher than that in the frame using the smaller columns. This means specimen that used the larger column size allowed the connections to develop higher bending moment capacities than the specimen that used the smaller column size. For the tested frames with other joint types (fin plate, web cleat, flexible endplate and extended endplate), similar observations have been obtained (figures are not presented here due to space limitation). Nevertheless, the temperature differences between these two sets (using different column sizes) of results are small as shown in *Fig. 4(b)*. *Fig. 4(b)* shows that the compressive axial forces in the test beams using the two different column sizes were drastically different with the large columns providing much greater axial restraint during the thermal expansion stage. However, if using the conventional limiting temperature, which is the temperature at which the beam's axial force is zero, and whose values are given in *Table 3*, the maximum difference between these two sets of results is 28 °C. Therefore, it appears that changing the steel column size is an unlikely source of improving the beam's fire resistance if adopting the conventional limiting temperature approach. According to the theoretical studies of Yin and Wang (2004,2005a,b), the catenary force will reach a peak and then decrease at increasing beam temperatures due to increasing beam deflection as well as decreasing mechanical properties of steel. However, due to connection failure in some tests (see *Table 2*) and limitations in the test setup it was not possible to observe this stage of beam behaviour.

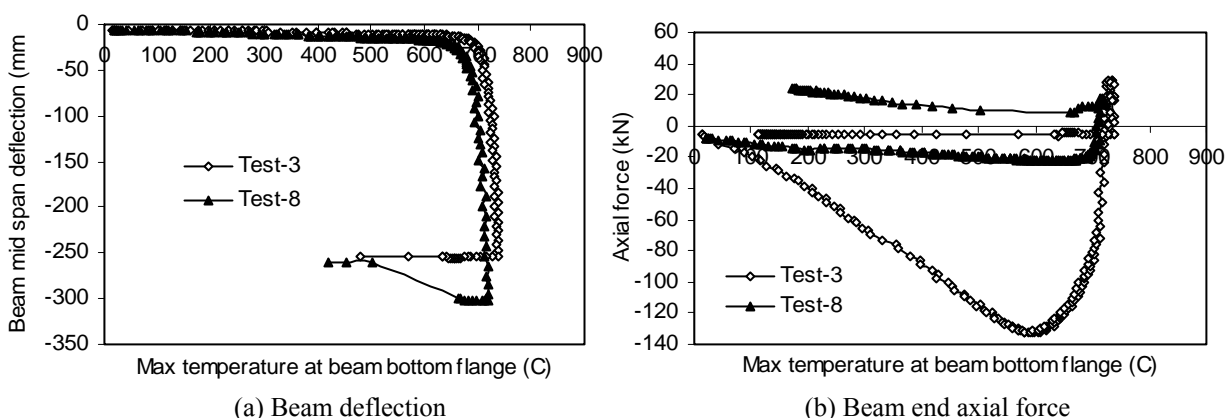


*Fig.4:* Comparisons of beam mid span deflection and axial forces to show the effects of different column sizes (flush end plate connection)

Table 3: Summary of beam limiting temperatures (with axial force=0)

|   |        |        |        |        |         |  |
|---|--------|--------|--------|--------|---------|--|
| Test ID                                   | Test-1 | Test-2 | Test-3 | Test-4 | Test-5  | Max temp difference by connection type ( C ) |
| Temperature ( C )                         | 748    | 728    | 728    | 750    | 753     | 25   |
| Test ID                                   | Test-6 | Test-7 | Test-8 | Test-9 | Test-10 |  |
| Temperature ( C )                         | 733    | 700    | 710    | 725    | 745     | 45   |
| Max temp difference by column sizes ( C ) | 15     | 28     | 18     | 25     | 8       |  |

### 3.2 Effects of joint types on structural fire behaviour

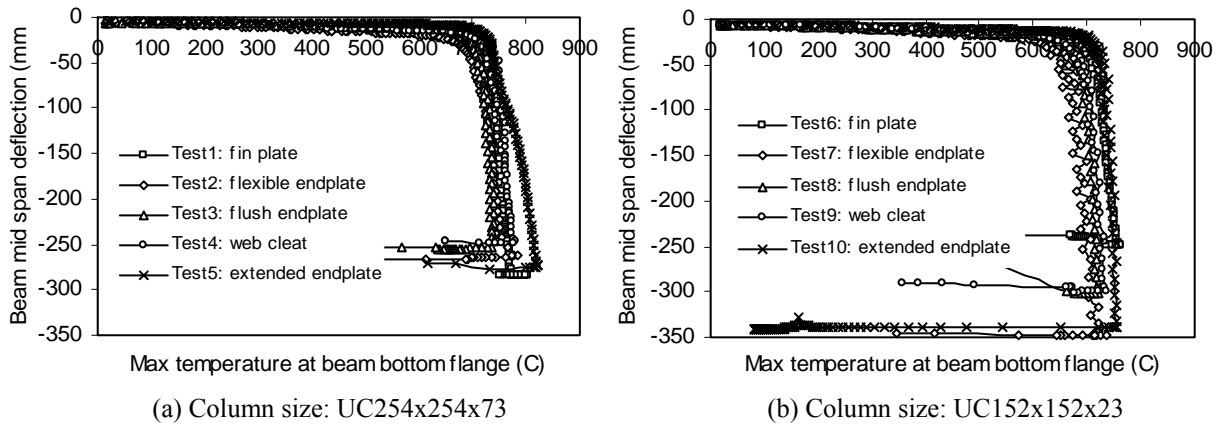


Fig. 5: Comparisons of beam deflections for different joint types

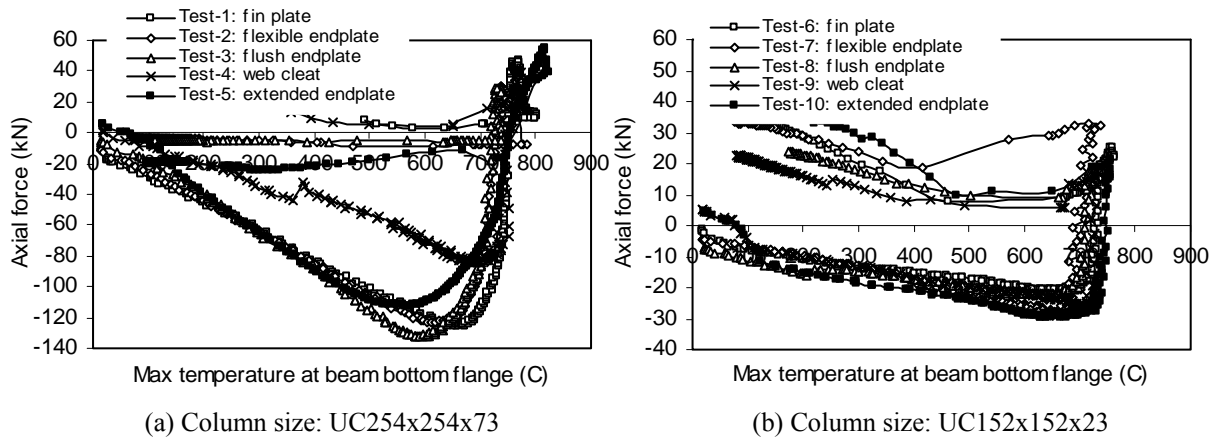


Fig. 6: Comparisons of beam axial forces for different joint types

Fig. 5 compares the beam mid-span deflections for using different joint types. It can be seen the difference is relatively small comparing to the large difference in joint types, ranging from nominal pin joints (fin plate, flexible endplate) to the relatively rigid extended end plate joints. Due to bearing between the beam lower flange and the column flange when using the fin plate connection, the nominally pinned fin plate connection resulted in a much more rigid behaviour. The poor behaviour of flush end plate in Test-3 is a result of severe asymmetrical heating in the testing furnace. Fig. 6 compares the beam axial forces for the five different connection types. It is very clear that during the compression phase, the joint type had little effect on the axial force development except for the specimen using web cleat when the large columns were used. This is clearly an indication that due to the small joint zone, the joint may be considered to possess almost infinite axial restraint stiffness to the beam compared to the column size. This may be used to considerably simplify the whole frame analysis model when using springs to represent the effects of the joints. Again, if using the temperature at which the beam's axial force returns from compression to zero as its limiting temperature, the beam's limiting temperatures from the different tests are very

similar, the maximum difference being 45 °C as given in *Table 3*. Considering the large range in connection bending behaviour (from nominally pinned to almost full strength), this indicates that it is not worthy using stiffer and stronger joints to increase the limiting temperature of the connected beam, if the beam's limiting temperature is based on its bending moment resistance.

#### 4. CONCLUSIONS

This paper presents some results on test observations, connection failure modes and effects of different column sizes and joint types on the behaviour of the joints and the connected beams. Although due to limitations of the test set up, the structural behaviour during the entire phase of beam catenary action has not been fully captured, it is still possible to achieve some tangible conclusions with regard to robust joint design and fire resistant design of steel framed structures. The main conclusions are:

- The fire tests have revealed a number of joint failure modes, including weld tearing, beam web fracture and bolt thread stripping. The test data will provide valuable insight in detailed understanding of joint behaviour and failure.
- The test beams were able to experience very large deflections (span/8~span/6) without fracture.
- If beam limiting temperature is calculated based on its bending moment resistance, the effect of using different joints (ranging from nominally pinned to almost full strength) has very little effect, with the changing in beam limiting temperature being less than 50°C. The effect of column size is even smaller, less than 30°C.
- Using different joint types had very little effect on the beam's axial force in compression. But using different column sizes had great effect. However, irrespective of the great effect of using different column sizes, the structure was able to sustain the applied load throughout the beam-in-compression phase.
- If catenary action in the beam is considered in fire resistant design (e.g. to consider structural robustness), the effects of different columns and different joints should be considered.
- If using the ability of a joint to allow the connected beam to develop catenary action without joint failure as criterion to assess joint robustness, the flexible end plate connection performed the poorest, then followed by flush end plate connection, fin plate connections, web cleat and extended end plate connections.

#### 5. ACKNOWLEDGEMENTS

This research reported in this paper is funded by a research grant from the UK's Engineering and Physical Science Research Council (EP/C003004/1). The fire tests were conducted at the University of Manchester's Fire Test Laboratory, with technical assistance from Mr. Jim Gorst, Mr. Jim Gee, Mr. Martin Cruikshank and help from a number of PhD students including Jifeng Yuan, Pinyu Yan, Henry He, Penjun Wang in the authors' research group.

#### REFERENCES

- [1] International Organization for Standardization (ISO 834 1975): Fire Resistance Tests, Elements of Building Construction, Geneva: International Organization for Standardization.
- [2] Wang Y.C. (2002), Steel and composite structures, behaviour and design for fire safety. London: Spon Press; 2002.
- [3] Yin, Y.Z. and Wang, Y.C. (2004), "A numerical study of large deflection behaviour of restrained steel beams at elevated temperatures". *Journal of Constructional Steel Research* 60(2004) 1029-1047. 2004.
- [4] Yin, Y.Z. and Wang, Y.C. (2005a), "Analysis of catenary action in steel beams using a simplified hand calculation method, Part 1: theory and validation for uniform temperature distribution". *Journal of Constructional Steel Research* 61(2005) 183-211. 2005.
- [5] Yin, Y.Z. and Wang, Y.C. (2005b), "Analysis of catenary action in steel beams using a simplified hand calculation method, Part 2: validation for non-uniform temperature distribution". *Journal of Constructional Steel Research* 61(2005) 213-234. 2005.

## EFFECTS OF FLAME RADIATION ON TEMPERATURE ELEVATION of Steel Members in Large Space Building Fire

Du Yong <sup>a</sup>, Li Guo-qiang <sup>b</sup>

<sup>a</sup> Nanjing University of Technology, School of Architecture and Urban Planning, Nanjing, China

<sup>b</sup> Tongji University, School of Civil Engineering, Shanghai, China

### INTRODUCTION

A significant amount of research work shows that in small compartments the temperature conditions at a given time are considered to be uniform and can be approximate as the flame temperature. However, temperature fields are non-uniform in large space building fires and lower than small compartment fires generally[1]. Then the histories of temperature of steel members unprotected are difference under various temperature fields in fires.

For *Ref.2* propose, in the large space building fires if the distance from the flame to the surface of steel members is far enough, heat transfer between the flame and the steel member may be disregarded. Otherwise the radiant heat transfer from the flame to steel members must be considered in the heat equilibrium equation based on the lumped differential formulation. The incremental rise in temperature of an uniformly heated unprotected steel section in time interval  $\Delta t$  due to heat transfer from hot smoke and flame radiant is given by

$$\frac{\Delta T_{sf}}{\Delta t} = \frac{\varepsilon_r \varepsilon_s c_0 F [(T_g + 273)^4 - (T_{sf}(t) + 273)^4] + \varepsilon_r \varepsilon_s \varphi_{sf} \xi F (1 - \varepsilon_g) \varepsilon_0 [(T_f + 273)^4 - (T_{sf}(t) + 273)^4] + F \varepsilon_c (T_g - T_{sf}(t))}{V \rho_s c_s} \quad (1)$$

where  $c_s$ ,  $\rho_s$  specific heat of steel [J/ (kg · °C) ] and the density of steel [7850kg/m<sup>3</sup>] respectively

$\Delta t$  time interval (recommended  $\Delta t$  is not more than 5 seconds)

$\varepsilon_r$  resultant emissivity representing the radiation transmitted between the hot smoke and the steel member surface [ $\varepsilon_r = 0.5$ ]

$\varepsilon_s$ ,  $\varepsilon_f$  emissivity of steel members and flames respectively [ $\varepsilon_s = 0.8$ ,  $\varepsilon_f = 0.7$ ]

$\varepsilon_c$  convective heat transfer coefficient [25W/(m<sup>2</sup> · °C) ]

$c_0$  Stefan-Boltzmann constant [ $5.67 \times 10^{-8}$  W/m<sup>2</sup> · K<sup>4</sup>]

$F$  surface area of the unprotected steel member per unit length [m<sup>2</sup>/m]

$V$  volume of the unprotected steel member per unit length [m<sup>3</sup>/m]

$T_{sf}(t)$  temperature of the unprotected steel member, which is due to heat transfer by convection and radiant from hot smoke and by flame radiant

$T_f$  average temperature of flame [°C]

$\varphi_{sf}$  configuration factor in the particular case of two parallel surfaces

$\xi$  ratio of the surface area of the unprotected steel member exposed to flame radiation given by

$$\xi = F_{sr} / F$$

where  $F_{sr}$  surface area of the unprotected steel member exposed to flame radiation

$T_g(t)$  temperature of hot smoke in the large space building fire at a particular time given by

$$T_g(t) - T_g(0) = T_g^{\max} \left[ 1 - 0.8e^{(-\beta t)} - 0.2e^{(-0.1\beta t)} \right] \cdot \left[ \eta + (1-\eta)e^{\left(\frac{b-x}{\mu}\right)} \right] \quad (2)$$

where  $T_g(0)$  ambient temperature [ $^{\circ}\text{C}$ ]

$T_g^{\max}$  maximum temperature of smoke depended on the fire load and the dimension of compartment [ $^{\circ}\text{C}$ ]

$B, \eta, \mu$  temperature gradient factors relevant to the growth rate and the heat release rate of design fires, given by CECS200:2006 (the Technical code for fire safety of steel structures in buildings of China)

$b$  distance from the centre to the edge of the fire source [m]

*Eq.(2)* is a regression formula[3], which is solved statistically over the set of data from the computer program FDS based on field model and adopted by CECS200:2006[4].

With step-by-step method, solution of the incremental *Eq.(1)* formulates the time history of temperature of steel members  $T_{sf}(t)$ . If the second term at the right side of *Eq.(1)* is neglected, the temperature of steel members generated by the hot smoke could be solved by the same method. This traditional method does not lend to rapid calculation of the temperature rise in steel members for fire resistance design, so an alternative simplified approach for temperature calculation is developed in this paper.

## 1 PROPOSED SIMPLIFIED FORMULA

*Eq.(3)* is defined to describe the effect of flame radiation on the elevated temperature in steel members. The typical temperature history based on *Eq.(3)* is shown in *Fig.1*

$$T_{sf}' = T_{sf}(t) - T_s(t) \quad (3)$$

where  $T_{sf}'$  temperature of the steel member generated by the flame radiation alone

$T_s(t)$  temperature of the steel member generated by the hot smoke

The simple expression for typical temperature course of  $T_{sf}'$  shown in *Fig.1* is gotten by

$$T_{sf}' = T_m \left( k_1 e^{-k_2 \lg^2(t/t_m)} + k_3 e^{-k_4 \lg^2(t/t_m)} \right) \quad (4)$$

where  $T_m$  maximum temperature generated by the flame radiation lonely

$t_m$  time at maximum temperature

$k_i$  shape coefficient for  $i=1,2,3,4$

$\lg$  logarithm as base to 10

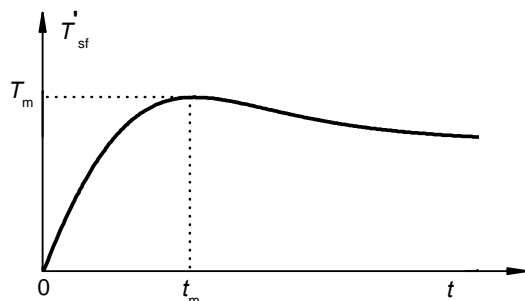


*Fig. 1.* Typical temperature course of steel members

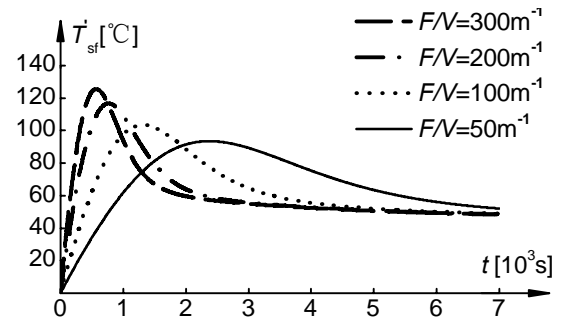


*Fig. 2.* Relationship of time with temperature of steel members for factor  $F/V$

## 2 KEY PARAMETERS DUE TO FLAME RADIANT ALONE

A large number of curves for temperature elevated in steel members formed from *Eq.(1)* to

Eq.(3), which are provided for analysis the key parameters affecting temperature histories of steel members generated by flame radiation alone in large space building fire are discussed further as follows.

### 2.1 Effects of the section factor $F/V$

Fig.2 shows the temperature history  $T_{sf}'$  with a range of  $F/V$  between  $300\text{m}^{-1}$  and  $50\text{m}^{-1}$ . Here the other factors are given as  $\varphi_{sf} = 0.9$ ,  $\xi = 0.7$ ,  $\beta = 0.003$ ,  $T_g^{\max} = 500\text{ }^\circ\text{C}$ .

A series of temperature course shows that the maximum temperature  $T_m$  is increase and the time at the maximum temperature  $t_m$  is early with the developed  $F/V$  for given other factors.

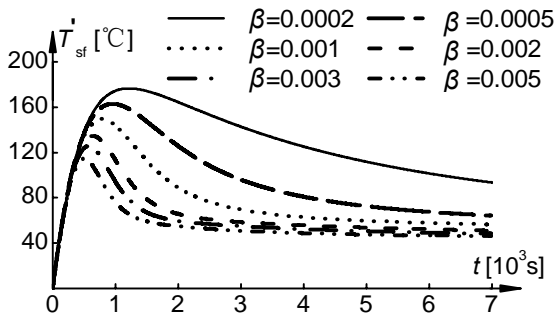


Fig. 3. Relationship of time with the temperature  $T_{sf}'$  for factor  $\beta$

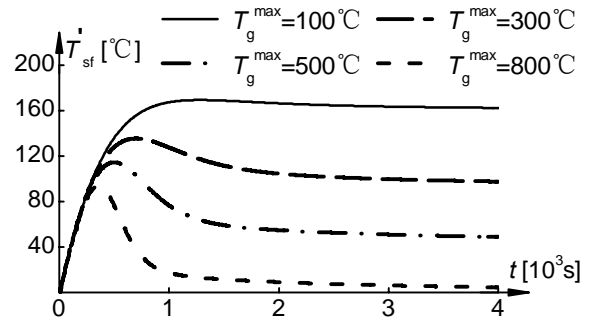


Fig. 4. Relationship of time with the temperature  $T_{sf}'$  for factor  $T_g^{\max}$

### 2.2 Effects of the temperature gradient factor of the smoke $\beta$

Fig.3 shows the temperature history  $T_{sf}'$  with a range of  $\beta$  between 0.0002 and 0.005. Here the other factors are given as  $\varphi_{sf} = 0.9$ ,  $\xi = 0.7$ ,  $F/V = 300\text{m}^{-1}$ ,  $T_g^{\max} = 500\text{ }^\circ\text{C}$ . A series of temperature course shows that the maximum temperature  $T_m$  is decrease and the time at the maximum temperature  $t_m$  is early with the developed  $\beta$  for given other factors.

### 2.2 Effects of the maximum temperature of smoke $T_g^{\max}$

Fig.4 shows the temperature history  $T_{sf}'$  with a range of  $T_g^{\max}$  between  $100\text{ }^\circ\text{C}$  and  $800\text{ }^\circ\text{C}$ . Here the other factors are given as  $\varphi_{sf} = 0.9$ ,  $\xi = 0.7$ ,  $F/V = 300\text{m}^{-1}$ ,  $\beta = 0.003$ . A series of temperature course shows that the maximum temperature  $T_m$  is decrease and the time at the maximum temperature  $t_m$  is early with the developed  $T_g^{\max}$  for given other factors.

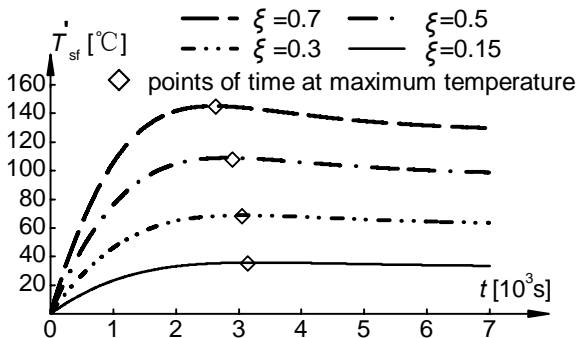


Fig.5. Relationship of time with temperature of steel members for factor  $\xi$

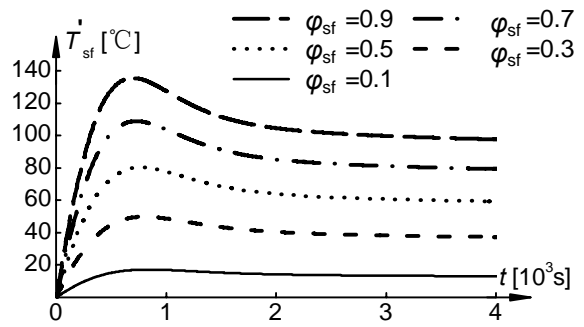


Fig.6. Relationship of time with temperature of steel members for factor  $\varphi_{sf}$

## 2.4 Effects of the rate of the surface area under flame radiant $\xi$

Fig.5 shows the temperature history  $T_{sf}'$  with a range of  $\xi$  between 0.15 and 0.70. Here the other factors are given as  $\varphi_{sf} = 0.9$ ,  $F/V = 100\text{m}^{-1}$ ,  $T_g^{\text{max}} = 200^\circ\text{C}$ ,  $\beta = 0.003$ . A series of temperature course shows that the maximum temperature  $T_m$  is increase and the time at the maximum temperature  $t_m$  is late with the developed  $\xi$  for given other factors.

## 2.5 Effects of the configuration factor $\varphi_{sf}$

Fig.6 shows the temperature history  $T_{sf}'$  with a range of  $\varphi_{sf}$  between 0.1 and 0.9. Here the other factors are given as  $T_g^{\text{max}} = 300^\circ\text{C}$ ,  $\xi = 0.7$ ,  $F/V = 300\text{m}^{-1}$ ,  $\beta = 0.003$ . A series of temperature course shows that the maximum temperature  $T_m$  is increase and the time at the maximum temperature  $t_m$  is the same with the developed  $\varphi_{sf}$  for given other factors.

## 3 REGRESSION COEFFICIENTS FOR DESIGN PROPOSES

### 3.1 Determine the shape coefficient $k_i$

Fig.1 shows the curve shape is deference between growth and decay phase. The shape coefficient with Eq.4 can be gotten by fitting the curves shown in Fig.2 for given  $T_m$  and  $t_m$ . Although the curves in Fig.2 differ in  $T_m$  and  $t_m$ , all the shape coefficients  $k_i$  mentioned above are approximate with each other. Then two rows of average value for  $k_i$  are given in table 1 to describe the curve shape through growth and decay phase respectively.

Table 1. Values of shape coefficients

| Curve shape                   | $k_1$ | $k_2$ | $k_3$ | $k_4$ |
|-------------------------------|-------|-------|-------|-------|
| Growth phase ( $t \leq t_m$ ) | 0.624 | 1.253 | 0.364 | 0.134 |
| Decay phase ( $t > t_m$ )     | 0.430 | 0.075 | 0.576 | 0.116 |

### 3.2 Determine maximum temperature $T_m$ and the time at maximum temperature $t_m$

With the step-by-step method, a series of temperature histories of steel members due to flames radiant alone could be calculated from Eq.(1) to Eq.(3) for various key parameters, which are similar to curves discussed in chapter 2. The  $T_m$  and  $t_m$  can easily be obtained from each temperature history curve to form the curves shown in Fig.7 to Fig.9.

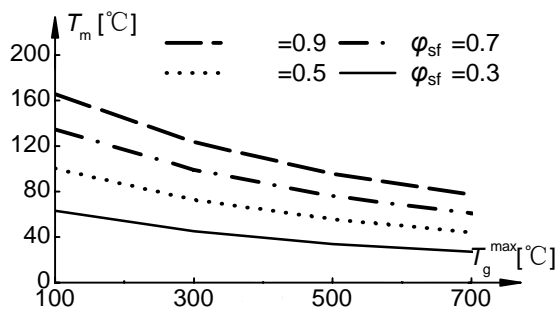


Fig.7. Relation of  $T_g^{\text{max}}$  between  $T_m$  for a rang of  $\varphi_{sf}$

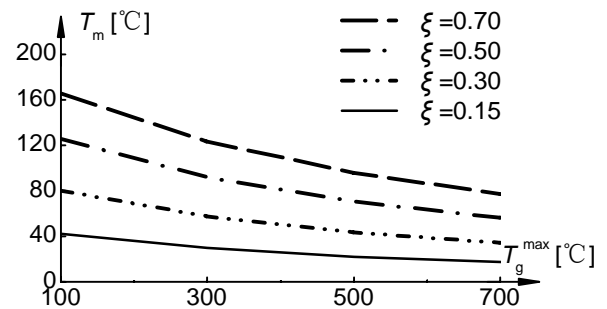


Fig.8. Relation of  $T_g^{\text{max}}$  between  $T_m$  for a rang of  $\xi$

Shown in Fig.4 to Fig.6 the maximum temperature  $T_m$  is depend on,  $\xi$  and  $T_g^{\text{max}}$  for given factors  $F/V$  and  $\varphi_{sf}$ , in the meantime the time at maximum temperature  $t_m$  is determined by  $T_g^{\text{max}}$  and  $\xi$  mainly. Shown in Fig.7 to Fig.9 curves for various factor  $\varphi_{sf}$  and  $\xi$  follow

the same form as an exponential function of  $T_g^{\max}$  with Eq.(5) and Eq.(6) respectively.

$$T_m = A + Be^{-T_g^{\max}/C} \quad (5)$$

$$t_m = A' + B'e^{-T_g^{\max}/C'} \quad (6)$$

Where  $A, B, C$  and  $A', B', C'$  are functions of the parameter  $\xi$  and  $\varphi_{sf}$  given by Eq.(7) and Eq.(8) respectively

$$\begin{cases} A = a_1 + a_2\xi^2 + (a_3 + a_4\xi)\varphi_{sf} \\ B = b_1 + b_2\xi^2 + (b_3 + b_4\xi)\varphi_{sf} \\ C = c_1 + c_2\xi^2 + (c_3 + c_4\xi)\varphi_{sf} \end{cases} \quad (7) ; \quad \begin{cases} A' = a'_1 - a'_2\xi \\ B' = b'_1 - b'_2\xi \\ C' = c'_1 - c'_2\xi \end{cases} \quad (8)$$

Where  $a_i, b_i$  and  $c_i$  ( $i=1\sim 4$ ) regression coefficients given in Table 2  
 $a'_i, b'_i$  and  $c'_i$  ( $i=1\sim 2$ ) regression coefficients given in Table 3

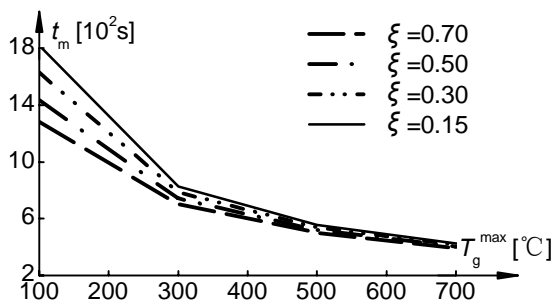


Fig.9. Relation  $t_m$  between  $T_g^{\max}$  for a range of parameter  $\xi$

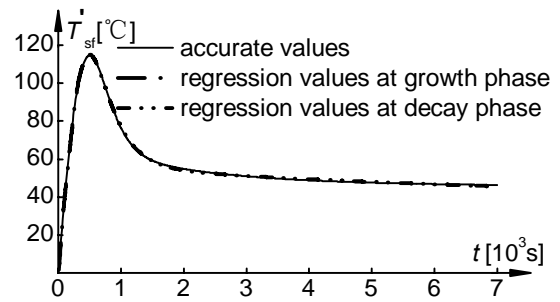


Fig.10. Comparison between the accurate value and the application result

#### 4 APPLICATION

It is important to estimate the temperature in steel members conveniently for engineer to assess fire resistance. A simple approximate formula is presented as

$$T_{sf}(t) = T_m \left( k_1 e^{-k_2 \lg^2(t/t_m)} + k_3 e^{-k_4 \lg^2(t/t_m)} \right) + T_s(t) \quad (9)$$

where  $T_s(t)$  is provided by CECS200:2006 as

$$T_s(t) = T_g(t) - [T_g(t) - T_g(0)] \cdot \left[ -a + (1+a) \cdot e^{(-b \times 10^{-4} t)} \right] \quad (10)$$

Where  $a, b$  regression coefficients given by CECS200:2006 for  $T_g^{\max}$ ,  $\beta$  and  $F/V$

It has been proved that the Eq.(10) is precise enough to estimate the temperature in unprotected steel members due to hot smoke heat entering by Ref.5. To verify the accuracy of Eq.(4) a common fire scenario is designed as  $T_g^{\max} = 500$  °C,  $\xi = 0.7$ ,  $F/V = 300\text{m}^{-1}$ ,  $\beta = 0.005$  and  $\varphi_{sf} = 0.9$ . The regression coefficients list in Table 2. and Table 3 for given  $F/V$  and  $\beta$  are induced into Eq.(7) or Eq.(8) to calculate  $T_m$  and  $t_m$ , and the shape coefficients  $k_i$  are given in Table 1. Then the temperature history derived from Eq.(4) is shown in Fig.10 as regression values. Referring to Fig.10 the exact solution with Eq.(1) and Eq.(3) for temperature  $T_{sf}'$  and the approximate solution from empirical formula Eq.(4) almost merge into one another. The compare shown that Eq.(9) can give a very good prediction of unprotected steel member temperatures caused by both hot smoke and flame heat entering and provide a simple calculation method for engineers concerned with structural fire safety.

Table 2. Values of regression coefficients for the maximum temperature

| $\beta$ | $F/V$<br>[m <sup>-1</sup> ] | A      |       |       |       | B     |        |        |       | C     |         |        |       |
|---------|-----------------------------|--------|-------|-------|-------|-------|--------|--------|-------|-------|---------|--------|-------|
|         |                             | $a_1$  | $a_2$ | $a_3$ | $a_4$ | $b_1$ | $b_2$  | $b_3$  | $b_4$ | $c_1$ | $c_2$   | $c_3$  | $c_4$ |
| 0.005   | 300                         | -0.027 | 3.024 | 2.429 | 108.6 | 0.356 | 16.330 | 21.399 | 153.7 | 402.3 | -5.84   | 15.56  | 160.1 |
|         | 200                         |        |       |       | 90.6  |       |        |        | 172.1 | 397.3 | -5.69   | 15.48  | 155.4 |
|         | 100                         |        |       |       | 57.1  |       |        |        | 203.6 | 405.1 | -1.77   | 17.34  | 162.4 |
|         | 50                          |        |       |       | 35.7  |       |        |        | 245.3 | 444.9 | 0.00    | 18.00  | 157.5 |
|         | ≤30                         | -0.026 | 2.951 | 1.728 | 34.9  | 0.348 | 15.957 | 20.910 | 239.7 | 444.9 | 0.00    | 18.00  | 157.5 |
| 0.001   | 300                         | -0.049 | 5.334 | 4.033 | 176.1 | 0.233 | 16.170 | 17.760 | 85.0  | 552.6 | -57.71  | 6.09   | 208.7 |
|         | 200                         |        |       |       | 159.7 |       |        |        | 100.0 | 494.9 | -21.41  | -12.77 | 152.3 |
|         | 100                         |        |       |       | 130.7 |       |        |        | 131.8 | 425.0 | -5.72   | 22.67  | 149.9 |
|         | 50                          |        |       |       | 86.7  |       |        |        | 168.0 | 465.1 | 0.00    | 35.96  | 139.2 |
|         | ≤30                         | -0.045 | 4.897 | 3.703 | 79.6  | 0.214 | 14.845 | 16.304 | 154.2 | 465.1 | 0.0     | 35.96  | 139.2 |
| 0.0002  | 300                         | -0.040 | 8.305 | 6.627 | 229.5 | 0.037 | 12.409 | 11.525 | 45.0  | 878.5 | -251.84 | -26.93 | 406.2 |
|         | 200                         |        |       |       | 218.2 |       |        | 13.020 | 56.5  | 771.0 | -167.74 | -11.13 | 311.5 |
|         | 100                         |        |       |       | 195.4 |       |        | 15.180 | 75.6  | 634.3 | -89.57  | -0.13  | 239.3 |
|         | 50                          |        |       |       | 155.0 |       |        | 21.421 | 90.1  | 651.2 | 0.00    | 18.99  | 235.3 |
|         | ≤30                         | -0.037 | 7.667 | 6.118 | 143.1 | 0.035 | 11.459 | 19.772 | 83.2  | 651.2 | 0.00    | 18.99  | 235.3 |

Table 3. Values of regression coefficients for the time at maximum temperature

| $\beta$ | $F/V$<br>[m <sup>-1</sup> ] | $a_1'$<br>[10 <sup>3</sup> ] | $a_2'$ | $b_1'$<br>[10 <sup>3</sup> ] | $b_2'$<br>[10 <sup>3</sup> ] | $c_1'$ | $c_2'$ |
|---------|-----------------------------|------------------------------|--------|------------------------------|------------------------------|--------|--------|
| 0.005   | 300                         | 0.382                        | 71.4   | 3.427                        | 2.321                        | 167.1  | 73.3   |
|         | 200                         | 0.487                        | 89.6   | 5.419                        | 3.618                        | 165.6  | 69.8   |
|         | 100                         | 0.860                        | 247.1  | 11.815                       | 8.150                        | 152.5  | 84.0   |
|         | 50                          | 0.828                        | 182.5  | 13.597                       | 6.849                        | 255.6  | 74.5   |
|         | ≤30                         | 1.252                        | 338.2  | 23.687                       | 12.200                       | 244.0  | 80.0   |
| 0.001   | 300                         | 0.684                        | 124.8  | 2.248                        | 1.311                        | 233.3  | 49.8   |
|         | 200                         | 0.887                        | 174.8  | 3.620                        | 2.179                        | 210.9  | 69.8   |
|         | 100                         | 1.454                        | 317.7  | 9.043                        | 6.068                        | 166.5  | 80.8   |
|         | 50                          | 1.646                        | 268.2  | 12.050                       | 6.342                        | 263.9  | 80.3   |
|         | ≤30                         | 2.203                        | 361.7  | 17.623                       | 6.304                        | 267.2  | 51.0   |
| 0.0002  | 300                         | 1.213                        | 322.5  | 2.114                        | 1.198                        | 292.3  | 20.1   |
|         | 200                         | 1.592                        | 401.3  | 3.177                        | 1.803                        | 277.0  | 37.0   |
|         | 100                         | 2.527                        | 561.8  | 6.385                        | 3.657                        | 245.4  | 47.9   |
|         | 50                          | 3.171                        | 515.2  | 9.801                        | 4.932                        | 355.6  | 76.0   |
|         | ≤30                         | 4.459                        | 724.4  | 13.780                       | 6.934                        | 355.6  | 76.0   |

## REFERENCES

- [1] Guo-qiang Li, Yong Du, Analyses the parameters of fire temperature elevation at the top of large space buildings, *Fire Science and Technology* (in chinese)2005; Vol.24 No.1:19-21
- [2] Yong Du, Guo-qiang Li, Fire radiation effect on steel member at elevated temperature in large space fire, *Fire Safety Science* (in chinese) 2006; Vol.15 No.4:189-199
- [3] Yong Du, Guo-qiang Li, Utility temperature elevation empirical formula in large space fire, *Fire Science and Technology* (in chinese)2005; Vol.24 No.3:283-287
- [4] National Institute of Standards for Engineering, *Technical code for fire safety of steel structures in buildings, CECS 200: 2006 China*
- [5] Yong Du, Guo-qiang Li, Simplified algorithm of steel members at elevated temperature in large space fire based on field model, *Fire Science and Technology* (in chinese)2006; Vol.25 No.3:299-303

## **APPLICATION OF STRUCTURAL FIRE DESIGN TO STEEL BUILDINGS New Zealand Experience 1986 to 2008**

Martin Feeney <sup>a</sup> and G Charles Clifton <sup>b</sup>

<sup>a</sup> Senior Fire Engineer and Principal, Holmes Fire & Safety, Auckland, New Zealand.

<sup>b</sup> Associate Professor of Civil Engineering, Department of Civil and Environmental Engineering, University of Auckland, Auckland, New Zealand.

### **INTRODUCTION**

This paper outlines the application of structural fire design to apartment buildings, hotels, shopping centres, grandstands, offices and parking buildings in New Zealand since the introduction of a performance based Building Control System in 1992, through a series of case studies illustrating the various design approaches and bases for regulatory approval.

New Zealand's long-standing requirements for seismic design and detailing, which require steel structures to withstand inelastic demand without failure, mean that these structures have a dependable ability to redistribute load when heated during a severe fire. This ability has been exploited in the development of structural fire engineering solutions for steel framed buildings. This has been supplemented more recently by design procedures developed from research focussed specifically on experimental testing of structures exposed to fire.

The processes for regulatory approval are also covered in the case studies. This aspect of the process has highlighted the importance of education for the authority having jurisdiction. Comments on this part of the process are also included in the paper.

### **1. HISTORY OF BUILDING REGULATORY CONTROLS AFFECTING FIRE SAFETY**

Prior to the introduction of the performance-based building control system in 1992, building fire safety in New Zealand was controlled by a prescriptive Model Building Bylaw NZS1900 Chapter 5 [1]. The Standard prescribed a specific and simplistic solution that took no account of performance of structures or materials in fire. This regulatory approach was used in most parts of the world at the time, as there were no accepted calculation methods available.

In 1992, the Model Building Bylaws were all replaced with a fully performance based Building Control System (BCS) as regulated by the 1992 (since revised in 2004) Building Act and the current national Building Code [2]. The NZ Building Code specifies mandatory functional requirements and performance criteria, but these may be achieved by any means. A prescriptive fire safety Compliance Document is available, produced by the Department of Building and Housing (the relevant Government department). This provides designers with one option for a solution which is deemed to comply with the Building Code, but is non-mandatory. Alternative solutions using other performance verification methods can be used. Routine fire safety design for most buildings is undertaken in accordance with the Compliance Document.

### **2. DEVELOPMENT OF ANALYSIS AND DESIGN METHODS FOR STRUCTURAL FIRE ENGINEERING**

A consequence of the lack of flexibility characterised in the traditional prescriptive approach to structural fire design was a two stage design process: structure design and then subsequently ensuring adequate fire resistance were carried out as two separate activities. Structures were analysed and

designed to withstand all other environmental loads and effects, using whatever materials and methods considered appropriate for each specific case, but for structural fire safety the only solutions available were construction in concrete, or applied insulative fire protection of the structure. For example, the Standard [1] prescribed that “internal columns and main beams supporting concrete floors...shall be of concrete or masonry..(or)..other materials when the equivalent fire resistance rating is provided by the use of protective material”.

The 1992 performance based Building Control System offered the option of quantifying the expected fire severity (fire threat) on an individual building basis, subject to knowing the building use (hence fire load energy density) and characteristics such as firecell geometry and features of the external walls. Although some calculations can be carried out, the most common simplified design approach is still semi-prescriptive, as the method itself and the range of values used as input parameters are tightly constrained. The assessment of structure performance is also most commonly done with reference to individual structural element/member fire resistance as measured by the standard fire test eg. ISO 834 [3]. Structure fire safety solutions derived in this way almost always use externally applied fire protection to achieve the calculated fire resistance rating.

Since 1996, more advanced analyses have based fire exposure on natural fires (not the time-temperature curve used in the Standard Fire test) eg. the parametric fire curve described in Eurocode ENV 1991-2-2 [4]. While the fire time-temperature equations are a function of many of the same variables as simpler methods, such as firecell geometry, fire load, external ventilation area, etc. the fire curve includes a cooling phase. Maximum steel temperatures in fire depend on duration of the heating phase. For some steel structures, in which the fire load is low and ventilation conditions good, or the building is sprinkler protected, adequate performance is achieved without externally applied fire protection as the fire temperature does not increase indefinitely (as it does in the standard fire test). Assessment of limiting temperature hence period of structural adequacy takes into account the reduced likelihood of maximum effect from other loads occurring during a fire [5]. Although performance is assessed on an individual structural element basis, in some cases a nominal level of inelastic structure behaviour has been included in the assessment of member capacity eg. partial moment capacity from simple (pinned) end connections.

Building on work by Bailey [6], Lim [7] and others, the HERA Slab Panel Method [8] (based on the tensile membrane model of Bailey [6]) was released in 2006. This HERA method is the result of New Zealand experimental and theoretical research programme as well as overseas research and testing. It applies to steel framed buildings with composite concrete floors and for structural members which may be subjected to high temperatures, considerable inelastic demand and large deformation of the floor system. A dependable proportion of the additional reserve of strength available from the structure when the floor system undergoes large deformation is included in the structure assessment. This consideration of three dimensional structure behaviour goes beyond an assessment which considers only individual structural elements basis and strength contribution from one material (steel) and provides a much better understanding of overall behaviour of steel structures in fire. In special circumstances, 3D finite element modelling of structure sub-assemblages with partial fire protection has been carried out [9].

### **3. CASE STUDIES**

Open-sided steel carpark buildings, which have low fire load and are well ventilated, in effect being a firecell (the car) within a firecell, have been constructed without passive fire protection since 1986. Approval under the earlier prescriptive Building Code requirements was achieved with detailed submissions to the approving authority referring to results of full scale experimental tests and citing

overseas design recommendations. Since 1992, under the performance based Building Control System, enclosed sprinklered carparks have also been designed with unprotected steel structure. Studies of sprinkler reliability and more recent full scale experimental test results have been referenced to support the design basis. Quantitative analysis methods include calculation of fire effects using measured car fire heat release rates and assessment of steel structure stability using limiting temperature concepts.

Apartment and hotel buildings in New Zealand are characterised by low fire load, a high degree of internal compartmentation, relatively small firecell area and moderate to high levels of external glazing. Accordingly, the structural fire severity in these types of buildings is usually very low and with the high compartment into multiple firecells on each floor, the extent of structure influenced by a fully developed fire in one firecell is limited to only part of a floor.

Most of these multi-storey accommodation buildings are sprinklered, because of trade-offs permitted by the fire safety compliance document for non-structural aspects of fire safety. A natural fire concept has been applied to a number of steel framed buildings (since 1996, [10]) in conjunction with an analysis of the limiting steel temperatures for steel beams, to determine which structural elements remain stable with no passive fire protection and those which need applied fire protection. Beam design is based on assessment of the period of structural adequacy of individual members in the standard fire test, in accordance with the current Steel Structures Standard, NZS 3404 [11]. Steel columns are almost invariably concealed with fire protection materials.

In some apartment and hotel buildings where a plasterboard ceiling is required for Building Code compliance for non-fire safety reasons (eg. acoustic separation between floors), the effectiveness of the ceiling as a radiation shield has been included in the analyses. Performance of the ceiling in fire conditions has been determined from a series of natural fire tests [12] and further supported by observations of performance of the same types of ceiling assembly in standard furnace tests.

Another category of building types that have been the subject of performance based structural fire engineering are large, low rise, public assembly buildings in which the occupants are awake, alert, and predominantly ambulant and in many cases familiar with their immediate environment. Examples include shopping centres, conference facilities, grandstands, stadia and low rise office buildings. Where there is no requirement for structure to remain stable to protect other property, structure performance criteria relate to safety of occupants while escaping and protection of fire fighters. Fire design for life safety usually requires high capacity escape routes for short evacuation time, or else the building covers a large plan area so that performance of structure impacts only a small area of the building. These buildings are also usually sprinklered because of their large firecell area and high occupant load, and to take advantage of trade-offs that benefit occupant safety. Structure design for these buildings has applied a natural fire concept to compare on a time line the 'real time' at which fire conditions threaten structure stability (assuming sprinklers do not operate) with the time required for safe egress. A conservative safety margin has been applied to account for uncertainty in predicting fire effects. In most cases the regulators have also requested an assessment of 'equivalent time' fire resistance ratings to benchmark against more familiar prescriptive requirements. This approach is similar to that proposed in Australia [13, 14]. Performance based structure design has been applied in New Zealand to these types of buildings since 1998.

High rise office buildings present a more complex challenge for structural fire engineering. These buildings are characterised by medium level fire load energy density, firecell area ranging from small to large, firecell ventilation ranging from minimal to highly ventilated and occupant egress times that are often in the range 30 to 60 minutes after an emergency is declared. Understanding actual structure performance in fire is important because of the potentially disastrous consequences of overall structure

instability, even when full compliance is achieved for Building Code approval with a deemed to comply prescriptive solution. The actual duration of exposure to severe fire is often long when compared with fire resistance ratings based on exposure to the standard fire test. Also, modes of structure failure that are not apparent from individual element furnace tests have an influence on overall structure behaviour.

Because of the magnitude and variability of fire severity for this type of occupancy, assessment of the impact of a natural fire on structure stability based on performance of individual members in the standard fire test is neither sufficiently conservative nor accurate to assess whole structure performance with partial fire protection. For these buildings, the design approach considers 3D structure performance when exposed to elevated temperatures. The HERA Slab Panel Method has been used to assess performance in fire with partial structure protection (some beams not protected; all columns protected at office levels) for at least three recent high rise office buildings in Auckland. For one of these buildings 3D finite element analysis was used to model non-typical parts of the structure (slender cellular beams and large capacity seismic dominated frames) which did not fit within typical structure parameters assumed for the Slab Panel Method. Time-temperature relationships for these finite element analyses considered equivalent time fire resistance (the standard fire test) as prescribed by the non-mandatory Compliance Document and also natural fire time-temperature profiles.

Most of the new office buildings assessed to date have had extensive area of external walls with curtain wall glazing, providing a high floor area to ventilation area ratio and lower fire severity. Sensitivity analyses have been undertaken varying the ventilation area from 50% to 100% of the actual glazed area to gauge the effect this would have on structure performance when subjected to natural fires. The prescriptive solution assumes 100% of glazed wall area contributes to effective fire ventilation.

A consequence of this more complex design optimisation approach to assess the extent where fire protection provides no real benefit to structure performance is a requirement for more thorough on-site inspection of applied fire protection. The building constructor and fire protection applicator need greater quality control to ensure that the specification for structure fire protection is correctly interpreted and implemented. Not all contractors are prepared for this increased demand on their on-site resources.

For existing buildings, the NZ Building Control System allows for compliance with the Building Code performance requirements to be 'the same as a new building as nearly as is reasonably practicable'. This allows the particular circumstances for each building to be taken into account when assessing the extent of compliance. A first-principles approach concentrating on the objectives and functional requirements of the Building Code has provided more flexibility in design approach.

For example, where asbestos-based fire protection material needs to be removed for public health reasons or where the structure of an historic building cannot be easily insulated with fire protection in the usual way, then other factors have been considered to compensate for the constraints associated with the existing construction. For office buildings this has included a comparison with performance outcomes from experimental testing [15] where structure and firecell details are similar. In other cases, where existing unsprinklered buildings have had sprinkler systems installed to improve occupant life safety, an improvement in the reliability of the sprinkler system (which reduces the likelihood of the fire threatening structure stability) has been accepted as compensation for not being able to provide formal certification of fire resistance rating of existing fire protection materials. By necessity these judgements of compliance for existing buildings are frequently qualitative.

#### **4. STRUCTURE REQUIRING SPECIAL CONSIDERATION**

Special structural elements such as load transfer beams, transfer trusses, slender columns or any other part of structure whose deformation or collapse during a fire would result in a disproportionate extent of damage or collapse are designed with greater caution, and usually receive insulative fire protection, even if the strength of the member is sufficient without it. This applies particularly to structural elements which could endanger fire fighters located in other firecells during fire fighting operations (eg. columns supporting large areas of roof in buildings without open plan internal layout).

The more sophisticated 3D modelling of structure behaviour in fire has highlighted the importance of structure robustness, rather than strength at elevated temperature, which is likely to be the dominant feature characterising adequate performance. While adequate strength at elevated temperature is necessary, in design it is unwise to assume that it is sufficient. To date, excessive reliance is still placed on a semi-prescriptive calculation of equivalent fire rating (required fire resistance). But in natural fires, as our understanding of modes of failure in fire improves, the cooling phase arguably becomes more important to more accurately determine where and how structural failure might occur. Careful structural detailing to accommodate inelastic demand assumes greater importance than an analysis concentrating on performance of a structure ‘heated’ to failure.

#### **5. EXPERIENCE WITH REGULATORY REVIEW AND APPROVAL**

The change to performance based Building Codes and advances in structural fire engineering analysis that have occurred over the last 15 years now provide different solutions in many to those that have become familiar from prescriptive approaches. The knowledge gap between building control officials more familiar with historical designs and structural fire engineers proposing the new methods is wider than ever. The necessary level of expertise is not available within the authorities with jurisdiction for building approvals. It is no longer sufficient just to understand the impact of fire effects, or simple elemental response to standard fire tests. The assessment of adequacy of structural fire designs requires greater reliance on independent peer review. This has been the experience in New Zealand. However, even the level of understanding within the regulatory organisations that is necessary to identify the need for peer review varies widely across the country.

Accordingly where there is a lack of full understanding there is greater suspicion of the adequacy of the outcome – especially where a solution is different to that produced by historical approaches. Confusion also arises between the meaning of ‘equivalent time’ such as the period of structural adequacy (measured with reference to performance in the standard fire test) and ‘real’ time relating to fire development or occupant evacuation time or Fire Service response time. The difference between fire protection (usually applied insulative coatings or concealment) and fire resistance – a measure of a structure or member’s ability to resist fire effects is still a common misunderstanding.

Misconceptions about performance of various structural materials in fire (steel, concrete and timber) are still widespread. Structures provided with traditional solutions for insulative fire protection are usually assumed by regulators to be immune from the effects of fire, and structures without such protection are therefore regarded as highly vulnerable. It is of interest to note that 3D finite element analyses for natural fire exposure which compared the performance of partially protected structure with fully protected structure [9] showed better performance with partial fire protection. The structure with full fire protection exhibited a much less desirable potential failure mode for the same fire exposure.

## 6. IMPLEMENTATION INTO THE STEEL STRUCTURES STANDARD

The current Steel Structures Standard [11] provides only a simplistic and element based approach to the design for fire, as this material was written for application under the previous prescriptive based system. This is one reason for the problems with the regulatory approval process described in the previous section.

A complete revision of this standard commenced late in 2008 and the design provisions for fire are to be presented in an expanded new stand-alone part, which will incorporate the steel based fire engineering design methods described above directly into the Standard as an Approved Document means of compliance with the NZ Building Code [2]. An outline of this amended part has been produced and it is expected to be released for public comment towards the end of 2009.

## REFERENCES

- [1] NZS 1900 Chapter 5 Model Building Bylaw: Fire, Standards New Zealand, Wellington, NZ
- [2] New Zealand Building Code, 1992, Department of Building and Housing, Wellington, NZ
- [3] ISO 834, (1975), Fire resistance tests – elements of building construction, International Organisation for Standardisation, Geneva, Switzerland
- [4] ENV 1991-2-2:1995, (1995), Eurocode 1: Basis of Design and Actions on Structures, Part 2.2 Actions on Structures Exposed to Fire, British Standards Institution, London, England.
- [5] NZS 4203, (1992), Code of Practice for General Structural Design and Design Loadings for Buildings, Standards New Zealand, Wellington, New Zealand.
- [6] Bailey, C. G. (2000). Design of steel members with composite slabs at the fire limit state, Building Research Establishment, United Kingdom
- [7] Lim, L. (2003). Membrane Action in Fire Exposed Concrete Floor Systems, Fire Engineering Research Report 03/02. Dept of Civil Engineering, University of Canterbury, Christchurch, New Zealand
- [8] Clifton, G.C., (2006), Slab Panel Method – Design of composite steel floor systems for severe fires, 3rd Edition, HERA Report R4-131, Heavy Engineering Research Association, Manukau City, New Zealand.
- [9] Feeney, M.J., Clifton, G.C. and Mago, N., (2008), Dependable Performance of Steel Structures in Fire – The Britomart East Office Building, *Structures in Fire Conference 08*, Singapore.
- [10] Feeney, M.J., (1998), Design of Steel Framed Apartment and Hotel Buildings for Fire, Proceedings 1998 *Australasian Structural Engineering Conference, Auckland*, Vol. 2, pp 563-570, New Zealand Structural Engineering Society, Auckland, New Zealand
- [11] NZS 3404:1997 Steel Structures Standard, incorporating Amendment No 1:2001 and No 2:2007, Standards New Zealand, Wellington, New Zealand
- [12] Brown, N.C., (2005), Steelwork Partially Protected from Post-Flashover Fires in Gib@Board Lined Compartments: Research Proposal for ME (Fire) Thesis, Dept of Civil Engineering, University of Canterbury, Christchurch, New Zealand.
- [13] Bennetts, I.D., Poh, K.W., Poon, S.L., Thomas, I.R., Lee, A.C., Beever, P.F., Ramsay, G.C. and Timms, G.R., (1998), Fire Safety In Shopping Centres, Final Research Report Project 6, Fire Code Reform Centre Ltd, Sydney, Australia
- [14] Bennetts, I.D., Goh, C. C., Thomas, I.R. and Poh, K.W. (2000), Low Rise Office Construction - A Guide to Fire Safety, One Steel Market Mills, Newcastle, Australia
- [15] Thomas, I.R., Bennetts, I.D., Poon, S.L., and Sims, J.A, (1992), *The Effect of Fire in the Building at 140 William Street*, BHP/ENG/R/92/044/SG2C, BHP Research, Melbourne, Australia

## INFLUENCE OF FIRE ON STEEL BRIDGE Over Vistula River In Puławy

Grzegorz Głuch <sup>a</sup>

<sup>a</sup> Wrocław University of Technology, Institute of Civil Engineering, Wrocław, Poland

### INTRODUCTION

The conclusion from the traffic studies shows that the probability of fire in the area of bridge is relatively low. However, the importance of bridge structures, as a parts of road and transportation systems, for local economy and industry is significant. Damaged bridges are usually hard to detour and affect traffic quality in the region. It seems to be reasonable to consider the fire danger of bridges during design process, especially for structures along main roads and highways.

Although bridges are usually made of flame resist materials, traffic accidents can lead to fire develop, Fig 2.. High temperatures occurring during fires, cause additional stresses and thermal strains in structure [1, 2]. Steel is one of the most popular materials in civil engineering, the world's biggest bridges are made of steel. Unfortunately it is very sensitive to high temperatures, it's loads capacity is decreasing in fire's conditions. It can result in damage of bridge elements or, in case of large fires, the structure may even collapse, Fig. 1.

In extreme cases the bridge equipment, as a plastic cover of suspension system or paint on the steel elements, may begin to burn. The bridge fires cause usually no human casualties but the costs of bridge repair or road close due to fire damage are significant and highly disturb traffic in the area.



*Fig. 1.* Bridge collapsed after fire [12]



*Fig. 2.* Fire on the Big Four Bridge [13]

Fires are uneasy to modelling due to the complexity of the phenomena, the number of physical and chemical processes involved in combustion and the size of structure subjected to fire. In case of buildings and industry facilities fire engineering is well developed [7, 8, 9]. Unfortunately fires in open space, as on the bridges, are more difficult to simulate and analyse because of atmospheric and terrain influence on model.

The paper presents the algorithm for estimation the temperature of the suspended bridge when fire appears on deck. As an example the new build steel arch bridge over Vistula river in Puławy was analysed. The main span of bridge is 212m long, deck is suspended to two steel arches by the 28 hangers. The arch is a box in cross section. Each hanger is build from 4 steel bars, 82 mm in diameter. The deck is composed with concrete slab and steel grill. It was assumed the temperature, caused by the fire, affects only elements above deck as arch elements and suspension cables. The other issues are fires under bridges, especially in case of girders bridges, where main structure elements ale located below the deck.

## FIRE SIMULATIONS ON THE BRIDGE

There are many mathematical models describing fires in civil engineering structures. Most of them are prepared for fires in closed area of rooms in buildings [7, 8, 9]. Only several models can be used in open space [10, 11] for example to simulate bridge's fires. Complex geometry of bridge and the surrounding terrain can be modelled with use of CFD, the algorithm based on fluid dynamics. The computation space is divided in to finite volumes and for each volume algorithm solves system of differential equations of mass, momentum, energy conservation and the equation of state (1) [8]:

$$\begin{aligned} \frac{\partial \rho}{\partial t} + \nabla \rho u &= 0 \\ \frac{\partial}{\partial t}(\rho u) + \nabla \rho u u + \nabla p &= \rho f + \nabla \tau_{ij} \\ \frac{\partial}{\partial t}(\rho h) + \nabla \rho h u + \nabla p &= \frac{Dp}{Dt} + \dot{q}''' - \nabla q + \Phi \\ p &= \frac{\rho RT}{M} \end{aligned} \quad (1)$$

where unknowns are:  $\rho$  – fluid density,  $u$  – fluid velocity vector,  $T$  – temperature,  $p$  – pressure. All functions depend on space coordinates and time. As the result of simulations various information can be received, including the temperature of elements contained in computation domain. The received temperatures of the bridge elements can be written as:

$$t_i = \{T_d^i, T_z^i, T_g^i, T_w^i\} \quad (2)$$

where  $t_i$  – temperature of element  $i$  exposed to fire,

$T_d, T_z, T_g, T_w$  – temperatures in element's cross section, as in Fig. 3

When the fire affects more then one bridge element, temperature can be presented as a vector:

$$T = col\{t_1, \dots, t_i, \dots, t_k\} \quad (3)$$

where  $k$  – number of elements exposed to high temperature.

The temperature  $t_i$ , as in (2), can be transformed into thermal loads for structure (4). Transformation rules are placed in [4].

$$d_i = \{\Delta t_i, \delta t_z^i, \delta t_y^i\} \quad (4)$$

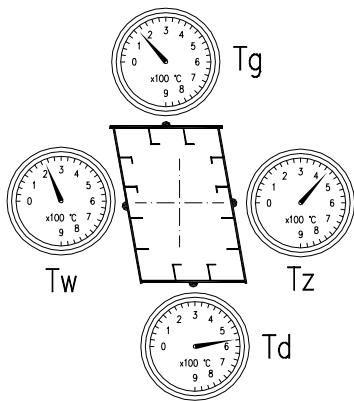


Fig. 3. Temperature of bridge element

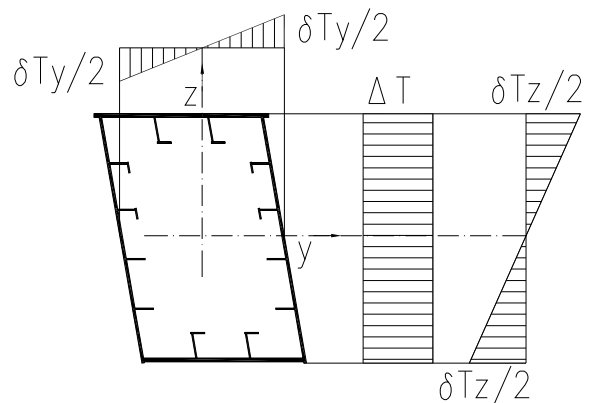


Fig. 4. Thermal loads

Forces, as shown in Fig 8 and in equations (5), cause deformation of whole bridge structure, also the element  $e$ , which deformed shape is presented in Fig 9. Displacement on direction of any force, as in Fig. 9 is equivalent to stresses in element  $E$  as in (6), it is the direct result form definition of influence function.

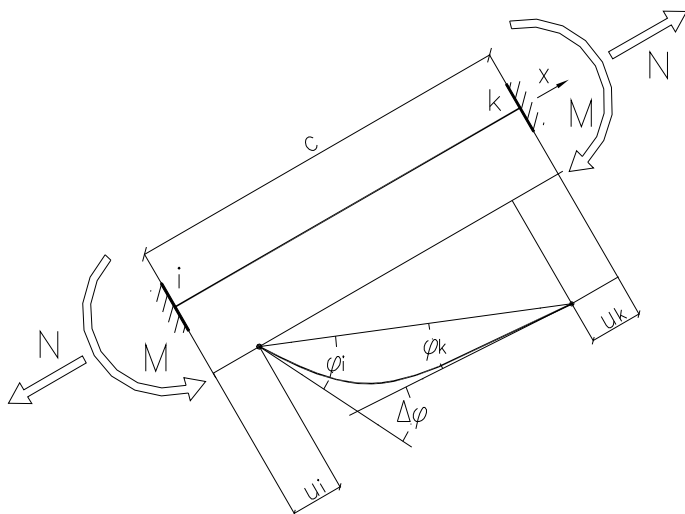


Fig. 9. Deformed bridge element

$$S_u = \frac{EA}{a} \cdot \frac{1}{A} = \frac{E}{A} \quad (5)$$

$$S_\varphi = \frac{EJ}{a} \cdot \frac{v}{J} = \frac{Ev}{a}$$

where

$a$  – length of element  $E$ ,  
 $A$  – cross section of element  $E$ ,  
 $E$  – elasticity modulus,  
 $J$  – moment of inertia,  
 $v$  – half of cross section height.

$$\sigma_u = N \cdot \Delta c_{ik} \quad (6)$$

$$\sigma_\varphi = M \cdot \Delta \varphi$$

The length change  $\Delta c_{ik}$  of element  $e$  (7) corresponds with the normal stress in element  $E$  generated by axial force  $N$ , as in Fig. 9. The angle between tangents  $\Delta \varphi$  (7) corresponds with the normal stress in element  $E$  generated by bending moments  $M$ , as in Fig. 9.

$$\Delta c_{ik} = u_i - u_k \quad (7)$$

$$\Delta \varphi = \varphi_i + \varphi_k$$

where

$u_i, u_k$  – displacement of nodes  $i, k$  of element  $e$  in  $x$  direction,  
 $\varphi_i, \varphi_k$  – rotations of nodes  $i, k$  of element  $e$ .

The element's  $e$  length change  $\Delta c_{ik}$  can be caused by axial force  $N$  or by temperature change  $\Delta t$ :

$$\Delta c(\Delta t)_{ik} = \alpha \cdot \Delta t \cdot c_{ik}$$

$$\Delta c(N)_{ik} = \frac{N}{EA_{ik}} \cdot c_{ik} \quad (8)$$

$$\Delta c(\Delta t)_{ik} = \Delta c(N)_{ik} \Rightarrow N = \alpha \cdot EA_{ik} \cdot \Delta t$$

Analyses were carried out for new build steel arch bridge over Vistula river in Puławy [3]. The truck fire on the bridge deck was assumed as a heat source. During simulations truck was stopped. Different fire powers were considered. HRR curve shape was assumed according to [5]. The influence of high temperature on construction elements below deck was neglect, because of high thermal capacity of concrete slab. Fires were placed in 30 locations on the deck and temperature were calculated in 76 points on the steel arch. Example results are presented below. Figure 5 shows the temperature of suspension cable versus time and distance from the fire. The highest value of temperature  $T=470\text{ }^{\circ}\text{C}$  is significant for the bridge safety. Figure 6 shows temperature of arch element versus time. The influence of fire on the different sides of box cross section is various. Temperature of top and inner side reaches value of  $250\text{ }^{\circ}\text{C}$ , and other sides are practically in ambient temperature. The inequality of temperatures on bottom, outer, top and inner sides of arch cross section generates bending moments.

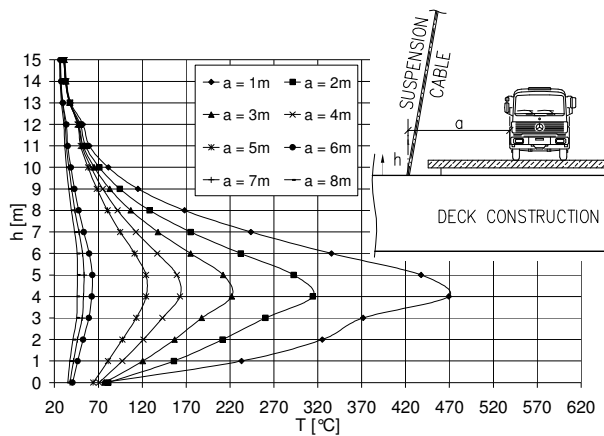


Fig. 5. Hanger temperature

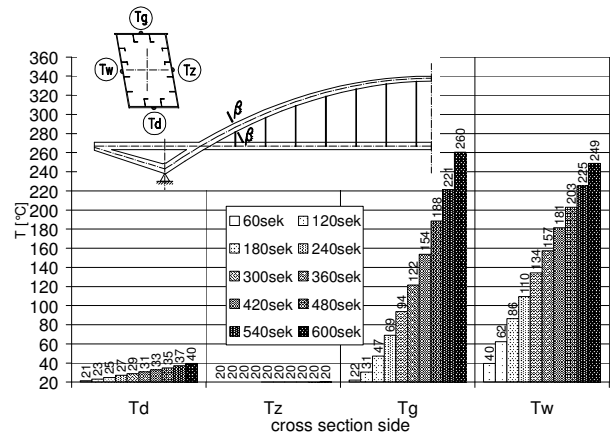


Fig. 6. Temperature of arch's cross section

## THERMAL INFLUENCE FUNCTIONS

The scheme of analysed bridge and the example locations of elements  $E$  and  $e$  are shown in Fig. 7. Stresses are analysed in element  $E$ , heat is acting on element  $e$ . Bridge's elements  $e$ , exposed to fire influence, are subjected to high temperatures and are being heated. The differences of the temperature of structure generate thermal stresses in element  $E$ . However size of fire is usually smaller than the bridges and it can be located in various places on bridge deck. When the most dangerous location of fire, for the stresses in element  $E$ , is known, it makes the analyses faster and easier because the only one location of fire could be simulated. To find such a location the influence function and kinematical excitations for stresses [6], as in (5) and in Fig 8, can be used.

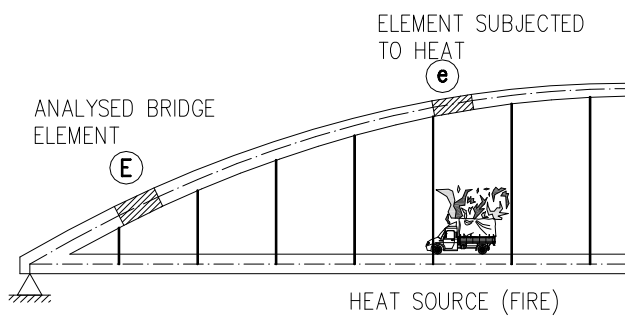


Fig. 7. Fire on the bridge scheme

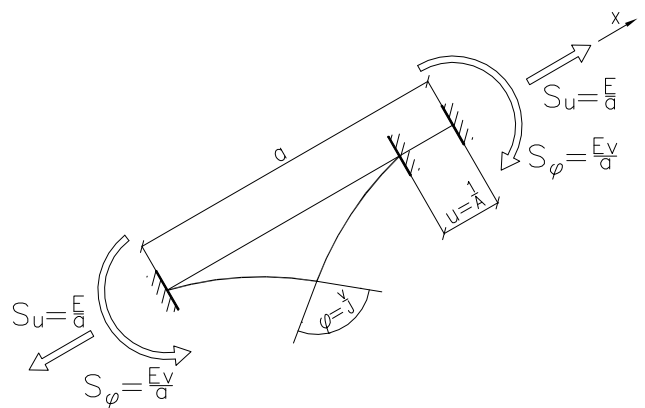


Fig. 8. Kinematical stress excitation

Finally the stresses in element  $E$  (6) generated by temperature change  $\Delta t$  can be written as:

$$\sigma_u = \alpha \cdot EA_{ik} \cdot \Delta c_{ik} \cdot \Delta t \quad (9)$$

The angle between tangents  $\Delta\varphi$  can be caused by bending moments  $M$  or by temperature  $\delta t$ :

$$\Delta\varphi(\delta t)_{ik} = \frac{\alpha \cdot \delta t \cdot c_{ik}}{h_{ik}}$$

$$\Delta\varphi(M)_{ik} = \frac{M}{EJ_{ik}} \cdot c_{ik} \quad (10)$$

$$\Delta\varphi(\delta t)_{ik} = \Delta\varphi(M)_{ik} \Rightarrow M = \frac{\alpha \cdot EJ_{ik}}{h_{ik}} \cdot \delta t$$

Eventually the stresses in element  $E$  (6) generated by temperature  $\delta t$  can be written as:

$$\sigma_\varphi = \frac{\Delta\varphi_{ik} \cdot \alpha \cdot EJ_{ik}}{h_{ik}} \cdot \delta t \quad (11)$$

If the temperatures  $\Delta t$  and  $\delta t$  work in element  $e$  simultaneously the stress in element  $E$  is the sum of components generated by  $\Delta t$  and  $\delta t$ :

$$\sigma = \sigma_u + \sigma_\varphi$$

$$\sigma = \alpha EA \Delta c_{ik} \cdot \Delta t + \frac{\Delta\varphi_{ik} \alpha EJ_{ik}}{h_{ik}} \cdot \delta t \quad (12)$$

When more than one element  $E$  is analysed and temperature acts on more than one element  $e$ , the equation in (12) becomes a matrix equation:

$$s = I_\Delta \cdot \Delta t + I_\delta \cdot \delta t \quad (13)$$

Vectors  $I_\Delta$  and  $I_\delta$  in (13) are the thermal influence vectors and can be used to locate most dangerous fires location for stresses in analysed bridge element  $E$ . Influence vectors are shown below, the  $\beta$  cross section of arch was chosen as an example:

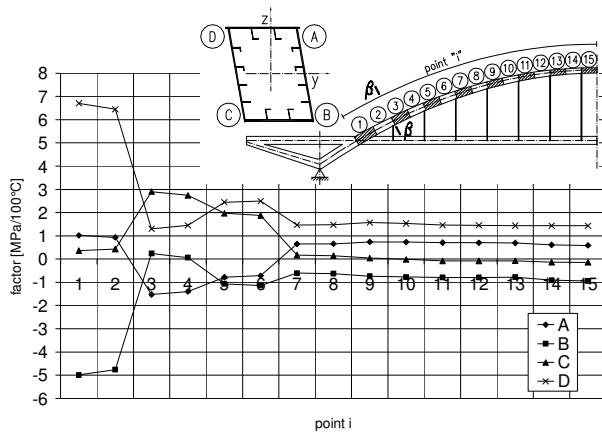


Fig. 10. Thermal influence vector  $I_\Delta$

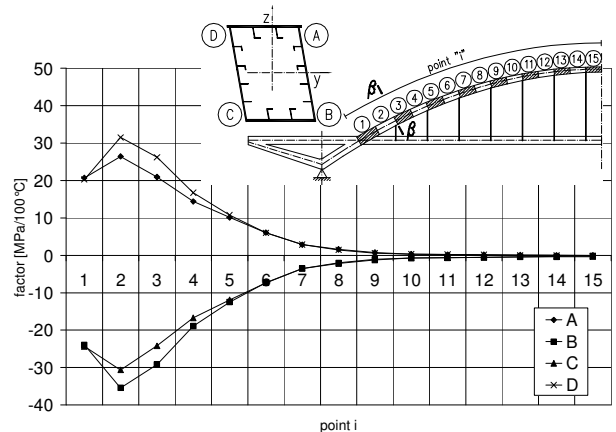


Fig. 11. Thermal influence vector  $I_\delta$

## BRIDGE SAFETY ESTIMATION

To estimate bridge safety the  $\mu$  coefficient (14) was proposed. This parameter compares thermal stresses with the stresses generated by the live loads in analysed element  $E$ . Live loads match the class A loads from polish design code for bridges.

$$\mu = \frac{\sigma(T)}{\sigma(P)} \quad (14)$$

If  $\mu < 1$  safety of the bridge is preserved, values of thermal stresses are lower than live loads stresses. If  $\mu > 1$  the thermal stresses in arch elements exceed stresses generated by live loads. If  $\mu > 1$  thermal stresses can lead to bridge's elements or equipment damage. For example, if  $\mu = 3,03$  the thermal stress is three times greater than live loads stress. As shown in *Table 1*, fires with 30 MW peak HRR are not hazardous for analysed bridge. However 120 MW peak HRR fire generate dangerous thermal stresses in bridge structure.

*Table 1.* Values of  $\mu$  coefficient

| distance from deck edge to fire [m] | Peak HRR      |          |          |            |               |          |          |            |
|-------------------------------------|---------------|----------|----------|------------|---------------|----------|----------|------------|
|                                     | 30 MW         |          |          |            | 120 MW        |          |          |            |
|                                     | cross section |          |          |            | cross section |          |          |            |
|                                     | $\beta$       | $\gamma$ | $\delta$ | $\epsilon$ | $\beta$       | $\gamma$ | $\delta$ | $\epsilon$ |
| 2,40                                | 3,03          | 0,51     | 0,34     | 0,44       | 7,31          | 3,28     | 3,26     | 4,41       |
| 5,70                                | 1,23          | 0,46     | 0,31     | 0,40       | 2,80          | 2,08     | 1,96     | 2,75       |
| 9,00                                | 0,67          | 0,31     | 0,17     | 0,17       | 1,81          | 1,43     | 1,10     | 1,13       |

Presented algorithm shows the bridge's structure stresses dependence on high temperature generated by fires on the deck. The temperatures during fire reach significant value for bridge safety and should be considered. Use of thermal stress influence functions simplifies the simulations and analyses.

## REFERENCES

- [1] Głuch G., Efekty oddziaływania wysokiej temperatury na dźwigary mostowe, *Zeszyty Naukowe Politechniki Śląskiej. Seria „Budownictwo”*, z. 104, Gliwice 2005.
- [2] Głuch G., Ocena zagrożenia pożarowego mostu łukowego w Puławach, *Wrocławskie Dni Mostowe*, Wrocław 2008.
- [3] Bąk J., Grej K., Oleksiak C., Sałach W., Nowy most przez rzekę Wisłę w Puławach. Wybrane zagadnienia projektowe, *Wrocławskie Dni Mostowe*, Wrocław 2008.
- [4] Biliszczyk J., Machelski Cz., Głuch G., Modelowanie pożaru na moście łukowym w Puławach, *Instytut Inżynierii Lądowej Politechniki Wrocławskiej Raport serii SPR 10/2008*, Wrocław, marzec 2008.
- [5] Schleich J. B., Cajo L. G., Pierre M., Brasseur M., Development of Design Rules for Steel Structures Subjected to Natural Fires in Closed Car Parks, *European Commission*, Luxembourg 1999.
- [6] Machelski Cz., Zastosowanie macierzy wpływu do projektowania kładki podwieszanej, *Inżynieria i Budownictwo*, nr 3-4/2002.
- [7] Mangs J., On the fire dynamics of vehicles and electrical equipment, *VTT Building and Transport Department of Physical Sciences Faculty of Science*, University of Helsinki 2004.
- [8] McGrattan K., Klein B., Hostikka S., Floyd J., Fire Dynamics Simulator (Version 5) User's Guide NIST Special Publication 1019-5 U.S., *Department of Commerce National Institute of Standards and Technology*.
- [9] Yuguang L., Assessment of Vehicle Fires in New Zealand Parking Buildings, *Fire Engineering Research Report 04/2 May 2004*, Department of Civil Engineering University of Canterbury.
- [10] Zobel H., Golubińska A., Symulacja pożaru mostu podwieszanego, *Drogownictwo*, nr 4/2002.
- [11] Zobel H., Golubińska A., Pożary mostów, *Prace IBDiM*, Warszawa 2000.
- [12] [www.vermontbridges.com](http://www.vermontbridges.com)
- [13] [www.google.com](http://www.google.com)

## DESIGN METHOD FOR RESTRAINED STEEL COLUMNS IN FIRE

Guo-Qiang Li<sup>a,b</sup>, Peijun Wang<sup>b</sup>, Yong-Chang Wang<sup>c</sup>

<sup>a</sup> State Key Laboratory for Disaster Reduction in Civil Engineering, No.1239 Siping Road, Shanghai, 200092, China

<sup>b</sup> College of Civil Engineering, Tongji University, Shanghai, 200092, China

<sup>c</sup> School of Mechanical, Aerospace and Civil Engineering, the University of Manchester, PO Box 88, Manchester, M60 1QD, UK

### INTRODUCTION

Present fire resistance design codes [1, 2] are mainly based on isolated structural members, only adopt the design procedure at ambient temperature by using the reduced strength and stiffness of steel at elevated temperatures in fire. In fire situation, design method should consider the interactions among structural members.

Wang [3] presented an advanced design method for axially restrained column under axial load in fire. Huang et al. [4], Neves [5], Valente and Neves [6], and Li et al. [7] proposed different procedures to produce the axial force-temperature curve of a restrained column in fire. All the procedures have similar precision in predicting the failure temperature of restrained columns. The advanced design method is simple compared to the Finite Element Method (FEM). However, for design purpose, it may be necessary to further simplify the problem because the main target of design calculation is to find the buckling and failure temperatures of the restrained column.

Among the efforts that have been made in order to present analytical design formulae for restrained columns in fire, the early contribution presented by CTICM [8] should be highlighted. However, the design method of CTICM [8] did not include the post-buckling phase. Based on a limited numerical study, Franssen [9] found that if the axial restraint ratio was higher than a certain value the failure temperature of a restrained column could not reduce any more with the increase in the axial restraint stiffness ratio. Wang [10] presented a design proposal to consider the effect of structural continuity on behaviours of steel columns in fire. He proposed that there is no need to explicitly consider the effect of axial restraint and rotational restraint to the column in fire. Neves et al. [11] presented a simple method to calculate failure temperatures of restrained steel columns under axial load.

Despite many research results on the design of restrained columns in fire, a method is still necessary for axially and rotationally restrained columns under combined axial load and bending moment.

### 1. DESIGN METHODS FOR RESTRAINED COLUMNS

#### 1.1 Equivalent bending moment factor

When a column is loaded by end bending moments, the maximum bending moment may not occur at the mid-height of the column when the two end bending moments are not the same. On the other hand, for design purpose, the value of the maximum bending moment is more important than its position on the column. The equivalent moment factor,  $\beta_{mx}$ , is used to calculate the maximum bending moment in a simplified way. At ambient temperature,  $\beta_{mx}$  is calculated by [12]:

$$\beta_{mx} = 0.65 - 0.35\alpha_M \quad (1)$$

*Fig.1* shows the maximum bending moments in the restrained column at failure temperature with different end bending moment ratio. It can be seen that the end bending moment ratio has little

effects on the maximum bending moments in the column at failure temperatures.

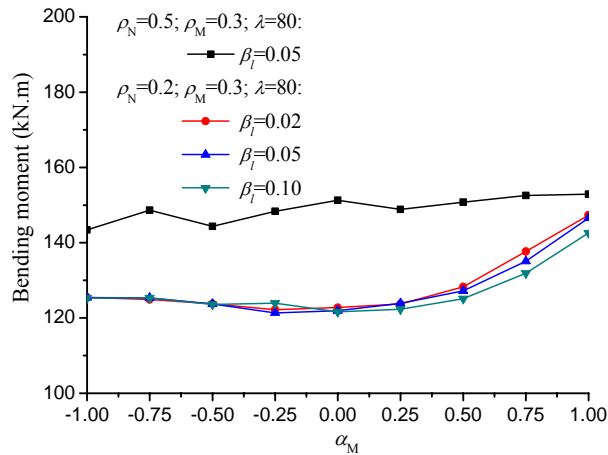


Fig. 1. Maximum bending moments at failure temperature

## 1.2 Structural behaviours of the restrained column

ABAQUS simulations on restrained columns under combined axial load and bending moment were carried out for the following cases: (1) slenderness ratio is 80; (2) axial restraint stiffness ratios 0.02; (3) bending moment load ratio is 0.3; (4) end moment ratio is -1.0; and (5) axial load ratios are 0.1, 0.2, 0.3, 0.4, 0.5, 0.6, 0.7, 0.8, and 0.9.

The simulation results are shown in Fig.2. As shown in Fig.2(a) and Fig.2(b), before the restrained column buckles, the axial force in the restrained column increases linearly and the bending moment changes little. Hence, for determining the buckling temperature of the restrained column, the design equations for the unrestrained column can be used, but with increased column axial load due to restraint thermal expansion. After buckling, the axial force in the restrained column drops, and the bending moment increases. Again, as shown in Fig.1(c) and Fig.1(d), at the column failure the  $N/N_{cr,T}+M/M_{p,T}$  value is greater than 1.0, but the value  $N/N_{u,T}+M/M_{p,T}$  is close to 1.0.

## 1.3 Design method for the buckling temperature

### (1) Design Equations

Before the restrained column buckles, the axial force increases linearly and the bending moment changes little. The design equation is

$$\frac{N}{N_{cr,T}} + \frac{\beta_{mx} M_x}{\gamma_x W_{1x} \left( 1.0 - 0.8 \frac{N}{N'_{EX}} \right)} = 1.0 \quad (2)$$

$$N = P_0 + k_l u_l \quad (3)$$

where,  $\gamma_x$  is the plastic factor of the section.  $W_{1x}$  is the elastic modulus of the cross-section; and  $u_l$  is the displacement of the axial restraint and it is calculated by

$$u_l = \frac{k_c}{k_c + k_l} \left( \varepsilon_{th} l - \frac{P_0}{k_c} + \frac{P_0}{k_{c,0}} \right) \quad (4)$$

The buckling temperature of the restrained column should not be higher than the failure temperature of the unrestrained column.

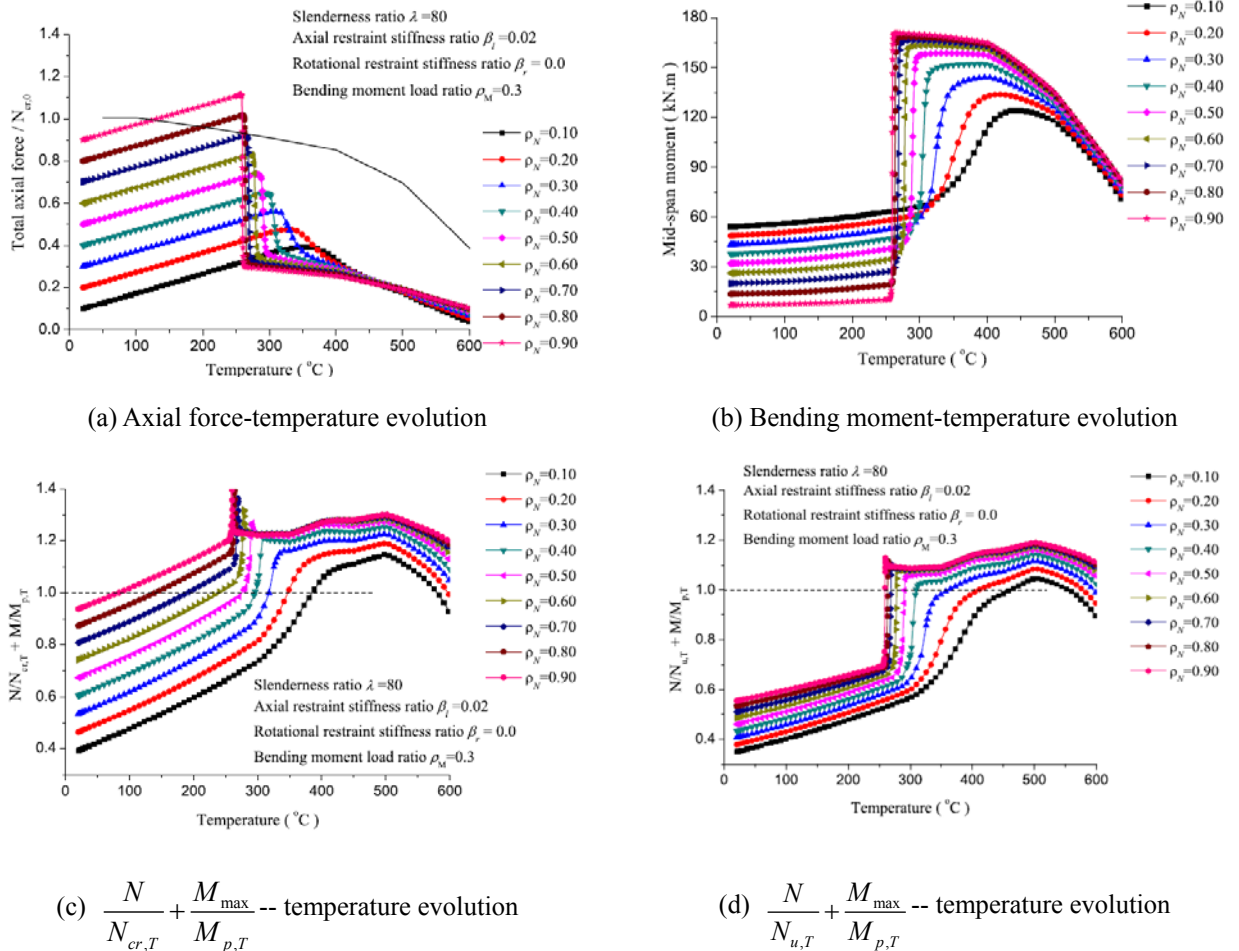


Fig. 2 Behaviours of restrained columns

## (2) Verification of the buckling temperature equation

To check the accuracy of the proposed method, ABAQUS simulations have been run. The simulation results are shown in Fig.3. From Fig.3(a), it can be seen that, for columns with axial restraint stiffness ratio less than 0.05, the buckling temperature predicted by the proposed method is greater than that of ABAQUS by about 80°C. However, for columns with axial restraint stiffness ratio greater than 0.1, the buckling temperature predicted by the proposed method is less than that of ABAQUS by about 50°C. The difference between buckling temperature predicted by ABAQUS and the simplified method becomes greater for columns with bigger bending moment ratio, as shown in Fig.3(a) and Fig.3(b). Again the difference is primarily due to the difference between ABAQUS simulation results and CECS200 calculations of column buckling resistance at high temperature. Fortunately, in practice the initial axial load ratio rarely exceeds 0.6.

### 1.4 Design method for the failure temperature

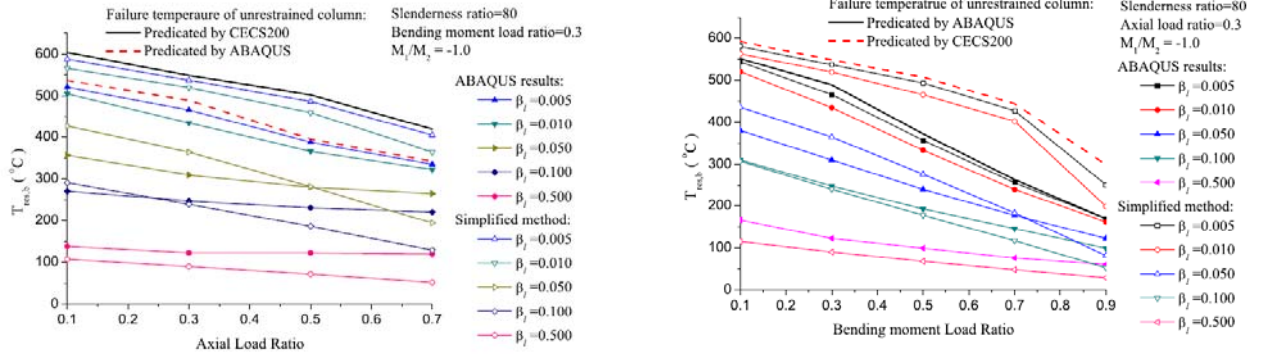
#### (1) Design equations

The design equation for failure temperature of the restrained column is

$$\frac{N}{N_{u,T}} + \frac{N \cdot w + \beta_{mx} M_x}{M_{p,T}} = 1.0 \quad (5)$$

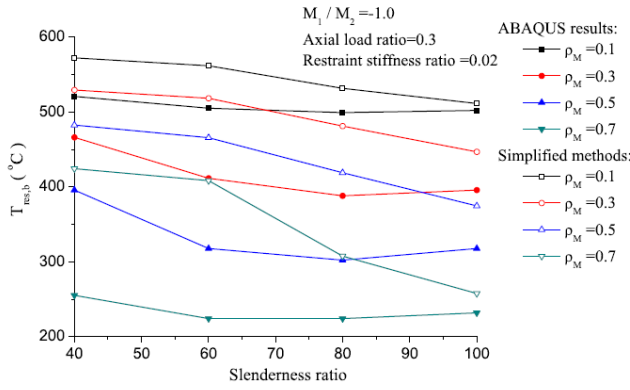
here

$$N = P_0 \quad (6)$$

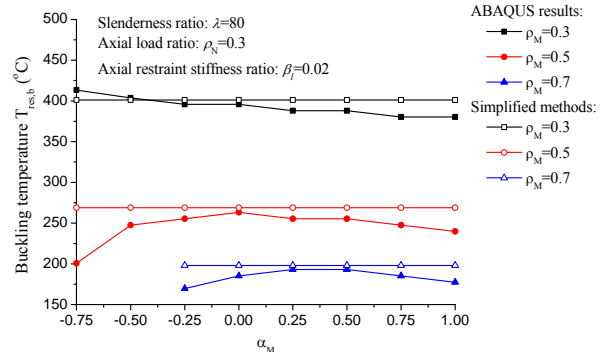


(a) Effects of axial force

(b) Effects of bending moment



(c) Effects of slenderness



(d) Effects of end moment ratio

Fig.3 Verification of the buckling temperature equation

The maximum column lateral deflection can be related to the axial restraint displacement  $u_l$  in the following way:

$$w = \sqrt{\frac{u_l \cdot l}{\alpha}} \quad (7)$$

where  $u_l$  is calculated using Eq.(7);  $\alpha$  is a function of slenderness ratio ( $\lambda$ ), the axial restraint stiffness ratio ( $\beta_l$ ), the axial load ratio ( $\rho_N$ ), the bending moment load ratio ( $\rho_M$ ) and the end moment ratio ( $\alpha_M$ )

$$\alpha = (\rho_N, \rho_M, \lambda, \beta_l, \alpha_M) \quad (8)$$

Here the expression of  $\alpha$  is obtained by curve fitting ABAQUS results. The following equations are obtained:

$$\begin{aligned} \alpha &= c_{\rho_N} c_{\rho_M} c_{\beta_l} c_{\lambda} \geq 2.5 \\ c_{\rho_N} &= 1.10\rho_N + 0.06 \\ c_{\rho_M} &= -1.60\rho_N + 2.10 \\ c_{\beta_l} &= 4.72e^{\frac{\beta_l}{0.002}} + 205.35e^{-\frac{\beta_l}{136.81}} - 203.32 \\ c_{\lambda} &= 10.87e^{-\frac{\beta_l}{406.80}} - 7.70 \end{aligned} \quad (9)$$

## (2) Verification of the failure temperature equation

To check accuracy of the proposed method, ABAQUS simulations have been carried out. Fig.4 compares the column failure temperatures obtained by the proposed method and from ABAQUS

simulations.

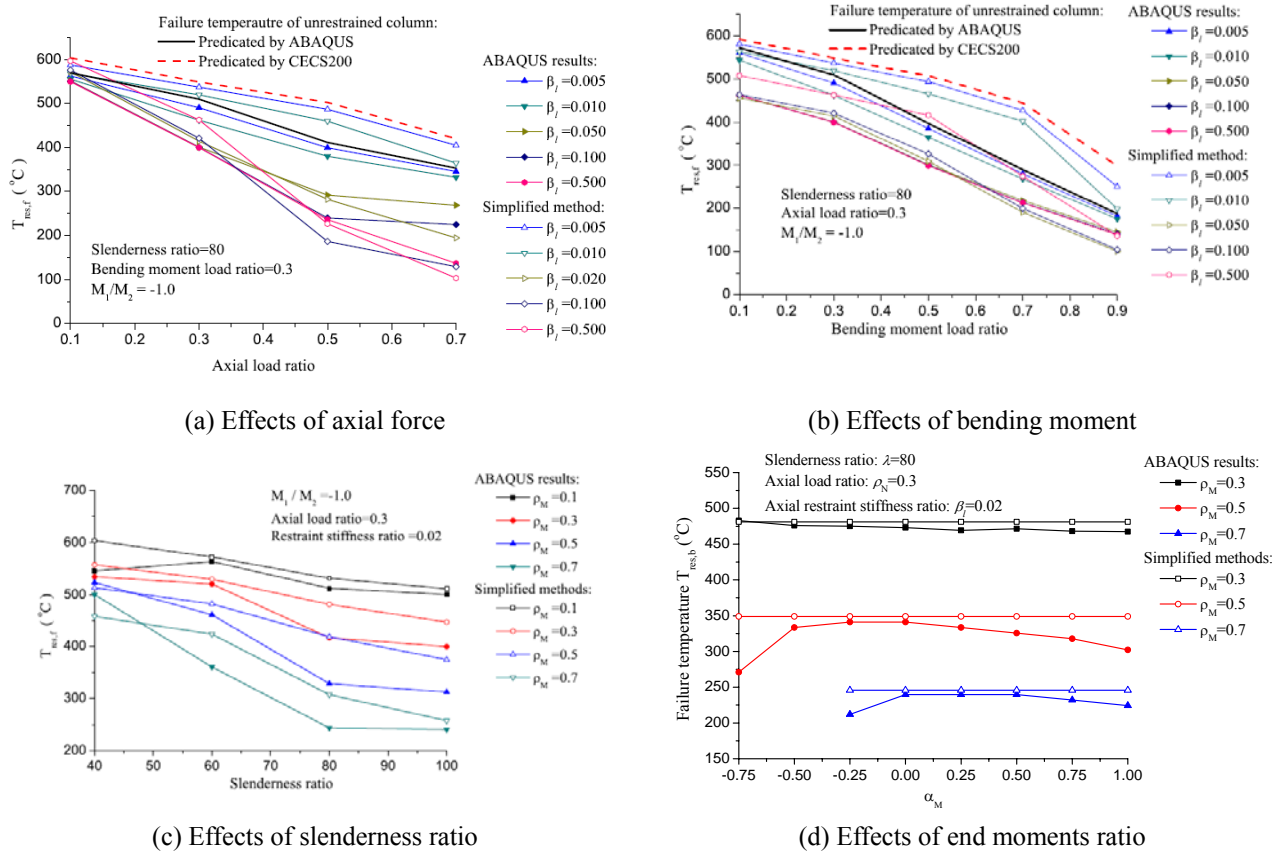


Fig. 4 Verification of the failure temperature equation

For columns with axial restraint stiffness lower than 0.02, the failure temperature predicted by the proposed method is greater than the prediction of ABAQUS. At increasing load ratio, the difference between the failure temperature obtained by the two methods increases, as shown in Fig.4(a) and Fig.4(b). For columns with great axial restraint stiffness, the failure temperatures predicted by the proposed method is slightly lower than those by ABAQUS. For columns with different slenderness ratio, the failure temperatures predicted by the proposed method are greater than that by ABAQUS by about 80°C, as shown in Fig.4(c). Except for  $\alpha_M = -0.75$ , the failure temperature predicted by the proposed method is not affected by the end moment ratio, as shown in Fig.4(d). The simplified method gives a slightly higher failure temperature.

### 3. CONCLUSIONS

This paper has studied the behaviour and developed a new method for calculating the buckling and failure temperatures of restrained columns under axial load or combined axial load and bending moment in fire. Results from the proposed calculation methods are compared with ABAQUS simulations for different cases. The main works and conclusions of this paper are:

1. simplified methods to calculate the buckling and failure temperature of restrained columns under combined axial load and bending moment are proposed.
2. by including the additional axial force due to restrained thermal elongation, the design equation for unrestrained column is used to predict the buckling temperature of restrained columns. For calculating the failure temperature, the yield axial strength-plastic bending moment interaction curve is adopted. The failure criterion is defined as the temperature at which the axial force returns to its initial value.

3. For the restrained column with realistic parameters, the buckling and failure temperatures predicted by the proposed method agree well with those of ABAQUS.

#### **ACKNOWLEDGEMENT**

The work reported hereinabove was financially supported by the National Natural Science Foundation of China under contracts 50621062, 50738005 and 50728805. The support is gratefully acknowledged.

#### **REFERENCES:**

- [1] EN1993-1-2. Eurocode 3: Design of steel structures, Part 1-2: General rules--structural fire design. European committee for standardization, 2005.
- [2] CECS200. Technical Code for fire safety of steel structural in buildings (CECS200:2006). China Planning Press, Beijing, 2006.
- [3] Y. C. Wang. Post-buckling behaviour of axially restrained and axially loaded steel columns under fire conditions. *Journal of Structural Engineering*, 130(3):371--380, 2004.
- [4] Z. F. Huang, K. H. Tan. Structural response of restrained steel columns at elevated temperatures. Part 2: Fe simulation with focus on experimental secondary effects. *Engineering Structures*, 29(9):2036--2047, 2007.
- [5] I. C. Neves. The failure temperature of steel columns with restrained thermal elongation. *Fire Safety Journal*, 24(3):211--227, 1995.
- [6] J. C. Valente, I. C. Neves. Fire resistance of steel columns with elastically restrained axial elongation and bending. *Journal of Constructional Steel Research*, 52(3):319--331, 1999.
- [7] G. Q. Li, P. J. Wang, H. T. Hou. Behaviour of axially restrained steel columns incorporating strain reversal effects of steel at elevated temperatures in fire. *Steel & Composite Structures*, In Press.
- [8] CTICM. Méthode de prévision par le calcul du comportement au feu des structures an acier. Document Technique Unifié, *Construction Métallique*, 3, 1982.
- [9] J. M. Franssen. Failure temperature of a system comprising a restrained column submitted to fire. *Fire Safety Journal*, 34(2):191--207, 2000.
- [10] Y. C. Wang. Effects of structural continuity on fire resistant design of steel columns in non-sway multi-storey frames. *Fire Safety Journal*, 28(2):101--116, 1997.
- [11] I. C. Neves, J. C. Valente, J. P. C. Rodrigues. Thermal restraint and fire resistance of columns. *Fire Safety Journal*, 37(8):753--771, 2002.
- [12] GB50017. Design of Steel Structure (GB50017-2003). China Building Industry Press, Beijing, 2003.

# INTEGRATED FIRE ENGINEERING OF STEEL SKELETON

## USING WELL ESTABLISHED FIRE SOURCES

Heinisuo M.<sup>a</sup>, Hietaniemi J.<sup>b</sup>, Kaitila O.<sup>c</sup>, Laasonen M.<sup>a</sup>, Outinen J.<sup>d</sup>

<sup>a</sup> Tampere University of Technology, Department of Civil Engineering, Tampere, Finland

<sup>b</sup> Technical Research Centre of Finland, Espoo, Finland

<sup>c</sup> Finnish Constructional Steelwork Association, Helsinki, Finland

<sup>d</sup> Rautaruukki Oyj, Vantaa, Finland

### INTRODUCTION

Representation of all the information needed to describe buildings throughout the whole life cycle has long been an objective for those applying information technology to building construction. One discipline involving a considerable amount of computing effort in building projects has so far been missing both from the commonly used product modelling softwares and from the product model standards. This topic is fire engineering. Considerable efforts have been put to enhance this discipline during the last 20 years.

The natural fire safety concept [1] has now been accepted in many countries as a valid method to perform the structural design in fire. To do this, some level of fire simulation has to be done for the building in order to obtain the temperatures and other quantities in fire.

The basic question is how to integrate fire engineering to the product model? The basic idea of this paper (see also [2], [3] and [4]) is that all the information needed in the fire simulation is derived from the physical model of the building. This means that we use a single program to model both the geometrical and material entities of the building and all the data needed in the fire simulation and then map this data to the separate fire simulation program using special interface softwares.

The product model software used in this study is Tekla Structures (TS). The fire simulation program is FDS, Version 5 [5]. FDS includes both the fire fluid dynamics and the evacuation module. Only the fire dynamics module is applied in this study. Virtual thermometers are modelled in the fire simulation input file. The locations of these are determined on the basis of the structural analysis model. In this study, the thermometers are located at the centre points of each steel member. It is worth noting that typically the steel skeleton is so slender that its inclusion in the fire simulation model is not necessary [3], [6]. If desired, however, the steel skeleton can be included in the fire simulation. Difficulties when modeling the steel skeleton to the fire simulations have been considered in [2]. If there are important changes in steel skeleton layout during the design, the fire simulation should be done again, if it is modeled to the fire simulations, which can cause extra work.

After fire simulations the temperatures of the virtual thermometers are transferred into the structural analysis program and the resistance of the steel skeleton is checked using these temperatures. In this study the linear analysis resistance checks of the steel members were done using the program SCIA Engineering and its fire engineering module. Some cases have been checked using the program ABAQUS Standard in order to verify the analyses and obtain information on the geometrically and materially non-linear 3D behaviour of the building. Joint resistances are not dealt in this study.

The essential features when running the fire simulations are the applied fire sources. In this study, well established fire sources, called fuel packages [7], based on experimental and

theoretical bases are proposed for the cases under consideration, and fulfilling the safety level of the Eurocodes.

The developed tool has been applied in this paper to a typical warehouse steel skeleton for a heavy-good vehicle fire and for other fire scenarios. The resistance times for the unprotected steel skeleton have been defined using the simple engineering tool, i.e. checking of members individually, and comparisons on the results of the non-linear analysis are carried out.

The goal is to demonstrate how to enhance the fire design of steel structures by the integration of different disciplines applying product modelling techniques.

## 1 DEVELOPED INTEGRATED FIRE ENGINEERING TOOL

This project is an industrial project financed by the Finnish steel company Rautaruukki Oyj and the Finnish Funding Agency for Technology and Innovation (Tekes). The main goal of the project was to integrate fire engineering to the practises and softwares presently used in the company without the need to introduce new softwares to the end user. Figure 1 illustrates the integration completed in this study.

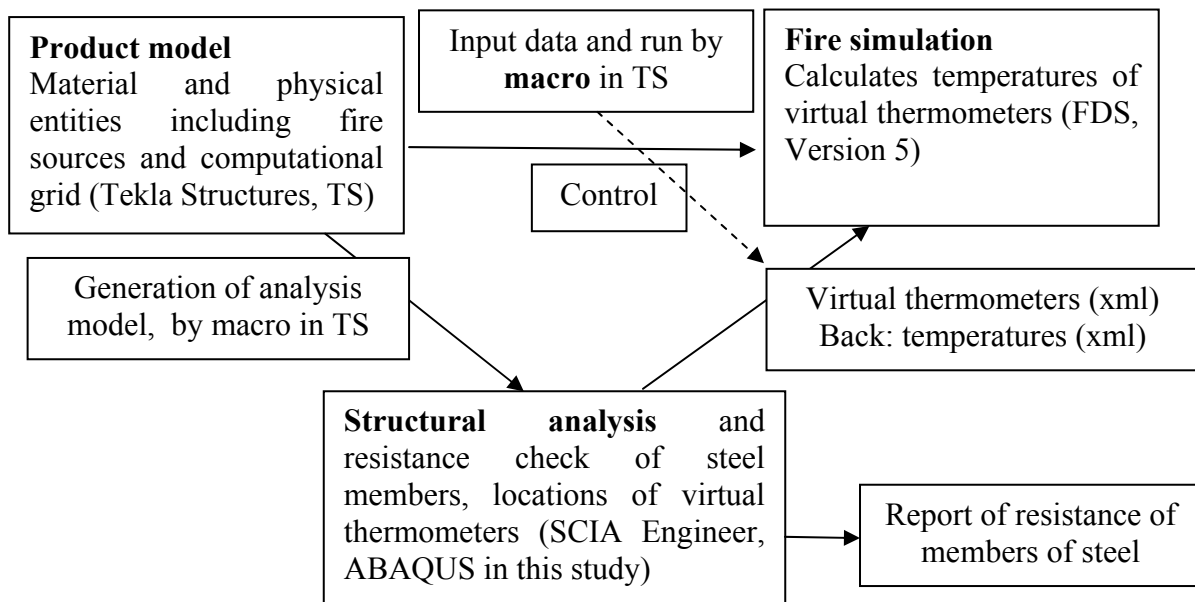


Fig. 1. Fire engineering in product modelling

Constant values for the convection coefficient ( $h = 25 \text{ W/(mK)}$ ) and emissivity ( $\epsilon = 0.7$ ) at the steel surfaces were used in this study. The specific heat of the steel members varied according to the steel temperature according to EN 1993-1-2. The increment time 30 seconds was found to be suitable for all calculations.

## 2 FUEL PACKAGES

VTT has developed a fuel-package-based approach [7] to characterise fire scenarios in buildings with different end uses such as car parks, offices, shops and warehouses. The basic problem is the assessment of the heat release rate (HRR). The fuel-package-based approach employs two ways to assess the heat release rate in fires.

1. Analysis and synthesis of experimental data.
2. Modelling and fire simulation.

The approach 1 is the primary way so that whenever there is reliable and relevant data available, it should be used. There is abundantly of experimental data available but in general, the larger fires one has consider, the less there is relevant data.

The approach 2 can be used where *no directly relevant HRR* data is found. It is also based on experimental data, but now the data is used so that first, the fire load is broken down to its basic constituents and then, using small-scale experiments on HRR per unit area, heat of combustion, ignition delays, thermal properties, etc., the HRR model is constructed using appropriate mass, volume and area weighted properties; and *before use validated against some experimental results*.

In this study, the following fire scenarios for typical warehouses were considered

- ISO fire,
- heavy-good-vehicle (HGV) fire,
- local and global wood fire,
- local and global plastic fire.

The local fire describes the fire in the building with sprinklers, but with the worst scenario: the sprinkler just above the fire ignition location is not working. It is believed that the above three cases include the most severe fire scenarios, which may be occur in typical warehouses. As an example the next figure illustrates the estimate for HGV fire corresponding to 95% fractiles of the maximum HRR (50 MW) and the fire load (245 GJ).

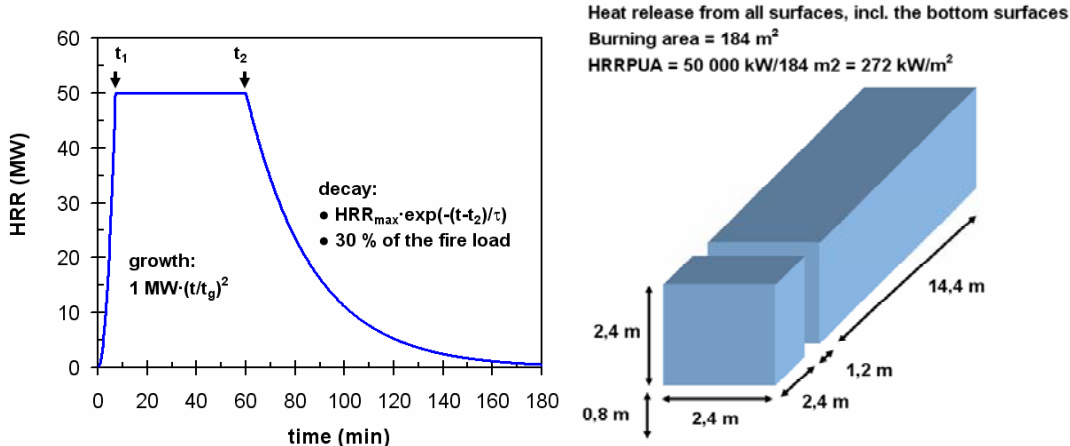


Figure 2. HGV fire source

2 EXAMPLES

Consider the steel skeleton shown in the next figures. Here it is used for the demonstrations of the developed tool. The building is 24 m wide and 41 m long. The height at the eaves is about 6.5 m and at the top about 8.8 m.

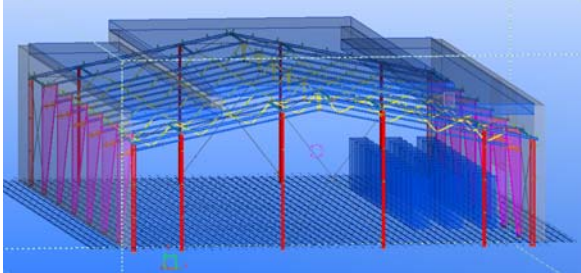


Fig. 3. View of product model

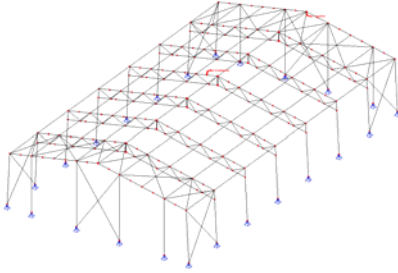


Fig. 4. View of analysis model

The main frame is a two hinge frame with hinges at the base bolt joints. The top chord and the bottom chord of the frame are connected (hinges) to the tapered columns. The steel skeleton is stiffened at the roof level, at the ends of the building and at the long outer wall lines with X-braces, as shown in the figure. The floor, walls and the roof were modeled using INERT coding of FDS, meaning non-combustible material. In the wall near the fire ignition location are two openings  $6 \times 3 \text{ m}^2$  portraying open doors. In the roof just above the fire ignition location is an opening  $2 \times 5 \text{ m}^2$ .

The entire steel skeleton with all the members was modelled. The X-braces and roof purlins were modelled as tubular members, which are not as in the real building. The main columns were modeled using the uniform IPE500 profiles, not as welded tapered members, as in the real building. All the other members were modeled as they are in the real building. All the members but the columns are rectangular steel tubes and the columns are I-profiles. The detailed data for the building is available from Rautaruukki Oyj.

The mechanical load combination used in all structural analyses was the dead load ( $28 \text{ kg/m}^2$  applied to the whole roof area) plus 40 % of the uniform characteristic snow load on the entire roof ( $100 \text{ kg/m}^2$ ). All the loads are acting on the roof; purlins and mid points at top chords between purlins.

The following fire scenarios were applied:

- ISO fire all around the building,
- HGV fire so that the vehicle is just below one frame as shown in the figure 5,
- Local and global wood fire starting from the local fire source as shown in the figure 6,
- Local and global plastic fire starting from the local fire source as shown in the figure 7.

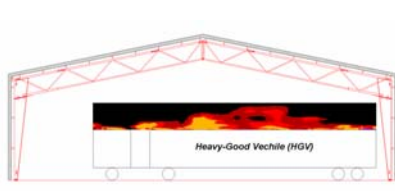


Fig. 5. Heavy-good vehicle fire

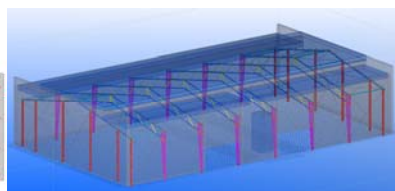


Fig. 6. Local fire

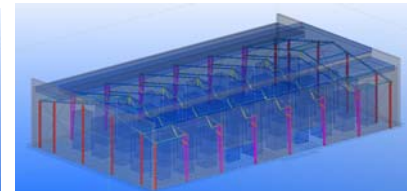


Fig. 7. Global fire

The global fires start from one ignite fire source (same as in the local fire) and then spread following the given ignition temperatures to other fire sources modelled as rectangular boxes in the figure 6. The size of one fire source in the local and global fire is  $2 \times 2 \times 5 \text{ m}^3$  and the c/c distances between the sources in the global fire is 2 m. The size of the HGV fire source is as given in figure 2 representing the real vehicle. The heat release rates were given using the coding HRRPUA to the FDS program and the ramps described in [7].

In the ISO fire case the resistance of the steel skeleton was about 12-14 minutes in both SCIA Engineer and ABAQUS analyses. The resistance time in the ABAQUS calculations was defined as the time when vertical displacement rates of critical points were radically increasing.

The simplified analysis using the program SCIA Engineer showed that the entire steel skeleton could resist the HGV fire 2 hours, but for the second brace of the truss from the outer wall. Its resistance was 19.5 minutes and the temperatures of that member are shown in the next figure. The second largest utility ratio during the entire fire (2 hours) was at the top chord member nearest the ridge of the skeleton and it was 0.7, meaning that it can resist the fire.

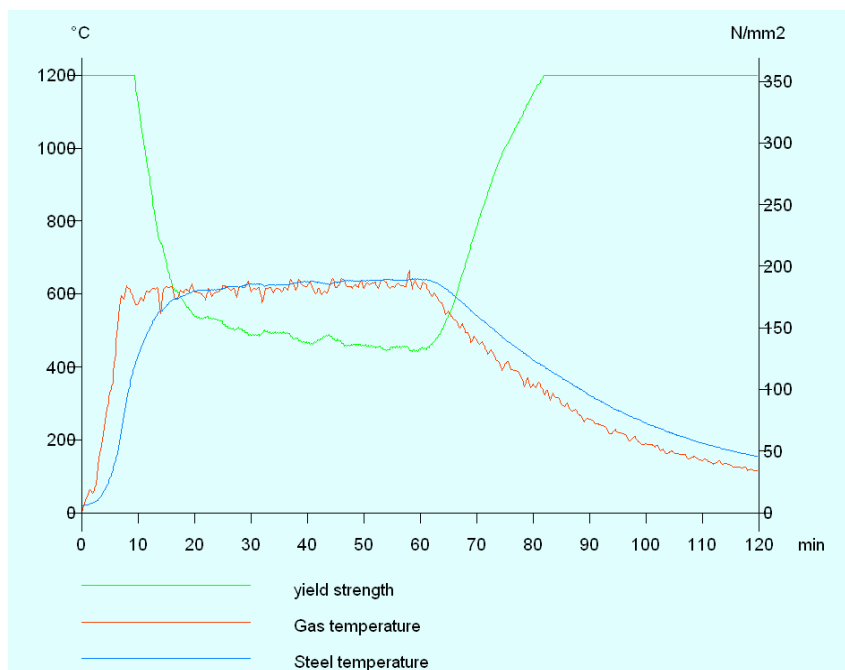


Fig. 8. Temperatures of the critical steel member in HGV fire

This means, that by changing the second braces of the trusses to the rectangular hollow sections with a little bit larger wall thicknesses (from 4 mm to 6 mm), the whole skeleton can resist the HGV fire for 2 hours. The reason for this is that the heat release rate for the area of the vehicle is just  $272 \text{ kW/m}^2$  and the vehicle is rather low, so that the hot gases do not reach the roof structures. The total heat release rate was 50 MW for the vehicle. After one hour the fire starts to decrease. This case was not analysed using ABAQUS.

The global wood and plastic fires are quite different from each other both in the time scale (one plastic fire source lasts longer) and in the intensity (one wood source: 35 MW, one plastic source: 62 MW). Moreover, the start ramp was quicker in both fires compared to the ISO fire. The global wood fire firstly increases and then descends near the doors.

The global plastic fire did not descend during the simulation times up to 4700 seconds (78 minutes) but after about 2000 seconds it was rather constant and reaching the entire simulation space.

In both global fires the resistance of the steel skeleton is very low without applied fire protection. Due to the rapid temperature increase in the global fires, the fire resistance times are lower than in the ISO fire. The resistance times using the program SCIA Engineer and ABAQUS were about 10 minutes for the global wood fire. The global plastic fire is more severe and it was calculated only using the program SCIA Engineer.

In the local wood fire case the resistance of the steel skeleton was about 10 minutes for the most critical member using the program SCIA Engineer. However, in this case the resistance duration of the steel skeleton using the program ABAQUS is infinite! Practically the calculations were stopped at 2400 s when the fire was already practically over. This considerable difference in analysis results is explained by the use of non-linear analysis techniques in ABAQUS, which allow for the redistribution of actions during the analysis.

### 3 CONCLUSIONS

The developed tool worked well in the cases considered and it is considered by the authors that the developed tool enhances the fire design of steel structures considerably. However, the

joint behaviour and the resistance checks of joints should be included in the analyses in the future.

The local wood fire analysis case was based on a realistic fire scenario in an industrial hall or a warehouse equipped with sprinklers. In order to provide a more severe approach, the sprinkler device closest to fire ignition was assumed to be out of order. The analysis showed that the structure survives this type of fire safely due to three-dimensional structural behaviour and the redistribution of loads and stresses during the fire. The catenary actions in the purlins play an important role in providing support for the most severely affected frame. No structural failure was observed during the whole analysis that included the decreasing phase of the fire.

However, in an actual design case special consideration should be paid on the strength of connections between structural members, which are of primary importance when considering the 3D-behaviour of a complete structure and the catenary actions present in the fire situation. The effects of connections have not been considered in this study.

The results of the cases considered showed that

- The skeleton can resist the HGV fire with a slight structural modification without applied fire protection,
- The skeleton can resist without applied fire protection a typical cellulose based fire with sprinklers and by taking into account the worst scenario: the sprinkler just above the fire ignition is considered to be out of order during the fire (local wood fire). This is due to the catenary action and the three dimensional behaviour of the skeleton during the fire, meaning that these should be taken into account when seeking good solutions for steel skeletons in fire.

In order to get reliable results from the fire simulations, the used fire sources should be well defined and based on experimental and theoretical data. Obviously, the user of tools of this type should have both fire engineering and structural engineering skills and access to detailed information on all factors considered.

## REFERENCES

- [1] Natural fire safety concept – Valorisation project, Dissemination of Structural Fire Safety Engineering Knowledge – DIFISEK, RFS-C2-03048, 2005.
- [2] Heinisuo M., Laasonen M., Product modeling, part of the fire safety concept in the future for metal structures?, Advanced Research Workshop, Fire Computer Modeling, Santander 18-20 October, Universidad de Cantabria, 2007, pp. 261-272.
- [3] Heinisuo M., Laasonen M., Hyvärinen T., Berg T., Product modeling in fire safety concept, effects of grid sizes and obstacles to steel temperatures, Proceedings of IABSE Conference on Information and Communication Technology (ICT) for Bridges, Buildings and Construction Practice, Helsinki, Finland, June 4-6, 2008.
- [4] Heinisuo M., Laasonen M., Hyvärinen T., Product modeling in fire safety concept, calculation of steel temperatures, Proceedings of 15<sup>th</sup> Workshop of the European Group of Intelligent Computing in Engineering (EG-ICE), Plymouth, July 2-4, 2008, pp. 460-469.
- [5] McGrattan, K., Hostikka, S., Floyd, J., Baum, H. and Rehm, R., Fire Dynamics Simulator (Version 5), Technical Reference Guide (Draft: may 30, 2007), NIST Special Publication 1018-5, 2007.
- [6] Prasad, K. and Baum, H.R., Coupled Fire Dynamics and Thermal Response of Complex Building Structures, Proceedings of the Combustion Institute 30, 2005, pp. 2255-2262.
- [7] Hietaniemi J., Fuel Packages for Structural Fire Safety Design, To be published in the VTT Working Papers Series, Espoo, 2009.

## **BUCKLING BEHAVIOUR OF STEEL COLUMNS IN FIRE CONDITIONS AND COMPARISON WITH EUROCODE 3**

Tomaž Hozjan<sup>a,b</sup>, Luka Kurnjek<sup>a</sup>, Igor Planinc<sup>a</sup>, Miran Saje<sup>a</sup>, Stanislav Srpčič<sup>a</sup>

<sup>a</sup> University of Ljubljana, Faculty of Civil and Geodetic Engineering, Ljubljana, Slovenia

<sup>b</sup> Trimis d.o.o., Prijateljeva cesta 12, 8210 Trebnje, Slovenia

### **INTRODUCTION**

Steel columns are efficient structural elements both in terms of construction time and load bearing capacity. Steel is vulnerable to fire, however, and steel structures, potentially exposed to fire, require a particularly careful design. This especially holds true for steel columns as they are loaded in compression and are thus prone to buckling. With an increase of temperature, strength of steel and the stiffness of columns decrease leading to buckling at an even much lower level of external loading than at room temperature. We can find numerous results of experiments on steel columns in fire. Yet extensive parametric studies of behaviour of steel columns in fire can only be performed with numerical programs previously validated with the results of experiments. These programs are rather complex and not appropriate for a routine engineering usage. Therefore engineers will rather use simplified, practical methods such as those given in building codes, e.g. Eurocode 3 [3], and BS5950 [1]. These codes offer methods for the fire analysis for isolated columns, which, however, may not result in sufficiently reliable quantitative predictions of the fire bearing capacity of a column.

A deeper insight into the thermo-mechanical behaviour of a column during fire can be achieved by the use of sophisticated mathematical models and modern numerical tools. These formulations make it possible to consider and analyse various material models, fire load scenarios, boundary conditions, restraints and geometric imperfections. Such models have been applied to steel columns subjected to elevated temperatures [2, 4, 10, 15]. Although they have been performed only for simple boundary conditions their results have shown that the critical temperature depends on slenderness of the column and on material model of steel at elevated temperatures.

Analytical solutions are much more difficult to obtain and are only limited to the determination of fire resistance. The majority of analytical solutions revolves around the Merchant-Rankine equation and the second-order theory of beams. Skowronski [13] derived an analytical formula for the fire resistance of a simple steel column. Tang et al. [14] improved their formulae by taking into account the effects of an initial crookedness, residual stresses, material models and the load eccentricity. Huang et al. [6] significantly improved their results by additionally considering axial restraints.

The present article presents a systematic analytical procedure for the determination of the critical temperature of a straight, geometrically perfect and axially loaded steel column exposed to fire. A series of standard simplifications and assumptions need to be introduced, however, to enable the analytical solution to be derived. In particular, we assume that a steel column can be realistically modelled by a kinematically exact planar beam model of Reissner [12] neglecting the effect of shear strain. Next, we assume a non-linear, temperature dependent material law, which accounts for both viscous and plastic strains. The mathematical expressions for the stress-strain law of steel at high temperatures are taken from EC 3 [3] along with the explicit expressions for temperature-dependent material parameters. As the walls of the steel sections are thin, we further assume that the temperature field in the column is uniform, but somewhat delayed with regard to temperature of the surrounding gas. After the thermo-mechanical equations are set up, the fundamental equilibrium solution of the column is obtained and the set of linearized equations at the fundamental equilibrium state is

derived. The condition for the existence of the non-trivial solution of the linearized equations supplies us with the value of the critical temperature.

The basic equations for the derivation of determination of the critical temperature for steel columns in fire conditions are presented in Sec. 1. The parametric analyses and the comparisons with the results of the European standard EC 3 [3] are given in Sec. 2.

## 1 FIRE ANALYSIS OF RESTRAINED STEEL COLUMNS

### 1.1 Preliminaries

We consider a straight steel column of initial, undeformed length  $L$  and a constant I-shaped cross-section. The column is centrally loaded with an axial force  $F$  while simultaneously being exposed to fire (*Fig. 1*). The plane of deformation of the column is the plane  $(x, z)$  of the Cartesian coordinate system  $(x, y, z)$ . The reference axis of the column is assumed to coincide with its centroidal axis.

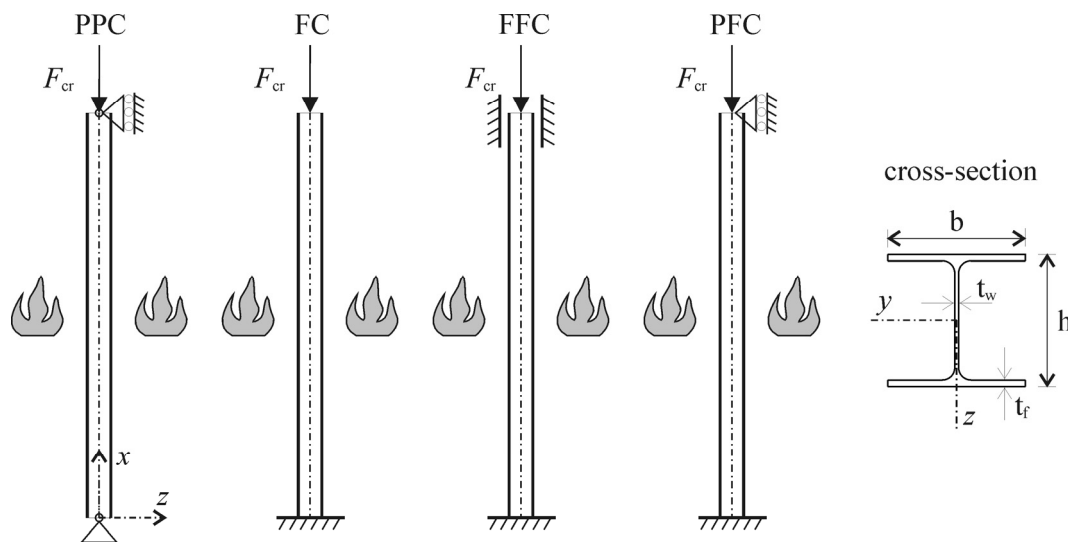


*Fig 1.* Euler's columns and typical I-shaped cross-section

In modelling the interaction between fire and a structure, we assume two independent analysis steps, the first one being the determination of the temperature field in the column and the second one consisting of the determination of the stress and strain field due to a combined effect of mechanical and temperature loads.

### 1.2 The temperature field

The development of gas temperature in the fire compartment depends on many parameters and is therefore both a complex task to do and unreliable. That is why convenient, yet very much simplified parametric temperature-time curves are introduced for the engineering design practice, which uniquely define explicit relationships between gas temperature in the compartment and time for a number of typical situations, including the amount of fire load and the thermo-dynamical and geometrical properties of the compartment [9]. Once the variation of gas temperature in the compartment has been obtained, we can determine the temperature distribution within the structure by integrating the differential equation of heat conduction. For a typical I-shaped steel cross-section uniformly heated over all surfaces, it is appropriate to assume an instantaneously uniform temperature distribution over the cross-section. One such simplified solution, which is also used in this article, is proposed by the EC 3 standard [3]. *Fig. 2a* shows some typical parametric temperature-time curves, while on *Fig. 2b* displays the development of temperature with time in the typical steel cross-sections for standard fire curve ISO 834 [7].

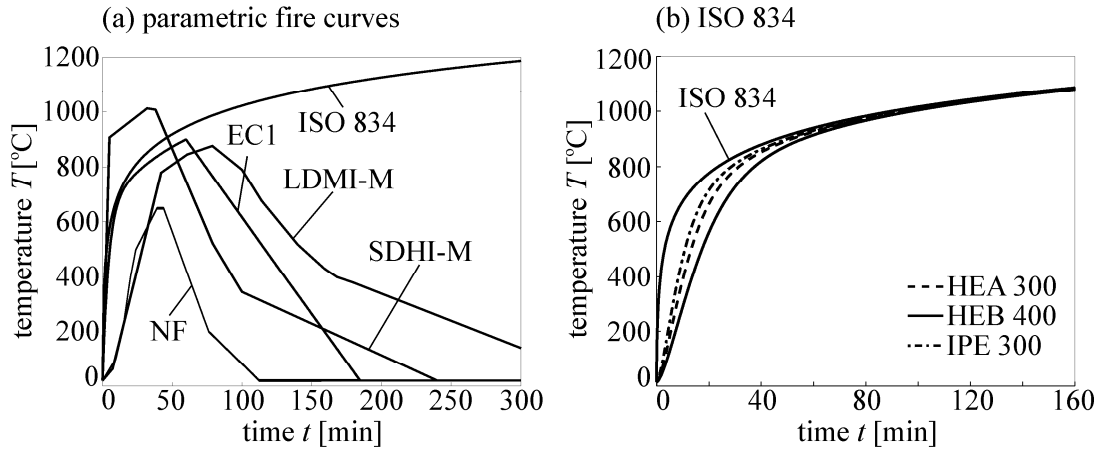


Fig 2. (a) Parametric fire curves. (b) Temperature-time curves for different steel profiles for fire curve ISO 834

### 1.3 The stress-strain field

Once the temperature variation in time has been obtained, we may start the mechanical analysis of the structure. We find the solution in an incremental way. We divide the time of the duration of fire into time intervals  $[t^{i-1}, t^i]$  ( $i = 1, 2, 3, \dots$ ) and determine iteratively the stress and strain state at each time  $t^i$ . The column is modelled by Reissner's geometrically exact beam theory [12], but with the effect of shear deformations being neglected. The corresponding governing equations of such a beam model are:

$$1 + u^{i'} - (1 + \varepsilon^i) \cos \varphi^i = 0, \quad (1)$$

$$w^{i'} + (1 + \varepsilon^i) \sin \varphi^i = 0, \quad (2)$$

$$\varphi^{i'} - \kappa^i = 0, \quad (3)$$

$$\mathcal{H}^{i'} = 0, \quad (4)$$

$$\mathcal{V}^{i'} = 0, \quad (5)$$

$$\mathcal{M}^{i'} - (1 + \varepsilon^i) Q^i = 0, \quad (6)$$

$$\mathcal{N}^i = \mathcal{H}^i \cos \varphi^i - \mathcal{V}^i \sin \varphi^i = 0, \quad (7)$$

$$Q^i = \mathcal{H}^i \sin \varphi^i + \mathcal{V}^i \cos \varphi^i = 0, \quad (8)$$

$$\mathcal{N}^i = \int_{\mathcal{A}} \sigma^i dA, \quad (9)$$

$$\mathcal{M}^i = \int_{\mathcal{A}} z \sigma^i dA, \quad (10)$$

where  $(\bullet)'$  denotes the derivative with respect to  $x$ ;  $u^i$  and  $w^i$  are the components of the displacement vector of the centroidal axis of the column in  $x$  and  $z$  directions,  $\varphi^i$  is the cross-sectional rotation around  $y$ . Deformations  $\varepsilon^i$  and  $\kappa^i$  are the extensional strain of the centroidal axis and its bending strain (also termed the 'pseudocurvature').  $\mathcal{N}^i$  and  $Q^i$  are the axial and the shear force and  $\mathcal{M}^i$  is the bending moment.  $\mathcal{H}^i$  and  $\mathcal{V}^i$  are the components of the resulting cross-sectional force with respect to spatial axes  $x$  and  $z$ , respectively.

Based on the given stress and strain state at time  $t^{i-1}$  and temperature at  $t^i$ , we can determine the strain  $D^i$  at time  $t^i$  of any point of the column by the equation

$$D^i = D^{i-1} + \Delta D^i, \quad (11)$$

where  $\Delta D^i$  is the increment of the total strain (also termed the 'geometrical deformation') in time interval  $i$ . Considering the principle of additivity of strains and the material model of steel at elevated temperatures according to EC 3 [3], we propose that the strain increment  $\Delta D^i$  is the sum of the strain increments due to temperature,  $\Delta D_{th}^i$ , and stress,  $\Delta D_{\sigma}^i$ :

$$\Delta D^i(T^i) = \Delta D_{th}^i(T^i) + \Delta D_{\sigma}^i(T^i). \quad (12)$$

In this material model, viscous strains are assumed to be included in  $\Delta D_{\sigma}^i$  and are thus not treated separately. The temperature strain increment,  $\Delta D_{th}^i$ , is calculated from the EC 3 formula [3], where the total temperature strain,  $D_{th}$ , is given with a formal expression  $D_{th} = f(T^i)$ ; thus,  $\Delta D_{th}^i = f(T^i) - f(T^{i-1})$ . The stress-dependent strain increment,  $\Delta D_{\sigma}^i(T^i)$ , also termed the ‘mechanical strain increment’, is assumed to be equal to the sum of elastic and plastic strains,  $\Delta D_{\sigma}^i(T^i) = \Delta D_{\epsilon}^i(T^i) + \Delta D_p^i(T^i)$ . Here we use the stress-strain law for steel at high temperatures according to EC 3; for full description of the model, see [3].

#### 1.4 Linearized buckling analysis

We wish to find the buckling load or critical temperature of a column with the help of the linear theory of stability [8]. By the linearization of the governing equations, Eqs. (1)–(10), around the fundamental solution, which is characterized by the condition  $\varphi^i = 0$ , we get a system of 10 algebraic-differential equations. For the complete derivation of the equations, see [5]. After a systematic elimination of the unknowns is made, we end up with the system of two linear differential equations with constant coefficients

$$\delta u^{i'''} = 0, \quad (13)$$

$$\delta w^{i''''} + k^{i^2} \delta w^{i''} = 0, \quad (14)$$

in which the buckling load parameter  $k^i$  is introduced as

$$k^{i^2} = \frac{(1 + \varepsilon^i) |\mathcal{N}^i|}{E_t^i J} \geq 0. \quad (15)$$

In Eq. (15)  $E_t^i$  is the tangent modulus of steel at time  $t^i$  and temperature  $T^i$  and  $J$  is the momentum of inertia of the cross-section. The general solutions of Eqs. (13) and (14) are

$$\delta u^i(x) = \mathcal{K}_1^i x + \mathcal{K}_2^i, \quad (16)$$

$$\delta w^i(x) = C_1^i \cos k^i x + C_2^i \sin k^i x + C_3^i x + C_4^i. \quad (17)$$

The unknown integration constants,  $\mathcal{K}_1^i, \mathcal{K}_2^i, C_1^i, C_2^i, C_3^i$  and  $C_4^i$ , are obtained with the help of boundary conditions. the implementation of the boundary conditions into Eqs. (16) and (17) results in the homogeneous system of six linear algebraic equations for the unknown constants. It is well known that the non-trivial solution of the homogeneous system of linear algebraic equations is possible only if the determinant of the system matrix is zero [11]

$$\det \mathbf{L}_T^i = \det \mathbf{H}_T^i \det \mathbf{K}_T^i = 0. \quad (18)$$

Matrix  $\mathbf{H}_T^i$  depends solely on  $\mathcal{K}_1^i, \mathcal{K}_2^i$ , while matrix  $\mathbf{K}_T^i$  only on  $C_1^i, C_2^i, C_3^i$  and  $C_4^i$ . It is easy to show that  $\det \mathbf{H}_T^i \neq 0$  for any  $\mathcal{K}_1^i$  and  $\mathcal{K}_2^i$  thus requiring condition (18) to imply  $\det \mathbf{K}_T^i = 0$ . Finally, to determine the buckling load, the following set of non-linear algebraic equations for the three unknowns, critical axial force  $\mathcal{N}_{cr}$ , critical axial strain  $\varepsilon_{cr}$  and critical temperature  $T_{cr}$ , has to be solved

$$\mathcal{N}_{cr} + F_{cr} + \mu_H \varepsilon_{cr} L = 0, \quad (19)$$

$$\mathcal{N}_{cr} - \sigma_{cr} A = 0, \quad (20)$$

$$\det \mathbf{K}_T^i = 0. \quad (21)$$

Eqs. (19)–(21) are solved with the Newton iterative solution method for three critical values,  $\mathcal{N}_{cr}$ ,  $\varepsilon_{cr}$  and  $T_{cr}$ . Once critical temperature  $T_{cr}$  is known, we determine the critical time  $t_{cr}$  directly from the known temperature field of steel column [7], which is possible only because the time-independent material model of steel at elevated temperatures has been employed.

## 2 NUMERICAL EXAMPLE

We analyze the effect of the adopted material model on the buckling resistance of Euler's columns (*Fig. 1*). The columns are made of section HEA 300 and steel S 235. In *Fig 3* the critical stress ratio,  $\sigma_{cr}/\sigma_{y,20}$  vs the column slenderness,  $\lambda$ , is depicted for the range of temperatures from 20°C to 800°C. Results for our model are presented with full lines, while the dotted lines present the results of the simplified method proposed by EC 3 [3]. For a full description of the simplified method, see EC 3 [3], section 4.2.3.2.

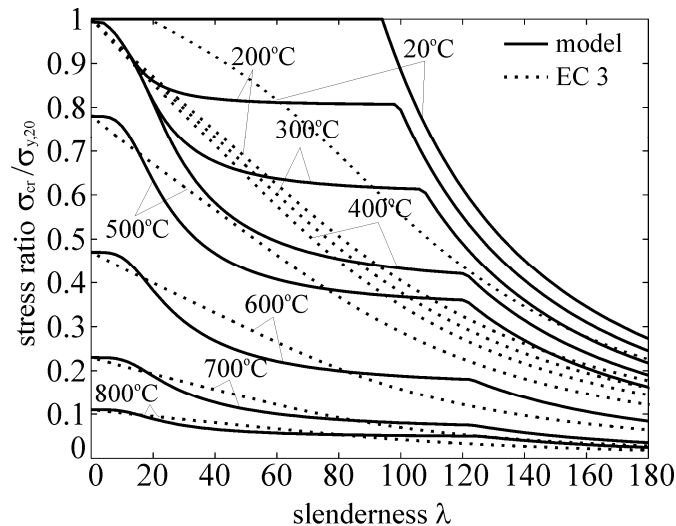


*Fig 3.* Euler's columns. Relationships between the critical stress ratio,  $\sigma_{cr}/\sigma_{y,20}$ , and the slenderness,  $\lambda$ , at different temperatures

The results (*Fig. 3*) show that the drop of the critical stress ratio with temperature is significant. For instance, the buckling resistance of a column with slenderness  $\lambda=60$  at  $T=500^\circ\text{C}$  is about 40% and at  $T=800^\circ\text{C}$  only about 5% of the related resistance at room temperature. The point, separating elastic and plastic buckling regimes, also notably varies with the slenderness. Somewhat unexpected is the position of the point separating the loss of stability by buckling and by the material failure of the column. At room temperature, the slenderness as high as 93 triggers buckling, while at temperatures higher than 200°C, the slenderness of about 2 is already sufficient for buckling. Hence, in practice buckling will appear to be the only mode of fracture of columns due to fire.

*Fig. 3* further shows the difference between the critical stress, obtained by the present model and the one determined by simplified method from EC 3. The behaviour of columns with slenderness up to 20 at room temperature is similar for the two models. For the slendernesses  $\lambda < 20$  and  $\lambda > 90$  the EC 3 method gives lower values of the critical stress. This difference is probably due to neglecting imperfections in the present model. By contrast for slendernesses  $20 < \lambda < 90$ , the EC 3 gives bigger critical stress than the one determined by the present procedure. The largest difference is about 20% at  $T = 500^\circ\text{C}$ . This may be due to the fact that present model accounts for the dependence of tangent modulus  $E_t$  on deformation. Namely, once deformation is in the non-elastic range, the tangent modulus significantly decreases. Because the critical temperature depends on the tangent modulus, it also decreases when the tangent modulus decreases. By contrast, in simplified method EC 3, the tangent modulus does not depend on deformation and hence remains constant if the temperature is constant. As a result the EC 3 method is proved to be not conservative in this case.

### 3 CONCLUSIONS

We presented an analytical procedure for the determination of the critical temperature of an axially loaded, axially restrained, geometrically perfect steel column, if exposed to a temperature increase, which is characteristic for the standard or natural fire. Within the assumption that steel at high temperature behaves in accordance with the material model proposed by European standard EC 3 [3], the critical temperature is determined exactly. From numerical example we can conclude that the critical temperature highly depends on both the slenderness of a column and the material model of steel at elevated temperatures. We could also see that the simplified method proposed by EC 3 can be unsafe for moderate slendernesses.

### 4 ACKNOWLEDGMENT

The work of T. Hozjan was financially supported by the Ministry of Education, Science and Sport and by the Ministry of the Economy of the Republic of Slovenia under contract 3311-04-831816. The support is gratefully acknowledged.

### REFERENCES

- [1] BS5950-8. Structural Use of Steelwork in Building - Part 8: Code of Practice for Fire Resistant Design. London: British Standard Institution; 2003
- [2] Burgess IW, Olawale AO, Plank RJ. Failure of steel columns in fire. *Fire Safety J*, 1992;18:183–201
- [3] Eurocode 3. Design of Steel Structures, Part 1.2: Structural fire design (draft). *European Committee for Standardization* 2003
- [4] Franssen JM, Dotreppe JC. Fire resistance of columns in steel frames. *Fire Safety J*, 1992;19:159–175
- [5] Hozjan T, Planinc I, Saje M, Srpčič S. Buckling of an axially restrained steel column under fire loading. *Fire Safety J*, 2007, submitted for publication
- [6] Huang ZF, Tan KH. Analytical fire resistance of axially restrained steel columns. *J Struct Eng ASCE*, 2003;129(11):1531–1537
- [7] ISO 834 Fire resistance tests – elements of building constructions. *International Standard ISO 834*; 1975
- [8] Keller HB. Nonlinear bifurcation. *J Diff Eq*, 1970;7:417–434
- [9] Ma ZC, Mäkeläinen P. Parametric temperature–time curves of medium compartment fires for structural design. *Fire Safety J*, 2000;34:361–375
- [10] Oda H, Usami T. Stability design of steel plane frames by second-order elastic analysis. *Eng Struct*, 1997;19:617–627
- [11] Planinc I, Saje M. A quadratically convergent algorithm for the computation of stability points: the application of the determinant of the tangent stiffness matrix. *Comp Meth Appl Mech Eng*, 1999;169:89–105
- [12] Reissner E. On one-dimensional finite-strain beam theory: The plane problem. *J Appl Math Phys (ZAMP)*, 1972;23:795–804
- [13] Skowronski W. Buckling fire endurance of steel columns in fire. *J Struct Eng ASCE*, 1993;119(6):1712–1732
- [14] Tang CY, Tan KH, Ting SK. Basis and application of a simple interaction formula for steel columns under fire conditions. *J Struct Eng ASCE*. 2001;127(10):1206–1213
- [15] Vila Real PMM, Hopes N, da Silva S, Piloto P, Franssen JM, Numerical modelling of steel beam-columns in case of fire–comparison with Eurocode 3. *Fire Safety J*, 2004;39:23–39

## **BEHAVIOUR OF HIGH STRENGTH GRADE 10.9 BOLTS UNDER FIRE CONDITIONS**

Dipl.-Ing. Fernando González <sup>a</sup>, Prof. Dr.-Ing. Jörg Lange <sup>b</sup>

<sup>a, b</sup> Technische Universität Darmstadt, Department of Civil Engineering and Geodesy, Darmstadt, Germany

### **INTRODUCTION**

In the last decades structural fire design has changed essentially. In the past the structural integrity of single elements was mostly proven by load tables which were based on fire tests. The introduction of the “hot” Eurocodes (Parts 1-2) offers the possibility to assess the resistance even of complex structural systems under fire conditions. For this purpose a calculation can be made according to the Eurocodes taking into account the relevant material behaviour which is mainly known for structural steel and concrete elements. The material behaviour is defined in the ECs by stress – strain curves, depending on the affecting temperature. Even for connections design rules are given in the Eurocodes. The resistance of bolts and welding seams under fire conditions can easily be calculated using global reduction factors which depend on the element temperature. The global reduction factors for bolts are currently valid for all grades. The experience shows that either differing alloying materials or varying treatment methods can lead to a relevant change in the stress – strain curve. These two points have an important influence on the production process of high strength grade 10.9 bolts. Due to this tension tests on specimens and bolt assemblies have been carried out in order to evaluate the behaviour under fire conditions. The results will give on one hand the possibility to verify the reduction factors for grade 10.9 bolts given in the Eurocode and on the other hand give a more precise understanding of high strength bolt behaviour under fire conditions.

The paper will describe the state of the art, the elaborated tests in more depth and present first results.

### **1. STATE OF THE ART**

The joint behaviour under fire exposure has currently moved into the focus of researchers. The global aim of forecasting the behaviour of complete structures under fire conditions can only be achieved by merging the knowledge of all single structural elements. The behaviour of the joint area is very complex and still not fully predictable in the hot stage. On that background various publications have been published in recent years dealing with the behaviour of bolted connections like fin plate or endplate connections ([1], [2]). Research concerning the behaviour of pure bolt assemblies is rare. In [3] and [4] series of tests are presented using grade 8.8 bolts, analysing the pure material and the bolt assembly behaviour. Experiences respectively test series for grade 10.9 bolts are not existent. The reason for this is, that from the international point of view the grade 10.9 bolts are rarely used and therefore not in the focus of investigations. In Germany and France by contrast grade 10.9 bolt assemblies are very common for endplate connections. Globally very little knowledge exists in this area. In [5] high-strength fire resistant (FR) bolts have been tested, showing similar properties at room temperature compared to grade 10.9 bolts. But due to some differences concerning the alloy and fabrication the test results at high temperatures are not fully comparable.

Eurocode 3 Part 1-2 Annex D [6] proposes for the connection area a design concept providing strength reduction factors for bolts and welding seams. The factors depend on the local temperature of the connection area and are valid for all bolt grades. The local temperature at the connection can be estimated using a method given in Annex D. It has to be stated that the handling is not transparent and leads at least to very rough solutions.

## 2. HIGH TEMPERATURE TESTS OF SPECIMENS AND GRADE 10.9 BOLT ASSEMBLIES

### 2.1 General Procedure

Due to the obvious lack of knowledge concerning the behaviour of grade 10.9 bolt assemblies under fire conditions a large test series was planned to be executed in order to fill up this gap. Some of the tests are already completed, others are outstanding or still in course. Due to this

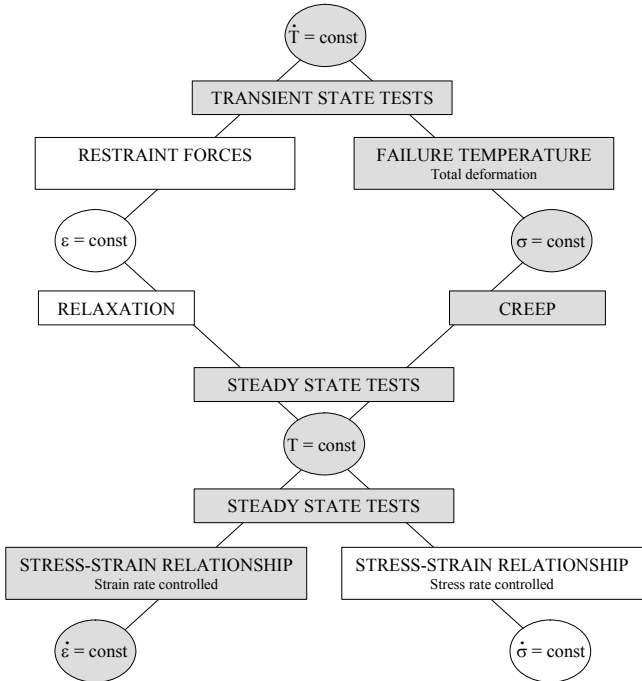


Fig. 1. Different testing methods according to [8]

the paper will show the pure material and the first 10.9 bolt assembly tension test results. The specimens used have been milled of grade 10.9 bolts. As described in numerous publications, the high temperature test procedure itself has an enormous impact on the outcome and can lead to clearly differing results. Therefore the specification of the test procedure is fundamental for the outcome. In [8] different high temperature test methods are listed and described. Figure 1 shows the different test methods. During a fire the material is normally subjected to a transient process which is directly depending on the applied temperature sequence. Therefore the transient test will normally lead to more realistic results, but it has to be noted that the temperature curve is not exactly defined and correlates with various factors like ventilation, thermal conductivity of the elements etc. The steady state test on the other hand is strain rate controlled and the results depend severely on this parameter. Due to the great sensitivity of the results concerning the heating velocity as well as the strain rate, it was decided to perform both steady state tests and transient state tests in order to be able to compare and to verify the results. At first glance a direct comparison of the two tension test results is not possible. The strain of the transient state test is composed of the thermal strain, the stress related strain and the creep strain, where thermal strain can easily be eliminated measuring the thermal elongation of an unstressed specimen. In comparison to the steady state test the strain is mainly composed by the stress related strain. The creep effects are negligible because of the short duration of the test. In order to make the results comparable additional creep tests have been performed. The grey shaded boxes in Figure 1 show the specimen tests realized by now. The bolt assemblies have only been tested under steady state conditions in order to determine the maximum failure load at the hot stage. For the bolt assemblies a much higher testing load (app. 270 kN at room temperature) was necessary to reach the failure, than in comparison to

the milled specimens (app. 18 kN at room temperature). This made the realization of the tests quite difficult. A measurement of the strain was not possible and even not useful due to the varying diameter along the bolt length. As it will be shown further on the creep effect has in a certain margin no significant influence on the ultimate strength of the material, so it can be stated, that the test procedure used gives a realistic failure load for the bolt assemblies.

**2.2 Test Arrangement and Test Method**

The round milled test specimens were made from high strength grade 10.9 bolts with a diameter of 16 mm. The bolts were manufactured by cold forging followed by a quench and temper heat treatment in order to achieve the required minimum mechanical properties as shown in *Table 1*. The chemical composition of the bolt material complies with the DIN EN ISO 898-1 [10].

*Table 1: Mechanical properties of grade 10.9 bolts*

| Steel grade | minimum tensile strength | minimum strength at strain of 0,2% | minimum expansion | minimum lateral contraction | Vickers hardness, HN; F ≥ 98 N |
|-------------|--------------------------|------------------------------------|-------------------|-----------------------------|--------------------------------|
| 10.9 bolt   | 1040 N/mm <sup>2</sup>   | 940 N/mm <sup>2</sup>              | 9 %               | 48 %                        | 320 - 380                      |

The dimensions of the specimens used for the different tests are in accordance with DIN EN 10002 Part 5 [9] and are shown in *Figure 3*. The gauge length was 30 mm. The extensometer which was fixed on the specimen was able to measure a maximum extension of 3 mm. The furnace in which the specimen was situated during the tests is equipped with three separate controlled resistor elements and three thermocouples (*Figure 2*). For the steady state test the specimens were heated to a given temperature and held for approximately half an hour. During this time the thermal expansion was permanently controlled due to the fact that this indicates the completion of the warming phase of the specimen. If no further thermal expansion occurs, the warming is completed. The tension test was performed at a strain rate of 0,001/min to provide proof stress values up to 2 %, after that the strain rate was raised to 0,025/min and maintained until rupture. The chosen strain rates correspond to the values given in [9]. The results of this testing method can be shown in a stress strain curve. Three specimens were tested under steady state conditions at each temperature.

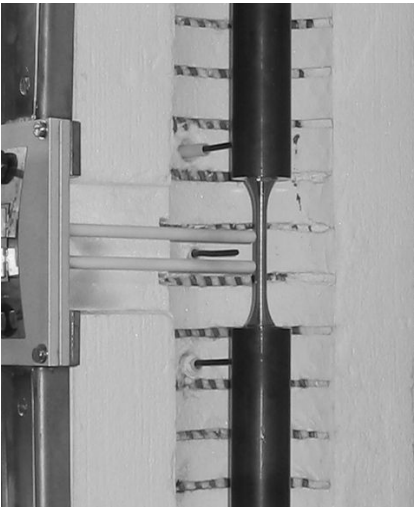


*Fig. 2: Testing device specimen*

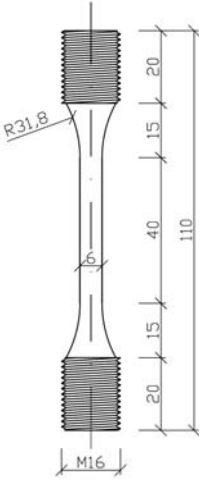


*Fig. 3: Dimensions of specimen in mm*

For the transient test the specimens were located accordingly in the testing device and stressed with a constant load. The steel temperature was additionally measured by a K-Type thermocouple which was directly fixed on the surface of the specimen. The test was performed using a constant heating rate of 10 K/min. The results can be shown in a temperature strain curve. It has to be kept in mind that under these testing conditions the thermal expansion is included in the results which can be eliminated easily as explained before. For the transient tests two specimens were tested at different stress levels. The additionally performed creep tests require a constant loading and a constant temperature. Due to this the specimens were heated up to a certain temperature and loaded subsequently. After applying the load the occurring strain was recorded constantly.

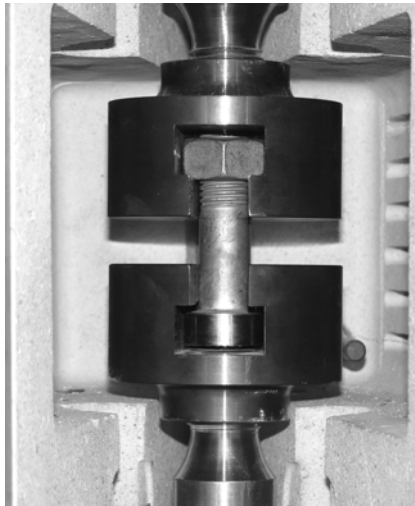


*Fig. 4: Testing device bolt*

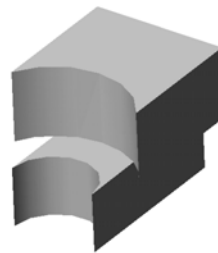


*Fig. 5: Fitting*

The bolt assemblies have been tested in a different device with a maximum traction load of 1000 kN. The load transfer into the bolt assemblies was realized by a bracket made of Nimonic 80A which has been designed to fit with all the constraints like furnace and bolt dimensions. The bracket is shown in *Figure 4*. First tension tests showed that the opening on the front of the bracket, which is necessary to put the bolt in place, has a big impact on the outcome. Due to this an additional fitting was produced to realize a rotation symmetric load transfer to the bolt (*Figure 5*). The bolt temperature was constantly measured by two K-type thermocouples which were fixed on the nut and on the shank of the bolt. Due to the big mass of the brackets the heating phase was very long and a small temperature gradient between shank and nut was not avoidable. Even though, the temperature gradient during the tension tests was smaller than 5°C. After reaching the target temperature it has been maintained constant about half an hour. The tension test of the bolts was performed using a constant strain rate of 0,001/min which was held constant until the end of the test. A code for tension tests of bolt assemblies is not existent and therefore the test procedure follows closely DIN EN 10002 Part 5 [9].

### **2.3 Test Results**

The results of the high temperature tests on the round milled specimens are shown in *Figure 6*. The indicated curves describe the stress-strain relation up to a strain of 2% and are based on the steady state tests. From 300°C onwards the strength reduction is significant and clearly visible, see also *Fig. 7*. At 700°C respectively 800°C the strength is only about 5% in comparison to the strength at room temperature. As indicated before the strain rate was increased after an extension of 2% in order to obtain the tensile strength. The strain rate

acceleration occurs relatively early and leads to a considerably hardening of the material. Comparing the 2% strain stress ratio at 600°C with the tensile strength ratio at the same temperature a hardening of about 70% occurs (Fig. 7). This effect is very interesting comparing it with the results in [3]. There the strain rate was held constant until an expansion of 5% was reached. The maximum strength was obtained within this range, so that a significant hardening effect after 5% was not noticeable. During a transient test this effect will not occur, due to this the tensile strength ratios shown in Figure 7 have to be used very carefully. But on the other hand it is interesting to see, that the tensile strength ratios are fitting with the reduction factors given in the Eurocode 3 Part 1-2 Annex D. Comparing the stress ratio curve at 2% of extension with the Eurocode curve a significant difference can be noticed. The tension tests on bolt assemblies show in comparison to the Eurocode reduction factor curve up to 450°C a similar behaviour, but from that point on the bolt assemblies behave more like the strength ratio curve at 2% strain. From 550°C onwards the 10.9 bolt strength ratio behaves a bit stronger than expected due to the pure material tests. First tests on bolts of a different manufacturer show a similar behaviour. Nevertheless the 10.9 bolt strength ratio runs significantly underneath the Eurocode reduction factor curve given in Annex D. In Figure 6 some additional values resulting from the transient tests are indicated by dots. The values belonging to a temperature of 200°C (Transient test Tr.t. 200°C) are following quite well the curve obtained by a steady state test. This is understandable comparing it with the results of the creep tests. At low temperatures none or just negligible creep deformation occur, so that the transient test results fully correspond with the results of the steady state tests. For higher temperatures the transient test values are quite beneath the corresponding steady state results, due to the fact that from 300°C upwards a creep effect is visible and not further negligible. The horizontal distance in Figure 6 between the transient test values and the steady state curve is approximately the creep deformation tested in the corresponding tests.

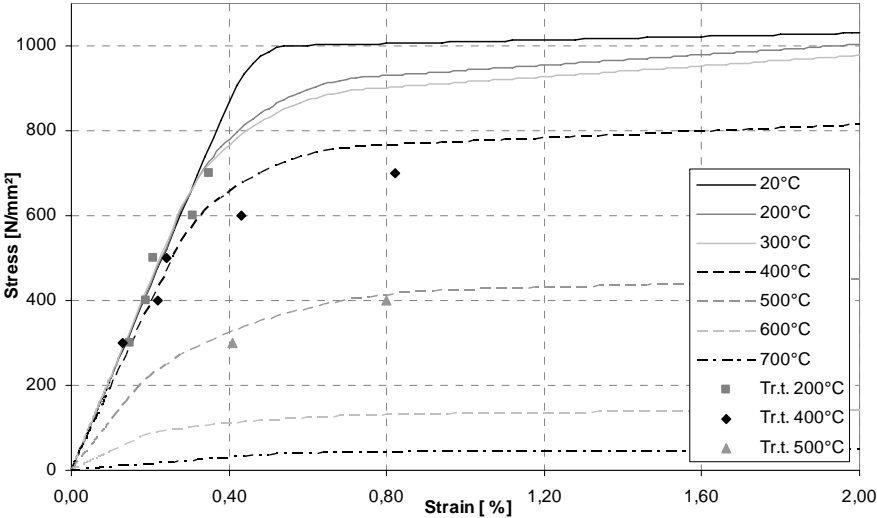


Fig. 6: Stress-Strain Curve

### 3 SUMMARY AND OUTLOOK

The performed tension tests show that high temperatures have a strong effect on the grade 10.9 bolt material behaviour. Comparable tests for this material are nearly not existent. Further examinations will be performed using more bolt assemblies for tension and shear tests.

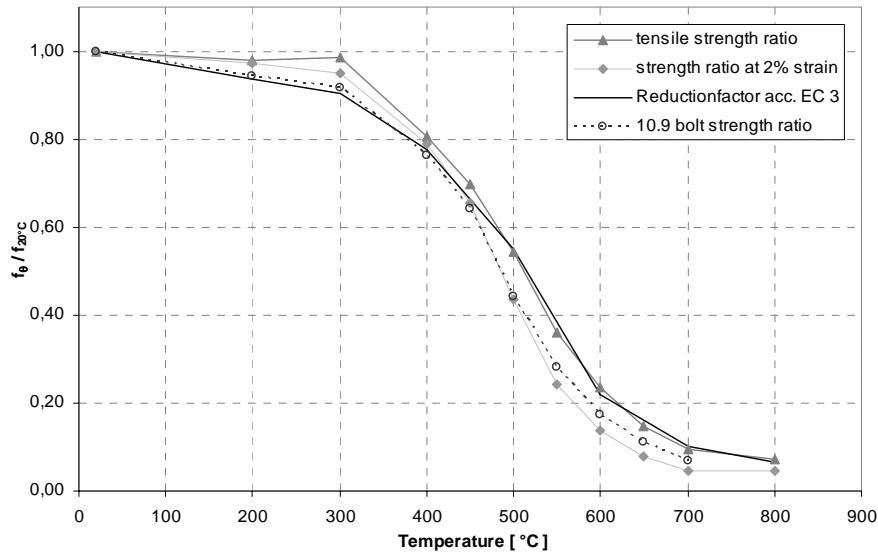


Fig. 7: Reduction factors

## REFERENCES

- [1] Heddrich, Rolf, „Untersuchungen zum Trag- und Verformungsverhalten von Schraubverbindungen bei feuerwiderstandsfähigen Verbundprofil-Konstruktionen unter Brandeinwirkung“, Doctoral thesis D17, *Konstruktiver Ingenieurbau der Technischen Universität Darmstadt*, 1990
- [2] Hongxia Yu, I.W. Burgess & J.B. Davison, “Experimental investigation of the behaviour of fin plate connections in fire”, Proceedings of the 3<sup>rd</sup> International Conference on Steel and Composite Structures (ICSCS07) Manchester, *Taylor and Francis*, 2007
- [3] Kirby, B.R., “The behaviour of high-strength grade 8.8 bolts in fire”, J. Construct. Steel Research 33, *Elsevier Science Limited*, 1995
- [4] Hu Y, J.B. Davison & I.W. Burgess, “Comparative study of the behaviour of BS 4190 and BS EN ISO 4014 bolts in fire”, Proceedings of the 3<sup>rd</sup> international conference on steel and composite structures (ICSCS07) Manchester, *Taylor and Francis*, 2007
- [5] Sakumoto Y., “Test of fire resistant bolts and joints”, Journal of Structural Engineering Vol. 119 No. 11, *ASCE Publication*, 1993
- [6] DIN EN 1993-1-2, “Eurocode 3: Bemessung und Konstruktion von Stahlbauten, Teil 1-2 Allgemeine Regeln – Tragwerksbemessung für den Brandfall”, *Beuth Verlag*, 2006
- [7] BS 5950-8, “British Standard: Structural use of steel work in building – Part 8: Code of practice for fire resistant design”, *British Standards Institution*, 2003
- [8] Anderberg, Yngve, “Modelling Steel Behaviour”, Report LUTCDG/(TVBB-3028), *Lund Institute of Technology*, 1986
- [9] DIN EN 10002-5, “Metallische Werkstoffe Zugversuch Teil 5: Prüfverfahren bei erhöhter Temperatur”, *Beuth Verlag*, 1992
- [10] DIN EN ISO 898-1, “Mechanische Eigenschaften von Verbindungselementen aus Kohlenstoffstahl und legiertem Stahl- Teil 1: Schrauben”, *Beuth Verlag*, 2007

## STAINLESS STEEL BEAM-COLUMNS INTERACTION CURVES IN CASE OF FIRE WITH AND WITHOUT LATERAL TORSIONAL BUCKLING

Nuno Lopes <sup>a</sup>, Paulo Vila Real <sup>a</sup>, Luís Simões da Silva <sup>b</sup>, J.-M. Franssen <sup>c</sup>

<sup>a</sup> University of Aveiro, LABEST-Department of Civil Engineering, Aveiro, Portugal

<sup>b</sup> University of Coimbra, ISISE-Department of Civil Engineering, Coimbra, Portugal

<sup>c</sup> University of Liege, Structural Engineering, Belgium

### INTRODUCTION

The use of stainless steel in construction is increasing [1]. However, it is still necessary to develop the knowledge of its structural behaviour. Stainless steels are known by their non-linear stress-strain relationships with low proportional stress and extensive hardening phase. The EN 1993-1-4 “Supplementary rules for stainless steels” [2] gives design rules for stainless steel structural elements at room temperature, and only makes mention to its fire resistance by referring to the fire part of the Eurocode 3 (EC3), EN 1993-1-2 [3], stating that stainless steel structural members subjected to high temperatures must be designed with the same formulae as those used for carbon steel members. However, as these two materials have different constitutive laws, it can be expected that different formulae for the calculation of member stability should be used for fire design.

In previous papers, [4] and [5], new proposals for the flexural buckling of stainless steel columns and LTB of stainless steel beams were made.

It is the purpose of this paper to evaluate the accuracy and safety of the currently prescribed design rules in EC3: Part 1.2 for the evaluation of the resistance of stainless steel beam-columns with and without lateral-torsional buckling (LTB). In this evaluation the new carbon steel beam-column formulae at room temperature were also tested [6, 7, 8], after being adapted to deal with stainless steel in fire situation.

A parametric study of the behaviour of the several stainless steel grades (austenitics, austenitic-ferritic and ferritics grades) beam-columns subjected to fire are presented, and new proposals for the design of these structural elements are made.

This evaluation is carried out by performing numerical simulations on Class 1 and Class 2 stainless steel H-columns subjected to compression plus uni-axial bending. It is considered buckling in the two main cross-section axes and different bending moments diagrams ( $\psi = 1$ ;  $\psi = 0$  and  $\psi = -1$ ), with and without lateral-torsional buckling. The stainless steel mechanical and thermal properties at high temperatures used in this paper can be found in Part 1.2 of EC3 [3]. The following welded cross-sections were used: HEA200, HEB280 and HEB200. The types of stainless steel grade used were: 1.4301, 1.4003 and 1.4462. An average of 5 beam lengths and 8 bending moment / axial load ratios were analysed for each case. A uniform temperature distribution of 600°C in the cross-section was used.

In the numerical simulations, a sinusoidal lateral geometric imperfection was considered [4]. The adopted residual stresses follows the typical pattern for carbon steel welded sections [4, 9, 10], considered constant across the thickness of the web and flanges.

The program SAFIR [11], a geometrical and material non linear finite element code, which has been adapted according to the material properties defined in EN 1993-1-4 [2] and EN 1993-1-2 [3], to model the behaviour of stainless steel structures, was used in the numerical simulations.

It is shown an evaluation of the performance of the interaction curves obtained with part 1.2 of EC3 [10], concluding that these interaction curves don't provide a good approximation to the numerical results obtained with SAFIR. Therefore it was necessary to find other curves that could fit better these numerical results, testing the new formulae from part 1.1 of EC3 [6] and finally proposing new formulae.

## 1 BEAM-COLUMN WITHOUT LTB

### 1.1 EC3 proposals for fire situation

The EC3 states that the safety evaluation should be made with the same expressions as those used in carbon steel elements, which are

$$\frac{N_{fi,Ed}}{\chi_{i,fi} A k_{y,\theta} \frac{f_{y,\theta}}{\gamma_{M,fi}}} + k_i \frac{M_{i,fi,Ed}}{W_{pl,i} \frac{f_{y,\theta}}{\gamma_{M,fi}}} \leq 1 \quad (1)$$

where,  $i = y$  or  $z$ , and

$$k_i = 1 - \frac{\mu_{i\theta} N_{fi,Ed}}{\chi_{i,fi} A k_{y,\theta} \frac{f_y}{\gamma_{M,fi}}} \leq 3 \quad (2)$$

with, according to [12],

$$\mu_{y,\theta} = (2\beta_{M,y} - 5)\bar{\lambda}_{y,\theta} + 0.44\beta_{M,y} + 0.29 \leq 0.8 \text{ with } \bar{\lambda}_{y,20^\circ C} \leq 1.1 \quad (3)$$

$$\mu_{z,\theta} = (1.2\beta_{M,z} - 3)\bar{\lambda}_{z,\theta} + 0.71\beta_{M,z} - 0.29 \leq 0.8 \quad (4)$$

The equivalent uniform moment factor  $\beta_{M,y}$  and  $\beta_{M,z}$  is determined according to the expression (5), in function of the bending diagram shape.

$$\beta_{M,i} = 1.8 - 0.7\psi_i \quad (5)$$

The curves obtained with these formulae are denoted "EN 1993-1-2" in Figure 2, while the curve "EN 1993-1-2 mod" was obtained together with the new proposal for columns [4].

From figure 2 it can be concluded that the interaction curves from part 1.2 of Eurocode 3 together with the new proposal for columns [4], is closer to the numerical results but still can be improved.

### 1.2 Formulation of a new proposal

Based in the procedure adopted by Talamona [13] for the determination of the carbon steel interaction curves at high temperatures, new formulae for the stainless steel beam-columns safety evaluation were developed and are here presented.

Comparing with EC3 [3, 14] the main changes appear in the determination of the interactions factors  $K_{i,fi}$  ( $K_{y,fi}$  or  $K_{z,fi}$ ).

$$K_{i,fi} = 1 - \frac{\mu_{i,\theta} N_{fi,Ed}}{\chi_{i,fi} A k_{y,\theta} \frac{f_y}{\gamma_{M,fi}}} \text{ with } K_{i,fi} \leq 0.8\bar{\lambda}_{i,\theta} + 0.9 \quad (6)$$

Now the limits for  $K_{i,fi}$  are dependent of the Slenderness. Figure 1 shows the influence in the interaction curves due to those limits.

The interaction curve given by (1) can be written in the following schematic way.

$$N^* + M^* - \mu N^* M^* = 1 \quad (7)$$

Figure 1 shows the shape of the interaction curves for different values of the coefficient  $\mu$ . It is concave for positive values of  $\mu$  (meaning that higher resistance is available) and turns convex with negative values of  $\mu$  (meaning that lower resistance is available). The linear branch near the  $N^*$  axis comes from the limitations of  $k_i = 1 - \mu N^*$  in equations (2) and (6).

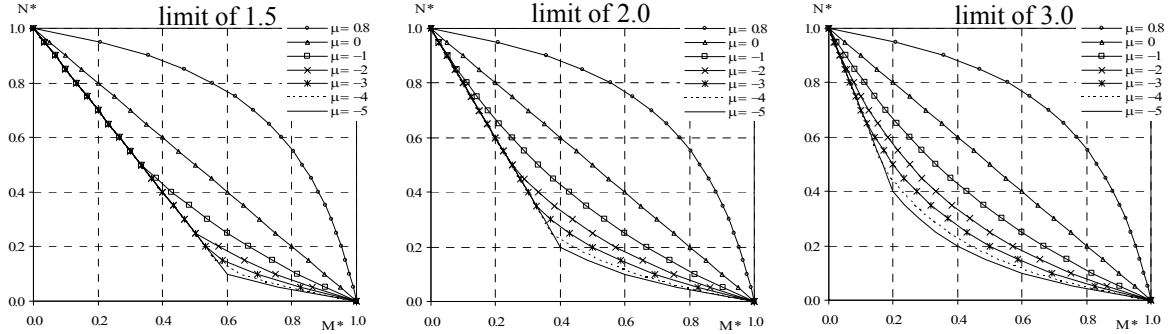


Fig. 1. Interaction curve shape for different interaction factor limits.

To determine the values of  $\mu_{y,\theta}$  and  $\mu_{z,\theta}$  the following equations should be used for the stainless steel grades 1.4301 and 1.4003:

$$\mu_{y,\theta} = (4.33\beta_{M,y} - 8.56)\bar{\lambda}_{y,\theta} + 0.33\beta_{M,y} + 0.11 \leq 0.7 \quad (8)$$

$$\mu_{z,\theta} = (3.03\beta_{M,z} - 6.33)\bar{\lambda}_{z,\theta} + 1.93\beta_{M,z} - 2.45 \leq 0.7 \quad (9)$$

It was found that for the duplex grade, the changes introduced in the flexural buckling curves [15], when compared to the other grades, were not enough to approximate satisfactory the beam-columns numerical results. Therefore, for the duplex stainless steel grade 1.4462 different formulae should be adopted.

$$\mu_{y,\theta} = (1.27\beta_{M,y} - 2.63)\bar{\lambda}_{y,\theta} + 0.66\beta_{M,y} - 0.49 \leq 0.8 \quad (10)$$

$$\mu_{z,\theta} = (1.53\beta_{M,z} - 3.20)\bar{\lambda}_{z,\theta} + 0.41\beta_{M,z} + 0.24 \leq 0.9 \quad (11)$$

The equations from (8) to (11) were developed to approximate the numerical results being on the safe side when compared to them, as shown in the next section.

### 1.3 Accuracy of the proposals

#### Numerical validation

Due to space limitations only few results of the parametric study are shown.

The graphics from Figure 2 were obtained for beam-columns with welded cross-sections equivalent to an HEA200 at 600°C of the stainless steel grade 1.4301, for the buckling modes about the y and z axis, with uniaxial bending in the strong and weak axis respectively. Here, the length of 7m corresponds to  $\bar{\lambda}_{y,\theta} = 0.84$  and was used  $\bar{\lambda}_{z,\theta} = 1.39$ .

The four interaction curves in the graphics from Figure 2 are obtained from: a) part 1-2 of EC3 “EN 1993-1-2”; b) part 1-2 of EC3 with the new proposal for columns [4] “EN 1993-1-2 mod”; c) part 1-1 of EC3 for carbon steel beam-columns with the new proposal for columns

[4] “Method 1” and “Method 2” [6, 7, 8]; and d) the formulated interaction curves presented in the previous section “New proposal”.

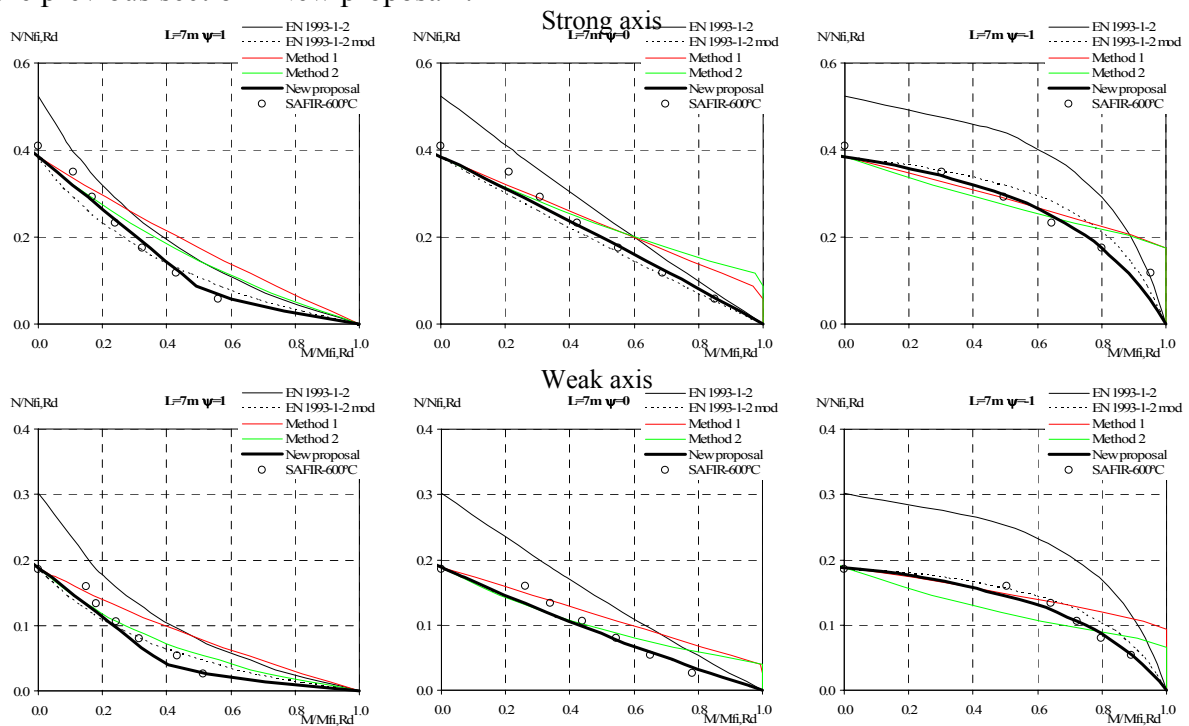


Fig. 2. Comparison between different interaction curves for welded HEA200 beam-columns of the stainless steel grade 1.4301.

The method that is the best approximation of the numerical results from SAFIR is the method “New proposal”. As it can be seen in Figure 2 the other methods present unsafe approximations compared with numerical results.

It can be also observed that the new proposal for columns [4] introduces a significant improvement in the interaction curves.

#### Statistical evaluation

All the obtained results, with the several proposals for the interaction curves (“EN 1993-1-2”, “EN 1993-1-2mod”, “Method 1”, “Method 2” and “New proposal”), are shown in Figure 3.

Table 1 presents the average and standard deviation obtained with the different methods for determining the austenitic and the ferritic stainless steel beam columns interaction curves at high temperatures.

Table 1. Statistical results of beam-columns without LTB at high temperatures.

|             |                    | EN 1993-1-2 | EN 1993-1-2 mod | Method 1 | Method 2 | New proposal |
|-------------|--------------------|-------------|-----------------|----------|----------|--------------|
| Strong axis | Average value      | 1.355       | 1.017           | 1.185    | 1.122    | 0.961        |
|             | Standard deviation | 0.312       | 0.218           | 0.320    | 0.272    | 0.162        |
| Weak axis   | Average value      | 1.342       | 0.973           | 1.188    | 0.951    | 0.903        |
|             | Standard deviation | 0.281       | 0.195           | 0.270    | 0.261    | 0.154        |

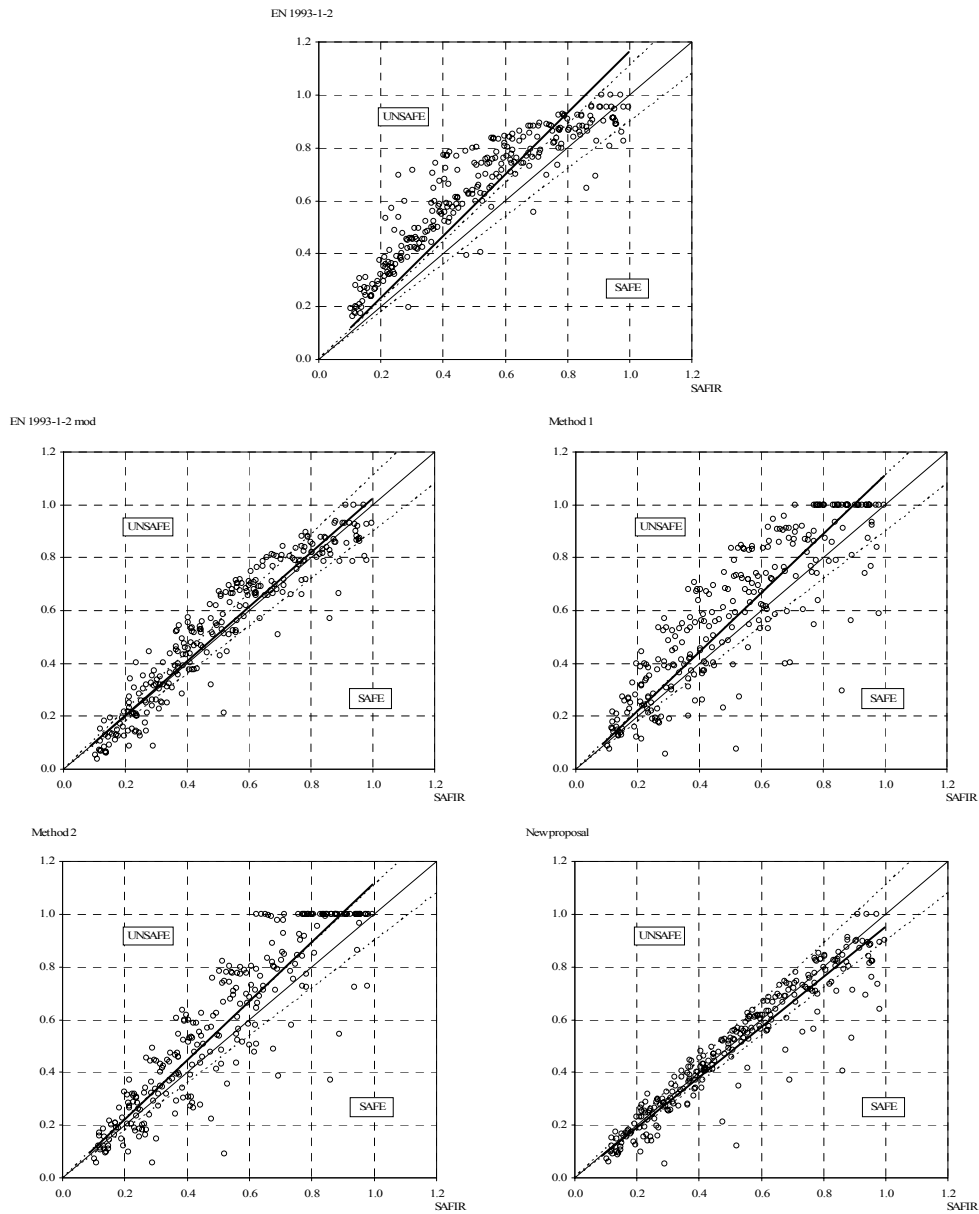


Fig. 3. Comparison with the numerical results for the strong axis for steel grade 1.4301 and 1.4003.

Table 2 presents the average and standard deviation obtained with the different methods for determining the duplex stainless steel beam columns interaction curves at high temperatures.

Table 2. Statistical results of duplex beam-columns without LTB at high temperatures.

|             |                    | EN 1993-1-2 | EN 1993-1-2<br>mod | Method 1 | Method 2 | New<br>proposal |
|-------------|--------------------|-------------|--------------------|----------|----------|-----------------|
| Strong axis | Average value      | 1.004       | 0.860              | 1.065    | 0.993    | 0.956           |
|             | Standard deviation | 0.153       | 0.173              | 0.230    | 0.246    | 0.122           |
| Weak axis   | Average value      | 1.004       | 0.753              | 0.912    | 0.711    | 0.896           |
|             | Standard deviation | 0.132       | 0.181              | 0.223    | 0.236    | 0.178           |

It can be observed that, although having a few unsafe results, the new proposal presents the best agreement with the numerical results for all the stainless steel grades. It is also clear that specific interaction formulae are needed for the 1.4462 stainless steel grade.

## 2 BEAM-COLUMN WITH LTB

### 2.1 EC3 proposals for fire situation

The EC3 states that the safety evaluation should be made with the same expressions as those used in carbon steel elements, which are

$$\frac{N_{fi,Ed}}{\chi_{z,fi} A \frac{k_{y,\theta} f_y}{\gamma_{M,fi}}} + K_{LT,fi} \frac{M_{y,fi,Ed}}{\chi_{LT} W_{pl,y} \frac{k_{y,\theta} f_y}{\gamma_{M,fi}}} \leq 1 \quad (12)$$

where,

$$K_{LT,fi} = 1 - \frac{\mu_{LT,\theta} N_{fi,Ed}}{\chi_{z,fi} A k_{y,\theta} \frac{f_y}{\gamma_{M,fi}}} \quad \text{with} \quad K_{LT,fi} \leq 1 \quad (13)$$

with,

$$\mu_{LT,\theta} = 0.15 \bar{\lambda}_{z,\theta} \beta_{M,LT} - 0.15 \leq 0.9 \quad (14)$$

The equivalent uniform moment factor  $\beta_{M,LT}$  is determined according to the expression (5), in function of the bending diagram shape in the strong axis.

### 2.2 Formulation of a new proposal

It is proposed that the safety evaluation of elements subjected to bending and axial compression with LTB should satisfy expression (12), using the new proposal for LTB presented in [5], and a new  $\mu_{LT,\theta}$  given by

$$\mu_{LT,\theta} = (-0.14 \beta_{M,LT} + 0.11) \bar{\lambda}_{z,\theta} + 0.50 \beta_{M,LT} - 0.09 \leq 0.8 \quad (15)$$

The equation (15) was developed to be a good approximation to the numerical results. In this case it was not necessary to differentiate the duplex 1.4462 stainless steel grade, because of the high values obtained for  $\mu$ .

### 2.3 Accuracy of the proposals

The graphics from Figure 4 were obtained for beam-columns with welded cross-sections equivalent to an HEA200 of the stainless steel grade 1.4301, with the possibility of LTB, with bending in the strong axis. Here, the length of 7m corresponds to  $\bar{\lambda}_{z,\theta} = 1.39$ . The non-dimensional slenderness values for the LTB phenomena are 0.89 for  $\psi = 1$ , 0.67 for  $\psi = 0$ , and 0.55 for  $\psi = -1$ . Again, due to space limitations only few results, of the parametric study, are shown here.

The interaction curves named “EN 1993-1-2 mod” in the graphics from Figure 4 were obtained from part 1-2 of EC3 with the new proposal for columns presented in [4] and with the new proposal for LTB presented in [5], as for the other methods studied (“Method 1”, “Method 2” and “New proposal”).

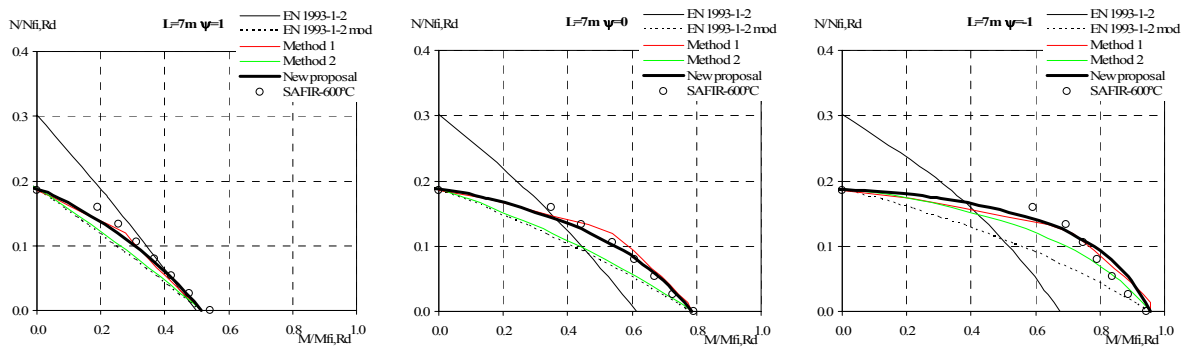


Fig. 4. Comparison between different interaction curves for welded HEA200 beam-columns of the stainless steel grade 1.4301, for beam-columns with LTB.

Figure 4 shows that the best approximation to the numerical results is given by the “New proposal”.

The “Method 1” and “Method 2” [6, 7] also present good approximations. From these two methods, the one that has a better behaviour is the “Method 1”.

It can be also observed that the new proposals, for columns [4] and for LTB of beams [5], introduce significant improvements in the models.

In Figure 5 all the obtained results with the different proposals for the interaction curves (EC3, “Method 1”, “Method 2” and “New proposal”), are shown

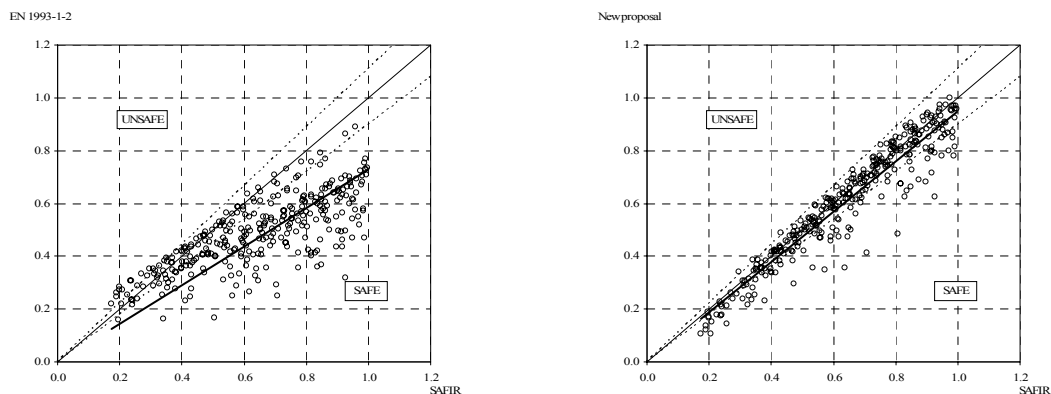


Fig. 5. Comparison with the numerical results for all steel grades, for beam-columns with LTB.

It can be observed that the new proposal presents the best agreement with the numerical results, providing at the same time safety.

### 3 CONCLUSIONS

In this paper, new approaches for evaluating the safety of stainless steel elements subjected to axial compression and bending in the fire situation were presented. These approaches address the influence of global buckling phenomena (flexural buckling and LTB).

The studies on stainless steel beam-columns concluded that the direct adaptation of the new carbon steel interaction curves to stainless steel in case of fire didn't give good results. As a consequence, new interaction curves for the design of stainless steel beam-columns with and without LTB, and at high temperatures, were proposed, providing safe and economic approximations to the obtained numerical results.

The studies presented in this paper were made in different stainless steel grades. Due to the fact that they have different stress-strain relationships at high temperatures, it was necessary to account for this influence, mainly in the ferritic and duplex grades.

## REFERENCES

- [1] Euro Inox and Steel Construction Institute, “Design Manual for Structural Stainless Steel”, 3rd edition, 2006.
- [2] CEN, EN 1993-1-4, Eurocode 3: Design of steel Structures – Part 1-4: General rules – Supplementary Rules for Stainless steels, Belgium, 2006.
- [3] CEN, EN 1993-1-2, Eurocode 3, Design of Steel Structures – Part 1-2: General rules – Structural fire design, Belgium, 2005.
- [4] Lopes, N., Vila Real, P., Silva, L., Franssen, J.-M., Mirambell, E., Numerical modelling of axially loaded stainless steel members under fire conditions, proceedings of the *International Colloquium SDSS’06*, Lisboa, Portugal, 2006.
- [5] Vila Real, P., Lopes, N., Simões da Silva, L., Franssen, J.-M., Lateral-torsional buckling of Stainless steel I-beams in case of fire, *Journal of Constructional Steel Research*, ELSEVIER, 2008.
- [6] CEN, “EN 1993-1-1, Eurocode 3, Design of Steel Structures – Part 1-1: General rules and rules for buildings”, Belgium, 2005.
- [7] Boissonnade, N., Greiner, R., Jaspart, J. P., Rules for Member Stability in EN1993-1-1 Background documentation and design guidelines, *ECCS Technical Committee 8 – Stability*, 2006.
- [8] Lopes, N., Vila Real, P., Simões da Silva, L., Franssen, J.-M., Stainless steel beam-columns in case of fire, proceedings of the *ICSAS’07*, Oxford, United Kingdom, 2007.
- [9] Chen, W. F. and Lui, E. M., Stability design of steel frames, CRC Press, 1991.
- [10] Gardner, L., Nethercot, D., Numerical Modelling of Stainless Steel Structural Components - A consistent Approach, *Journal of Constr. Engineering*, ASCE, 2004.
- [11] Franssen, J.-M., SAFIR. A Thermal/Structural Program Modelling Structures under Fire, *Engineering Journal*, A.I.S.C., 2005.
- [12] Talamona, D., Franssen, J.-M., Schleich, J.-B., Kruppa, J., Stability of Steel Columns in Case of Fire: Numerical Modeling, *Journal of Structural Engineering*, 1997.
- [13] Talamona, D., Flambement de poteaux métalliques sous charge excentrée, à haute température, (in french); *Ph.D. thesis*, Université Blaise Pascal Ecole Doctorale Sciences pour l’Ingenieur de Clermont-Ferrand, 1995.
- [14] Talamona, D.; Castagne, S.; Lopes, N.; Vila Real, P.; Franssen, J.-M. “Comparative study of analytical formulae for the fire resistance of steel beam-columns”, proceedings of the 5th International Conference on Structures in Fire SiF’08, pp. 101 a 112, ISBN 978-981-08-0767-2, Singapore, Singapore, 28 to 30 of May of 2008.
- [15] Lopes, N., Vila Real, P., Simões da Silva, L., Franssen, J.-M., duplex stainless steel columns and beam-columns in case of fire, proceedings of the *SiF’08*, Singapore, 2008.

## **FIRE PROTECTION OF STEEL STRUCTURES USING SPRINKLER SYSTEMS**

Jyri Outinen <sup>a</sup>, Jouko Kansa <sup>b</sup>

<sup>a</sup> Rautaruukki Oyj, Ruukki Construction, Vantaa, Finland

<sup>b</sup> Rautaruukki Oyj, Ruukki Construction, Seinäjoki, Finland

### **INTRODUCTION**

An experimental research program has been carried out in Finland in order to study the cooling effect of two different sprinkler systems in fire situation to steel structures. The aim was to study how the temperatures of the load-bearing structures develop in fire situation, when there's a sprinkler system present. The aim is to have the possibility to use unprotected steel trusses, beams and columns within certain limits when a specified sprinkler network is installed.

The research was based on experimental fire tests [1,2] carried out in a small building built from steel structures in Finland year 2007. The building was constructed only for this research's purposes. The study consists of two kind of different sprinkler systems. One is a traditional sprinkler system and the other is a hi-fog sprinkler system using a lot less water than the previous one. The temperature inside the building was tried to follow the standard fire curve and the temperatures from the surrounding structures were studied.

### **1 BACKGROUND**

It is very common to have a 1 hour fire resistance requirement to load-bearing structures in typical buildings in Finland and also in other European countries. To fulfil this requirement using steel structures needs normally passive fire protection, e.g. intumescent coating, gypsum or other boards to cover and protect the structure. These are naturally simple ways of achieving the fire resistance, but there are also some problems with these.

The aim of this research was to study whether the cooling effect of normal and also the hi-fog sprinkler systems is enough to ensure the temperatures of steel structures to be so low that there is no need for passive fire protection. It is known that automatic water suppression also keeps the fire local in most cases when functioning properly[4].

The fire protection is always expensive whether it is done by passive or active measures. That is why there's also a financial benefit when either of these can be totally or partly left out. The sprinkler system is more important when talking about protecting the people, which of course is more essential than the building itself. Naturally in some cases the passive protection is more reasonable than using active measures.

When the automatic water suppression is required to the building for common fire safety reasons, the use of it also as structural fire protection can be very cost-effective, still not risking the life safety of the occupants or users of the building. When the fire sprinkler system is designed, installed and maintained properly, the risk that it won't work is very little [4]. As it is known the sprinkler systems are required in certain types of buildings with certain criteria. This differs from country to another, even within EU countries.

In some countries the structural fire resistance can be lowered when the fire sprinklers are present. Almost in every country some other benefits in fire safety design can be gained, e.g.

bigger fire-compartments, compromises in smoke extraction etc. This is also the case in Finland and especially the fire-compartment size is a normal compensation.

The Authorities can then decide whether the water suppression system can also be used to lower e.g. the structural fire resistance requirements. These differences in various countries and different building types can be seen from the next Table taken from the European Sprinkler Organisations's homepages [3]. This is just a clip of the original table, which covers more countries and building types. As can be seen e.g. in Germany the Fire rating can be lowered 60 minutes, which is actually one aim of this study also.

Table 1. Summary of Legislative Incentives for Fire Sprinklers. Part of the original Table [3].

| Summary of Legislative Incentives for Fire Sprinklers |                                |   |   |   |  |
|---|--------------------------------|---|---|---|--|
| Construction Alternatives are in red                  |                                |   |   |   |  |
|   | Major airports<br>sprinklered? | Places of<br>assembly   | Shopping<br>Centres   | Industry  | Warehouses   |
| Austria   | No                             |   |   | Larger compartments.  | Depends on height and size of goods but generally requires sprinklers >1800m <sup>2</sup>  |
| Belgium   | Yes                            |   | >2,000m <sup>2</sup>  |   |  |
| Czech Republic  | No                             | Exhibition halls with compartment > 5,000m <sup>2</sup>             | >1,000m <sup>2</sup>  | >20m <sup>3</sup> of flammable liquids  | Postal stores >800m <sup>2</sup><br>>50m <sup>3</sup> of flammable liquids   |
| Denmark   | Yes                            |   | >1,000m <sup>2</sup> multi-floor<br>>2,000m <sup>2</sup> one floor  | >2,000m <sup>2</sup> high fire load<br>>5,000m <sup>2</sup> other fire load<br>Can increase compartment from 1,000m <sup>2</sup> to 10,000m <sup>2</sup>  | >2,000m <sup>2</sup> high fire load<br>>5,000m <sup>2</sup> other fire load<br>Can increase compartment from 1,000m <sup>2</sup> to 10,000m <sup>2</sup> |
| Finland   | Yes                            | Unlimited compartment or halve fire rating and 25% smoke extraction | Unlimited compartment or halve fire rating and 25% smoke extraction   | Unlimited compartment or halve fire rating and 25% smoke extraction   | Unlimited compartment or halve fire rating and 25% smoke extraction  |
| France  | No                             |   | >3,000m <sup>2</sup> or with restaurant or >10,000kg paint<br>Can increase storage of dangerous goods from 1,000m <sup>3</sup> to 2,000m <sup>3</sup>                                     |   | >3000m <sup>2</sup> and less than 6000m <sup>2</sup><br>>6000m <sup>2</sup> with risk assessment and approval from Prefect                               |
| Germany   | Yes                            | >3,600m <sup>2</sup> * or >22m high or below ground                 | >3000m <sup>2</sup> or underground floors >500m <sup>2</sup><br>60 minutes less fire resistance for walls and ceilings; no need for smoke extraction; can increase travel distance by 35m | fire load >15kWh/m <sup>2</sup> and >400m <sup>2</sup><br>fire load >45kWh/m <sup>2</sup> and <400m <sup>2</sup><br>Width >40m & structure not rated<br>Halve fire service water needs<br>Increase compartment area 3-10 times depending on fire resistance<br>Increase first basement floor from 1,000m <sup>2</sup> to 3,500m <sup>2</sup> ; lower floors from 500m <sup>2</sup> to 1,750m <sup>2</sup><br>Can increase travel distances by 15m <5m high; 20m <10m high<br>Need less smoke extraction | >1,200m <sup>2</sup><br>Storage > 7.5m high<br>fire load >15kWh/m <sup>2</sup> & >4<br>fire load >45kWh/m <sup>2</sup> & <4                              |
| Hungary   |                                |   | >8,000m <sup>2</sup><br>>13.65m height  |   | Double compartments  |

## 2 TESTING FACILITIES

### 2.1 Tested building

The fire tests were conducted in Finland in the summer of 2007. A 8mx8mx8m sized steel framed hall was constructed, the sprinkler system was installed to the ceiling and the studied steel trusses, beams and columns and other parts of the building were equipped with temperature detectors. The outer walls were left enough open from the bottom so that there

would be enough oxygen for the fire. In Figures 1 and 2 the basic geometry and the sprinkler locations of the tested system are presented. The outer walls were constructed from sandwich panels and the roof was built from load-bearing corrugated steel sheets with insulations above it. Temperatures were measured also from the corrugated steel sheeting.

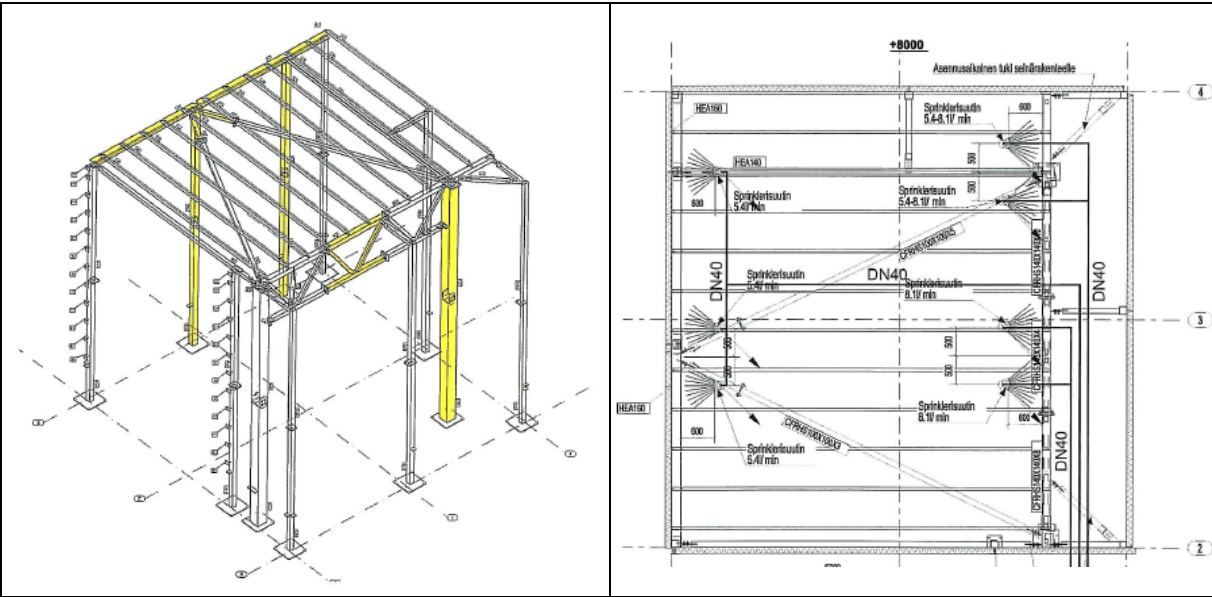


Fig. 1. Skeleton of the structures

Fig 2. Sprinkler nozzles in one test

**2.2 Fire scenario**

The system was to be tested against standard ISO-fire. The fire load was produced by heptan-spray burner, which was situated centrally under the studied structures spreading the fire with three nozzles. The aim was to run the test over 1 hour to get the needed data for the product approval of the system.

**2.3 Tested structures**

The temperatures were measured from tubular steel trusses , beams and columns. Also the temperatures from the connections, bracing and steel sheeting were measured. The height of the steel truss was about 1,5m and it was built from different sized cross-sections. The temperatures were measured from different parts of the truss. The other structures were also selected so that they represented the smaller sized structures normally used, in order to widen the use of the results to bigger sections.

**2.4 Fire sprinkler systems**

Two kinds of sprinkler systems were used in the tests, a traditional water sprinkler system and hi-fog sprinkler system. The nozzles were installed with 3mx3m distances. The water flow of the normal fire sprinkler system was put to very low level in order to define the minimum water flow to the structures that would be needed for the cooling in this kind of a system. In the hi-fog system the sprinklers produce water mist that fulfils the space and with that keeps the fire and the structures cooled during the fire. This system has previously mainly

been used in cruise ships, tunnels and e.g. historic buildings [5] and the aim is to begin to use this system also in wider range of buildings.

### 3. RESULTS

The standard fire exposure was set by using heptan-spray burners underneath the structure system. Temperatures from the installed structures were measured during the test. For the defined set of cross-sections, the temperatures of the steel structures did not raise above critical level in standard fire exposure [1,2].

In figure 3 the temperatures from the steel trusses top chord in one test and in figure 4 the temperatures of the steel sheeting temperatures in another test with hi-fog sprinklers are presented.

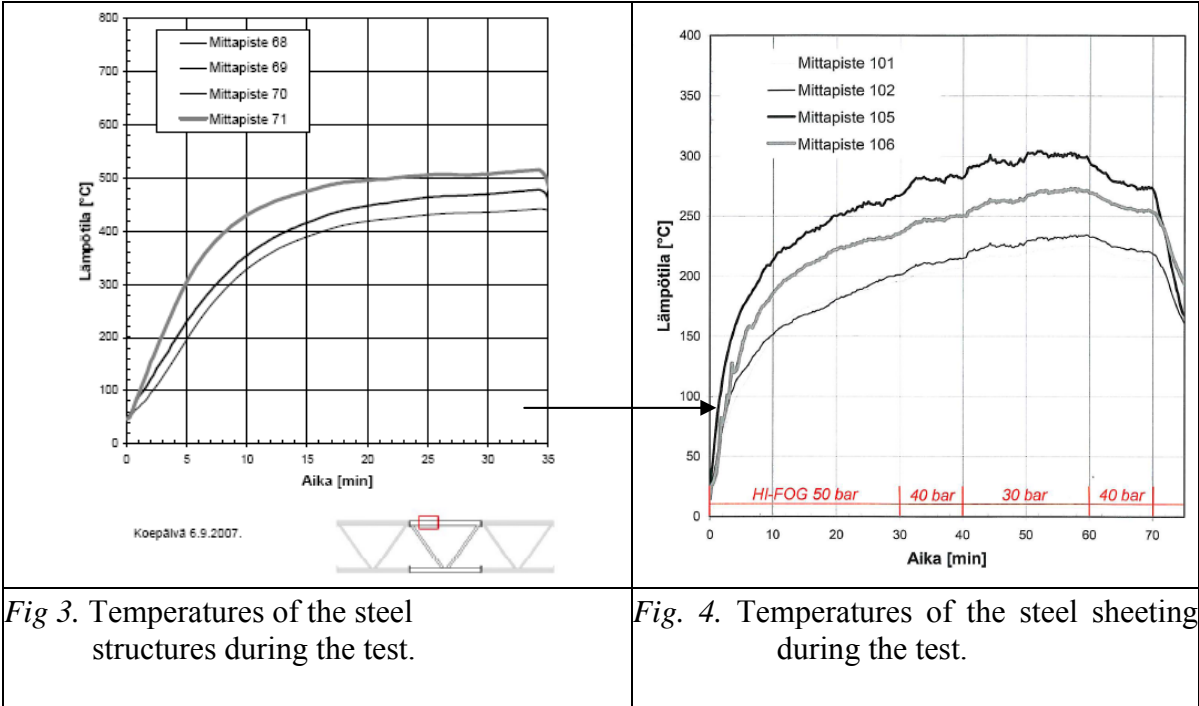


Fig 3. Temperatures of the steel structures during the test.

Fig 4. Temperatures of the steel sheeting during the test.

All in all the temperatures of the structures stayed at adequate level. On the basis of these tests product approvals for 1 hour fire rating were got to the systems. The tests went well and the measurements were carried out successfully.

On the basis of the tests a short design guide for structural design and also for the design of the water sprinkler system was introduced. In these instructions the limitations to the structures, cross-sections, structure dimensions are set. For the water sprinklers the design principles concerning the water flow, number and location of the sprinkler nozzles are instructed.

Some of the tested steel structures and sprinkler system are presented in the next figure 5.

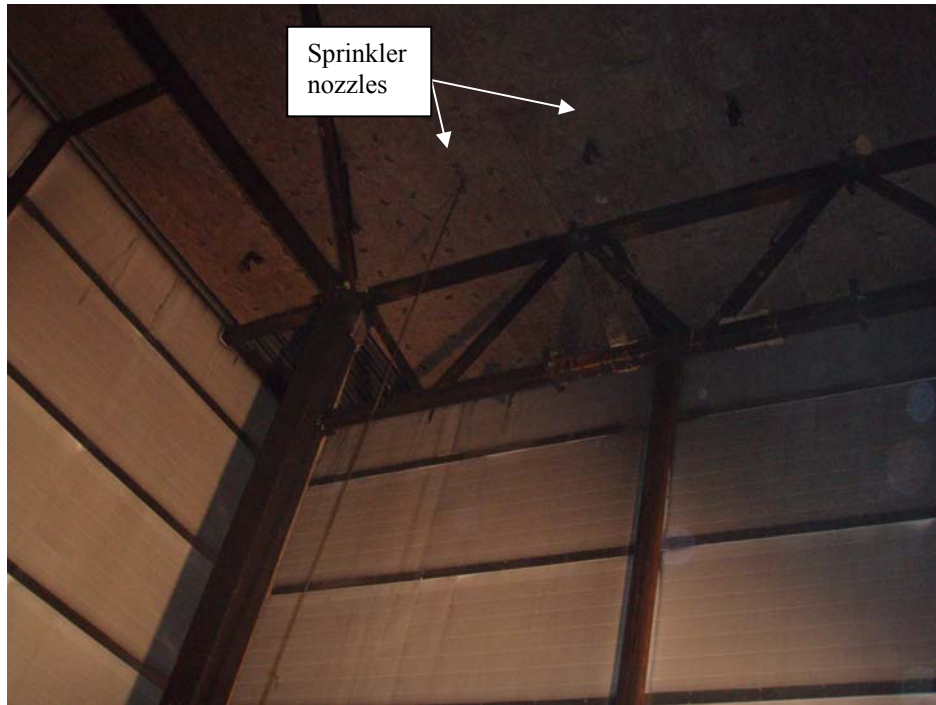


Fig. 5. Tested structures and sprinkler system.

#### 4 SUMMARY AND ACKNOWLEDGMENT

A small experimental study concerning the fire protection of steel structures in standard fire exposure was carried out in Finland. Structural fire protection of steel structures was studied using fire sprinkler systems. Two different sprinkler types were used to study the temperatures in selected steel structures.

The aim was to get fire resistance rating of 1 hour to the system and this was accomplished. The temperatures of the steel structures stayed at very low level so that there is no need for additional fire protection in this kind of case.

As a result the systems got product approvals of 1 hour fire resistance [6]. These systems will be used typically in 1-2 storey building at the moment, but the field of application will be widened in the future.

The writers want to acknowledge the Marioff Corporation, Tampere University of Technology and also Finnish Constructional Steelwork Association for a good co-operation.

#### REFERENCES

- [1] Tampere University of Technology, Fire protection of steel structures with water sprinklers, Report 404/2007/463, Tampere, Finland, 2007
- [2] Tampere University of Technology, Fire protection of steel structures with hi-fog sprinklers, Report Palo 1645/2008, Tampere, Finland, 2008
- [3] European sprinkler organisation homepage, [www.eurosprinkler.org](http://www.eurosprinkler.org)
- [4] Hietaniemi, J., Cajot, L.-G., Pierre, M., Fraser-Mitchell, J. Joyeux, D. & Papaioannou, K. Risk-Based Fire Resistance Requirements. Final Report. Luxembourg: *Office for Official Publications of the European Communities* 2005.
- [5] Marioff Corporation, [www.marioff.com](http://www.marioff.com)
- [6] Finnish Constructional Steelwork Association, FCSA, [www.fcsa.fi](http://www.fcsa.fi)

## FSE ANALYSIS OF A 19th CENTURY CAST-IRON BRIDGE STRUCTURE A performance based analysis of a solution that combines water suppression and ventilation to avoid passive protection.

Ramón Ugartetxe<sup>a</sup>, Fernando Morente<sup>a</sup>, Jon Aurtenetxe<sup>a</sup>, Christian Pérez<sup>a</sup>  
Jesús De la Quintana<sup>b</sup>

<sup>a</sup> Labein-sai. Derio, Spain

<sup>b</sup> Head of Labein-sai. Derio, Spain.

### 1. INTRODUCTION AND GENERAL APPROACH

A cast-iron massive structure enters Bilbao city centre from one of it's iconic bridges to an underground level underneath an English-style park. This underground space has been silent for decades, but new access demands in the city were asking for the shelter that this unexpected "cast-iron tunnel" was giving them.



i

Fig.: Deusto Bridge. Circa 1950

This volume is also giving road path and access to three different buildings, an underground parking, a commercial centre, and the headquarters of an important electrical company. This mean that several hundreds of cars and some small trucks and vans will move in and out through it, and can even collapse it in rush-hours, creating a potentially harmful scenario for people involved there, and for the rest of inhabitants in the surroundings.

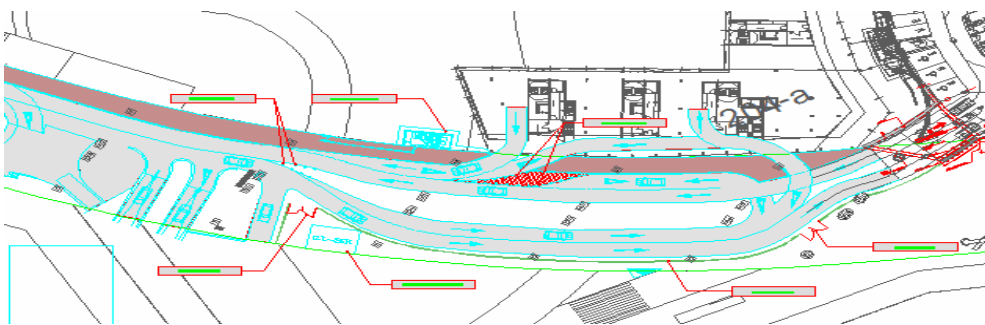


Fig.: General view of the "tunnel" case study.

The mayor problem that arises was that the new function of this structure was exponentially increasing the fire load under it, others than cars, small trucks must be

taken into account reaching a 30Mw value, and thus turning a beautiful bridge into a dangerous tunnel.

Then, last but not least, this nineteenth century cast-iron riveted structure, was in the way to disappear under a thick sturdy layer of intumescent protection required for a one hundred and twenty minutes resistance to ISO fire according to regulatory prescriptions.



Fig.: Structure details.

Bilbao town council architects implore heaven (and technicians) for an alternative safe solution which might fulfil regulatory requirements without destroying structural harmony.

Labein was asked to do a complete “research-meets-practice” work identifying, defining and validating an integrated solution based on a combined fire suppression and ventilation systems. A zone-detection-activation-sprinkler system was proposed together with mechanical ventilation for smoke evacuation.

## 2. FIRE SCENARIOS

Firstly, a risk analysis of the whole infrastructure was made, in which five fire design scenarios were identified as the most extremely dangerous because of their high impact on the structural stability and people’s safety.

It has to be commented that the objective for this fire safety engineering analysis, was holistic in the sense that not only the structural stability has to be assessed, but the final safety of people attending to tenability conditions during escape, and last but not least, safe operation of Fire Brigades were key aspects to be demonstrated.

So fires that block the openings of the tunnel, or the escape routes of people were considered, together with critical fires attending to their position regarding structural elements.

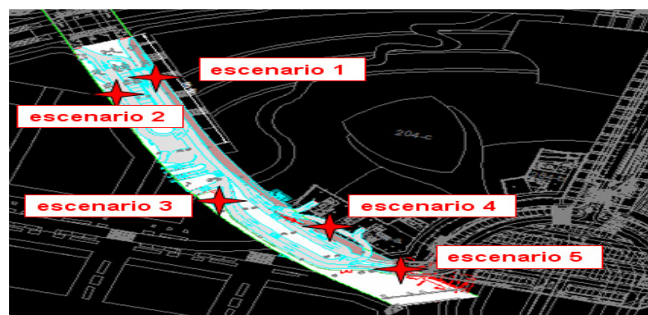


Fig.: Fire scenarios

### 2.1. Fire load and R.H.R. curve

A medium sized van loaded with wood pallets has been considered as the most critical fire load expected, experimental data was obtained to define R.H.R. curve



Fig.: fire load

The R.H.R. (Rate of Heat Release) curve represents the evolution of the fire, for this case the addition of the previous two loads, give the R.H.R. that is shown in the next figure.

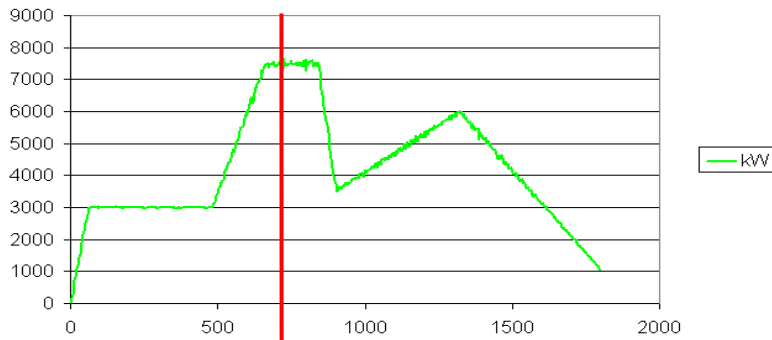


Fig.: Rate of heat release curve.

### 3. ALTERNATIVE SOLUTION

The solution proposed for this case was to turn from a passive protection to an active one including detection, ventilation and fire suppression through sprinklers. Thus early detection and activation of sprinklers will drastically limit the fire to an extent compatible with the structure performance. A performance based analysis is needed to demonstrate that an equal safety level is reached with this solution.

### 4. CFD ANALYSIS

A numerical model of the case study has been prepared in order to calculate the evolution of the fire in the defined scenarios, considering also the interaction of the active systems that need to be assessed.

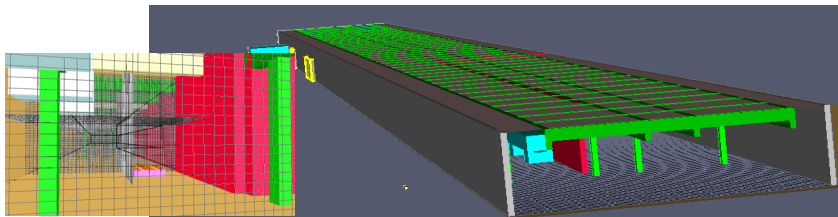


Fig.: Numerical model of the “tunnel”

Thermal and non-thermal effects are obtained. The heat flux over the structure is the key data to establish the thermal actions in the structural analysis and from them to calculate the thermal and thus the mechanical response. Other effects are the visibility, and toxicity of the smoke, so the smoke movement is analysed in detail.

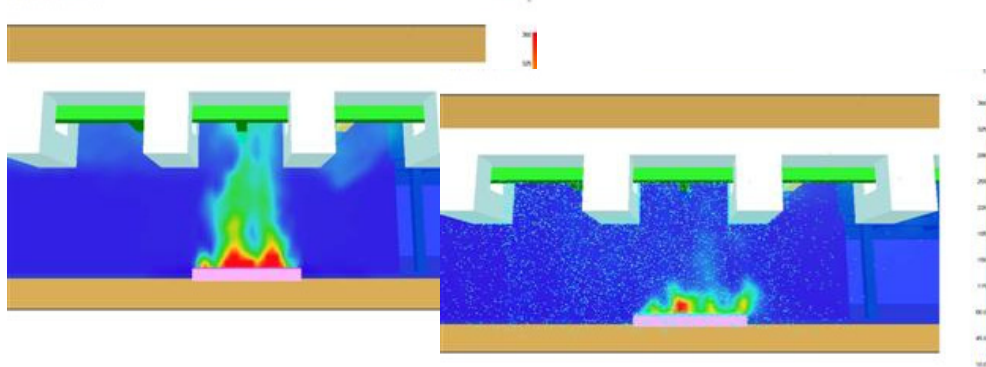


Fig.: Analysis of the fire suppression system performance

## 5. ADVANCED EVACUATION ANALYSIS

This kind of analysis allows the designer to consider how the environmental conditions modified by fire are endangering the escape of people, and how their behaviour is also being modified towards the objective of a safe escape.

A population design is considered including physical and psychological characteristics, and the time changing conditions are inputs from the CFD analysis including both thermal and non-thermal effects.

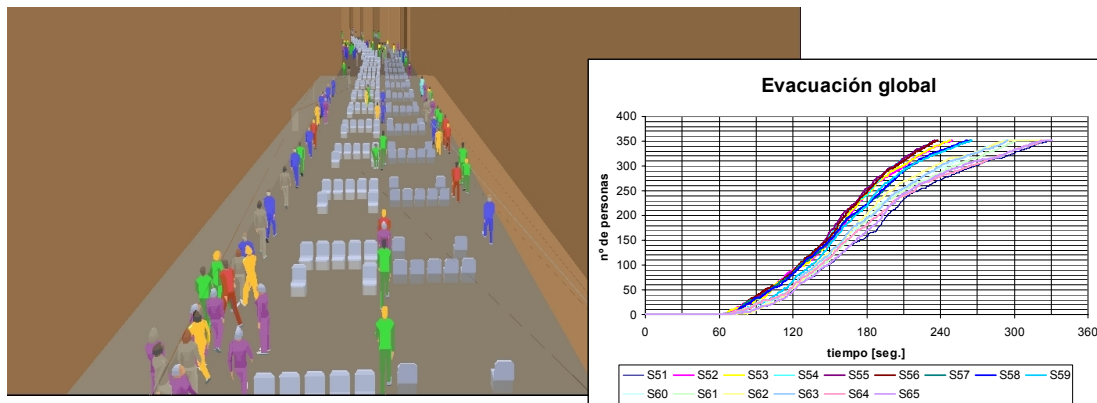


Fig.: Evacuation model and results: Persons / time

## 6. STRUCTURAL ANALYSIS

The structural analysis started with the construction of the structural global model, that include the search of the original drawings, dated 1930, and several topographic studies, and material analysis to determine the state and properties of the iron, elements, and rivets.

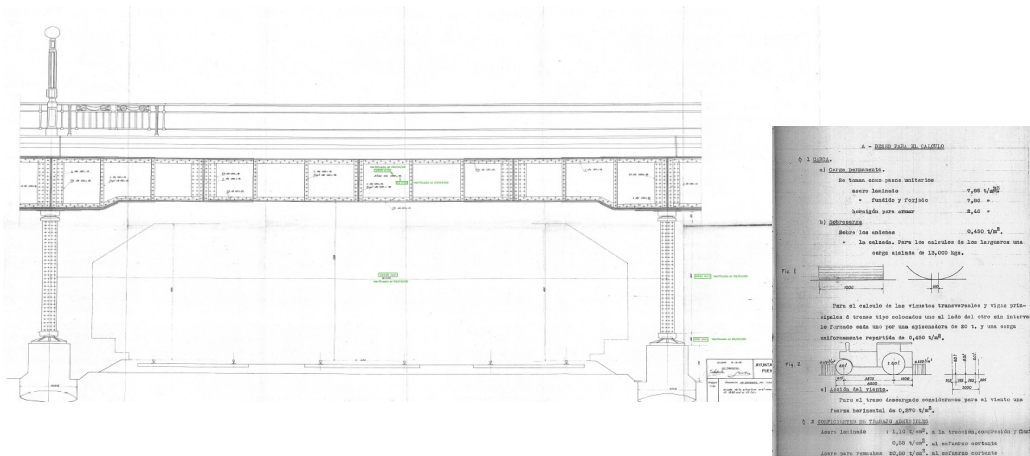


Fig.: Original drawings and calculations. Dated 1930

A global structural model was needed to take the maximum advantage of the interaction of all elements in a combined working performance, as it happens in reality.

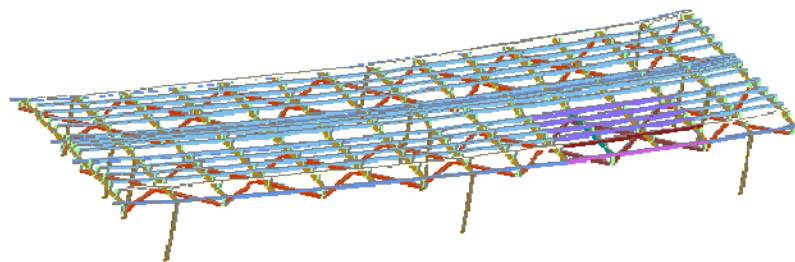
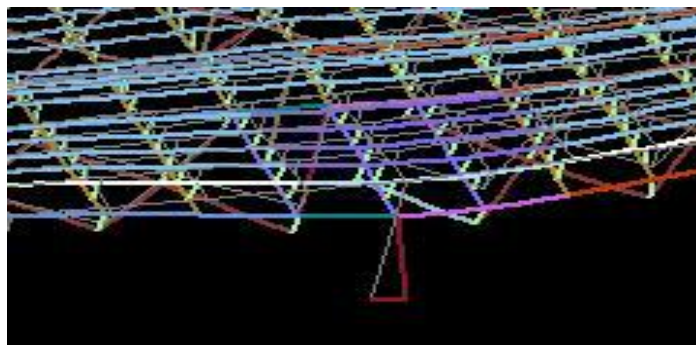
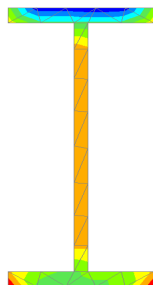


Fig.: Numerical model F.E.M. (beam elements)

Natural Fire Safety Concept was considered according to fire scenarios, but also ISO fire analysis was performed to determine failure modes.



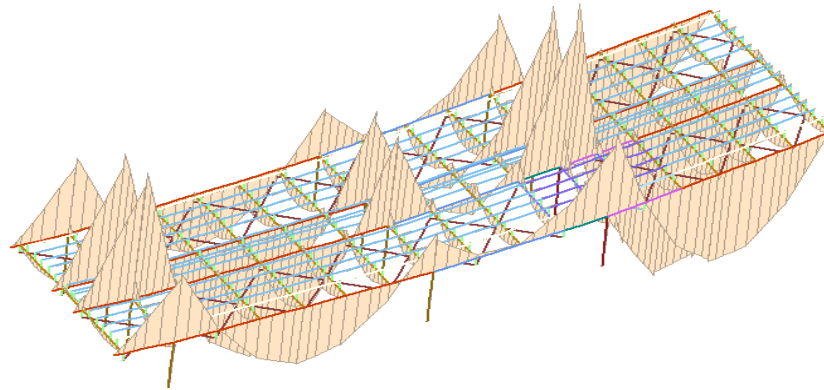


Fig.: Structural results: Thermal response and mechanical response.

## 7. CONCLUSION

No passive protection of the structure was required. A performance based analysis of an alternative solution has allowed to assess structural behaviour and people safety demonstrating that heritage can survive to fire without jeopardizing its beauty and splendour.

### *Acknowledgements:*

*Labein wants to thank Bilbao Ria 2000, for entrusting us in this interesting work with the aim of a safer environment for people using the most advanced technologies for a performance based design .*

## **EXPERIMENTAL RESEARCH ON THE FIRE BEHAVIOUR OF STEEL COLUMNS EMBEDDED ON WALLS**

António J. P. Moura Correia<sup>a</sup>, João Paulo C. Rodrigues<sup>b</sup> & Valdir Pignatta e Silva<sup>c</sup>

<sup>a</sup>Faculty of Sciences and Technology of University of Coimbra & Superior School of Technology and Management of Oliveira of the Hospital. Portugal.

<sup>b</sup>Faculty of Sciences and Technology of University of Coimbra. Portugal.

<sup>c</sup>Polytechnic School of University of S. Paulo, Brazil.

### **INTRODUCTION**

The fire resistance of a steel column is strongly influenced by the conditions in which it is inserted in the building. Beyond other parameters the contact of the column with the building walls has a great influence on its behaviour in fire. The walls, on one hand, have a favourable influence on the fire resistance of the steel columns because they protect a large part of its lateral surface from heating, but on the other hand, they will have an unfavourable influence because they lead to differential heating of the cross-section. The design methods considered in Eurocode 3 part 1.2 do not take into account this fact and the fire resistance is determined as if the heating was uniform [1].

In this paper, the results of fire resistance tests in steel columns embedded on walls, carried out at the Laboratory of Testing Materials and Structures of the University of Coimbra, are presented. The evolution of temperatures registered in the experimental models are compared with the ones obtained in numerical simulations performed with the FEM program SUPERTEMPCALC (STC), developed by Y. Anderberg of Fire Safety Design, Lund, Sweden [2]. SUPERTEMPCALC is a thermal finite element program that solves two-dimensional, non-linear, transient, heat transfer differential equation, incorporating thermal properties which vary with temperature. This program allows the use of rectangular or triangular finite elements, in cylindrical or rectangular co-ordinates. Heat transfer by convection and radiation at the boundaries can be modelled as a function of time.

### **1. EXPERIMENTAL PROGRAM**

The aim of this study was to analyse the thermal behaviour of steel columns embedded in walls. Fire resistance tests with two different column cross-sections, two orientations of the inertia axis in relation to the fire and two thicknesses of the building walls, were tested [3].

The columns had cross-sections of HEA160 and HEA200, steel class S355 and the walls different thicknesses and were made of bricks (fig. 3). The bricks were placed by ordinary cement mortar.

The columns in the test were placed on the center of a 3D restraining frame (fig. 2 a). This frame was composed by columns HEB200 of 3m high and beams HEB200 of 6m span, steel class S355. Two brick walls were then built, one of each side of the column (fig. 2b).

The specimens were instrumented with thermocouples type k (chromo-alumel) in different positions of the cross-section of the columns and on the walls (fig.1).

The thermal action was applied only on one side of the element, in such a way as to permit the analysis of the thermal gradient produced through the wall and across the cross section of the column. The evolution of temperatures in the furnace followed the ISO 834 standard fire curve. The temperatures inside the furnace were measured by shielded probe thermocouples type K in the first 4 tests (cases 1 to 4 in fig. 3) and were later exchanged for plate thermometers in the last 4 tests (cases 5 to 8 in fig. 3). This change was due to the fact that a small delay in the heating of the furnace was observed in the first 4 tests and so the decision to change the thermocouples that controlled the furnace had to be taken.

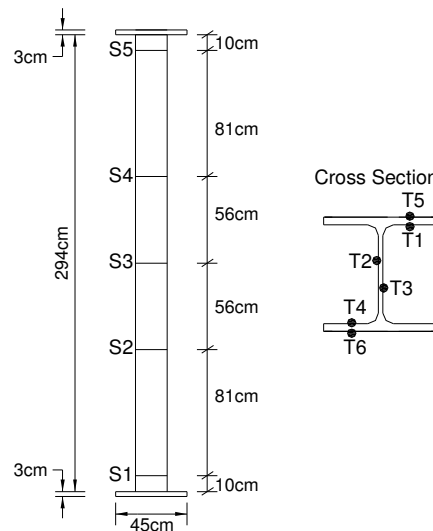


Figure 1 – Specimen and position of thermocouples

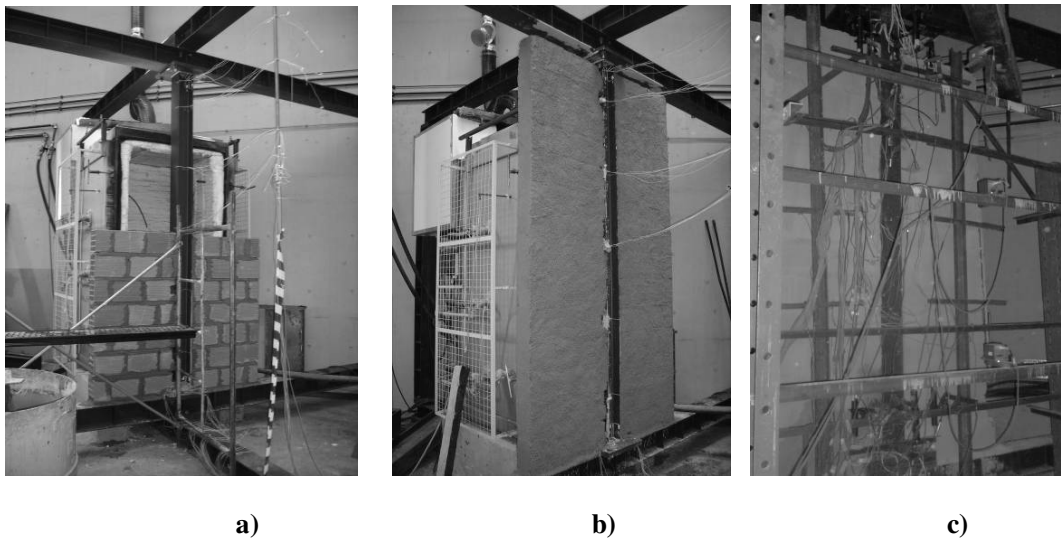


Figure 2 – a) Construction of the test model, b) Column embedded on the wall, c) Instrumentation of the specimen.

## 2. NUMERICAL MODELLING

The computational modelling was performed using the computer code SUPERTEMPALC (STC) – Temperature Calculation and Design v.5, developed by ANDERBERG [2] for thermal two-dimensional analysis of sections exposed to heat of any elements.

The thermal properties of the materials, adopted in this work for the numerical analysis, were the ones presented in Eurocode 3 [1] for steel and Eurocode 2 [4] for concrete parts 1.2. For the mortar covering the bricks the same properties for the concrete recommended by the Eurocode 2 were adopted.

The thermal properties adopted for the masonry were the same as the values adopted in the computer program Ozone developed in the University of Liège, which are: thermal conductivity = 0,7 W/m°C, specific heat = 840 J/kg°C; specific weight = 1600 kg/m<sup>3</sup>; specific heat x specific mass = 1344000 J/m<sup>3</sup>°C.

The emissivity was  $\varepsilon = 0.7$ , for the steel profile, as well as for the masonry and the mortar.

The coefficient of heat transmission by convection in the face exposed to the fire was  $\alpha_c = 25$  W/m<sup>2</sup>°C. For the non-exposed face, the values recommended by Eurocode 1 [5] were used:  $\alpha_c = 4$  W/m<sup>2</sup>°C and  $\varepsilon = 0.7$ .

The models were meshed in finite rectangular elements of 4 mm or 5 mm of side. The computer code STC can draw isothermals, temperature fields, for each instant of time, and, punctually, give the value of the temperature in function of the time.

The cases studied are summarized in figure 3.

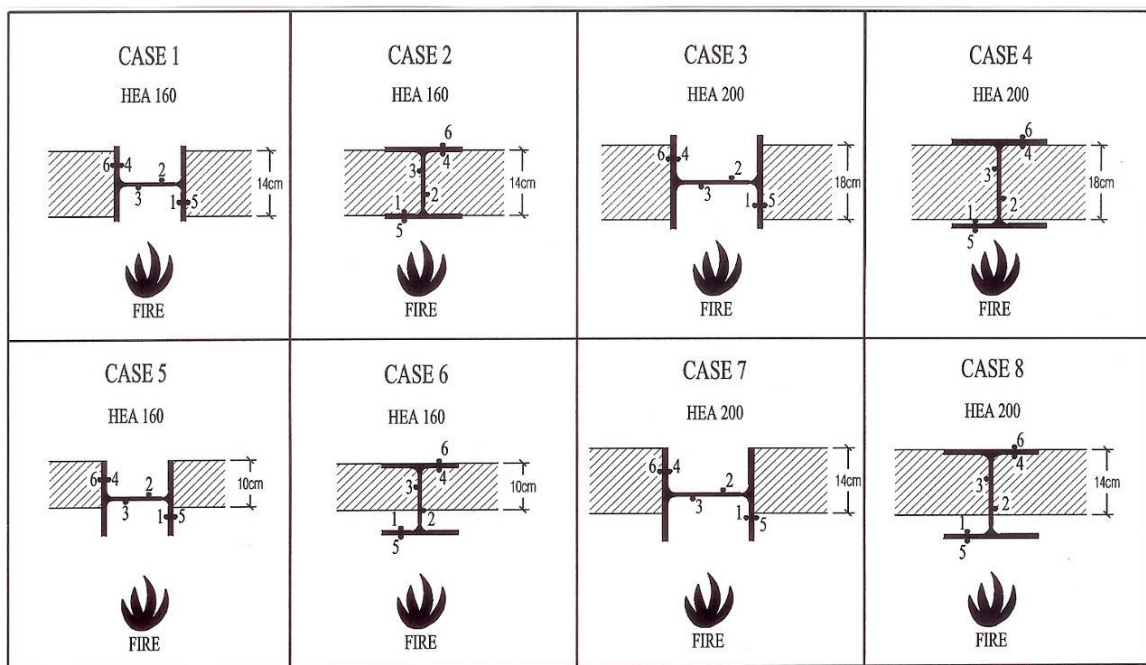


Figure 3 – Cases studied

### 3. COMPARISONS EXPERIMENTAL vs NUMERICAL ANALYSIS

#### 3.1. Furnace temperatures

The temperatures inside the furnace were very uniform in both series of tests (cases 1 to 4 and 5 to 8) however a small delay to the ISO 834 fire curve is observed in the first series of four tests (cases 1 to 4) (fig. 4). As already explained, this delay is maybe related to the type of thermocouples used in the furnace on the first series of tests.

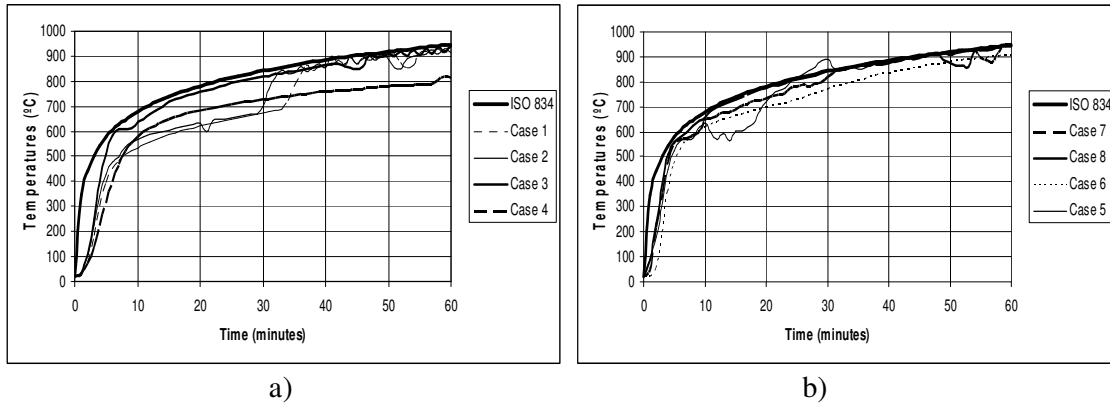


Figure 4 – Furnace curves a) cases 1 to 4 b) cases 5 to 8

### 3.2. Thermal gradients in the cross-sections

Figure 5 shows the isothermals on the cross-section for cases 6 and 7. In case 6 the wall was 10cm thick and in case 7 was 14cm thick. In the figure, one can observe higher thermal gradients in the cross-section for case 6 than case 7. The mechanical resistance of the steel profile is maybe more affected in case 7.

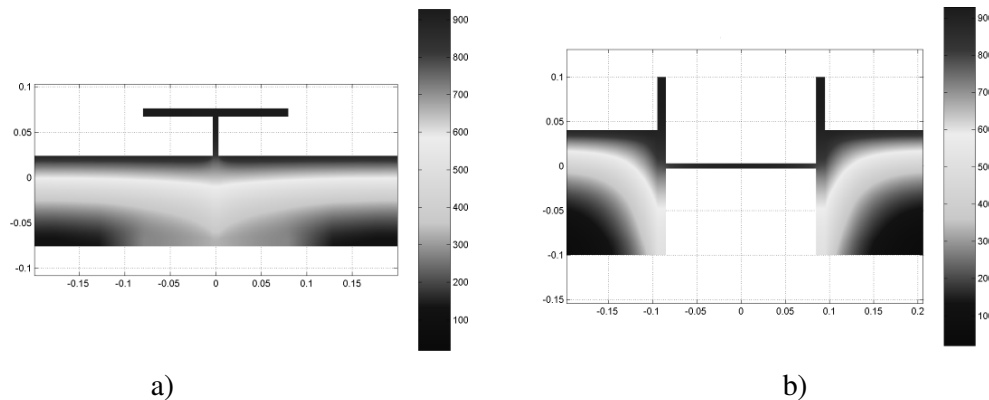


Figure 5 – Isotherms in the cross-section a) case 6 b) case 7

### 3.3. Evolution of temperatures in the middle height section of the steel columns

The temperatures in the experimental tests were measured in 6 points on 5 sections of the steel column (fig. 1). The temperatures in the middle height section of the columns were compared with the ones obtained in numerical simulations for 60min (figs. 6 to 9).

In the case of the web parallel to the wall surface, the temperature in the flange not exposed to the fire (thermocouple 6), is smaller in the case of the walls of smaller thicknesses (figs. 6a and 8a). For the HEA160 the difference is nearly 400°C for the ST calculations and 300°C for the experimental tests (fig. 6a) while for the HEA200 the difference is nearly 300°C for the ST calculations and 150°C for the experimental tests (fig. 8a).

In the face of the web exposed to the fire, the temperatures are higher for the thin than for the thick walls (thermocouple 3), presenting a difference of almost 500°C in the ST simulations and 200°C in the experimental tests (fig. 8b).

In the case of the web perpendicular to the wall surface, the temperature in the exposed flange (thermocouple 5) is higher in the case of the thin wall than in the thicker wall (figs. 7 a and 9a). For HEA160 the difference is approximately 100°C both in the ST simulations and in the experimental tests (fig. 7a). For HEA200 the difference is 300°C in both analyses (fig. 9a).

Curiously in the flange not exposed the temperatures are higher for the thick wall (thermocouple 6). For HEA160 the difference is 200°C in the experimental test and 150°C in the ST simulation (fig. 7b) and for HEA200 the difference is almost 200°C in both analyses (fig. 9b).

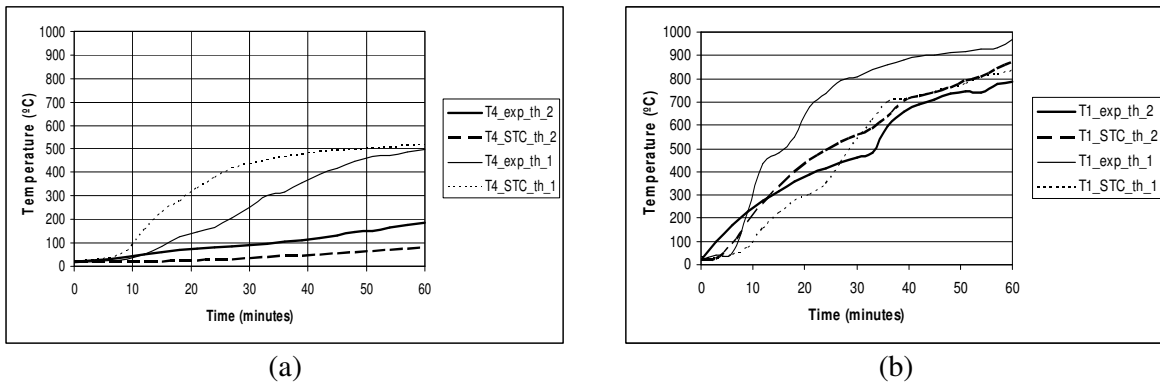


Figure 6– Temperatures vs time for HEA160 with the web parallel to the wall (cases 1 and 5);  
 a) thermocouple T4 ; b) thermocouple T1

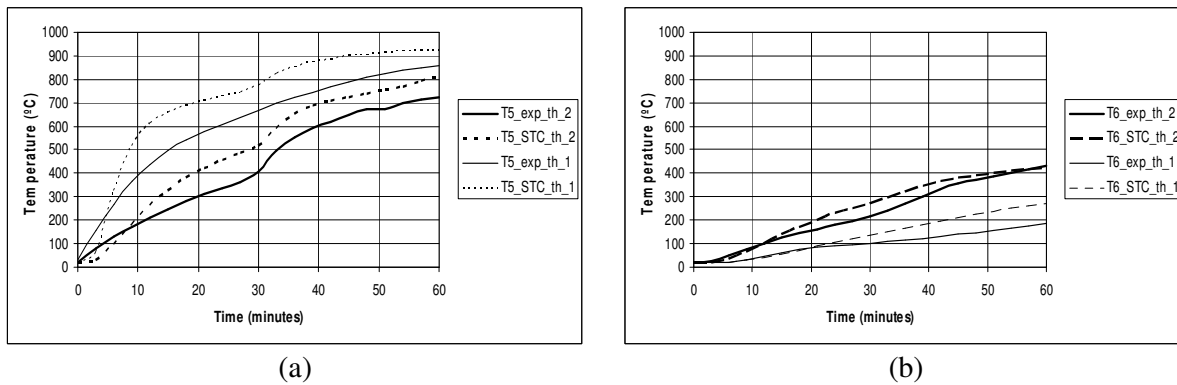


Figure 7 – Temperatures vs time for HEA 160 with the web perpendicular to the wall (cases 2 and 6);  
 a) thermocouple T5 ; b) thermocouple T6

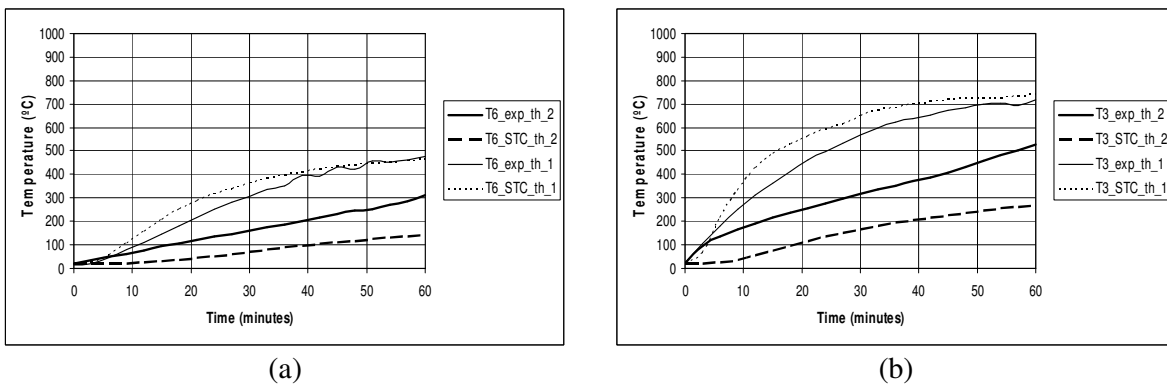


Figure 8 – Temperatures vs time for HEA 200 with the web parallel to the wall (cases 3 and 7);  
 a) thermocouple T6 ; b) thermocouple T3

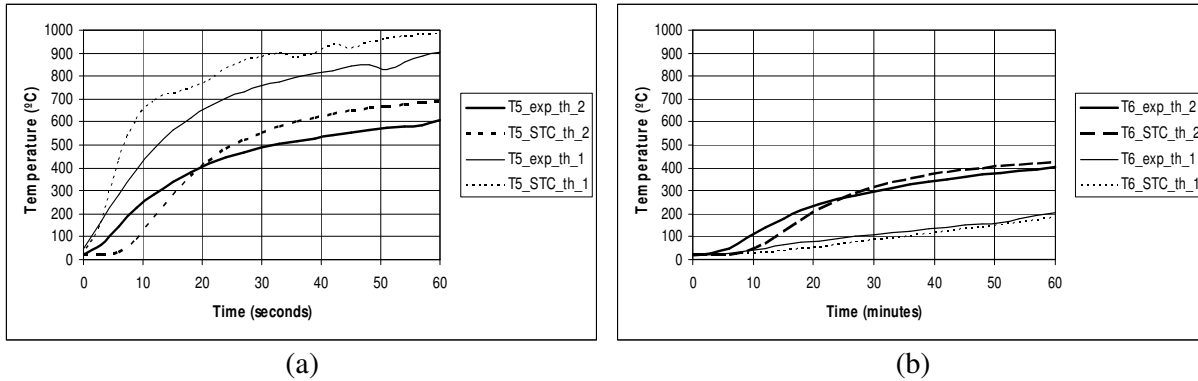


Figure 9 – Temperatures vs time for HEA 200 with the web perpendicular do the wall (cases 4 and 8);  
a) thermocouple T5 ; b) thermocouple T6

#### 4. CONCLUSIONS

For cases with web parallel to the wall surface it was concluded that the thicker wall plays a very important role in reducing the temperatures on the unexposed half of the flange and also in the web.

While for cases with the web perpendicular to the wall surface a quite interesting result was observed, in the unexposed face of the flange the temperatures were slight higher on the thicker wall. On the contrary on the exposed flange the temperatures were much higher for the thinner walls.

#### AKNOWLEDGMENTS

The authors gratefully acknowledge to CBCA, Brazil, FCT - MCTES, PRECERAM S.A., METALOCARDOSO S.A. and A. COSTA CABRAL S.A., Portugal, for their support.

#### REFERENCES

- [1.] Eurocode 3, *EN 1993-1-2, Design of Steel Structures, Part 1.2: General Rules - Structural Fire Design*, European Community (EC), Brussels, Belgium, 2004.
- [2.] Anderberg, Y.; *TCD 5.0 - User's Manual*, Fire Safety Design, Lund, 1997.
- [3.] Correia, A. M, Rodrigues, J. P. C, Silva, V. P.; *Studies on the fire behaviour of steel columns embedded on walls*, 11th International Conference on Fire Science and Engineering - Interflam, London. 2007.
- [4.] Eurocode 2, *EN 1992-1-2, Design of Concrete Structures, Part 1.2: General Rules - Structural Fire Design*, European Community (EC), Brussels, Belgium, 2004.
- [5.] Eurocode 1, *EN 1991-1-2, Basis of Design and Actions on Structures, Part 1-2: Actions on Structures - Actions on Structures Exposed to Fire*, European Community (EC), Brussels, Belgium, 2002.
- [6.] Silva, V. P., Correia, A. M, Rodrigues, J. P. C., *Simulation on fire behaviour of steel columns embedded on walls*, XXXIII Jornadas Sudamericanas de Ingenieria Estructural, Maio 2008, Santiago, Chile.

## NUMERICAL SIMULATION OF STEEL COLUMNS IN FIRE

Luís T. Carvalho<sup>a</sup>, João Paulo C. Rodrigues<sup>a</sup>, Miguel C. Gonçalves<sup>b</sup> & A. Moura Correia<sup>a</sup>

<sup>a</sup> Faculty of Sciences and Technology, University of Coimbra, Portugal

<sup>b</sup> University of Porto, Faculty of Engineering, Porto, Portugal

### INTRODUCTION

The fire resistance of steel columns has been studied for years. A lot of numerical and experimental tests have been performed on single steel columns without thermal restraint. However this does not represent the real behaviour of a steel column in fire. Fire resistance is influenced by thermal restraint forces that are developed in a column when inserted in a building.

In order to clarify the phenomena an experimental program on the fire resistance of steel columns with restrained thermal elongation was carried out in the University of Coimbra. The experimental tests were simulated using the finite element program SAFIR developed by Jean Marc-Franssen, in the University of Liège, in Belgium.

The results of several experimental tests are compared with numerical simulations and several conclusions on the behaviour of steel columns in fire are outlined [1].

### 1. BASES OF CALCULATION OF SAFIR

The design of steel columns in fire can be assessed by means of experimental tests, simplified and advanced calculation methods. The first two are normally devoted to single elements while the third to the entire structure. There are already several advanced calculation models available to calculate structures in fire. SAFIR is one of those programs that perform thermal and the mechanical non-linear analysis of building elements in fire.

The process of calculation of SAFIR consists of two steps, a thermal and a structural analysis. The thermal analysis allows readings of the distribution of temperature in the section exposed to the fire. The mechanical analysis determines displacements and stresses (axial forces and bending moments) in the section. For each element can be defined a different material since they are known its thermal and mechanical properties at high temperatures.

#### 1.1 The thermal analysis

The heat transfer by conduction is described in SAFIR by the Fourier equation that is calculated according to the standard finite element [2]. In this calculation procedure the following hypotheses are considered:

- The materials are isotropic, not submitted to movements, not compressible and have no mechanical dissipation;
- No contact thermal resistance exists in the interface between adjacent materials

The local equation describing conduction in solid materials follows the equation:

$$K \left( \frac{\partial^2 T}{\partial x^2} + \frac{\partial^2 T}{\partial y^2} + \frac{\partial^2 T}{\partial z^2} \right) + Q - C\rho \frac{\partial T}{\partial t} = 0 \quad (1)$$

where:

$$\begin{aligned} K &= \text{thermal conductivity, W/m.K} \\ T &= \text{temperature, K} \\ x, y, z &= \text{coordinates, m} \\ Q &= \text{internally generated heat, W/m}^3 \\ C &= \text{specific heat, J/kg.K} \\ \rho &= \text{specific mass density, kg/m}^3 \\ t &= \text{time, s} \end{aligned}$$

The classical shape functions,  $N$ , are used in the formulation.

If in equation (1) the temperature is replaced by the approximation  $T = N_i T$  and then multiplied by a weighting function and integrated on the volume of the element the equation becomes:

$$\int_{\text{element}} k \{ \nabla N_i \} \{ \nabla N_j \} dv T_i + \int_{\text{element}} C \rho N_i N_j dv \dot{T}_i + \int_{\text{element}} Q N_j dv = \int_{\text{boundary}} N_j q_n dS \quad (2)$$

Where  $\nabla$  means  $\langle \partial/\partial_x; \partial/\partial_y; \partial/\partial_z \rangle$  and  $q_n$  is the heat flux at the boundary of the element.

Finally, when the contributions from all the elements are summed, the matrix (equation 3) is obtained, describing the equilibrium of heat fluxes in the structure at any given instant of time:

$$[K]\{T\} + [C]\{\dot{T}\} = \{g\} \quad (3)$$

where:

$$\begin{aligned} [K] &= \text{matrix of conductivity} \\ [C] &= \text{matrix of capacity} \\ \{\dot{T}\} &= \text{vector of the temperatures at nodes} \\ \{g\} &= \text{vector of heat exchanges at boundaries} \end{aligned}$$

The fact that the thermal properties are temperature dependent is taken into account in equation 3 that expresses the thermal equilibrium at a given time.

## 1.2 The mechanical analysis

The bases of mechanical analysis of structures that experience large displacements is the incremental form of the principal of virtual work. If a total co-rotational configuration is used it is given by equation 4 in which the forces applied on the surface of the structure have not been considered:

$$\int_V (\bar{D}_{ijkl} d\bar{E}_{kl} \delta \bar{E}_{ij} + S_{ij} \delta d\bar{E}_{ij}) dV = \int_V (d\bar{f}_i \delta \bar{u}_i + \bar{f}_i \delta d\bar{u}_i) dV \quad (4)$$

where:

- $V = \bar{V}$  = the undeformed volume of the element
- $S_{ij}$  = tensor of the second Piao-Kirchoff stress
- $\bar{D}_{ijkl} = D_{ijkl}$  = tensor defining the incremental constitutive law of the material
- $\delta \bar{E}_{ij}$  = tensor of the Green virtual field of displacement
- $\bar{f}_i$  = volume forces
- $\delta \bar{u}_i$  = virtual field of displacements from the deformed position of the element

In order to solve this equation in a displacement based finite element formulation we obtain the matrix equation that governs the iteration from one position to the next position of equilibrium:

$$\int_v B^T DBdVdp + \int_v S^T \delta ledVdp = (K_u + K_s)dp = f^{ext} - f^{int} \quad (5)$$

where:

- $B$  = matrix that contains not only spatial derivatives of the shape functions but also the nodal displacements
- $K_u$  = comprises the linear elastic and the geometric stiffness matrices
- $K_s$  = is the stress generated stiffness matrix
- $f^{ext}$  = nodal forces energetically equivalent to the applied forces
- $f^{int}$  = nodal forces obtained from integration of the internal stresses

## 2. EXPERIMENTAL TESTS

In the experimental tests, a new set-up for fire resistance of columns with restrained thermal elongation was developed and used by the Faculty of Sciences and Technology of University of Coimbra (fig. 1).

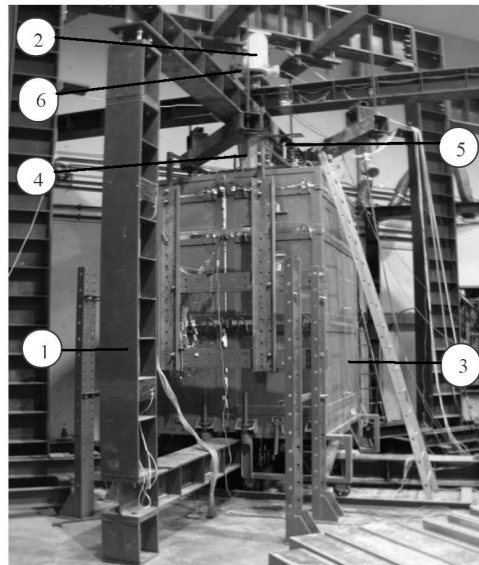


Figure 1. Test set-up for fire resistance tests on building columns

This system comprises a restraining frame of variable stiffness (1) with the function of simulating the stiffness of the surrounding structure to the column in fire.

The columns were subjected to a constant compressive load of 70% of the design value of buckling resistance of the column at room temperature. This load was controlled by a load cell of 1MN located on the head of the hydraulic jack (6). This load simulated the serviceability load of the column when part of a real structure. The load was applied by the hydraulic jack (2) controlled by a servo hydraulic system.

The thermal action was applied by a modular electric furnace (3) that could closely follow the ISO 834 fire curve.

The restraining forces generated in the column due to heating were measured by a load cell of 3 MN located into a steel piston (4). This piston was placed between the testing column and the restraining frame (1).

The axial displacements and rotations on the top and base of the column were also measured by displacement transducers (5) orthogonally arranged in three different points, forming a deformation plane.

In the experimental programme tests were carried out on steel and composite steel and concrete columns with cross-sections of HEA160 and HEA200 with stiffness ratios of 3, 13, 39, 68 kN/mm.

### 3. NUMERICAL SIMULATIONS

The conditions of the experimental tests were reproduced in SAFIR as most rigorous as possible. The 3m column tested was discretized in 14 beam elements with variable lengths, between 100 mm and 280 mm. In the upper part of the column a piston was placed to measure the restraining forces simulated by a solid cylinder of steel measuring 565 mm in length and 300mm in diameter.

The beams and columns of the restraining frame HEB300 that were used to simulate the stiffness of the surrounding structure of the column, were discretized in 60 beam elements with lengths that varied between 375 and 0935mm.

The temperatures considered in the numeric simulations were the ones registered in the steel of the columns in the experimental tests, although the furnace temperature followed the curve ISO 834. In the cross-section it was considered a uniform distribution of temperatures, since the gradient of temperatures for these sections was very small.

The applied axial loads to the columns were the ones in table 1.

Table 1 – Initial loads

|         |         |
|---------|---------|
| HEA 160 | HEA 200 |
| 640 kN  | 1025 kN |

The mechanical and thermal properties of the materials are the ones presented in EC1 and EC3 parts 1.2.

#### Comparison of results

Figure 2 presents the evolution of the restraining forces related to the initial load in function of the mean temperature of the steel of the column. In this figure it can be observed that some difference of values exists, between the experimental tests and the numeric simulations, although the global development of the curves is similar.

In a global analysis, it can be observed that the HEA 200 section suffers a smaller increment of the restraining forces in relation to the HEA 160 section. However the critical temperature in both sections is nearly the same in the tests and the numerical simulations, around 400°C.

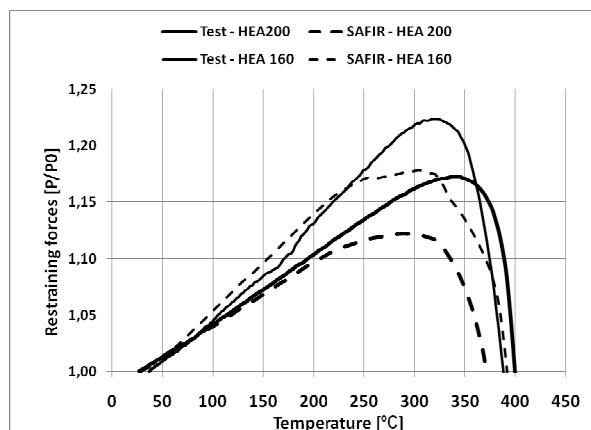


Figure 2 – Restraining forces in function of the mean temperature of the steel

Figure 3 presents the increment of vertical displacements of the columns in function of the mean temperature of the columns.

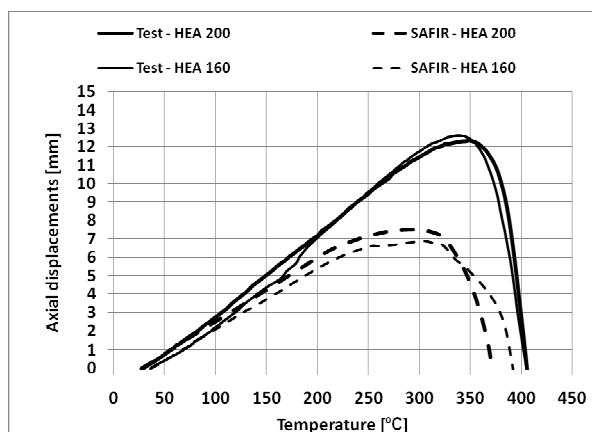


Figure 3 – Axial displacements in function of the mean temperature of the steel

In figure 3 some discrepancy can be observed between the results of the numerical simulations and the results of the experimental tests, although the results of the simulations are very close to each other as well as the results of the tests. For the case of the HEA 160 section, the maximum axial displacement was of 12.63 mm in the tests and 6.87 mm in the numerical simulations. For the case of the HEA 200 section, the maximum axial displacements were 12.35 mm for the test and 7.52 mm for the numerical simulation. A difference in average of 5.30 mm between the numerical simulations and the experimental tests is observed.

The rotations in the top of the column between the tests and the numerical simulations were also compared. In figure 4 the development of the rotations is presented in function of the mean temperature of the steel.

In figure 4 it can be verified that the rotations suffered similar developments in the tests and in the numerical simulations, with values of order of greatness slightly different, mainly in later phases of the tests. Values obtained in tests were of maximum rotations of  $117 \times 10^{-5}$  rad for the HEA160 sections and  $66 \times 10^{-5}$  for the HEA 200 sections. In the numerical simulations, the maximum rotation was of  $16 \times 10^{-5}$  rad for the HEA160 sections and  $5 \times 10^{-5}$  rad for the HEA 200 sections.

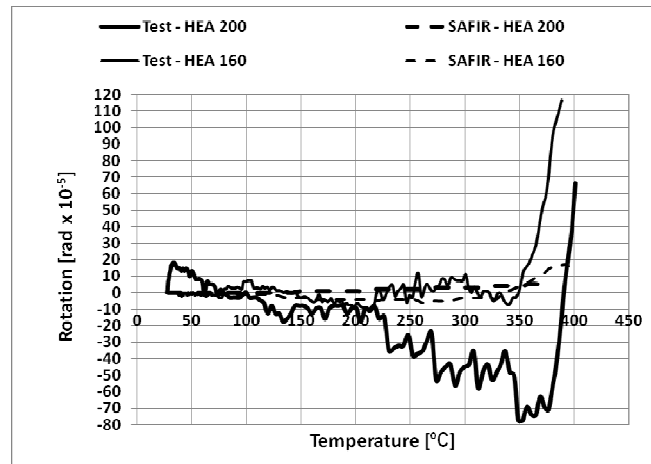


Figure 4 – Rotations in the top of the column in function of the mean temperature of the steel

The values obtained for the rotations of the two cross-sections demonstrate that the superior central node has smaller rotational stiffness in the tests than in the numerical simulation.

#### 4. CONCLUSIONS

The numerical simulations using the program SAFIR described the experimental tests quite well. The differences observed in the restraining forces and in the axial displacements possibly results from the model used and the assumptions made in the numerical simulations for the real test conditions. Some of the differences could be due to the fact that the model cannot correctly foresee the axial and rotational stiffness of the ends of the column.

To sum up, it should be highlighted that in these experiments, there were a large number of factors that could disturb the results. The difference of results obtained between the numeric simulations and the experimental tests can be more or less significant. Factors such as the deviations of straightness of the elements and measurement errors of the sensors are not possible to simulate numerically.

#### REFERENCES

- [1] Carvalho, M. C., *Numerical modelling of steel columns in fire*, MSc Thesis, Faculty of Sciences and Technology of University of Coimbra, 2008.
- [2] Franssen, J.-M.; *SAFIR: A thermal/structural program for modelling structures under Fire*, Engineering Journal, third quarter 2005, pp 143-158.
- [3] EN 1992-1-2, “Eurocode 2: Design of Concrete Structures – Part1-2: General Rules - Structural Fire Design”, European Committee for Standardization, English version, Brussels, Belgium, December 2004.

## UNPROTECTED STEEL IN MULTI-STOREY CAR PARKS 15 min Fire Resistance of Unprotected Steel and Composite Members in a Multi-Storey Car Park System

Prof. Peter Schaumann, Thomas Kirsch

Leibniz University Hannover, Institute for Steel Construction, Hannover, Germany

### INTRODUCTION

Visible steel structures are aesthetically appealing and cost effective. These advantages can often not be used because steel constructions must be protected for reasons of the structural fire safety. Due to numerous examinations no fire resistance of the support structure is



*Fig. 1:* Open multi-storey car park  
(©GOLDBECK)

required in Germany for open car parks. For the reason of high ventilation and low fire load densities even the low fire resistance of unprotected steel is adequate.

Thus, unprotected steel is used by a number of providers of multi-storey car parks in Germany during the last decade (Fig. 1). In some European countries, for example the Czech Republic, the fire resistance level R15 for open car parks is required. The objective of the investigation presented in this paper is to check whether the steel or the composite construction fulfils this requirement. For that purpose the authors calculated the fire resistance time of several steel columns and

composite beams applying different structural fire design methods according to the Eurocodes [1, 2, 3].

### 1 FIRE RESISTANCE REQUIREMENTS IN EUROPEAN OPEN CAR PARKS

A survey of the fire resistance requirements in open car parks in Europe is provided in [4]. It becomes obvious that there is a wide scatter of fire resistance times required in different countries. For example in France there is no differentiation made between open and closed car parks or between car parks above or below ground. So the required fire resistance class is R90 in general. If advanced performance based design methods are applied the requirements to steel members may be reduced. In Finland R60 is required. Other countries for example Great Britain and the Czech Republic accept a shorter fire resistance time of 15 min (R15) for car parks above ground with sufficient ventilation openings (cf. Table G1, [5]).

The use of unprotected steel columns and composite beams in German open car parks is applicable because the building regulations do not require any fire resistance. These boundary conditions have been the reason that in Germany the steel/composite construction has become the standard construction method for open car parks. The company GOLDBECK provided the structural data of its system GOBACAR for the investigations dealt with in this paper. These constructions are designed for room temperature conditions according to the European steel

and composite design codes. The question was whether these unprotected steel members are able to withstand ISO standard fire exposure for short duration of 15 min.

## 2 CALCULATION METHODS

### 2.1 Simple Calculation Method

According to the Eurocodes there are two possible simplified assessment methods to calculate the fire resistance of steel and composite members. The first method is based on the critical temperature. The second method bases on the load bearing capacity at elevated temperatures. Due to possible stability problems especially for columns the second method was used for this investigation. For the steel columns the method of EC3 part 4.2.3.5 [2] and for the composite beams the method of EC4 annex E [3] was used, respectively.

The temperature of the members was calculated by a formula of Eurocode 3 part 4.2.5.1 [2] using heat transfer conditions according to EC1 part 3.1 [1]. As some input parameters are temperature dependent, the calculation has to be carried out incrementally.

Schaumann developed an approximation that allows an explicit algebraic formulation of the heating curves. These formulae are very helpful because they decrease the computing time compared to the incremental method. The

limitation of the area of validity has to be considered (cf. Table 1).

Table 1: Approximation of temperature increase in an unprotected steel section

|  |  |   |
|--|--|---|
| $\theta_{a,t} = \frac{c_1 \cdot c_2 + c_3 \cdot t^{c_4}}{c_2 + t^{c_4}}$ |  |   |
| $c_1 = \theta_0 = 20^\circ\text{C}$                                      | $c_3 = \frac{9875}{0.486 + 1.89 \cdot \ln\left(k_{sh} \frac{A_m}{V}\right)}$ |   |
| $c_2 = 11890 \cdot \left(k_{sh} \frac{A_m}{V}\right)^{-1.12}$            | $c_4 = 1.253 + 0.071 \cdot \ln\left(k_{sh} \frac{A_m}{V}\right)$             |   |
| $\left(\frac{A_m}{V}\right) [\text{m}^{-1}]$                             | Area exposed to fire divided by volume                                       | Min: 25 m <sup>-1</sup><br>Max: 300 m <sup>-1</sup> |
| t [min]  | Time   | Max: 30 min   |
| $\Theta_{a,t} [^\circ\text{C}]$  | Steel temperature  | Max: 700°C  |

### 2.2 Advanced Calculation Method

The more sophisticated and presumably more exact way to achieve the fire resistance time for steel and composite members is the advanced calculation method. At the Institute for Steel Construction the software BoFire is used for this task in most cases. BoFire is a finite-element software based on work done by Schaumann [6] in 1984. It allows simulating the load bearing behaviour of two dimensional bars and frames of steel, concrete and composite constructions. Therefore BoFire is a "Level-3"-method concerning EC3 [2] and EC4 [3]. In 2001 the software was modified by Upmeyer [7] to implement actual material properties concerning the Eurocodes and to give a possibility to use design fires instead of the ISO standard fire.

### 3 CALCULATION OF FIRE RESISTANCE OF COMPOSITE BEAMS

The study included two different composite beams and twelve columns belonging to the GOBACAR system. The members of the construction system and the applied loads were taken out of the static calculation for a completed car park in Dresden. The two beams consist of a steel section and a concrete slab with a thickness of 103 mm and an effective width of 2500 mm. According to Fig. 2 the first section comprises a hot rolled beam (IPE400a) while the second comprises a welded beam. The slab is connected to the steel section by headed

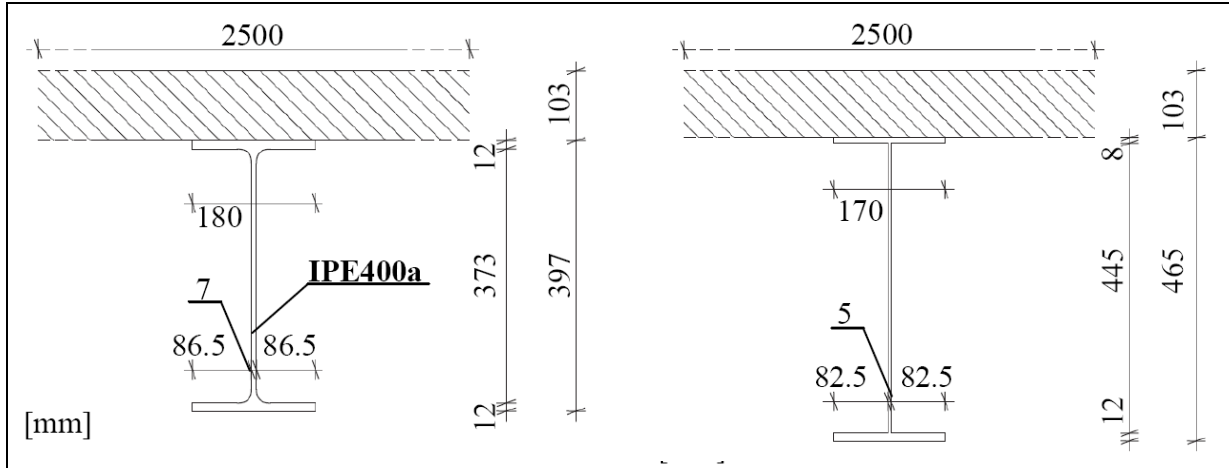


Fig. 2: Dimensions of composite beam with IPE400a profile (left) and welded profile (right)

studs. The materials of both composite beams are equal. Steel grade S355J2G3 and concrete grade C35/45 are used. The headed studs have a maximum tensile strength of 450 N/mm<sup>2</sup>. According to the load, the assumption of the characteristic dead load is obligatory. The live load is normally multiplied by the combination factor  $\Psi_2$  in case of fire. For traffic areas a value of  $\Psi_2=0.3$  is taken for this in general. Alternatively a more realistic approach of applying the characteristic values of the live load limited to the parking bay area was conducted. In this approach live loads on the lane between the slots were not taken into account. The resulting bending moments are nearly identical. For the further investigation the bending moment calculated by the realistic approach was used. This led to a total design moment of 315 kNm for the hot rolled composite beam (IPE400a) and due to less self weight 311 kNm for the welded one. For the reason that the assembly of the car park is symmetric, the beams can be used for most parts of a storey. Only a few beams in the ramp area are shorter and for that reason not relevant. The load on the beams is also practically equal for each storey. So it was possible to calculate just one beam exemplarily for all beams in the car park.

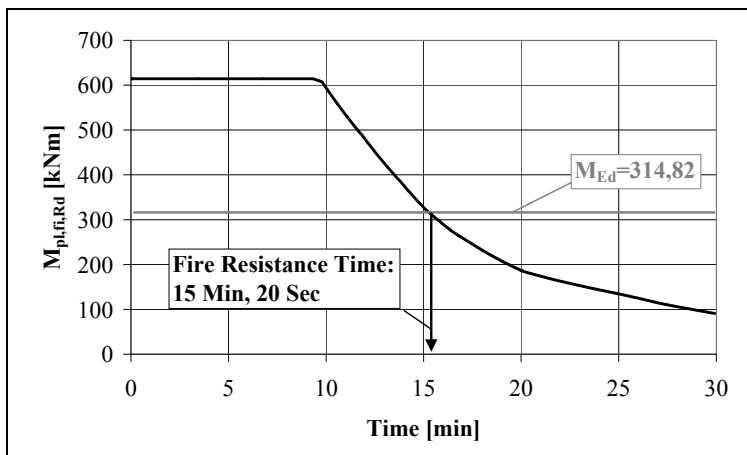


Fig. 3: Time dependent plastic moment capacity of composite beam with hot rolled section IPE400a

explicit formulae for calculation of the steel temperature were also used and verified. As the

next step the procedure concerning EC4 annex E [3] was used. So the cross sectional area of any part was multiplied by the yield stress decreased by the reduction factor for steel members  $k_{y,\Theta}$  concerning Table 3.2 of EC4 [3]. In this way a resulting force was found for the web and both flanges. By calculating the dependent compressive force of the concrete slab and the inner lever arm, the plastic bending moment was found for every increment. That way the exact time when the plastic moment decreased to a value less than the applied moment of 315 kNm was determined to 15 min and 20 sec (cf. Fig. 3). The plastic moment at 15 min is 328 kNm. So the fire resistance class R15 is reached by the composite beam with the IPE400a section.

Because the flanges and the web of the welded profile are thinner than the parts of the IPE400a profile, the heating of the member is faster. This leads to a fire resistance time of only 14 min and 5 sec. Because of this result advanced calculation methods were applied.

The thermal material properties, the heat transfer coefficient  $\alpha=25 \text{ W/m}^2\text{K}$  and the emissivity coefficient  $\epsilon_r=0.8$  were taken from the Eurocodes. The configuration factor  $\Phi$  was set to 1.0 according to EC1 [1]. The plastic moment capacity after 15 min calculated by BoFire is 251 kNm. This is less than the needed plastic moment of 311 kNm and even less than the plastic moment of 272 kNm calculated by the simple calculation method of EC4 [3]. Reason for the difference is a difference in the steel temperatures. The shadow factor  $k_{sh}$  taken into account in the simplified calculation method causes lower steel temperatures than the heat transfer assuming a configuration factor  $\Phi = 1.0$  in the advanced calculation method. This conflicts with EC4-1-2 cl.4.1(3) which reads: "Tabulated data and simple calculation models should give conservative results compared to relevant tests or advanced calculation models." The shadow factor  $k_{sh}$  has been established to consider the fact that not every part of the open section is equally and directly exposed to the fire. Concerning advanced calculation methods, there is a possibility to reduce the heat flux into the member by reducing the configuration factor  $\Phi$ , but there is no default value given in the Eurocodes for this purpose. Improvement may be based on experimentally checked configuration factors  $\Phi < 1.0$ . For the time being the fire resistance time calculated by advanced calculation methods is less than calculated by the simple method in this case.

#### 4 CALCULATION OF FIRE RESISTANCE OF STEEL COLUMNS

In contrast to the beams there are differences in the load and thus in the cross section of the columns for the different storeys. In higher car parks the columns of the ground storey need to have a higher load bearing capacity. There are also four different types of columns in any storey. For this reason at least twelve types of columns were analysed including car parks with 2, 4 and 6 storeys. The most interesting four columns are shown in Table 2.

Table 2. Column types for different positions and loads

| Number of storeys | Position of column | Normal force [kN] |                 | Bending moment[kNm] |                 | Profile |
|-------------------|--------------------|-------------------|-----------------|---------------------|-----------------|---------|
|                   |                    | at 20°C           | in case of fire | at 20°C             | in case of fire |         |
| 2                 | Edge column        | 311               | 202             | 9                   | 6               | HE-140A |
|                   | Internal column    | 614               | 399             | 7                   | 5               | HE-180A |
| 6                 | Edge column        | 932               | 606             | 9                   | 6               | HE-220A |
|                   | Internal column    | 1841              | 1197            | 7                   | 5               | HE-280A |

The columns with highest load utilisation ratios are the internal columns while the columns exposed to the maximum bending moment are the edge columns. The two other types of columns are located in the ramp area and their number is lower.

The buckling length of all columns for calculation at 20°C is 2.7 m. This is equal to the height of every storey. In case of fire the static system changes for the ground storey to 0.7 times of the length at 20°C. This leads to a buckling length of 1.89 m.

The constant temperature field of the columns was calculated by the simple method of EC3 [2]. The calculation of the fire resistance was carried out by comparing the load bearing capacity to the applied load using the calculation method of EC3 part 4.2.3.5. The method implies the lateral and the lateral torsional buckling by decreasing the resistance against normal forces. The temperature dependent load capacity was determined for every timestep. So in Table 3 the time is given at which the load capacity becomes less than the applied load. This time is defined as the fire resistance time.

Table 3. Calculated fire resistance time and required profiles (R15) for different column types

| Number of storeys | Position of column | Used profile | Calculated fire resistance time | Required profile (R15) | Calculated fire resistance time |
|-------------------|--------------------|--------------|---------------------------------|------------------------|---------------------------------|
| 2                 | Edge column        | HE-140A      | 10:01                           | HE-200A                | 15:50                           |
|                   | Internal column    | HE-180A      | 11:15                           | HE-220A                | 15:00                           |
| 6                 | Edge column        | HE-220A      | 12:33                           | HE-260A                | 15:45                           |
|                   | Internal column    | HE-280A      | 13:03                           | HE-320A                | 15:53                           |

The fire resistance time for all actual used profiles is less than 15 min. This is caused by the high load utilisation factor of nearly 1.0 calculated at 20°C. The advanced calculation by BoFire leads to a shorter fire resistance time than the calculation by the simple method of EC3 [2]. This is caused by the use of the shadow factor  $k_{sh}$ , again.

The minimum required profile to reach the aim of R15 is also given in Table 3. For all columns there are profiles needed which are minimum two classes bigger than the already used. This leads to the assumption that it is cheaper to use fire protection materials instead of increasing the size of the steel columns. However, it is possible to use unprotected steel columns for car parks if the fire resistance class R15 is required.

## 5 CONCLUSIONS

The calculation of the fire resistance time by the simple and advanced calculation methods showed that the more sophisticated method leads to a more conservative solution in this case. This is presumably caused by the shadow factor  $k_{sh}$ . This factor is not applicable to advanced calculation methods. The average decrease of the steel temperatures caused by the shadow factor is determined to 95% for the columns ( $k_{sh}=0.85$ ) and 93% for the composite beams ( $k_{sh}=0.7$ ). It is obvious that a calculation with advanced methods can not compensate this reduction of temperatures unless taking into account this shadow effect. So the calculated fire resistance time was not increased for the analysed members.

The exact calculation of the fire resistance time of the analysed members by simple calculation methods according to the Eurocodes showed that it is possible to meet the fire resistance class of R15 for composite and steel members. To reach this aim it is necessary that the steel part of the members has either a minimum thickness or a maximum load utilisation factor. It is shown that the investigated hot rolled IPE beam can be used without any fire protection for car parks with a required fire resistance class of R15. In contrast the welded beam with thinner web and flanges is not reaching the required fire resistance class. Concerning the columns the load utilisation factor at 20°C is very high for economic reasons and the fire resistance time is less than 15 min. The class R15 can be reached by using profiles with an increased cross sectional area (overdesign).

## 6 SUMMARY AND ACKNOWLEDGEMENT

The standard construction method for multi storey car parks in Germany is the steel and composite construction. This is caused by the fact that no structural fire resistance is required according to the building regulations for open car parks. In some other European countries, for example the Czech Republic, a fire resistance class of R15 is obligatory. This leads to the question whether the steel structure of German car park systems withstands this short fire exposure. So the fire resistance time of two composite beams and twelve steel columns was calculated in this investigation.

The calculation of the steel temperature was conducted by the incremental simple method of Eurocode 3 and by an approximated explicit formulation. It has become obvious that the approximated formulae are adequate to calculate the steel temperature in its application range. Because the required fire resistance class was not reached in any case, the advanced calculation method BoFire was applied. The fire resistance time calculated by the advanced calculation method was found to be more conservative than calculated by the simple method in this case. Reason for this is the shadow factor  $k_{sh}$  in the simplified calculation method. An adequate reduction of the heat transfer is not regulated for practical use when advanced calculation methods are applied. So the calculated fire resistance was not increased for the analysed members.

The calculation of the fire resistance time by simple calculation methods according to the Eurocodes showed that it is possible to gain a fire resistance time of 15 min for composite and steel members. One of the investigated composite beams reached the class R15, while the second failed for the reason of a thinner web and flanges.

The load utilisation factor of the analysed columns at 20°C is very high for economic reasons. Thus the fire resistance time was determined to less than 15 min. It is also shown that it is possible to reach the class R15 by increasing the cross sectional area of the columns (overdesign).

This investigation was initiated by the German company GOLDBECK. The authors would like to acknowledge the company for the support in this research.

## REFERENCES

- [1] Eurocode 1: Actions on structures – Part 1-2: General actions – Actions on structures exposed to fire; German version EN 1991-1-2:2002; Beuth Verlag, Berlin 2002
- [2] Eurocode 3: Design of steel structures – Part 1-2: General rules – Structural fire design; German version EN 1993-1-2:2005 + AC:2005; Beuth Verlag, Berlin, 2006
- [3] Eurocode 4: Design of composite steel and concrete structures – Part 1-2: General rules – Structural fire design; German version EN 1994-1-2:2005; Beuth Verlag, Berlin, 2006
- [4] Innovation in Steel, Parking Structures around the World; International Iron and Steel Institute (IISI), Bruxelles, 2001
- [5] CSN 73 0804; Pozarni bezpecnost staveb – Vyrobní objekty; Fire Protection of buildings – Industrial buildings, Cesky normalizacni institut, Praha, 2002
- [6] Schaumann, P.: Zur Berechnung stählerner Bauteile und Rahmentragwerke unter Brandbeanspruchung, Technisch-wissenschaftliche Mitteilungen Nr. 84-4, Institut für konstruktiven Ingenieurbau, Ruhr-Universität Bochum, Dissertation, Bochum, 1984
- [7] Upmeyer, J.: Nachweis der Brandsicherheit von kammerbetonierten Verbundbauteilen über Grenzbrandlasten, Schriftenreihe Heft 19, Institut für Stahlbau, Universität Hannover, Dissertation, Hannover, 2001, Shaker Verlag

# **STEEL BEAM-COLUMN UNDER THERMAL GRADIENT**

## **Combined axial-bending capacity of steel double-T cross-sections subjected to non-uniform temperature distribution**

C. Tsalikis <sup>a</sup>, E. Koltsakis <sup>b</sup>, C.C. Baniotopoulos <sup>c</sup>

<sup>a,b,c</sup> Aristotle University of Thessaloniki, Institute of Steel Structures, Thessaloniki, Greece

### **1 INTRODUCTION**

Beam-column is a term which is used to describe a structural member which is simultaneously subjected to an axial compressive force and a bending moment [1]. This type of element is commonly met in steel frame buildings. A beam in such buildings tries to expand due to thermal loading that is induced to it, but the restraints prevent this expansion and as a result, a compressive force develops on the member, in addition to the bending moment in place due to the gravity load. Similarly, a possible expansion of a beam can cause additional moments to the column of the structure, apart from the axial force already imposed to it. Contemporary provisions of the Eurocodes assume a uniformly distributed temperature over the steel members for the estimation of their capacity [2]. Such a hypothesis, for the members that are located on the borders of the fire room, may lead to disproportional results in relation to the true situation. This paper investigates the way that a thermal gradient on a cross-section of a steel beam-column member affects its mechanical strength.

### **2 STATE OF THE ART**

Wang et al. examined the limiting temperatures for elements of frames and found that the presence of thermal gradients and other types of temperature profiles cause significant alterations of the respective results [3]. It was noticed that the non-uniformity of the temperature profiles affect the limiting temperatures depending on the type of the profile, the load ratio and the slenderness of the columns. As the slenderness increases, the limiting temperature goes down. In addition, Wang et al. observed the presence of high bending moments because of the thermal gradient, but refrained from investigating the behaviour of the axial-load moment-capacity envelope in such a situation.

Garlock and Quiel made one more step towards the study of the influence of thermal gradients on beam-columns under several load cases [4]. Neglecting global buckling, local buckling and residual stresses, they loaded the steel members up to their plastic limit and they came up with two forms of normalized axial load – moment capacity envelopes depending on the reference axis of the cross-section. Both forms of graphs point out the alteration of the conventional capacity envelope in the case of a non-uniform temperature over the entire depth of the section. The first one assumes the plastic neutral axis as reference for the estimation of the axial load and bending moment capacity, whilst the second one is based on the centre of gravity being the reference axis. This assumption generates additional bending moment because of the eccentric induction of the axial load, which will result in a more or less conservative capacity envelope depending on the type of external loading and on the slope of the thermal gradient.

The current study poses again the same question of load capacity but deals with it from a different point of view: starting from the assumption of Bernoulli for the strains and combining it with precise material models attempts to estimate capacity envelopes and compare them with those of the Eurocodes. This approach sets forth new questions to further investigations.

### **3 DESCRIPTION OF THE PROBLEM**

As starting point for the formulation within the context of the present work, the planarity of the cross section was assumed in order to remain inside the framework of a beam theory. As known, according to the hypothesis of Bernoulli and Navier, during deflection, the cross-section remains

plane and normal to the deflected centroidal axis [5]; any transverse normal stresses are negligible. Other phenomena, such as creep deformation, thermal elongation, geometric non-linearities and residual stresses are not to be accounted for as the present work is to focus on the strength at a cross section level: introduction of the influence these may have on the bending and axial capacity of the beam-column would exceed the limits of the current study.

The cross-sections that were studied are double T cross-sections and the field of temperatures introduced to them was taken linear over the weak axis (i.e. the  $z$ -axis according to the Eurocode notation). This means that at the bottom of the lower flange there is the lowest temperature which rises up linearly and reaches its maximum value at the highest part of the top flange. The upper flange is the one assumed to face the internal part of the building and therefore absorbing the maximum temperatures. As no thermal analysis has been made, the assumption of the linear distribution of the temperature is merely a working assumption made in order to obtain an assessment of the phenomenon: the divergence from the real situation is not the issue of the current paper. The later is difficult to estimate as it depends to a number of uncertain factors as the rate of heat release, the position of the plume, the thicknesses of the flanges and the web and, generally, the thermal conditions inside the examined room.

In a cross-section under thermal gradient the relationship describing the material depends on the position of a certain point in the temperature field. For the determination of the beam-column resistance under a specified elevated temperature, EC3-Part 1.2, which addresses the structural fire design for steel elements, proposes the use of the ambient temperature stress-strain relationship with some additional reduction factors [2]. These reduction factors affect the yield strength, the modulus of elasticity and the proportionality limit of the material and they are inversely proportional to the increase of the temperature, as shown in *Fig. 2*. This relationship of EC3-1.2, may be used to determine the resistances to tension, compression, moment or shear. For this investigation, apart from the use of the formulae that are proposed by EC3 without taking into account the strain-hardening, another stress-strain relationship is formulated by the authors which is based on the combination of two other publications. Burgess et al. studied the behaviour of steel beam in fire with the use of a constitutive model based on a Ramberg-Osgood type of equation [6], [7]. The formula, which had been adopted, represents the stress-strain relationship as given in *Eq. (1)* and the parameters, that depend on the temperature, were obtained from test data [7], [8]:

$$\varepsilon_{(T)} = \frac{\sigma_{(T)}}{A_{(T)}} + 0.01 \left( \frac{\sigma_{(T)}}{B_{(T)}} \right)^{n_T} \quad (1)$$

where  $\varepsilon$  is the strain,  $\sigma$  is the stress and  $A(T)$ ,  $B(T)$  and  $n(T)$  are the parameters which depend on the temperature

In order to attain similarity between the two material descriptions, the Ramberg-Osgood equation was inverted using Mostaghel's method [9]. According to this method, equation (1) was divided into two parts: the first part consists of the elastic strains and the second one of the plastic strains. Following a first order approximation for the plastic dominated region, Mostaghel et al. came up with a stress-strain relationship that describes both the elastic and the plastic region with negligible errors. By substituting the parameters that Burgess et al. proposed into the new stress-strain relationship, a new formula was created which provides the stress as a function of both the strain and the temperature as following:

$$\varepsilon = f(\sigma, T) \rightarrow \sigma = f(\varepsilon, T) \quad (2)$$

This formula is created for the verification and the comparison of the material model proposed by the Eurocode (*Fig. 3*).

The core of the procedure used in the present work was to compute (through integration over the cross section) internal forces corresponding to a set of assumed strain and temperature fields that span the possible operational conditions expected for a structural element to face. Knowing the temperature and the strain in every point of the section, the next step is to calculate the stress at

every single point using either the relationship that Eurocode proposes or the inversed Ramberg-Osgood formula (Fig. 1(b), 1(c)). As mentioned, these relationships change their parameters (yield strength, modulus of elasticity and proportional limit of the material) in relation to the temperature (Fig. 3). This procedure will reveal the true stresses that develop at every single point of the cross-section. It has to be mentioned that due to the fact that stress depends on both the strain and the temperature, which is a function of the position of a point, the stress field will be neither uniform nor linear type but a complex higher-order field, as shown in Fig. 1(d).

After the calculation of the stress field, the internal forces are obtained by means of the evaluation of integrals: first, the axial force is computed as the integral of the stress field over the area of the cross-section:

$$N = \int_A \sigma_x dA \tag{3}$$

where  $\sigma_x$  is the stress at each point and  $A$  is the total area of the section. For the estimation of the bending moment that is carried by the section, the stresses that cause the above axial force should be subtracted from the general stress field in order for the stresses that create the bending moment to be revealed. Specifically, the normalized stress  $\sigma_o$  which is responsible for the axial force derives from the following expression Eq. (4):

$$\sigma_o = \frac{N}{A} \tag{4}$$

where  $N$  is the axial force as described in Eq. (3) and  $A$  is the total area of the section. Subtracting the uniform stress  $\sigma_o$  from  $\sigma_x$ , the new stress field  $\sigma_M$  is obtained (Fig. 1(f)). The integration of the stress  $\sigma_M$  multiplied by the distance from the “zero stress” axis over the whole area of the section will give us the bending moment, as seen in Eq. (5):

$$M = \int_A (\sigma_y - \sigma_o) z_{ZSA} dA \tag{5}$$

where  $Z_{ZSA}$  is the distance of a point from the “zero stress” axis (i.e. the points which have  $\sigma_M=0$ ). The traditional neutral axis is where the strains are zeroed and, in our model, it is applied by the user in order to represent every possible combination of external loading, as described above. On the other hand, the “zero stress” axis is where the  $\sigma_M$  reaches zero. At that point, the integration of the positive stresses over the area that are distributed equals the integration of the negative ones. Apparently, the distribution of  $\sigma_M(z)$  is not linear, as in that case the ZSA will always be located at the centre of the cross-section. At this point, it is necessary to mention that there are strong indications that the stress field that we are getting from the above analysis cannot be described only with the first-order moment, but higher-order moments are needed: this line of investigation is not within the scope of the present study but a goal for further investigation.

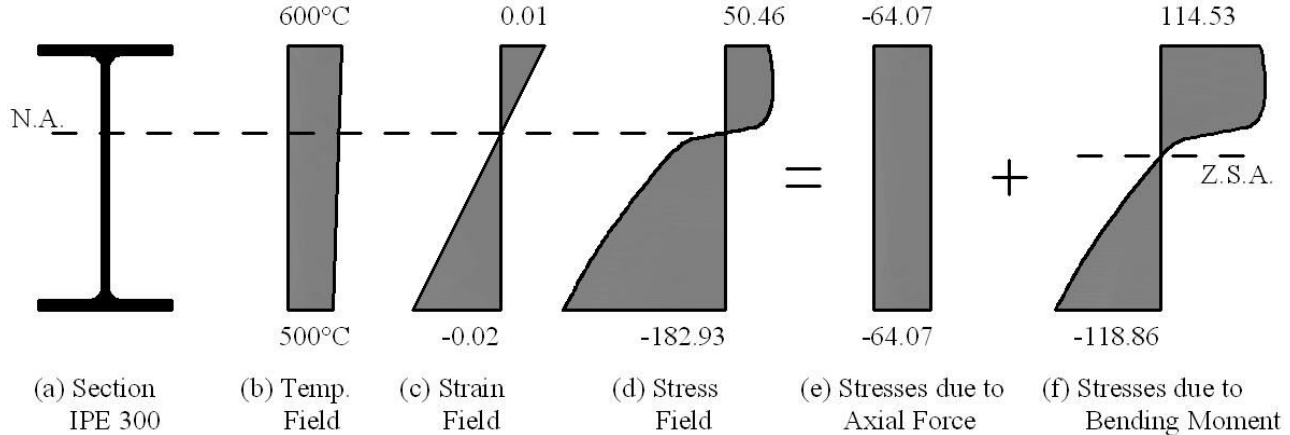


Fig. 1. Temperature, Strain and Stresses fields through the depth of an IPE300 cross-section

## 4 IMPLEMENTATION AND CONCLUSIONS

### 4.1 Implementation

All the above theoretical approach was modelled in a code using the program CAST3M. CAST3M is a computer code for structural analysis using the finite elements method. The cross-sections that were modelled are IPE300, HEA300 and IPE200. Each section was discretized using a suitable mesh for the most precise solution to be achieved. As far as the temperature is concerned, SCI's technical report proposes the practical rates of heating to be 5°C/min for well insulated sections and 20°C/min for unprotected sections [10]. Taking this for granted, the temperatures, which are applied on the top and bottom edge of the sections, obtained various values from 300°C to 700°C, to represent an unprotected structural member in fire between the 15<sup>th</sup> and the 35<sup>th</sup> minute. The distribution of the temperature field onto the cross-section was made as described above. For the strain field, an effective strain limit of 2% was adopted for determining the strength at elevated temperatures [10]. This means that the values at the extreme fibres of the cross-section fluctuate from -0.02 to 0.02.

### 4.2 Results and conclusions

The stress-strain relationship that the Eurocode proposes for elevated temperatures is depicted in (Fig. 2). In Fig. 3 one can see the differences between the EC and the Ramberg-Osgood approach. In particular, the EC produces higher values for the modulus of elasticity for the elastic region than the R-O equation. This fact changes as the cross-section enters the plastic region where the R-O modulus of elasticity shows a more prominent hardening, a fact that makes the R-O seem more optimistic, especially, when the temperatures are not the highest that may develop during a fire.

Each point in the N-M plane of Figs.4-6 corresponds to a pair of strains imposed to the upper / lower fibre of the cross section. The step used for the coverage of the strain domain is constant; therefore the increase of the density of the images of strain points in the N-M space represents a reduction of the stiffness of the cross section due to partial plastification. Using the EC relationship for the estimation of the axial load-bending moment capacity, it was found that the capacity envelope that EC 3 (Part 1.1 – cl.(6.36)) proposes may be conservative or non-conservative in relation to the real situation [11]. As being described in the example that Fig. 4 shows, the thermal gradient alters the capacity of the cross-section. Each point on this figure represents the normalized N-M value and derives from the combination of a distribution of strains and a thermal gradient. The normalization of N-M values was made for the (constant) mean value of the temperature field. EC envelopes illustrate the capacities of the beam-column elements, assuming uniformly distributed temperatures [11]. On the one hand, in the region where the accumulation of the points falls outside the safety envelopes, EC appears conservative, whilst in the opposite situation, the EC approach appears to be optimistic. Similarly, in Fig. 5 these discrepancy regions become greater. Therefore, as the slope of the thermal gradient increases, so does the discrepancy between the EC capacity envelopes and the true ones.

Furthermore, the alteration of the N-M values, as the slope of the thermal gradient rises, is clearly shown in Fig. 6. In Fig. 7, the evaluation of the stress field was made according to R-O's formula. The N-M images of the two approaches are quite similar, apart from the difference the density increase in the edges of the strain span, a fact easily attributable to the difference of the two stress-strain relationships. This observation is, also obvious at Fig. 8 and Fig. 9. The temperatures of these last figures represent a possible fire history scenario. The alteration of the region of points shows the way that the growth of the fire affects the capacity of the cross-section.

As conclusion, it can be said that:

- the region of safe operation of the cross section presents under that presence of thermal gradient shows a differentiation in shape that is not accounted for by the present regulatory framework;
- extensive parametric research is needed in order to obtain N-M interaction safety regions for the commonly used structural steel cross sections;

- the absence of a distinct hardening form of the stress-strain curve at elevated temperatures requires, to the authors opinion, a reconsideration of the concept of allowable stress so as to obtain the same safety margin with the low temperatures range.

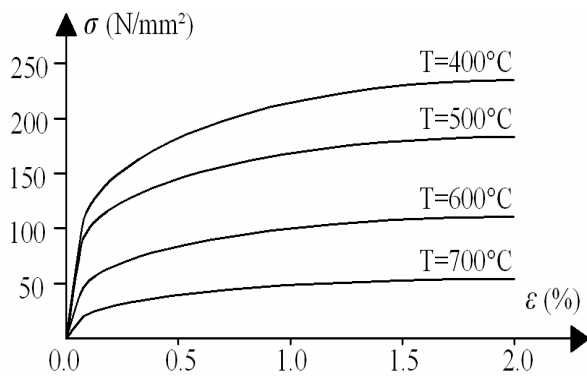


Fig. 2. Stress-strain relationship at elevated temperatures according to EC3

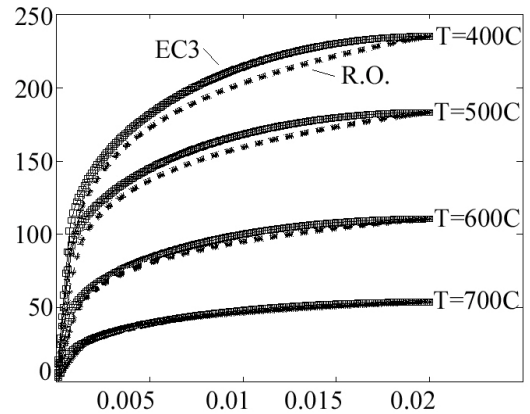


Fig. 3. Stress-strain relationships at elevated temperatures (EC3 + Ramberg-Osgood)

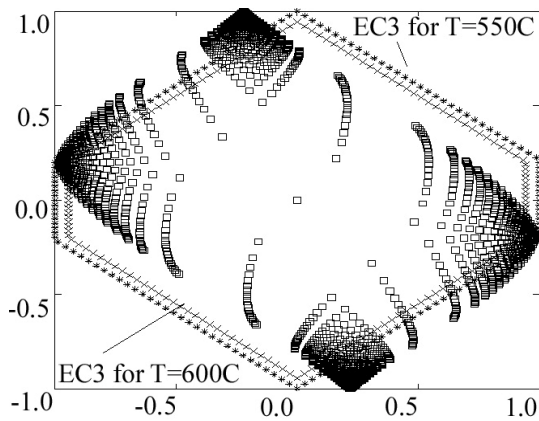


Fig. 4. Normalized M-N capacity for non-uniform temperature ( $T_{max}=600C/T_{min}=500C$ ) and EC3 capacity envelopes ( $T=550 \rightarrow$  External /  $T=600C \rightarrow$  Internal)

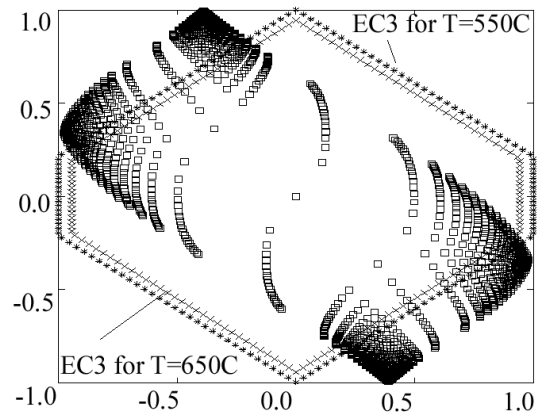


Fig. 5. Normalized M-N capacity for non-uniform temperature ( $T_{max}=650C/T_{min}=450C$ ) and EC3 capacity envelopes ( $T=550 \rightarrow$  External /  $T=650C \rightarrow$  Internal)

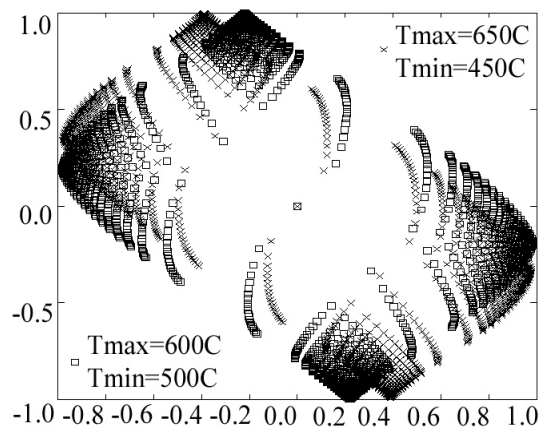


Fig. 6. Normalized M-N capacities for non-uniform temperatures using EC3 stress-strain relationship

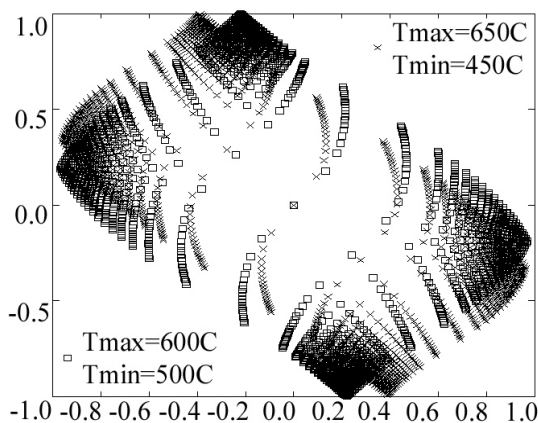


Fig. 7. Normalized M-N capacities for non-uniform temperatures using Ramberg-Osgood stress-strain relationship

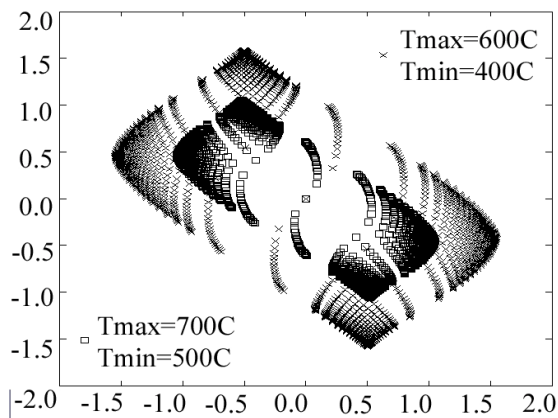


Fig. 8. Normalized M-N capacities for non-uniform temperatures using EC3 stress-strain relationship

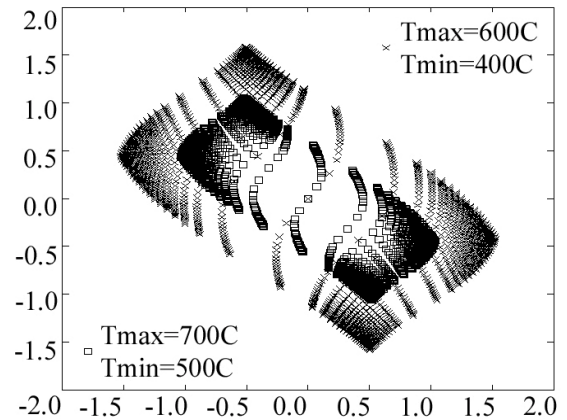


Fig. 9. Normalized M-N capacities for non-uniform temperatures using Ramberg-Osgood stress-strain relationship

## REFERENCES

- [1] W.F. Chen, T. Atsuta, Theory of beam-columns, *J. Ross publishing*, 2008
- [2] Eurocode 3: Design of steel structures, Part 1.2: General Rules – Structural Fire Design, *European Committee for Standardisation*, Brussels 2003
- [3] Y.C. Wang, T. Lennon & D.B. Moore, The Behaviour of Steel Frames Subject to Fire, *J. Construct. Steel Research* 35, p. 291-322, 1995
- [4] M. E.M. Garlock, S.E. Quiel, Combined axial load and moment capacity of fire-exposed beam-columns with thermal gradients, *Fourth International Workshop “Structures in Fire”*, Aveiro, Portugal, 2006
- [5] Z.P. Bazant, L. Cedolin, Stability of Structures: Elastic, Inelastic, Fracture and Damage Theories, *Dover Publications*, 2003
- [6] I.W. Burgess, J. El Rimawi & R.J. Plank, Studies of the Behaviour of Steel Beams in Fire, *J. Construct. Steel Research* 19, p. 285-312, 1991
- [7] C.G. Bailey, I.W. Burgess & R.J. Plank, Analyses of the Effects of Cooling and Fire Spread on Steel-framed Buildings, *Fire Safety Journal* 26, p. 273-293, 1996
- [8] B.R. Kirby & R.R. Preston, High Temperature Properties of Hot-rolled Structural Steels For Use in Fire Engineering Design Studies, *Fire Safety Journal* 13, p.27-37, 1988
- [9] N. Mostaghel, R.A. Byrd, Inversion of Ramberg-Osgood equation and description of hysteresis loops, *International Journal of Non-Linear Mechanics* 37, p.1319-1335, 2002
- [10] R.M. Lawson, G.M. Newman, Structural Fire Design to EC3&EC4, and comparison with BS 5950, *Technical Report – SCI publication 159*, 1996
- [11] Eurocode 3: Design of Steel Structures, Part 1-1: General rules and rules for buildings, *European Committee for Standardisation*, Brussels 2005

## BEHAVIOUR OF SCREWED SHEAR SHEETING CONNECTION IN FIRE

Wei Lu, Pentti Mäkeläinen <sup>a</sup>, Jyri Outinen <sup>b</sup>

<sup>a</sup> Helsinki University of Technology, Department of Structural Engineering and Building Technology, Espoo, Finland

<sup>b</sup> Rautaruukki Oyj, Ruukki Construction, Vantaa, Finland

### INTRODUCTION

Corrugated steel sheets are normally attached to the underlying purlins or more commonly straight to the steel trusses by self-drilling or self-tapping screws. The behavior of sheeting connections in fire conditions is important because of the maximum compression force during thermal expansion and maximum tension force in catenary action exerted to the screw connectors at supports [1]. In this paper, the performance of screwed connections between a thinner plate and a thicker plate are investigated to simulate the structural application of connecting the roof sheeting to underneath truss members. The investigations are carried out via both single lap shear tests and Finite Element (FE) modeling both at room temperature and at elevated temperature. The aims of this study are (1) to understand the failure mechanism of the screwed connection and (2) to get the load-displacement curves so that they can be used in the further research.

### 1 SINGLE LAP SHEAR TEST

*Fig. 1* shows the standard testing set-up according to ECCS recommendations [2]. However, due to the limitation of dimensions of the furnace available, the dimensions of the specimens are reduced accordingly (*Fig. 2*). Two kinds of tests have been carried out: one is to validate the testing results of specimens with Reduced Dimensions (RD) with Standard Dimensions (SD); and the other is to do the tests for a group of temperatures, i.e. 20 °C, 200 °C, 400 °C and 600 °C. Since the displacement of the specimen inside furnace is recorded as the plate end displacement, measurement setting (dotted lines in *Fig. 1*) has been removed in the SD test.

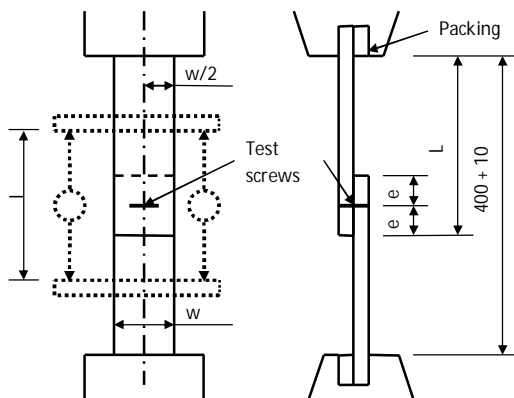


*Fig. 1.* Standard testing set-up

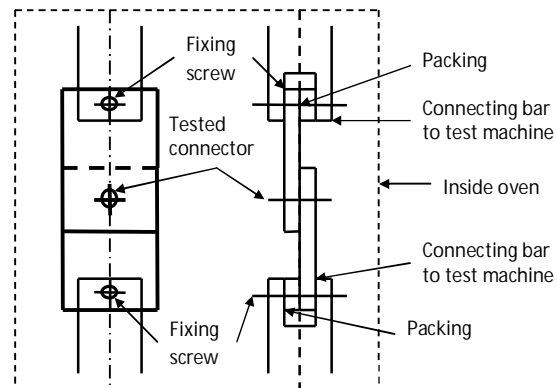


*Fig. 2.* Testing set-up in this research

In the room temperature tests, the rate of loading in the initial stage of testing shall not exceed 1 kN/min. Until the ultimate load is reached the rate of straining shall not exceed 1 mm/min [2]. The displacement control is used. At elevated temperatures, the tests are carried out in two steps. Firstly, the temperature is raised to a given temperature. Then the loading is applied to the specimen with the rate of 0.1 to 0.3% per minute. According to [2], the maximum load is reached in a deformation of 3 mm in order to avoid the extra deformations in the connection. However, in fire case the large deformation is an alternative mechanism to avoid the failure of the structure. Thus, the tests have been stopped when the displacement of 20 mm is reached at room temperature and 15 mm at elevated temperature. The maximum load is recorded as the one in this range of deformation.

The deformation histories for SD specimens at room temperature are shown in *Fig. 3*. It can be seen that the deformation of connection starts from the progressively curling or tilting of thinner plate because of the eccentricity of single lap shear joint (a). Then the slipping in the thinner plate is observed when the slipping is out of the cover of screw. The slipping is due to the local yielding of material when the bearing of screw fastener against thinner plate (b). Because of the large local strain, the cracking appeared in the thinner plate when the ultimate strength of material is reached. The tearing of thinner plate continues and in the later stage the base plate of screw cut into the thinner plates (c). The same deformation histories for RD specimens have been observed and the final failure mode is shown in (d).

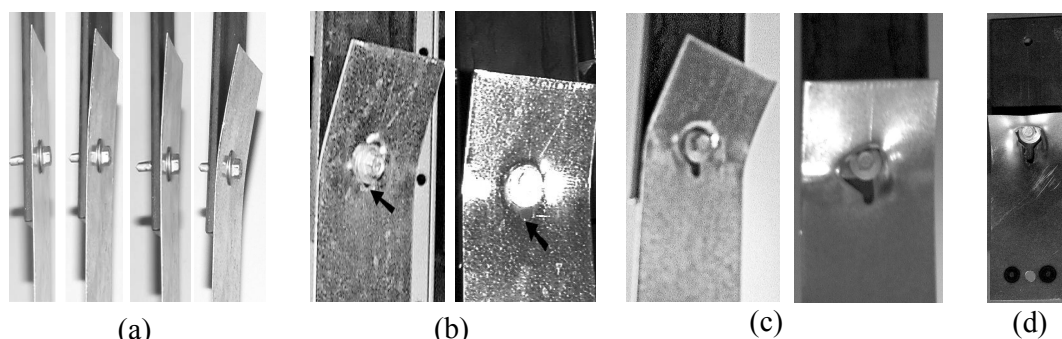


*Fig. 3.* Deformation histories of SD specimen (a), (b), (c), failure mode of RD specimen (d)

In order to show the feasibility of testing results with RD specimens, a load-deflection curve is taken out respectively for SD and RD specimens as shown in *Fig. 4* (a). According to 7 points (0-6) marked on the curves, it can be seen that the deformation histories of two types of specimens are the same due to the same shapes of two curves. The maximum loads of the connections (point 5) are at about the same level. However, due to the displacement of SD specimen has been measured at the end of the plate instead of around the connection area, the RD specimens are more stiff than SD ones. The load-displacement curves for other RD and SD testing specimens are shown in *Fig. 4* (b).

Due to the limitation of the testing furnace, the deformation histories of specimen at elevated temperatures cannot be observed. Only the final failure modes of the specimens are shown in *Fig. 5*. Two failure modes have been observed: bearing and tearing failure of thinner plate below at 200 °C (a) and shearing failure of screw connector at 400 °C (b) and 600 °C (similar mode to 400 °C). The main factor that determines the final failure mode in the connection might be the relative material strength involved in the connections. At room temperature, the material strength of thinner plate is lower than that of screw connector. Thus the failure mode is Mode 1 failure. When the temperature is above 400 °C, the material properties for screw

connector might drop dramatically because the ways of increasing of material strength to be used as screws (for instance heat treatment).

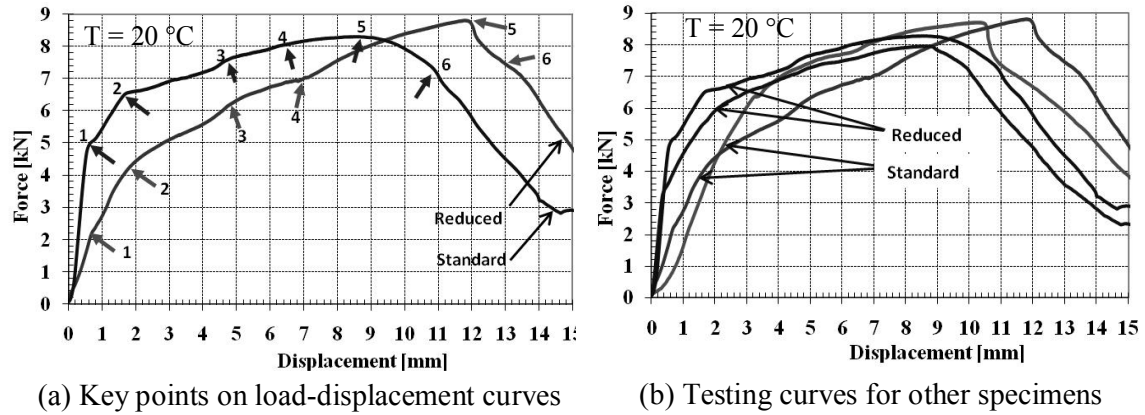


Fig. 4. Load-displacement curves of SD and RD specimens

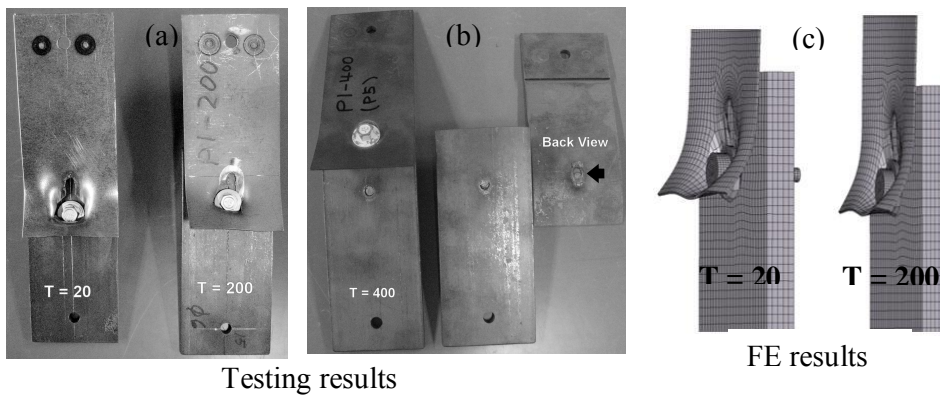


Fig. 5. Failure modes of testing results and FE results

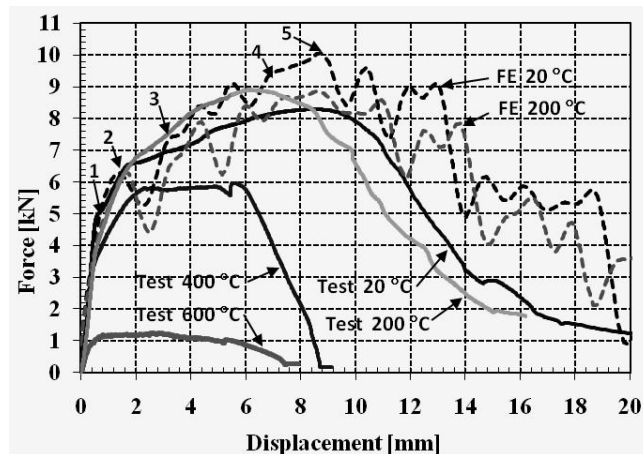


Fig. 6. Load-displacement curves from tests and from FE modelling

The load-displacement curves from tests are shown in Fig. 6. When comparing load-displacement curves at 20 °C to that at 200 °C, it can be seen that up to point 2 these two curves are very close because both strength and modulus of elasticity are not much reduced at

200 °C. Then load-deformation curves at 200 °C are higher than those of at 20 °C but with reduced ductility. The stiffness and maximum load at 400 °C and 600 °C are lower than those at room temperature because of the reduction of strength and modulus of elasticity of materials at elevated temperatures. The ductility has been reduced as well due to the brittle failure mode of screw connectors when comparing to the bearing tearing failure of thinner plate at 20 °C and 200 °C respectively.

## 2 FINITE ELEMENT MODELLING

*Fig.7* shows the structural assembly of the single lap shear screw connection and connection details. Thinner sheet with thickness 0.8 mm simulates the steel sheeting in roofing system. The thicker sheet (10 mm) represents the top chord (structural hollow section) of the roof truss to which the sheeting is connected. The lengths of the two sheets are 150 mm, respectively. One screw connector  $\phi$  5.5 mm x 26 mm with head diameter 11 mm is used to connect two sheets. The main function of screw thread is to prevent the screw from being moved along its axial direction, thus only three threads are modelled in order to improve the computational efficiency. The steel washer with diameter 15 mm is used between the screw connector and thinner sheet. The distances of centre of the screw connector to the sheet edges are both transversely and longitudinally 30 mm. Commercial FE software, ABAQUS/Explicit, is used as an analysis tool. Three dimensional eight nodes solid elements with reduced integration point (C3D8R) are chosen for modelling the thicker sheet, the thinner sheet, the screw, the screw thread and the washer. The description of mesh details, the loading steps and boundary conditions are presented in reference [3].

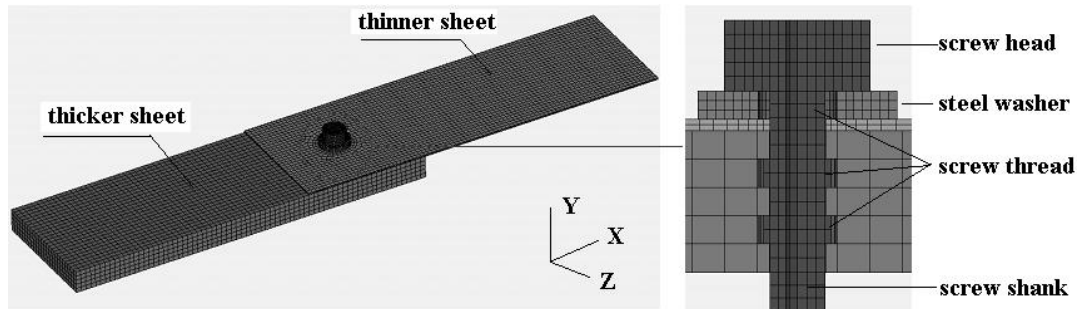


*Fig. 7.* Structural modelling of single lap shear screw connection and connector details

In order to simulate the real behaviour of material, true-stress and true-strain curves are used. Due to the high local strain in the thinner sheet in vicinity of screw connector, the progressive damage and failure of material are included in the analysis. From our trial simulations, it is assumed that the damage initiation starts when the equivalent plastic strain is 0.45 and the material failure is reached when the equivalent plastic strain is 0.5. The damaged elements are not removed from the analysis. The reduction factors for the yield strength and modulus of elasticity follow the values defined in the main text of EN 1993-1-2 [4].

Researches [5] have revealed that failures normally do not take place in the screw connector itself. So the following assumptions are made in FE analysis: the screw connector has the higher strength and rigidity than other materials in the connection assembly. Therefore, the screw connector and washer have the linear elastic material properties with the same values of yield strength and modulus of elasticity as those of steel sheet at 20 °C. However, from our testing, the failure of screw occurred at 400 °C and 600 °C. Thus, the material model of screw

connectors needs to be modified in order to further apply the FE modelling. Therefore, in the following sections, only results at 20 °C and 200 °C are compared.

### 3 VERIFICATION OF FE MODEL

*Fig. 5* shows that at 20 °C and 200 °C the failure modes from FE analysis is the same as those from testing results. Similar to 7 points in *Fig.4*, the load-displacement curves from FE analysis at 20 °C and 200 °C can be divided also by 6 points up to maximum load (*Fig.6*). It can be concluded that FE model simulates the deformation history very well.

*Table 1* shows the comparisons of the maximum load from tests and from FE analysis. It can be seen that at 20 °C, the FE results are about 20% higher than testing results. At 200 °C, due to the differences of real material properties and model used in FE modelling, the maximum load values are the same but the ductility from FE analysis is larger than that from tests.

*Table 1.* Comparisons of maximum load and corresponding deformation from FE analysis to those from tests

|        | Test         |                  | FE Analysis  |                  | Comparisons<br>MaxLoad (FE/Test) |
|--------|--------------|------------------|--------------|------------------|----------------------------------|
|        | MaxLoad [kN] | Deformation [mm] | MaxLoad [kN] | Deformation [mm] |                                  |
| 20 °C  | 8.5          | 9.1              | 10.0         | 8.7              | 1.17                             |
| 200 °C | 8.8          | 6.1              | 8.8          | 8.6              | 1.00                             |

### 4 ANALYSIS OF FAILURE MECHANISM

The verified model has been used to understand the failure mechanism of connection at 20 °C and 200 °C. According to the 5 points in *Fig. 6*, the following mechanisms at 20 °C are illustrated in *Fig.8*. (1) The yielding of thinner plate due to the bearing of screw connector starts early, for instance, it has been observed at the deformation of 0.6 mm and initial slip happened due to material yielding (Point 1). (2) Then the local buckling of thinner plate around screw connector has been observed at 1.2 mm (Point 2). However, in order to show it clearly, the deformation of 3.0 mm has been chosen. At the same time the thinner plate tilts due to the eccentricity of single lap shear connection. (3) At point 3 (deformation of 3.6 mm or better to show with 4.2 mm), the buckling of the thinner plate has been observed. (4) With the continuation of buckling, bending stresses appeared at the edge of thinner plate (ex. deformation of 7.2 mm). At point 4, the thinner plate slips out of washer. (5) When the maximum load is reached (point 5), the material failure occurred. This can be seen from the reduction of bending effects at deformation of 8.4 mm. (6) At deformation of 15 mm, it has been shown clearly the tearing of the thinner plate and the washer's cutting into the thinner plate. The locations of maximum stresses have been transferred due to the tensioning of thinner plate. The failure mechanism at 200 °C is similar to that described at 20 °C. The differences are as follows: (1) yielding of material occurred earlier (2) the maximum load is lower. These differences are due to the reduction of strength at elevated temperatures.

### 5 SUMMARY AND ACKNOWLEDGMENT

The test results have shown that (1) It is reasonable to use the specimens with reduced dimensions. (2) The failure modes of connections at room temperature is bearing and tearing failures of thinner plates. The maximum load is reached when the first tearing appeared in the thinner plate. (3) Two failure modes are observed at elevated temperatures: Mode 1 is the bearing and tearing failure of thinner plate at 200 °C; Mode 2 is the shearing failure of screw connectors at temperature equal or higher than 400 °C. (4) Mode 2 is unfavourable mode

because of connector's brittle failure. This failure mode can be avoided when using such as shot-nailed connections. (5) The 6 points can be used to describe the load-displacement curves of connections at temperatures of 20 °C and 200 °C.

With the testing results, it has been shown that FE modelling can predict the behaviour of connection well at 20 °C and 200 °C. The verified FE model has been used to understand the failure mechanism of the screwed connection at 20 °C and 200 °C.

The Finnish company Rautaruukki Oyj financially supported this research. Mr. Reijo Lindgren in CSC Finland provided many helps in using ABAQUS Commercial software when creating the connection models.

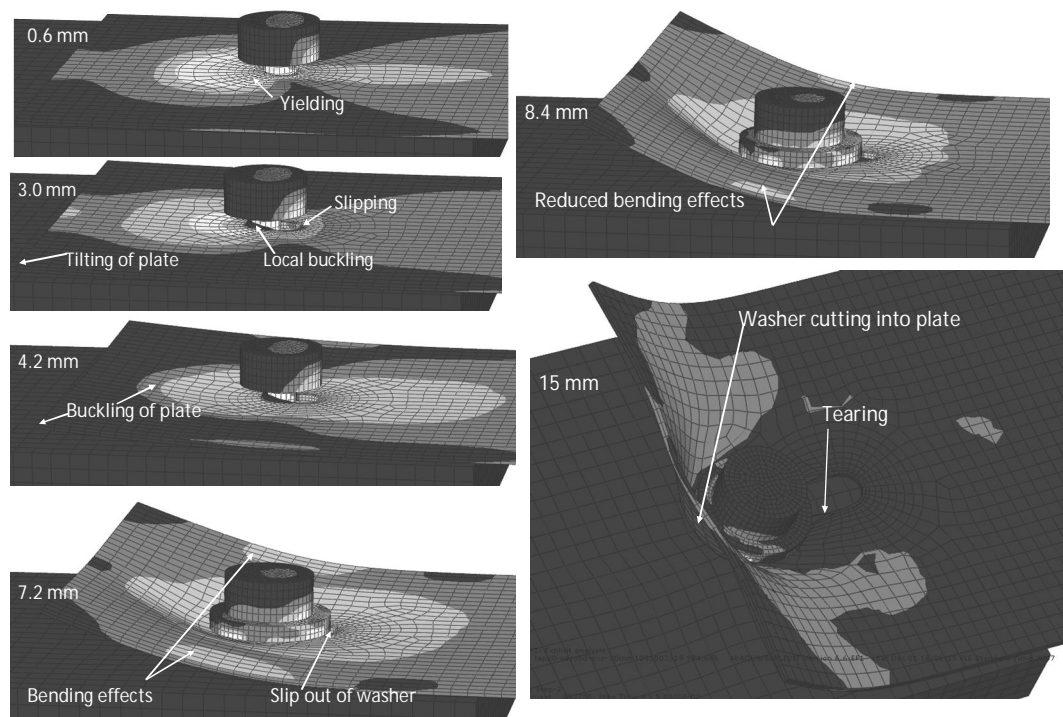


Fig. 8. Failure mechanism at 20 °C according to FE analysis

## REFERENCES

- [1] Lu, W., Mäkeläinen, P. and Outinen, J., Numerical Simulation of Catenary Action in Cold-Formed Steel Sheeting in Fire. Proceedings of 5<sup>th</sup> International Conference on Thin-Walled Structures: Recent Innovations and Developments, Edited by M. Mahendran, Gold Coast, Australia, June 18-20, pp. 713-720, 2008.
- [2] ECCS-TC7.10, The Testing of Connections with Mechanical Fasteners in Steel Sheeting and Sections, ECCS Publication 124, 2008.
- [3] Lu, W., Mäkeläinen, P. and Outinen, J., Single Shear Screw Connections in Steel Sheeting in Fire – Finite Element Modeling. Proceedings of 5<sup>th</sup> European Conference on Steel and Composite Structures, Graz, Austria, September 3-5, pp.1031-1036, 2008.
- [4] EN 1993-1-2, Eurocode 3: Design of steel structures, Part 1.2: General rules – structural fire design, 2005.
- [5] Sokol Z., Wald F., Structural integrity of corrugated sheets exposed to fire. Steel - a new and traditional material for building, edited by Dubina and Ungureanu, Taylor & Francis Group, London, 561-566, 2006.

# UNPROTECTED BI-AXIALLY LOADED STEEL COLUMNS UNDER FIRE CONDITIONS

Yao Yao<sup>a</sup>, \*Tan Kang Hai<sup>b</sup>

<sup>a</sup>ExxonMobil Upstream Research Company, Houston, Texas, USA

<sup>b</sup>Nanyang Technological University, School of Civil and Environmental Engineering, Singapore

(\*corresponding author)

## INTRODUCTION

Up till now, there has been limited research work conducted on bi-axially loaded steel columns under fire conditions. Under normal ambient temperature, the load-bearing capacity of steel columns is governed by the interaction of strength and stability considerations, which gives rise to Rankine method. The authors extended this method to predict the fire resistance of steel columns subjected to bi-axial loading under standard fire curve. Basically, the authors developed an interaction equation based on column failure surface to account for the effects of axial load and bending moments in two directions. Predictions from the proposed approach were benchmarked against a well-established finite element program SAFIR for steel columns under standard fire conditions. The same approach is then extended to include natural fire curves. To model a compartment fire with different geometries, thermal characteristics of boundary walls, different fire loads and ventilation factors, a zone fire modelling program Ozone was used. Coupling Ozone to SAFIR, the failure times of steel columns in a compartment fire were predicted. These numerical predictions were compared with those from the proposed approach and reasonable agreement was obtained.

## 1 EXTENDED RANKINE METHOD FOR BI-AXIALLY LOADED STEEL COLUMNS UNDER FIRE CONDITIONS

In the European and the American codes, the design of steel columns exposed to fire is generally based on the national and international code recommendations. In buildings, due to initial imperfection, most of the columns are bi-axially and eccentrically loaded. It is necessary to develop a rational design method for structural engineers to calculate the fire resistance of such columns under realistic fire conditions, herein referred to as natural fire curves. For columns subjected to biaxial load and elevated temperature conditions, the traditional Rankine formula can be modified to:

$$\frac{1}{P_R(T)} = \frac{1}{P_{R_x}(T)} + \frac{1}{P_{R_y}(T)} - \frac{1}{P_{R_o}(T)} \quad (1)$$

where  $P_R(T)$  is an approximate value of ultimate load in biaxial bending with eccentricities  $e_x$  and  $e_y$ ;  $P_{R_y}(T)$  is the ultimate load at temperature  $T$  when only eccentricity  $e_x$  is present ( $e_y = 0$ );  $P_{R_x}(T)$  is the ultimate load at temperature  $T$  when only eccentricity  $e_y$  is present ( $e_x = 0$ );  $P_{R_o}(T)$  is the ultimate load at temperature  $T$  for concentrically loaded column;

Incorporating the effect of load eccentricity, a plastic load reduction factor  $u_p$  is defined:

$$P_p(T) = u_p P_p(T) \quad (2)$$

To consider the effect of initial crookedness, residual stress and thermal gradient, the elastic critical load reduction factor  $u_e$  is defined as follows:

$$P_e(T) = u_e P_e(T) \quad (3)$$

From Eqs. (1) to (3), the biaxial bending formula based on Rankine method can be derived:

$$\frac{1}{P_R(T)} = \frac{u_{px}P_p(T) + u_{ex}P_e(T)}{u_{px}u_{ex}P_p(T)P_e(T)} + \frac{u_{py}P_p(T) + u_{ey}P_e(T)}{u_{py}u_{ey}P_p(T)P_e(T)} - \frac{P_p(T) + P_e(T)}{P_p(T)P_e(T)} \quad (4)$$

where  $u_{px}$  and  $u_{py}$  are the plastic load reduction factor of major and minor axis, respectively;  $u_{ex}$  and  $u_{ey}$  are the elastic critical load reduction factor of major and minor axis, respectively. For convenience, this equation can be transformed to:

$$\frac{1}{P_R(T)} = \alpha_p \frac{1}{P_p(T)} + \alpha_e \frac{1}{P_e(T)} \quad (5)$$

where  $\alpha_p = 1 + 1/u_{px} + 1/u_{py}$  and  $\alpha_e = 1 + 1/u_{ex} + 1/u_{ey}$ , which considers the effect of biaxial bending based on Rankine approach.

The values of  $u_p$  for I- or H-sections were proposed by Horne (1979):

1) For I-sections or H-sections bending about the major axis,

$$u_p = \frac{1}{5} \left( \sqrt{(eA/S)^2 + 10} - eA/S \right) \text{ for } eA/S \geq 4.5; \quad u_p = \left( 1 + \frac{eA/S}{1.125} \right)^{-1} \text{ for } eA/S \leq 4.5 \quad (6)$$

2) For I-sections or H-sections bending about the minor axis,

$$u_p = \sqrt{(eA/S)^2 + 2} - eA/S \text{ for } eA/S \geq \sqrt{4.5};$$

$$u_p = \frac{1}{2.25} \left( \sqrt{(eA/S)^2 + 2.25^2} - eA/S \right) \text{ for } eA/S \leq \sqrt{4.5} \quad (7)$$

where  $S$  is the plastic modulus of column sections.

The elastic critical load reduction factor  $u_e$  can be found from the following equation (Gere and Timoshenko, 1991):

$$1 = \frac{e_{equ}}{\Delta_f} \left( \sec\left(\frac{\pi}{2} \sqrt{u_e}\right) - 1 \right) + \frac{a_{equ} / \Delta_f}{1 - u_e} \quad (8)$$

where  $e_{equ}$  and  $a_{equ}$  are the equivalent load eccentricity and equivalent initial crookedness, respectively;  $\Delta_f$  is the control deflection or the allowable deflection and is taken as  $L/C$ ;  $C$  is a parameter related to fire conditions and is a function of  $\frac{eA}{S}$ ; for biaxial bending, the maximum value of  $func(e_x A/S_x)$  and  $func(e_y A/S_y)$  is used.

Based on Eq. (8), the following equation is recommended to calculate  $u_e$ :

$$u_e = \left( \frac{2}{\pi} \arccos\left(1/\left(\frac{L_e}{eC} + 1\right)\right) \right)^2 \quad (9)$$

where for ISO 834 fire curve:  $C = 76.1 \times \frac{eA}{S}$  if  $\frac{eA}{S} \leq 1$ ;  $C = 0.24 \left(\frac{eA}{S}\right)^2 - 6.14 \frac{eA}{S} + 82$  if

$\frac{eA}{S} > 1$ , obtained by curve fitting the column test results (Tang et al. 2001) and  $0 < u_e \leq 1$ .

For natural fire conditions, the authors propose the following formula for  $C$ :

$$C_{natural} = 0.7v_f^{0.5} Q_f^{0.25} C \quad (10)$$

Due to the lack of experimental data for column tests under natural fire conditions, Eq. (10) is obtained from least-squares regression analysis by curve fitting zone modeling program Ozone and finite element program SAFIR predictions to a large group of steel columns under different natural fire conditions.

It is expedient to formulate the method in terms of the buckling coefficient  $N(T)$ , which can be obtained as a ratio of Rankine load  $P_R(T)$  (taken as the applied load  $P$  at the critical temperature) to the plastic collapse load  $P_p(T)$ :

$$N(T) = P_R(T) / P_p(T) = P / P_p(T) \quad (11)$$

Thus, a simple expression for  $N(T)$  can be obtained:

$$N(T) = 1 / (1 + \lambda(T)^2) \quad (12)$$

where  $\lambda(T)$  is the normalized slenderness ratio of columns defined by the following equation:

$$\lambda(T) = \sqrt{\alpha_e P_p(T) / \alpha_p P_e(T)} \quad (13)$$

It is convenient to express  $P_p(T)$  and  $P_e(T)$  in terms of their respective values at ambient temperature  $P_p(20)$  and  $P_e(20)$ : where  $P_p(T) = \phi_p(T)P_p(20)$ ;  $P_e(T) = \phi_e(T)P_e(20)$ . Thus:

$$\lambda^2(T) = [\phi_p(T) / \phi_e(T)] \cdot \lambda^2(20) \quad (14)$$

Since

$$N(T) = N(20) / \phi_p(T), \quad N(20) = \phi_p(T) / (1 + \frac{\phi_p(T)}{\phi_e(T)} \cdot \lambda^2(20)) \quad (15)$$

where  $N(20)$  is the modified buckling coefficient at ambient temperature ( $T = 20^\circ\text{C}$ ) and  $\lambda(20)$  is the modified normalized slenderness ratio.

In Eq. (15), the terms  $\phi_p$  and  $\phi_e$  are the respective load reduction factors of plastic collapse load and elastic critical load, accounting for the material deterioration at elevated temperatures. Thus,  $\phi_p(T) = P_p(T) / P_p(20)$  and  $\phi_e(T) = P_e(T) / P_e(20)$ . For steel columns, the plastic collapse load  $P_p(T)$  is equivalent to its squashing load  $f_y(T)A$ , where  $f_y(T)$  is the effective yield strength of steel at temperature  $T$ , and  $A$  is the cross-sectional area. The term  $f_y(T)$  can be expressed in terms of its initial value at ambient temperature  $f_y(20)$  by  $f_y(T) = k_y(T)f_y(20)$ , where  $k_y(T)$  is the reduction factor for effective yield strength of steel at temperature  $T$ . This research adopts the EC3 material model for the values of reduction factors for strength  $k_y(T)$  (Euro code 3: Part 1.2, 2003). There is no reduction in strength for steel less than  $400^\circ\text{C}$ , but beyond which it reduces rapidly. At  $1200^\circ\text{C}$ , steel ultimately loses all its strength and  $k_y(T)$  is practically 0. Apparently, the following relationship can be established between  $\phi_p(T)$  and  $k_y(T)$ :

$$\phi_p(T) = f_y(T)A / f_y(20)A = k_y(T) \quad (16)$$

On the other hand, the elastic critical load  $P_e(T)$  is equal to the Euler buckling load:

$$P_e(T) = \pi^2 E_s(T)I / L_e^2 \quad (17)$$

where  $E_s(T)$  is the elastic modulus of steel at temperature  $T$ ;  $I$  is the second moment of area of the cross-section about its neutral axis;  $L_e$  is the effective column length taking account of different support conditions.

Once again, the term  $E_s(T)$  can be expressed in terms of its value at ambient temperature  $E_s(20)$  by  $E_s(T) = k_E(T)E_s(20)$ , where  $k_E(T)$  is the reduction factor for elastic modulus of steel at temperature  $T$ . The value of  $k_E(T)$  starts to reduce at a temperature of  $100^\circ\text{C}$  and eventually reaches 0 at  $1200^\circ\text{C}$ . It can be shown that:

$$\phi_e(T) = k_E(T) \quad (18)$$

Thus, the column failure load at ambient temperature  $N(20)$  can be defined:

$$N(20) = k_y(T) / (1 + \frac{k_y(T)}{k_E(T)} \cdot \lambda^2(20)) \quad (19)$$

## 2. DISCUSSIONS OF RESULTS FROM PROPOSED APPROACH & SAFIR

Generally, the reduction factors  $\phi_p$  and  $\phi_e$  are functions of the steel temperature  $T$ . Thus,  $N(20)$  can be expressed as a function of steel temperature and column slenderness  $\lambda(20)$ . For a given column, the magnitude of  $N(20)$  and  $\lambda(20)$  can be estimated by performing simple structural analysis at ambient temperature. Thus, the column failure temperature can be determined graphically or by a trial-and-error method. Due to the scarcity of test data for columns subjected to biaxial loading, the proposed method was verified by SAFIR program. Fig. 1 shows the prediction of Rankine method for a group of steel columns (slenderness ratio from 22 to 271, load ratio from 10% to 80%, cross section from HE100A to HE500B, load eccentricity from (25mm, 25mm) to (100mm, 100mm)) subject to bi-axial bending under ISO 834 fire conditions. The results are compared with SAFIR predictions. It is found that the prediction of Rankine method is conservative and consistent. It is also found that the Rankine method can only be applied for steel columns with a slenderness ratio smaller than 200; with higher slenderness ratio, the proposed method will give unsafe predictions compared with SAFIR. This is partly due to the increasing importance of secondary effect with increasing column slenderness ratio.

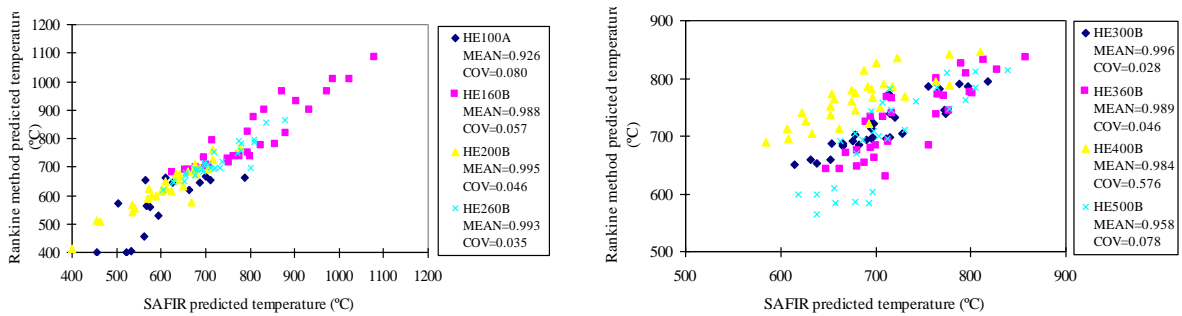


Fig. 1. Predictions of failure temperature for bi-axial loaded steel columns under standard fire conditions

After determining the column failure temperatures, Eq. (20) can be used to calculate the failure times of columns under standard fire conditions; this information can also be obtained from the New Zealand steel element design guide (NZS3404 1997):

$$t = (-4.7 + 0.0263T_R + \frac{1.67T_R}{A_m/V}) \quad (20)$$

where  $T_R$  is the temperature predicted from Rankine method;  $A_m$  is the exposed surface area of member per unit length;  $V$  is the volume of member per unit length.

Eq. (20) is valid in the temperature range of 500°C to 850°C, and has a limit for the size of the steel section factor, with the  $A_m/V$  value between 15 and 275  $m^{-1}$ .

## 3. COMPARTMENT FIRE MODELLING

Up till now, there is limited research work conducted on natural fire conditions. It is useful to extend the proposed Rankine method for biaxially-loaded steel columns subjected to natural fire conditions. Fire modelling is required which takes account of actual fire load, ventilation conditions and thermal characteristics of compartment walls. In the absence of available test results for columns subjected to natural fire conditions, the authors used zone fire modelling program Ozone and finite element program SAFIR as benchmark tests as a basis of comparison with predictions from proposed approach based on Rankine. There are three

phases in the fire resistance calculations, viz. fire modelling, heat transfer and structural analysis. The benchmark tests consist of fire modelling using Ozone software. Through heat transfer process, the predicted thermal field is input into SAFIR to determine the mechanical responses of steel columns subject to elevated temperature. For heat transfer analysis, the authors proposed a simplified empirical formula (Eq. (10)), which incorporates heat transfer analysis directly into Rankine formula. The authors proposed Eq. (21) to predict the failure times of columns under natural fire conditions, considering the effects of fire load, ventilation factor and thermal properties of boundary walls. A compartment fire can basically be characterized by these three parameters. Similar to Eq. (10), Eq. (21) is obtained from least-squares regression analysis by curve fitting Ozone and SAFIR predictions to a large group of steel columns under different natural fire conditions.

$$t_{natural} = 0.9Q_f^{-0.1}v_f^{-0.25}\Gamma \times t \quad (21)$$

where  $Q_f$  = the fire load (MJ/m<sup>2</sup>);  $v_f$  = the ventilation factor;  $\Gamma = \sqrt{\frac{(v_f/0.04)}{(b/1160)}}$ ;  $v_f = A_v \sqrt{H_v} / A_t$  (m<sup>1/2</sup>);  $H_v = (A_1H_1 + A_2H_2 + \dots) / A_v$ ;  $A_v = A_1 + A_2 + \dots$ ;  $b = \sqrt{c \rho \lambda}$  (J/m<sup>2</sup>s<sup>1/2</sup>K) ;  $A_v$  is the area of vertical openings (m<sup>2</sup>);  $A_1, A_2, \dots$  are the respective area of opening 1, 2... (m<sup>2</sup>);  $H_v$  is the weighted average height of vertical openings (m);  $H_1, H_2, \dots$  are the respective height of opening 1, 2... (m);  $A_t$  is the total area of enclosure, i.e., walls, ceiling and floor, including openings (m<sup>2</sup>);  $c$  is the specific heat capacity of enclosure (J/kg K);  $\rho$  is the density of enclosure (kg/m<sup>3</sup>);

$\lambda$  is the thermal conductivity of enclosure (W/m K), and  $t$  is obtained from Eq. (20) for standard fire condition. The predictions of the proposed method are compared and validated with numerical predictions from SAFIR and Ozone. The geometry, ventilation size and thermal characteristics of boundary walls of a fire compartment are given in Table 1.

Table 1. Geometrical and thermal conditions of the analyzed fire compartment

|                                  |  |
|----------------------------------|--|
| Compartment Length $L_1$         | 5.0 m  |
| Compartment Width $L_2$          | 5.0 m  |
| Compartment Height $H_c$         | 3.0 m  |
| Ventilation Opening Height $H_v$ | 2.0 m  |
| Ventilation Opening Width $B_v$  | 0.778, 1.556, 3.111, 4.667 m                   |
| Enclosing Boundary               | Walls, ceiling and floor all of heavy concrete |
|                                  | Density $\rho$ 2300 kg/m <sup>3</sup>          |
|                                  | Specific Heat $c$ 1230 J/kg K                  |
|                                  | Thermal Conductivity $\lambda$ 1.3 W/mK        |
|                                  | Thickness 0.200 m                              |

A large pool of steel columns has been investigated. The columns have different slenderness ratios (from 22 to 271), load levels (from 10% to 80%), load eccentricities in both axes (from (25 mm, 25 mm) to (100 mm, 100 mm)). In addition, the compartment is subjected to a range of fire loads  $Q_f$  from 200 MJ/m<sup>2</sup> to 1200 MJ/m<sup>2</sup> and different ventilation factors  $v_f$  from 0.02 to 0.12. Predicted failure temperatures from the proposed approach (vertical axis) and SAFIR coupled with Ozone (horizontal axis) are given in Fig. 2a. Only the case of  $v_f=0.08$  is presented in this paper. It shows that the Rankine approach is able to provide accurate and safe predictions of critical temperatures of steel columns under different heating conditions.

Based on Eq. (21), the failure times can be obtained. This information is useful for assessing the adequacy of evacuation of occupants in a fire compartment. From Fig. 2b, the proposed approach is conservative compared to SAFIR predictions but should not be applied to rooms with a ventilation factor less than 0.02, in which case, the method will give ultra-conservative predictions compared with numerical predictions using SAFIR (with Ozone). This is partly due to inaccuracy of zone modeling predictions within this range.

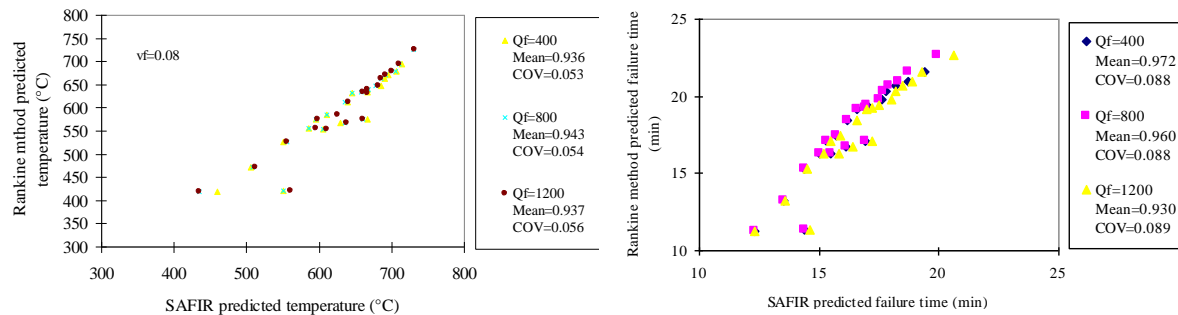


Fig. 2. Comparison of bi-axial loaded steel columns failure temperature and time under different heating conditions predicted by the proposed method and SAFIR (with Ozone modelling) (for the case of  $v_f=0.08$ )

#### 4 CONCLUSIONS

A theoretical model based on Rankine method is proposed to predict the fire resistance of bi-axially-loaded steel columns under both standard and natural fire conditions. A large pool of columns with different slenderness ratios, load levels, eccentricities, cross sectional areas, and material strengths has been analyzed with Ozone and finite element program SAFIR. Comparisons of predictions between the proposed method and SAFIR (with fire curves predicted by Ozone) are performed. The results show that the proposed method can be safely applied for most fire curves and for different thermal boundary conditions.

#### 5 ACKNOWLEDGMENT

The authors would like to acknowledge funding support from the ministry of education, Singapore, for research project titled “failure modes and ultimate strength of tubular joints under elevated temperatures” with account number arc 2/07.

#### REFERENCES

- [1] Euro code 3 (2003). “Design of Steel Structures”. Part 1.1& Part 1.2 London: British Standard Institution.
- [2] Gere, J.M. and Timoshenko, S.P. (2000). “Mechanics of Materials” 5th Ed. Chapman & Hall, London.
- [3] Horne, M.R. (1979). “Plastic Theory of Structures”, Oxford: Pergamon Press Ltd.
- [4] SNZ (1997), Steel Structures Standard NZS 3404: Part 1 & Part 2 1997, Standards, New Zealand Wellington.
- [5] Tang, C. Y., Tan, K. H. and Ting, S. K. (2001). “Basis and Application of a Simple Interaction Formula for Steel Columns under Fire Conditions,” J. of Struct. Engrg., ASCE, 127, 1214 –1220.

## COMPUTER PROGRAM FOR FIRE CHECK OF CONCRETE MEMBERS

Radek Štefan, Jaroslav Procházka

Czech Technical University in Prague, Faculty of Civil Engineering, Department of Concrete and Masonry Structures, Prague, Czech Republic

### INTRODUCTION

Structural fire resistance is one of the most important requirements that have to be fulfilled by a structural design. Concrete has excellent fire resistance properties, but that does not mean that concrete and reinforced concrete (RC) structures are not adversely affected by a fire or high temperatures. According to the European Standard EN 1992-1-2 [1], if a mechanical resistance in the case of a fire is required, RC structures shall be designed and constructed in such a way that they maintain their load bearing function during the required time in fire exposure.

For a fire design of RC structures, a member analysis is usually sufficient. For the verification of members under fire conditions, tabulated data, simplified calculation methods or advanced (general) calculation methods are suitable. The member analysis by means of the tabulated data given in EN 1992-1-2 [1] is very simple, but it can be very conservative. Another objection that might be raised against the design using the tabulated data is that these data are valid for specific types of members and only for a standard fire exposure. Also, the tabulated method can't be used for a fire design of members with a protective layer (insulation).

For more realistic member analysis, simplified or advanced calculation methods may be used, provided that a temperature distribution through the cross section is known. Temperatures in RC members exposed to fire may be determinate from tests or calculations. As a simplification, the temperature profiles given in the Annex A of EN 1992-1-2 [1] may be used, but these profiles are valid only for members (slabs, beams and columns) exposed to the standard fire and the profiles can't be used for members with a protective layer.

In this paper, the computer program FRCB500 (**F**ire **R**esistance of **C**oncrete **B**eams – **500**°C Isotherm Method) for fire check of RC beams is described. A temperature distribution through a cross section to-be-checked is calculated by means of the finite elements method (FEM) using the material models suggested by EN 1992-1-2 [1]. A design resistance in the fire situation is determined by means of the 500°C isotherm method given in the Annex B.1 of EN 1992-1-2 [1]. The program may be used in a conjunction with both standard and parametric fires (see EN 1991-1-2 [2]) and it is possible to enter cross sections with a protective layer.

The program FRCB500 is developed in the MATLAB environment. It is a non stand-alone application (that means the program FRCB500 can't run without MATLAB), but presently, a stand-alone version will be developed. The source files (so-called M-files) of the application FRCB500 are available in the Department of Concrete and Masonry Structures, Faculty of Civil Engineering CTU in Prague. Together with the program FRCB500, the application for fire check of RC slabs (FRCS500) was developed. Stand alone versions of the programs FRCB500 and FRCS500 will be available via the CTU web pages.

### 1 TEMPERATURE ANALYSIS

Before a fire resistance check can be performed, it is necessary to determine temperatures in the cross section to-be-checked. The dialog window "FRCB500 – Temperature Analysis" is shown in the Fig. 1. A user can define dimensions of a beam, properties of concrete, a thickness and properties of insulation (if the cross section is considered insulated), a design fire scenario, a fire exposure (two- three- or four-sided) and a time in fire exposure.

By means of the window "FRCB500 – Temperature Analysis", the temperature-time curve or the temperature profile can be displayed and the temperature in a point given by coordinates ( $x$ ,  $y$ ) can be calculated.

**FRCB500 - Temperature Analysis**

**FRCB500** Fire Resistance of Concrete Beams - 500 °C Isotherm Method

**Dimensions, Concrete**

Width (m)  Height (m)

Density (at 20 °C) (kg/m<sup>3</sup>)

Moisture Content (%)  <0,3>

Thermal Conductivity  
 Lower Limit  Upper Limit

**Protective Layer**

Enter Protective Layer  
 No  Yes

Thickness of the Insulation (m)

Thermal Conductivity (W/mK)

Density (kg/m<sup>3</sup>)

Heat Capacity (J/kgK)

**Design Fire Scenario**

Temperature-Time Curve:  
 Standard  
 Parametric (Natural)

Design Fire Load Density \* (MJ/m<sup>2</sup>)  <50,1000>

\* Related to the total surface area of the fire enclosure

Opening Factor (m<sup>1/2</sup>)  <0.02,0.20>

Thermal Inertia (J / m<sup>2</sup> s<sup>1/2</sup> K)  <100,2200>

Fire Growth Rate

**Temperature-Time Curve**

**Calculation of Temperatures**

Fire Exposure:  
 Two-Sided (Corner)  
 Three-Sided  Four-Sided

Time in Fire Exposure (min)

**Calculation**

... please wait!

Calculation of the Temperature in a Point (x,y)

x (m)  y (m)

Temp. (°C)

**Temperature Profile**

**CHECK OF RESISTANCE**

**Error Notification**

OK

Made by Radek Štefan, CTU in Prague, 2008. Version 1.0.  
The program can be used on your own responsibility!

Fig. 1 Dialog window “FRCB500 – Temperature Analysis”

### 1.1 Dimensions, Concrete

The beam to-be-checked is given by a width,  $b$  (m), and a height,  $h$  (m), of the beam’s cross-section.

Concrete is defined by a density at 20 °C,  $\rho(20)$  (kg·m<sup>-3</sup>), by a moisture content,  $u$  (% of concrete weight), and by a thermal conductivity,  $\lambda_c$  (W·m<sup>-1</sup>·K<sup>-1</sup>). The thermal conductivity is defined by means of the lower or upper limit suggested by EN 1992-1-2 [1]. A variation of a density with a temperature and a variation of a heat capacity (specific heat) with a temperature and with a moisture content is described in EN 1992-1-2 [1].

### 1.2 Protective Layer

If the cross section is considered insulated, the protective layer is given by a thickness of the insulation,  $d_{iz}$  (m), and by constant values of a thermal conductivity,  $\lambda_{iz}$  (W·m<sup>-1</sup>·K<sup>-1</sup>), a density,  $\rho_{iz}$  (kg·m<sup>-3</sup>), and by a heat capacity (specific heat),  $c_{p,iz}$  (J·kg<sup>-1</sup>·K<sup>-1</sup>). The protective layer is considered on all sides of the cross section that are exposed on fire.

### 1.3 Design Fire Scenario

A fire exposure is represented by the standard temperature-time curve (ISO 834) or alternatively by the parametric temperature-time curve given by a design fire load density,  $q_{t,d}$  ( $\text{MJ}\cdot\text{m}^{-3}$ ), related to the total surface area of the fire enclosure, by an opening factor,  $O$  ( $\text{m}^{1/2}$ ), by a thermal inertia,  $b$  ( $\text{J}\cdot\text{m}^{-2}\cdot\text{s}^{1/2}\cdot\text{K}^{-1}$ ), and by a fire road rate, according to EN 1991-1-2 [2].

Using the push button “Temperature-Time Curve”, the design fire scenario is displayed (*Fig. 2a, b*).

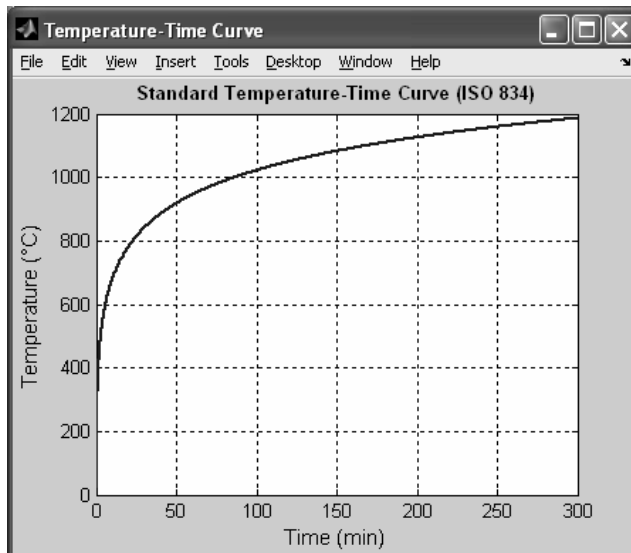


*Fig. 2a* Window with the standard temperature-time curve

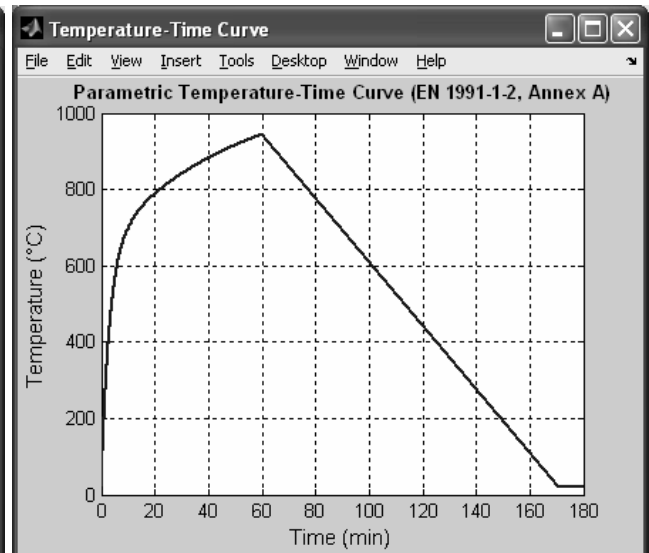


*Fig. 2b* Window with the parametric temperature-time curve

### 1.4 Calculation of Temperatures

At first, it is necessary to define a fire exposure (two-sided, three-sided or four-sided exposed cross section) and a time in fire exposure,  $t$  (min).

The temperature distribution through the cross section to-be-checked is calculated by means of the finite elements method (time approximation is based on the finite difference method).

The problem is solved as a one-dimensional heat transfer (finite element’s dimension 10 mm). At first, it is calculated with respect to  $x$ , after that with respect to  $y$ . The temperature in a point  $(x, y)$  is given in *Eq. (1)*,

$$\theta(x, y) = \theta(x) + \theta(y) - \frac{\theta(x) \cdot \theta(y)}{\theta(0)}, \quad (1)$$

where  $\theta(x, y)$  the temperature in the point  $(x, y)$ ,

$\theta(x)$  the temperature in the depth  $x$  of the “slab” with the width  $b$  (+insulation),

$\theta(y)$  the temperature in the depth  $y$  of the “slab” with the width  $h$  (+ insulation),

$\theta(0)$  the surface temperature.

The approximation given in *Eq. (1)* is explained in *Fig. 3*. The temperature distribution through the cross section is determined without taking into account steel bars. The reinforcement temperature is assumed to coincide with the concrete temperature in the same point.

Using the push button “Calculation” (see *Fig. 1*), the temperature analysis is started. After calculation, the temperature profile (or temperature field, see *Fig. 4a, b*) can be displayed and the temperature in the point given by coordinates  $(x, y)$  can be calculated. Also, using the push button “CHECK OF RESISTANCE”, the window “FRCB500 – Check of Resistance” (see *Fig. 6*) is displayed.

As shown in *Fig. 5*, the temperature profiles provided by the program FRCB500 (for the standard fire) are in agreement with the temperature profiles given by EN 1992-1-2 [1].

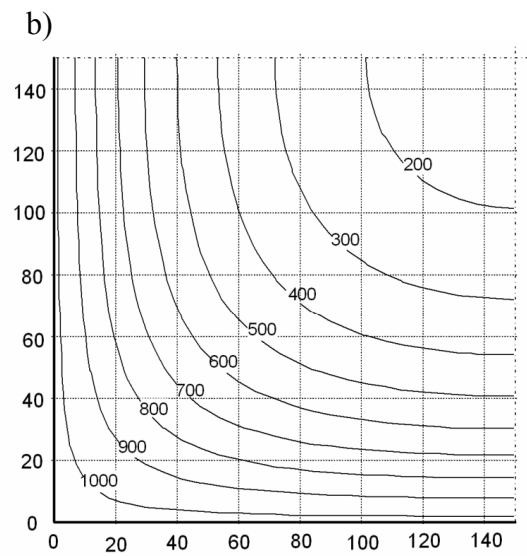
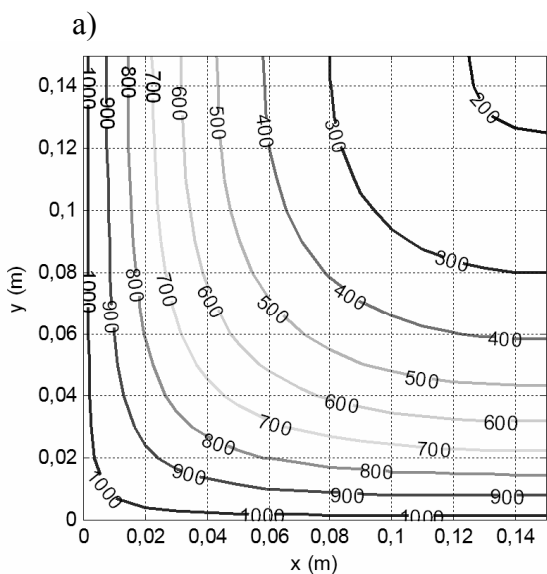
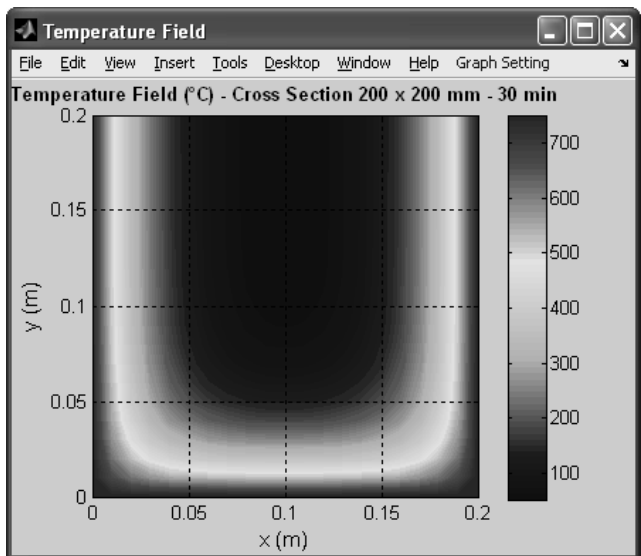
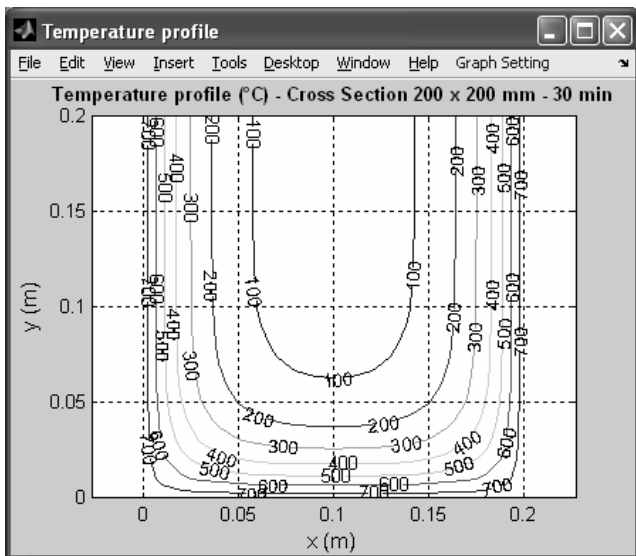
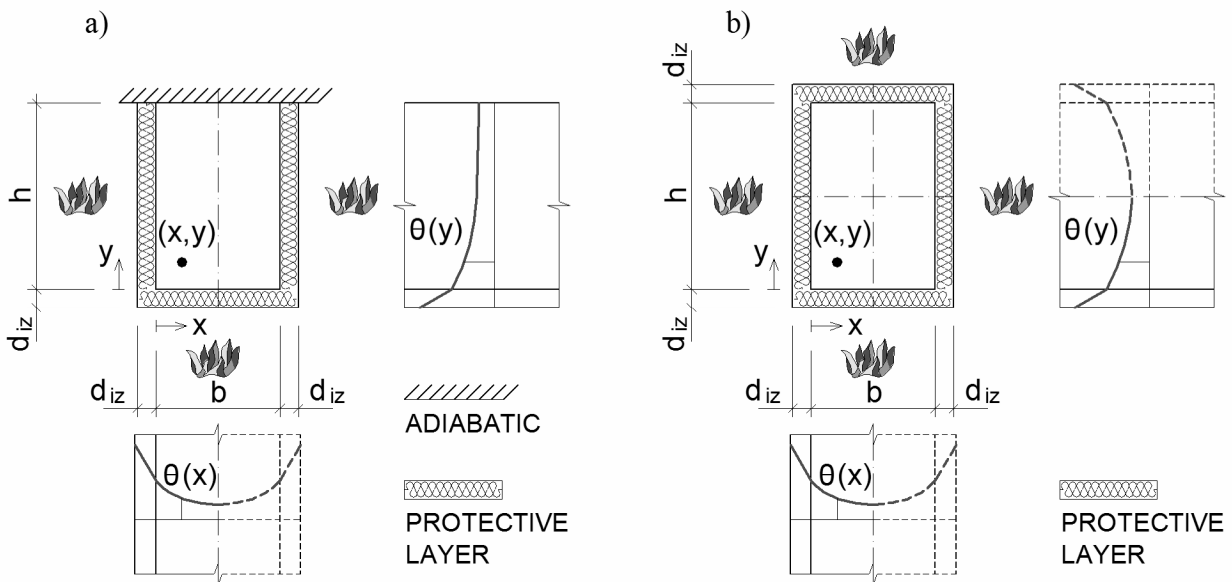


Fig. 5 Comparison of the temperature profiles for the cross section 300 x 300 mm,  $t = 120$  min, a) FRCB500, b) EN 1992-1-2 [1]

## 2 CHECK OF RESISTANCE

It is possible to check only three- or four-sided exposed cross sections. Also, the requirements on a minimum width of the cross-section as a function of a fire resistance (for the standard fire exposure) or a fire load density (for the parametric fire exposure) have to be fulfilled. The dialog window “FRCB500 – Check of Resistance” is shown in the Fig. 6.

Fig. 6 Dialog window “FRCB500 – Check of Resistance”

### 2.1 Load-bearing Function at Normal Temperature

At first, an assessment of the load-bearing function at normal temperature is determined. The beam to-be-checked (see Fig. 7) is defined by a bending reinforcement (characteristic yield strength,  $f_{yk}$  (MPa), frontal cover,  $c_1$  (mm), lateral cover,  $c_2$  (mm), bar diameter,  $\phi$  (mm), number of bars,  $n$ ), by a concrete class, and by a design value of an applied internal bending moment (absolute value),  $|M_{Ed}|$  (kNm). The assessment consists of verification of detailing rules and comparing the design bending moment with the moment of resistance, according to EN 1992-1-1 [3]. Outputs are displayed on the right part of the window.

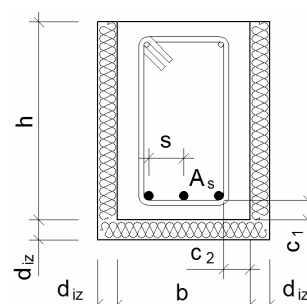


Fig. 7 Beam

## 2.2 Fire Resistance

The beam can be checked at fire situation, if all requirements at normal temperature are fulfilled. A design effect of actions for the fire situation (bending moment  $M_{Ed,fi}$ ) is determined using a reduction factor  $\eta_{fi}$ . The reduction factor is computed using the equation (2.5) given in EN 1992-1-2 [1]. Alternatively, a value  $\eta_{fi} = 0,7$  may be used.

The moment of resistance  $M_{Rd,fi}$  is calculate using the 500°C isotherm method. The method is based on the hypothesis that a concrete at a temperature more than 500 °C is neglected in the calculation of the load-bearing capacity. Concrete at a temperature below 500 °C is assumed to retain its full strength. The strength of the reinforcement is reduced with the temperature according to EN 1992-1-2 [1]. For the standard fire exposure, the fire check is performed at the time  $t$  in the fire exposure. For the parametric fire exposure (if  $t > t_{max}$ ), the fire check is performed at the time  $t_{max}$  (see Fig. 2b,  $t_{max} = 60$  min) and than repeatedly in the interval 60 seconds, until the time  $t$  (or until the fire resistance is not satisfied). Outputs are displayed on the right part of the window (see Fig. 8).

The screenshot shows a software window for fire resistance checking. At the top, there are input fields for diameter (16 mm), moment (140 kNm), and number of bars (5). Below these are buttons for 'Check' and 'Modify'. The main area is titled 'Fire Resistance' and contains several sections: 'Location of Reinforcement' with radio buttons for 'On Exposed Side' (selected) and 'On Un-Exposed Side'; 'Reduction Factor' with radio buttons for '0.7' and 'Compute' (selected); 'Assessment of Fire Resistance Moment (kNm)' showing calculated values for |MRd,fi| and |MEd,fi|. At the bottom, there is a 'Check' button and a message 'Fire resistance R 30 is satisfied!'.

Fig. 8 Check of fire resistance

## SUMMARY

Member analysis using the 500°C isotherm method is one of the methods suggested by EN 1992-1-2 for a verification of structural fire resistance of concrete members. The calculation method can be used provided that a temperature distribution through a cross section is known.

In this paper, the computer program FRCB500 for fire check of RC beams was described. A temperature distribution through the cross section to-be-checked is calculated by means of the finite elements method using the material models suggested by EN 1992-1-2 [1]. The program may be used in a conjunction with both standard and parametric fires. A design resistance in the fire situation is determined by means of the 500°C isotherm method given in EN 1992-1-2 [1].

*This work was supposed by project MSM 6840770001.*

## REFERENCES

- [1] Eurocode 2: Design of concrete structures – Part 1-2: General rules – Structural fire design (EN 1992-1-2). CEN, Brussels, 2004.
- [2] Eurocode 1: Actions on structures – Part 1-2: General actions – Actions on structures exposed to fire (EN 1991-1-2). CEN, Brussels, 2002.
- [3] Eurocode 2: Design of concrete structures – Part 1-1: General rules and rules for buildings (EN 1992-1-1). CEN, Brussels, 2004.

## **CONNECTIONS OF TRAPEZOIDAL SHEETS AT ELEVATED TEMPERATURE**

Petra Kallerová, Zdeněk Sokol, František Wald

Czech Technical University in Prague, Department of Steel and Timber Structures, Prague, Czech Republic

### **INTRODUCTION**

The behaviour of steel structure under fire situation differs from the behaviour under ambient temperature. The mechanical properties and the thermal expansion are changing with increasing temperature. Especially the yield stress and the modulus of elasticity have significant influence on the bearing capacity of steel members. This is significant especially for thin-walled elements. The corrugated sheet is able to transfer the bending moments at the early phase of the fire. The thermal expansion of steel leads to extension of the sheet and results in increased deflection. At this stage the bolted connection is loaded by forces induced by thermal expansion. At higher temperatures the bending moment resistance is reduced and major part of the load is transferred by tension membrane. At this moment the resistance and stiffness of the bolted connection has significant influence on the sheet behaviour. The connections transfer the membrane force to the supports. The performance of the connection is important also at the cooling phase of the fire.

The resistance of the connection is expressively influenced by the change of the mechanical properties of corrugated sheet. The increase of the temperature leads to the decrease of the yield stress and the modulus of elasticity of thin-walled cold formed steel members. The decrease of these mechanical properties leads to the reduction of the load bearing capacity of the structure. However, the ultimate strength is slightly increased for higher temperatures. The maximum strength is reached at 250 °C and the original value is obtained at about 350 °C. Additional increase of the temperature leads to decrease of the bearing capacity. For temperatures higher than 400 °C the yield stress on the force-deformation diagram is not visible. Buckling of the thin walled elements is influenced by reduced value of modulus of elasticity.

### **1 DESCRIPTION OF EXPERIMENT AND TESTED SPECIMENS**

#### **1.1. Experiments with screwed connections**

It the laboratory of Faculty of Civil Engineering of Czech Technical University in Prague there were carried out two sets of tests with screwed connections under ambient and elevated temperatures. Within these experiments the mechanical properties of screwed connections at steady state conditions were determined. The steady state tests (SST) are faster and simpler in comparison with the transient state tests. The SST can be used for the prediction of behaviour under fire situation when the temperature is changing in time [1]. The experiments were focused on stiffness, resistance, deformation capacity and collapse mode of the connections during fire.

By this time, four sets of experiments were performed. In the year 2005 two sets of tests were carried out [2]. The set A was with screws E-VS BOHR 5-5.5x38 and sealed washer  $\varnothing$  19 mm, in the set B the same screws were used and the sealed washer was replaced by steel

washer with diameter 29 mm. The thickness of trapezoidal sheet for sets A and B was 0.75 mm. The next two sets of experiments were carried out in 2007 [3]. The tested screwed connections were made by self-drilling screws from carbon steel with marking SD8-H15-5.5x25 (set C and set D). Test specimens were cut out from the trapezoidal sheet with nominal thickness 0.75 mm. In the set of tests C the trapezoidal sheets with measured thickness 0.75 mm, width 75 mm and length 500 mm were tested. The specimens for the set of tests D were from measured sheet thickness 0.80 mm, width 50 mm and length 350 mm. The values of material properties of used trapezoidal sheet were obtained by material experiments. For measured sheet thickness 0.75 mm was the yield stress 338 MPa and ultimate strength 428 MPa, for measured sheet thickness 0.80 mm these values reached 327 MPa for the yield stress and 426 MPa for the ultimate strength.

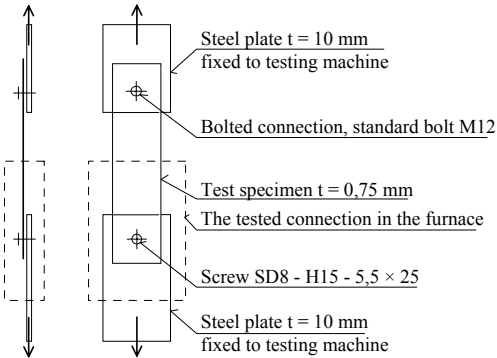


Fig. 1. The test set up



Fig. 2. The electric furnace for tests in 2007

In each sets of tests there were made experiments with two specimens for ambient temperature 20 °C and for constant elevated temperatures 200 °C, 400 °C, 500 °C, 600 °C and 700 °C. The steel sheets with thickness 10 mm simulated the bearing roof structure and they were anchored into grips of the testing machine, see Fig. 1. Due to these thicker sheets the force from testing machine to the specimens was transferred. The tested screwed joints were situated in the middle in the electrical furnace. The specimens tested in 2006 were heated in electric furnace with internal diameter 150 mm and height 300 mm. The temperatures of the connection were measured by thermocouple attached to steel sheet close to the bolt.

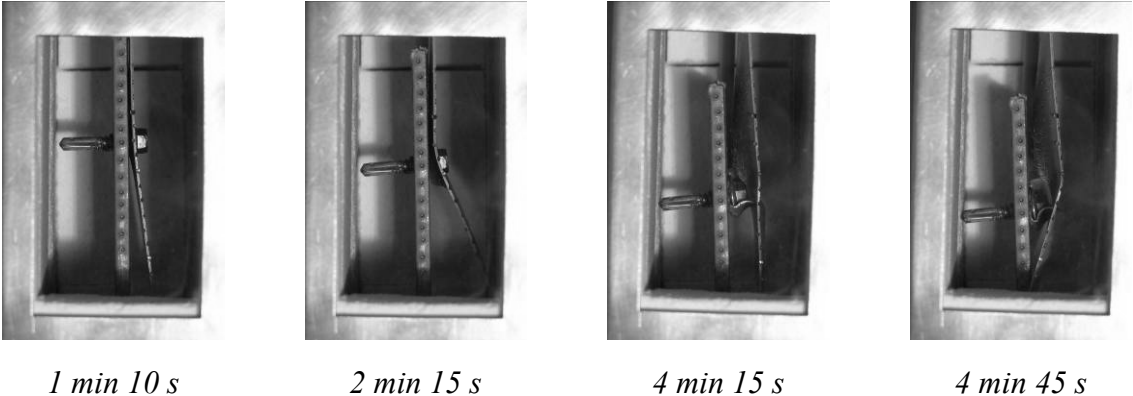


Fig. 3. The deformation of the connection

The experiments from 2007 were carried out in a smaller furnace with one opening and internal dimensions 50x130x125 mm, see Fig. 2. The thermocouple for measuring the temperature of connection was located in a hole drilled in the screw head. The air

temperatures in the furnaces and the temperatures of the tested connections were measured by one thermocouple. The electrical furnace had one opening which was filled with glass with high temperature protection. During the fire tests there was the possibility to see the behaviour and the deformation of the tested connections. In the course of the experiments the photo documentation in interval 5 seconds was provided. On Fig. 3 you can see four photos which were taken during one of the tests. The edges of the specimens were marked at the spacing 5 mm for displacement measurement. The constant rate of movement was established.

## 1.2. Experiment with the trapezoidal sheet and its catenary action

In 2007 in the laboratory of PAVUS in Veselí nad Lužnicí there was provided one fire experiment for check of the catenary effect of the thin-walled trapezoidal sheet. The specimen for fire experiment was from the trapezoidal sheet with sheet thickness 0.75 mm and the height of the waves was 55 mm. This sheet was put above the furnace with diesel burners. The specimen was fastened by self-drilling screws SD8-H15-5,5x25 to the bearing steel frame which was made from HEB200 profiles. The inner dimension of this frame was 800 x 3000 mm. In each lower wave of trapezoidal sheet two self-drilling screws were used. The frame was protected by the thermal insulation against the effect of the high temperatures.

Four rectangular iron plates with thickness 30 mm, dimensions 450 x 580 mm and weight 60 kg each were used as the mechanical load. The total load on the tested specimen was 240 kg which corresponds to 1 kN/m<sup>2</sup>. The iron plates were uniformly distributed on the trapezoidal sheet. The distance between the load and the edge of the specimen was 300 mm and the distance from each other was 200 mm. On Fig. 4 there is a view of the tested specimen before the fire experiment. There can be seen the trapezoidal sheet, the mechanical load, the bearing frame and the thermal insulation of the whole specimen.



Fig. 4 The tested specimen before fire experiment

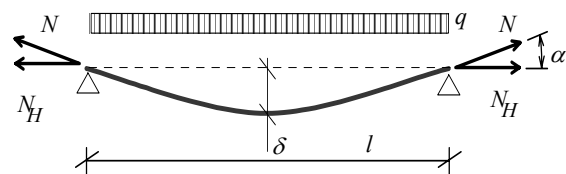


Fig. 5 The catenary action on simply supported beam

The thermocouples and a vertical deflectometer in the half of the span of the simple beam were located directly on the sheet. The thermocouples were placed in the midspan and in the quarter of the span of the trapezoidal sheet, three on the screws and three near the screws on the sheet. Two thermocouples were used for measuring the gas temperature in the furnace; they were placed at the distance of 350 mm from the upper surface of the upper wave of the sheet.

## 2 RESULTS OF EXPERIMENTS

### 2.1. Experiments with screwed connections

The resistance of the connection with sealed washer (set A) was limited by bearing resistance of the thin sheet. The sealant washer does not have any influence on the behaviour because the sealant burns at higher temperatures. The stiffness of the connection with steel washers (set B) was much higher and the resistance was almost doubled compared to the previous set. The thin sheet was deformed and accumulated in front of the washer which was accompanied by creation of two shear zones on both sides of the washer, see Fig. 6. This failure mode is characterized by deformation capacity larger than 30 mm. However, at temperatures higher than 500°C shear failure of the bolt was observed, see Fig. 7.



Fig. 6. The collapse mode of connection from the set B, temperature 200°C

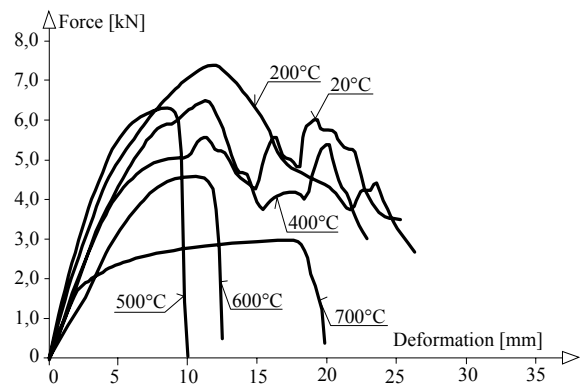


Fig. 7. The force-displacement diagrams of the screwed connections from the set B

On Fig. 8 there is the force-deformation diagram of the connections from set D and the collapse mode for connection from set C is on Fig. 9. For all specimens with the measured thickness of sheet 0.75 mm the failure in bearing was reached which occurred by tearing of trapezoidal sheet. Two modes of failure were observed for the sheet thickness 0.80 mm. For the temperatures from 20°C to 600°C the failure of sheet in bearing occurred, whereas for the temperature 700°C the mode of failure was the shear failure of the screw.

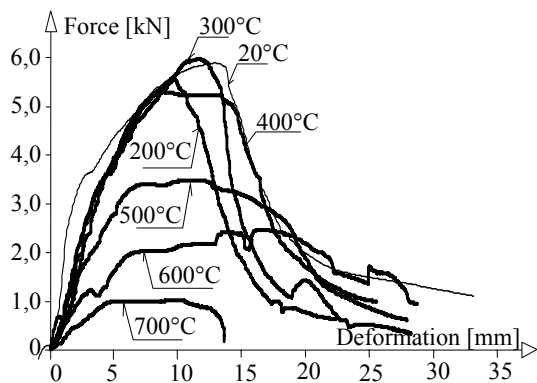


Fig. 8 The force-displacement diagrams of the screwed connection from the set D



Fig. 9 The collapse mode of the connection from set C, temperature 200°C

In the initial phase of loading the elastic behaviour can be seen. Then the force was increasing until the maximum bearing capacity was achieved and the tearing of sheet occurred. In the next phase of force-deformation diagram the decrease of force can be noticed. Due to

accumulation of deformed sheet in front of the screw the increase and subsequent decrease of force can be seen on the diagram. The deformation capacities of connections were high. Due to the dimensions limits of the electrical furnace all the experiments were terminated before their ultimate failure, but after the exhaustion of the residual bearing capacity.

The results of these experiments show how the temperature increase leads to decrease of the bearing capacity of the connections. For the temperature 550°C is the bearing capacity of the connection reduced approximately to half of the bearing capacity under ambient temperature and for the temperature 700°C the bearing capacity is less than 20% from the bearing capacity under the ambient temperature. The reduction of 45% for temperature 500°C and 90% for 700°C is used for calculations of connections with bolts and nuts. The experiments confirm the higher reduction of the resistance of the self-drilling screws in bearing in the initial phase of heating (up to temperature 550°C) and smaller reduction for higher temperatures. These two things mentioned above lead to unfavourable brittle failure of connection in shear [4]. Temperatures lower than 500°C don't have significant influence on the initial stiffness of the connection. The deformation capacity for higher temperatures is reduced by failure of the screw in shear. This mode of failure occurred only for screwed connection with the sheet thickness 0.80 mm and temperature 700°C.

## 2.2. Experiment of the trapezoidal sheet and its catenary action

The fire load was modelled by multilinear fire curve which simulated fire load used for the fire tests in Cardington. The usage of the similar fire curves is helpful for subsequent comparison of the results from different fire experiments. The maximum measured gas temperature in the furnace was 1096°C. This value was reached in the 55 minute, the total length of fire experiment was 2 hours. The temperature of the trapezoidal sheet above the support was 447°C and this temperature is about 58% lower than temperature of the trapezoidal sheet in the midspan (1084°C), see Fig. 10. In case of unprotected load bearing structure the temperature would be higher.

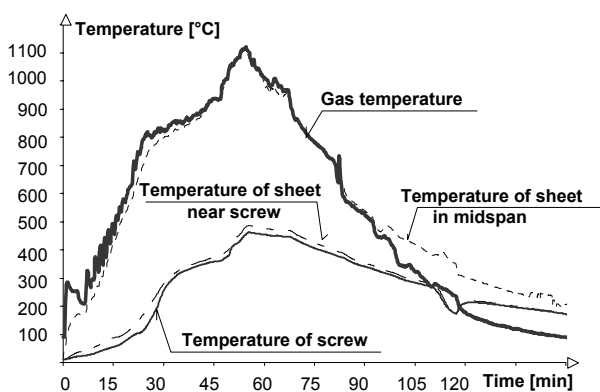


Fig. 10 The measured temperature on the specimen

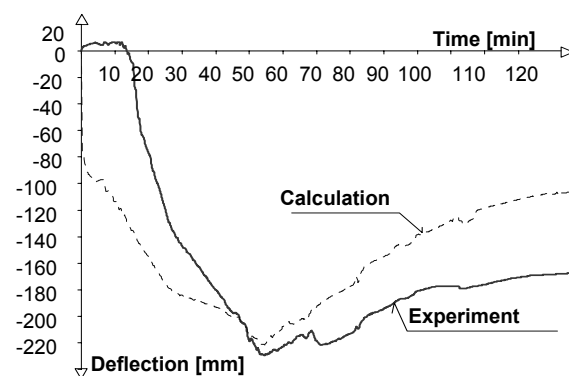


Fig. 11 The vertical deformations in midspan of trapezoidal sheet

The behaviour of trapezoidal sheet during fire experiment was quite the same as the behaviour of simple beam on which the elongation is restrained. At the beginning of the fire test the temperatures are low and the trapezoidal sheet isn't deflecting by the influence of the temperature. The sheet is elongating in its plane and the screws in supports are loaded in shear. As the temperature increases, the extension as a result of the thermal expansion of material occurs and the yield stress and the modulus of elasticity decrease. As a result of these effects the deflection is increased. By increase of the deflection and decrease of bending

stiffness there is a change of tensile forces in the supports and the sheet starts to behave like a tensile membrane. This effect is known as catenary action. On Fig. 5 there is a scheme of catenary action on simply supported beam.

The collapse of structure depends on the bearing capacity of the connections and on the ability of the load bearing structure to carry the tensile forces. On Fig. 11 there is a comparison of the deflection as a function of time for the values calculated by equations and those obtained during the experiment. The comparison of maximum deflections and the times where the deflection are obtained are in a good agreement. The maximum measured deflection of trapezoidal sheet was 229 mm, the calculated vertical deformation was 222 mm.

### 3 SUMMARY AND ACKNOWLEDGMENT

Resistance of the connection in relation to temperature is shown on Fig. 12. Resistance is reduced at higher temperatures; the reduction is small at temperatures up to 400°C but significant at temperatures higher than 500 °C. The diameter of the washer or of the screw head has significant influence on the resistance. The resistance of screwed connection from set A is approximately 40 % lower than resistance of the screwed connection from set D. When the connection from set B is used the resistance is similar to connection from set C. Shear failure of the screw may lead to low deformation capacity at temperature higher than 500 °C. These experiments will be used for development of design model of the connections at high temperatures.

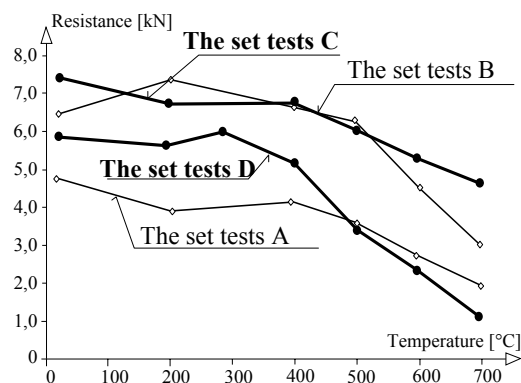


Fig. 12. The resistance of the connections

By the experiment with trapezoidal sheet supported like a simple beam the catenary action was confirmed. High fire resistance of the trapezoidal sheet which depends on suitable design of screwed connection to bearing structure was also confirmed.

This outcome has been achieved with the financial support of the Ministry of Education, Youth and Sports, project no. 1M0579.

### REFERENCES

- [1] Outinen J., Mechanical properties of structural steels at high temperatures and after cooling down, *Espoo*, 2007.
- [2] Sokol, Z., Design of Corrugated Sheets Exposed to Fire, *Progress in Steel, Composite and Aluminium Structures*, 2006.
- [3] Kallerová, P., Experiments with bolted connections – experiments at normal and elevated temperatures, *research report CTU in Prague*, 2007.
- [4] Wald, F. et al., Calculation of the fire resistance of structures, *CTU in Prague*, 2005.

## **STRUCTURAL ANALYSIS OF STEEL STRUCTURES UNDER FIRE LOADING**

Chiara Crosti, Luisa Giuliani, Konstantinos Gkoumas, Franco Bontempi

University of Rome "La Sapienza", School of Engineering, Rome, Italy

### **INTRODUCTION**

This paper builds on assumptions and findings from a second paper presented at the same conference [1], and focuses on the structural analysis of steel structures under fire loading. The use of analysis with thermo-plastic materials and with geometric nonlinearities and the modelling of the fire action using parametric curves, allow the faithful evaluation of the effective behaviour of steel structures subject to fire. In this context, once these two basic aspects are clarified, they are applied in steel structures under fire loading. For these structures the collapse can be quantified when they are subject to localized fire, modelled using a parametric curve. The evaluation of the structural collapse is very tricky and depends from many aspects; in particular, in a Performance Based approach for buildings subject to fire, it is important to consider the global vision of the structure itself. The prescriptions derived by the exploitation of the Fire Safety Engineering, come as an aid to the above.

### **1 CONSIDERATIONS ON THE PERFORMANCE BASED APPROACH**

The European Standard [2] classifies the fire action as an accidental action, intended as an action occurring after an accident. In the above sense, the design of a structure subject to fire must highlight the capacity of the structural system in achieving the objective of safety related to different performance levels. The designer is called to make a responsible choice of the performance to assign. This liberty of decision allows finding the more effective solution, one that avoids useless operations, which is the case of when following a prescriptive approach.

It is common, when assessing the performance of a structure subject to fire, to define a conventional collapse connected to the typology of structural elements and to the function that each element must perform.

It is important though to highlight that the performance based approach is not easy and immediate as is the case of a prescriptive approach. In fact, the latter approach involves the understanding of the safety levels and the accomplishment of a precise prescription and in this sense it seems to be easy to apply. On the contrary, the performance based approach requires specific knowledge from the designer. Moreover, another important difference between these two kinds of approaches is that the prescriptive one divides the situations in "checked" or "not checked", while the performance one allows to graduate the consequence on the structure and to the persons, in function of accepted risk levels.

A step very important to guarantee a determinate level of safety is to verify that the resistance of the structure under fire loading is higher than the fire severity (fire resistance > fire severity). In the particular case of steel beams, it is possible to define the conventional collapse when, the maximum vertical displacement of one node of the element, becomes equal to  $L/20$ , where  $L$  is the length of the beam. The temperature and the time of fire exposition corresponding to this displacement are defined as the critical temperature and time for the considered element.

## 2 STRUCTURAL ANALYSIS OF STEEL STRUCTURES UNDER FIRE

In this paragraph the structural behaviour of two steel structures is investigated. The structures under inquiry, although both in steel, characterised by distinctive features due to their different construction and complexity, the first one being a simple frame structure, while the second a somewhat more complex structure in truss.

Objective of the analyses is, in a first place, to highlight some of the peculiar effects arising from the fire loading, and to some extent, provide a starting point for the characterisation of the collapse resistance of the structures. The performed analyses (implemented in commercial FEM codes) account for the material and geometry nonlinearities, thus being able to accurately describe the actual behaviour of the structure.

In both cases, some aspects of the process are common. In order to assess the safety of these structures in case of fire, for the specific case, the performance level that does not contemplate collapse for all the duration of fire has to be guaranteed. As a consequence, in order to evaluate the fire resistance, a check is done by modelling the fire action using the nominal standard curve (ISO834) provided by [2]. This curve has been applied only to the elements directly involved to the fire action. Thus, the (localized) fire interests a limited area of the whole structure, in which, the release of heat, remains concentrated in the area itself.

### 2.1 Structural analysis of a single storey steel framed open deck car park under fire

The structure under inquiry is a single storey steel framed open deck car park. The facility shown in *Fig. 1*, is 32 meters long, 15 meters wide and has a maximum height of 3 meters. The deck consists in three rows of primary beams supporting seven rows of secondary beams, while the vertical elements are contemplated by appropriate steel braces.



*Fig. 1.* Picture of the steel framed car parking under inquiry

The FEM of the structure (modelled in STRAND<sup>®</sup> [3]) can be seen in *Fig. 2*.

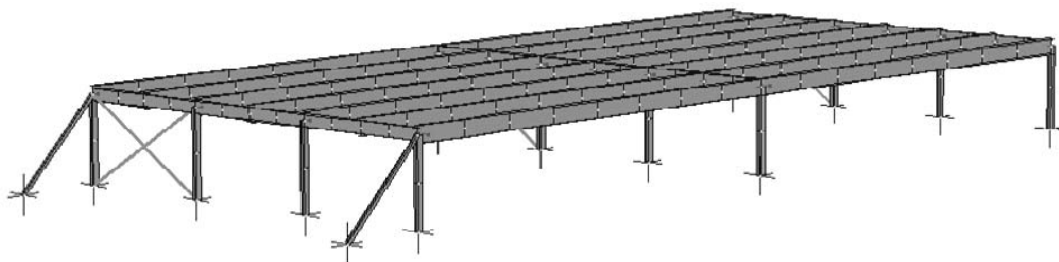


*Fig. 2.* Finite element model of the structure

Due to the simplicity in the configuration of the structure and of its particular utility, a comprehensive risk analysis has not been performed, thus being the fire scenarios identified during a process of preliminary risk analysis. For the sake of brevity, only one fire scenario is briefly presented (refer to [4] for further analyses), the one involving three vehicles eventually catching fire in the proximity of the intermediary of the primary beams, in the area delimited by the four external secondary beam rows (*Fig. 3*), with two columns influenced by the fire.

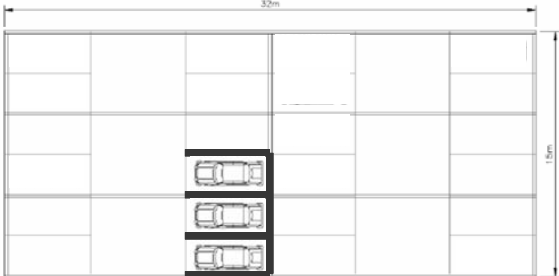


*Fig. 3.* Deformed configuration of the structure

The vertical displacements in time of a node at the middle of the beam in correspondence to the central column is shown in *Fig. 4*. As can be seen various phases can be identified. In a first phase, the terminal excursion leads to the uplifting of the node. This terminates at about 600 sec. after the fire ignition, with the column abruptly failing due to buckling in two distinct time points. Part of the displacement has to be attributed to the thermal bowing effect (see for example [5]) resulting from differential thermal expansion over the cross-section of the non-uniformly heated supported beam.

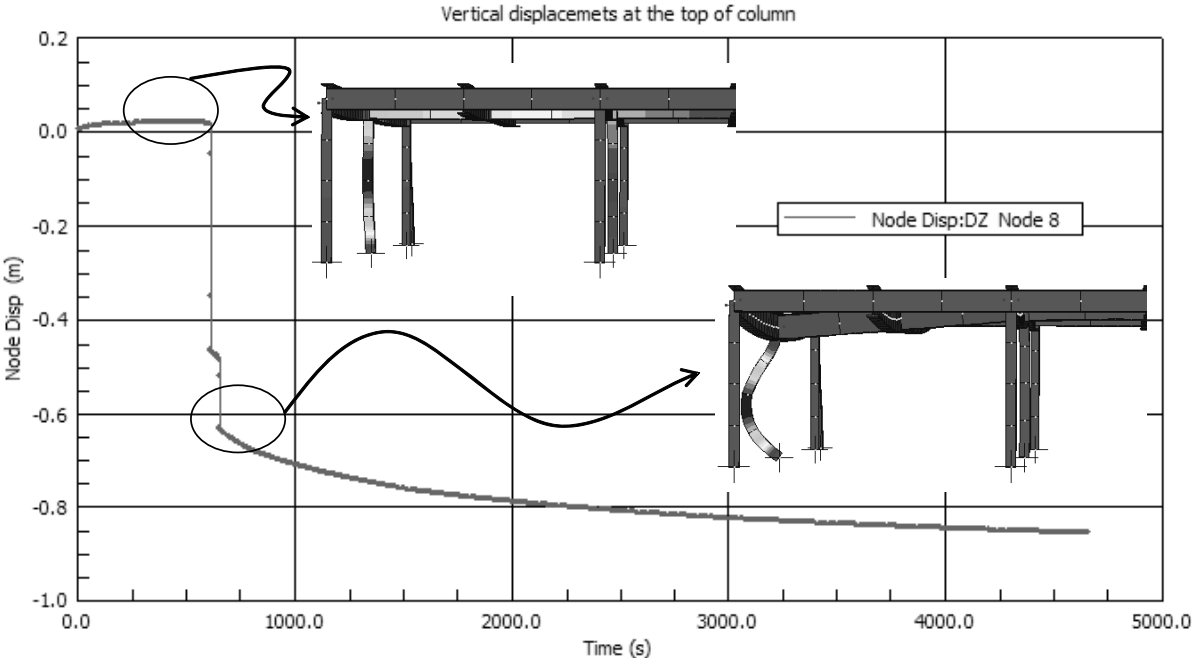


*Fig. 4.* Vertical displacements of a node of the column and corresponding deformed shape

The column continues to sag, leading to the final configuration of *Fig. 5*, where the inner column is also deformed.

For the sake of brevity, at this point, no further considerations are made on the front of the collapse resistance of the structure.

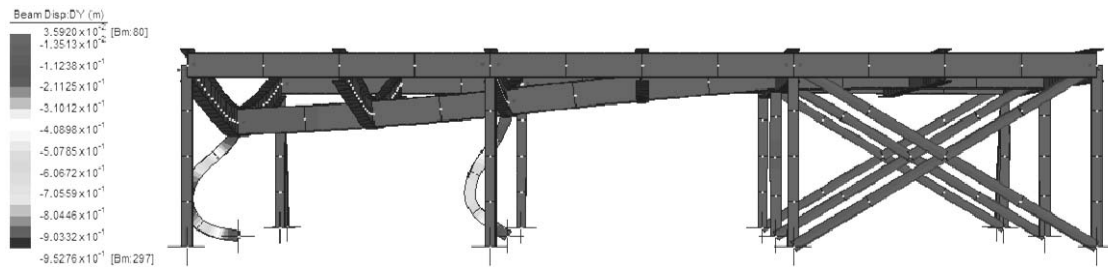


Fig. 5. Deformed configuration of the structure

## 2.2 Structural analysis of an industrial facility under fire

The structure under inquiry is an industrial facility in steel, used for the storage and maintenance of helicopters, therefore it presents with an elevated fire risk. The facility is 64.64 meters long, 32.85 meters wide and has a maximum height of 12.9 meters as shown in Fig. 6.

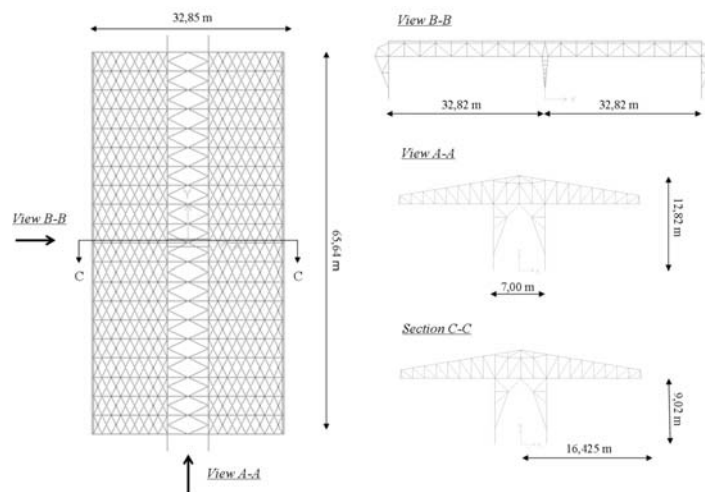
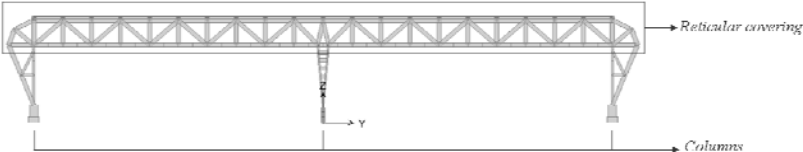


Fig. 6. Geometry of the facility

This facility presents a relatively complex geometry. The structure is isolated, it presents symmetry both in the x and in the y direction and it has a truss covering. There are six vertical elements, composed by a block of concrete at the end of these, start steel elements, those composes the column.

Some initial considerations are necessary on the front of the structural dependability of the facility [6], in terms of collapse resistance [7]. If a structure is redundant, then there are many alternative load paths, large deformations can develop without a loss of its load bearing capacity, and structural failure must be accounted for in a different way. This phenomenon creates sufficient reserve capacity to allow most of such structures to survive fires with little structural damage. For the above reason, it is important to make some considerations about the facets of structural collapse. It is possible to verify that the collapse of a single metal bar, although of a certain significance, doesn't compromise the global behaviour of the whole structure. Therefore, the local collapse of a single (or a limited number) of the covering bars has to be dealt with differently compared to the collapse (or loss of resistance) of the vertical elements (columns) which do not offer redundancy in this building. The collapse can be evaluated as a function of the global behaviour of the whole structure, assigning particular importance to the more resistant elements, and after that, to the columns.

To evaluate the fire resistance of this structure, three fire scenarios are considered, as indicated in [1]. For the sake of brevity, only the 1<sup>st</sup> scenario is presented, in which fire is concentrated in the central zone of building, involving also the central columns. However, similar considerations can be made for the 3<sup>rd</sup> scenario, considering the nodes of the extreme columns subject to fire (presented in [8]), while results referring to the 2<sup>nd</sup> scenario are omitted since this scenario doesn't involve the columns, therefore, it doesn't lead to structural collapse. FEM analyses are performed on the ADINA<sup>®</sup> [9] commercial code, and involve a large engagement in terms of time and memory on the computer: for example, for the specific model with 1205 nodes, corresponding to 7230 degrees of freedom, the analysis lasts five hours with a normal processor. Particular attention is given also to the static scheme of this structure, composed by a reticular covering and it is so very redundant, as shown in *Fig. 7*.



*Fig. 7.* Identification of the structural elements of the building, view B-B

The trend of the node displacement corresponding to the column affected by the fire is reported referring to the 1st scenario (*Fig. 8*). For this scenario, the trend of one node of the central column is evaluated.

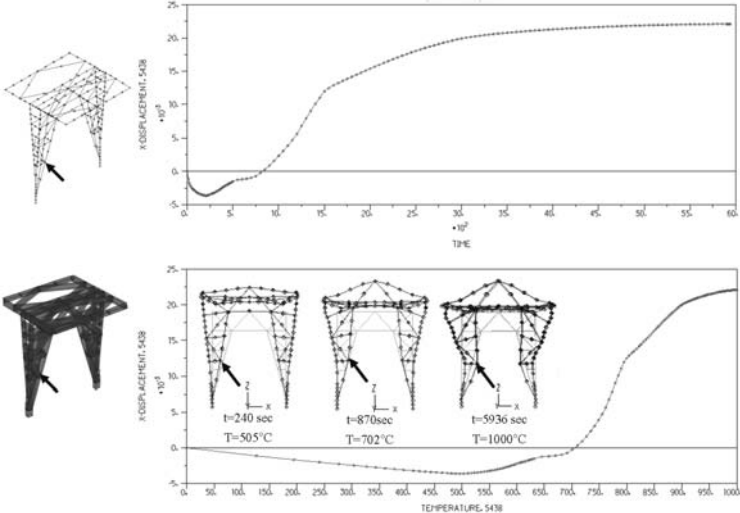


*Fig. 8.* Displacements of a node of the column along the x axis

For this trend a point of discontinuity seems easily to single out. In fact, after 800 seconds, which corresponds to a temperature of approximately 700°C, the trend of displacements of the x axis of the node goes through negative values, for the effect of temperature that initially produces large thermal expansion, to positive values.

This passage is due to loss of stiffness and resistance produced by the elevated temperature, in this way the element starts to skid towards the weakest direction. From what said, it is not possible to suggest that after 13 minutes the structure collapses, but it is reasonable to think that over this time limit, the column suffers a modification of stiffness and resistance that, in a Performance Based approach, highlights the possibility that the safety of the structure cannot be guaranteed.

In *Fig. 9* and *Fig. 10* the initial and deformed configurations along the x and y axis are shown, with reference to this scenario.

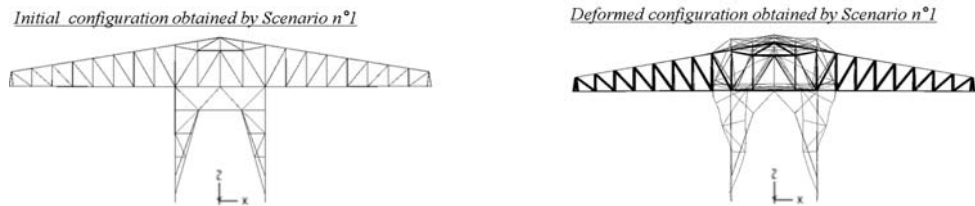


*Fig. 9.* Initial configuration, view A-A *Fig. 10.* Deformed configuration, view A-A

From these considerations it is possible to conclude that for the scenarios involving the columns, after 800 seconds, which correspond to a temperature of 700°C, the structure shows an abrupt change in stiffness, and therefore, this temperature represents a critical state that can make this structure less safe regarding to its stability.

### 3 CONCLUSIONS

In this paper, some initial thoughts about the performance of two distinctive structures under fire loading are presented. To this aim, the application of nonlinear analysis on the thermo-mechanic behaviour of materials and on the structures as a whole, together with the appropriate fire modelling in pragmatic scenarios, consents to demonstrate and verify the performance of the structure in terms of resistance to fire during the design phase.

The effective behaviour of steel structures subject to fire is rather complex, and therefore, their evaluation must to be assessed considering the global behaviour of the structure, considering also that the definition of collapse of a structure is connected to many aspects.

### REFERENCES

- [1] Gkoumas, K., Crosti, C., Giuliani, L., Bontempi, F. Definition and selection of design fire scenarios. Book Proceedings: Applications of Structural Fire Engineering, Prague 19-20 February 2009.
- [2] Eurocode 3 - Design of steel structures, Part 1.2: Structural fire design, Commission of the European Communities, Brussels, 1993.
- [3] STRAND<sup>®</sup>, [www.strand7.com](http://www.strand7.com)
- [4] Crosti, C., Bontempi, F., Benchmarking/Betatesting di codici di calcolo utilizzabili per l'analisi strutturale in caso di incendio (in Italian), available online on 01/2009 at <http://dx.medra.org/10.3267/HE2008>
- [5] Cooke, G.M.E., Morgan, P.B.E., Thermal bowing in fire and how it affects building design, BRE Information Paper 21/88, Building Research Establishment, 1988.
- [6] Bontempi, F., Giuliani, L., Gkoumas, K., Handling the exceptions: dependability of systems and structural robustness, in Recent Developments in Structural Engineering, Mechanics and Computation, Alphonse Zingoni (Ed.), Millpress, Rotterdam, 2007.
- [7] Starossek, U., Wolff, M., Design of collapse resistant structures, Workshop on robustness of structures (JCSS and IABSE), November 28-29, 2005.
- [8] Crosti C., Bontempi F., Safety performance evaluation of steel structure under fire action by means of nonlinear analysis, in Proceedings of the CST2008 & ECT2008 Conferences, Athens, 2-5 September 2008.
- [9] ADINA<sup>®</sup>, [www.adina.com](http://www.adina.com)

## CONNECTION TEMPERATURES DURING THE FIRE TEST IN MOKRSKO

Jiří Chlouba, František Wald

Czech Technical University in Prague, Department of Steel and Timber Structures, Czech Republic

### INTRODUCTION

The fire test in Mokrsko was focussed mainly to the overall behaviour of the structure and the connection temperatures, both of which may not be observed on the separate elements. Except for the three types of flooring systems, six wall structures with mineral wool were tested.

The fire experiment was conducted in Mokrsko in Central Bohemia, Czech Republic, 50 km south from Prague 18 September 2008, see [1]. The new building was made in front of the Czech technical University in Prague educational centre Joseph gallery, see [www.uef-josef.eu](http://www.uef-josef.eu). The experiment follows the seven large fire tests in Cardington laboratory on steel frame from 1998 – 2003, see [2]. During the experiment were used the knowledge learned during the Ostrava fire test, see [3] and [4] as well. The structure was designed by the design office EXCON a.s. Prague with cooperation of the all parties involved into the structural parts delivery. The fire design of the structure was prepared at Czech Technical University in Prague, The University of Sheffield and Slovak Technical University in Bratislava. The behaviour of slender castellated beams and beams with the corrugated web were simulated including the concrete slab and the connection behaviour at the elevated temperature by the VULCAN programme.



Fig. 1 Experimental building

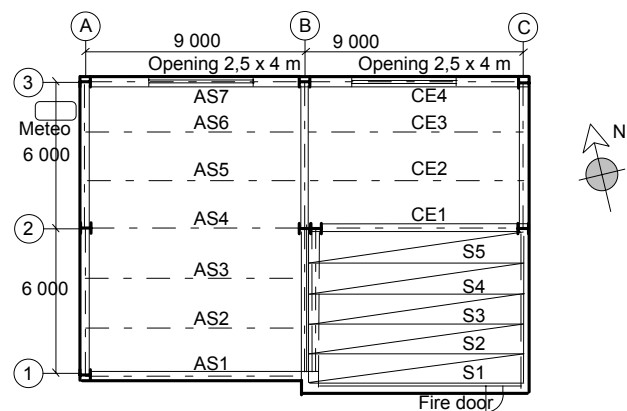


Fig. 2 Plan view of the structure

### 1 EXPERIMENTAL STRUCTURE

The structure represents one floor of the administrative building of size 18 x 12 m, see Fig. 1 and Fig. 2. The composite slab on the castellated beams was designed with a span 9 to 12 m and on beams with corrugated webs with a span 9 to 6 m. The deck was a simple trapezoidal composite slab of thickness 60 mm with the height over the rib 120 mm with sheeting CF46 (Cofraplus 0.75 mm) and concrete of measured cubic strength  $34 \text{ N/mm}^3$  in 28 days reinforced by a smooth mesh  $\phi 5 \text{ mm } 100/100 \text{ mm}$ , with strength 500 MPa and coverage 20 mm. The prefabricated panels Spiroll of height 320 mm with hollow core openings formed a span 9 m. The panels were supported by concrete wall and primary hollow beam from the welded double IPE 400 section. The height of the castellated beams with sinusoid openings

Angelina, design by ArcelorMittal, made of IPE 270 section from steel S235 was 395 mm. The beams with corrugated webs, design by Kovové profily s.r.o., have flanges 220 x 15 mm and web 2.5 mm thick with height 500 mm steel S320. The edge beams were from sections IPE 400 steel S235. The fire protected columns were prepared from HEB 180 sections. The horizontal stiffness of the frame was reached by concrete walls with 250 mm thickness made of concrete C30/37 and two cross braces of L 80x80x8. The beam to beam and beam to column connections were designed as header plate, plate 10 mm with four bolts M16 class 8.8. The improved fire resistance was reached by encasing two bolts in the concrete of the slab.

Two walls were composed from cladding, linear trays, mineral wool and external corrugated sheets. In two 6 m spans was compared the system with the internal grid and horizontal sheeting and with vertical sheeting without the internal grid. Two other walls were made of sandwich panels of thickness 150 mm filled with mineral wool. In front of the concrete wall was a brick wall made of plaster blocks. The fire protection of columns, primary and edge beams as well as bracings was designed for R60 by board protection 2 x 15 mm Promatect H.

## 2 MECHANICAL AND FIRE LOAD

Mechanical load was designed to comply with regular administrative building. The dead load of tested structure reached  $2.6 \text{ kN/m}^2$ . The variable load  $3.0 \text{ kN/m}^2$  was simulated by 78 sand bags with road metal. The weight of the bags varied from 793 kg to 1087 kg. They were coupled on pallets by three to reach an average weight 900 kg, see Fig. 3. The applied load represented the characteristic value of the variable action at elevated temperature  $3.0 \text{ kN/m}^2$  and the characteristic value of flooring and partitions  $1.0 \text{ kN/m}^2$ .



*Fig. 3* Position of mechanical load

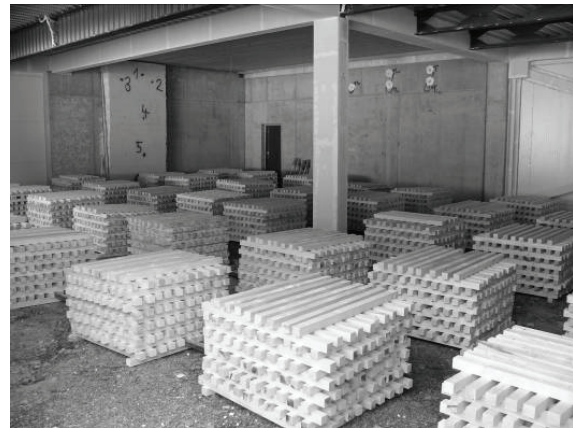


*Fig. 4* Distribution of fire load

The  $15 \text{ m}^3$  unwrought wooden cribs  $50 \times 50 \text{ mm}$  of length 1 m of softwood dried to moisture till 12% represented the fire load. The cribs were placed into 50 piles, see Fig. 4. Each pile consisted of 12 rows with 10 cribs, which means  $35.5 \text{ kg/m}^2$  of timber and simulates the fire load  $620 \text{ MJ/m}^2$ . The design characteristic fire load of administrative building is calculated as  $420 \text{ MJ/m}^2$ . The simultaneous ignition of piles was reached by their connection by the steel thin-walled channels filled by a mineral wool and penetrated by paraffin. The channels were located on the second layer of cribs and connected three/four piles together. The fire test starts by reaching the gas temperature  $50 \text{ }^\circ\text{C}$ . The openings of height 2.54 m and total length 8.00 m with parapet 1 m ventilated the compartment. To allow a smooth development of fire no glazing was installed.



*Fig. 5* Thermocouples for gas and steel temperatures



*Fig. 6* Thermocouples on beam to column connection

### 3 MEASUREMENTS

The gas temperature in the fire compartment was measured by 14 jacketed 3 mm thermocouples located 0.5 m below the ceiling in the level of the beams lower flanges, see Fig. 5. Two thermocouples were placed in the openings. The temperature profile along the compartment height was measured between the window and in the back of the fire compartment below the secondary beam. For measuring the temperature of the structure 2 mm jacketed thermocouples were used. In the composite slab were designed 12 thermocouples, on beams 11, in bolted connections 37, see Fig. 6, in the hollow core panels 6, in concrete wall 16, in external cladding 24, in the fire protected internal column 7, and on the external column 24. On the West linear scaffold a meteorological station was installed to record the external temperature and the wind direction and its speed. The behaviour was documented by photographs, video and thermo imaging records.

#### 3.1 Temperatures

The prediction of the gas temperatures by the parametric fire curve and by the zone model expected conservatively in 60 min of the fire the temperature 1057 °C, see Fig. 7. Under the composite slab with castellated beams was measured in 60 min the temperature 935°C. At the beginning of the fire the highest gas temperatures were reached in the front of the fire compartment and during the full developed fire in the back of the fire compartment. The East and West part of the compartment showed different temperature development. In the Eastern part of the fire compartment with the concrete wall reached in 21 min temperature 810°C, in 30 min temperature 935°C, and in 58 min temperature 855°C. In the Western part of the fire compartment the developed gas temperature was very similar to the nominal standard fire curve [5]. The temperatures in both parts of the fire compartment were different due to the different walls and a small change in the wind direction during the test.

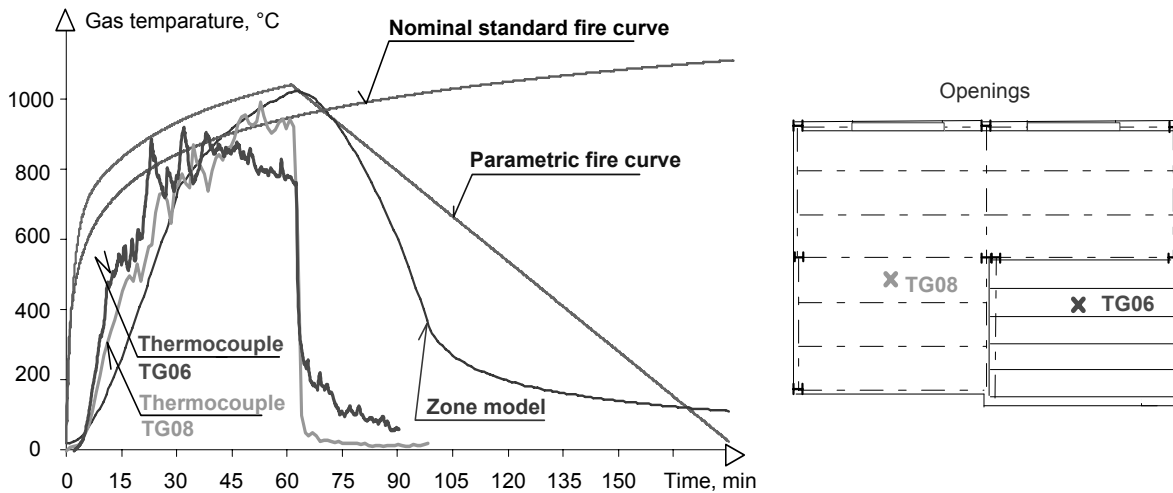


Fig. 7 Comparison of predicted and measured gas temperatures

### 3.2 Response of the structure

The lower flange at the midspan of the unprotected castellated beam AS4 reached in 23 min 487 °C with deformation 135 mm, see Fig. 8 and 9. In 34 min of the fire were the temperature 790 °C and the deflection 378 mm. The failure of the slab occurred in 62 min of the test in the cooling phase of the fire with the measured temperature of the beam's lower flange at the mid span 895 °C. The damage of the ceiling started in the Southeast corner. The slab lost the resistance in compression in 62 min of the experiment. The edge beam buckled on its developed free length. Due to the spalling of the top of the concrete column the anchors lost the tensile resistance. The bolted connection of the primary box girder was exposed to torsion, which leads its lost of its bolt shear resistance.

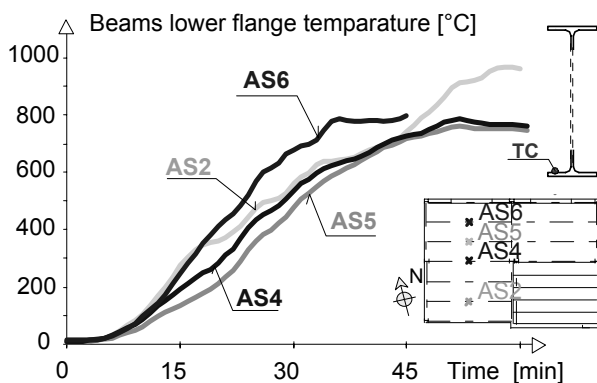


Fig. 8 Temperatures of the lower flanges of cellular beams

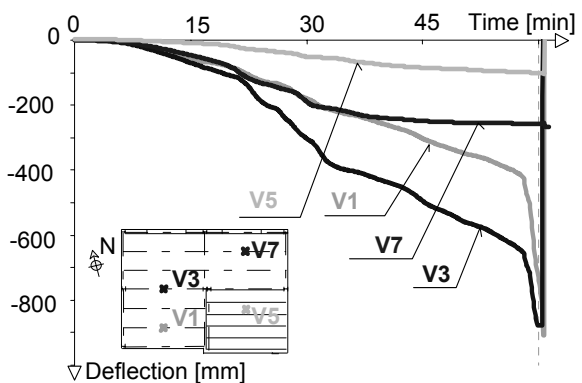


Fig. 9 Deflection of the ceiling

### 3.3 Connection temperatures

One of the goals of this experiment was to examine connections with higher fire resistance, which is reached by encasing them in the concrete slab. The maximal temperature of the lower part of the beam to column joint was 520°C, whereas the upper encased part reached 157°C. The highest temperature of the lower flange of the beam in the midspan was 932°C. In the case of beam to beam connection, the temperatures differences were similar; the lower part of the joint reached the maximal temperature 410°C, the upper encased part 198°C, whilst the lower flange at the beam's midspan 881°C. The connections end plate plastically

deformed before the collapse of the slab, see Fig. 10. On Fig. 11 there is presented temperature in the connection of castellated beam AS4 to column and Fig. 12 shows temperatures of the connection of castellated beam AS5 to primary beam.

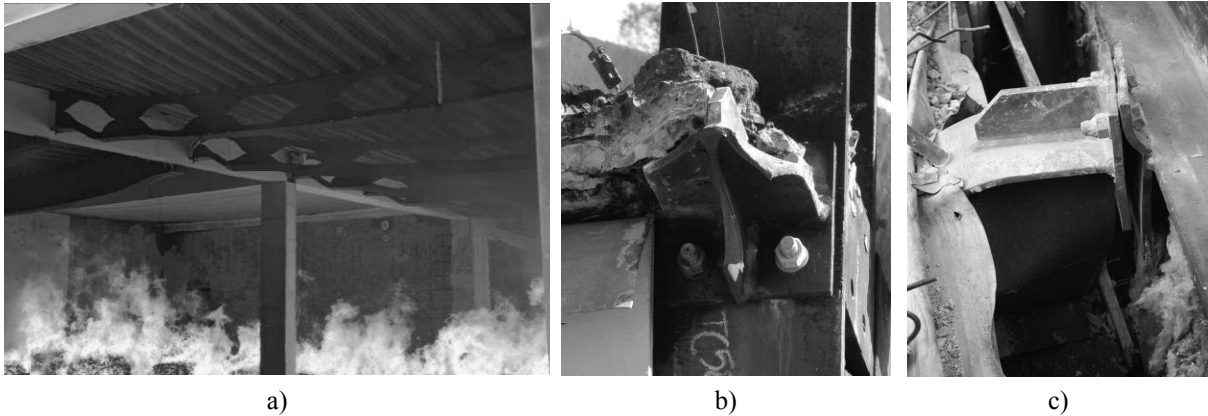


Fig. 10 a) Deflections of the structure in 58 min, b) the beam to column connection after the test, c) the deformation of the end plate of the beam to beam connection

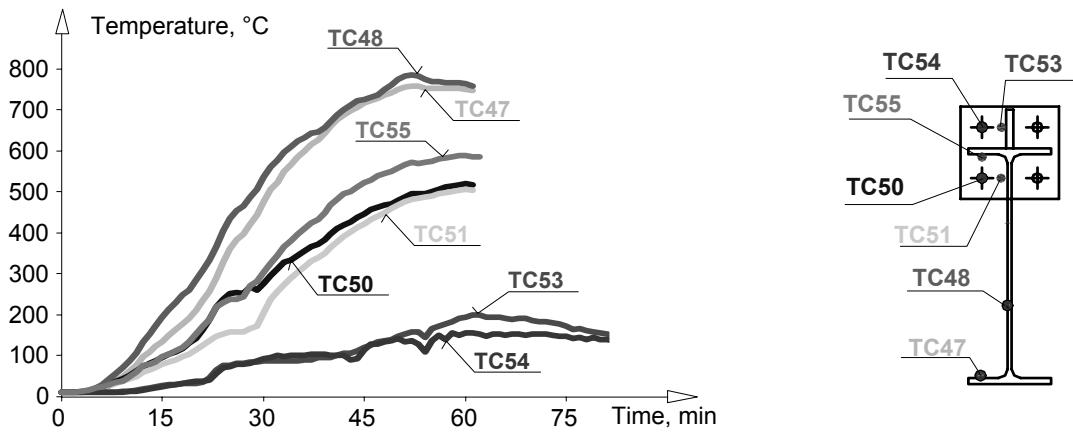


Fig. 11 Temperatures in the beam to column connection of the castellated beam AS4

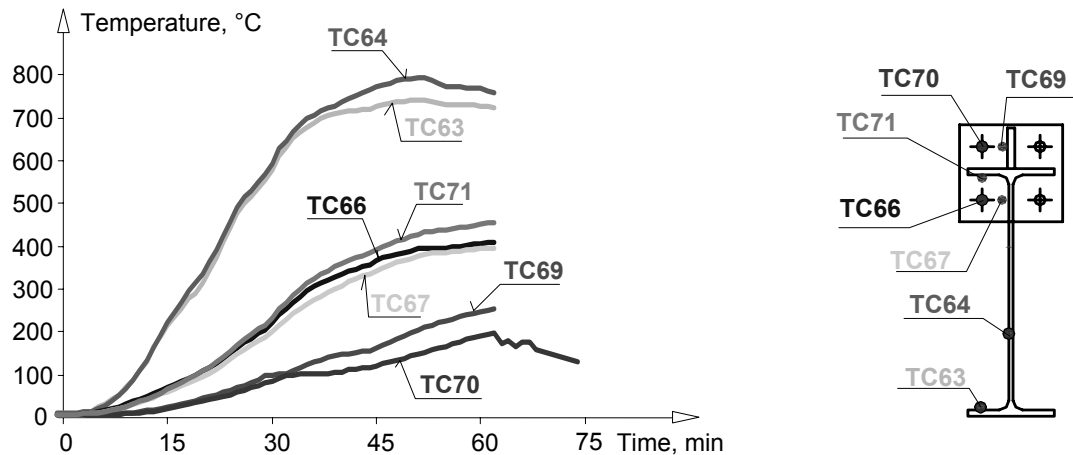


Fig. 12 Temperatures in the beam to beam connection of the castellated primary beam AS5

To predict the temperature in the connection, which is partially encased into the concrete slab, the program SAFIR, see [6], was selected. The 3D model of the joint is shown on Fig. 13. The fire was modelled by program Ozone 2.2, see [7]. The predicted temperatures in the connection can be seen on Fig. 14.

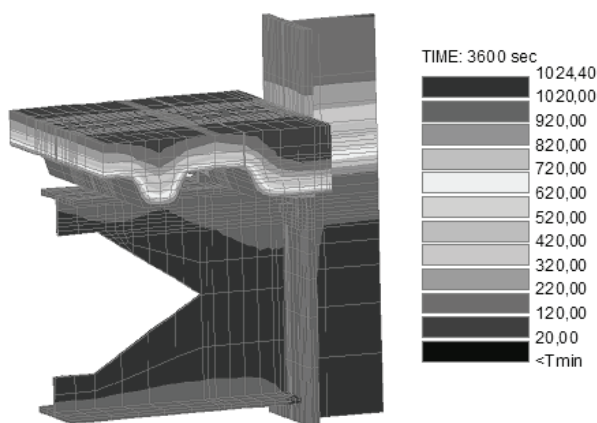


Fig. 13 Simulation of temperatures of the beam to column connection in 60 min

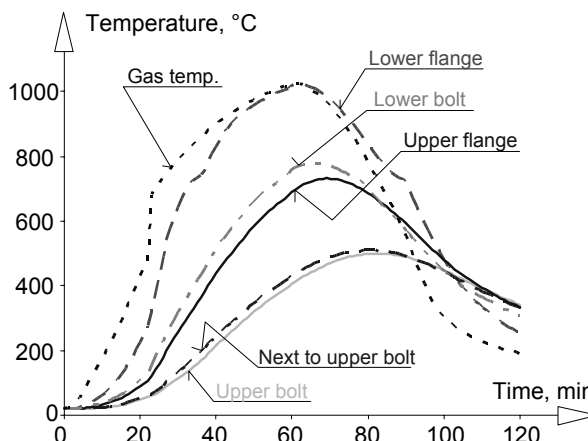


Fig. 14 Predicted temperatures in the connection

#### 4 SUMMARY

The fire test shows the differences between the behaviour of the element and of the structure exposed to high temperatures during fire. The collapse of the composite slab was reached.

The maximum temperature of the lower bolt in the beam to column connection reached 56% of the temperature in the lower flange in the beam midspan, the upper encased bolt 17% of the midspan maximum in the flange. In case of beam to beam connection, the temperature in the lower unprotected bolt was 46% of the maximal temperature in the beam's flange in the midspan, whilst the upper protected bolt 22% of the same maximal temperature.

#### 5 ACKNOWLEDGEMENT

This work was supported by grant Fire improved joints No. OC 190 and by the research centre of Ministry of education, youth and sports CIDEAS No. 1M0579.

#### REFERENCES

- [1] Kallerová P. a Wald F., Požární zkouška na experimentálním objektu v Mokrsku, *ČVUT v Praze*, srpen 2008, ISBN 978-80-01-04146-8.
- [2] Wald F., Simões da Silva L., Moore D.B., Lennon T., Chladná M., Santiago A., Beneš M. and Borges L., Experimental behaviour of a steel structure under natural fire, *Fire Safety Journal* 2006, Volume 41, Issue 7, pp. 509-522.
- [3] Kallerová P. and Wald F., Ostrava fire test, *Czech Technical University in Prague*, CIDEAS report No. 3-2-2-4/2, p.18, [www.cideas.cz](http://www.cideas.cz).
- [4] Chlouba J., Wald F., Sokol Z., Temperature of connections during fire on steel framed building, *International Journal of Steel Structures*, accepted for printing.
- [5] EN 1991-1-2: 2002. Eurocode 1: Basis of design and actions on structures – Part 2-2: Actions on structures – Actions on structures exposed to fire, *CEN, Brussels*.
- [6] Franssen J.M., Kodur V.K.R., Mason J., User's Manual for SAFIR 2004: A Computer Program for Analysis of Structures Subjected to Fire, *University of Liège*, 2005.
- [7] Ozone V2, *University of Liège*, URL: <http://www.argenco.ulg.ac.be/logiciel.php>.

Proceedings of International Conference  
Applications of Structural Fire Engineering  
Prague, 19-20 February 2009

**Session 6**

**Composite Structures**

## ASSESSMENT OF STEEL – CONCRETE – STEEL SHEAR WALL

David Dunne <sup>a</sup>, Dr. Nutan Subedi <sup>b</sup>

<sup>a</sup> University of Dundee, School of Engineering, Physics & Mathematics, Civil Engineering, Dundee, Scotland.

<sup>b</sup> Reader Structural Engineering (Retired), University of Dundee, Dundee, Scotland.

### 1 INTRODUCTION

Fire safety is an important consideration in design. Concrete as a construction material is extensively used in structures. Its inherent fire resistance property provides protection for life, property and the environment we live in [1]. Moreover, concrete is a material possessing low thermal conductivity and high specific heat capacities. These properties render its heat transfer rate very slow and fire resistance very good [2]. Steel-Concrete-Steel, S-C-S, construction has the capacity to contribute and enhance this function as in the case with steel deck composite floors. The steel plates on both sides of the concrete core can provide good insulation to concrete retarding the heat flow and early spalling of concrete [3,4].

S-C-S is a robust form of construction in which the composite action can be achieved in a number of ways, such as: the use of shear studs, overlapping shear studs, overlapping J-hooks, bi-steel welded stud system and epoxy resin plate bonding. The applications include beams in common structures, wall panels, tunnels and aircraft hangars to name but a few [5]. In S-C-S composite construction the conventional reinforcement is replaced by external steel plates; its main advantage being its robustness, derived from the composite action between these steel plates on the outside and the concrete core on the inside. The current research programme was to extend the application of S-C-S system to shear walls in tall buildings. The main aim was to investigate the behaviour of two different structural forms of shear walls, a conventionally reinforced shear wall and a S-C-S composite construction. It was considered that the S-C-S system would fully utilise the properties of both the steel and concrete making it a more efficient, robust and durable form of structural system and performing better under variable loading conditions. An experimental study was carried out using one of each of the two systems of wall and subjected to static and impact loadings. The main conclusion from this preliminary study was that the S-C-S composite system possesses significantly greater stiffness and thus significantly reduced degree of deflection compared to that of a conventionally reinforced shear wall system. Other significant design parameters such as strain development, crack patterns and their effects are also discussed.

### 2 EXPERIMENTAL MODEL

The model depicted in Figures 1 and 2 and in more detail elsewhere [5], consists principally of two shear walls of the same size 900mm x 40mm x 300mm, one conventionally reinforced with the second containing a S-C-S form of construction which consists of two external plates as reinforcement. The walls were cast into a specially designed concrete block providing a rigid foundation for testing. For testing purpose the walls were laid horizontal while still being restrained at the base.

The conventional reinforcement consisted of 6mm diameter and 1180mm length mild steel, placed longitudinally and spaced at 23mm centres. Additionally, two horizontal reinforcement bars were placed at the top and bottom of the wall increasing both tensile and compressive zones of the wall respectively. Furthermore, 6mm diameter link bars at 50mm centres and at lengths of 260mm were placed at staggered centres either side of the main horizontal steel vertically tying the reinforcement together. The second form of reinforcement to be employed was that of steel plates, which were placed on both sides of the externally reinforced wall, 1180mm x 0.7mm x 300mm in size. There was also reinforcement required for the concrete block which was to consist of a steel cage of eight links of 10mm diameter steel bar. The final element in the steel reinforcement was the addition of four reinforcing plates along the top of each wall, 50mm x 40mm x 10mm in size with each plate having two number 100mm lengths of 6mm

diameter steel bar welded to its base. These plates which can be seen in Figure 1 and in greater detail elsewhere [5], were placed at loading locations on the top of both walls, their purpose being to distribute the applied loads to reduce the local damage under the bearing plate.

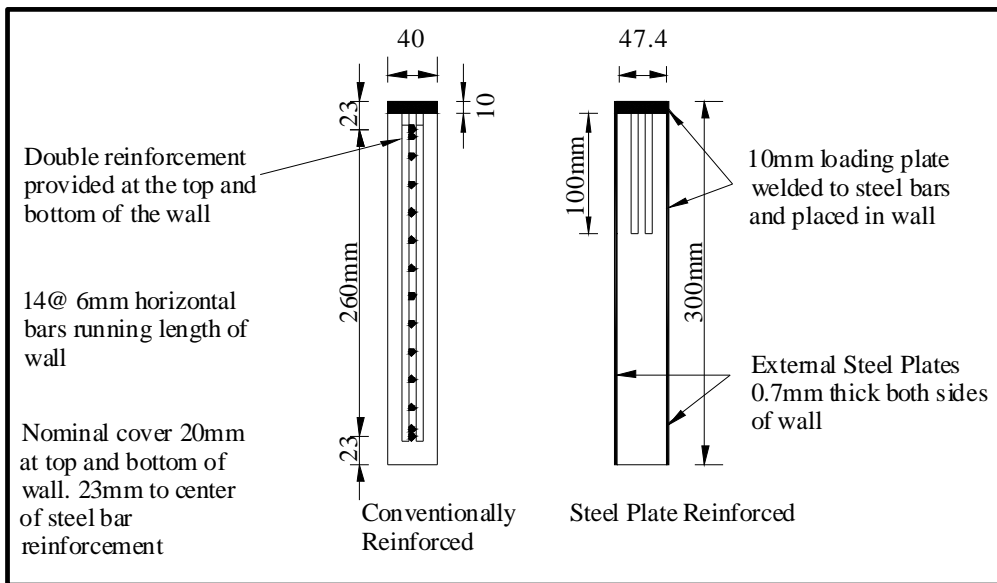


Figure 1 Shear Walls cross sections

### 3 MATERIAL PROPERTIES AND TEST PROCEDURES

The material properties were chosen to be representative of full size structures.

#### 3.1 Concrete & Steel

Two different grades of concrete were used, with the first, used in the restraint block being a standard RMC Ready-Mix design C50 grade concrete. Secondly, the concrete in the shear walls was a specially designed micro-concrete mix with a w/c ratio of 0.4. Two cubes and two cylinders, one from each wall, were tested for strength development at designated periods up to day of testing as in Table 1, where the average of the two results are presented. For reinforcement two standard 0.7mm grade S275 mild steel plate sections and two 6mm (for the shear wall) diameter bars were tested. Tensile test properties for the steel are also given in Table 1.

Table 1 Concrete and Steel properties

| Day<br>Strength | Concrete             |          |                       | Steel           |       |       |
|-----------------|----------------------|----------|-----------------------|-----------------|-------|-------|
|                 | $f_{cu}$             | $f_{ct}$ | $E_c$                 | Materials       | $f_y$ | $E_s$ |
|                 | (N/mm <sup>2</sup> ) |          | (kN/mm <sup>2</sup> ) |                 |       |       |
| 7               | 48.0                 | ----     | 31.1                  | 6.0 mm          | 490.0 | ----  |
| 28              | 52.0                 | ----     | 32.4                  | 0.7 mm<br>plate | 373.5 | 225.0 |
| 44              | ----                 | 3.9      | ----                  | ----            | ----  | ----  |
| Test Day        | 54.0                 | 4.0      | 33.1                  | ----            | ----  | ----  |

#### 3.2 Epoxy Resin

A two part cold cure epoxy resin, manufactured and supplied by Sika and commonly used for structural bonding purposes in the UK was employed to attach the steel plates to the concrete surface.

### 3.3 Instrumentation

Common LVDT transducers were used to measure the wall deflections under static loading. A SPECTRA data logger system was used for data recording. Additionally a dial indicator gauge was employed to record readings of end deflection of both walls during the static testing experiment, to an accuracy of 0.01mm.

### 3.4 Static & Impact Testing

The static testing apparatus shown in Figure 2(A), consisted of a number of weights 1, 2, 5 and 10 kilograms applied manually to the walls. The measurements consisted of deflection from the transducers, strain readings from the strain gauges and the dial gauge positioned beneath the front of each wall. The main piece of equipment required in the impact test was the use of an impactor. This consisted of a cylindrical steel section of 2.5kg weight which could be manually placed onto a threaded bar allowing incremental increase in weights to be applied. The first steel section has a domed end as this impacted the wall with the remaining sections being cylindrical in shape, 100mm long and 63.5mm in diameter as can be seen in Figure 2(C). A hook located on the top of the bar allowed a rope to be threaded and for a pulley mechanism to be employed. Finally, a guidance tube was used, its function being to guide the impactor over the loading location, with the testing mechanism layouts impact loading detailed in Figure 2(B).

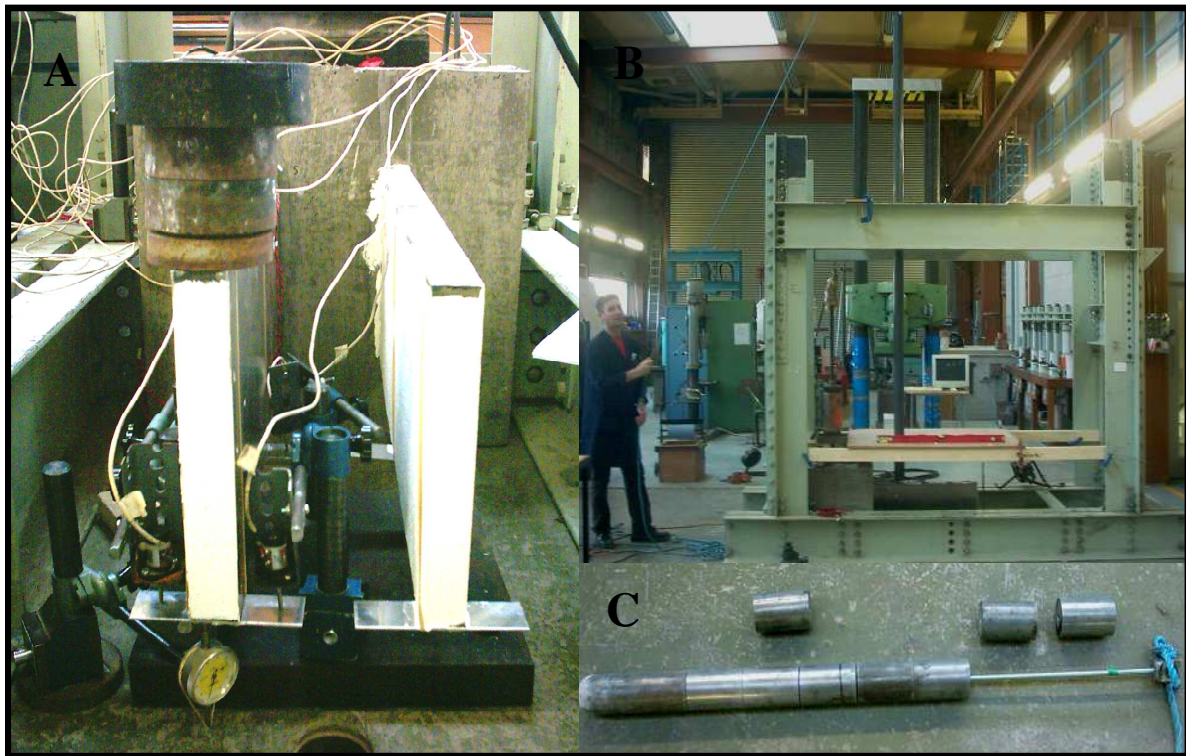


Figure 2 (A) Static test setup (B) Impact test setup (C) Impactor

## 4 RESULTS AND DISCUSSION

### 4.1 Deflection: Static testing

The plots of the deflection readings for both systems of the wall are shown in Figure 3. The load cycles represent the load values from 1kg up to 40kg. It is clear from the figure that the deflections of the S-C-S wall are considerably lower as well as linear over the span of the wall. The conventionally reinforced wall demonstrated a greater mid span deflection and greater end span deflection. The main finding from the presented graph is that under static loading the stiffness of the S-C-S wall is much greater compared to the conventionally reinforced wall and over the range of the applied load its behaviour is more or less described as linear.

### 4.2 Strain: Static testing

Strain readings for the cantilever S-C-S shear wall showed that the top of the wall was in tension and the bottom of the wall in compression under loading, as expected and can be seen in Figures 4. These Figures also illustrate that the action of elastic deformation is taking place, with the strains increasing gradually under increased loading in a linear fashion. Furthermore, the strains in both plates were also similar which infers that the epoxy resin bonding gave an even distribution of strain built up in the steel plates under static loading as also supported by the findings of Barnes et al [6]. It is noted that the obtained values were of a very small magnitude signifying that the plates were grossly under stressed.

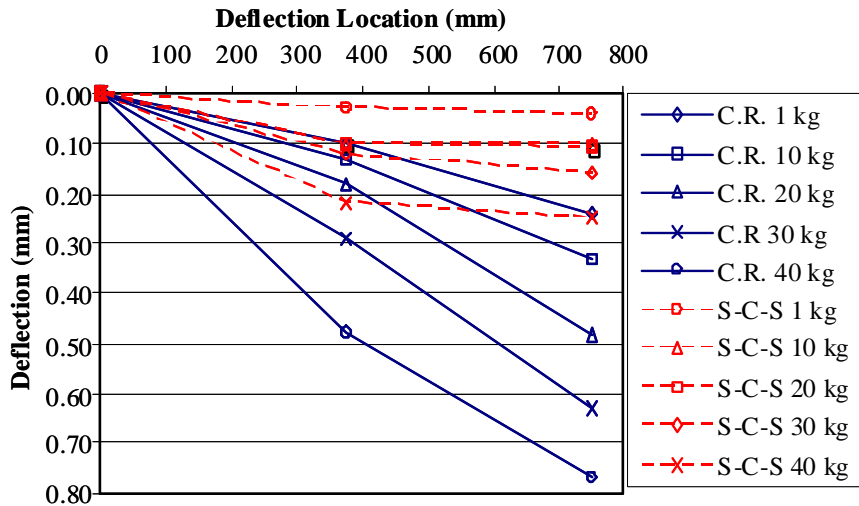


Figure 3 Deflection of both systems under 1kg - 40kg static loading

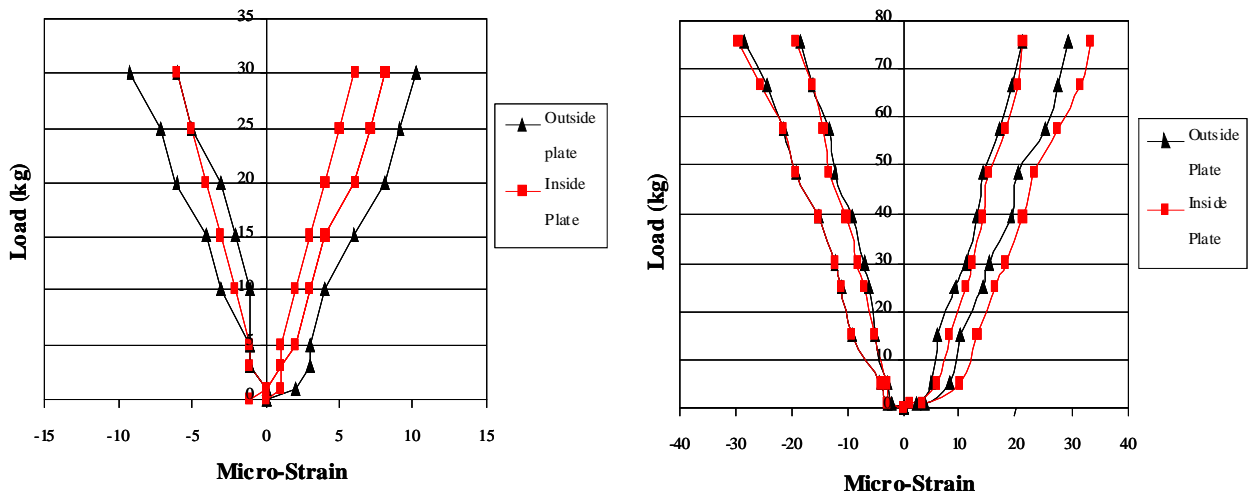
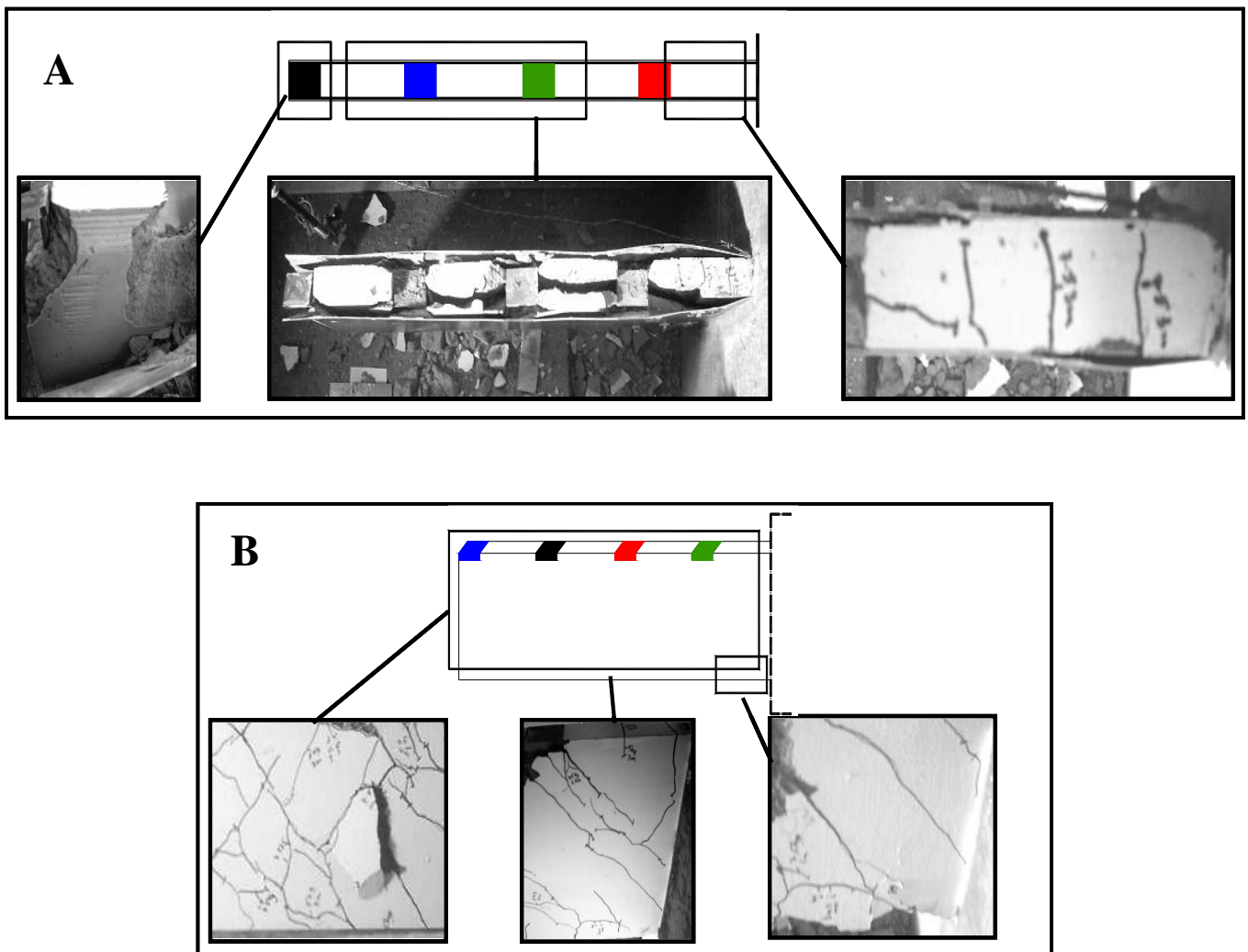


Figure 4 Strain in steel plates under static loading cycles 1 and 3 (left – right)

### 4.3 Crack Inspection: Impact Testing

The behaviour of the walls under impact loading was recorded as observed. This being a preliminary study no instrumentation was incorporated. All reinforced concrete structures possess cracks in order for reinforcement to function properly, however it is important to limit the developments of these cracks in order to achieve serviceability requirements. Throughout the experimental procedure it was visible that although extensive cracks had formed in the S-C-S wall it was still structurally sound and the widths of the cracks remained visually small until ultimate failure mechanism developed. At failure the behaviour was somewhat brittle. This can be attributed to the early peeling and onset of separation of the plates near the base from the concrete surface. In the conventional wall however, as the load increased large deflections were taking place accompanied by wider main cracks.



**Figure 5 (A) Failure of S-C-S shear wall, (B) Failure of conventionally reinforced shear wall on impact loading**

Throughout the experiment the S-C-S system possessed a visible resistance to the effects of impact loading with little disturbance to the wall. Plate separation, reduction in shearing, small deflections and increased ultimate strength were the characteristics at failure as observed by Oh et al [7] in their study. All of the above mechanisms were also observed here during the test. In particular at a fairly early stage the onset of plate peeling initiated by local buckling of the plates near the base where high compressive stress was present was noted. It was evident from the experiment that extensive cracking of the tensile zone of the wall took place which can be seen in Figure 5(A), which was attributed to a high tensile stress build-up at the top of the wall caused due to a confinement of stresses. Plate buckling was also visible from an early stage, which would imply an unsatisfactory transfer mechanism of shear flow from the concrete to the epoxy. The ultimate failure was attributed to the plate peeling accompanied by concrete rip-off as the contact area of concrete with the steel plate was reduced, Figure 5(A). The main observations from the study were (a) Early peeling of plates initiated by the local buckling of the plate on the compression side is a real possibility. (b) As the peeling progresses, the plate-concrete composite action is reduced and appears to be controlled by brittle behaviour of the concrete. It is clear that adequate means of preventing early buckling of plates near the base is a very important consideration in the design of S-C-S walls.

With respect to the conventional reinforced system severe cracking was evident from an early stage as expected in a normal R.C. construction, Figure 5(B). The impact effect caused the initiation of diagonal cracking as well as some cracks forming in the web at the rebound effect of the impact force. The ultimate failure mechanism was as a result of diagonal shear failure, which occurred as a continuation of shear cracking towards the restraint position leading to local crushing in the bottom corner of the wall

attached to the concrete block. The shear crack formed as a diagonal splitting crack inclined at 45° from the loading plate to the compressive zone of the wall where final compression failure took place through the break-off of concrete as can be seen in Figure 5(B).

## 5 CONCLUSION

The following conclusions are drawn from the preliminary study of conventionally reinforced and steel-concrete-steel shear walls subject to static and impact loading:

(a) S-C-S offers enhanced overall economical structural system with a reduction in construction time, due in the main to reduced, less complicated cross-sections, a direct consequence of conventional reinforcement omission.

(b) S-C-S reinforcement was found to be an inherently stronger and more robust system than the conventional reinforcement.

(c) Plated elements can resist large degrees of static and impact loading through composite action.

(d) Failure of the S-C-S system was due to the initiation of local buckling of the plates in the lower highly compressed area of the wall. The progress of peeling reduced the composite action causing concrete to fail in a brittle manner.

(e) To take full advantage of the S-C-S system early buckling of the plates should be delayed. This can be done by taking extra precaution in detailing near the base.

(f) S-C-S is a system highly suitable for tall buildings and other structures where robustness against impact, fire and terrorist activities are the main design considerations.

## ACKNOWLEDGEMENTS

The first author would like to sincerely thank and acknowledge the support and help of Dr. Nutan Subedi, both in the undertaking of this study which formed part of the said authors Bachelors Degree study and in the preparation of this paper.

## REFERENCES

- [1] Chana, P., Fire safety with Concrete, Proceedings, *International conference held at the University of Dundee, Scotland, UK, 2008*, Concrete for Fire Engineering, pp. 13-26.
- [2] Khoury, G. A., Passive fire protection of concrete structures, Proceedings, *Institution of Civil Engineers Structures & Buildings*, Vol. 161, June 2008, pp. 135–145.
- [3] Corus, Fire resistance of steel-framed buildings, *Corus Construction & Industrial*, 2006 edition.
- [4] Bostrom, L., Concrete exposed to fire, Proceedings, *International conference held at the University of Dundee, Scotland, UK, 2008*, Concrete for Fire Engineering, pp. 319-328.
- [5] Dunne, D., Assessment of steel – concrete - steel shear wall, *B.Eng. Dissertation*, University of Dundee, 2005.
- [6] Barnes, R.A., Baglin, P.S., Mayes, G.C. and Subedi, N.K., External steel plate systems for the shear strengthening of reinforced concrete beams, *Journal of Engineering Structures*, Vol. 23, No. 9, 2001, pp.1162-1176.
- [7] Oh, B.Y., Cho, J.Y. and Park, D.G., Failure behaviour and separation criterion for strengthened concrete members with steel plates, *Journal of Structural Engineering*, Vol. 129, No. 9, 2003, pp. 1991-1198.

## **LONG SPAN COMPOSITE BEAMS SUBJECTED TO FIRE**

### **Effects of Fire on Lateral Stability**

Graeme Flint<sup>a</sup>, Barbara Lane<sup>a</sup>

<sup>a</sup> Arup, 13 Fitzroy Street, London UK, W1T 4BQ

#### **INTRODUCTION**

With the recent increase in fundamental knowledge of structures coupled with the ease of use of modern design tools, building designers are able to create ever more efficient structures in the modern urban landscape. Structural design is typically governed by the well understood static load cases in the normal range of ambient temperatures, i.e. gravity, wind and snow.

By creating highly efficient and optimised structures for very specific ambient load conditions, the inherent strength reserve of a structure can be reduced. It is this strength reserve that a composite steel structure relies on when subjected to abnormal loading conditions such as severe fire. Therefore, it becomes necessary to explicitly consider fire loading during the design process to ensure that an acceptable level of safety is maintained in the structure.

This paper reports on the case study of a failure mechanism which was observed during a structural fire assessment of a new office building design. The structure includes long span, composite floor systems supported by a unique connections and a highly optimised structure. When subjected to fire, failure of the floor system occurred due to a mechanism which involved lateral stability failure of the bottom flange of the highly optimised long span beams. This resulted in a loss of load carrying capacity and failure of the structure.

The building presented as part of this study was a proposed design for a high-rise office building in the City of London. This paper concentrates on a local study of the response of long span cellular beams. The investigation was conducted using the ABAQUS Finite Element Analysis software.

A detailed investigation of the structure indicated a potential failure mechanism in the beams at the fire limit state. The failure mechanism was further investigated using a parametric study in order to better understand the causes of the failure mechanism. The paper shows the value of advanced structural fire analysis for the structural design and assessment of the robustness of this highly optimised structure with its unique beam connections.

#### **1. STRUCTURAL DETAILS**

The structural system of the proposed building is a perimeter braced frame. Vertical support around the perimeter of the building was provided through the use of a robust diagrid megaframe. The diagrid members were typically single- and double-web fabricated I sections.

One important structural detail is that the load bearing megaframe is located outside the main floor plate perimeter, as indicated in Figure 1 which shows part of a typical floor plant. Therefore the primary beam connecting into the perimeter column has an extension of approximately 1m beyond the normal floor-plate and thus is unrestrained by the floor slab. Additionally the support of the primary beam includes a substantial movement joint, comparable to a bridge movement joint. This joint acts to de-couple displacements between the floor structure and the megaframe. This movement joint allows movement in the direction indicated in Figure 1.

Internal columns were generally single- and double-web fabricated I sections.

The composite floor slabs were supported by fabricated beams that work compositely with the concrete floor plates. The floor I-beams spanned up to 16m and were generally 700mm deep with 200mm wide flanges. They have cellular web openings and gained additional strength by acting compositely with the concrete slab. The single spanning composite slab consisted of 150mm thick lightweight concrete cast onto a Ribdeck 80 trapezoidal profiled metal deck that acted as permanent formwork. The slab span ranges from 3m to approximately 4.85m.

## 2. STRUCTURAL FIRE PROTECTION

The structural fire analysis of the model was primarily intended to assess the robustness of the floor system assuming a reduced level of structural fire protection compared to code requirements. In this case, primary and secondary beams attached to columns were provided with 90 minute protection while intermediate secondary beams were left unprotected.

It has been shown in a number of recent analyses of tall office buildings (e.g. [1]) that this type of fire protection layout is a safe and efficient alternative to “code compliant” generic solutions. The analysis presented here was conducted in order to gain an understanding of the response of the building to fire under this engineered structural fire protection scheme. Such detailed knowledge of the building would not be gained from merely applying standard fire protection. The analysis utilized cutting edge modelling techniques and the latest analysis software.

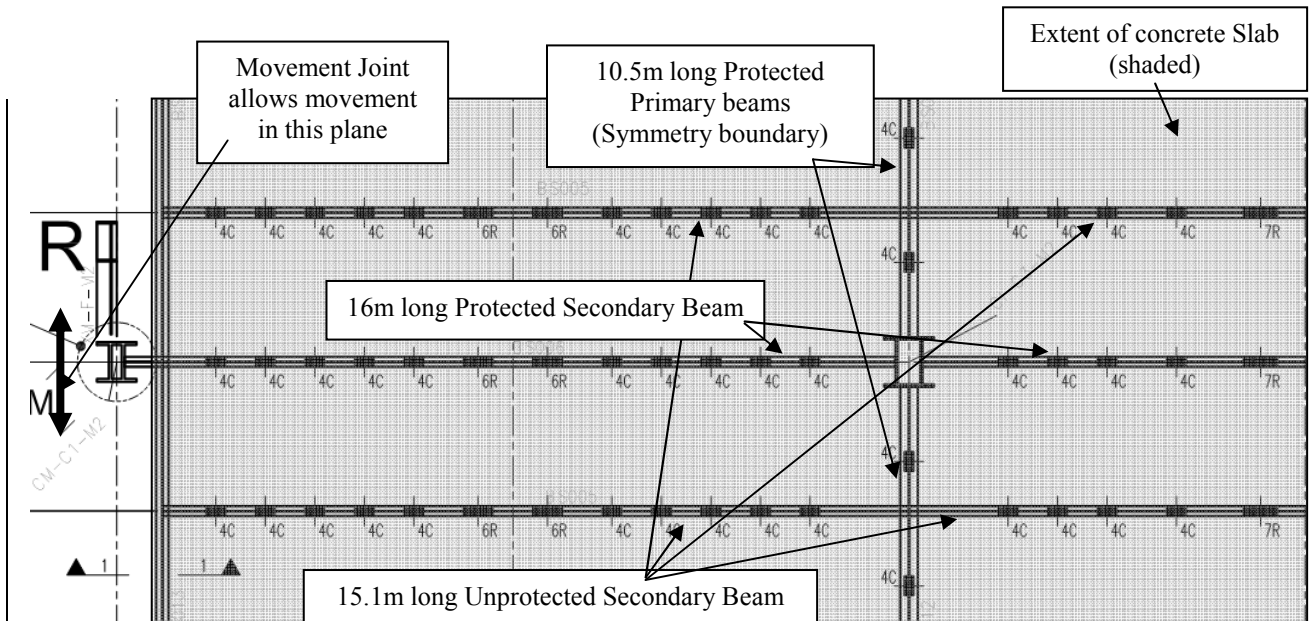


**Figure 1: Extent of Structural Model**

## 3. DESIGN FIRE

Our experience as consultants investigating the response of structures to Fire Limit State loading is closely linked to the use of the Eurocode Parametric Fire equation [2]. The Authorities Having Jurisdiction require the Eurocode Parametric Fire (PD6688.1-2)[3] to be used as the design fire. This method often leads to an extensive design fire including a substantial heating phase and an extended cooling phase to be applied simultaneously throughout the entire office floor plate. This type of temperature-time curve is considered onerous and may be unrealistic for the large compartments common in modern, open plan office buildings.

This conservatism is evident in the significant increase in temperature of protected steel members during the cooling phase until gas phase and solid phase temperatures are equal. Combined with the other conservatism included as part of the Eurocode calculation process, it is deemed to bring the design basis beyond that considered a reasonable worst case.

Therefore, the decay phase of the design fire of this case study was based on the results of the Cardington Office Fire Demonstration test. As the Cardington test was also conducted in a compartment that is considerably smaller than the office floors that are studied here, some modification to the Cardington test results were included to ensure the cooling phase was more representative.

As can be seen in Figure 2, the heating phase of the design fire was follows the standard fire curve up to 90 minutes. Previous experience has shown that the most conservative results of the Eurocode parametric equations for this type of building gives very similar results to the standard fire curve. To implement an appropriate cooling phase, the Cardington fire curve for the “office demonstration test” was conservatively translated until the start of the cooling phase coincides at 90 minutes. A

simple bi-linear curve was then fitted to the resulting test profile. As may be seen in Figure 2, the bi-linear curve is on the conservative side of the Cardington results throughout the duration of the cooling phase, until temperatures drop below 200°C.

The proposed design fire was compared with a number of full scale, natural fire tests (3 of the Cardington Tests and 1 test from the 140 William Street series performed in Australia) to ensure the cooling phase proposed captures the worst case of currently available test data from real compartment fires in the cooling phase. The proposed bi-linear cooling phase was observed to be consistent with the cooling phases of each of these tests. The design fire was applied to a single fire floor only.

#### 4. HEAT TRANSFER

The heat transfer calculations for the steelwork were conducted using the Eurocode heat transfer equations in Eurocode 3 Part 1.2 [4] for the protected and unprotected steel members. Thermal gradients over the depth of the beams were included to introduce additional thermal curvature effects. Additionally, it was assumed that the voids between the beams and the underside of the trapezoidal deck would be left unfilled, thereby increasing the temperature in the top flange of the beams. The code [5] requires that the voids be filled with fire rated infill.

Columns were modelled assuming a uniform temperature throughout their cross section effectively assuming that all columns will be simultaneously heated from 4 sides. These are considered to be conservative assumptions. The temperature gradient through the depth of the slab varying with time was modelled using a 1D heat transfer model in ABAQUS.

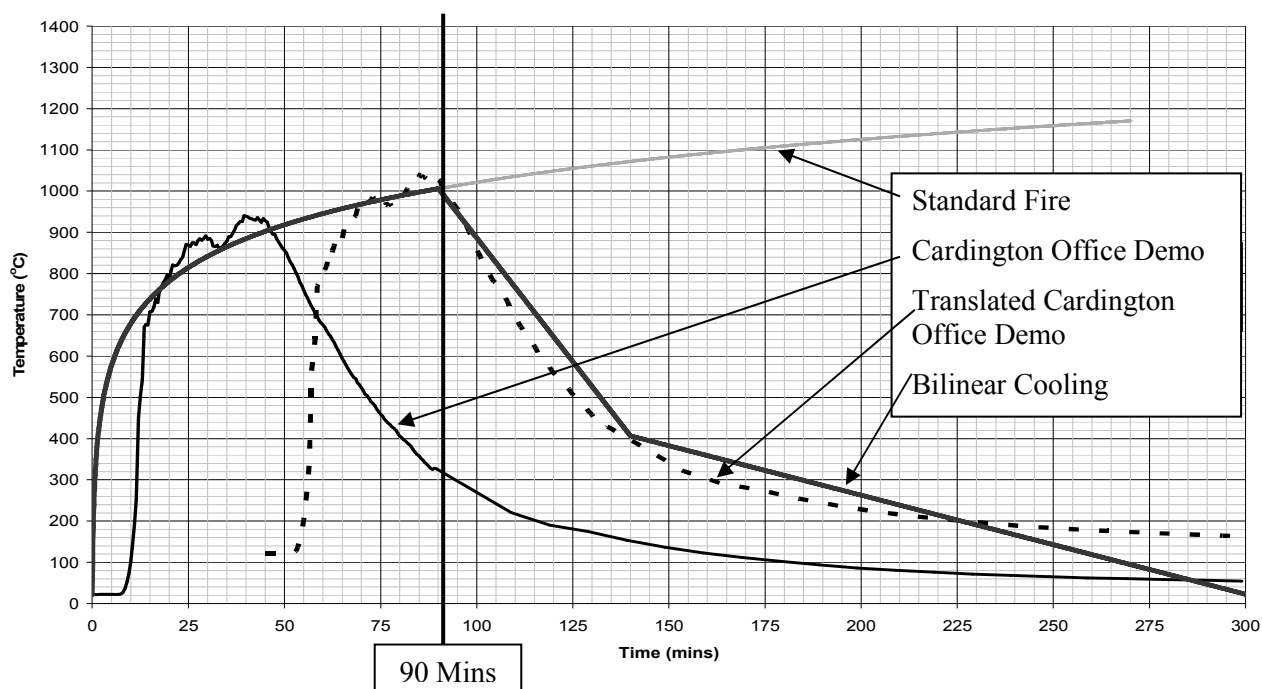
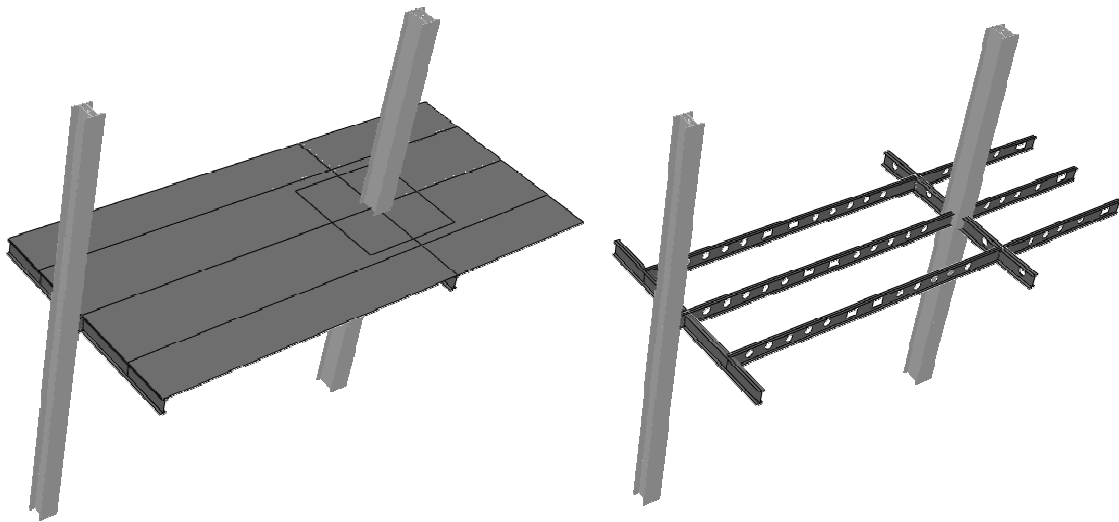


Figure 2: Modified Design Fire

#### 5. MODEL CONSTRUCTION

The model investigated for the case study is presented in Figure 3. The model is shown both with and without the concrete slab for clarity.



**Figure 3: Structural Model (shown with and without slab)**

In the model, the beams and slab were represented using 4-noded reduced integration shell elements. Columns were represented by 2-noded linear beam elements. Shell elements were used for the beams in order to capture local buckling behaviour, which would not be detected by beam structural elements. All material models for the analyses were based on Eurocode recommended values [4,6&7].

## 6. STRUCTURAL FIRE RESPONSE

The primary response identified by the analysis is the significant lateral deformation of the protected primary beam, as indicated in Figure 4 and also Figure 5 which shows the deformed shape of the beam at the onset of failure. Figure 5 shows the local buckling of the top flange and upper web. This behaviour occurred towards the end of the heating phase, starting at approximately 45 mins into the design fire. At this point, the temperature of the bottom flange was approximately 375°C while the web was at 400°C. This temperature is significantly lower than the temperature that a beam would normally be expected to fail (Usually 620°C). The resulted in twisting of the entire protected beam which led to failure of the connections between the beams and the megaframe (external perimeter) column, and subsequently collapse of the floor system.

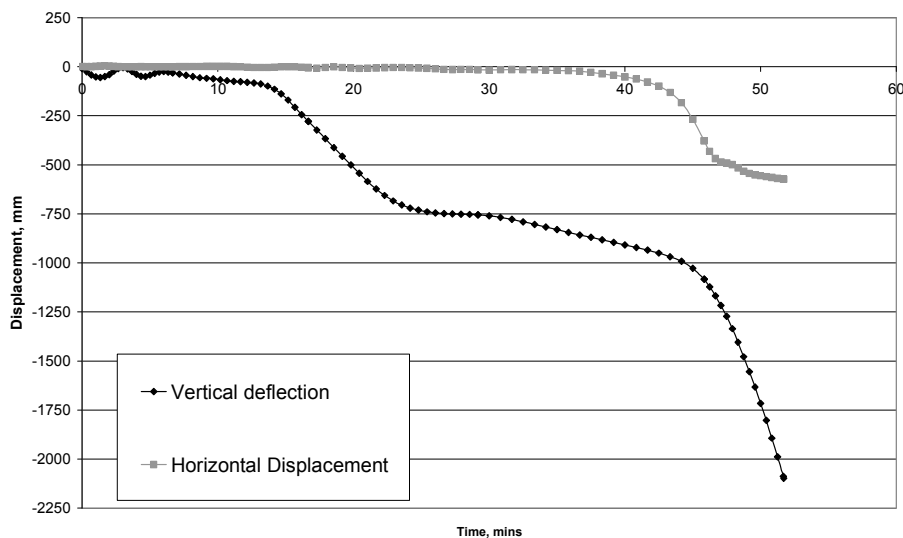


**Figure 4: Protected Primary Beam Deflections at Mid-span**

This type of lateral failure mechanism has been observed in real testing, for example the live fire test at Mokrsko testing facility conducted on the 18th September 2008, indicated in Figure 6.

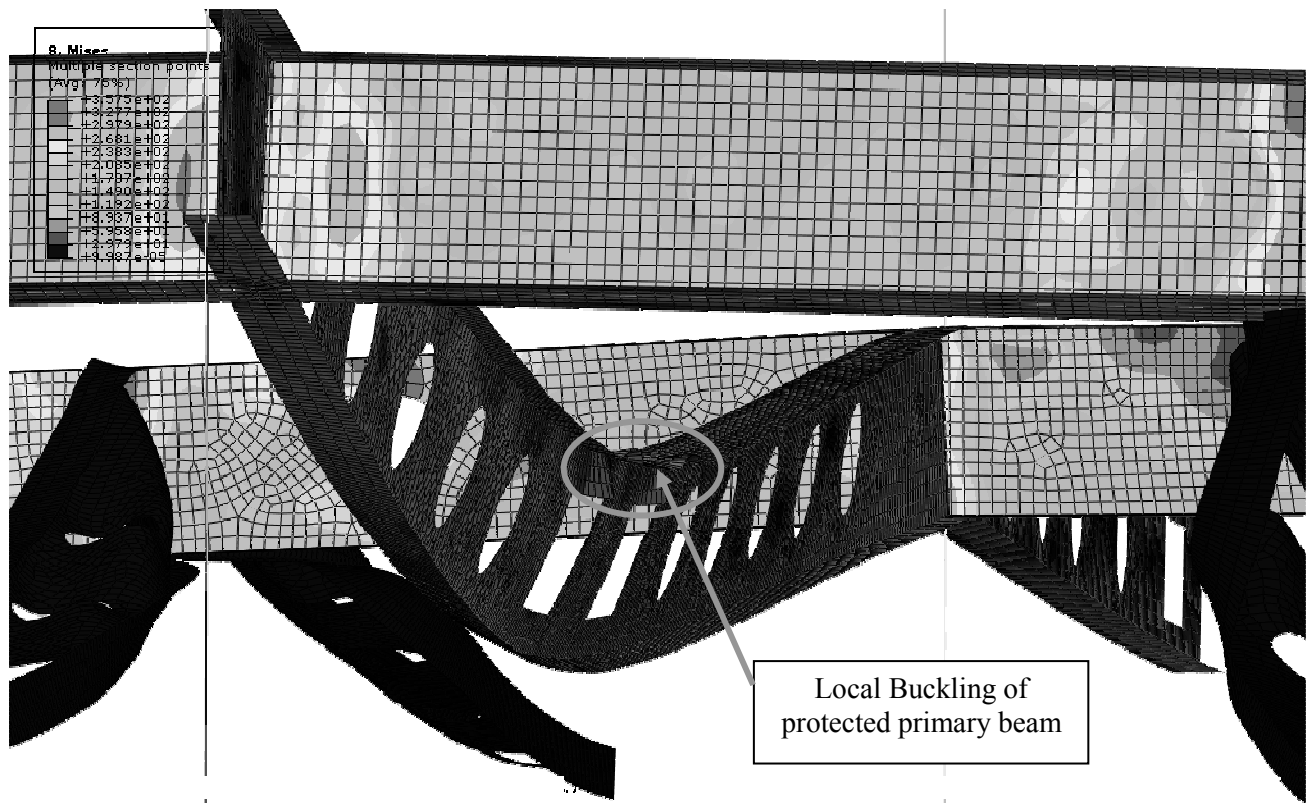


**Figure 5: Protected Secondary Beam Failure (Slab not shown)**

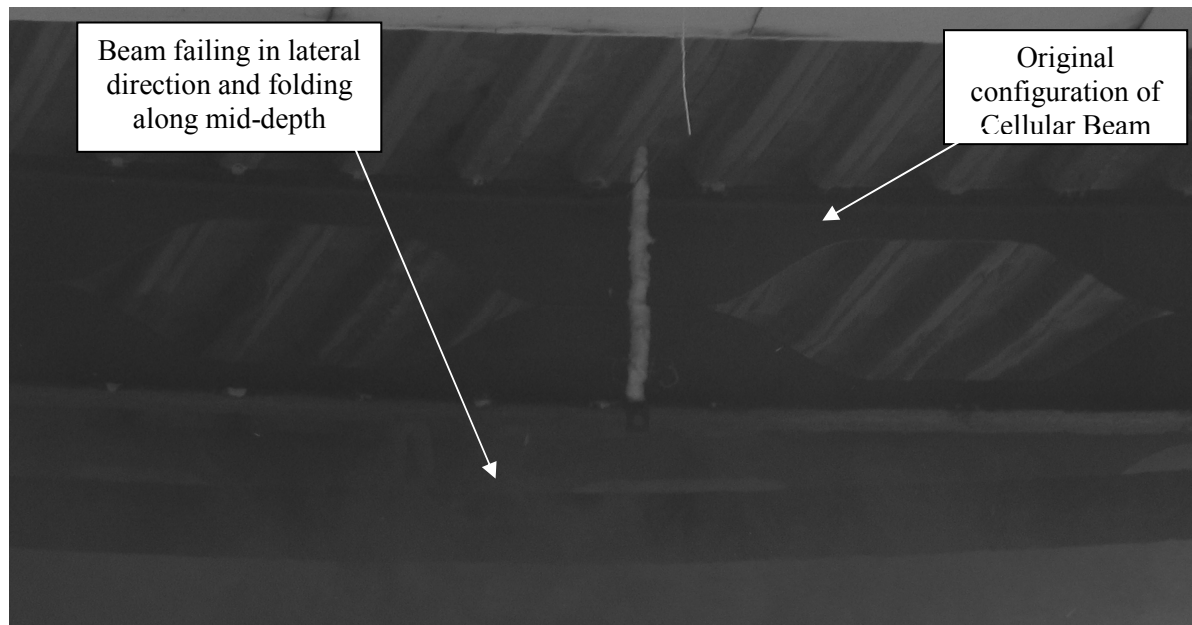


**Figure 6: Lateral failure of comparable beam in Mokrsko live fire test**

A parametric study was undertaken to determine the cause of the instability of the protected beam. The parameters investigated are indicated in Table 1. It should be noted that the increase in web thickness and structural fire protection to steel were also incorporated in models 3-8. The parametric study showed that failure was linked to the use of a deep beam (700mm deep) in combination with a relatively narrow bottom flange (200mm wide). This particular section geometry leads to a lateral instability of the beam at the fire limit state reducing the overall robustness of the floor system.

This kind of instability has not been observed in previous projects due to the unique nature of the building design.

**Table 1: Parametric Study**

| Model    | Parameter                     | Detail Changed  | Result                      |
|----------|-------------------------------|---|-----------------------------|
| 1*       | Web thickness                 | Protected secondary beam web thickness increased from 12 to 14mm  | Fails                       |
| 2*       | Increased protection to steel | Thickness of fire protection on protected secondary beams increased by 10%  | Fails                       |
| 3        | Holes in web                  | Central rectangular holed filled  | Fails                       |
| 4        | Top flange temperature        | Trapezoidal Deck voids assumed filled   | Fails                       |
| 5        | Rebar location                | Rebar moved to slab mid-depth to reduce temperatures  | Fails                       |
| 6        | Secondary beam location       | Unprotected secondary beams moved to equalize slab spans to 3.5m each.  | Fails                       |
| 7        | Mid-span stiffener            | Stiffener included at the mid-span of the protected secondary beam.   | Fails                       |
| <b>8</b> | <b>Bottom flange width</b>    | <b>Width increased from 200mm to 300mm (flange thickness reduced to 16mm to maintain original overall section area)</b> | <b>Stability maintained</b> |

Note: \* - The detail altered was incorporated in all following models.

## 7. CONCLUSIONS

This investigation was designed to assess the structural robustness of the of a proposed office building design. The structure designed for use under the standard ambient limit states (i.e. gravity, wind, etc) was subjected to a severe compartment fire.

The key response of the structure was a lateral failure mechanism in the protected long span primary beams during the heating phase of the design fire. This mechanism has also been observed in a recent large scale tests and is considered to be a realistic failure mechanism for beams with tall, relatively narrow sections.

A parametric study was conducted and the analysis indicated that in order to maintain stability throughout the design fire, the following alterations would need to be applied to the protected beams spanning onto the perimeter columns:

- Web thickness increased from 12mm to 14mm
- Fire protection thickness increased by approximately 10% above the typical 90 minute rating
- Width of the bottom flange of the beam would have to be increased from 200mm to 300mm (flange thickness may be reduced to 16mm to maintain original overall section area)

This paper has shown that detailed structural fire analyses can provide significant value in the design for robustness of highly unconventional and unique buildings. By analysing the structure in detail a failure mechanism was observed that would not have been detected if the structure had been protected to the usual code provisions without such an analysis.

## REFERENCES

- [1] A. Heise, G. Flint & B. Lane, Effect of fire on tall buildings: Case study, *Proceedings of the 3<sup>rd</sup> International Conference on Steel and Composite Structures (ICSCS07)*, 2007
- [2] BSI, Eurocode 1: Actions on structures. General actions - Actions on structures exposed to fire, BS EN 1991-1.2:2002, 2002
- [3] BSI, Background paper to the UK National Annex to BS EN 1991-1.2, PD 6688-1.2:2007, 2007
- [4] BSI, Eurocode 3: Design of steel structures. General rules - Structural fire design, BS EN 1993-1.2:2005, 2005
- [5] ASFP, Fire protection for structural steel in buildings 4th edition, ASFP Publications, Revised April 2008
- [6] BSI, Eurocode 2: Design of concrete structures. General rules - Structural fire design, BS EN 1992-1.2:2004 2004
- [7] BSI, Eurocode 4: Design of composite steel and concrete structures. General rules - Structural fire design, BS EN 1994-1.2:2005, 2005

## PERFORMANCE OF SHEAR STUDS IN FIRE

Sengkwan Choi<sup>a</sup>, Sanghoon Han<sup>a</sup>, Sungbae Kim<sup>b</sup>, Ali Nadjai<sup>a</sup>, Faris Ali<sup>a</sup> & Joungyoon Choi<sup>c</sup>

<sup>a</sup> FireSERT, School the Built Environment, University of Ulster, Newtownabbey, BT37 0QB, UK

<sup>b</sup> R & D Division, Sen Structural Engineering, Seoul, Republic of Korea

<sup>c</sup> Centre of Reliability Research, Korea Institute of Construction Materials, Gunpo, Republic of Korea

### INTRODUCTION

There have been significant improvements in the structural design of multi-storey buildings in recent years, many of which have been the result of developments in composite construction. The wide variety of automatically fabricated long-span composite structures not only has economic benefits due to fast, light-weight and accurate construction, but also maximizes the potential for flexibility in internal layout, which is a greatly desired feature in modern buildings. In particular, understanding and technology surrounding fire safety design for steel and concrete composite structures has been noticeably advanced due to the introduction of new insulation materials, the improvement of computational modelling technology and advanced design methodologies obtained through extensive full scale experiments in fire.

Structural fire safety calculations have been traditionally based upon prescriptive methods – according to hourly ratings, on code requirements with respect to standard fires such as ASTM E119 [1], BS 476 Part 20 [2] or ISO 834 [3]. Now, however, both domestic (UK) and international regulations permit design for structural fire safety to be carried out according to performance based concepts. This approach can be particularly beneficial when considering various types of composite structures, such as composite truss, slim floor, cellular beams, as these can be shown to obtain potentially significant structural performance benefits by adopting an optimal configuration of structural sections and relevant insulation requirements.

A wide-ranging investigation of the in-fire performance of such composite structures has highlighted various local instabilities that are deemed to likely govern the overall flexural performance of the structures. The research presented here aims to act as a pilot study to examine the in-fire performance of headed shear studs. These are commonly used in composite structures over the world and appear to be a key element in maintaining the global structural integrity of composite structures.

### CONTEXT OF RESEARCH

The flexural performance of composite structures depends on the effective transfer of longitudinal shear stress and control of uplift force at the interface between the steel and concrete constituents. The mode of collapse initiated by failure of the bond at this interface is brittle and often catastrophic and the appropriate use of mechanical shear connectors is therefore essential when trying to achieve composite action of the two materials at the ultimate limit state. Similarly, there is a requirement for the capacity of shear connectors to be maintained in fire to prevent premature brittle failure. It is furthermore preferable for the structure be resistant to local buckling and load carrying mechanism transition.

Although various configurations of shear connectors have been proposed and used over the last half century, a headed stud (commonly 19 mm diameter and 100 to 125 mm pre-welded length) is now the most widely used type of flexible shear stud in composite construction in buildings due to the speed, convenience and reliability of the welding process involved in their placement

The strength and ductility performance of headed stud shear connectors are typically investigated by push-out tests using a solid slab and by using the load – slip relationship obtained from the test, composite action can be reliably designed into a flexural member. The capacities of stud shear connectors embedded in a solid slab were first evaluated by Ollgaard, Slutter and Fisher [4]. Through the use of empirical methods, the authors developed a formula to assess the strength of a

stud as a function of the stud area and concrete properties, with an upper limit equal to the tensile strength of the stud:

$$Q_u = 0.5A_{sc}\sqrt{f_{ck}E_c} \leq A_{sc}f_u \quad (1)$$

where  $A_{sc}$  is the cross-sectional area of the stud shear connector  
 $f_{ck}$  is the cylinder compressive strength of the concrete ( $= 4730\sqrt{f_{ck}}$ )  
 $E_c$  is the modulus of elasticity of concrete  
 $f_u$  is the ultimate tensile strength of the stud material

Eq. 1 is included in both the AISC [5] and CSA [6] codes of practice as a fundamental formula to assess the strength of studs. In Eurocode 4 Part 1.1 [7], however, the strength of headed studs in solid slabs is based on the simplified engineering assumption that a stud fails either in the concrete alone (height / diameter of stud > 4) or in the steel alone as follows.

$$Q_u = 0.37A_{sc}\sqrt{f_{ck}E_c} \leq 0.8A_{sc}f_u \quad (2)$$

Stark et al [8] determined the coefficient of 0.37 used in Eq. 2 by means of a statistical study, and the upper limit is taken as 80% of the tensile strength of the stud. The design capacity of the shear connector is introduced with a partial safety factor of 80% of the nominal strength to ensure that the material ductility requirements and discrete nature of resistance are met [7].

In the UK, Menzies' regression analysis of standard push-out experiments [9] is used to determine the design strength of headed studs embedded in solid concrete slabs (provided in tabulated form in BS5950 Pt 3 [10]). A large number of additional tests have been conducted in Europe and North America with the aim of identifying the strength reduction effects of studs embedded in various shapes of profiled deck slabs. However, as this work is beyond the scope of current publication, the detail is not included. It is noted that, as the force developed in composite beams is not identical to that developed in push-out tests, caution needs to be taken if applying the test results to beams. It is nevertheless known that the performance of shear connectors in beams is much better than in push-out tests.

Zhao and Kruppa [11] conducted experiments to determine the shear capacity of headed studs and angled connectors, subject to the standard ISO fire, in conjunction with solid slabs and composite slabs with profiled sheets. The results of this study suggest that the strength of headed studs at elevated temperatures must be assessed using an absolute 20% strength reduction and that the strength retention of steel material in relation to the ultimate tensile strength is:

$$Q_{u\theta} = 0.8(0.8A_{sc}f_u)SRF_{u\theta} \quad (3)$$

Where  $SRF_{u\theta}$  is the strength retention of steel at  $\theta^\circ\text{C}$  with respect to the ultimate tensile strength

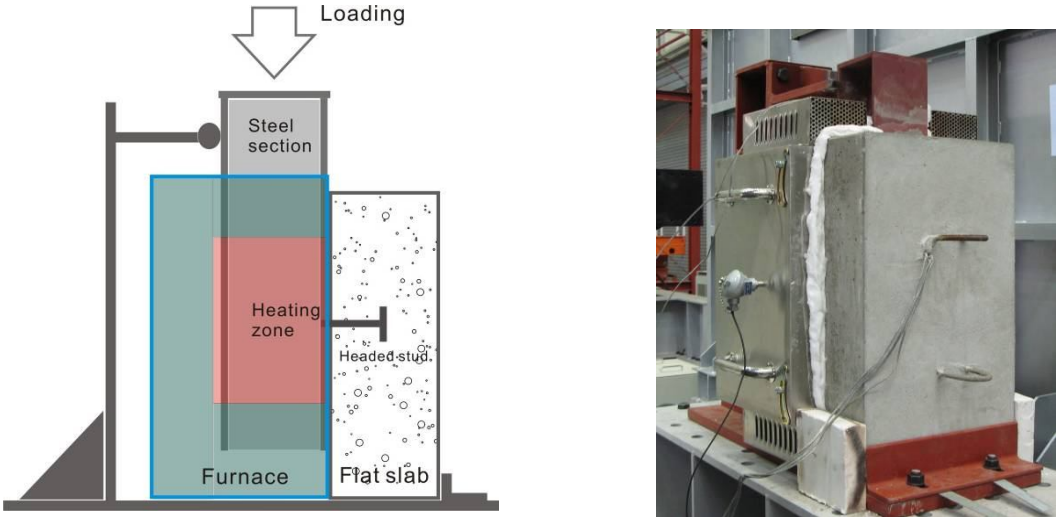
Eq. 3 is used in Eurocode 4 Part 1.2 [12] as verification of the shear resistance of studs in fire and, whilst concrete crushing failure at elevated temperatures is also considered in the code, it is generally considered that the stud failure governs the performance in fire.

The plastic resistance of composite beams (found using rectangular stress blocks) is determined with the provision that the shear connectors have sufficient capacity to deform - hence they must maintain resistance to shear at slips. A design application rule to accept the ductility of the connector is implemented in a form of 5 mm available slip. Since the deflection of composite beam in fire is often significantly larger (commonly up to span/20), care is also considered in the subsequent levels of the stud slip.

## EXPERIMENTAL PROGRAMS

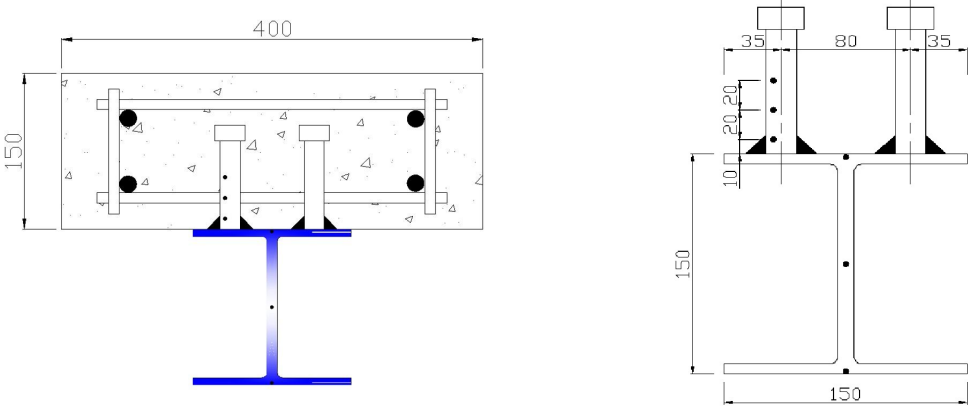
In order to investigate the performance of the stud connectors in fire, the standard push-out test was

modified to use half of the standard set-up [13]. In the modified experiment (Figs. 1a and 1b), one side of the solid concrete block in the standard push-out specimen was replaced with an electric furnace to expose the steel member to fire from 3 sides. Vertical loading was applied downward from the top of the steel section and the relative displacements were measured between the top of the steel section and the top of concrete slab. To provide appropriate stability to the test assembly under loading, lateral movements of the slab base and top of the steel section were restrained. Under these boundary conditions, the development of uplift forces in the connectors could be limited to acceptably low levels.



(a) Schematic drawing of the modified push-out test (b) Instrumentation arrangements  
 Fig. 1. Modified push-out tests in fire

The specimen (Fig. 2a) consisted of a 650 mm length of S355 steel section (150×150×30 UC) connected to a C30 flat concrete slab (400 mm width × 150 mm depth × 500 mm height), using two headed studs of 19 mm diameter × 100 mm depth. A natural bond at the interface was prevented by greasing the steel flanges before casting the slab. K-type thermocouples were installed to measure temperature developments of the flanges and web in the steel section and locations at 10 mm, 30 mm and 50 mm depths of the headed studs from the fire exposed surface (Fig. 2b). Tension testing of the studs reported that the average characteristic properties of the steel were yield strength of 349 N/mm<sup>2</sup>, an ultimate tensile strength of 427 N/mm<sup>2</sup> and an elongation of 25 %. Two specimens were loaded until collapse for cases of room temperatures (20°C), 30 minutes and 60 minutes of the standard ISO fire.



(a) Cross-section of specimen (b) Locations of thermocouples (marked by •)  
 Fig. 2. Specimen for modified push-out test

## ANALYSIS OF RESULTS

In order to establish the shear capacity of the headed stud when subjected to the standard ISO fire the temperature developments of the specimen were obtained for the duration of the tests, as shown in Figure 3. It was found that the temperature difference between the 10 mm and mid-depth (50 mm) reference points was in excess of 200 °C within 30 minutes of the standard fire and approximately 300 °C at 60 minutes. As the temperature rise at 10 mm was over 400 °C at 30 minutes, a corresponding and significant reduction of strength was seen in this area. Further, as the temperature rise of concrete slabs is generally much lower than that of steel elements in fire, it could be expected that the collar area of the shank will experience the highest levels of strength reduction due to the temperature increase.

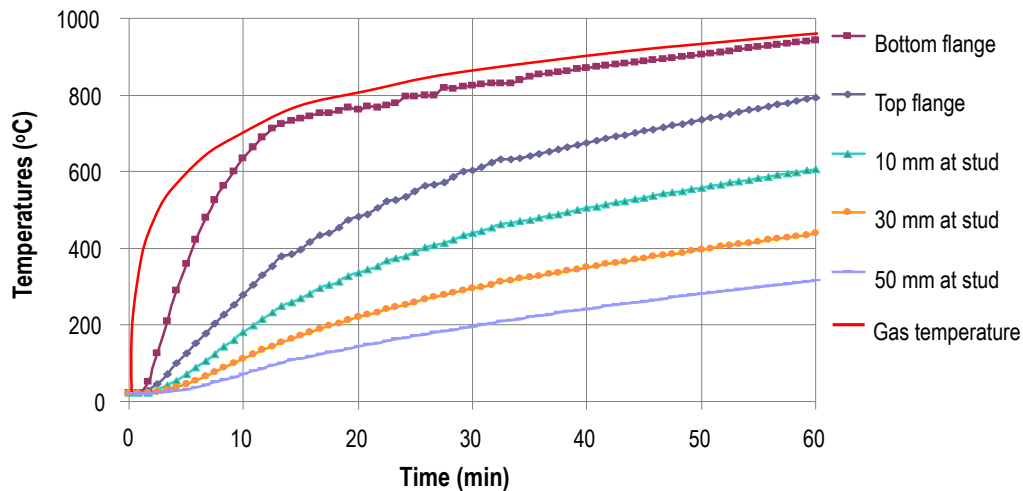


Fig. 3. Temperature-time curves in steel and stud connector for standard fire

The load-slip relationship for stud shear connectors was monitored at ultimate limit state, 30 and 60 minutes of the standard ISO fire; the relationship per stud is plotted in Figure 4. At a slip of 5 mm, the ultimate capacity of the stud was measured to be 120 kN at 0 minutes, 85.0 kN at 30 minutes and 38.0 kN at 60 minutes respectively. By modifying Eq. 1 an equation can be proposed to evaluate the stud strength at elevated temperatures:

$$Q_{u\theta} = A_{sc} f_u SRF_{u\theta} \quad (4)$$

The strength of the stud at ULS when estimated using Eq. 1 (121 kN), shows very good agreement with the test result of 120 kN at ULS. Using Eq. 4, the residual strength of the studs at 30 and 60 minutes in fire is calculated as 88.7 kN and 38.0 kN respectively, which also demonstrates excellent agreement with the experimental results of 85.0 kN and 38.0 kN respectively.

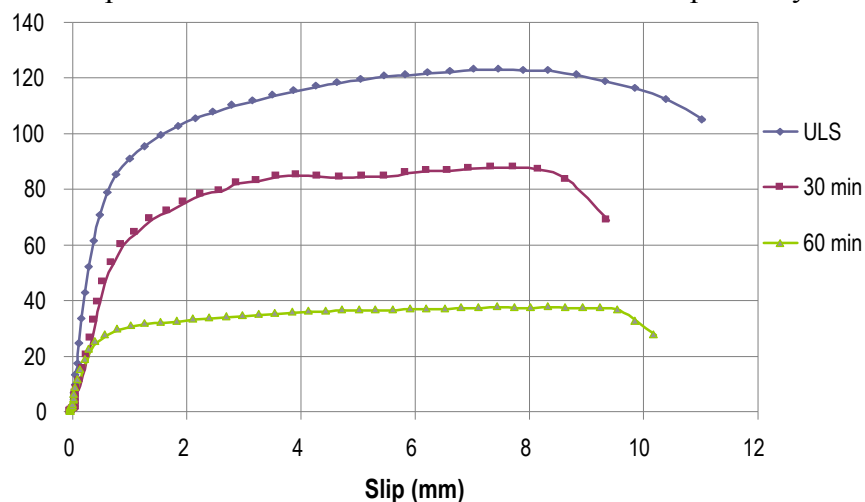


Fig. 4. Load-slip curves for stud connectors at elevated temperatures

Examination of the failure mechanism exhibited by the studs, as the resistances estimated using Eq. 1 for crushing of the concrete surrounding the connector and connectors shearing off at the base are similar, interaction of the failure modes occurred at ultimate limit state. At elevated temperatures, shear failure consistently occurred at the weld-collar/shank interface, as shown in Figure 5. The reasons for this behaviour are that at the weld-collar/shank interface (1) a concentration of high stress occurs in the push-out tests and (2) a higher temperature rise develops in the area due to the heat flux through the top flange of steel section in fire. When compared to the research of Zhao and Kruppa [11], the observed failure mode of headed studs in fire is generally alike, but in the tests reported here a higher strength was recorded due to the presence of lateral restraint at the bottom of the slab.



Fig. 5. Failure of stud shear connector after push-out test at 60 minutes of the standard fire

## CONCLUSIONS

This pilot project was designed to investigate the capacity of headed shear studs at elevated temperatures through the use of a modified push-out test with a solid concrete slab. An electric furnace attached to the test assembly provided three-sided fire exposure to the specimen. At room temperature, 30 and 60 minutes of the standard ISO fire, tests were conducted to identify the strength retention properties of the studs. Temperature developments were measured across the steel section and along the stud shank. The headed studs failed at elevated temperatures due to shear of the weld-collar/shank interface. An equation was proposed to allow assessment of the residual strength of the stud in fire and this demonstrated a very good agreement with the test results.

## REFERENCES

- [1] American Society for Testing and Materials, ASTM E119-95a Standard Test Methods for Fire Tests of Building Construction and Materials, West Conshohocken, PA, 1995
- [2] British Standards Institution, BS476: Fire Tests on Building Materials and Structures: Part20: Method for Determination of the Fire Resistance of Elements of Construction (General Principles), UK, 1987
- [3] International Organization for Standardization, ISO834: Fire resistance tests - Elements of building construction, Geneva, 1975
- [4] Ollgaard, J.G., Slutter, R.G. and Fisher, J.W., Shear strength of stud connectors in lightweight and normal weight concrete, engineering Journal, AISC, 8(2), 1971, pp. 55-64
- [5] American Institute of Steel Construction, Load and Resistance Factor Design Specification for Structural Steel Buildings, Chicago, IL., 1993
- [6] Canadian Standards Association, Steel Structures for Buildings – Limit State Design, CAN3-S16.1-M84, Rexdale, Ontario, 1994
- [7] European Committee for Standardisation, ENV 1994-1-1: Eurocode 4: Design of Composite Steel and Concrete Structures. Part 1.1: General Rules and Rules for Buildings, BE, 1994

- [8] Stark, J.W. and von Hove, B.W.E.M., Statistical Analysis of Pushout Tests on Stud Connectors in Composite Steel and Concrete Structures, TNO Buildings and Construction Research, Delft, Report BI-91-163, 1991
- [9] Menzies, J.B., CP117 and shear connectors in steel-concrete composite beams made with normal-density or lightweight concrete, Structural Engineers, 49(3), pp. 137-153
- [10] British Standards Institution, BS 5950: Structural use of steelwork in building Part 3: Design in composite construction Section 3.1: Code of Practice for design of simple and continuous composite beams, UK, 1990
- [11] Zhao, B. and Kruppa, J. EUR 16822-Properties and Service Performance: Fire resistance of composite slabs with profiled steel sheet and of composite steel concrete beams Part2: composite beams, Luxembourg, 1997
- [12] European Committee for Standardisation, ENV 1994-1-2: Eurocode 4: Design of Composite Steel and Concrete Structures. Part 1.2: General Rules: Structural Fire Design, Brussels, BE, 1994
- [13] British Standards Institution, BS 5400: Steel, concrete and composite bridges Part 5: Code of practice for design of composite bridges, UK, 1979

## FIRE COMPOSITE FLOOR CELLULAR STEEL BEAMS FOR BUILDINGS

Nathan Goodfellow<sup>a</sup>, Ali Nadjai<sup>a</sup>, Kong Fah Tee<sup>a</sup>, Faris Ali<sup>a</sup>, Sengkwon Choi<sup>a</sup>,

<sup>a</sup> Ulster University, School Built Environment, FireSERT Block 27, Shore Road, Jordanstown, Belfast BT37 0QB, United Kingdom

### INTRODUCTION

Cellular beams (CBs) are currently being widely used in multi-storey buildings where, as well as reducing the total weight of the steelwork, they help decrease the depth of floors by accommodating pipes, conduits and ducting. They are also used in commercial and industrial buildings, warehouses and portal frames. CBs produced by modern automated fabrication processes can be competitive for the construction of both floor and roof systems.



*Fig. 1. Use of cellular beams in buildings*

A composite concrete floor-slab has the effect of significantly increasing the flexural resistance of a steel section; however its effect on shear resistance is more complex. Investigation of the behaviour of composite beams with isolated web openings in otherwise solid webs has shown that the slab significantly increases the shear-carrying capacity beyond that of the steel beam alone. This is due to the enhanced flexural and shear capacity of the upper part of the beam across an opening, although an unsupported web-post is more susceptible to buckling. In fire, the temperature distribution across a composite member is non-uniform, since the web and bottom flange have thin cross-sections and a greater exposed perimeter than the top flange. The deterioration of the material properties of the web will therefore become an important effect on the overall performance of the member in the event of fire (Figure 1). The structural behaviour of beams with opening is relatively complex and involves the main failure modes which are included in the design model for ULS design at ambient temperature and in fire conditions described in the literature review [1-9]

This paper describes an experimental study at elevated temperatures on the behaviour of full scale composite floor cellular steel beams. A total of four specimens, comprising two different steel geometries, applied load ratios and different temperature time curves. The beams were designed to fail by web buckling, which was observed in all the tests. Failure temperature observed in the fire tests indicated that failure by web post buckling of cellular beams in fire cannot simply be estimated by applying temperature dependent reduction factors on stiffness, as given in codes. Simple model was developed to calculate the deflections and ultimate loads for cellular beams in fire situations. Also, a finite element model using DIANA was then established with both material and geometrical non-linearity using shell elements to compare the experimental results and the simple model. The comparison between the finite element prediction, actual tests results and simple model are quite good in terms of failure modes, load deflection behaviour and ultimate loads.

## 1 EXPERIMENTAL RESULTS TESTS AT ELEVATED TEMPERATURES

Initially two composite cellular steel beams were tested under the same fire slow curve [7]. This fire curve was set up in order to produce lower peak temperatures but of longer duration sufficient to permit significant heat conduction, which may produce a large build up of vapour pressure and the creation of significant thermal expansion producing a restraint force coming from the concrete slab. Whereas, the last two composite beams were tested under the ISO 834 temperature – time curve subjected to 0.3 x failure load obtained from the cold tests given respectively as 108 kN and 126 kN [7]. The positions of the thermocouples (Figure 2) were located at each web post along its depth of the section and also around the openings.

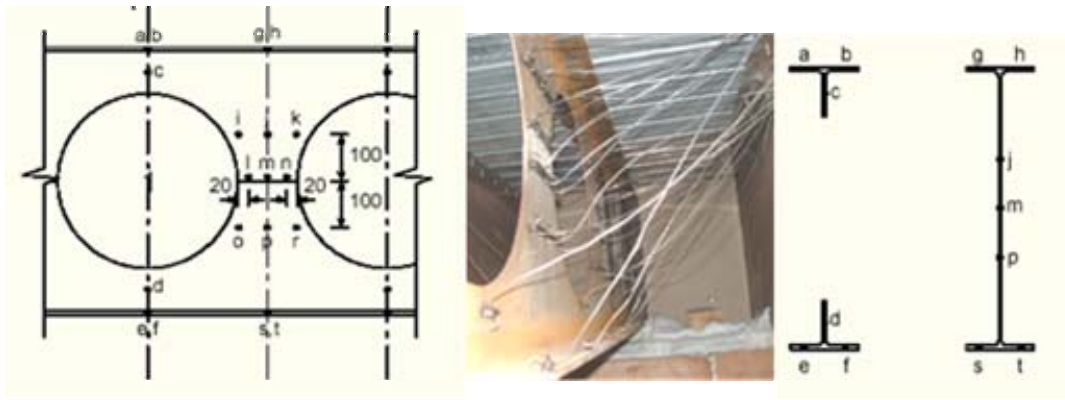


Fig. 2. Typical Thermocouples locations

The stiffness in beam (Fig 3) is linear elastic up to 13 minutes ( $T_{\text{fir}}=717\text{ }^{\circ}\text{C}$ ) with a reading deflection of 23 mm, whereas Figure 4 stayed linear up to 16 minutes ( $T_{\text{fir}}=748\text{ }^{\circ}\text{C}$ ) with a deflection equal to 26 mm. At 30 minutes of time ( $T_{\text{fir}}=842\text{ }^{\circ}\text{C}$ ) both beams A and B failed with a recording different respectively 179 mm and 235 mm. The instability of the beams and the rapid loss of stiffness of web post capacity occur faster than the beams tested during the slow fire curve [7] and this is due to the severity of the ISO834 temperature time curve.

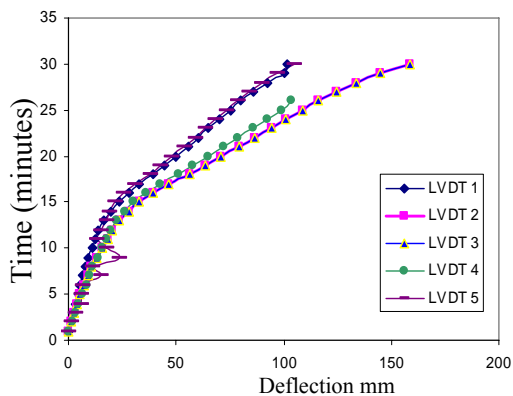


Fig. 3. Time versus deflection of test A

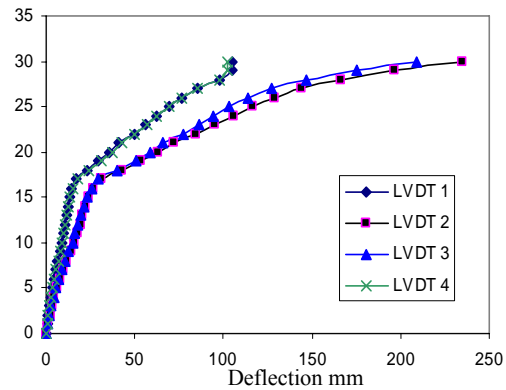


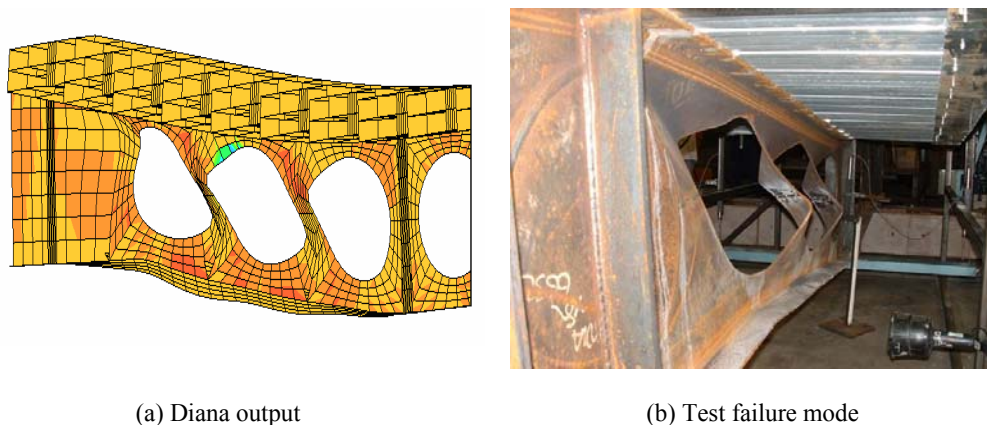
Fig. 4. Time versus deflection of test B

## 2 FINITE ELEMENT MODEL AND COMPARISONS

The composite cellular steel beams in ambient and fire tests were modelled using the commercial finite element software DIANA [10] at the University of Ulster. Shell elements with the ability to handle large strains, large deformations, and plasticity were used to model the cellular steel beam. Composite brick elements were used, incorporating a smeared crack approach for the concrete, to model the composite slab. Both the steel deck, as a bottom layer, and the reinforcing mesh as a layer within the concrete was included within the composite shell element. Due to the high density of the shear connectors used in the test, full interaction between the beam and supporting composite slab was assumed. This assumption is also justified from test observations [7] which confirmed that no stud failure occurred before web-post buckling of the beam.

Imperfections were introduced, based on an Eigen value buckling analysis, with the amplitude of the imperfections being governed by the thickness of the steel plate for local buckling and the overall length of the section for global buckling [13]. An implicit analysis was conducted in two steps, where the load was applied in the first step and the temperature was applied in the second step.

Figure 5 shows the output deformed shape of the Diana program compared with the actual failure mode of the symmetric test specimen. It is obvious when comparing the two that the same failure mode has occurred as the web post buckles under the applied load forming an S shape caused by the formation of hinges around the openings.



(a) Diana output

(b) Test failure mode

*Fig. 5. Asymmetric section at point of failure*

The measured yield and ultimate tensile strength of the steel was used in the simulation. The beam geometry was based on measured dimensions. The stress-strain curve at elevated temperatures for steel given by EN1994-1-2 [11] was adopted. For the stress-strain of the concrete in compression, at elevated temperatures, the relationship given in EN1994-1-2 [11] was adopted. For concrete in tension, at both ambient and elevated temperatures, the fracture energy concept [12] is used to estimate the ultimate tensile strain of the concrete.

Thermocouples positioned in the top, middle and bottom of the concrete composite slab recorded the relevant values. These were applied to the model directly by defining temperature points through the shell thickness. The temperature variation along the beam section was modelled. In the last 10 minutes of the tests a decrease in temperature was recorded due to heat loss through a window.

Figure 6 shows the time-deflection comparison between the test and FEA at elevated temperatures. A very good correlation was obtained between the predictions and test results. In both cases (Figure 7) web post buckling is clearly observed in the modelling corresponding to the failure mode witnessed in the tests.

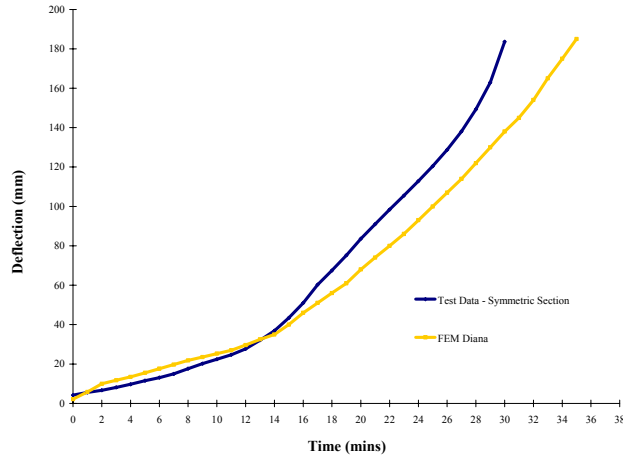


Fig. 6. Graph for symmetric section – ISO fire

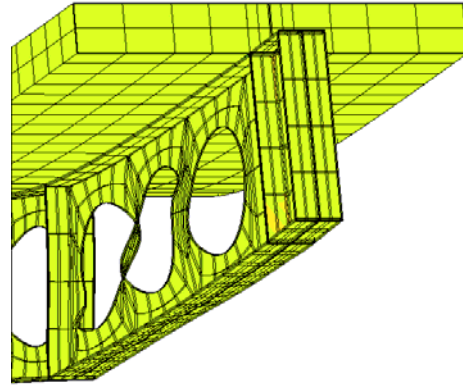


Fig. 7. Mesh Deformation

### 3 DEFLECTION

A method to estimate the beam mid-span (maximum) deflection is presented based on the ratio of applied moment to moment capacity as well as a new reduction factor for the second moment of area. The maximum deflections obtained from the experimental tests and different equations for the symmetric and asymmetric cellular composite beams are shown in Figures 8 and 9, respectively. The maximum deflections at the centre for simply supported beams at both ends with one centre load and two equal loads symmetrically placed are

$$\delta = \frac{Pa}{24EI} (3L^2 - 4a^2) \quad (1)$$

$$\delta = \frac{PL^3}{48EI} \quad (2)$$

Where  $P$  is the applied load,  $L$  the beam length,  $a$  the distance between the load and the support,  $E$  the Young's Modulus and  $I$  the second moment of area. The reduction factor for  $E$  at elevated temperatures is based on the Eurocode EN1993-1-2 [14]. The maximum thermal bowing deflection at the beam centre can be calculated as

$$\delta_t = \frac{\alpha \Delta T L^2}{8d} \quad (3)$$

Where  $\alpha$  is the coefficient of thermal expansion,  $\Delta T$  the temperature difference between the top and bottom of the beam cross-section and  $d$  the height of the cross-section. The ratio of the applied moment to the moment capacity [8] can be expressed as

$$MR = \frac{M_A}{M_\theta} \quad (4)$$

If this moment ratio is less than 1 (before the web post buckles), the moment capacity is greater than the applied moment. Thus the deflections of the beams can be reasonably determined from the summation of Eqs. (1) and (3) or Eqs. (2) and (3). However, when the moment ratio is greater than 1 (after the web post buckles), the beam deflections can not be accurately determined from the above equations. Beyond these points the applied moment is resisted by the concrete slab. Therefore, the moment ratio has to be taken into account in the calculation of beam deflections.

Another important issue in the calculation of beam deflections is the reduction factor for  $I$  at elevated temperatures. For simplicity, only one-thirds of  $I$  are reduced when the moment ratio is greater than 1 (when the temperatures at the bottom flange and bottom web are greater than 550°C). It is shown that  $I$  reduction factor is even larger (approximately three-fifths of  $I$ ) for the asymmetric section as shown in Figure 9. Before comprehensive conclusions can be drawn, further research studies regarding the accurate  $I$  reduction factor at elevated temperatures will be necessary.

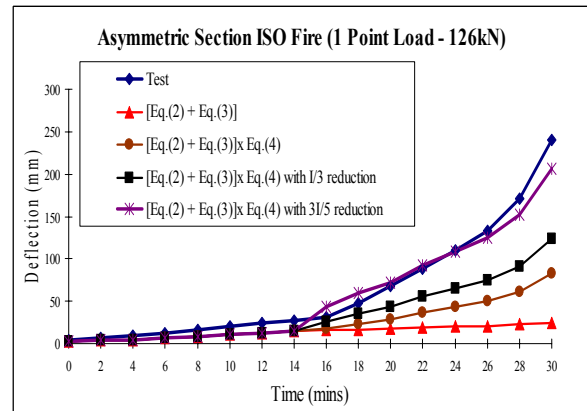
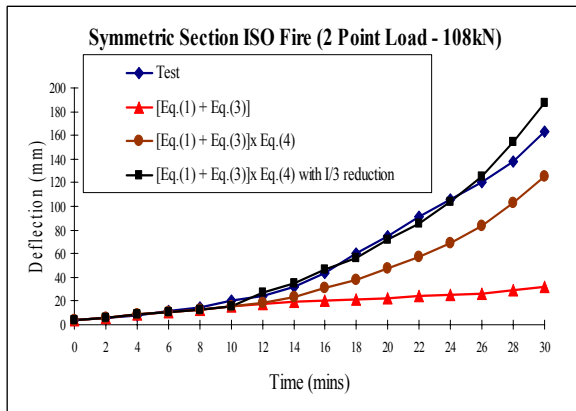


Fig. 8. Maximum deflections for the symmetric cellular composite beam

Fig. 9. Maximum deflections for the asymmetric cellular composite beam

#### 4 CONCLUSION

This paper describes an analytical study of the behaviour of composite floor cellular steel beams in fire conditions conducted at the FireSERT, University of Ulster. The study suggests the following:

- The beams failed due to web post buckling and the instability resulted in sudden loss of stiffness and strength in the beams
- The experimental data has compared well with the results from the Finite Element Modelling, giving confidence that it can be used for further parametric studies.
- The numerical model is capable to simulate the mechanical behaviour of composite Cellular beam sections in both cold and at elevated temperature conditions with a relatively high accuracy.
- The deflection hand calculation approach compared very well with the experimental tests but needs to be improved to include the concrete cracking at elevated temperatures and the effects of the shear connectors. It is still necessary to validate the proposed approach with more numerical and experimental data.

## REFERENCES

- [1] Liu, TCH, Liew, KH, Behaviour of Cellular Steel Beams in Fire, Interflam 2004, pp157-168, 2004.
- [2] SCI, 2004. RT1006 Version 02 - Fire Design of Cellular beams with Slender Web Posts, SCI, Ascot, 2004.
- [3] Bitar, D.; Demarco, T.; Martin, P.O. 2005. Steel and non composite cellular beams – Novel approach for design based on experimental studies and numerical investigations, Proc. 4<sup>th</sup> Eurosteel Conference, Maastricht, June 2005.
- [4] Lawson et al, Design of composite asymmetric cellular beams and beams with large web openings, Journal of Constructional Steel Research, V62, N6, June 2006
- [5] BS5950-8:2003 Structural use of steelwork in building - Part 8: Code of practice for fire resistant design
- [6] BS5950-1:2000 Structural use of steelwork in building - Part 1: Code of practice for design - Rolled and welded sections
- [7] Nadjai, A.; Vassart, O.; Faris, A.; Talamona, D.; Allam, A. & Hawes, M. 2006. Performance of cellular composite floor beams at elevated temperatures, Proc. SIF 2006, pp. 813-823.
- [8] Nadjai, A, Goodfellow, N, Vassart, O, Ali, F and Choi, S, Simple calculation method of composite cellular beams at elevated temperatures, Proc. SIF 2008, pp. 551-559.
- [9] Vassart, O. , Bouchair, A., Muzeau, J.-P. and Nadjai, A, Analytical model for the web post buckling in cellular beams under fire, Proc. SIF 2008, pp. 3-11.
- [10] TNO Building and Construction Research. DIANA finite element analysis. User's Manual release 9, Delft, 2005.
- [11] ENV 1993-1-2:200, Design of steel and composite structures, Part 1-2: Structural fire design, 2003
- [12] Ceb-Fip Model Code 1990: Design Code, Comit E Euro-International Du Beton, 1993.
- [13] Schafar BW, Pekoz T. Computational modelling of cold-formed steel: characterizing geometric imperfections and residual stresses. Journal of Constructional Steel Research, 1998.
- [14] Eurocode EN1993-1-2 Eurocode 3: Design of steel structures – Part 1-2: General rules – Structural fire design, 2005.

# EXPERIMENTAL STUDY ON FULL SCALE COMPOSITE FLOOR SLABS UNDER FIRE CONDITION

Na-Si Zhang <sup>a</sup>, Guo-Qiang Li <sup>a</sup>, Guo-Biao Lou <sup>a</sup>, Shou-Chao Jiang <sup>a</sup>, Kun-Chao Hao <sup>b</sup>

<sup>a</sup> College of Civil Engineering, Tongji University, Shanghai, China

<sup>b</sup> China Jingye Engineering corporation Limited, Beijing, China

## 1 INTRODUCTION

Cardington test and real fire disaster show that, the performance of concrete floor slabs composited with unprotected steel decks and beams in fire condition was much better than the prediction without considering membrane action. The observation and analyses show that, during a fire, with the strength and stiffness decrease of the steel decks, the reinforcement and the concrete, the load capacity of the slab offered by traditional bending mechanism will not be enough to bear the applied load. Instead of bending mechanism, membrane action will contribute to keep the stability of the slab by forming an elliptical tensile reinforcement mesh in the center of the slab and a concrete compressive ring at the boundary of the slab. The development of the membrane action is shown in Fig.1. <sup>[1]</sup>

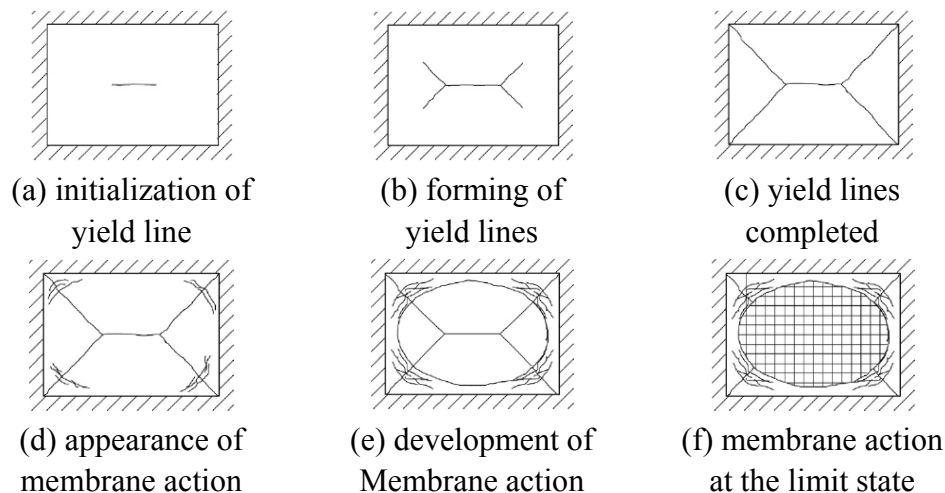


*Fig.1.* The development of membrane action in a floor slab

In the past decades years, many theoretical and experimental researches were performed to analyze membrane action.

From 1995 to 1996, six localized fire tests were conducted in a full-scale, eight-storey, steel frame building at Building Research Establishment Laboratory at Cardington. The test results showed that although the temperature of unprotected beam was higher than 1000°C, the slabs maintained their load bearing capacity during all the tests owing to membrane action. <sup>[2-3]</sup>

In 1999, to prove the existence of membrane action, Bailey performed a destructive test on a 9.5m\*6.5m composite floor slab at ambient temperature based on the data of Cardington test. <sup>[4]</sup> After that, in order to validate the theoretical analysis, he performed some small scaled tests on 15 reinforced concrete floor slabs. However, all of Bailey's tests were under ambient temperature, which might not be appropriate to verify the validity of membrane theory. <sup>[5]</sup>

In 2008, ArcelorMittal and CTICM launched a project FRACOF in which an 8.735m\*6.660m composite floor slab was tested under ISO standard fire. The test lasted for more than 120 minutes. Finally, the slab failed because of the fracture of the reinforcement bar. But, the fracture of the reinforcement was due to the failure of welding line at the joint of reinforced bars, which can be avoid by construction measures. Therefore, it caused a limitation to analyze the limit state and failure of the slab. [3]

In 2008, Guo-Qiang Li and Na-Si Zhang developed a new method to estimate the load capacity of composite floor slab under fire condition with considering membrane action. In order to observe the development of membrane action, analyze the membrane mechanism and verify the new method, 4 full-scaled slab tests were performed at Tongji University in China under the sponsoring from National Natural Science Foundation of China. [6]

## 2 GENERAL SITUATION OF THE TESTS

The test specimens were 4 pieces of 5.232m\*3.72m composite floor slabs with steel decks unprotected. The specimens were numbered from S-1 to S-4. The slabs were contributed with the profiled steel sheet YX76-344-688 which is commonly used in China. The thickness of the deck was 1mm, and its strength was larger than 270N/mm<sup>2</sup> (270 N/mm<sup>2</sup> was considered in the calculation [7]). The decks were fixed on the primary beams and secondary beams (if existed) by shear connector with a diameter of 16mm and a height of 125mm. Total depth of the slabs was 146mm and the thickness of the concrete on the top of the decks was 70mm. The reinforcing mesh of the slabs was made by smooth reinforcement bar with the grid size of 150mm\*150mm. The diameter of the reinforcement bar was 8mm, and the steel grade was Q235. The thickness of the protective layer of reinforcement was 21mm for S-1 and 30mm for S-2 to S-4. S-1 and S-2 had an unprotected secondary beam supporting the slabs in the middle, while S-3 and S-4 did not have. The cross section of the secondary beam was I25b, and the steel grade was Q235. The slabs, the primary beams and secondary beams were designed in according with the Chinese Code GB50017-2003 [8] and YB 9238-92 [9]. The general situations of the specimens were shown in *Table 1*. The arrangement of the specimens and the cross section of the composite slab are shown in the *Fig.2* and *Fig.3* respectively. The grade of the reinforcement was Q235 and the grade of the concrete was C25. The result of material property test for reinforcement and concrete are shown in *Table 2* and *Table 3* respectively (Where  $f_y$ ,  $f_u$  and  $\delta$  are the yield strength, ultimate strength and the ultimate elongation of the reinforcement respectively.  $f_{cu}$  is the cubic compressive strength of concrete).

In Cardington test, it was found that the reinforcement at the boundary of the slabs was fractured. In order to simulate this phenomenon, the reinforcement in these tests was not anchored at the boundary of the slabs, but exceeded the edge of the slab with a length of 150mm. The anchorage of the reinforcement is shown in *Fig.4*.

*Table 1.* Constructional information of test slabs [mm]

| No. | Specimens size | Total depth | Thickness on the top of decks | Arrangement of the reinforcement | Thickness of the protective layer of reinforcement | Direction of the rib        | Secondary beam                              |
|-----|----------------|-------------|-------------------------------|----------------------------------|--|-----------------------------|---|
| S-1 | 5232*3720      | 146         | 70                            | φ8@150                           | 21   | Along the <b>long</b> edge  | In the middle of the long edge, unprotected |
| S-2 | 5232*3720      | 146         | 70                            | φ8@150                           | 30   | Along the <b>long</b> edge  | In the middle of the long edge, unprotected |
| S-3 | 5232*3720      | 146         | 70                            | φ8@150                           | 30   | Along the <b>short</b> edge | No secondary beam                           |

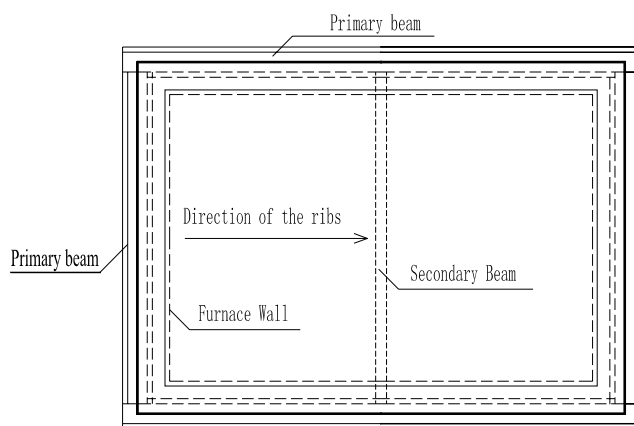
|     |               |     |    |              |    |                               |                   |
|-----|---------------|-----|----|--------------|----|-------------------------------|-------------------|
| S-4 | 5232*<br>3720 | 146 | 70 | $\phi 8@150$ | 30 | Along the<br><b>long edge</b> | No secondary beam |
|-----|---------------|-----|----|--------------|----|-------------------------------|-------------------|

Table 2. Properties of reinforcement bar at ambient temperature

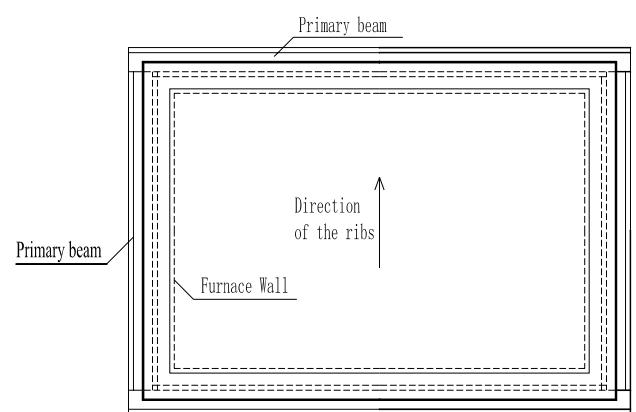
| No.           | S-1    | S-2    | S-3、S-4 |
|---------------|--------|--------|---------|
| $f_y(N/mm^2)$ | 579.06 | 531.84 | 557.04  |
| $f_u(N/mm^2)$ | 632.05 | 604.85 | 661.35  |
| $\delta(\%)$  | 33.3   | 36     | 31.33   |
| $f_y/f_u$     | 0.92   | 0.88   | 0.84    |

Table 3. Cubic compressive strength of concrete

| No.              | S-1  | S-2  | S-3   | S-4   |
|------------------|------|------|-------|-------|
| $f_{cu}(N/mm^2)$ | 26.1 | 21.0 | 22.37 | 22.87 |



(a) specimens S-1 and S-2



(b) specimens S-3 and S-4

Fig.2. Arrangement of the specimens

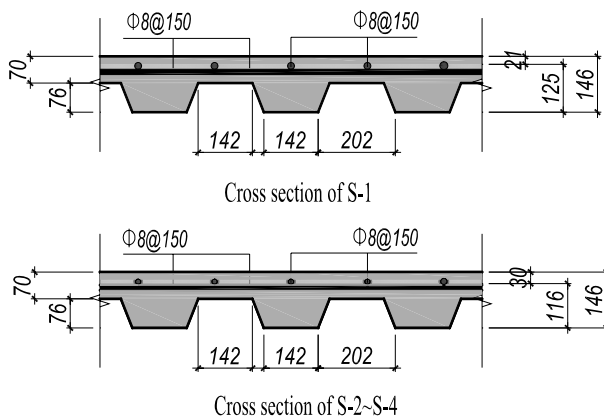


Fig.3. Cross section of the slabs



Fig.4. Anchorage of the reinforcement at the boundary of the slabs

The slabs were loaded at 24 points to stimulate uniform load (as shown in Fig.5 and Fig.6) with the load ratio of 0.60~0.65 over the load-bearing capacity of the slabs at the room temperature. The temperature-time curve of the furnace used for the tests followed ISO834 standard fire. The displacement of slabs, the temperature at the surface and bottom of the slabs, the temperature and strain of the reinforcements in the slabs, as well as the strain of concrete were measured in the tests. The arrangements of the measuring points are shown in Fig.7 to Fig.10.

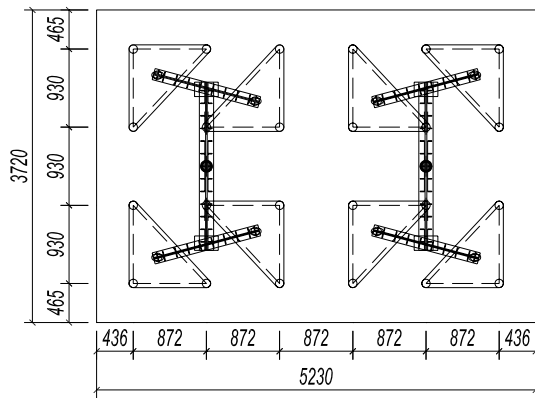


Fig. 5. The planform of loading system



Fig. 6. Loading system

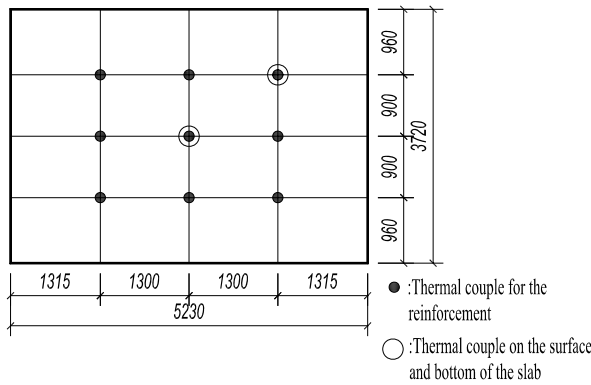


Fig. 7. Arrangement of thermal couples

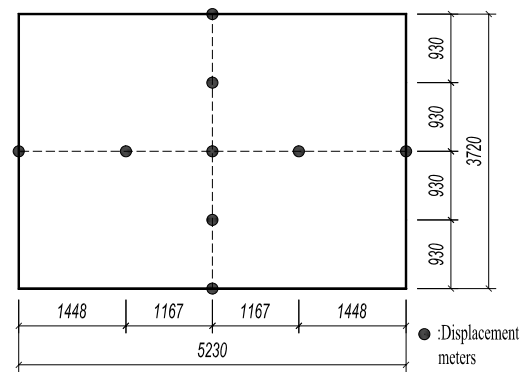


Fig. 8. Arrangement of displacement meters

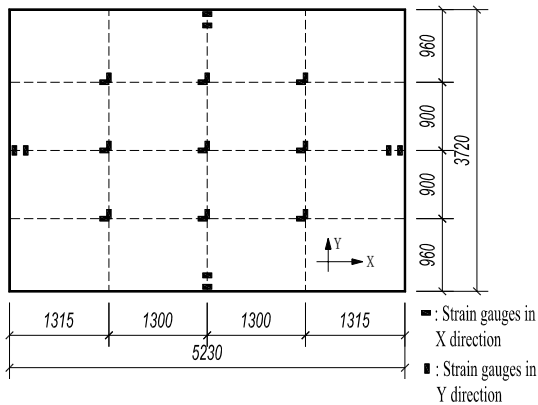


Fig. 9. Arrangement of strain gauges for the reinforcement

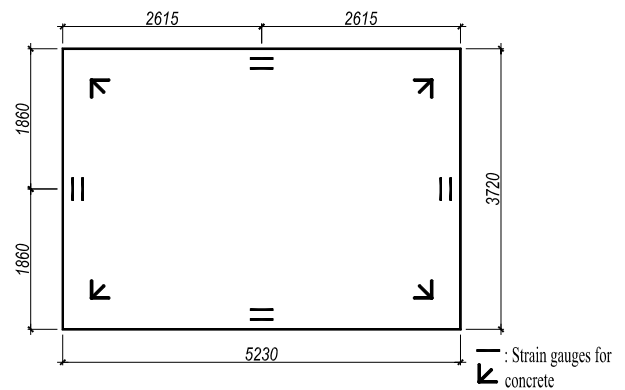


Fig. 10. Arrangement of strain gauges for the concrete

### 3 TEST PHENOMENA

The tests were performed under ISO834 standard fire with uniform load which was applied on the slabs in 10 steps. After all the load was applied at ambient temperature, there was only slight deflection found in the middle of the slabs. No crack and other failure phenomena were found on the slabs. Tests began until load and deflection were stable at room temperature. The test load and duration for the 4 tests were shown in *Table 4*.

Table 4. Test load and duration for 4 tests

| No. | Ultimate bearing capacity of design value<br>(kN/m <sup>2</sup> ) | Test load<br>(kN/m <sup>2</sup> ) | Load ratio<br>(%) | Duration<br>(min) |
|-----|---|-----------------------------------|-------------------|-------------------|
| S-1 | 30.64   | 18.38                             | 60                | 75                |
| S-2 | 29.51   | 17.71                             | 60                | 90                |
| S-3 | 14.57   | 8.75                              | 60                | 100               |
| S-4 | 14.57   | 9.47                              | 65                | 100               |

\* Terminated without fail.

In test S-1 and S-2, cracks appeared beside secondary beam firstly due to the negative moment which was caused by the decrease of the strength and stiffness of the slabs. Then, significant cracks were found along the long edge of the slabs because of negative moment which was induced by the large deflection in the center of the slabs. These cracks located at the weakest cross section of the slabs (shown in *Fig. 11*). Meanwhile, some cracks occurred along the short edge of the slabs. These cracks developed not only on the surface of the slabs, but also extended to the side face of the slabs (shown in *Fig. 12*). After the test, significant yield lines were founded at the corner of the slabs. The concrete along the yield line was crushed (shown in *Fig. 13*).

The deflection of the slabs was very large. The deformation of the slabs presented as an elliptic parabolic after the tests which validate that during the test membrane action was developed to bear the applied load (shown in *Fig. 14*).

*Fig. 15* shows the distribution of the cracks on S-2 after the test, where cracks caused by the membrane action can be found both at the center and at corner of the slabs. *Fig. 16* shows the deflection of S-2. Although the deflection of the unprotected secondary beam was huge, no failure was found on the secondary beam. *Fig. 17* shows the condition at the bottom of S-2. It is found that the profiled steel decks did not melt down, which help the decks to keep the stability of the slabs after 90 min under standard fire.

Water vapor sweated seriously during the test. Even after the test was finished, some water vapor continued to sweat for a long time.

The test's phenomena of test S-3 and S-4 were similar to that of S-1 and S-2. Since there was no secondary beam in the center of the slabs, the concrete began to crack at the boundaries of the slabs in test S-3 and S-4 instead of beside secondary beam in test S-1 and S-2. The distributions of the cracks on S-3 and S-4 were shown in *Fig. 18* and *Fig. 19* respectively. The cracks in the center of S-3 and S-4 were not caused by the negative moment but by membrane action.

No collapse was found in these 4 tests, which shows that membrane action occurred to carry applied load on the slabs and to keep the stability of the floor system.



Fig. 11. Cracks along the long edge



Fig. 12. Cracks along the short side face



*Fig.13.* The yield line at the corner



*Fig.14.* The deformation of the slab after the test



*Fig.15.* The cracks on the S-2 after the test



*Fig.16.* The deformation at the bottom of S-2 after the test



*Fig.17.* The steel deck after the test

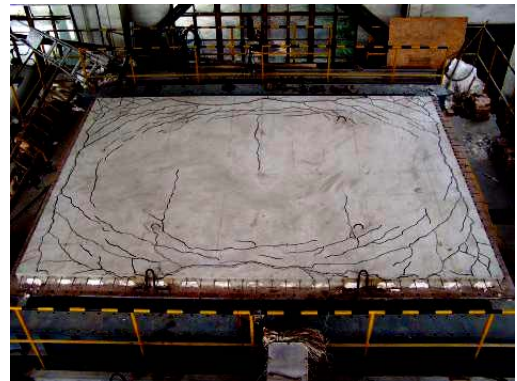


*Fig.18.* The cracks on S-3 after the test



*Fig.19.* The cracks on S-4 after the test

## 4 TEST RESULTS AND ANALYSES

### 4.1 Temperature

*Fig.20* is the furnace temperature curve, which shows that the furnace temperature coincided well with the ISO834 fire curve.

*Fig.21* is bottom temperature curve in the middle of the slabs. It shows that at the beginning of the test, the temperature of the slab at the bottom was low, and then it increased along with time. At the time of 75 minutes, the temperature can reach to 700 or 800°C. At the time of 90 minutes to 100 minutes, the bottom of the slab can be heated up to around 800°C or 900°C.

*Fig.22* is surface temperature curve in the middle of the slabs. It shows that during the whole test, surface temperature of the slab is very low. At the time of 90 minutes, the temperature was only around 100°C.

*Fig.23* is the average temperature curves of the reinforcement. It can be found that the distance between the reinforcement and the bottom of the slab has a great impact to the temperature of the reinforcement.

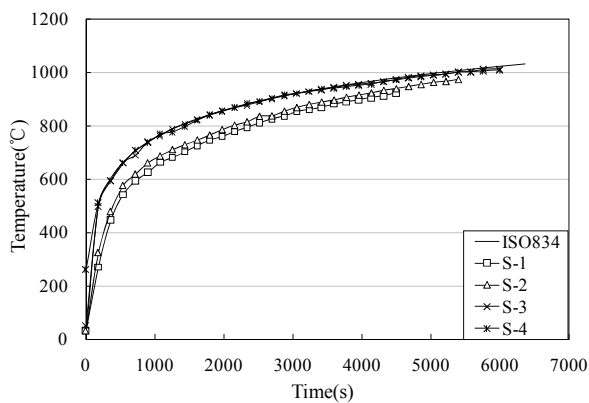


*Fig.20.* Furnace temperature curve

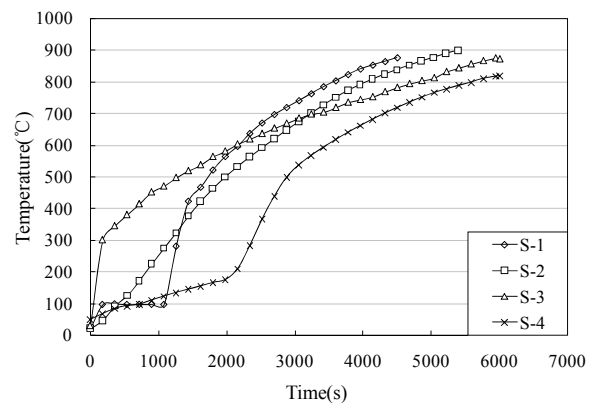


*Fig.21.* Bottom temperature in the middle of the slabs

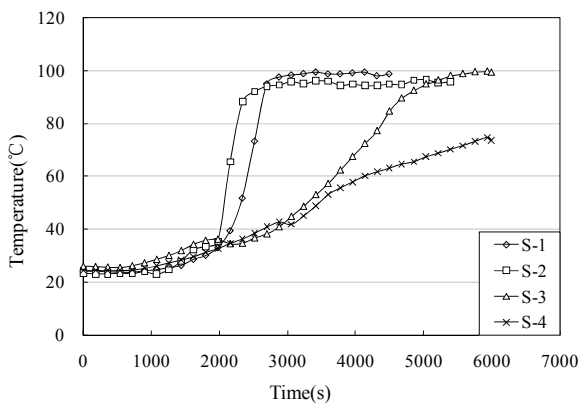


*Fig.22.* Surface temperature in the middle of the slabs

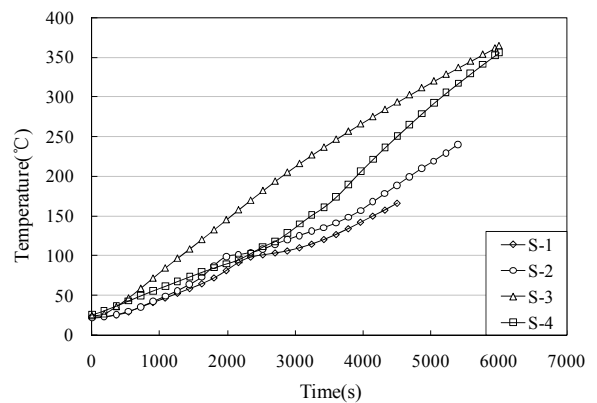


*Fig.23.* Average temperature of the reinforcement of S-1 to S-4

### 4.2 The strains of reinforcement and concrete

*Fig.24* and *Fig.25* show the strains of the reinforcement along the short edge and long edge respectively. Since the effective working temperature of the strain gauges is less than 60°C, the data when the temperature was higher than 60°C are taken out in the figures. According to the yield line theory, the reinforcement of these tests was located at the compression zone in the cross section of

the slabs, therefore the reinforcement should be under compression. However, the data show that the reinforcement was under tension during most of the test except for the beginning. This phenomenon proves the occurrence of tensile membrane action in the test.

*Fig.26* is the strains curve of the concrete at the boundary of S-4. It can be found that the concrete in the middle of the boundary was under compression. It validates the existence of the concrete compressive ring which can provide the anchorage for the reinforcement.

According to analysis of the data taken by the strain gauges at the corner of the slab (see *Fig.10*), compressive strains were found at the corner at the angle between 30° and 60°, which coincides with the failure phenomenon shown in *Fig.13*.

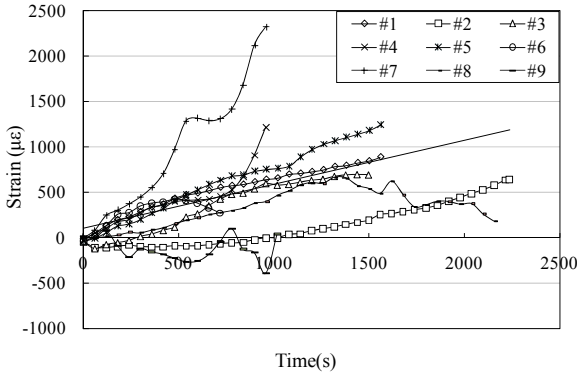


*Fig.24.* The strains of the reinforcement along short edge in S-1

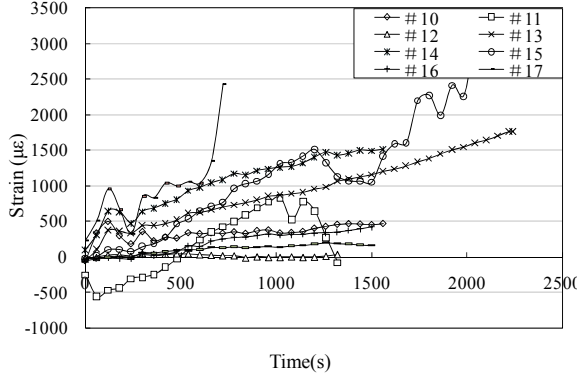


*Fig.25.* The strains of the reinforcement along long edge in S-1

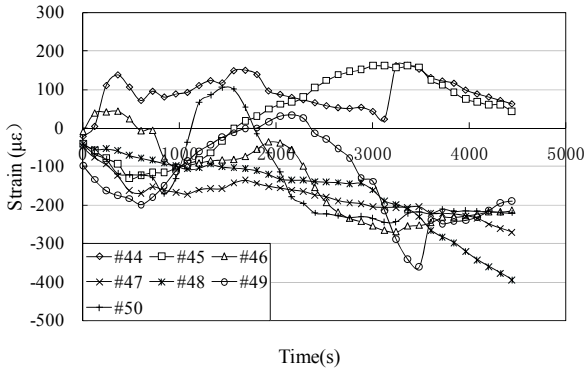


*Fig.26.* The strains of the concrete at the boundary of S-4

**4.3 Deflection in the middle of the slabs**

*Fig.27* and *Fig.28* show the deflections in the middle of the slabs. It is found that the deflection can arrive at 1/25 of the short edge of the slabs. Therefore, it is reasonable to deduce that the load-bearing mechanism of the slabs has been changed from bending mechanism to membrane action one under such large deflection in the tests.

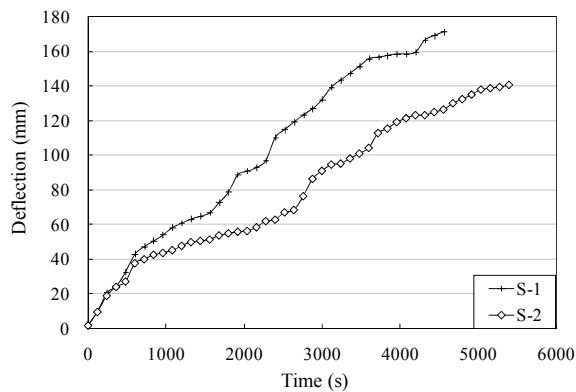


Fig.27. The deflection of S-1 and S-2

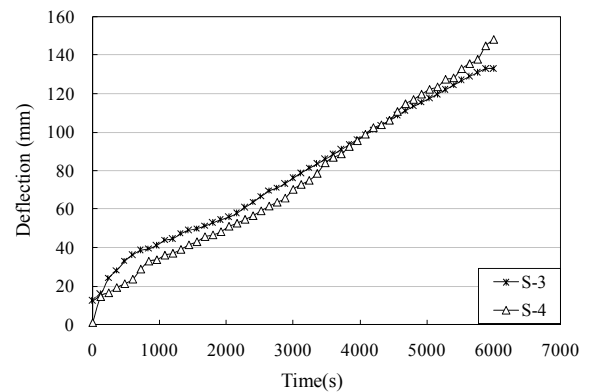


Fig.28. The deflection of S-3 and S-4

## 5 CONCLUSION

In this paper, full-scale tests were performed on 4 steel-concrete composite floor slabs. In the tests, the temperature of the furnace, slabs, and reinforcement, the strains of the reinforcement and concrete, and the deflection of the slabs were measured. Important conclusions can be presented as follow:

1. Membrane action will occur to carry the applied load instead of bending mechanism due to large deflection, when the composite floor slabs are subjected to fire. This membrane action can help to keep the load capacity of the slabs and maintain the stability of the floor system under fire condition.
2. Based on the data measured in the tests, the reinforcement in the slabs will be under tensile force and form an elliptical paraboloid tensile mesh which can bear the load on the slabs. A concrete compressive ring will be formed at the boundary of the slabs to provide anchorage for the reinforcement.
3. Due to the membrane action, the existence of secondary beams to support the slab is not necessary in fire condition, which can save the fire protection for secondary beams.

## REFERENCES

- [1] Guo-Qiang Li, Shi-Xiong Guo, Hao-Sheng Zhou, Modeling of membrane action in floor slabs subjected to fire, *Engineering Structure*, 2007
- [2] Huang Zhaohui, Modeling Membrane Action of Concrete Slabs in Composite Buildings in Fire II: Validations, *Journal of Structural Engineering*, Vol.129, No.8, 2003
- [3] Zhao Bin, Roosefid Mohsen, Vassart Olivier, Full scale test of a steel and concrete composite floor exposed to ISO fire, *Proceeding of the Fifth International Conference on Structures in Fire (SiF'08)*, 2008
- [4] Bailey Colin G, White D. S., Moore D. B., The tensile membrane action of unrestrained composite slabs simulated under fire condition, *Engineering Structures*, 2000
- [5] Foster S. J., Bailey C. G., Burgess I. W., Plank R. J., Experimental behavior of concrete floor slabs at large displacement, *Engineering Structures*, 2004
- [6] Na-Si Zhang, Guo-Qiang Li, A new method to analyze the membrane action of composite floor slabs in fire condition, *Proceeding of the Fifth International Conference on Structures in Fire (SiF'08)*, 2008
- [7] Continuously Hot-Dip Zinc-Coated Steel Sheet and Strip. GB/T 2518-2004, China
- [8] Code for design of steel structures. GB50017-2003, China

- [9] Specification for design and construction of steel-concrete composite floor system, YB 9238-92, China

#### **ACKNOWLEDGEMENT**

The work reported in this paper was financially supported by the National Natural Science Foundation of China under contract 50621062, 50738005 and 50728805. The support is gratefully acknowledged.

## **THERMAL RESTRAINT EFFECTS ON THE FIRE RESISTANCE OF STEEL AND COMPOSITE STEEL AND CONCRETE COLUMNS**

Manfred Korzen<sup>a</sup>, João Paulo C. Rodrigues<sup>b</sup> & António Moura Correia<sup>b</sup>

<sup>a</sup> Federal Institute for Materials Research and Testing, Berlin, Germany.

<sup>b</sup> Faculty of Sciences and Technology, University of Coimbra, Portugal

### **INTRODUCTION**

The recently approved parts of Eurocodes concerning structural fire design, opens to the designer the possibility of using analytical and numerical methods as a way of guaranteeing the adequate fire resistance of the structures, apart from the expensive experimental tests. Although those documents foresee the possibility of making the use of advanced calculation methods for the analysis of the global behaviour of the structures subjected to fire, they also allow an analysis of single elements or parts of the structures, which is easier and more attractive for the common designer. In an analysis of single elements, the mechanical action of the surrounding structure, where the elements are inserted, is taken into account by the so-called “indirect fire actions”. However, the Eurocodes allow that these actions are not taken into account in the case of an analysis of single elements subjected to the normalized fire. Tests and numerical studies carried out previously concerning steel columns with restrained thermal elongation indicate that the fire resistance of these elements can be significantly reduced with respect to the situation of free elongation [1].

This paper presents a comparison of results of fire resistance tests on steel and composite steel and concrete columns with restrained thermal elongation carried out at the Laboratory of Testing Materials and Structures of the Faculty of Sciences and Technology of University of Coimbra (FCTUC), Portugal and other ones carried out at the Federal Institute for Materials Research and Testing (BAM), in Berlin, Germany.

New three-dimensional experimental set-ups are under development in both Institutions to test building columns in conditions similar to the ones in real buildings. In the system of FCTUC, the stiffness of the surrounding structure to the column in fire is realized by a three-dimensional restraining frame while in the system of BAM it is done by the so-called substructuring method. Due to this concept the entire building is divided into two parts, which are connected through a special hardware-software interface. One part is represented by the column under testing in a special furnace, whereas the remaining building environment is simulated online by a model on a computer [2].

### **1. EXPERIMENTAL SET UP OF FCTUC**

A new test set-up was used at FCTUC to measure the fire resistance of columns with restrained thermal elongation that are under development at this Institution (fig. 1).

The system comprised a restraining frame of variable stiffness (1) that had the function of simulating the stiffness of the surrounding structure to the column in fire.

The columns were subjected to a constant compressive load of 70% of the design value of buckling resistance of the column at room temperature. This load was controlled by a load

cell of 1MN located on the head of the hydraulic jack (6). This load simulated the serviceability load of the column when part of a real structure. The load was applied by the hydraulic jack (2) controlled by a servo hydraulic system.

The thermal action was applied by a modular electric furnace (3) that could closely follow the ISO 834 fire curve.

The restraining forces generated in the column due to heating were measured by a load cell of 3 MN located on a steel piston (4). This piston was placed between the testing column and the restraining frame.

The axial displacements and rotations on the top and base of the column were also measured by displacement transducers (5) orthogonally arranged in three different points, forming a deformation plane.

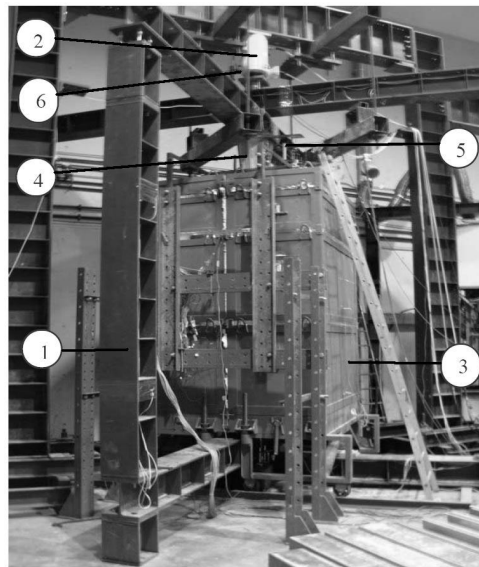


*Figure 1.* Test set-up of FCTUC

In the experimental programme, tests were carried out on steel and composite steel and concrete columns, with cross-sections of HEA160 and HEA200 and with stiffness ratios of 3, 13, 39, 68 kN/mm.

## **2. EXPERIMENTAL SET UP OF BAM**

A central role of the substructuring method plays the *BAM* column furnace (Fig. 2 (a) – (b)). Mechanical and thermal actions are applied through this device to the specimen under test. Whereas the thermal set point is a known function of time for the mean gas temperature before starting the test, the mechanical set point has to be calculated online during a fire test in substructuring mode. Six electro-hydraulic control channels equipped with displacement and force sensors are available to influence the mechanical boundary conditions, i.e. two bending rotations each at top and bottom, one axial displacement at the bottom and one horizontal displacement at the top. During a substructuring test, forces and moments at the boundaries of the specimen, i.e. at the upper and lower bearings of the column, are measured and utilized for the computation of the corresponding displacements and angles, which are sent to the specimen in order to keep the entire building in mechanical equilibrium with its prescribed overall boundary conditions [2].

This closed loop for only one channel in substructuring mode is displayed in Fig. 2 (b) – (c). According to the free body diagram in Fig. 2 (c), the experiment is *driven* by the thermal displacement, which is diminished by the mechanical displacement  $u^{mech}$  due to the stiffness  $c^{mod}$  of the surrounding environment resulting in a compressive force on the column under test. The function of the control loop is to change the (total) displacement  $u$  by moving the position of the electro-hydraulic axial cylinder in such a way that the model force  $f^{mod}$  is equal to the measured force  $f$ .

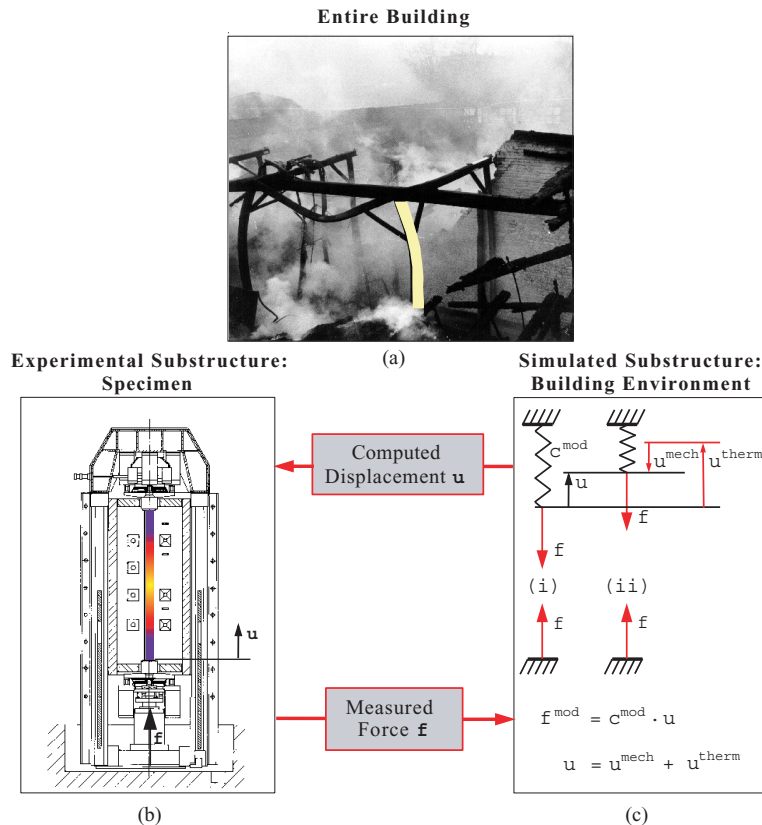


Figure 2 – BAM system - substructuring method

### 3. SPECIMENS

In order to compare the performance of both experimental systems several fire resistance tests on steel and composite steel and concrete columns were carried out.

In FCTUC fire resistance tests, the specimens were steel and composite steel and concrete columns HEA160 and HEA200, 3m high. The steel had the class S355 and the concrete C25/30. In BAM fire resistance tests the specimens were HEA140 and HEB180 for the steel columns and HEA200 for the composite columns, 3.60m in height. The steel of the steel columns had the class S235 and the composite S355 and the concrete C25/30 (fig. 3).

The specimens were fitted with thermocouples type k (chromo-alumel) to measure the temperatures in different points of the cross-section. All the specimens were subjected to an initial load, constant all over the test, of 70% of the design value of the buckling load at room temperature.



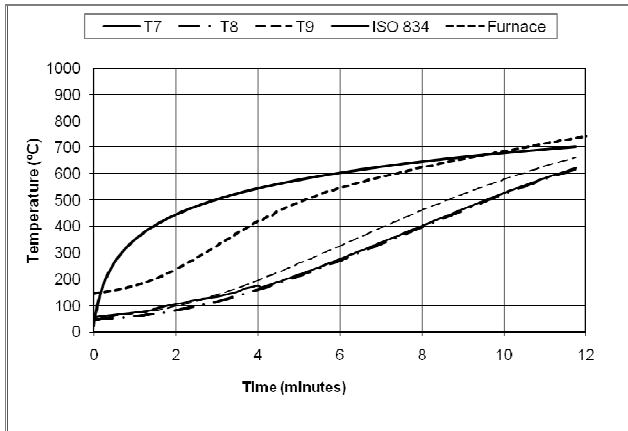


Figure 4 – Temperatures – FCTUC2 - Section S3

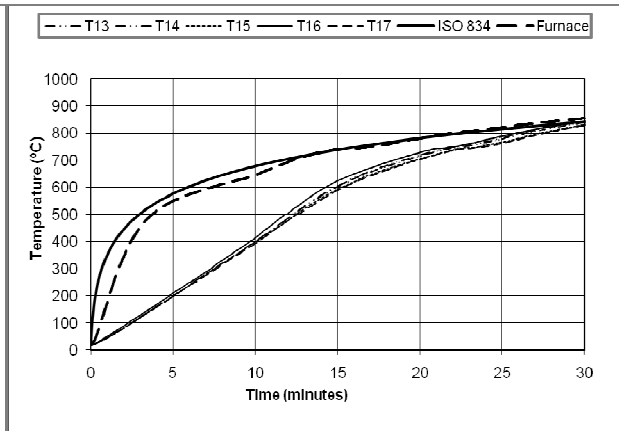


Figure 5 – Temperatures – BAM2 - Section S5

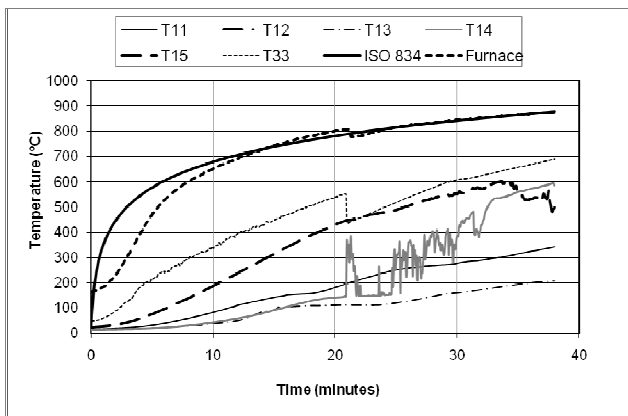


Figure 6 – Temperatures – FCTUC4 - Section S3

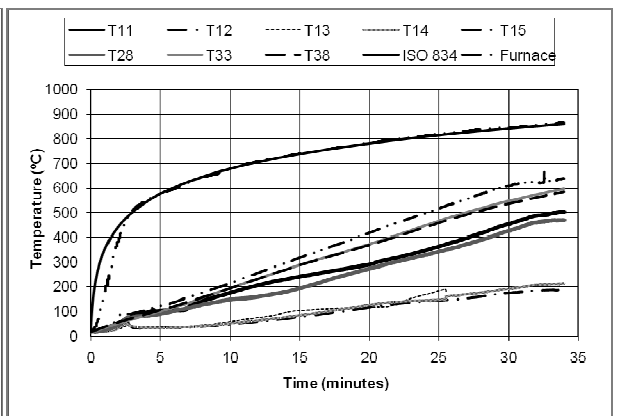


Figure 7 – Temperatures – BAM3 - Section S3

#### 4.2. Evolution of restraining forces

Figures 8 and 9 present the evolution of the restraining forces related to the initial load in function of the test duration.

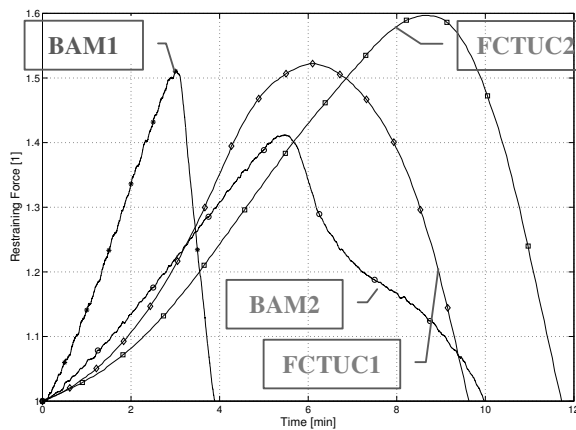


Figure 8 – Restraining forces – steel columns

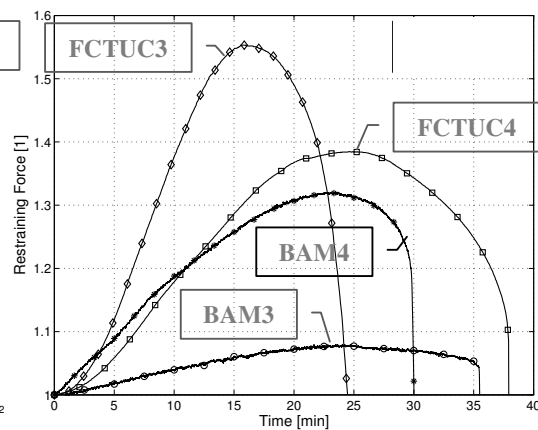


Figure 9 – Restraining forces – composite columns

In figure 8, for the steel columns, comparing the FCTUC tests between them, the HEA200 (*FCTUC2*) registered higher restraining forces and fire resistance than the HEA160 (*FCTUC1*). The comparison of the HEB180 (*BAM2*) with HEA200 (*FCTUC2*) and the HEA140 (*BAM2*) with the HEA160 (*FCTUC1*) that have nearly the same slenderness, show some differences on the pattern of the curves and in the values of the restraining forces and the fire resistance. This is maybe explained by the different distribution of mass around the inertia axis of the section.

In figure 9, for composite columns, comparing the FCTUC tests, the HEA200 (*FCTUC4*) showed higher fire resistance than the HEA160 (*FCTUC3*). The *BAM4* and the *FCTUC4* that were tested with identical conditions, presented curves for the restraining forces of the same pattern and the values of the fire resistance and the restraining forces were very close. Comparing the *BAM* tests, *BAM4*, tested with higher stiffness, presented higher restraining forces and shorter fire resistance than *BAM3*.

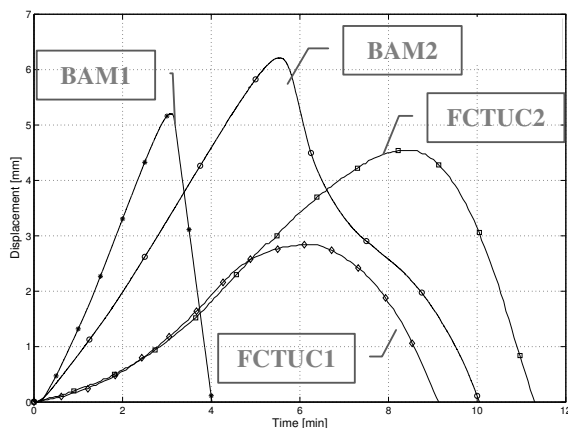


Figure 10 – Axial displacements – steel columns

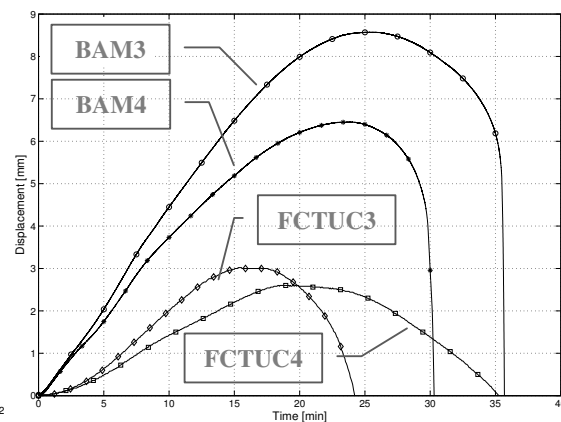


Figure 11 – Axial displacements – composite columns

Figures 10 and 11 present the development of the axial displacements in function of the test duration. The main finding in these graphs is that the axial displacements experienced by the *BAM* specimens were in general higher than the ones of *FCTUC* specimens.

## 5. FINAL REMARKS

These fire resistance tests allowed us to understand not only the real behaviour of steel and composite steel concrete columns in fire, but also find specific problems of the performance of both systems. As a main conclusion of this work it can be pointed out that the higher stiffness of the surrounding structure induces higher restraining forces and lesser fire resistance for steel and composite columns. Moreover, the less slender columns presented higher fire resistance.

## REFERENCES

- [1] Rodrigues, J.P.C.; I. Cabrita Neves; J. C. Valente – “Experimental research on the critical temperature of compressed steel elements with restrained thermal elongation”, *Fire Safety Journal*, Vol. 35 No. 2, 2000, pp. 77-98.
- [2] Korzen, M.; G. Magonette; Ph.Buchet – “Mechanical Loading of Columns in Fire Tests by Means of the Substructuring Method” - *Zeitschrift für Angewandte Mathematik und Mechanik*, Vol. 79, 1999, pp. S617-S618.

## **FIRE RESISTANCE OF BAR-REINFORCED CONCRETE-FILLED STEEL TUBE COLUMNS**

Su-Hee Park<sup>a</sup> Kyung-Chul Song<sup>a</sup> Kyung-Soo Chung<sup>b</sup> Byung-Yeol Min<sup>c</sup> Sung-Mo Choi<sup>a</sup>

<sup>a</sup> Department of Architectural Engineering, University of Seoul 130-743, Seoul, Korea

<sup>b</sup> Research Institute of Industrial Science & Technology Steel Structure Research Laboratory, Kyungkido, Korea

<sup>c</sup> Korea Institute of Construction Technology, Kyungkido, Korea

### **INTRODUCTION**

thanks to the thermal storage effect created inside the steel tube, the CFT structure has better fire resistance than that of conventional steel structures. In this regard, In this study, we conducted an experimental evaluation and analytical study on the fire resistance of a non-coated square tubular steel as well as a circular tubular column (Chung K.S., et al, 2008, Park S.H., et al, 2007), and identified that it sufficiently resisted fire for two hours or less under high axial force. We also proposed a simple design formula with a range limitation.

However, in the Ministry of Land, Transport and Maritime Affairs Notice No. 2005-1225, the standard of fire resistance structure under the regulation 'Fire Resistance Accreditation and Management Standards' states that every column used in the construction of high-rise buildings with more than 12 floors is required to secure a three-hour fire resistance. Accordingly, in order to apply a non-coated CFT column to a high-rise building, additional repairs and reinforcement for fire resistance should be suggested. To secure fire resistance, a steel-reinforced non-coated steel square CFT column was set.

In a related foreign research study, Kodur (V.K.R. Kodur 1999) conducted an experiment and analytical study on a concrete-filled steel square column or circular column specimens that were unreinforced, fiber-reinforced and steel-reinforced. With major parameters such as the presence or not of concrete reinforcement, external diameter, working axial force, effective length and concrete strength, a parameter analysis was conducted. Through this, a simple design formula with range limitation was proposed, which identified that steel-reinforced concrete-filled steel square column offers improved fire resistance.

In this study, we designed specimens of a steel-reinforced non-coated steel square CFT column based on existing researches, and projected the fire resistance of each specimen. A fire resistance test under load was conducted on the steel-reinforced non-coated square CFT columns. Through this, the study attempted to evaluate the effect of steel reinforcement in applying cross-section diameter and axial force ratio and high-strength concrete, along with determining the effect of applying steel reinforcement.

## **1 EXPERIMENT DESIGN**

### **1.1 Specimen Design**

Fig. 1 shows the details of specimens used in the experiment, which are the following: square steel tubular column with 280mm and 360mm in cross-section diameter: 2902 mm of member length, sectional members and sizes. The thickness of the steel column was set to be 6 mm and 9 mm whereas width thickness ratio was set to be 46.6~40, sufficient deformation capacity being expected at room temperature. The end-plate of a steel column was set to be 50 mm. In the case of steel reinforcing concrete cover, the concrete cover was set to be 50mm in order to perform full fire resistance. In order to emit internal steam of a CFT column heated at the height of 340 mm, 1311 mm and 1011 mm at the lower end-plate of an upper column, a paired hole was made (Fig. 1). A SS400-grade steel column was used. Table. 1 shows the result of a coupon tensile test in accordance with KS B 0810. The design

strength of in-filled concrete used normal strength and high strength of 35MPa and 55MPa, whereas slump was measured at 21.5 cm and 25 cm, respectively. The column was filled with concrete by inserting a tremie pipe into the top of a steel column. After concrete pouring, the top of the column was covered, followed by curing. Fire resistance cover at the steel column was done. Table 2 shows the parameters of specimens, which are the following.

Table 1. Material Characteristics of Steel and Concrete

| Concrete  |                            | Steel          |       |                      |                  |
|-----------|----------------------------|----------------|-------|----------------------|------------------|
| Age (day) | compressive strength (MPa) | thickness (mm) | grade | Yield Strength (Mpa) | Tensile strength |
| 28        | 36.1                       | 6              | SS400 | 240                  | 422              |
| 28        | 56.8                       | 9              | SS400 | 237                  | 410              |

Table 2. Specimen Parameter

| Name     | size (mm) | Concrete strength $f_{ck}$ (Mpa) | Steel strength $F_y$ (Mpa) | Axial force ratio $N_a/N_c$ | Effective length KL (mm) | Reinforcement ratio (%) | Fire resistance time FR (min) |
|----------|-----------|----------------------------------|----------------------------|-----------------------------|--------------------------|-------------------------|-------------------------------|
|          |           |                                  |                            |                             |                          |                         | Test time                     |
| APL1     | □-360×9   | 36.1                             | 240                        | 0.4                         | 2902                     | -                       | 99                            |
| ARL1     |           | 36.1                             | 237                        | 0.4                         |                          |                         | 171                           |
| BRL1     | □-280×6   | 36.1                             | 237                        | 0.4                         |                          | 2%                      | 158                           |
| BRL2     |           | 36.1                             | 237                        | 0.6                         |                          |                         | 80                            |
| BRH1     |           | 56.8                             | 237                        | 0.4                         |                          | 146                     |                               |
|          |           |                                  |                            |                             |                          |                         |                               |
| D×t (mm) |           | Reinforcement (concrete)         |                            |                             | $f_{ck}$ (MPa)           |                         |                               |
| A        | B         | P                                | R                          | H                           | L                        |                         |                               |
| 360×9    | 280×6     | Plain                            | Bar-reinforced             | High                        | Low                      |                         |                               |

D: cross-section diameter, t: steel thickness,  $f_{ck}$ : concrete strength,

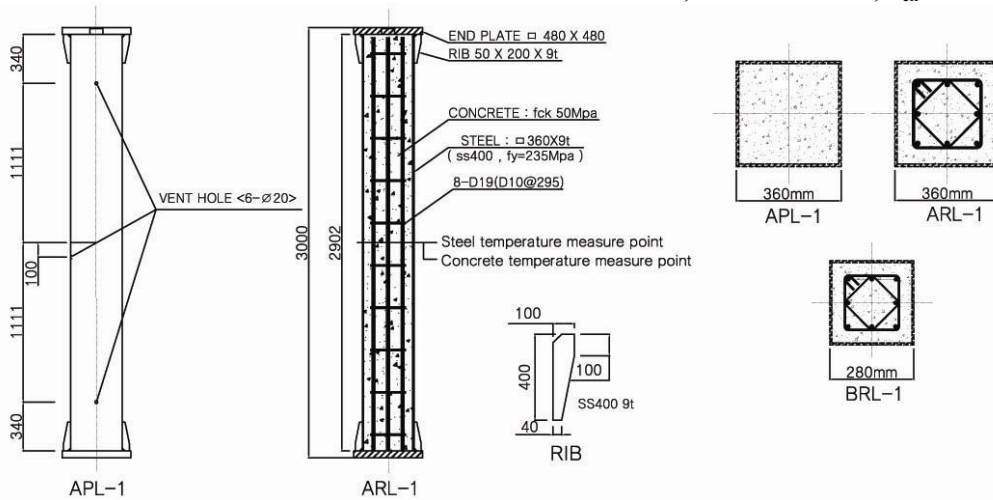


Fig. 1. Section and Size of Column Specimens

## 1.2 Experiment Method

The outline of the experimental equipment is shown in Fig. 2. A loading equipment that can exert axial force with a column-used reheating furnace from top to bottom, in other words, a compression tester with a loading capacity of 3000kN, was installed. Specimens were vertically installed in the center of a reheating furnace. Oriented amounts by heat expansion and shrinkage were measured by the linear variable differential transformer (LVDT) attached to a hydraulic cylinder. Items for temperature measurement were Fig. 4. The experiment proceeded as follows:

- (1) A CFT square column in the reheating furnace is vertically set up after fitting in the center of a hydraulic jack.
- (2) 15 minutes prior to heating, compressive force is introduced in the column center.
- (3) The surface temperature of a steel column before the experiment is set to be approximately 5°C, whereas the reheating furnace's temperature is set according to the heating curve of ISO 834 during the experiment.

(4) If shrinkage reaches  $L/100$  or more of the total shrinkage, or targeted fire resistance time is met, the experiment ends.

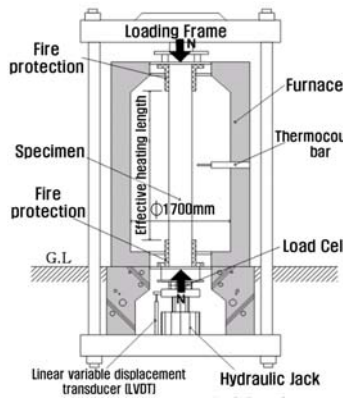


Fig. 2. The Loading device

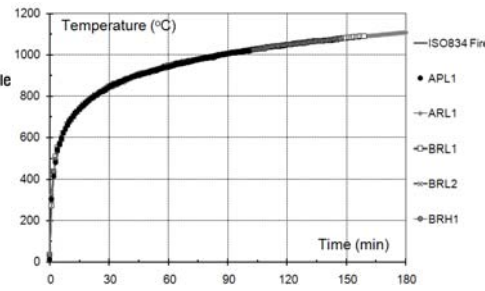


Fig. 3. Comparison of ISO Standard Fire Curve and test Curve

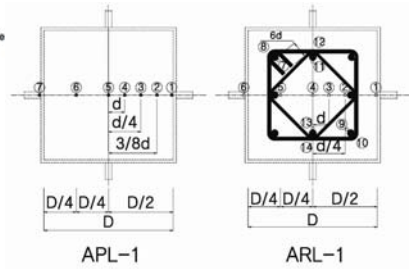


Fig. 4. Temperature Measurement Position

## 2 EXPERIMENT RESULT OF FIRE RESISTANCE TEST UNDER LOAD

### 2.1 Temperature Distribution

As for temperature distribution by heating, specimens were compared at the surface of the steel column, 1/4 of the concrete cross-section center and surface, and internal and external point of steel. In looking into the temperature distribution, data regarding the steel surface in Fig. 5-(a) and concrete surface in Fig. 5-(b) show that the distribution of average temperature is located at the position lower than that of the standard fire curve. However, it shows a pattern similar to the standard fire curve after the middle section. This is attributable to having little influence of the initial parameters. The spot, 1/4 of concrete cross-section in Fig. 5-(c), shows that the temperature distribution of the BRH1 specimen drastically increases after 80 minutes of heating due to the spalling effect. The concrete cross-section center in Fig. 5-(d) shows that the temperature distribution of a steel-reinforced CFT column is higher than that of a non-reinforced CFT column after 40 minutes. Steel has a higher thermal conductivity than concrete. This is because steel-reinforced CFT column has smaller concrete-only area than that of the non-reinforced one.

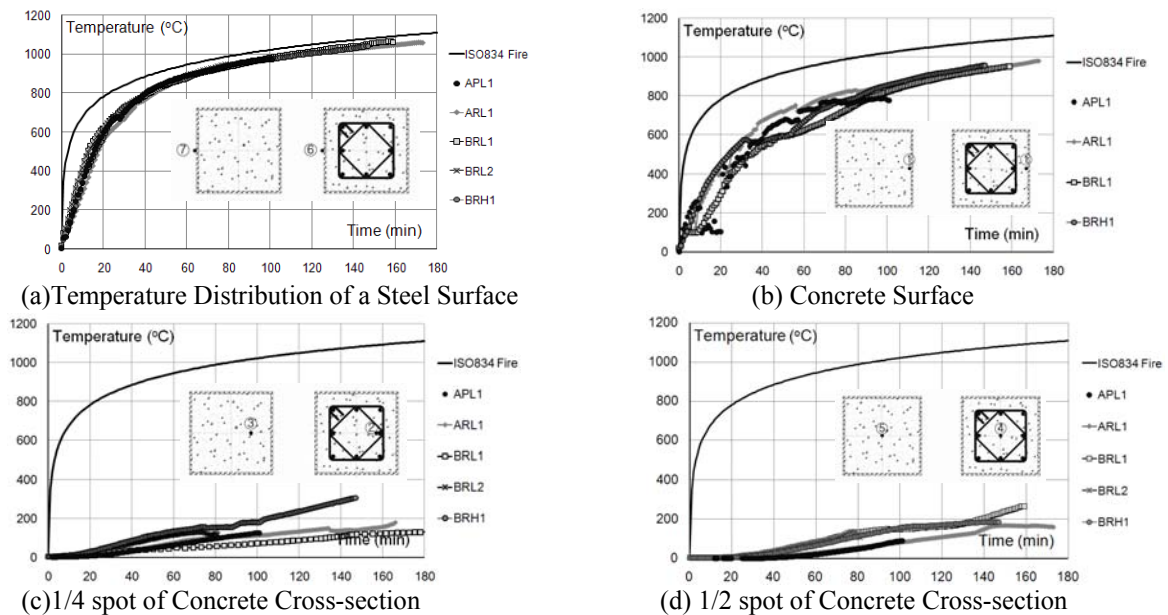


Fig. 5. Temperature Distribution of Steel and Concrete

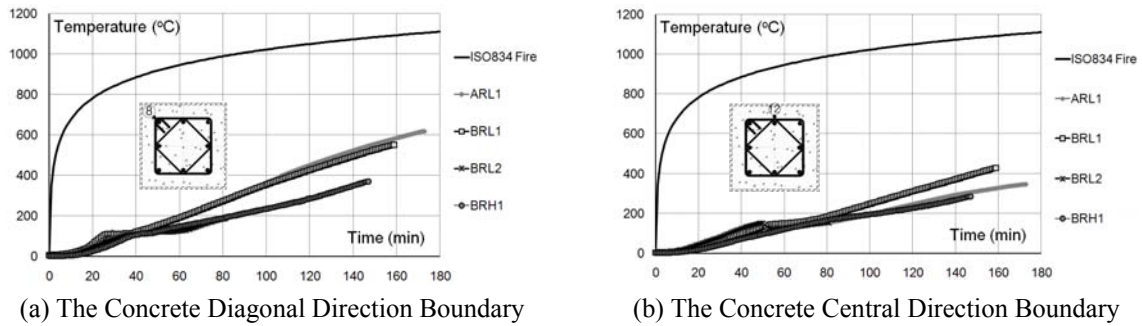


Fig. 6. The Temperature Distribution of Internal and External Boundary of Steel

In Fig. 6-(a) of the concrete diagonal direction boundary, the BRH1 specimen shows a reduction in the rate of temperature change in comparison with other specimens. This is attributable to a reduction of heat transfer by high-strength concrete, which has high density but minimal moisture content. With the ARL1 specimen, it is considered that the thermocouple location has changed due to the effect of concrete pouring after the installment of the thermocouple. In Fig. 6-(b) of the external concrete central direction boundary, there was the same distribution of temperature before 80 minutes, whereas other specimens show a higher increase rate of temperature except for ARL1 after 80 minutes. This is because of the thermal storage effect of the internal concrete area in which specimens with a smaller cross-section diameter than the others tend to have a higher temperature distribution.

## 2.2 Axial Deformation

To classify time–axial displacement relations, there are four stages: the section for steel resistance; load dislocation section; concrete resistance section; failure section. The section with the largest resistance against loading is the concrete resistance section. Fig. 8 shows the concrete resistance section collected from the Time–Curve Graph with the rate of each specimen. The 360mm cross-section steel-reinforced ARL1 specimen had a high resistance of 89%, demonstrating longer resistance as compared with the 77% of a non-reinforced APL1 specimen. This is because concrete-coated steel has the effect of thermal storage, thereby creating a long resistance to loading, as shown in the temperature distribution. Moreover, the BRL1 specimen is 79% resistance, showing a short section in comparison with the ARL1 specimen. This is because the steel area decreased by 65%. In the case of the BRL2 specimen, the loading rate against the strength of specimens is 0.6, which is the case of overloading, showing a significantly low fire resistance. The BRH1 specimen is a steel-reinforced CFT column with the application of high-strength concrete. High-strength concrete has low fire resistance due to its lower moisture content than that of normal-strength concrete. However, with steel reinforcement, fire resistance can be improved, thanks to the confining effect of steel. The BRH1 specimen has approximately 89% of concrete resistance section.

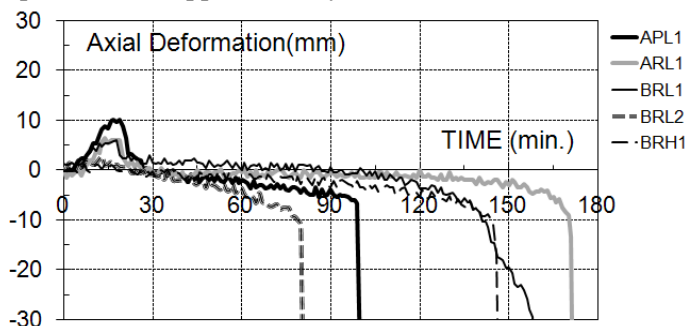


Fig. 7. The Axial Displacement by CFT column in fire resistance under load

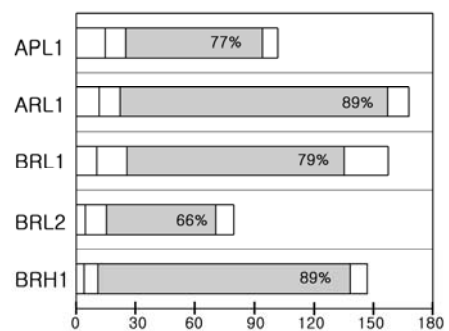


Fig. 8. The Sectional Ratio of Concrete Load resistance by each Specimen

### 2.3 Failure Mode

The APL1, ARL1, BRL1 specimens were set to have an axial force rate of 0.4 for fire resistance test under load, and 1/3 spot from the upper had local buckling. In the case of BRH1, which had steel-reinforcement and high-strength concrete, steel column fractured at the 1/3 spot where local buckling took place. The BRL2 specimen with an axial force rate of 0.6 had a total buckling of a column. Except for BRL2 specimen with 90 minutes or less in terms of fire resistance time, all other four specimens had separation on the surface of steel columns.



(a) A CFT column before the Experiment (b) BRH1 Specimen after the Experiment (c) BRL2 Specimen after the Experiment (d) Separation and column Fracture of BRH1 Specimen

Fig. 9. A CFT Column Before and After the Experiment

## 3 ANALYSIS OF FIRE RESISTANCE INFLUENCING FACTORS

### 3.1 The Effect of Steel Reinforcement

Fig. 10 compares a non-reinforced CFT square column (APL1) and steel-reinforced CFT square column (ARL1). Both specimens were set to have an axial force rate of 0.4. In the case of the ARL1 specimen, working axial force increased approximately by 14% due to the 2% increase in steel reinforcement. As for the fire resistance, it was identified to have an approximately 70% increase, from 99 minutes to 171 minutes. This is because the steel is coated in concrete as in Fig. 6 of the Temperature Distribution of Boundary of Steel with up to 160 minutes of thermal storage effect, and concrete and steel create a composite effect, securing the target three-hour fire resistance until local buckling occurs.

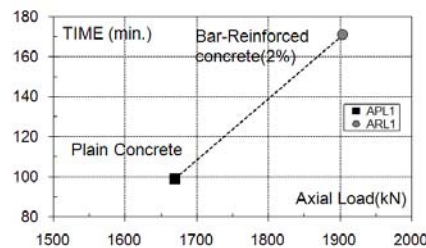


Fig. 10. The Effect of Concrete Reinforcement

### 3.2 The Effect by Parameters in Steel Reinforcement

Fig. 11 summarizes the comparison of a steel-reinforced CFT square column according to each major influencing factor, such as cross-section diameter, axial force ratio and concrete strength. As the cross-section diameter increases from 280 mm to 360 mm, the area of a CFT column increased approximately by 65%, whereas fire resistance increased approximately by 8%, from 158 minutes to 171 minutes. As axial force ratio was set to be 0.6 from 0.4, the working axial force increased by 607kN, whereas fire resistance decreased approximately by 50%. Moreover, as concrete strength from 36.09Mpa to

56.81MPa increased from normal strength to high strength, fire resistance decreased by approximately 6%, from 158 minutes to 147 minutes. The result of the analysis shows that the axial force ratio appeared to have the largest portion in determining the fire resistance of specimens. Moreover, as in Fig. 9 of failure mode, when the axial force ratio was 0.4 of low axial force, local buckling occurred at the end of fire resistance. However, when the axial force ratio was 0.6 of high axial force, total buckling on a column occurred.

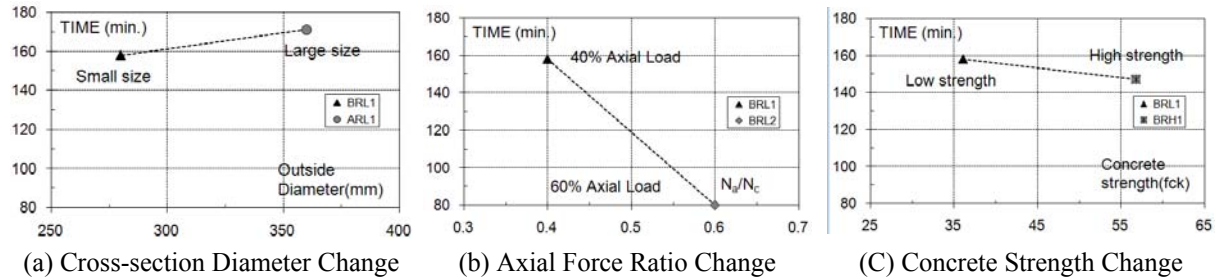


Fig. 11. The Effect of Influencing Factors in Steel Reinforcement

#### 4 CONCLUSION

The study was conducted to evaluate the fire resistance of a steel-reinforced CFT square column under a certain degree of axial force. In order to meet the required three-hour fire resistance, non-reinforced CFT square column and a steel-reinforced CFT square column were compared. The effects of the major influencing factors in steel reinforcement on the fire resistance of the inside column, such as cross-section diameter, axial force ratio and concrete strength change, were compared and analyzed.

The result of the fire resistance comparison between a non-reinforced CFT square column and a steel-reinforced CFT square column shows that in the case of a CFT column with a 2% steel reinforcement, working axial force increased approximately by 14%, whereas fire resistance increased approximately by 70%, from 99 minutes to 171 minutes when the axial force ratio was set at 0.4. Accordingly, it was determined that the target three-hour fire resistance was achieved.

Following the comparison of the major influencing factors with a steel-reinforced CFT square column, it was found that 8% of fire resistance increased when increasing the area by 65%, and the cross-section diameter from 280 mm to 360 mm. When increasing the axial force ratio from 0.4 to 0.6, fire resistance decreased by 50%. Moreover, when increasing concrete strength from 36.09MPa to 56.81MPa, there was a strength decrease of approximately 6%. Accordingly, in the case of fire resistance experiment designed in the study, the effect of cross-section diameter and concrete strength appeared to be minimal, whereas the axial force ratio appeared to play a significant role as the major parameter.

#### REFERENCES

- [1] Park S.H., Ryoo J.Y., Chung K. S., Choi S.M., An Evaluation for the Fire Resistance of Concrete-filled Steel Square Tube Columns under Constant Axial Loads, *KOREAN SOCIETY OF STEEL CONSTRUCTION*, 2007
- [2] Park S.H., Chung K. S., Choi S.M., A Study on Failure Prediction and Design Equation of Concrete Filled Square steel Tube Columns under fire Condition, *International Journal of STEEL STRUCTURES*, 2007
- [3] Chung K. S., Park S.H., Choi S.M., Material effect for predicting the fire resistance of concrete-filled square steel tube column under constant axial load, *Journal of Constructional Steel Research*, 2008
- [4] V.K.R Kudur., Design Equations for Evaluating Fire Resistance of SERC-filled HSS Columns, *Journal of Structural Engineering*, 1998
- [5] Y.C Wang., Steel and Composite Structures-Behaviour and Design for Fire Safety, *Spon press-Taylor & Francis Group*, 2002
- [6] ISO, Fire Resistance Test-Elements of Building Construction, *ISO 834*, 1975

## CALCULATION OF TEMPERATURE DISTRIBUTION IN COMPOSITE COLUMNS

Yuan Weifeng, Tan Kang Hai

School of Civil & Environmental Engineering, Nanyang Technological University, Singapore 639798

### INTRODUCTION

An accurate prediction of temperature distribution across a section for a given fire condition plays a key role in the simulation of thermal effect in structural analyses [1, 2]. In numerical modeling, fiber model is frequently applied to column members since it offers a good balance between simplicity and accuracy [3, 4]. According to this model, the cross-section of a column member is divided into a matrix of fibers; each of these fibers can have different material, thermal and mechanical properties. Normally, to simplify the simulation, the temperature in a fiber is assumed to be uniform along the longitudinal direction of members. Currently, several existing methods can be used to predict the temperature distribution on column members in numerical analysis that is based on fiber model, such as finite element analysis (FEA) [5], boundary element method (BEM), analytical approach [6] and engineering assumption [7]. Among these methods, FEA is the most popular tool used by engineers to conduct heat transfer analysis. However, due to the meshing of the cross-section, it is tedious to incorporate FEA of heat transfer into fiber model formulations. Compared with FEA, BEM seems more convenient to be used since it only requires discretization on the boundaries of the cross-sections of beams and columns. But, BEM will become inefficient if the fibers have many different types of material properties. Although analytical approach is the basis of numerical validations for FEA and BEM, its use is rather limited. Engineers resorting to analytical approach will encounter great difficulties when dealing with a cross-section of complex shape consisting of anisotropic material. The fourth approach — engineering assumption supposes that the temperature distribution on a cross-section follows a linear or quadratic function in spatial domain. This method is easy to use but lacks rigor. To overcome the difficulties mentioned above, the authors propose a mesh-free method based on cellular automaton (CA). The history of CA can be traced back to 1940s when Von Neumann et al. studied biological reproduction and crystal growth [8]. Since then, CA has been used to model complex phenomena in various areas such as fluid dynamics [9], biology [10] and emergency evacuation [11, 12]. Basically, CA is a discrete model which consists of a regular grid of cells, each cell in one of a finite number of states. In a CA model, time is also discretized into finite number of steps, and the current state of a specific cell is influenced and determined by the states of its neighboring cells at the last time step. When CA is applied to heat conduction problems, the rules which dominate the simulation are deduced directly from physical phenomenon instead of solving differential equations. To implement the CA approach, random nodes are generated within a domain and along its boundary as well. Since meshing is not required, this approach can be used to model domains with arbitrary boundaries. Moreover, it can also be used to calculate the temperature distribution in non-homogeneous materials. Therefore, the proposed approach provides a useful and practical numerical tool to simulate heat conduction in composite structural members, such as composite concrete columns with embedded I-section steel.

# 1 FORMULATION

Generally, a CA model requires the spatial domain to be discretized into regular cells. Besides, the time domain is divided into a series of intervals. As a main feature, a CA model is established based on several local rules which relate the current state of a particular cell to the states of its neighbouring cells at the last time step. To analyze heat conduction in solids, this basic concept of CA is extended in the present study. Firstly, irregular grid of random nodes in spatial domain is used to replace regular cells in traditional CA. Secondly, a virtual time domain is generated and divided into constant intervals to match the features of CA. In this paper, only steady-state heat conduction is discussed, although with some modifications, the method may also be extended to transient-state heat conduction.

Consider an arbitrary 3-dimensional solid domain  $\Omega$  as shown in Figure 1. The term  $T_i$  is the temperature at an arbitrary point  $P_i$  within  $\Omega$ . The point  $P_i$  is located at the centre of its neighbouring area which is illustrated by a sphere with a radius  $r_0$ . Within the sphere,  $P_j$  is a typical node among  $N_i$  monitoring points. Similar to  $P_i$ , the temperature at point  $P_j$  is denoted by  $T_j$ . To construct a CA model, the relationship between point  $P_i$  and other points within its neighbouring sphere is defined by Eq. (1).

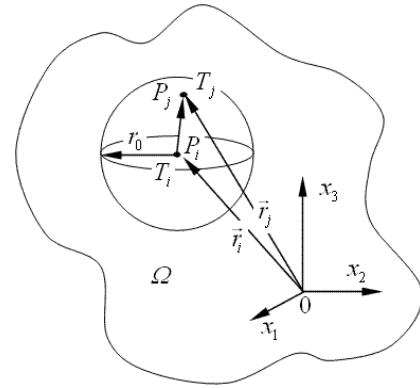


Figure 1. Illustration of an arbitrary three-dimensional domain

$$T_i = \sum_{j=1}^{N_i} \omega_{ij} T_j \tag{1}$$

where  $\omega_{ij}$  is weighting factor where subscript i denotes point  $P_i$  and j relates the congregate effects of temperatures at neighbouring points  $P_j$ . Thus, clearly, from Eq. (1), the temperature at point  $P_i$  is determined by temperatures at its neighbouring points. This rule is based on the assumption that the variable  $T_i$  will not vary too much within a very small sphere. It is assumed that there is continuous variation of temperature over distance within the sphere. Eq. (1) also indicates that the influence of point  $P_j$  to  $T_i$  is dependant on the value of weighting factor  $\omega_{ij}$ . Assuming that the material in the domain is non-homogeneous,  $\omega_{ij}$  is given by Eq. (2):

$$\omega_{ij} = (k_i + k_j) / \sum_{l=1}^{N_i} (k_i + k_l) \tag{2}$$

where  $k_i$ ,  $k_j$  and  $k_l$  are thermal conductivities at points  $P_i$ ,  $P_j$  and  $P_l$ , respectively. One

observes that  $\sum_{j=1}^{N_i} \omega_{ij} = 1$ .

From Eqs. (1) and (2), one finds that the temperature of each point within the neighbouring area of  $P_i$  affects the value of  $T_i$ . The definition given in Eq. (2) accords with physical law in that, the larger the average thermal conductivity between points  $P_i$  and  $P_j$ , the closer are the temperatures at these two points.

To complete the construction of the CA model, Eq. (1) is extended to Eq. (3) by incorporating virtual time steps t:

$$T_i(t_m) = \sum_{j=1}^{N_i} \omega_{ij} T_j(t_{m-1}) \quad (3)$$

The interpretation for Eq. (3) is that the temperature at  $P_i$  at  $t_m$  is determined by the temperatures at neighbouring points of  $P_j$  at previous time step  $t_{m-1}$ .

To implement the CA model described above, similarly to points  $P_i$  and  $P_j$ , one can define randomly many points within  $\Omega$  and on its boundary. During an analysis, the temperature at each point is updated according to Eq. (3) until it converges to a stable value. The final values of the temperature at each point form a state which represents the solution of the particular domain. One may realize that Eqs. (1) ~ (3) are entirely based on physical intuition of the heat conduction phenomenon. Differential equations are not involved in the derivation. Like traditional CA model, the procedure to calculate the distribution of temperature forms a loop which contains the following steps:

- (1) Generate random nodes in the modelled domain and on its boundary.
- (2) Assign an initial value to each node where temperature is unknown.
- (3) Based on the state at time  $t_{m-1}$ , calculate the temperature at each node at  $t_m$  using Eq. (3).
- (4) Repeat step (3) till the final time step  $t_M$ . At  $t_M$ , temperature at each node cannot be updated compared with previous time  $t_{M-1}$ .

## 2 NUMERICAL EXAMPLES

**Example 1:** As shown in Figure 2, a rectangular two-dimensional domain a-b-d-c is subjected to thermal conditions. In the domain, the varying thermal conductivity of the material is described by the function  $k(x, y) = e^{x^2 - y^2}$  where  $x$  and  $y$  represent the physical domain. On the boundaries, it is assumed that the temperatures are known as  $T_{ab} = 0$ ,  $T_{ac} = 0$ ,  $T_{bd} = 2y$  and  $T_{cd} = x$ .

For comparison purpose, the analytical solution is derived for this example. From the heat transfer theory, one knows that Eq. (4) is the governing partial differential equation for example 1.

$$\partial(k \partial T / \partial x) / \partial x + \partial(k \partial T / \partial y) / \partial y = 0 \quad (4)$$

The solution of Eq. (4) can be obtained without difficulty. Its expression is:

$$T = xy \quad (5)$$

The diagonals a-c and d-b can be respectively described by  $y = x/2$  and  $y = 1 - x/2$ . Hence, the temperature distributions on the diagonals of rectangle a-b-d-c can be derived:

$$T = \begin{cases} x^2/2, & (y = x/2) \\ x - x^2/2, & (y = 1 - x/2) \end{cases} \quad (6)$$

On the other hand, to evaluate the temperature distribution using CA method, 1200 points inside the domain and 120 points along the four edges are generated randomly, as shown in Figure 3. In the figure, there are 21 points (in red dots) distributed along the two diagonals of rectangle a-b-d-c. Temperatures at these points are used for comparison with analytical answers given by Eq.(6). The value of spatial distance of the sphere  $r_0$  is set to 0.1 in the calculation.

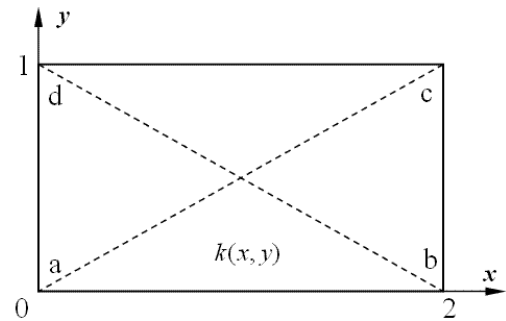


Figure 2: A rectangular domain under thermal conditions

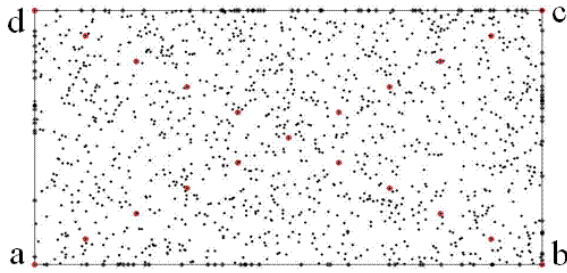


Figure 3 Distribution of points generated randomly in example 1

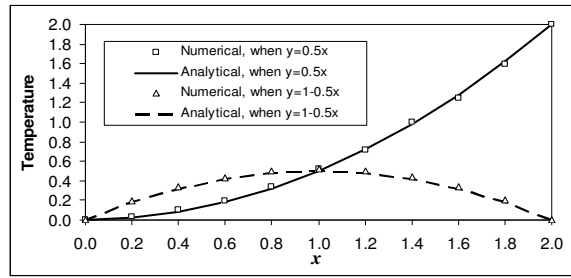


Figure 4: Numerical and analytical temperatures on diagonal lines

Both numerical and analytical results are depicted in Figure 4. It can be seen from the figure that the CA predictions agree very well with the analytical results. In fact, to minimize numerical errors, one can conduct several trial runs based on different distribution of random points. The average values of all trial run results will be more accurate.

During the study, it has also been found that the accuracy of simulation is affected by the number of nodes and the value of  $r_0$ . In general, more nodes will result in more accurate results. This feature of CA model is no different from FEA or BEM. However, large amount of random nodes will require longer CPU time.

**Example 2:** Figure 5 shows the cross-section of a rectangular composite concrete column modelling using fiber model. It can be seen that an I-section steel is embedded in the concrete interior. The dimensions and the thermal boundary conditions are illustrated in the figure. In the analysis, it is assumed that the temperatures on the top and bottom boundaries are  $T_1 = 100^\circ C$  and  $T_2 = 500^\circ C$ , respectively. It is also defined that  $k_C / k_S = 1/50$  where  $k_C$  and  $k_S$  denote the thermal conductivities of concrete and steel, respectively.

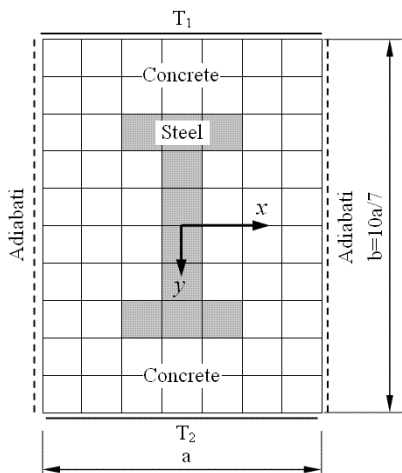


Figure 5. The cross-section of a composite concrete column

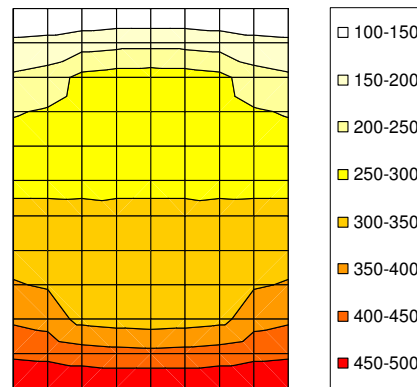


Figure 6. Temperature distribution on the cross-section of a composite concrete column

It should be mentioned that the segments on the cross-section are generated for fiber model. However, if heat conduction is required, these segments can be used to calculate the temperature distribution based on the proposed CA model. In this problem, the central points of all segments coincide to form a grid of CA cells, as shown in Figure 5. Thus, the present CA approach can be directly applied.

As shown by the temperature contour in Figure 6, the temperature distribution on the cross-section is symmetric about the column centroid  $x = 0$ . Along  $y$  direction, between  $y = b/2$

and  $y = -b/2$ , the temperature increases gradually from  $T_1$  to  $T_2$ . More details can be seen in Figures 7 and 8. However, it is noteworthy that the temperature on the column cross-section is not linearly distributed.

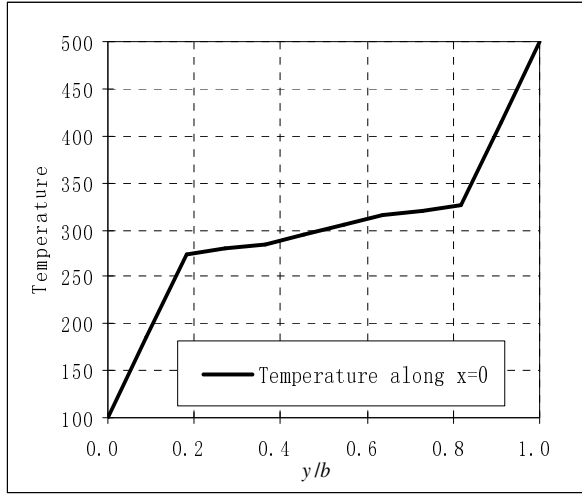


Figure 7. Temperatures along  $x = 0$

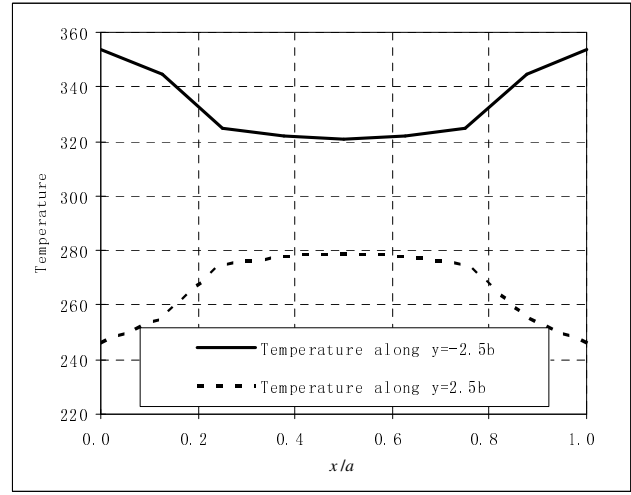


Figure 8. Temperatures along  $y = \pm 2.5b$

### 3 THE RELATIONSHIP BETWEEN DIFFERENTIAL EQUATION AND CA

The two examples illustrate that the proposed CA model can be used as a numerical tool to analyze steady-state heat conduction, although the local rules incorporated into the CA model are deduced without the consideration of differential equation. However, it should be realized that differential equation is an analytical tool applied to the same problem. Hence, it is believed that there exists a relationship between the present CA model and classical differential equation since they both describe the problem correctly. It is well-known that one-dimensional heat conduction is governed by:

$$d(k dT/dx)/dx = 0 \quad (7)$$

Based on this, one infers that  $k dT/dx = C_1$  where  $C_1$  is a constant. Applying classical limit theorem to Eq. (7), one obtains:

$$\lim_{x_j \rightarrow x_i} (k_j T_j - k_i T_i)/(x_j - x_i) = C_1 \quad (8)$$

Let spatial distance  $\Delta_{ji} = x_j - x_i$  and thermal conductivity  $k_j = k_i = (k_j + k_i)/2 = \eta_{ji}$  arbitrarily. By applying Eq. (8) to all points within the neighbouring domain of point  $P_i$ , one obtains Eq. (9).

$$\sum_{j=1}^{N_i} \eta_{ji} (T_j - T_i) = C_1 \sum_{j=1}^{N_i} \Delta_{ji} \quad (9)$$

Thus,

$$\sum_{j=1}^{N_i} (\eta_{ji} T_j) - \left( \sum_{j=1}^{N_i} \eta_{ji} \right) T_i = C_1 \sum_{j=1}^{N_i} \Delta_{ji} \quad (10)$$

It should be noted that  $P_j$  is a random point in the neighbourhood of  $P_i$ . Therefore, according to statistics, the term  $C_1 \sum_{j=1}^{N_i} \Delta_{ji} \rightarrow 0$  when  $N_i$  is large enough. For this situation, one obtains:

$$T_i = \frac{\sum_{j=1}^{N_i} (\eta_{ji} T_j)}{\sum_{l=1}^{N_i} \eta_{li}} = \sum_{j=1}^{N_i} \omega_{ij} T_j \quad (11)$$

## 4 CONCLUSION

Based on the concept of cellular automata, a new numerical approach is developed without the consideration of differential equation for analyses of heat conduction in anisotropic domain. Numerical examples show that this approach can be applied to steady-state heat conduction. Since CA is a mesh-free method, the proposed approach is convenient to use when it is incorporated into the fiber model in structural analyses for composite concrete beams or columns. Additionally, no complicated mathematical derivation is required during the development of the proposed approach. The numerical implementation of this model is simple because it is based on one local rule (Eq. (1)). After necessary improvement, such a methodology can be used in other fields, for instance, columns subjected to torsion since this kind of problems is governed by Poisson equation. In this study, only steady-state heat conduction is discussed. So it would be more meaningful to develop a new CA model for transient problems in the future.

## REFERENCES

- [1] Tan KH, Yuan WF, Buckling of Elastically Restrained Steel Columns under Longitudinal Non-Uniform Temperature Distribution, *Journal of Constructional Steel Research*, (2008) 64: 51-61.
- [2] Tan KH, Yuan WF, Inelastic Buckling of Pin-ended Steel Columns under Longitudinal Non-uniform Temperature Distribution, *Journal of Constructional Steel Research*, (2009) 65 (1): 132-141.
- [3] Spacone E, Filippou FC, Taucer FF, Fibre Beam-column Model for Non-linear Analysis of R/C Frames: Part I. Formulation, *Earthquake Engineering and Structural Dynamics*, (1996) 25: 711-725.
- [4] Spacone E, Filippou FC, Taucer FF, Fibre Beam-column Model for Non-linear Analysis of R/C Frames: Part II. Applications, *Earthquake Engineering and Structural Dynamics*, (1996) 25: 727-742.
- [5] Huang ZF, Tan KH, Phng GH, Axial Restraint Effects on the Fire Resistance of Composite Columns Encasing I-section Steel, *Journal of Constructional Steel Research*, (2007) 63 (4): 437-447.
- [6] Wang ZH, Tan KH, Radiative Heat Transfer for Structural Members Exposed to Fire: An Analytical Approach, *Journal of Fire Sciences*, (2008) 26 (2): 133-152.
- [7] Tan KH, Ting SK, Huang ZF, Visco-elasto-plastic Analysis of Steel Frames in Fire, *Journal of Structural Engineering-ASCE*, (2002) 128 (1): 105-114.
- [8] Von NJ, Burks AW, *Theory of Self-reproduction Automata*, University of Illinois Press, Urbana, (1966).
- [9] Wolfram S, Cellular Automaton Fluids 1: Basic Theory, *Journal of Statistical Physics*, (1986) 45 (3/4): 471-526.
- [10] G. Bard Ermentrout and Leah Edlestein-Keshet. *Journal of Theoretical Biology*, 160, January (1993) 97-133
- [11] Yuan WF, Tan KH. An Evacuation Model using Cellular Automata, *Physica A*, (2007) 384 (2): 549-566.
- [12] Yuan WF, Tan KH. A Novel Algorithm of Simulating Multi-velocity Evacuation Based on Cellular Automata Modeling and Tenability Condition, *Physica A*, (2007) 379 (1): 250-262.

## PARAMETRIC NUMERICAL ANALYSIS OF STEEL AND CONCRETE COMPOSITE FLOORS EXPOSED TO ISO FIRE

Mohsen Roosefid and Bin Zhao

CTICM - Centre Technique de la Construction Métallique, Paris, France

### INTRODUCTION

In recent years, increasing interest has been observed throughout Europe in developing steel and concrete composite construction, i.e. the floors are constructed using composite slabs with profiled steel decking attached through shear connectors like headed studs to downstand beams. Indeed, the full-scale natural fire tests in the steel framed buildings have shown the beneficial effects of membrane forces in improving the load-carrying capacity of composite floor system, compared to estimates of capacity based on only flexural behaviour. From observation and analysis of these full scale natural fire tests, a new fire design concept (design method and corresponding design guide) was developed in UK concerning modern multi-storey steel-framed buildings using composite floor systems [1]. This design method is aimed at fire resistance assessment of partially protected composite floors not only under natural fire condition but also in a standard ISO fire situation. In order to extend this design concept to other European countries, the dissemination project FRACOF [2] has been launched in 2007 and within the scope of this project, a demonstration full scale fire test was carried out to show the fire behaviour of steel and concrete composite floors exposed to the ISO fire. The steel and concrete composite floor used in this test was supported by four columns, occupying an area of 7.35 m by 9.53 m, so around 70 m<sup>2</sup>. All steel structural members were designed in accordance with the requirement related to simple design rules of EN1994 [3, 4].

The mechanical loading of the floor is applied using fifteen sand bags uniformly distributed over the floor, each of which weighs exactly 15.0 kN leading therefore to an equivalent uniformly distributed load of 3.87 kN/m<sup>2</sup> (see *Fig. 1*).

In compliance with the existing simple engineering design method of such type of floor, the two secondary beams and the composite slab are unprotected. However, all the boundary beams of the floor (all beams in direct connection with columns) are fire protected to ensure a global structural stability under fire situation.

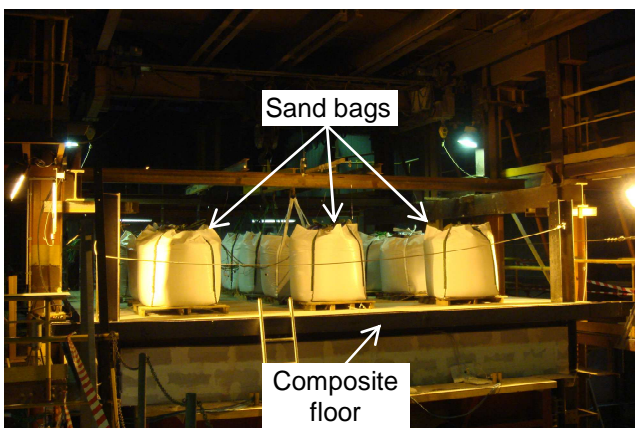


*Fig. 1.* Loading of the floor with sand bags



*Fig. 2.* View below the floor inside fire furnace after the test

The states of the floor before and after the fire are shown in Fig. 2. The experimental results illustrated clearly the excellent fire performance of partially protected composite floors with adequate reinforcing steel mesh under membrane action for a long ISO fire duration exposure. Further to above fire test, based on a 3D numerical modelling validated against the experimental results within this research project, a numerical parametric investigation is performed in order to enlarge the verification field of the design method.

### 1 VALIDITY OF DEVELOPED NUMERICAL MODELLING

Before the presentation of the parametric study, it is important to get an idea about the validity of adopted numerical model from the computer code ANSYS. In fact, the developed numerical model is composed of two different parts, one for heat transfer analysis and another one for structural analysis.

#### 1.1 Heat transfer analysis

The heating of all structural members is predicted with help of 2D models using their typical cross sections. As the validation of the numerical model concerns mainly the structural behaviour of the floor, the thermal properties of insulation material is adjusted so that the prediction of a heating of protected steel members is as close as possible to reality. However, as far as steel and concrete are concerned, their thermal properties are those given in EN1994-1-2 [4].

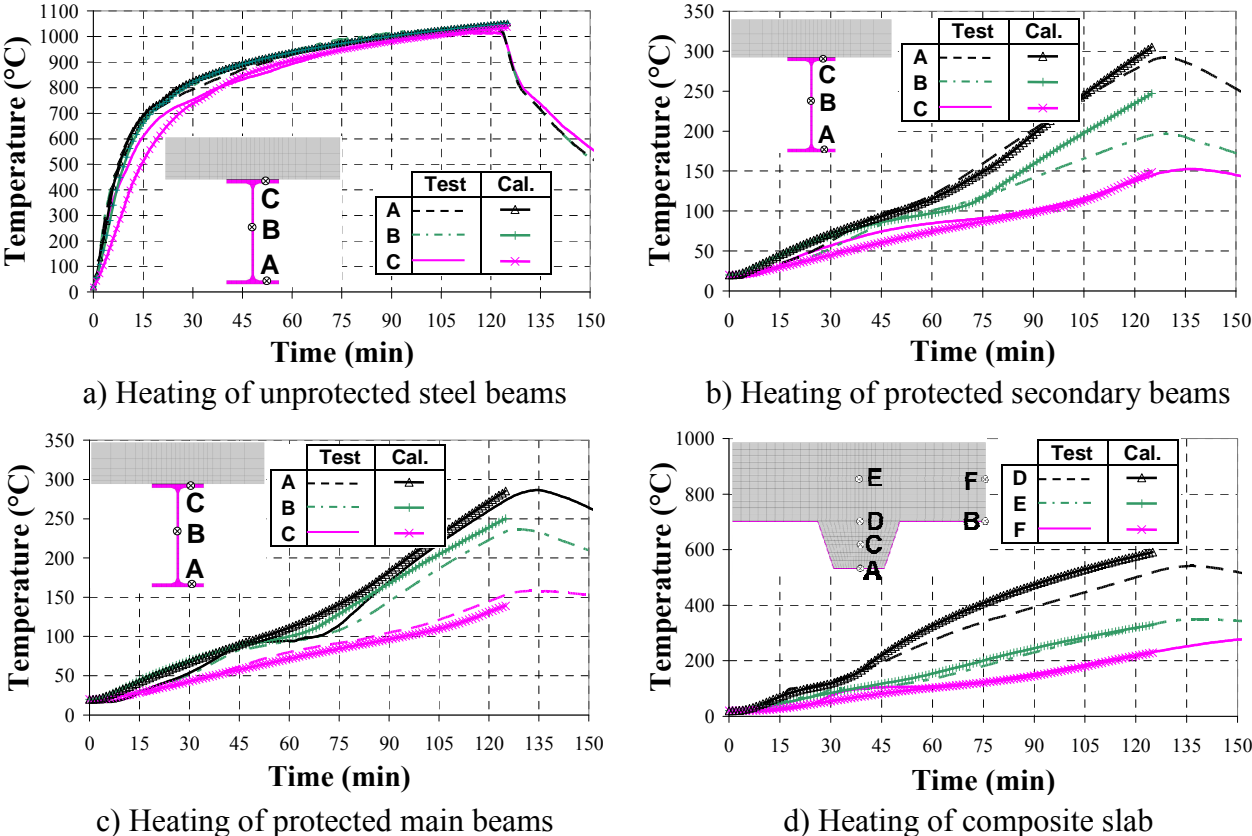


Fig. 3. Temperature comparison between test and numerical calculation

A comparison of calculated temperatures with measured ones during the test for different structural members is illustrated in Fig. 3. From this comparison, can be found an excellent agreement between test and numerical modelling which constitutes also a good basis for mechanical analysis.

## 1.2 Mechanical behaviour of structural members

The analysis is based on a hybrid structural model which takes account of steel beams, steel sheet, concrete rib, concrete slab and reinforcing steel mesh (see Fig. 4).

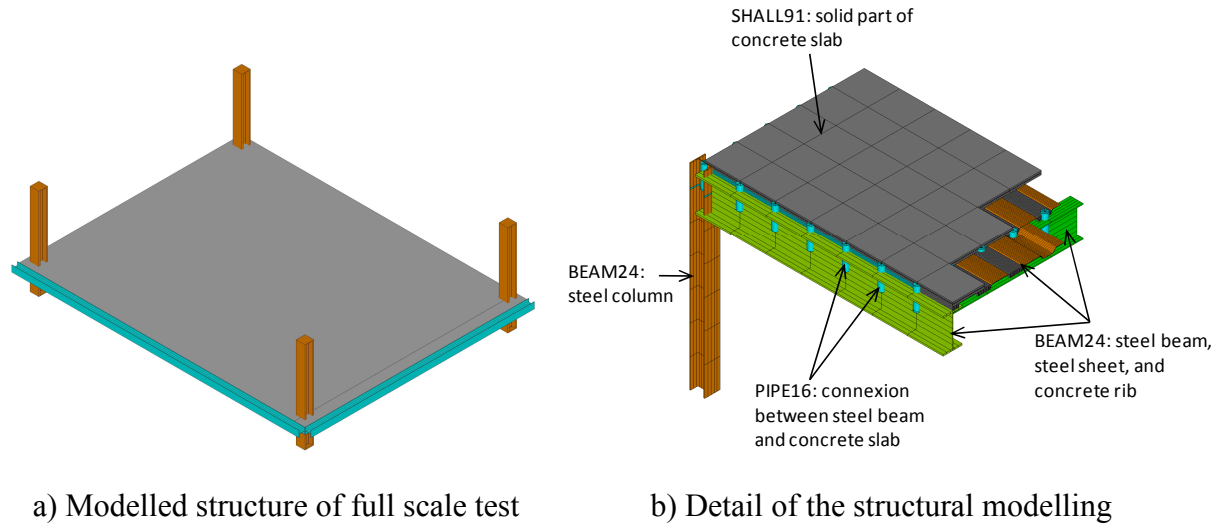


Fig. 4. Numerical modelling for structural analysis of full scale ISO fire test

In this structural modelling, the steel structural members are represented by 3D non-linear line element of BEAM24. As for concrete part over the steel sheet, a layered orthotropic shell element SHELL91 was used. The connection between steel beam and concrete slab was modelled using 3D linear line element PIPE16.

The structural behaviour of the floor is then analysed on the basis of previously calculated temperatures and a global structural model. The simulated structural behaviour of the floor is shown in Fig. 5 which illustrates the deformed shape predicted by the numerical model at 120 minutes of ISO fire.

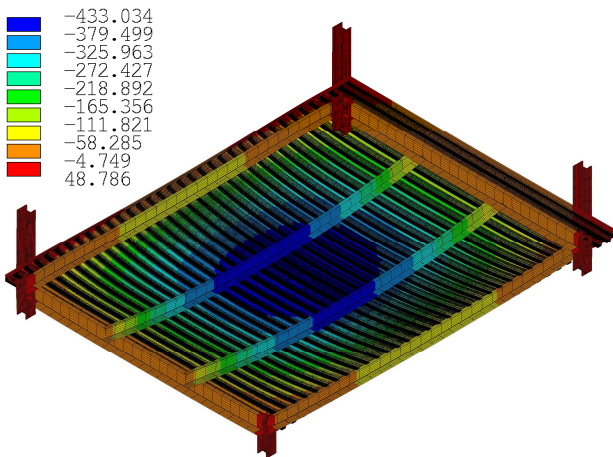


Fig. 5 Simulated deformed shape of the floor

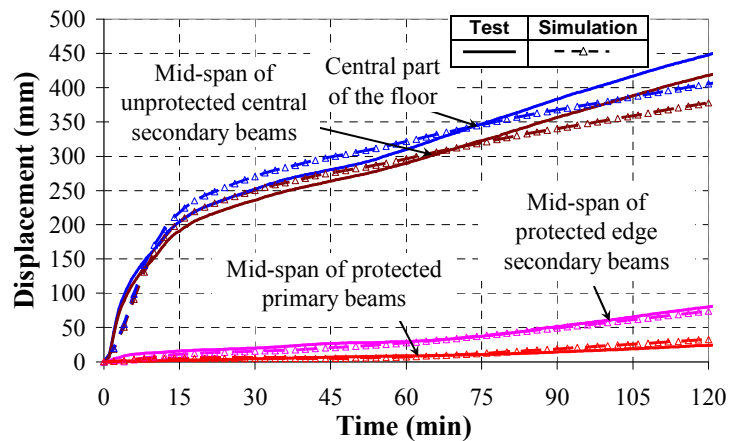


Fig. 6 Comparison of the predicted deflection and the floor recorded during the heating period of test

A comparison of floor vertical displacements between numerical calculation and test is shown in Fig. 6. It can be observed that globally the numerical modelling follows very closely the test results. However, a very slight discrepancy seems to occur after 75 minutes of fire for unprotected steel beams due to the fact that at about 50 minutes of fire test one of welded joints between two steel reinforcing meshes started to break which induces a small change in

the floor behaviour. Despite this small difference, the validity of the numerical model as well as its capacity of predicting in good way the fire behaviour of the composite floor is proved without any doubt. In consequence, the adopted numerical model can be applied more widely for global parametric investigation for a deeper check of the simple design method.

## 2 PARAMETRIC NUMERICAL STUDY

In order to take advantage of the tensile membrane action with composite floor systems subjected to fire, a new simple design method was proposed [1]. This simple design method gives designers access to whole floor behaviour and allows them to determine which members can remain unprotected while maintaining the safety level at least equivalent to that obtained with traditional design methods. This method is based on the yield-line approach of slab panels, which takes account of the enhancement due to membrane action of the slab and the beam systems. The details of the formulation are given in [6].

In order to extend the verification of this assessment method to its full application domain, a numerical parametric study on the basis of above advanced calculation model is performed, in which several specific features, such as deflection limit of the floor and maximum elongation of reinforcing steel are systematically checked.

### 2.1 Input data for parametric study

With the parametric study, the investigation of the simple design method may be extended to its full application domain. However, a full parametric study means at least several hundreds even more than thousand of numerical simulations, which necessitate a huge computation cost. Considering this situation is carried out only a reduced parametric study in which the following parameters are considered as the most representative or sensitive, resulting thus in a total of 112 numerical simulations.

#### 2.1.1 Grid size of the floor

With respect to grid size of floor investigated in the parametric study, were adopted seven values, which are respectively (in m) 6x6, 6x9, 6x12, 9x9, 9x12, 9x15 and 7.5x15 (Fig. 7). All boundary beams are assumed protected but all central secondary beams are supposed unprotected.

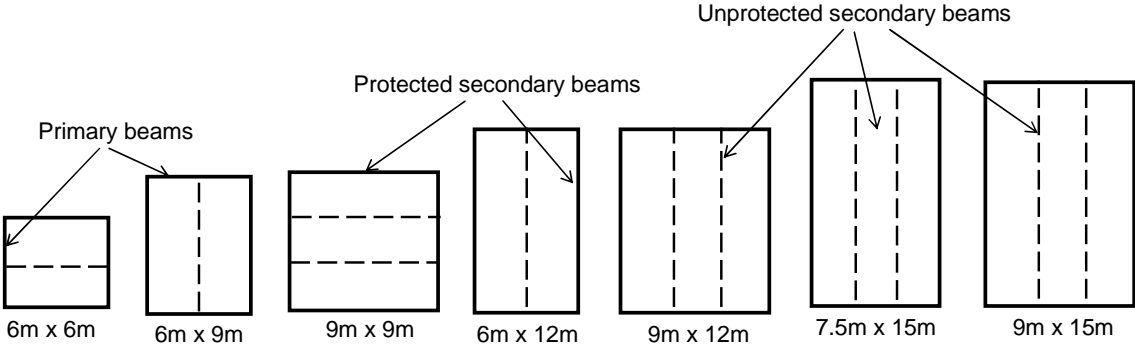


Fig. 7 Floors considered in the Parametric numerical study

#### 2.1.2 Load levels

Two load combinations corresponding to load values commonly used in room temperature design over French market, are considered in this study which are given in Table 1.

Table 1. Load combinations considered in this parametric study

| Case | Permanent load G                     | Live load Q           |
|------|--------------------------------------|-----------------------|
| 1    | Self weight + 1.25 kN/m <sup>2</sup> | 2.5 kN/m <sup>2</sup> |
| 2    | Self weight + 1.25 kN/m <sup>2</sup> | 5.0 kN/m <sup>2</sup> |

### 2.1.3 Link condition between floor and steel columns

The numerical analysis is conducted with two link assumptions, one of which considers that the composite slab is mechanically linked to steel columns with help of additional reinforcing bars and another one assumes that this link does not exist at all.

### 2.1.4 Fire duration

Four standard fire durations, that is 30, 60, 90 and 120 minutes, are investigated. As the necessary total depth of the composite slab depends directly on these fire durations, the minimum values according to the simple design method are adopted which are respectively 120, 130, 140 and 150 mm in case of open trapezoidal steel decking. Also, the size of all reinforcing steel mesh is derived directly from this simple design method. In addition, their axis distance is always taken as 45 mm. It has to be pointed out here that this parametric study considers only the steel decking of COFRAPLUS60. The reason of using such steel decking is due to the fact that it is not only, for the time being, the most commonly used one over French market but also the most open trapezoidal steel decking for composite slabs. One can understand easily that the composite slab using such steel decking will be the most critical from the point of view of mechanical resistance under fire situation. Therefore, if the simple design method is checked with this steel decking, the conclusion will be equally valid for any other types of steel decking.

### 2.1.5 Heating of boundary beams

In this parametric study, all peripheral beams are supposed to be heated up to 550 °C which corresponds to the critical temperature proposed for French market using such design concept.

## 2.2 Results of parametric study

For each numerical analysis, two special points of corresponding numerical results have been systematically checked, which are related to:

- maximum deflection of floor
- maximum mechanical strain of reinforcing steel

Concerning the deflection of floor, the first step of current investigation is to check whether the maximum allowable deflection is reached or not. In consequence, the maximum deflection obtained by numerical analysis in two cases, that is with and without link condition between floor and steel columns is compared to the maximum allowable deflections according to simple design method (SDM limit) and the results are illustrated in *Fig. 8*. It can be found that in any case, the maximum allowable deflection used as the validity limit of the simple design method is beyond the maximum deflection according to numerical analysis by assuming that the composite slab is mechanically linked to steel columns. Even if this link condition does not exist, the simple design method remains still valid as its deflection limit is exceeded only in very few cases.

In addition to the deflection of the floor, the elongation of reinforcing steel is the second feature which is investigated in detail in this parametric study. In reality, as the reinforcing

steel mesh is put over the whole area of the floor, it is certainly continuous across all beams including protected boundary beams. In this case, as the central part of the floor deflects largely under fire situation and meanwhile the protected boundary beams bows much less with their reduced heating, the reinforcing steel will then subject to important stretching in particular at the supports of protected boundary beams and around columns. If the elongation becomes too important, the failure could occur which may lead to following consequences: firstly the loss of integrity and insulation performance of the floor and secondly the reduced load bearing capacity as the continuous condition of the slab disappears. However, the question arises about the criterion to be applied to elongation capacity of reinforcing steel. According to EN1992-1-2 [5], the minimum elongation capacity among all types of reinforcing steel is at least 5%. Therefore, this value is taken as the maximum elongation that one can accept in this parametric study for reinforcing steel mesh.

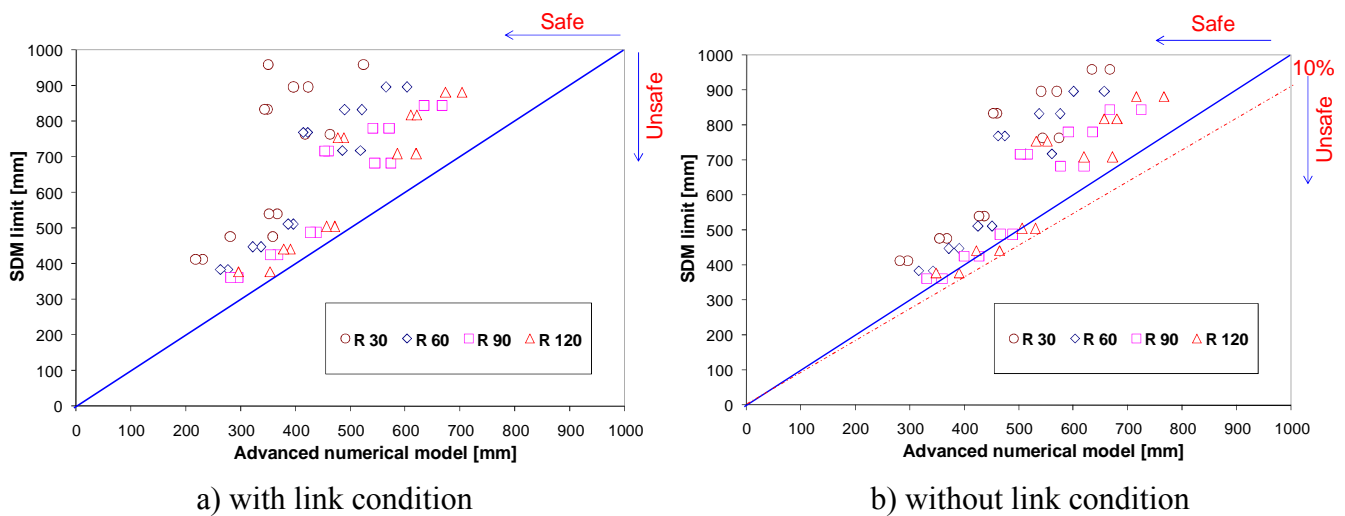


Fig. 8. Comparison of the deflection predicted by ANSYS with SDM limit

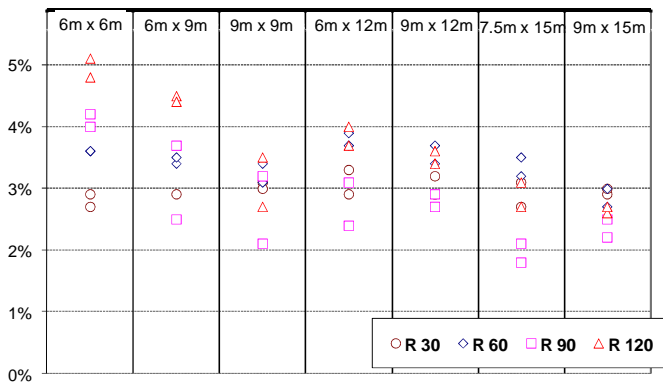


Fig. 9. Predicted maximum mechanical strain of reinforcing steel assuming no link condition

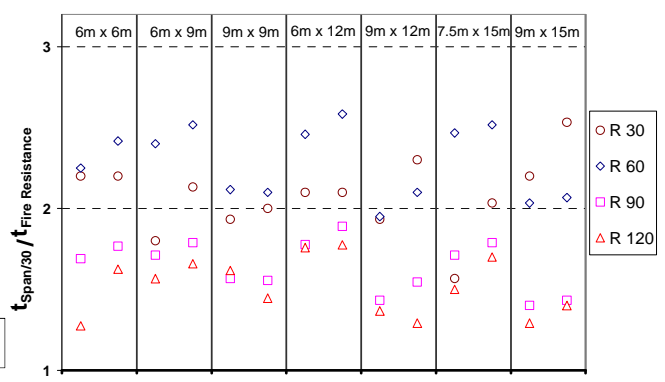


Fig. 10. Comparison between predicted fire ratings according to deflection criterion of span/30

Fig. 9 shows the predicted maximum mechanical strain of reinforcing steel according to numerical analysis by assuming no link condition, considering the most critical case. It can be found that the predicted maximum deflection of the floor varies in general between 2% and 5% which once again is satisfactory.

In addition, the fire resistance of a beam can be also expressed by fire ratings based on a total deflection limit not exceeding span/30 of all assembled structural members (primary beams, secondary beams, slabs). A special investigation is made in the numerical analysis to check

the necessary duration to reach this deflection criterion. If these durations are compared to corresponding standard fire ratings to be looked for (see *Fig. 10*), one can find that the ratio between them is always beyond one and in certain cases even more than two. Such results are very meaningful to show the validity of the simple design method which apparently provides the conservative fire ratings in comparison with advanced calculation tools.

## Conclusion

The objective of the parametric study is to make a detailed investigation of simple design method with help of advanced calculation models validated against ISO fire test. This investigation should lead to the improvement of simple design method if necessary. From obtained results, it can be concluded that:

- with respect to deflection criterion, the simple calculation method gives conservative results compared to advanced calculation models;
- concerning the elongation of reinforcing steel mesh, it remains generally below 5%, the minimum allowable elongation capacity recommended by EN1992-1-2 for all types of reinforcing steel.

The results derived from this parametric study show clearly that the simple design method is capable of predicting in a safe way the structural behaviour of composite steel and concrete floor subjected to ISO fire condition and there is no need to include additional limitation to this simple design method in its application to assess the fire performance of composite floor.

## Acknowledgements

The authors would like to give their acknowledgement to ArcelorMittal of which the financial support is highly appreciated.

## References

- [1] Fire Safe design: A new approach to multi-storey steel-framed buildings, Steel Construction Institute Publication no 288.
- [2] Zhao B., Roosefid M. and Vassart O., Full scale test of a steel and concrete composite floor exposed to ISO fire, SIF Conference proceeding, 2008
- [3] CEN, EN 1994-1-1, Eurocode 4: Design of composite steel and concrete structures" – Part 1-1: General rules and rules for buildings, *European Committee for Standardisation*, 2004
- [4] CEN, EN 1994-1-2, Eurocode 4: Design of composite steel and concrete structures, Part 1-2: General rules - Structural fire design, *European Committee for Standardisation*, 2005
- [5] CEN, EN 1992-1-2, Eurocode 2 "Design of concrete structures" – Part 1-2: Structural fire design, *European Committee for Standardisation*, 2003
- [6] Bailey C.G. and Moore D.B., The structural behaviour of steel frames with composite floor slabs subject to fire, Part 1: Theory, Part 2: Design, *The Structural Engineer*, 2000

## CELLULAR COMPOSITE BEAMS AT ELEVATED TEMPERATURES Experimental investigation

Gisèle BIHINA <sup>a</sup>, Bin ZHAO <sup>a</sup> and Olivier VASSART <sup>b</sup>

<sup>a</sup> CTICM, Saint-Aubin, France

<sup>b</sup> Arcelor Mittal, Luxembourg

### INTRODUCTION

Cellular beams offer long uninterrupted clear spans, which are ideal for offices. However, increasingly, questions are being asked about the performance of cellular beams in fire situation.

In order to overcome the present lack of knowledge, a research project, FIRE resistance of long span Cellular Beams (FICEB), has been carried out for more than one year [1]. In this project, four full-scale fire-tests of composite steel and concrete cellular beams were conducted over a fire furnace at the test facilities of Efectis France, the subsidiary of CTICM which is one of the partners of the project. These experiments aimed at investigating the fire behaviour of cellular beams under different configurations.

All these beams were made of a steel profile with circular and/or elongated web openings, connected by shear studs to a composite slab composed of a reinforced concrete part and a trapezoidal re-entrant deck spanning perpendicularly to the profile. The steel profile consisted of two “tees” from standard I-sections, which were welded together.

The first part of this paper describes the experimental set-up, whereas the results of the tests are given and discussed in the second part.

## 1 EXPERIMENTATION SET-UP

### 1.1 Beam geometric and material properties

An overall view of the four beams is shown in *Fig. 1*. As parts of composite floors, beams 1, 3 and 4 were considered to be secondary beams, and beam 2 was considered as a primary beam. They were fire designed according to [2].

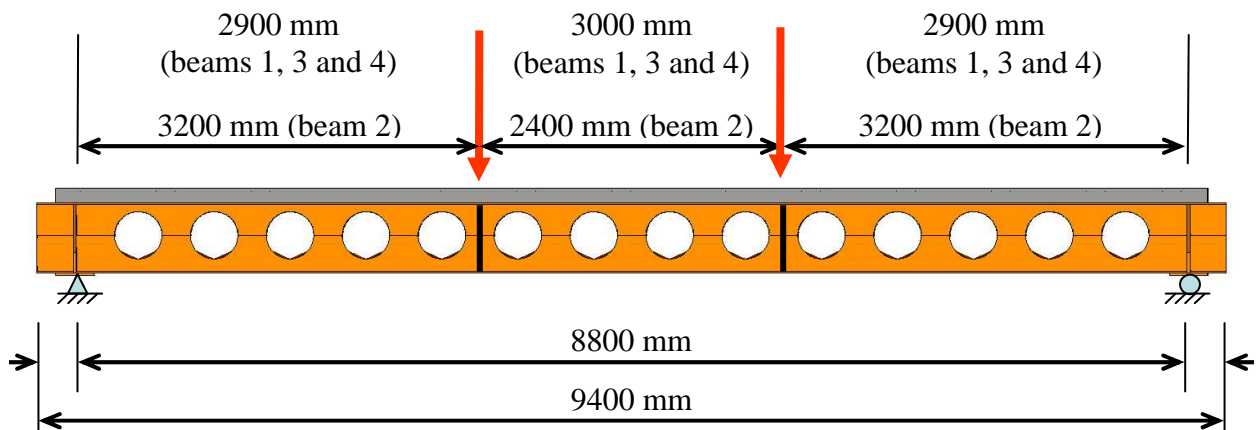


*Fig. 1.* Elevation view of the composite beams

The main geometric and material properties of the beams are shown in *Table 1* [1, 2, and 3]. In addition to the web stiffeners at load points and at its end supports, For beam 4, there was a one-side stiffener at each web-post. The upper steel flange was fully connected to the 120 mm deep composite slab, which comprised a COFRASTRA 40 ® re-entrant deck, via Nelson headed studs. The slab width was 2.20 m which equals to the effective width  $b_{eff}$  according to Eurocode 4 part 1.1 [4], i.e.  $2 \times L/8$ . As for the reinforcement steel, a mesh of 252 mm<sup>2</sup>/m was used.

|   | Beam 1  | Beam 2  | Beam 3  | Beam 4  |
|---|---------|---------|---------|---------|
| <b>Top tee section</b>                            | IPE 360 | IPE 450 | IPE 360 | IPE 360 |
| <b>Top tee depth <math>h_{top}</math> (mm)</b>    | 255     | 275     | 255     | 255     |
| <b>Bottom tee section</b>                         | IPE 450 | IPE 450 | HEB 450 | IPE 450 |
| <b>Bottom tee depth <math>h_{bot}</math> (mm)</b> | 300     | 275     | 300     | 300     |
| <b>Stiffener thickness (mm)</b>                   | 20      | 20      | 20      | 20 / 15 |
| <b>Span : <math>L</math> (mm)</b>                 | 8800    |         |         |         |
| <b>Overall slab length: <math>L_t</math> (mm)</b> | 9100    |         |         |         |
| <b>Slab width : <math>b_{eff}</math> (mm)</b>     | 2200    |         |         |         |
| <b>Number of openings</b>                         | 13      | 13      | 13      | 14      |
| <b>Number of circular openings</b>                | 12      | 11      | 12      | 14      |
| <b>Number of elongated openings</b>               | 1       | 2       | 1       | 0       |
| <b>Number of semi-infilled openings</b>           | 0       | 2       | 0       | 0       |
| <b>Cell diameter (mm)</b>                         | 375     | 335     | 375     | 375     |
| <b>Reinforcement mesh</b>                         | A252    |         |         |         |
| <b>Number of shear studs</b>                      | 59      |         |         |         |
| <b>Shear stud diameter (mm)</b>                   | 19      |         |         |         |
| <b>Shear stud length (mm)</b>                     | 100     |         |         |         |
| <b>Shear stud spacing (mm)</b>                    | 150     |         |         |         |
| <b>Mechanical load (kN)</b>                       | 140     | 160     | 160     | 140     |
| <b>Steel grade</b>                                | S355    |         |         |         |
| <b>NWC compressive strength (MPa)</b>             | 31.0    | 33.0    | 33.5    | 29.5    |

Table 1. Geometric and material properties of the fire-tested beams

## 1.2 Mechanical load

A mechanical load was applied through a hydraulic pump, and then distributed via a steel beam to 2 horizontal steel cylinders, providing two loading lines corresponding to the stiffeners' location. The hydraulic jack had a 400 mm stroke.

## 1.3 Thermal load

The thermal load was applied from beneath: hence, the steel profile was fire-exposed on 3 sides, while only the lower side of the slab was fire-exposed (see Fig. 2).

None of the four beams was fire-protected. For beams 1, 3 and 4, a 30-min exposure to the standard fire was assumed, whereas a specific bi-linear fire curve was used for beam 2, in order to simulate the heating regime of a fire protected beam.

For beams tested under ISO fire condition, despite their failure criterion occurred prior to 30 minutes, the thermal load was maintained until 30 minutes (see Table 2) in order to investigating the heating of the beams to the lowest standard fire rating commonly defined by the fire regulations. The average furnace temperatures are given in Fig. 3.

|                            | Beam 1 | Beam 2 | Beam 3 | Beam 4 |
|----------------------------|--------|--------|--------|--------|
| <b>Heating phase (min)</b> | 30     | 80     | 30     | 30     |
| <b>Collapse time (min)</b> | ~18    | ~73    | ~26    | ~19    |

Table 2. Test duration

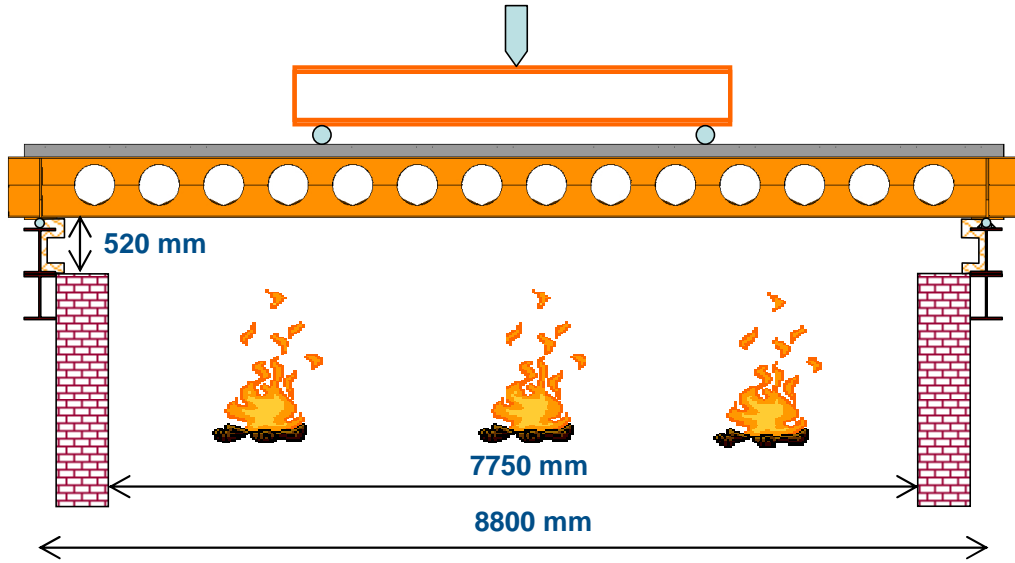


Fig. 2. Schematic view of the furnace

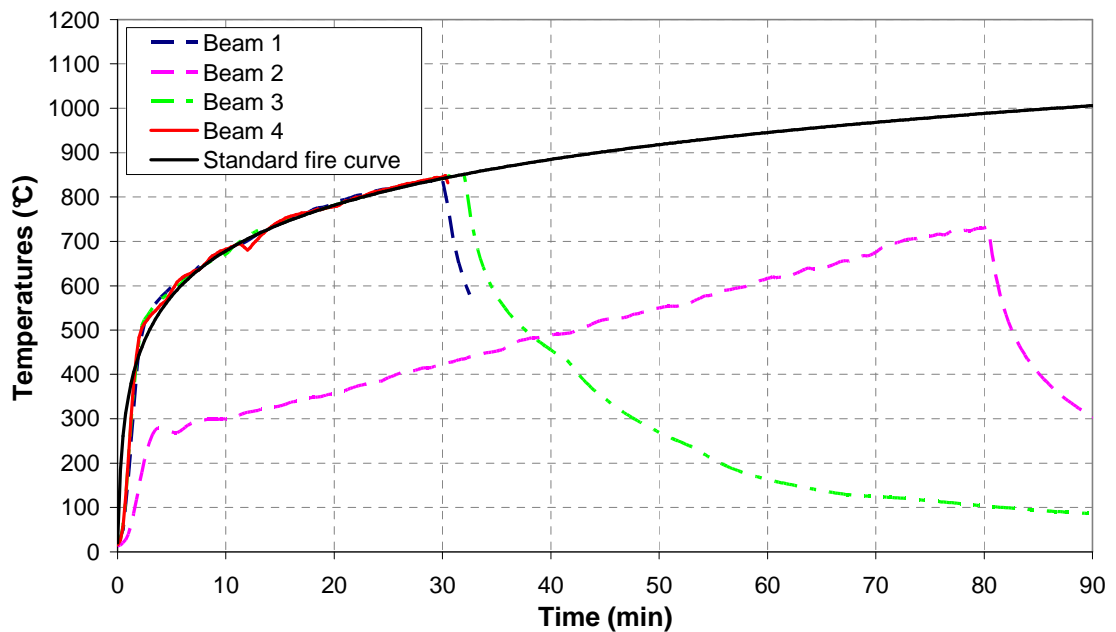


Fig. 3. Furnace average temperature vs. time

### 1.3 Measurement of experimental results

For each test, about 100 thermocouples were disposed in the furnace and at various locations along the beams in both the steel profile and the composite slabs, though most of them were located in the steel profile. Transducers were also used to check the rotations near the supports, the bond-slip between the steel profile and the slabs, and the vertical displacements in the central part of the slab.

## 2 RESULTS AND DISCUSSION

### 2.1 Temperatures

Fig. 4. shows the temperatures of a steel cross-section around mid-span of all tested beams [3] (cross-section without cell in the central zone of webs), which was the hottest one due to the shadow effect. In each graph, the failure time is given by the vertical line.

It is observed that there was always a significant thermal gradient, i.e. about 150 °C, between the top flange, which was the “coolest” steel part, and the remained parts of the cross-section, especially for beam 1 and 4, which underwent very close temperature rises. Moreover, the maximum temperature values were recorded in the web, reaching up to 820 °C in the secondary beams after 30 minutes of ISO fire and up to 690 °C in the primary beam after 80 minutes of fire (fire temperature: 735 °C).

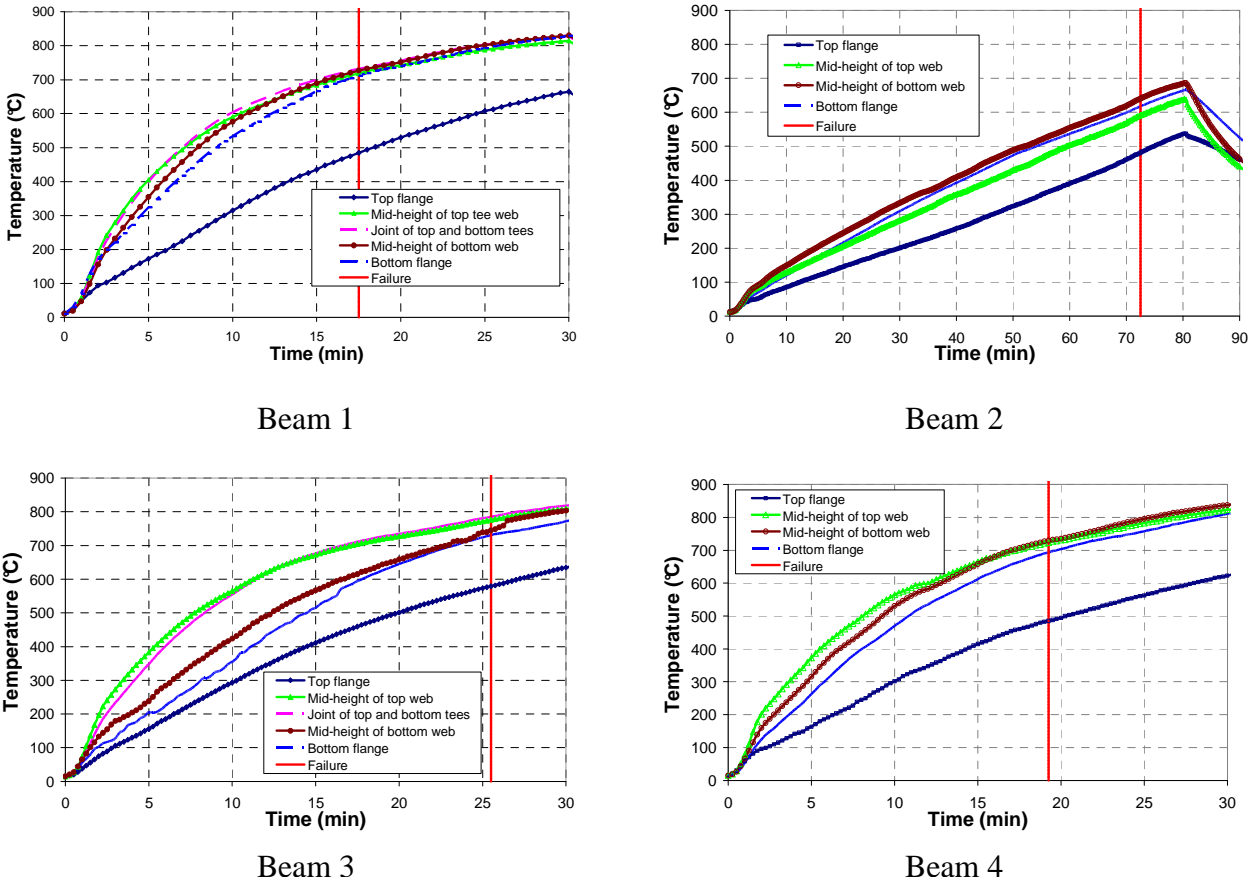


Fig. 4. Temperatures in a central cross-section

### 2.2 Deflections

The deflections recorded at a  $L/4$  distance from the supports and at mi-span are shown in Fig. 5 [3]. As long as a mechanical load was applied, the beams underwent vertical displacements increasing progressively and linearly until a heating around 700 °C for beams exposed to ISO fire and 550 °C for beam subject to protected situation. Afterward, their deflections increased very quickly with the temperature rising until the collapse.

A slight deflection decrease was observed once the hydraulic jack reached its stroke limit and was taken away. However, after this decrease, some beams continue bending downwards under their self-weight without any additional mechanical load until maximum thermal load.

It must be reminded that all the beams exposed to ISO fire had the same top tee section and in particular the beams 1 and 4 had exactly the same cross-section. Nevertheless, in spite of its one-side additional stiffeners, beam 4 underwent approximately the same deflections as beam 1. In fact, the behaviour of these two beams is very close if it is related to the their heating instead of the time. Besides, beam 3 behaved stiffer than both beam 1 and beam 4, as its bottom tee section was more resistant.

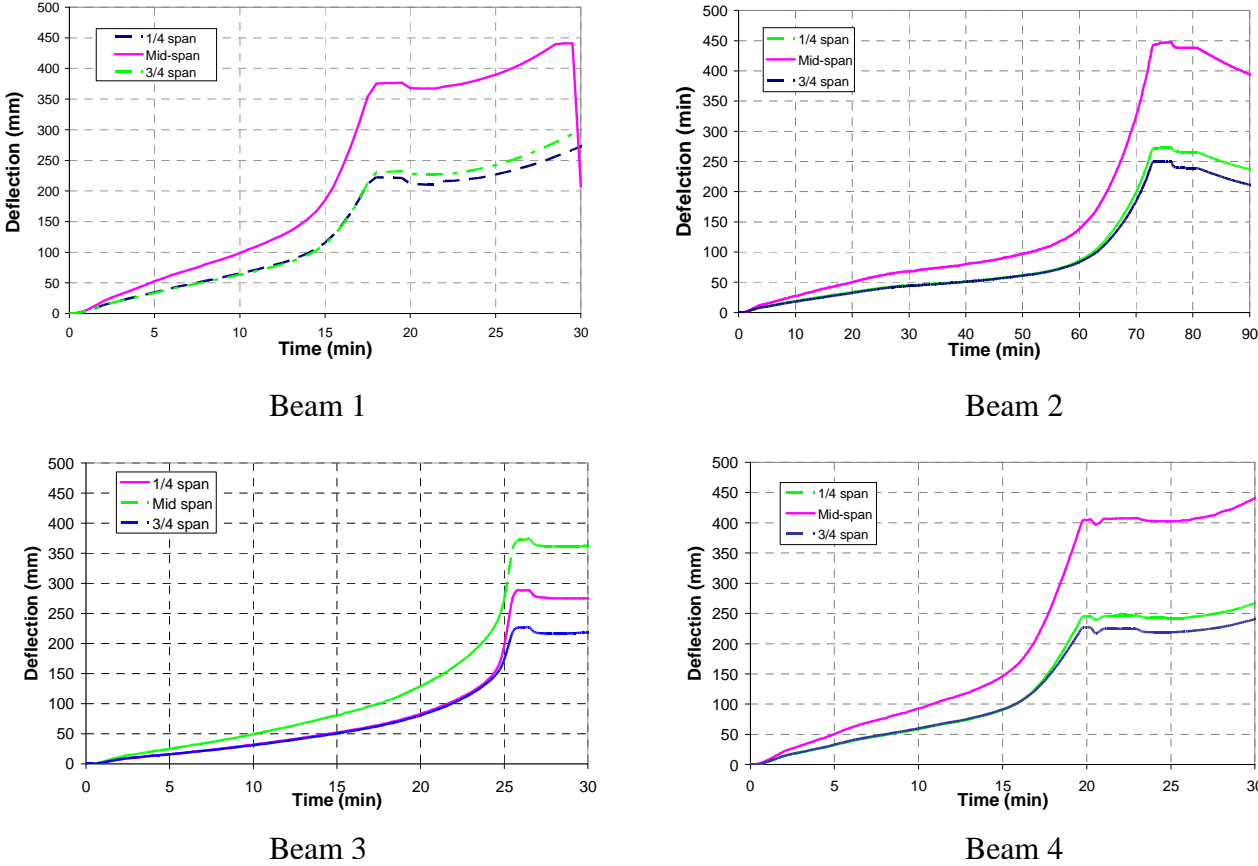


Fig. 5. Deflection vs. time

**2.3 Failure mode**

For both beam 1 and beam 3, the failure was due to web-post buckling near the beam supports (see Fig. 6), which is one of the usual modes of failure observed for such beams in fire situation. This web-post buckling could even generate a tee welding breakage.

Besides, because of its web-post stiffeners, beam 4 could only have a flexural bending failure, as it behaved like an “ordinary” beam. Hence, as beam 1 and beam 4 had the same cross-section, and as their deflection vs. time graphs are very close, beam 1’s collapse might have been caused by combined web-post buckling and flexural bending.

As for the primary beam, i.e. beam 2, no web-post buckling was observed, which leads to the conclusion that this beam also failed by flexural bending.



Beam 1



Beam 2



Beam 3



Beam 4

*Fig. 6. Deformed beams*

## CONCLUSION

The tests carried out on cellular composite steel and concrete beams at elevated temperatures have highlighted two modes of failure:

- a web-post buckling near beam supports, when the web stiffeners were located only in the loading zone (and at the beam ends);
- a flexural bending, when the beam's web was thicker, or when its web-post was stiffened, making the beam behave like an "ordinary" beam without cells.

It should be noticed that no particular damage, such as concrete crushing, occurred in the composite slabs.

The next step of actual investigation is to use these results for validating finite element models such as *ANSYS*, *Cast3M* and *Safir* to predict the fire resistance of this type of structural members. Afterwards, these models will be used to conduct parametric studies for the development of corresponding simple fire design rules.

## REFERENCES

- [1] Technical annex of RFCS project FICEB (FIRE RESISTANCE OF LONG SPAN CELLULAR BEAM MADE OF ROLLED PROFILES), ArcelorMittal, WESTOK, SCI, CTICM, ULG, Ulster University, 2006
- [2] Westok Limited, Input data – design summary, 2008
- [3] Rapports d'essais 08-G-399, 08-G-431, 08-G-407, 08-G-419, Efectis France, 2009
- [4] CEN, Eurocode 4 - Design of composite steel and concrete structures – Part 1-1: General rules and rules for buildings, 2005

## CONCRETE AND COMPOSITE SLABS IN FIRE Discussion of the Load Bearing Characteristics

Martin Mensinger, Martin Stadler

Technische Universität München, Faculty of Civil Engineering and Geodesy,  
Chair of Metal Structures, Munich, Germany

### INTRODUCTION

In the last years several research results have been published which discuss the load bearing characteristics of composite floor systems in case of fire. Diverse design methods were presented to calculate the load bearing capacity using assumptions that the slabs behave like a membrane due to large deflections (e. g. [1]-[3]). However, results of fire tests performed on such structures in the last years show some discrepancies between the available design methods and the real behaviour (e. g. [4]). Therefore, this paper presents some new approaches which may describe the influence factors on the load bearing characteristics.

### 1 STRESSES DUE TO TEMPERATURE CHANGES OVER THE CROSS-SECTION

The temperature distribution in concrete and composite slabs which are exposed to fire at one side is highly nonlinear. In addition, the thermal strains of concrete are not straight proportional to the temperature of the material. Therefore, also the strains in a concrete slab are distributed nonlinearly. Fig. 1 shows such a temperature and strain curve of a 100 mm thick unprotected concrete slab which is exposed to the standard fire curve (ISO 834). The temperatures and temperature-strain relations can be found in Eurocode 4 [5].

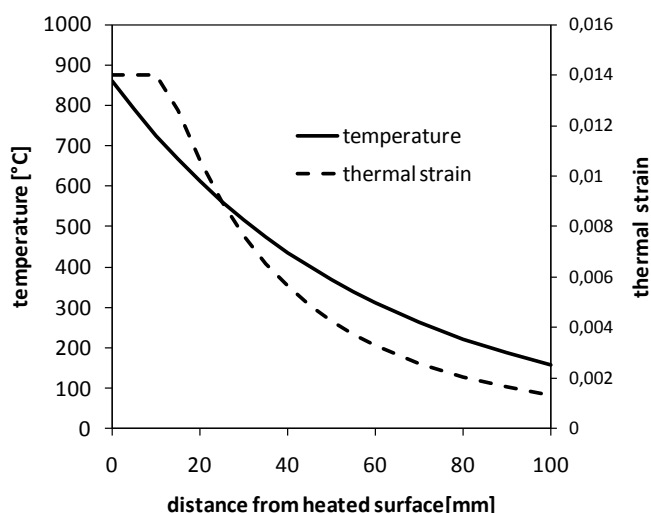


Fig. 1. Temperature and resulting strain distribution in a concrete slab

If these curves are used to analyse larger structures, a very high effort of calculation is necessary. A calculation by hand is virtually impossible. It is more practical to use linear strain distributions but not easy to find an appropriate approach. Furthermore, it is necessary to take into account that the nonlinear strain distribution leads to additional stresses. Related effects occur in hot-rolled steel sections during its production where non-uniform cooling generates self-equilibrating stresses. In contrast to steel sections a concrete slab cannot yield in such a way that these stresses can be neglected at design.

## 2 INTERNAL FORCES AND LOAD TRANSFER

Some of the following thoughts are mentioned in [3] and described in more detail in [6]. Here some new aspects shall be discussed. The temperature distribution over the depth of a cross-section is simplified considered as linear and the thermal expansion factor  $\alpha_T$  as constant. This leads to linear thermal strains which can be divided into a constant part  $\Delta\varepsilon_{unif}$  and a linear strain gradient  $\Delta\kappa$ .

$$\Delta\varepsilon_{unif} = \alpha_T \cdot \frac{\Delta\theta_{top} + \Delta\theta_{bottom}}{2}$$

$$\Delta\kappa = \alpha_T \cdot \frac{\Delta\theta_{top} - \Delta\theta_{bottom}}{h}$$

In a simple beam which is horizontally unrestrained the constant part causes a longitudinal extension  $u_{unif}$  and the gradient causes a uniform curvature and bowing of the beam.

$$u_{unif} = \Delta\varepsilon_{unif} \cdot L$$

For fast heating like the standard fire curve, large curvatures result and geometrical nonlinear approaches are necessary to calculate deformations. Second order theory assumes small deformations and is not sufficient. An unrestrained beam with uniform curvature deforms to a circular arc.

$$w_m = \frac{1}{\Delta\kappa} \left[ 1 - \cos\left(\Delta\kappa \cdot \frac{L}{2}\right) \right]$$

The arc length is the original length of the beam and the ends must move together ( $u_{grad}$ ). In Fig. 2 these relations are illustrated.

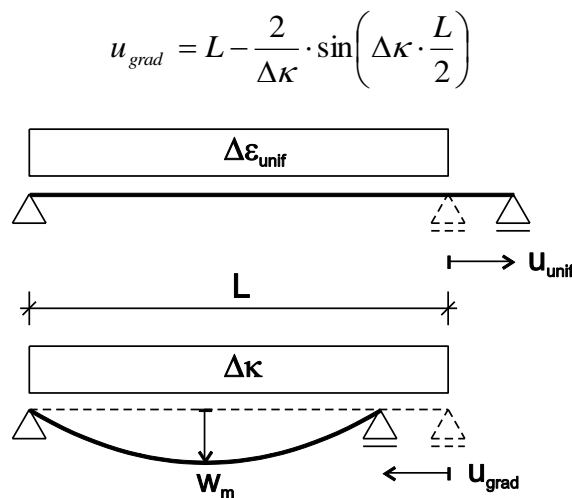


Fig. 2. Horizontal displacement of an unrestrained beam under uniform extension and curvature

If the beam is horizontally fixed on both ends, constraining forces occur. This can be visualized as an unrestrained beam which deforms under thermal loading and afterwards the support is shifted back to its initial position. Depending on whether the total horizontal extension  $u_{tot}$  is positive or negative the constraining forces are either an almost uniform compressive normal force with a positive bending moment in curved shape or a tensile force with a negative bending moment. In the special case when both extensions are the same size there will be no constraining forces (see Fig. 3).

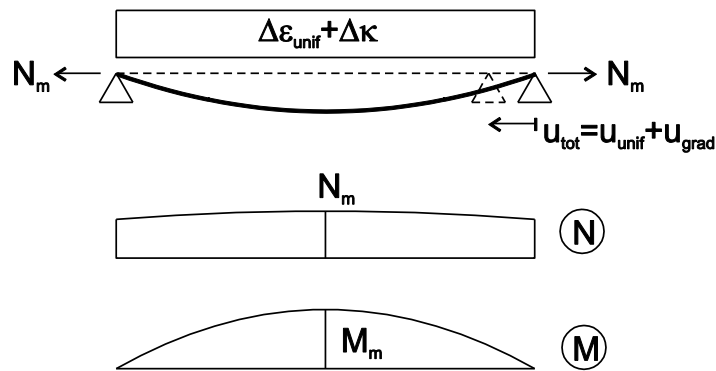


Fig. 3. Resulting constraining forces in a horizontally fixed beam

Slabs which are subjected to the fast heating of the standard fire curve will get a high curvature and in relation a small uniform extension. The curvature changes in both directions of the slab but even at unrestrained slabs the edges cannot move together. The deformations are restrained due to the development of a compression ring around the perimeter of the slab. In this case the thermal loading leads to a tensile force and a negative bending moment in the slab. The height of these forces depends on the bending stiffness of the slab but the tensile force easily reaches the tensile strength of the reinforcement. The negative bending moment generates cracks on the top surface of the slab unless mechanical loads generate contrary moments. On the basis of these facts, it is imaginable that working loads can have positive effects on the structural integrity of slabs or even that slabs fail without any working load only due to the exposure to thermal loading. The influence of the height of the load has not been sufficiently investigated by fire tests until now. If the reinforcement already yields under thermal loading, the contribution to the transfer of mechanical loads becomes very small. It seems that mechanical loads like the dead load of the slab or working loads are mainly transferred by reduction of the bending moment. This kind of load transfer can be compared with the behaviour of prestressed concrete structures.

If the slab is heated slower like it probably is in real fire conditions, the uniform expansion becomes more important and the slab will get under compression. In this case the additional loads can be transferred by reducing the compression force and after that, generating membrane tensile forces.

### 3 TENSION STIFFENING

In most engineering models only the reinforcement makes contribution to the load transfer because the concrete cracks at tension. Thus, the deflection of the slab only depends on thermal and mechanical strains of the reinforcement. But actually the concrete does not completely crack. Between the cracks stresses occur in the concrete and in the cracks the strains of the reinforcement increase. The slab becomes stiffer and the reinforcement is not stretched constantly. This so-called tension stiffening, which is well-known at ambient temperatures, also appears at elevated temperatures. For the design of beams and plates in bending, this effect does not influence the load bearing capacity but only the deflection. But in the engineering models using membrane action the load bearing capacity depends decisively on the deflection. Therefore tension stiffening must be included when the slabs are designed. In [7] approaches are published how these effects can be handled at ambient temperatures and for high reinforcement ratios  $\rho = A_s / A_c$ . Here it is discussed what happens at low reinforcement ratios.

Fig. 4 shows the stresses in a rebar related to its strain. Line a) is for a simple rebar without concrete. The curve is linear until it reaches the yield stress  $f_y$  with the related yield strain  $\epsilon_y$ . Then it begins to yield, the stresses only rise slowly until the bar cracks at the ultimate stress  $f_u$  and strain  $\epsilon_u$ . It is the well-known simplified stress-strain curve of steel with a linear elastic part and a hardening slope.

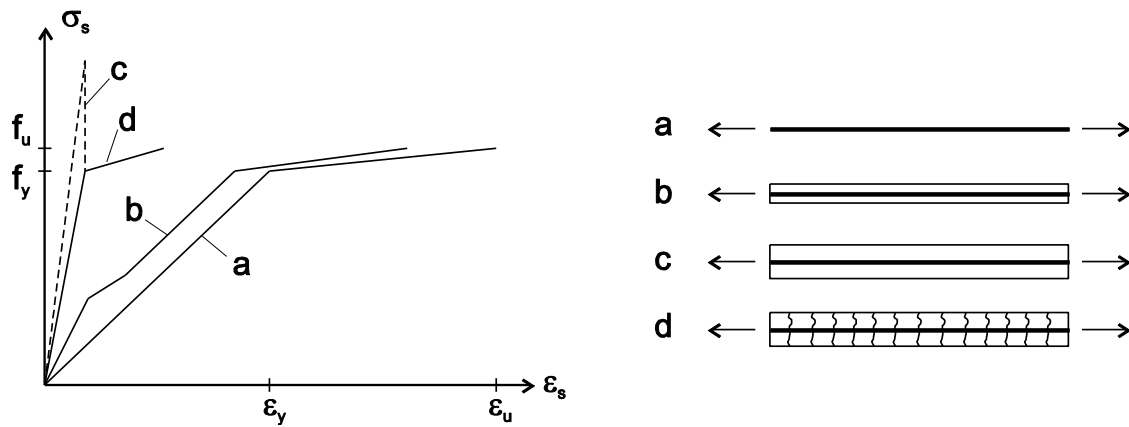


Fig. 4. Tension stiffening

If the rebar is embedded in a small concrete section, the reinforcement ratio is high and the stress-strain curve of the rebar looks like line b) in Fig. 4. In the first part the concrete is not cracked, it acts together with the rebar and the beam is very stiff. At the first bend of the curve the tensile strength of the concrete is reached and the first cracks appear. The stress in the rebar at this point can be calculated as follows:

$$\sigma_{s,cr} = f_{ct} \left( \frac{1}{\rho} + \frac{E_s}{E_{ct}} \right)$$

After the second bend the cracking is finished and the curve runs parallel to line a). The yield and ultimate stresses are the same as for line a) but the related strains are smaller. The reason is that the strains are concentrated in the cracks and in Fig. 4 an average strain over the length of the beam is shown.

Line c) shows the behaviour of a slightly reinforced beam. With rising strains the stress in the rebar theoretically rises higher than the yield stress. The reason is that the force which is necessary to reach the tensile strength of the concrete cross-section is higher than the force which the rebar can absorb. If the beam is stretched further, a first crack appears in the concrete and the force falls down to the tensile strength of the rebar. After a short hardening the beam fails with a small elongation. This curve can only be generated in a displacement-controlled test and is rather theoretical.

More realistic is line d). There the concrete beam is pre-cracked like it is the case at composite slabs in fire. The stiffness of the beam is higher than the stiffness of a simple rebar but lower than the stiffness of a reinforced concrete beam without cracks. Like for line c) the total possible deformation is much smaller than for a simple rebar.

Transferred to slabs in fire the tension stiffening effects can explain why some specimen in tests failed before the estimated deflection was reached. Reaching the yield stress of the reinforcement cannot be the only failure criterion. The ductility of the whole slab must also be taken into account. This ductility is influenced by the reinforcement ratio and the ductility of the reinforcement itself. The load bearing capacity of concrete and composite slabs in fire can be increased on the one hand by increasing the reinforcement ratio. It not only increases the bearable load of the reinforcement but also the tension stiffening effects decrease and the slab becomes softer. On the other hand, reinforcement with higher ductility enables larger displacements and hence higher load bearing capacities without need of additional reinforcement. Unfortunately most fire tests were not run until the slabs failed. The estimated deflections and load bearing capacities are therefore difficult to prove.

## REFERENCES

- [1] Bailey, C. G.: Membrane action of slab / beam composite floor systems in fire. *Engineering Structures* 26 (2004), 1691-1703
- [2] Li, G.-Q., Guo, S.-X., Zhou, H.-S.: Modeling of membrane action in floor slabs subjected to fire. *Engineering Structures* 29 (2007), 880-887
- [3] Cameron, N. J. K, Usami, A. S.: New design method to determine the membrane capacity of laterally restrained composite floor slabs in fire, Part 1: Theory and method. *The Structural Engineer* 83 (2005), 28-33
- [4] Bailey, C. G., Toh, W. S.: Small-scale concrete slab tests at ambient and elevated temperatures. *Engineering Structures* 29 (2007), 2775-2791
- [5] EN 1994-1-2 August 2005: Eurocode 4: Design of composite steel and concrete structures – Part 1-2: General rules – Structural fire design
- [6] Lamont, S.: The Behaviour of Multi-storey Composite Steel Framed Structures in Response to Compartment Fires. *PhD Thesis, University of Edinburgh, 2001*
- [7] CEB-FIP Model Code 1990. *Comité Euro-International du Béton, 1993*



Proceedings of International Conference  
Applications of Structural Fire Engineering  
Prague, 19-20 February 2009

**Session 7**

**Timber Structures**

## TESTS AND MODELLING OF WOOD IN SHEAR AT ELEVATED TEMPERATURES

Maxime Audebert<sup>a,b</sup>, Abdelhamid Bouchaïr<sup>a</sup>, Dhionis Dhima<sup>b</sup>

<sup>a</sup> LaMI, Civil Engineering, Blaise Pascal University, Clermont-Ferrand, France

<sup>b</sup> CSTB, Centre Scientifique et Technique du Bâtiment, Marne-la-Vallée, France

### INTRODUCTION

Fire safety remains a major subject of interest for the development of the use of wood in building structures. Wood is a combustible material but several research works showed that the thermo-mechanical behaviour of timber structures exhibit an interesting behaviour in fire situations [1-3]. In fact, the charring rate of timber elements is generally well known. Consequently, the decrease of the fire resistance of structures can be predicted if the evolution of the wood properties, with temperature, is known.

Besides, the structural joint are characterised by various complex geometrical and material configurations due mainly to the orthotropic character of wood. However, a limited number of studies are available concerning the timber joints. Thus, a modelling approach combined with experimental tests is chosen to evaluate the behaviour of dowelled steel-to-timber joints with the aim of developing simple design rules [8]. The modelling needs many data about the material characteristics of wood mainly in shear. In EN 1995-1-2 [4], the reduction factors for strength (compression, tension and shear) are given for softwood, in the direction parallel to grain. For compression perpendicular to grain or shear parallel to grain, the same reduction of strength may be applied as for compression parallel to grain. In this study, an experimental study is used to validate this hypothesis. Thus to provide the material characteristics to be used in the numerical model of the timber-to-timber and the steel-to-timber dowelled connections, tests are performed to determine the shear reduction factors of glulam under high temperatures.

This paper presents the results of shear tests of glulam samples under high temperatures. At first, these original tested specimens are described and their geometry justified. Then, the testing program and the results are discussed and compared to the values given by EC5. The final aim of the study is to analyse the thermo-mechanical properties of wood in shear to be included in a more extensive study on the modelling of the thermo-mechanical behaviour of timber connections.

### 1 SHEAR TEST SPECIMENS AND TEST ARRANGEMENT

The experimental tests carried out at CSTB (Marne-la-Vallée, France) concern 9 specimens taken from glulam members with a moisture content of 8%. The average density measured varied between 433 and 462 kg/m<sup>3</sup> which correspond to wood in class GL24h [5]. The specimens are characterised by an original geometry (Fig. 1). The cylindrical geometry was chosen to allow the development of a thermal gradient within material, around the shear section, as during a real combustion of timber members. Furthermore, it guarantees a uniform distribution of temperature in the shear section concerned by the tests.

On Fig. 1,  $T_1$  and  $T_2$  represents the positions of the thermocouples used to measure the temperatures at the section in shear. Three additional thermocouples ( $T_{S1}$ ,  $T_{S2}$ ,  $T_{S3}$ ) are positioned on the surface of the specimen.

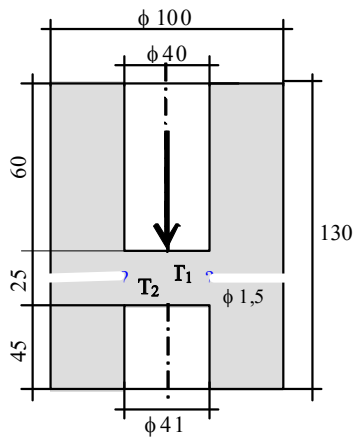


Fig. 1. Geometry of the specimen and a view after test



Fig. 2. Testing device at high temperatures

To obtain a full cutting of the shear section and a uniform distribution of stresses during test, the height of the shear section was selected using different values. This choice was operated on the basis of a numerical study based on a 2D finite element elastic model, due to the symmetry of the specimen. The finite element model was implemented in the finite element code MSC MARC [6]. So, the evolution of the stresses along a shear section of 35 mm in height show that uniform distribution of stress is already reached for a 24 mm height (Fig. 3). Thus the height of the shear section was chosen equal to 25 mm.

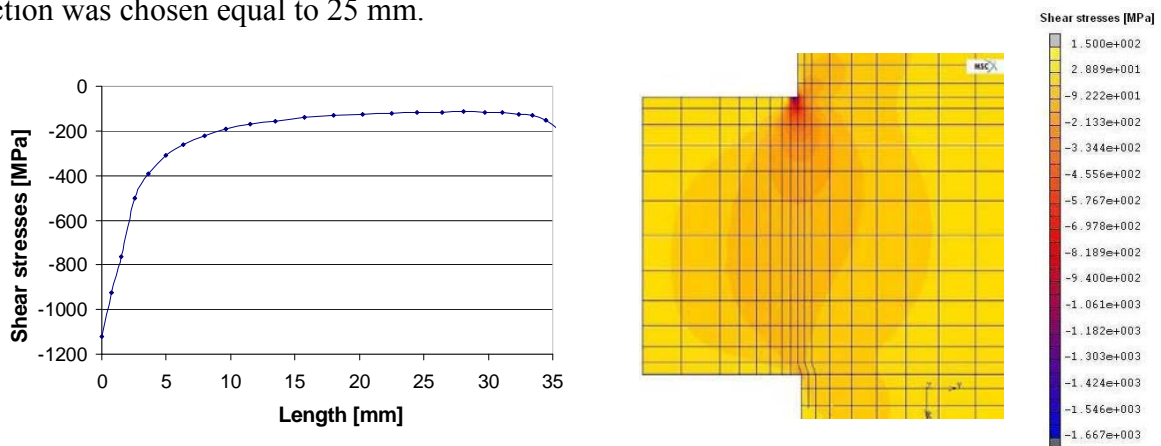


Fig. 3. Evolution of stresses along the shear section

The shear force was applied experimentally on the specimens using the test arrangement shown in Fig. 2. The wood specimens were introduced into the furnace which allowed the required temperature to be kept constant during the loading. The load is applied using a steel cylinder of diameter equal to 39,8 mm to allow its free displacement without friction inside the wood whole. On the top of the furnace, the gap between the steel cylinder and the boundary of the furnace was insulated with mineral wool to guarantee the homogeneity of the temperature inside the furnace (Fig. 2.).

## 2 TESTING PROGRAMM

The rate of loading of the specimens, managed by imposed displacement, was equal to 0,3 mm/min for all the tests. Four different types of tests were carried out considering the normal conditions or the fire conditions with the specimens dried or not before test with two different temperatures. The types of specimens are described hereafter.

- Tests in fire conditions:
  - Tests 1 to 4

For these four tests, the temperature of the furnace was fixed to 250°C. The loading of the specimen began when the temperature measured by the thermocouples T1 and T2 reached 100°C. This process allows obtaining a thermal gradient inside the specimen (between the surface and the shear section).

- Tests 5 and 6

For these two tests, the specimens were dried in a heating room to reach a moisture content equal to 0%. Then, the mechanical test in the furnace was conducted. The temperature of the furnace was fixed to 105°C. The loading began when the temperatures inside the specimen were stabilized to a temperature close to 100°C. Thus, the temperature inside the specimens can be considered homogeneous and constant.

- Test 7

The conditions of the test are similar to those of tests 1 to 4 but the loading begins when the temperature at the sheared section reached 150°C. The specimen is dried before the test in the same conditions as for the specimens of tests 5 and 6.

- Tests in normal conditions
  - Tests 8 and 9

These two tests are realized in cold conditions with normal room temperature (20°C) to obtain a reference.

### 3 TESTS RESULTS AND DISCUSSION

#### 3.1 Thermal results

During the tests in fire conditions, three thermocouples ( $F_1$ ,  $F_2$ ,  $F_3$ ) were used to measure the temperatures inside the furnace. Three other thermocouples were positioned on the surface of the specimen ( $T_{S1}$ ,  $T_{S2}$ ,  $T_{S3}$ ). Finally, the thermocouples  $T_1$  and  $T_2$  were used to measure the temperatures at the sheared section. The values of temperature measured by these thermocouples showed the homogeneity of the temperatures around the specimen and in the shear section. An example of the measured temperatures is shown in Fig. 4. It can be observed a good correlation between the different measures and a good homogeneity of the temperatures in each zone of measurement.

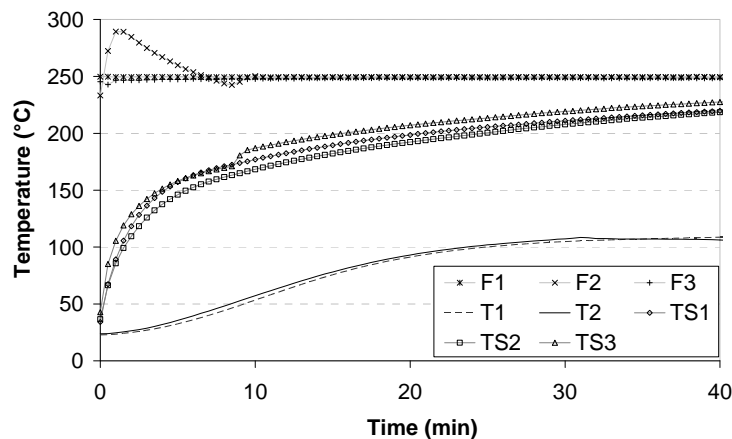


Fig. 4. Temperatures measured (furnace, specimen surface and shear section): test 2

A numerical approach of modelling of the heat transfers within the tested specimens was carried out using the recommendations of EN 1995-1-2 for the thermal properties of timber. The results of the numerical simulations (Fig. 5.) show a good approximation of the temperatures below 100°C.

Beyond this temperature, a plateau is observed on the experimental results, due to the evaporation of the water contained in wood. Besides, the use of the fictitious properties of timber provided by EN 1995-1-2 seems to not be enough to represent exactly the distribution of temperature inside the wood specimen. Thus, this difference can be explained by the fact that the numerical model does not take into account the phenomena of mass transfer within material [7]. This aspect has to be improved.

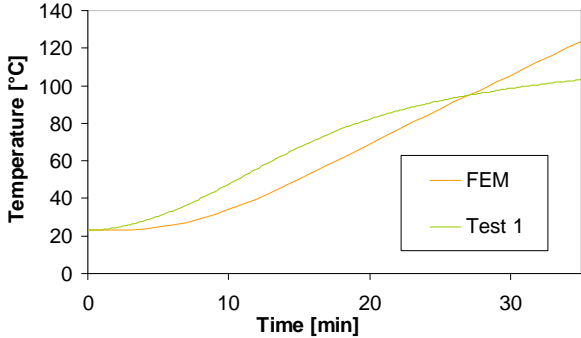


Fig. 5. Comparison between FEM and experiment (temperature)

3.2 Load-displacement results

- Tests 1 to 4 and 7

Fig. 6 shows the load-displacement curves for the tests 1-4 and 7. Fig. 7 shows the evolution of the temperature and the load versus time for test 1.

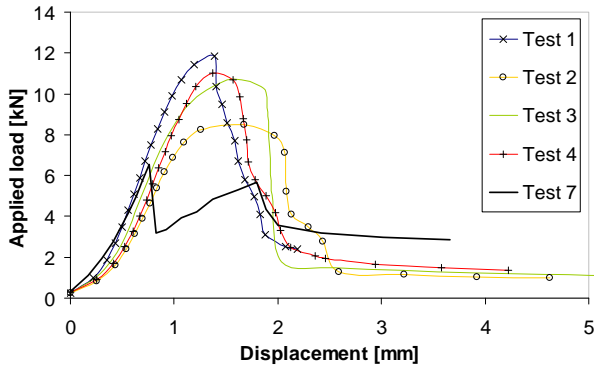


Fig. 6. Load-displacement curves ( tests 1-4 and 7)

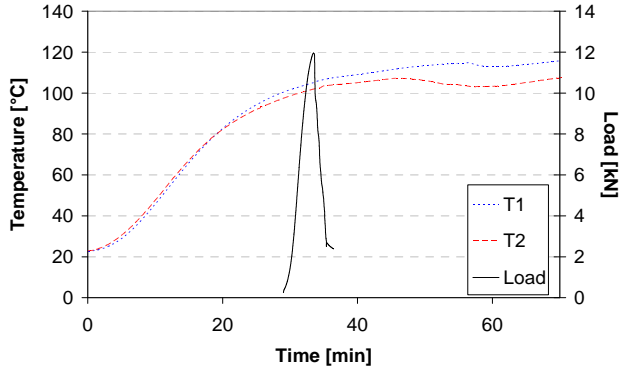


Fig. 7. (Load, temperatures)-time curves (test 1)

From Fig. 6 and 7, the following remarks can be drawn:

1. For tests 1-4, a good homogeneity of the results is obtained with the exception of the test 2 for which the value of the shear strength is weaker (Tab. 1.).

| Tests              | Test 1 | Test 2 | Test 3 | Test 4 |
|--------------------|--------|--------|--------|--------|
| $F_{failure}$ [kN] | 118,3  | 84,9   | 107,3  | 110    |

Tab. 1. Failure loads for tests 1 to 4

2. Tests (1-4) present a progressive failure of the specimens. This can be explained by the fact that the water contained in wood migrates toward the sheared section. Then, the moist fibers of wood fail gradually and increase the friction at the sheared interface. The observation of the

failure profile of the specimen confirms this remark (Fig. 8.). In fact, a brown colour is observed inside specimens 1-4, due to the migration of water against the steel cylinder, and the visible failure surface is not smooth.



Fig.8. View of a cut of specimen 3 after the test

3. A decrease of the shear strength of about 40% is observed for the test 7, realised at 150°C, in comparison with the values of tests 1-4 realised at 100°C.
4. The load-displacement curve for test 7 is appreciably different from that of tests 1-4. It can be observed a first brittle failure and then a second at a weaker level of strength. Thus, the absence of water inside the material seems to be influencing the failure mode. This observation is confirmed by the results of tests 5-6.

- Tests 5-6

Fig. 9 shows the load-displacement curves for the tests 5 and 6, realised at 100°C with dried specimens.

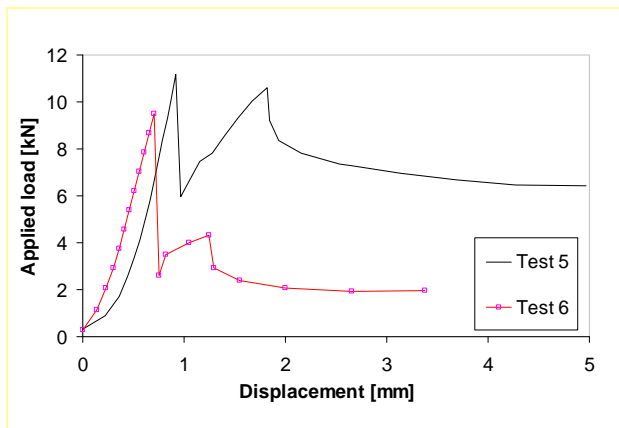


Fig. 9. Load-displacement curves (tests 5-6)



Fig. 10. Views of a cut specimen after test (test 5)

The observation of the specimen after the test shows that the failure profile is different (Fig. 10.). In fact, the brown colour observed with tests 1 to 4 does not appear in the case of the dried specimen. It can be observed a clear and smooth failure surface at the sheared section.

Fig. 9 shows that the moisture content of wood doesn't affect the shear strength of specimens. The same strength is obtained for tests 1 to 4 (2,8 to 3,8 MPa). It appears that the wood moisture content does not affect the strength but the presence of water within material changes the failure mode of tested specimens. However, it should be noted that the initial moisture content of the specimen was relatively weak (8%). This observation will have to be confirmed later with other tests carried out on specimens having higher moisture content (12%).

- Cold tests 8-9

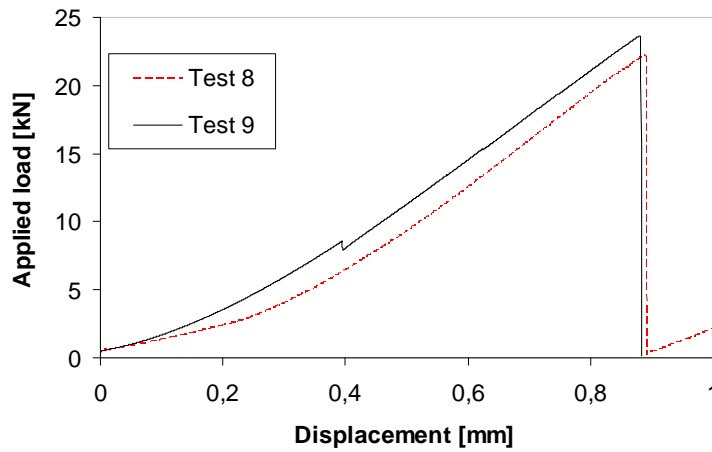


Fig. 11. Load-displacement curves (tests 8 and 9)

A low dispersion is obtained with the two tests in cold conditions (Fig. 11). The comparison of the strength values at high temperature with those given by cold tests, shows that the shear strength at 100°C decreases by 40 to 50%. At 150°C, this resistance is reduced by 65% (only one value from test 7).

### 3.3 Comparison with the results of Eurocode 5

The values of strength obtained by tests in fire conditions are compared with those given by the reduction factors provided by EN 1995-1-2 (Fig. 12.). It can be observed a good agreement between the experimental results and the values of Eurocode.

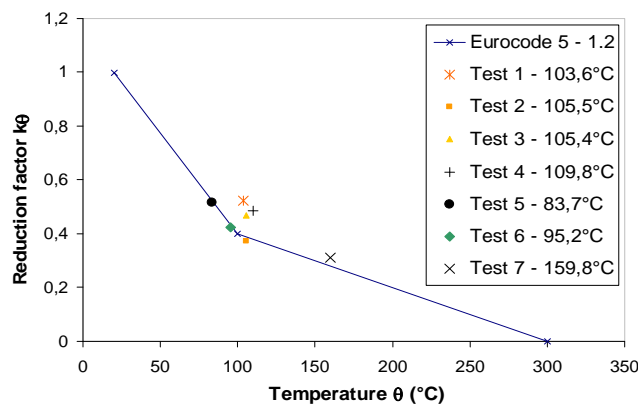


Fig. 12. Reduction factors of the shear strength (tests and EC5)

## CONCLUSIONS

The present study presented shear results to be used in the thermo-mechanical modelling of timber connections. Some tests were carried out to study the shear behaviour of glued laminated timber at high temperatures. These tests were performed using specimens with a specific cylindrical geometry to reproduce various experimental conditions. Four different types of tests were performed. The results of these tests show that the moisture content of the material does not affect the shear strength, but influences the failure mode. It appears in fact that the moist fibers of wood fail gradually. These results, obtained with a limited number of tests, realized on specimens with

weak moisture content (8 %), must be confirmed by additional tests which allow analyzing the effects of higher moisture contents of wood specimens.

For fire design of timber connections, it is necessary to know the decrease of shear strength with the increase of temperature. At 100°C, the obtained results show that the shear strength of the tested specimens decreases by 40 to 50%. At 150°C, the decrease is about 65%. These reduction factors are comparing with the values given by Eurocode 5-1-2. Homogeneous results and a good agreement between experimental results and Eurocode values are obtained. The results of this study show that the reduction factor for shear strength of parallel to grain of softwood, given by Eurocode 5-1-2, is valid for the glulam in strength class GL24h. The geometry of the specimens selected for the shear tests appears as relevant for the study.

As further developments, the preliminary results obtained by this study will be confronted with the results of another experimental campaign, realized on a larger number of specimens with the same geometry but different moisture contents. The final aim of this research work is to integrate the shear properties of wood into a modelling of thermo-mechanical behaviour of dowelled timber connections [8].

## REFERENCES

- [1] Buchanan A. H., Structural design for fire safety, *John Wiley & Sons, ISBN 0471 89060 X, 421 pages*, 2004
- [2] König J., Effective thermal actions and thermal properties of timber members in natural fires, *Journal of Fire and Materials, Vol. 30, pp. 51-63*, 2005
- [3] König J., Structural fire design according to Eurocode 5 – Design rules and their background, *Journal of Fire and Materials, Vol. 29, pp. 147-163*, 2004
- [4] EN1995-1-2, Design of timber structures – General rules Structural fire design”, *CEN TC250-SC5*, Brussels, 2004
- [5] NF P 21-400, Structural timber and wood-based products - resistance classes and related permissible stresses, *pp. 21-400*, 2003
- [6] MSC.Software Corporation, MSC.Marc, User Manual, A: theory and user information, 2005
- [7] Fredlund B., Modelling of Heat and Mass Transfer in Wood Structures During Fire, *Fire Safety Journal 0379-7112/92/\$05-00*, 1992
- [8] Audebert M., Bouchaïr A., Dhima D., Taazount M., Modelling of the behaviour of timber joints in fire, 24<sup>th</sup> *Civil Engineering University meetings*, Nancy, France, 2008 [In French].

## **TIMBER CONNECTIONS UNDER FIRE LOADING**

### **A component model for numerical modelling**

Paulo Cachim <sup>a</sup>, Jean-Marc Franssen <sup>b</sup>

<sup>a</sup> University of Aveiro/LABEST, Department of Civil Engineering, Aveiro, Portugal

<sup>b</sup> University of Liege, Department of Structural Engineering, Liege, Belgium

## **INTRODUCTION**

Connections are key elements in structures. Consequently, understanding the behaviour of the connections is fundamental for an adequate modelling of structures, because the load-deformation behaviour of the connections will influence the overall stress distribution in the structure. Timber connections are usually considered in analysis either as fully rigid or fully hinged, however, only the use of a semi-rigid behaviour will allow a more realistic structural modelling.

For the design at room temperatures, the current design methodology of many codes, e.g. EC 5 [1], is based on a plastic limit state design that allows the calculation of the ultimate load bearing capacity of the connections. However, only a simple expression that is function only of the timber density and fastener diameter is proposed for the load-slip characterization of the connections. This expression doesn't consider some effects, such as the load to grain angle or the geometry of the connection, that are fundamental for an accurate modelling of timber connections.

The goal of this paper is the development of a simple component model for the behaviour of dowelled timber connections under fire loading. In order to reach this goal, constitutive models were implemented for room and fire temperatures. Finite element simulations were performed using a finite element code for structural analysis under fire loading and EC 5 values and experimental data were used to calibrate the model.

## **1 THE COMPONENT MODEL FOR TIMBER CONNECTIONS**

The component model considers the connection as an assembly of individual components. Once the individual constitutive components are identified and characterized, the overall behaviour of the connection can be obtained through the so-called assembly procedures. Each of the components behaves in a way that is independent of the other components, of the connection layout and of the loading type. Therefore, each component can be modelled separately, with its own stiffness and strength. When the connection is loaded, the distribution of forces in the connection is determined by the relative stiffness/strength and by the position of the individual components. Application of the component model to timber connections requires the knowledge of the behaviour of all individual components of the timber connection. For a dowel type connection with a single fastener, a timber component and a dowel component can be identified.

The behaviour of the timber component can be determined by embedding tests that relate the force applied to a fastener to the corresponding embedding in timber. The dowel component is represented as a beam model. The materially non linear behaviour of the section can be captured if the section is discretized by a fibre model. The components can be assembled into the connection model. Fig. 1 shows the case of a fastener in double shear. A typical finite element modelling of the component model of the connection uses a series of beam elements

to discretize the dowel with a spring connected at each node and representing the behaviour of the timber.

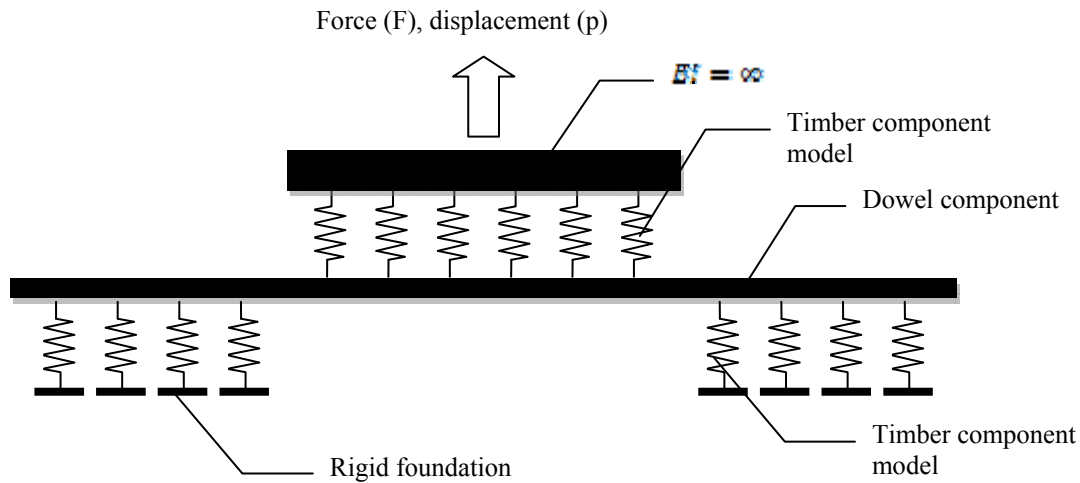


Fig. 1. Model of a single fastener connection

## 2 PARAMETERS OF THE MODEL AT ROOM TEMPERATURE

All parameters of the model should ideally be determined experimentally. However, in this paper, the available formulas presented in EC 5 are used, complemented by additional information obtained from available experimental data to derive generic properties of the timber component.

The general constitutive model for the timber component is shown in Fig. 2 on which the relevant parameters are indicated. The parameters are mainly dependent of the force to grain direction,  $\alpha$ . A total of four parameters are necessary to completely define the model, for each  $\alpha$  value, but, by using the well-known Hankinson expression, a property value at an angle  $\alpha$  to the grain can be obtained from the parallel (subscript 0) and perpendicular (subscript 90) to grain directions.

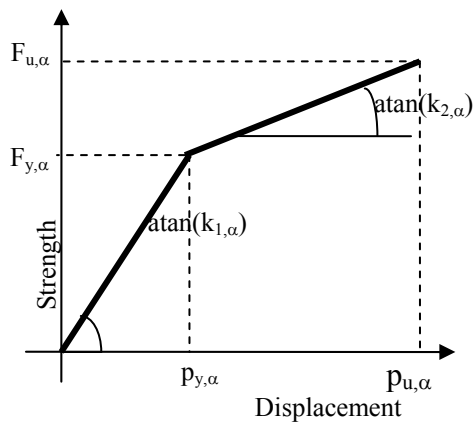


Fig. 2. Idealized force displacement curve for dowel-timber interaction

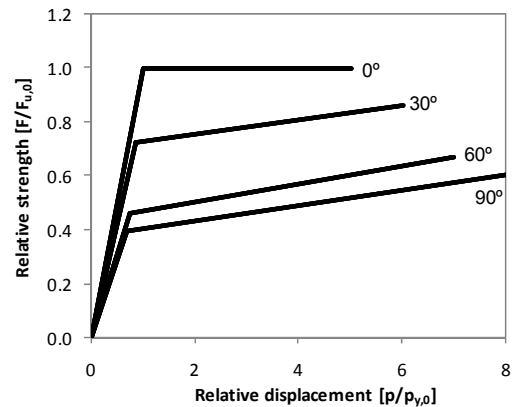


Fig. 3. Relative strength-relative displacement curves for 0, 30, 60 and 90°

The ultimate strength for dowels or bolt fasteners,  $F_{u,\alpha}$ , is derived from EC5 [1] expressions for dowel-type bolts as

$$F_{u,\alpha} = f_{h,\alpha} d = \frac{f_{h,0} d}{k_{90} \sin^2 \alpha + \cos^2 \alpha}, \quad k_{90} = 1.35 + 0.015d \quad (1)$$

where  $d$  is the fastener diameter in mm and  $f_{h,\alpha}$  is the embedding strength at an angle  $\alpha$  to the grain,  $f_{h,0}$  is the embedding strength parallel to grain and  $k_{90}$  is the parallel/perpendicular embedding strength ratio ( $f_{h,0} / f_{h,90}$ ). When no experimental data is available for  $f_{h,0}$  and  $f_{h,90}$ ,  $F_{u,\alpha}$  can be obtained using the EC5 embedding strength for dowels expression:

$$F_{u,\alpha} = \frac{F_{u,0}}{k_{90} \sin^2 \alpha + \cos^2 \alpha} = \frac{0.082(1 - 0.01d) \rho_k d}{k_{90} \sin^2 \alpha + \cos^2 \alpha} \quad (2)$$

where  $d$  is in mm and  $\rho_k$  is the timber density in kg/m<sup>3</sup>. The yield strength,  $F_{y,\alpha}$ , can be related to the ultimate strength by multiplying the latter by  $F_{y,\alpha} = \eta_\alpha F_{u,\alpha}$ . Experimental results [2, 3] show that  $\eta_0 = 1.0$  and that  $\eta_{90}$  ranges from 0.5 to 0.8 (an average value of 0.65 is recommended in absence of experimental data). By knowing the values  $\eta_0$  and  $\eta_{90}$  it is possible to calculate  $F_{y,0}$  and  $F_{y,90}$  and with help of Hankinson equation the value  $F_{y,\alpha}$  can be related to  $F_{u,0}$  as:

$$F_{y,\alpha} = \frac{\eta_0}{\frac{\eta_0}{\eta_{90}} k_{90} \sin^2 \alpha + \cos^2 \alpha} F_{u,0} \quad (3)$$

The expression for  $\eta_\alpha$  as a function of  $\eta_0$  and  $\eta_{90}$  finally reads

$$\eta_\alpha = \frac{F_{y,\alpha}}{F_{u,\alpha}} = \frac{k_{90} \sin^2 \alpha + \cos^2 \alpha}{n_{90} k_{90} \sin^2 \alpha + \cos^2 \alpha} \eta_0, \quad n_{90} = \eta_0 / \eta_{90}. \quad (4)$$

The values for the yield displacement,  $p_{y,\alpha}$ , must be determined from available experimental results. Lam [2] stated that stiffness is independent of the dowel diameter (diameters of tested dowels ranged from 10 to 20 mm). Using again the results of [2, 3], the displacement  $p_{y,0}$  can be described by the following proposed expression

$$p_{y,0} = 0.1(1 - 0.01d)d \quad (5)$$

Using the fact that  $\eta_0 = 1$ , the value  $k_{1,0}$  can be calculated using EC 5 expression as:

$$k_{1,0} = \frac{F_{y,0}}{p_{y,0}} = 0.82 \eta_0 \rho_k = 0.82 \rho_k \quad (6)$$

The stiffness  $k_{1,90}$  can be assumed to be related to the stiffness  $k_{1,0}$  by a factor  $\zeta_{90}$  as  $k_{1,0} = \zeta_{90} k_{1,90}$ . Experimental data shows  $\zeta_{90}$  in the range 1.5 to 2.0 and, for analysis purposes, in the absence or experimental data, can be estimated as  $\zeta_{90} = 1.8$ . The value  $k_{1,\alpha}$  then reads

$$k_{1,\alpha} = \frac{k_{1,0}}{\zeta_{90} \sin^2 \alpha + \cos^2 \alpha} \quad (7)$$

From Fig. 2 and using previous equations, the yield displacement  $p_{y,\alpha}$  is given by

$$p_{y,\alpha} = \frac{F_{y,\alpha}}{k_{1,\alpha}} = \frac{\zeta_{90} \sin^2 \alpha + \cos^2 \alpha}{n_{90} k_{90} \sin^2 \alpha + \cos^2 \alpha} p_{y,0} \quad (8)$$

There is, to our knowledge, no reliable information about the ultimate displacements  $p_u$ . In fact, the embedding strength tests performed according to EN 383 stop at an ultimate displacement of 5 mm. However, experimental results indicate that timber continues to sustain load beyond this value, especially for loads applied perpendicular to the grain. In the

absence of more consistent data, the values of  $p_{u,0} = 5$  mm and  $p_{u,90} = 8$  mm are suggested. The ultimate stiffness  $k_{2,\alpha}$  then reads

$$k_{2,\alpha} = \frac{F_{u,\alpha} - F_{y,\alpha}}{p_{u,\alpha} - p_{y,\alpha}} \quad (9)$$

Fig. 3 shows the relative strength-relative displacement curves for  $\alpha = 0, 30, 60$  and  $90^\circ$  obtained with the proposed model using default values for  $n_{90}, \zeta_{90}, p_{u,0}$  and  $p_{u,90}$ .

### 3 PARAMETERS OF THE MODEL AT ELEVATED TEMPERATURES

A two-step approach is used for the component model for timber connections under fire loading. Initially, a three-dimensional thermal analysis of the connection is carried out that allows the determination of the temperature field in fasteners and timber. Afterwards, the component model previously described for the connection is used to determine the mechanical behaviour of the connection. The three-dimensional thermal analyses of the connections were carried out using program SAFIR [4] with material thermal properties defined in Eurocodes.

The determination of the mechanical parameters for the timber component at elevated temperatures was based on the reduced mechanical properties at elevated temperatures proposed in the structural fire design part of EC 5 [5]. Since shear fasteners in timber connections work by compressing the timber, the reduction factors for compressive stiffness and strength were adopted for the timber component. By applying these factors for material properties described previously, the strength-displacement curves of the timber component at elevated temperatures can be obtained. The ultimate displacement was kept independent of temperature. Examples of these curves at selected temperatures are shown in **Erro! A origem da referência não foi encontrada.**

The non linear mechanical properties at elevated temperature for the dowels are obtained from recommendations of EC 3 [6].

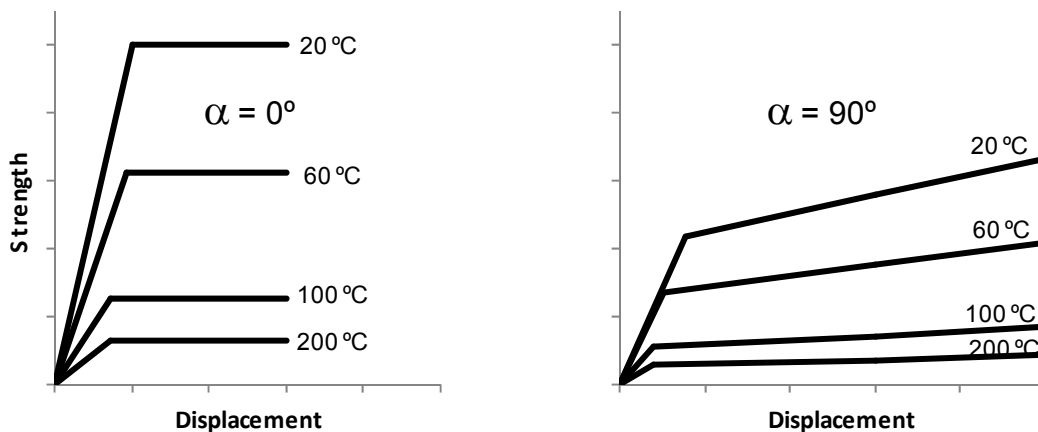


Fig. 4. Relative strength-displacement curves at selected temperatures for  $\alpha = 0^\circ$  and  $90^\circ$ .

### 4 MODEL PERFORMANCE UNDER FIRE CONDITIONS

The model performance under fire conditions was compared with experimental tests with dowels and bolts. The results used for comparison purposes were those from Laplanche *et al.* [7] and Kruppa *et al.* [8]. Summary of side member thickness, fastener type, applied load level and time to failure are presented in Table 1. In dowelled connections, some of the dowels (usually one in four) were replaced by bolts to prevent separation of members during fire tests.

The methodology used for the analysis of fire resistance was as previously described: first a thermal analysis is performed and then obtained temperatures are applied in the mechanical model. Numerical simulations were carried out using a single fastener, since the effect of the number of fasteners for the calculation of the load ratio-time to failure curves is very small and, as a consequence, the use of a single dowel should provide similar results.

Table 1. Summary of experimental and numerical test results

| Author                         | Type  | Thickness    |                | Fastener diameter<br>[mm] | Number of fasteners<br>[dowel+bolt] | Load ratio<br>[%] | Time to failure       |                    |                    |              |    |    |   |    |
|--------------------------------|-------|--------------|----------------|---------------------------|-------------------------------------|-------------------|-----------------------|--------------------|--------------------|--------------|----|----|---|----|
|                                |       | Side<br>[mm] | Center<br>[mm] |                           |                                     |                   | Experimental<br>[min] | Numerical<br>[min] | Deviation<br>[min] | Error<br>[%] |    |    |   |    |
| Laplanche<br><i>et al.</i> [7] | Dowel | 84           | 160            | 16                        | 6+2                                 | 29.9              | 54                    | 48                 | -6                 | -11.1        |    |    |   |    |
|                                |       |              |                |                           |                                     | 9.9               | 79                    | 76                 | -3                 | -3.8         |    |    |   |    |
|                                | Dowel | 64           | 112            | 16                        | 6+2                                 | 30.1              | 41                    | 35                 | -6                 | -14.6        |    |    |   |    |
|                                |       |              |                |                           |                                     | 30.0              | 38                    | 35                 | -3                 | -7.9         |    |    |   |    |
|                                |       |              |                |                           |                                     | 20.0              | 46                    | 42                 | -4                 | -8.7         |    |    |   |    |
|                                |       |              |                |                           |                                     | 19.8              | 45                    | 42                 | -3                 | -6.7         |    |    |   |    |
|                                |       |              |                |                           | 9.7                                 | 57                | 54                    | -3                 | -5.3               |              |    |    |   |    |
| Kruppa <i>et al.</i> [8]       | Dowel | 50           | 80             | 12                        | 6+2                                 | 56.0              | 13                    | 16                 | 3                  | 23.1         |    |    |   |    |
|                                |       |              |                |                           |                                     | 28.0              | 32                    | 26                 | -6                 | -18.8        |    |    |   |    |
|                                | Dowel | 60           | 100            | 20                        | 6+2                                 | 65.0              | 7                     | 20                 | -                  | -            |    |    |   |    |
|                                |       |              |                |                           |                                     | 33.0              | 35                    | 30                 | -5                 | -14.3        |    |    |   |    |
|                                |       |              |                |                           | 12+4                                | 62.0              | 22                    | 20                 | -2                 | -9.1         |    |    |   |    |
|                                |       |              |                |                           |                                     | 31.0              | 41                    | 31                 | -10                | -24.4        |    |    |   |    |
|                                |       |              |                |                           | Bolt                                | 50                | 80                    | 12                 | 0+8                | 42.0         | 23 | 26 | 3 | 13 |
|                                |       |              |                |                           |                                     |                   |                       |                    |                    | 21.0         | 38 | 38 | 0 | 0  |
|                                | Bolt  | 60           | 100            | 20                        | 0+8                                 | 57.0              | 13                    | 11                 | -2                 | -15.4        |    |    |   |    |
|                                |       |              |                |                           |                                     | 24.0              | 22                    | 20                 | -2                 | -9.1         |    |    |   |    |
|                                |       |              |                |                           | 59.0                                | 15                | 17                    | 2                  | 13.3               |              |    |    |   |    |
|                                |       |              |                |                           | 30.0                                | 24                | 25                    | 1                  | 4.2                |              |    |    |   |    |

Numerical results obtained with the component model and deviations to experimental results are also presented in the last columns of Table 1. Ignoring the case of dowels loaded at a load ratio of 65 % that fail after 7 min and for which there should be some problem in the tests (according to [8]) the absolute average error for the time to failure is 3.55 min and the standard deviation is 2.33 min. It can be seen that a good agreement was found between the numerical and experimental results both for the case of dowels and bolts.

## 5 CONCLUSIONS

A component model for dowelled type timber connections subjected to fire has been developed. A generic constitutive model for the timber component can be defined with two parameters, namely the timber density and the dowel diameter. The constitutive model was calibrated with available experimental embedding tests. The component model showed good accuracy when used in several types of connections and compared with experimental results collected from two different sources.

When applied to timber connections under fire loading, the component model showed interesting possibilities, allowing the identification and characterization of the main mechanisms of the connection behaviour, indicating that regardless of its simplicity the model is quite capable of modelling the load-deformation behaviour of connections at room temperature and under fire conditions.

## REFERENCES

- [1] EN 1995-1-1:2004. Eurocode 5: Design of timber structures - Part 1-1: General - Common rules and rules for buildings. CEN, Belgium.
- [2] Lam LY. Développement de modèles analytiques pour la prédiction du comportement élastique des assemblages mécaniques à broches dans la construction en bois (in French), PhD dissertation, University of Liege, Belgium, 2006.
- [3] Pederson MU. Dowel Type Timber Connections – Strength Modelling, PhD dissertation, Rapport BYG·DTU R-039, Technical University of Denmark, Denmark, 2002.
- [4] Franssen J-M. SAFIR. A Thermal/Structural Program Modelling Structures under Fire, Engineering Journal, A.I.S.C., 2005: 42 (3), pp. 143-158.
- [5] EN 1995-1-2:2004. Eurocode 5: Design of timber structures - Part 1-2: General - Structural fire design. CEN, 2004.
- [6] EN 1993-1-2: 2005. Eurocode 3: Design of steel structures – Part 1-2: General rules - Structural fire design. CEN, 2005.
- [7] Laplanche, K., Dhima, D. & Racher, P. 2004. Predicting the behaviour of dowelled connections in fire: Fire test results and heat transfer modelling. 8th World Conference on Timber Engineering, WCTE 2004, Lahti Finland
- [8] Kruppa, J., Lamadon, T. & Racher, P. 2000. Fire resistance tests of timber connections. CTICM, INC-00/187-JK/NB..

# EVALUATION OF NATURAL AND PARAMETRIC TEMPERATURE-TIME CURVES FOR THE FIRE DESIGN OF CROSS-LAMINATED WOOD SLABS

Kathinka Leikanger Friquin

National University of Science and Technology, Dept. of Civil and Transport Engineering, Trondheim, Norway

## 1 INTRODUCTION

Many temperature-time curves for performance-based fire design have been developed, but most of them are only applicable to concrete, brick, lightweight concrete and steel structures. As most of the methods for determining the temperature-time development in a fire compartment only include the fire load of the furniture and other contents in the fire compartment, few of the temperature-time curves developed give a correct picture of the temperature development in a compartment surrounded by combustible wooden structures. The contributions made to the fire load by the wooden boundaries and structures are very often ignored, resulting in an optimistic temperature development. In the present article, temperature-time curves found in the literature for complete fires, including growth stage, flashover, fully developed fire and decay stage, have been evaluated based on their ability to describe the temperature development in compartments with boundaries of cross-laminated slabs, their applicability and suitability to these types of structures. Four models for determining temperature-time curves that might be applicable to wooden structures were found. The project is funded by the Norwegian Research Council.

## 1 DESCRIPTION OF TEMPERATURE-TIME CURVES FOR WOODEN STRUCTURES

As many of the temperature-time curves for fires in compartments are developed mainly for testing and design of non-combustible structures, such as concrete and steel, the applicability of these curves to wooden structures must be evaluated. There are a few different types of wooden structures, like light frame walls, glue-laminated structures with insulation and plasterboards between the columns, fully exposed glue-laminated structures, and partly or fully exposed cross-laminated slabs. The different structures will give different temperature-time curves, and the charring rate may vary. In this paper only cross-laminated slabs have been considered. The curves consider various parameters, and for wooden structures the important parameters might be different from steel and concrete structures. The applicability to wooden structures therefore has to be considered for each and every temperature-time curve.

### 1.1 The “Swedish curves”

Magnusson and Thelandersson [1] developed temperature-time curves describing all stages of the fire (growth, flashover, fully developed and decay/cooling) for seven different compartments, designated A-G, based on their bounding surfaces, see *Fig. 1*. Curves for compartments with wooden boundaries are not developed. The curves are developed based on the fire load density ( $\text{MJ}/\text{m}^2$  of bounding surface area), the area and height of the ventilation openings, the thermal properties of the bounding surfaces, and the heat balance in the compartment, i.e. heat transfer through the structures bounding the enclosed space, radiation through the openings, and the replacement of combustion gases by cold air. *Fig. 1* below shows temperature-time curves for compartment A with opening factors  $0.04$  and  $0.08 \text{ m}^{1/2}$ , and various fire loads.

The curves developed by Magnusson and Thelandersson [1] are based upon a few assumptions:

- a) The temperature in the interior of the whole enclosed space is uniform at any given instant.
- b) The coefficient of heat transfer to the interior bounding surfaces of the enclosed space is uniform at every point.
- c) The heat flow through the bounding structures of the enclosed space is one-dimensional and, except for the window and door openings, if any, uniformly distributed.

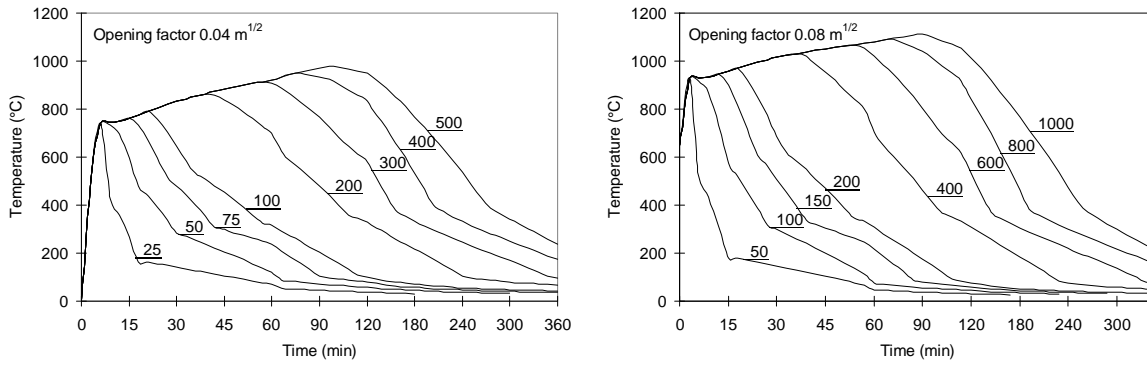


Fig. 1. Temperature-time curves for a complete fire developed by , for compartment A with opening factors  $0.04$  and  $0.08 \text{ m}^{1/2}$ . The numbers on each curve are the fire load densities distributed on the total surface area.

Pettersson and Ödeen [2] developed correction factors,  $k_{fict}$ , to convert the curves for the standard compartment A into curves for the other defined compartments. The correction factors range from 1.0, for bounding surfaces with thermal properties averaging between concrete, brick and lightweight concrete, to 3.0, for steel sheets and mineral wool. The correction factors are based upon thermal differences in the bounding surfaces of the compartments. Magnusson and Thelandersson [1] did not calculate curves for compartments with wooden boundaries, and Pettersson and Ödeen [2] did not calculate correction factors for such compartments. However, according to König et al. [3] the correction factors can be calculated based on the thermal properties of the boundaries of the compartments, as given in Eq. (1):

$$k_{fict} = \frac{1160}{\sqrt{\lambda \rho c}} \quad (1)$$

where  $\lambda$  is the thermal conductivity of the enclosure [W/mK],  $\rho$  is the density of the enclosure [kg/m<sup>3</sup>] and  $c$  is the specific heat of the enclosure [J/kgK]. For a fire compartment with uniform boundaries of cross-laminated wooden elements of pine or spruce typically used in Scandinavia, with density 500 kg/m<sup>3</sup>, specific heat 1900 J/kgK, and thermal conductivity 0.12 W/mK, the correction factor  $k_{fict}$  will therefore be 3.44. Procedure:

1. Calculate the opening factor,  $O$ :

$$O = A_v \sqrt{h} / A_t \quad (2)$$

where  $A_v$  is the total area of vertical openings on all walls [m<sup>2</sup>],  $A_t$  the total area of the enclosure (walls, ceiling and floor, including openings) [m<sup>2</sup>], and  $h$  the weighted average of window heights on all walls [m].

2. Determine the fire load density,  $q_{t,d}$  (fire load density per unit total surface area):

$$q_{t,d} = \Sigma(M_{k,i} \cdot H_{ui} \cdot m) / A_t \quad [\text{MJ/m}^2] \quad (3)$$

where  $M_{k,i}$  is the amount of the combustible material  $i$  in the compartment [kg],  $H_{ui}$  the net calorific value of material  $i$  [MJ/kg],  $m$  the combustion factor, and  $A_t$  the total area of the enclosure (walls, ceiling and floor, including openings) [m<sup>2</sup>].

3. Calculate the correction factor,  $k_{fict}$ , as given in Eq. 1.

4. Find corrected opening factor,  $O_{fict}$ , and fire load density,  $q_{t,d,fict}$ , by multiplying  $O$  and  $q_{t,d}$  with  $k_{fict}$ .

5. Find the curve for compartment A with  $O_{fict}$  and  $q_{t,d,fict}$ , and use it as the temperature-time curve for the fire. For fire compartments with  $O_{fict}$  and  $q_{t,d,fict}$  other than those found in the curves, interpolation can be used to determine the temperature-time development.

The curves can be found in Magnusson and Thelandersson [1] and Pettersson and Ödeen [2].

## 1.2 EN 1991-1-2 Standard temperature-time curve

The standard temperature-time curve in [4] is given by:

$$\theta_g = 20 + 345 \log_{10}(8t + 1) \quad (4)$$

where  $\theta_g$  is the gas temperature in the fire compartment [°C] and  $t$  the time [min].

In Sweden a cooling rate of 10°C/min has been used.

## 1.3 EN 1991-1-2 Parametric temperature-time curve

The procedure to calculate a temperature-time curve based on EN 1991-1-2 [4] is as follows:

1. Calculate temperature-time curve for the heating stage, found in EN 1991-1-2 Annex A(3):

$$\theta_g = 20 + 1325 (1 - 0.324e^{-0.2t^*} - 0.0204e^{-1.7t^*} - 0.472e^{-19t^*}) \quad (5)$$

where  $\theta_g$  is the gas temperature in the compartment [°C]. The gas temperature is a function of time, opening factor, and thermal properties (density, specific heat and thermal conductivity) of the boundary of the compartment.

2. Calculate the maximum temperature,  $\theta_{max}$ , in the heating stage using EN 1991-1-2 Annex A(7). If  $t_{max} = t_{lim}$  the fire is fuel controlled, and if  $t_{max} > t_{lim}$  the fire is ventilation controlled.

3. The cooling stage of the fire is calculated based on the maximum temperature,  $\theta_{max}$ , the opening factor,  $O$ , the product of the density and thermal properties,  $b, t_{max}^*$ , and a factor  $x$ , which express whether the fire is fuel controlled or ventilation controlled. Three different equations describe the cooling stage, based on the duration of the fire. The cooling stage is a function of time, opening factor, and thermal properties of the boundary of the compartment.

## 1.4 iBMB parametric fire curve

The iBMB parametric fire model is described by Zehfuss and Hosser [5] and Zehfuss [6] as a model that considers the actual boundary conditions of the fire compartment concerning fire load, ventilation conditions, geometry and thermal properties of the enclosure. The parametric equations for the temperature-time curve were developed for a reference fire load density of  $q'' = 1300 \text{ MJ/m}^2$  (upper value for residential and office buildings). The procedure when determining iBMB parametric fire curves:

1. Calculate opening factor  $O$ , fire load density  $q$ , total fire load  $Q$ , averaged thermal property of the boundaries, total area of boundaries incl. openings  $A_t$ , total area of boundaries excl. openings  $A_T$ .

2. Calculate the maximum rate of heat release  $\dot{Q}_{max} = \min[\dot{Q}_{max,v}; \dot{Q}_{max,f}]$  and determine whether the fire is ventilation or fuel controlled during the fully developed fire stage.

3. The curves have three distinct points at the times  $t_1$ ,  $t_2$  and  $t_3$ , where the slope of the curves changes, see Fig. 2. Growth stage: From the initiation of the fire until  $t_1$ , the RHR rises quadratically,  $\dot{Q}(t) = \dot{Q}_0 (t/t_g)^2 [\text{MW}]$ , where  $\dot{Q}_0 = 1 \text{ MW}$  and  $t_g = 300 \text{ s}$  (for residential and office buildings). The upper layer temperature increases rapidly at this stage. Fully developed fire: At  $t_1$  the RHR has reached its maximum,  $\dot{Q}_{max}$ , and remains constant until  $t_2$ . Between  $t_1$  and  $t_2$  the upper layer temperatures increases moderately, reaching its maximum at  $t_2$ . Cooling stage: 70% of the fuel is consumed at  $t_2$  and the RHR drops off linearly, at the same time the upper layer temperature starts to decline. At  $t_3$  the total fire load is consumed and the RHR decreases to 0, and the upper layer temperature-time curve bends and declines slower than before. The times  $t_1$ ,  $t_2$  and  $t_3$  must be calculated for both the maximum fire load density,  $q''$ , for the actual building category, and the actual fire load density for the specific compartment,  $q''_x$ . The first point,  $t_1$ , is common for both fire load densities. For fire load densities less than the maximum  $q''$ , the maximum temperature is achieved accordingly earlier, see Fig. 2.

4. The temperatures  $T_1$ ,  $T_2$  and  $T_3$  for the maximum fire load density of  $q'' = 1300 \text{ MJ/m}^2$  can be calculated based on the RHR curve, and the temperature-time curve can be calculated based on the

parametric equations for ventilation or fuel controlled fires, according to the results from bullet No. 2 above. The equations are given in [5,6].

5. When the temperature-time curve for the maximum fire load density  $q''$  is drawn, the temperatures  $T_{2,x}$  and  $T_{3,x}$  can be found.  $T_{2,x}$  is found on the curve at time  $t_{2,x}$ .  $T_{3,x}$  is found on the  $T_{3,x}$  Log<sub>10</sub>-curve described by  $T_{3,x} = (T_3 / \log_{10}(t_3 + 1)) \cdot \log_{10}(t_{3,x} + 1)$  at time  $t_{3,x}$ . The temperature-time curve for a fire compartment with a fire load density  $q'' \leq 1300 \text{ MJ/m}^2$  can now be drawn based on the parametric equations given in [5,6].

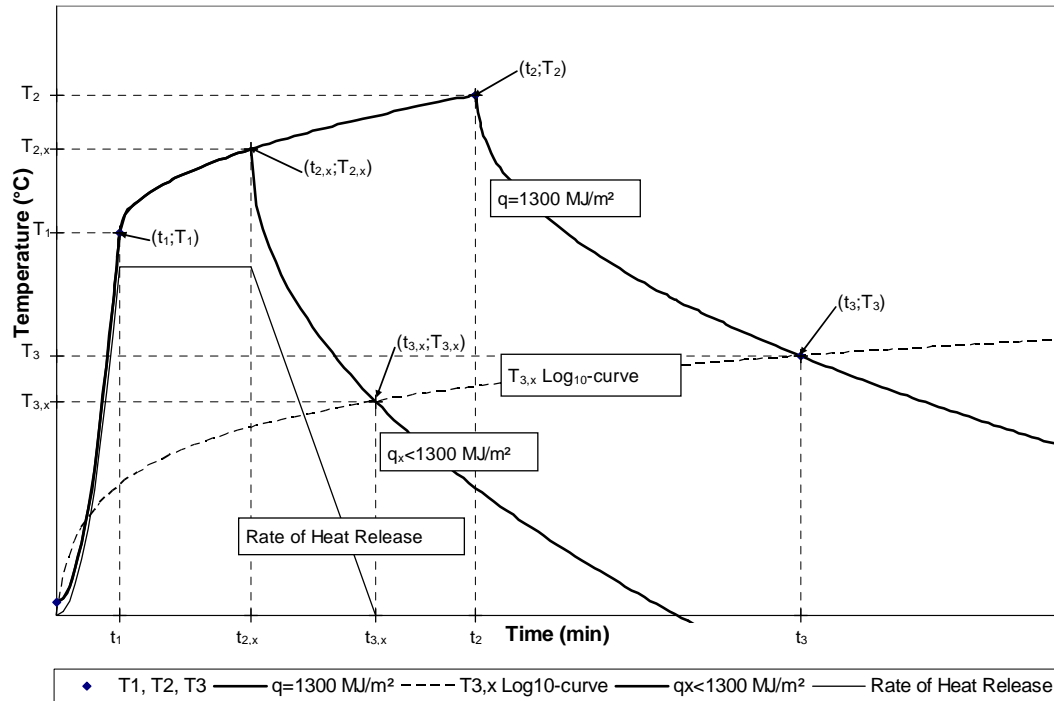


Fig. 2. Determination of the temperatures  $T_{2,x}$  and  $T_{3,x}$ . Rate of Heat Release and temperature-time curve for  $q < 1300 \text{ MJ/m}^2$ , and the temperature-time curve for  $q = 1300 \text{ MJ/m}^2$ .  $T_{3,x}$  Log<sub>10</sub>-curve for determination of  $T_{3,x}$ .

The trend of some of the curves described in this paper is shown in Fig. 3.

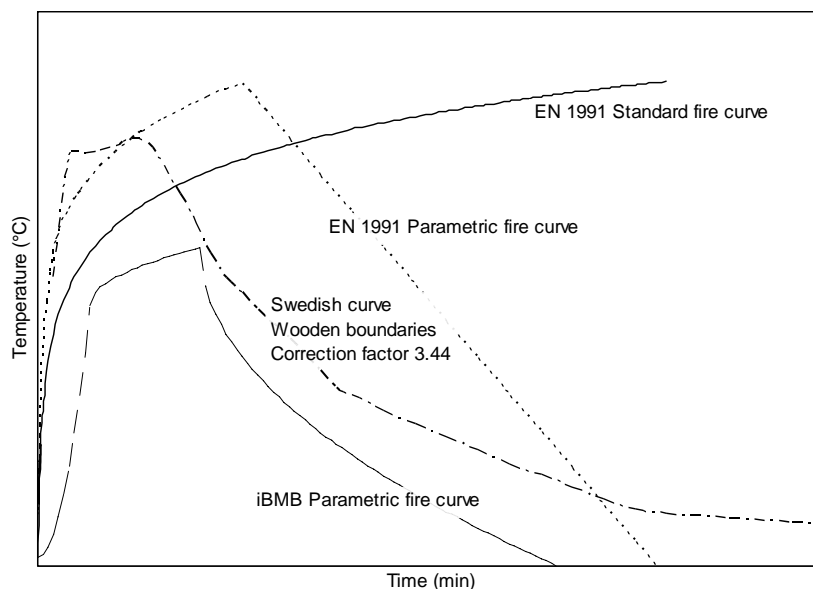


Fig. 3. The typical trend of some of the temperature-time curves described; EN 1991-1-2 Standard fire curve and Parametric fire curve, “Swedish fire curve”, and iBMB Parametric fire curve. The curves are not to scale with each other.

## 2 SUMMARY AND DISCUSSIONS

The models and curves described above have been evaluated based on their ability to describe the temperature development in compartments with boundaries of cross-laminated slabs, their applicability and suitability to these types of structures. Five models for determining temperature-time curves that might be applicable to wooden structures were found. Most of the curves are initially developed for testing and design of non-combustible structures, but have later also been assigned for combustible structures. Experimental research, performed through the years by various laboratories, has shown that the accuracy of the temperature-time development compared to real fires is not always good. And from time to time new models for determination of temperature-time curves are developed. It is therefore necessary to study the various models and determine which ones are more applicable to wooden structures.

### 2.1 The “Swedish curves”

Magnusson and Thelandersson [1] and Pettersson and Ödeen [2] have not given correction factors for fire compartments with wooden boundaries, but König et al. [3] describes how to calculate the correction factor for compartments with boundaries of various thermal properties. For a compartment with exposed cross-laminated slabs on all surfaces, the correction factor was here calculated to be 3.44. This correction factor considers the thermal properties of the boundaries, i.e. the density, the thermal conductivity and the specific heat capacity of the material. The charring rate and fire load of the boundary material is not considered. It might be reasonable to first determine the temperature-time curve only based on the fire load of the inventory to find the fire duration, and then add the fire load from the boundaries calculated based on the nominal charring rate from EN 1991-1-2 and the fire duration first found. A new curve can then be found based on the new fire load density and the old opening factor. The assumptions made when developing the method simplify the curves considerably.

### 2.2 EN 1991-1-2 Standard temperature-time curve

The development of the fire is very dependant on the type of building you are designing. The standard temperature-time curve given by EN 1991-1-2 [4] is very conservative for slow growing fires, less so for medium growth fires and only a little for fast growing fires. The curve only describes the heating stage, and does not consider the boundary conditions or the fire load density. A cooling stage of 10°C/min has been used in Sweden, but the real cooling stage for combustible structure is not linear.

### 2.3 EN 1991-1-2 Parametric fire

There are many limitations to the use of the parametric fire curve given by EN 1991-1-2 [4]. For example, the maximum floor area is 500 m<sup>2</sup>, maximum compartment height 4 m, thermal properties  $b = \sqrt{\rho c \lambda}$  between 100 and 2200 J/m<sup>2</sup>s<sup>1/2</sup>K, and opening factor between 0.02 and 0.20. To incorporate the charring of the structure, the maximum fire duration is 120 min, with a maximum char depth of ¼ of the height or width of the structural member. The thermal properties can be taken at ambient temperature, but for most materials these properties are strongly temperature dependant. The fire load density is calculated based on the combustible inventory in the compartment and “the relevant combustible parts of the construction, including linings and finishing. Combustible parts of the construction which do not char during the fire need not to be taken into account” [4]. The “relevant combustible parts of the construction” can only be found when we know the development of the fire, which in turn can only be found when we know the total fire load density. Through iterations the temperature-time development and the contribution from the construction to the fire load density can be found.

## 2.4 iBMB model

The iBMB parametric fire curves can be used to determine the occurrence of flashover, breakage of windows with additional ventilation, a failure of the enclosure with loss of compartmentation, or the effect of fire fighting and sprinkler systems. The connection between the design fire and the parametric fire curve makes it possible to consider all events influencing on the natural fire and resulting in a variation of the RHR.

Experiments performed by Hakkarainen [7] show that the temperature-time curve for a small compartment with exposed heavy timber structures a relatively small opening factor can have a plateau at a relatively low temperature due to insufficient ventilation. As much as 50% of the pyrolysis gases burnt outside the compartment. When most of the movable fire load has burnt, the temperature might increase as the generation of pyrolysis gases decrease, allowing more oxygen into the compartment. None of the curves above show this phenomenon.

## 2 CONCLUSIONS

Four temperature-time curves have been evaluated based on their applicability to exposed wooden structures. Based on the evaluation of the temperature-time curves, the following conclusions can be drawn:

1. The geometry of the compartment, and the position and size of the ventilation openings will have a great effect on the temperature, flashover and decay stage of the fire.
2. Many of the curves have growth rates much higher than real fires.
3. Linear cooling stages are not realistic. Fire curves with linear cooling stage give too fast cooling for compartments with large surfaces of exposed wooden structure.
4. None of the curves include the fire load from the structure directly. Iterations have to be made to incorporate this contribution to the fire.
5. Assumptions can be made to determine a relevant part of the structure to be part of the fire load.
6. The “Swedish curves” and the iBMB curves resemble a real fire in a compartment with exposed wooden structures most.

Using a realistic fire development and determining the overall structural behaviour can lead to an efficient and aesthetical construction.

## 3 REFERENCES

- [1] Magnusson, S. E. and Thelandersson, Sven. Temperature-time curves of complete process of fire development. Theoretical study of wood fuel fires in enclosed spaces. *Acta Polytechnica Scandinavica* 1970; Ci 65, pp. 181 pp.-
- [2] Pettersson, Ove and Ödeen, Kai. *Brandteknisk dimensionering. Principer, underlag, exempel (In Swedish)*. LiberFörlag; Stockholm, Sweden. (1978)
- [3] König, Jürgen, Norén, Joakim, Olesen, Frits Bolonius, and Hansen, Finn Toft. Timber frame assemblies exposed to standard and parametric fires. Part 1 : Fire tests, *Report No. I 9702015*. SP Wood Technology: Borås, Sweden; Borås, Sweden. (1997)
- [4] *EN 1991-1-2, Eurocode 1: Actions on structures - Part 1-2: General actions - Actions on structures exposed to fire*. European Committee for Standardization; Brussels, Belgium. (2003)
- [5] Zehfuss, Jochen and Hosser, D. A parametric natural fire model for the structural fire design of multi-storey buildings. *Fire Safety Journal* 2007; **42**, Issue 115-126. 10.1016/j.firesaf.2006.08.004.
- [6] Zehfuss, Jochen. *Bemessung von tragsystemen mehrgeschossiger gebäude in stahlbauweise für realistische brandbeanspruchung*. Dr.-Ing., Carolo-Wilhelmina University of Technology at Brunswick, Lower Saxony, Germany; 2004)
- [7] Hakkarainen, Tuula. Post-Flashover fires in light and heavy timber construction compartments. *Journal of Fire Sciences* 2002; **20**, Issue March, pp. 133-175. [10.1177/0734904102020002074](https://doi.org/10.1177/0734904102020002074).

## EXPERIMENTAL STUDY ON FIRE PROTECTION OF TIMBER ASSEMBLIES

Ni Zhaopeng<sup>a</sup>, Qiu Peifang<sup>b</sup>, Jim Mehaffey<sup>c</sup>, Stan Winter<sup>d</sup>

<sup>a</sup> Senior Researcher of Code Division, Tianjin Fire Research Institute of China;

<sup>b</sup> Assistant senior Researcher, Tianjin Fire Research Institute of China.

<sup>c</sup> Scientist of Forintek Canada Corp., Canada;

<sup>d</sup> Professor of Technical University of Munich, Germany.

### INTRODUCTION

In the history of China, timber was once the main material for building dwellings. Even now, there are still lots of historic buildings built with heavy timbers. They have been standing there for hundreds of years.

Masonry, reinforced concrete and steel structures became the fashion of the last century. Therefore, fire protection researches were mostly focused on them, while timber fire protection was more or less neglected, especially during the last thirty years of 20th century. Accordingly, fire code of China at that time was focused on the requirements for masonry, concrete and steel structures too.

However, after China joined WTO, more and more wood councils and companies from North America, Europe and so on set up offices or branches in China to find market opportunities or promote cooperation with some research institutes and organizations with the purpose of studying the applicability and sustainability of wood frame buildings in China. As a result, a certain number of wood frame buildings (mostly single-family dwellings) have been built in Beijing, Tianjin, Shanghai, Hangzhou, Qingdao, Dalian, Guangzhou etc. In order to provide proper regulations for the construction and fire protection of wood frame buildings, a series of codes have been issued. For example, *Code for Quality Acceptance of Timber Structure Engineering* in 2002, *Code for Design of Timber Structures* in 2003, *Technical Code for Partitions with Timber Framework* in 2005 and *Code of Design on Building Fire Protection and Prevention* in 2006. However, the fire protection requirements in these codes need to be further improved and coordinated.

The requirements of current national fire code *Code of Design on Building Fire Protection and Prevention* (2006 edition) for timber fire protection are not specific enough. They can't meet the need of current China building construction market.

Therefore, Tianjin Fire Research Institute of MPS set up a joint technical committee with Canada Wood Council, European Wood Council and AF&PA from USA in September of 2005 to study the fire protection of timber structures. The cooperation has brought us great achievements and verification tests of timber elements were one of them. The data acquired from the tests can provide scientific support for the revision of current national fire code *Code of Design on Building Fire Protection and Prevention*.

The test assemblies were designed by European Wood council and constructed by Canada Wood council. The studs for wall assemblies, beams and columns were provided by European Wood Council, but all the other materials such as gypsumboard and rock fibre etc. were produced in China. These tests were done according to GB 9978 (equivalent to ISO 834) and observed by experts from Joint Technical Committee of China, Canada and Germany.

### 1. DESCRIPTION OF TEST ASSEMBLIES

Twelve full-scale timber building elements were tested in the lab of Tianjin Fire Research Institute.

They include 7 load-bearing or non-load-bearing exterior or interior wood stud walls, one independent ceiling, two floors, one gluelam beam and one gluelam column. Here only one wood stud wall test (load-bearing exterior wall) is introduced in detail. The furnace for conducting full-scale loaded/unloaded wall fire tests is shown in Figure 1. The opening of the wall furnace is 3m×3m. The details of the assemblies are given in Table 1.

Figure 1 Wall Furnace



Floor Furnace



Column Furnace



Table 1 Details of the tested assemblies

| Time of testing | Name of the assembly      | Fabrication  | Dimension      | Load | Result |
|-----------------|---------------------------|--|----------------|------|--------|
| Dec.19, 2007    | Non-bearing exterior wall | gypsumboard -12mm; stud-89mm, glass wool -89mm; gypsumboard -12mm; | 3270 ×3270×113 |      | 59min  |
| Dec.20, 2007    | Non-bearing exterior wall | Gypsumboard-15mm; stud-140mm Rock fiber-140mm; gypsumboard -15mm;  | 3270 ×3270×170 |      | 99min  |
| Jan.11,2008     | Ceiling                   | gypsumboard-12mm; 30×50mm timber batten,                           | 3500 ×4500     |      | 43min  |

|             |                               |   |                       |   |        |
|-------------|-------------------------------|---|-----------------------|---|--------|
|             |                               | 38×235 Truss rafter construction<br>gypsumboard-12mm;   | ×289                  |   |        |
| Jan.12,2008 | Load-bearing<br>exterior wall | Gypsumboard-15mm; wood<br>stud-140mm, rock fibre-140mm;<br>OSB-15mm OSB                                     | 3600<br>×3300×170     | 22.5kN/m  | 64min  |
| Jan.13,2008 | Load-bearing<br>interior wall | Gypsumboard-12mm; wood<br>stud-89mm; glasswool-40mm;<br>gypsumboard-12mm                                    | 3300<br>×3600×113     | 11kN/m  | 47min  |
| Jan.13,2008 | Floor                         | Gypsumboard-12mm; Resilient<br>metal slat-13mm; Beams-235mm<br>Glass fibre>60mm; OSB-12mm                   | 3065<br>×4500<br>×275 | 4kN/m   | 36min  |
| Jan.16,2008 | Load-bearing<br>exterior wall | Gypsumboard-12mm; wood<br>stud-89mm; glass fibre-80mm;<br>OSB-12mm OSB                                      | 3600<br>×3300×113     | 12.5kN/m  | 34min  |
| Jan.17,2008 | Load-bearing<br>interior wall | Gypsumboard-15mm;<br>Resilient metal slat-13mm;<br>wood stud-89mm;<br>rock fibre-80mm;<br>Gypsumboard-15mm  | 3300<br>×3600×132     | 2.5kN/m<br>After reaching<br>to 60min,<br>increase 2.5kN<br>every 5min. | 72min  |
| Jan.18,2008 | Non-bearing<br>interior wall  | Gypsumboard-15mm;<br>Wood stud-89mm;<br>rock fibre-80mm;<br>Gypsumboard-15mm;                               | 3600<br>×3300×243     |   | 183min |
| Jan.19,2008 | Beam                          | Gluelam   | 200×400×5100          | 19kN/m  | 83min  |
| Jan.20,2008 | Floor                         | Two layers of gypsumboard-12mm<br>Resilient metal slat-13mm<br>Beam-235mm; rock fibre-80mm;<br>OSB-18mm OSB | 3065×4500<br>×290     | 2.5kN/m   | 72min  |
| Jan.23,2008 | Column                        | Gluelam   | 200×280               | Design load is<br>80kN , 4-face<br>exposure                             | 90min  |

## 2. DETAILS OF THE LOAD-BEARING EXTERIOR WOOD STUD WALL

### 2.1 Dimensions

The load-bearing wood stud wall assembly is 3600mm(wide)×3300mm(high)×170mm (thick).

### 2.2 Materials

The materials used in this wall assembly were gypsum boards, wood studs, rock fibre and OSB. Type H gypsum-board, conforming to the requirements of GB/T 9775 [EN 520 (Type F)] was used. The thickness of this kind of gypsum board was 15 mm. The framing materials of the wall assembly were wood studs (Solid Timber NH C24, conforms to EN 14081-1), 38 mm thick by 140 mm deep. The insulation for the assembly was rock fibre (density  $\rho \geq 50 \text{ kg/m}^3$ , melting point  $>1000^\circ\text{C}$ , which conformed to EN 13162 and GB/T 19686). OSB used in the unexposed surface of the wall assembly conformed to EN 300.

## 2.3 Fabrication

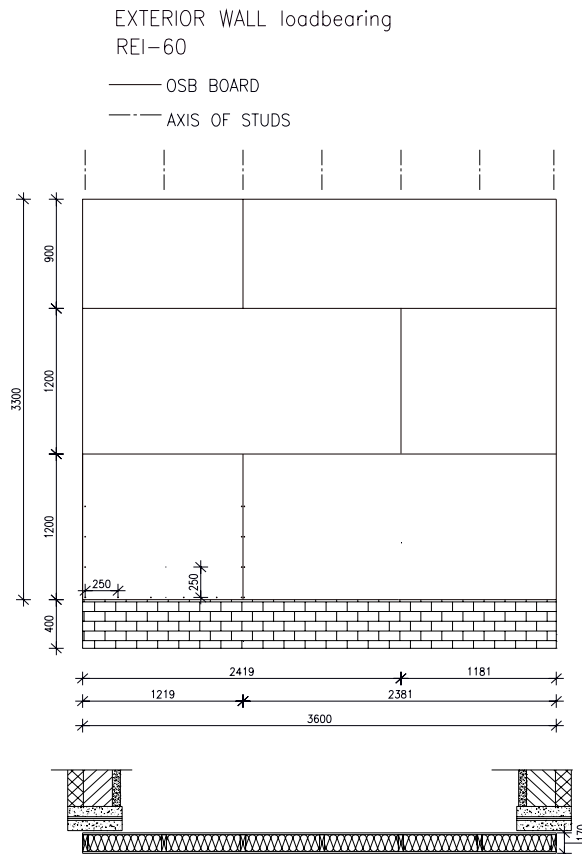
Fabrication details on the assembly is presented in Table 2.

Table 2 Fabrication of load-bearing exterior wall

| No. | Component  | Specification according to            | Thickness [mm] | Cross section |
|-----|--|---------------------------------------|----------------|---------------|
| 1   | Gypsum plasterboard<br>Fastening: dry wall screw 3,5x50 all 250mm                                | EN 520 (Type F)<br>GB/T 9775 (Type H) | 15,0           |               |
| 2   | Studs b/h = 38/140 mm <sup>2</sup> ,<br>e = 600 mm<br>Fastening: (nails 3,8x75)                  | Solid Timber NH C24<br>EN 14081-1     | 140,0          |               |
| 3   | Mineral fibre insulation (rock fibre)<br>density ≥ 50 kg/m <sup>3</sup><br>Melting point >1000°C | EN 13162<br>GB/T 19686                | 140,0          |               |
| 4   | OSB<br>Fastening: (nails 3,3x65)<br>all 250mm  | EN 300<br>EN 13986                    | 15,0           |               |

All the test assemblies were constructed in the processing workshop of the lab. In this wall assembly, one layer of 15mm thick Type H gypsum board was attached vertically to the wood studs on the exposed side with drywall screws, 50mm long, and spaced at 250 mm O.C. along the edges and in the field of the board. Screw locations and gypsum board joints are shown in Figure 2. The screw heads on both the exposed and unexposed faces were covered with joint compound. The gypsum board joints were finished with fibre tape and covered with joint compound.

Figure 2 Screw locations and gypsum board joints



### 3. TEST CONDITIONS AND PROCEDURES

#### 3.1 Instrumentation

Type K (20 gauge) chromel-alumel thermocouples were used for measuring temperatures at a number of locations throughout an assembly.

Thermocouple locations on the unexposed surface of the wall assembly are shown in Figure 3.

Figure 3 Locations of thermocouples

Figure 4 Loading device



#### 3.2 Loading System

The loading device used in this study is illustrated in Figure 4. The components of this device are a strong steel frame, in which the wall assembly is placed, and 9 hydraulic jacks fitted at the top to simulate vertical structural loads. The applied loading on the wall assembly used in this assembly was 22.5Kn/m.

#### 3.3 Test Procedure

The test was carried out by exposing the assemblies to heat in a diesel-fired vertical furnace as shown in Figure 1. The assembly was sealed at the edges against the furnace using ceramic fibre blankets. The furnace temperature was measured by 7 shielded thermocouples in accordance with GB/T 9978. The average of the 7 thermocouple temperatures was used to control the furnace temperature.

#### 3.4 Fire Exposure

During the test, the wall assembly was exposed to heating on the exposed side, in such a way that the average temperature in the furnace followed, as closely as possible, the GB/T 9978 [10] (equivalent to ISO 834) standard time-temperature curve.

#### 3.5 Failure Criteria

The failure criteria were derived from GB/T 9978 [10]. The assembly was considered to have failed if a single point thermocouple temperature reading on the unexposed face rose 180°C above ambient or the average temperature of the 9 thermocouple readings under the insulated pads on the unexposed face (see Figure 3) rose 140°C above the ambient temperature or there was passage of flame or gases hot enough to ignite cotton waste. The test assembly was also deemed to have

structurally failed if there was excessive (>150 mm) deflection.

### 3.6 Recording of Results

The furnace and wall assembly temperatures were recorded at 1 minute intervals through computer data acquisition system. The gauge pressure of the loading system was also recorded at 1 minute intervals.

### 3.7 Observations

Observation during fire test 12th of January 2008, exterior wall REI-60

| time [min:s] | Observation during fire test   | Side of observation |
|--------------|--|---------------------|
| 0:00         | start (manual burner start)  | -                   |
| 2:00         | black coloring of paper lamination fire exposed gypsum board   | E                   |
| 7:30         | surface of gypsum boards becomes white again, cracks in puddy  | E                   |
| 22:00        | puddy in joints fall down  | E                   |
| 25:00        | flammable gases escapes from joints inside the furnace   | E                   |
| 32:00        | visible burning of studs under joints  | E                   |
| 45:00        | escape of Smoke at horizontal OSB joint  | UE                  |
| 55:00        | increase of smoke  | UE                  |
| 64:00        | stop of testing, (break off by test institute)<br>large horizontal deflection, escape of flames between furnace and assembly<br>no integrity failure of assembly only brown colouring at OSB joint | UE                  |

\*) E = fire exposed side

UE = fire unexposed side

## 4. TEST RESULTS

For this exterior wall assembly, the design time was REI 60min. The ultimate result was 64min, which was within our expectation. It failed structurally through excessive deflection. The unexposed surface temperature at the time of structural failure was below the temperature failure criteria.

## 5. CONCLUSIONS

With the help of these verification tests, we have obtained the fire resistance ratings of some typical wood stud walls, floor and gluelam beams and columns as well as their burning behaviors under standard fire. The data obtained from these tests agree well with those obtained from the similar assembly tests done in Canada and Germany. It indicates that China building and fire code can adopt the data of those timber assemblies listed in the building codes of those countries like Canada. Of course, we will do further research on timber fire protection so as to provide more scientific supports for the revision of China building and fire code.

## 6. REFERENCE

1. GB/T 9978-2008: Fire-resistance tests-Elements of building construction-Part 1: General requirements (ISO 834-1: 1999, MOD).
2. NO.2008-0217: Testing Report. National Center for Quality Supervision and Test of Fixed Fire-fighting Systems and Fire-resisting Building Components of China, 2008.

## FIRE RESISTANCE OF TRUSSES WITH PUNCHED METAL PLATE FASTENERS

Petr Kuklík<sup>a</sup>, Jan Starý<sup>b</sup>, Aleš Tajbr<sup>a</sup>, Miloš Vodolan<sup>b</sup>

<sup>a</sup> Czech Technical University in Prague, Faculty of Civil Engineering, Prague, Czech Republic

<sup>b</sup> FINE s.r.o., Prague, Czech republic

### INTRODUCTION

Great attention in the Czech Republic is paid to development of software and methodology of analysis of timber structures with punched metal plate fasteners. Company FINE s.r.o. in cooperation with the fastener producer BOVA Březnice and CTU in Prague, Faculty of Civil Engineering, has been developing program TRUSS for analysis and design of these structures using the modern technology. At the same time, a research of behaviour of punched metal plate fasteners at normal temperature and in fire has been carried out.

### 1 DESCRIPTION OF FIRE TESTS

Geometry and load layout of tested structures were designed to represent common conditions of real structures. The aim of the first experiment was to find the real fire resistance of timber structures connected by punched metal plate fasteners. The second test was performed to determine the influence of simple construction arrangements on increase of fire resistance of the same structure.

#### 1.1 Fire test No. 1

The structure consisted of three flat trusses – see *Fig. 1*. The thickness of timber members was 50 mm, the truss span was 6,0 m and the truss spacing was 1,0 m. The trusses were made of timber of grade S10 (C24) and punched metal plate fasteners BV15 and BV20 were used. The structure was diagonally braced by 120x24 mm members installed in planes of all verticals and upper chords. The top chord was sheathed with 120x24 mm boards and there was no ceiling. The load was determined according to EN 1990 and the trusses were designed in program TRUSS 4. The temperature during the fire test corresponded to the time-temperature curve according to EN 1995-1-2. *Fig. 2* and *Fig 3* show the tested structure.

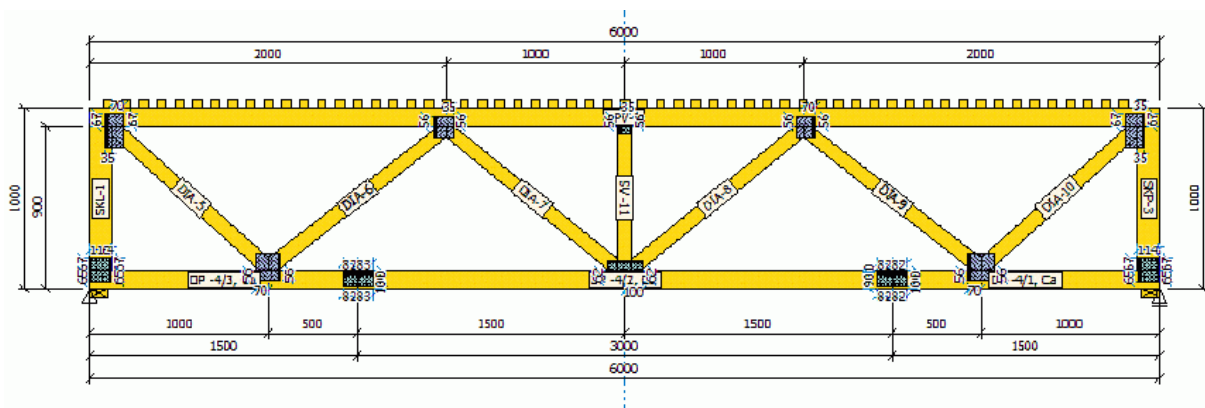


*Fig.1.* Drawing of the truss used for the fire test



*Fig.2.* Structure No. 1 before the fire test



*Fig.3.* Structure No.1 during the fire test

The test results demonstrated that fire resistance of timber structures with punched metal plate fasteners is not insignificant. The second limit state (deflection and rate of deflection increase) was reached after 8 minutes. The structure collapsed (reached the first limit state) in the 11<sup>th</sup> minute of the test. These results were quite encouraging therefore it was decided to perform a second test on the same structure but with some arrangements to increase its fire resistance.

## 1.2 Fire test No. 2

The first fire test indicated that the decisive elements for fire resistance of the structure are the punched metal plate fasteners located in splice of lower chords of trusses. They are the most fire-exposed elements in the structure and their failure quickly leads to collapse of the structure. So it is expected that if this critical point is improved, the fire resistance could increase. Therefore fire test No. 2 was performed. The second structure was the same as the first one except that the punched metal plate fasteners in splice of lower chords of trusses were overlapped with timber elements as shown in *Fig. 4*.



*Fig.4.* Detail view of overlap of a lower chord splice

Test No. 2 was performed at the same conditions as the test No. 1 and the results were positive. The second limit state was reached after 11 minutes and it means the 35% increase of fire resistance with respect to the test No. 1.

## 2 SUMMARY AND ACKNOWLEDGMENT

Two fire tests, performed in the Fire laboratory of PAVUS in Veselí nad Lužnicí, proofed that structures with punched metal plate fasteners by themselves have some fire resistance, which is not insignificant and could be taken into account in structure fire-design. Fire test No. 2 showed that the overlap of splice joint of lower chords with timber elements is a simple and cheap modification, which positively affects fire resistance of these structures.

It is expected to perform sufficient number of similar tests required for significant statistical evaluation. However the two tests are useful pieces in the puzzle of knowledge of fire behaviour of these structures.

The anchorage strengths (5-percentile values) of punched metal plate fasteners BV15 and BV20 produced by BOVA Březnice and determined from tests at normal temperature according to EN 1995-1-1 and EN 14545 are showed in *Fig. 5*.

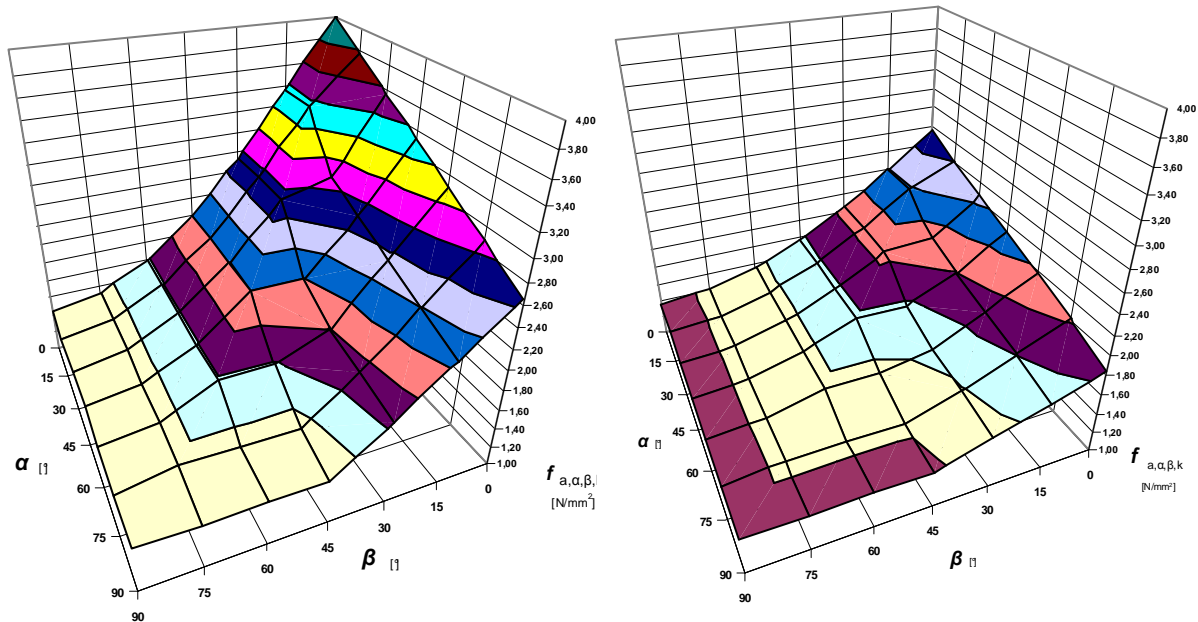


*Fig.5.* Anchorage strengths of punched metal plate fasteners BV15 and BV20

The article was created under the support of the research aim of CTU in Prague MSM 6840770005 "Sustainable Construction".

## REFERENCES

- [1] EN 1990 Eurocode: Basis of structural design
- [2] EN 1995-1-1 Eurocode 5: Design of timber structures - Part 1-1: General rules and rules for buildings
- [3] EN 1995-1-2 Eurocode 5: Design of timber structures - Part 1-2: Structural fire design
- [4] EN 14545 Timber structures - Connectors - Requirements

Proceedings of International Conference  
Applications of Structural Fire Engineering  
Prague, 19-20 February 2009

**Session 8**

**Other Questions**

# SEISMIC AND FIRE DESIGN OF COMPOSITE FRAMES

## A multi-disciplinary approach for an integrated design

Elisabetta Alderighi <sup>a</sup>, Walter Salvatore <sup>a</sup>

<sup>a</sup> University of Pisa, Department of Civil Engineering, Pisa, Italy

### INTRODUCTION

Seismic and fire design of a building structure may be two very demanding tasks especially if included in a performance-based design philosophy, so that a multidisciplinary approach is needed. For the time being, the harmonization on the regulations for these two design fields is almost missing; moreover, while performance-based approach to seismic design has widely developed in last years and introduced by many countries into standards and regulations, the same cannot be said for performance-based design of structures in fire whose application is still limited in scope.

In addition, while many studies have been done on risk assessment for daily fires, there have been very few works on risk assessment and damage evaluation of a building after an earthquake.

In present work, a comprehensive methodology for the evaluation of the structural fire performance of earthquake resistant frames including post-earthquake fire scenarios is presented and applied to a set of composite frames in order to identify an optimized solution with respect to all design actions. Seismic and fire are at first considered as independent hazards, this allowing for the identification of the key structural parameters governing each design phase and thus for their correlation.

Once seismic and fire design issues are met, post-earthquake fire scenarios are investigated showing that control of fires in a building after earthquakes can be possible if the buildings are designed with good earthquake resistance, good fire resistance rating and good overlap between the two.

### 1 THE PROPOSED PERFORMANCE-BASED DESIGN METHODOLOGY

Actual code provisions such as the Eurocodes develop seismic and fire design of structures according to completely independent tools, this preventing the possibility of obtaining an integrated design. It's only in the last years that adopting the idea developed in performance-based earthquake engineering some design procedures have been developed ([1], [2]) accounting for the integration of structural fire safety into the design of framing systems and analyzing buildings subjected to an earthquake and to the subsequent fire (see Figs. 1 and 2). However, even if the evaluation of the state of the structure after the earthquake was posed as a fundamental step, no indication was given of means of quantifying the seismic-induced damage. Moreover, no attention was paid to the necessary harmonization between seismic and fire design fields to promote an integrated design.

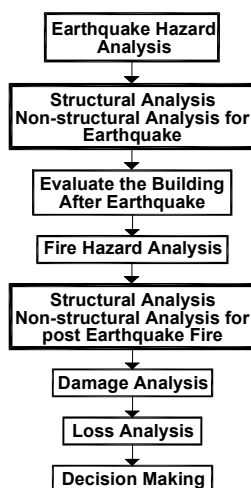


Fig. 1. Lee et al., 2004 [1]

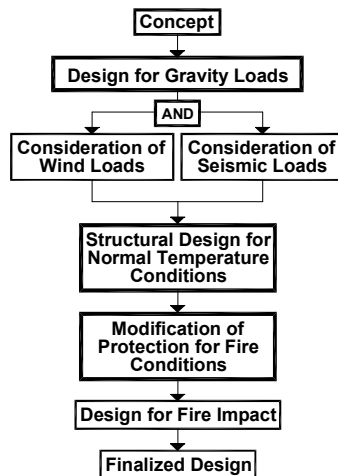


Fig. 2. Johann et al., 2006 [2]

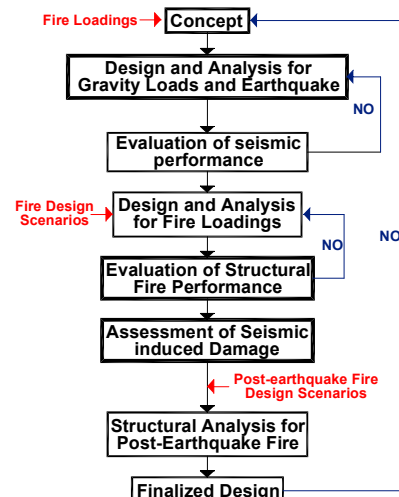


Fig. 3. Proposed methodology

In present paper, a comprehensive methodology for the assessment of the fire performance of earthquake resistant frames including post-earthquake fire design scenarios is presented (see Fig. 3). The starting point is represented by the conceptual design of the building structure meaning that all design issues are carefully evaluated and taken into account since the early design stages, this being very important in order to gather information on the effectiveness of different possible structural solutions. The obtained result is the definition of a set of composite frames to which the proposed methodology is applied in order to identify an optimized solution with respect to all design actions. Afterwards, the process is divided into two main macro-steps consisting in design and evaluation of the structural performance under seismic and fire loadings when these two are considered as independent hazards. In this way, the related design actions are applied in separate conditions and the resulting structural behaviour is carefully evaluated. The importance of separating these two design/performance evaluation phases consists in the identification of the most relevant structural parameters governing each design phase, in order to correlate them for the obtainment of an integrated design solution. In the last step, the post-earthquake fire performance of the frame is re-evaluated by taking into account suitably defined design scenarios.

## 2 THE COMPOSITE FRAMES: CONCEPTUAL DESIGN

In order to choose the most suitable structural solution with respect to all design actions, several frames with the same geometric layout, but different members typologies as defined in the framework of a Europeans Research Project [3] were investigated and summarized in Table 1.

Table 1. Analyzed structural solutions for beam and column elements

| Frame Type | Main beams                                 | Composite Columns              |
|------------|--|--------------------------------|
| Type A1    | IPE (bare steel)                           | HEB (partially encased)        |
| Type A2    | IPE (composite with ribbed steel sheeting) | HEB (partially encased)        |
| Type B1    | IPE (bare steel)                           | CHS (circular concrete filled) |
| Type B2    | IPE (composite with ribbed steel sheeting) | CHS (circular concrete filled) |

For each solution, the main frame was made out of two bays spanning 7,5 and 10 m, respectively while the secondary beams, spanning 7,5 m each, were placed at a distance of 2,5 m and were designed according to a simply supported scheme (see Fig.4) so that the frame resulted braced in transversal direction. For what concerns the elevation, a medium-rise solution was adopted including five floors with 3,5 m inter-storey height.

At this stage, a preliminary investigation on the load bearing capacity at elevated temperature of the two kinds of composite columns was developed and obtained results showed [4,5] that the concrete filled solution offered a more satisfactory behaviour in fire with respect to the partially encased one.

## 3 DESIGN AND PERFORMANCE FOR VERTICAL AND SEISMIC LOADINGS

In the first macro-step of the design procedure, gravity loads in the static combination of actions were applied and afterwards, seismic design was developed according to the lateral force method of analysis with reference to the so called “strong column – weak beam” concept. Seismic design actions were determined considering a behaviour factor  $q = 6$ , meaning high ductility class (HDC). An extensive presentation of the obtained results is reported in previous works [4, 5, 6], anyway the main findings in terms of members’ sizing are summarized in Table 2.

Table 2. Members’ sizing according to different combinations of actions

| Frame   | Static combination of actions (EC3 / EC4) |                  | Seismic combination of actions (EC8) |                            |
|---------|---|------------------|--------------------------------------|----------------------------|
|         | Main beam                                 | Composite Column | Main beam                            | Composite Column           |
| Type A1 | IPE450 (bare steel)                       | HEB340           | IPE450 (bare steel)                  | HEB450                     |
| Type A2 | IPE400 (composite)                        | HEB340           | IPE400 (composite)                   | HEB400                     |
| Type B1 | IPE450 (bare steel)                       | CHS355/10        | IPE450 (bare steel)                  | CHS508/14 (not commercial) |
| Type B2 | IPE400 (composite)                        | CHS355/10        | IPE400 (composite)                   | CHS457/12                  |

It was observed that in the static combination the use of a composite section for the main beams did not allow for a substantial reduction of the steel joist with respect to the bare steel solution and this because the adoption of a moment resisting scheme do not allow taking advantage of the composite action in hogging bending regions, especially for long spans. Afterwards, when passing from static to seismic design, the size of beams' cross sections was unchanged meaning that their sizing is governed by the static combination of actions. Moreover, in the framework of the adopted linear elastic analysis, severe limitations were imposed on the selection of columns cross-sections, especially when coupled with bare steel beams (type A1, type B1) since the last do not add a significant contribution to the global lateral stiffness of the frame. This phenomenon was evident for type B1 frame where no commercial column cross-section with the required amount of flexural stiffness satisfying the serviceability limit states was available. Conversely, the combination with composite beams (type B2) allowed for smaller columns cross-sections, this limiting both frame self-weight and fundamental period.

Afterwards, the seismic performance of each structural solution was evaluated by means of static non linear analysis; obtained results [4, 5] showed that all the analyzed solutions offered a satisfactory behaviour under seismic actions.

**4 DESIGN AND PERFORMANCE FOR FIRE LOADINGS**

In the second macro-step of the procedure, the structural fire performance of the unprotected frames was evaluated by using the program SAFIR [7]. Considering that in seismic design the importance of the relative stiffness between beam and column elements was outlined, three situations accounting for different values of the flexural stiffness ratio  $r$  were investigated to assess its influence in fire situation, and thus setting a correlation between the two design fields.

In particular, the analyzed frames were Type B2 ( $r \sim 1$ ) and Type A1 ( $r < 1$ ) designed for the seismic combination of actions and Type B2 ( $r > 1$ ) designed for the static combination of actions.

Tracing an analogy with performance-based seismic design, a stiffness hierarchy criterion was defined being the condition  $r > 1$ , identified as “soft columns – stiff beams” and the condition  $r < 1$  identified as “stiff columns – soft beams”.

Thermo – mechanical analyses were performed with reference to the same fire design scenario considering fire applied to beam and column elements at the second floor level; the obtained results were expressed in terms of evolution of the axial force in the longest span beam, this being the most representative curve of the global frame behaviour in fire, as shown in Fig. 5.

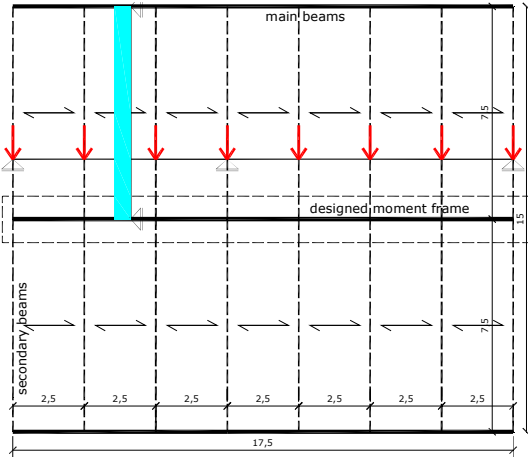


Fig. 4. Typical floor layout

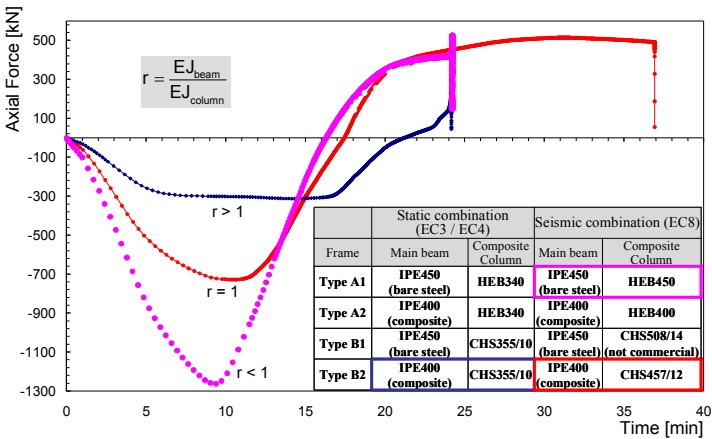


Fig. 5. Axial force in the heated beams

It was observed that the frames designed with  $r > 1$  and  $r < 1$ , possess a quite lower global fire resistance rating than the frame with  $r \sim 1$ ; besides, the obtained curves have quite different shapes. The “static” Type B2 frame ( $r > 1$ ) was not able to develop catenary action since the column elements, being too flexible, were not able to provide a sufficient axial restraint to the heated beam; moreover, the compressive peak was replaced by a constant field characterized by a low intensity.

Conversely, the behaviour of the “seismic” Type A1 frame ( $r < 1$ ) was characterized by a sharp compressive peak and a reduced duration of the developed catenary action; in this case, because of the high flexural stiffness of column elements high values of the axial compressive force are induced in the heated beam, this causing its premature failure. The adopted numerical model wasn’t able to catch local buckling phenomena, but it’s clear that having high values of compressive force in the beam can induce early local buckling of the compressed steel flanges at supports, especially for earthquake resistant frames where the continuity of joints increases such phenomenon [4].

Finally, the performed analysis showed that the “seismic” Type B2 frame ( $r \sim 1$ ) offer the best performance with respect to both seismic and fire actions when these are considered as independent hazards, since it offered near 40 minutes of fire resistance rating even if unprotected [8].

Therefore, such a solution was chosen as reference study case and thermo – mechanical analyses in the post-earthquake fire situation were developed, as reported in the next section.

In present work, no account is taken of the earthquake induced structural damage, anyway extensive details and results on the matter may be found in [9].

## 5 POST-EARTHQUAKE STRUCTURAL FIRE PERFORMANCE

When considering post-earthquake fire situations, different design scenarios have to be taken into account; this would require a comprehensive post-earthquake fire risk assessment involving both analysis and prediction of fire spreading inside the building.

This work focused on structural issues only and some earthquake “indirect” effects were taken into account in a simplified way, namely: the debonding of the steel sheeting from the concrete slab and the possibility of fire spreading between two adjacent compartments.

In each case, the fire performance of the “damaged” frame was evaluated in terms of its global fire resistance rating and compared with the performance in “undamaged” conditions.

### 5.1 Debonding of the steel sheeting from the concrete slab

The cyclic action of earthquake loadings may induce a debonding effect of the steel sheeting from the concrete slab; for this reason, considering the presence of the steel sheeting in a post-earthquake fire situation could not represent a safe-sided choice.

In present work, the fire resistance rating of the frame is re-evaluated neglecting the presence of the steel sheeting in order to assess its influence on the global frame structural fire behaviour.

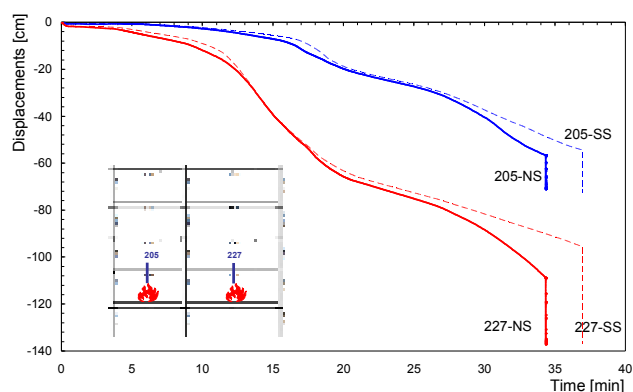


Fig. 6. Vertical displacements at mid-span

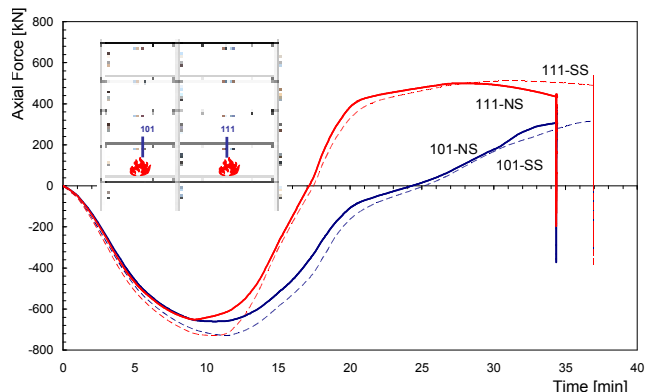


Fig. 7. Axial force in the heated beams

The evolution of vertical displacements at mid-span of heated beams is shown in Fig. 6. When neglecting the steel sheeting (NS), the beams undergo higher displacements at mid-span, especially in the catenary action regime, the steel sheeting offering additional tensile strength and stiffness to the composite beam when loads are carried in tension. It’s worth to notice that the contribution of the steel sheeting is relevant mainly in the later stages of fire this being in contrast with standard design practice where because of elevated temperatures the sheeting is supposed to have lost its strength and its contribution is neglected.

The evolution of internal actions was checked as well; with particular attention to the evolution of axial force, as shown in Fig. 7. In this case, neglecting the steel sheeting caused a reduction of the peak compressive force due to the limited expansion of the beam in the heating phase, this inducing a lower restraining force offered by column elements.

Comparing the global fire resistance rating in the two situations, it was shown that the presence of steel sheeting can partly enhance the structural fire behaviour by adding a 7% to the surviving time. Moreover, the Code assumption of considering the steel sheeting bonded to the concrete slab for all the duration of the fire is revealed to be not on the safe side in a post-earthquake fire situation.

**5.2 Simultaneous fire spreading in two adjacent compartments**

The loss of separating function normally covered by the slab due to extensive seismic-induced concrete cracking may be considered a realistic post-earthquake fire situation increasing the possibility of fire spreading between two adjacent compartments.

In present analysis, it is supposed that a fire can simultaneously start at the first (F1) and second (F2) floor levels, these representing the “weakest” parts of the frame at an earthquake as showed by the distribution of plastic hinges obtained by non-linear static analysis [4, 6].

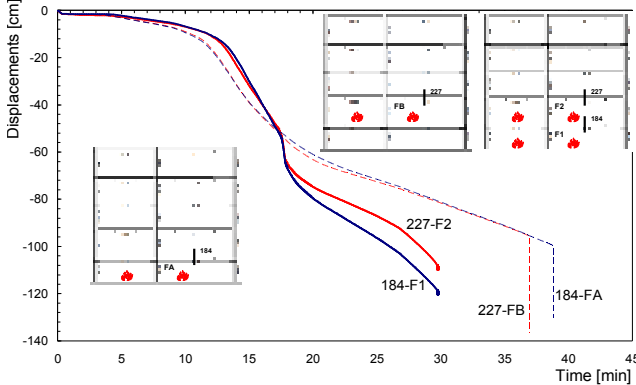


Fig. 8. Vertical displacements at mid-span

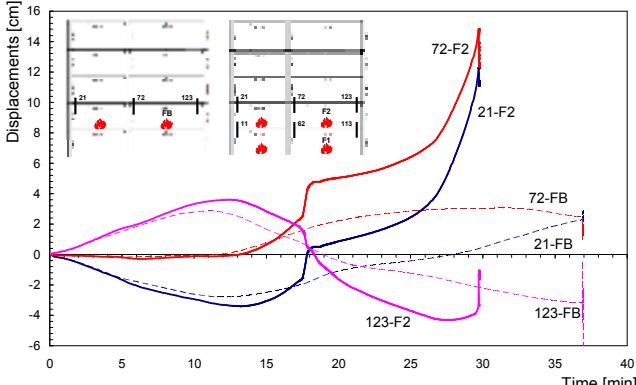


Fig. 9. Horizontal displacements at supports

The evolution of displacements and the distribution of stresses at critical cross-section for the longest span beam were deeply investigated; obtained results were compared with two “undamaged” situations: FA - fire at first floor level only and FB - fire at second floor level only.

The evolution of vertical displacements at mid-span is shown in Fig. 8; the picture shows the tendency of the beams F1 and F2 to move into run-away deflections once the catenary action begins. This is prevented by column elements allowing for higher vertical displacements if compared with the beams FA and FB. For the same reason, vertical displacements are lower in the early stages since beam elements are allowed higher expansion and there is less need to accommodate the restrained thermal elongation through bowing deflections.

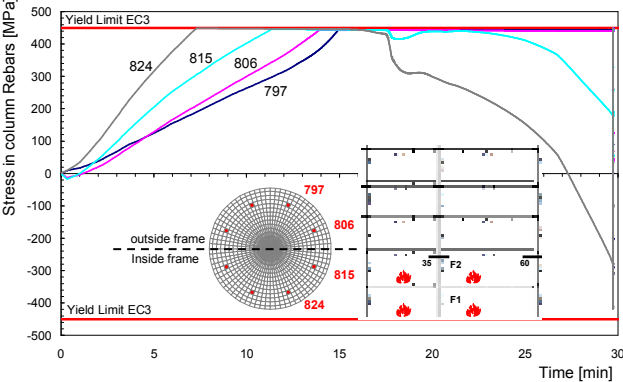


Fig. 10. Top interior column (35): re-bars stress

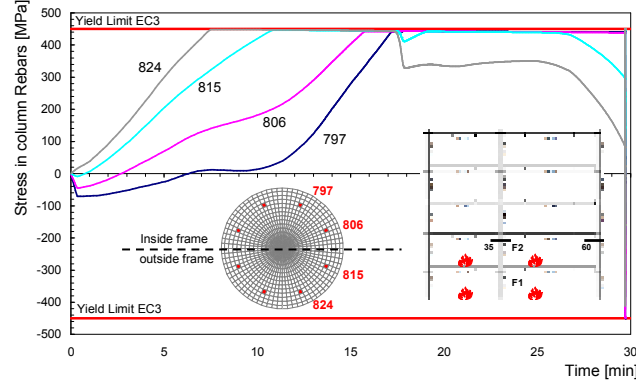


Fig. 11. Top exterior column (60): re-bars stress

The evolution of horizontal displacements at beam ends is shown in Fig. 9; in particular, beams F2 (“damaged”) and FB (“undamaged”) are compared. The two beams show a quite similar behaviour until the beginning of catenary action; only at this point, the shape of displacements of beam F2 changes completely outlining the tendency of the left side and central columns to deflect inwards since they are pulled by the rapidly bowing down heated beam.

For what concerns the state of stress, several critical cross-sections were investigated [4,9]; in particular, the state of stress in the steel re-bars for the top interior (35) and top exterior (60) columns is shown in Figs. 10 and 11, respectively.

The state of stress in steel re-bars is very high near the connection to the beams probably because the column elements heated on two floors are more flexible and hence subjected to higher displacements. This relieves in some way tensile stresses in the top flanges of heated beams, while the re-bars in the column elements yield quickly in tension.

Further investigation is needed, anyway it seems that for this design scenario, failure was due not only to extensive damage in the heated beams but in the heated columns as well, anyway the frame global behaviour was satisfactory, this achieving a fire resistance rating of nearly 30 minutes and showing a time reduction of 23% with respect to FA and of 20% with respect to FB scenarios.

## 6 SUMMARY AND ACKNOWLEDGMENT

The presented comprehensive performance-based design methodology had two main goals. The first was integrating seismic and fire design issues since the early stages; the second was providing an assessment method for the evaluation of the post-earthquake fire performance. The application of such a methodology to a suitably defined set of composite frames showed its effectiveness; in fact, the resulting optimized solution showed a satisfactory behaviour with respect to seismic and fire loadings as independent hazards and in the post-earthquake fire situation, as well.

Results presented in this work were obtained in the framework of the following European research project: RFCS Steel RTD Programme, Contract n. RFSR-CR-03034 [3]. Nevertheless the opinions expressed in this paper are those of the writers and do not necessarily reflect those of the sponsors.

## REFERENCES

- [1] Lee George C., Chen S., Li G., Tong M., On Performance-based Analysis of Buildings for Multi-Hazard Mitigation. *Steel Structures* 4, 231-238, 2004.
- [2] Johann A.M., Albano L.D., Fitzgerald R.W., Meacham Brian J., Performance-Based Structural Fire Safety. *Journal of Performance of Constructed Facilities*, Vol. 20, No. 1, pp. 45-53, 2006.
- [3] RFCS Steel RTD Programme: PRECIOUS, Prefabricated composite beam-to-column concrete-filled tube or partially reinforced-concrete encased column connections for severe seismic and fire loadings. *Technical Steel Research, Science, Research, Development*. Brussels, 2008.
- [4] Alderighi E., Performance of unprotected Composite Frames with Concrete Filled Columns under Seismic and Fire Loadings, *Ph.D. Thesis, Dep. of Structural Engineering Pisa*, 2007.
- [5] Alderighi E., Braconi A., Salvatore W., Design and performance evaluation of bare steel and composite Moment Resisting Frames subjected to seismic and fire loadings, *Proceedings. XII Italian National Conference on Earthquake Engineering, ANIDIS, Pisa, Italy*. Ed. Plus, 2007.
- [6] Alderighi E., Salvatore W., Structural fire performance of earthquake-resistant composite steel-concrete frames. *Engineering Structures* (2009), doi:10.1016/j.engstruct.2008.12.001.
- [7] SAFIR. A Thermal/Structural Program Modelling Structures under Fire, Franssen J.-M., *Engineering Journal*, A.I.S.C., Vol 42, No. 3 (2005), 143-158
- [8] Alderighi E, Franssen J.M., Salvatore W., Performance of unprotected composite frames with CHS columns submitted to fire loadings. *Eurosteel 2008 - 5<sup>th</sup> European Conference on Steel and Composite Structures – Graz (Austria) 3<sup>rd</sup>-5<sup>th</sup> September, 2008*.
- [9] Alderighi E, Franssen J.M., Salvatore W., Post-earthquake structural fire performance of composite steel-concrete frames. *Engineering Structures* (under review),

## FIRE ANALYSIS OF STRUCTURES IN SEISMIC AREAS

Raul Zaharia <sup>a</sup>, Dan Pinteau <sup>a</sup>, Dan Dubina <sup>a</sup>

<sup>a</sup> The "Politehnica" University of Timisoara, Romania

### INTRODUCTION

Fire following earthquake is the most concerning earthquake-related hazard. In some previous papers [1-4], a state-of-art of the risk management related aspects as well as of the available research concerning the structural aspects of the problem, was presented. On another hand, even in case no fire develops immediately after an earthquake, the possibility of later fires affecting the structure must be adequately taken into account, since the earthquake induced damages make the structure more vulnerable to fire effects than the undamaged one. In the present paper, the authors present a study on the influence of the damage induced by the earthquake and of the collapse mechanism of the damaged or undamaged structures under fire action, on the fire resistance. Both standard and natural fire scenarios are considered. The design fire load density for the natural fire scenarios are determined according to Annex E in EN1991-1-2 [5], considering or not the active fire fighting measures, which could be all available in a normal fire situation, but could be partially available immediately after the occurrence of an earthquake.

### 1 ANALYSED STRUCTURES

The moment resisting steel plane frames considered for the present study have the dimensions given in *Fig. 1*. The structures are made using European steel profiles of S235 steel grade and all beam-to-column connections are rigid. Both frames were dimensioned for the same fundamental load combinations of actions (4 kN/m<sup>2</sup> for dead load and 2 kN/m<sup>2</sup> for the live load of the current storey, 3.5 kN/m<sup>2</sup> for dead load and 1.5 kN/m<sup>2</sup> for the live load of the top storey, 0.5 kN/m<sup>2</sup> for the wind action). The frames were further verified for two seismic regions in Romania, with different ground motions: a near-field type (Banat region) and a far-field type (Vrancea region). The design was made according to the Romanian seismic code [6], adapted from EN1998. The elastic spectral analysis was applied considering the response spectrum for the Romanian Banat region (moderate seismic area with the design peak ground acceleration  $a_g=0.16g$  and control period  $T_c=0.7$  seconds), and for Vrancea region (severe seismic area with the design peak ground acceleration  $a_g=0.32g$  and control period  $T_c=1.6$  s). The behaviour factor for the moment resisting frames was considered  $q=6$ . The design of the Frame A - Banat structure was governed by the fundamental load combination (no changes in elements dimensions after the seismic design verification). For all other cases (Frame A – Vrancea and Frame B – Banat and Vrancea) the design of the structures was governed by the seismic combination. *Fig. 1* shows the steel sections of both frames. The values in parathesis represent the profiles used for Vrancea structures, which resulted with stronger beams for some levels and with stronger columns on the height of the building, due to the higher seismic demand.

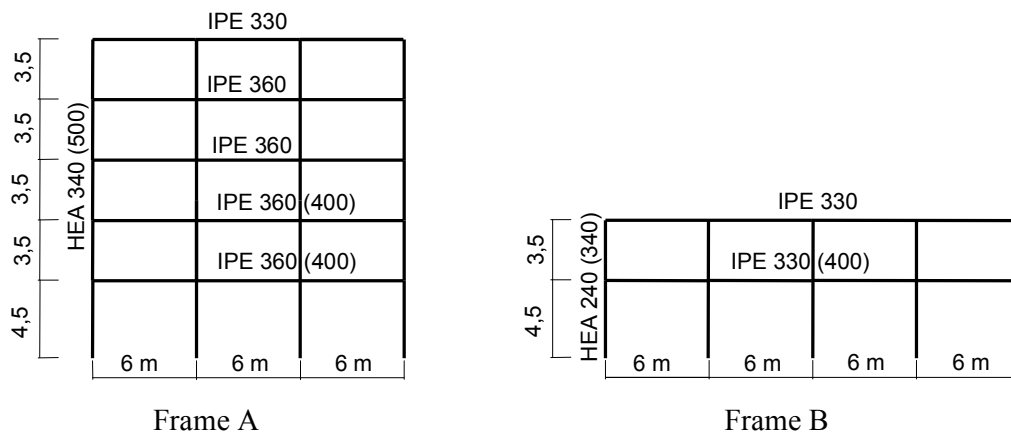


*Fig. 1.* Steel frame dimensions

The seismic response of the structures was evaluated using a pushover analysis, while the displacement demand under the corresponding seismic event was determined using the N2 method [7]. Figures 2-5 show the procedure used to determine the displacement demand (target displacement) of the equivalent SDOF systems for frame B. The entire procedure was presented by the authors in [3].

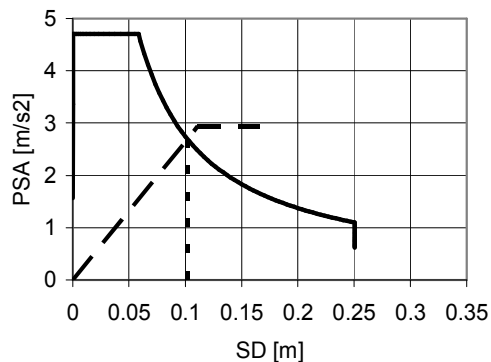


Fig. 2. Seismic demand spectra vs. capacity diagram for Frame A - Banat

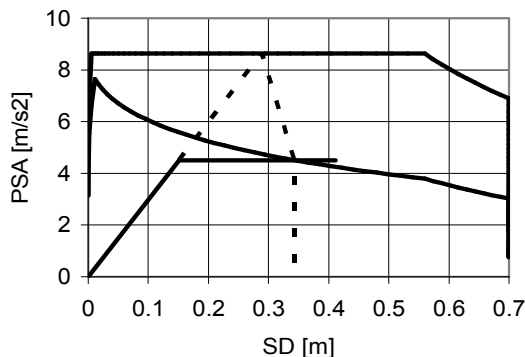


Fig. 3. Seismic demand spectra vs. capacity diagram for Frame A - Vrancea

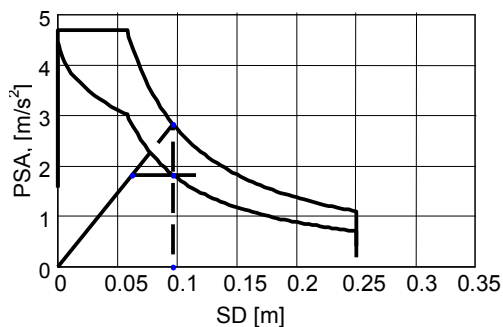


Fig. 3. Seismic demand spectra vs. capacity diagram for Frame B - Banat

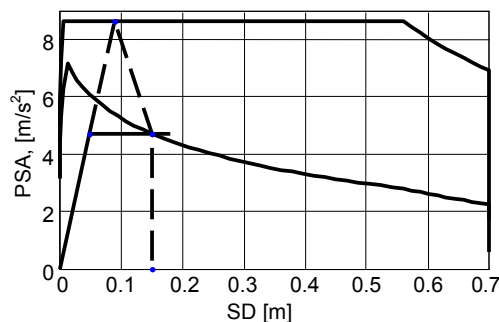


Fig. 4. Seismic demand spectra vs. capacity diagram for Frame B - Vrancea

The Banat Frame A remains elastic after the occurrence of the corresponding earthquake. The Banat frame A was dimensioned from the fundamental load combination, being sensitive to the horizontal wind action, and the steel sections remained the same after the verification for the code seismic action. Frame A - Vrancea responded to the seismic motion in inelastic range, experiencing maximum interstorey drifts of 2.7%, slightly larger than the 2.5% limit corresponding to “Life safety” performance level according to the informative classification given by FEMA 356 [8]. This means that the structure is expected to present important damages of non-structural elements and moderate damages of structural elements, but the safety of the people is guaranteed. The same performance level was attained for Frame B (1.8% maximum drifts for Banat frame and 2.2% maximum drifts for Vrancea frame).

Consequently, after the earthquake, the Frame A - Banat structure remains undamaged, while for the other structures in fire analysis, two hypotheses will be considered:

- a lower intensity earthquake occurs and the structure remains undamaged;
- an earthquake with the intensity given by the Romanian code for Banat and Vrancea regions occurs and the structures suffer the damage determined by the above procedure.

## 2 FIRE ANALYSIS

The standard ISO 834 fire and the natural fires were applied only for the columns and beams of the first storey, in the hypothesis that the ground floor represents a fire compartment. The steel elements have no fire protection. On the beams, the fire was applied on three sides (the top being

protected by the concrete slab). In the mechanical analysis, the collaboration between the steel beam and the concrete slab was not considered.

The natural fire curves were obtained using the OZone v2 computer model [9]. Frame A was considered as part of a structure of 18mx18m in plane, while Frame B was considered as part of a structure of 24mx24m. The walls are made out of normal concrete having a thickness of 20 cm, and the following thermal characteristics: conductivity 0.8 W/mK and specific heat of 840 J/kgK. As shown in Fig. 6 the windows (openings) in three adjacent walls have a sill height of 1 m and a soffit height of 3 m. In the fourth wall the sill height is 2 m and the soffit is 2.5 m. A linear variation of the openings was considered, i.e. the glass panes. At 300°C 30% of the windows were considered broken, while at 500°C all the windows are broken, based on available research presented by the authors in [3, 4].

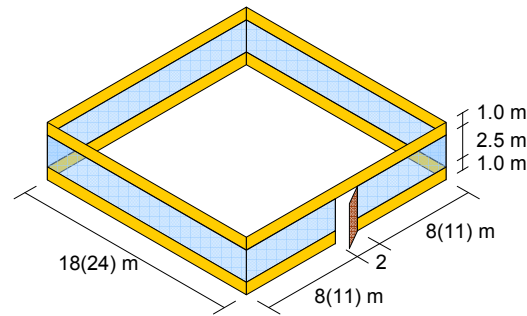


Fig. 6. Fire compartment

The occupancy of the fire compartment is office with a characteristic fire load density  $q_{f,k}$  of 511 MJ/m<sup>2</sup>. The design fire load density, according to Annex E in EN1991-1-2 [8] is

$$q_{f,d} = q_{f,k} \cdot m \cdot \delta_{q1} \cdot \delta_{q2} \cdot \delta_n \quad (1)$$

in which  $m$  is the combustion factor,  $\delta_{q1}$  is a factor taking into account the fire activation risk due to the size of the compartment (1.51 for frame A and 1.65 for frame B),  $\delta_{q2}$  is a factor taking into account the fire activation risk due to the type of occupancy (1.00 for both frames - offices) and  $\delta_n = \prod_{i=1}^{10} \delta_{ni}$  is a factor taking into account the different active fire fighting measures  $i$  (sprinkler, detection, automatic alarm transmission, firemen, etc.).

Table 1 gives the values of the active fire fighting measure factors considered. Before the earthquake, the building being provided with sprinklers, the coefficient which takes into the account the existence of automatic water extinguishing system ( $\delta_1$ ) and the coefficient which takes into account the existence of the independent water supplies ( $\delta_2$ ) are both sub unitary. After the earthquake, considering the possible disruptions, the sprinkler system and the automatic fire detection are no more considered, and the corresponding coefficients are both 1.00. In relation with the prompt intervention of the fire brigades, which is no more possible due to the number of emergencies and traffic congestion, associated to the possible lack of the active fire measures, the coefficients  $\delta_{5,9}$  are considered with the unit value.

Table 1. Fire fighting measures before and after the earthquake

| Fire Scenarios | Autom. Water Exting. | Indep Water Supply | Auto Fire Detection | Alarm Fire Brigade | Fire Brigade   | Access Routes | Fire Fight Devices | Smoke Exhaust | Total         |
|----------------|----------------------|--------------------|---------------------|--------------------|----------------|---------------|--------------------|---------------|---------------|
|                | $\delta_1$           | $\delta_2$         | $\delta_{3/4}$      | $\delta_5$         | $\delta_{6/7}$ | $\delta_8$    | $\delta_9$         | $\delta_{10}$ | $\Pi\delta_n$ |
| Before         | 0.61                 | 0.87               | 0.73                | 0.87               | 0.78           | 1.0           | 1.0                | 1.0           | 0.26          |
| After          | 1.0                  | 1.0                | 1.0                 | 1.0                | 1.0            | 1.5           | 1.5                | 1.0           | 2.25          |

Using these parameters and running the Ozone software [9], two fire curves were produced for each building (Fig. 7). For both buildings, the “before earthquake” curves, for which no flashover occurs, are ventilation controlled. The “after earthquake” curves are fuel controlled. The peak temperatures for Frame B are higher than those of the Frame A, due to the higher design fire load density and to the size of the compartment.

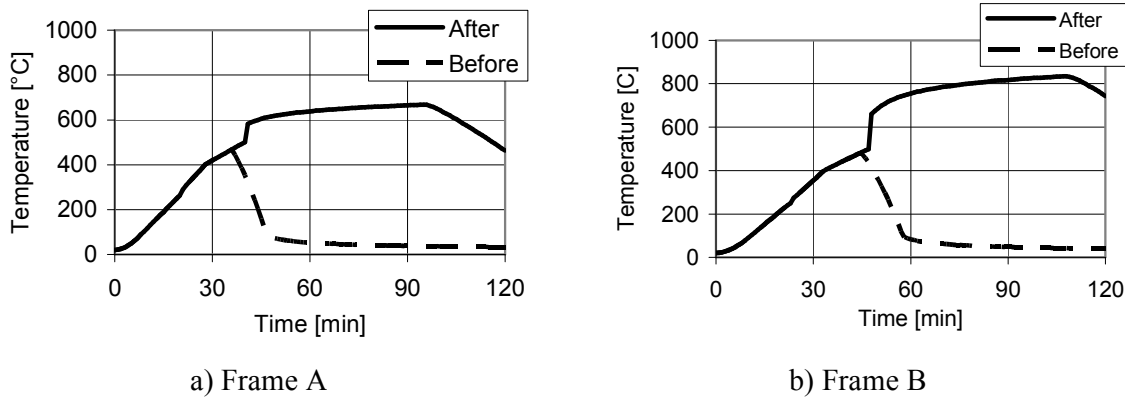


Fig. 7. Temperature-time evolution

These curves were used in SAFIR programme [10] to find the temperature evolutions on each of the exposed profiles, without fire protection. On the beams the fire was applied on three sides (the top being protected by the concrete slab). In the mechanical analysis, the collaboration between the steel beam and the concrete slab was not considered.

The analysis procedure for damaged structures is shown in figure 8b for the damaged Frame B – Banat under ISO fire. The structure subjected to vertical loads corresponding to the fire load combination is loaded with the lateral forces (push-over by applying an inverted triangular distribution of lateral forces, as described previously) up to the target displacement for the MDOF system, determined using the N2 method. The structure is then discarded of the lateral loads and, because the frame responded in the inelastic range, presents residual displacements. At this stage of structural damage, starts the fire analysis under vertical loads corresponding to the fire load combination. Figure 8 shows the response of both damaged and undamaged Frame-B Banat structure under ISO fire, in terms of displacement – time characteristics.

Two types of collapse modes were observed during the fire analysis using standard or natural fire: a global mode and a mode characterised by the collapse of the beams. For all fire analyses, frame A presented a global collapse mechanism, while frame B presented both modes, as shown in figure 9.

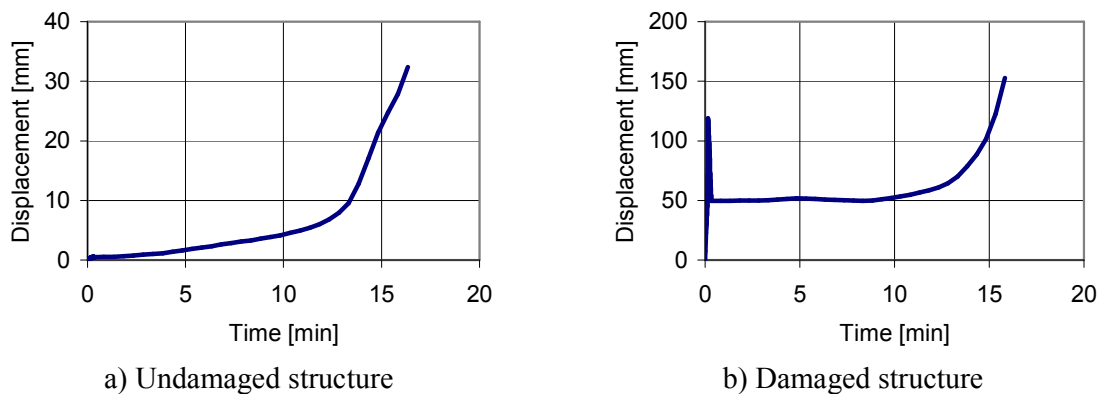


Fig. 8. Displacement-time characteristics for Frame B – Banat under ISO fire

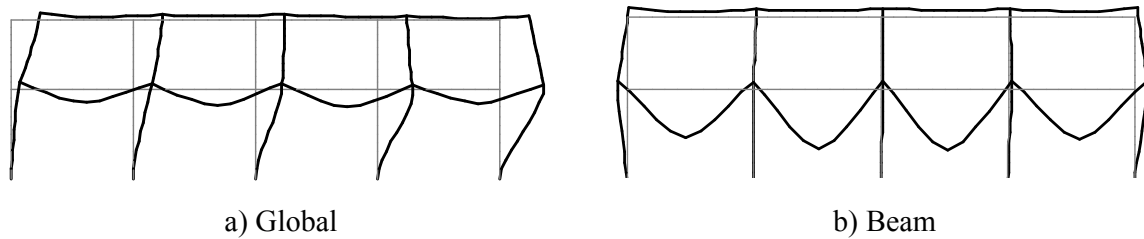


Fig. 9. Collapse mechanisms for frame B

For all cases, considering all fire fighting measures active (in a situation before an earthquake) both frames, designed for the two seismic regions, resist to the fire action. Therefore, no collapse is produced for “before earthquake” natural fire scenario, for which no flashover occurs. Table 2 summarizes the fire resistance times and collapse modes for the standard and natural “after earthquake” fire scenarios for each frame.

Table 2. Fire resistance times and collapse modes

| ISO fire                           | Frame A           |                   | Frame B           |                   |
|------------------------------------|-------------------|-------------------|-------------------|-------------------|
|                                    | Banat             | Vrancea           | Banat             | Vrancea           |
| Undamaged                          | 16' 10"<br>global | 26' 10"<br>global | 16' 30"<br>global | 26' 20"<br>global |
| Damaged                            |                   | 20' 40"<br>global | 15' 40"<br>global | 23' 20"<br>global |
| Natural fire<br>(after earthquake) | Frame A           |                   | Frame B           |                   |
|                                    | Banat             | Vrancea           | Banat             | Vrancea           |
| Undamaged                          | 74' 00"<br>global | no collapse       | 56' 20"<br>beam   | 71' 40"<br>beam   |
| Damaged                            |                   | no collapse       | 54' 40"<br>global | 71' 20"<br>beam   |

It may be observed that there are important differences of time resistance under standard and natural fire, between the undamaged structures (before earthquake, or for an earthquake of lower intensity than the code seismic action for the corresponding region) and the damaged structures. The differences in fire resistance times between the damaged and undamaged structures are affected by the damage level. Under ISO fire, the differences are ranging from around 5% for the Banat frame B (experiencing maximum inter-storey drifts of 1.8% in the inelastic range), 11% for the Vrancea frame B (experiencing maximum inter-storey drifts of 2.2% in the inelastic range), to around 21% for the Vrancea frame A (experiencing maximum inter-storey drifts of 2.7% in the inelastic range). In case of frame B for Banat region under natural fire, the difference is lower, but it is to be also taken into account that for the damaged and undamaged structures, the collapse mechanism is different. In case of frame B for Vrancea region under natural fire, for both damaged and undamaged structures, the collapse mechanism is local (beam) and the fire resistance time is not influenced in a significant way by the damage of the structure.

For both structures and under both fire scenarios, the Vrancea frame, designed for stronger seismic action, presents higher fire resistance times than the corresponding structures designed for the Banat region. Moreover, in case of frame A, for a natural fire scenario after earthquake, the stronger Vrancea frame resists the fire, even if the structure is damaged after the seismic action, while the Banat frame collapses, even if its structure remains undamaged after the code earthquake.

Therefore, it must be underlined that the structures designed for seismic action (or for stronger seismic action) have an important reserve of resistance into a fire situation.

### 3 CONCLUSIONS

The study emphasised that there are important differences in time resistance under standard and natural fire between the undamaged structures and the damaged structures, in case of a fire after an earthquake. The fire resistance time of the damaged structures is influenced by the damage level. The highest differences in terms of fire resistance appear between the damaged and undamaged structures experiencing a global type of collapse mechanism. For the fire scenarios with all fire fighting measures available in a regular fire situation, both structures resisted to the fire action (considering all measures available, the fire does not reach flashover). The structures adapted for seismic action, or designed for stronger seismic action, have an important reserve of resistance in case of a fire after an earthquake, but also in case of a regular fire situation.

### REFERENCES

- [1] Faggiano B., Esposito M., Zaharia R., Pintea D, Risk management in case of fire after earthquake, Urban habitat constructions under catastrophic events, COST Action C26, Malta University Publishing, ISBN 978-99909-44-40-2, 75-80, 2008
- [2] Faggiano B., Esposito M., Zaharia R., Pintea D, Structural analysis in case of fire after earthquake, Urban habitat constructions under catastrophic events, COST Action C26, Malta University Publishing, ISBN 978-99909-44-40-2, 75-80, 2008
- [3] Zaharia R, Pintea D, Dubina D, Fire after earthquake, Proceedings of the Fifth International Conference Structures in Fire, Singapore, 28-30 May, 2008
- [4] Pintea D, Zaharia R, Dubina D, Fire after earthquake- a natural fire approach, Proceedings of the Fifth International Conference EUROSTEEL, 3-5 September, Graz, Austria, 2008
- [5] EN1991-1-2: Eurocode 1 - Actions on structures - Part 1-2: General actions - Actions on structures exposed to fire, 2005, European Committee for Standardization, Brussels
- [6] P100-1/2004, 2005. Seismic design code – Part 1: Rules for buildings (in Romanian) Indicativ P100-1/2004, Buletinul Constructiilor, Vol. 5, 2005
- [7] Fajfar P., A non linear analysis method for performance based seismic design, Earthquake Spectra, vol. 16, no. 3, pp. 573-592, August, 2000
- [8] FEMA 356, Guidelines for Seismic Rehabilitation of Buildings, Vol. 1: Guidelines, FEMA 356, Washington DC, 2002 (formerly FEMA 273).
- [9] Cadornin, J.F, Pintea, D., Dotreppe, J.C, Franssen, J.M, 2003, A tool to design steel elements submitted to compartment fires- Ozone V2, Fire Safety Journal, Elsevier, 38, 439-451.
- [10] J.M. Franssen, VK. R. Kodur, J. Mason, User Manual for SAFIR. A computer program for analysis of structures submitted to the fire. University of Liege, 2004.

## **INCORPORATION OF LOAD INDUCED THERMAL STRAIN IN FINITE ELEMENT MODELS**

Angus Law<sup>a</sup>, Martin Gillie<sup>a</sup>, Pankaj Pankaj<sup>a</sup>

<sup>a</sup> The University of Edinburgh, BRE Centre for Fire Safety Engineering, Edinburgh, UK

### **INTRODUCTION**

Load induced thermal strain (LITS) is an integral part of the behaviour of concrete in fire. The existence of LITS has been well documented and modelled by different researchers. It is vital that this strain development is correctly represented in structural models, as the locked in strains due to LITS constituents are significant. Current methods of modelling LITS involve incorporating the strains into constitutive curves. This approach allows the total strains developed due to LITS to be simply included in a finite element analysis. More thorough representation is needed to accurately represent the plastic components in loading directions, and the total strains in non-loading directions. This paper presents a technique to allow the evolution of LITS in accordance with the rules developed in several academic material models [1-3]. The technique is implemented with a simple Drucker-Prager yield surface and the results assessed.

### **1 CURRENT METHODS**

Inclusion of LITS in a concrete constitutive curve is a convenient way of representing LITS in finite element analyses. It allows the modeller to make the LITS constituents temperature dependent and stress dependent – through the use of multiple curves and by giving strains for different stresses respectively. A number of models are available from different sources and for different concretes [1-4]. Failure to represent LITS will result in the modeller not modelling the strains developed in the material accurately, thereby giving an excessively stiff structure. In fact, it could be argued that since LITS is an integral part of concrete behaviour, a modeller failing to include it will not be modelling concrete but some other, non-physical, material.

Once the total strains caused by LITS have been represented, one can then think about the division between elastic and plastic strains. It has been observed that the largest LITS constituents are irrecoverable [5], i.e. they are plastic strains. Therefore, to accurately model these plastic strains it is necessary to determine the elastic modulus of the material as a function of temperature. If the modulus is too stiff, the plastic strains will be overestimated; too soft, and they will be underestimated. The correct modelling of plastic strain constituents becomes increasingly important as a structure cools as the plastic strains will induce greater tension on strain reversal.

Some authors have presented their material models in parts, allowing the user to build the strain constituents into the full curve. The elastic modulus is, therefore, a precisely identifiable constituent of the material model and can be included in a structural model as such; henceforth, this will be termed the “actual” modulus. Other material data such as that presented in the Eurocode do not specify the value of the elastic modulus. In this case, extra care must be taken to represent the strain components accurately. Where the elastic modulus is the initial gradient of the constitutive curve, this will be termed the “apparent” modulus.

## 2 MULTIPLE DIMENSIONS

The primary focus for research has been on total and plastic strains in the direction of loading. However, attention must also be paid to the non-loading directions. Depending on the model in use, failure to carefully consider the elastic modulus of the material will result in unrepresentative plastic strains, unexpected strains in the non-loading directions, or a mixture of both. The potential for these effects to manifest themselves can be demonstrated by simple example.

### 2.1 Simple Example

Consider a small cube of concrete, subject to a displacement controlled loading in principle direction 2, but free to move in the transverse directions with a Drucker-Prager yield surface and a perfectly plastic material behaviour, as shown in Figure 1. The associative isotropic flow rule (used here for simplicity) dictates that once the yield surface is reached, plastic strain must occur in a direction orthogonal to the yield surface in stress space. This means that plastic strains are induced in directions other than the one in which the load is applied.

Since the location of trial stress is a function of the elastic modulus, the implications of this for the implementation of LITS via a constitutive curve are significant. The inclusion of LITS whether implicitly (with an “apparent” elastic modulus) or explicitly (with an “actual” elastic modulus) will result in a proportion of that LITS becoming active in the transverse directions. The magnitude of the extra strain would depend on the stress state of the material, and on the degree of plasticity developed in the principle direction. For example: should the element described above be at a stress state at point A, no plastic strains would be induced in the 1-direction.

In the case of the apparent modulus, a large proportion of the extra transverse strain may be elastic; while in the case of the actual modulus, the major constituent of the incremental strain would be plastic.

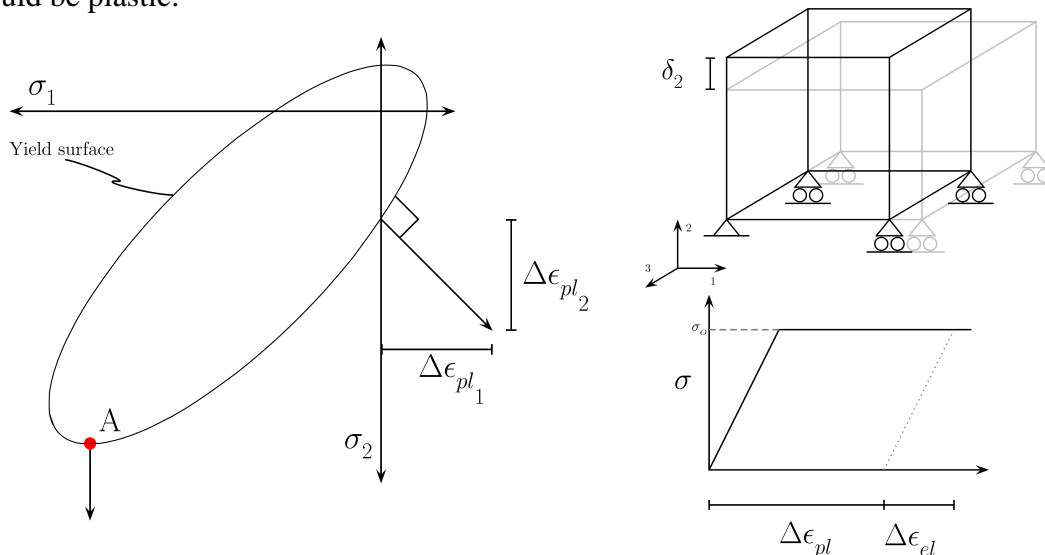


Fig. 1. Plastic flow, and model setup.

The impact of this difference is demonstrated below using the Drucker-Prager yield criterion with a constitutive curve corresponding to that of the 200°C Terro [2] LITS curve. This temperature was used as there is a significant difference between the actual and apparent

moduli, but the temperature is not too extreme. Two different models were created each with a different elastic modulus – apparent or actual – but with the same constitutive curve (Figure 2(a)). The numerical models consisted of a single cubic finite element, restrained at the base in the 2-direction (but free to displace in the 1 and 3-directions) and were strained in the 2-direction. The corresponding deformations and plastic strains were recorded.

Figure 2(b) shows the total strains in the lateral deformation direction. The strains in the 2-direction (i.e. the direction of strain control) are the same for both of the models. In the unrestricted directions, however, there are significant differences in the total strains, particularly in the inelastic phase of the constitutive model. The origin of these differences can be clearly seen from Fig. 2(c). In the “apparent” model the plastic strains do not develop until much later in the deformation process. The “actual” model on the other hand – because of the difference between the elastic modulus and the shape of the constitutive curve – activates the plastic strain constituents immediately. This difference in plastic strain is entirely due to the activation of the flow rule at a much lower stress. Consequently, though the plastic strain in the loading direction is what would be expected from using the “actual” modulus in the constitutive curve, the impact of this approach can be clearly seen in the non-loading directions.

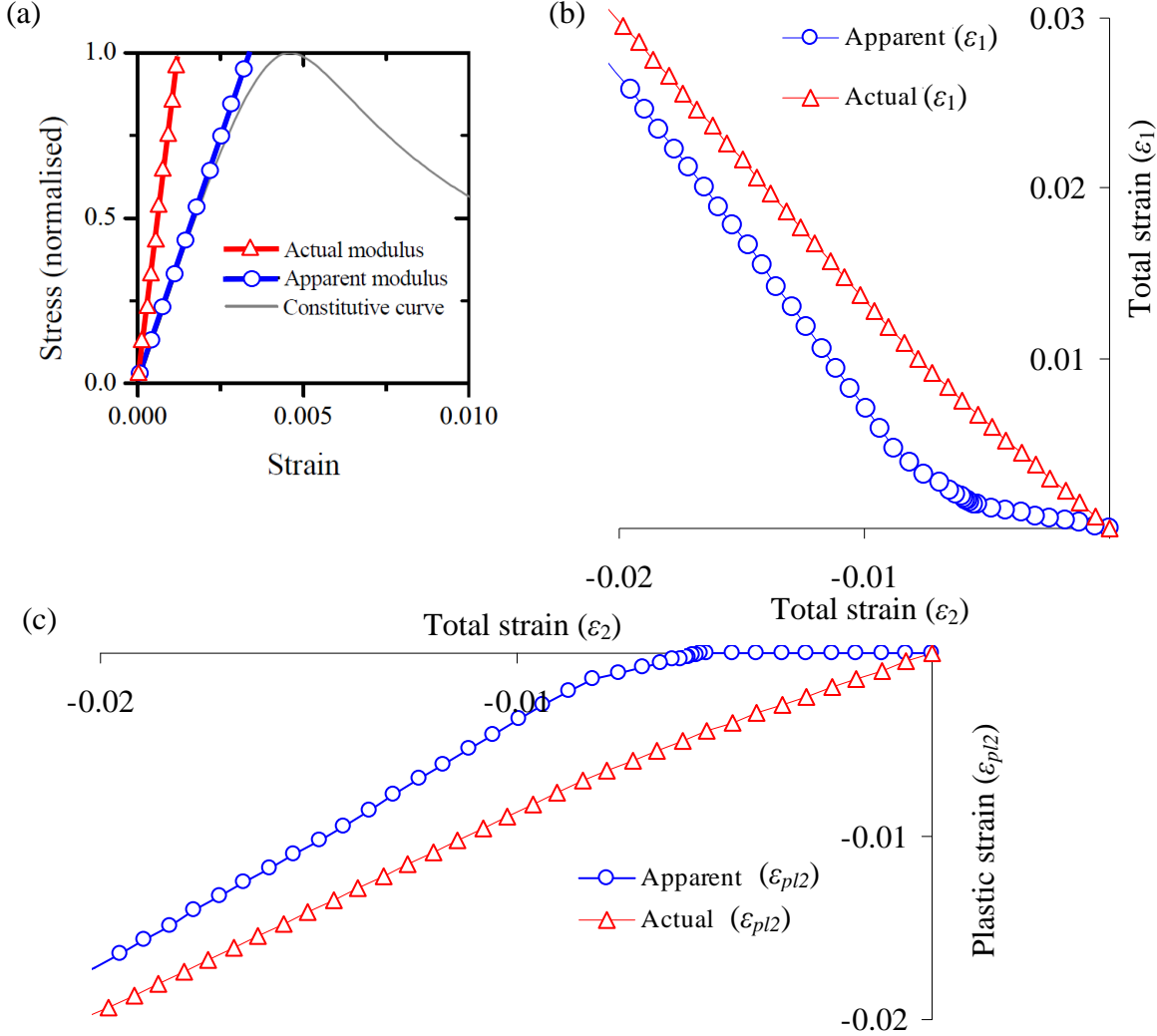


Fig. 2. The same constitutive curve with different elastic moduli gives different lateral deformations and direct plastic strains.

Since equations to represent LITS are all functions of temperature and direct stress, the use of either the apparent or the actual modulus is inadequate if one wants to model the plastic strains accurately, whilst limiting the lateral deformations.

### 3 THE EMBEDDED MODULUS

To allow the modelling of LITS to be more representative, a new method for the inclusion of LITS in the constitutive model while avoiding the transverse strain issue outlined above is proposed. The Drucker-Prager yield criterion and plasticity equations are solved in a two step method: first, the elastic strains and corresponding plastic strains are calculated using the apparent modulus and the normal solution methods (Figure 3); secondly, the elastic ( $\epsilon_{el1}$ ) and plastic ( $\epsilon_{pl1}$ ) strains are recalculated using the actual modulus (Fig. 4). As such, the actual modulus is *embedded* within the solution procedure. This second stage can be expressed simply as:

$$\epsilon_{el1} = \frac{\sigma}{E_{em}} \quad (1)$$

where  $E_{em}$  is the embedded actual modulus and  $\sigma$  is the stress calculated from the previous solution. Since:

$$\epsilon_{el0} + \epsilon_{pl0} = \epsilon_{total} \quad (2)$$

where  $\epsilon_{el0}$  and  $\epsilon_{pl0}$  are the original elastic and plastic strains, and  $\epsilon_{total}$  is the total strain. The new plastic strain can be directly calculated from:

$$\epsilon_{pl1} = \epsilon_{total} - \epsilon_{el1} \quad (3)$$

The new plastic and elastic strains are then used in the subsequent analysis. The equivalent plastic strain is not, however, changed. Consequently, the strains developed in the transverse directions are in line with those that would occur when using an apparent modulus, but the plastic strains developed in the principle direction are as would be expected from using the actual modulus. It should also be noted that where plastic strain has occurred, but the yield function is found to be negative (i.e. the total strain is reduced), the corresponding elastic stresses must be recalculated using the embedded modulus. Otherwise, the redistributed strains would be reabsorbed into the elastic region on return to zero stress.

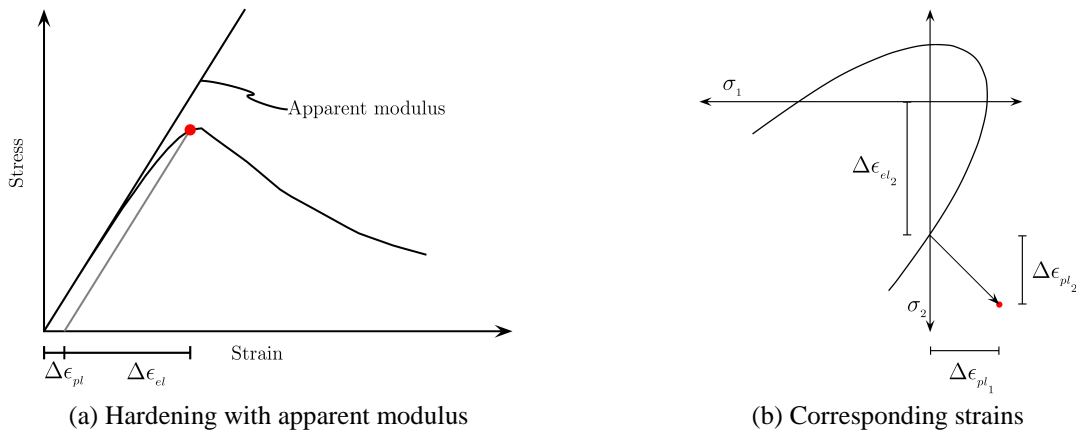


Fig. 3. Calculation of plastic and elastic strains.

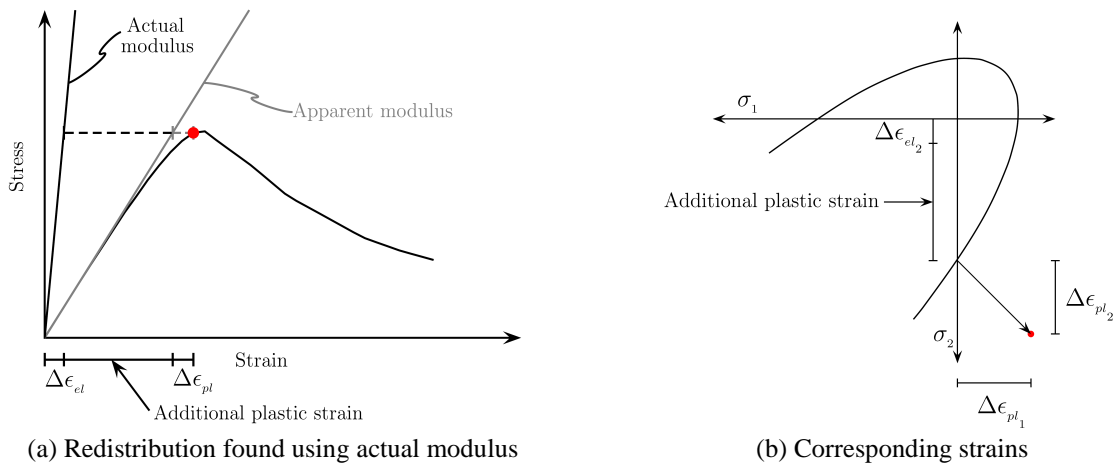


Fig. 4. Redistribution of strains due to the difference between actual modulus and apparent modulus.

A Drucker-Prager model was created [6-12] which incorporated this method of modification by the embedded modulus. A model with an apparent elastic modulus and an embedded actual modulus was subjected to the previously described test. The results were compared with the previous models (Figure 5).

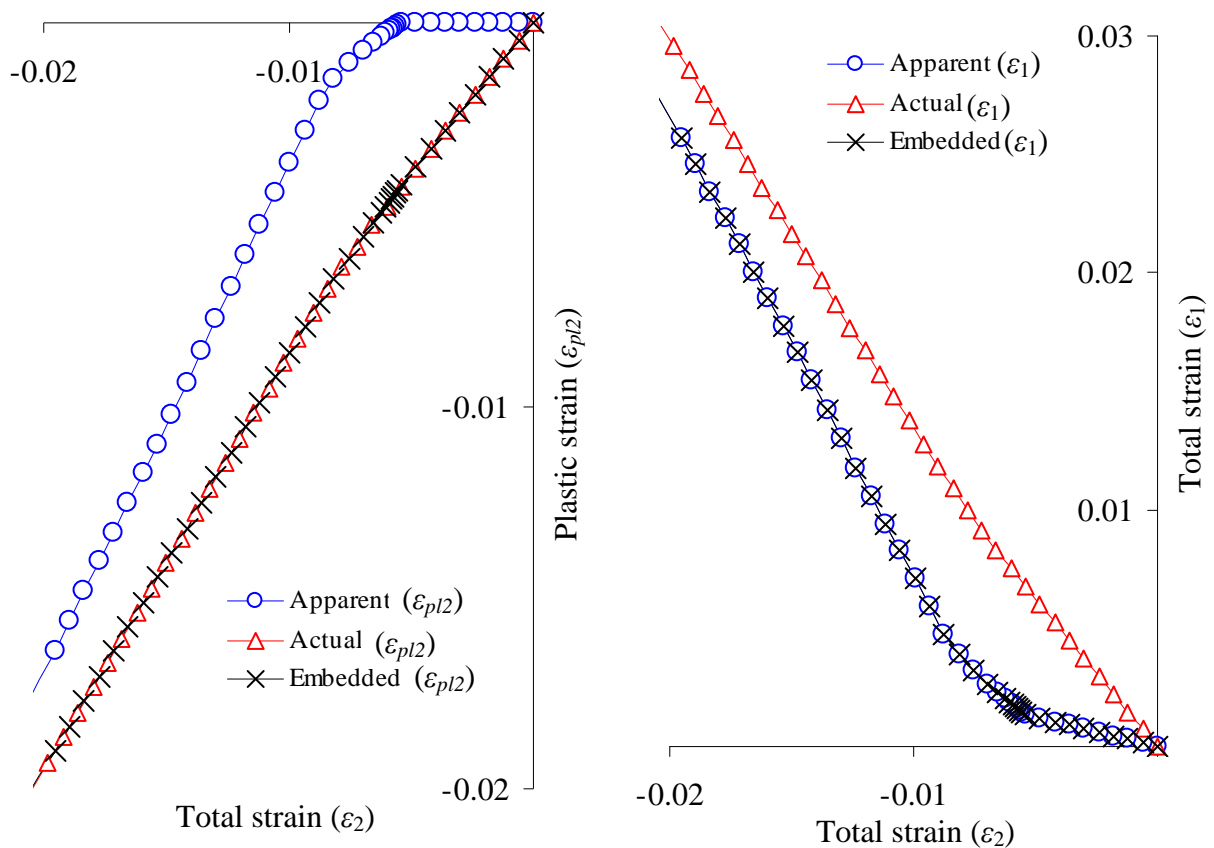


Fig.5. Comparison of two stage approach with results from original models.

The total lateral strains experienced by the “embedded” material are the same as those experienced by the “apparent” material. Equally, the total plastic strain experienced in the loading direction is the same as those experienced by the “actual” material. Thus, a fully

plastic, transient strain constituent has been included in the model without affecting the deformations in the non-loading directions. This allows the plastic LITS effect to be successfully modelled uni-axially and in proportion to the applied stress in the way stated in the governing LITS equations.

#### 4 CONCLUSION

There are several conclusions to be drawn from this study:

- There are significant differences between a constitutive curve which includes LITS, and a full constitutive model which accurately represents LITS components.
- Inclusion of the plastic strains by means of an “apparent” modulus is useful in one dimension; however, plastic flow rules cause unwanted strains to develop laterally when more than one dimension is considered
- Use of a two step model with an “apparent” modulus, and an embedded “actual” modulus within the material model is one approach which can be used to correctly model the plastic strain due to the LITS equations, while allowing the strain in the lateral directions to be modelled correctly. This model has been demonstrated in the case of an element deformed uniaxially.

The authors of this work would like to gratefully thank the project sponsors; BRE Trust, and the EPSRC.

#### 5 REFERENCES

- [1] Anderberg Y, Thelandersson S: Stress and Deformation Characteristics of Concrete, 2 - Experimental Investigation and Material Behaviour Model. Sweden, University of Lund, 1976
- [2] Terro MJ: Numerical Modeling of the Behaviour of Concrete Structures in Fire. *ACI Structural Journal* 95:183-193, 1998
- [3] Nielsen CV, Pearce CJ, Bicanic N: Theoretical Model of High Temperature Effects on Uniaxial Concrete Member under Elastic Restraint. *Magazine of Concrete Research* 54:239-249, 2002
- [4] EN1992-1-2: Design of Concrete Structures - Part1-2: General Rules- Structural Fire Design, 1992
- [5] Khoury GA, Grainger BN, Sullivan PJE: Transient Thermal Strain of Concrete: Literature Review, Conditions within Specimen and Behaviour of Individual Constituents. *Magazine of Concrete Research* 37:131-144, 1985
- [6] Calladine CR: Plasticity for Engineers: Theory and Applications. Chichester, Horwood Publishing, 2000
- [7] Crisfield MA: Non-Linear Finite Element Analysis of Solids and Structures. Chichester, Wiley, 1991
- [8] Crisfield MA: Non-Linear Finite Element Analysis of Solids and Structures: Advanced Topics. Chichester, Wiley, 1997
- [9] Cook RD, Malkus DS, Plesha ME, *et al.*: Concepts and Applications of Finite Element Analysis. Chichester, Wiley, 2002
- [10] Hill R: The Mathematical Theory of Plasticity. Oxford, Oxford University Press, 1950
- [11] Pankaj: Finite Element Analysis in Strain Softening and Localisation Problems, in Department of Civil Engineering. Swansea, University College of Swansea, 1990
- [12] Zienkiewicz OC: The Finite Element Method (ed 3). London, McGraw-Hill, 1977

## FIRE RESISTANCE ASSESSMENT FOR DIFFERENTIATED SAFETY REQUIREMENTS

Mariusz Maślak <sup>a</sup>

<sup>a</sup> Cracow University of Technology, Faculty of Civil Engineering, Cracow, Poland

### INTRODUCTION

Classical methodology of structural member fire resistance evaluation, proposed by the standard EN 1991-1-2 [1], is connected with a comparison between the design value of unfavourable action effect  $E_{fi,d,t}$  of a combination of external loads applied to the structure together with internal forces and moments induced as a result of thermal strains constraint, and the design value of resistance  $R_{fi,d,t}$ , reduced in high temperature. In such an approach the fire resistance limit state is reached if  $E_{fi,d,t} = R_{fi,d,t}$ . In the present paper the safety level of simply supported steel floor beam is studied for fire situation. Such elementary example is selected specially for simplicity and clarity of the interpretations. The permanent load  $g[kN/m]$  as well as the only one variable load  $q[kN/m]$ , both uniformly distributed, are applied to the member. The bending moment, calculated according to the rules of accidental design situation, can be considered as a conclusive action effect:

$$E_{fi,d,t} = M_{fi,d,t} = (g_k + \gamma_Q \psi_2 q_k) L^2 / 8 \quad (1)$$

where  $L[m]$  is the span length,  $\gamma_Q$  is the partial safety factor defined for variable loads, and  $\psi_2 q_k$  is a quasi-permanent value of variable action (in some countries a frequent value of this action  $\psi_1 q_k > \psi_2 q_k$  is suggested to be used). Let us notice that the value of  $E_{fi,d,t}$  remains constant during the whole fire time provided that the beam has the possibility of unlimited thermal deformation. In reality this is only the approximation because load changes generated by evacuation of building occupants or furnishings combustion are not taken into consideration in the analysis. Design value of member resistance  $R_{fi,d,t}$  is obtained based on its characteristic value  $R_{fi,k,t}$ . In fact  $R_{fi,d,t} = R_{fi,k,t} / \gamma_{M,fi}$ ; however, a suggestion to accept  $\gamma_{M,fi} = 1,0$  is given in the standard [1]. In simple load cases  $R_{fi,k,t}$  is proportional to steel yield point  $f_y = f_{y,k} [MPa]$ . The bending modulus  $W$  is adopted as a proportionality factor in the considered example. When steel temperature  $\Theta_a [^\circ C]$  grows,  $f_y$  decreases as follows:

$$f_{y,\Theta} = k_{y,\Theta} f_{y,20} \quad (2)$$

The quantity  $f_{y,20}$ , defined for the room temperature  $\Theta_a = 20^\circ C$ , is then understood as a reference value. Parameter  $k_{y,\Theta}$  is a suitable reduction coefficient. Its values, determined for particular steel temperatures, are given in EN 1993-1-2 [2]. Finally, the beam resistance can be calculated by means of the following formula:

$$R_{fi,d,t} = R_{fi,k,t} / \gamma_{M,fi} = W k_{y,\Theta} f_{y,20} \quad (3)$$

## 1 REQUIRED SAFETY LEVEL

Failure probability  $p_f$  is usually adopted as the reliable safety measure in design of steel members for fire situation. If maximum value of such probability, acceptable by the user of the structure, is described as  $p_{f,ult}$ , then the global safety condition has the following form:

$$p_f < p_{f,ult} \quad (4)$$

This formula is frequently rearranged to the equivalent inequality:

$$\beta > \beta_{req} \quad (5)$$

in which  $\beta$  is the global reliability index. Its required (target) value  $\beta_{req}$  is explicitly connected with ultimate failure probability. If random variables  $E$  and  $R$  are described by means of normal or log-normal probability distribution, then:

$$p_{f,ult} = \Phi(-\beta_{req}) \rightarrow \beta_{req} = -inv\Phi(p_{f,ult}) \quad (6)$$

Symbol  $\Phi()$  means the cumulative distribution function of standardized normal probability distribution. The notation  $inv\Phi$  is understood as an inverse function of  $\Phi$ . Probability  $p_{f,ult}$  is unequivocally determined only if corresponded reference period  $n$ [years] is given. Usually it is assumed that  $n = 50$  years; however, period  $n = 1$  year is also considered in many cases. In general, if the probability  $p_{f,ult}$  identified within 50 years period is known, then its respective value, adequate for  $n \neq 50$  years, may be calculated from the equation:

$$\Phi(\beta_{50}) = 1 - \Phi(-\beta_{50}) = \Phi(\beta_n)^{50/n}, \text{ hence if } n = 1 \text{ year we have: } \Phi(\beta_1)^{50} = \Phi(\beta_{50}) \quad (7)$$

Values of  $\beta_{req}$  are differentiated depending on real safety requirements. Such a methodology leads to the specification of various kinds of reliability classes  $RC$ . They are the most frequently related to the consequences of failure or to the relative cost of safety measure [3]. In the standard EN 1990 [4] only three reliability classes are defined (Table 1).

Table 1. Reliability classes according to EN 1990 [4]

| Reliability class | Safety requirements | $\beta_{req}$ for reference period equal:                                  |  |
|-------------------|---------------------|--|--|
|                   |                     | one year   | 50 years   |
| RC3               | range               | $\beta_{1,req} = 5,2 \left( p_{1,f,ult} \approx 9,9 \cdot 10^{-8} \right)$ | $\beta_{50,req} = 4,3 \left( p_{50,f,ult} \approx 8,5 \cdot 10^{-6} \right)$ |
| RC2               | moderate            | $\beta_{1,req} = 4,7 \left( p_{1,f,ult} \approx 1,3 \cdot 10^{-6} \right)$ | $\beta_{50,req} = 3,8 \left( p_{50,f,ult} \approx 7,2 \cdot 10^{-5} \right)$ |
| RC1               | minor               | $\beta_{1,req} = 4,2 \left( p_{1,f,ult} \approx 1,3 \cdot 10^{-5} \right)$ | $\beta_{50,req} = 3,3 \left( p_{50,f,ult} \approx 4,8 \cdot 10^{-4} \right)$ |

## 2 PARTIAL SAFETY FACTOR FOR VARIABLE LOADS

The component safety factor  $\gamma_Q$  specified for variable load is the basic safety measure necessary to obtain design value of the action effect  $E_{f,d,t}$  (see Eq. 1). Its constant value  $\gamma_Q = 1,5$  is accepted in design methodology based on the standard recommendations. However, such statement is not precise enough. In reality, its minimum value  $\gamma_{Q,min}$  is greater for greater coefficient  $\nu_Q$ . Action  $q$  applied to the beam is a random variable described by

means of *Gumbel* probability distribution  $G(\tilde{q}, u_Q)$  -  $\tilde{q}$  is the modal value of load intensity whereas  $u_Q$  is *Gumbel* standard deviation. It is well known that:

$$u_Q = \sigma_Q \sqrt{6}/\pi = 0,78\sigma_Q \text{ and } \tilde{q} = \bar{q} - 0,577u_Q = \bar{q} - 0,45\sigma_Q \quad (8)$$

where  $\bar{q}$  and  $\sigma_Q$  are the parameters of normal probability distribution - the mean value and the standard deviation, respectively. Design load intensity  $q_d$  depends on the component value of global safety index  $\beta_E = \alpha_E \beta$  (it is a partial safety index determined for the action effect). Ultimate limit state is reached if  $\beta = \beta_{req}$ . Furthermore, according to design format proposed by [4] constant value  $\alpha_E = 0,7$  is fixed as a result of calibration process presented in many papers. Finally, for *Gumbel* probability distribution, we have:

$$q_d = \tilde{q} - u_Q \ln[-\ln \Phi(\alpha_E \beta)] = \bar{q} \{1 - 0,78v_Q [0,577 + \ln(-\ln \Phi(0,7\beta))]\} \quad (9)$$

where  $v_Q = \sigma_Q/\bar{q}$ . Characteristic value  $q_k$  is defined as a 95% fractile, therefore:

$$q_k = \tilde{q} - u_Q \ln[-\ln(0,95)] = \bar{q} \{1 - 0,78v_Q [0,577 + \ln(-\ln(0,95))]\} = \bar{q}(1 + 1,867v_Q) \quad (10)$$

Consequently:

$$\gamma_Q = \frac{q_d}{q_k} = \frac{1 - 0,78v_Q \{0,577 + \ln[-\ln \Phi(0,7\beta)]\}}{1 + 1,867v_Q} \quad (11)$$

Substituting particular values of  $\beta_{50,req}$  and  $\beta_{1,req}$  from Table 1 into the place of  $\beta$  in Eq. 11 gives the set of functions  $\gamma_{Q,min} = \gamma_{Q,min}(v_Q)$  presented in Fig. 1a for 50 year and in Fig 1b for one year reference periods. They are the minimum values of  $\gamma_Q$  for which the component safety condition  $E_{fi} < E_{fi,d,t}$  (its equivalent is the inequality  $\beta_E \geq \beta_{E,req} = 0,7\beta_{req}$ ) is satisfied. Let us notice that the standard value  $\gamma_Q = 1,5$  is in general much greater than  $\gamma_{Q,min}$ , even if the range safety requirements are assumed and load variability is considerable ( $v_Q \geq 0,2$ ).

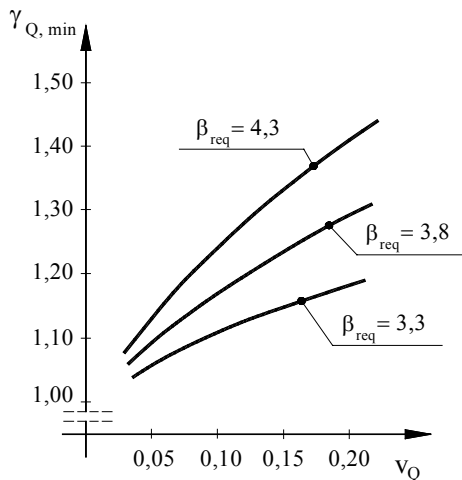


Fig. 1a. Minimum values of  $\gamma_Q$  for 50 year reference period

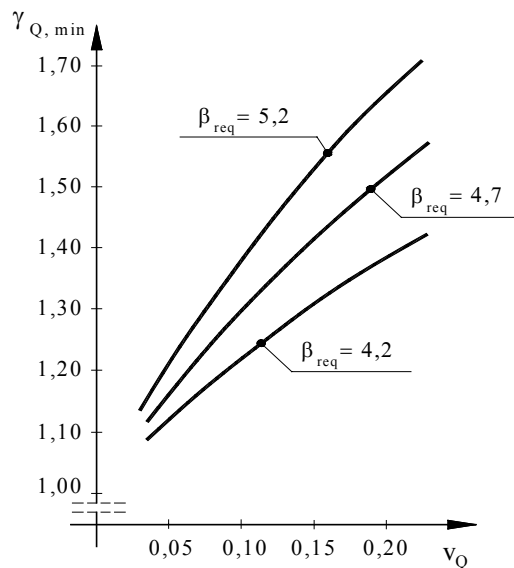


Fig. 1b. Minimum values of  $\gamma_Q$  for one year reference period

### 3 LIMITATIONS RELATED TO MEMBER RESISTANCE

Analogous condition  $R_{fi} > R_{fi,d,t}$ , in other words  $\beta_R > \beta_{R,req} = \alpha_R \beta$ , leads to the specification of minimum values of partial safety factor  $\gamma_{M,fi}$ . In the standard [4] a constant value  $\alpha_R = 0,8$  is suggested. Random variable  $R$  is characterized by log-normal probability distribution  $LN(\bar{R}, \nu_R)$  -  $\bar{R}$  is the median value, whereas  $\nu_R$  - the log-normal coefficient of variation. Characteristic value  $R_{fi,k,t}$  is assumed as a 95% fractile. Consequently:

$$\gamma_{M,fi} = \frac{R_{fi,k,t}}{R_{fi,d,t}} = \frac{\bar{R} \exp(-1,645 \nu_R)}{\bar{R} \exp(-0,8 \beta \nu_R)} = \exp[(0,8 \beta - 1,645) \nu_R] \quad (12)$$

Taking particular  $\beta_{50,req}$  from Table 1 as a  $\beta$  value in Eq. 12 gives curves  $\gamma_{M,fi,min} = \gamma_{M,fi,min}(\nu_R)$  presented in Fig. 2. Let us underline that those values are always greater than constant value  $\gamma_{M,fi} = 1,0$  proposed in [1] and [2].

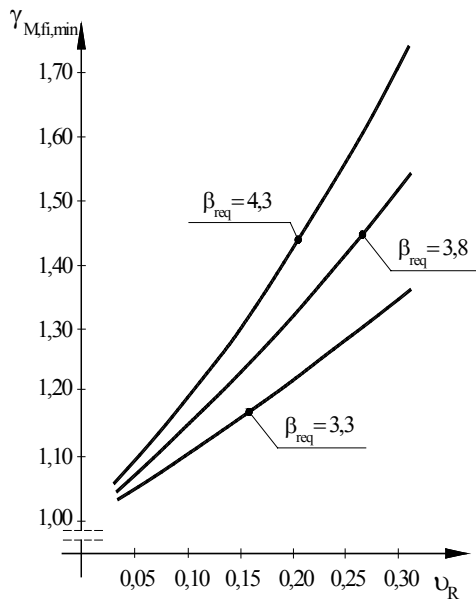


Fig. 2. Minimum values of  $\gamma_{M,fi}$

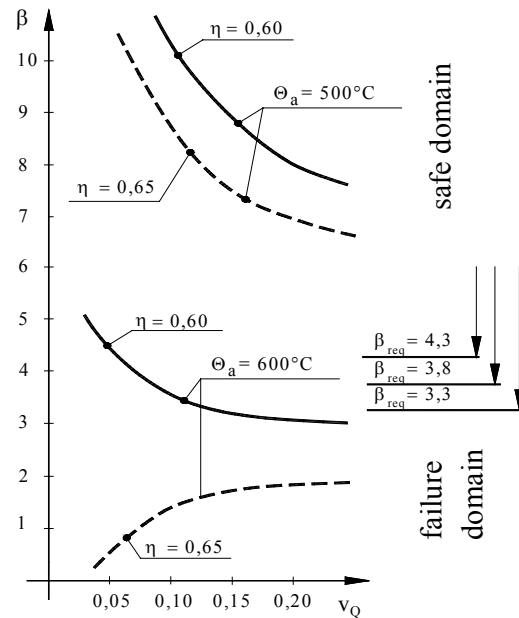


Fig. 3. Global reliability index  $\beta = \beta(\nu_Q)$  for selected temperatures of steel

### 4 GLOBAL SAFETY CONDITION

Basic safety condition has the form  $E_{fi,d,t} < R_{fi,d,t}$ . It means that the safety margin can be calculated as  $g = R_{fi} - E_{fi} > 0$ , hence in ultimate limit state we have:

$$g = R_{fi,d,t} - E_{fi,d,t} = 0 \quad (13)$$

Let  $\eta = q_k / (g_k + q_k)$  be the parameter which reflects the importance of variable action in relation to the total load. Value  $\eta = 0$  means that  $q_k = 0$ , on the other hand if  $\eta = 1$  then  $g_k = 0$ . Furthermore  $\bar{R} = \bar{W} \bar{k}_y \bar{f}_y$ , where  $\bar{f}_y = f_{y,k} \exp(2\nu_f)$  - as a 98% fractile,  $\nu_f = 0,08$  (it is a measure of variability of  $f_y$ ),  $\bar{k}_y$  is adopted as a nominal value  $k_y$  from [2],  $\bar{W}$  is also

equal to the nominal value taken from tables. Random variability of  $k_y$  and  $W$ , described by means of the coefficients  $\nu_k$  and  $\nu_A$  respectively, is summed with  $\nu_f$  giving  $\nu_R = \sqrt{\nu_f^2 + \nu_A^2 + \nu_k^2}$ . It is accepted that  $\nu_A = 0,06$  and  $\nu_k = 0,20$ , then  $\nu_R = 0,22$ . Such a great value of variability of  $k_y$  is the reflection of considerable uncertainty of a model describing mechanical properties of steel under fire conditions. For example *M. Holicky* [5] suggests to use in this field  $\nu_k = 0,10 \div 0,30$ . Finally, Eq. 13 can be rearranged to the form:

$$g(\eta, \Theta_a, \beta, \nu_R, \nu_g, \nu_Q) = R_{fi,k,t} - \left( \frac{g_k \cdot L^2}{8} \right) \left( 1 + \gamma_Q \psi_2 \frac{\eta}{1-\eta} \right) = 0 \tag{14}$$

This condition has been solved for the beam made of IPE300 and the span length equal  $L = 6m$ . Many diagrams can be presented as a result of such calculation. Dependence between the index  $\beta$  and coefficient  $\nu_Q$ , determined for selected temperatures  $\Theta_a$ , is given in Fig. 3. Functions  $\beta = \beta(\nu_Q)$  specified for particular values of  $\eta$  parameter are shown in Fig. 4 (for  $\Theta_a = 400^\circ C$  in Fig. 4a, and for  $\Theta_a = 600^\circ C$  in Fig. 4b). Last of all, curves  $\beta = \beta(\eta)$  are demonstrated in Fig. 5 for various temperatures  $\Theta_a$  (let us notice that variability  $\nu_Q = 0,1$  is adopted in Fig. 5a, whereas  $\nu_Q = 0,2$  in Fig. 5b). It is extremely important that all values of  $\beta$  index, obtained from Eq. 14 and presented in Figures 3, 4 and 5, have to be compared with suitable levels of safety margin, which are defined by the ultimate values of  $\beta_{req}$  (those levels are marked separately in analysed diagrams).

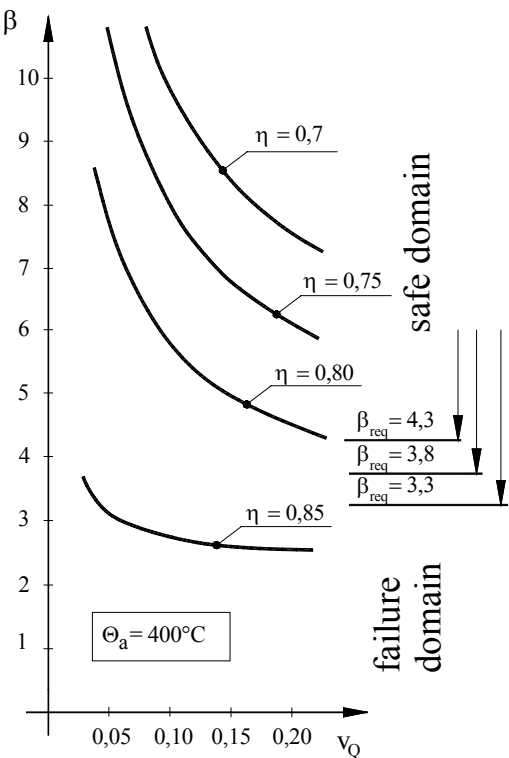


Fig. 4a. Reliability index  $\beta = \beta(\nu_Q)$  for particular values of  $\eta$  parameter ( $\Theta_a = 400^\circ C$ )

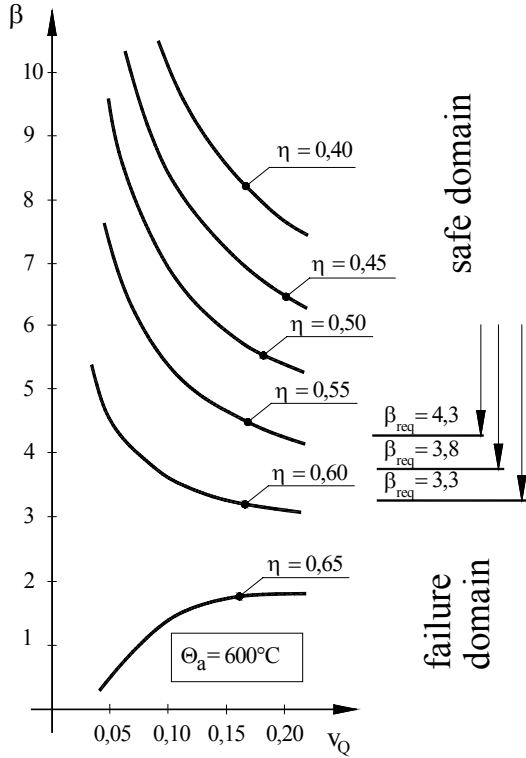


Fig. 4b. Reliability index  $\beta = \beta(\nu_Q)$  for particular values of  $\eta$  parameter ( $\Theta_a = 600^\circ C$ )

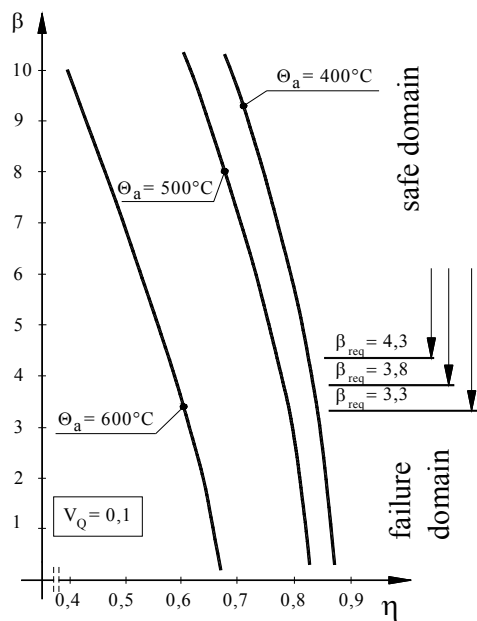


Fig. 5a. Reliability index  $\beta = \beta(\eta)$  for selected temperatures of steel ( $v_Q = 0,1$ )

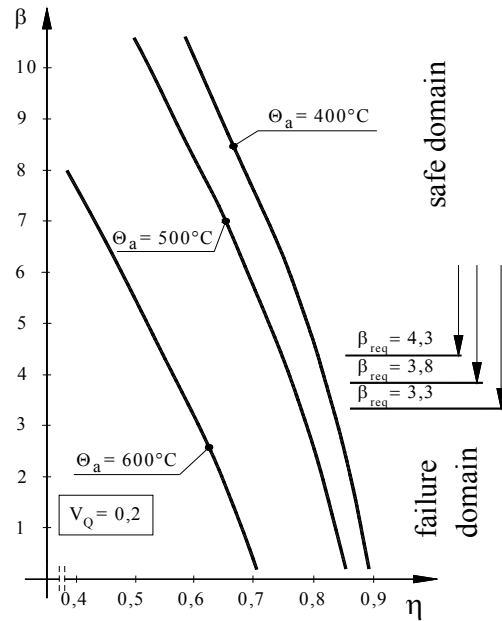


Fig. 5b. Reliability index  $\beta = \beta(\eta)$  for selected temperatures of steel ( $v_Q = 0,2$ )

## 5 SUMMARY AND CONCLUSIONS

The aim of this paper is to show the ratio of the transformation of real safety level during fire. The global reliability index  $\beta$  is adopted as a reliable measure which allows to determine the member failure probability  $p_f$  in particular fire moments described by means of different steel temperatures  $\Theta_a$ . Not only the global safety condition  $E_{d,fi,t} < R_{d,fi,t}$  but also two component limitations:  $E_{fi} < E_{fi,d,t}$  and  $R_{fi} > R_{fi,d,t}$ , have to be taken into account in such semi-probabilistic design approach. Inserted figures show the functions  $\beta = \beta(v_Q)$  and  $\beta = \beta(\eta)$  and their dependence on steel temperature growth. Differentiated safety requirements are considered due to the specification of various reliability classes which is an equivalent of the acceptance of different values of required index  $\beta_{req}$ . The simplified design approach proposed by standards [1] and [2] is not fully compatible with classical methodology of member safety evaluation. In the present paper it is shown that the suggested value  $\gamma_{M,fi} = 1,0$  is too small to secure required safety level of the resistance. On the other hand, this lack is partly compensated by the acceptance of constant value  $\gamma_Q = 1,5$ , greater then necessary.

## REFERENCES

- [1] EN 1991-1-2, Eurocode 1: Action on structures – Part 1-2: General actions – Actions on structures exposed to fire,
- [2] EN 1993-1-2, Eurocode 3: Design of steel structures – Part 1-2: General rules – Structural fire design,
- [3] JCSS Probabilistic Model Code, Joint Committee on Structural Safety, 2001,
- [4] EN 1990, Eurocode – Basis of structural design,
- [5] Holicky M., Decision on fire safety measures based on risk assessment, Proceedings of 9<sup>th</sup> International Conference on Structural Safety and Reliability *ICOSSAR*, Rome, Italy, June 19-23, 2005.

## PERFORMANCE OF STRUCTURAL SYSTEMS IN FIRE

H. Mostafaei , M. A. Sultan, N. Bénichou

National Research Council Canada, Institute for Research in Construction, Ottawa, Canada

### INTRODUCTION

Traditionally, fire-resistance tests of structures have been employed based on individual element tests and without consideration of interactions among structural elements and systemic structural response. Recent studies indicate that systemic interactions and boundary conditions of a structure can have significant effects both on the performance of the entire structural system and on the response of the individual structural elements. Therefore, to achieve a comprehensive understanding of the structural response, application of a proper performance-based evaluation and design methodology is inevitable.

One of the most important systemic phenomena, barely considered previously in the design of building structures exposed to fire, is the effect of thermal expansion on the behaviour of structures in fire [1]. Effects of thermal expansion on structural performance could not be evaluated based on the traditional fire-resistance tests, in which structural elements such as beams, floors, or columns, are exposed to the standard fire, individually, disregarding the boundary conditions. Therefore, to investigate the behaviour of structures subjected to thermal expansion, a performance-based evaluation approach would be perhaps the best methodology to apply.

Thermal expansion is not a new term in structural engineering, as it has been considered in the design of bridge structures for many years at ambient temperature. However, such consideration has not been extended to the design of building structures exposed to fire. A recent study on the collapse of World Trade Centre Building 7 revealed that thermal expansion has a major effect on the structural response and can induce even progressive collapse of a structure [1]. A study on the results of survey on several past collapses of moderate-high building structures [2] revealed the fact that most of these structural failures seem to share a similar pattern of collapse with significant thermal expansion effects on the structural performance. Results of the studies on the collapse of structures in fire, such as the World Trade Center Towers, illustrate a collapse sequence in which the elevated temperature due to fire causes initial thermal expansion of the building floors following by the floors sagging and pulling inward on the exterior columns, resulting in a progressive collapse of the buildings [3,4].

These recent research findings indicate two important issues; 1) thermal expansion plays a very important role in the performance of structures in fire, and 2) to simulate and assess realistic 3D structural response of structures in fire, performance of the entire structural system should be investigated using a proper performance-based evaluation methodology and technique.

The objective of this article is to provide results of a literature review on the performance evaluation of buildings in fire considering the effects of thermal expansion, structural systems and material properties. As a result of this study, new avenues for future research on collapse mitigation of structures in fire are identified and suggested.

### 1 THERMAL EXPANSION

One of the major terms that should be considered in the design of large-scale structures, such as bridges, is the thermal expansion of the structures. For bridges, for instance, this will result

in the design of thermal expansion joints located along the bridge deck, which seems to be one of the most effective solutions to mitigate effects of thermal expansion on the deck due to variation of ambient temperature through the year. As for building structures, thermal expansion due to ambient temperature has not been a major design concern. However, when it comes to structural performance exposed to fire, thermal expansion would play a major role in the response and behaviour of structures. Recently, the National Institute of Standards and Technology of the United States has revealed results of a study on the collapse assessment and simulation of World Trade Centre Building 7 [5], concluding:

“Thermal expansion is a new phenomenon that can cause structural collapse. For the first time we have shown that fire can induce a progressive collapse. Currently thermal expansion effects are not explicitly considered in design practice for fire resistance ratings.”

This result reveals the fact that currently, there is a clear lack of knowledge and design methodology relating to the effects of thermal expansion on performance of structures in fire. Furthermore, results from previous experimental studies [6], and from observed collapses of structures in fire [2], also indicate that such structures can experience significant floor expansion at high temperatures inducing large lateral deformation or drift to columns or resulting in floor sagging in compression. These, in turn, can result in the collapse of partial or entire structures.

Fig. 1 illustrates a photo taken after a major fire at the US Military Personnel Records Centre building [2]. This photo shows a lateral deformation of about 60 cm for a column on the sixth floor of the building induced by the floor expansion due to the fire. In fact, this is very similar to a reinforced concrete column failure under extreme lateral loads such as earthquakes. This deformation is the result of floor thermal expansion during the fire. Usually temperatures at the ceiling level of the fire compartment are much higher than that at the floor level of the compartment. This temperature difference induced different thermal expansions for the floors at the upper and lower levels, which resulted in a significantly larger deformation at the top of the columns compared to the base causing significant shear forces and end moments on the elements. If the induced drift to the element exceeds the upper bond of the column deformation capacity, it will fail either in shear or buckling.



Fig. 1. Large drift and shear failure of a column due to thermal expansion of floor [2]

In the case of the US Military Personnel Records Centre building, shown in Fig. 1, the column drift is significantly larger than the shear deformation capacity of the element and a clear shear failure occurred at the top of the column. Such column response and failure mode could not be predicted using the traditional column furnace test method, in which a single column is exposed to a standard fire and subjected to only constant axial load.

Lateral deformations of columns due to floor thermal expansion have also been observed in a full-scale fire test [6]. Previously, a full-scale reinforced concrete building in fire was tested at the Cardington test facility of BRE, UK. Fig. 2 shows a plan of first floor of the building, fire compartment location, and burning of the fire compartment. During the test, lateral deformations of the floor at the top of the first floor columns have been measured, shown also

on the floor plan in Fig. 2. The maximum lateral deformation at the first floor measured during the fire was about 67 mm. This is still a relatively large lateral deformation and drift induced on the columns. This deformation compared to that of the column at the US Military Personnel Records Centre is relatively small. This is mainly because of the small size of the fire compartment and the floor dimensions. Typically the larger the floor size is the larger thermal expansion and lateral deformation can occur. Practically, floor size of conventional moderate-rise buildings is relatively larger than that of the building specimen in Fig. 2. This in fact could be one of the reasons that thermal expansion effect has been hardly observed in previous moderate or small size tests.



Fig. 2. Fire test of a full-scale reinforced concrete building, 2001 (BRE) Cardington [6]

The National Institute of Standards and Technology of the United States reported 22 fire-induced multi-story building collapses since 1970; fifteen cases were from the USA, two from Canada, and 5 from Europe, Russia and South America [2]. Out of the 22 building collapses, 7 buildings had reinforced concrete structures, 6 steel frames, 5 masonry systems, 2 wood structures and 2 unknown materials. A study on these building collapses could reveal that the main reason for most of these building collapses could be not only due to strength degradation of the materials exposed to elevated temperature but also to the significant effects of thermal expansion on the entire structural performance and thermal stresses and strains on the individual elements. Therefore, further studies are recommended to investigate the behaviour of structures in fire considering the effects of thermal expansion.

## 2 REINFORCED CONCRETE STRUCTURES IN FIRE

Reinforced concrete structures have been categorized as structures with very good reliability and fire resistance properties. As mentioned in the previous section, surprisingly, the National Institute of Standards and Technology of the United States reported the largest number of collapses of structures among conventional structures, since 1970, belonged to reinforced concrete buildings [2]. This would be mostly due to the brittle nature of concrete materials. However, there is currently a significant lack of information and analytical tools for performance evaluation and design of reinforced concrete structures especially under design fire, realistic loading and failure scenarios [7].

A failure mechanism of reinforced concrete structures in fire is the loss of capacity due to spalling of cover concrete resulting in failure of the element or sometimes even partial or the entire structure. The phenomenon of spalling is very complex and not well understood. Experiments have shown that spalling of cover concrete exposed to fire is essentially due to high moisture content, high rates of heating, and high concrete stresses [8,9]. There are studies showing that spalling rate is dependant on the size of the elements and specimen

scales [10]. The type of aggregate also has some effects on the mechanical properties and spalling of concrete. Spalling is generally much less for carbonate aggregate concrete compared to that of siliceous aggregate concrete [11]. Studies show, spalling of high strength concrete is considerably higher than that for normal strength concrete exposed to fire, as shown in Fig. 3. This is in fact referred to as one of the major concerns with high strength concrete, which could be due to its low water/cement ratio [12]. Recent studies on post-tensioned structures such as post-tensioned beams and slabs have revealed that the effect of spalling on these structural elements can be very significant and could result in the collapse of the structure. Further studies in this area are urgently suggested [13].

The issue of thermal expansion of floors would be significantly important for both reinforced concrete columns and floors. Depending on the stiffness and load capacity of the structural elements, collapse of reinforced concrete structures in fire could be initiated as a result of shear failure or buckling of beam due to large floor sagging, shear failure or buckling of columns, or even shear failure of the connections. In all these three failure modes, shear mechanism plays the major role and governs the performance of reinforced concrete structures in fire.

As mentioned earlier, drifts of columns due to thermal expansion of floor are very similar to the response of a column to an extreme lateral load such as an earthquake. This means buildings located in and designed for a low seismic risk area are even more vulnerable to thermal expansion than those in high seismic zones. This is mainly because reinforced concrete buildings designed for high risk of earthquake have relatively high shear and deformation capacity against lateral force and deformation. Therefore, studies on this subject would be extremely important for reinforced concrete buildings designed with low lateral loads such as earthquake. However, this would not entirely resolve the thermal expansion effects in buildings designed for high lateral force. In fact for such buildings, interaction of fire and earthquake, during the main shock and aftershocks, would be a major structural response, in which little knowledge and information is available. Thus, further studies are also needed to take into account the fire-earthquake interaction of the structures in the design or assessment process [14].

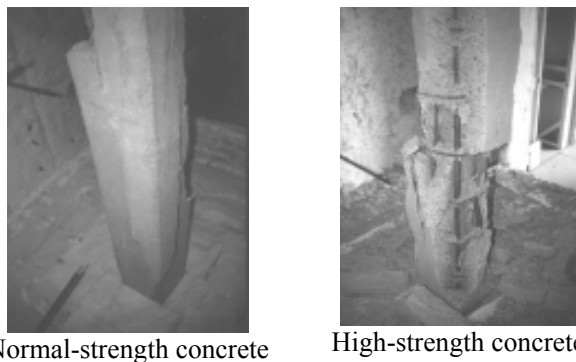


Fig. 3. Spalling of concrete column after fire-resistance tests [12].

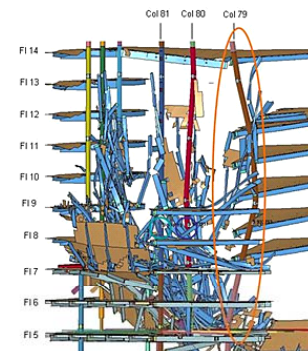


Fig. 4. Collapse simulation of WTC Building 7 [1].

### 3 STEEL STRUCTURES IN FIRE

Compared to reinforced concrete structures, steel framed buildings exposed to fire tend to perform poorly [15]. This is mainly because structural steel elements are relatively much thinner and have a higher thermal conductivity compared to concrete elements. Common failure modes of steel frames in fires are squashing, overall buckling, bending and lateral torsional buckling of columns, local buckling and bending failure of beams, and shear and

local buckling failure of the connection elements [16]. Studies on behaviour of steel structures in fire show that end restraint and continuity of structural elements and membrane action of the floor slab would enhance performance of steel structures in fire [17, 18].

Axial restraint has a less profound influence on steel structures than on concrete structures. This is because the more rapid heating and the more ductile behaviour of steel structure can result in larger vertical deflections, floor sagging, which reduce the horizontal axial resistance force [15]. In other words, horizontal deformations as a result of thermal expansion of structural elements are relatively larger for reinforced concrete structures compared to steel-framed buildings. Therefore in steel structures, unlike reinforced concrete structures, most likely, floor sagging or deflection of beams is larger than column deformation or drift, which in fact coincides with the basic design philosophy of beam failure prior to column.

Recent study on the collapse of World Trade Centre steel frame Building 7, has demonstrated that thermal expansion could be one of the major grounds for progressive collapse of steel buildings [1]. Fig. 4 illustrates progressive collapse simulation of Building 7, initiated by buckling of a column.

Results from an analytical study on behaviour of a steel structural system with perimeter moment resisting frame also indicate that floor thermal expansion can cause large out-of-plate displacement and inelastic stresses in the perimeter columns [19]. Studies also have been carried out on the effects of heating rate on the structural response. The results of these studies show that a slow heating rate could produce higher compressive forces in the connections of steel structures due to less thermal gradient and therefore less curvature to take out the thermal expansion of the beam [20]. In other words the heating rate has an important effect on the floor expansion; the slower the heating rate the higher floor thermal expansion is expected. This would convey that the decay or cooling down rate could also have significant effects on the thermal expansion of structural elements. Further studies are needed to investigate the effects of heating and cooling rates on performance of structures exposed to fire.

Currently, there are thermal transfer analytical tools available, such as SAFIR [21], for prediction of steel beam temperature during fire. However, available analytical tools for heat transfer analysis of concrete could not provide proper accuracy. For instance, the SAFIR program predicts higher temperatures for concrete, compared to the test data, which could be due to effects of the concrete moisture content property [22]. Further investigations are required to examine the problem and to develop proper analytical tools for heat transfer analysis of concrete slab and composite structures.

#### **4 CONCLUSIONS**

A literature review was carried out to explore a number of current studies on performance of structures in fire. The main considerations are primarily directed toward performance-based evaluation and design approaches. Among the research avenues recommended in this study, thermal expansion of structure was identified as one of the most important phenomena that requires a comprehensive research in order to understand the thermal expansion mechanism and its effects on the structural performance and to develop proper analytical and design approaches. There is currently a lack of design tools in buildings codes and standards for consideration of thermal expansion. For reinforced concrete structures there are very few models for material properties and shear failure mechanism at elevated temperature. Spalling mechanism of post-tensioned concrete structures requires further research. Studies are suggested on the effects of heating and cooling rates on the thermal stress and strain properties of structures. The cooling and heating rate would affect the magnitude of vertical and lateral deformations of structures. Effects of thermal properties and moisture content on

spalling of concrete require further studies. The study on the collapse of Building WTC 7 showed the importance of a performance-based approach for the evaluation and design of structures in fire. Further studies are suggested on developing simple analytical approaches for modelling the response of 3D structural systems in fire. Studies are also recommended on developing thermal analytical approaches for reinforced concrete elements considering factors such as moisture content. Performance of structures exposed to different fire scenarios, including post-earthquake fire, requires assessment and research to develop realistic design fires and loading.

## REFERENCES

- [1] NIST, Final Report on the Collapse of World Trade Center Building 7, *National Institute of Standards and Technology*, www.nist.gov, November 2008.
- [2] Beitel J., Iwankiw N, Analysis of Needs and Existing Capabilities for Full-Scale Fire resistance testing, *National Institute of Standards and Technology*, NIST GCR 02-843, 2002.
- [3] Gross J. L., McAllister T. P., Structural Fire Response and Probable Collapse Sequence of the World Trade Center Towers, *National Institute of Standards and Technology*, NCSTAR 1-6, Federal Building and Fire Safety Investigation of the World Trade Center Towers 2005
- [4] Usmani A., A Very Simple Method for Assessing Tall Building Safety in Major Fires, *Proceedings of the Fifth International Conference on Structures in Fire*, May 2008.
- [5] Sunder S., Report on the Collapse of World Trade Center Building 7, Opening Statement Press Briefing - August 21, 2008, *National Institute of Standards and Technology*, wtc.nist.gov, 2008
- [6] Bailey C., Holistic behaviour of concrete buildings in fire, *Proceedings of the Institution of Civil Engineers. Structures and buildings*, vol. 152, Issue 3, pp. 199-212, 2002.
- [7] Kodur V.K.R., Dwaikat M., Performance-based Fire Safety Design of Reinforced Concrete Beams, *Journal of Fire Protection Engineering*, Vol. 17, pp. 293-320, 2007
- [8] Malhotra H.L. Spalling of Concrete in Fires. Technical report. 118. *Construction Industry Research and Information Association*: London, 1984.
- [9] Phan, L. T., Fire Performance of High-Strength Concrete: A Report of the State-of-the-Art, *National Institute of Standards and Technology*, NISTIR 5934, 1996
- [10] Bostrom and Jansson, Results from Two Research Program on Spalling of Concrete, *Proceedings of the Fifth International Conference on Structures in Fire*, May 2008.
- [11] Kodur V.K.R., McGrath R., Leroux P. and Latour J.C., Experimental Studies for Evaluating the Fire Endurance of High-Strength Concrete Columns, *National Research Council Canada*, No. 197, 2005.
- [12] Kodur V.K.R., Fire Performance of High-Strength Concrete Structural Members, *National Research Council of Canada*, Construction Technology Update No. 31, 1999.
- [13] Rowson J., Fire test exposes flaws in post-tensioned floor slabs, *New Civil Engineer*, www.nce.co.uk, 2008.
- [14] Mousavi S., Bagchi A., Kodur V.K.R., Review of post-earthquake fire hazard to building structures. *Canadian Journal of Civil Engineering*, Vol.35, pp. 689–698, 2008.
- [15] Buchanan A. H., Structural Design for Fire Safety, *John Wiley & Sons*, 2001.
- [16] British Steel plc, Swinden Technology Centre, The Behaviour of Multi-Story Steel Framed Buildings in Fire, *British Steel plc, Swinden Technology Centre*, 1999.
- [17] Nwosu D.I., Kodur V.K.R., Behaviour of Steel Frames Under Fire Conditions, *Canadian Journal of Civil Engineering*, 26, 156-167 (1999).
- [18] Nwosu D.I., Kodur V.K.R., Steel Structures Exposed to Fire – A State-of-the-Art Report, *National Research Council Canada*, Report No. 749, 1997
- [19] Varma, A.H., Agarwal A., Hongo S., Prasad K., Behaviour of Steel Building Structures With Perimeter MRFs Under Fire Loading Effects, *Proceedings of the Fifth International Conference on Structures in Fire*, May 2008.
- [20] Selamet S., Garlock M. E. M., Behaviour of Steel Plate Connections Subjected to Various Fire Scenarios, *Proceedings of the Fifth International Conference on Structures in Fire*, May 2008.
- [21] Franssen J. M., User's Manual For SAFIR 2007a Computer Program For Analysis of Structures Subjected to Fire, *University of Liege*, Belgium, 2007.
- [22] Alfawakhiri F., Kodur V.K.R., Frater G., Temperature Field Modeling of the First Cardington Test, *National Research Council Canada*, NRCC-46898, 2004.

## **INTEGRITY OF FIRE RESISTANT CONSTRUCTION**

### **- Developing A Methodology To Control Fire Induced Progressive Structural Collapse**

Yong C Wang

University of Manchester, School of Mechanical, Aerospace and Civil Engineering, Manchester, UK

#### **ABSTRACT**

This paper is intended to initiate a discussion to develop a suitable framework within which design to control fire induced progressive structural collapse may be undertaken. There are two levels of integrity of fire resistant construction: prevention of fire spread (fire integrity) and control of progressive collapse (structural integrity). These two requirements have traditionally been considered in isolation with the former being a purely fire but non-structural problem and the latter a purely structural problem. Using a few well-publicised recent examples of fire induced progressive structural collapse, this paper argues that while fire integrity should be achieved under “normal” fire design condition, when assessing structural integrity under exceptional fire loading, it may be necessary to assume some fire integrity failure and the simultaneous actions of fire and mechanical loading (structural response) should be considered. This may be likened to acceptance of local structural failure when assessing structural integrity in general. Modern structural fire engineering is seen by many to offer significant advantages (reduced construction cost, better understanding of structural behaviour leading to rational decision making on fire safety level) than the traditional prescriptive approach of fire resistant design. However, its inappropriate use could lead to increased risk of fire induced progressive collapse. Using tensile membrane action in floor slabs as an example, this paper suggests that the key element approach, similar to that in design for structural robustness, should be adopted.

#### **1 INTRODUCTION**

Under normal fire design condition, a building should have sufficient integrity so as to prevent fire spread through the building’s fire resistant compartments. This is required to ensure that the risk to life safety and building damage is limited. Under exceptional fire exposure, the building structure should possess sufficient robustness so that the building does not suffer from progressive collapse. These requirements will be termed “fire integrity” and “structural robustness” respectively in this paper. Currently, design for “fire integrity” is poorly informed, with supporting information being mainly from standard fire resistance tests of building components. On the other hand, although there are some design guidelines on “structural robustness”, they have not been developed with fire exposure in mind and may not be adequate for applications under exceptional fire condition. Furthermore, when these two aspects are considered, they are usually treated independently, with the fire engineer/architect responsible for “fire integrity” and the structural engineer responsible for “structural robustness”. However, the recent high profile cases of fire induced progressive structural failure suggest that these two aspects are closely linked: fire integrity failure caused progressive structural collapse. In particular, multiple floor fires drastically increased the risk

of progressive structural collapse. In order to establish that fire integrity failure and multiple floor fires should be considered as credible scenarios of exceptional fire loading, the next section will present a brief analysis of a few case studies.

## 2. A BRIEF ANALYSIS OF RECENT FIRE INDUCED PROGRESSIVE COLLAPSE

In the World Trade Center 1 and 2 buildings [1], airplane impact destroyed a number of floors and simultaneously ignited these floors. Furthermore, destruction of fire protection to the floor trusses by airplane impact caused the floor trusses to exceed their limiting temperatures in bending so that these floor trusses experienced very high deflections and developed catenary action. Simultaneous catenary action in these floor trusses meant that instead of them providing the edge structure with lateral restraint, the edge structure of WTC 1 & 2 buildings acted as compressive members with unrestrained lengths of a number of floor heights, with additional lateral forces acting on them. Progressive collapse of the buildings was inevitable.

In WTC 7 building [2], fire integrity of the building was also breached because the fire was present on a number of floors, Figure 1. In addition, the fire on each floor appeared to be travelling, reaching different intensities at different locations at different times. This resulted in fracture of the weak seated connection to column 79 (Figure 2), which led this column to become laterally unsupported at the floor level (Figure 3), which ultimately resulted in its buckling and progressive collapse of the building.

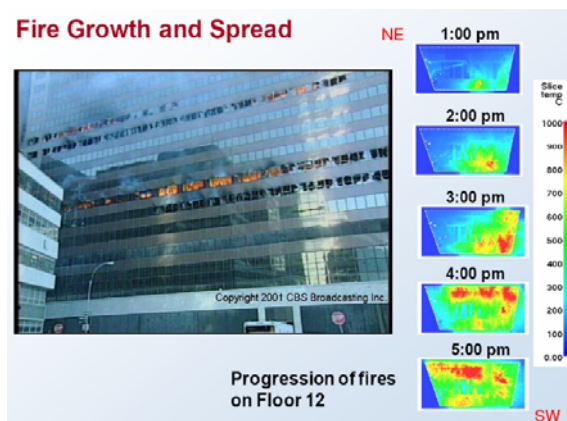


Figure 1: Multiple floor and travelling fire



Figure 3: Unsupported column 79

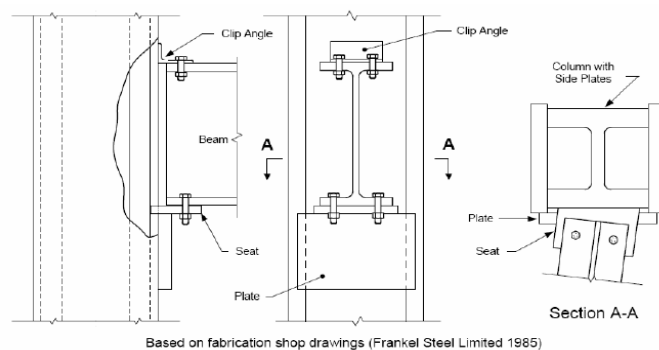
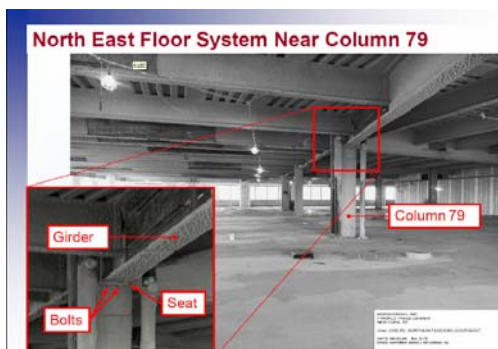


Figure 2: Seated connection to column 79 in WTC7 (FEMA 2008)

During the fire attack on the Madrid Windsor tower [3], poor fire stop between different fire compartments caused the fire to engulf a number of floors, which caused partial collapse on a number of floors, Figure 4. Fortunately, the strong and stiff core and floor slabs prevented total collapse of the structure.

These three cases of fire induced partial or complete structural collapse share one thing in common: the fire attack caused fire integrity failure and involved multiple floors. Whilst it would not be impossible for fires within one floor height to induce complete structural collapse, as will be postulated later, the risk of progressive structural collapse under multiple floor fires must be drastically higher than that under one floor fire. As has been demonstrated above, the exceptional fire loading scenario of fire integrity failure and multiple floor fire must be considered.



**Fig 4: Madrid Windsor tower (Intermac 2005)**

Multiple floor fires in the WTC buildings were caused by ignition on multiple floors (airplane impact on WTC1 and WTC2 and firebands from WTC1/WTC2 to WTC7), which by-passed the buildings' fire resistant compartmentation designed to prevent fire spread through floors. For some extremely important buildings, design for airplane impact may be a realistic scenario. If so, the probability of multiple floor fire must be very high. Other similar causes of multiple floor fires could include: explosion followed by fire and vehicle impact followed by fire.

In the Madrid Windsor tower, multiple floor fire was caused by poor compartmentation in the building. Although in general fire safety design, this cause may be eliminated through proper design and construction of the building's fire resistant compartmentation, it may be difficult to achieve because fire integrity is still rooted in the prescriptive framework of standard fire resistance testing and consideration of element performance. Although experiences so far may be used to indicate satisfactory performance of the current method of specifying fire integrity, as evidenced by infrequent report of fire integrity failure, this may have been purely good luck or underreporting as fire integrity failure has been observed in fire tests in buildings which have been constructed according to the prevailing specification and technology.

Other credible causes of multiple floor fires include fire spread through façade, either externally or internally in atrium construction, arson attack and fire following an earthquake.

### **3. OTHER POSSIBLE PROGRESSIVE COLLAPSE SCENARIOS**

Under normal fire resistant design condition, it is assumed that the fire resistant compartmentation remains intact. Therefore, fire exposure is contained within the fire resistant compartment. Usually, a fire resistant compartment is within one storey of the building so the design assumption is that only the structure within the fire resistant compartment is exposed to fire. Furthermore, it is assumed that only one fire exposure is dealt with at a time, therefore, the accumulative effect of fire attack is not considered. But such an effect may lead to progressive collapse. For example, consider the 2-D skeletal structure

shown in Figure 5, assuming each bay being a fire resistant compartment. Under normal fire design, the fire exposure will be in each of the bays and will be considered individually. Suppose fire is in bay 2. Further assume that the connection between the beam B2 and the column C2 is fractured due to axial force in the beam. It is possible that progressive collapse may occur following this event. But for the sake of argument, assume the structure is robust enough to limit the structural and fire damage to the connection only. Therefore, the buckling length of the column will not be changed because beam B1 will still be able to offer lateral support to the column. Now suppose fire design is now dealing with fire exposure in bay 1. The effect of fire exposure in bay 2 will now not be considered. Suppose the connection between beam B1 and column C2 is now fractured. The buckling length of column C2 will still not be changed because beam B2 is now providing lateral support to the column. Therefore, if fire in bay 1 and in bay 2 is considered separately, column C2 will be able to support the structure. However, if the fire is moving and travels from bay 1 to bay 2, or vice versa, then the connections on both sides of column C2 would be fractured and the column buckling length would be doubled, increasing the risk of progressive collapse. This appears to have contributed to progressive collapse of the WTC7 building.

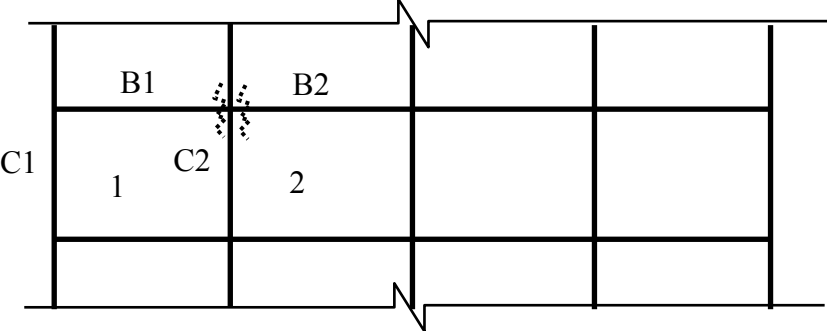


**Figure 5: Illustrative example of loss of lateral support to columns**

To summarise, fire integrity is concerned with prevention of fire spread. Design for fire integrity is necessary under “normal” fire scenario to limit the loss of fire damage. However, under exceptional fire attack, fire integrity failure may occur and this should be assumed when assessing structural integrity under exceptional fire exposure. Although it will not be possible to prescribe the number of multiple floor fires, the case of fire spread to adjacent fire resistant compartments should be considered. In addition, as illustrated above, it is possible for the supporting columns to become laterally unsupported over two floors even if fire exposure is contained within one floor height. Therefore, design for structural integrity under exceptional fire loading should consider the case of the vertical members being unsupported over two floor heights.

**4. KEY ELEMENTS**

A further potential source of progressive collapse is the continued push to extract the last possible source of reserve in capacity of the structure. Traditionally, fire resistant design has followed a rather elementary approach, in its treatment of the structure (based on structural elements, not the entire structure) as well as structural behaviour (according to the familiar small deflection theory, not large deflection behaviour). The result of this historical ignorance is that there is usually a substantial amount of reserve in fire resistance in the structure, which may become useful in controlling progressive collapse under exceptional fire conditions. Recently, refined methods have been developed to allow the reserve in structural capacity to be exploited, principally to reduce the need for fire protection. However, it is important that pushing the boundary in research is accompanied by appropriate caution and understanding in applications so that the risk of progressive structural collapse is not unduly increased.

Consider two recent developments in structural fire engineering: catenary action in beams and tensile membrane action in floor slabs. Tensile membrane action exploits the ultimate strength of a floor slab under very large deflections. One of the main assumptions is that the slab has to be vertically supported around all the edges. Under the normal design fire condition, it may be assumed that this key assumption is satisfied and that the benefit of tensile membrane action can be safely utilised. However, should an exceptional fire or other loading condition result in the loss of one of the edges of the slab, the slab would fold without being able to develop tensile membrane action and the applied load on the floor slab (designed according to tensile membrane action) could be much higher than the actual load carrying capacity of the slab, thereby greatly increasing the risk of progressive collapse. To a watchful engineer who is aware of this issue, the risk of progressive structural collapse may be reduced if the engineer takes appropriate actions. However, the commercial interest in utilising tensile membrane action has been such that it is now becoming routine application with decreasing level of understanding of the fundamental assumptions of structural behaviour. Contrast this with exploitation of catenary action. This load carrying mechanism is activated when an axially restrained beam undergoes very large deflections. If the connections between the beam and the surrounding structure are sufficiently strong, it is possible for the steel beam to survive virtually any fire attack without fire protection, which makes it possible to eliminate fire protection to steel beams [4]. However, since this load carrying mechanism relies on the close interaction between the restrained steel beam and other structural members, the beam cannot be considered in isolation (as can the floor slab when utilising tensile membrane action), therefore, utilising catenary action will force the potential user to thoroughly analyse the behaviour of the whole structure to ensure that the entire structure is stable. Furthermore, if this load carrying mechanism were disrupted under an extreme loading situation, it may be argued that damage would be local to the structure because the catenary action force (axial tension in the beam) would be relieved, thus reducing the load on the rest of the structure.

It is in the nature of researchers to push the boundary of understanding and quantification of structural behaviour and for practitioners to take advantage of any new found reserve in structural resistance. However, it is important that when exploiting advanced analysis methods, the designer develops an understanding of the potential of increased risk in progressive collapse. To mitigate the potential risk of progressive collapse, the key element or element removal approach may be adopted.

## **6. A POSSIBLE FRAMEWORK FOR ASSESSMENT OF PROGRESSIVE STRUCTURAL COLLAPSE UNDER EXCEPTIONAL FIRE LOADING**

Whilst design for fire integrity is a well defined requirement, design for structural robustness is ill-defined due to the unknown nature of the initiating accidental event. Coupled with a lack of detailed research on structural robustness under exceptional fire condition, it is not possible at this stage to offer detailed recommendations for design. However, based on the discussions in the preceding sections of this paper, the following framework may be considered:

- (1) Under exceptional fire loading, some fire integrity failure should be allowed. The design task then becomes how to prevent progressive collapse of the structure following the assumed fire integrity failure.
- (2) It appears that the main cause of progressive structural collapse in fire is buckling of the columns as a result of loss of the lateral support to the columns in fire. Assuming fire integrity failure of the fire resistant compartments is immediately above or sideways on the same floor, the likely increase in the column buckling length is to make it unsupported over two storeys. In a braced multi-storey building of equal floor height, this would lead to doubling of the

column buckling length. For this type of construction under normal design fire, the current European standards (EN 1993-1-2 [5], EN 1994-1-2 [6]) recommend the column buckling length to be 0.5 times the floor height. Doubling this value would make the column buckling length the same as the floor height, which would be the column buckling length for ambient temperature design. Therefore, to enhance structural robustness under exceptional fire loading, one specific action is to use the same column buckling length for fire design as for ambient temperature design.

(3) Similar to normal consideration of structural robustness at ambient temperature, it is necessary to consider the scenario of elemental removal. This may have some impact on structures that have been fire engineered using tensile membrane action. Should an element removal lead to extensive structural failure, this element should be treated as a key element for fire resistance.

## **7. SUMMARY**

The main objective of this paper is to initiate a discussion and debate on integrity of structures under fire exceptional attack. It has outlined the difference in considerations for fire integrity and structural integrity. Structural integrity failure (progress collapse) appears to be closely related to fire integrity failure (fire spread). It may not be possible to prevent fire integrity failure under exceptional fire loading. Therefore, it is recommended that when assessing progressive structural collapse under exceptional fire loading, some fire integrity failure immediate to the fire resistant compartment under design should be assumed. Design to achieve structural integrity should then aim to prevent progressive structural collapse based on the new fire exposure condition. It is further recommended that the key element approach for ambient temperature design be adopted so that structural elements that are critical to the viability of a particular critical load carrying mechanism (e.g. the edge members of a floor plate designed using tensile membrane action) are offered additional protection/strengthening or the consequence of its failure is clearly understood and explicitly considered.

## **REFERENCES**

- [1] Federal Emergency Management Authority (FEMA 2002), World Trade Center Building Performance Study, FEMA, USA.
- [2] National Institute of Standards and Technology (NIST 2008), Federal Building and Fire Safety Investigation of the World Trade Center Disaster: Structural Response and Probable Collapse Sequence of World Trade Center Building 7, Volume 2, National Institute of Standards and Technology Report NIST NCSTAR 1-9.
- [3] Instituto Tecnico De Materiales Y Construcciones (Intemac 2005), Fire in the Windor building, Madrid: Survey of the fire resistance and residual bearing capacity of the structure after the fire, Intemac
- [4] Yin, Y.Z. and Wang, Y.C. (2004), "A numerical study of large deflection behaviour of restrained steel beams at elevated temperatures", Journal of Constructional Steel Research, Vol. 60, No. 7, pp. 1029-1047
- [5] Committee of European Standardisation (CEN 2005a), Eurocode 3: Design of steel structures, Part 1-2: General rules – structural fire design, BS EN 1993-1-2, British Standards Institution
- [6] Committee of European Standardisation (CEN 2005b), Eurocode 4: Design of composite steel and concrete structures, Part 1-2: General rules – structural fire design, BS EN 1994-1-2, British Standards Institution

## **SUPER ELEMENT IN STRUCTURAL ANALYSIS**

Yuan Weifeng, Tan Kang Hai

School of Civil & Environmental Engineering, Nanyang Technological University, Singapore 639798

### **INTRODUCTION**

The computing cost in FEM analysis is dependant on the number of degrees of freedom (DOF) in the model under investigation. To increase computational efficiency, one direct way is to reduce the number of elements. However, the FEM theory indicates that fewer elements will cause poorer accuracy in general cases. To achieve a better balance between accuracy and processing time, several special techniques have been developed without altering the accuracy of numerical findings, for instances, the spectral finite element method [1] and the transfer matrix method [2]. Alternatively, super element method has been widely applied in the FEM analyses for various problems [3, 4, 5]. Briefly, the basic concept of super element method is to treat the structural members as a continuous body, and then discretize this continuous body into super elements using traditional FEM techniques [6, 7]. In this way, each super element may consist of different types of members which may have various shapes, material properties and boundary conditions. In this paper, the procedure of constructing super elements is introduced based on numerical examples. To implement the proposed approach, an entire structure has to be divided into several zones according to the requirement of numerical investigation and the expected behavior of the structure. Among all the zones defined by the user based on his judgment, some zones consist of linear members and the others have nonlinear members. The advantage of the proposed method is that all the linear zones can be grouped into one super element, regardless whether they are connected or not. The nodes of the super element include i) all the boundary nodes between linear and nonlinear zones and ii) an additional node which only has one DOF, if there are external loads acting on the members within the linear zones. Thus, the total number of DOF of the original FEM model can be reduced significantly. It is noteworthy that the same approach can also be applied to linear analyses although the saving may not be as remarkable as a non-linear analysis.

### **1 DEFINITION OF SUPER ELEMENT**

#### **1.1 Basic Concept**

To illustrate the approach, recourse is made to a frame example as shown in Figure 1. The frame is evenly divided into twenty two-node three-dimensional beam elements, and three forces are applied at nodes 3, 9 and 21, respectively. It is assumed that in such a structure, greater attention is needed for key elements between node 6 and node 21. The zone comprising the key elements is denoted as a non-linear zone. In this case, all the elements between node 1 and node 11 can be merged into one super element, if only linear analysis is required for these elements. This is also the linear zone.

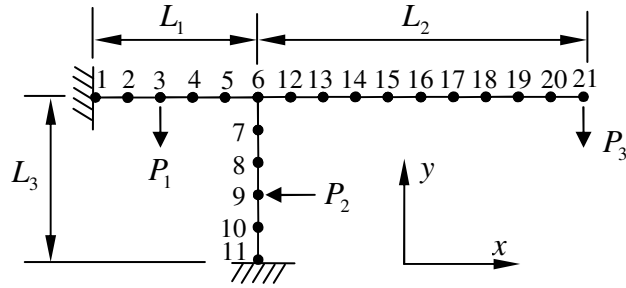


Figure 1. A two-dimensional frame subjected to external forces

Consider the linear zone shown in Figure 2, with the key elements including the force applied on them removed from the original model. To construct a super element, its nodes must be determined at the beginning. For the FEM model in Figure 1, node 6 is the only joint shared by the nonlinear and linear zones. Thus, the super element under construction will have only two nodes, viz. node 6 which has six DOFs and an additional node, which is in linear zone. Without loss of generality, node 8 is selected to be the second node of the super element.

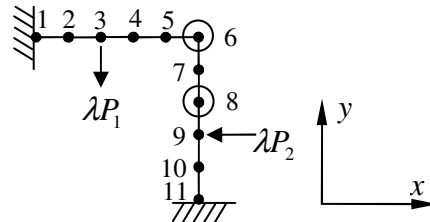


Figure 2. The linear zone of the two-dimensional frame under real forces

To obtain the stiffness matrix of the super element, a series of linear analyses has to be conducted based on the configuration shown in Figure 2:

Firstly, forces  $\lambda P_1$  and  $\lambda P_2$ , where  $\lambda$  is an arbitrary nonzero factor are applied to the frame and the associated deformations at node 8 and node 6 are calculated. Denoted by  ${}^0U$ , where the superscript indicates the load case number, the corresponding deformation vector induced by the combination of all scaled forces applied on the linear zones ( $\lambda P_1$  and  $\lambda P_2$  in this example) is expressed by  ${}^0U = ({}^0u_{8-x}, {}^0u_{6-x}, {}^0u_{6-y}, {}^0u_{6-z}, {}^0\theta_{6-x}, {}^0\theta_{6-y}, {}^0\theta_{6-z})^T$ , where the terms  $u$  and  $\theta$  represent the nodal displacements and rotations, respectively. The Arabic number in the subscript denotes the node number, while the Latin letters indicate the respective coordinate axis. It should be mentioned that all the six components of the deformation at node 6 are stored in  ${}^0U$  but only one component of the deformation of node 8 needs to be considered. In fact, among the six components of the deformation of node 8, any nonzero component can be selected to form  ${}^0U$ .

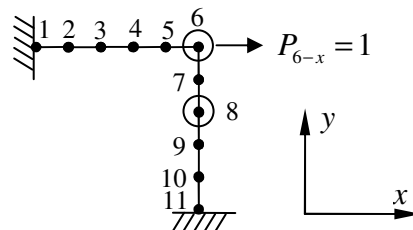


Figure 3. The linear zone of the two-dimensional frame under virtual force scenario

Secondly, as shown in Figure 3, the forces  $P_1$  and  $P_2$  are removed and a unit load  $P_{6-x}$  is applied to node 6 at the  $x$  direction. Similar to the first step, the deformations at node 8 and 6 are calculated and stored in  ${}^1U = ({}^1u_{8-x}, {}^1u_{6-x}, {}^1u_{6-y}, {}^1u_{6-z}, {}^1\theta_{6-x}, {}^1\theta_{6-y}, {}^1\theta_{6-z})^T$ .

Thirdly, repeat the second step to generate five more load cases, viz. two unit loads (along the  $y$  and  $z$ -axis) and three unit moments (about  $x$ ,  $y$  and  $z$ -axis) are applied to node 6 in sequence. The corresponding deformation vectors are stored as  ${}^2U, {}^3U, {}^4U, {}^5U$  and  ${}^6U$ . It should be mentioned that the global stiffness matrix of the linear zone shown in Figure 2 and 3 can be factorized during the calculation. Hence,  ${}^1U \sim {}^6U$  can be obtained without additional effort compared with the solution procedure of  ${}^0U$ . Based on the characteristic of linear elasticity, the above three steps can be described by one equation given by:

$$K\psi = \begin{pmatrix} \uparrow & \mathbf{0} \\ \mathbf{0} & \mathbf{I}_{6 \times 6} \end{pmatrix}_{7 \times 7} = \mathbf{I}_{7 \times 7} \quad (1)$$

where  $\psi = ({}^0U, {}^1U, {}^2U, {}^3U, {}^4U, {}^5U, {}^6U)$  and  $K$  is an unknown matrix.

It should be mentioned that in Eq. (1), the load case of the combination of  $\lambda P_1$  and  $\lambda P_2$  is represented by a unit virtual force “ $\uparrow$ ” acting at node 8 in the  $x$  direction.

In the end, the inverse matrix of  $\psi$  is calculated. Based on Eq. (2), one obtains  $K = \psi^{-1}$  where  $K$  performs as the stiffness matrix of the super element. For this example, the super element has seven DOFs, including six DOFs at node 6 and one DOF at node 8.

## 1.2 General Approach

Special attention must be paid to the case that the remaining structure is unstable after the part under investigation is removed from the original structure. For instance in Figure 4 (a), an elastic block is supported at points A and B by columns 1 and 2, respectively. In FEM modeling, the block may be meshed into many elements. However, to conduct an efficient analysis, all the elements on the block can be merged into just one super element. According to the present approach, points A and B must be selected to be the nodes of the super element. Moreover, another point, assuming to be point C, is also selected. To calculate the stiffness matrix of the super element, the proposed approach requires that the two columns must be removed from the original model. But the problem arising in this procedure is that the block above the two columns becomes unstable since it is hanging in the air without any physical support. Based on such a configuration, the deformation vectors of nodes A, B and C cannot be obtained.

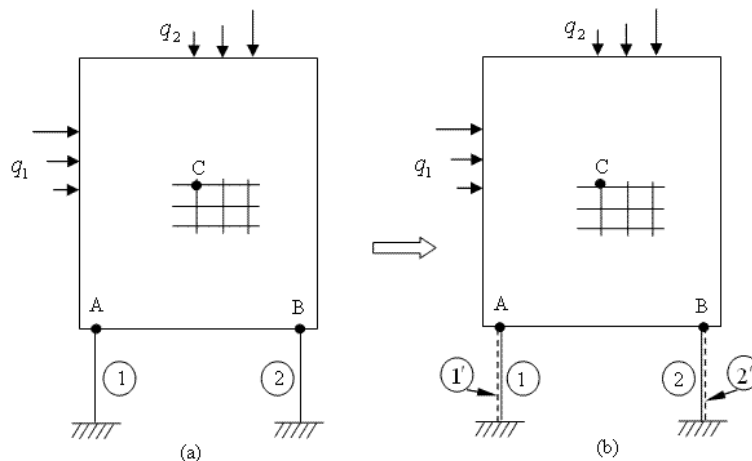


Figure 4. Calculate the stiffness matrix of super element using weak member method

To overcome the problem, a so-called “weak member method” is proposed in this paper. As illustrated in Figure 4 (b), two columns, viz. 1' and 2' are added to the original structure given in Figure 4 (a). The dimensions and locations of the old and new columns overlap each other, but columns 1' and 2' are much weaker than original columns 1 and 2. Theoretically, the numerical result based on (b) will not differ much from the one based on (a). Therefore, structure (b) can be used to replace structure (a) in ensuing analyses without affecting the accuracy of findings. Obviously, for structure (b), the remaining structure is still stable even if columns 1 and 2 are removed. Thus, based on structure (b), the stiffness matrix of super element can be carried out following the four steps described in Section 1.1.

## 2 NUMERICAL VALIDATION

### 2.1 Linear Analysis

Once the super element is constructed, the global stiffness matrix can be assembled using traditional approach. Meanwhile, the original frame given in Figure 1 is replaced by an equivalent structure shown in Figure 5. Please note that a fictitious force is applied at node 8. Its value is set to  $1/\lambda$  since the actual forces  $P_1$  and  $P_2$  are scaled up to  $\lambda P_1$  and  $\lambda P_2$ , respectively. In a nonlinear analysis, this fictitious force and  $P_3$  are applied to the structure proportionally.

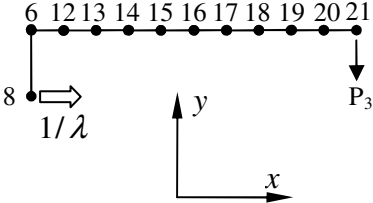


Figure 5. A FEM frame model consists of beam and super elements

To verify the correctness of the proposed approach, linear analyses are first conducted for the original frame using normal and super element approaches. In the simulation in Figure 1, it is defined that  $L_1 = L_2/2 = L_3 = 0.5$ . The dimension of the cross-section of each beam is set to be  $0.05 \times 0.05$ . The material properties of both super and normal elements are the same. Young’s modulus is set to  $1 \times 10^6$  and Poisson’s ratio is set to 0.3. The loads applied to the original frame are  $P_1 = P_2 = 10$  and  $P_3 = 0.1$ . During the calculation, the factor  $\lambda$  is set to 10.

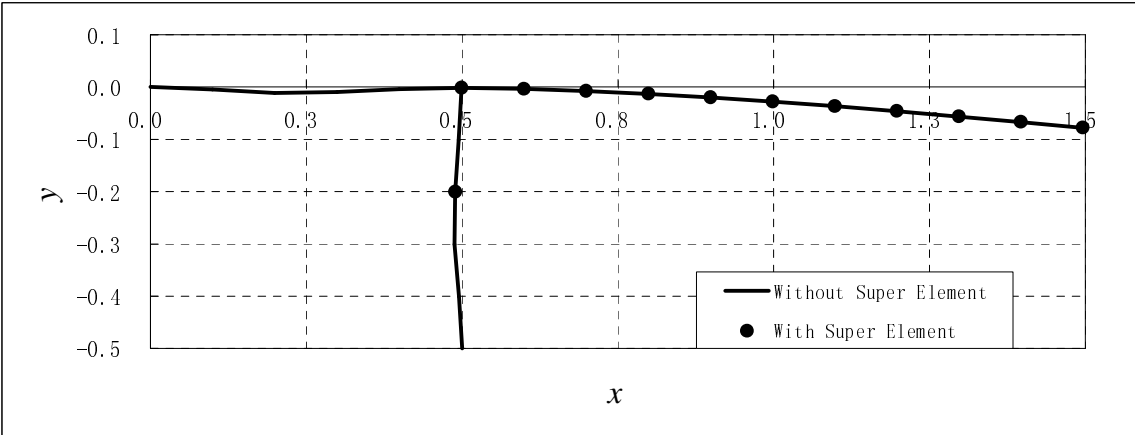


Figure 6. Comparison between the deformations obtained by FEM and super element method

The comparison between normal FEM and the proposed super element approach is depicted in Figure 6. In the figure, the deformations of the structure obtained by normal and the present FEM methods are compared. Obviously, with or without super element, the two results are almost the same.

**2.2 Nonlinear Analysis**

It is now assumed that nonlinear analysis is required for the frame shown in Figure 1. The geometry and the material properties are identical as the problem in Section 2.1. However, the forces at node 3 and node 9 are all zero, viz.  $P_1 = P_2 = 0$ . Meanwhile,  $P_3$ , the force at node 21 is replaced by a bending moment about z-axis. In this situation, the nonlinear response of the frame can be calculated using the model given in Figure 7. One finds that the fictitious force applied at node 8 is set to zero.

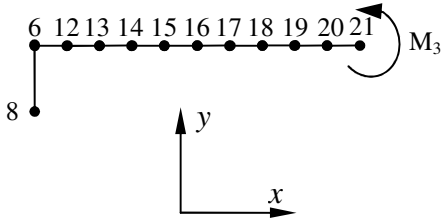


Figure 7. A FEM frame model with super element under bending moment

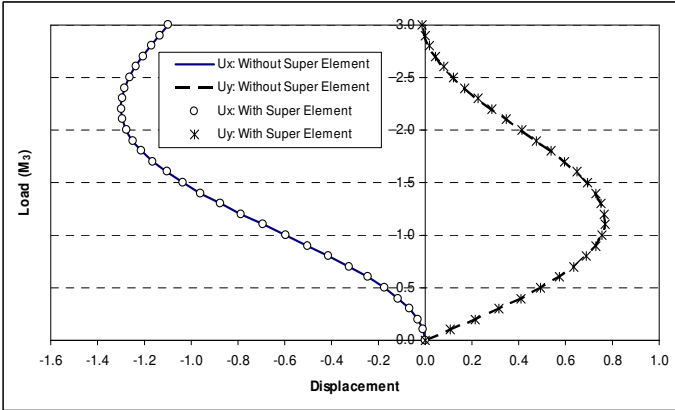


Figure 8. The load-displacement curves obtained by FEM and super element method

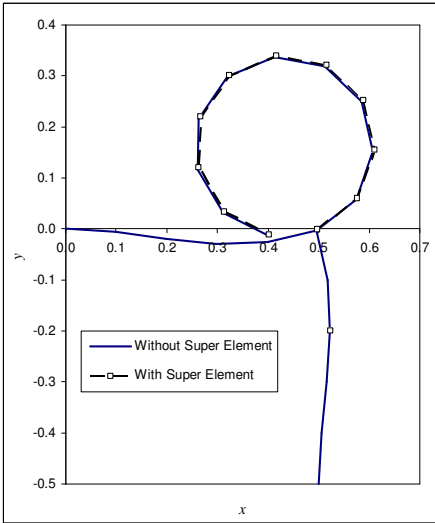


Figure 9. The shapes of the deformed frame obtained by FEM and super element method

Using load-control algorithm, a full nonlinear analysis is conducted for the model for 30 steps. In the simulation, the load increment in each step is set to 0.1. As a comparison, the model shown in Figure 7 is analyzed by super element method. The load-displacement relationships at node 21 are depicted in Figure 8. From the figure, one finds that the results obtained by super element method are very close to traditional FEM results. However, as shown in Figure 9, slight differences between the two kinds of results can be observed. This is caused by the assumption of linearity for super element.

### 3 CONCLUSION

This manuscript presents a method to construct super element. The advantage of the present method is that, with weak element formulation, different parts which may not be connected in a structure can be merged into one linear element to reduce the number of DOFs. Numerical examples show that this method is easy to be implemented and it has great potential in the simulation of large complex structures.

In traditional FEM, the global stiffness matrix is generally symmetric. However, it should be mentioned that this characteristic of the system matrix is damaged in the present method since the stiffness matrix of the super element is non-symmetric. On the other hand, although non-symmetric system matrix may cause additional requirements for CPU time, the overall calculation is efficient because the total number of DOFs is reduced significantly. Moreover, some techniques, such as iteration algorithm can be used to minimize the loss induced by non-symmetric matrix.

### REFERENCES

- [1] Finnveden S, Exact Spectral Finite Element Analysis of Stationary Vibrations in Rail Way Car Structure, *Acta Acustica*, (1994) 2: 461-482.
- [2] Lin YK, Donaldson BK, A Brief Survey of Transfer Matrix Techniques with Special Reference of Aircraft Panels, *Journal of Sound and Vibration*, (1969) 10: 103-143.
- [3] Ju F, Choo YS, Super Element Approach to Cable Passing Through Multiple Pulleys, *International Journal of Solids and Structures*, (2005) 42: 3533-3547.
- [4] Jiang J, Olson MD, Nonlinear Analysis of Orthogonally Stiffened Cylindrical Shells by A Super Element Approach, *Finite Elements in Analysis and Design*, (1994), 18: 99-110.
- [5] Lukasiewics SA, Geometrical Super-Elements for Elasto-Plastic Shells with Large Deformation, *Finite Elements in Analysis and Design*, (1987) 3: 199-211.
- [6] Huang Y, Ma KJ, Chen B, The Study of Dynamic Behavior for Multi-Storied Vierendeel Sandwich Plate-Column Structure, *Journal of Building Structures*, (2000) 3: 23-29
- [7] Cao ZY, Super Element Method for Complex Structure Analysis, *Mechanics and Practice*, (1992) 14 (4): 10-14.

## Authors Index

|   |                  |   |                       |
|---|------------------|---|-----------------------|
| Abramowicz M., <i>Poland</i>            | 134              | Correia A.J.P.M., <i>Portugal</i>       | 417                   |
| Abrantes V., <i>Portugal</i>            | 222; 228         | Correia A.M., <i>Portugal</i>           | 423; 512              |
| Abu A.K., <i>United Kingdom</i>         | 338              | Crosti Ch., <i>Italy</i>                | 66; 465               |
| Alderighi E., <i>Italy</i>              | 580              | Cvetanovski P., <i>Macedonia</i>        | 190; 196              |
| Ali F., <i>United Kingdom</i>           | 240; 490;<br>496 | Cvetkovska M., <i>Macedonia</i>         | 190; 196              |
| Alonso C., <i>Spain</i>                 | 110              |   |                       |
| Anderson K., <i>United Kingdom</i>      | 332              | Dai X.H., <i>United Kingdom</i>         | 350                   |
| Annerel E., <i>Belgium</i>              | 172              | Davie C.T., <i>United Kingdom</i>       | 301                   |
| Audebert M., <i>France</i>              | 550              | de Korte A.C.J., <i>The Netherlands</i> | 158                   |
| Aurtenetxe J., <i>Spain</i>             | 411              | De la Quintana J., <i>Spain</i>         | 411                   |
|   |                  | Deeny S., <i>United Kingdom</i>         | 202                   |
|   |                  | Dhakal R., <i>United Kingdom</i>        | 202                   |
| Babu C.R., <i>India</i>                 | 318              | Dhima D., <i>France</i>                 | 550                   |
| Bacinskas D., <i>Lithuania</i>          | 258              | Ding S.J., <i>United Kingdom</i>        | 53                    |
| Bailey C.G., <i>United Kingdom</i>      | 350              | Domański T., <i>Poland</i>              | 116                   |
| Bamonte P., <i>Italy</i>                | 60; 234          | Du Y., <i>P. R. of China</i>            | 356                   |
| Baniotopoulos C.C., <i>Greece</i>       | 435              | Dubina D., <i>Romania</i>               | 586                   |
| Bayer P., <i>Czech Republic</i>         | 146              | Dudáček A., <i>Czech Republic</i>       | 96                    |
| Bénichou N., <i>Canada</i>              | 604              | Dunne D., <i>United Kingdom</i>         | 478                   |
| Bhargava P., <i>India</i>               | 318              |   |                       |
| Bićanić N., <i>United Kingdom</i>       | 301              | Espinós A., <i>Spain</i>                | 184                   |
| Bihina G., <i>France</i>                | 537              | Ewald K., <i>Germany</i>                | 18                    |
| Bisby L., <i>United Kingdom</i>         | 178              |   |                       |
| Block F.M., <i>United Kingdom</i>       | 338              | Faure L., <i>United Kingdom</i>         | 72                    |
| Bontempi F., <i>Italy</i>               | 66; 465          | Feeney M., <i>New Zealand</i>           | 362                   |
| Bouchair A., <i>France</i>              | 550              | Felicetti R., <i>Italy</i>              | 60; 208               |
| Brouwers H.J.H., <i>The Netherlands</i> | 158              | Fike R., <i>USA</i>                     | 264                   |
| Buchanan A., <i>New Zealand</i>         | 202              | Flint G., <i>United Kingdom</i>         | 484                   |
| Burgess I.W., <i>United Kingdom</i>     | 338; 344         | Fontana M., <i>Switzerland</i>          | 216                   |
| Butterworth N.A., <i>United Kingdom</i> | 338              | Frangi A., <i>Switzerland</i>           | 216                   |
|   |                  | Franssen J.M., <i>Belgium</i>           | 222; 289;<br>398; 557 |
|   |                  | Friquin K.L., <i>Norway</i>             | 563                   |
| Cachim P., <i>Portugal</i>              | 557              |   |                       |
| Čajka R., <i>Czech Republic</i>         | 313              | Gambarova P.G., <i>Italy</i>            | 234                   |
| Carvalho L.T., <i>Portugal</i>          | 423              | Geda E., <i>Lithuania</i>               | 258                   |
| Chlouba J., <i>Czech Republic</i>       | 471              | Gillie M., <i>United Kingdom</i>        | 72; 332;<br>592       |
| Choi J., <i>Korea</i>                   | 490              |   |                       |
| Choi J.Y., <i>Korea</i>                 | 128              | Giuliani L., <i>Italy</i>               | 66; 465               |
| Choi S., <i>United Kingdom</i>          | 490; 496         | Gkoumas K., <i>Italy</i>                | 66; 465               |
| Choi S.M., <i>Korea</i>                 | 518              | Głuch G., <i>Poland</i>                 | 368                   |
| Chun Ch., <i>Korea</i>                  | 128              |   |                       |
| Chung K.S., <i>Korea</i>                | 518              |   |                       |
| Cinař R., <i>Czech Republic</i>         | 164              |   |                       |
| Clifton G.Ch., <i>New Zealand</i>       | 362              |   |                       |

|                                      |          |                                     |                    |
|--------------------------------------|----------|-------------------------------------|--------------------|
| Gonçalves M.C., <i>Portugal</i>      | 222      | Laasonen M., <i>Finland</i>         | 380                |
| Gonçalves M.C., <i>Portugal</i>      | 228; 423 | Lackner R., <i>Austria</i>          | 295                |
| González F., <i>Germany</i>          | 392      | Laím L., <i>Portugal</i>            | 271                |
| Goodfellow N., <i>United Kingdom</i> | 496      | Lakshmipathy M., <i>India</i>       | 252                |
| Gribniak V., <i>Lithuania</i>        | 258      | Lane B., <i>United Kingdom</i>      | 22; 484            |
| Gupta V.K., <i>India</i>             | 318      | Lane B., <i>United Kingdom</i>      | 34                 |
|                                      |          | Lange J., <i>Germany</i>            | 18; 392            |
|                                      |          | Law A., <i>United Kingdom</i>       | 592                |
| Hajpál M., <i>Hungary</i>            | 122      | Li G.Q., <i>P. R. of China</i>      | 356; 374;<br>502   |
| Han S., <i>United Kingdom</i>        | 490      |                                     |                    |
| Hao K.Ch., <i>P. R. of China</i>     | 502      | Liang H., <i>United Kingdom</i>     | 72                 |
| Hardie B., <i>United Kingdom</i>     | 240      | Lim L., <i>United Kingdom</i>       | 22                 |
| Harries D., <i>United Kingdom</i>    | 53       | Lopes N., <i>Portugal</i>           | 41; 398            |
| Heinisuo M., <i>Finland</i>          | 380      | Lou G.B., <i>P. R. of China</i>     | 502                |
| Hermouet E., <i>United Kingdom</i>   | 53       | Lu S., <i>P.R.of China</i>          | 90                 |
| Hietaniemi J., <i>Finland</i>        | 380      | Lu W., <i>Finland</i>               | 441                |
| Horiguchi T., <i>Japan</i>           | 325      |                                     |                    |
| Hospitaler A., <i>Spain</i>          | 184      | MacDougall C., <i>Canada</i>        | 178                |
| Hozjan T., <i>Slovenia</i>           | 386      | MacLean K., <i>Canada</i>           | 178                |
| Huang X., <i>P.R.of China</i>        | 90       | Mäkeläinen P., <i>Finland</i>       | 441                |
| Huang Z., <i>United Kingdom</i>      | 344      | Martins A.M.B., <i>Portugal</i>     | 277                |
| Huisman S., <i>Germany</i>           | 246      | Maślak M., <i>Poland</i>            | 598                |
|                                      |          | Matečková P., <i>Czech Republic</i> | 313                |
| Ibáñez C., <i>Spain</i>              | 184      | Mehaffey J., <i>Canada</i>          | 569                |
|                                      |          | Mensing M., <i>Germany</i>          | 543                |
| Jang H.M., <i>Korea</i>              | 128      | Mesquita L.M.R., <i>Portugal</i>    | 140                |
| Jayasree G., <i>India</i>            | 252      | Mihailovschi G., <i>Argentina</i>   | 271                |
| Jiang S.Ch., <i>P. R. of China</i>   | 502      | Mihajlov V., <i>Macedonia</i>       | 190; 196           |
| Jowsey A., <i>United Kingdom</i>     | 22       | Min B.Y., <i>Korea</i>              | 518                |
|                                      |          | Morente F., <i>Spain</i>            | 411                |
|                                      |          | Moss P., <i>United Kingdom</i>      | 202                |
|                                      |          | Mostafaei H., <i>Canada</i>         | 604                |
| Kaiser R., <i>Czech Republic</i>     | 13       |                                     |                    |
| Kaitila O., <i>Finland</i>           | 380      | Nadjai A., <i>United Kingdom</i>    | 240; 490;<br>496   |
| Kaklauskas G., <i>Lithuania</i>      | 258      |                                     |                    |
| Kallerová P., <i>Czech Republic</i>  | 459      | Ni Z., <i>P. R. of China</i>        | 78; 84;<br>90; 569 |
| Kan Q., <i>P.R.of China</i>          | 78; 84   |                                     |                    |
| Kansa J., <i>Finland</i>             | 406      | Outinen J., <i>Finland</i>          | 380; 406;<br>441   |
| Kim S., <i>Korea</i>                 | 490      |                                     |                    |
| Kirsch T., <i>Germany</i>            | 429      | Pada D., <i>Finland</i>             | 28                 |
| Klingsch E., <i>Switzerland</i>      | 216      | Pankaj P., <i>United Kingdom</i>    | 592                |
| Kodur V., <i>USA</i>                 | 264      | Park S.H., <i>Korea</i>             | 518                |
| Koltsakis E., <i>Greece</i>          | 435      |                                     |                    |
| Korzen M., <i>Germany</i>            | 246; 512 |                                     |                    |
| Kowalski R., <i>Poland</i>           | 134      |                                     |                    |
| Kuklík P., <i>Czech Republic</i>     | 575      |                                     |                    |
| Kurnjek L., <i>Slovenia</i>          | 386      |                                     |                    |

|   |  |                                     |                       |
|---|--|-------------------------------------|-----------------------|
| Pearce Ch.J., <i>United Kingdom</i>       | 301  | Strejček M., <i>Czech Republic</i>  | 164                   |
| Pérez Ch., <i>Spain</i>                   | 411  | Subedi N., <i>United Kingdom</i>    | 478                   |
| Piloto P.A.G., <i>Portugal</i>            | 140  | Suhaendi S.L., <i>Singapore</i>     | 325                   |
| Pintea D., <i>Romania</i>                 | 586  | Sultan M.A., <i>Canada</i>          | 604                   |
| Pinto T.M.G., <i>Portugal</i>             | 140  |                                     |                       |
| Planinc I., <i>Slovenia</i>               | 386  | Taerwe L., <i>Belgium</i>           | 172                   |
| Plank R., <i>United Kingdom</i>           | 344  | Tajbr A., <i>Czech Republic</i>     | 575                   |
| Procházka J., <i>Czech Republic</i>       | 453  | Tan K.H., <i>Singapore</i>          | 307; 447;<br>524; 616 |
|   |  | Tee K.F., <i>United Kingdom</i>     | 496                   |
| Qiu P., <i>P. R. of China</i>             | 569  | To E.Ch.Y., <i>Hong Kong</i>        | 47                    |
|   |  | Toledo R., <i>Brazil</i>            | 283                   |
| Rahmanian I., <i>United Kingdom</i>       | 152  | Torrero J.L., <i>United Kingdom</i> | 34                    |
| Rein G., <i>United Kingdom</i>            | 34   | Tsalikis C., <i>Greece</i>          | 435                   |
| Ring T., <i>Austria</i>                   | 295  |                                     |                       |
| Rodrigues C., <i>Spain</i>                | 110  | Ugartetxe R., <i>Spain</i>          | 411                   |
| Rodrigues J.P.C., <i>Brazil</i>           | 417  |                                     |                       |
| Rodrigues J.P.C., <i>Portugal</i>         | 222; 228;<br>271; 277;<br>283; 423;<br>512 | Vassart O., <i>Luxembourg</i>       | 537                   |
| Romero M.L., <i>Spain</i>                 | 184  | Vaz M.A.P., <i>Portugal</i>         | 140                   |
| Roosefid M., <i>France</i>                | 530  | Veljkovic M., <i>Sweden</i>         | 102                   |
| Rovnanik P., <i>Czech Republic</i>        | 146  | Vila Real P., <i>Portugal</i>       | 41; 398               |
| Rovnaniková P., <i>Czech Republic</i>     | 146  | Vodolan M., <i>Czech Republic</i>   | 575                   |
|   |  |                                     |                       |
| Saje M., <i>Slovenia</i>                  | 386  | Wald F., <i>Czech Republic</i>      | 13; 164;<br>459; 471  |
| Salvatore W., <i>Italy</i>                | 580  | Wang P., <i>P. R. of China</i>      | 374                   |
| Sandström A., <i>Sweden</i>               | 102  | Wang Y., <i>United Kingdom</i>      | 152; 350;<br>374; 610 |
| Santhanaselvi S., <i>India</i>            | 252  | Welch S., <i>United Kingdom</i>     | 72                    |
| Santos S.O., <i>Portugal</i>              | 283  | Wickström U., <i>Sweden</i>         | 102                   |
| Schaumann P., <i>Germany</i>              | 429  | Winter S., <i>Germany</i>           | 569                   |
| Schneider M., <i>Austria</i>              | 289  |                                     |                       |
| Schneider U., <i>Austria</i>              | 289  | Yao Y., <i>USA</i>                  | 307; 447              |
| Sharma U.K., <i>India</i>                 | 318  | Young B., <i>Hong Kong</i>          | 47                    |
| Silva V.P., <i>Portugal</i>               | 417  | Yuan W., <i>Singapore</i>           | 524; 616              |
| Simões da Silva L., <i>Portugal</i>       | 398  |                                     |                       |
| Sokol Z., <i>Czech Republic</i>           | 459  | Zaharia R., <i>Romania</i>          | 586                   |
| Song K.Ch., <i>Korea</i>                  | 518  | Zeiml M., <i>Austria</i>            | 295                   |
| Song Y., <i>United Kingdom</i>            | 344  | Zhang H., <i>United Kingdom</i>     | 301                   |
| Srpčič S., <i>Slovenia</i>                | 386  | Zhang N.S., <i>P. R. of China</i>   | 502                   |
| Stadler M., <i>Germany</i>                | 543  | Zhao B., <i>France</i>              | 530; 537              |
| Starý J., <i>Czech Republic</i>           | 575  |                                     |                       |
| Štefan R., <i>Czech Republic</i>          | 453  |                                     |                       |
| Stern-Gottfried J., <i>United Kingdom</i> | 34   |                                     |                       |
| Stratford T., <i>United Kingdom</i>       | 202  |                                     |                       |